Proceedings of META'13

The 4th International Conference on Metamaterials, Photonic Crystals and Plasmonics

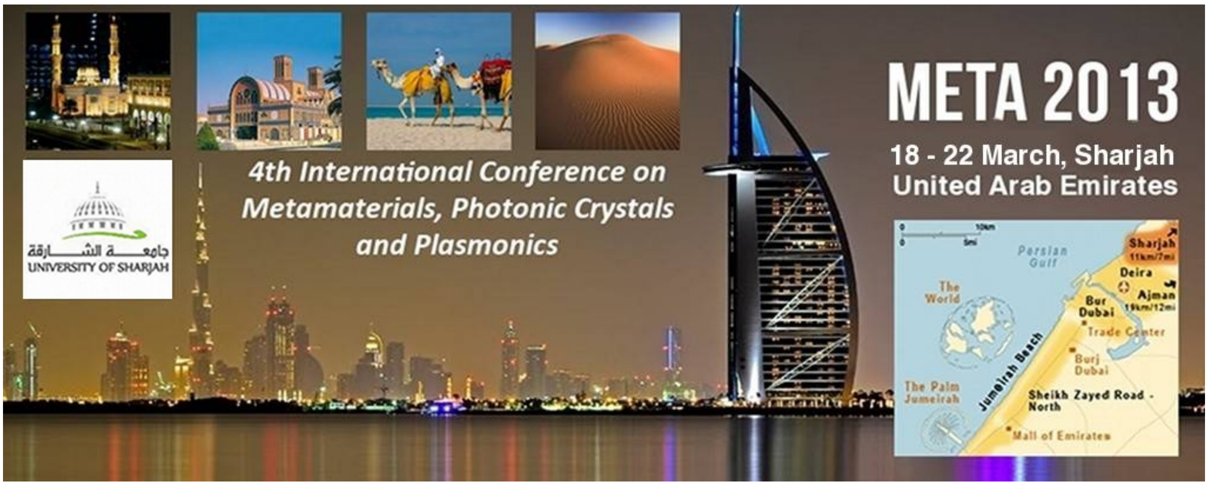

ISBN : 978-2-9545460-0-1

March 18 – 22, 2013
Sharjah, United Arab Emirates

www.metaconferences.org

Proceedings of META'13

The 4th International Conference on Metamaterials, Photonic Crystals and Plasmonics

ISBN : 978-2-9545460-0-1

Edited by

Said Zouhdi | Paris-Sud University, France
Hamid Al-Naimiy | University of Sharjah, UAE

META'13 General Chair

Said Zouhdi, Paris Sud University, France

META'13 General Co-Chair

Hamid Al-Naimiy, University of Sharjah, UAE

Organizing Committee

Hussein M. Elmehdi (Chair), UAE
Laurent Santandrea (Co-Chair), France

Nadjib Brahimi, UAE
Ihsan Shehadah, UAE
AbdulKadir Hamid, UAE
Muhammad Bawa'aneh, UAE
Omar Adwan, UAE
Rafea Haffa, UAE
Kifah Taqez, UAE
Khadijah Al Housani, UAE
Ghada Amer, UAE
Romain Corcolle, France
Tahsin Akalin, France
Mohamed Ahachad, Morocco
Mounia Ajdour, Morocco

International Advisory Committee

Hamid M. K. Al-Naimiy, UAE
Nader Engheta, USA
Mathias Fink, France
Sailing He, Sweden
Tatsuo Itoh, USA
Yuri Kivshar, Australia
Ricardo Marques, Spain
Graeme W. Milton, USA
Raj Mittra, USA
Susumu Noda, Japan
Masaya Notomi, Japan
Yahya Rahmat-Samii, USA
Vladimir Shalaev, USA
Ari Sihvola, Finland
Sergei Tretyakov, Finland
J. C. Vardaxoglou, UK
Alexey Vinogradov, Russia
Martin Wegener, Germany
Nikolay Zheludev, UK

Technical Program Committee

S. Maier (Chair), UK
J.Aizpurua, Spain
T. Akalin, France
A. Alu, USA
W. L. Barnes, UK
X. Begaud, France
S. Bozhevolnyi, Denmark
K. Busch, Germany
C. T. Chan, Hong Kong
A. Chipouline, Germany
J. Christensen, Spain
C. Craeye, Belgium
A. Dmitriev, Sweden
I. El-Kady, USA
D. Felbacq, France
W. Fritzsche, Germany
F. J. Garcia, Spain
H. Giessen, Germany
O. Hess, UK
R. Hillenbrand, Spain
D. Kim, Rep. Of Korea
J. Krenn, Austria
K. Leosson, Iceland
J. Li, Hong Kong
M. McCall, UK
L. M. Moreno, Spain
P. Nordlander, USA
T. Odom, USA
D. Pawlak, Poland
C.-W. Qiu, Singapore
M. Qiu, Sweden
D. R. Smith, USA
T. Tanaka, Japan
A. Urbas, USA
J. K. W. Yang, Singapore
A. V Zayats, UK
X. Zhang, USA
L. Zhou, China

Special Session Organizers

Tahsin Akalin, France
Samel Arslanagic, Denmark
Henri Benisty, France
Pai-Yen Chen, USA
Christophe Craeye, Belgium
Johan Christensen, Denmark
Beatrice Dagens, France
Mady Elbahri, Germany
Nayla El-Kork, UAE
Mohamed Farhat, Saudi Arabia
Vicent Romero Garcia, Spain
Jiaming Hao, France
Mustafa Kuzuoglu, Turkey
Zhengtong Liu, Singapore
Anatole Lupu, France
Radu Malureanu, Denmark
Fernando Moreno, Spain
Manuel Nieto-Vesperinas, Spain
Ozlem Ozgun, Turkey
Wounjhang Park, USA
Dorota A. Pawlak, Poland
Carsten Rockstuhl, Germany
Mohamed Swillam, Egypt

SPONSORS AND SUPPORTERS

We wish to thank the following organizations for their contribution to the success of this conference :

University of Sharjah, UAE
LGEP-SUPELEC, France
Paris-Sud University, France
Institut Français, UAE
Office of Naval Research Global, UK
IOP Publishing, UK
EPL, UK
CST-ME , Egypt
IEEE-APS, USA
URSI, Belgium

META'13 VENUE

META'13 will be held on March 18-22, 2013, at the University of Sharjah, Sharjah, United Arab Emirates.

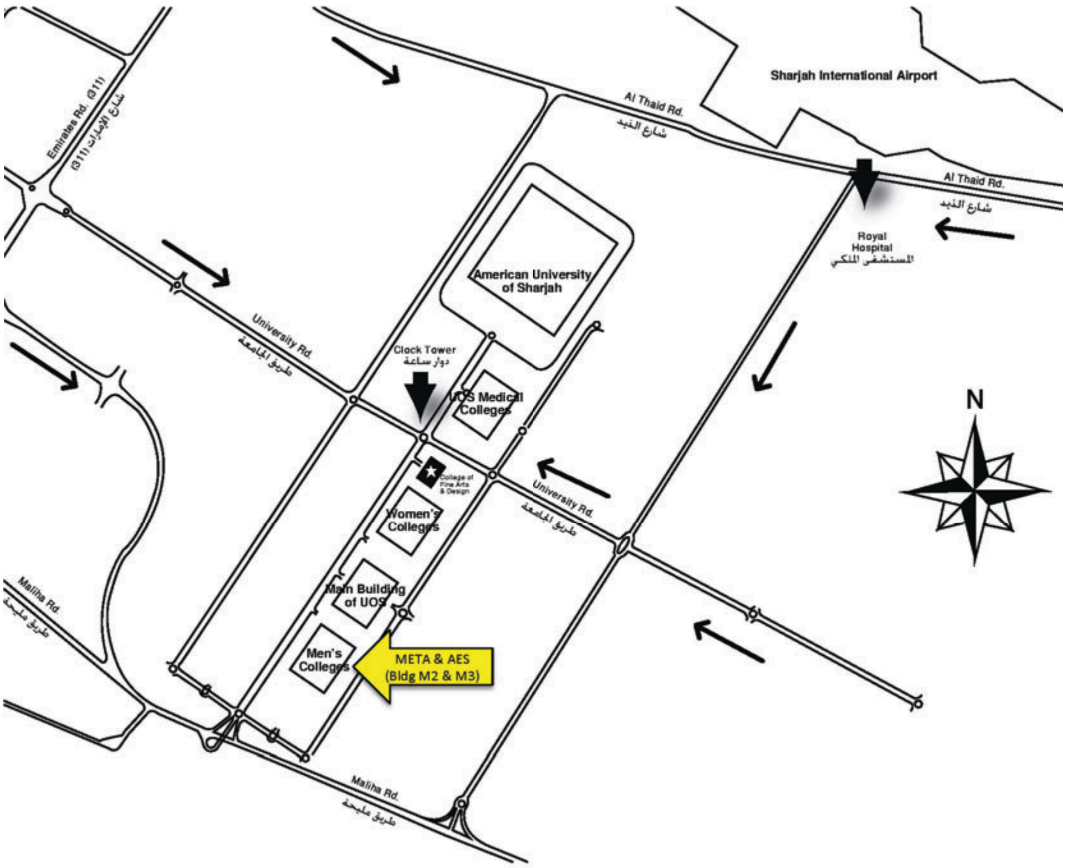

GUIDELINES FOR PRESENTERS

Oral Presentations

Each session room is equipped with a stationary computer connected to a LCD projector. Presenters must load their presentation files in advance onto the session computer. Technician personnel will be available to assist you.

Scheduled time slots for presentation are 20 mn for regular and invited prensentations, 45 mn for plenary talks, and 30 mn for keynote talks, including questions and discussions. Presenters are required to report to their session room and to their session Chair at least 15 minutes prior to the start of their session.

The session chair must be present in the session room at least 15 minutes before the start of the session and must strictly observe the starting time and time limit of each paper.

Poster Presentations

Presenters are requested to stand by their posters during their session. One panel will be available for each poster. Pins or thumbtacks are provided to mount your posters on the board. All presenters are required to mount their papers one hour before the session and remove them at the end of their sessions.

TABLE OF CONTENTS

General Papers

Metamaterials and negative index materials

Graphene metamaterials

Acoustic metamaterials

Biophotonic materials

Plasmonics and nanophotonics

Nanophotonics with gain media for loss compensation and spasing

Hybrid and quantum materials

Photonic crystals

Chiral and bianisotropic materials

Plasmon-enhanced photovoltaics, photocatalysis, and solar fuels

Structured and disordered media

Transformational electromagnetics

Extraordinary transmission

Frequency selective structures and high impedance surfaces

Near-field optics and nano-optics

Analytical and numerical modelling of complex materials and structures

Experimental characterization techniques

Technologies and applications

Plenary Session

Recent progress on numerical methods for metamaterial analysis

Novel applications of transformation electromagnetics

Plasmonic antennas

Active Terahertz Metamaterials

Recent Advances in Nano-Particle Configurations

A bottom-up approach towards metamaterials and plasmonics

Plasmonic Nanocomposites

Tunable metamaterials and plasmonics devices

New Advances in Optically Magnetic Materials for Nanophotonics

Emerging technology in plasmonics

Singularities & broken symmetries of systems with gain and loss structures

Plasmonic Biosensors

Plasmonic metamaterials and applications

Acoustic metamaterials and phononic crystals

Nanoparticles and nanosystems

General Papers

Giant magnetoimpedance in thin amorphous and nanocrystalline microwires.

A. Zhukov[1,2], M. Ipatov[1], M. Churyukanova[3], S.Kaloshkin[3] and V. Zhukova[1+]

[1]Dpto. Física de Materiales, Universidad del País Vasco, San Sebastián, Spain
[2]IKERBASQUE, Basque Foundation for Science, 48011 Bilbao, Spain
[3]National University of Science and Technology «MISIS», Moscow, 119049, Russia
[*]corresponding author: valentina.zhukova@ehu.es

Abstract- We present the results on Giant magneto-impedance effect (GMI) effect in amorphous and nanocrystalline microwires at frequencies till 4 GHz paying special attention to tailoring the frequency and magnetic field dependence of GMI effect . Correlation between magnetoelastic anisotropy and magnetic field dependences of diagonal and off-diagonal impedance components are observed.

Ferromagnetic thin wires (with typical diameters from 5 till 120 μm) gained considerable interest owing to their good soft magnetic properties and giant magneto-impedance, GMI, effect [1,2]. Industrial applications required miniaturization of the magnetic sensors. Therefore soft magnetic wires with reduced dimensionality recently gained much attention [1,2]. GMI effect, consisting of large sensitivity of the impedance of magnetically soft conductor on applied magnetic field, attracted great attention [1,3] due to excellent magnetic field sensitivity. The shape of magnetic field dependence of the GMI effect i the magnetic anisotropy [1-3] Magnetic anisotropy of amorphous and nanocrystalline microwires is determined mostly by the manetoelastic term and can be tailored by thermal treatment [1,2].

We present results on the GMI effect (GMI ratio, $\Delta Z/Z$,) and magnetic properties in amorphous and nanocrystalline glass-coated microwires and possibilities to tailor magnetic field dependence of GMI effect. We observed the optimum frequency for highest GMI effect (Fig.1).

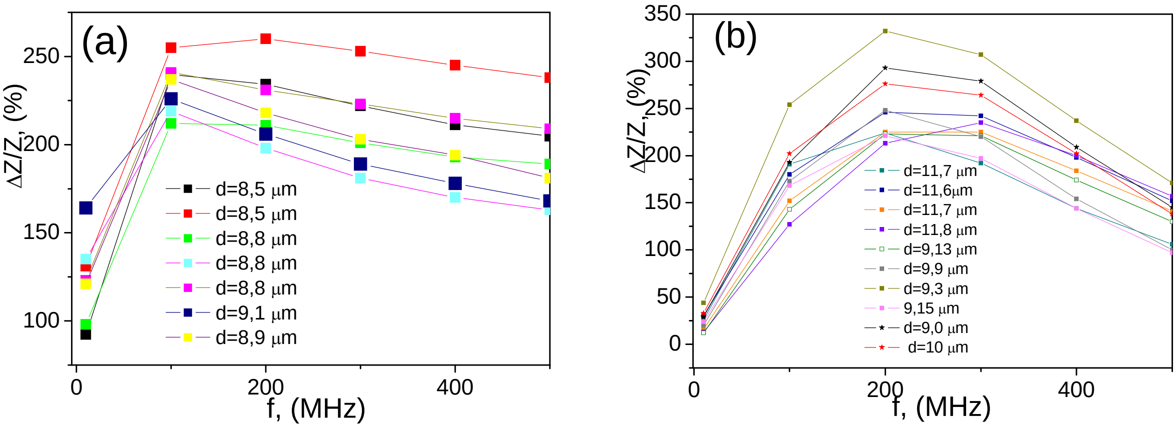

Fig.1. Frequency dependence of $Co_{66.87}Fe_{3.66}Ni_{2,14}Si_{11.47}B_{13.36}Mo_{1.52}C_{0.98}$ microwires with different metallic nucleus diameters.

For microwires of the same composition and different diameters the frequency dependence of maximum GMI ratio, $\Delta Z/Z_m(f)$ the highest GMI ratio, $\Delta Z/Z_m$, presents optimum at different frequencies. Thus, for metallic nucleus diameters ranging between 8,5 and 9,0 μm the optimal frequency is about 100 MHz, while for microwires with metallic nucleus diameters between 9 and 11,7 μm the optimal frequency is about 200 MHz. Nanocrystallization results in increasing of the GMI ration in Fe-rich FeSiBCuNb finemet-type microwires.

Acknowledgements, This work was supported by EU ERA-NET programme under project DEVMAGMIWIRTEC (MANUNET-2007-Basque-3), by Spanish MICINN under Project MAT2010-18914 by the Basque Government under Saiotek 09 MICMAGN (S-PE09UN38) and MEMFOMAG (S-PE12UN139) projects and by federal target program “Scientific and scientific-pedagogical personnel of innovative Russia”, state contract no 14.A18.21.0762.

REFERENCES

1. Zhukova, V; Ipatov, M. & Zhukov A., Thin Magnetically Soft Wires for Magnetic Microsensors. *Sensors* Vol. 9, No. 11, pp. 9216-9240, 2009
2. Vazquez, M.; Chiriac, H.; Zhukov, A; Panina, L. & Uchiyama T., On the state-of-the-art in magnetic microwires and expected trends for scientific and technological studies. *Phys. Status Solidi A*, Vol. 208, No. 3, pp. 493–501, 2011
3. L.V. Panina L.V. and K. Mohri K, Magneto-impedance effect in amorphous wires” *Appl. Phys. Lett.* 65: 1189-1191, 1994.

Magnetic nanoparticles: hybrid architectures with GMR response

A. D. Crisan[1], C. Luculescu[2], F. Dumitrache[2], R. Muller[3], A. Dinescu[3] and O. Crisan[1*]

[1]National Institute for Materials Physics, PO Box MG-7, 077125 Magurele, Romania

[2]National Institute for Laser, Plasma and Radiation Physics, Bucharest, Romania

[3]National Institute for Microtechnologies, Bucharest, Romania

[*]corresponding author: ocrisan@yahoo.com

Abstract-A novel hybrid magnetic-semiconductor structure obtained from magnetic core-shell nanoparticles deposited onto prepatterned Si (111) substrate with basic logic circuitry made of metallic conductive lines is created and its capabilities are demonstrated in terms of magnetotransport properties. The laser pyrolysis method was employed for synthesis of magnetic core-shell Fe/FeC nanoparticles. For the first time, a significant giant magnetoresistive (GMR) effect has been observed for the hybrid device. This opens possibilities for the use of such devices as magnetic GMR-based sensors.

Among the most recent and innovative approaches for synthesis of advanced functional materials at a nanometric scale, nanoparticle organization has proven to be one of the most effective ways for obtaining mono-dispersed nanoparticles (NP's), dispersed onto extended areas [1]. Such arrays of dispersed NP, obtained by a simple and extremely cost effective procedure, may constitute the building blocks for complex-architecture nanostructures for applications in nanoelectronics, applications that uses spin manipulation, and for creation of devices with high added value. On the other hand, one of the newest sciences, related to spin manipulation in magnetic materials, is spintronics [2]. Spintronics utilizes the spin dependent scattering of conduction electrons caused by the direction and magnitude of spontaneous magnetization in magnetic-conductive two-phase materials, at a nanometric scale. The effects exploited in such nanostructures are giant magnetoresistance GMR and spin dependent tunneling SDT [3]. We propose in the present work to create a hybrid architecture structure where a logic conditioned pre-patterned Si substrate is used as a support for regularly dispersed magnetic core-shell nanoparticles and allows detection of magnetoresistive signal along metallic conductive predefined lines. The synthesis method chosen for the core-shell Fe/FeC nanoparticles is the laser pyrolysis technique [4] which is basically a chemical laser precipitation method.

In order to prepare the logic conditioned substrates for the hybrid architectures, Si(111) wafers have been used. A protective 500 nm oxide layer has been grown on top by baking the wafers in induction furnace at 1100C. On the oxide layer a 20 nm thick Cr layer has been grown by e-beam evaporation.

The layout of the polymer masks has been designed as an alternate disposal of 2 different configurations. As a consequence, independent units of 4 x 4 mm covering a total area of 8 x 16 mm have been designed. The layout 1 consists of 4 pads, 300 x 400 μm, connected through thin conductive 50 μm conductive lines with 5 μm spacer disconnecting the lines. The layout 2 contains parallel 2 μm thick lines separated by 5 μm spacer. The lines are connected to the large contact pads, on top and bottom of the figure. The as-designed mask has been made of PMMA photoresist. The pre-patterning has been performed using e-beam lithography. The metallic layer deposited onto the conductive lines was CrAu. After lift-off and corroding the metallic layer, parallel conductive line configurations, as exemplified by SEM image in Fig. 1, are obtained.

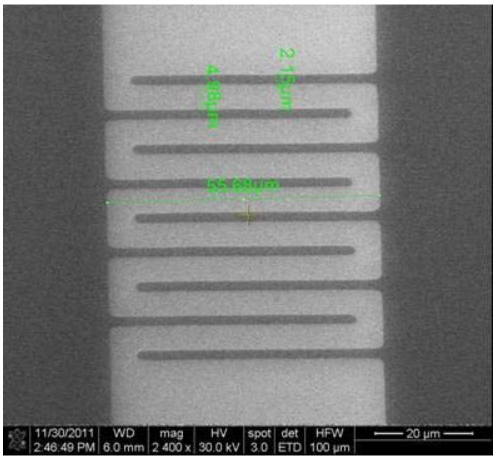

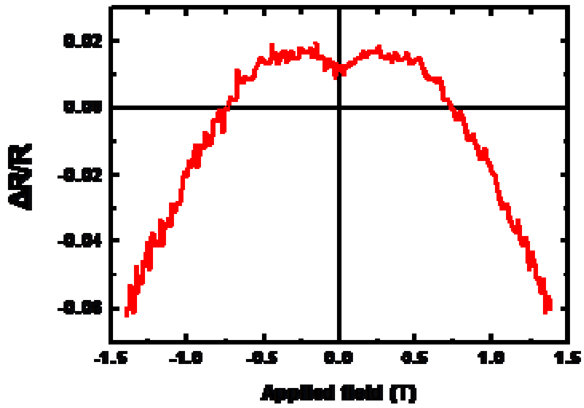

Figure 1: Scanning electron microscopy images of unit with layout 2

Figure 2: GMR response of the hybrid structure at 4.2 K, in CIP configuration.

For the magnetoresistance measurements of the hybrid structure, we have chosen the unit having the layout 2, with 4, 300 microns wide, pads, and 1.5 microns wide conductive lines.

Fig. 2 shows the magnetoresistive curve as a function of the applied field, recorded at 4.2 K, in CIP configuration. The magnetoresistance is given by the ΔR/R ratio defined as:

$$\frac{\Delta R}{R}(T.H) = \frac{R(T,H) - R(0)}{R(0)}$$

where R(T,H) is the resistance at a value H of the applied field and a a temperature T and R(0) is the resistance at the temperature T in the absence of the applied field. In the CIP configuration the hybrid structure shows the highest GMR, of about 6% at 4.2 K. It is a significantly high GMR value that may allow the use of such hybrid structures as magnetic GMR sensors.

In conclusion, a combined approach of nanoelectronics methods and chemical vapour precipitation routes has been undertaken in order to build a hybrid architectured logic device of magnetic core-shell nanoparticles deposed onto prepatterned, logic conditioned, Si substrate. It has been shown that such hybrid architectured structure exhibit a significant giant magnetoresistance effect of about 6% at 4.2 K. This makes such hybrid structures suitable for advanced applications as magnetic GMR sensors.

Acknowledgements: Financial support from Romanian Ministry of Education and Research, through PN II IDEI grant no. 291/2011 is gratefully acknowledged.

REFERENCES

1. Sun, S. and Murray C.B, *Journal of Applied Physics*, Vol. 85, 4325, 1999.
2. Shinjo, T., *Nanomagnetism and Spintronics*, Elsevier Science, Dordrecht, 2009.
3. Moodera, J. S. and Mathon, G., *Journal of Magnetism and Magnetic Materials,* Vol. 200, 248, 1999.
4. Cannon, W.R., Danforth, S.C, Flint, J.H., Haggerty, J.S., Marra, R.A., *J. Am. Ceram. Soc.,* Vol. 65, 324, 1982.

Multi-Band, Highly Absorbing, Microwave Metamaterial Structures

T. M. Kollatou*, A. I. Dimitriadis, S. D. Assimonis, N. V. Kantartzis, and C. S. Antonopoulos

Department of Electrical and Computer Engineering, Aristotle University of Thessaloniki, GR-54124 Thessaloniki, Greece

*corresponding author: fanikollatou@gmail.com

Abstract- The idea presented in this paper concerns the design of new, ultra-thin, polarization-insensitive metamaterial absorbers that operate in mutli-frequency bands within the microwave regime. The basic structure geometry is presented firstly and used to create multi-band higly absorbing structures exploiting the scalability property of the metamaterials. Simulation results verify the high absorption of the structure.

Metamaterials (MTMs) are artificial substances, usually consisting of metallic particles, embedded on a host dielectric medium that exhibit unique electromagnetic properties, not usually encountered in natural media, such as negative refractive index. Those unusual electromagnetic features have gained them worldwide attention and inspired various applications in different engineering fields like antennas, substrates, cloaking and shielding [1], [2]. They are frequently described via effective-medium theories, i.e. by extracting effective electromagnetic parameters [3]. Recently, various metamaterial structures have been proposed in order to achieve almost perfect absorption in the microwave, terahertz, and infrared regions [4]. Initial designs were fabricated in low-cost FR-4 substrate by means of standard photolithographic techniques and have been very sub-wavelength (around $\lambda_0/35$ at the resonant frequency). However, their performance has often been angle- and polarization-dependent, while the absorption bandwidth is usually narrow, due to the resonant behavior of metamaterial elements. Since there is still need for improvement of their performance, a lot of research is still expected to be carried out. This is a subject of huge importance for many different electromagnetic interference/electromagnetic compatibility (EMI/EMC) problems. The purpose of this paper is to present ultra-thin, polarization-insensitive metamaterial structures that can achieve high absorption in multiple frequencies within the microwave regime. To this end, an electric ring resonator (ERR) [5] is imprinted at the front face of a 1 mm thick FR-4 dielectric substrate with a relative permittivity of 4.1 and loss tangent 0.025, as in Fig. 1(a). The opposite side of the dielectric is covered by a full copper plane to ensure zero transmission through the slab and enhance the absorption since it is necessary to minimize both reflection and transmission of incident waves to obtain efficiency. The metallic parts are made of copper, which behaves as a perfect electric conductor (PEC) at the microwave regime. The ERR has been chosen to have rotational symmetry around the propagation axis which makes the structure polarization insensitive. The basic structure geometry is used to create mutli-band absorbers by exploiting the scalability property of the metamaterials.

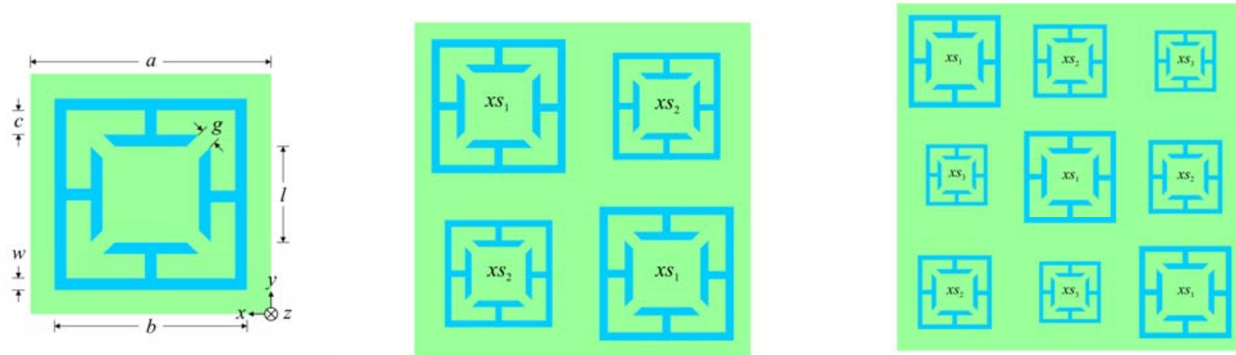

(a) (b) (c)

Figure 1 The original unit cell (a), the unit cell of a dual-band absorber (b) and the unit cell of a triple-band absorber (c).

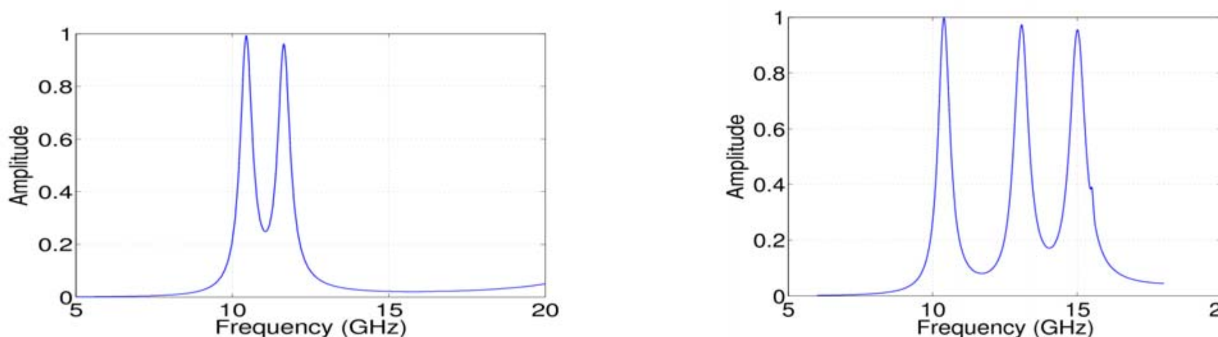

(a) (b)

Figure 2 Absorption spectrum of the dual-band structure (a) the absorption peaks of the triple-band(b)

The geometry of a dual- and triple-band MTM absorber is shown in Fig. 1 (b), (c). The absorption curve of the multi-band absorbers is depicted in Fig. 2 (a), (b). If the design frequencies can be selected to be close enough so as to result in overlapping absorption patterns, bandwidth-enhanced performance can be achieved. Future work could focus on the experimental verification of the simulated structures as well as an insight into which factors influence the absorptive spectra.

REFERENCES

1. C. Caloz and T. Itoh, *Electromagnetic metamaterials: transmission line theory and microwave applications.* Wiley-IEEE Press. 2005.
2. R. Marques, F. Martin and M. Sorolla, *"Metamaterials with negative parameters: theory, design and microwave applications"*, Wiley-Interscience, 2008, Vol. 183.
3. D. Smith, S. Schultz, P. Markos and C. Soukoulis, *" Determination of effective permittivity* And permeability of metamaterials from reflection and transmission coefficients, " Phys. Rev. B, vol. 65, no. 19, p. 195104, 2002.
4. F. Bilotti, A. Toscano, K. Alici, E. Ozbay and L. Vegni, *"Design of miniaturized narrowband absorbers based on resonant-magnetic inclusions,"* IEEE Trans. Electromagn. Compat. vol. 53, no. 1, pp. 63-72, 2011.
5. H. Chen, J. O' Hara, A. Taylor, R. Averitt, C. Highstrete, M. Lee and W. Padilla, "Complementary planar terahertz metamaterials," Opt. Express, vol. 15, no. 3, pp. 1084-1095, 2007.

Toroidal Lasing Spaser

Y.-W. Huang[1], W. T. Chen[1], P. C. Wu[1,] C. Y. Liao[2*], V. A. Fedotov[3], N. I. Zheludev[3,4], and D. P. Tsai[1,2,5]

[1]Graduate Institute of Applied Physics, National Taiwan University, Taipei 10617, Taiwan

[2]Department of Physics, National Taiwan University, Taipei 10617, Taiwan

[3]Optoelectronics Research Centre and Centre for Photonic Metamaterials, University of Southampton, Southampton SO17 1BJ, UK

[4]Centre for Disruptive Photonic Technologies, Nanyang Technological University, Singapore 637371, Singapore

[5]Research Center for Applied Sciences, Academia Sinica, Taipei 11529, Taiwan

[*]corresponding author: r00222042@ntu.edu.tw

Abstract-Toroidal structures can support exotic high-frequency electromagnetic excitations that are neither electric nor magnetic multipoles. Using a model toroidal metamaterial system, we show that coupling optical gain medium with high *Q*-factor toroidal resonance mode can enhance the single pass amplification to up to 65dB. This offers an opportunity of creating the "toroidal" lasing spaser, a source of coherent optical radiation that is fueled by toroidal plasmonic oscillations in the nanostructure.

Spaser is a quantum amplifier of surface plasmons based on stimulated emission of radiation[1]. In a further development of the spaser concept the stimulated plasmonic oscillations were suggested to power up a nanoscale source of coherent radiation, the lasing spaser[2]. The key element of the lasing spaser is a plasmonic metamaterial, a two-dimensional array of plasmonic nano-resonators, which can support a high-*Q* collective and low radiation mode of excitation[2]. In this paper we propose a lasing spaser that is fueled by previously overlooked toroidal dipolar mode of plasmonic coherent oscillations[3]. This peculiar electromagnetic mode is formed by poloidal currents and cannot be described in terms of the standard multipole expansion; it couples very weakly to electromagnetic radiation and until recently remained elusive at microwave[2] and optical frequencies[3]. We show that compare to the conventional magnetic dipolar response, engaging toroidal dipolar resonance in a near-IR active metamaterial enables to lower the levels of gain for loss compensation, optical amplification and lasing. The resonant toroidal mode also ensures stronger collective response of the metamaterial, which will lead to better spatial coherency and narrower diversion of the beam produced in the self-starting regime.

Figure 1(a) shows a schematic diagram of the proposed toroidal lasing spaser. It is based on a two-dimensional array of plasmonic toroidal metamolecules embedded into a dielectric slab with optical gain. Each metamolecule occupies a rectangular unit cell $t \times a_x \times a_z$ and is formed by four identical U-shaped gold nano-resonators suspended in the dielectric with alternating orientations yielding 2-fold rotoinversion axis parallel to *z*-axis. The dimensions of the metamolecules ensure non-diffractive resonant operation of the metamaterial in the near-IR spectral range (see Fig. 1(b)). The optical response of the toroidal metamaterial was modeled by solving 3D Maxwell equations with full-wave finite-element method (COMSOL Multiphysics 3.5a). The permittivity of gold was described by Drude model with the damping constant γ set to $2\pi \times 6.5 \times 10^{12}$ s^{-1} and the plasma frequency $\omega_p = 2\pi \times 2.175 \times 10^{15}$ s^{-1}. Refractive index of the dielectric slab was $n = 1.39$, while its gain coefficient was assumed to be independent of frequency.

In conclusion, we have proposed and numerically studied near-IR toroidal lasing spaser, a metamaterial-based optical amplifier/source of coherent radiation fuelled by toroidal plasmons. Switching from magnetic to toroidal dipolar response at around 110 THz allows to achieve better coherency and bring the gain threshold down to the level of 366 cm^{-1}, which can be provided by quantum cascade amplifiers in near-IR, such as quantum dots (QDs), quantum wells, and organic dyes. Such a high Q-factor of toroidal metamolecule with a narrow bandwidth of gain has applications, such as single pass amplifier which the certain frequency of incident wave can be amplified up to 65 dB ($\sim 3.16\times10^6$ times).

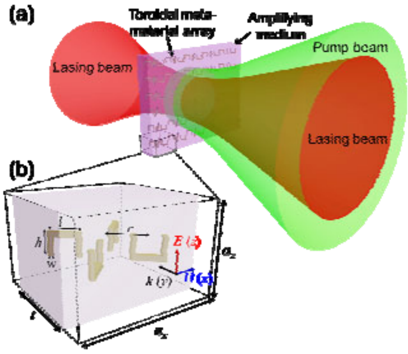

Figure 1. Toroidal lasing spaser: (a) Schematic diagram of the plasmonic toroidal lasing spaser. The structure comprises an amplifying medium slab (purple) supporting an array of plasmonic toroidal metamolecules. (b) Unit cell of the toroidal metamaterial, where a_x = 1200 nm, a_z = 800 nm and t = 800 nm (thickness of the gain medium slab). It contains four gold U-shaped nano-resonators forming toroidal metamolecule with the following dimensions: l = 300 nm, h = 250 nm, r = 300 nm and w = 50 nm. **K**(y), **E**(z) and **H**(x) denote the direction of incident wave, polarization direction of electric and magnetic fields, respectively.

REFERENCES

1. Bergman, D. J. and M. I. Stockman, “Surface plasmon amplification by stimulated emission of radiation: Quantum generation of coherent surface plasmons in nanosystems,” *Phys. Rev. Lett.* Vol. 90, 027402, 2003.
2. Zheludev, N. I., S. L. Prosvirnin, N. Papasimakis and V. A. Fedotov, “Lasing spaser,” *Nat. Photonics* Vol. 2, 351-354, 2008.
3. Huang, Y.-W., W. T. Chen, P. C. Wu, V. A. Fedotov, N. I. Zheludev and D. P. Tsai, “Toroidal lasing spaser,” *Scientific Reports*, Vol. 3, 1237, 2013.
4. Kaelberer, T., V. A. Fedotov, N. Papasimakis, D. P. Tsai and N. I. Zheludev, “Toroidal dipolar response in a metamaterial,” *Science*, Vol. 330, 1510-1512, 2010.
5. Huang, Y.-W., W. T. Chen, P. C. Wu, V. Fedotov, V. Savinov, Y. Z. Ho, Y.-F. Chau, N. I. Zheludev and D. P. Tsai, “Design of plasmonic toroidal metamaterials at optical frequencies,” *Opt. Express*, Vol. 20, 1760-1768, 2012.

Acknowledgements: The authors thank financial aids from National Taiwan University, National Science Council, Taiwan under grant numbers 101-3113-P-002-021, 100-2923-M-002-007-MY3 and 101-2112-M-002-023. Authors are grateful to EPSRC, UK and the Royal Society, London, the National Center for Theoretical Sciences, Taipei Office, Molecular Imaging Center of National Taiwan University and National Center for High-Performance Computing, Taiwan for their support.

Metamaterials and negative index materials

MICROWAVE PROPAGATION IN NONLINEAR MTMS FILM SURROUNDED BY ANISOTROPIC MATERIALS

Hala J. El-Khozondar[1] , Rifa J. El-Khozondar[2], Said Zouhdi

[1]Department of Electrical Engineering, IUG, P. O. Box 108, Gaza, Palestine.

[2]Physics Department, Al-Aqsa University, P.O. box 4051, Gaza, Palestine

[3]Laboratorie do Génie Electrique de Paris, Université Paris Sud 11, France

[*]corresponding author: hkhozondar@iugaza.edu

Abstract- Metamaterials which have both negative permeability and negative permittivity have potential applications in optoelectronics and communications. These materials are fabricated in laboratories which is an added advantage. In this work, we studied the characteristics of waveguide consists of nonlinear MTMs surrounded by anisotropic materials. The dispersion equation is derived from Maxwell's equations. The dispersion equation is solved numerically to study the characteristics of the propagated wave. In this study, we considered only TE modes in the microwave range. Results display the different behavior of the propagating waves as the refractive index of refraction of MTMs change and as the thickness of the film changes.

Keywords: MTMs, anisotropic, microwave, optical waveguide

Unidirectional amplification and shaping of optical pulses by three-wave mixing with negative phonons

A. K. Popov[1*], M. I. Shalaev[2], S. A. Myslivets[3], and V. V. Slabko[2]
[1]University of Wisconsin-Stevens Point, Stevens Point, WI 54481, USA
[2]Siberian Federal University, Krasnoyarsk 660041, Russian Federation
[3]Institute of Physics of the Russian Academy of Sciences,
Krasnoyarsk 660036, Russian Federation
[*]corresponding author: apopov@uwsp.edu

Abstract- A family of photonic amplifiers and switching devices are proposed which mimic and utilize extraordinary coherent nonlinear-optical frequency conversion processes commonly attributed to plasmonic metamaterials.

Optical negative-index metamaterials (NIMs) form a class of electromagnetic media that promises revolutionary breakthroughs in photonics. The possibilities of such breakthroughs originate from backwardness, the extraordinary property that electromagnetic waves acquire in NIMs. Unlike ordinary materials, energy flow, **S**, and wave-vector, **k**, become contradirected in NIMs. This determines their unique linear and nonlinear optical (NLO) propagation properties. Usually, NIMs are nanostructured metal-insulator composites with a special design of their building blocks at the nanoscale that enables negative magnetic response at optical frequencies. Metal component imposes strong absorption of optical radiation in NIMs, which presents a major obstacle towards their numerous prospective exciting applications. Extraordinary features of coherent NLO energy conversion processes in NIMs that stem from wave-mixing of ordinary and backward electromagnetic waves (BW) and the possibilities to apply them to compensating the outlined losses have been shown earlier (for a review, see [1]). Most remarkable feature of NLO propagation processes in such metamaterials is distributed feedback behavior which allows for sharp huge resonance-type increase of conversion efficiency by adjusting strength of the input control field and/or the material slab thickness. Such a property is in strict contrast with the commonly known exponential dependence in ordinary NLO materials. Essentially different properties of three-wave mixing (TWM) and harmonic generation have been shown in [1-3]. Herein, we propose and investigate a different approach to photonic amplification and switching through TWM of ordinary and BWs. It builds on stimulated Raman scattering (SRS) whereby two ordinary electromagnetic waves excite backward elastic vibration wave in a crystal, which results in TWM. The existence of such *crystal building blocks* which support BW optical phonons with *negative* group velocity was predicted in [4]. *Our work* is to show the possibility to substitute sophisticatedly fabricated negative index metal-dielectric composites by the extensively studied ordinary crystals in order to simulate unparallel properties of *coherent NLO energy exchange* between the ordinary and backward waves and related novel possibilities for photonic amplification and switching.

Basic idea that underlies the proposed concept is as follows [5]. The dispersion curve $\omega(k)$ for phonons in the crystals containing more than one atom per unit cell consists of two branches - acoustic and optical. For optical branch, the dispersion is negative in the range from zero to the boundary of the first Brillouin's zone. Hence, the group velocity of optical phonon, $\mathbf{v}_{gr}$, appears antiparallel with respect to its wave-vector, $\mathbf{k}_v$, and phase velocity,

$\mathbf{v}_{ph}$. This is a consequence of the relationship $\mathbf{v}_{gr}= \text{grad}_{\mathbf{k}}\, \omega(\mathbf{k}) < 0$. Optical vibrations can be excited by the light waves through SRS. The latter gives the ground to consider such a crystal as the analog of the NIM at the phonon frequency and to examine the processes of parametric interaction of the three waves. Two of them are ordinary electromagnetic waves. The third one is the BW of elastic vibrations with negative group velocity. Extraordinary propagation and output properties of the Stokes wave were shown to appear in the phase-matching configuration where energy fluxes of Stokes and vibration waves are counter-directed [5]. On the contrary, standard SRS behavior occurs in the opposite case. Both options utilize backward elastic waves. However, it was also found that fast optical phonon relaxation causes the required intensity of the fundamental (control) field to bappear close to the optical breakdown threshold in the continuous-wave regime. Here, we investigate *short-pulse regime* for the fundamental pulse duration shorter than the phonon lifetime. Counterintuitive behavior and the possibility to tailor the output Stokes pulse shape dependent on the difference of group velocities for fundamental and Stokes waves have been shown which are in a striking contrast with those attributed to the counterparts in the standard schemes. They are also different from the properties of the phase-matched mixing of light and acoustic waves for the case where the latter has energy flux and wave vector directed against those of one of the optical waves. BW optical phonons can be excited, for example, in diamond crystals at frequency ω_v = 1332 cm^{-1} with the lifetime $\tau_v \sim 10^{-11}$s. We show that the detrimental role of the phonon relaxation can be eliminated by making use of femtosecond control field pulses. The results of numerical simulations will be presented. The revealed properties can be utilized for creation of optical switches, filters, unidirectional amplifiers and cavity-free optical parametric oscillators based on the readily available Raman crystals without the requirement of periodically poling at the nanoscale [9] (and references therein).

In conclusion, the possibility to exploit ordinary crystals instead of plasmonic NLO NIMs is shown in order to mimic similar extraordinary coherent NLO frequency-conversion processes. Their exotic properties stem from backwardness of optical phonons in the proposed family of crystals. Unparallel properties of coherent energy exchange between electromagnetic and backward vibration waves with the negative group velocity are predicted for one of the possible phase matching options. Both continuous wave and pulsed regimes are investigated and compared. Unique photonic amplifiers and switches with the unparallel properties similar to those achievable with the plasmonic NIMs are proposed. Short-pulse regime is shown to enable overcoming formidable limitations associated with phonon damping. Many orders increase of amplification and extraordinary pulse shaping properties become possible.

Acknowledgements: This work was supported in parts by the US National Science Foundation under Grant No ECCS-1028353, by the US AFOSR Grant No FA950-12-1-298 and by the Russian Federal Program on Science, Education and Innovation under Grant No 14.A18.21.1942.

REFERENCES

1. Popov, A. K. and V. M. Shalaev, ``Merging nonlinear optics and negative-index metamaterials,,'' *Proc. SPIE* vol. **8093-06**, pp. 1-27, 2011, arXiv:1108.0867.
2. Shadrirov, I. V., A. A. Zharov and Yu. S. Kivshar, ``Second-Harmonic Generation in Nonlinear Left-Handed Metamaterials," *J. Opt. Soc. Am. B* vol. **23**, pp. 529-534 (2006).
3. Maimistov, A. I. and I.R. Gabitov, ``Nonlinear optical effects in artificial materials," *Eur. Phys. J. Spec. Top*. **147**, 265–286, 2007.
4. Mandelstam, L. I., ``Group velocity in a crystall lattice," *ZhETF* vol. **15** pp. 475-478, 1945.
5. Shalaev, M. I., S. A. Myslivets, V. V. Slabko and A. K. Popov, "Negative group velocity and three-wave mixing in dielectric crystals," *Optics Lett*. Vol. **36,** pp. 3861-3863, 2011.
6. Khurgin, J. B., ``Mirrorless magic," *Nat. Photonics* Vol. **1**, pp. 446-447, 2007.

Oblique total transmission through epsilon-near-zero materials

J. Luo and Y. Lai*
Wave-functional Materials Lab,
School of Physical Science and Technology,
Soochow University, Suzhou, China
*corresponding author: laiyun@suda.edu.cn

Abstract- Zero-index metamaterials with near zero permittivity and/or permeability usually cannot transmit oblique incident waves due to total reflection. Here, we show that if a tiny disturbance changes the metamaterial into an anisotropic one, it is possible to achieve oblique total transmission at certain angles. Our work may have potential applications for angular filters, ultra-sensitive sensors and switches.

Zero-index metamaterials usually maintain a uniform field inside and thus reflect oblique incident waves[1-2]. However, when parameters are near zero, it is easy to change sign. If an anisotropic disturbance changes the sign of one component of the permittivity tensor, the whole dispersion curve is changed from a tiny circle to hyperbolas. Such a dramatic change may make oblique total transmission through epsilon-near-zero materials possible. In this work, we have investigate this problem analytically and numerically [3].

In Fig. 1, we demonstrate the dispersion surfaces of certain types of epsilon-near-zero materials. Fig. 1(a) shows the model of our study. Fig. 1(b) shows the case when $\varepsilon_x = \varepsilon_y = 0.001$. Figs. 1(c) and 1(d) show the cases when $\varepsilon_x = -\varepsilon_y = 0.001$ and $-\varepsilon_x = \varepsilon_y = 0.001$. It is seen that under a tiny disturbance of 0.002. The dispersion can change dramatically into hyperbolic dispersions.

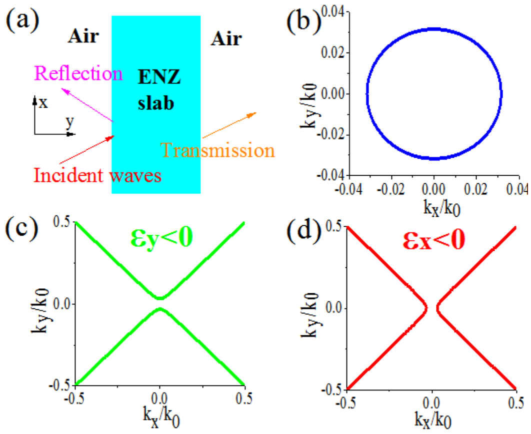

Fig. 1. (a) Schematic graph of ENZ metamaterial slab placed in air. Dispersion curves of ENZ metamaterials with (b) $\varepsilon_x = \varepsilon_y = 0.001$, (c) $\varepsilon_x = -\varepsilon_y = 0.001$ and (d) $-\varepsilon_x = \varepsilon_y = 0.001$.

We apply transfer matrix method to obtain the transmission properties of such epsilon-near-zero materials with hyperbolic dispersions. It is found that the total transmission angles can be obtained from the formula

$\theta = \arcsin\frac{k_x}{k_0} = \pm\arcsin\sqrt{\varepsilon_y\mu - \left(\frac{m\lambda_0}{2d}\right)^2\frac{\varepsilon_y}{\varepsilon_x}}$. Here m is an arbitrary integer and d is the slab thickness.

In Fig. 2, we plot the numerical results of oblique transmission. It clear that several transmission peaks associated with $|m|$=0,1,2,3 are observed. $|m|$=0 does not depend on the slab thickness, while $|m|$=1,2,3 peaks are dependent on the slab thickness. These peaks are very sharp in angle and very sensitive to permittivity change. Therefore, they might be applied for angular filters, ultra-sensitive sensors and switches.

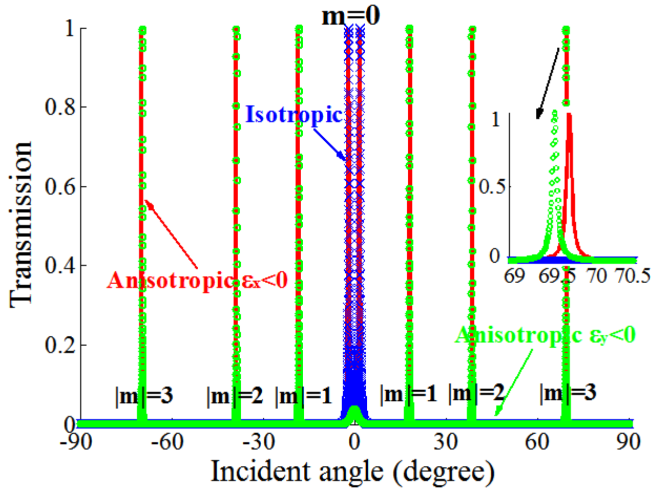

Fig. 2. Transmission coefficients of the isotropic (blue crosses) and anisotropic ENZ metamaterials with $-\varepsilon_x = \varepsilon_y = 0.001$ (red lines) and $\varepsilon_x = -\varepsilon_y = 0.001$ (green circles).

We have also verified our theory by using the finite element method (COMSOL Multiphysics). Numerical simulations with an example using Lorentz model have demonstrated the appearance of such sharp peaks under a tiny anisotropic disturbance.

REFERENCES

1. Silveirinha, M. and N. Engheta, "Tunneling of electromagnetic energy through subwavelength channels and bends using "ε-near-zero materials," Phys. Rev. Lett. 97, 157403 (2006).
2. Huang, X., Y. Lai, Z.H. Hang, H. Zheng, and C. T. Chan, "Dirac cones induced by accidental degeneracy in photonic crystals and zero-refractive-index materials," Nat. Mater. 10, 582–586 (2011).
3. Luo , J., Y.D. Xu, H.Y. Chen, B. Hou, and Y. Lai "Oblique total transmissions through epsilon-near-zero metamaterials with hyperbolic dispersions" unpublished.

Tuniable microwave filter Using Split Ring resonator

Mondher LABIDI, Oussama TABBEBI and Fethi CHOUBANI

Innov'com Research Laboratory, Higher School of Communications of Tunis,
Sup'Com University of Carthage, Tunisia

Abstract— The idea aim of this paper is to describe the potentiality of sub-wavelength resonators, namely, Split-Ring Resonators, complementary split-ring resonators, and related structures to the suppression of undesired spurious bands in microwave filters, a key aspect to improve their rejection bandwidths. The utilization of such resonant structures as efficient microwave filter is also demonstrated. The coupling between 7- SRRs can be quite complex and strongly depends on their geometrical arrangement. These materials have in certain bands a frequency of negative permittivity and permeability with promising applications in the field of microwaves such as: antenna, waveguides, filter…First of all we will examine the electromagnetic behavior of those materials focusing mainly on their response on an external electric field and its crucial role in the achievement of left-handed behavior. Later we will study the applications of these metamaterials in the filter design.

A band-pass filter is a device that passes frequencies within a certain range and rejects (attenuates) frequencies outside that range. An example of an analogue electronic band-pass filter is an RLC circuit. These filters can also be created by combining a low-pass filter with a high-pass filter

This section is devoted to a band-pass filter under SRRs [1-5] and microstrip resonators. here, we represent the characteristics of band-pass structure composed of microstrip resonators. Then, we associate the SRRs with the microstrip resonators and we comment on the results of simulation. In the first part we describe a filter-pass using microstrip resonator only [6]. Several values for width and length of microstrip resonators are taken to behave band-pass to22 GHz. The resonators are five in number and each have a length of 3.43 mm and a width of 1.2 mm. The input lines and output have the same width and a length of 9.825 mm. The width of gaps is 0.2 mm. The total length of the circuit is 38 mm as shown in Figure 1 (a) and the substrate used is ROGERS RO4003C with 3.38 of permittivity and 0.0027 of tangδ. The results obtained from numerical simulations using Ansoft's HFSS show a band-pass character for the filter on use around 22 GHz frequency. Noticing transmission curve, structure shows high insertion loss. This does not in any way considered a problem. In fact, the frequency band of interest here is below the band-pass, where the signal is not transmitted. The second part is devoted to describe the second type of the filter in use. Here, structure represented is made from a blend of microstrip resonators, Split Ring Resonators and an electrical shielding (Figure 1.(b)). The microstrip resonators are used to realize the band-pass filter modeled in the previous section, whose center frequency is 22 GHz with a bandwidth of 0.8 GHz (Figure 2(a)). The input and output lines of band-pass filter can also feed SRRs. Indeed, SRRs produce a resonance effect mainly when magnetic field penetrates through the rings. Thus, an electromotive force is generated around the ring giving rise to the creation of a current flowing on them. This current disappears in the cut rings and many charges of opposite sign accumulate at the ends of each ring. In our case, the magnetic field of the fundamental mode, from microstrip resonators forms a loop around the ribbons. As a result, SRRs must be placed along the axis of propagation perpendicular to the tape drivers to ensure good magnetic coupling. The type of substrate used for SRRs is the same as for the band-pass filter in Figure 1.(a), in other words the RO4003C having a relative permittivity of 3.38, tangential loss of 0.0027, a thickness of 0.81 mm, a height of

3.63 mm, a length of 25.41 mm, a copper layer on each side of 35µm thickness and periodicity of elements is 3.63 mm.

The guide shaped shield has a cross section of 4, 475 × 10 mm2. This shielding reduces the insertion loss of the structure by creating a capacitive effect. As the dimensions of SRRs were calculated for a resonance X-band [8.2 GHz, 12.4 GHz], simulation results (figure 2.(b) show behavior band-pass centered around 10 GHz instead of 22 GHz (figure 2.(a)) with a bandwidth of 0.3 GHz.

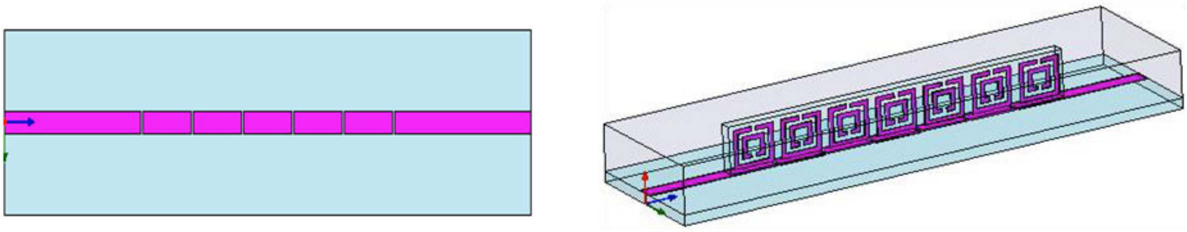

(a) (b)

Figure 1. (a) Pass-band filter using microstrip resonator. (b) Associated SRRs to microstrip resonator

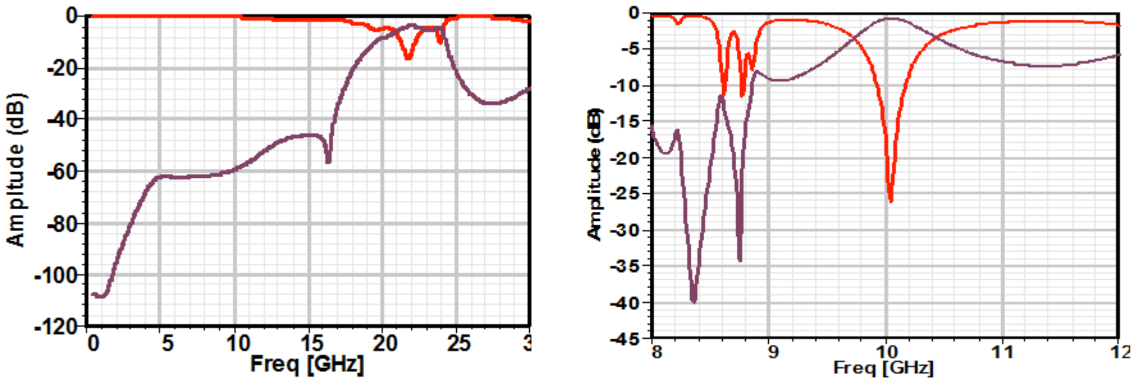

(a) (b)

Figure 2. (a) Transmission and Reflection Coefficients for pass band filter without SRRs, (b) Transmission and reflection Coefficients for band pass filter using SRRs.

REFERENCES

1. J. B. Pendry, “Negative refraction makes a perfect lens”, Physical Review Letters, vol. 85, no.18, pp. 3966–3969, October 2000.
2. D. R. Smith and N. Kroll, “Negative refractive index in left-handed materials”, Physical Review Letters, vol. 85, no. 14, pp. 2933–2936, October 2000.
3. D. R. Smith, D. C. Vier, N. Kroll, and S. Schultz, “Determination of effective permittivity and permeability of metamaterials from reflection and transmission coefficients”, Physical Review B,vol. 65, no. 19, April 2002.
4. V. G. Veselago, “The electrodynamics of substances with simultaneously negative values of ε and μ”, Soviet Physics USPEKHI, vol. 10, no. 14, pp. 509–514, January-February 1968.
5. J. B. Pendry, A. J. Holden, D. J. Robbins, and W. J. Stewart, “Magnetism from conductors and enhanced nonlinear phenomena”, IEEE Transactions on Microwave Theory and Techniques, vol.47, no. 11, pp. 2075–2084, November 1999.
6. S. N. Burokur, M. Latrach, and S. Toutain, “Split Ring Resonators and Slot Split Ring Resonators: Influence on microstrip line transmission and possible applications”, in 11th International Symposium on Antenna Technology and Applied Electromagnetics, St-Malo, June 2005.

SRR Array for Energy Harvesting in the Infrared Regime

Mohammed R. AlShareef*and Omar M. Ramahi
Department of Electrical and Computer Engineering, University of Waterloo, Canada
*corresponding author: mohammed.alshareef@uwaterloo.ca

Abstract-Energy harvesting has recently received much attention since it is an environmental-friendly source of energy. Currently, rectenna systems, which are mainly based on the concept of electromagnetic radiation, can harness ambient energy. In this work, a resonance-based novel structure for harvesting infrared energy is proposed. A new scheme to channel the infrared waves from an array of SRRs is proposed, whereby a wide-bandwidth collector is realized by employing this new channeling concept.

Introduction

Exploiting solar energy effectively, which is a sustainable and pollution-free source, is decisively demanded for our planet. Although producing electricity from solar cells is a promising way to get environmental-friendly energy, its production cost needs to be fallen by a factor of 2-5 compared with fossil fuel. However, a rectenna, which is a significant element in Wireless Power Transmission (WPT) systems, has become an emerging technology for harvesting and collecting ambient RF and solar wave energy. Many publications have focused on WPT using classical antennas [1-5]. Typically, power harvesting using a classical rectenna is still not providing a considerable energy and has disadvantage of design complexity. The necessity of miniaturizing and maximizing power harvesting efficiency in rectenna systems is important to exploit another technology for power collecting purposes. Artificial engineered structures (metamaterials) have received much attention in recent years owing to the uniqueness of their electromagnetic properties [6].

Resonance-based concept has many advantages over the classical approaches. These advantages include, but not limited to, miniaturization, low production cost, coupling effect and more importantly the potential collected power. From that point, our novel concept based on resonator coupling and utilizing metamaterials, which is meeting these demands, is proposed to collect infrared energy.

Array Harvester of Infrared Energy

An array of three SRRs extended over a wide bandwidth (420-550 GHz) is proposed. This structure is utilizing a Silicon (S_i) substrate with thickness ($h=100\ \mu m$) and dielectric constant ($\varepsilon_r=11.9$). Figure 1 depicts the layout of the proposed energy collector. The microstrip line that comes beside the SRRs couples the resonators. In other words, it channels the energy from each SRR and feed it towards the resistive load terminated at the end of the microstrip. Figure 2 represents the scattering parameters of the array structure after loading the microstrip line with a 185Ω rsistance. The last plot shows the calculated power efficiency of the array after loading it with a 185 **Ω** as depicted in Figure 3. This resistance is connected at a one terminal of the strip line, where its value is chosen, at which, the maximum power transfer can occur. The highest power efficiency happens around 540 GHz, which reads above 38%.

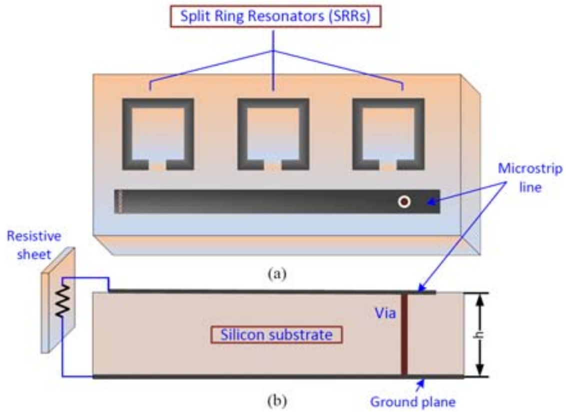

Figure 1: Layout of the far-infrared array energy harvester, (a) top view and (b) side view.

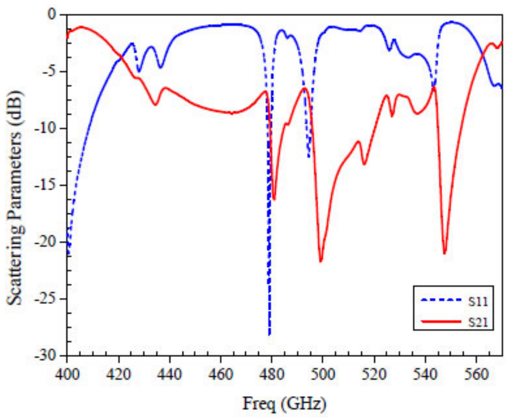

Figure 2: Simulated scattering parameters for the far-infrared array energy harvester

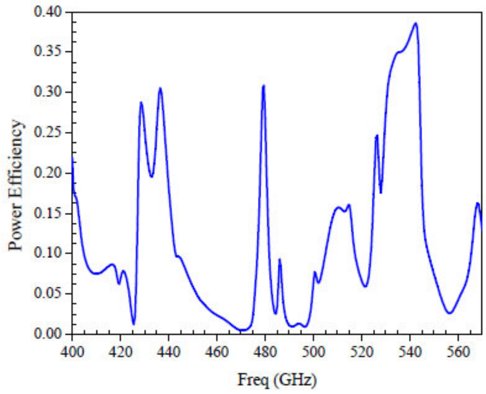

Figure 3: Calculated power efficiency of the array

Acknowledgements: This work was supported in part by the Saudi Arabian Ministry of Higher Education.

REFERENCES

[1] J. McSpadden, T. Yoo, and K. Chang, "Theoretical and experimental investigation of a rectenna element for microwave power transmission ", *Microwave Theory and Techniques*, IEEE Transactions on 40, 2359, 1992.

[2] W.-H. Tu, S.-H. Hsu, and K. Chang, "Compact 5.8-GHz Rectenna Using Stepped-Impedance Dipole Antenna", *Antennas and Wireless Propagation Letters*, IEEE 6, 282, 2007.

[3] Y.-J. Ren and K. Chang, "New 5.8-GHz circularly polarized retrodirective rectenna arrays for wireless power transmission", *Microwave Theory and Techniques*, IEEE Transactions on 54, 2970 , 2006.

[4] N. Shinohara and H. Matsumoto, "Experimental study of large rectenna array for microwave energy transmission", *Microwave Theory and Techniques*, IEEE Transactions on 46, 261, 1998.

[5] D.-G. Youn, Y.-H. Park, K.-H. Kim, and Y.-C. Rhee, "A study on the fundamental transmission experiment for wireless power transmission system", inTENCON 99. *Proceedings of the IEEE Region 10 Conference*, Vol. 2 (1999) pp. 1419-1422 vol.2.

[6] D. R. Smith, J. B. Pendry, andM. C. K. Wiltshire, "Metamaterials and Negative Refractive Index", *Science* 305, 788, 2004.

Total Transmission in Multi-Channel Systems using Tunneling Effect in Epsilon Near Zero Materials

A. Ourir[1*], A. Maurel[1], and V. Pagneux[2]

[1]Institut Langevin LOA, UMR CNRS 7587 - ESPCI - UPD Univ. Paris 7, 10 rue Vauquelin, 75005 Paris, France

[2]Laboratoire d'Acoustique de l'Université du Maine, UMR CNRS 6613, Avenue Olivier Messiaen, 72085 Le Mans, France

[*]corresponding author: a.ourir@espci.fr

Abstract- A realization of a reflectionless power splitter is proposed by use of a metamaterial junction. A closed analytical form is derived for the scattering matrix of any geometry of the interconnected leads. We show that the use of a junction made of ε-near-zero material (ENZ) allows to produce perfect transmission. This can be achieved by reducing the area of the ENZ junction (squeezing effect) and by tuning the widths of the output leads with respect to the input lead.

Recently, zero index metamaterials (ZIM) have been the subject of a growing interest. ZIMs are structures consisting of permittivity ε near zero media (ENZ), permeability μ near zero media (MNZ), or matched impedance zero-index material (MIZIM) where ε and μ vanish simultaneously over a specific frequency band. Original devices and applications involving ZIMs have been investigated experimentally and theoretically [1,2, 3,4]. Other interesting applications concern the tunneling and squeezing of electromagnetic waves in ZIM channels to realize total transmissions or total reflections. This has been considered first in [5] for subwavelength channels and bends. The authors solved the problem of the impedance mismatch for ENZ material by using the so-called squeezing effect, which consists in choosing the area of the channel filled with ENZ electrically small.

In this paper, from closed form expressions of the scattering matrix, we show that tunneling and squeezing effects can be used to control the scattering of a ZIM junction connected to multiple leads. It appears that by properly choosing the widths of the leads, it is possible to get perfect transmission allowing the design of nearly perfect power splitters.

We first characterize the scattering matrix of an arbitrary junction with ZIM material connecting multiple leads, as shown on Fig. 1(a). The whole geometry is two dimensional, invariant to translation along the z-direction and we consider TM polarization of the magnetic field $\mathbf{H}(x, y) = \mathbf{H}(x, y)\, \mathbf{e}z$. The scattering matrix S can be determined using the variational formulation and the continuity of $\mathbf{H}$ at the lead boundaries, $a_n + b_n = \mathbf{H}_0$, where a_n and b_n denote the amplitudes of the incoming and of the outgoing waves in the lead n (Fig.1). In particular, we solve the problem of a power splitter shown in Fig.1(b). We discriminate the inlet of height h_0 connecting the ZIM junction at L_0 from the remaining N outlets. The wave is incident from the inlet lead. The reflection and transmission coefficients r and t_n, $n = 1, \ldots, N$ are given by Eq. (1).

According to Eq. (1), low reflection occurs for $\Sigma h_n = h_0$ and $k\mu A/h_0 \ll 1$. We can use the squeezing effect for a non magnetic ($\mu = 1$) ENZ material to achieve a small reflection by reducing the area of the ENZ junction. Denoting L the typical length of the junction, the low phase variation condition that achieves low reflection, reduces to $\sqrt{\varepsilon} kL \langle\langle 1$ for the an ENZ junction and $\varepsilon kL \langle\langle 1$ for the MIZIM junction.

$$
\begin{cases}
r = \dfrac{1 + ik\mu A / h_0 - \sum_{n=1}^{N} h_n / h_0}{1 - ik\mu A / h_0 + \sum_{n=1}^{N} h_n / h_0}, \\
t_n = 1 - r,
\end{cases}
\tag{1}
$$

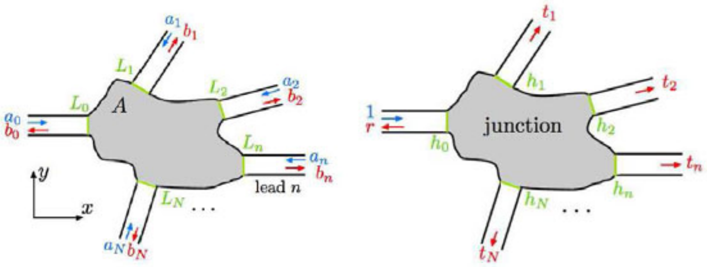

(a) (b)

FIG. 1. a) Geometry of the leads connected to a ZIM junction. b) The Power Splitter with N outlets.

We confirm our analytical results in a particular geometry of power splitter, by comparison with numerical simulations using finite element software package (Comsol). We set the widths of the inlet and outlet leads $h_0 = 0.3\ m$ and $h_n = h_0/3,\ n = 1, 2, 3$. The frequency f varies between 0 and 2 GHz. This corresponds to a dimensionless frequency kh_0 between 0 and 4π. Fig 2 shows the magnetic field distribution when a TM plane wave is incident from the left in the lead 0 connecting a MIZIM junction with $\varepsilon = \mu = 0.001$ compared to a squeezed ENZ junction with $\varepsilon = 0.001$ and μ=1. The incoming wave transmits through the junction with very low reflectivity and a transmission with an equal repartition of the energy in the three output leads is obtained in the two configurations.

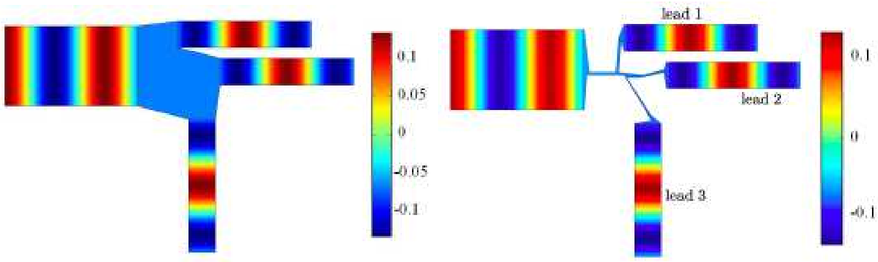

(a) (b)

FIG. 2. Real part of the magnetic field **H**(x, y) for a three output power splitter based on a MIZIM (a) and an ENZ (b) junctions.

We have shown that efficient multiple output dividers can be designed using ZIM-materials. These dividers have the advantage of being compact for any geometry, without restriction on the number and on the directions of the outlets. We have considered here the case of an equipartition of the power but one can design easily configuration with other power repartition. Finally, note also that such divider can work as combiner as well in symmetric modes.

Acknowledgements, The authors acknowledge the financial support of the Agence Nationale de la Recherche through the grant ANR ProCoMedia, project ANR-10-INTB-0914.

REFERENCES

1. J. Li, L. Zhou, C. T. Chan, and P. Sheng. Phys. Rev. Lett., 90: 083901 (2003).
2. R W. Ziolkowski. Phys. Rev. E, 70: 046608 (2004).
3. A. Al`u, M G. Silveirinha, A. Salandrino, and N. Engheta. Phys. Rev. B, 75: 155410 (2007).
4. J. Luo, P. Xu, L. Gao, Y. Lai, and H. Chen. Plasmonics, 7: 353–358 (2012).
5. M. Silveirinha and N. Engheta, Phys. Rev. Lett., 97:157403 (2006).

Sub-Wavelength Imaging with Non-Spherical Plasmonic Nano-particles

Y. Kiasat[1, 2*], Zs.Szabo[3], and E. P. Li [1]

[1] Institute Of High Performance Computing (IHPC), Singapore

[2] National University of Singapore, Singapore

[3] Department of Broadband Info communications and Electromagnetic Theory, BME, Hungary

[*] corresponding author: g0900296@nus.edu.sg

Abstract- The design of single and multi layer composite superlenses is presented herein to image objects with sub-wavelength features. The dependence of the optical property of the composite on the shape, size, and orientation of nano-particles provides high degree of freedom to fabricate the superlens according to the wavelength of the available laser source. It is shown that properly designed aligned ellipsoid nano-particle leads to low loss composites with improved sub-wavelength imaging capabilities. This observation makes the ellipsoid nano-particles a prospective candidate for low loss tunable sub-wavelength imaging.

The state-of-the-art fabrication techniques and the suitable optical property of noble metals have facilitated the science and the engineering community to extend the techniques of the sub-wavelength imaging in the recent years [1-3]. However due to the monotone nature of the noble metals dispersion curve, the metal-based superlenses are only able to perform imaging at a specific frequency, where the electric permittivity equals minus one. In contrast to the fixed electric permittivity of the metallic thin films, where the imaging can be successful, the composite lens provides the possibility to tune the effective permittivity. Consequently in this paper we present the design of single and multi layer composite superlenses to image objects with sub-wavelength features.

The composite thin film is made of deep sub-wavelength metallic nano-particles, which can support dipolar plasmonic modes, embedded in a dielectric host. The optical properties of the composite depend on the shape, size, and orientation of the nano-particles, which provide sufficient degree of freedom to optimize the superlens according to the wavelength of the available laser source. This novel structure not only offers tunability but may eliminate the hot spots created by the localized surface plasmons supported by the surface imperfections of the bulk metallic thin films.

To design the multilayer superlens, the optical transfer function is calculated based on the transfer matrix method. This method provides the exact solution of Maxwell equations for waves propagating in isotropic and anisotropic multilayer structures. The optical properties of the metal-dielectric composite are described with an extended effective medium theory, which takes into account the higher order scattering in the averaging procedure of the field quantities. The composite slab with spherical or randomly oriented elliptical nano-particles has isotropic effective optical parameters, while aligned elliptical nano-particles leads to anisotropic materials tensors. It is shown that in lenses with properly designed layers of anisotropic material, the evanescent waves can be converted to propagating waves and the sub-wavelength imaging process is less sensitive to the material loss of individual constituents. This observation makes the ellipsoid nano-particles intriguing option for low loss tunable sub-wavelength imaging. To achieve the highest possible resolution of the lensing system, the geometrical parameters and the orientation of the nano-particles, the filling fraction and the thickness of the individual layers are determined with differential evolution optimization algorithm [5].

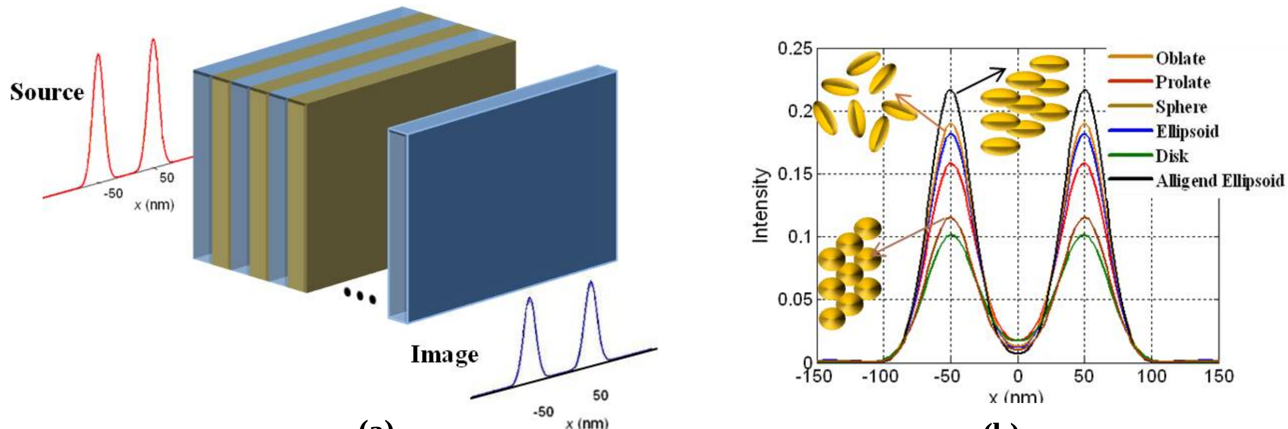

(a) **(b)**

Figure 1 The image formation of the imaging system made of composite thin film layers separated with dielectric. The imaging object is a two slit modeled with a double Gaussian intensity distribution in the source plane. The geometry of the imaging system is presented in (a). The optimized intensity distribution in the image plane in function of the shape and orientation of the metallic inclusions (spherical ($\lambda = 357nm$), nano-particles randomly oriented ($\lambda = 488nm$) and aligned ellipsoidal ($\lambda = 429nm$), nano-particles) are presented in (b).

Acknowledgements, The support of Agency for Science Technology and Research (A*STAR) Singapore, Metamaterial Research Program Grant No. 0821410039 is acknowledged. Zsolt Szabó is grateful as well for the support of the János Bolyai Research Fellowship of the Hungarian Academy of Sciences.

REFERENCES

1. Fang, N *et al*, “Sub-diffraction-limited optical imaging with a silver superlens”, *Science* **308**, 534 (2005).
2. Wood *et al*, “directed sub-wavelength imaging using a layered metal-dielectric system”, *Phys. Rev. B* **74**, *(*2006).
3. Smolyaninov *et al*, “Magnifying superlens in the visible frequency range,” *Science* **315**, 1699 (2007).
4. Zs. Szabó, Y. Kiasat, E. P. Li, Isotropic Metal-Dielectric Composites for Subwavelength Imaging, META’12 the 3rd International Conference on Metamaterials, Photonic Crystals and Plasmonics, Paris, France, 19-22 April (2012).
5. K. V. Price, R. M. Storn, J. A. Lampinen, “Differential Evolution, A Practical Approach to Global Optimization”, *Springer*, (2005).

Microwave metamaterials with competing nonlinearity

P. V. Kapitanova[1], **A. P. Slobozhanyuk**[1], **I. V. Shadrivov**[1,2], **P. A. Belov**[1], **and Yu. S. Kivshar**[1,2]
[1]National Research Univ. of Information Technologies, Mechanics, and Optics, St. Petersburg, 197101 Russia
[2] Nonlinear Physics Center, Australian National University, ACT 0200 Canberra, Australia

Abstract- We suggest an approach for creating metamaterials with sign-varying nonlinear response. We demonstrate that microwave metamaterials with such competing nonlinearities can be created by loading split-ring resonators (”meta-atoms” of the structure) with pairs of varactor diodes and photodiodes exhibiting nonmonotonic resonance frequency shift on incident microwave power. Additionally, the nonlinear response of such metamaterials can be controlled by illuminating the meta-atoms by light.

Recently emerged physics of metamaterials offers exceptional opportunities for creating artificial materials with a wide range of macroscopic parameters through appropriate arrangement of their subwavelength elements [1-3]. However, it has not been recognized yet that the concept of metamaterials allows engineering a nonlinear response as well. In this paper we study the nonlinear behavior of a light-tunable split-ring resonator (SRR) recently proposed in [4]. We demonstrate that the effective nonlinearity can change its sign as we increase the intensity of a microwave signal. Moreover, the nonlinear response can be controlled additionally by illuminating photodiode with an external light source. We demonstrate that such nonmonotonic nonlinear response corresponding to the competing nonlinearities is caused by effective switching between the two nonlinear regimes.

Schematic of the SRR is shown in Fig. 1 (a), with the photograph of the experimental setup presented in Fig. 1 (b). The SRR is formed by two side-coupled broken rings made of copper, which are printed on a dielectric substrate (FR4 fiberglass, $\varepsilon_r \cong 4{:}4$). To achieve tunability, we solder a varactor diode (D1) in an additional gap, which we made in the outer ring of the SRR. The bias voltage for the varactor diode is produced by two photodiodes (D2 and D3), which operate in the photovoltaic mode. The polarity of the photodiodes is chosen so that they provide the reverse voltage on the varactor. To prevent shunting the varactor by the large capacitance of the photodiodes, we use chip inductors (L) connected in series with the photodiodes. The more details on the SRR geometrical size and components used can be found in [4].

We experimentally investigate the reflection coefficient measured by an Agilent PNA E8362C vector network analyzer when the loop antenna is coupled to the SRR is shown in Fig. 1 (b) for the incident power changing from 0 dBm up to 24 dBm and for the light intensities illuminating photodiodes 0 lx (dark state) and 17 klx (bright state). The resonant frequency is determined from the minimum of the reflection coefficient, and its shift is represented in Fig. 1 (c). In the dark state the resonant frequency grows when the input power increases up to 14 dBm and decreases with further power increase. In the bright state, the resonant frequency decreases monotonically with the increase of the input power. This result indicates that the type of the nonlinear response of the SRR can be changed by light illumination.

In order to understand the nonlinear behavior of the SRR we measure the current vs. voltage (I – U) characteristic of the photodiode. In the dark state, the observed I – U behavior is similar to that of a conventional rectifier diode. However, when the photodiode is illuminated, the I – U curve shifts. If the circuit is open

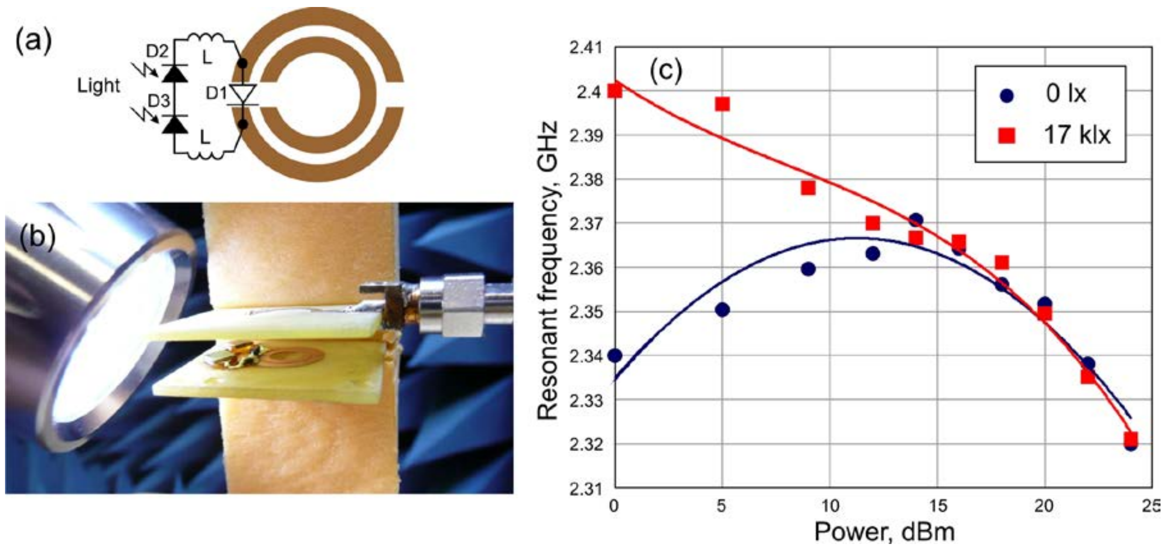

Figure 1. (a) Schematic of the light-tunable SRR and attached electronic components. (b) Photograph of a SRR sample (bottom dielectric board) excited by a loop antenna (top dielectric board) and illuminated by a light source. (c) Experimentally measured shift of the SRR resonant frequency as a function of input power, for two values of light source intensity. Measured data are shown by markers, whereas the lines are guide for eye.

(operation in a photovoltaic mode), the open circuit voltage 0.4 V will be generated with positive polarity at the anode. On the other hand, if the circuit operates in a biased regime and the forward voltage is applied to the photodiode, the breakdown voltage can be estimated as U_d=0.44 V.

Thus, a change in the sign of nonlinear frequency shift can be explained by the regimes of the photodiodes operation. In the dark state, when the input power is low, the photodiodes operate in the bias-free regime providing zero reverse voltage to the varactor. The constant voltage across the varactor appearing due to the signal rectification shifts the operating point of the varactor to the region of the $I - U$ curve with low effective conductance and lower capacitance, and the SRR resonant frequency grows. After the input power increases up to 15 dBm, the voltage rectified by the varactor is of the order of 1 V which is above $2U_d$. This bias applied to photodiodes is sufficient to make them conducting. As soon as this happens, the characteristic impedance of photodiodes significantly decreases and DC current may flow via this network causing the varactor discharge. As a result, with further power increase the resonance frequency decreases. In the light illuminated state the varactor operates around the zero voltage point, this leads only to the negative sign of nonlinearity.

In conclusion, we have demonstrated that the split-ring resonator incorporating electronic components may exhibit nonmonotonic dependence of its resonant frequency on the incident microwave power. In addition, by employing photodiodes it becomes possible to tune the overall nonlinear response by illuminating the structure with light. The proposed meta-atoms would allow creating metamaterials with competing nonlinearity, the type of material that was long considered by theoreticians, but which was never found in nature. We believe that our approach will be useful for other types of nonlinear metamaterials also allowing to control and engineer both wave mixing and second-harmonic generation.

REFERENCES

1. D.R. Smith, W.J. Padilla, D.C. Vier, S.C. Nemat-Nasser, and S. Schultz, *Phys. Rev. Lett.*, **84**, 4184 (2000).
2. M. Gorkunov, M. Lapine, E. Shamonina and K.H. Ringhofer, *Eur. Phys J. B*, **28**, 263 (2002),
3. D. Powell, M. Lapine, M. Gorkunov, I. Shadrivov, and Yu. Kivshar, *Phys. Rev. B*,**82**, 155128-8 (2010).
4. P. Kapitanova, S. Maslovski, I. Shadrivov, P. Voroshilov, D. Filonov, P. Belov, and Yu. Kivshar, *Appl. Phys. Lett.*, **99**, 251914 (2011).

Determination of the effective material parameters of PMMA filled with gold, silver, and mixed nano-particles for a cylindrical cloak

M.M. Sadeghi [1], H. Nadgaran[1*]
[1]Physics Dep., Shiraz University, Shiraz 71454, Iran
[*]corresponding author: nadgaran@susc.ac.ir

Abstract *This work investigates the quality and quantity of a cylindrical cloak made of PMMA material filled with gold, silver, and mixed nano-particles. The effective material parameters together with their transformed permittivity and permeability are calculated by a home-made computational code. The form of the three different cloaks will be compared pictorially.*

Form-invariant Maxwell's equations are usually transformed optically to describe the relations between field, sources, and materials [1,2]. Often optical transformation can well lead to new permittivity and permeability tensors that are the main tools for cloaking [2,3]. For a cylindrical cloak we have:

$$\mu_z = (\frac{b}{b-a})^2\ \frac{r-a}{r}\ ,\varepsilon_\theta = \frac{r}{r-a}\ ,\ \varepsilon_r = \frac{r-a}{r} \tag{1}$$

that finally reduces to [4, 5, 6]:

$$\mu_z = 1\ ,\varepsilon_\theta = (\frac{b}{b-a})^2\ ,\ \varepsilon_r = (\frac{b}{b-a})^2\ (\frac{r-a}{r})^2 \tag{2}$$

where ε and μ show the permittivity and permeability of the material, *a* and *b* denote the outer and inner radius of the cylinder respectively [6].
In this work we assume a cylindrical cloak whose unit cells are filled with spherical nano-gold particles, nano-silvers, and a combination of nano-gold and nano-silvers to investigate the quantity and quality of cloaking mechanism. All the above nano-particles are supposed to be embedded in a PMMA host medium. A home-made simulation code was prepared to determine the effective material parameters.
The cylindrical cloaking shell is assumed to be a composite structure of unit cells consisting of one golden sphere in a PMMA host medium (figure 1). The shape of every unit cell has a small curvature, but it can be approximated as a rectangular prism since the curvature is small. This is due to the small dimensions of the unit cell compared to the cloaking shell. In simulating the special material mentioned, we made use of the so-called parameter-retrieval method of Smith *et al* [7, 8] in which knowledge of S_{11} and S_{12} can provide the effective refractive index n_{ret} and the effective impedance z_{ret} of the unit cell. These two important parameters can well give the effective permittivity and permeability.
We used two independent configurations with incident TM-polarized light, first light propagate along the r –direction (figure1) and second along φ-direction (figure 2). This allows us to independently derive the ε_φ and ε_r components of the permittivity tensor. The permittivity of PMMA has been set to 2.25.

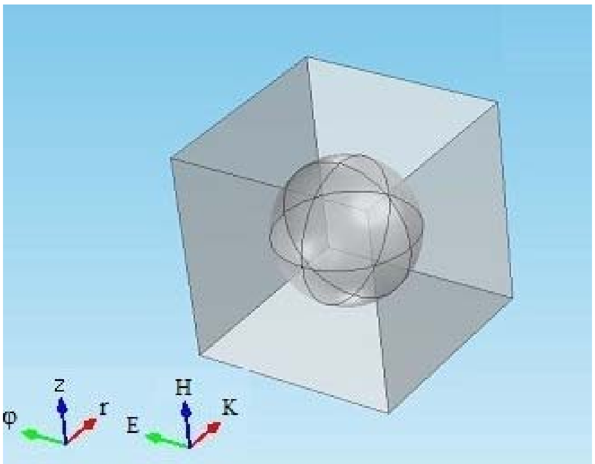

Figure 1

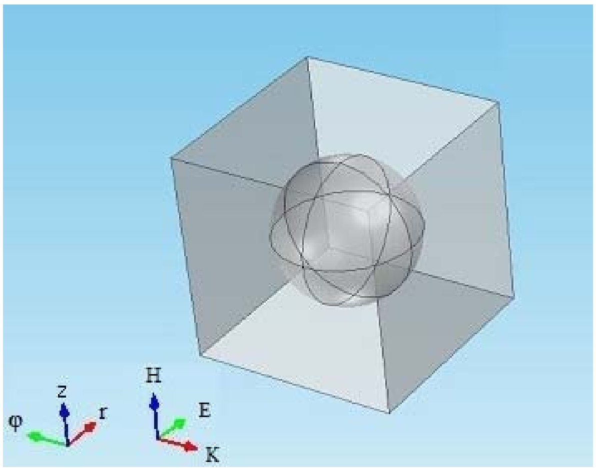

Figure 2

Final part of the paper is devoted to comparison between the three special cloaks (silver, gold, and mixed) by pictorial methods of so-called continuous-ideal, continuous-reduced, and discrete-reduced parameter [9,10].

REFERENCES

1. Ward, A.J., Pendry, J. B. "Refraction and geometry in Maxwell's equations". *J. Mod Opt*. 43:773–793, 1996.
2. Leonhardt,Ulf, Tomas Philbin., *Geometry and Light:The science of invisibility*, Dover Publication, New York, 2010.
3. Leonhardt U , "Optical conformal mapping", *Science* 312:1777–1780, 2006.
4. Tamm IE, "Electrodynamics of an anisotropic medium in the special theory of relativity", *J. Russ Phys Chem Soc.* 56:248, 1924.
5. Cai, Wenshan., *Optical Metamaterials*, Springer, New York, 2010.
6. Pendry J.B., Schurig, D., Smith D.R. "Controlling electromagnetic fields", *Science*, 312: 1780–1782, 2006.
7. Romero, I., F. J. Garcia de Abajo, "Anisotropy and particle-size effects in nanostructured plasmonic metamaterials," *Opt. Express,* **17** 22012–22, 2009.
8. Smith D R, S. Schultz , P. Markov and C. M. Soukoulis, "Determination of effective permittivity and permeability of metamaterials from reflection and transmission coefficients", *Phys. Rev.* B **65** 195104, 2002.
9. Schurig D, Mock J.J, Justice B.J., Cummer S.A., Pendry J.B., Starr A.F., Smith D.R., " Metamaterial electromagnetic cloak at microwave frequencies". *Science* 314:977–980, 2006.
10. Diedrich, D., A. Rottler., D. Heitmann and S. Mendach, "Metal–dielectric metamaterials for transformation-optics and gradient-index devices in the visible regime", *New J. Phys.* 14 053042, 2012

Finite Difference Time–Domain Modelling of Metamaterials: GPU Implementation of Cylindrical Cloak

A. Dawood[1]

[1]National University of Computer and Emerging Sciences (FAST), Pakistan
attique.dawood@nu.edu.pk

Abstract— Finite difference time–domain (FDTD) technique can be used to model metamaterials by treating them as dispersive material. Drude or Lorentz model can be incorporated into the standard FDTD algorithm for modelling negative permittivity and permeability. FDTD algorithm is readily parallelisable and can take advantage of GPU acceleration to achieve speed–ups of 5x–50x depending on hardware setup. Metamaterial scattering problems are implemented using dispersive FDTD technique on GPU resulting in performance gain of 10x–15x compared to conventional CPU implementation.

Standard FDTD algorithm cannot cater for negative values of permittivity or permeability. This is because of the Courant stability criterion. As soon as the permeability or permittivity becomes less than unity the algorithm will not be stable. A metamaterial object can be modelled as a dispersive substance using either the Lorentz or Drude dispersive models. These models can yield negative values of permittivity (or permeability) for certain frequency ranges [1]. Using these dispersive models, FDTD update equations are modified and permittivity and permeabilities are replaced with terms dependent on frequency of operation.

Two problems are chosen for GPU implementation. First is the electromagnetic wave scattering by a slab with negative permittivity and permeability; also known as DNG (double negative) medium. Second problem is the simulation of cylindrical cloak. An incident Gaussian pulse on DNG slab will undergo dispersion resulting in different frequency components being separated. Refractive index and transmission coefficient are calculated numerically to ascertain the validity of implementation. The cylindrical cloak was first proposed and tested by Pendry et. al. [2]. The first FDTD implementation was by Zhao et. al [3] and implemented on Comsol, a commercial electromagnetic simulation software. Simulations are implemented on Matlab, C++ and GPU. Performance comparison reveals a 10–15 times increase in performance with GPU implementations. Performance gain is greater for larger problem sizes and greater simulation times.

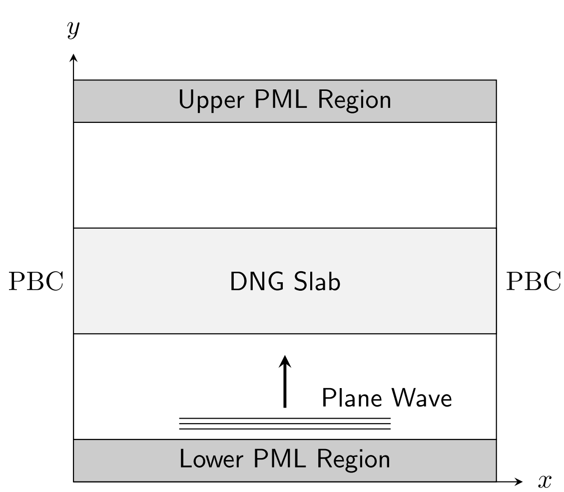

(a) DNG slab problem

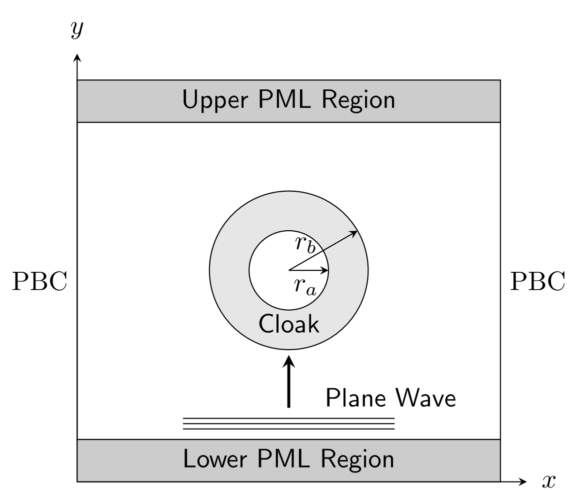

(b) Cylindrical cloak

Figure 1: Simulation geometries

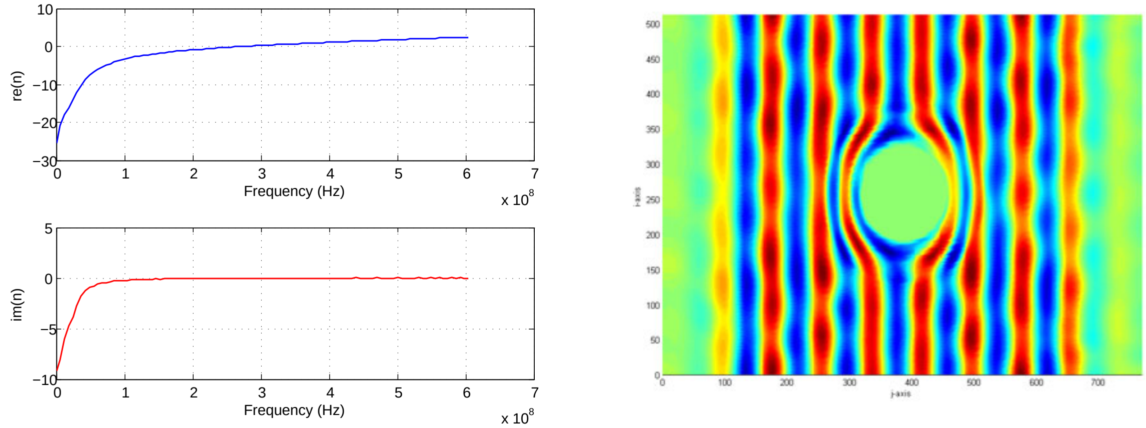

(a) Refractive index of DNG slab

(b) Cylindrical cloak simulation

Figure 2: Simulation results

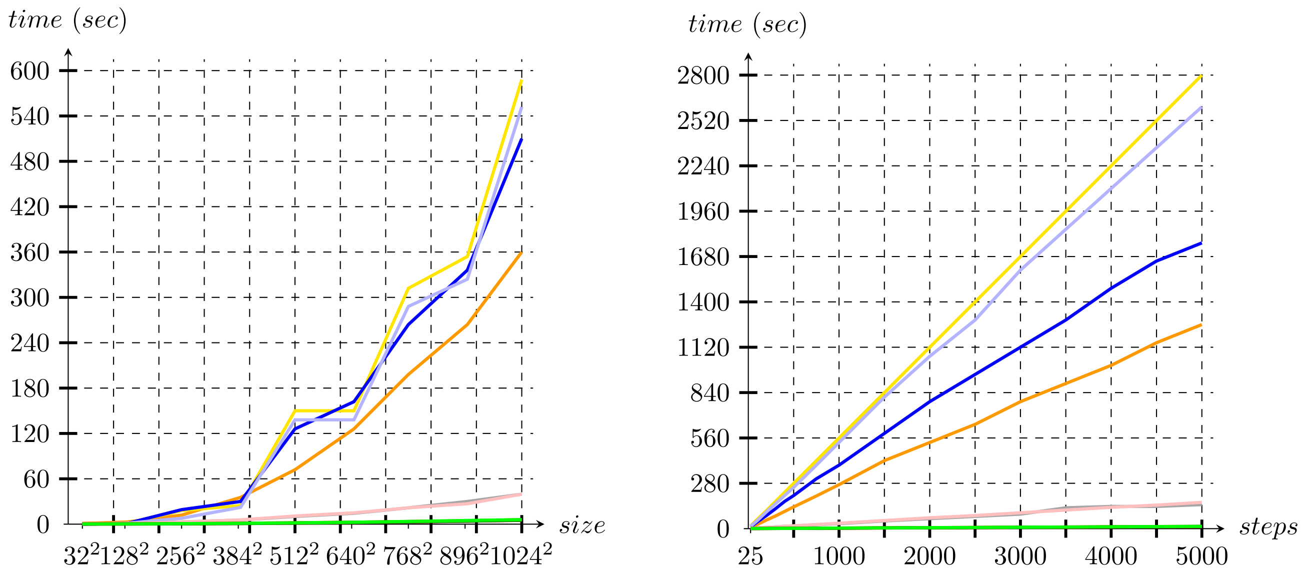

(a) Spatial performance times

(b) Temporal performance times

Figure 3: Performance comparison

REFERENCES

1. S. G. et al, “Metamaterials and fdtd based numerical modeling studies,” *ELECO*, Sep 2007.
2. D. Schurig, J. J. Mock, B. J. Justice, S. A. Cummer, J. B. Pendry, A. F. Starr, and D. R. Smith, “Metamaterial Electromagnetic Cloak at Microwave Frequencies,” *Science*, vol. 314, no. 5801, pp. 977–980, 2006.
3. Y. H. Argyropoulos C., Yan Zhao, “A radially-dependent dispersive finite-difference time-domain method for the evaluation of electromagnetic cloaks,” *IEEE Transactions on Antennas and Propagation*, vol. 57, pp. 1432–1441, May 2009.
4. K. Yee, “Numerical solution of inital boundary value problems involving maxwell’s equations in isotropic media,” *IEEE Transactions on Antennas and Propagation*, vol. 14, pp. 302–307, May 1966.
5. R. W. Ziolkowski and E. Heyman, “Wave propagation in media having negative permittivity and permeability,” *Physical Review*, vol. 64, October 2001.

Frequency conversion and time reversal via a dynamic metamaterial

A. V. Chumak[1*], A. D. Karenowska[2], V. S. Tiberkevich[3], A. A. Serga[1], J. F. Gregg[2], A. N. Slavin[2], and B. Hillebrands[1]

[1] Fachbereich Physik and Landesforschungszentrum OPTIMAS, Technische Universität Kaiserslautern, Kaiserslautern 67663, Germany

[2] Department of Physics, Clarendon Laboratory, University of Oxford, Oxford OX1 3PU, UK

[3] Department of Physics, Oakland University, Rochester, Michigan 48309, USA

[*]corresponding author: chumak@physik.uni-kl.de

Abstract-We report on an all-linear frequency conversion and time reversal process which occurs when the transmission properties of a waveguide containing a traveling wavepacket are rapidly switched from a spatially homogeneous state to one in which they vary periodically on a lengthscale comparable to the wavelength of the wavepacket carrier. We describe the experimental observation of the phenomenon in a spin-wave system incorporating a one-dimensional dynamic magnonic crystal, and explain how the results might be generalized to any physical domain.

The time reversal of pulsed signals or propagating wavepackets has long been recognized to have profound scientific and technological significance. Until now, all experimentally verified time-reversal mechanisms have been reliant upon nonlinear phenomena such as four-wave mixing. In this paper, we report the experimental realization of all-linear time reversal. The time-reversal mechanism we present is based on the dynamic control of an artificial crystal structure, and is demonstrated in a spin-wave system using a dynamic magnonic crystal.

Metamaterials with spatially periodic variations in their magnetic properties – magnonic crystals (MCs) – are the magnetic analog of photonic or sonic crystals. The spin-wave excitation spectra of such structures exhibit a range of interesting features including band gaps. Especially interesting in the context of both fundamental research and microwave signal processing are dynamic magnonic crystals (DMC) – magnetic artificial crystals having lattices with properties that can be modified while a wavepacket propagates through them [1]. We have demonstrated such a structure based on a ferrite spin-wave waveguide placed in a periodically varying current-controlled magnetic field (see Fig. 1a). We have shown that the rejection band depth and width in such a crystal

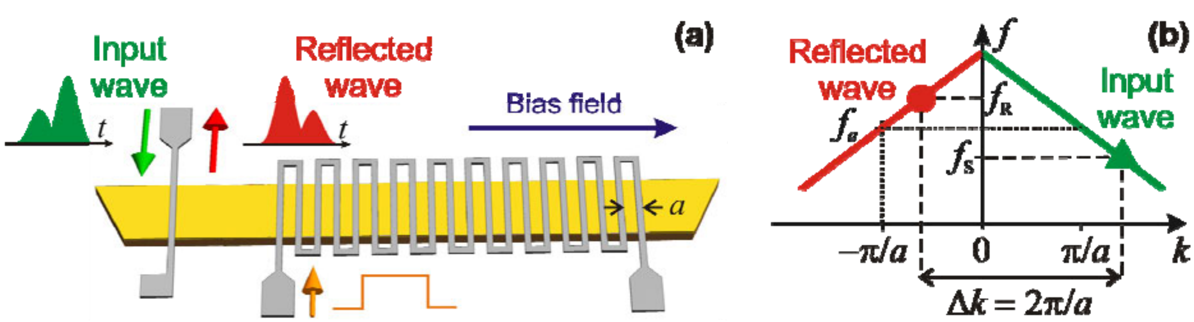

Fig. 1. All-linear time reversal by a dynamic magnonic crystal. (a) The experimental DMC system which comprises a planar current-carrying meander structure positioned close to a spin-wave waveguide. (b) Schematic illustration of the frequency inversion process.

can be tuned using the applied current. Furthermore, the crystal can be switched from full transmission to full rejection with a transition time ten times smaller than the spin-wave relaxation time and ten times smaller than the time required by the spin-wave packet to propagate through the magnonic-crystal area [1].

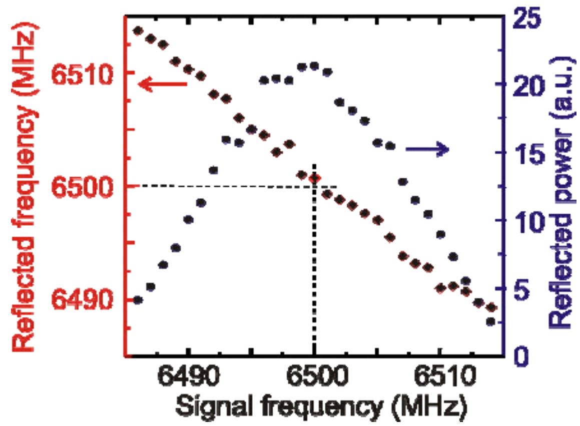

Fig. 2. The frequency (left axis) and the power (right axis) of the reversed via the DMC spin-wave packet.

We have demonstrated that a DMC provides a linear means to perform spectral transformations, including frequency inversion and time reversal [2] which, until now, have only been possible through nonlinear mechanisms (Fig. 1b). If the crystal is switched from a homogeneous state to one in which its properties vary with spatial period a while an incident wavepacket having a frequency lying inside the band gap is inside, a linear coupling between wave components with wave vectors $k \approx \pi/a$ and $k' = k - 2\pi/a \approx -\pi/a$ results [3]. This coupling leads to the production of a counter propagating "reflected" wavepacket (see Fig. 2). If the carrier frequency of the incident packet is detuned from the band-gap centre frequency (6500 MHz in the data of Fig. 2), the frequency of the reflected signal is inverted about this value (left ordinate axis, red diamonds). The frequency inversion shown in Fig. 2 directly implies reversal of the time profile of the signal packet [2, 3]. The time reversal mechanism is entirely general and so applicable to metamaterials of any physical nature [4].

Financial support from the Deutsche Forschungsgemeinschaft (Grant No. SE 1771/2), from the ECCS and DMR Programs of the U.S. National Science Foundation, and from the Defense Advanced Research Projects Agency (DARPA) is gratefully acknowledged.

REFERENCES

1. A. V. Chumak, T. Neumann, A. A. Serga, B. Hillebrands, and M.P. Kostylev, "A current-controlled, dynamic magnonic crystal, " *J. Phys. D: Appl. Phys.*, Vol. 42, 205005, 2009.
2. A. V. Chumak, V. S. Tiberkevich, A. D. Karenowska, A. A. Serga, J. F. Gregg, A. N. Slavin, and B. Hillebrands, "All-linear time reversal by a dynamic artificial crystal," *Nat. Commun.*, Vol. 1:141 doi: 10.1038/ncomms1142, 2010.
3. A. D. Karenowska, V. S. Tiberkevich, A. V. Chumak, A. A. Serga, J. F. Gregg, A. N. Slavin, and B. Hillebrands, "Oscillatory energy exchange between waves coupled by a dynamic artificial crystal," *Phys. Rev. Lett.* , Vol. 108, 015505, 2012.
4. Y. Sivan and J. B. Pendry, "Broadband time-reversal of optical pulses using a switchable photonic-crystal mirror," *Opt. Expr.*, Vol. 19, No. 15, 14502-14507, 2011.

Storage-recovery phenomenon in a magnetic artificial crystal

A. A. Serga[1], **A. V. Chumak**[1], **V. I. Vasyuchka**[1], **M. P. Kostylev**[2], **V. S. Tiberkevich**[3], **and B. Hillebrands**[1]

[1]Fachbereich Physik and Landesforschungszentrum OPTIMAS, Technische Universität Kaiserslautern, 67663 Kaiserslautern, Germany
[2]School of Physics, University of Western Australia, Crawley, Western Australia 6009, Australia
[3]Department of Physics, Oakland University, Rochester, Michigan 48309, USA
serga@physik.uni-kl.de

Abstract— The coherent wave trapping and restoration is demonstrated experimentally in a magnetic artificial crystal. Unlike the conventional scheme used in photonics, the trapping occurs not due to the deceleration of the incident wave in a periodic structure but due to excitation of the quasinormal modes of the spatially localized crystal which is the most effective in narrow frequency regions near the edges of the band gaps of the crystal.

The deceleration of light due to the modification of the light dispersion in photonic crystals (PCs) is a topic of intense experimental and theoretical studies over the last decade. It has been demonstrated that the slow light can be used for time-domain processing including buffering (storage and recovery) of optical signals as well as for an enhancement of nonlinear effects due to the spatial compression of optical energy [1, 2]. Magnonic crystals (MCs) are the magnetic counterpart of photonic crystals which operate with spin waves, i.e. the collective oscillations of the spin lattice of a magnetic material [3, 4, 5]. These oscillations can be efficiently excited by a microwave magnetic field. However, due to sufficient intrinsic damping the excited spin wave propagates only the limited number of MC structure periods. The small number of periods (up to 20) implies that the slope of MC dispersion does not become zero at the edges of the magnonic band gap and the group velocity of spin waves only slightly decreases in these spectral areas. This makes the realization of long-time storing a signal in a MC using the *slow* spin-wave mode practically impossible.

As an alternative solution, we show that the storage-recovery phenomenon can be successfully realized in an artificial crystal with a limited number of periods by the use of a quasi-normal mode (QNM) of this structure [6]. This mode is excited by the incident wave and conserves oscillation energy for a long time after the propagating wave has left the MC area. Upon subsequent parametric amplification the internal mode irradiates part of its energy back into the propagating wave allowing the restoration of the stored signal.

The magnonic crystal used in our experiment had been produced in the form of a stripe of a low-damping magnetic insulator (5.1 μm-thick yttrium iron garnet (YIG) film) with an array of parallel grooves chemically etched into its surface (see Fig. 1(a)) [5]. The array comprises ten 300 nm-deep and 30 μm-wide grooves placed 270 μm apart (lattice constant 300 μm). The bias magnetic field is applied along the stripe in order to form conditions for propagation of backward volume magnetostatic spin waves (BVMSW) [7].

The experiment was performed in the following way. A 100 ns-long microwave pulse of $f_\mathrm{s} = 7.212$ GHz frequency is applied to the input antenna in order to excite a traveling spin-wave packet which propagates toward the output antenna. The waveform of the output signal is shown in Fig. 1(c). First, the output antenna receives a practically rectangular pulse without any delay, caused by a direct electromagnetic leakage from the input antenna at the time $t = 0$. Approximately 0.3 μs afterwards a pulsed signal carried by spin waves arrives at the output antenna. Well after this took place we apply a 10 μs-long pumping pulse at the frequency of $f_\mathrm{p} = 2f_\mathrm{s} = 14.424$ GHz. This pulse selectively amplifies a stored signal and is resulted in the appearance of an additional bell-shaped pulse at the output antenna. This is the restored signal. Our measurements show that the signal stored inside the MC is phase correlated to the input microwave signal: in spite of the distortion of the time profile of the original pulse its phase information is conserved.

It is important that the restored pulse appears only at the edges of the band gaps. We have calculated the group velocity v_gr and compared it with the experimental data. Both the measured and the calculated group velocities decrease at the edges of the band gaps. At the same time this decrease is 20 percent at most and cannot be used in a slowing-down approach to store information

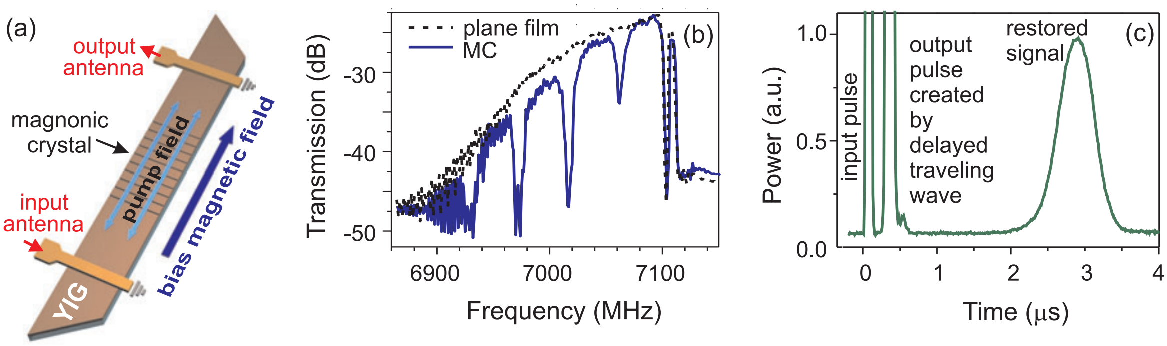

Figure 1: (a) Sketch of the experimental setup. The MC is fabricated in the form of YIG spin-wave waveguide with 10 grooves on its surface. The microwave magnetic field, which is used for parametric amplification of stored signals, is parallel to the bias field H. (b) Measured transmission characteristics (the ratio of the output signal intensity to the input) of the plane YIG film and MC for the magnetic field $H = 1800$ Oe. Several band gaps are seen. (c) The time profile of the restored signal measured at field $H = 1860$ Oe.

for a reasonably long time. The phenomenon can be understood if we assume that the storage of the spin-wave signal is based on quasi-normal modes [8] of the magnonic crystal. Any artificial crystal of finite length L presents an *open* system which is coupled to the outside medium. Respectively, internal excitations of such crystal can be excited from outside (in contrast to normal modes of a *closed* system) and, in turn, lose their energy by radiating traveling waves. The life time of a QNM can be substantially larger than the corresponding traveling time $T_{\text{gr}} = L/v_{\text{gr}}$ in homogeneous medium. Moreover, there is the principal difference between the traveling time T_{gr} and the life time τ for the storage purposes. In the case of a traveling wave packet the storage time does not exceed the time T_{gr} at which the spin-wave energy completely leaves the magnonic crystal. On the contrary, in the case of QN mode the time τ characterizes its decay rate only. Since this mode does not propagate its energy is stored in the crystal as long as the mode amplitude falls down to the level of thermal fluctuations. As a result the storage time can significantly exceed the lifetime τ.

We have calculated QNM eigenfrequencies numerically as complex eigenvalues of the crystal's transfer matrix taking into account the SW coupling with the groove structure which value can be obtained from half-width of the MC band gap. It has been found that the life time is maximal for the mode which is closest to the band gap edge. Furthermore, for our experimental conditions the frequency of this mode coincides with the global minima of v_{gr}. Thus, this $n = 1$ QNM conserves energy for the longest time ($\tau_{n=1}/T_{\text{gr}} \simeq 5$) and can interact with the parametric pumping long after the exciting traveling spin wave packet has passed. As a result, the restoration phenomenon is observed only at the global minima of v_{gr}.

The results presented here provide deeper understanding of the storage-recovery mechanisms in periodic lattices in general and evidence a perspective of magnonic crystals for buffering of microwave information.

ACKNOWLEDGMENT

We acknowledge financial support by Deutsche Forschungsgemeinschaft (SE 1771/1-2) and the Australian Research Council.

REFERENCES

1. T. Krauss, *J. Phys. D.*, Vol. 40, 2666, 2007.
2. T. Baba, *Nat. Photon.*, Vol. 2, 465, 2008.
3. Nikitov, S. A., P. Tailhades and C. S. Tsai, *J. Magn. Magn. Mater.*, Vol. 236, 320, 2001.
4. Kruglyak, V. V. and R. J. Hicken, *J. Magn. Magn. Mater.*, Vol. 306, 191, 2006.
5. Chumak, A. V., A. A. Serga, B. Hillebrands and M. P. Kostylev, *Appl. Phys. Lett.*, Vol. 93, 022508, 2008.
6. Chumak, A. V. *et al.*, *Phys. Rev. Lett.*, Vol. 108, 257207, 2012.
7. Serga, A. A., A. V. Chumak and B. Hillebrands, *J. Phys. D.*, Vol. 43, 264002, 2010.
8. Ching, E. S. C. *et al.*, *Rev. Mod. Phys.*, Vol. 70, 1545, 1998.

Stability and Noise in Metamaterials with Non-Foster Inclusions

K. Z. Rajab[1*], **Y. Fan**[1], **and Y. Hao**[1]
[1]Queen Mary University of London, United Kingdom
[*]corresponding author: Khalid.rajab@eecs.qmul.ac.uk

Abstract-Metamaterials loaded with active inclusions can exhibit increased bandwidth and reduced loss as compared to their passive counterparts. However, fundamental and practical aspects of their design will constrain their implementation. Namely, the active metamaterials may suffer from instability and increased noise figures. In this presentation we will detail the investigation of these issues as implemented with non-Foster loads, and in particular to the effective constitutive parameters.

Active metamaterials have been proposed as a means for overcoming the fundamental physical limitations of passive metamaterials with near-zero or negative material parameters; namely narrow bandwidth and high loss. These limitations are a result of their highly dispersive, typically resonant nature that is a fundamental characteristic of these properties, as detailed in [1]. While passive metamaterials are limited in this manner, their counterparts with active inclusions may be design to overcome these limitations, at the expense of possible instability [2]. A promising approach to implementing these active inclusions was proposed in [3], where it was suggested that non-Foster loads, in the form of negative impedance converters (NICs) may be used to increase the bandwidth of metamaterials with negative permittivity or permeability.

An ideal NIC is a device in which the input impedance is the negative of the load impedance. There are a number of different implementations based on a variety of active components, including vacuum tubes, operational amplifiers, and field-effect transistors. However, the most common implementation is based on Linville's bipolar junction transistor-based circuit [4]. These circuits had been widely used in the amplification of long-distance analog telephony transmissions, and there is a wide body of research into their application for the broadband impedance matching of receive antennas [5]. Recently however, their potential for the improvement of metamaterial performance has been recognised with the investigation of the bandwidth improvement of both magnetic [6] and electric [7] materials.

Stability has been the primary issue in implementing these, and other active metamaterials. In (Rajab et al. 2010) it was demonstrated that stability can be maintained in infinitely periodic NIC-loaded magnetic metamaterials. The stability was analysed using the Routh-Hurwitz technique, while in [8] the Nyquist criterion was used for more robust, practical investigation of stability. In the technique presented in that paper, the source impedance (for example an open-circuit stable NIC) and the load admittance (for example the passive components of the metamaterial) are defined seperately, but analysed in conjunction by plotting:

$$G(s) = Z_s(s)Y_l(s) \quad (1)$$

in the complex plane with $s \equiv j\omega$. Cauchy's argument principle states that

$$N = Z - P \tag{2}$$

where Z and P are, respectively, the number of zeros and poles of $Z_s(s)Y_l(s)$, while N represents the number of loops of the origin. Therefore, a stable closed-loop system will not make and clockwise encirclements of the -1 point on the complex plot. A benefit of this method is that it can comfortably handle complex circuits, and the source and load can be varied to parametrically analyze effects on stability.

Johnson-Nyquist noise has been investigated previously in magnetoinductive materials with both passive, and amplifying (negative resistance) loads [9]. By investigating the noise waves travelling along a metamaterial, one may also analyze the effects of NICs on the noise figure. As with the earlier analysis of stability, the system may be interpreted as an impedance matrix. Johnson-Nyquist noise sources may be imposed at all resistances. It can then be shown that the noise figure will increase with the inclusion of the NIC loads. However, it may still be reduced through design, even for the cases of active near-zero and negative material parameters.

In summary, we have shown that non-Foster NIC loads can be used to increase the bandwidth of both negative and near-zero parameter metamaterials. Most importantly, we have dealt with the issues of stability and noise in these implementations. We have shown that stability can be maintained, and in certain cases the noise can be kept relatively low. This comes, however, at the expense of a reduced effective bandwidth. In this presentation, we will show our methods for investigating these effects in any material for which an equivalent circuit model may be described.

REFERENCES

[1] M. I. Stockman, "Criterion for Negative Refraction with Low Optical Losses from a Fundamental Principle of Causality," *Physical Review Letters*, vol. 98, no. 177404, 2007.

[2] B. Nistad and J. Skaar, "Causality and Electromagnetic Properties of Active Media," *Physical Review E*, vol. 78, no. 036603, 2008.

[3] S. A. Tretyakov, "Meta-materials with wideband negative permittivity and permeability," *Microwave and Optical Technology Letters*, vol. 31, no. 3, pp. 163-165, Nov. 2001.

[4] J. G. Linvill, "Transistor negative-impedance converters," *Proceedings of the IRE*, vol. 41, no. 6, pp. 725-729, June 1953.

[5] S E Sussman-Fort and R M Rudish, "Non-Foster Impedance Matching of Electrically-Small Antennas," *IEEE Trans. Antennas Propag.*, vol. 57, p. 2230, 2009.

[6] K. Z. Rajab et al., "Stability of Active Magnetoinductive Metamaterials," *Journal of Applied Physics*, vol. 108, no. 054904, 2010.

[7] S Hrabar, I Krois, and A Kiricenko, "Towards active dispersionless ENZ metamaterial for cloaking applications," *Metamaterials*, vol. 4, pp. 89-97, 2010.

[8] K. Z. Rajab, Y. F. Fan, and Y. Hao, "Characterization of active metamaterials based on negative impedance converters," *Journal of Optics*, vol. 14, p. 114004, 2012.

Focusing Effect Measurements of Artificial Dielectric Lens with Metal Rectangular Chips for Terahertz Wave Band

Yuki Takebayashi[1], Takuya Konno[1], Shouhei Shimada[2], Fumiaki Miyamaru[2], John C. Young[3], Hideaki Kitahara[4], Keisuke Takano[4], Masanori Hangyo[4] and Takehito Suzuki[1*]

[1]Department of Electrical & Electronic Engineering,
Ibaraki University, 4-12-1 Nakanarusawa, Hitachi, Ibaraki 316-8511, Japan
[2]Department of Physics, Shinshu Universtiy, 3-1-1 Asahi, Matsumoto, Nagano 390-8621, Japan
[3]Electrical and Computer Engineering, University of Kentucky, Lexington, Kentucky 40506-0046, USA
[4]Institute of Laser Engineering, Osaka University, 2-6 Yamadaoka, Suita, Osaka 565-0871, Japan
[*]E-mail: takehito@mx.ibaraki.ac.jp

Abstract- This paper presents the focusing effect measurements of an artificial dielectric lens with metal rectangular chips for the terahertz wave band. The focusing effect is produced by the rectangular metallic chips which macroscopically act as electrical dipoles. The measurement results are obtained by terahertz near-field spectroscopy. We confirm the focusing effect at 4.5 mm from the front of the lens at 0.67 THz by measurements.

Due to the increasing use of the terahertz wave band, the need for high-performance optical devices in the terahertz band is increasing. However, the realization of a desired refractive index using naturally-occurring materials can be quite difficult. When a material is directly used to construct an optical device, the material properties themselves determine the optical characteristics. High density polymer lenses, Tsurupica lenses, and silicon lenses with refractive indices of 1.52, 1.56, and 3.41, respectively, are typical terahertz band lenses. Microwave-band lenses composed of electromagnetic metamaterials were proposed in [1] and [2]. For terahertz-band, a metamaterial with an unnaturally high refractive index is presented in [3] and an antireflection coating is presented in [4]. The work in [5] presented an artificial dielectric lens with metallic rectangular chips for the terahertz wave band. The fabrication of terahertz electromagnetic metamaterials by laser processing, metallic processing and semiconductor etching is relatively easy compared with fabrication of metamaterials in the optical range since the dimensions of the unit element are on the order of microns. Furthermore, the unit cell of the electromagnetic metamaterial, which controls the refractive index, is of prime importance with respect to design flexibility and cost performance.

This paper measures the focusing effect [5] of a terahertz-band artificial lens with 10 layer metal rectangular chips, as shown in Figure 1. The focusing effect is produced by the rectangular metallic chips which macroscopically act as an electrical dipole. Figure 2 shows the unit cell model. Figure 3 shows the full wave analysis result by Ansys HFSS where the input electric filed is 1 V/m. The dimensions of the analysis model are small compared with those of the actual lens in order to escaping the time-consuming due to the problem size. Both of the curvature radii are same. The focusing length is 2.77 mm (6.23λ) for 0.67 THz. The effective refractive index is estimated as 2.09.Table 1 shows the lens parameters. As shown in Figure 4, the rectangular chips are fabricated from copper films by laser processing. A Chrome layer with a thickness of 10 nm, which produces losses, exists as buffer layer. Copper is sputtered on ZEONEX film with a refractive index of 1.53. The measurement results are obtained by terahertz near-field spectroscopy [6]. Figure 5 shows the measurement results at 2.0 mm (4.5λ) and 4.5 mm (10.1λ) from the front of the lens for 0.67 THz. The amplitude of the white color is 40 times that of the black color. The amplitude is expressed in decibels in Fig. 5. We confirm the focusing effect at 4.5 mm (10.1λ) at 0.67 THz by the measurements, which is estimated as an effective refractive index of 1.67, even though fabrication errors cause the difference between the analysis and measurement results.

ACKNOWLEDGMENT

This research was partially supported by a Grant-in-Aid for Scientific Research on Innovative Areas "Electromagnetic Metamaterial" (No. 23109505) from the Ministry of Education, Culture, Sports, Science and Technology (MEXT), Japan, the Strategic Information and Communications R&D Promotion Programme (SCOPE) (No. 122103011) from the Ministry of Internal Affairs and Communications, Accelerating Utilization of University IP Program (No. 439) from Japan Science and Technology Agency (JST), Program for Revitalization Promotion (No. 241FT0462) from Japan Science and Technology Agency (JST), the Takayanagi Memorial Foundation, the Yazaki Memorial Founda-tion for Science & Technology, and the Iketani Science and Technology Foundation. The authors wish to thank Dr. Ishikawa at Industrial Technology Institute of Ibaraki Prefecture in fabrication.

REFERENCES

1. W. E. Kock, Bell Syst. Tech. J. **27**(1), 58-82 (1948)
2. S. S. D. Johns and J. Brown, Nature, **163**, 324-325 (1949)
3. M. Choi, et al., Nature 470, 369–374 (2011)
4. H.-T. Chen, et al., Phys. Rev. Lett. **105**, 073901-1–073901-4 (2010)
5. T. Suzuki, et al., Appl. Phys. A **109**(4), 825-830 (2012)
6. H. Kitahara, et al., The 73th Autum Meeting, 2012; The Japan Society of Applied Physics and Related Societies, 13a-PA6-15, 04-211 (2012) (in Japanese)

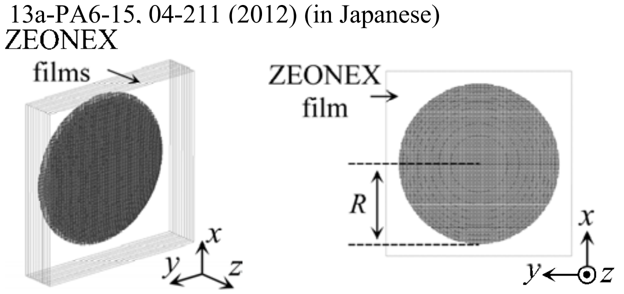

(a) Bird's-eye view (b) Top view

Fig. 1 Artificial lens with 10 layer metal rectangular chips.

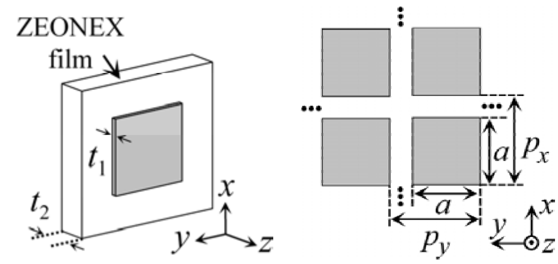

(a) Bird's-eye view (b) Top view

Fig. 2 Unit cell models.

Table 1 Lens parameters.

a	75 µm	t_1	0.35 µm
p_x	100 µm	t_2	100 µm
p_y	100 µm	R	4.3 mm

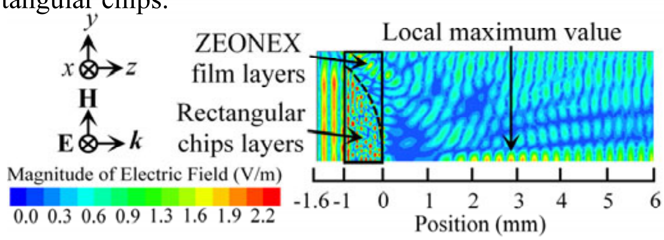

Fig. 3 Full wave analysis result.

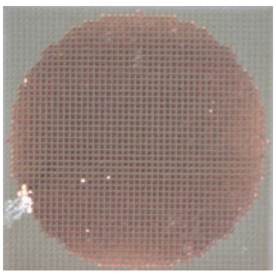

Fig. 4 Lens fabricated by laser processing.

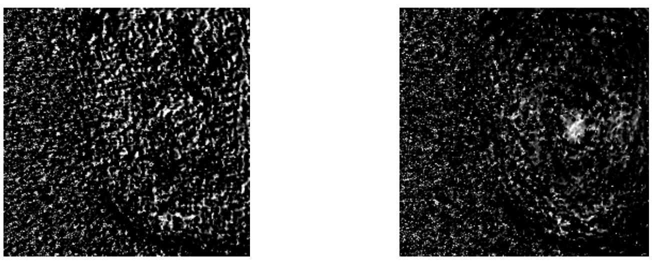

(a) 2.0mm position (b) Focusing effect at 4.5 mm position

Fig. 5 Measurement results of focusing effect at 0.67 THz.

Analysis and Design of Concave Lens with Metallic Slit Array for Terahertz Wave Band

Takehito Suzuki[1*], Hiroki Yonamine[1], Takuya Konno[1], John C. Young[2],
Kotaro Murai[3], Fumiaki Miyamaru[3], Keisuke Takano[4], Hideaki Kitahara[4], and Masanori Hangyo[4]

[1]Department of Electrical & Electronic Engineering,
Ibaraki University, 4-12-1 Nakanarusawa, Hitachi, Ibaraki 316-8511, Japan

[2]Electrical and Computer Engineering, University of Kentucky, Lexington, Kentucky 40506-0046, USA

[3]Department of Physics, Shinshu Universtiy, 3-1-1 Asahi, Matsumoto, Nagano 390-8621, Japan

[4]Institute of Laser Engineering, Osaka University, 2-6 Yamadaoka, Suita, Osaka 565-0871, Japan

[*]E-mail: takehito@mx.ibaraki.ac.jp

Abstract- This paper presents the analysis and design of a three-dimensional concave lens with metallic slit array for the terahertz wave band. The full wave analysis at a design frequency of 0.5 THz is performed by Ansys HFSS. The fast wave effect can be controlled by the slit array space. The light focusing due to the fast wave effect is verified by the analysis.

The need for optical devices in the terahertz wave band from 0.1 to 10 THz is rapidly growing. The ability to arbitrarily realize a given refractive index using naturally-occurring materials can be difficult. When materials are directly used for optical devices, the material properties themselves determine the optical characteristics. A metamaterial's unit cell, which controls the refractive index [1], [2], is an important parameter for design flexibility and cost performance. In the terahertz wave band, the work in [3] presented experimental results of a two-dimensional concave lens with metallic slit array and that in [4] presented the analysis results of a three-dimensional one. Various research [1], [5], [6] is performed in microwave frequency bands because the fabrication is relatively easy compared with that of the terahertz electromagnetic metamaterials.

This paper presents the design of a three-dimensional concave lens that includes the effect of the dielectric material, ZEONEX, with refractive index of 1.53, as shown in Figure 1. The lens is hollow with a hemispherical shape of radius of R. The three-dimensional structure is useful for the implementation of a photoconductive antenna. The excitation is a TEM mode with E field parallel to the metallic plate such that TE_1 mode propagates as the dominant mode in the parallel plate. The fast wave effect [1], [5]-[7], which can produce a focusing effect, is controlled by the slit spacing. The effective refractive index n is estimated as $0<n<1$. Table 1 shows the lens parameters. From the calculation of TE_1 mode wavelength in the slit array , the effective refractive index n with a slit spacing of 0.188 mm (0.34λ) is estimated as 0.49 and that with a spacing of 0.180 mm (0.33λ) is estimated as 0.22. The full wave analysis results are obtained by Ansys HFSS using an incident electric field amplitude of 1 V/m. For a slit spacing of 0.188 mm (0.34λ), the local maximum value is 4.3 times that of the incident wave at 1.80 mm (3.3λ) from the front of the lens, as shown in Figure 2. The results verify that the three-dimensional concave lens with metallic slit array produces a focusing effect in the terahertz wave band. From the lens parameters and focal length, the effective refractive index n is estimated as 0.55 from the lens. For a slit spacing of 0.18 mm (0.33λ), the local maximum value is 3.1 times that of the incident wave at 0.76 mm (1.3λ) from the front of the lens. The effective refractive index n is 0.31. To reduce problem size and analysis time, only one quarter of the analysis model is analyzed due to symmetry and the dimensions of the full analysis model are small compared with those of the actual lens. Figure 3 shows the effective refractive index from the TE_1 mode wavelength and full wave analyses. The refractive index becomes smaller with narrower slit spacing even though the small errors exist. We plan to fabricate the concave lens with metallic slit array and measure the focusing effect in the terahertz wave band.

ACKNOWLEDGMENT

This research was partially supported by a Grant-in-Aid for Scientific Research on Innovative Areas “Electromagnetic Metamaterial” (No. 23109505) from the Ministry of Education, Culture, Sports, Science and Technology (MEXT), Japan, the Strategic Information and Communications R&D Promotion Programme (SCOPE) (No. 122103011) from the Ministry of Internal Affairs and Communications, Accelerating Utilization of University IP Program (No. 439) from Japan Science and Technology Agency (JST), Program for Revitalization Promotion (No. 241FT0462) from Japan Science and Technology Agency (JST), the Takayanagi Memorial Foundation, the Yazaki Memorial Founda-tion for Science & Technology, and the Iketani Science and Technology Foundation.

REFERENCES

1. W. E. Kock, Bell Syst. Tech. J. **27**(1), 58-82 (1948)
2. S. S. D. Johns and J. Brown, Nature, **163**, 324-325 (1949)
3. R. Mennndis, et al., IEEE Trans. Microw. Theory Tech., **58(7),** 1993-1998 (2010).
4. H. Yonamine, et al., The 73th Autum Meeting, 2012; The Japan Society of Applied Physics and Related Societies, 11p-B1-6, 04-164 (2012) (in Japanese)
5. W. E. Kock, Proceedings of the I. R. E and Waves and Electrons, **34**(11) 828-836 (1946)
6. Kamiya, et al. IEICE general Conference 2012 C-2-51, 92 (2012) (in Japanese)
7. L. Josefsson, IEEE Trans. Antennas Propag., **41**(7), 845-850 (1993)

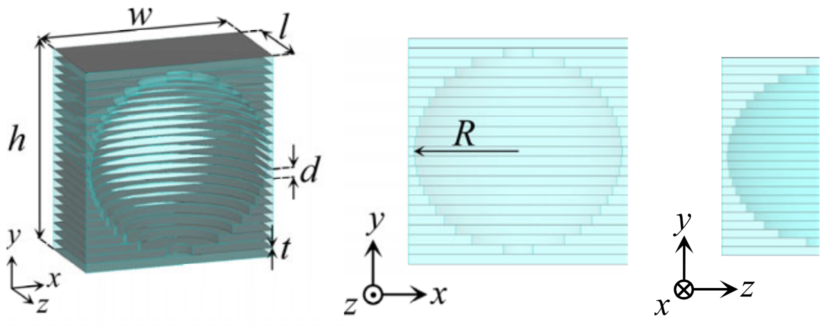

(a) Bird’s-eye view (b) Top view (c) Side view

Fig. 1 Three-dimensional concave lens with metallic slit array.

Table 1 Concave lens parameters.

t	0.5 μm
R	2.0 mm (3.7 λ)
l	2.1 mm (3.9 λ)
w	4.2 mm (7.7 λ)

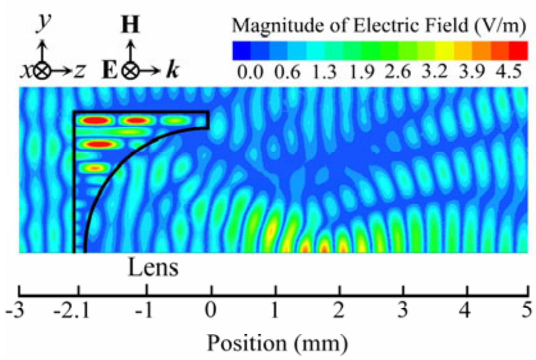

Fig. 2 Full wave analysis result.

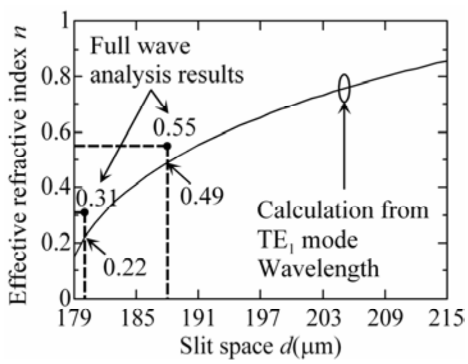

Fig. 3 Effective refractive index.

Controlling Förster energy transfer with the density of photonic states

T. U. Tumkur[1], J. K. Kitur[1], C. E. Bonner[1], E. E. Narimanov[2], M. A. Noginov[1]*
[1] Center for Materials Research, Norfolk State University, Norfolk, VA 23504
[2] Birck Nanotechnology Center, Department of Electrical and Computer Engineering, Purdue University, West Lafayette, IN 47907
*corresponding author: mnoginov@nsu.edu

Abstract - We demonstrate control over Förster energy transfer in the vicinity of media that possess a high density of photonic states, such as metals and hyperbolic metamaterials. We observe that such media, which enhance spontaneous emission rates, inhibit Förster energy transfer.

Hyperbolic metamaterials can support the propagation of waves with large wavevectors, owing to the anisotropy of the dielectric permittivity components in orthogonal directions [1]. Correspondingly, they possess a broadband singularity in the density of photonic states, and thus provide an excellent platform to control optical phenomena such as spontaneous emission [2] and reflection off rough surfaces [3]. Here, we show that media with high density of photonic states can influence Förster energy transfer.

Förster energy transfer is a non-radiative transfer of electronic excitation from a donor molecule to an acceptor molecule, Fig. 1a. At dipole-dipole approximation, at fixed positions of donors and acceptors, and random spatial distributions of acceptors around donors, the emission kinetics of donors $I(t)$ (excited by short laser pulses) is given by $I(t)= I_0 \exp(-(A+W)t-\gamma\sqrt{t})$, where I_0 is the initial emission intensity, A and W are radiative and non-radiative emission decay rates of donors, respectively; t is time; $\gamma \approx 6.28 R_0^3 N / \sqrt{\tau_0}$ is the energy transfer constant; N is the concentration of acceptors; $\tau_0 = \left(A+W\right)^{-1}$ is the decay-time of donors in the absence of acceptors; and R_0 is the characteristic distance at which the transfer probability in a pair of donor and acceptor molecules equals the probability of spontaneous emission of the donor molecule [4]. Note that $R_0^3 \propto \gamma \propto n^{-2}$ [4] and $A \propto n$ [5] depend differently on the index of refraction n. Thus, dielectric environments, which enhance A, inhibit γ. Since the density of photonics states in dielectric materials is proportional to n, we hypothesize that hyperbolic metamaterials and metals which enhance spontaneous emission rates A, should reduce Förster energy transfer rates γ.

We fabricate the metamaterial structures by depositing alternating layers of Ag and MgF_2. Such multilayer structure has hyperbolic dispersion in the visible and infrared spectral regions [6-8], which was confirmed experimentally at 543 nm. Other substrates included glass, 200 nm Ag film on glass, and 200 nm Au film on glass. On the top of each substrate, we deposited thin (<80 nm) films of polymethyl methacrylate (PMMA) doped with donor (DCM dye, 10 g/l) and acceptor (DOTC, 10 g/l) molecules. This donor-acceptor combination was ideal for our measurements because of a strong overlap between the emission band of the donor, and the absorption band of the acceptor, Fig. 1b. Polymeric films doped with donors only and co-doped with donors and acceptors were excited with ~150 fs pulses of a frequency doubled Ti:sapphire laser into the absorption band of DCM (at λ = 392 nm), and the emission kinetics of donors were measured using a streak camera.

By dividing the emission kinetics of donor molecules in the co-doped (with donors and acceptors) sample, $\propto \exp(-(A+W)t-\gamma\sqrt{t})$, by that in the film doped by donor molecules only, $\propto \exp(-(A+W)t)$, we singled out the contribution of the Förster energy transfer. The resulting function $\propto \exp(-\gamma\sqrt{t})$ plotted as ln(-ln($I(t)$)) *vs* ln(t) has slope 1/2, and the corresponding energy transfer constant γ can be determined by fitting the experimental curve to the theoretical model (Fig. 2a) [4].

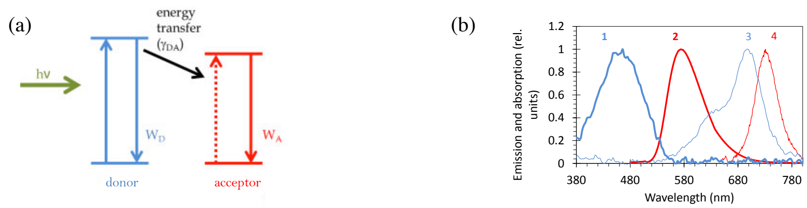

Fig. 1: (a) Energy level diagram of donor and acceptor molecules showing a combination of radiative and non-radiative relaxation processes in donor (W_D), Förster donor-acceptor energy transfer (γ_{DA}), and relaxation in acceptor (W_A). (b) Absorption (1,3) and emission (2,4) spectra of DCM (1,2) and DOTC (3,4) dyes doped into PMMA.

In accord with the theoretical prediction [1], we notice enhanced emission rates of the donors τ^{-1} (which are presumably proportional to spontaneous emission rates A) on top of hyperbolic metamaterials and metallic films, Fig. 2b. Simultaneously, we see that the same environments that enhance emission inhibit Förster energy transfer, which is much weaker on top of hyperbolic metamaterials and metals than on top of glass. The pairs of data points (γ,τ_0^{-1}) measured on metamaterial, metallic, and glass substrates are plotted in Fig. 2c. The slope of the curve plotted in logarithmic coordinates is equal to -2.5, in a fair agreement with the heuristic prediction.

To summarize, we have demonstrated that environments with high local densities of photonic states (like hyperbolic metamaterials and metals), which enhance emission decay rates, inhibit Förster energy transfer.

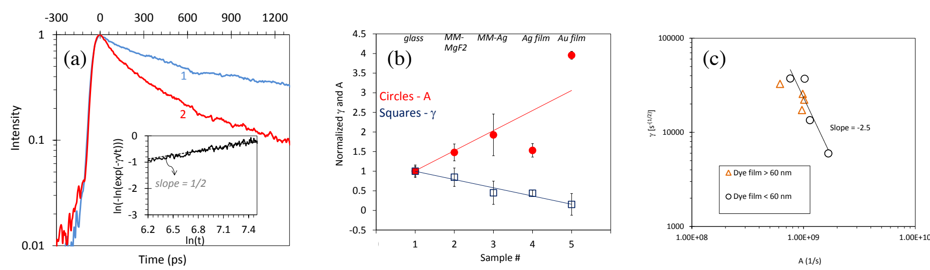

Fig. 2: (a) Spontaneous emission kinetics of donors (DCM) in single doped (1) and co-doped with donors and acceptors (2) PMMA films deposited on glass substrates. Inset: trace 2 divided by trace 1, fitted with a straight line, which slope is 1/2. (b) Emission decay rates τ^{-1} and Förster energy transfer constants γ in dye-doped films deposited on top of glass (1), metamaterial with MgF_2 as the outermost layer (2), metamaterial with Ag as the outermost layer (3), Ag film (4), and Au film (5). All data points are normalized to that on glass. (c) Values τ^{-1} plotted against corresponding values γ in the dye-doped PMMA films deposited on the top of samples 1, 2, 3 and 4 in Fig. b.

The authors acknowledge the NSF PREM grant # DMR 1205457, NSF IGERT grant #DGE 0966188, and AFOSR grant # FA9550-09-1-0456.

1. Jacob, Z., Smolyaninov, I., Narimanov E. E., Appl. Phys. Lett., (2012).
2. Noginov, M. A., *et al*., Opt. Lett. **11**, 1863 (2010).
3. Narimanov, E. E., *et al*., *arXiv*:1109.5469 [physics.optics] (2011).
4. Agranovich, V. M., Galanin, M. D., Electronic Excitation Energy Transfer in Condensed Matter, North-Holland, New York, 1982
5. Pantell, R. H., Puthoff, H. E., Fundamentals of Quantum Electronics, Wiley, New York, 1969.
6. Hoffman, A. J., *et al*., Nature. Mater.6, 946 (2007).
7. Jacob, Z., *et al*., Appl. Phys. B100, 215 (2010).
8. Tumkur, T., *et al*., Appl. Phys. Lett. 99, 151115 (2011).

Graphene metamaterials

Silver nanoparticle distribution with the dependence of graphene layer number

Hsing-Ying Lin[1], Chen-Han Huang[1*], and Hsiang-Chen Chui[2]
[1]Center for Nano Bio-Detection, National Chung Cheng University, Taiwan
[2]Department of Photonics, National Cheng Kung University, Taiwan
[*]corresponding author: chenhan512@gmail.com

Abstract-The size distribution of silver nanoparticles (AgNPs) deposited on the monolayer, bilayer, and trilayer graphene substrates are studied. Thermal evaporation method was used to deposit silver. Graphene layers were obtained by using the mechanical splitting of graphite. Systematic analyses revealed that the average size of nanoparticles increased with the number of graphene layers. The mechanisms of formation of these layer-dependent morphologies of silver on n-layer graphene are related to the surface free energy and surface diffusion of the n-layer graphene.

A single atomic layer of graphene is the thinnest sp^2 allotrope of carbon. It, therefore, has various unique electrical and optical properties of interest to scientists and technologists [1]. Graphene samples are widely fabricated by the micromechanical cleavage of highly oriented pyrolytic graphite (HOPG) with scotch tape. Layers of oxides such as SiO_2 and Al_2O_3 with special thickness between graphene and the substrate are typically used to make graphene optically visible [2]. The effect of the substrate on Raman measurements has been widely investigated [3]. Raman and surface-enhanced Raman spectroscopy have been widely utilized to elucidate the vibration properties of materials [4]. Recently, they have been used as powerful techniques for characterizing the phonons of graphene. The profile and peak position of the Raman second-order (2D) band can be used to determine the number of graphene layers.

In this work, layers of graphene were fabricated in a sample by micromechanical cleavage. The number of layers of graphene was determined by micro-Raman spectroscopy and optical microscopy. After silver nanoparticles were deposited on the sample using a thermal deposition system, the distribution and sizes of the particles on flakes with different numbers of layers were systematically analyzed. To analyze the effect of the substrate, suspended graphene was fabricated, and the size and density thereof were found to be similar to those of supported graphene. The different results for the mono-, bi-, and tri-layer graphene are theorized to be caused only by the variation among the diffusion barriers of the various graphene layers, which provides a method of determining the number of graphene layers and provides information that can be utilized to elucidate the interaction between a graphene flake and its substrate.

A graphene flake was fabricated by micromechanical cleavage with scotch tape. It was capped with 300-nm-thick layer of SiO_2 over a Si substrate. Graphene flakes that contained different numbers of graphene layers were distributed on different areas on the same sample. The variation in the color contrast with the number of graphene layers is observed under an optical microscope, as presented in Figure 1(a). In the determination of the number of graphene layers, various shapes and 2D bandwidths of graphene were observed by obtaining Raman spectra of different areas, as presented in Figure 1(b). A 633-nm He-Ne laser was the excitation light source.

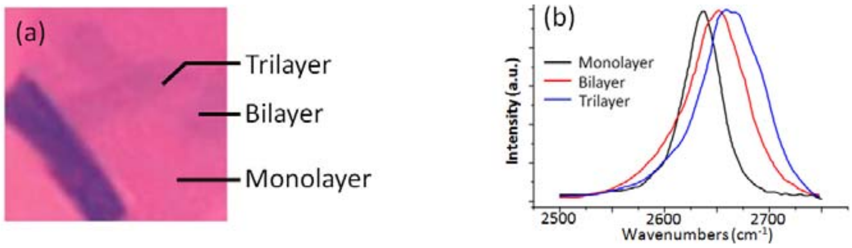

Figure 1. Graphene with different layers. (a) Optical image and (b) Raman spectra.

To investigate the density and size of the nanoparticles, average size and density were determined by histogram analysis. The histograms, on the left-hand sides of Figure 2(a)~2(d), demonstrate the distributions of nanoparticles on the SiO_2/Si substrate, monolayer, bilayer, and trilayer graphene. The sizes of the nanoparticles on the monolayer graphene flake are distributed in the range of 0 to 50 nm, whereas those of the nanoparticles on the trilayer graphene flake were distributed in the range of 10 to 70 nm. Whereas the sizes of the nanoparticles on the SiO_2/Si substrate were distributed in the range of 0 to 50 nm, the majority of them were in the range of 10 to 30 nm.

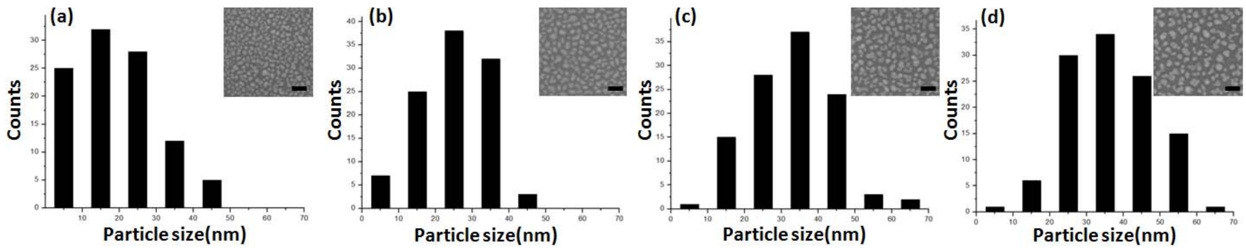

Figure 2. Histograms and SEM images of silver nanoparticles. (a) Substrate, (b) monolayer, (c) bilayer, and (d) trilayer graphene flakes.

In summary, a systematic analysis revealed that the average size of the nanoparticles increased, and the area density and the difference between diffusion barriers of the nanoparticles decreased as the number of graphene layers increased. To analyze the effect of a substrate such as SiO_2, suspended graphene was also fabricated. The size and density of suspended graphene were found to be similar to those of the supported graphene. According to these results, only variations in the interactions between n-layer graphene and the silver nanoparticles were responsible for the variation in their distribution.

Acknowledgements

This work is supported by National Science Council of Taiwan (NSC100-2622-E-006-039-CC3).

REFERENCES

1. Geim A.K., "Graphene: status and prospects," *Science*, Vol. 324, 1530–1534, 2009.
2. Wang Y.Y., Ni Z.H., Yu T., Shen Z.X., Wang H.M., Wu Y.H., Chen W., Wee A.T.S., "Raman studies of monolayer graphene: the substrate effect," *J. Phys. Chem. C*, Vol.112, 10637–10640, 2008.
3. Novoselov K.S., Jiang D., Schedin F., Booth T.J., Khotkevich V.V., Morozov S.V., Geim A.K., "Two-dimensional atomic crystals," *Proc. Natl. Acad. Sci. USA*, Vol.102, 10451–10453, 2005.
4. Huang C.H., Lin H.Y., Chen S.T., Liu C.Y., Chui H.C., Tzeng Y.H., "Electrochemically fabricated self-aligned 2-D silver/alumina arrays as reliable SERS sensors," *Opt. Express*,Vol.19, 11441–11450, 2011.

Effective Modeling of Graphene as a Conducting Sheet in the Finite-Difference Time-Domain Method

V. Nayyeri[1, 2], M. Soleimani[2] and O. M. Ramahi[1*]

[1] Department of Electrical and Computer Engineering, University of Waterloo, Waterloo, ON, Canada

[2] School of Electrical Engineering, Iran University of Science and Technology, Tehran, Iran

[*]corresponding author: oramahi@uwaterloo.ca

Abstract- An effective approach for Finite-Difference Time-Domain modeling of graphene as a conducting sheet is proposed. A novel technique for implementing a conducting sheet boundary condition in the FDTD method which is based on use of backward- and forward-difference schemes for the spatial derivatives is used for modeling of graphene sheet.

Graphene, which is a planar monoatomic layer of carbon bonded in a hexagonal structure, has recently gained significant interest due to its potential in enabling new technologies and addressing key technological challenges [1]. For electromagnetic fields, graphene behaves as a surface with conductivity that depends on chemical doping or external field bias [2]. To understand the scattering, radiation and waveguiding properties of grapheme, Maxwell equations need to be solved either in two-dimensional or three-dimensional space. Analytical solutions for simple canonical problems involving grapheme layers are available; however, for most problems, numerical solutions of Maxwell equations are inevitable. Modeling graphene in FDTD can be performed in different ways with dramatic variation in the efficiency and resource requirements of the simulation. Two approaches have been so far used for modeling of graphene sheets in the FDTD method which are: 1) regular FDTD method with fine enough discretization of the fields inside the sheet [3] and 2) subcell FDTD approach [4-5]. In both approaches, graphene sheets were considered as thin layers occupying some (in the first one) or a fraction (in the second one) of the FDTD cells and the surface conductivity of graphene was converted to volumetric conductivity. The first approach needs the spatial discretization of computational domain to be at least as fine as the thickness of the layer which can be considered around $1nm$. This extremely fine discretization requires huge computing resources for running simulations and hence is impractical in some cases. The second approach using subcell FDTD method also suffers from this problem but not as strong as the first one. Furthermore, modeling of infinite graphene sheets using subcell method requires a special type of PML [5].

The idea behind this work is based on modeling of graphene as a conducting sheet boundary condition. Implementation of a resistive (or conducting) sheet boundary condition was introduced in [6] but suffered from field polarization restrictions, was applicable to purely resistive sheets, and suffered from instability [7]. In this paper we propose a method for implementing a conducting sheet boundary condition. The proposed method is not polarization restricted, applicable to sheets having complex conductivity and does not suffer from instability.

To briefly describe the proposed method, let see Fig. 1 which shows a 3-D FDTD cell including a conductive surface (which can be a graphene sheet). Due to the possibility of current and net charge at the conducting surface, a pair of each of the tangential components of the magnetic field (H_x and H_y) and a pair of the normal component of electric field (E_z) are considered immediately to the bottom and top sides of the surface. The updating equations for these field components can be derived by first using backward and forward difference schemes for the spatial derivative normal to the sheet, and then applying the conducting sheet boundary condition ($[{}^2\mathbf{H}- {}^1\mathbf{H}] = \sigma_s \mathbf{E}$).

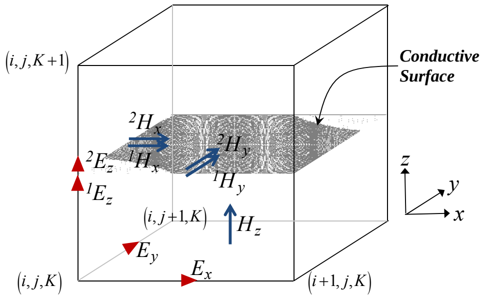

Fig. 1. A 3-D FDTD cell including a conductive boundary at grid K+ ½.

As an example, the method is evaluated by simulating normal incidence of a plane wave on an infinite graphene sheet and extracting the transmission and reflection coefficients. We consider a grapheme sheet of T= 300K, μ_c= 0.5eV and Γ= 0.65$meV/\hbar$. FDTD technique is applied in this example in which a wideband Gaussian pulse is used as the source. The values of electric field are recorded at both sides of the boundary and Discrete Fourier Transform is used to obtain the transmission and reflection coefficients. These coefficients are also calculated analytically. The comparison between the results of our proposed FDTD algorithm and the analytic solution is shown in Fig. 2 demonstrating a strong agreement. In our simulations, the spatial mesh size was $\lambda_{\min}$ / 20. Since the graphene is modeled as a boundary, the size of the FDTD mesh can be chosen completely independent of the graphene sheet. We also found that classical PML is applicable to the FDTD method proposed. To test the stability of the method, the simulation was run for 30,000 time steps without any trace of instability.

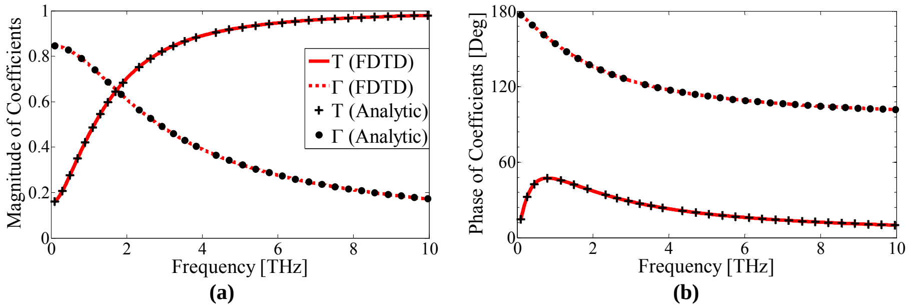

Fig. 2. Transmission (T) and reflection (Γ) coefficients for normally incident plane wave on a graphene sheet, (a) magnitude, and (b) phase.

REFERENCES

1. K. S. Novoselov *et al*, "A roadmap for graphene," *Nature*, Vol. 490, 192-200, 2012.
2. G. W. Hanson, "Dyadic Green's functions and guided surface waves for a surface conductivity model of graphene," *J. Appl. Phys.*, Vol. 103, 064302, 2008.
3. A. Mock, "Pade approximant spectral fit for FDTD simulation of graphene in the near infrared," *Opt. Mater. Exp.*, Vol 2, 164810, 2012.
4. G. D. Bouzianas *et al*, "Optimal modeling of infinite graphene sheets via a class of generalized FDTD schemes," *IEEE Trans. Magn.,* Vol. 48, 379–382, 2012.
5. X. Yu and C. D. Sarris, "A perfectly matched layer for subcell FDTD and applications to the modeling of graphene structures*," IEEE Antennas Wireless Propag. Lett.*, Vol. 11, 1080-1083, 2012.
6. L. Wu and L. Han, "Implementation and application of resistive sheet boundary condition in the finite-difference time-domain method," *IEEE Trans Antennas Propag.*, Vol. 40, 628-633, 1992.
7. J. G. Maloney and G. S. Smith, "A comparison of methods for modeling electrically thin dielectric and conducting sheets in the finite-difference time-domain method," *IEEE Trans. Antennas Propag.*, Vol. 41, 690- 694, 1993.

Spontaneous nonparametric down-conversion of plasmon-polaritons

V. Hizhnyakov, H. Kaasik, I.Tehver*

Institute of Physics, University of Tartu, Riia 142, 51014 Tartu, Estonia
*corresponding author: tehver@fi.tartu.ee

Abstract-The spontaneous down-conversion of laser light focused on metal-dielectric interface is considered. In this case the working second-order susceptibility is enhanced due to excitation of plasmon-polaritons. It is found that strong enhancement of the process takes place for the laser intensity close to the critical intensity. The further increasing of intensity will cause weakening of the process. The crossover of the efficiency takes place if the amplitude of oscillations of the eikonal coincides with the wavelength of excitation.

Spontaneous nonparametric down-conversion of photons - the creation of photon pairs on the expense of the single photon in case of absence of the feedback is the nonlinear quantum phenomenon which takes place due to existence of the zero-point fluctuations. The process belongs to the phenomenon of general importance,- the Dynamical Casimir effect (the emission of photon pairs due to time-dependent perturbation of the zero-point state of the electromagnetic field). It is of remarkable interest also from practical point of view while generated photon pairs are in the entangled state. At the usual conditions the process has extremely low probability and is observed only in case of positive feedback, e.g. in parametric oscillators. However, at present there exist possibilities to enhance strongly both, the intensity of laser light and the interaction of it with the matter, and in this way to increase the intensity of the down-conversion. In this communication we consider how the efficiency of this process changes with increase of the intensity of excitation. The theoretical method developed in [1, 2] is used. We consider the case of laser light focused at a small spot of a dielectric with non-zero second-order susceptibility. It is found that strong enhancement of the process takes place for the laser intensity close to the critical intensity I_0. If the intensity I of the laser light is less than I_0 then increasing of the intensity I of the laser light will result in the increasing of the down-conversion. However, if I exceed I_0 then further increasing of I will cause decreasing of the down-conversion. The crossover of the efficiency takes place if the amplitude of oscillations of the optical length (eikonal) coincides with the wavelength of excitation. This condition may be fulfilled e.g. using femto-pulse excitation with 10^{-6} J of pulse energy.

Acknowledgements. Acknowledged is the support by Estonian IRF project IUT2-27 and by the European Union through the European Regional Development Fund (project 3.2.0101.11-0029).

REFERENCES

1. Hizhnyakov, V. and Kaasik, H. “Emission of dielectric with oscillating refractive index,” *Journal of Physics D: Applied Physics*, Vol. 21, 155–160, 2005.
2. Hizhnyakov, V. and Kaasik, H. “Dynamical Casimir effect: quantum emission of a medium with time-dependent refractive index,” in: *IEEE Conference Proceedings: Northern Optics*, Bergen, Norway, June 2006, 7–11.

Acoustic metamaterials

On the feasibility of a 2D acoustic cloak using layers of elastic materials

C. Dutrion[1], **F. Simon**[1]

[1]Onera Toulouse, France
cecile.dutrion@onera.fr

Abstract— This paper examines the possibility of creating an acoustic cloak using a multilayered elastic cylindrical shell to eliminate the acoustic field scattered from a rigid cylinder impinged by plane waves. This scattered field is calculated by a semi-analytical code and depends on the dimensional and mechanical characteristics of the elastic layers. Optimization by genetic algorithm is led to determine the characteristics of the layers minimizing the scattering. Realizable elastic coatings leading to scattering reduction are eventually proposed.

For a few years, researchers have been investigating the possibility of making an acoustic cloak using metamaterials. Thanks to a coordinate transformation method similar to that employed by Pendry [1] in the electromagnetic domain, Cummer and Schurig [2] demonstrated that perfect acoustic cloaking could be achieved in surrounding the obstacle with a specific anisotropic and inhomogeneous fluid. One popular approach consists in designing a material which has the effective properties of this theoretical fluid, but other methods can also be proposed to reduce strongly the acoustic scattering. In this study, an alternative approach is examined: the feasibility of a 2D acoustic cloak with layers of elastic materials in the case of an infinite rigid cylinder submitted to normal plane waves, as represented in figure 1.

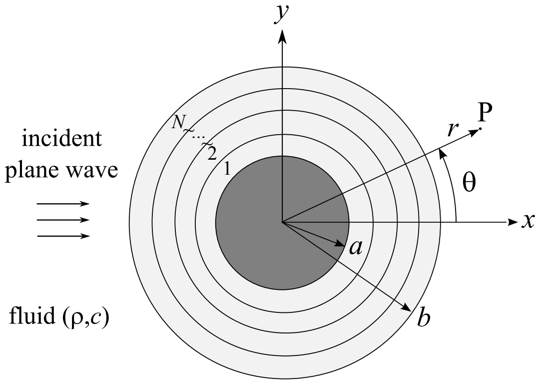

Figure 1: Problem geometry

A semi-analytical code has been developed to calculate the pressure field around a cylinder on which a multilayered orthotropic elastic coating has been fixed. Two approaches have been employed. The first one, based on a method described by Skelton [3], combines the wave-number domain approach and the finite element method; the second uses the method of wave function expansion in conjunction with the transfer matrix approach [4], and is less CPU time consuming when a significant number N of layers is considered. It has been numerically shown that both methods provide very similar results for the scattered pressure field. To keep a reasonable number of parameters, the study has then been restricted to a bi-layer coating, and next simulations have been carried out with Skelton's method.

The coupling of a genetic algorithm with the vibro-acoustic code shows that a strong scattering reduction can be achieved with only 2 layers: the exterior one being isotropic and stiff, the interior one being orthotropic and soft. Thus, in the case of a rigid cylinder 30 cm in diameter placed in air, a scattering reduction of 96% in comparison to the uncloaked case theoretically occurs at 380 Hz as represented in figure 2.a and 2.b. However, it is very unlikely that materials having precisely the set of characteristics obtained through optimization could be found in practice. So, further investigations have been conducted using a 10 mm orthotropic polyethylene foam for the internal layer, the aim being to find an existing or realizable material for the external layer that could lead to a substantial reduction of the acoustic scattering. According to simulations and for an appropriate choice of obstacle size and frequency, a thin isotropic layer of polymer like polymethylpentene, polycarbonate or poly(methyl methacrylate) can in this case enable scattering reduction (see figure 2.c and 2.d).

These simulations show that a reduction of the scattering around a cylinder can be obtained thanks to a multilayered orthotropic cylindrical shell. Experiments are to be conducted in order to validate these numerical results. Further works in material design would then be necessary to develop materials giving a better attenuation of the scattering.

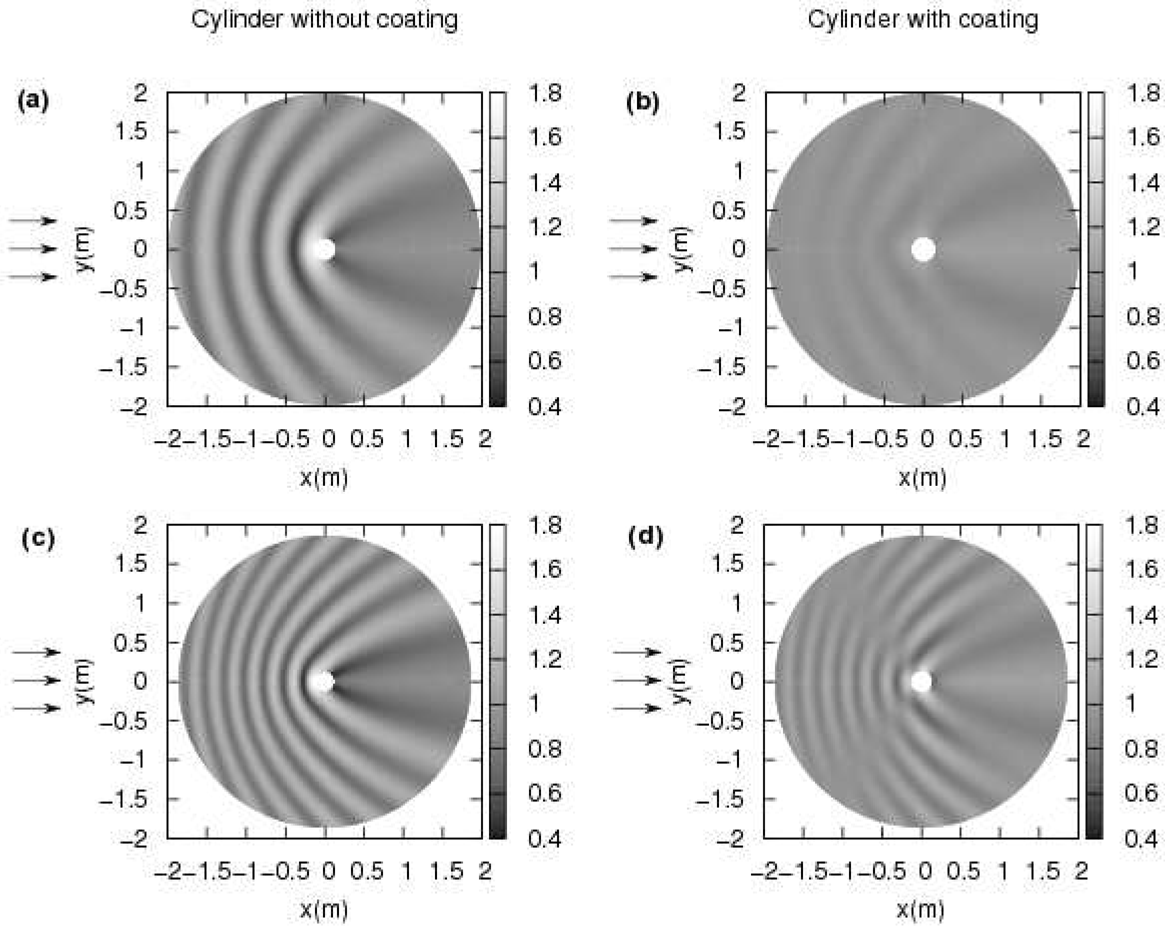

Figure 2: Amplitude of the pressure field around an uncloaked (left) or a cloaked (right) cylinder insonified by a unit plane wave. (a), (b): 380 Hz, cylinder 30 cm in diameter, coating entirely determined by optimization. (c), (d): 680 Hz, cylinder 26.6 cm in diameter, coating with an internal layer of orthotropic polyethylene foam and an external layer determined by optimization.

REFERENCES

1. Pendry, J. B., D. Schurig, and D. R. Smith, "Controlling electromagnetic fields," *Science*, No. 312, 2006.
2. Cummer, S. A. and D. Schurig, "One path to acoustic cloaking," *New J. Phys.*, Vol. 9, No. 45, 2007.
3. Skelton, E. A. and J. H. James, "Acoustics of an anisotropic layered cylinder," *J. Sound Vib.*, Vol. 161, No. 2, 1993.
4. Jamali, J., M. H. Naei, F. Honarvar, and M. Rajabi, "Acoustic scattering from functionally graded cylindrical shells," *Arch. Mech.*, Vol. 63, No. 1, 2011.

Axisymmetric periodic systems for beam forming in acoustics

A. Cebrecos[1], V. Romero-García[1], R. Picó[1], V. Sánchez-Morcillo[1], L.M. Garcia-Raffi[2] and J.V. Sánchez-Pérez[3]

[1]Instituto de investigación para la Gestión Integrada de zonas Costeras,
Universitat Politècnica de València, Spain
[2]Instituto Universitario de Matemática Pura y Aplicada,
Universitat Politécnica de València, Spain
[3] Centro de Tecnologías Físicas: Acústica, Materiales y Astrofísica,
Universitat Politécnica de València, Spain.
virogar1@gmail.com

Abstract— Numerical and experimental evidences of the advantages of axisymmetric systems made of concentric toroidal rigid scatterers embedded in air for beam forming in acoustics are reported in this work. Several effects as focusing, beam forming, spatial filtering and frequency filtering are observed and discussed in this work. The structure has been designed for the audible frequencies, however the results are independent of the scale, therefore the system can be redefined for the ultrasound regime.

Axial symmetric structures are receiving increasing interest in last years due to the fact that they seems to be relevant in wave propagation applications because of the symmetry of the system source-object. Axial symmetric devices to focus acoustic waves making use of the scattering of waves in the diffraction regime by an optimized arrangement of toroidal elements have been proposed [1]. On the other hand, in the long wavelength regime, an axial symmetric gradient lens for electromagnetic and acoustic waves has been theoretically studied [2, 3, 4]. More recently, axial symmetric lenses have been used to obtain subwavelength imaging in the far field regime [5].

In this work we numerically and experimentally analyse an axisymmetric structure based on a transformational design from a two-dimensional (2D) SC. Applying an axial rotation of the 2D SC made of rigid cylindrical scatterers with respect to its symmetry axis, we create a three dimensional (3D) axial symmetric system made up of concentric toroidal rigid scatterers (Fig. 1). Although this system presents a geometric periodicity, the wave equation for the axisymmetric system is not invariant under periodic transformations and cannot be rigorously considered as a periodic medium. However, due to the fact that the effective properties in the long wavelength regime are not sensible to the arrangement of the scatterers but to the filling fraction [6], we can use the homogenization formulas to design an axial symmetric medium with effective parameters. In that way, one can control the refraction of acoustic waves by means of axial symmetric structures.

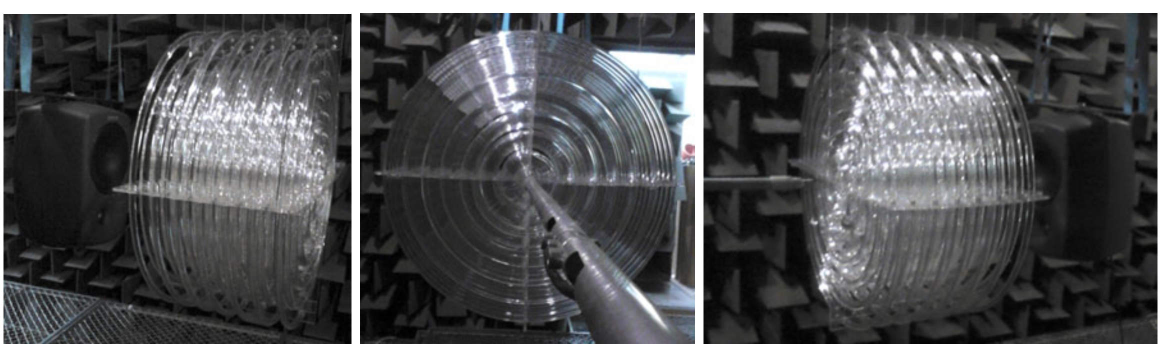

(a) (b) (c)

Figure 1: Pictures of the experimental setup. (a) Source and sample. (b) In-plane view of the sample and microphone. (c) Complete setup.

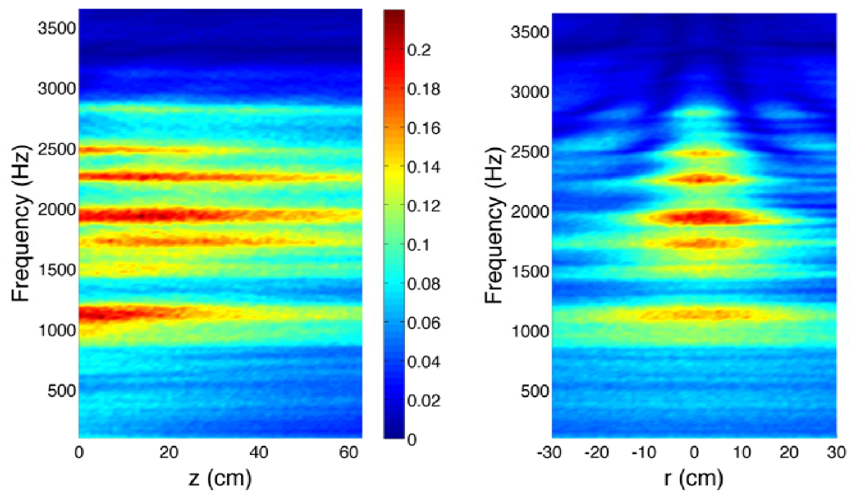

(a) (b)

Figure 2: Experimental results. (a) Frequency analysis through the longitudinal z-axes. Distances measured from the end of the lens. (b) Frequency analysis at the r-radial axes at point z =20 cm. Distances measured from the center of the lens. In (a) and (b) the color scale shows the measured Pressure in Pa.

Figure 2 show the experimental frequency analysis through the longitudinal (z-axis) (a) and radial (r-axis) axis (b). In the long wavelength regime, the system behaves as a refractive lens. The effective parameters are controlled by means of a gradient variation of the filling fraction in the radial direction (see the design details in Ref. [4]), so being the system a gradient refractive index lens. In agreement with the numerical predictions, one can see around 1000 Hz, the focusing behaviour due to the modulation of the effective parameters.

The analysis has been also extended to higher frequencies. Interesting questions arise from several effects observed in Figure 2. One can see evidences of phenomena related with several aspects of the system as for example the finite size of the axisymmetric structure or the frequency and spatial filtering produced in some regions of the spectra. Specially the results presented in this work can be use to design axisymmetric systems for beam forming in acoustics independently of the range of frequencies.

ACKNOWLEDGMENT

The work was supported by Spanish Ministry of Science and Innovation and European Union FEDER through projects FIS2011-29734-C02-01 and -02, MAT2009-09438 and GVA/2011/55. V.R.G. is grateful for the support of post-doctoral contracts of the UPV CEI-01-11.

REFERENCES

1. Sanchis, L., Yánez, A., Galindo, P. L., Pizarro, J. and Pastor, J. M. "Three-dimensional acoustic lenses with axial symmetry", *Appl. Phys. Lett.*, Vol. 97, 054103, 2010.
2. Chang, T.-M.; Guenneau, S.; Hazart, J. and Enoch, S. "Focussing light through a stack of toroidal channels in PMMA" *Opt. Exp.*, Vol. 19, 16154, 2011.
3. T M Chang and G Dupont and S Enoch and S Guenneau, "Enhanced control of light and sound trajectories with three-dimensional gradient index lenses", *New Jour. Phys.*, Vol. 14, 035011, 2012.
4. V. Romero-García, R. Picó, A. Cebrecos, L.M. Garcia-Raffi, J.V. Sánchez-Pérez and V. Sánches-Morcillo, "Focusing properties of axisymmetric acoustical metamaterials made of toroidal scatterers", *IMECE2012, ASME 2012 International Mechanical Engineering Congress and Exposition*, Vol. , , 2012.
5. Rogers, E. T. F., Lindberg, J., Roy, T., Savo, S., Chad, J. E., Dennis, M. R. and Zheludev, N. I. "A super-oscillatory lens optical microscope for subwavelength imaging", *Nat. Mat.*, Advanced Online Publication, 1-4, 2012.
6. Torrent, D., Hakansson, A., Cervera, F. and Snchez-Dehesa, J. "Homogenization of two-dimensional Cluster of Rigid Rods in Air" *Phys. Rev. Lett.*, Vol. 96, 204302, 2006.

Heuristic homogenization to overcome the homogenization limit of the effective parameters of two dimensional Sonic Crystal slabs.

J.-P. Groby[1], **V. Tournat**[1], **V. Romero-García**[2] **and O. Umnova**[3]

[1]Laboratoire d'Acoustique de l'Université du Main, France
[2]Instituto de investigación para la Gestión Integrada de zonas Costeras, Universitat politècnica de València, Spain
[3]School of Computing, Science and Engineering, University of Salford, United Kingdom.
virogar1@gmail.com

Abstract— A heuristic homogenization procedure to determine the effective properties (wave number and impedance or related ones such as effective density and bulk modulus) of sonic crystal slabs (finite-length acoustic periodic structures) is proposed in this work. The method shows a frequency range of validity which largely exceeds that of the classical procedures obtaining the effective properties of the system even inside the band gap. In this range of frequencies the effective wave number matches with both the real and imaginary parts of the band structure obtained using the Plane Wave Expansion method.

Most of the homogenization methodologies have been developed in the long wavelength limit [1]. The frequency limit of these methods has recently been overtaken by using of an asymptotic homogenization procedure specifically developed for the high frequencies [2]. In this work we use the heuristic homogenization procedure, often referred to as the Nicolson-Ross-Weir procedure,[3] which consists of heuristically replacing the heterogeneous sample by a body of the same shape and size filled with uniform continuous medium with unknown properties.

Consider a finite-depth sonic crystal composed of N d-periodic rows containing an infinite number of infinitely long rigid cylinders with circular cross section (radius r) arranged to mimic a square lattice crystal slab, as depicted Figure 1 (left panel). The total reflected (transmitted) pressure in the sub-domain Ω^u (Ω^l) follows as,

$$p^u(\mathbf{x}) = p^i(\mathbf{x}) + \sum_{q\in\mathbb{Z}}\sum_{j\in N}\sum_{m\in\mathbb{Z}} \frac{2(-\mathrm{i})^m}{k_{2q}d} B_m^{(j)} e^{\mathrm{i}k_{1q}\left(x_1-x_1^{(j)}\right)+\mathrm{i}k_{2q}\left(x_2-x_2^{(j)}\right)+\mathrm{i}m\theta_q},$$
$$p^l(\mathbf{x}) = p^i(\mathbf{x}) + \sum_{q\in\mathbb{Z}}\sum_{j\in N}\sum_{m\in\mathbb{Z}} \frac{2(-\mathrm{i})^m}{k_{2q}d} B_m^{(j)} e^{\mathrm{i}k_{1q}\left(x_1-x_1^{(j)}\right)-\mathrm{i}k_{2q}\left(x_2-x_2^{(j)}\right)-\mathrm{i}m\theta_q}, \tag{1}$$

where $k_{1q} = k_1^i + 2q\pi/d$, $k_{2q} = \sqrt{k^2 - k_{1q}^2}$, so that $\mathrm{Re}(k_{2q}) \geq 0$ and $\mathrm{Im}(k_{2q}) \geq 0$ to satisfy the Sommerfeld radiation condition, and $ke^{\mathrm{i}\theta_q} = k_{1q} + \mathrm{i}k_{2q}$. Below the lowest d-periodic grating mode frequency or Cutler's mode which satisfies $f_g = \frac{c}{d(1+\cos\theta^i)}$, only the specular reflected and transmitted waves can propagate in respectively Ω^u and Ω^l,being the higher order Bloch waves evanescent, with purely imaginary k_{2q}. In this situation one can identify the reflection and transmission coefficients as

$$R = \sum_{j\in N}\sum_{m\in\mathbb{Z}} \frac{2(-\mathrm{i})^m}{k_2^i d} B_m^{(j)} e^{-\mathrm{i}k_1^i x_1^{(j)}+\mathrm{i}k_2^i\left(H-x_2^{(j)}\right)+\mathrm{i}m\theta_q},$$
$$T = e^{\mathrm{i}k_2^i H} + \sum_{j\in N}\sum_{m\in\mathbb{Z}} \frac{2(-\mathrm{i})^m}{k_2^i d} B_m^{(j)} e^{-\mathrm{i}k_1^i x_1^{(j)}+\mathrm{i}k_{2q}x_2^{(j)}-\mathrm{i}m\theta_q}. \tag{2}$$

Assuming these coefficients being those of an homogeneous fluid plate, as it is usually hypothesized in case of the heuristic homogenization procedure of metamaterials, effective impedance and projection of the effective wave number can be derived analytically as

$$\widetilde{Z}_{eq} = \pm\frac{Z}{\sin\theta^i}\sqrt{\frac{(1+R)^2-T^2}{(R-1)^2-T^2}}\ , \quad k_{2eq} = -\frac{-\mathrm{i}}{H}\ln\left(\frac{(1+R)+(R-1)\widetilde{Z}_{eq}\sin\theta^i/Z}{T-T\widetilde{Z}_{eq}\sin\theta^i/Z}\right) + \frac{2n\pi}{H}\ . \tag{3}$$

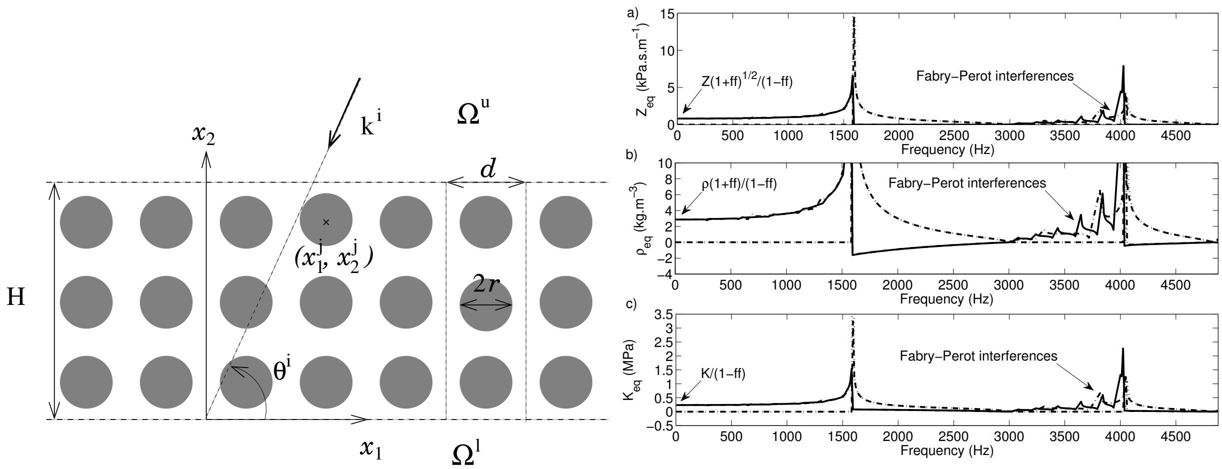

Figure 1: Left panel: Scheme of a d-periodic sonic crystal slab made of circular rigid inclusions excited by a plane wave. Right panels: Real and imagniary parts of the equivalent impedance Z_{eq} (a), density ρ_{eq} (b) and bulk modulus K_{eq} (c) of a sonic crystal slab of 3 [(-.-) and $(\cdots)$] and 7 [(—) and $(- - -)$] rows.

These two parameters can be used to recover the effective density and bulk modulus,

$$\rho_{eq} = \widetilde{Z}_{eq} k_{2eq}/\omega \ , \quad K_{eq} = \frac{\widetilde{Z}_{eq}\omega/k_{2eq}}{1+(k\cos\theta^i/k_{2eq})^2} \ . \tag{4}$$

from which, the equivalent impedance and wavenumber can finally be calculated by $Z_{eq} = \sqrt{K_{eq}\rho_{eq}}$ and $k_{eq} = \omega/\sqrt{K_{eq}/\rho_{eq}}$.

Right panel of Figure 1 shows the effective impedance (a), density (b) and bulk modulus (c) of a sonic crystal slab. In this work we show that the effective wavenumber matches both the real and imaginary part of the PWE calculations and that the equivalent density becomes negative inside the bandgaps. This is analyzed as being the result of a dipolar diffraction of the fundamental element of the finite depth sonic crystal. This means that negative density can be reached not only with dipolar resonances but also with dipolar diffracted fields. It is also shown that this effective parameters depend on the frequency, the angle of incidence and on the thickness of the material, leading to quite interesting questions concerning the development of non-local models for metamatrials and of the Cosserat's theory of the elasticity to acoustics. Moreover, the analysis of the results points out some intrinsic differences between a sonic crystal, which cannot be studied in practice, and a finite depth sonic crystal: the influence of the interfaces which lead not only to grating modes but also to index of refraction makes impossible to study sonic crystal properties at oblique incidence, the existence of quasi-bandgap at oblique incidence, the impossibility of exciting odd mode at normal incidences when mimicking the behavior of a sonic crystal along the ΓM direction. Moreover, this article offers a clear definition of the interface location of the effective material for square lattices. The current procedure can also be helpful in optics, both in TM and TE polarization, the fundamental equations being identical to those of acoustics for two-dimensional problems.

ACKNOWLEDGMENT

The authors would like to thank the Région Pays de la Loire for granted the invitation of O. Umnova as Senior Researcher in Le Mans University. V. Romero-García is grateful for the support of "Programa de Contratos Post-Doctorales con Movilidad UPV del Campus de Excelencia Internacional (CEI-01-11)" and of the grant "BEST2012" of the Generalitat Valenciana.

REFERENCES

1. Wu, Y., Li, J., Zhang, Z.-Q. and Chan, C. "Effective medium theory for magnetodielectric composites: Beyond the long-wavelength limit". *Phys. Rev. B*, Vol. 74, 085111, 2006.
2. Craster, R., Kaplunov, J. and Pichungin, "A. High-frequency homogenization for periodic media". *Proc. R. Soc. A*, Vol. 466, 2341-2363, 2010.
3. Nicolson, A. and Ross, G. "Measurement of the intrinsic properties of materials by time-domain techniques". *IEEE Trans. Instr. and Meas.*, Vol. 19, 377-382, 1970.

Dissipative Phononic Materials:

Mathematical Models and Physical Phenomena

M. J. Frazier and M. I. Hussein*
University of Colorado Boulder, USA
*corresponding author: mih@colorado.edu

Abstract-We present rigorous formulations for the treatment of viscous and viscoelastic damping in the analysis of elastic wave propagation in phononic crystals and acoustic metamaterials. For simplicity, we consider mass-spring-dashpot models and obtain exact formulae for the frequency and damping factor band structures. Our analysis sheds light on the effects of these two types of damping on the dispersive characteristics in the presence of Bragg scattering or local resonance.

Phononic crystals (PnCs) and acoustic metamaterials (AMs) are periodic materials that exhibit distinct frequency characteristics, such as the possibility of the formation of *band gaps.* Within a band gap, wave propagation is effectively prohibited. In the case of AMs, it is possible for a band gap to open up at wavelengths smaller than the unit cell size. This inherent dynamical phenomenon, in PnCs and/or AMs, can be utilized in a broad range of technologies at different length scales (see [1] for a review of theory, concepts and applications).

In this work we consider two mass-spring-dashpot models, one in which the damping is represented simply by a single viscous dashpot (as depicted in Fig. 1) and one that incorporates viscoelasticity. For the latter, we use Boltzmann's hereditary theory whereby the damping force depends upon the past history of motion via a convolution integral over a kernel function $G(t)$:

$$\mathbf{f}_d(t) = \mathbf{C}\int_0^t G(t-\tau)\dot{\mathbf{u}}(\tau)d\tau. \tag{1}$$

The kernel function, $G(t)$, may take several forms, while recognizing that in the limit where $G(t\text{-}\tau) = \delta(\text{t-}\tau)$, the familiar viscous damping model is recovered [2]. In particular we consider a Maxwell damping element for which we assume the following form for the kernel function [3]:

$$G(t) = \mu_1 e^{-\mu_2 t} H(t). \tag{2}$$

The choice of parameters for the viscous damping model is given in the caption of Fig. 1. For the viscoelastic model, we assume

$$\mu = \mu_1 = \mu_2. \tag{3}$$

where we choose $\mu = 10^3$ which is a value that reflects viscoelastic behavior very well. Higher values of μ leads to a more standard viscous-like behavior (i.e., less dependence on the past history), whereas low values of μ represent more viscoelastic behavior (i.e., more dependence on the past history).

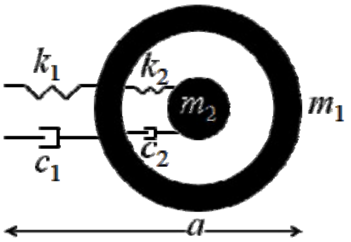

Figure 1. Mass-spring-dashpot model of a one-dimensional viscously damped acoustic metamaterial

In Fig. 2, we show a sample of our results; in particular we present the frequency and damping ratio band diagrams for the acoustic metamaterial model depicted in Fig. 1. A similar study on damped phononic crystals was conducted by the authors in an earlier publication [4].

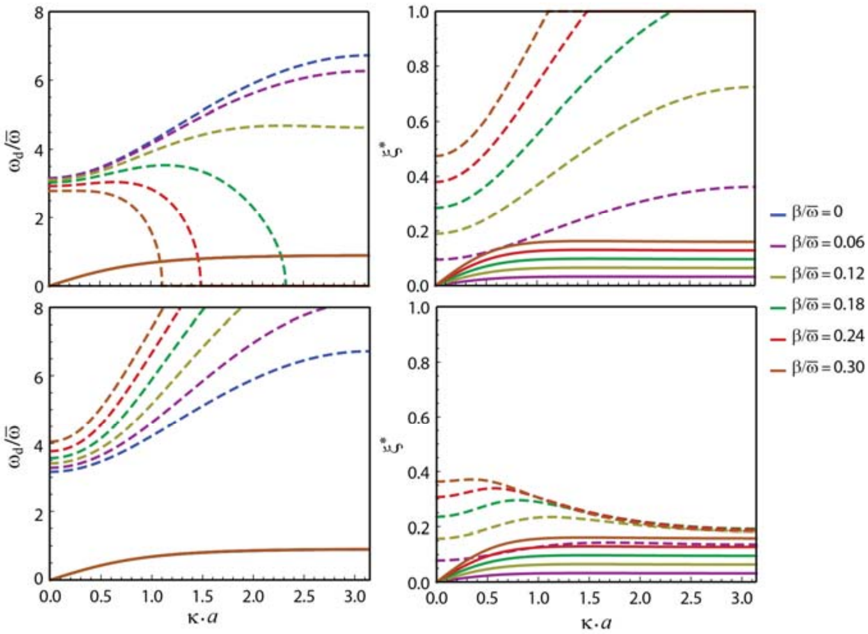

Figure 2. Frequency (left) and damping factor (right) dispersion band structures for the viscous damping model (top) and the viscoelastic damping model (bottom).

Acknowledgement

This research is partially funded by the DARPA Young Faculty Award grant YFA N66001-11-1- 4134.

REFERENCES

1. Deymier, P.A. (Ed.), *Acoustic Metamaterials and Phononic Crystals*, Springer Physics, New York, in press.
2. Woodhouse, J. "Linear Damping Models for Structural Vibration," *J. Sound Vib.* Vol. 215, 547-569, 1998.
3. Fung, Y.C. and Tong, P., *Classical and Computational Solid Mechanics*, World Scientific Publishing Co., 2001.
4. Hussein, M.I. and Frazier, M.J., "Band structure of phononic crystals with general damping," *Journal of Applied Physics*; Vol. 108, 093506, 2010.

Biophotonic materials

Fabrication of amorphous-diamond photonic crystals and their optical properties

Yafeng Zhang[1*], Biqin Dong[1], Feng Liu[2], Xiaohan Liu[1], and Jian Zi[1]
Department of Physics, Fudan University, Shanghai 200433, P. R. China
[2]Laboratory of Opto-electrial Material and Device, Department of Physics, Shanghai Normal University, Shanghai 200234, P. R. China
[*] E-mail: 09110190012@fudan.edu.cn

Abstract-We successfully fabricate SiO_2, ZnO, and TiO_2 amorphous-diamond photonic crystals (ADPCs) that have optical response in the visible regime by using sol-gel and atomic layer deposition (ALD) methods based on templates of parrot feather barbs. We find that SiO_2, ZnO, and TiO_2 ADPCs retain amorphous-diamond structures and display bright structural colors.

Photonic crystals of diamond structures are regarded as the champion structure for opening up photonic bandgaps [1-4]. On the other side, ADPCs show some unique optical properties due to the lack of long-range order [2,5,6]. The fabrications of such structures in the visible and near-infrared regimes are still rather challenging.

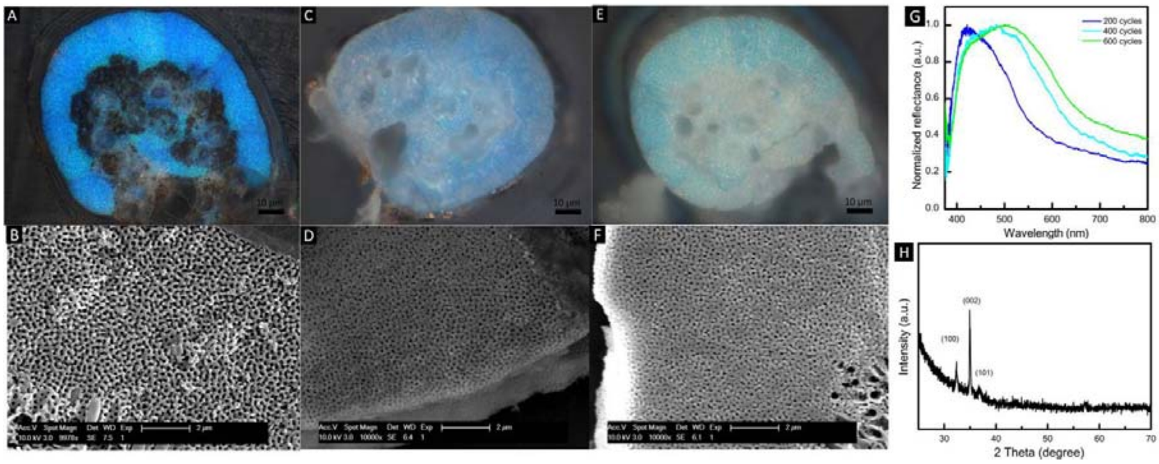

Fig. 1 Fabricated ZnO PADCs by ALD. (A) Optical microscopic image of the transverse cross-section of a blue barb. (C) and (E) Optical microscopic images of the transverse cross-section of inversed PADCs with 200 and 600 infiltration cycles, respectively. The corresponding SEM images are shown in (B), (D), (F). (G) and (H) Spectral and XRD measurements, respectively.

In a previous study, we found that there exists a well-defined ADPC in blue feather barbs of the scarlet macaw, responsible for the blue structural coloration [6]. Here, based on the barbs as templates we successfully replicate ADPCs with SiO_2, ZnO and TiO_2 by using sol-gel and ALD methods. By controlling the infiltration or deposition cycles, the heating rate, and the calcination time, the inversed ADPCs of SiO_2, ZnO, and TiO_2 are found to retain the amorphous-diamond structure, confirmed by scanning electron microscopy (SEM) observations. Bright structural colors can be observed, further confirming the good structural quality of the inversed ADPCs. Figure 1 shows the inversed ZnO ADPCs. Obviously, the inversed structures retain the amorphous-diamond structure. The volume fraction can be controlled by infiltration cycles, together with a change in structural color.

ADPCs possess only short-range order, showing interesting optical response [2,5,6]. As a result, inversed ADPCs may find potential applications in photonics and can be exploited to study unusual light transport such as light localization.

Acknowledgements: This work was supported by the 973 Program (Grant Nos. 2013CB632701 and 2011CB922004). The research of J.Z. and X.H.L. is further supported by the NSFC.

REFERENCES

1. M. Maldovan and E. L. Thomas, "Diamond-structured photonic crystals", Nat. Mater. 3, 593-600, 2004.
2. K. Edagawa, S. Kanoko, and M. Notomi, "Photonic Amorphous Diamond Structure with a 3D Photonic Band Gap", Phys. Rev. Lett. 100, 013901, 2008.
3. S. Imagawa, K. Edagawa, "Polarization conversion by a three-dimensional photonic crystal mirror with a diamond structure", Photonics and Nanostructures-Fundamentals and Applications 10, 281–286, 2012.
4. M.R. Jorgensen, J.W. Galusha, and M.H. Bartl, "Strongly Modified Spontaneous Emission Rates in Diamond-Structured Photonic Crystals", Phys. Rev. Lett. 107, 143902, 2011.
5. S. F. Liew, J.-K. Yang, H. Noh, C.F. Schreck, E.R. Dufresne, C.S. O'Hern, and H. Cao, "Photonic band gaps in three-dimensional network structures with short-range order", Phys. Rev. A 84, 063818, 2011.
6. H. Yin, B. Dong, X. Liu, T. Zhan, L. Shi, J. Zi, and E. Yablonovitch. "Amorphous diamond-structured photonic crystal in the feather barbs of the scarlet macaw", PNAS, vol. 109, no. 27, 10798–10801, 2012.

Surface-Enhanced Raman Spectroscopy in Silver Nanowire-based transparent films

R. Capasso[1], M. Pannico[2], P. Musto[2], W. Shen[3], W. Song[3], J. Zhou[4], P. Mormile[1] and L. Petti[1*]
[1]Institute of Cybernetics "E. Caianiello" of CNR, Via Campi Flegrei 34, 80072 Pozzuoli, Italy
[2]Institute of Chemistry and Technology of Polymers of CNR, Via Campi Flegrei 34, 80072 Pozzuoli, Italy
[3]Institute of Material Technology and Engineering, Chinese Academy of Sciences, Ningbo, China
[4]Institute of Photonics, Faculty of Science, Ningbo University, Ningbo 315211, Zhejiang, China
[*]corresponding author: luciapetti@hotmail.com / L.petti@cib.na.cnr.it

Abstract- Silver nanowires (NWs) can exhibit unique optical properties known as localized surface plasmon resonance (LSPR) and surface enhanced Raman scattering (SERS). An effective and facile method for the fabrication of a SERS-active film with Silver NWs is proposed by drop casting of Silver NWs on glass with ethanol as the inducer. The dropped Ag NWs exhibit very efficient Raman scattering enhancement estimated using pMA (p-mercaptoaniline) as a probe molecule which is attributed to the coupling electromagnetic SERS enhancement mechanism with additional localization field within Silver NWs on glass.

Since the initial discovery of surface-enhanced Raman scattering (SERS), an increased amount of work has been done on the research of substrates for highly efficient Raman scattering enhancement due to their extraordinary potential for trace analysis and biological tags[1]. The optical properties of noble metals with nanostructures have attracted enormous attention because of their potential application in optical sensing[2], biosensor[3] and cell diagnostics[4]. Recently, the plasmonic optical responses of metal nanoparticles, based on localized surface plasmon resonances (LSPR) and significant fluorescence enhancement in the visible and near IR region, have been intensively researched. Many groups have demonstrated that the plasmon resonance is closely related to the size and shape of metal nanoparticles and the dielectric properties of the surrounding medium[5]. A great deal of work has been reported with their developments on the synthesis of Au and Ag nanoparticles with all kinds of shapes, such as spheres, cages, rods, and bipyramids. Especially, Au and Ag nanorods exhibit a very good tunability of plasmon resonance wavelength and high optical sensitivity to the dielectric environment, which is associated with the anisotropy of nanorods. Herein, we report our successful attempt to utilize a very simple drop casting process to fabricate Ag NW films (with areas over 2 cm^2) on glass from a dispersion of silver nanowires that are ~190 nm in diameter and 7-8 μm in length diluted with ethanol. We have dispersed Ag NWs in ethanol where they show a very good dispersibility and are easier to redispersion. Figure 1 shows the SEM and TEM images of the AgNWs on glass.

Figure 2 shows the Stokes Raman spectra of pMA molecular monolayers deposited on top of Ag films collected with different acquisition times (3-10s). The three dominant Stokes modes (390, 1077, 1590 cm^{-1}), arising from bending and stretching modes in the benzene rings of the pMA molecule, can clearly be distinguished in all the spectra. SERS spectra were collected with a 785-nm laser resulting in power at the sampling point of ~1.7 mW. The high SERS signals are attributed to the electromagnetic coupling effect on AgNW arrays when the probe molecules are trapped in the vicinity of AgNWs.

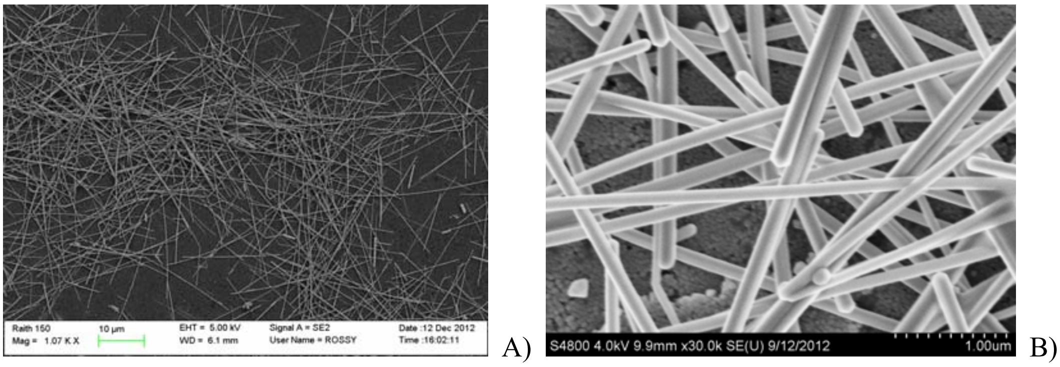

Figure 1. Scanning electron microscopy (A) and TEM (B) images of the Ag NW film deposited on a glass substrate: d=190nm and L=7-8µm.

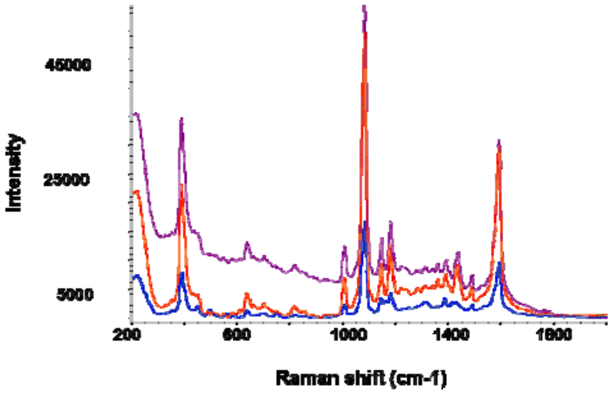

Figure 2. Experimental Stokes SERS spectra of pMA on the Ag NW film collected with near-infrared excitation (785 nm, 1.7 mW) and different acquisition times: 3s (blue curve), 5s (red curve), 10s (magenta curve).

The resulting nanowire film can serve as good surface enhanced Raman spectroscopy (SERS) substrates, exhibit large electromagnetic field enhancement factors for p-mercaptoaniline, and can readily be used in ultrasensitive, molecule-specific sensing utilizing vibrational signatures.

REFERENCES

1. Jarvis, R. M., Brooker, A. and Goodacre, R. “Surface-Enhanced Raman Spectroscopy for Bacterial Discrimination Utilizing a Scanning Electron Microscope with a Raman Spectroscopy Interface,” *Anal. Chem.* 76, 5198, 2004.
2. Chen, C.D., Cheng, S.F., Chau, L. K., Wang, C. R. C. “Sensing capability of the localized surface plasmon resonance of gold nanorods,” *Biosensors and Bioelectronics*, 22, 926–932, 2007
3. Liu, J.; Lu Y. “A colorimetric lead biosensor using DNAzyme-directed assembly of gold nanoparticles,” *J. AM. CHEM. SOC.*, 125, 6642-6643, 2003.
4. Huang, X.; El-Sayed, I. H.; Qian, W.; El-Sayed, M. A. “Cancer Cells Assemble and Align Gold Nanorods Conjugated to Antibodies to Produce Highly Enhanced, Sharp, and Polarized Surface Raman Spectra: A Potential Cancer Diagnostic Marker,” *Nano Lett.*, 7, 1591-1597, 2007.
5. Huang, X.; Neretina, S.; El-Sayed, M. A. “Gold nanorods: from synthesis and properties to biological and biomedical applications,” *Adv. Mater.*, 21, 4880-4910, 2009.

Plasmonics and nanophotonics

Study on PL enhancement of GaAs/InGaAs Quantum Well Emission by Gold Nanoparticle Arrays

Hongwei Gao[1], Jinghua Teng[2], SooJin Chua[1, 2], and Ning Xiang[1]

[1] Department of Electrical and Computer Engineering, National University of Singapore, Singapore 117576, Singapore
[2] Institute of Material Research and Engineering, Singapore 117602, Singapore

Abstract: Enhancement of photoluminescence (PL) intensity from InGaAs/GaAs quantum well (QW) is achieved experimentally by coupling surface plasmon (SP) resonance with QW emission. The SP resonance is generated by fabricating a periodic Au nanodisk arrays and a thin spacer layer of SiO_2 between Au nanodisk and GaAs surface. 4.16-fold QW PL enhancement is observed. Theoretical simulations confirm that the PL emission is enhanced by surface plasmon coupling.

The enhancement of electron-hole recombination rate in a semiconductor quantum well (QW) through the coupling between the dipoles in the QW and the surface plasmons generated by metallic structure has the potential to play important role in future optical devices [1-3]. Recently, there has been great progress in enhancing the efficiency of spontaneous emission (fluorescence) using SPR effect in the vicinity of a metal-dielectric boundary. The first important example of the improvement was achieved in GaN photoluminescence by depositing a thin layer of Ag film on top of the GaN [4]. Subsequently, 90-fold enhancement of the spontaneous recombination rate from a similar structure was reported [5]. Since then, SPR was employed in many different light emitting media [6-10] to enhance the spontaneous emission, for example, Si emitters [11]. The coupling of surface plasmon polariton (SPP) modes with the radiation mode has been obtained by one dimensional (1D) dielectric gratings [6,7,10], two-dimensional (2D) corrugated silver films [9,12], and more complicated cavity like structures [13]. This interaction could be accomplished in two ways to enhance the photoluminescence (PL) intensity. The first approach occurs during the optical excitation stage, which is to couple the incident light directly into tightly confined SPs modes generated by metallic nanostructure to increase the excitation energy density in the vicinity of the quantum well (QW) region [14-17]. The second approach takes place during the emission stage, which is to enhance energy-emission efficiency of the QW through Purcell effect [18]. Those effects have already been demonstrated in visible region through InGaN/GaN and AlGaAs/GaAs systems. However, no such effect has been reported and confirmed in near infrared (NIR) range, a very important spectrum region for communication and other applications.

InGaAs is a very important optoelectronic materials emitting in NIR spectrum range. So far there has been very few reports regarding the SP effects on InGaAs/GaAs QWs systems, maybe due to the fabrication challenge. If one wants to locate SPR wavelength into NIR range on GaAs, very small feature (sub-100 nm) metallic structure should be designed which causes a fabrication challenge. In this letter, we report our approach to overcome the fabrication challenge by simply introducing a thin SiO_2 layer between GaAs and Au nanodisk arrays. This thin SiO_2 layer leads to a relatively larger metallic structure for the SP resonant wavelength in NIR region due to the smaller refractive index of SiO_2 (n=1.46) as compared to that of GaAs (n=3.5), thus can reduce the fabrication difficulty. More than 2 fold enhancement of light emitting from the InGaAs/GaAs QWs by Au SPR has been observed. To our best knowledge, this is the first report on the SPR enhanced emission from InGaAs/GaAs QWs.

Acknowledgement: This work is supported by Singapore Ministry of Education (grant number MOE2009-T2-1-086).

References

1 S.Schwieger, P.Vasa and E.Runge, Theory of the surface plasmon polariton-exciton interaction in multi-layer systems, *Phys. stat. sol (b)* 245, No. 6, 1071–1075 (2008)
2 K.Tanka, E.Plum, J.Y.Ou, Multifold Enhancement of Quantum Dot Luminescence in Plasmonic Metamaterials, *PRL* 105, 227403 (2010)
3 Dominc Lepage and Jan J. Dubowki, Surface plasmon effects induced by uncollimated emission of semiconductor microstructures, *Proc. of SPIE* Vol. 7586 758607-1 (2010)
4 I. Contijo, M. Boroditsky, E. Yablonovich, S. Keller, U. K. Mishra, and S. P. DenBaars, Phys. Rev. B **60**, 11564 (1999).
5 A. Neogi, C. W. Lee, H. O. Everitt, T. Kuroda, A. Takemuchi, and E. Yablonovich, Phys. Rev. B **66**, 153305 (2002).
6 K. Okamoto, I. Niki, A. Shvartser, Y. Narukawa, T. Mukai, and A. Scherer, Nat. Mater. **3**, 601 (2004).
7 K. Okamoto, I. Niki, A. Scherer, Y. Narukawa, T. Mukai, and Y. Kawakami, Appl. Phys. Lett. **87**, 071102 (2005).
8 T. D. Neal, K. Okamoto, and A. Scherer, Opt. Express **13**, 5522 (2005).
9 J. Feng, T. Okamoto, and S. Kawata, Opt. Lett. **30**, 2302 (2005).
10 S. Wedge, J. A. E. Wasey, W. L. Barnes, and I. Sage, Appl. Phys. Lett. **85**, 182 (2004).
11 S. Pillai, K. R. Catchpole, T. Trupke, G. Zhang, J. Zhao, and M. A. Green, Appl. Phys. Lett. **88**, 161102 (2006).
12 P. T. Worthing and W. L. Barnes, Appl. Phys. Lett. **79**, 3035 (2001).
13 J. Vuckovic, M. Loncar, and A. Scherer, IEEE J. Quantum Electron. **36**, 1131 (2000).
14 N. E. Hecker, R. A. Hopfel, N. Sawaki, T. Maier, and G. Strasser, Appl. Phys. Lett. **75**, 1577 (1999).
15 H. R. Stuart and D. G. Hall, Appl. Phys. Lett. **69**, 2327 (1996).
16 T. W. Ebbesen, H. J. Lezec, H. F. Ghaemi, T. Thio, and P. A. Wolff, Nature _London_ **391**, 667 (1998).
17 J. A. Porto, F. J. Garcia-Vidal, and J. B. Pendry, Phys. Rev. Lett. **83**, 2845 (1999).
18 G. Sun,J. B. Khurgin,and R. A. Soref,APPLIED PHYSICS LETTERS **94**, 101103 (2009)

Imaging Plasmon Modes over Isolated Metal Nanoparticle: A Combined Approach using Electron Microscopy and FDTD simulation

Pabitra Das[1] **and Tapas Kumar Chini**[1*]
[1]Surface Physics Division, Saha Institute of Nuclear Physics, 1/AF Bidhannagar, Kolkata, India
[*]corresponding author: tapask.chini@saha.ac.in

Abstract- We study localized surface plasmon (LSP) modes on individual gold nanoparticles with various shape and size by Cathodoluminescence (CL) spectroscopy and imaging. We experimentally resolve distinct LSP modes in the far-field radiation acquired via CL. Detail analysis using FDTD simulation helps us to identify the origin of the plasmon modes.

The striking feature of a resonantly excited LSP is to undergo a radiative decay process and to show highly localized enhancement of near field and similar enhancement of the far-field intensity. Often the local EM field enhancement in the plasmonic structures is confined spatially on length scales of ∼10−50 nm that cannot always be accessed by the sub-diffraction limited optical imaging techniques. Alternatively, electron beam induced radiation emission (EIRE) or CL in a scanning electron microscope (SEM) has been shown to constitute an excellent probe of plasmons with a spatial resolution better than 20 nm [1]. The CL-SEM as a probe of plasmonics is based on the fact that energy is coupled from incident electron to the plasmonic modes of the nanostructure and subsequently to propagating light modes that constitute one of the prominent decay channels for the plasmons. While a light source excites the whole volume of a metal nanoparticle (MNP), a finely focused e-beam on the otherhand can act as a local probe to excite plasmons and consequently the monochromatic CL map gives the information about the EM local density of states (LDOS). This is related to the local electric field intensity at a particular wavelength at a fixed point. Consequently, EM-LDOS reflects the EM field enhancement in the metallic nanostructure. In the present paper, we show how CL-SEM can be utilized as a unique single particle spectroscopy tool with a high spatial resolution imaging capability of plasmonic modes of a metal nanoparticle.

Detail analysis of the experimental data on the surface plasmon assisted photon emission from MNPs requires solutions of Maxwell equations for the geometry of the MNP under consideration. However, analytical solutions exist only for simple geometries, like the sphere or the infinite cylinder. For the complex shaped Au nanoparticles such as truncated tetrahedron (TT) and decahedra considered in this study, we have performed 3D-FDTD numerical simulations. For numerical investigation of the e-beam excited photon emission in a CL setup, the e-beam can be modeled as a line current density source. In the simulation, this current density is modeled as a series of dipoles with temporal phase delay that is related to the electron velocity. To simulate the emission spectra, the radiative energy component of the induced electromagnetic field is calculated by integrating the Poynting vector normal to an arbitrary large surface in the upper z half-plane for wavelength ranging from 400 to 700 nm. Our method of obtaining the simulated radiation intensity maps mimics the equivalent raster scanning situation of the e-beam as done for CL mapping in the actual experiment. A more detailed description of the CL spectroscopy and imaging using FDTD can be found in our recent work [2].

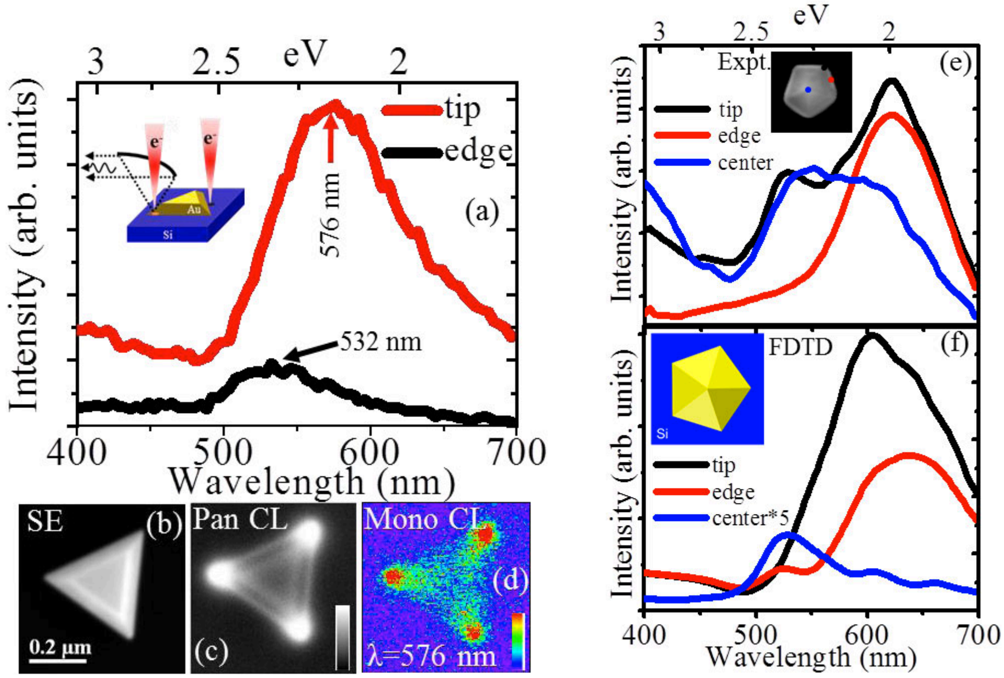

FIGURE 1: (a) CL spectroscopy on a single Au TT NP on Si, (b-d) SE, Pan, and mono CL images of the same particle, (e-f) experimental and FDTD simulated CL spectra of a decahedral Au nanoparticle. The e-beam energy is 30 keV, beam current ~15 nA and beam diameter ~5 nm.

Gold nanoparticles used in the present study were synthesized using a seed mediated chemical growth method [2,3]. We have done CL spectroscopy and imaging on two different asymmetric (TT and decahedra) geometries and demonstrate that the plasmon peak intensity and peak position strongly depends on the particle size and shape and also on the substrate on which they are sitting. More importantly, it also depends on the e-beam impact point on the MNP. We show that for the polyhedral particle considered in the present study, luminescence intensity enhances dramatically at the sharp tips/apexes, edges and corners. The experimental CL spectra and photon maps agree well results with those obtained from detailed FDTD numerical simulations. Further investigation using FDTD reveals that in the case of tetrahedral particle, the prominent emission peak at ~ 576 nm originates due to a higher order out of plane plasmon mode. However, for the decahedral particle, the major peak at ~ 620 nm is associated with the azimuthal dipole mode and the lower intensity peaks at ~ 540 nm is linked with the polar dipolar mode or quadrupolar mode of plasmon oscillation [3].

The approach and methodology presented here could be used to investigate a wide range of nanoparticle geometries and associated surface plasmon modes.

REFERENCES

1. García de Abajo, F. J. "Optical excitations in electron microscopy" *Rev. Mod. Phys.* **82**, 209-275 (2010).
2. Das, P., Chini, T. K. and Pond, J. "Probing Higher Order Surface Plasmon Modes on Individual Truncated Tetrahedral Gold Nanoparticle Using Cathodoluminescence Imaging and Spectroscopy Combined with FDTD Simulations" *J. Phys. Chem. C*, **116**, 15610 (2012).
3. Das, P. and Chini, T. K. "Spectroscopy and Imaging of Plasmonic Modes over a Single Decahedron Gold Nanoparticle: A Combined Experimental and Numerical Study" *J. Phys. Chem. C*, DOI 10.1021/jp3103782.

Light intensity modulation in magneto-plasmonic crystals by a novel longitudinal magneto-photonic effect

V.I. Belotelov[1,2], L.E. Kreilkamp[3], I.A. Akimov[3,4], A.N. Kalish[1,2], D.A. Bykov[5], S. Kasture[6], Y.V.Jayasurya[6], Achanta Venu Gopal[6], A.M. Grishin[7], S.I. Khartsev[7], L.L. Doskolovich[5], D.R. Yakovlev[3,4], A.K. Zvezdin[2], and M. Bayer[3]

[1] Lomonosov Moscow State University, 119991 Moscow, Russia

[2] Prokhorov General Physics Institute, Russian Academy of Sciences, 119991 Moscow, Russia

[3] Experimental Physics 2, TU Dortmund University, D-44221 Dortmund, Germany

[4] Ioffe Physical-Technical Institute, Russian Academy of Sciences, 194021 St. Petersburg, Russia

[5] Image Processing Systems Institute, Russian Academy of Sciences, 443001 Samara, Russia

[6] Tata Institute of Fundamental Research, 400005 Mumbai, India

[7] Royal Institute of Technology, SE-164 40 Stockholm-Kista, Sweden

[*]corresponding author: Belotelov@physics.msu.ru

Abstract- Here we postulate a novel magneto-optical phenomenon which originates solely from suitably designed nanostructured metal-dielectric material, so called magnetoplasmonic crystal. For the considered configuration the effect cannot occur in smooth samples. The effect shows up as a change of the optical transmission/reflection when the sample is magnetized in-plane. Though the effect is second order in magnetization, the experimentally achieved light intensity modulation is giant and reaches 24% at around frequencies of the waveguide modes excitation.

Magnetic field control of light is among the most intriguing methods for efficient modulation of light intensity and polarization on sub-nanosecond time scales. The implementation in nanostructured hybrid materials provides a remarkable increase of magneto-optical effects. However, so far only the enhancement of already known effects has been demonstrated in such materials. Here we demonstrate a novel magneto-optical phenomenon originating solely from properly designed nanostructured metal-dielectric material.

In particular, we fabricated and studied a hybrid metal-dielectric structure consisting of a one-dimensional gold grating on top of a magnetic waveguide layer (see insets in Fig.1c,d). It is shown that a magnetic field applied in the longitudinal configuration (perpendicularly to the slits in gold) to the metal-dielectric structure modifies the field distribution of its optical modes and thus changes the mode excitation conditions. In the optical far-field, it manifests in the alteration of the optical transmission or reflection coefficients when the structure becomes magnetized. Such magneto-optical effect is shown to represent a novel class of the effects related to the magnetic field mediated modification of the Bloch modes of the periodic hybrid structures. That is why we propose to call the effect the Longitudinal Magneto-Photonic Intensity Effect (LMPIE). The LMPIE is described by the relative difference between the transmission coefficients T_M and T_0 of the magnetized and the demagnetized structure: $\delta = (T_M - T_0)/T_0$.

Two principal modes of the magnetic layer − TM- and TE-modes – acquire in the longitudinal magnetic field additional field components and thus turn into quasi-TM and quasi-TE-modes, respectively. The key point in that respect is that due to the appearance of the TM-components in the quasi-TE-mode this mode can be excited by light of TM-polarization. This means that a combination of external magnetic field application and TM-polarized illumination allows one to switch on the quasi-TE-mode or to switch it off. The excited quasi-TE-mode takes some amount of the incident optical energy and carries it away where this energy is finally absorbed.

The largest LMPIE is observed at the excitation of the anti-symmetrical quasi-TE mode (at 842 nm and 825 nm, Fig.1 c,d) by TM-polarized illumination. In this case the measured value of LMPIE is as large as 24 % for the even effect.

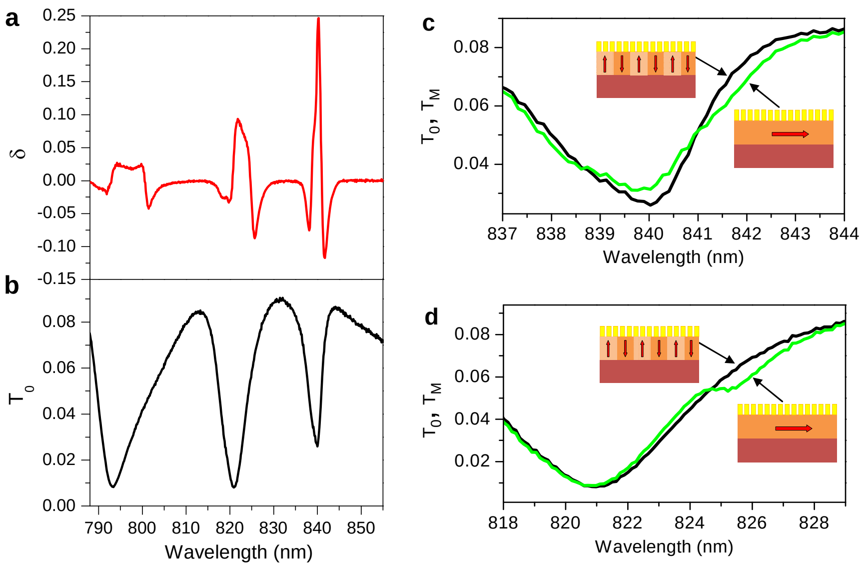

Figure 1. a, Spectrum of the LMPIE taking place when saturating magnetic field B = 320 mT is applied. b–d, Spectra of the optical transmission coefficient for the demagnetized (T_0, black curves) and fully magnetized (T_M, green curves) structures: overall spectrum of T_0 (b) and large-scale spectra of T_0 and T_M near the resonances at around 842 nm (c) and 825 nm (d). In (d) the difference in spectra of T_0 and T_M due to the magnetic field is increased by 2 times in order to be easily visualized. The light is TM-polarized and hits the sample under normal incidence. The MPC is based on the 1270 nm thick magnetic film of $Bi_{2.97}Er_{0.03}Fe_4Al_{0.5}Ga_{0.5}O_{12}$. The MPC has gold grating with period d=658 nm, height h_{gr}=65 nm and slit width r=150 nm.

The LMPIE can be further increased by properly choosing the magnetic film thickness and composition. For realistic parameters of a fully Bi-substituted iron garnet magnetic film the LMPIE exceeding 100% should be achievable. Thus, the nanostructured material described here can be considered as a novel ultrafast magneto-photonic light valve.

Acknowledgements. The work was supported by the Deutsche Forschungsgemeinschaft, the Russian Foundation for Basic Research (No. 12-02-33100, 12-02-31298, 11-02-00681), the Russian Federal Targeted Program "Scientific and Scientific-Pedagogical Personnel of the Innovative Russia", and the Russian Presidential Fellowship (No. SP-124.2012.5).

REFERENCE

1. Belotelov, V. I. et al. "Enhanced magneto-optical effects in magnetoplasmonic crystals", *Nature Nanotechn.*, Vol. 6, 370–376, 2011.
2. Belotelov, V. I., Doskolovich, L.L. & Zvezdin, A.K. "Extraordinary magneto-optical effects and transmission through metal-dielectric plasmonic systems", *Phys. Rev. Lett.*, Vol. 98, 77401(4), 2007.

Deep subwavelength double metal disk cavity and applications

Soon-Hong Kwon
Department of Physics, Chung-Ang University, South-Korea
*corresponding author: soonhong.kwon@gmail.com

Abstract-We propose a deep subwavelength plasmonic double metal disk cavity. By reducing radius and thickness carefully, the surface-plasmon-polariton cavity mode with a resonant wavelength of 1550 nm can be confined in a disk with a radius of 88 nm and a thickness of 10 nm, where the physical size is 0.000064 λ^3 (λ: free space wavelength). The cavity mode has a deep subwavelength mode volume of 0.010 $(\lambda/2n)^3$ with high Q of 1900.

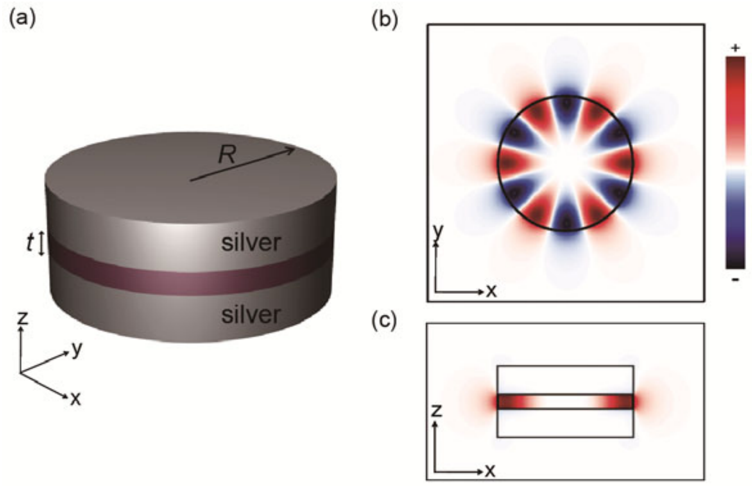

Figure 1. (a) Schematic diagram of the plasmonic disk cavity consisting of silver/dielectric/silver. (b) Horizontal and (c) cross-sectional views of the electric field (Ez) profiles of the plasmonic WGM mode with the azimuthal number, N = 6 for the cavity with R = 476 nm and t = 100 nm.

In this talk, we propose a plasmonic whispering-gallery-mode cavity comprising of a dielectric disk with sub-hundred nanometer thickness sandwiched by two silver disks as shown in Fig. 1(a) [1]. In a cavity with R = 476 nm and t = 100 nm, plasmonic whispering-gallery-mode (WGM) with an azimuthal number (N) of 6 can be excited at a resonant wavelength of 1550 nm (Fig. 1(b) and 1(c)). In order to further reduce cavity size while resonant wavelength is maintained, resonant wavelength, Q factor, and mode volume (V_m) are systematically investigated by varying the structure parameters, radius and thickness for the cavity mode with N = 6 in Fig. 2. At a fixed thickness of 100 nm, the resonant wavelength decreases linearly with decreasing radius in Fig. 2(a). On the other hand, at a fixed radius of 476 nm, the resonant wavelength increases significantly for a thinner thickness due to the stronger coupling of SPPs excited at the two silver/dielectric interfaces in Fig. 2(b) [2]. Dependencies of the resonant wavelength on R and t are plotted as 2D color map in Fig. 2(c) where black squares indicate (R, t) sets to have the resonant wavelength of 1550 nm. It is remarkable that the resonance wavelength is kept to be constant while the physical volume ($\pi R^2 t$) of the dielectric layer reduces considerably for the cavities with (R, t) ranging from (476 nm, 100 nm) to (214 nm, 10 nm). In Fig. 3(d), Q factors at 40 K and V_{mode} were calculated as a function of the physical volume for the cavities with (R, t) sets indicated by the black squares in Fig. 3(c). The Q factor decreases to 3 times the size from 5500 to 1900 as the physical volume decreases 50 times smaller from 1.6 $(\lambda/2n)^3$ to 0.044 $(\lambda/2n)^3$, because of the increasing metallic absorption in the thinner cavity. In addition, the plasmonic WGM with N = 2 could be confined in the deep subwavelength cavity with (R, t) = (88 nm, 10 nm), having Q of 1900 and V_m of 0.010 $(\lambda/2n)^3$. These extremely small plasmonic cavities, which suppress radiation loss strongly, would be widely applicable for the biochemical sensing and ultra-compact photonic integrated circuits.

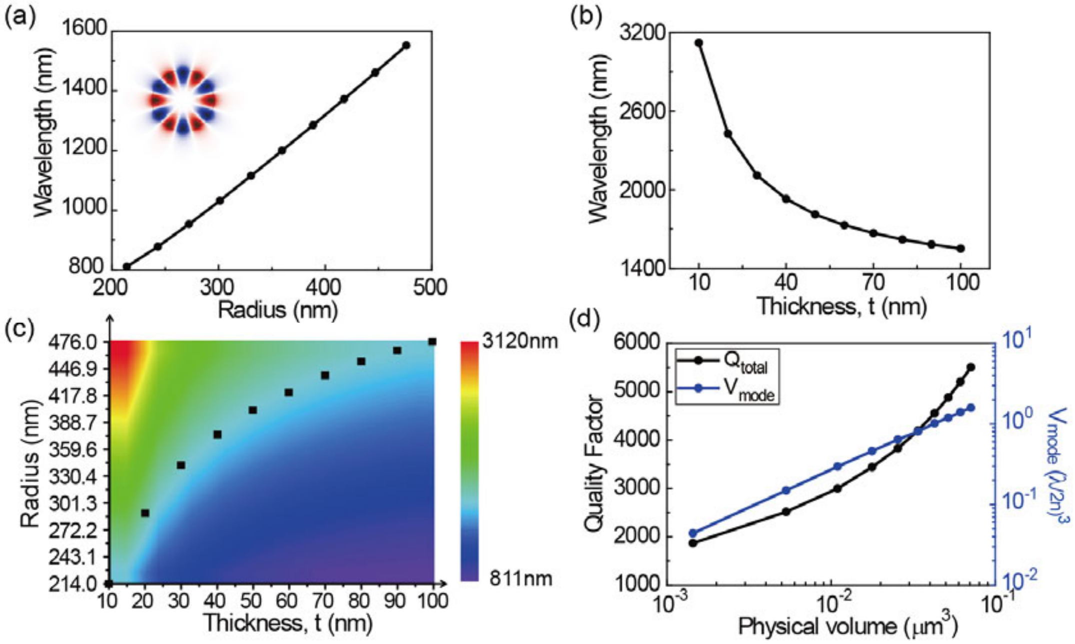

Figure 2. Optical properties of the plasmonic WGM with the azimuthal number, N = 6. (a) Resonant wavelength vs. radius. (b) Resonant wavelength vs. gap thickness. (c) Resonant wavelength color map as a function of R and t. Black squares indicate (R, t) sets having the wavelength of 1550 nm. (d) Q factors at 40 K (black) and V_{mode} (blue) as a function of the physical volume ($\pi R^2 t$) of the dielectric disk. (R, t) varies from (476 nm, 100 nm) to (214 nm, 10 nm), corresponding to black squares in (c).

Acknowledgements, This research was supported by the Basic Science Research Program through the National Research Foundation of Korea (NRF) funded by the Ministry of Education, Science and Technology (Grant No. 2012-0003438).

REFERENCES

1. Kwon, S.-H. "Deep subwavelength plasmonic whispering-gallery-mode cavity," *Opt. Express*, Vol. 20, No. 22, 24918–24924, 2012.
2. Miyazaki, H. T. and Y. Kurokawa, "Squeezing visible light waves into a 3-nm-thick and 55-nm-long plasmon cavity," *Phys. Rev. Lett.* Vol. 96, No. 9, 097401, 2006.

Coupled nano-plasmons

M. Apostol[1,2,*], **L. Cune**[1], **S. Ilie**[2,3], **A. Petrut**[3], **M. Savu**[b], **and S. Toba**[3]

[1]Department of Theoretical Physics, Institute of Atomic Physics, Magurele-Bucharest MG-6, POBox MG-35, Romania
[2]MiraTechnologies Ltd, Teiul Doamnei 2, Bucharest
[3]MiraTelecom, Grigorescu 13, 075100 Otopeni-Bucharest
*corresponding author: apoma@theory.nipne.ro

Abstract— A simple model of coupled plasmons arising in two neighbouring nano-particles is presented. It is shown that the plasmons may be periodically trasferred between the two particles. For larger separation distances between the two particles the retardation is included. The van der Waals-London-Casimir force is estimated for the two particles; it is shown that for large distances the force is repulsive.

The motion of the mobile charges in polarizable matter can be described by a displacement field $\mathbf{u}(t, \mathbf{r})$, which is a function of the time t and position $\mathbf{r}$. In the classical limit of small and slow variations (corresponding to classical electromagnetism), this displacement field generates a polarization charge density $\rho = -nqdiv\mathbf{u}$ and a corresponding current density $\mathbf{j} = nq\dot{\mathbf{u}}$. These charge and current densities generate in matter an electric field $\mathbf{E}$ and a magnetic field $\mathbf{H}$; but we still have two independent equations and three unknowns: $\mathbf{E}$, $\mathbf{H}$ and $\mathbf{u}$. However, the displacement field obeys an equation of motion, which, in this classical limit, is the Newton equation of motion

$$m\ddot{\mathbf{u}} = q(\mathbf{E} + \mathbf{E}_0) - m\omega_c^2\mathbf{u} - m\gamma\dot{\mathbf{u}} \ ; \tag{1}$$

$\mathbf{E}$ is the internal (polarization) electric field, $\mathbf{E}_0$ is an external electric field, ω_c is a characteristic frequency and γ is a damping coefficient (much smaller than any relevant frequency). The magnetic part of the Lorentz force is absent in equation (1) because the velocities of the charges in matter are much smaller than the speed of light; the internal magnetic field is also absent, in accordance with our assumption of small $\mathbf{u}$ and non-magnetic matter. Equation (1) is the missing equation (the third equation), which helps solving the Maxwell equations.[1]-[3]

Obviously, $\mathbf{P} = nq\mathbf{u}$ is the polarization (density of dipole moments); equation (1) leads immediately to the well-known Drude-Lorentz (plasma) model.

The longitudinal internal (polarization) electric field in Gauss equation $div\mathbf{E} = -4\pi nqdiv\mathbf{u}$ is given by $\mathbf{E} = -4\pi nq\mathbf{u}$ (*i.e.*, $\mathbf{E} = -4\pi\mathbf{P}$). In the long-wavelength limit, the finite size of the body is usually taken into account by a (de-) polarizing factor f, such as the field is given by $\mathbf{E} = -4\pi nqf\mathbf{u}$; for instance, for a sphere $f = 1/3$. Introducing this polarization field in equation (1), taking the Fourier transform and leaving aside the coefficient γ, we get

$$(\omega^2 - \omega_c^2 - f\omega_p^2)\mathbf{u} = -\frac{q}{m}\mathbf{E}_0 \ ; \tag{2}$$

we can see that we have a plasmon resonance at frequency $\sqrt{\omega_c^2 + f\omega_p^2}$; for a conducting sphere with $\omega_c = 0$ and $f = 1/3$, we get the plasmon frequency $\omega_p/\sqrt{3}$.[4]

We consider two point particles, denoted by 1 and 2, each with its own plasmon frequency $\omega_{1,2}$, separated by the position vector $\mathbf{d}$. We describe the motion of the mobile charges in each particle by a displacement vector $\mathbf{u}_{1,2}$; equation (2) becomes

$$(\omega^2 - \omega_{1,2}^2)\mathbf{u}_{1,2} = -\frac{q}{m}\mathbf{E}_{02,1} \ \ , \tag{3}$$

where $\mathbf{E}_{01,2}$ is the electric field generated by particle 1 (2) at the position of the particle 2 (1). In the long wavelength limit this is the field generated by a point dipole

$$\mathbf{E}_{01,2} = v_{1,2}n_{1,2}q\frac{3(\mathbf{u}_{1,2}\mathbf{d})\mathbf{d} - \mathbf{u}_{1,2}d^2}{d^5} \ \ , \tag{4}$$

where $v_{1,2}$ are the volumes of the two particles and $n_{1,2}$ are the concentration of the mobile charges in the particles; equation (4) is valid in the near-field region $c/\omega \gg d$, where c is the speed of light. Since the particles are considered point-like, we have also $v_{1,2}^{1/3} \ll d$. Introducing this field in equations (3) and taking the projections on $\mathbf{d}$ (longitudinal, l) and perpendicular to $\mathbf{d}$ (transverse, t) we get, for the longitudinal ones,

$$(\omega^2 - \omega_{1,2}^2)u_{l1,2} = -\frac{\omega_{p2,1}^2 v_{2,1}}{2\pi d^3} u_{l2,1} \ . \tag{5}$$

The solution of these coupled-oscillators equations is straightforward.

An interesting situation occurs for two identical conducting particles $\omega_{c1} = \omega_{c2} = 0$, $\omega_{p1} = \omega_{p2} = \omega_p$ and $v_1 = v_2 = v$. In this case the eigenfrequencies are given by

$$\Omega_{1,2} = \omega_p \left(1 \pm \frac{v}{2\pi d^3}\right)^{1/2} \simeq \omega_p \left(1 \pm \frac{v}{4\pi d^3}\right) \ . \tag{6}$$

The displacement vectors for the initial condition $u_{l2}(t=0) = 0$ is given by

$$\begin{aligned} u_{l1}(t) &= 2Ae^{i\omega_p t} \cos \tfrac{v}{4\pi d^3} t \ , \\ u_{l2}(t) &= -2iAe^{i\omega_p t} \sin \tfrac{v}{4\pi d^3} t \ ; \end{aligned} \tag{7}$$

we can see that the two coupled oscillations exhibit "beats", and the plasmons can be transferred periodically between the two particles, as expected. A similar situation holds for the transverse oscillations, with the factor 2π replaced by 4π in the above formulae.

The retardation can be included for two point dipoles. We limit ourselvs heer to give the result for the force acting between the two particles, due to the zero-point fluctuations:

$$F = \frac{\hbar\omega_p v^2}{32\pi^2} \left(\frac{3\omega_p^4}{c^4 d^3} + \frac{10\omega_p^2}{c^2 d^5} - \frac{9}{d^7} \right) \ . \tag{8}$$

We can see that in the non-retarded limit ($\omega_p d/c \ll 1$) the force is attractive and goes like $-1/d^7$; this is the van der Waals-London force; it comes from the longitudinal degrees of freedom. In the opposite, retarded limit $\omega_p d/c \gg 1$ the force is repulsive and goes like $1/d^3$; this is the limit of the Casimir force, coming entirely from the transverse oscillations.[5] The force changes sign around $\omega_p d/c \preceq 1$ and has a maximum for $\omega_d d/c \succeq 1$.

ACKNOWLEDGMENT

The authors are indebted to the members of the Seminar of the Institute of Atomic Physics and the Laboratory of Theoretical Physics, Magurele, Bucharest, for useful discussions and a careful reading of the manuscript. This work was supported by the Romanian Government Research Agency Grant #306/SMIS 26614.

REFERENCES

1. M. Apostol and G. Vaman, "Electromagnetic field interacting with a semi-infinite plasma," J. Opt. Soc. Am. A, Vol. 26, 1747-1753, 2009.
2. M. Apostol and G. Vaman, "Reflection and refraction of the electromagnetic field in a semi-infinite plasma," Opt. Commun., Vol. 282, 4329-4332, 2009.
3. M. Apsotol and G. Vaman, "Plasmons and diffraction of an electromagentic palne wave by a metalli sphere," Progr. Electrom., Res. (PIER), Vol. 98, 97-118, 2009.
4. M. Apostol, S. Ilie, A. Petrut, M. Savu and Stefan Toba, "A generalization of the dipolar force," J. Appl. Phys. Vol. 12, 024905, 2012.
5. M. Apostol, "On the molecular forces acting between macroscopic bodies," Physica B, Vol. 40, 57-62, 2013.

Optical property of double-layered metal films with periodic structure

M. Boutria* and R. Oussaid*
Houari Boumediene University of Sciences and Technology, Instrumentation Laboratory
Box n°32 El Alia Bab Ezzouar 16111 Algiers, Algeria
*corresponding author: roussaid@usthb.dz

Abstract- This paper reports optical property of double-layered metal films with periodic structure, which works as a half-wave plate by itself. The advantage of this structure is that it can tune the rotation angle of optical activity, with high transmittance, by changing the relative angle of two films. We analyze the optical property of the structure using numerical calculation with conventional transfer matrix method and FDTD method. We propose the design of an anisotropic and chiral structure (3-D). The chirality is controlled by simply changing the angle between the two plates. The optical rotation is accompanied by a transmission up to 80%. The proposed structure opens the way to the design of a new kind of chiral plates in the terahertz or microwave domains.

The optical activity characterizes the rotation of the polarization plane of linearly polarized waves. The main objective in the development of artificial chiral periodic structures is to produce simultaneously a large optical activity and a high transmittance. Many researches were done in this field [1, 2]. In these studies, a large optical rotation is sometimes achieved, but often with relatively low transmission. In this paper, we present a design of a chiral structure based on a 3-D metamaterial composed of two identical nanostructured metallic films each one playing the role of a half-wave plate and working at normal incidence. Chirality is obtained through a provoked optical rotation induced by breaking the symmetry of one plate to get artificial intrinsic chiral material with an enhanced transmission up to 80%. In the proposed Structure**, t**he second plate is rotated by an angle (α) with regard to the first one (see fig. 1). We assume that the two plates are spaced by a distance *d*. For a seek of simplicity, we assume that the two plates are free-suspended in vacuum and that the cavities are also devoid of dielectric. Each layer consists of a perfectly conducting metallic film similar to the one studied in ref [3]. With the geometrical parameters of that reference, the metallic layer behaves as a half-wave plate for a wavelength around $\lambda=1.223p$. The optical activity is demonstrated through a semi-analytical approach combining *FDTD* and multi-reflection algorithms. An exalted transmission (up to *80%)* at the operating wavelength is obtained accompanied by a tunable rotation corresponding to twice the angle between the two plates. The results obtained are shown in figures 1 to 4.

REFERENCES

1. F. I. Fedorov. ”on the theory of optical activity in crystals”. *Opt. Spectrosc.* 6: 49, 1958.
2. Thomas Paul Christoph Menzel, Carsten Rockstuhl and Falk Lederer. ”retrieving effective parameters for quasiplanar chiral metamaterials”. *Applied Physics Letters*, 93:233106, 2008.
3. F. I. Baida, M. Boutria, R. Oussaid, and D. Van Labeke. “Enhanced-transmission metamaterial as anisotropic plates”. *Phys. Rev. B*, 84:035107, 2011.
4. M. Boutria, R. Oussaid, D. Van Labeke and F. I. Baida, “Tunable artificial chirality with extraordinary transmission metamaterials”. *Phys. Rev. B, 86*, 155428, 2012**.**

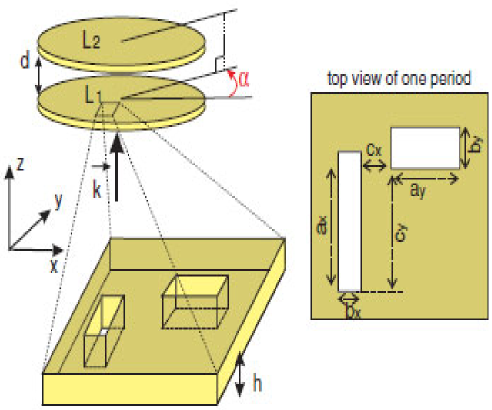

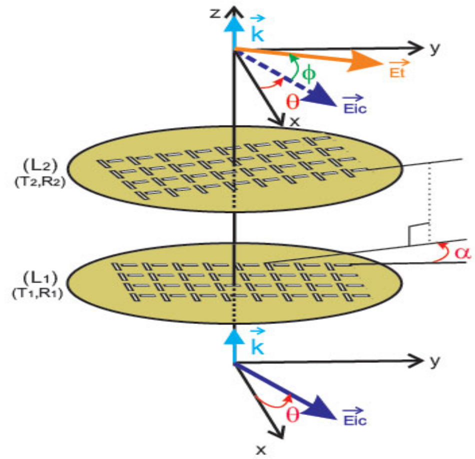

Figure1**:** Schematic of the proposed structure composed of two half-wave plates (L_1,L_2) rotating by an α one with regard to the other. A zoom-in over one unit cell of L_1 is presented to show one array pattern composed of two rectangular apertures. The top view made over one period shows the geometrical parameters of the slits.

Figure2: Cascaded structure consisting of two plates (L_1 and L_2), the second is rotated by (α) with respect to the first one. The polarization plane rotation is named ϕ.

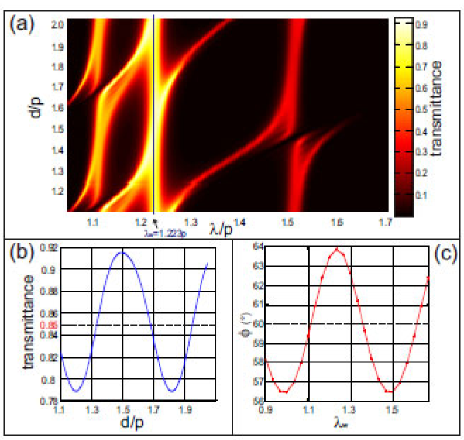

Figure3: (a) Semi-analytical calculated transmission spectra versus the distance d separating the two plates. The incident beam is polarized at theta=45° from Ox and the angle between the two plates is set to α=30°. (b) Transmission variations at the operating wavelength of $\lambda=1.223p$ as a function of d. (c) Rotation angle ϕ function of the operating wavelength.

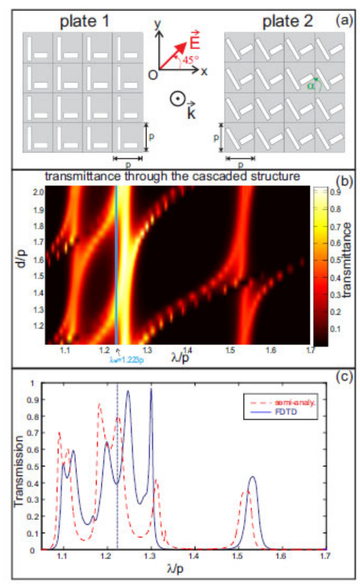

Figure 4: (a)Schema of $4x4$ periods of the plate with non-rotated (left) and rotated (right) rectangular apertures.

(b) Transmission spectra of the two plates calculated by FDTD with the same parameters as in fig.3b .

(c) Comparison between the spectra obtained by the two methods for $d=1.8p$.

Surface plasmon and bound plasmon-waveguide resonances with As_2S_3 light sensitive films in four layers configuration

A.A. Popescu, D. Savastru[c)], S. Miclos, Simona Dontu
National Institute of R&D for Optoelectronics INOE 2000, 077125, Magurele, Romania
[c)] corresponding author: dsavas@inoe.ro

Abstract. The surface plasmon resonance calculations were made in Kretschmann configuration that contains four layer. The third layer consists of a thin As_2S_3 vitreous film. The sensitivity to the refractive index was calculated. The pick sharpness analyses of plasmonic resonance and bounded plasmon-planar waveguide resonance give the road to improve the sensibility to the refractive index changes in four layer plasmonic structure.

In the chalcogenide glasses (ChG) changes of the optical constants arise under the action of light with the photon energy exceeding the band gap. Stationary and dynamic photoinduced absorption may be distinguished [1]. The modifications of the optical absorption correlate with the modifications of the refractive index by Kramers–Kronig relation. However, the change of the refractive index in chalcogenide films is small and a sensitive experimental method has to be used. As was demonstrated early the surface plasmon resonance (SPR) is very sensitive to small, up to 10^{-4}-10^{-5} changes of the refractive index.

Among the several SPR sensing structures, the most prominent is the Kretschmann configuration in which a thin metallic layer is deposited directly on the base of the prism. In a recent investigation the authors [2] proposed and have experimentally demonstrated the light modulation by use of thin As_2S_3 chalcogenide light sensitive vitreous film in four layer SPR configuration. The authors called this interaction “active plasmonic”.

As the chalcogenide materials have a high value of the refractive index (2,45-2,50 for As_2S_3, GaLaS), this film can form a planar waveguide also. We have studied the resonances of the bounded plasmon-waveguide modes and the sensibility to the film’s refractive index change in a 4-layer plasmonic structure. The obtained results can motivate the application of chalcogenide glasses as high sensitive media for plasmonic optical modulators or optical storage devices.

Software for numerical SPR calculations of four layer structure was developed by use transfer matrix formalism. Calculations of the reflectivity Rp and Rs for p-polarization and respectively s-polarization were performed for a four-layer system made up of a GaP prism, a 50 nm silver layer, a ChG layer with variable thickness and air. Two different thicknesses for the ChG As_2S_3 layer were considered: d_{ChG} = 50 nm and d_{ChG} = 250 nm. Gallium phosphate is an optically isotropic material, has the refractive index n_{pr}=3,317 and is transparent for the wavelength of 633 nm. We used such prism earlier for the characterization of planar chalcogenide waveguides [3]. An average refractive index value for this class of ChG films was taken to be 2,47. The refractive index data n=0.057+ 4.27i for silver layer are that one presented in E.D.Palik’s Handbook.

The relation between the reflectivity spectra and the incidence angle θ was simulated for the 632.8 nm wavelength (the irradiation of HeNe laser). Reflectivity was computed for a large range of incidence angles with a very small step (0,005°) in order to sense the narrowest peaks. The results are presented in below.

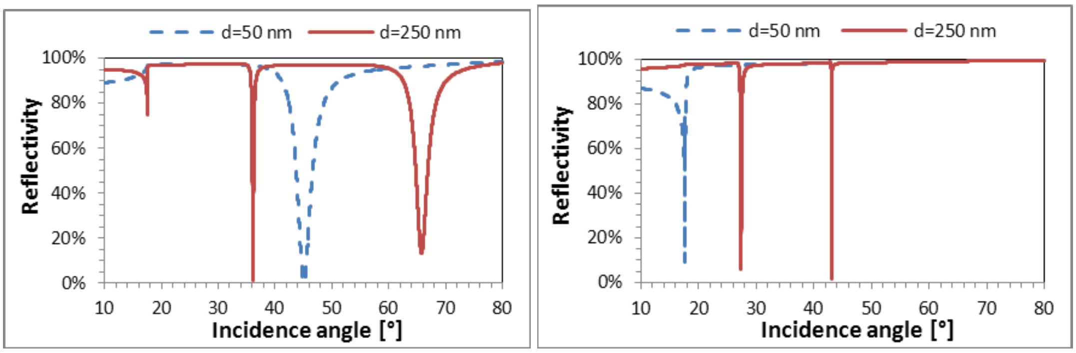

Fig. 1. Calculated resonance angles with As_2S_3 for p-polarization (left) and s-polarization (right).

Only one pick (blue line, left) exists for small thickness that coresponds to true plasmonic interaction. While for thicknesses of 250 nm, besides plasmonic pick at the approx. 65^0 resonance angle, a pick at 36^0 exists. It corresponds to to bound plasmon-planar waveguide mode. Waveguide mode resonances for s-polarisation also exist. For low thicknesses the resonance angle lowers up to 20-30°. This means that more convenient silica or borosilicate glass may be used as prism material. The mode coupled resonances are sharper than plasmon-polariton modes. Such peculiarity can indicate to greater sensitivity. However, in order to make a decision the picks shift $\Delta\Theta/\Delta n_f$ due to changes of the film refractive index have to be calculated. The results are presented below.

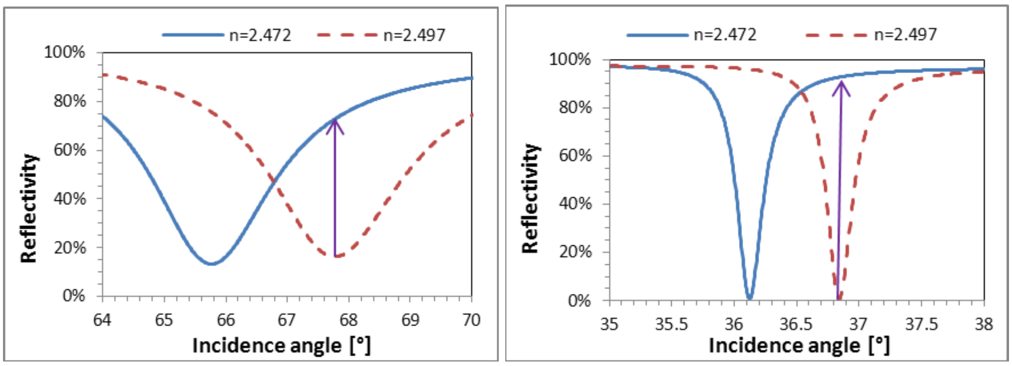

Fig.2. The resonance sensibility to the modification of the film's refractive index.

The reflectivity values corespond to two values of ChG film refractive indices which have a difference of 1%. Simulations are done for p-polarisation plasmonic mode (left) and for coupled waveguide mode (right). It can be seen that for the bounded plasmon-waveguide modes the same variation of the film refractive index is better distinguished. The SPR experiments that use As_2S_3 thermally evaporated films are in progress.

Acknowledgements. This work was supported by a grant of the Romanian National Authority for Scientific Research, CNDI – UEFISCDI, project number PN-II-PT-PCCA-2011- 25 / 2012.

References

[1] J. Orenstein, M. Kastner, "Photocurrent Transient Spectroscopy: Measurement of the Density of Localased States in a-As_2S_3", Phys. Rev. Lett. **46,** 1421-1424, 1981.

[2] Zsolt L. Sámson, Shih-Chiang Yen, Kevin F. MacDonald, Kenton Knight, Shufeng Li, Daniel W. Hewak, Din-Ping Tsai, Nikolay I. Zheludev, "Chalcogenide glasses in active plasmonics", Phys. Status Solidi RRL, **4**(10), 274-276, 2010.

[3] A.A. Popescu, D. Savastru, S. Miclos, "Design and realization of low losses chalcogenide As_xS_{1-x} planar waveguides", J. Optoelectron. Adv. Mater. 13(3), 213-217, 2011.

Surface-enhanced infrared spectroscopy of CBP-molecules based on nano-sized gaps

C. Huck[1*], F. Neubrech[1,2], A.Toma[3], D. Gerbert[1], T. Härtling[4], E. di Fabrizio[3], and A. Pucci[1]
[1]Kirchhoff-Institute for Physics, Heidelberg, Germany
[2]4th Physics Institute and Research Center SCoPE, Stuttgart, Germany
[3]Istituto Italiano di Tecnologia (IIT), Genova, Italy
[4]Fraunhofer Institute for Non-Destructive Testing, Dresden, Germany
[*]corresponding author: christian.huck@kip.uni-heidelberg.de

Abstract-We report on an increased infrared vibrational signal enhancement in nanoantenna-assisted surface-enhanced infrared spectroscopy (SEIRS) induced by inter-particle near-field coupling. Individual nanoantenna dimers with gaps sizes down to 4 nm were prepared by electron beam lithography and subsequent photochemical metal deposition. Afterwards the dimers were covered with a thin layer of CBP acting as a near-field probe. Our experiments show an increasing vibrational signal enhancement for decreasing gap sizes demonstrating the additional enhancement induced by nanometer-sized gaps.

1. Introduction

Infrared (IR) spectroscopy is well suited for label-free and direct characterization of molecular species. One disadvantage of the IR-spectroscopy is the small absorption cross-section of molecular vibrations in the IR which hampers the detection of minute amounts of molecules. One possibility to overcome this limitation is the use of surface-enhanced IR absorption spectroscopy (SEIRS) [1], where metal nanoparticles are employed to enhance the electromagnetic field in their vicinity. If the resonance frequency of such nanoantennas matches IR vibrations of molecules, the IR vibrational signal can be enhanced up to 5 orders of magnitude [2]. Additional enhancement is theoretically predicted and can be achieved by exploiting the extraordinary field enhancement of two antennas interacting across a very small gap (nm range).

2. Sample preparation

Individual nanoantenna dimers with dimensions of L=1460 nm, w=h=60 nm and a gap-size of 20 nm were fabricated by means of standard electron beam lithography (see Figure 1a). To diminish the gap-size further photochemical metal deposition was carried out on the lithographically prepared dimers. Covering the nanorods on the substrate with a solution of $HAuCl_4$ and illuminating them by a focused 532 nm laser beam leads to the reduction of the gold salt and to a gradual growth of the nanorods [3,4]. Applying this approach final gap sizes down to 4 nm were successfully prepared as checked by SEM (see Figure 1b) and IR spectroscopy in combination with FDTD simulations.
The dimers thus prepared were covered with a 5 nm layer of CBP which was evaporated in a UHV-chamber.

3. Nanoantenna-assisted SEIRS

Typical relative transmittance spectra of an individual dimer and an antenna-array measured by means of microscopic IR spectroscopy are shown in Figure 1c. The enhanced IR vibrational signals of various CBP-vibrations are clearly visible for both cases. The additional enhancement of the dimers with small gaps is clearly visible.

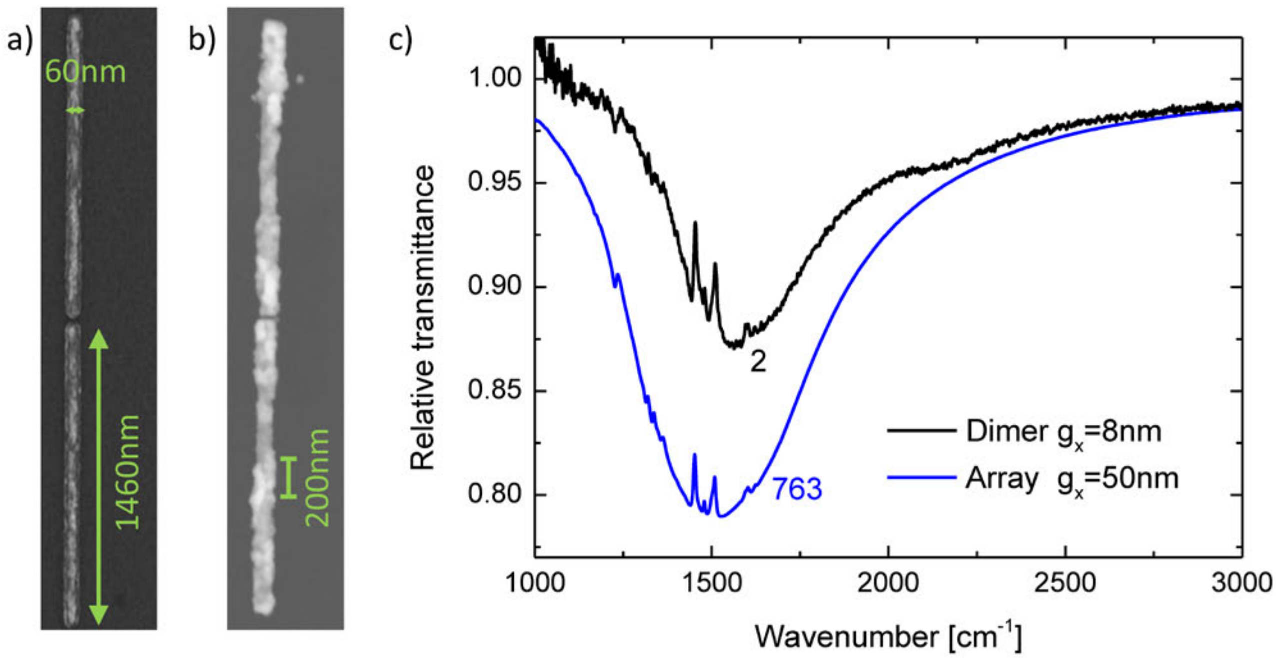

Figure 1 SEM-image of a) untreated lithographically prepared dimer b) photo-chemically grown dimer c) Typical IR relative transimttance of nanoantennas in dimer configuration (black) and arragned in arrays (blue) featuring enhanced vibrational signals of a 5nm thick CBP layer. The numbers indicate the quantities of rods contributing to the signals.

Acknowledgements: We acknowledge SOLEIL for provision of synchrotron radiation facilities and we would like to thank P. Dumas and F. Jamme for assistance in using the beamline SMIS. CH, FN, AT, AP, EF acknowledge financial support by the NANOANTENNA project (Health-F5-2009-241818). CH acknowledges financial support by the HGS-HIRe and HGSFP.

REFERENCES

1. Wang, H. et al., Plasmonic Nanoshell Arrays Combine Surface-Enhanced Vibrational Spectroscopies on a Single Substrate, *Angew. Chem.*, Vol.46, No. 47, 9040-9044, 2007.
2. Neubrech, F. et al., Resonant Plasmonic and Vibrational Coupling in a Tailored Nanoantenna for Infrared Detection, *Phys. Rev. Lett.*, Vol. 101, No. 15, 157403, 2008.
3. Härtling, T. et al., Controlled photochemical particle growth in two-dimensional ordered metal nanoparticle arrays, *Nanotechnology*, Vol. 21, No. 14, 145309, 2010.
4. Neubrech, F. et al., Infrared Optical Properties of Nanoantenna Dimers with Photochemically Narrowed Gaps in the 5 nm Regime, *ACS Nano*, Vol. 6, No. 8, 7326-7332, 2012.

Strong Emission From Nano-Iron
Using Laser Induced Breakdown Spectroscopy Technique

A.M.ELSherbini[1], F.F.Rashid[2*],A.Al-Muhamady[1]

[1]: Lab. of Lasers and New Materials, Faculty of Science, Cairo University, Dep. of Phys., Giza, Egypt
[2*]: Department of Laser and Opto-Electronic Engineering, University of Technology, Baghdad, IRAQ
Corresponding author : fareedfrasheed@yahoo.com

Abstract

In this paper we report a strong emission from laser produced plasma from iron oxide nanomaterials compared with bulk samples. The analysis showed that such enhancement increased exponentially with the plasma evolution time, while, it declines as the laser fluence increased. The enhancement strength differs with different Nd:YAG laser harmonics wavelengths. Experimental data analysis clearly showed that the observed enhancement is mainly associated with the change in the plasma electron density. We claim that this strong enhanced optical emission from laser produced plasma is due to surface plasmon resonant excitation preferably on nano oxide materials. Such results could improve the LIBS-sensitivity to detect materials at very low concentrations.

LIBS technique can be used for many analytical applications [1,2]. The light emitted from plasma produced by the interaction of pulsed lasers with matter is used for such analysis. The spectral shape and radiance can provide both of plasma electron density and temperature, respectively.

In the present work we will demonstrate the application of the LIBS technique to get enhancement in nano Iron oxide (Fe_3O_4) emission compared to the bulk samples. The experimental set-up is explained in details elsewhere[3].The Fe_3O_4 (MKN-Fe3O4-025) nano material powder with particle size of 25 nm was used. A comprehensive preview to the observed enhanced spectral lines emission from laser produced iron plasma at 532nm laser wavelength, under constant fluence (34 J/cm^2), gate and delay time (5 μs), is shown in figure (2), (Red color represents bulk sample while green for nano sample).

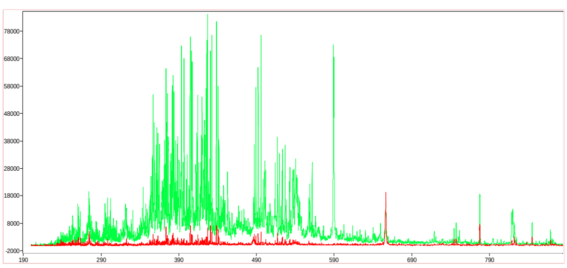

Figure (2)

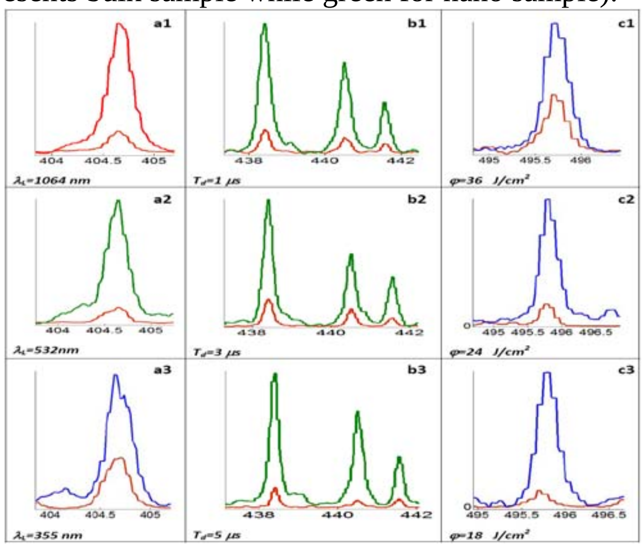

Figure (3)

The spectrum details can be seen in figure 3(*a1, a2*,*a3*), were a general comparison between emitted signal intensity from Fe I lines from both of nano and bulk targets shows the effect different laser harmonics, (b1, 2, 3) shows the behavior with delay time in the range from 1 to 5 μs. The effect of

Surface enhancement raman scattering under external electric field by composited nanogrid and nanopartical

Y. J. Wang[1], W. J. Sun, X. X. Xia[1], Z. Liu[1], J. J. Li[1], H. F. Yang[1], and C. Z. Gu[1*]

[1]Beijing National Laboratory for Condensed Matter Physics, Institute of Physics, Chinese Academy of Sciences, Beijing 100190, China

[*]corresponding author: czgu@aphy.iphy.ac.cn

Abstract- An oscillating and gate voltage were separately applied during the SERS measurement by introducing interdigitated electrodes and back-gate. The response of the Raman peak intensity to the applied field shows evident dependence on the intensity and frequency of external electric field, which reveals a new direction for fabricating the controllable SERS.

Surface Enhanced Raman Scattering(SERS) has been discovered for several decades [1], and the development of micro/nano-fabrication technologies have made SERS more and more widespread in the field of chemical and biological analysis. Generally, the SERS process is observed for molecules adsorbed on the surfaces of noble metal substrate with nanoscale structure or simply irregular nanoparticles, which can trap the light as surface plasmons and form the so-called 'hot spots' [2]. The interaction between the local enhanced electromagnetic field near the 'hot spots' and the molecular will result in the enhancement of characteristic Raman signal. S. Sriram et al has announced that the external oscillating electric field can have influence on the SERS peak intensity [3], which supplies a new method to control the SERS process. The electrode pairs are used to apply external field in most of SERS devices, however, they can't ensure the uniformity of external field to the majority of metal nanoislands.

In this paper, we introduce a method modulating the SERS process under external electric field by using both the interdigitated electrode and back gate, the schematic is shown in Fig. 1. Al_2O_3 or SiO_2 layer was deposited by atomic layer deposition (ALD) or plasma enhanced chemical vapor deposition (PECVD) on the low-resistance silicon substrate, which was used as back gate. With a series of fabrication process consisting of ultraviolet lithography and thermal evaporation, the gold interdigitated electrodes with the spaces of 2μm and 5μm were fabricated on the substrate. After that, discrete silver nanoislands were deposited by electron beam evaporation. The diameter of the silver islands can be controlled by changing deposition time and rate. By applying the oscillating electric field and the gate voltage during SERS measurement, distinct impact can be observed from the response of the specific Raman shift intensity. The multi-parameter control under the external field for this kind of SERS device makes it possible to have more high sensitivity.

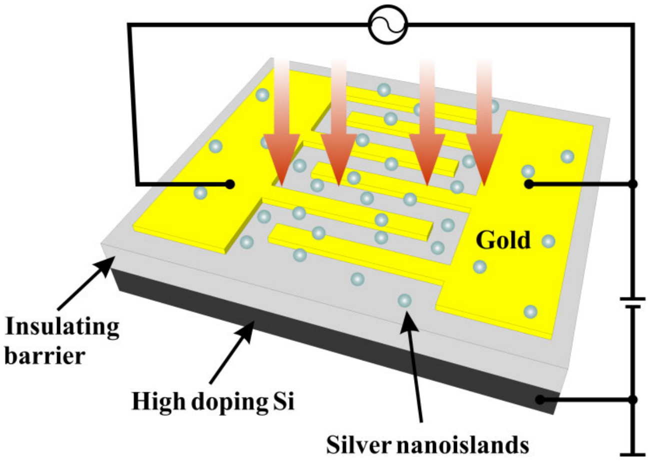

Figure 1.Schematic of the composited grid-particle structure with gate electrode used in SERS measurement.

Acknowledgements, This work was supported by National Natural Science Foundation of China (Grants No. 50825206, 1083401, 60871045，61001045, 50825206 and 91023041) and the National Basic Research Program of China (Grant No.2009CB930502) and the Knowledge Innovation Project of CAS (Grant No. KJCX2-EW-W02).

REFERENCES

1. Fleischmann, M., P.J. Hendra, and A.J. McQuillan, "Raman spectra of pyridine adsorbed at a silver electrode," *Chem. Phys. Lett.*., Vol. 26, No. 2, 163-166, 1974
2. Jeanmaire, D.L. and R.P. Van Duyne, "Surface raman spectroelectrochemistry: Part I. Heterocyclic, aromatic, and aliphatic amines adsorbed on the anodized silver electrode," *J.Electroanal. Chem*., Vol. 84, No. 1, 1-20, 1977
3. Sriram, S., et al.,"Influence of Electric Field on SERS: Frequency Effects, Intensity Changes, and Susceptible Bonds," *J.Am.Chem. Soc.*, Vol. 134, No. 10, 4646-4653, 2011.

Four Vertical Prolate Spheroids with a Center Gap as Nanoantenna

M. Khosravi[1*], R. A. Sadeghzadeh[1], and M. S. Abrishamian[1]
[1]Department of Electrical and Computer Engineering, K. N. Toosi University of Technology, Shariati Street, PO Box 16314, Tehran, Iran

[*]corresponding author: m_khosravi@ee.kntu.ac.ir

Abstract-In this paper, we first investigate the properties of a single prolate nanospheroid of different materials to determine basic element. Next, we study the behavior of a structure of four vertical prolate spheroids of same dimension with a center gap (g). Finally, simulation results for different parameters variation (element size and gap distance) have been presented by order. As a result, this semi-turnstile nanoantenna produces intense optical field enhancement when illuminated at the resonant wavelength.

Properly designed plasmonic nanoantennas could have various applications in many fields such as optical communications, biological and medical sensors. Basically, an optical antenna is a dramatically miniaturized version of its much larger RF counterpart [1-2]. In antenna theory, antenna parameters are directly related to the wavelength λ of incident radiation, but this scaling fails at optical frequencies where metals behave as strongly coupled plasmas [3]. Recent advances in nano technology have opened doors to several next generation devices and sensors. Characterizing nanoplasmonic particles and structures in a simple and effective way is imperative for monitoring and detecting processes at nano scale in a variety of environments.

As stated above, the development of plasmonic structures as nanoantennas has become an important topic, and different numerical simulations have been used for their design and optimization. CST is a convenient software for this purpose. An important requirement of this software for the study of dispersive media is the need of an analytical law of dispersion. Here, it seems good to use Drude model for describing the dispersion of metals at optical frequencies [4]. However, the parameters of modeled materials have to be applicable over broad frequency bands in order to perform broadband calculations. Since the constitutive parameters (ε, μ, σ, and τ) must be specified as constants in simulations, the modified Debye model (MDM) is used here to describe the frequency-dependent behavior of metals [5].

As first step, we investigate the properties of a single prolate nanospheroid of different materials to make best choice for basic element (Fig.1 (a)). Main advantage of using the spheroidal particle is providing a means of adjusting the scattering resonant frequency by changing the ratio of radii. Also, what metals to use for optical antenna design is an open question, since metals behave very differently in optical domain. As an answer, noble metals such as gold and silver are good candidates for optical antenna design, mainly due to their specific optical property. The final choice for metal is silver whose permittivity at the frequencies of interest is well described by modified Drude model. In conclusion, a concentric (core-shell) spheroidal nanoparticle made of a given plasmonic material (silver) and an ordinary dielectric (silica) is employed to be the structural block of semi-turnstile nanoantenna in next step. This is because of the fact that one can tailor the resonant frequency in a wide range by properly controlling the geometrical parameters (the cover thickness and the ratio of radii).

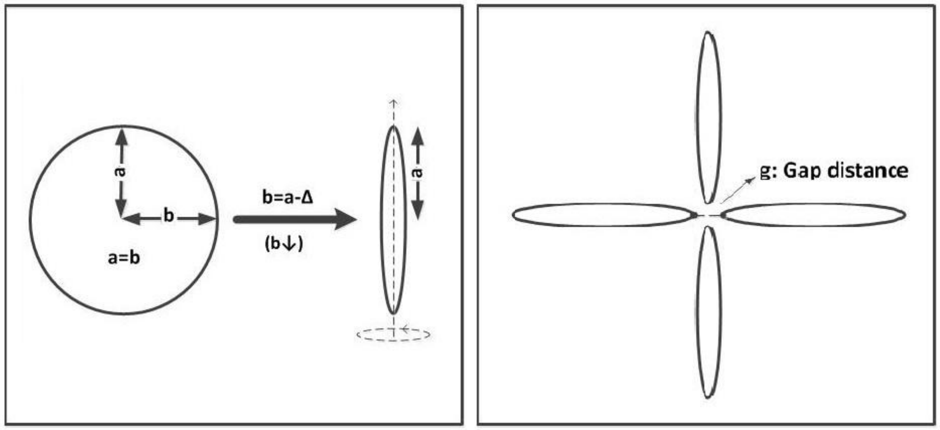

Fig.1 (a) Single prolate spheroid as basic element **(b)** Semi-turnstile arrangement

During the rest of this paper, we model a structure of four vertical prolate spheroids of same dimension (a [major axis] $\times$ b [minor axis] $\times$ b) having common feed gap of width g at its center (Fig.1 (b)). This structure of vertical nanoparticles is normally illuminated by a plane wave source. Before performing calculations for our actual structures, we verify our model by the results published by the researchers in recent years [5-6]. The overall goal of this work is to investigate effects of cover thickness (h), the ratio of radii (a/b) and gap size (g) using CST Microwave Studio. The field profiles were calculated at resonance wavelengths for each size of the particle.

All over this paper, we study the resonances behavior of nano-sized models under study. Special attention is focused on Extinction Cross Section (ECS) as output of simulations, because it experiences a peak at resonance frequency and its enhancement is also considerable for dimensions of this scale. We also calculated the electric field distribution around the nanoparticles and also around the vertical assembly of them in the presence of an incident electromagnetic field (a linearly polarized plane wave). And as final result, simulation outputs verify that a wise adjustment of gap size and two other parameters will lead to a considerable field enhancement in center gap of this novel structure of offered element.

Acknowledgements The authors have special thanks to Microelectronic Research and Development Center of Iran (MERDCI), an R&D organization set up by Industrial Development and Renovation Organization (IDRO) of Iran, for financial supports.

REFERENCES

1. Bharadwaj, P.; B. Deutsch, and L. Novotny, "Optical antennas," *Adv. Opt. Photon,* No. 1, 438–483, 2009.
2. Guzatov, D., and V. Klimov, "Optical properties of a plasmonic-nano-antenna: an analytical approach," *New JNL. of Phys.,* 2011.
3. Novotny, L., "From near-field optics to optical antennas feature," *Physics Today,* 47-52, July 2011.
4. Ordal, M. A., "Optical properties of the metals Al, Co, Cu, Au, Fe, Pb, Ni, Pd, Pt, Ag, Ti, and W in the infrared and far infrared", *J. App. Optics,* Vol. 22, No. 7, Apr. 1983.
5. Gai, H., J. Wang, and Q. Tian, "Modified Debye model parameters of metals applicable for broadband calculations", *Applied Optics,* Vol. 46, No. 12, 2229-2233, 2007.
6. Thomas, R., J. Kumar, R. S. Swathi, and K. G. Thomas, "Optical effects near metal nano structures: towards surface-enhanced spectroscopy," *Current Science,* Vol. 102, No. 1, Jan. 2012.

Hetero-plasmons coupling resonators

Masanobu Iwanaga[1,2*] **and Bongsoek Choi**[1]
[1]National Institute for Materials Science (NIMS), 1-1 Namiki, Tsukuba 305-0044, Japan
[2]JST PRESTO, 4-1-8 Honcho, Kawaguchi 332-0012, Japan
[*]corresponding author: IWANAGA.Masanobu@nims.go.jp

Abstract-We introduce a new class of plasmonic resonators having constructive coupled resonant modes of heterogeneous plasmons. The structure comprises two stacked layers with a nanogap spacer; each layer includes periodic array of plasmonic resonators and is complementary concerning metal. The unique structure has advantages in enhancement of optical responses with help of Babinet's principle and in realizing novel coupled plasmonic states that have been hardly explored. The new plasmonic resonators are shown with experimental evidences.

Plasmonic resonances in metallic nanostructures have been extensively investigated over 30 years [1,2]. Nevertheless, the diversity is quite limited. Most plasmonic structures consist of simple structures such as dots, rods, wires, rings, the aggregations, and perforated metallic films. Coupled plasmonic states were explored with sets of dots, rings, and so on [3,4].

Here we introduce a new class of plasmonic structures, which comprise two stacked layers including metallic nanostructures as drawn in Fig. 1. The feature is seen in the point that the two layers are complementary in terms of metallic nanostructures, enabling us to access new plasmonic states. The complementary structure produces complementary optical properties; the property is called Babinet's principle. As a result, the two layers have same resonant energies. The plasmonic eigen states in the two layers interplay in the nanogap spacer (or middle layer) and form constructive couple states. Recently, a few features were clarified: transmission enhancement and very large extinction ratio in anisotropic unit structures [5,6]. Such enhanced optical responses were found in the stacked complementary (SC) structures of transparent spacer of low refractive index 1.5. In this study, we show experimental and numerical results on a newly fabricated SC plasmonic structure of high-index spacer of Si as illustrated in Fig. 1, and clarify the plasmonic states. The SC structure has unique spacer, which is a Si photonic crystal slab of in-plane full photonic bandgap. It is an intriguing issue to elucidate how the bandgap affects plasmonic coupling via near-fields.

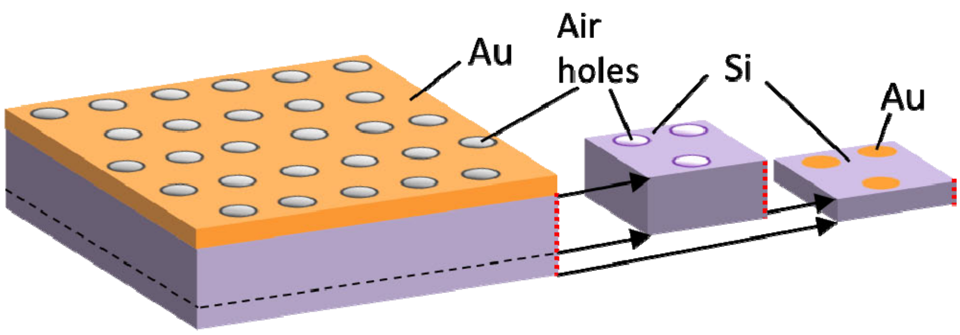

Figure 1. Schematics of a SC structure. The top and bottom layers are complementary regarding metallic nanostructures. The middle layer works as a spacer of hundreds nm thickness.

Figure 2(a) shows a top-view scanning electron microscope (SEM) image of a fabricated SC structure. The scale bar (white) denotes 100 nm. The periodicity of the hexagonal array was 410.5 nm and the diameter of the holes was 200 nm. Figure 2(b) presents measured reflectance spectrum of the sample in Fig. 2(a). Incident angle was 5 degrees and incident polarization was set to be *p* polarization or parallel to the *xy* plane, defined in Fig. 2(a). Several reflectance dips were explicitly observed, indicating resonant plasmonic states. The dips at the near-infrared range are located near the bandgap of the middle layer (or Si photonic crystal slab). The dispersion diagrams on the wavenumber–energy plane reveal that the states are almost local modes, suggesting that the full bandgap suppresses dispersive modes. Also, the local modes mean that each hole serves as a plasmonic resonator and that huge number of local electromagnetic hot spots is available in the SC structure.

At the presentation, the features of the plasmonic states will be reported. In addition, the potential for enhanced spectroscopy will be examined.

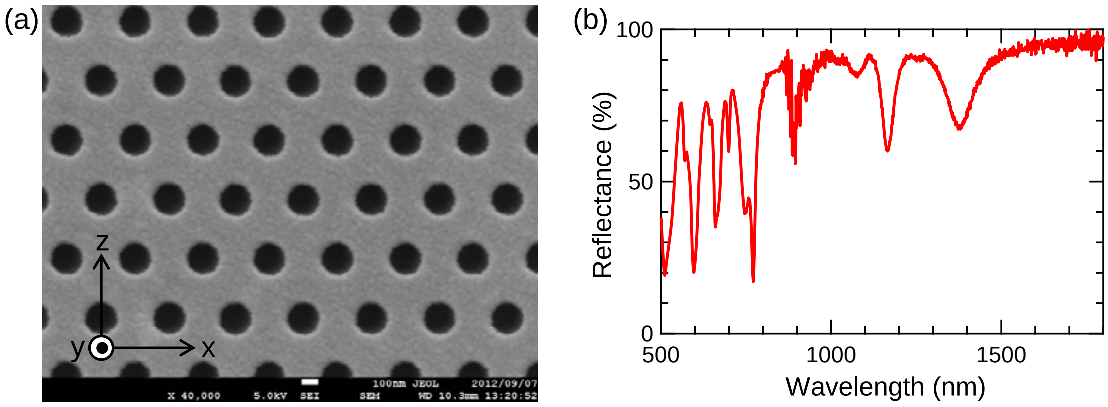

Figure 2. (a) A top-view SEM image of a SC structure. (b) Measured reflectance spectrum of the sample (a). Incident angle was 5 degrees and the incidence was *p* polarization.

Acknowledgements This study was partially supported by Cyberscience Center, Tohoku University and by a Grant-in-Aid (no. 22109007) from the MEXT, Japan. A part of nanofabrication was conducted at NIMS nanofabrication platform.

REFERENCES

1. Maier, S. A. and H. A. Atwater, "Plasmonics: Localization and guiding of electromagnetic energy in metal/dielectric structures," *J. Appl. Phys.*, Vol. 98, No. 1, 011101, 2005.
2. Murray, A. and W. L. Barnes, "Plasmonic Materials," *Adv. Mater.*, Vol. 19, No. 22, 3771–3782, 2007.
3. Prodan, E., C. Radloff, N. J. Halas, and P. Nordlander, "A Hybridization Model for the Plasmon Response of Complex Nanostructures," *Science*, Vol. 302, No. 5644, 419–422, 2003.
4. Hentschel, M., M. Saliba, R. Vogelgesang, H. Giessen, A. P. Alivisatos, and N. Liu, "Transition from Isolated to Collective Modes in Plasmonic Oligomers," *Nano Lett.*, Vol. 10, No. 7, 2721–2726, 2010.
5. Iwanaga, M., "Polarization-selective transmission in stacked two-dimensional complementary plasmonic crystal slabs," *Appl. Phys. Lett.*, Vol. 96, No. 8, 083106, 2010.
6. Iwanaga, M., "Subwavelength electromagnetic dynamics in stacked complementary plasmonic crystal slabs," *Opt. Express*, Vol. 18, No. 15, 15389–15398, 2010.

Atomistic approach for simulating plasmons in nanostructures

A. Sakko[1], **T. Rossi**[1], **J. Enkovaara**[1], **and R. M. Nieminen**[1]

[1]COMP Centre of Excellence, Department of Applied Physics, Aalto University, Finland
arto.sakko@aalto.fi

Abstract— Electronic structure calculations are used to study quantum mechanical effects behind the optical properties of small nanoscale (0–10 nm) systems. The optical response of metal nanostructures and graphene nanoflakes is shown to depend on their precise composition. Open-source computer code GPAW is used for the simulations, which can be done for systems of thousands of electrons, and which automatically include quantum effects such as tunneling, nonlocal response, and molecular orbital hybridization.

1. INTRODUCTION

Present-day materials design benefits from reliable computer simulations, which yield the materials' characteristics only from the knowledge of their structure and composition. Optical properties are typically calculated using Maxwell's equations, which describe the scattering, absorption, and propagation of light in materials whose dielectric permittivity and permeability are known.With sophisticated nanofabrication techniques (litography, self-assembly, surface chemistry, etc.), it is possible to create materials with sub-nm-scale structures, leading to a new regime where quantum mechanical effects must be accounted for in order to understand the optical response.[1, 2] One efficient strategy for adding quantum effects in optical response is to extend Maxwell's equations by incorporating nonlocality in the dielectric permittivity.[3] A more general approach is to use fully quantum mechanical electronic structure calculations. Some pioneering works have recently used time-dependent version of density functional theory (TDDFT) for such situations, and explored the tunneling and nonlinear response between nanoparticles in close contact.[2, 4] Our calculations are similar, but whereas the cited works employ the "jellium" approach (i.e. ions are replaced by positive charge continuum), we also account for the atomistic structure of the material. Our approach thus describes molecular orbital hybridization and the bonding between atoms, which can be significant for nanoparticles with sub-nm separations.

2. METHOD

The optical properties of the nanostructure depend on how the electrons respond to applied light. In the TDDFT approach, one calculates the time-dependent electron density under the influence of external electric field, by using a Schrödinger-type equation for single-particle electronic states (Kohn-Sham orbitals). Through linear response functions and perturbation theory, the time-dependent density can be directly related to the material's optical properties, such as the photoabsorption spectrum. TDDFT is a successful method for predicting valence electron excitations in molecules as well as plasmonic properties of solids.

The calculations in this work are carried out using open-source GPAW computer code. In this approach the time-dependent wavefunctions, electron density, and potentials are expressed on uniformly distributed real space grid points. The derivative operators are generated by finite-difference method, and since they are almost local, the approach provides exceptionally good parallelizability. The structure of the material is given as atom coordinates, although also jellium calculations are possible.[5]

3. RESULTS AND DISCUSSION

The simplest systems that contain plasmon-type electronic excitations are metal atom chains. In Fig. 1 we show the optical response (photoabsorption spectrum) of these structures, and the electron density change that is associated with the L_0 resonance. The energy of this longitudinal excitation clearly redshifts with increasing chain length, as expected from the classical plasmon theory and previous works.[6] The density profile that is typical for nearly-free electron gas, is evident from the shown transition charge density.

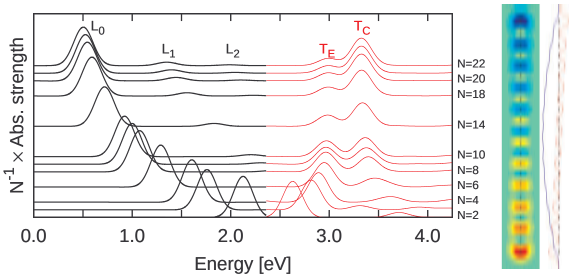

Figure 1: The photoabsorption spectrum of Na_N chains (left), separated into longitudinal (black) and transversal (red) parts, and the transition charge density associated with the L_0 transition (right).

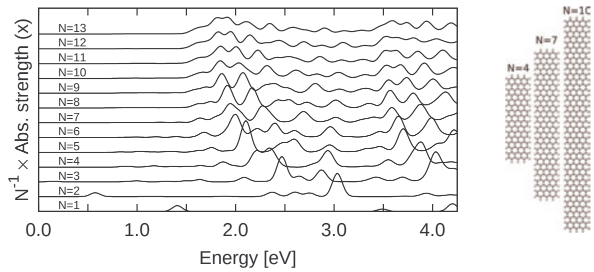

Figure 2: The length dependence of the photoabsorption spectrum of graphene nanoflakes, for the polarization along the long axis of the flake.

In addition to the metallic nanoclusters and wires, also many other types of nanostructures have tunable optical response. Graphene nanoflakes have attracted wealth of interest lately, as their electrical and optical properties depend strongly e.g. on their size and termination type. Fig. 2 shows how the photoabsorption spectrum of graphene flakes evolves as the length of the ribbon increases. The calculation demonstrates that the optical properties of graphene nanoflakes can be tailored systematically by changing the flake length. This is actually possible with chemical synthesization methods.[7]

Thanks to the improving nanofabrication techniques, the need for including quantum effects in the optical materials design can be expected to increase. Free access, good performance, and user-friendly Python scripting interface make GPAW an attractive tool for studying these effects. This work paves way for studying nano-optics with atomistic TDDFT simulations. In addition to the direct atomistic effects demonstrated here, we expect electronic structure calculations to be useful in many related problems in nano-optics and engineering. For example, they could give insight into the coupling of surface plasmons and light emitters. Nonlocality of the response can also be studied using TDDFT, by exploring the q-dependence of the density response function (the energy loss spectrum).[8] Moreover, the real space grid approach of GPAW could also be advantageous for embedding quantum and classical simulations of the optical response.[9]

ACKNOWLEDGMENT

We thank the Academy of Finland (Centres of Excellence Program) for the financial support, and Aalto Science-IT project and Finnish IT Center for Science (CSC) for computational resources.

REFERENCES

1. Scholl., J. A. and Koh, A. L., and Dionne, J. A., "Quantum plasmon resonances of individual metallic nanoparticles," *Nature*, Vol. 483, 421, 2012.
2. Zuloaga, J. and Prodan, E. and Nordlander, P. "Quantum Description of the Plasmon Resonances of a Nanoparticle Dimer" *Nano Lett.*, Vol. 9, No. 2, 887–891, 2009.
3. McMahon, J. M. and Gray, S. K. and Schatz, G. C. "Nonlocal Optical Response of Metal Nanostructures with Arbitrary Shape," *Phys. Rev. Lett.*, Vol. 103, 097403, 2009.
4. Savage, K. J. *et al.*, "Revealing the quantum regime in tunnelling plasmonics," *Nature*, Vol. 471, 574, 2012. Marinica, D. C. *el al.* "Quantum Plasmonics: Nonlinear Effects in the Field Enhancement of a Plasmonic Nanoparticle Dimer," *Nano Lett.* Vol. 12, 1333, 2012.
5. Enkovaara, J. and Rostgaard, C. and Mortensen, J. J. *et al.*, "Electronic structure calculations with GPAW: a real-space implementation of the projector augmented-wave method," *J. Phys.: Condens. Matter*, Vol. 22, 253202, 2010.
6. Yan, J. and Yuan, Z. and Gao. S., "End and Central Plasmon Resonances in Linear Atomic Chains," *Phys. Rev. Lett.* Vol. 98, 216602, 2007.
7. Cocchi, C. *el.*, "Optical Properties and Charge-Transfer Excitations in Edge-Functionalized All-Graphene Nanojunctions," *J. Phys. Chem. Lett.* Vol. 2, 1315–1319, 2011. Cai, J. *et al.*, "Atomically Precise Buttom-Up Fabrication of Graphene Nanoribbons," *Nature Letters* Vol. 466, No. 22, 470–473, 2010.
8. Sakko, A. and Rubio, A., and Hakala, M. and Hämäläinen, K., "Time-Dependent Density Functional Approach for the Calculation of Inelastic X-Ray Scattering Spectra of Molecules," *J. Chem. Phys.*, Vol. 133, 174111, 2010.
9. Gao, Y. and Neuhauser, D. "Dynamical Quantum-Electrodynamics Embedding: Combining Time-Dependent Density Functional Theory and the Near-Field Method," *J. Chem. Phys.*, Vol. 137, 074113, 2012.

Artefact free constant distance near field optical microscopy

Nayla El-kork*[1,2], Feiran Lei[3], Mohammad Ismail Elnaggar[1,3],Paul Moretti[2], Bernard jacquier[2]

.

[1]Khalifa University of Science, Technology and Research, Sharjah, UAE.

[2]Laboratoire de Physico Chimie des Matériaux Luminescents, Lyon, France.

[3]Ohio State University, Columbus, Ohio, U.S.A.

[*]corresponding author: nayla.elkork@kustar.ac.ae

Abstract-This paper aims at showing how constant distance Scanning Near Field Optical Microscopy (SNOM) can be genuinely used for the study of a Local Surface Plasmon Resonance (LSPR) biosensor through hot spots imaging. We present a verification procedure that would allow one to assert the validity of SNOM measurements without referring to constant height scans. SNOM images of LSPR hot spots on gold nanoplots, in addition to corresponding Finite Element Method (FEM) simulations, will demonstrate the veracity of the verification method.

I- Introduction

SNOM artefacts have been the cause of several debates, especially in the case of microscopes with an auxiliary gap width regulation (shear force, tunneling) due to the fact that the produced images can represent the path of the probe rather than optical properties of the sample[1, 2]. More specifically, constant distance SNOM brings doubts concerning optical and topographic coupling. Still, one cannot deny the importance of this tool and the high resolution that it can offer, in applications such as the detection and sensing of nanosized object or nanoparticles.

II- Materials and methods

Electron Beam Lithography was used for the fabrication of Au spheroid disc arrays. Each dot has a height of about 70 nm, a diameter of 140nm and is distant by 340nm from its neighbours.

Hybrid nanoparticles were chemically synthesised by Nano-H company[3]. They are composed of a gadolinium oxide core, covered with a polysiloxane shell, containing fluorescent molecules. Their diameter is about 20 nm.

Near field images have been performed using a commercial Omicron Twin SNOM (Figure 1). Measurements were done using a shear force constant distance regulation system. The sample is excited by a He-Ne laser and the emanating light is directed through a system of lenses, leading to a (C31034 series Burle type) photomultiplier tube; for fluorescence imaging, special notch filters are placed in the trajectory of the collected light.

III- Results

At least one of the following requirements has to be satisfied by a constant gap mode near field image to be genuine[4]: a) Topographic and near field optical images are highly uncorrelated.-b) Topographic and near field optical images correlate but are shifted with respect to one another by a constant distance- c) The resolutions of near field optics and shear force images are clearly different.

Figure 1 Shows a SNOM fluorescence image of the sample. Each dot is characterised by two luminescent point sources (or 'hot spots'), that seem opposite to one another. These correspond to emission emanating from gold LSPR emission. Figure 3 shows the corresponding simulation- both experimental results and simulation correspond well.   . Both criteria (a) and (c) are fulfilled. Criteria (b) and (c) have been fulfilled by measurements done on chemically synthesized hybrid nanoparticles.

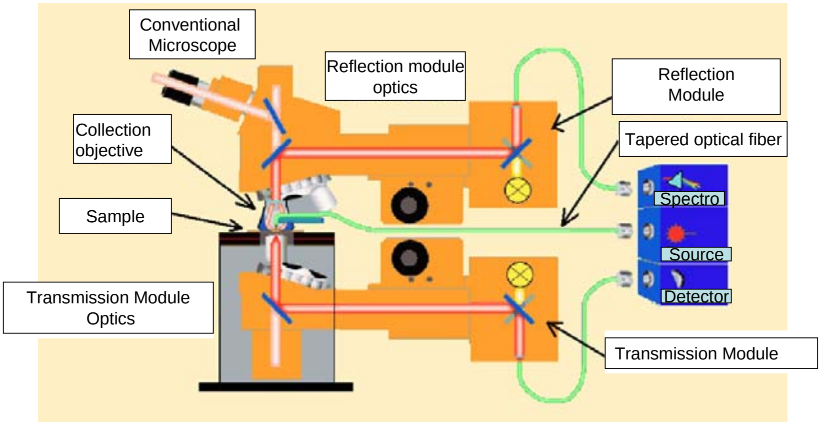

Figure1: SNOM setup

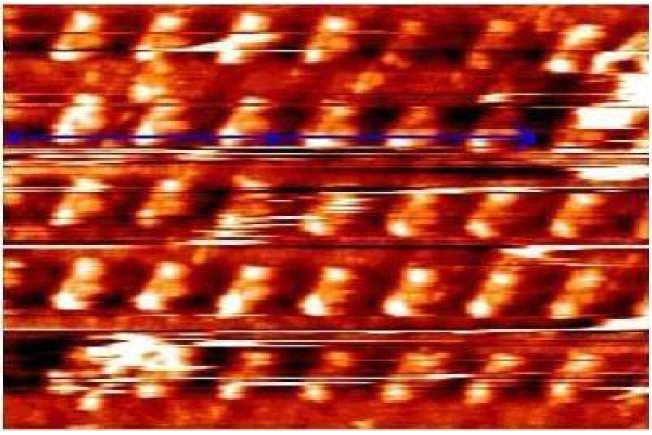

Figure 2: Gold nanoplots SNOM optical image

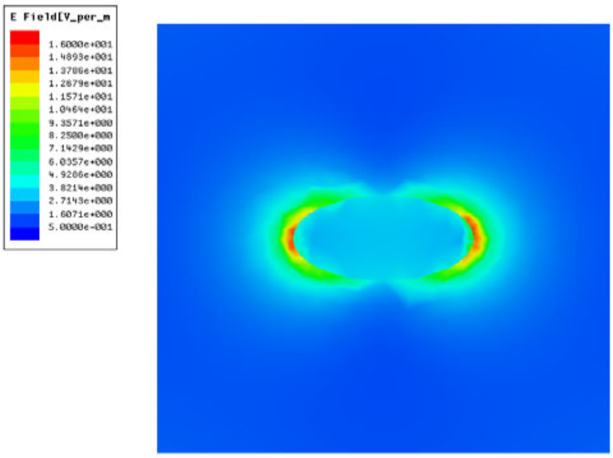

Figure 3: LSPR emission simulation

REFERENCES

1. B. Hecht , H. Bielefeldt, Y. Inouye, and D. W. Pohlc., "Facts and artifacts in near-field optical microscopy," *Journal of Applied Physics*,Vol 81, no. 6 , 2492-2498,1997.
2. G. Kaupp, A.Hermann, and M. Haak, "Artifacts in Scanning Near-field Optical Microscopy (SNOM) Due to Deficient Tips," *Journal of Physical Organic Chemistry* , Vol.12, no. 11, 797–807,1999.
3. http://www.nano-h.com/.
4. B. Hecht, B. Sick, U. P. Wild, V. Deckert, R. Zenobi, O. J. F. Martin, and D.W. Pohl," Scanning near-field optical microscopy with aperture probes.", *Journal of Chemical Physics*", Vol.**112**, 7761,2000.

Plasmonic Smart Dust for Probing Local Chemical Reactions

A. Tittl[1*], X. Yin[1], H. Giessen[1], X. Q. Tian[2], C. Kremers[3], D. N. Chigrin[3], Z. Q. Tian[2], and N. Liu[4]
[1]4th Physics Institute and Research Center Scope, University of Stuttgart, 70569 Stuttgart, Germany
[2]State Key Laboratory for Physical Chemistry of Solid Surfaces and Department of Chemistry, College of Chemistry and Chemical Engineering, Xiamen University, Xiamen 361005, China
[3]Institute of High-Frequency and Communication Technology, Faculty of Electrical, Information and Media Engineering, University of Wuppertal, 42119 Wuppertal, Germany
[4]Max Planck Institute for Intelligent Systems, Heisenbergstrasse 3, 70569 Stuttgart, Germany
[*]corresponding author: a.tittl@pi4.uni-stuttgart.de

Abstract We demonstrate an all-optical probing technique based on plasmonic smart dust for monitoring local chemical reactions. Our smart dust consists of silica shell-isolated gold nanoparticles which can work as strong light concentrators and optically report subtle changes at their pinning sites on the probed surface. In particular, we investigate the hydrogen dissociation and subsequent absorption in neighboring palladium films. Our single particle measurements offer a real-time, label-free, and high-resolution method for probing local reaction kinetics on various surface morphologies.

The rapid progress of energy and chemical conversion technologies calls for a comprehensive understanding of physical and chemical processes on the nanoscale [1]. As size decreases, localized features such as shapes, facets, defects, and boundaries in nanostructures play a pivotal role in the behavior of such systems [2].

Here, we demonstrate optical probing of local chemical reactions along with hydrogen uptake in palladium using single shell-isolated gold nanoparticles [3]. By recording the scattering spectra of such single plasmonic smart dust particles using dark-field microscopy, chemical reactions can be tracked in-situ and in real time.

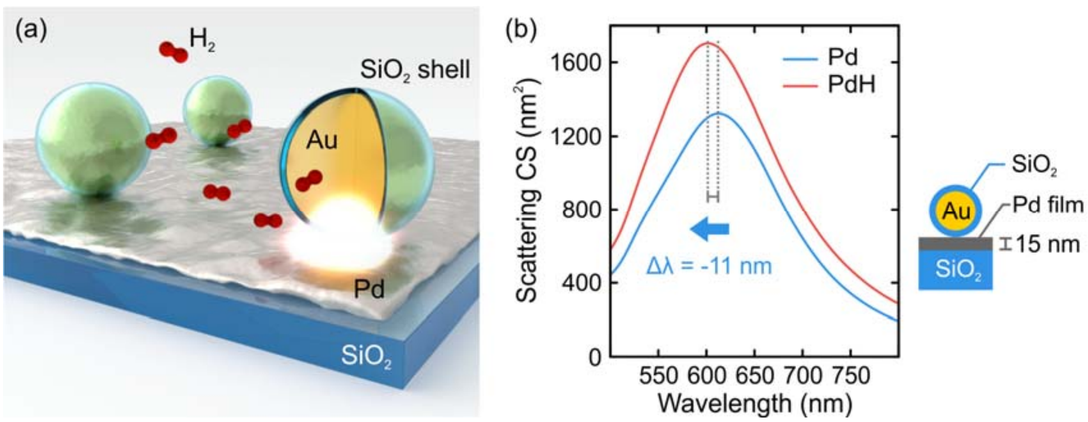

Figure 1: (a) Sketch of the “dust-on-film” sensor platform. Highly localized plasmonic near-fields are used to probe chemical reactions on an adjacent Pd film. (b) Calculated sensor response of the same geometry. A pronounced sensor response can be observed for the transition from pure to fully hydrided Pd (PdH).

In our system, the Au core concentrates strong electromagnetic near-fields into a subwavelength volume adjacent to the Pd film, where the chemical reactions take place. Simultaneously, the Au core serves as a plasmonic probe to report the local reaction processes during hydrogen uptake through the dielectric changes of Pd at varying hydrogen concentrations. Importantly, the ultra-thin SiO_2 shell of the smart dust separates the Au core from direct contact with the probed agents.

To emphasize the high sensitivity of our method to variations in the local environment, we study two sensor platforms: “dust-on-film”, where the smart dust particles are dispersed on the Pd film, and “film-on-dust”, where the smart dust is covered with a highly curved Pd layer using tilted rotating angle evaporation.

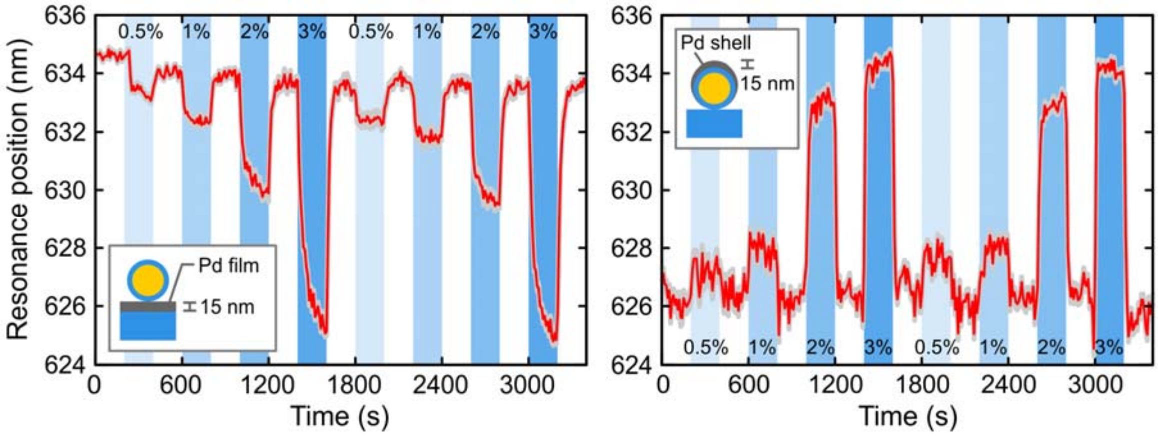

Figure 2: Experimental time-response of the resonance peak position for a single smart dust particle exposed to hydrogen concentrations ranging from 0.5 to 3% in nitrogen. All concentration steps can be clearly identified with response times on the order of seconds in both “dust-on-film” (left) and “film-on-dust” (right) platforms.

In both cases, the resonance position undergoes a pronounced spectral shift upon hydrogen exposure. In addition, the film placement strongly influences the direction of the spectral shifts, resulting in a blueshift for the “dust-on-film” case and a redshift for the “film-on-dust” case. This disparate behavior elucidates that our plasmonic smart dust can sensitively distinguish subtle changes in surface morphology at its probing site, yielding large associated optical changes. Thus, our method can be easily extended to investigate a plethora of chemical reactions on surfaces in industrially relevant systems, ranging from fuel cells to catalytic water splitting

Acknowledgements A.T., X.Y. and H.G. acknowledge financial support by the DFG (SPP1391, FOR730, and GI 269/11-1), the BMBF (13N9049 and 13N10146), the Baden-Württemberg Stiftung (Kompetenznetz Funktionelle Nanostrukturen), and the MWK Baden-Württemberg. N.L. was supported by the Sofia Kovalevskaja Award of the Alexander von Humboldt Foundation.

REFERENCES

1. Linic, S., et al., “Plasmonic-metal nanostructures for efficient conversion of solar to chemical energy.,” *Nature Mater.*, Vol. 10, No. 12, 911–921, 2011.
2. Watanabe, K., et al., “Photochemistry on metal nanoparticles.,” *Chem. Rev.*, Vol. 106, No. 10, 4301–4320, 2006.
3. Li, J. F., et al., “Shell-isolated nanoparticle-enhanced Raman spectroscopy,” *Nature*, Vol. 464, No. 7287, 392–395, 2010.

Optical forces induced by metal nanoparticle clusters

J. Sancho-Parramon[1,2*] **and S. Bosch**[2]
[1]Rudjer Boskovic Institute, Croatia
[2]Universitat de Barcelona, Spain
[*]corresponding author: jsancho@irb.hr

Abstract- The strong field localization generated between closely placed metal particles excited by radiation induces intense forces on small polarizable objects. In this study we investigated the optical forces that can be generated in the vicinity of metal nanoparticle clusters using fully electrodynamic numerical simulations. The influence of the cluster configuration (material, numer of particles and geometrical arrangement) as well as the excitation parameters (polarization distribution and degree of focusing) is investigated.

Optical trapping appears to be a promising way to control the position of small objects with nanometric precision. In this sense, optical tweezers has been shown to be a useful tool to trap objects in the focal region of tightly focused beams. The key issue is the gradient of electromagnetic field generated at the focus that induces a dipole force on polarizable particles. This force, proportional to the field intensity gradient, drives the particles towards the region with largest field. However, due to the diffraction-limited field distribution that can be achieved with conventional optics, nanometric control of the position of small objects requires large laser power beams, preventing the application to objects that might be damaged when exposed to strong irradiation, for instance, biological samples.

In order to surpass this restriction, the use of optical near-fields for trapping has been proposed as alternative, since near-field distributions are not diffraction-limited. In this sense nanometric optical tweezers have been suggested for precise trapping of very small objects based on the strong field gradient generated around nanoparticle surfaces[1]. Using this principle, nanoscale control of objects has been experimentally demonstrated at nanostructured substrates containing metal particle pairs[2,3]. Such trapping configurations exploit the strongly enhanced and localized near field generated at the gap between particles as result of the coupling of individual particle plasmon resonances[4].

In the present study we analyze the potential of different metal clusters for efficient optical trapping of small objects. In particular, we focus on the influence of different particle configurations (number of particles and geometrical arrangement) as well as on the radiation exciting the cluster (plane wave, focused radiation, cylindrical vector beams). The evaluation of the trapping potential for each configuration is performed by calculating the near field distribution in the cluster structure. For this purpose we use fully electrodynamic simulations, i.e., a generalized Mie theory that can take into account different particles and illumination conditions[5].

Acknowledgements, JSP acknowledges the financial support of the Government of Catalonia through a “Beatriu de Pinos” grant.

REFERENCES

1. Novotny, L., Bian, R. X. and Xie, X. S. "Theory of nanometric optical tweezers," *Phys. Rev. Lett.*, Vol. 79, 645–648, 1997.
2. Grigorenko. A. N., Roberts, W. W., Dickinson, M. R and Zhang, Y. "Nanometric optical tweezers based on nanostructures substrates," *Nat. Photonics*, Vol. 2, 365–670, 2008.
3. Righini, M., Ghenuche, P., Cherukulappurath, S., Myroshnychenko, V., García de Abajo, F. J., and Quidant, R. "Nano-optical Trapping of Rayleigh particles and Escherichia coli bacteria with resonant optical antennas," *Nano Lett.*, Vol. 9, No. 10, 3387–3391, 2009.
4. Krenn, J. R., Dereux, A. Webber, J. C., Bourillot, E., Lacroute, Y. Goudonnet, J. P., Schider, G., Gotschy, W. Leitner, A., Aussenegg, F. R. Girard, C. "Squeezing the optical near-field zone by plasmon coupling of metallic nanoparticles," *Phys. Rev. Lett.* Vol. 82, No. 12, 2590–2593, 1999.
5. Sancho-Parramon, J. "Near-field coupling of metal nanoparticles under tightly focused illumination," *Opt. Lett.*, Vol. 36, No. 17, 3527-3529, 2011.

Effect of ordered and disordered gold nanoporosity on dispersion control of propagating surface plasmons

Neha Sardana[1,2*] , Sven Schlenker [3], Carsten Reinhardt[4] and Jörg Schilling[1]

[1]Centre for Innovation Competence SiLi-nano®, Martin Luther University of Halle-Wittenberg, Karl-Freiherr-von-Fritsch-Str. 3, 06120 Halle (Saale), Germany
[2]International Max Planck Research School for Science and Technology of Nanostructures, Weinberg 2, 06120 Halle (Saale), Germany
[3]Interdisciplinary center of material science, Martin Luther University of Halle-Wittenberg, Heinrich-Damerow-Straße 4, 06120 Halle (Saale), Germany
[4]Laser Zentrum Hannover e.V., Hollerithallee 8, 30419 Hannover, Germany

[*]corresponding author: neha.sardana@physik.uni-halle.de

Abstract- Two types of nanoporous gold films (spongy bi-continuous network and hexagonally ordered nanopores in gold) are prepared by dealloying and evaporation of Au on nanoporous templates. Their optical properties, specifically the tuning of the surface plasmon resonances connected with the effective dielectric constant of the films, is investigated using angular resolved reflection measurements in the Kretchmann configuration (prism coupling). The experimentally determined dispersion relation of the surface plasmons on the nanoporous gold/air interfaces is compare with the Bruggeman & Maxwell Garnett effective medium theory. Ohmic and scattering losses leading to the attenuation of the surface plasmons at the nanoporous surface are also studied using leakage radiation microscopy.

Contemporary sub-wavelength optics of thin metal (with negative real part of dielectric constants) films, Surface Plasmons (SPs) are formed and strongly confined while propagating along their boundary. The dispersion relation of these SPs on plane metal/dielectric surfaces follows directly from Maxwell equations [1] and is given as

$$k_x = \frac{\omega}{c}\sqrt{\frac{\varepsilon_m \varepsilon_d}{\varepsilon_m + \varepsilon_d}} \tag{1}$$

Where, k_x describes the wave vector of the surface plasmon and ε_m and ε_d are the dielectric constants of the metal and the dielectric respectively.

For a fixed value of ε_d the dispersion of the surface plasmons can therefore still be controlled by changing ε_m. This can be achieved by introducing nanoporosity into the metal with structure sized well below the wavelength of light. In this way a "meta-metal" is created whose effective dielectric constant ε_m governs now the surface plasmon dispersion on its surface.

In order to achieve nanopores with diameters in the range of 10-50nm in gold we dealloyed 12 carat white gold leaf samples [2] which lead to spongy nanoporous gold films. To achieve a more regular hexagonal porosity we evaporated Au on a self-ordered nanoporous alumina template. The gold is deposited at the surface between the pores and SEM characterizations confirm a porosity of approx. 20%- 45% of the gold films depending on pore size distribution. Free hexagonally ordered gold films can be obtained by removing the template by selective wet etching.

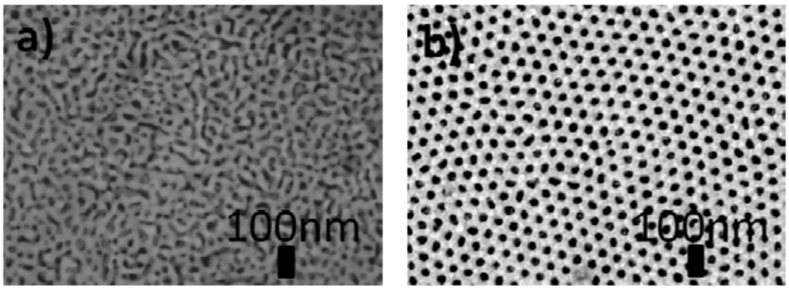

(a) (b)

Figure 1(a). SEM of Au and 60 min dealloyed 12 carat Au. (b) Au formed by wet etching of Alumina template.

To map the dispersion relation of the SPs at the nanoporous gold surface, angular resolved reflection measurements were carried out in the Kretchmann configuration (prism coupling). A characteristic dip in reflectivity that shifted to shorter wavelength with increasing angle of incidence was identified as the excitation of propagating SPs at the nanoporous gold/air interface [3]. A clear red shift of the SP dispersion relation on nanoporous gold is observed resulting in SPs near the infra-red region.

A good agreement is observed between the experimental shift of the dispersion relation towards infra-red wavelengths for nanoporous gold when compared with theoretical calculations in which the ε_m of the nanoporous gold layer is derived using the Bruggeman effective medium theory for spongy structure and Maxwell Garnett for more organized structure [4].

Furthermore, to image the SP propagating losses, leakage radiation microscopy in both direct and Fourier space are studied. It is observed that the ordered nanoporous Au has lesser scattering and therefore shows a lower attenuation.

The above set of experiments and analysis proves that the dispersion relation and scattering of the SPs can be controlled by manipulating the porosity of a metal. This could allow the tuning of the limiting surface plasmon frequency ω_{sp} into a specific desired spectral range where e.g. the luminescence of the adjacent specific dielectric material should be enhanced or the low group velocity of the SPs around ω_{sp} should be utilized.

Acknowledgment- The authors would like to thank International Max Planck Research School for Science and Technology of Nanostructures and the Federal Ministry for Education and Research (BMBF) for their financial support within the Centre for Innovation Competence SiLi-nano®

REFERENCES

1. Raether, Heinz. *Surface plasmons on Smooth and Rough Surfaces and on Gratings*. New york: Springer-verlag., 1988.
2. Erlebacher, J., M.J. Aziz, A. Karma, N. Dimitrov, K. Sieradzki. "Evolution of nanoporosity in dealloying." *Nature* 410, 2001.
3. Sardana, N., F. Heyroth, and J. Schilling. "Propagating surface plasmons on nanoporous gold." J*OSA B* 29(7), 2012.
4. Dixon, M.C., T.A. Daniel, M. Hieda, D.M. Smilgies, M.H.W. Chan, D.L. Allara. "Preparation , Structure , and Optical Properties of Nanoporous Gold Thin Films." *Thin Solid films* 2414-2422, 2007.

Simulating light transmission through a metallic thin film perforated with 2D periodic array of multiple-slit apertures

Hui-Hsin Hsiao[1] **and Hung-chun Chang**[1,2,3*]

[1]Graduate Institute of Photonics and Optoelectronics, National Taiwan University, Taipei, Taiwan 10617, R.O.C.

[2]Graduate Institute of Communication Engineering, National Taiwan University, Taipei, Taiwan 10617, R.O.C.

[3]Department of Electrical Engineering, National Taiwan University, Taipei, Taiwan 10617, R.O.C.

[*]corresponding author: hcchang@cc.ee.ntu.edu.tw

Abstract-The light transmission properties of a designated 2D array of multiple-slit apertures perforated on a metallic film are analyzed using the FDTD method. Different aperture shapes having different symmetry characteristics are studied. Some specific near-field features are found to be associated with three mechanisms underlying the transmission spectral profiles, providing a way in revealing the physical nature of the enhanced transmission phenomenon.

The physics and applications of extraordinary transmission through periodically arranged sub-wavelength holes in metal films have attracted considerable interest during past decades[1]. The excitation of surface plasmon polaritons (SPPs), or the surface electromagnetic (EM) modes, and Wood's anomalies (WAs) set up by periodically arranged holes have been widely believed to be the underlying main mechanisms. Moreover, it has been shown that shape resonances (SRs) related to the shape of aperture have a strong effect on the transmission spectra[2,3]. In this work, we study the optical properties of differently shaped apertures composed of one to three horizontal slits, named *x*-arm slits, and one vertical slit, named *y*-arm slit. Figure 1(a) shows the geometry of a unit cell of one structure example we study and Fig. 1(b) shows the top views and structural parameters of samples 1 to 5: the unit cell with lattice constants of $a_x = a_y = 14$ μm, where the length of each silt $l_x = 12$ μm and $l_y = 7$ μm, and the width of the silt $w = 1$ μm. Samples 1 to 3 possess twofold mirror symmetry with respect to the center of the *x*-coordinate (C_x) as well as the center of the *y*-coordinate (C_y), while samples 4 and 5 only possess the mirror symmetry with respect to C_x. The metal (silver) film with thickness 75 nm is coated on a silicon substrate. An in-house developed 3D finite-difference time-domain (FDTD) method numerical model is used to simulate the EM field distributions and transmission spectra under normal incidence of light. Periodic boundary conditions are applied to the *xz* and *yz* planes to simulate a square periodic array of apertures.

The SR wavelength might dominantly depend on the slit length. But for more complex-shaped apertures, the SR paths may have some ambiguities to be estimated by the modified cutoff wavelengths of the rectangular waveguide (i.e., $\lambda_{res} = 2n_{eff}L_{res}/m$, where $n_{eff} = \sqrt{(n_{substrate}^2 + n_{air}^2)/2}$ is the effective refractive index, L_{res} is the resonant length, and m is an integer) due to the slight difference of the L_{res} between those possible contours. We have found that analyzing the near-field features is helpful in distinguishing the SR modes[4]. For example, the modulus of the electric field, $|\boldsymbol{E}|$, defined by $\sqrt{|E_x|^2 + |E_y|^2 + |E_z|^2}$, contours clear geometry of the resonant length. Within the SR paths, the distribution of the phase component parallel to the polarization of the incident light (e.g., φ_{Ex} under *x*-polarized light) is quite homogeneous and the phase component along the propagation direction, φ_{Ez}, exhibits a 180° jump at the center of the slit width. By focusing on the anti-phase property of φ_{Ez} along the SR contours and the symmetry requirement preserved for certain polarization state of light, those SR paths that cannot meet the above two criteria together are obviated and the possible right ones are left. In order to testify the validity of such principles in determining the SR paths, we design a set of apertures with onefold or twofold mirror symmetry, as shown in Fig. 1(b). We find the FDTD-obtained field-profile predictions agree well with the real SR modes, which are validated by the near-field analyses.

We in particular discuss the broad-band peaks in the transmission spectra under y-polarized light. We discuss how the separation distance between slit elements in the apertures affects the SR wavelength, showing how the coupling between adjacent slits would play a role in the variation of the spectra. Figure 1(c) shows the transmission spectra for samples 1 to 5 under y-polarized light. To utilize the symmetry principle to predict the SR contours, φ_{Ez} now needs to be with even/odd symmetry with respect to C_x/C_y for twofold mirror symmetry apertures. In this case, the resonant paths are forbidden to across the y-arm slits for samples 1 to 5, which are all posited in the middle of the x-coordinate within the unit cell. Without the connection of the vertical y-arm slit, the possible SR paths are all along the horizontal x-arm slits. According to the experiential formula for SR, the resonant position would be the same for samples 1 to 5 due to the equivalence of the effective SR path, L_{res}. However, Fig. 1(c) shows that the separation distances between the x-arm slits, s_1 and s_2, specified in the inset have a strong effect on resonant wavelengths. By analyzing the near-field features, we found that the broad-band peaks at $\lambda \sim 56$ μm, 64 μm, and 68 μm correspond respectively to the first and third x-arm slits resonance with $s_1 = 5$ μm and $s_2 = 7$ μm (for both samples 1 and 2), the second and third x-arm slits resonance with $s_1 = 2$ μm and $s_2 = 10$ μm (for sample 4), and one x-arm slit resonance with $s_1 + s_2 + w = 13$ μm (for both samples 3 and 5). With the present study, we could manipulate the spectra with an additional degree of freedom, which could be important to structures with multi-holes or multi-slits in one unit cell.

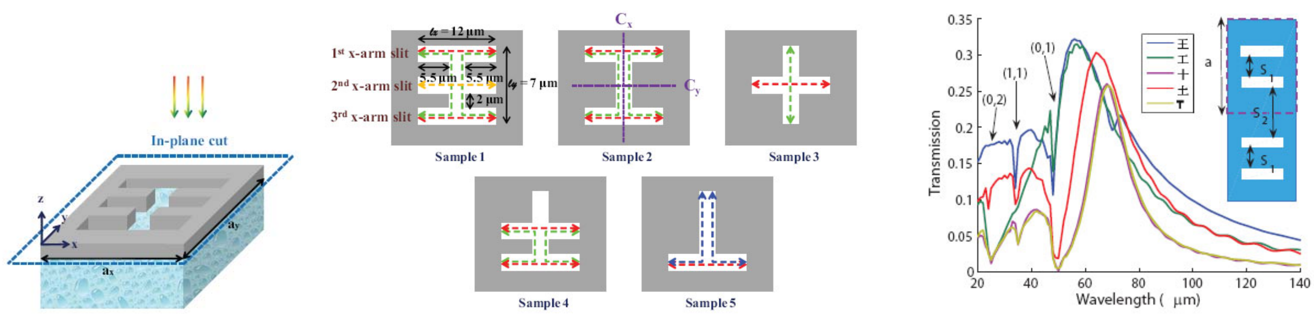

(a) (b) (c)

Figure 1 (a) The unit cell and the near-field plane cut in our simulation. (b) Top view and structural parameters of samples 1–5. (c) Transmission spectra with an y-polarized light under normal incidence. The inset shows two adjacent unit cells with separation distances between the x-arm slits, s_1 and s_2, specified.

REFERENCES

1. Ebbesen, T. W., H. J. Lezec, H. F. Ghaemi, T. Thio, and P. A. Wolff, “Extraordinary optical transmission through sub-wavelength hole arrays,” Nature, Vol. 391, 667-669, 1998.
2. Klein Koerkamp, K. J., S. Enoch, F. B. Segerink, N. F. van Hulst, and L. Kuipers, “Strong influence of hole shape on extraordinary transmission through periodic arrays of subwavelength holes,” Phys. Rev. Lett., Vol. 92, 183901, 2004.
3. Ruan, Z., and M. Qiu, “Enhanced transmission through periodic arrays of subwavelength holes: The role of localized waveguide resonances,” Phys. Rev. Lett., Vol. 96, 233901, 2006.
4. Hsiao, H. H., H. F. Huang, S. C. Lee, and H. C. Chang, “Investigating far-field spectra and near-field features of extraordinary optical transmission through periodic U to H shaped apertures,” IEEE Photon. J., Vol. 4, 387–398, 2012.

Frequency-dependent excitation of surface plasmon polaritons in Al-coated SNOM tips

V. Palm*, M. Rähn, J. Jäme, and V. Hizhnyakov
Institute of Physics, University of Tartu, Riia 142, 51014 Tartu, Estonia
*corresponding author: viktor@fi.tartu.ee

Abstract- The recently introduced technique of mesoscopic spectral modulation is used as an indicator of surface plasmon polariton generation in Al-coated SNOM tips. Application of SNOM tips of different output aperture diameters allows studying this effect in different spectral regions. Additionally, finding proper conditions for excitation of certain pairs of photonic fiber modes allows the studies to be performed in broader spectral region with a single tip sample. The observed wavelength dependence of the effect magnitude is consistent with theoretical considerations.

As it was recently demonstrated [1], the technique of mesoscopic spectral modulation (MSM) [2] can be applied to study photon-plasmon coupling effects in a metal-coated SNOM tip terminating a multimode optical fiber. Due to the mode-filtering effect [3], for a SNOM tip of certain output aperture diameter a spectral region exists where only two photonic fiber modes can be transmitted with significant and comparable amplitudes. This results in intermodal interference revealing itself as a sinusoidal spectral modulation.[4] The MSM technique allows finding the optical path difference (OPD) for the pair of modes from the estimated period of spectral modulation observed.[2] OPD generated in a SNOM tip can be attributed to a mode-selective coupling of photons to surface plasmons of the metal coating. Spectral measurements performed with different (gradually reduced) fiber tail lengths *l* allow taking into account the inherent modal dispersion of the fiber.

Due to technical reasons we started our MSM experiments using bent-type Al-coated SNOM tips (Nanonics). In addition to earlier reported results obtained for the ~800 nm spectral region using a 200 nm SNOM tip [1], we performed MSM experiments with a 150 nm SNOM tip [5], which allowed us studying the mode-selective excitation of surface plasmon polaritons by shorter-wavelength photons. In the latter case the output spectra were measured for different positions of the fiber tail input in relation to the focused spot of the broadband exciting light. It turned out that the number and intensity ratio of fiber modes excited and transmitted by our 150 nm SNOM tip strongly depends on the fiber input adjustments, which is reflected in the changing structure of spectral modulation. Still it was possible to find “proper” adjustment positions, which resulted in regular patterns of spectral modulation enabling application of the two-mode model for estimation of the corresponding OPD value. Shorter or longer spectral intervals with such regular modulation patterns could be observed within a broader spectral region between 640 and 760 nm We found that at least two different types of regular modulation patterns can be obtained, corresponding probably to different pairs of transmitted fiber modes. The first type (T1) seems to possess nearly constant period in the frequency domain regardless of the spectral location within the broader region, which is a similar behavior to the one earlier observed for our 200 nm SNOM tip [1,5], indicating that the regular modulation pattern observed there probably corresponds to the same pair of modes. Thus the comparison of OPD values *A* generated in Al-coated SNOM tips for this pair of modes in different spectral regions can be of interest. For ~800 nm spectral region (200 nm SNOM tip) we have A = –23(3) fs, [1];

for ~700 nm region (150 nm SNOM tip) we obtain A = –67(31) fs [5]. Taking into account that the plasmonic resonance frequency of Al lies in UV region, it seems quite logical that the absolute value of A is larger at lower wavelength, indicating stronger photon-plasmon coupling. Considering the weakness of this coupling, the result can be seen as an indication of the high sensitivity of MSM technique, inherently to interference techniques. Negative A values indicate that the OPD generated in a SNOM tip is of the opposite sign to the one generated in the fiber. The second pattern type (T2), which is harder to obtain due to its high sensitivity to the fiber input adjustments, exhibits larger modulation period and can be observed spanning over longer spectral intervals. In spite of the modulation regularity, T2 patterns clearly exhibit smooth linewidth dependence of the modulation period. The method we propose to analyze this spectral dependence will be discussed and analyses presented.

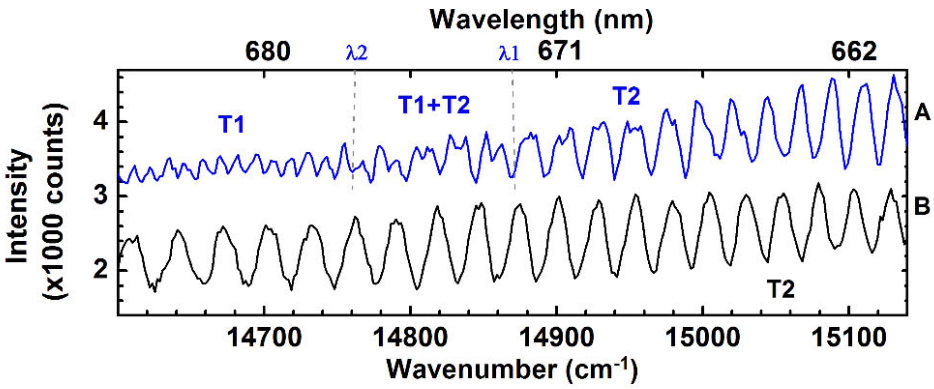

Figure 1. Two examples of spectra observed for our 150 nm SNOM tip with different fiber tail lengths: (A) l = 1488 mm, (B) l = 1330 mm. Spectrum A exhibits T2-type modulation pattern in the wavelength region $\lambda < \lambda 1$ and T1-type pattern in the region $\lambda > \lambda 2$; a mixed (T1+T2) “chaotic” pattern can be observed in an intermediate region $\lambda 1 < \lambda < \lambda 2$. Spectrum B exhibits T2-type pattern over the entire range displayed; the corresponding modulation period increases with λ. Signal collection time 3000 s.

Acknowledgements Acknowledged is the support by Estonian Science Foundation Grant nos. 7741 and 8167, by the project TLOFY0145, and by the European Union through the European Regional Development Fund (project TK114). MR acknowledges the support by Archimedes Foundation. and by graduate school “Functional materials and processes”, European Social Fund project 1.2.0401.09-0079 in Estonia.

REFERENCES

1. Palm, V., M. Rähn and V. Hizhnyakov, “Modal dispersion due to photon-plasmon coupling in a SNOM tip”, *Opt. Commun.*, Vol. 285, No. 21-22, 4579–4582, 2012.
2. Rähn, M., M. Pärs, V. Palm, R. Jaaniso and V. Hizhnyakov, “Mesoscopic effect of spectral modulation for the light transmitted by a SNOM tip”, *Opt. Commun.*, Vol. 283, No. 11, 2457–2460, 2010.
3. Novotny, L. and C. Hafner, “Light propagation in a cylindrical waveguide with a complex, metallic, dielectric function”, *Phys. Rev. E*, Vol. 50, No. 5, 4094-4106, 1994.
4. Hlubina, P. “Coherence of light at the output of a fibre waveguide analysed in the space-frequency domain“, *J. Mod. Opt.*, Vol. 42, No. 7, 2385-2399, 1995.
5. Palm, V., M. Rähn, J. Jäme and V. Hizhnyakov, “Excitation of surface plasmons in Al-coated SNOM tips”, *Proc. SPIE*, Vol. 8457, 84572S-1–84572S-10, 2012.

Magetostatic Surface Resonance in Anisotropic Spherical and Ellipsoidal Shapes

Z. Ren[1], **A. Kabiri**[2], **and O. M. Ramahi**[1]

[1]University of Waterloo, Canada
[2]Harvard University, U.S.A.
omar.ramahi@uwaterloo.ca

Abstract— We propose a magnetostatic surface resonance (MSR) solution and its conditions in electrically-small particles such as isotropic ellipsoid, ellipsoid with coating, anisotropic sphere and ellipsoid. The magnetostatic resonance is governed by the particle's dimensions, relative permeability of coating layers and that of the surrounding medium. The conclusions in this work are expected to help understand the interesting MSR phenomenon in isotropic or anisotropic spherical and ellipsoidal structures.

Magnetostatic surface resonance (MSR), which is the magnetic counter part of the well-known surface plasmon or surface plasmon polarition in optics, occurs in electrically small particles having negative real and small imaginary permeability. Such resonance phenomenon requires excitation frequency in the direction of the negative real permeability where the maximum magnetic moment happens. This phenomenon can be found in many metamaterials that process effective negative permeability over a wide range of frequencies, such as the well-known split ring resonator (SRR) [1], rose curve element [2], fishnet structure [3], circle aligned paired-nanoparticles [4], amongst others. In our earlier work [5], we demonstrated MSR for isotropic sphere and sphere with coatings, where strong magnetic energy confinement was found inside the volume and enhanced scattered field was observed in the neighborhood of the particles. Since most of metamaterials have anisotropic properties, in this work we propose MSR condition for isotropic ellipsoid, ellipsoid with coating, anisotropic sphere, and anisotropic ellipsoid.

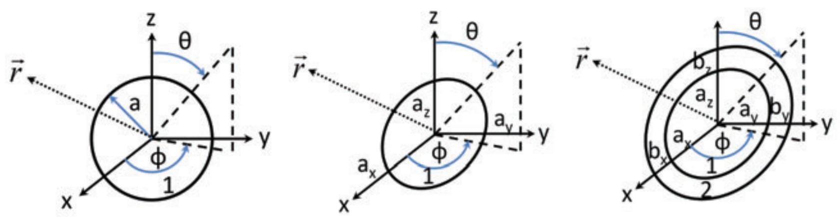

(a) (b) (c)

Figure 1: Particle scattering. The definitions of scattering angle θ and ϕ are considered as the vertical and horizontal angles. Particle dimensions are denoted as a and b. The distance from observation point to origin is represented as vector $\vec{r}$. (a) Single sphere. (b) Single ellipsoid. (c) Coated ellipsoid.

The magnetic field across an electrically small particle can be considered as constant such that $\nabla \times \vec{H} = 0$. Such wave particle interaction is governed by magnetostatic rather than magnetodynamics physics. The problem is then reduced to solving the Laplace's equation $\nabla^2\varphi = 0$, where φ is the magnetic potential. Then the magnetic field density can be obtained from the gradient of magnetic potential in reverse direction, $\vec{B} = -\nabla\varphi$:

$$\vec{B}(\vec{r}) = \frac{\mu}{4\pi}\left[\frac{3\hat{r}(\hat{r}\cdot\vec{m}) - \vec{m}}{|\vec{r}|^3} + \frac{8\pi}{3}\vec{m}\delta(\vec{r})\right]. \tag{1}$$

where $\vec{r}$ is the distance between the volume and observation point, $\hat{r}$ is the unit vector along $\vec{r}$ direction, μ is permeability of isotropic surrounding medium, and $\vec{m}$ is total magnetic moment within the volume. The delta function in Eq. (1) presents the hyperfine structure of atomic s states. Since the size of the volume is electrically very small, the magnetic moment m is actually a dipole magnetic moment which is related to the magnetic polarizibility $\bar{\beta}$ and in the direction of applied magnetic field $\vec{H}_0$.

$$\vec{m} = 4\pi\bar{\beta}\vec{H}_0 \tag{2}$$

In spherical coordinates, generally the solutions to Laplace's equation are spherical harmonics. Regardless of the observation position in the entire system, the induced magnetic field is represented as $\vec{H} = \vec{B}/\bar{\mu}$ for a homogenous magnetic material with small dimension. Note that this is also applicable to non-linear material with electrically small size as the non-linearity can be ignored within a small region. For a given shape, MSR solution can be approximated by Eq. (1). The corresponding magnetic polarizibility can be found from electrostatic theory due to electric-magnetic field duality.

In electrically small isotropic ellipsoid shapes, the MSR resonant condition can be calculated through finding the maximum magnetic polarizibility:

$$\mu_1 = \frac{L_i - 1}{L_i}\mu \tag{3}$$

where

$$L_i = \frac{a_x a_y a_z}{2}\int_0^\infty \frac{dq}{(a_i^2 + q)\sqrt{(q + a_x^2)(q + a_y^2)(q + a_z^2)}} \tag{4}$$

L_i is an integrable function, $Lx+Ly+Lz = 1$, $a_x \geq a_y \geq a_z$ are ellipsoid radius in x, y, z directions. Such inequality yields $L_1 \leq L2 \leq L3$. Similarly, MSR condition for coated ellipsoid can be also found as follows.

$$\mu_1 = \frac{\mu_2[\mu + (\mu_2 - \mu)L_i^{(2)}](L_i^{(1)} - fL_i^{(2)} - 1) + \mu_2^2 f L_i^{(2)}}{(L_i^{(1)} - fL_i^{(2)})[\mu + (\mu_2 - \mu)L_i^{(2)}] + fL_i^{(2)}\mu_2} \tag{5}$$

where

$$L_i^{(j)} = \frac{a_{jx} a_{jy} a_{jz}}{2}\int_0^\infty \frac{dq}{(a_{jz}^2 + q)\sqrt{(q + a_{jx}^2)(q + a_{jy}^2)(q + a_{jz}^2)}} \tag{6}$$

In Eq. (5), $f = a_{1x}a_{1y}a_{1z}/(a_{2x}a_{2y}a_{2z})$ represents the ratio between the inner and outer volume, and $j = 1, 2$ refers to the inner and outer radius a_1 and a_2.

Similar to above, to sustain MSR in an anisotropic sphere or ellipsoid, Eq. (7) and Eq. (8) need to be satisfied.

$$\mu_{j,i} = -2\mu \tag{7}$$

where $i = x, y, z$ is the direction of incident field, j is the direction where the quasi-static approximation is applicable. Eq. (7) is determined by the direction i $(= x, y, z)$ of applied magnetic field.

From the expression for isotropic ellipsoid above, it is not difficult to generalize the results to the anisotropic case:

$$\mu_{j,i} = \frac{L_i - 1}{L_i}\mu \tag{8}$$

REFERENCES

1. Smith, D. R., Padilla, W. J.,Vier, D. C., Nemat-Nasser, S. C., and Schultz, S., "Composite Medium with Simultaneously Negative Permeability and Permittivity," *Phys. Rev. Lett.*, Vol. 84, No. 18, 4184–4187, 2000.
2. Kabiri, A. and Ramahi, O. M., "nth order rose curve as a generic candidate for rf artificial magnetic material," *J. Appl. Phys. A.*, Vol. 103, No. 3, 831–834, 2011.
3. Valentine, J., Zhang, S., Zentgraf, T., Ulin-Avila, E., Genov, D. A., Bartal, G., and Zhang, X., "Three-dimensional optical metamaterial with a negative refractive index," *Nature*, Vol. 455, 376–379, 2008.
4. Alù, A., Salandrino, A., and Engheta, N., "Negative effective permeability and left-handed materials at optical frequencies," *Opt. Express* , Vol. 14, No. 4, 1557–1567, 2006.
5. Ren, Z. and Ramahi, O. M., "Scattering from Spherical Particles with Negative Permeability," in *IEEE International Symposium on Antennas and Propagation*, Chicago, U.S.A, July 2012, *in press.*

Quantitative mapping of plasmonic near-fields using infrared far-field vibrational spectroscopy

D. Dregely[1*], F. Neubrech[1], H. Duan[2], and H. Giessen[1]
[1]4th Physics Institute and Research Center SCoPE, University of Stuttgart, Germany
[2]Institute of Materials Research and Engineering, A*STAR, Singapore
[*]corresponding author: d.dregely@physik.uni-stuttgart.de

Abstract We present a new method to measure plasmonic near-field intensities in the mid-IR and THz region. We position a nanoscopic molecular probe at different locations of plasmonic structures with 10 nm accuracy and measure the resonantly enhanced molecular vibrational signal with far-field spectroscopy. In that way we map the near-field intensity along a dipole antenna and find that the vibrational strength in the gap of a gap-type antenna is 5.9 times enhanced when compared with the edge of the antenna.

Plasmonic nanoantennas confine electromagnetic fields at visible and infrared wavelengths to volumes of only a few cubic nanometers. Assessing their near-field distribution offers fundamental insight into light-matter coupling [1]. In particular resonantly enhanced near-field intensities in the IR and THz region are important for future sensing techniques in analytical science, medicine, and industry since the molecular fingerprints are situated in this spectral domain.

Surface enhanced infrared spectroscopy (SEIRS) with a variety of different geometries of nanoantennas was brought forward by several groups to identify very small quantities of molecular substances [2,3].

Here, we use antenna-enhanced SEIRS of a localized nanoscopic molecular patch to map plasmonic near-field intensities of rod and gap-type nanoantennas with 10 nm accuracy. Compared to scanning near-field optical microscopy techniques [4,5] our technique uses conventional FTIR far-field spectroscopy which avoids tip-sample interaction. Therefore, it is also suitable for measuring complex embedded three-dimensional plasmonic structures.

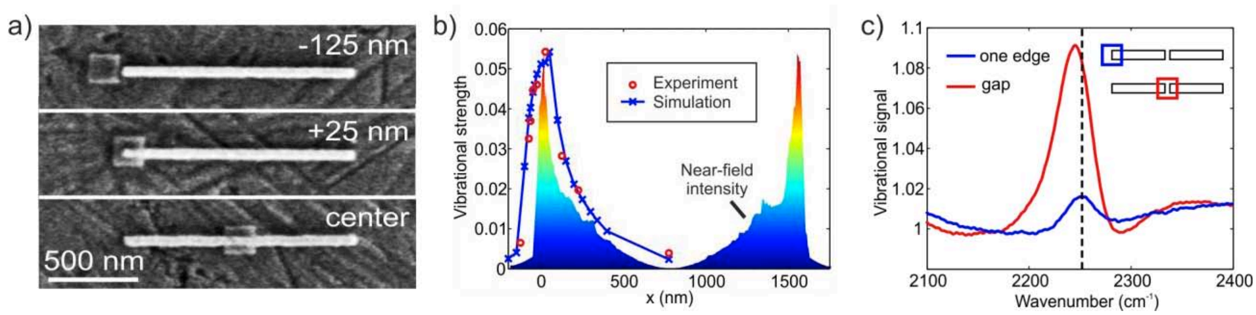

Figure 1: a) SEM images of plasmonic gold rod antennas in resonance with the vibrational band of HSQ at 2252 cm^{-1}. Three different exemplary patch positions with respect to the left antenna edge are shown. b) Measured (red dots) and simulated (blue crosses) far-field vibrational signal strength as a function of the patch position with respect to the left antenna edge. The rainbow-colored area plot is the numerically calculated total near-field

intensity of the gold rod antenna normalized to the experiment. c) Vibrational signal of a HSQ patch at the antenna gap (red curve) and at one edge of the gap-type antenna (blue curve). The inset is a schematic of the patch position in the gap (red square) and at one edge (blue square) of the gap-type antenna.

We patterned nanoscopic hydrogen silsesquioxane (HSQ) patches and shifted their position with respect to gold nanoantennas using a two-step electron beam process (see Fig. 1a). The vibrational Si-H band of HSQ at 2252 cm^{-1} is resonantly enhanced near the plasmonic nanoantenna, and the far-field vibrational strength depends directly on the local near-field intensity.

In experiment we realized 9 different patch positions along the dipole antenna. By extracting the vibrational strength as a function of the patch position we achieved accurate mapping of the plasmonic near-field intensity. We confirm our findings with numerical simulations and find excellent quantitative agreement (see Fig. 1b).

Additionally, for each patch position, we fabricated five different antenna lengths to shift the plasmon resonance with respect to the vibrational band, and hence tuned the lineshape of the Fano resonance. This assured that we accounted experimentally for detuning effects.

Furthermore, we applied our method to gap-type antennas and studied the near-field intensity in the gaps. We observe a 6-fold enhancement of the vibrational signal for a resonant gap-type antenna when the patch is positioned at the 55 nm wide gap compared to the patch positioned at one edge of the antenna (see Fig 1c).

Our method is capable to map plasmonic fields from the near infrared to the THz spectral region, since a large amount of molecular vibrational fingerprints is available in this spectral region. The variety of linewidth, vibrational strength, and spectral location available in the IR and THz region combined with the positioning accuracy of electron-beam lithography renders our technique an extremely versatile and quantitative analysis tool.

Acknowledgements We acknowledge funding by DFG (SPP1391, FOR730, and GI 269/11-1), BMBF (13N10146), and Baden-Württemberg Stiftung. D.D. additionally acknowledges support by the Carl-Zeiss-Stiftung. H.D. thanks for the partial support by A*STAR and NSFC (11274107 and 61204109).

REFERENCES

1. Novotny, L. and N. van Hulst, "Antennas for light," *Nat. Photonics*, Vol. 5, No. 2, 83-90, 2011.
2. Neubrech, F., et al., "Resonant plasmonic and vibrational coupling in a tailored nanoantenna for infrared detection," *Phys. Rev. Lett.*, Vol. 101, No. 15, 157403, 2008.
3. Wu, C., et al., "Fano-resonant asymmetric metamaterials for ultrasensitive spectroscopy and identification of molecular monolayers," *Nat. Mater.*, Vol. 11, No. 1, 69-75, 2012.
4. Schnell, M., et al., "Controlling the near-field oscillations of loaded plasmonic nanoantennas," *Nat. Photonics*, Vol. 3, No. 5, 287–291, 2009.
5. Dorfmüller, J., et al., "Fabry-Pérot resonances in one-dimensional plasmonic nanostructures," *Nano Lett.*, Vol. 9, No. 6, 2372-2377, 2009.

Enhanced Emission of Waveguide Thermal Emitter by Incorporating Metal Nanoparticles in Periodic Hole Arrays

Pei-Wen Wu, Che-Hsuan Cheng, Hung-Hsin Chen, and Si-Chen Lee*
Graduate Institute of Electronics Engineering, National Taiwan University, No. 1, Sec. 4, Roosevelt Road, Taipei, 10617 Taiwan. , TEL:886-2-33662000, FAX:886-2-23621877, * sclee@ntu.edu.tw

Abstract- Recently, numerous studies have been conducted to investigate the emission and transmission properties through the periodic hole arrays by using various metallic nanoparticles (NPs) [1,2] and coupled structures [3]. However, very few researches focused on the mid-infrared regime due to the weak intensities of infrared sources. In this paper, we incorporate different kinds of nanoparticles into micro-scaled periodic hole arrays of the waveguide thermal emitter (WTE) [4] and investigate its emission properties in the mid-infrared regime.

Fig. 1 displays the fabrication processes of the WTE structure with embedded metal NPs (gold, silver, and chromium). The WTE consists of tri-layer 150nm gold/ 2μm SiO_2/ 80nm gold layers deposited on the front and Mo was on the back of the silicon substrate. The top gold film was perforated with periodic hole arrays with period of 2.3μm and hole diameter of 1.15μm. Next, different kinds of metal film were deposited inside holes and then rapid thermal annealed (RTA) at 450°C for 2 minutes to form randomly sized and distributed NPs, the SEM pictures of 3nm gold and chromium film after RTA are shown in Fig. 2 (a) and (b), respectively. The electric current was sent into Mo layer to heat up WTE and the waveguide mode was excited by black body radiation from oxide film and emitted through the holes on the top metal. Fourier Transform Infrared Spectrometer (FTIR) was used to measure the reflection and emission spectra in the normal direction.

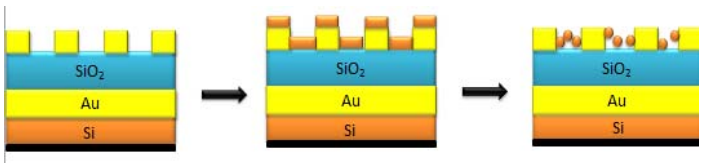

Fig. 1: Fabrication processes of the WTE with metal nanoparticles embedded.

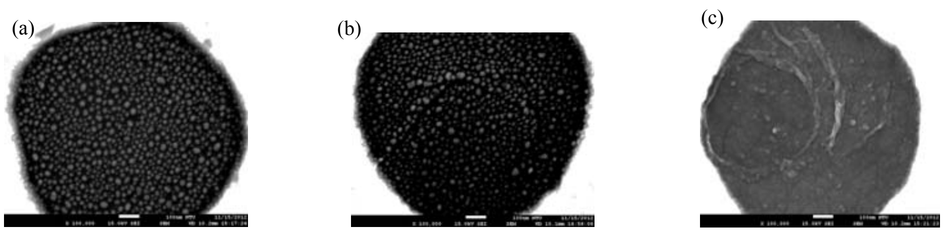

Fig. 2: SEM pictures of the random sized (a) gold, (b) silver, and (c) chromium NPs inside the perforated hole.

Figure 3(a) displays the normalized reflection spectra of the WTE without and with 3 nm gold film on top and after RTA. It is evident from Fig. 3(a) that the reflection intensity decreases with gold NPs embedded in holes. And the similar result was got as gold NPs replaced by silver NPs. WTE with chromium NPs showed a little bit dipper on reflection spectra but not that evident as gold and silver. Fig. 3(b) shows the emission spectra of WTE operated at 150^{o}C with different kinds of metal NPs. It is clear that the emission peak positions stay the same after metal NPs incorporated in structure. The maximum increase in emission intensity was found when gold NPs used. Theoretically, holes with random nanoparticles inside should screen out part of the emission and result in lower emission of light. However, the results are opposite. Random meatl NPs enhance the emission intensity. It is believed that the large accumulative scattering effect from all directions and plasmoinc-like resonance between different nano-sized particles may bring about the enhancement.

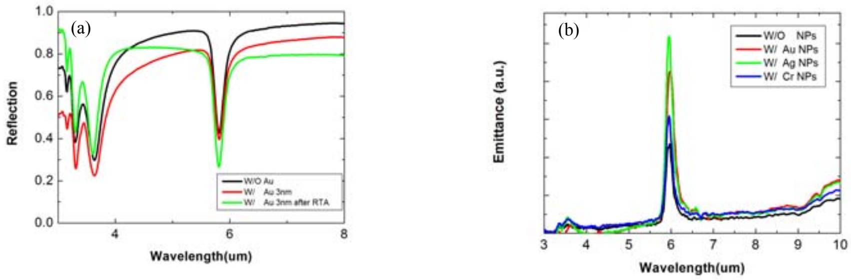

Fig. 3: (a) Reflection spectra of WTE incorporated with gold NPs.
(b) Emission spectra of WTE incorporated with different kind of metal NPs.

In conclusions, the enhanced emission with random metal nanoparticles embedded in periodic hole arrays were demonstrated. This unique design by integrating localized and propagating surface plasmons together provides an easy way to improve the emission intensity of WTE and a better device for IR application, such as biosensors, solar cells, and surface enhanced SERS.

Acknowledgements

The authors would like to thank the National Science Council of the Republic of China and the center of Advanced Nano-Materials of National Taiwan University for financial support under Contract Nos. NSC 99-2120-M-002-002 and“Novel Infrared devices and applications 99R80202”.

REFERENCES

1. Brian K Canfield, Sami Kujala, Konstantins Jefimovs, Tuomas Vallius, Jari Turunen, d Martti Kauranen, J. Opt. A: Pure Appl. Opt. **7,** 2005.
2. Hong Wei, Daniel Ratchford, Xiaoqin (Elaine) Li, Hongxing Xu, and Chih-Kang Shih, Nano Lett. Vol.9 No. 12, 2009.
3. Zhaoguang Pang, Xinping Zhang, and Tianrui Zhai, J. Appl. Phys., **110**, 074313, 2011
4. Y. T. Wu, Y. T. Chang, H. H. Chen, H. F. Huang, D. C. Tzuang, Y. W. Jiang, P. E. Chang, and S. C. Lee, IEEE Photon. Tech. Lett., **22**, 1159-1161, 2010

Surface Plasmon Waves for Subwavelength Far-Field Imaging at Visible Wavelengths

A. Ourir[1*], **and M. Fink**[1]

[1] Institut Langevin, Laboratoire Ondes et Acoustique, ESPCI, CNRS UMR 7587, 1 rue Jussieu, 75238, Paris Cedex 05

[*]corresponding author: a.ourir@espci.fr

Abstract- We present here a simple and original concept for subwavelength far field imaging at visible wavelengths. The proposed far field superlens consists of a finite size ultrathin metallic slab. We demonstrate that surface plasmon polaritons (SPPs) propagating on the interfaces lead to subwavelength Faby-Perot like modes in the case of a finite size slab. A numerical time reversal imaging process applied to this lens achieves far field imaging of objects with a resolution higher than $\lambda/10$ in the visible range.

We have proposed in recent work to use a finite collection of resonators to transmit efficiently subwavelength scale information in the far field [1, 2, 3]. The proposed metalenses can convert the near field of an object to diffraction limited waves that can be collected efficiently in the far field.

In this paper, we propose to use a metallic slab with finite sizes for subwavelength far field imaging at visible wavelengths. We study the properties of the surface plasmon polaritons (SPPs) that can propagate at the interfaces of the proposed ultrathin slab of platinum. We demonstrate that these SPPs lead to subwavelength Faby-Perot like modes in the case of a finite size slab. We show that subwavelength focal spot can be achieved using a time reversal far field focusing over the slab.

To obtain subwavelength SPPs at visible wavelengths, we consider the slab of platinum of a thickness h shown in Fig. 1(a). Actually, by using a mechanism for depression of the plasma frequency into the desired frequency band [4], other metals can be considered. The dispersion relation, plotted in Fig. 1(b) confirms that small wavelength of the SPPs can be obtained with a 10 nm-thick slab of platinum. Consequently, we use this slab for our subwavelength far field application.

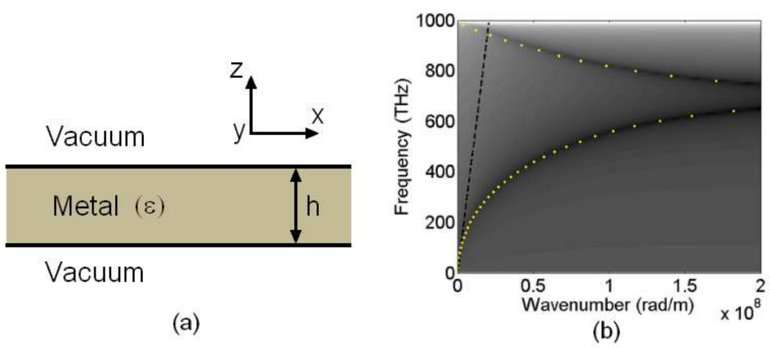

Fig. 1 : (a) Schematic view of the Metallic slab surrounded by vacuum. (b) Dispersion curves for 10 nm-thick slab. The black (dark) dotted curve is the light line and the yellow (bright) dots correspond to the electrostatic solutions.

The normal electric field propagating at each interface of the slab cannot escape because the period of the field is smaller than vacuum wavelength. In case of a finite size slab, the system behaves like a Fabry-Perot cavity for surface waves. A wavenumber quantification is then induced and a finite number of eigenmodes is generated. Because of the finite size of the structure, some components of the Fourier transform of these eigenmodes contain spatial periods that are equal or larger than the wavelength. Consequently, the generated subwavelength modes can radiate efficiently with their respective patterns[2, 5].

To show the "superlens" effect of our structure, we start by performing a far field subwavelength focusing of light using time reversal techniques [3, 6]. To that aim, we place 8 detectors in the far field all around the metallic slab. After exciting the structure using small evanescent wave source, we record the radiated field at each detector. Time reversed waves are then generated and emitted at the detectors positions. Fig. 2 illustrates the far field focusing results obtained by time reversal focusing (λ=460 nm to 545 nm) and with 8 transmitters placed in the far field. The thinnest focal spot (<$\lambda/10$) is obtained when combining spatiotemporal effects.

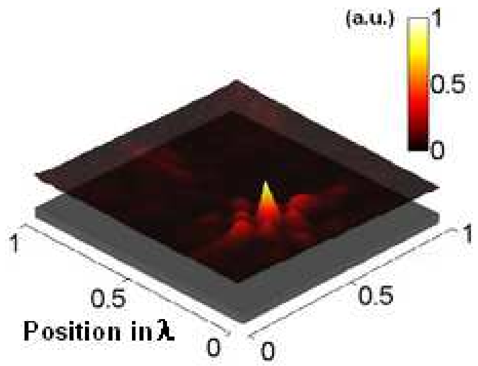

Fig. 2 : Focal spot obtained by time reversal focusing (λ=460 nm to 545 nm) and with 8 transmitters placed in the far field.

We have proposed to use a finite size metallic slab for subwavelength far field imaging at visible wavelengths. By using a time reversal techniques, we have achieved far field subwavelength imaging with this lens. The structure we have proposed is easy to realize and its response is not affected by the imaged objects. Moreover, this lens is less sensitive to losses than resonant metalenses.

REFERENCES

1. A. Ourir, G. Lerosey, F. Lemoult, M. Fink, and J. de Rosny, “Far field subwavelength imaging of magnetic patterns,” Applied Physics Letters, vol. 101, no. 11, p. 111102, 2012.
2. F. Lemoult, G. Lerosey, J. de Rosny, and M. Fink, “Resonant metalenses for breaking the diffraction barrier,” Phys. Rev. Lett., vol. 104, p. 203901, May 2010.
3. G. Lerosey, J. de Rosny, A. Tourin, and M. Fink, “Focusing beyond the diffraction limit with far-field time reversal,” Science, vol. 315, no. 5815, pp. 1120–1122, 2007.
4. J. B. Pendry, A. J. Holden, W. J. Stewart, and I. Youngs, “Extremely low frequency plasmons in metallic mesostructures,” Phys. Rev. Lett., vol. 76, pp. 4773–4776, Jun 1996.
5. C. Jouveaud, A. Ourir, and J. Rosny, “Surface waves radiation by finite arrays of magnetoelectric resonators,” Progress In Electromagnetics Research, vol. 132, pp. 177–198, 2012.
6. M. Fink, “Time reversed acoustics,” Physics Today, vol. 50, no. 3, pp. 34–40, 1997.

Nonreciprocal Plasmonics: Thin Film Faraday Rotator

Jessie Y. Chin[1], Tobias Steinle[1], Thomas Wehlus[2], Thomas Weiss[1], Daniel Dregely[1], Vladimir Belotelov[3], Bernd Stritzker[2], and Harald Giessen[1]

[1]4th Physics Institute and Research Center SCOPE, University of Stuttgart, 70569 Stuttgart, Germany

[2]Institute of Physics, University of Augsburg, 86135 Augsburg, Germany

[3]Lomonosov Moscow State University, Faculty of Physics, 119991 Moscow, Russia

[*]corresponding author: j.chin@physik.uni-stuttgart.de

Abstract We here demonstrate thin film Faraday effect enhanced by plasmonics. By hybridizing magneto-optics and plasmonics, we report experimental enhancement of Faraday rotation up to one order of magnitude. Numercial simulation is found to agree well with the experimental results and explains the mechanism behind the large Faraday effect.

The propagation of light is usually reciprocal. The Faraday effect, where light travels through a magnetized material experiences a rotation of the polarization plane, and when it travels back, the polarization plane does not resume but is further rotated, breaks this reciprocity. The Faraday effect in available materials is usually weak, and consequently Faraday rotators are rather bulky. Enhancing Faraday rotation is of particular importance as the recent development of integrated optics demands thin film devices that are easier to integrate. Previously, a plasmonic heterostructure [1] and a planar photonic crystal [2] were suggested for enhancement of the Faraday effect, but neither has been realized in experiment. Here we report the first experimental demonstration of Faraday rotation enhanced plasmonically by about one order of magnitude.

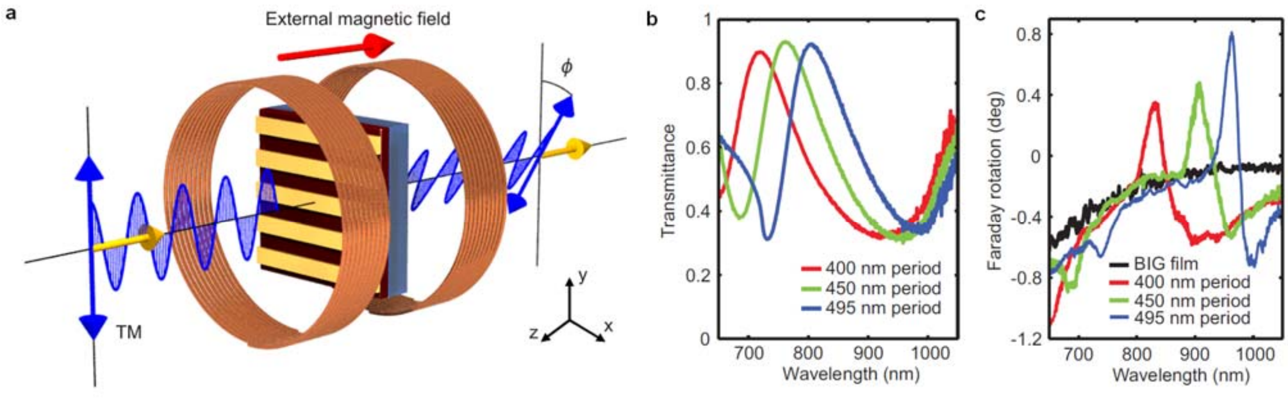

Figure 1: a) Faraday rotation by a magneto-plasmonic thin film Faraday rotator. TM polarization is defined as perpendicular to the wires. b) Measured transmittance for the three samples with different periods and a schematic of the magneto-plasmonic Faraday rotator (inset). (c) Measured Faraday rotation for the three samples compared with the bare BIG film.

We consider a plasmonic photonic crystal consisting of periodic gold nanowires structured on thin films of MO materials (Fig. 1a). A localized plasmon resonance is excited when the incident light is TM polarized. In such a configuration, the MO film acts as a photonic crystal waveguide for photons. The local plasmons and the waveguide interact strongly, contributing to a hybrid TM mode. When the incident light is TE polarized, there is only the waveguide resonance inside the MO photonic crystal, defined as TE mode. The coupling between the TM and the TE modes alters the MO properties of the system.

We fabricated three samples of magneto-plasmonic Faraday rotators, each of which consists of periodic gold nanowires, structured by electron beam lithography on a thin film of bismuth iron garnet (BIG). The samples have different periods of p=400 nm, p=450 nm, and p=495 nm, respectively. The gold nanowires have a constant width of 120 nm and height of 65 nm. The 150 MO thin film of BIG was prepared by pulsed laser deposition. The inset of Fig. 2a illustrates the profile of the magneto-plasmonic Faraday rotator.

We first characterize the transmittance spectra of the samples by white light transmission spectroscopy. The spectrum of each sample (see Fig. 2b) exhibits two pronounced transmission dips, corresponding to the interacting plasmonic and photonic crystal waveguide resonances. Spectral shifts of the features can be observed when the period increases from 400 nm to 495 nm. Faraday rotation is measured using a rotating-analyzer polarimeter, where a 140 mT magnetic field is applied normal to the film. Spectra of Faraday rotation are displayed in Fig. 2c for the samples and the reference BIG film. The maximum Faraday rotation increases gradually with the period p. For the sample with 495 nm period reaches the maximum Faraday rotation of 0.80° at λ=963 nm. Compared to the BIG film. The Faraday rotation is enhanced by 9 times. We achieve, to our knowledge, the largest enhancement of Faraday rotation by plasmonics. At λ=963 nm, the sample has 36% transmittance, which implies that the Faraday rotator is rather transparent. It also exhibits broadband properties as the half-value bandwidth of 0.8° Faraday rotation is 22 nm.

Numerical simulations using S-matrix methods agreed very well with measured spectra. Dispersion diagrams of the particle-plasmon-waveguide polaritons elucidate the detailed coupling mechanism: the maximum Faraday rotation of our hybrid sample takes place in the vicinity of the crossing of TM and TE modes. At TM incidence, the primary electric field component is along the y-axis (Fig. 1a), and a secondary electric field component comes into existence due to the off-diagonal elements of the MO film’s permittivity tensor. Near the TM/TE mode crossing, effective TM-to-TE conversion due to the Faraday rotation takes place.

Our magneto-plasmonic system can be further engineered and may lead to ultracompact device applications in optical systems. The concept could also be applied to large area plasmonic-enhanced optical rotators and isolators.

Acknowledgements Our work was supported by BMBF (3D Metamat and FARADAY), Carl- Zeiss Stiftung, BW Stiftung, AvH foundation, GIF and DFG.

REFERENCES

1. K. Fang, Y. Yu, V. Liu, and S. Fan, “Ultracompact nonreciprocal optical isolator based on guided resonance in a magneto-optical photonic crystal slab,” *Opt. Lett.* Vol. 26, 4254, 2011.
2. V. I. Belotelov, L. L. Doskolovich, and A. K. Zvezdin, “Extraordinary Magneto-Optical Effects and Transmission through Metal-Dielectric Plasmonic Systems,” *Phys. Rev. Lett.* Vol. 98, 077401 (2007).

Enhancement spectra of light emission caused by surface plasmon scattering in low-molecular-weight organic materials

S. Kawasaki[1], Y. Horikoshi[1], A. Yamazaki[1], H. Kawase[1], K. Kasahara[1*], N. Ikeda[2], and Y. Sugimoto[2]
[1]Graduate School of Science and Engineering, Ritsumeikan University, Kusatsu, Shiga 525-8577, Japan
[2]Nanotechnology Innovation Center, National Institute for Materials Science, Tsukuba 305-0047, Japan
kasahara@se.ritsumei.ac.jp

Abstract-Surface-plasmon-enhanced light emission spectra in low-molecular-weight organic materials were investigated by changing metals. For the interpretation of the spectra, the influence of an inhomogeneously broadened excited state present in disordered organic materials, and a intermolecular distance have to be taken into account. A peak wavelength shift which appeared in the enhancement spectra suggests some energy shift mechanism, such as Förster energy transfer, related closely to it.

The surface roughness naturally formed on an Ag film was reported to enhance the light extraction efficiency from coumarin 460 doped in PMMA[1]. There have been several experimental and theoretical studies of surface plasmon (SP) scattering[2-4]. It helps increase outgoing light of emitters with a medium-to-low luminescence efficiency. Since the SP density state affects the exciton-to-SP energy transfer rate, SP-induced emission should generally grow monotonously as wavelengths come close to the plasma wavelength. However, we noticed through experiments on the annealing of metals that the pitch and height of the surface irregularity exercise an influence on the position of the peak wavelength of enhancement brought by the SP scattering. The maximum enhancement occurred at wavelengths longer than the plasma wavelength, which we found appeared without annealing. Here, we report the detailed experimental results of the spectra of surface-plasmon-enhanced light emission in low-molecular-weight organic materials. A peak wavelength shift observed in the enhancement spectra indicates that Förster energy transfer had an impact on it in addition to self-absorption.

α-NPD was deposited by thermal deposition on a glass substrate, where a 200 nm-Ag (or Au) film was formed partially. The thickness of α-NPD was varied from 20 to 100 nm. The irregularity of the glass observed with an AFM was ~ 60 nm in the vertical direction. A 405 nm blue semiconductor laser diode was used as an excitation light source. Compared with the spectra without metal, whose peak wavelengths were ~440 nm and constant irrespective of the thickness, we found that the peak wavelengths for the α-NPD on the metal moved according to the thickness. Figures 1 (a) and (b) show the ratio of the PL enhancement with and without the metal on the glass. It is striking that the enhancement peak wasn't at the calculated respective plasma wavelengths, 380 nm and 530 nm for the organic film/Ag and Au, and that the shift of the peak wavelength to longer wavelengths was accompanied by an increase in the thickness of α-NPD. On the whole, enhancement peaks of the devices on Ag were located on the longer wavelengths than those on Au. PL enhancement was at a maximum with 40-nm devices, 7.8 at 480 nm and 5.2 at 580 nm for Ag and Au devices, respectively. We measured the enhancement data using an integration sphere, and the peak shift was observed with an increase in the thickness as well. Furthermore, these phenomena appeared with Alq_3.

The experimental results obviously indicated that a portion of energy in excited states in the α-NPD moved after the SP scattering. Aside from excitons, localized electronic states (traps) associated with chemical impurities, structural disorder, and surface states should be the source transferring its energy to the SP. However, if the trap level is positioned too deep from the LUMO level, energy exchange with the SP becomes difficult. It is reasonably anticipated that the region adjacent to the interface between the metal and organic material was in such a situation, and the small enhancements seen in the 20-nm devices in Figs. 1 (a) and (b) would be ascribed to this. The enhancement that followed 40 nm was smaller in thicknesses. This was natural since the contribution of the SP scattering was lowered, because it was too thick and exceeded the SP penetration depth.

In addition to the self-absorption, the Förster energy transfer mechanism, which occurs in inverse proportion to the molecular distance raised to the sixth power, should become involved in the spectral peak shift, and seems to have played a major role in the peak shift. For example, the absorption of the light generated from the SP scattering at 410 nm reaches 21% in the course of propagation across the 40 nm thick organic layer. This is, however, difficult to account for the spectral change between 20 nm and 40 nm devices on Ag in Fig. 1 (a). The input-output characteristics of optically pumped lasing from Alq_3: DCM system has been shown to be significantly distorted owing to the presence of inhomogeneous broadening. Intermolecular distance is short in low-molecular-weight organic materials such as α-NPD and Alq_3, as compared with the coumarin-doped PMMA. Accordingly, it is probable that energy transfer arises from an organic molecule in the state of relatively high LUMO level to a neighboring molecule in a low LUMO level due to Förster mechanism. This moves the enhancement peak towards long wavelengths with an increase in the thickness of an organic layer.

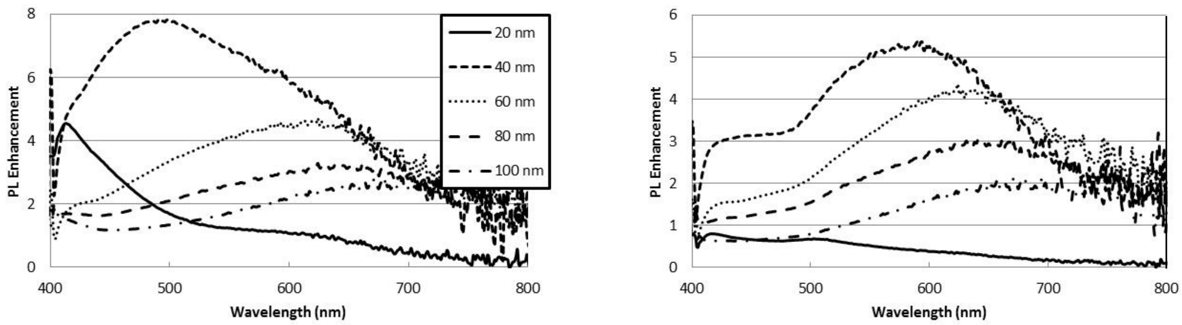

(a) (b)

Fig.1 Enhancement spectra of α-NPD defined by the PL ratio of with a metal to without the metal. (a) Ag and (b) Au. Light output of the blue laser diode was 4 mW and the spot size on the devices was ~1 mmϕ.

REFERENCES

1. Neal, T. D., K. Okamoto and A. Scherer, “Surface plasmon enhanced emission from dye doped polymer layers,” *Opt. Exp.*, Vol. 13, No. 14, 5522-5527, 2005.
2. Park, H.-J., D. Vak, Y.-Y. Noh, B. Lim and D.-Y. Kim, “Surface plasmon enhanced photoluminescence of conjugated polymers,” *Appl. Phys. Lett.*, Vol. 90, 161107-1-3, 2007.
3. Sun, G., J. B. Khurgin and R. A. Soref, “Practical enhancement of spontaneous emission using surface plasmons,” *Appl. Phys. Lett.*, Vol. 90, 111107-1-3, 2007.
4. Tam, M. C., H. Su, K. S. Wong, X. Zhu and H. S. Kwok, “Surface-plasmon-enhanced photoluminescence from metal-capped Alq_3 thin films,” *Appl. Phys. Lett.*, Vol. 95, 051503-1-3, 2009.

Dielectric Sensing based on Energy Tunneling in Wire-loaded Microstrip Cavities

Abdullah Nauroze[1], Omar Sidiqui[2]*, Rashad Ramzan[3], and Omar Ramahi[4]
[1]National University of Computer and Emerging Sciences (FAST-NU), Islamabad-44000, Pakistan
[2]Taibah University, Madinah, Saudi Arabia
[3]United Arab Emirates University, AlAin-15551, UAE
[4]University of Waterloo, Waterloo, Ontario, Canada

*corresponding author: omarsiddiqui2@gmail.com

Abstract-The electromagnetic energy tunneling which takes place in narrow channels and bends loaded with epsilon-near-zero materials or resonant wires is accompanied by very intensive electric fields. The resulting transmission response is, therefore, highly frequency selective. Hence such configurations can be employed in highly sensitive dielectric detection. In this paper, the energy tunneling set-up is created in a microstrip environment using resonant wires. The dependence of various wire and microstrip parameters on the sensitivity of the sensor is studied. The microstrip technology, compared to the rectangular waveguides, is low cost, robust, easily manufactureable and suitable for planar integration.

The dispersion regimes supporting energy tunneling are identified by diminishing group velocities along one of the structure's axes of symmetry and the flatness of the dispersion surfaces, leading to permittivities that are close to zero. Hence such materials have also been termed as epsilon-near-zero materials (ENZ) [1-3]. When these materials are interfaced with free space, a strongly directive electromagnetic propagation is observed where energy tunnels or squeezes through sub-wave length apertures [1-3]. The property of high field build-up in these narrow channels can be exploited to obtain highly sensitive dielectric sensors [4]. A rectangular waveguide arrangement that supports energy tunneling is depicted in Fig. 1a. It is a 180° short-circuited bend where two rectangular waveguides are connected through a narrow channel filled with an ENZ material. More recently, analogous energy-tunneling effects have also been observed in waveguide bend loaded with wires. The metallic wires, in such configuration are directed parallel to the electric (E) field [5]. It can be inferred, at least in a qualitative manner, that the tunneling can also take place in other guided media if the wires are placed to match the direction of dominant electric field component. To support this argument, a microstrip cavity is studied which is formed by placing two microstrip transmission lines on top of each other with a common ground, as shown in Fig. 1b. The wire is placed in front of the conductor backing inside the aperture that connects the two microstrip lines. Two simulation studies are performed using Agilent's HFSS, first with the air substrate and second with a Rogers 5880. As depicted in Fig. 2, the proposed cavity indeed supports the tunneling mode that is highly sensitive to the dielectric material that fills the cavity. A resonance frequency shift of −1.335 GHz is noted for the permittivity shift +1.2. Simulation studies are performed to determine the geometric parameters of the cavity that affect the sensitivity so that a practical sensor can be designed. The microstrip transmission lines are planar and are much easier to fabricate and electrically fed compared to the rectangular waveguides. .

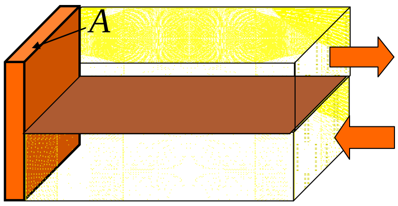

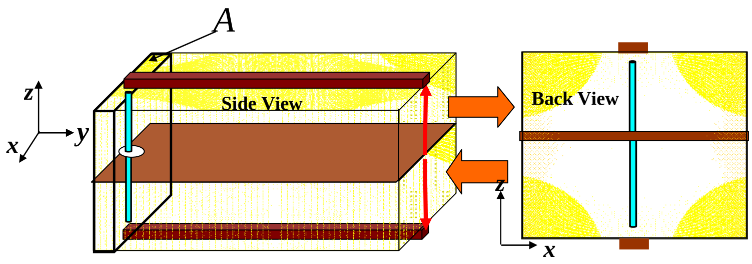

(a) (b)

Fig 1: (a) Two short-circuited wave guides connected with ENZ material and (b) Two views of the proposed microstrip wire-loaded cavity.

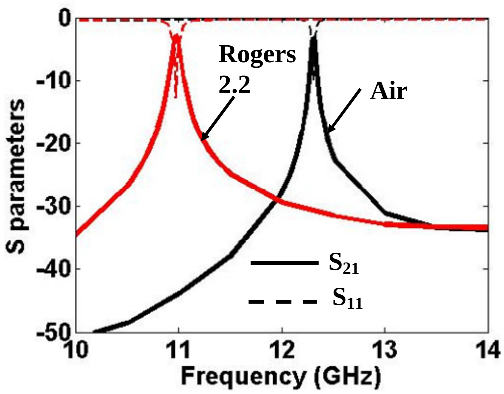

Fig. 2: Simulation Results for the microstrip cavity given in Fig 1b

REFERENCES

1. A. Alu and N. Engheta, "Light Squeezing through Arbitraily Shaped Plasmonic Channels and Sharp Bends," Physical Review B, vol. 78, pp. 035440-035445, July 2008
2. A. Alu, M. Silveirinha, and N. Engheta, "Transmission-Line Analysis of Epsilon-Near-Zero (ENZ)-Filled Narrow Channels" Phsyical Review E, Vol. 78, 016604 (10 pages), 23 July 2008
3. M. G. Silveirinha and N. Engheta, “Theory of supercoupling, squeezing wave energy, and field confinement in narrow channels and tight bends using ε near-zero metamaterials” Phys. Rev. B., vol. 76, no. 24, , pp. 245109 (1) -245109(17), Dec. 2007
4. A. Alu and N. Engheta, "Dielectric Sensing in Epsilon-Near-Zero Narrow Waveguide Channels," Physical Review B, Vol. 78, 045102 (5 pages), July 3, 2008.
5. O.F. Siddiqui and O. Ramahi,, "A Novel Dielectric Detection System Based on Wire-Loaded Waveguides", IEEE Microwave and Wireless Components Letters, vol. 21, no.2 ,Feb. 2011.

Metamaterial-Inspired Bandpass Filter for the Terahertz Goubau Line

Ali K. Horestani[1], **Withawat Withayachumnankul**[1], **Christophe Fumeaux** [1], **Derek Abbott**[1], **and Tahsin Akalin**[2]

[1]School of Electrical & Electronic Engineering, The University of Adelaide, Adelaide, Australia
[2]Institut d'Electronique de Microelectronique et de Nanotechnologie IEMN, France
akarami@eleceng.adelaide.edu.au, tahsin.akalin@iemn.univ-lille1.fr

Abstract— Recently, it has been shown that a single wire Goubau line that supports surface wave propagation can be used as an effective terahertz waveguide with low attenuation and low dispersion. In order to fully exploit Goubau lines in terahertz systems, for example for communication applications, structures such as different types of passive filters are required. This abstract demonstrates that metamaterial elements can be used as building blocks for realization of compact bandpass Goubau line filters.

Despite the emerging interest in terahertz systems and their applications in sensing, imaging and communications, there is still a need for efficient low-loss waveguides in the terahertz regime. Even though hollow waveguides and two-conductor transmission lines such as coaxial cables and microstrip lines are efficient for low to moderate radio-frequency operation, scaling these waveguides for terahertz applications is not an efficient solution because of the finite conductivity of metals at this higher frequency range. On the other hand, in spite of their high efficiency, conventional optical interconnections such as fiber cables are bulky and can not be integrated in planar technologies [1]. Surface electromagnetic waves that propagate along the interface of a dielectric and a conductor, so-called surface-plasmon polaritons (SPPs), are one possible solution that has been proposed for realization of high speed on-chip interconnections, where thin metal circuitry can be used for carrying both the optical signals and electrical currents [1]. In particular, it was shown in [2] that a bare Goubau-like single metal wire that supports the propagation of surface waves [3] can be used as an efficient terahertz waveguide with low attenuation and low dispersion.

In order to exploit the propagation of surface waves on single wire in real applications, effective passive structures such as various types of filters are required. A bandstop filter based on the corrugated planar Goubau line (PGL) has been studied in [4]. It was shown that the structure provides a stopband characteristic for surface plasmon polariton propagation. More recently, an application of metamaterial resonators for filtering was investigated in [5]. A stopband in the transmission characteristics of the guided surface electromagnetic waves on a PGL was demonstrated computationally and experimentally. However, to the authors' knowledge, no study has been conducted on bandpass structures for PGL. In this paper we present a metamaterial-inspired bandpass filter for a modified PGL operating at sub-terahertz frequencies around 200 GHz.

In previously published work [6] Akalin et al. have presented a high-efficiency planar launching structure for a plasmonic wave on a PGL. The structure consists of a coplanar waveguide with a tapered section, which effectively converts the coplanar waveguide mode to the Goubau mode. It was also shown that adding a gap in the Goubau line results in almost no energy transmission, proving that the transmitted energy in the original structure is not due to the direct coupling of the launching sections. In the present paper, it is shown that if the gapped Goubau line is properly coupled to a pair of split-ring resonators (SRRs), as illustrated in Fig. 1(a), at the resonant frequency of the ring resonators, the surface wave can be transmitted across the gap via coupling through the SRRs. Therefore, the resonance condition of the SRR creates a narrow passband, and there is virtually no transmission of energy in the rest of the spectrum.

The concept has been investigated with full-wave 3D electromagnetic simulation using a 400 μm thick quartz crystal with a relative permittivity $\epsilon_r = 3.78$ as the substrate. The dimensions of the coplanar waveguide to Goubau line launching structure are $w = 50$ μm, $w_{\text{gnd}} = 190$ μm, $s = 5$ μm and $l_l = 650$ μm. The Goubau line has a width $w_G = 5$ μm and a total length $l_G = 2100$ μm including the 50 μm gap in the middle. The gap is loaded with a pair of SRRs with $a = 140$ μm, $g = 10$ μm and $c = 10$ μm. Since the electromagnetic wave along the PGL propagates in a quasi-TEM mode, which is strongly confined around the line and decays exponentially in the transverse

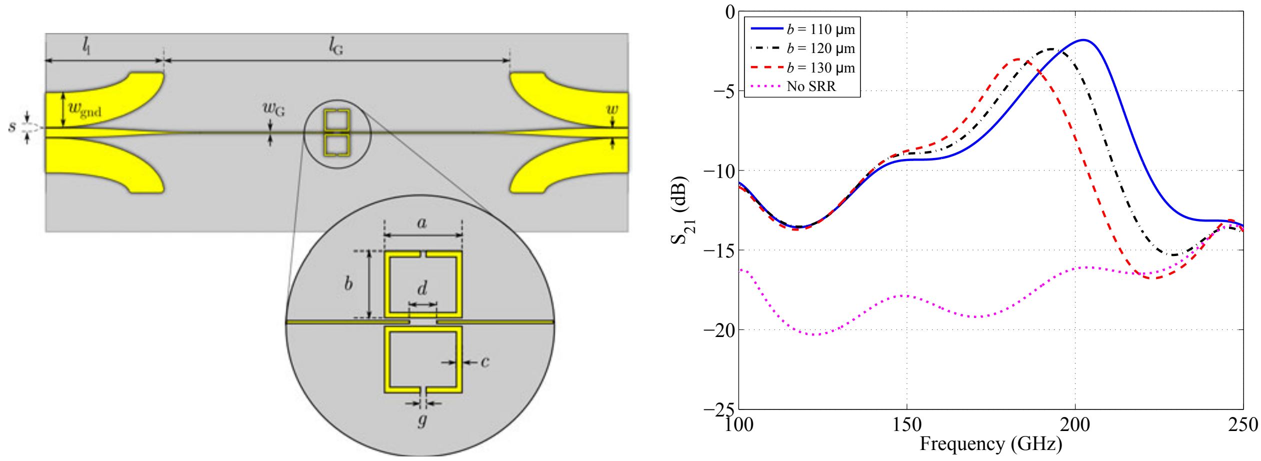

(a) (b)

Figure 1: (a) Top view of the metamaterial inspired bandpass Goubau line structure excited by coplanar waveguide launching sections. (b) simulated normalized transmission coefficients of the structure for three lateral dimensions of the SRRs, i.e. $b = 110\ \mu\text{m}, 120\ \mu\text{m}$, and $130\ \mu\text{m}$ as well as the structure without SRRs.

plane, the pair of single-ring SRRs are placed close to the PGL in order to maximize the magnetic coupling between both structures.

Fig. 1(b), depicts the simulated transmission coefficient of the structure for three different values of the SRRs' lateral dimension b. Note that in order to exclude the launching sections loss, the transmission coefficients of the bandpass structure are normalized to that of a structure without the gap and SRRs. Simulation results clearly demonstrate the bandpass behavior of the proposed structure with a with a central frequency that can be controlled by tuning the SRRs dimensions. More details about higher order bandpass filters for PGL and controlling the filter's bandwidth will be presented elsewhere.

Conclusion

This paper presents an application of metamaterial elements in the realization of bandpass filters for the PGL at sub-terahertz frequencies. Due to the exponentially decaying transverse electromagnetic field in the Goubau mode, a pair of SRRs needs to be placed in close proximity to a gapped Goubau line for strong coupling. This strong coupling results in transmission of energy exclusively in a narrow band around the SRRs resonance. The frequency and bandwidth of the passband can be controlled by optimizing the dimensions of the SRRs. Ongoing work includes structure fabrication and measurement.

REFERENCES

1. E. Ozbay, "Plasmonics: Merging photonics and electronics at nanoscale dimensions," *Science*, vol. 311, no. 5758, pp. 189–193, 2006.
2. K. Wang and D. Mittleman, "Metal wires for terahertz wave guiding," *Nature*, vol. 432, no. 7015, pp. 376–379, 2004.
3. G. Goubau, "Open wire lines," *IRE Transactions on Microwave Theory and Techniques*, vol. 4, no. 4, pp. 197–200, 1956.
4. T. Akalin, E. Peytavit, and J. Lampin, "Bendings and filters with single strip THz plasmonic waveguides," in *Joint 32nd International Conference on Infrared and Millimeter Waves, 2007 and the 2007 15th International Conference on Terahertz Electronics. IRMMW-THz.*, 2007, pp. 75–76.
5. W. Chen, J. Mock, D. Smith, T. Akalin, and W. Padilla, "Controlling gigahertz and terahertz surface electromagnetic waves with metamaterial resonators," *Physical Review X*, vol. 1, no. 2, 2011, art. no. 021016.
6. T. Akalin, A. Treizebré, and B. Bocquet, "Single-wire transmission lines at terahertz frequencies," *IEEE Transactions on Microwave Theory and Techniques*, vol. 54, no. 6, pp. 2762–2767, 2006.

Wide Band Silicon Mirror Based Grating Coupler for Silicon Integrated Photonics

Md Asaduzzaman[1,2], Masuduzzaman Bakaul[1,2], Stan Skafidas[1,2], Md Rezwanul Haque Khandokar[1,2]
(1) Department of Electrical & Electronic Engineering, The University of Melbourne, Parkville, Australia,
(2) NICTA (National ICT Australia Ltd.), Department of Electrical & Electronic Engineering, The University of Melbourne, Parkville, Australia
Author e-mail address: m.asaduzzaman@student.unimelb.edu.au

Abstract: A CMOS compatible Si grating waveguide coupler has been designed and simulated by finite difference time domain (FDTD) method. A highly efficient (90%) wide band (40 nm at 3dB) coupling has been achieved by exploiting the combined effects of surface grating and multilayer silicon mirrors.

Silicon-On-Insulator (SOI) provides the compatibility with well matured CMOS technology which opens the potentiality to integrate photonic devices with nano-electronic circuits. The high index contrast between silicon and oxide allows designing photonic devices in submicron scale with high density integration [1]. One of the key issues of such nano-scale devices is their integration with micro-scale optical links [2]. In this work, we have designed a high efficient, high bandwidth silicon coupler for interconnection between fiber and nano-scale waveguides by simultaneously applying techniques of light redirection, mirror-reflection, and surface gratings. The grating approach in designing such couplers exploits its fabrication simplicity and allows wafer level testing for mass production [4]. We took the advantages of using silicon-mirror in grating coupler that effectively overcome the efficiency limiting factors associated with coupling through the buried oxide (BOX) layer [5] and low bandwidth response of coupled light [6].

The structure of the proposed multilayer mirrored grating coupler is designed using a SOI wafer with dimensions of top-Si: 400nm and BOX: 1600 nm with grating at the top layer and a simple modification in the BOX layer as shown in Fig.1. The position of two 100 nm thin Si mirror layers is optimized for maximum efficiency. The grating period (Λ) is calculated using $\Lambda = \lambda / [n_{eff} - n_{top}\sin(\theta_{in})]$ [7] where λ is wavelength of incident light, n_{eff} is the effective refractive index of the structure, n_{top} is the refractive index of top cladding, θ_{in} is the incident angle normal to the surface (y-axis) of the structure. The extracted value of n_{eff} is found 2.38 using a fully vectorial mode solver „Lumerical Mode Solutions". The calculated value of Λ is 615 nm for the input optical wavelength of $\lambda = 1550$ nm, $n_{top} = 1$ (air) and, for incident angle $\theta_{in} = -8^0$. For clarity, this slight tilt angle helps enhancing the coupling of predominant first order diffraction by minimizing the effect of second order diffraction.

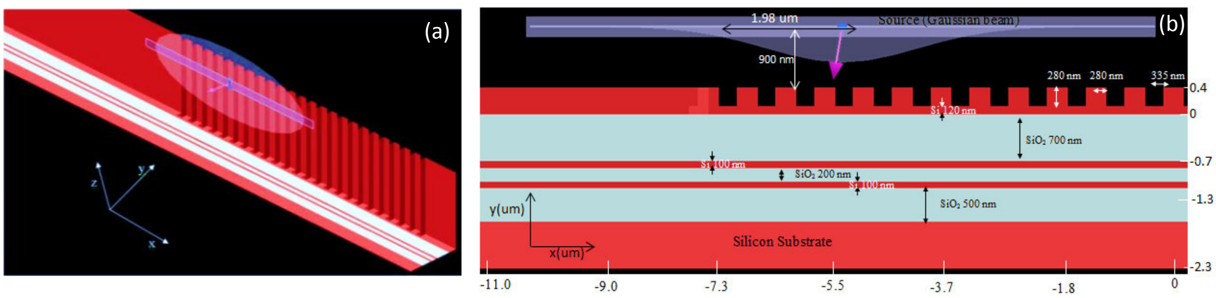

Figure 1: (a) Perspective view and (b) cross-section of the device structure

Based on the optimized design, the calculated grating depth (d) and width (w) are found 280 nm and 335 nm respectively using $\Lambda = 615$ nm and filling factor (w/Λ) = 0.545. The novel features of this design can be explained by analysing intensity profiles along three propagation directions.
Figure 2 and 3 show the TE mode intensity distribution in the BOX and the Si waveguide region including the impinging Gaussian beam region. For a clear visualization and comparison of coupling intensity between the point of incidence (grating region) and several microns away along the

waveguide (where a photo detector is assumed to be located), a wide region is covered. A significant enhancement intensity coupling occurs in presence of surface grating and Si mirrors in BOX region.

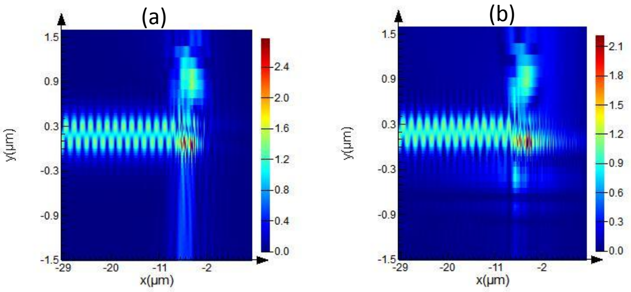

Figure 2: TE mode intensity distribution in the waveguide (grating region inclusive) at 1550 nm (a) without mirror (b) with mirror.

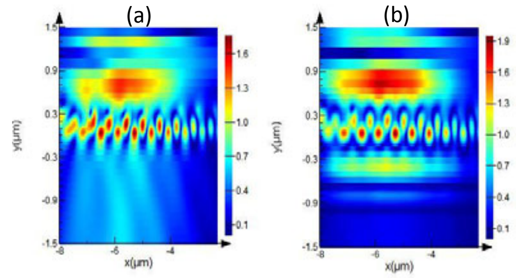

Figure 3: Enlarged view of TE mode intensity distribution in the grating region along the direction of incident at 1550 nm (a) without mirror (b) with mirror.

Figure 4 shows the intensity profiles in the same regions as in Fig. 2, which can further be explained by interference and scattering phenomena. The incident light is scattered by surface gratings and then fractionally coupled through +x, –x, and –y (direction of incidence) directions. The propagating waves along +x/-x directions are in the wave-guided modes reflect back from the periodic grating trench edges, resulting an interference with the incident light. Consequently, a standing wave forms with resonance around the point of incidence localized in the grating region. The period of modulated interference patterns is determined by the grating patterns (depth, width, and shape). Comparison of Fig. 4(a) and (b) indicates an efficient enhancement of light (from 50% to ~90%) in the waveguide region in presence of buried Si mirrors in the BOX layer. We have achieved >90% theoretical coupling efficiency in terms of intensity ratio in our novel design of Si grating coupler.

Figure 5 shows the wavelength dependent coupling efficiency of the coupler. The maximum efficiency (90%) is observed at 1565 nm and a wide frequency band is shown that coupled strongly around the standard telecommunication band.

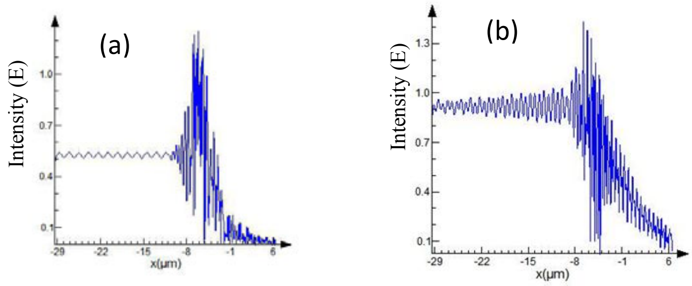

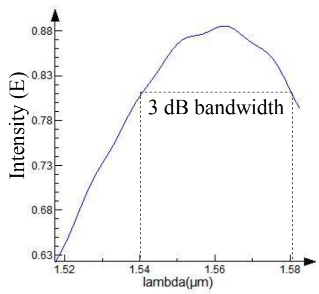

Figure 4: TE mode intensity profile (a) without mirror (b) with mirror. **Figure 5**: Wavelength dependent coupling efficiency.

In conclusion, we have designed a multilayer silicon mirror based grating coupler, which can couple the light efficiently between single-mode fiber and SOI waveguide. With this design we have achieved 85% coupling efficiency at telecom wavelength of 1550 nm and 3 dB bandwidth of 40 nm.

References:

[1] Xiaochuan Xu, Harish Subbaraman, John Covey, David Kwong, Amir Hosseini, "Complementary metal–oxide–semiconductor compatible high efficiency subwavelength grating couplers for silicon integrated photonics", *Appl. Phys. Lett.* 101, 0311091-4, 2012

[2] D. Vermeulen, S. Selvaraja, P. verheyen, G. Lepage, W. Bogaerts, P. Absil, D. Van Thourhout, G. Roelkens, "High-efficiency fiber-to-chip grating couplers realized using an advanced CMOS-compatible Silicon-On-Insulator platform", *Optics Express*, Vol. 18, No. 17, 18278-18283, 2010

[3] Chao Qiu, Zhen Sheng, Le Li, Albert Pang, Zhiqi Wang, Aimin Wu, Xi Wang, Shichang Zou, Fuwan Gan, "Poly-Silicon Grating Couplers for Efficient Coupling With Optical Fibers", *IEEE Photonics Technology Letters*, Vol. 24, No. 18, 1614-1617, 2012

[4] Neil Na, Harel Frish, I-Wei Hsieh, Oshrit Harel, Roshan George, Assia Barkai, Haisheng Rong, "Efficient broadband silicon-on-insulator grating coupler with low backreflection", *Optics Letters*, Vol. 36, No. 11, 2101-2103, 2011

[5] Dirk Taillaert, Wim Bogaerts, Peter Bienstman, Thomas F. Krauss, Peter Van Daele, Ingrid Moerman, Steven Verstuyft, Kurt De Mesel, Roel Baets, "An Out-of-Plane Grating Coupler for Efficient Butt-Coupling Between Compact Planar Waveguides and Single-Mode Fibers", *IEEE Journal of Quantum Electronics*, Vol. 38, No. 7, 949-955, 2002

[6] Liu Liu, Minhao Pu, Kresten Yvind, Jørn M. Hvam, "High-efficiency, large bandwidth silicon-on-insulator grating coupler based on a fully-etched photonic crystal structure", *Appl. Phys. Lett.*96, 0511261-3, 2010

[7] J. V. Galan, P. Sanchis, J. Blasco, J. Marti, "Study of High Efficiency Grating Couplers for Silicon-Based Horizontal Slot Waveguides", *IEEE Photonics Technology Letters*, Vol. 20, No. 12, 985-987, 2008

Enhanced Optical Confinement using an Array of Silica Nanoparticles Embedded in Ag Metallic Film

W. W. Ahmed, M. T. Mujahid and M. A. Alsunaidi*
King Fahd University of Petroleum & Minerals, Saudi Arabia

*corresponding author: msunaidi@kfupm.edu.sa

Abstract-Confinement of electromagnetic field in nanostructures is investigated by exciting the surface plasmon polaritons (SPPs) and plasmonic resonant cavities in silica nanoparticles embedded partially in a metallic layer. It is observed that confinement factor is highly sensitive to the thickness of the metallic film and the location, size and spacing between nanoparticles. It is shown that the proposed structure exhibits enhanced field confinement due to a combination of localized surface plasmon resonance and cavity resonance.

The confinement of the EM fields plays a significant role in many optical phenomena such as optical nonlinearity, optical limiting and optical wave guiding. Many structures have been proposed in literature to confine light in nanostructures with dielectric gratings [1] and metallic nanoparticles using SPPs [2-3]. In this work, dielectric nanoparticles instead of metallic particles are used to explore the confinement of EM fields. These dielectric nanoparticles have the potential to significantly confine the fields through trapping of light with the excitation of SPPs.

The proposed structure for field confinement in nanostructures is shown in Fig. 1. The structure consists of the silicon and silver layers in which silica nanoparticles of around 20~40 nm radius are embedded. The nanoparticles are partially embedded between silicon and silver interface. The thickness of Ag metallic film is comparable to the nanoparticles size and the spacing between the nanoparticles is around 20~30nm.

When an incident plane wave strikes the interface between the silicon and the nanoparticles it gets trapped inside the nanoparticles by the lensing effect, and surface plasmon polaritons are excited within the cavities, as shown in the inset of Fig.1. The shape, size and spacing between the nanoparticles play a crucial role in matching the resonance condition of plasmonic cavities at a given wavelength.

The Finite Difference Time Domain (FDTD) method is used to simulate and analyze the dynamics of the structure at an incident wavelength of 930 nm. The intensity of the trapped field is calculated within the nanoparticles and shown in Fig.2. It is found that intensity is enhanced over fifty times as compared to intensity in the absence of plasmonic resonance.

The proposed structure can be used for many applications such as light extraction from LED, light scattering, beam focusing and beam steering with specific orientation of dielectric nanoparticles. Quantum dots can also be embedded inside the nanoparticles for potential optical conversion.

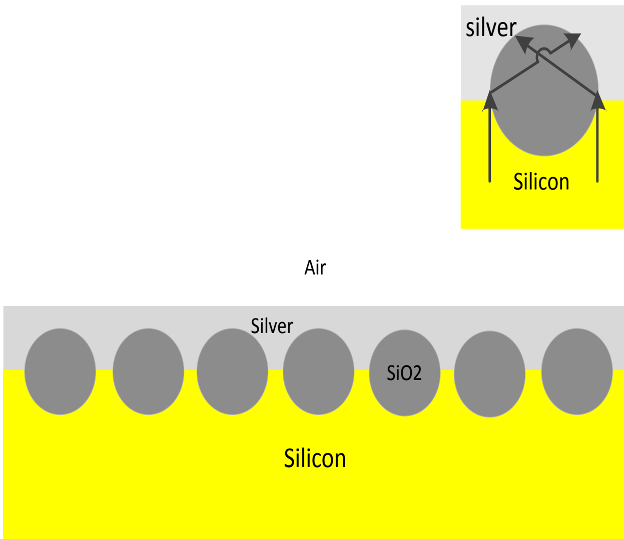

Fig.1. Structure of SiO_2 nanoparticles embedded in Ag Film

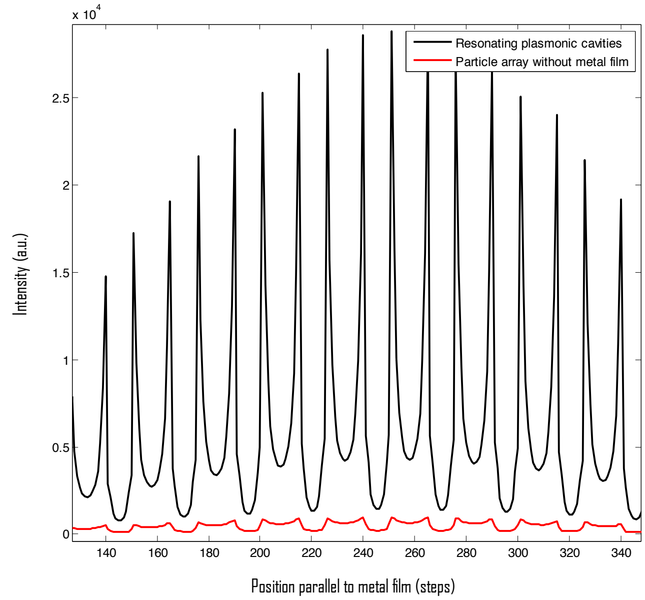

Fig.2. Intensity vs. position parallel to metal film

Optimization studies of silica nanoparticles embedded in Ag film with various sizes and inter-particle spacing has been carried out. The findings indicate that the size, thickness of metallic film and inter-particle spacing are key parameter to the enhancement of optical confinement in nanostructures, and to other optical effects such as beam focusing and steering.

Acknowledgements: The authors would like to acknowledge the support of King Fahd University of Petroleum & Minerals.

REFERENCES

1. Lee, B., S. Kim., H. Kim and L. YongJun, "The use of plasmonics in light beaming and focusing," *Progress in Quantum Electronics*, Vol. 34, No. 2, 47–87, 2010.
2. Toroghi, S. and P. G. Kik, "Cascaded plasmon resonant field enhancement in nanoparticles dimmers in point dipole limit," *Applied Physics Letters*, Vol. 100, No. 18, 183105, 2012.
3. Henson, J., J. DiMaria and R. Paiella, "Influence of nanoparticles height on plasmonic resonance wavelength and electromagnetic field enhancement in two dimensional array," *Journal of Applied Physics*, Vol. 106, No. 9, 093111, 2009.

Photonic TE Modes in Metal-Insulator-Metal Waveguides

M. Ziaullahkhan and M. A. Alsunaidi*
King Fahd University of Petroleum & Minerals, Saudi Arabia
*corresponding author: msunaidi@kfupm.edu.sa

Abstract- In this paper, the numerical analysis of the photonic TE mode in metal-insulator-metal plasmonic waveguide is performed and compared with plasmonic TM mode of the same structure. It was found that the TE photonic mode can have advantages over the plasmonic TM mode in terms of energy confinement, propagation loss and bend efficiency. These properties make the TE photonic mode a suitable candidate for signal propagation and processing in photonic integrated circuits.

The fraction of fields extending inside the metal side for plasmonic TM modes in a MIM waveguide is responsible for the huge propagation loss characterizing these modes. Also, the thickness of the core region in these structures has to be reduced to achieve high field localization; but this will shift the energy into the metal regions even more. The TE photonic modes are thus studied to overcome these factors. Photonic TE modes exist for certain core thicknesses and excitation wavelengths in MIM waveguides [1]. Only the fundamental mode is considered here. The numerical analysis is based on the generalized polarization algorithm of the FDTD auxiliary differential equation technique [2] where silver is modeled using the 6-pole Lorentz-Drude equation. The dielectric core is assumed lossless. The comparison between the photonic TE mode and the plasmonic TM mode is done at the same core thickness of 60 nm and the same wavelength of 530 nm.

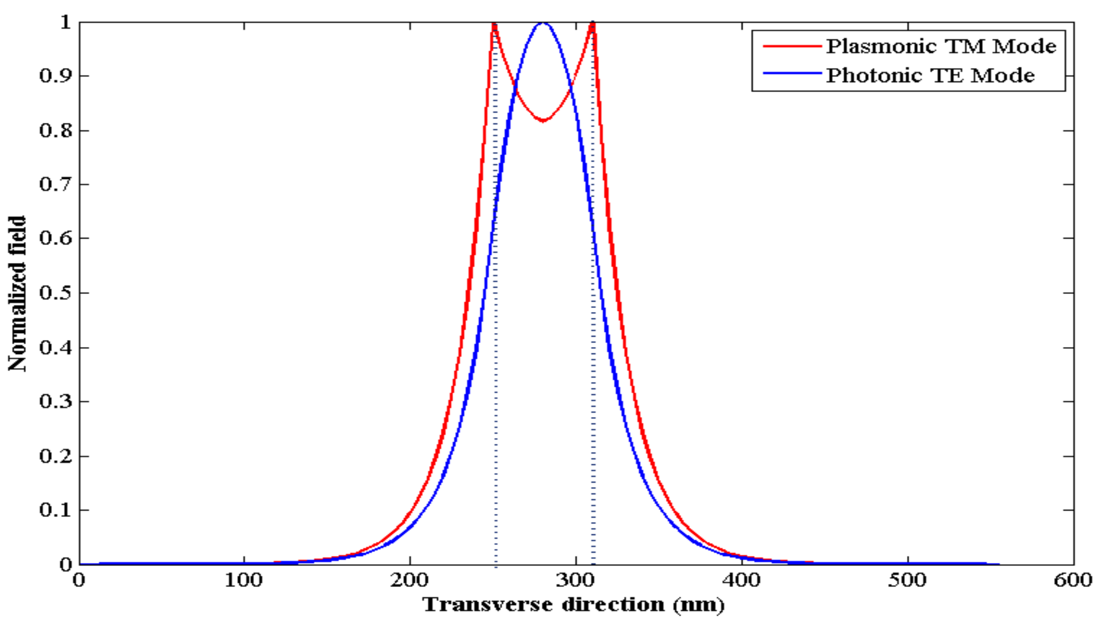

Figure 1. Mode confinement for photonic TE and plasmonic TM cases.

Results show that mode confinement in the core region is better for the photonics TE mode at these conditions, as shown in figure 1. Consequently, propagation losses due to metal are found significantly less as compared to the plasmonic mode as shown in figure 2. For the specific case considered here, the propagation length of the fundamental photonic TE mode is over three times larger than the corresponding plasmonic TM mode.

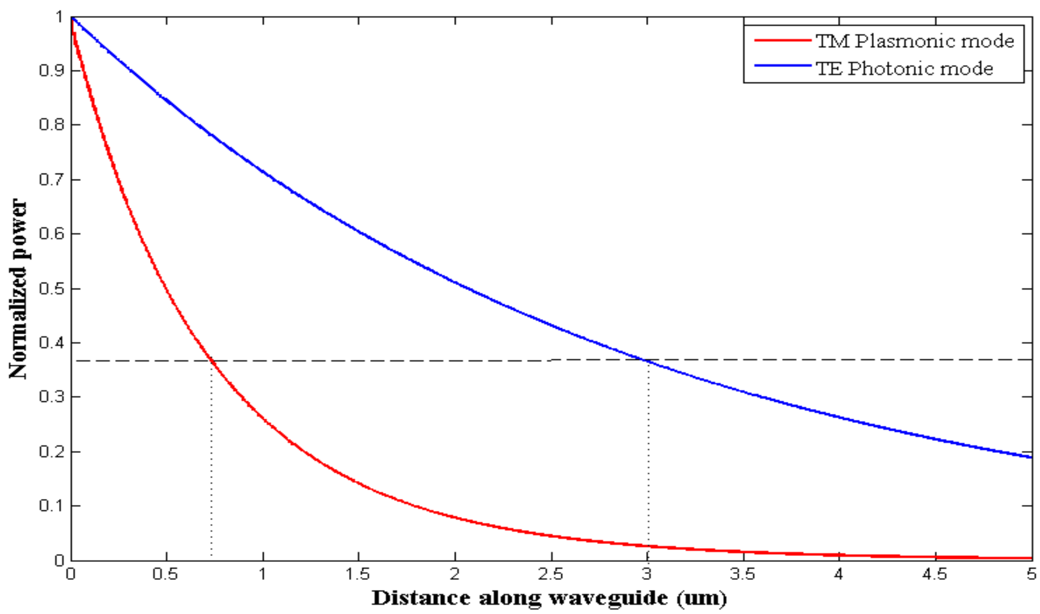

Figure 2. Normalized power for photonic TE and plasmonic TM modes versus distance.

The efficiency of field transmission over a 90^o bend has also been considered. The intensity of the transmitted wave was calculated just after the bend and normalized to the intensity of the incident wave. Around 80% transmission was achieved in the case of the photonic TE mode for the structure and wavelength under consideration, whereas only 45% transmission is recorded for the plasmonic TM mode.

The analyzed properties of the photonic TE mode in a typical nanoscale MIM structure are attractive for integrated photonics. Although this mode does not offer confinement at the metal surface, it can serve as an excellent candidate for signal transmission and signal processing in PIC circuits.

Acknowledgements. The authors would like to acknowledge the support of King Fahd University of Petroleum & Minerals.

REFERENCES

1. Dionne J. A., L. A .Sweatlock and H.A. Atwater, “Plasmon slot waveguides: Towards chip-scale propagation with subwavelength-scale localization,” *Physical Review B*, Vol.73,No.3, 035407, 2006.
2. Alsunaidi.M..A and A.A. Al-Jabr, “A General ADE-FDTD Algorithm for the Simulation of Dispersive Structures,” *IEEE Photonics Technology Letters*, Vol. 21, No. 12, June 15, 2009.

Magnetoplasmonic Management of Electromagnetic Near-Field

A. N. Kalish[1*], V. I. Belotelov[1], S. N. Andreev[2], V. P. Tarakanov[2], and A. K. Zvezdin[2]
[1]Lomonosov Moscow State University, Russia
[2]Prokhorov General Physics Institute of Russian Academy of Science, Russia
[*]corresponding author: kalish@physics.msu.ru

Abstract-In the paper a novel phenomenon is investigated that is magnetic management of plasmon tunnelling through a metallic film. A theory is developed and it is shown that the tunnelling efficiency and tunnelling length are sensitive to magnetization. Also the magnetoplasmonic properties in the near field such as polarization, dispersion and localization are considered.

Surface plasmon polaritons (SPP) provide energy transfer with small wavelengths and energy concentration at nanoscale volumes, leading to vast area of their possible applications [1]. Incorporating magnetic dielectrics into plasmonic structures leads to plasmon-assisted enhancement of magneto-optical effects [2]. In the present work we focus our attention on near-field properties of magnetoplasmonic structures and the possibility of management of plasmon electromagnetic energy transfer via magnetic field.

The magnetoplasmonic structures under consideration are shown in Fig. 1.

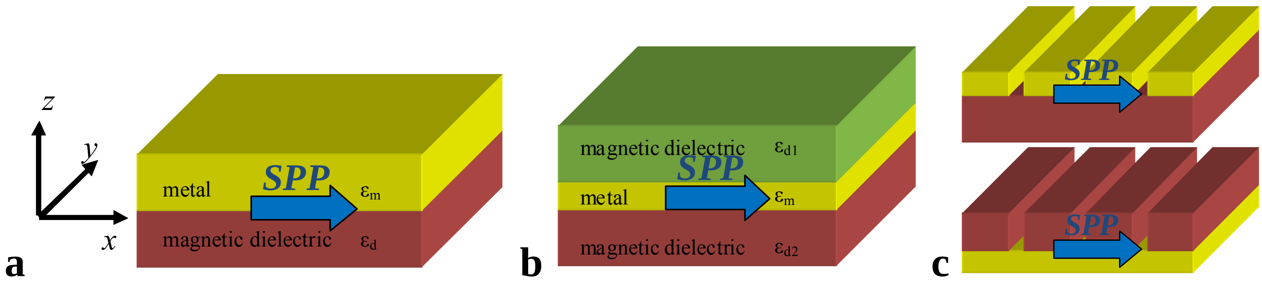

Fig. 1. Magnetoplasmonic structures under consideration. (a) The interface between a metal and a magnetic dielectric. (b) A metallic film placed between two magnetic dielectrics. (c) One-dimensional plasmonic crystals containing a magnetic dielectric.

The constituent equation for magnetic medium is the following [3]:

$$\mathbf{D} = \varepsilon\mathbf{E} - iQ\varepsilon[\mathbf{m} \times \mathbf{E}] \tag{1}$$

where $\mathbf{m}$ is the magnetization unitary vector and Q is magnetooptical Voigt parameter. For conventional magnetic dielectrics (such as Bi:YIG) its typical value is about 0.01 which allows linear in Q approximation for further analysis.

Magnetization directed along y-axis (transversal geometry) causes changes in magnetoplasmon dispersion and localization coefficients. It provides magnetic management of electromagnetic field tunnelling through a metallic film in the sandwiched structure (Fig. 1b). The equations for the magnetic field at the interfaces can be transformed to the following form:

$$\begin{aligned}\frac{\partial^2 H_+}{\partial x^2} + \beta_+^2 H_+ = \eta_+ H_- \\ \frac{\partial^2 H_-}{\partial x^2} + \beta_-^2 H_- = \eta_- H_+\end{aligned} \qquad (2)$$

Therefore, this effect can be fully described with the coupled oscillators theory. In such systems the energy can periodically transfer from one oscillator to another and backwards. In terms of the SPPs it implies periodic in x energy tunnelling between the two interfaces of the metallic film. As the partial frequencies $\beta_\pm$ and the coupling coefficients $\eta_\pm$ are dependent on magnetization the tunnelling becomes manageable via external magnetic field.

In particular, if the dielectrics are the same and their magnetizations are directed opposite to each other, the tunnelling efficiency is maximal and the same as for non-magnetized system. But if magnetizations are oriented in the same direction, the tunnelling efficiency decreases. The tunnelling length is also affected by magnetization. Depending on the film thickness it can be either linear or inversely proportional to magnetization.

The properties of the SPPs for magnetization directed along x- or z-axis (longitudinal or polar geometry respectively) are quite different. The propagation constant is independent on magnetization. However, the SPP polarization becomes different. The electromagnetic field acquires additional TE components that are proportional to Q. For example, their magnitudes at the single interface can be estimated by the following relations:

$$\frac{E_y}{H_y} = \frac{iQ}{2}\sqrt{\frac{\varepsilon_m}{\varepsilon_d\left(\varepsilon_m + \varepsilon_d\right)}} \quad \text{and} \quad \frac{E_y}{H_y} = \frac{Q}{2\sqrt{-\left(\varepsilon_m + \varepsilon_d\right)}} \qquad (3)$$

for the longitudinal and the polar geometries, respectively.

In conclusion, introducing magnetic materials in plasmonic crystals provides management of plasmon dispersion and near field distribution, as well as far field properties. The considered effects are prospective for light modulators, valves, magnetic field sensors, plasmonic interferometers and resonators etc.

The work is supported by the Russian Foundation for Basic Research (projects No. 12-02-33100, 12-02-31298, 12-02-31396, 11-02-00681), the Ministry of Education and Science of the Russian Federation (the Federal Targeted Program “Scientific and Scientific-Pedagogical Personnel of the Innovative Russia”) and the Russian Presidential Fellowship (No. SP-124.2012.5).

REFERENCES

1. Maier, S. A., *Plasmonics: fundamentals and applications*, Springer, New York, 2006.
2. Zvezdin, A. K. and V. A. Kotov, *Modern Magnetooptics and Magnetic Materials*, IOP Publishing, Bristol, 1997.
3. Belotelov, V. I., I. A. Akimov, M. Pohl, V. A. Kotov, S. Kasture, A. S. Vengurlekar, A. V. Gopal, D. R. Yakovlev, A. K. Zvezdin, and M. Bayer, “Enhanced magneto-optical effects in magnetoplasmonic crystals,” *Nature Nanotechnol.*, Vol. 6, No. 6, 370–376, 2011.

Bi-layered L-shaped plate toroidal metamaterial

Shi-Kang Tseng[1] **and Yih-Peng Chiou**[1,2,3*]
[1]Graduate Institute of Photonics and Optoelectronics
[2]Graduate Institute of Communication Engineering, and [3]Department of Electrical Engineering
Nation Taiwan University, Taipei 10617, Taiwan
ypchiou@ntu.edu.tw

Abstract- In this letter, we demonstrate an intrinsic toroidal dipolar plate metamaterial. Compared with other published plate toroidal dipolar MM structures, not only magnetic but also electric vortex distribution are generated in this structure.

Toroidal dipole moment with extraordinary electromagnetic property is investigated in recent years [1]. This moment can not be directly obtained by tradition multipole expansion. It can still be derived via some special mathematic technique. The character of toroidal moment field pattern is vortex distributed magnetic dipole surrounding a toroidal center. Due to toroidal dipolar moment violet symmetry, both of spatial inversion and temporal reversion, a lot of instinctive electromagnetic phenomenon be expected, such as directional dichroism [2], non-reciprocal refraction [3], and magnetoelectric effects [4].

Metamaterial (MM) is artificial structure arranging metal and dielectric in sub-wavelength scale. In this letter, we demonstrate an intrinsic toroidal dipolar plate metamaterial. Compared the design in [5], not only magnetic vortex distribution can be generated, but also electric vortex can be generated in this structure from the full-wave simulation.

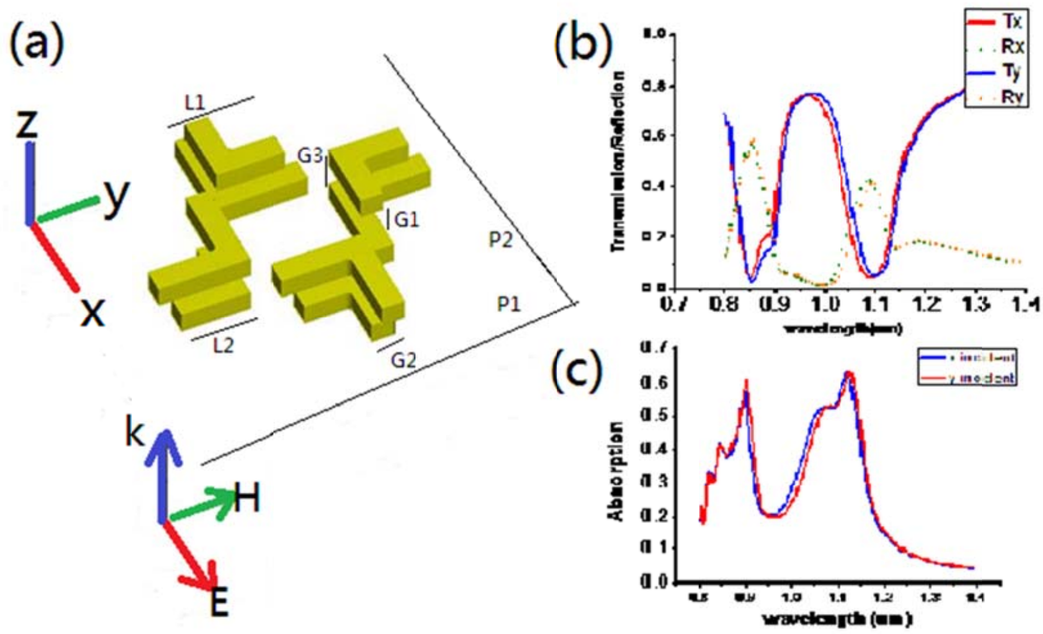

Figure-1 (a) Geometric structure of intrinsic anapolar metamaterial design. (b) The red solid curve and green dash curves are transmission and reflection for *x*-polarize incident plane waves, respectively. Solid blue and dash orange curves are those for y-polarize incident plane waves. (c) The absorption spectrum for two polarizations.

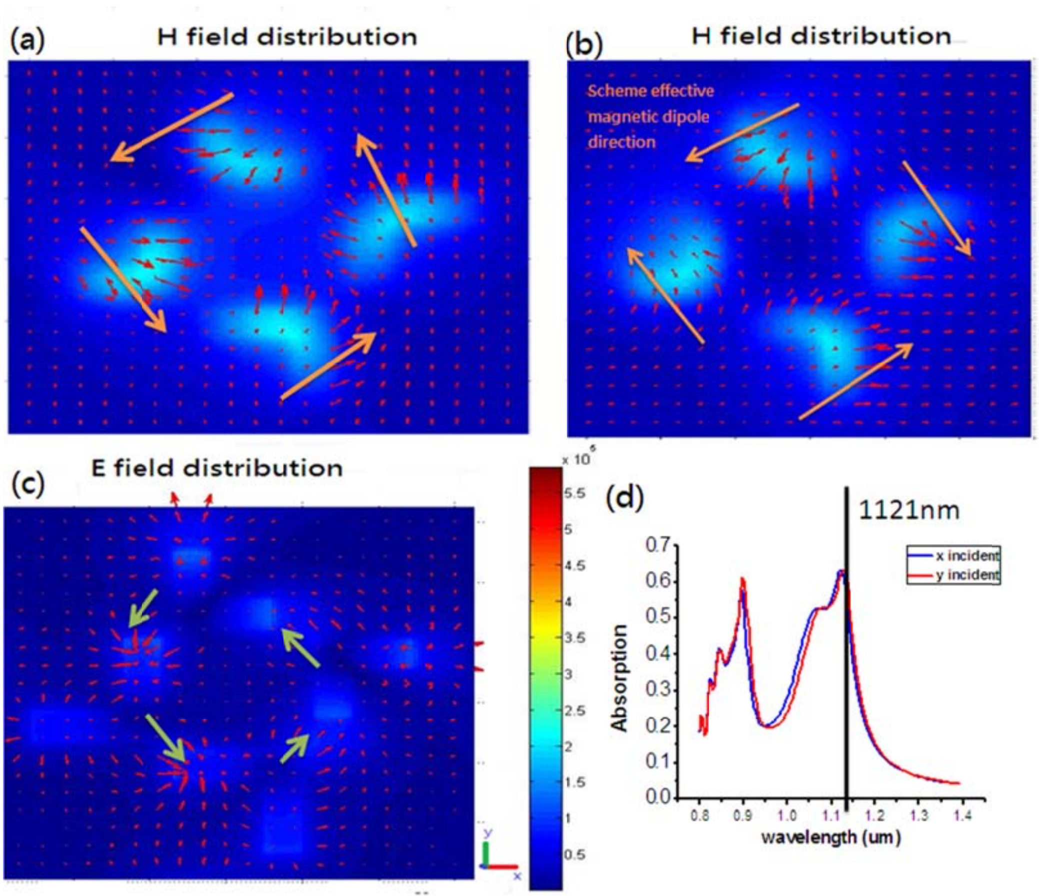

Figure-2 Magnetic field distributions for (a) *x*- and (b) *y*-polarized incident waves at wavelength 1121 nm. (c) Electric field distribution of (a). (d) Absorption spectrum for the two polarizations.

Both electric and magnetic toroidal dipole responses exist in our bi-layered L-shaped construction plate metamaterial system. The character of toroidal moment that is vortex field around an axis center is observed in our system. More details on the mechanism will be presented in the conference.

REFERENCES

1. Marinov, K., A. D. Boardman, V. A. Fedotov, and N. Zheludev, “Toroidal Metamaterial,” New J. Phys., Vol. 9, 324, 2007.
2. Takahashi1, Y., R. Shimano, Y. Kaneko, H. Murakawa and Y. Tokura, “Magnetoelectric resonance with Electromagnons in a Perovskite Helimagnet,” Nature, Vol.8, 121-125, 2012.
3. Sawada, K., and N. Nagaosa,“On the aromagnetism and anapole moment of anthracene nanocrystals ,“ Phys. Rev. Lett., Vol. 95, 237402, 2005.
4. Papasimakis, N., V. A. Fedotov, K. Marinov, and N. I. Zheludev,” Gyrotropy of a metamolecule: wire on a torus,” Phys.Rev. Lett., Vol. 103, 093901, 2009.
5. Dong, Z.G., J. Zhu, J. Rho, J.Q. Li, C. Lu, X. Yin,and X. Zhang,” Optical toroidal dipolar response by an asymmetric double-bar metamaterial,” App. Phys. Lett. 101, 144105, 2012.

Coupling colloidal nanocrystal emission to surface plasmons propagating in metallic nanowire structures

A. Giugni, A. Saeed, A. Toma, A. Alabastri, H. Li, E. Di Fabrizio, and R. Krahne*
Istituto Italiano di Tecnologià, Via Morego 30, 16163 Genova, Italia
*corresponding author: roman.krahne@iit.it

Abstract Colloidal core-shell nanorods absorbing in the blue and emitting in the red spectral range were positioned near metallic waveguides and stimulated by laser excitation. The nanorod emission coupled to propagating surface plasmon polaritons in the Au nanowire and the outcoupled emission at the opposite nanowire end was detected. We studied experimentally and theoretically the influence of light polarization and of the Au nanowire aspect ratio. Our approach allows us to decouple the nanowire light emission both spectrally and spatially from the excitation source.

Plasmonics in metallic nanostructures is generating increasing interest for the development of optics that beat the diffraction limit of standard dielectric optical components. In this respect photonic circuits based on surface plasmon polariton (SPP) propagation in metal nanowires have been explored and the exciton-plasmon coupling mechanisms have been investigated, using semiconductor[1] or metal [2] nanoparticles positioned in the vicinity of metal wires. Another approach consisted in photonic-plasmonic routing based on SnO_2 nanoribbons and Ag nanowires[3]. In particular, quantum dot emission from colloidal semiconductor nanocrystals has been successfully coupled into Ag nanowires, and both experimental and theoretical investigations have shown that the emission properties of QDs can be significantly modified near metallic nanostructures [1], that is within the range of the evanescent surface plasmon mode tail.

In this work we demonstrate the coupling of nanorod emission to Au nanostructures defined by electron-beam lithography. This top-down approach gives us precise control over the Au nanowire shape and the location of the nanorod deposition, which allowed to study the effects of nanowire length and width for the plasmon propagation, as well as the influence of the polarization of the excitation source on the near field coupling of the nanorod emission to the plasmons in the Au. The experimental data will be compared with the results obtained from finite elements (FEM) calculations on the propagation of SPPs in the metallic nanowires.

We positioned “dot-in-a-rod” colloidal core-shell nanorods in the vicinity of one tip of Au nanowires with 100 nm width and several microns in length fabricated by electron beam lithography. The exciting laser beam was coupled off-axis into the confocal imaging optics, which allowed us to illuminate the rod-functionalized tip of the nanowire while recording the emission from the opposite end. Spatially resolved conventional confocal luminescence mapping was used to verify the presence of nanorods solely at one tip of the nanowires. The architecture of the nanorods was chosen such that their absorption was in the UV-blue spectral range and the band edge emission of the core material in the range between 620-670 nm. The nanorods were excited locally by laser light in resonance with the band gap of the shell, and the far field light emission at the opposite end of the nanowire was detected.

We observed appreciable emission at the opposite end with a peak position that was slightly red-shifted with respect to the nanorod emission peak. This red-shift can be explained by convolution of the nanorod emission with the transmission dispersion of the nanowire. Furthermore we observed that in P-polarisation the intensity of the transmitted light was significantly stronger with respect to S-polarisation, which can be rationalized by the near field emission properties of the nanorods.

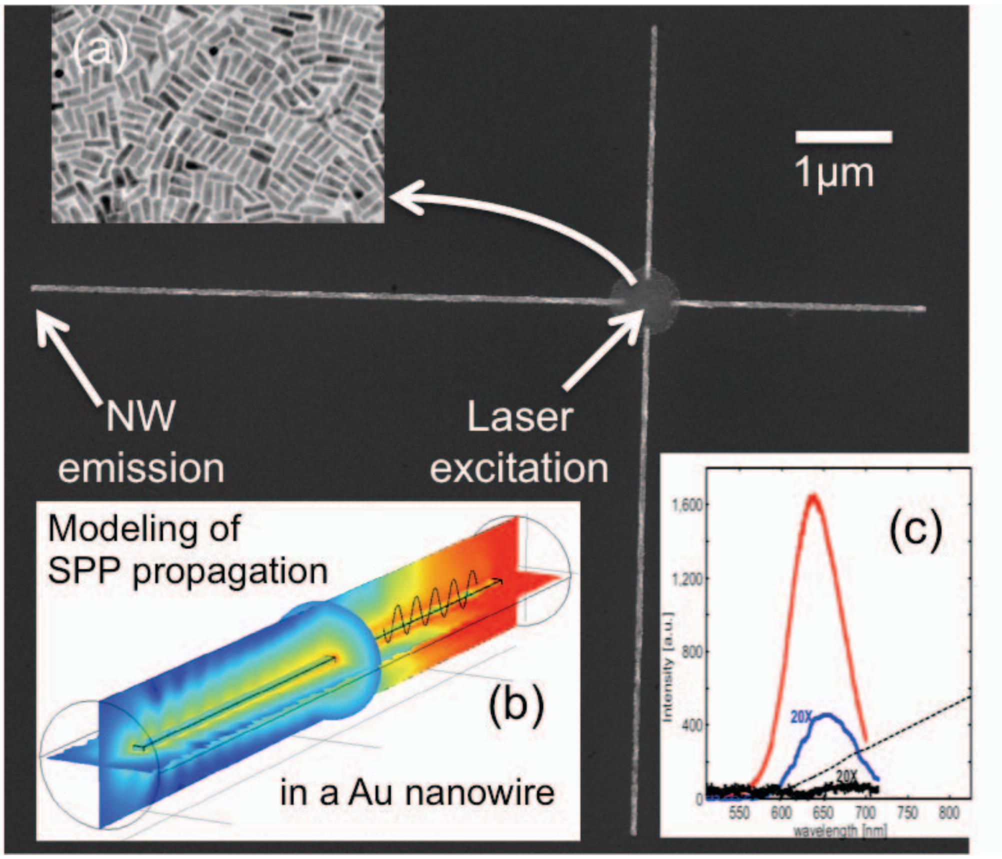

Figure 1. Scanning electron microscopy (SEM) image of four 100 nm wide Au nanowires pointing in orthogonal directions, top and right side with 3 µm, and bottom and left side with 7µm length. The central region of the cross has been covered with highly luminescent colloidal nanorods. The inset (a) shows a transmission electron microscopy image of the nanorods, (b) displays a result of finite elements modeling of the plasmon excitation along the Au nanowire, and (c) shows optical emission spectra recorded from the cross center (red) and the external tip of a 3 µm long nanowire while the laser excitation (λ= 488nm) remained fixed at the center.

REFERENCES

1. Akimov A. V., Mukherjee A., Yu C. L., Chang D. E., Zibrov A. S., Hemmer P. R., Park H. and Lukin M. D., *Nature*, "Generation of single optical plasmons in metallic nanowires coupled to quantum dots", 2007, **450**, 402-406.
2. Knight M. W., Grady N. K., Bardhan R., Hao F., Nordlander P. and Halas N. J., *Nano Letters*, "Nanoparticle-Mediated Coupling of Light into a Nanowire", 2007, **7**, 2346-2350.
3. Yan R. X., Pausauskie P., Huang J. X. and Yang P. D., *Proceedings Of The National Academy Of Sciences Of The United States Of America*, "Direct photonic-plasmonic coupling and routing in single nanowires", 2009, **106**, 21045-21050.

Blueshift of the surface plasmon resonance studied with Electron Energy Loss Spectroscopy (EELS)

N. Stenger[1,2], S. Raza[1,3], A.-P. Jauho[2,4], M. Wubs[1], and N. A. Mortensen[1,2]

[1]Department of Photonics Engineering, Technical University of Denmark, DK-2800 Kgs. Lyngby, Denmark
[2]Center for Nanostructured Graphene, Technical University of Denmark, DK-2800 Kgs. Lyngby, Denmark
[3]Center for Electron Nanoscopy, Technical University of Denmark, DK-2800 Kgs. Lyngby, Denmark
[4]Department of Micro and Nanotechnology, Technical University of Denmark, DK-2800 Kgs. Lyngby, Denmark
niste@fotonik.dtu.dk

Abstract— We used monochromated EELS to study the surface plasmon resonance of isolated silver nanoparticles with sizes ranging from 30 nm down to 3 nm. We observe a significant blueshift of 0.5 eV. We compare our experimental data with models going beyond the Drude model including the response of inhomogeneous electron density at the surface of noble metallic particles. We discuss the potential implications of this blueshift for nanometer scale plasmonic silver structures in general.

Recent experimental measurements performed on noble metallic nanostructures with feature sizes of the order of the nanometer have shown that the behavior of the Surface Plasmon (SP) resonances departs from the Drude model [1, 2, 3, 4]. These new results suggest that quantum and nonlocal effects start playing an important role for metallic structures with feature sizes below 10 nm. However, these effects are far from being understood and a better understanding of the physics behind them is needed. In this sense we used subnanometer spatial resolution Scanning Transmission Electron Microscope (STEM) equipped with a monochromated EELS to address quantum and nonlocal effects in tiny silver spheres.

We performed EELS on isolated silver nanoparticles dispersed on a silicon nitride membranes with sizes ranging from 30 nm down to 3.5 nm. We observe a clear blueshift of 0.5 eV of the SP

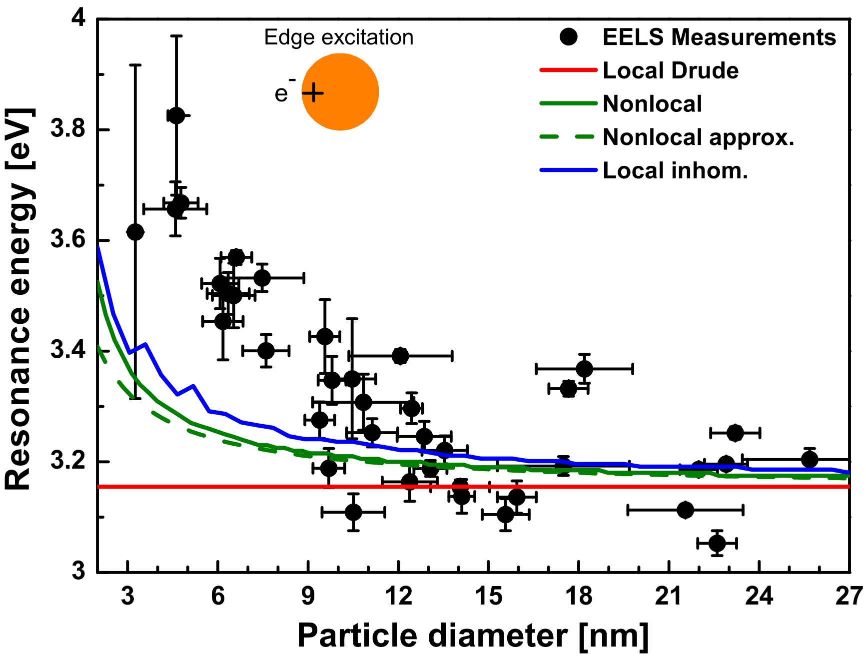

Figure 1: Nanoparticle SP resonance energies as a function of the particle diameter [4]. The dots are EELS measurements taken at the surface of the particle and analyzed using the reflected tail method, and the lines are theoretical predictions

resonance energy for decreasing diameters of the particles. It is known that in the quasistatic limit (valid for nanoparticle sizes much smaller than the excitation wavelength) the simple Drude model predicts that the SP resonance energy of the nanoparticles should remain constant with decreasing size.
In Figure 1 we compare our experimental results (black dots) with three different models, a classical Drude model with a homogeneous electron density profile in the metal (red line), a semiclassical model corrected for inhomogeneous electron density associated with quantum confinement (blue line), and a semiclassical nonlocal hydrodynamic description of the electron density (green line). We see that the two semiclassical model can describe qualitatively the blueshift observed experimentally. However, the theoretical predictions show a significantly smaller blueshift than expected. This discrepancy suggests that something beyond the semiclassical approach is at play at these scales. We discuss possible explanations and present future possible experiments in order to understand this large blueshift.

In conclusion the development of high-end spectroscopy techniques like STEM-EELS to study tiny noble metallic particles on the nanometer scale has enabled the possibility to observe new physics in the behavior of the SP resonances. This new physics will have significant implications in the design of future plasmonic devices with feature sizes on the nanometer scale.

ACKNOWLEDGMENT

N.S. is supported by the Lundbeck Foundation. The Center for Nanostructured Graphene is sponsored by the Danish National Research Foundation. The A. P. Møller and Chastine Mc-Kinney Møller Foundation is gratefully acknowledged for the contribution toward the establishment of the Center for Electron Nanoscopy.

REFERENCES

1. Scholl, J. A., Koh, A. L. and Dionne, J. A. "Quantum plasmon resonances of individual metallic nanoparticles" *Nature*, Vol. 438, 421, 2012.
2. Ciraci, C., *etal.*, "Probing the Ultimate Limits of Plasmonic Enhancement" *Science*, Vol. 337, 1072, 2012.
3. Kern, J., *etal.*, "Atomic-scale confinement of resonant optical fields" *Nano Lett.*, Vol. 12, 5504, 2012.
4. Raza, S., *etal.*, "Blueshift of the surface plasmon resonance in silver nanoparticles studied with EELS" *arXiv:1210.2535*, 2012.

Silicon nanowire photodetector enhanced by a bow-tie antenna

G. Klaric Felic[1*] and E. Skafidas[2]

[1]National ICT Australia (NICTA), Australia

[2]The University of Melbourne, Australia

[*]corresponding author: Gordana.klaricfelic@nicta.com.au

Abstract-

Excellent electronic transport properties of silicon nanowires can be exploited for biomolecule detection in the dc and frequency dependent detection system [1]. Germanium andand silicon-based nanowire devices can absorb and transduce light to photocurrent [2-3]. The addition of optical antennas in the nanowire device enhances photodetection by concentrating radiation into a semiconductor nanowire. This property of optical antenna comes from the unique optical behavior of metals that that enable collective electron excitations, known as surface plasmons [4].

In this paper we present and discuss how a bow-tie dipole antenna can be exploited to confine the radiated power into a silicon nanowire. Using principle of field enhancement by metal antenna structures a subwavelength metal-semiconductor-metal detector can be built [2]. Figure 1 show a silicon nanowire structure with a gold bow-tie antenna.

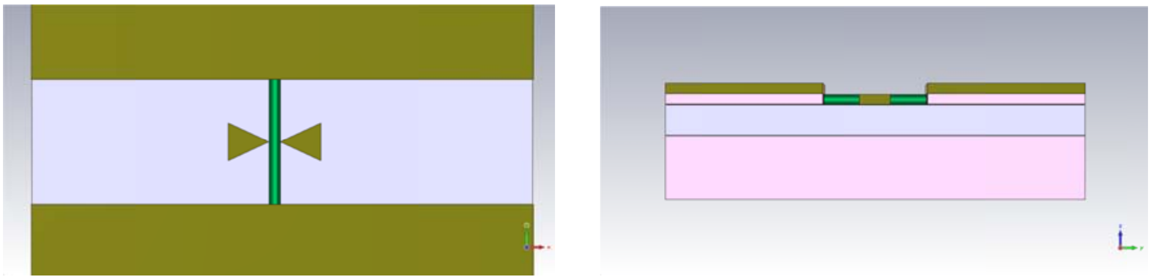

Fig. 1 Schematic illustration of the semiconductor nanowire device used for photodetection

To quantify the affect of light absorption enhancement CST calculations were performed for the near-field and power flow distribution of the detector with the plane wave excitations at wavelengths from 300 nm um to 1.6 um. The power flow configurations for the nanowire system with bow-tie antenna and dipole antenna are given in Fig 2.

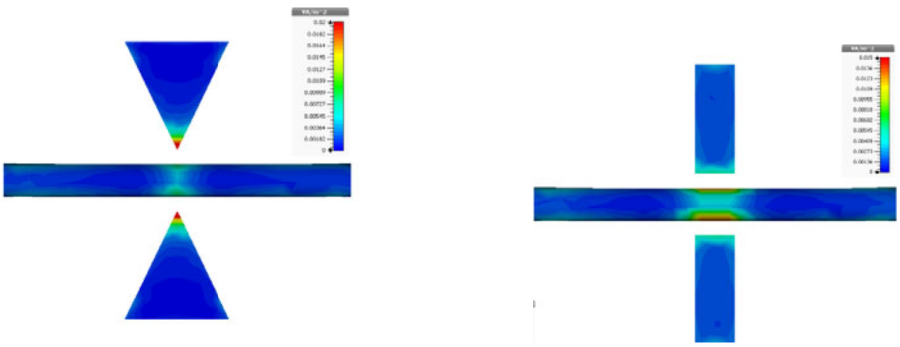

Fig 2 The configuration of power flow for the nanowire system with bow-tie antenna and with dipole antenna (antenna length, 380 nm, silicon wire diametre, 50 nm).

The ability of a bow tie antenna to concentrate radiation in the silicon element (absorption enhancement) is illustrated in Fig. 3. The plane wave polarised in the bow-tie direction was incident form the top of the nanowire system.

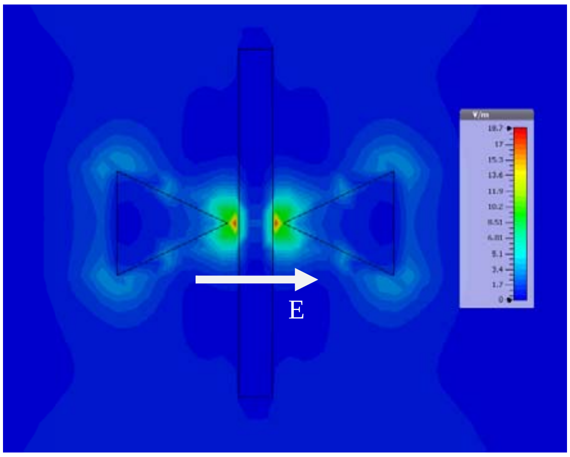

Fig 3 The configuration of electric field for the nanowire detection system with bow-tie antenna, l=850 nm.

The comparison between the power absorption a half-wave Herz dipole antenna and bow-tie antenna is given in Fig. 4.

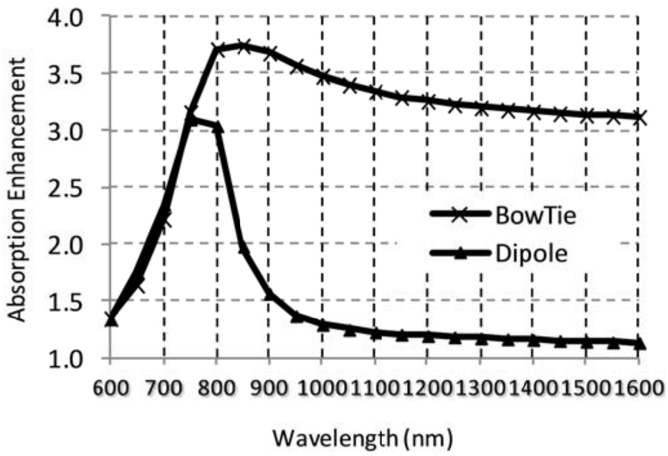

Fig 4 Spectra of light absorption enhancement for the nanowire system with bow-tie antenna and dipole antenna.

REFERENCES

1. Nguyen T.C, Qiu W. Z. and Skafidas E. "Functionalised Nanowire-Based Antigen Detection Using Frequency-Based Signals, *IEEE Transactions on Biomedical Engineering*, VOL. 59, NO. 1, January 2012
2. Tang, L. et al. "Nanometre-scale germnium photodetector enhanced by a near-infrared dipole antenna," *Nature Photonics*, VOL. 2, 226–229, 2008.
3. Fan P, Chettiar U. K., Cao L, Afsinmanesh F., Engheta N. and Brongersma M. L., "An invisible metal-semiconductor photodetector," *Nature Photonics*, VOL. 6, 380-385, 2012.
4. J.A. Schuller et al., "Plasmonics for extreme light concentration and manipulation", *Nature Materials*, VOL 9, 193-204, 2010.

Ultrafast interband nonlinear dynamics of surface plasmon polaritons in gold nanowires

Andrea Marini[1], **Fabio Biancalana**[1,2]

[1]Max Planck Institute for the Science of Light, Guenther-Scharowsky str. 1, 91058 Erlangen, Germany
[2]School of Engineering and Physical Sciences, Heriot-Watt University, EH14 4AS, Edinburgh, UK
f.biancalana@hw.ac.uk

Abstract— We theoretically model the nonlinear dynamics of surface plasmon polaritons on gold nanowires. We find that the thermo-modulational nonlinearity of gold leads to a strong spectral redshift of input pulses in a few nanometers of propagation.

The design and development of sub-wavelength photonic devices with metallic components has become a subject of intense research in the last decade. This trend is justified by the need for compact high-performance optical devices and is mainly driven by the enormous technological improvement in nano-fabrication techniques. Surface plasmon polaritons (SPPs) are hybrid electromagnetic waves propagating on metallic surfaces. They constitute the best candidates for manipulating light on the nanoscale and for the development of sub-wavelength all-optical devices. The nonlinear properties of SPPs can be used for second harmonic generation, active control and nanofocusing. In most of the nonlinear studies present in the scientific literature, the optical response of metals is assumed to be *linear*, while the nonlinearity originates from the dielectric medium; however, experimentalists know well that the Kerr nonlinearity of metals can be enormous. Experimental results indicate strong third-order nonlinear susceptibilities that vary by several orders of magnitude, with values of χ_3^m that vary between 10^{-14} and $10^{-18} m^2/V^2$ and that are much bigger than the third order susceptibility of bulk silica ($\chi_3^{Si} \approx 10^{-22} m^2/V^2$). Recently, the nonlocal ponderomotive nonlinearity for a plasma of free electrons has been proposed as a possible model for the interpretation of experimental results [1]. The predicted value for the ponderomotive third-order susceptibility at optical frequencies ($\chi_3 \approx 10^{-20} m^2/V^2$) is however insufficient to explain the experimental findings. In addition, the spectral dependence of the ponderomotive nonlinearity ($\chi_3 \propto 1/\omega^4$) does not fit with the enormous spectral variation (by several orders of magnitude) observed in the measurements, suggesting that the basic nonlinear mechanism for metals is *resonant*. Theoretical and experimental confirmation of this hypothesis is to be found in the results of Rosei, Guerrisi *et al.* on the thermo-modulational reflection spectra of thin films of noble metals [2, 3]. In their work, the authors theoretically predict and experimentally observe a strong modulation in the reflection spectrum due to light-induced heating. They demonstrate that the temperature change smears out the energy distribution of the conduction electrons, affecting the resonant interband absorption and hence the dielectric susceptibility. This process is intrinsically nonlinear, since the temperature change modulating the dielectric response depends on the optical power. Very recently, a complete analysis of the nonlinear optical response of noble metals, leading to the first theoretical derivation of a consistent model for the third-order nonlinear susceptibility of gold, was reported [4]. Following the semi-classical approach described in Ref. [5], we have calculated directly from the knowledge of the band structure of gold the spectral dependence of the nonlinear susceptibility $\chi_T^{(3)}$. The real and imaginary parts of $\chi_T^{(3)}$ are plotted as functions of optical wavelength λ in Fig. 1a. The nonlinear susceptibility is strongly dispersive at optical frequencies and can be much greater (≈ 7 orders of magnitude) than the Kerr susceptibility of bulk silica ($\chi_3^{Si} \approx 10^{-22} m^2/V^2$). We have also found that the nonlinear pulse propagation along a gold nanowire surrounded by silica glass can be modeled by a nonlinear Schrödinger equation for the field envelope $\psi(z,t)$:

$$i\partial_z\psi(z,t) + \hat{D}(i\partial_t)\psi(z,t) + \Upsilon_{Au}\int_0^{+\infty} \mathrm{d}t' h_T(t')|\psi(z,t-t')|^2\psi(z,t) = 0, \quad (1)$$

where $h_T(t) = (e^{-t/\tau_{th}} - e^{-t/\tau_r})/(\tau_{th} - \tau_r)$ is the temporal response function, τ_{th}, τ_r are the thermalization and relaxation times, $\hat{D}$ is the complex dispersion operator and Υ_{Au} is the nonlinear

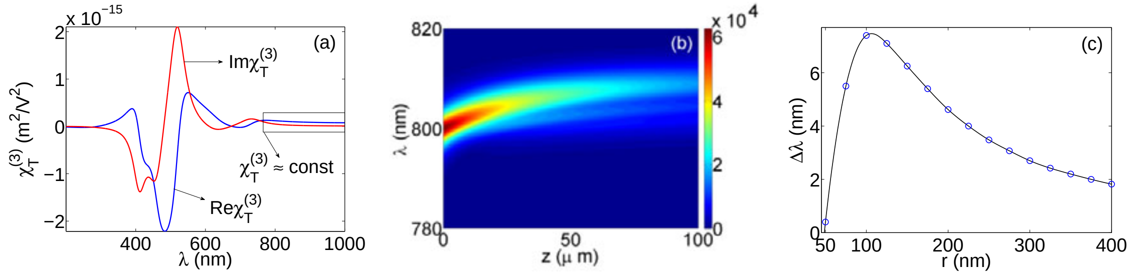

Figure 1: (a) Thermo-modulational interband nonlinear susceptibility $\chi_T^{(3)}$ as a function of the optical wavelength λ. Blue and red curves correspond to the real and imaginary parts of $\chi_T^{(3)}(\lambda)$. The region within which $\chi_T^{(3)}$ can be approximately considered to be a constant is also indicated. (b) Nonlinear propagation of an optical pulse along a gold nanowire with radius $r = 50nm$ surrounded by silica glass for $m = 1$ and an instantaneous input power $P_{in} = 5.3 \times 10^5 W$. The input pulse is a hyperbolic secant $\psi(0,t) = \sqrt{P_{in}} sech(t/t_0)$, with $t_0 = 106 fs$. The contour-plot displays the modulus of the Fourier transform of the optical amplitude: $|\psi(z,\omega)|$. (c) Wavelength red-shift $\Delta\lambda$ as a function of the wire radius r for the $m = 1$ long-range mode, fixed input power $P_{in} = 5.3 \times 10^4 W$ and the propagation length $L = 20\mu m$. Blue circles are the results of numerical simulations, while the full black curve is an interpolation of the numerical results.

coefficient measured in $m^{-1}W^{-1}$ [5]. In principle, also the Kerr and Raman nonlinearities from the silica should be included in order to model the propagation. However, these contributions are negligible with respect to the large third-order susceptibility of gold, and can be disregarded. The hybrid polarized $m = 1$ mode supports long-range SPPs. We have solved numerically Eq. (1) by using the split-step Fourier method and observing an intense spectral redshift of the pulse in few microns of propagation, which originates from the inherent delayed thermal response, analogously to the conventional Raman effect in silica fibers, but much more powerful in metals. Numerical results are depicted in Figs. 1b,c. The red-shift is the natural consequence of the intrinsic delayed mechanism governing the thermo-modulational interband nonlinear susceptibility of gold. In the time domain the frequency red-shift is accompanied by a small pulse delay of order $\approx 1fs$. We emphasize that neither the Kerr nor the Raman nonlinearities of silica are large enough to produce the reported red-shift for the propagation lengths considered. The strong red-shift is accompanied by a large time-delayed nonlinear loss. Our results will be useful in the design of micron-sized devices for frequency conversion purposes.

REFERENCES

1. P. Ginzburg, A. Hayat, N. Berkovitch and M. Orenstein, "Nonlocal ponderomotive nonlinearity in plasmonics", Opt. Lett. **35**, 1551 (2010).
2. R. Rosei and D. W. Lynch, "Thermomodulation Spectra of Al, Au and Cu", Phys. Rev. B **5**, 3883 (1972).
3. M. Guerrisi, R. Rosei and P. Winsemius, "Splitting of the interband absorption edge in Au", Phys. Rev. B **12**, 557 – 563 (1975).
4. M. Conforti and G. Della Valle, "Derivation of third-order nonlinear susceptibility of thin metal films as a delayed optical response", Phys. Rev. B **85**, 245423 (2012).
5. A. Marini, M. Conforti, G. Della Valle, H. W. Lee, Tr. X. Tran, W. Chang, M. A. Schmidt, S. Longhi, P. St. J. Russell and F. Biancalana, "Ultrafast nonlinear dynamics of surface plasmon polaritons in gold nanowires due to the intrinsic nonlinearity of metals", New J. Phys. **15**, 013033 (2013).

Nanophotonics with gain media for loss compensation and spasing

Dynamical model for gain-assisted Localized Surface Plasmons

A. Veltri[1,2], **A. Aradian**[2], **and A. Chipouline**[3]

[1]LICRYL- Liquid Crystal Research Center - University of Calabria, Italy
[2]Centre de Recherche Paul Pascal - CNRS - University of Bordeaux, France
[3]Institute of Applied Physics, Germany
alessandro.veltri@fis.unical.it

Abstract— We present a nonlinear, dynamical model for a classically treated metal spherical inclusion in a gain assisted medium described using quantum formalism. The model integrates geometry via a proper set of boundary conditions and it is shown to be consistent with the statical formula for polarizability, which can be obtained in the low amplitude linear approximation. This dynamical approach is able to account transient and nonlinear regimes.

The study of gain assisted Localized Surface Plasmons (LSP) is of growing interest in the field of metamaterials, in fact, the embedding of optical gain is possibly the most promising strategy to compensate the losses they show in visible-range [1,2]. Moreover, metallic nanostructures with gain elements are nanoscale source of strong optical fields, thus providing applications to nanoscale lithography, probing, microscopy and more [3,4].

The system we describe is the one presented in figure 1, consisting in a metal sphere of radius a and dipole momentum $\mathbf{p}$ described as a classical electromagnetic system, immersed in a medium consisting in a dielectric background made of molecules having a dipole momentum μ^b (blue in Fig. 1) in which active elements of dipole momentum μ^a (red in Fig. 1) are diluted. These two lasts are described as quantum systems. We will refer to the region inside the spherical inclusion

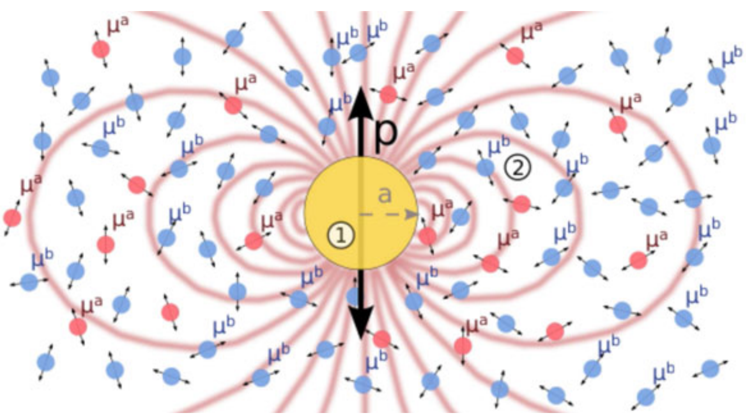

Figure 1: The system under study.

as region 1 while the region outside it will be referred as region 2. In region 1, both the electric field and the polarization are uniform and aligned to z-axis, while in region 2 we assume both the field and the polarization to have a uniform and a dipolar component:

$$\mathbf{E}_1 = E_1\hat{\mathbf{z}}, \qquad \mathbf{E}_2 = E_2\hat{\mathbf{z}} - \frac{\mathbf{p}}{r^3} + \frac{3(\mathbf{p}\cdot\mathbf{r})\mathbf{r}}{r^5}, \tag{1}$$

$$\mathbf{P}_1 = P_1\hat{\mathbf{z}}, \qquad \mathbf{P}_2 = P_2\hat{\mathbf{z}} - \frac{\mathbf{q}}{r^3} + \frac{3(\mathbf{q}\cdot\mathbf{r})\mathbf{r}}{r^5}. \tag{2}$$

The model can be easily expanded beyond the quasi static limit, to describe quadrupole or magnetic dipole resonances by adding the proper terms to these series.

We have used a system of equations based on the one presented in reference [5]:

$$\frac{d\rho_{12}^a}{dt} - \left(i\omega_{21}^a + \frac{1}{\tau_2^a}\right)\rho_{12}^a = -\frac{iH_{12}^a N^a}{\hbar} \tag{3}$$

$$\frac{dN^a}{dt} + \frac{N^a - N_0^a}{\tau_1^a} = -\frac{2iH_{12}^a(\rho_{12}^a - \rho_{21}^a)}{\hbar} \tag{4}$$

$$\rho_{12}^b = \frac{H_{12}^b N_0^b}{\hbar\omega_{21}^b} \tag{5}$$

$$\frac{d^2 z}{dt^2} + 2\gamma\frac{dz}{dt} = \frac{e}{m_e}E_1. \tag{6}$$

$$E_1 = E_0 - \frac{p}{a^3}, \tag{7}$$

$$E_1 + 4\pi P_1 = E_0 + 4\pi P_0 + \frac{2}{a^3}(p + 4\pi q). \tag{8}$$

Equations 3 and 4 describe the active molecules as a two level system, while equations 5 describes the molecules of the dielectric. Both are modeled using the density matrix formalism and are considered to be in a thermal bath. Here $\tau_2^{a,b}$ and $\tau_1^{a,b}$ are the constants describing phase and energy relaxation processes due to the interaction with the thermostat; $\omega_{21}^{a,b} = (E_2^{a,b} - E_1^{a,b})/\hbar$ is the transition frequency between levels 2 and 1; $H_{12}^{a,b}$ is the Hamiltonian matrix element responsible for the interaction of host medium molecules with the external field; $N^{a,b} = \rho_{22}^{a,b} - \rho_{11}^{a,b}$ where $\rho_{22}^{a,b}$ and $\rho_{11}^{a,b}$ are the diagonal matrix density elements and $N_0^{a,b} = (W^{a,b}\tau_1^{a,b} - 1)/(W\tau_1^{a,b} + 1)$ being $W^{a,b}$ a phenomenological pump rate. $H_{12}^{a,b}$ is the interaction matrix element $1,2$ of the Hamiltonian of interaction $H^{a,b}$ of the single quantum element (dielectric or dye molecule). Equation 6 is a free electrons model describing the motion of the charges in the metal inclusion. At $r = a$, the fields have to fulfill the boundary conditions described by equation 7 and 8. It's worth noting that the plasmonic resonance is not forced in equation 6 but it comes out naturally at the boundary between the metal inclusion and the host medium. We show that this set of equations reduce to the right formula for polarizability: $\alpha(\omega) = a^3(\varepsilon_m - \varepsilon_h)/(\varepsilon_m + 2\varepsilon_h)$ in the linear stationary approximation, thus ensuring the solidity of the model. We also present, as an example of the diverse applications of the model, a characterization of the transition between the linear and the non linear regime, discussing how the resonance spectra change in the two cases as a function of the probe field intensity. Moreover, this approach is designed to describe both stationary and dynamical couplings between a metal spherical inclusion and an active environment. It can be used to investigate transient regimes, instabilities and pulsed pump configurations allowing to analyze realistically the possibility of loss mitigation in LSP-based optical metamaterials and to study a wide range of cutting edge optical applications.

ACKNOWLEDGMENT

This work was supported by the FP7-NMP-2008 European project Metachem under grant agreement nr. 228762 and the Calabria Region (ROP) ESF-2007/2013 IV Axis Human Capital - Operative Objective M2 - Action D.5.

REFERENCES

1. N. M. Lawandy. Localized Surface Plasmon Singularities in Amplifying Media. *Appl. Phys. Lett.*, 85:5040–5042, 2004.
2. M. A. Noginov, G. Zhu, M. Bahoura, J. Adegoke, C. E. Small, B. A. Ritzo, V. P. Drachev, and V. M. Shalaev. Enhancement of surface plasmons in an Ag aggregate by optical gain in a dielectric medium. *Opt. Lett.*, 31(20):3022–3024, 2006.
3. M. A. Noginov, G. Zhu, A. M. Belgrave, R. Bakker, V. M. Shalaev, E. E. Narimanov, S. Stout, E. Herz, T. Suteewong, and U. Wiesner. Demonstration of a spaser-based nanolaser. *Nature*, 460(7259):1110–1112, 2009.
4. M. I. Stockman. Spasers explained. *Nature Photonics*, 2(6):327–329, 2008.
5. A Chipouline, S Sugavanam, V A Fedotov, and A E Nikolaenko. Analytical model for active metamaterials with quantum ingredients. *Journal of Optics*, 14(11):114005, 2012.

Hybrid and quantum materials

Light scattering by scatters of topological insulator

Lixin Ge*, Tianrong Zhan, Dezhuan Han, Xiaohan Liu and Jian Zi
Department of Physics, Fudan University, Shanghai 200433, P. R. China
* E-mail: 081019043@fudan.edu.cn

Abstract-We study theoretically Rayleigh and Mie scatterings by scatters of topological insulators (TIs). For both Rayleigh and Mie scattering, the pattern and polarization of scattered light differs considerably from those in scatters of conventional insulators, resulting from the topological magneto-electric effect.

In recent years, topological insulators (TIs) have attracted considerable attention[1, 2]. TIs are a new state of matter with an energy gap in the bulk and gapless states in the surfaces protected by the time-reversal symmetry[1]. Their optical properties differ considerably from those in conventional insulators due to the existence of the topological magneto-electric (TME) coupling[2].

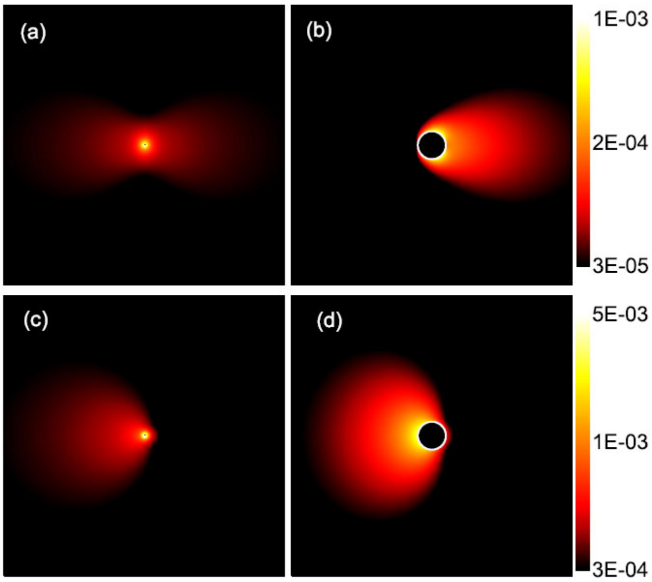

Fig. 1 Electric field distributions of scattered light for hollow cylinders with a dielectric constant of 30. Light is incident from left. (a) and (c) Rayleigh scattering for a conventional insulator and TI, respectively. (b) and (d) Mie scattering for a conventional insulator and TI, respectively.

By applying the Mie theory with the proper boundary conditions, we study theoretically Rayleigh and Mie scatterings for TI scatters. We find that the patterns of scattered light differ considerably from those in scatters of conventional insulators, showing enhanced backward scattering. Enhanced backward scattering has also been found in both metallic[3] and magnetic particles[4] in a very narrow frequency range due to their resonant nature. For TI scatters, however, this frequency range is very wide. Moreover, the polarization of scattered light is quite different from that in scatters of conventional insulators. Figure 1 shows the field distributions of scattered light for hollow cylinders of TI. In both Rayleigh and Mie scattering, the patterns of scattered light are characterized by strong backward scatterings. Our results show that the different behaviors of the pattern and polarization of scattered light for TI scatters stem from the TME effect.

Acknowledgements: This work was supported by the 973 Program (Grant Nos. 2013CB632701 and 2011CB922004). The research of J.Z. and X.H.L. is further supported by the NSFC.

REFERENCES

1. X.L. Qi, T. L. Hughes, and S.C. Zhang. “Topological field theory of time-reversal invariant insulators”. *Phys. Rev. B*, Vol. 78, No. 195424, 2008.
2. X.L. Qi, and S.C. Zhang. “Topological insulators and superconductors”. *Rev. Mod. Phys*, Vol. 83, No. 1057, 2011.
3. C.W. Qiu, L. Gao, J.D. Joannopoulos and M. Soljačić. “Light scattering from anisotropic particles: propagation, localization, and nonlinearity”. *Laser & Photon Rev*, Vol. 4, No. 268, 2010.
4. M. Kerker, D.S. Wang, and C. L. Giles. “Electromagnetic scattering by magnetic spheres”. *J. Opt. Soc. Am*, Vol. 73, No. 765, 1983.
5. C.F. Bohren and D.R. Huffman. “*Absorption and Scattering of Light by small Particles*” John Wiley and Sons, 1983.

The Influence of Debonding on The Mechanical Properties of Hybrid Nanocomposites

Waleed K. Ahmed[1,*]
[1] *United Arab Emirates University, Faculty of Engineering, EUR, Al Ain, UAE*
* *Corresponding author email: w.ahmed@uaeu.ac.ae*

Abstract: The present investigation explores the impact of the deponding in a hybrid nanocomposite on the mechanical properties under elastic condition.Finite element model of a representative volume element is adopted in the analysis.Mainly,RVE is consist of carbon nanofiber confined by matrix and subjected to axial tension. Moreover, a longitudinal debonding one time,and a transverse debonding in the second time are proposed along the interfacial nanofiber/matrix, are modeled and investigated individually.As a result,FE results demonstrate a significant influence on the mechanical properties.

Keywords: Debonding, hybrid, nanoccomposite, mechanical, properties.

Quantum-Dot Metamaterials

M. Decker[1], I. Staude[1], I. Shishkin[1,2], K. Samusev[1,2], P. Parkinson[3], V. K. A. Sreenivasan[4], A. Minovich[1], A. E. Miroshnichenko[1], A. Zvyagin[4], C. Jagadish[3], D. N. Neshev[1], and Y. S. Kivshar[1]

[1]Nonlinear Physics Centre, Research School of Physics & Engineering (RSPE), The Australian National University, Canberra, Australia

[2]National Research University for Information Technology, Mechanics and Optics (ITMO), St. Petersburg 197101, and Ioffe Physics-Technical Institute of the Russian Academy of Science, St. Petersburg194021, Russia

[3]Department of Electronic Materials Engineering, RSPE, Australian National University, Canberra, Australia

[4]MQ Photonics Centre, Macquarie University, Sydney, NSW, Australia

Control of spontaneous emission is crucial for a broad range of applications such as single-photon sources, efficient lasers, displays, solar energy harvesting, and biological markers. The quantum dot (QD) emission can be efficiently controlled through coupling to photonic structures, such as microcavities, photonic crystals, and plasmonic particles. Nanostructured plasmonic materials can be superior for emission enhancement due to their high local-field enhancement and good coupling to free space. A special class of such materials are metamaterials that allow for simultaneous control over the *electric and the magnetic interaction of light with the emitters*. While control of spontaneous emission of light in metamaterial has be the subject of intense recent interest, only a single channel of this interaction has been explored. Importantly, the control of QD emission via simultaneous coupling to the magnetic and the electric modes of the metamaterials remains unexplored.

Here, report on the coupling of QD emission to simultaneously to both electric and magnetic resonances of magnetic metamaterials. We compare the emission enhancement for the zero-order electric and the first-order magnetic resonances (matched spectrally to the QD emission, with the same strength but orthogonal polarisations) and observe three-fold enhancement of the QD emission into the magnetic mode in comparison to the electric one.

The system investigated in our work is a planar magnetic metamaterial composed of split-ring resonators (SRRs) covered by a 200nm-thick layer of polyvinyl alcohol (PVA) containing core-shell QDs emitting at 790nm. In order to investigate how the QD PL is influenced by coupling to the different modes of the magnetic metamaterial we have performed QD micro-photoluminescence (PL) spectroscopy and micro-PL spatial mapping on the SRR metamaterial. In our experiments, we observe broadening of the QD PL spectrum for the electric resonance, while for the magnetic resonance a narrowing of the QD PL emission spectrum is observed. In addition, while the PL intensity does not change when coupling to the electric resonance, a three-fold enhancement can be observed in the magnetic resonance. Furthermore, we have measured lifetime of QD PL for both metamaterial resonances and have found that the decrease in lifetime (in comparison to the unstructured reference areas) is more pronounced in the case of the magnetic resonance. Thus, remarkably, the magnetic mode, which exhibits weaker coupling to the far-field (deducted from transmittance measurements) and can be considered as a darker mode, becomes the brighter mode in QD emission due to its higher Purcell enhancement.

Our experimental results are in good qualitative agreement with theoretical expectations, paving the way towards an ultimate control of emission by magnetic metamaterials.

Photonic crystals

Photonic Crystal Fiber Propagation Characteristics

Dr.Raad.H.Thaher

Assistant Professor

Electrical Eng.Dept.-College of Eng.-AL-Mustansiriyah UNIV.

Baghdad-Iraq

Abstract

Photonic crystal fiber (PCF) is a new class of optical fiber based on the properties of photonic crystals, it have the ability to confine light in hollow cores. in this research paper the propagation characteristics of PCF described using different materials was investigated such as effective area, effective refractive index , numerical aperture and material dispersion for three different materials . It was concluded that zero dispersion occur at less wavelength when there is no silica in the constriction of PCF (i.e. 0.83μm for sapphire (extra ordinary wave).also the three dimension relation between dispersion ,bit error rate ,and fiber length for the three different materials was presented.

Keywords: BER, Dispersion, Numerical aperture, PCF

Summary

Over the past few years, photonic crystal fiber (PCF) technology has evolved from a strong research – oriented field to a commercial technology providing characteristics such as a wide single-mode wavelength range, a bend-loss edge at a shorter wavelengths, a very large or small effective core area, group velocity, dispersion at visible and near field arrangement of air holes running along the length of the fiber. PCF is now finding applications in fiber-optic communications, fiber lasers, non-linear devices, high-power transmission, highly sensitive gas sensors and other areas.

Research cover the last decades has generated a wide range of rigorous numerical algorithms for modeling PCF, such as plane wave expansion(PWE),finite difference time domaine, finite element methods. These versatile algorithms have been applied with success to study issues such as dispersion and losses for PC wave-guide.

The common term used in all these numerical methods is to calculate the effective refractive index of PCF because all linear and non-linear propagation properties of PCF can be analysed using effective refractive index.

We consider the type of PCF which consist of pure silica with a cladding and air holes of diameter (d) arranged in a triangular lattice with pitch (Λ).

The effective area is a quantity of great importance. It is originally introduced as a measure of non-linearities, a low effective area gives a high density of power needed for non-linear effect to be significant [1].the effective area can be related to the spot size and it is also important in the context of confinement loss [2],micro bending loss[3], macro bending loss splicing loss[4]and numerical aperture[5].The chromatic dispersion of the PCF s can be determined by:

$$D = -\frac{\lambda}{c}.\frac{d^2 n_{eff}}{d\lambda^2} + D_m \ , n_{eff} = \frac{\beta}{K_o} \ , \ k_o = \frac{2\pi}{\lambda}$$

Where λ, c are wavelength and speed of light respectively in free space

n_{eef} the effective refractive index of the PCF core

D_m the material dispersion

However , the material dispersion can by calculated using sellmeier equation[6].

Their combination leads to signal degradation in optical fibers for telecommunications because the varying delay in arrival time between different components of signal "smearont" the signal in time[7].

2. Theoretical Background [2,5,7]

Maxwell's equations predict the propagation of electromagnetic energy away from time varying source in the form of waves.They can be expressed by:

$$\nabla X\vec{E} = -\frac{dB}{dt} = -jw\mu\vec{H} \quad \text{..........} \quad (1)$$

$$\nabla X\vec{H} = J + \frac{d\vec{D}}{dt} = (\sigma + jw\epsilon)\vec{E} \quad \text{.........} \quad (2)$$

$$\nabla . \vec{D} = \rho_v \quad \text{.........} \quad (3)$$

$$\nabla . \vec{B} = 0 \quad \text{.........} \quad (4)$$

By taking the curl of equation (1) and substitute in equation (2), we get

$$\nabla^2 E = jw\mu(\sigma + jw\epsilon)\vec{E} = \beta^2\vec{E} \quad \text{.........} \quad (5)$$

And by taking the curl of equation (2)and substitute in equation (1)

$$\nabla^2 H = jw\mu(\sigma + jw\epsilon)\vec{H} \quad \text{.......} \quad (6)$$

Where β: is the propagation constant and can be expressed as

$$\beta = \sqrt{jw\mu(\sigma + jw\epsilon)} = \alpha + j\gamma \quad \text{........} \quad (7)$$

Where α the attenuation constant which defines the rate which the fields of the waves are attenuated as the wave propagates

γ is the phase constant which defines the phase rate at which the phase changes as the wave propagates. From the properties of the medium $(\mu,\epsilon,\sigma)$the attenuation and phase constants can be calculated (i.e. $\beta^2 = jw\mu(\sigma + jw\epsilon) = (\alpha + j\gamma)^2 = \alpha^2 + 2j\alpha\gamma - \gamma^2$

Therefore

$$\alpha = w \left(\sqrt{\frac{\mu\epsilon}{2}(1 + \left(\frac{\sigma}{w\epsilon}\right)^2 - 1)} \right.$$

And ....(8)

$$\gamma = w \left(\sqrt{\frac{\mu\epsilon}{2}\ (1 + \left(\frac{\sigma}{w\epsilon}\right)^2 + 1)} \right.$$

W is the signal frequency in rad/sec

The propagation constant can express the effective refractive index and the wavelength dispersion as

$$D_w(\lambda) = -\frac{\lambda}{c}.\frac{d^2 n_{eff}}{d\lambda^2}$$

And ....(9)

$$n_{eff} = \frac{\beta(\lambda, n_m)}{K_o}$$

Where n_m is the refractive index of any material, K_o is the wave number

Novel Design of Curved Silica Photonic Crystal Fiber Polarization Converter

B. H. Almewafy[1], M.F.O. Hameed[2], Nihal F. F. Areed[2], A. M. Heikal[2], S.S.A.Obayya[2*]
[1]Faculty of Engineering, Electronics and Communications Engineering Department, Mansoura University, Egypt
[2] Centre for Photonics and Smart Materials, Zewail City of Science and Technology, Sheikh Zayed District,
6th of October City, Giza, Egypt. E-mail: sobayya@zewailcity.edu.eg

Abstract- A novel design of multiple sectioned passive polarization rotator (PR) based on curved silica photonic crystal fibre (PCF) is studied and analyzed using numerically efficient finite difference based full vectorial modal and propagation approaches. The suggested curved PCF PR has a rectangular core region with two missing air holes. It is found that by careful adjustment of the structure geometrical parameters and the bending radius, nearly 100% polarization conversion ratio with a device length of 9.144 mm can be achieved.

Polarization rotators (PRs) play an important role in modern optoelectronic and communication systems. Therefore, PRs have attracted the interest of many researchers in recent years. The PRs are used to control the polarization states in the communication systems [1] such as polarization switches and polarization modulators Initially, PR based on multi-sections structure with periodically alternating asymmetric loading was reported [2]. In addition, cascaded configuration of curved waveguide sections each with an alternative curvature direction was introduced in [3]. Moreover, photonic crystal fibre (PCF) has been shown to have potential for polarization conversion [4].

In this paper, a novel design of multiple sectioned passive PR based on curved silica PCF with rectangular core region is introduced and analyzed. The simulation results are obtained using full vectorial finite difference method [5] as well as full vectorial finite difference beam propagation method [6] with perfect matched layer (PML) boundary conditions. Figure 1(a) shows cross section of the conventional rectangular lattice silica PCF while the suggested PCF PR with two missing air holes is shown in Fig.1 (b). All the cladding air holes have the same diameter d and are arranged with hole pitchesΛ_x and Λ_y in x and y directions, respectively. The axial layout of the PR device is also shown in Fig. 1(c) where it can be seen that it consists of a series of cascaded waveguide bends with alternating curvatures. Each section has a length equivalent to an arc length of 2φ, and the radius of curvature is R. The core region is similar to rib waveguide with two slanted side walls. However, the reported structure does not require a complex fabrication process like the semiconductor waveguide with slanted sidewalls [4] with strong polarization conversion ratio.

Initially, polarization conversion in a single section of curved PCF PR shown in Fig.1(b) is investigated. In the proposed structure, all the cladding air holes have the same diameter of 1.6 μm and are arranged with hole pitches Λ_x=Λ_y= 1.8 μm. In addition, the refractive index of the silica background is taken as 1.45 at the operating wavelength λ of 1.55 μm. Figure 2 shows the variations of the normalized TE (P_y) and TM (P_x) powers with the propagation distance at different bending radii R = 600 μm, 700 μm, and 800 μm. It is revealed from this figure that small polarization conversion occurs using the single section PCF PR shown in Fig.1(b). This is due to the low modal hybridness of the suggested single section PCF PR. Therefore, a configuration of cascaded curved

PCF waveguide sections shown in Fig.1(b) is proposed for the first time to the best of the authors' knowledge to obtain complete polarization rotation. Figure 3 shows the variations of the normalized TE and TM powers with the number of sections for cascaded configuration with cladding hole diameter d of 1.6 μm, $\Lambda_x=\Lambda_y=1.8$ μm, $2\varphi=83^o$ and R=700 μm. This figure shows that complete polarization conversion occurs at around device length of 9.144 mm at $\lambda=1.55$ μm with nine sections only. The suggested PR has a large radius of curvature which will be easy for fabrication. More results will be presented in the conference including the critical fabrication tolerance on each waveguide parameter, and the operating wavelength which show that the proposed PR has tremendous potential as a practical design for PR device.

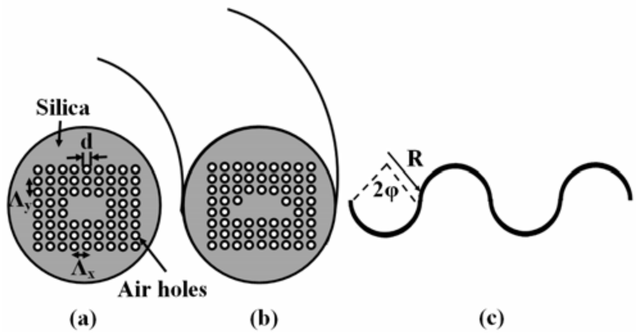

Fig. 1. Schematic diagram of the (b) conventional PCF with rectangular core region (b) bent PCF cross section. (c) Layout of the cascaded configuration of the bent waveguides in the longitudinal directions

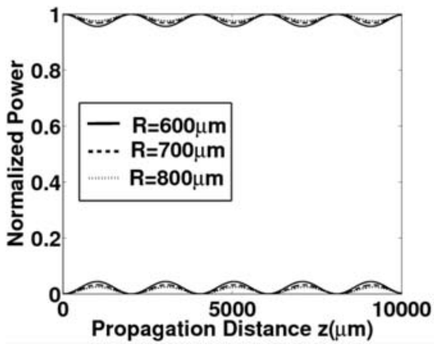

Fig. 2 Variation of the normalized TE and TM powers with the propagation distance at different bending radii R

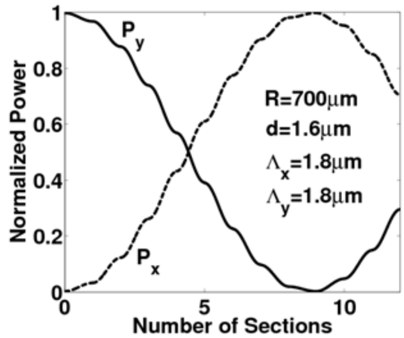

Fig. 3 Variation of the normalized TE and TM powers with the number of sections.

REFERENCES

1. Obayya, S., "Computational Photonics," first edition, John Wiley & Sons, 50-63, 2011
2. Shani, Y., R. Alferness, T. Koch, U. Koren, M. Oron, B. I. Miller and M. G. Young, "Polarization rotation in asymmetric periodic loaded rib waveguides," *Appl. Phys. Lett.*, Vol. 59, 1278–1280, 1991.
3. Obayya, S. S. A., N. Somasiri, B. M. A. Rahman and K. T. V. Grattan, "Full vectorial finite element modeling of novel polarization rotators," *Optical and Quantum Electronics*, Vol. 35, 297–312, 2003.
4. Hameed M. F. O., and S. S. A. Obayya,"Design of passive polarization rotator based on silica photonic crystal fiber," *Optics Letter*, Vol.36, No. 16, 3133-3135, 2011.
5. Fallahkhair, A. B., K. S. Li, and T. E. Murphy, "Vector Finite Difference Modesolver for Anisotropic Dielectric Waveguides," *IEEE J. Lightwave Technol.*, Vol.26, 1423-1431, 2008.
6. Huang, W. P., and C. L. Xu,"Simulation of three-dimensional optical waveguides by a full-vector beam propagation method," *IEEE journal of Quantum Electronics*, Vol. 29, 2639-2649, 1993.

Influence of Ag doping on structural and optical properties of ZnO thin films synthesized by sol-gel technique

H. Merzouk[1], A. Chelouche[1], D.djouadi[1] , A .Aksas[1], ,

[1] Laboratoire du Génie de l'Environnement (LGE), Université de Béjaia, Algérie

E-mail: hamid.merzouk@yahoo.fr

Abstract: Thin films of Ag-ZnO samples with different percentage of Ag content (1, 2 and 3 at %) were synthesized by a dip-coating sol-gel method. Samples present hexagonal wurtzite structure. The average grain size is about 15 nm. AFM shows a very low roughness of the layers for 2 at % Ag simples. Up to 3 at %, c-axis lattice parameter shifts towards higher value. The maximum transmission value is obtained for 2 at % simples.

The synthesis and applications of nanoscale structures based on zinc oxide was the subject of intense investigation in recent years. This is mainly due to the special properties of ZnO as a wide gap (3.37 eV) and large exciton binding energy (60meV) at room temperature. These features have made this material an excellent candidate for applications such as semiconductor luminescent emitting in the spectral region Blue-UV [1-3].

Among the different methods of preparation, the sol-gel method is easier to implement and is generally carried out at near room temperature. This technique should also be promising for doping ZnO nanostructures. The silver is one of the most promising dopant.

In this work, thin films of Ag doped ZnO were prepared by the sol-gel method and deposited on glass substrates by dip-coating technique. The effect of silver ions on the structural, morphological and optical properties of samples prepared was studied.

Experimental procedure:

Di-hydrate zinc acetate, ethanol, diethanolamine (DEA) and nitrate are used respectively as silver precursor, solvent, stabilizer and source doping. The doping level Ag / Zn is from 1 to 3%. The deposition of thin films was performed by dip-coating. The pulling speed was set at 20 mm / min. Finally, thin films prepared were annealed in air in a muffle furnace at 500 ° C.

Results and discussion:

ZnO and Ag-ZnO thin films X-ray diffraction spectra present hexagonal wurtzite structure. We note that doping favors c-axis orientation along planes (001) and (002). The calculated lattice parameter 'a' remains practically the same for all simples while the 'c' one increases from 5.177 Å (pure ZnO) to 5.300 Å (Ag3%-ZnO). This shows that the silver atoms introduced into the ZnO substitute Zn atoms in the crystal lattice [4]. The average grain size calculated by Scherrer formula is about 15 nm.

Scanning electron microscopy (SEM) images show a homogeneous distribution of crystallites for our prepared simples.

Silver doped ZnO thin films (1, 2 and 3%) topographies obtained by atomic force microscopy (AFM) are shown in Figure 1. The best roughness is found for ZnO layers doped with 2% silver atoms.

The UV-visible optical transmission spectra are given figure 2. The average value of the visible transmission is greater than 80%. The 2at% Ag doped layer shows the maximum transmission value.

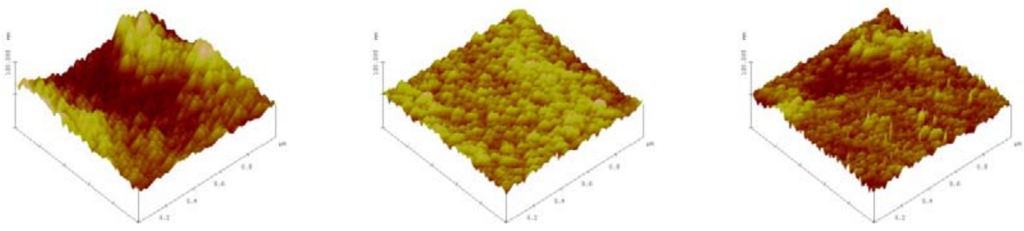

a) b) c)

Figure 1: Topography of Ag doped ZnO thin films: 1% (a), 2% (b) and 3% (c).

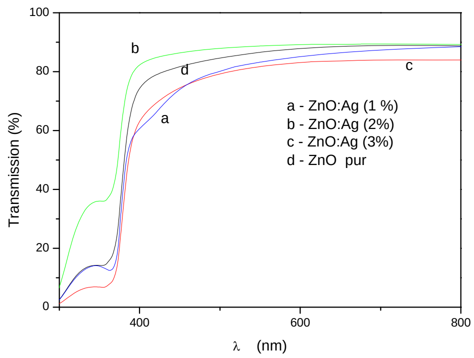

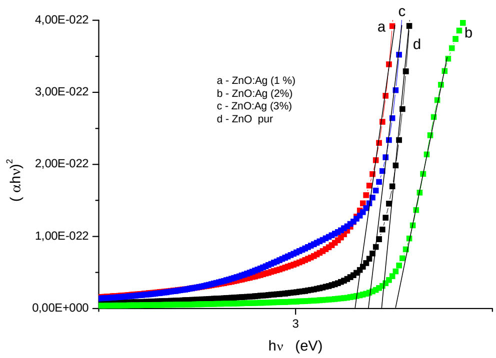

Figure 2: Transmittance spectra of ZnO and ZnO-Ag films Figure 3: Plot of $(\alpha h\upsilon)^2$ vs. photon energy

Optical band gap energy measurements, deduced from figure 3, vary between 3.15 and 3.25 eV. The wider gap is obtained for 1at% Ag-ZnO layer.

Conclusion:

The structural and optical properties of ZnO and ZnO-Ag films prepared by sol gel method were studied. The films exhibited the monocrystalline structure with hexagonal wurtzite. The surface morphology of the ZnO film is enhanced by incorporating Ag atoms. The best roughness is found for ZnO layers doped with 2% . . We note that doping favors c-axis orientation along planes (001) and (002). The 2at% Ag doped layer shows the maximum transmission value. The wider gap is obtained for 1at% Ag-ZnO layer.

[1]M. Krunks, A. Katerski, T. Dedova, I. OjaAcik, A. Mere, Solar Energy Materials and Solar Cells, Volume 92, Issue 9, 2008, pp- 1016-1019

[2] S.C. Ko, Y.C. Kim, S.S. Lee, S.H. Choi, S.R. Kim, Sensors Actuators A 103, (2003) pp-130-134;

[3] M.C. Carotta, A. Cervi, V. di Natale, S. Gherardi, A. Giberti, V. Guidi, D. Puzzovio, B. Vendemiati, G. Martinelli, M. Sacerdoti, D. Calestani, A. Zappettini, M. Zha, L. Zanotti, Sensors and Actuators B: Chemical, Vol. 137, Issue 1, 28 , 2009, pp- 164-169.

[4] X B Wang, C Song, K W Geng, F Zeng and F Pan, Luminescence and Raman scattering properties of Ag-doped ZnO films, JOURNAL OF PHYSICS D: APPLIED PHYSICS, 39 (2006) 4992–4996.

Numerical analysis of Whispering Gallery Mode Enhanced Light Absorption in amorphous silicon thin film absorber with Hemisphere and Nanocone Arrays

Gumin Kang, and Kyoungsik Kim*
School of Mechanical Engineering, Yonsei University,
262 Seongsanno, Seodaemun-gu, Seoul 120-749, South Korea
*corresponding author: kks@yonsei.ac.kr

Abstract- We numerically investigated the light absorption enhancement of amorphous silicon thin film absorber with dielectric hemisphere (HS) and nanocone (NC) arrays. The polystyrene (PS) HS and NC array have a graded index profile, resulting in broadband antireflection. Additionally, they can enhance light trapping by whispering gallery mode (WGM) resonances excited in the hemispherical or conical structure. FDTD simulation results show a confinement of incident light inside the HS or NC structure and resulting sharp resonance peaks verify the WGM resonance.

For optoelectronic devices such as photovoltaic (PV) solar cells and photodetectors, broadband light trapping enhancement is one of the important factors to improve the performance, especially in case of thin film semiconductors which have poor absorption. Amorphous silicon (a-Si) is a promising photovoltaic material as an active layer of thin film solar cells, and it has several advantages in large area coverage, light weight, and low manufacturing cost. For a-Si thin film solar cell with superior efficiency, thickness of a-Si layer should be at least a few microns to absorb visible light of solar spectrum, sufficiently. [1]

However, due to the very short minority carrier diffusion length (~100nm), bulk recombination process will occur in case of thick absorbing layer, resulting in reduction of photoelectron conversion efficiency.[2,3] In addition, in case of thick a-Si layer, there exist the light-induced degradation (the Staebler-Wronski effect) which is well known effect that lead to decrease in the final efficiency of a-Si solar cell (15~30%) by prolonged exposure of light. [4]

Therefore, light trapping enhancement in thin film absorber is very important to solve all problems that we mentioned above. Recently, Atwater's group theoretically proposed a new concept for absorption enhancement in thin film solar cells by using whispering gallery modes (WGM) in dielectric nanosphere array.[5]

In this study, we numerically investigate the light trapping enhancement effect of a-Si thin film (100nm) absorber with and without the dielectric hemisphere (HS) and nanocone (NC) array. HS and NC geometry is the mimicking structure of moth eye that has a graded-index profile, resulting in broadband antireflection effect. In addition, the light is highly reflected not only at the PS HS (NC)-amorphous silicon interface originated from the high refractive index of a-Si, but also at the PS HS (NC)-air interface due to the total internal reflection caused by higher index of PS compared to air.[6] Therefore, the incident light can be confined and trapped into the HS (NC) structures, resulting in excitation of WGMs. We perform 3D FDTD simulation to calculate the absorption characteristics of thin film with HS (NC) structures. Figure 1 (a) and (c) represents the scheme of thin film absorber with HS and NC array. The electric field intensity distributions of whole structure in x-z plane and absorption spectra of HS and NC array are shown as Fig 1(a'), 1(c') and Fig 1(b), 1(d), respectively. The localized e-field distribution in the HS and NC and several sharp resonance peaks appeared in absorption spectrum, are the evidences of WGM resonance.

The conclusion to be drawn here is that, the dielectric hemisphere and nanocone array can enhance broadband light absorption enhancement by antireflection effect from graded-index profile of geometry, and light trapping effect caused by the WGM resonance. We theoretically investigate the light absorption enhancement in thin film absorber with dielectric nanostructures which can be easily fabricated with low-cost and time-efficient soft nanoimprint lithography methods. 3D FDTD simulation results show a confinement of incident light inside the HS or NC structure and resulting sharp resonance peaks verify the WGM resonance.

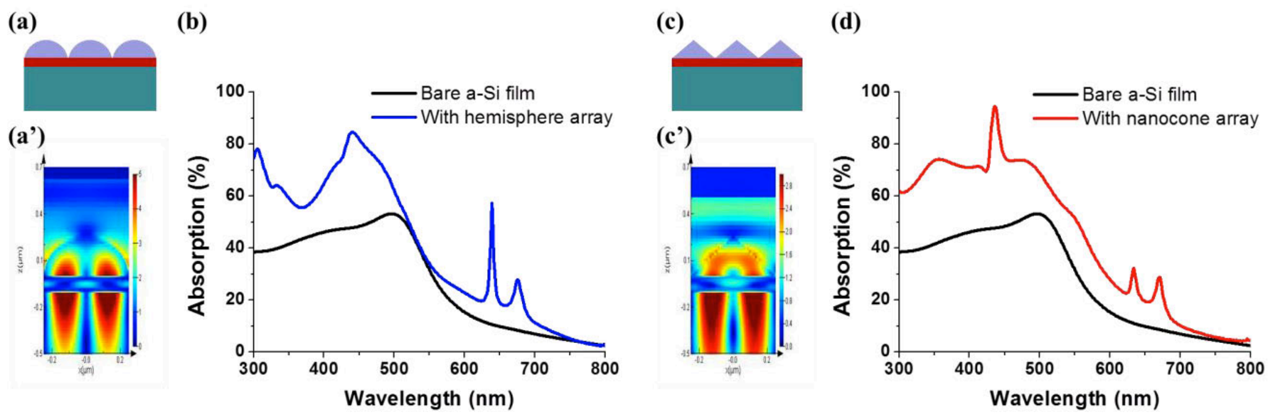

Fig. 1: Scheme of the a-Si thin film absorber with PS (a) hemisphere and (b) nanocone array. (a') and (c') represent electric field distribution of (a) and (c) in the x-z plane, respectively. (b) and (d) represent the simulated absorption spectra of a-Si thin film absorber with hemisphere and nanocone array compared to bare sample.

REFERENCES

1. Wang, W. Wu, S. Reinhardt, K. Lu, Y. Chen, S., “Broadband Light Absorption Enhancement in Thin-Film Silicon Solar Cells,” *Nano Lett.*, Vol. 10, 2012–2018, 2010.
2. Atwater, H. A., Polman, A., “Plasmonics for improved photovoltaic devices,” *Nat. Mater.*, Vol. 9, 205–213, 2010.
3. Zhu, J. Hsu, C.-M. Yu, Z. Fan, S. Cui, Y., “Nanodome solar cells with efficient light management and self-cleaning,” *Nano Lett.*, Vol. 10, 1989–1984, 2010.
4. Staebler, D. L., Wronski, C. R., “Reversible conductivity changes in discharge-produced amorphous silicon,” *Appl. Phys. Lett.*, Vol. 31, 292–294, 1977.
5. Grandider, J., Callahan, D., Munday, J. N., Atwater, H. A., "Light Absorption Enhancement in Thin-Film Solar Cells Using Whispering Gallery Modes in Dielectric Nanospheres," *Adv. Mater.*, Vol. 23, 1272–1276, 2011.
6. Ta, V. D., Chen, R., Sun, H. D., "Self-assembled flexible microlasers," *Adv. Mater.*, Vol. 24, OP60–OP64, 2012.

Ultrasensitive optical bio- and gas- sensor based on Photonic Crystal Surface Waves

T. Karakouz[1], V. N. Konopsky[2], E. V. Alieva[2], D. V. Basmanov[2], S. K. Sekatskii[1*], and G. Dietler[1]

[1] Laboratoire de Physique de la Matière Vivante, IPSB, BSP, Ecole Polytechnique Fédérale de Lausanne, CH1015 Lausanne, Switzerland

[2] Institute of Spectroscopy Russian Academy of Sciences, Moscow, Troitsk, Fizicheskaya str. 5, 142190 Russia

[*]corresponding author: Serguei. Sekatski@epfl.ch

Abstract- We report our recent results on design and development of ultrasensitive optical bio- and gas- sensor based on a properly designed Photonic Crystal (PC) supporting the propagation of bounded electromagnetic Surface Waves (SW) along the PC – medium to be studied interface.

We report our recent results on design and development of ultrasensitive optical bio- and gas- sensor based on a properly designed Photonic Crystal (PC) supporting the propagation of bounded electromagnetic Surface Waves (SW) along the PC – medium to be studied interface [1].

For gas sensing, this approach was used either with thin Pd or Au layer deposited onto the surface of a PC, which in this case, for certain wavelength and light incidence angle, is characterized by the same refractive index as the external medium thus enabling the ultralong surface plasmon propagation [1]. For the case of Pd, this enabled us to realize ultrasensitive detection of hydrogen [2, 3] and establish the size-dependent character of the hydrogen uptake for Pd-nanoparticles as well as the donation of hydrogen electrons to the collective electronic band of the metal [3]. Ultralong surface plasmon propagation for the ***blue*** laser line at 405 nm and sensitive detection of nitrogen dioxide was realized for the case of gold layers (paper in preparation). Schematic of these experiments is presented in the self-explanatory Figure 1.

For biosensing, we use bare (no metal coating) PC – external medium interface, specially treated to chemisorb protein layers, for the study of kinetics of the interprotein interactions. Besides quite large sensitivity, 0.2 pg/mm^2, this approach has additional advantages due to the possibility to excite simultaneously *s*- and *p*-polarized surface electromagnetic waves having very different penetration depths into an external medium. This enables to segregate surface and volume effects, thus drastically increasing both the sensitivity and reliability of the data obtained, and also to study interactions involving rather thick (of the order of one micron) objects such as bacteria, viruses, and certain cell organells – option unattainable for usual surface plasmon resonance-based detectors due to the short penetration depth of such plasmons. At present, this device has been successfully tested first for kinetic measurements of a few standard receptor – ligand interactions (streptavidin-biotin and IgG antigen – antibody pairs mouse/antimouse, rabbit/antirabbit) and then applied for the study of yet uncharacterized interactions between different fragments of faviviral (e.g. tick born encephalitis) surface glycoprotein E with its putative cell receptors (laminin binding protein, human $\alpha V\beta 3-$ integrin; this work is done together with the State Research Center of Virology and Biotechnology “Vector”, Koltsovo, Novosibirsk region, Russia; paper in preparation). These results and future perspectives of the method will be discussed.

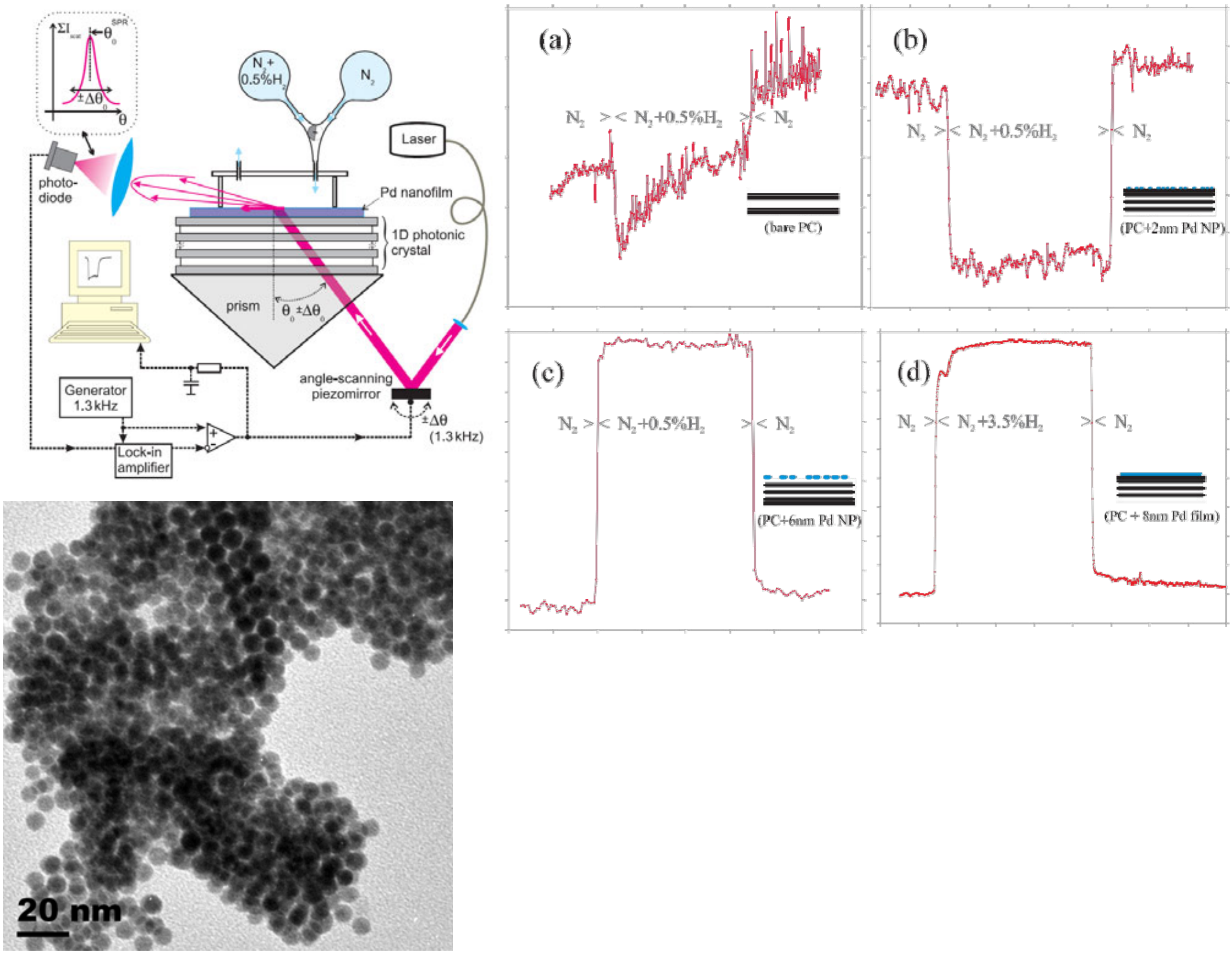

Fig. 1. Schematic of the ultrasensitive gas detector based on ultralong surface plasmons propagation along the gas – specially designed photonic crystal interface. Sensograms attesting the change of the signal upon hydrogen absorption are presented to the right; note the different signs of the signal for (mono)layers of 2-nm diameter Pd nanoparticles (b) and 6-nm diameter Pd nanoparticles (HRTEM image is presented below).

REFERENCES

1. V. N. Konopsky and E. V. Alieva, *Phys. Rev. Lett.*, **97**, 253904 (2006); V. N. Konopsky, *New J. Phys.* **12**, 093006 (2010).
2. V. N. Konopsky, D. N. Basmanov, E. V. Alieva *et al.*, *New J. Phys.* **12**, 063049 (2009).
3. V. N. Konopsky, D. N. Basmanov, E. V. Alieva *et al.*, *Appl. Phys. Lett.*, **100**, 083108 (2012).

Simple normalization for complete photonic bandgaps in two-dimensional photonic crystals with square lattice

Jong-Bin Yeo, and Hyun-Yong Lee
The Research Institute for Catalysis and Faculty of Applied Chemical Engineering,
Chonnam National University, Yongbong-dong, Gwangju, 500-757, Korea
*corresponding author: jbyeo@chonnam.ac.kr

Abstract- The characteristics of the photonic band gaps(PBGs) in two-dimensional photonic crystals(2D PCs) were theoretically studied using a FDTD simulation method. A novel concept of an optical coverage ratio(OCR) was proposed as a criterion parameter to determine whether the complete PBGs. The OCR is an optically compensated parameter given as a function of index contrast and filling factor. For PCs with the same OCR, but the different n_D, n_B, and η, the frequency range of the complete PBG could be normalized.

Proper photonic crystals (PCs) structure has been designed by the 'try to again' method with the calculation/estimation of the optical characteristics for the designed PC structures. The finite-difference time-domain (FDTD) method is very suitable for investigation into the calculation/estimation of the optical characteristics for the designed PC structures. There are several important factors of PCs that dominate their optical characteristics, such as refractive indices of the PC materials, type of periodic structure, periodic size, and radius of hole/dot. It is very capricious to design the PC structure, as well as estimate the properties of PCs intuitively, prior to their calculation, due to change in the optical characteristics originated by the complex combination of these important factors. Therefore, normalization of the several parameters influencing the optical characteristics of PCs is required as one factor to design PCs for various and easy applications. Only the well-designed PCs can obtain the property of PBGs, while the general periodic PC structures cannot show the properties of the PBGs. Application of the normalized factor towards confirmation of the existence and region of PBGs can become simple because of reduced application of the 'try to again' method. In the previous study, the authors demonstrated the normalized factor in the one-dimensional (1D) PCs, which is the normalized frequency. In this study, the novel concept of normalized factor is proposed for the 2D PCs with an optical coverage ratio (OCR) as a new structural parameter to determine the PBGs for TE-polarized light.

Figure 1 shows the schematic diagram of the studied square-lattice 2D PCs and the structural parameters. The left side of Fig. 1 is the real structure for the square array of dielectric columns, with radius r and index constant n_B (or n_D). The material is homogeneous in the perpendicular direction, and periodic along the horizontal with the lattice constant (periodic size) Λ. The right inset shows the Brillouin zone, with the irreducible zone shaded gray. Along the horizontal axis the in-plane wave vector k// proceeds along the edge of the irreducible Brillouin zone, from Γ to X to M. The equation in Fig. 1 is a definition of the OCR factor proposed in this study. For instance, a PBG of noticeable extent requires a large index contrast and geometric filling factor (η), which is typically implemented by combining two or more of the different materials (for example, air and dielectric materials such as SiO_2). The OCR indicates an integrated factor. Both η and OCR are given by:

$$\eta = 4\pi r^2/(2\Lambda)^2 \tag{1}$$

$$OCR = 4\pi (n_D r)^2/(2n_B \Lambda)^2 \tag{2}$$

$$r/\Lambda = (n_B/n_D)\sqrt{OCR/\pi} \tag{3}$$

Figure 2 shows the OCR and η of the square-lattice 2D PC as a function of the ratio of radius (r/Λ). The dashed line is the case of OCR = 1.13, with a variable index contrast (n_D/n_B). The condition of OCR = 1.13 denotes that the complex factors consist of n_B =1, n_D = 3, and r/Λ = 0.2. The same ratio of the radius shows the same filling factor, but possessing a different OCR with various index contrasts because the OCR factor includes the index factor. Solid lines show the OCR changes in each index contrast. The OCR value linearly simultaneously increased as the index contrast increased at the same filling factor, while the filling factor decreased as the index contrast increased under identical OCR conditions.

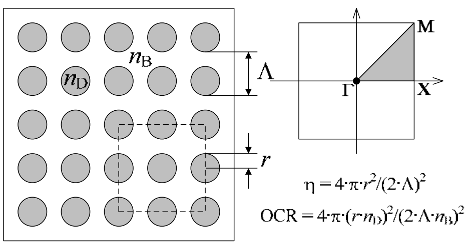

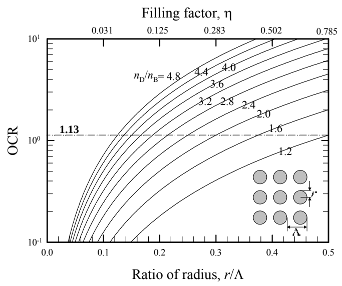

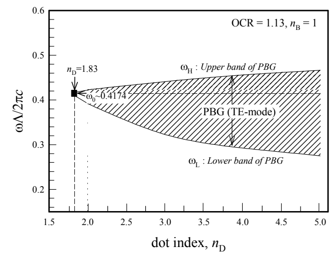

Fig 1. Schematic view of the studied square-lattice photonic crystal and the irreducible portion of the 1st Brillouin zone.

Fig 2. Dependency of optical coverage ratio (OCR) according to the ratios of radius and index contrast in the square-lattice photonic crystal.

Fig 3. Changes in upper and lower bands of the PBGs (OCR=1.13) as a function of n_D;upper and lower bands are representative n_B and n_D region properties, respectively.

Figure 3 shows the changes in the upper and lower bands in the PBG (at OCR = 1.13 and n_B = 1) as a function of n_D. The PBGs occurred at the above region of n_D = 1.83. This frequency was defined by ω_0 and the threshold index contrast. The PBGs were expanded when n_D increased. This is the expansion of PBG due to the increase in difference in the refractive index as reported previously. In particular, the lower band was more widely expanded than the upper band, because the fundamental frequency spectrum was decided by the following equation:

$$\omega(k) = ck/(\varepsilon^{1/2}) \quad (4).$$

The spread frequency region was calculated by Eq. (4), where ε is the dielectric constant factor and therefore, the spread frequency change is a function of refractive index. Accordingly, the upper band is defined by the n_B characteristic (in the case of n_B = 1, the air band), while the lower band is defined by the n_D characteristic. Thus, rapid expansion of the lower band in the PBGs was decided by a change in n_D (*i.e.*, ω_0 was not located in the center region of ω_H and ω_L, but leaned toward the lower refractive index region of ω_H). In the case of Fig. 3, the critical conditions for PBGs are n_D/n_B >= 1.83 in OCR = 1.13 (in this case, ω_0 = 0.4174). This indicates that ω_0 is 0.4174 at n_B = 1, n_D = 1.83, and $r = 0.65557/\Lambda$ in 2D-square lattice PCs. Accordingly, λ is 2.12 μm ($\lambda = \Lambda/\omega_0$) at Λ = 1.0 μm.

This novel approach with an OCR is appropriate and simple for designing 2D PCs. The approach proposed in this study can also be readily extended to address a greater variety of periodic structure designs, such as optimization of PCs in combined TE and TM fields, handling other types of lattices (triangular and photonic quasi-crystals), as well as modeling and optimizing the design of 3D PCs.

Acknowledgements, This research was supported by Basic Science Research Program through the National Research Foundation of Korea(NRF) funded by the Ministry of Education, Science and Technology(No. 2012037897)

REFERENCES

1. E. Yablonovitch, *Phys. Rev. Lett*. **58**, 2059 (1987)
2. J.D.Joannopoulos, R. Meada, and J. Winn, *Photonic Crystals* (Princeton University Press, Princeton, 2nd edition, 1995)
3. J. B. Yeo, S. D. Yun, and H. Y. Lee, *J. Appl. Phys*., 102, 084502 (2007)
4. J. B. Yeo, S. D. Yun, N. H. Kim, and H. Y. Lee, J. *Vac. Sci. Tech*., **B 27** (4), 1886 (2009)

Polymer microtips fabricated at the extremity of different type optical fibers

P. Pura[1], B. Wiśniowski[2], A. Spadło[1], L. R. Jaroszewicz[1*], P. Marć[1], and M. Kujawinska[2]
[1]New Technologies and Chemistry Faculty, Military University of Technology, Poland
[2]Institute of Micromechanics and Photonics, Warsaw University of Technology, Poland
[*]corresponding author: jarosz@wat.edu.pl

Abstract- In this paper we present a simple method of manufacturing micrometer-sized polymer elements at the extremity of both photonic crystal and polymer fibers and their possible modifications in order to provide requested functionalities. Exemplary polymer microtips manufactured from the polymeric material will investigate as coupling elements between different types of optical fibers including silica and polymer materials and standard single-mode and photonic crystal, also.

In recent decades, many fabrication methods of microtips which may serve as microlenses at the extremity of the optical fiber, have been developed: electric arc melting, laser micromachining, chemical etching or exposition of a photosensitive film to the UV light. All of these techniques are time and energy consuming, and impose an accurate control of experimental parameters[1]. From the above reason presented firstly in 2001 by Bachelot et al.[2] a new method consists of growing a micro polymer tip which is a an extension of the optical fiber core which seems to be much better practice. In this method, the light is exposed through the optical fiber on a photopolymer liquid solution put at the other end of the optical fiber[3]. In this way, a new attractive technique can be discussed as a method for fabrication flexibile coupling between two optical fibers[4].

The last method has been used for fabrication of polymer microtips at the extremity of photonic crystal fibers (PCFs). It is a new idea which should improve a manufacture patch cord with PCF fibers coupled with the SMF-28[5] or polymer optical fiber. As an initial structure we used the large mode area PCF type LMA-10 (fabricated by NKT Photonics) characterized by a 10±1 μm core diameter, 7.5±1.0 μm MFD and 0.10 NA at wavelength 980 nm.

The photopolymerizable formulation is made up of three basic components: sensitizer dye (Eosin Y disodium salt), co-initiator (MDEAN - methyldiethanolamine) and multifunctional acrylate (triacrylate) monomer (PETA - penthaerythritoltriacrylate), mixed in a weight proportion described by Bachelot et al.[2] Such mixture has high sensitivity for the wavelength in range from 450 nm to 550 nm (maximum for 530 nm), hence, the green laser with wavelength of 532nm can be used for photopolimerization. Since light distribution in the short section of PCF strongly depends on external conditions, the special method has been taken for protection it during a drop of the mixture deposition at the end of the fiber. This drop has been maintained by surface tension and polymerization carried by light exposure with an intensity of 5 μW and time in range from 20 s to 60 s. After polymerization, the polimer tip on the PCF end was washed in ethanol.

Figure 1 shows focusing properties of the example 28.5 μm length microtip manufactured at LMA-10 PCF end according to the above procedure. As one can see the structure has direct influence on focusing properties, strong reflections around the central part (right image in Fig. 1). In this example, light propagates in core as well as in the first ring of PCF's air-holes (left image in Fig. 1). Hence the manufactured microtip (middle image in Fig. 1) has guiding properties in all above regions (core and the first ring of air-holes).

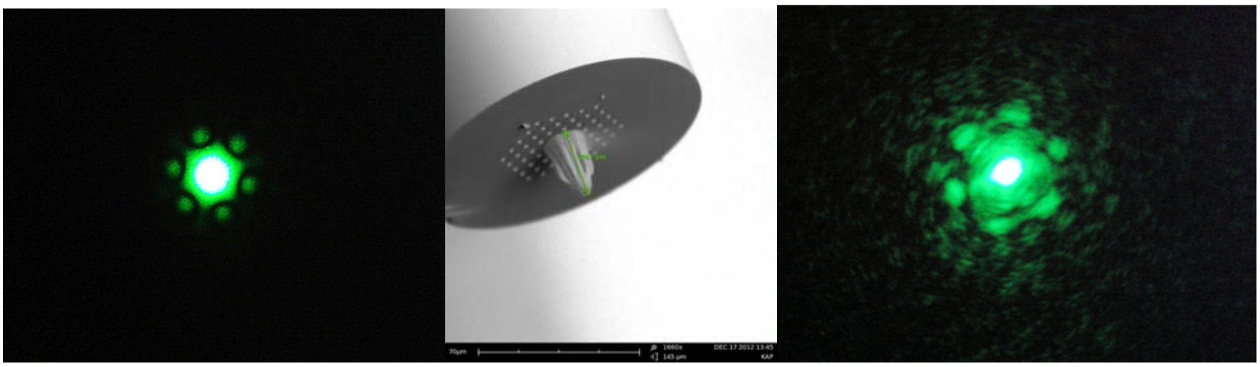

Figure 1 Power distribution in the far field from LMA-10 without (left) and with (right) monomer tips. The general view of 28.5 μm long microtip formulated on this fiber is shown in the middle of SEM image of the PCF end.

The mixture composition together with light exposure parameters (power and time) have general influence on microtip formulation - see Fig. 2. In this way it is a way for manufacturing the coupling elements between different type fibers which results will be presented at the conference after finalizing the patent application.

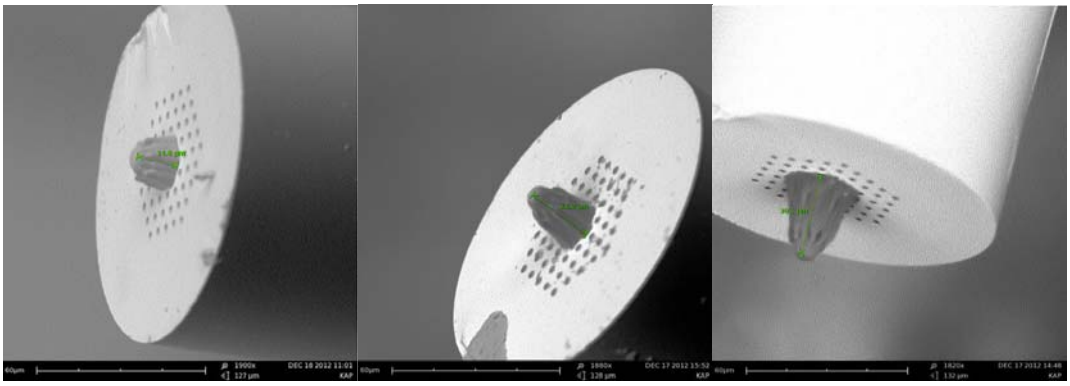

Figure 2 Influence of exposure time for microtip length growing from 14.6 μm for 20 s, via 23.9 μm for 45 s up to 30.5 μm for 60 s. All processes have the same other parameters.

Acknowledgements
Work described in this paper was partially supported by the EU FP7 as the COST action TD1001, and by the National Centre for Research and Development within the Innovative Economy Programme as the key project POIG.01.03.01-14-016/08-07 and InnoTech-2 research programme ID 18369.

REFERENCES

1. Kujawińska M., V. Parat, et al. "Interferometric and tomographic investigations of polymer microtips fabricated at the extremity of optical fibers", *Proc. SPIE*, Vol. 8494, DOI:10.1117/12.940779, 2012.
2. Bachelot R., C. Ecoffet, et al. "Integration of micrometer-sized polymer elements at the end of Optical fibres by free-redical photopolymerization", Appl. Opt., Vol. 40, No. 32, 5860-5871, 2001.
3. Soppera O., C. Truck and D. J. Lougnot, "Fabrication of micro-optical devices by self-guiding photopolymerization in the near IR", *Opt. Lett.,* Vol. 34, No. 4, 461-463, 2009.
4. Jradi S., O. Soppera and J. Lougnot, "Fabrication of polymer waveguides between two optical fibres using spatially controlled light-induced polymerization", *Appl. Opt.*, Vol. 47,No. 22, 3987-3993, 2008.
5. Jaroszewicz, L. R., M. Murawski, et al., "Low-Loss Patch Cords by Effective Splicing of Various Photonic Crystal Fibers With Standard Single Mode Fiber", *J. Lightwave Techn.,* Vol. 29, No. 19, 2940-2946, 2011.

One-way waveguide base on magnetoplasmonic chiral edge states

Rui-xin Wu[1*], Yin Poo[1], and Zhifang Lin[2]
[1] School of Electronic Sciences and Engineering, Nanjing University, Nanjing 210093, China
[2] Key Laboratory of Micro and Nano Photonic Structures (Ministry of Education), Fudan University, Shanghai 200433, China
[*]corresponding author: rxwu@nju.edu.cn

Abstract- In the photonic band gap induced by magnetic surface plasmon resonance, magnetic photonic crystals may have self-guiding electromagnetic chiral edge states whose dispersion curves are insensitive to the surface morphology when magnetic crystals are truncated. The unique characteristic of the MSP induced edge states enable flexible design of robust unidirectional subwavelength waveguides that contain bends at various angles, providing an alternative way for manipulating electromagnetic waves at subwavelength scales.

Robust unidirectional transportation due to chiral edge states (CESs) in quantum Hall effect is one of the most fascinating phenomena in electronic systems [1]. The CES carries current in one direction and the transport is robust against scattering from disorder [2]. Such one-way state is usually realized by applying a strong magnetic field perpendicular to two-dimensional (2D) electron systems to break time-reversal symmetry (TRS).

Based on the analogy to the electronic systems, Haldane and Raghu [3-4] theoretically predicted the existence of topological electromagnetic (EM) CESs in two-dimensional (2D) photonic crystals (PCs) made of nonreciprocal media, which also exhibit robust one-way propagation characteristics similar to their electronic counterpart. Since then, both theoretical and experimental works have been devoted to explore the unique wave propagation property of the EM edge states [6-9]. The one-way waveguide is realized by the magnetic PCs with square and honeycomb lattice [8-9].

Meanwhile, there was proposed [10] another type of one-way edge states associated with magnetic surface plasmon (MSP). Compared with the EM edge states based on the analogy of QHE, the MSP based edge states do not need to rely on the periodicity of photonic crystals and can work even on homogeneous bulk system. As a result, such edge states exhibit surface-morphology-independent characteristic, adding considerable flexibility to wave manipulation.

In this talk, we report using the surface-morphology-independent characteristics it is possible to realize one-way waveguide in subwavelength. We adopt a two-dimensional (2D) magnetic photonic crystal composed of magnetic ferrite rods to compose waveguide. The rods can have much smaller demagnetization effect, allowing for a significant decrease of the required static bias magnetic field and therefore enabling experimental realization. The studies show that in the frequency range of chiral edge states associated with MSP, the waveguide demonstrate a robustness of wave propagation against disorder on the edge and morphology of the edge of the MPC waveguide. Based on these advantages, we implement sub-wavelength one-way waveguides with bends of various angles. The theoretic result shown in Fig.1 illustrates that the robust feature of wave propagation due to the magnetoplasmonic CESs guarantees nearly full power transmission at the sub-wavelength scale although the bends cause some kind of disorder at the turning on the edge of the MPC, demonstrating considerably flexible ways for EM wave manipulation even at subwavelength scale. The study is further proved by the experiments and show additional advantage of the magnetoplasmonic CESs, the flexible magnetic tenability. These features potentially open up a new avenue towards applications of MPCs as spin wave or magnonic logic devices.

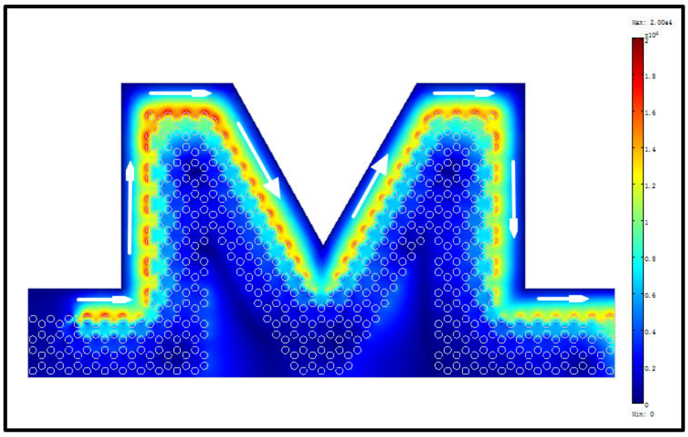

Figure 1 Magnitude of the electrical field distribution in the M-shaped waveguide at 5.5 GHz. The arrows represent the wave direction propagating along the edge of the M-shaped waveguide.

Acknowledgements: This work is supported by the NSFC (61271080, 61071007, and 61001017) and RFDP (20110091110030, 20100091120045). RXW thanks partial support from STP of Jiangsu Province (BK2012722).

REFERENCES

1. K. V. Klitzing, G. Dorda and M.Pepper, Phys. Rev. Lett. 45, 494 (1980).
2. D. J. Thouless et al., Phys. Rev. Lett. 49, 405 (1982).
3. F. D. M. Haldane and S. Raghu, Phys. Rev. Lett. 100, 013904 (2008).
4. S. Raghu and F. D. M. Haldane, Phys. Rev. A 78, 033834 (2008).
5. Z. Wang, Y. D. Chong, J. D. Joannopoulos and M. Soljačić, Phys. Rev. Lett. 100, 013905 (2008).
6. T. Ochiai and M. Onoda, Phys. Rev. B 80, 155103 (2009).
7. K. J. Fang, Z. F Yu, and S. H. Fan, Phys. Rev. B 84, 075477 (2011).
8. Z. Wang, Y. D. Chong, J. D. Joannopoulos and M. Soljačić, Nature (London) 461, 772 (2009).
9. Y. Poo, R. X. Wu, Z.F. Lin, Y. Yang and C.T. Chan, Phys. Rev. Lett. 106, 093903 (2011).
10. Z. F. Yu, G. Veronis, Z. Wang and S. H. Fan, Phys. Rev. Lett. 100, 023902 (2008).

Hybrid propagation in a polymer-based photonic liquid crystal fiber

T. R. Wolinski[1], M.Tefelska[1*], K. Milenko[1], A. W. Domanski[1], S. Ertman[1], K. Orzechowski[1], K. Rutkowska[1], M. Sierakowski[1], E. Nowinowski-Kruszelnicki[2], and R. Dabrowski[2]

[1]Faculty of Physics, Warsaw Univ. of Technology, Koszykowa 75, 00-662 Warszawa, Poland

[2]Military Univ. of Technology, Warszawa, Poland

[*]corresponding author: martef@if.pw.edu.pl

Abstract-Hybrid propagation in a polymer photonic crystal fiber (FM-340 KIRIAMA) infiltrated with a specially designed liquid crystal (1781A-2' nematic mixture) has been demonstrated for the first time. In lower temperatures index guiding governed whereas in higher temperatures the photonic band gap effect was responsible for propagation.

Over the past decade, photonic crystal fibers (PCFs) [1] have attracted an increasing scientific interest, due to a great number of potential applications. Optical wave guiding in a PCF is governed by one of two principal mechanisms responsible for light trapping within the core: a classical propagation effect based on the modified total internal reflection (mTIR or index guiding) and the photonic band gap (PBG) effect, that occurs if the refractive index of the core is lower than the mean reflective index of the cladding region. Infiltrating the air-holes with liquid crystals (LCs) introduces highly-tunable photonic structures, called photonic liquid crystal fibers (PLCFs) [2-6]. Due to high electro-, magneto-, and thermo-optic responses of LCs, their refractive indices may be relatively easily changed by physical fields and can highly influence propagation conditions within PLCFs. One of the most spectacular phenomena was successful realization of temperature-induced switching between two mechanisms of light propagation that was demonstrated for silica-glass based PLCFs [3].

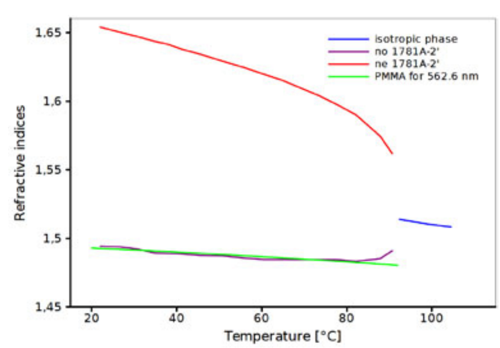

Figure 1 Thermal dependence of refractive indices of the nematic 1781A-2' LC mixture

The paper presents for the first time temperature-induced hybrid propagation in a polymer PCF infiltrated with a specially designed nematic 1781A-2' LC mixture. (Fig. 1). The polymer host fiber was commercially available FM-340 KIRIAMA PCF composed of polymethylmethacryle (PMMA) core/cladding material and polycarbonate (PC) outer coating. In the temperature range ($28^{o}\div69\,^{o}$ C) index-guiding (mTIR) propagation (Figs. 2a and 3a) dominates due to the fact that the PMMA core refractive index is higher the LC ordinary index. With increasing temperature contrast between the cladding inclusions and the core refractive indices diminishes and, consequently, the mTIR effect disappears. The transmitted spectrum fades into a lack of propagation when the average refractive index of the cladding region is close to the PMMA core index. When the temperature is above a critical point, the average effective refractive index of the polymer cladding with LC cylindrical holes decreases sufficiently above the PMMA core refractive index and propagation reappears. Consequently, the PLCF becomes a typical PBG fiber characterized by a selective wavelengths propagation (Figs 2b and 3b).

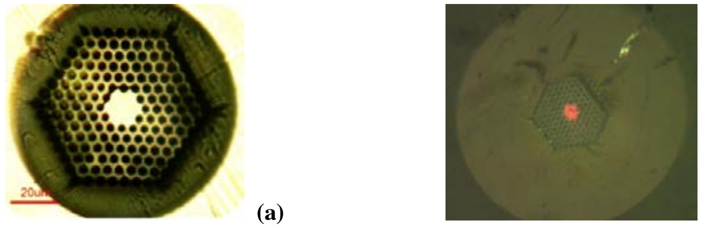

(a) (b)

Figure 2 End face of the FM-340 KIRIAMA polymer PCF (a) and after infiltration with the 1781A-2' LC mixture (b)

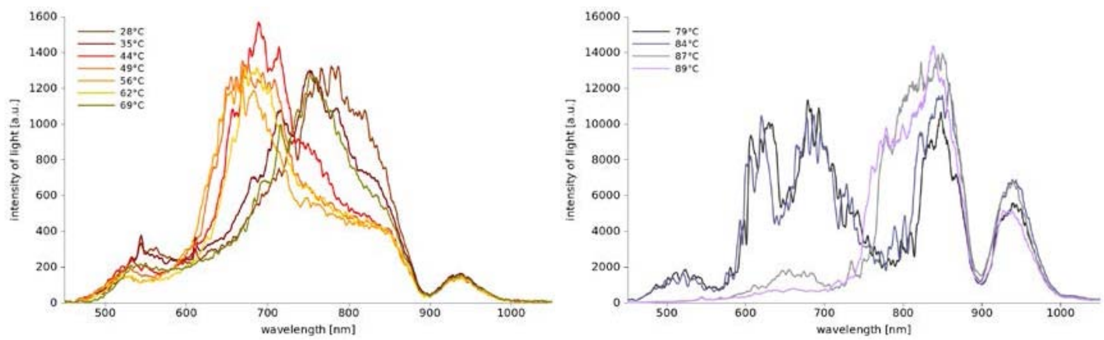

(a) (b)

Figure 3 Temperature-induced hybrid propagation in FM-340 KIRIAMA polymer PCF infiltrated with the 1781A-2' LC: index guiding (a) and the PBG effect (b)

Acknowledgements This work was supported by the Polish National Science Centre (NCN) under the grant no. 2011/01/B/ST7/05015.

REFERENCES

1. Russell, P. St. J. "Photonic Crystal Fibers, " *Science*; Vol. 299, No. 5605, 358-262, 2003.
2. Larsen T.T., A. Bjarklev, D. S. Hermann, and J. Broeng "Optical devices based on liquid crystal photonic bandgap fibers". *Opt. Exp.*, Vol. 11, No. 20, 2589-2596, 2003.
3. Wolinski T.R., K. Szaniawska, S. Ertman, P. Lesiak, A. W. Domanski, R. Dabrowski, E. Nowinowski-Kruszelnicki, and J. Wojcik "Influence of temperature and electrical fields on propagation properties of photonic liquid crystal fibers", *Meas. Sci. Techn.*, Vol. 17, 985–991, 2006.
4. Milenko, K. , T. R. Wolinski , P. Shum, and J. J. Hu "Temperature sensitive photonic liquid crystal fiber modal Interferometer", *IEEE Photonics J.* , Vol. 4, No. 5, 1855-1860, 2012.
5. Tefelska, M. M., S. Ertman, T. R. Wolinski, P. Mergo, and R. Dabrowski "Large area multimode photonic band gap propagation in photonic liquid crystal fiber", *IEEE Phot. Techn. Lett.,* Vol. 24, 631 – 633, 2012.
6. Wolinski, T. R. "Photonics Liquid Crystal Fiber Sensors for Safety and Security Monitoring", in *Photonics sensing: principle and applications for safety and security monitoring*, Eds. G. Xiao and W. J. Bock, John Wiley and Sons, pp 147-182, 2012.

Using metallic photonic crystals as visible light sources

S. Belousov[1], **M. Bogdanova**[1], **A. Deinega**[1], **S. Eiderman**[1], **I. Valuev**[1], **Yu. Lozovik**[1], **I. Polishchuk**[1], **B. Potapkin**[1], **B. Ramamurthi**[2], **T. Deng**[2], **and V. Midha**[2]

[1]Kintech Lab Ltd., Russia
[2]GE Global Research Center, USA
belousov@kintechlab.com

Abstract— We study the possibility of using metallic photonic crystals (PCs) as visible light sources. We achieve a substantial reduction of the emissivity in the infrared along with its increase in the visible with an optimal direct opal PC geometry. We take into account disorder of the PC, and we get quantitative agreement between the numerical and experimental results. Finally, we discuss how the results are affected by absorption in known refractory host materials necessary for fixing the PC elements.

Recently it was proposed to use PCs as a source of visible light [1, 2, 3]. Suppression of the IR emission of such sources may increase their efficiency in comparison with conventional incandescent lamps which emit mostly (about 95%) in the IR.

In this work we focused on practically achievable PC-based visible light emitters, namely the three- and two-dimensional PC structures with tungsten emitting elements. We analyze a number of possible three-dimensional tungsten PC geometries, perform numerical simulations, and support the obtained results experimentally.

We use Kirchhoff's law of thermal radiation and obtain the emissivity of a PC layer from its absorption coefficient [4, 5, 6]. The emitted energy flow from the PC layer at a given ambient temperature can be found by integrating the emissivity weighted with the blackbody spectral radiation density, in the hemisphere above the layer. The efficiency of light emission E is obtained as the ratio of the emitted energy flow in the visible J_{vis} to the total energy flow J_{tot}. We apply the finite-difference time-domain (FDTD) method [7, 8] to obtain the absorption coefficient of the PC layer numerically as a function of wavelength and incident angles.

We found that the highest emission efficiency $E \approx 15\%$ is achived for a direct opal PC, consisting of $N = 2$ layers of spheres arranged in the FCC lattice, stacked along (111) crystallographic direction. Each layer of this structure is a 2D triangular lattice with the period equal to $a = 0.45$, and radius of the spheres $R = 0.07\ \mu m$. The absorption spectra of the PC features a pronounced peak due to the resonant absorption of the electromagnetic waves in the 2D triangular layers constituting the opal PC (Fig. 1). The obtained efficiency is three times greater than that for the bulk tungsten ($E_{bulk} \approx 5\%$).

Further, a PC monolayer sample was fabricated on top of the quartz substrate. The sample consisted of tungsten spherical segment caps on top of cylindrical quartz posts arranged in the triangular lattice with $a = 0.55\ \mu m$. The absorption coefficient of the sample at the normal incidence was measured at the room temperature. The disorder inherent to the fabricated sample is modeled with random shifts of PC elements from their respective lattice nodes (ρ_{max} is the lattice disorder parameter - the maximum absolute displacement). The value of $\rho_{\mathrm{max}} = 0.3a$ yields the best agreement of the calculated peak height with the experimental data (Fig. 2).

The "imperfectness" of the experimental PC leads to decrease of the emission in the visible, however, the IR emission is still small.

The scattering elements of a PC should be embedded in a refractory material (host). There is only a small number of refractory materials, resistant to high temperatures and applicable for this purpose (i. e., yttrium-stabilized zirconia and hafnia). However, when being heated, these materials emit in the IR. We found that it leads to a substantial efficiency reduction of the whole structure (not shown for brevity).

In conclusion, we studied the possibility of using PCs as high-efficiency light sources. We found that the direct opal PC geometry provides the highest emission efficiency in the visible. In real PC

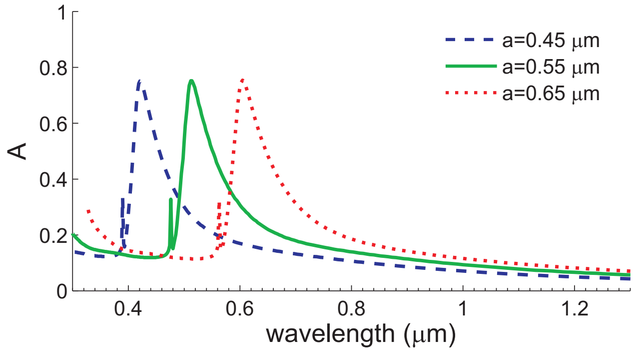

Figure 1: The absorption spectra of PC at normal incidence for varying lattice constant a, and $R = 0.156a$. $N = 2$, $T = 2400K$.

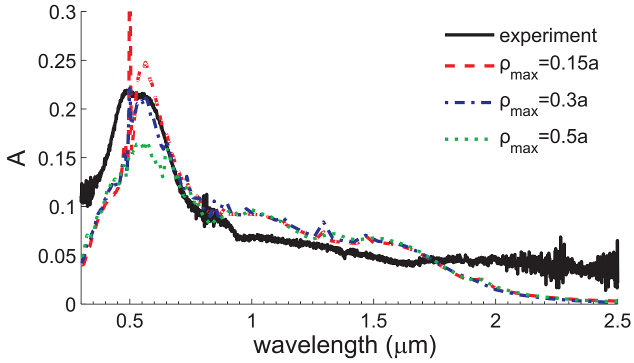

Figure 2: The tungsten PC monolayer absorption spectrum at normal incidence at the room temperature ($T = 298K$). The PC parameters: $a = 0.55$ μm, sphere segments radius 0.1 μm, and height 0.02 μm, the quartz posts radius is 0.17 μm and the height is 0.15 μm.

samples, a lattice disorder and a size dispersion of the constituent elements are present. This leads to a decrease of the peak emissivity in the visible, however, emissivity in the IR remains small.

For a practical application, the direct opal lattice needs to be embedded in a refractory host matrix. Known refractory materials are characterized by a high emissivity at the temperatures of interest. This leads to a lower PC peak emissivity in the visible. Therefore, implementing PC based light sources requires that low-absorbing refractory materials should be explored.

ACKNOWLEDGMENT

The work was partially supported by The Ministry of Science and Education of Russia under the contract No.16.523.11.3004.

REFERENCES

1. J. G. Fleming and S. Y. Lin and I. El-Kady and R. Biswas and K. M. Ho, "All-metallic three-dimensional photonic crystals with a large infrared band gap," *Nature* 417, 52–55, 2002.
2. Z.-Y. Li, "Modified thermal radiation in three-dimensional photonic crystals," *Phys. Rev. B* 66, 241103, 2002.
3. S. John and R. Wang, "Metallic photonic-band-gap filament architectures for optimized incandescent lighting," *Phys. Rev. A* 78, 043809, 2008.
4. C. M. Cornelius and J. P. Dowling, "Modification of Planck blackbody radiation by photonic band-gap structures," *Phys. Rev. A* 59, 4736, 1999.
5. D. L. C. Chan, M. Soljacic, and J. D. Joannopoulos, "Direct calculation of thermal emission for three-dimensionally periodic photonic crystal slabs," *Phys. Rev. E* 74, 036615, 2006.
6. C. J. Schuler, C. Wolff, K. Busch, and M. Florescu, "Thermal emission from finite photonic crystals", *Appl. Phys. Lett.* 95, 241103, 2009.
7. A. Taflove and S. H. Hagness, *Computational Electrodynamics: The Finite Difference Time-Domain Method*, Artech House, Boston (2005).
8. Electromagnetic Template Library (EMTL), Kintech Lab Ltd, `http://fdtd.kintechlab.com`

Eigenmodes Analysis in 2-D Lorentz-Type Frequency-Dependent Photonic Crystals

Amin Gul HANIF[1*], Toru UNO[2], and Takuji ARIMA[3]
Tokyo University of Agriculture and Technology
2-24-16 Naka-cho, Koganei-shi, Tokyo, Japan 184-0012
[*]50009834203@st.tuat.ac.jp

Abstract- Electromagnetic wave propagation in metamaterials including photonic crystals has been widely investigated due to their inherent capabilities for developing novel devices in optics, microwave and antenna engineering. In reality, most of the materials are frequency-dependent; on the other hand, it is necessary to investigate how the performance of photonic crystals depends on frequency. In this paper, it is shown that the eigenmodes can be clearly ad accurately calculated in two-dimensional (2-D) Lorentz-type frequency-dependent photonic crystals using a new finite-difference frequency-domain (FDFD) algorithm.

Summary- Recently, remarkable progress has been made in the research of photonic crystals (PCs) due to their various applications in optics, microwave, and antenna engineering [1, 2]. Lately, interest has grown in the analyzing dispersive or frequency-dependent PCs for novel applications. Therefore, accurate models of the band structure of PCs structures composed of frequency-dependent materials is highly desirable for efficient analysis of wave propagation phenomena over a wide range of frequencies in microwave and optical fields.

Several numerical methods have been used to compute the band structure of 2-D PCs. The most commonly used methods are the plane-wave expansion (PWE) method [3], the finite-difference time-domain (FDTD) method [4, 5], and the finite-difference frequency-domain (FDFD) method [2]. However, these methods have limitations in band structure calculation. The resultant matrix of the PWE method is dense and large, thus making its computation heavy for large problems. The FDTD has limitations in resolving the degenerate eigenmodes [2, 4].

The FDFD method is highly accurate in band structure calculations of 2-D PCs [2]. Because the FDFD method does not use spectral analysis. The FDFD method simply uses the eigenvalue equation. However, it has not been possible to calculate the band structure for frequency-dependent materials with the FDFD method. Lately, we developed a new 2-D FDFD algorithm for band structures calculation of Debye-type PCs [6].

In this paper, we propose a new FDFD algorithm for band structure analysis of 2-D PCs composed of Lorebtz-type frequency-dependent materials. The formulation of the new FDFD algorithm, for Lorentz-type frequency-dependent PCs, is developed using Lorentz complex relative permittivity instead of real relative permittivity used for frequency-independent materials [2]. The Lorentz relative permittivity is shown in (1).

$$\varepsilon_r^*(\omega) = \varepsilon_\infty + (\varepsilon_s - \varepsilon_\infty)\frac{\omega_p^2}{\omega_p^2 + 2j\omega\delta_p - \omega^2} \tag{1}$$

where ε_∞ is the relative permittivity at infinite frequency, ε_s is the relative permittivity at zero frequency, δ_p is the frequency of the pole pair, ω_p is the damping frequency, and ω is angular frequency. Replacing the Lorentz relative permittivity in usual FDFD [2], and performing some algebraic manipulations, we obtain

$$\mathbf{H}\,\mathbf{Z} = \omega\,\mathbf{Z} \tag{2}$$

where

$$\mathbf{H}=\begin{bmatrix} \mathbf{C} & \mathbf{D}+\mathbf{E}+\mathbf{F} & \mathbf{G} & \mathbf{H} \\ \mathbf{I} & 0 & 0 & 0 \\ 0 & \mathbf{I} & 0 & 0 \\ 0 & 0 & \mathbf{I} & 0 \end{bmatrix}; \quad \mathbf{Z}=\begin{bmatrix} \omega^3\mathbf{E}_z \\ \omega^2\mathbf{E}_z \\ \omega\mathbf{E}_z \\ \mathbf{E}_z \end{bmatrix} \quad ; \quad \mathbf{B}=\mathbf{\Delta\,\varepsilon\omega_p^2} \quad ; \quad \Delta\varepsilon=\varepsilon_s-\varepsilon_\infty$$

$$\mathbf{C}=2\,j\,\boldsymbol{\varepsilon}_\infty^{-1}\mathbf{B}\,\boldsymbol{\delta}_\mathbf{p}\mathbf{B}^{-1}\boldsymbol{\varepsilon}_\infty \quad ; \quad \mathbf{D}=\boldsymbol{\varepsilon}_\infty^{-1}\mathbf{B}\,\boldsymbol{\omega}_\mathbf{p}^2\,\mathbf{B}^{-1}\boldsymbol{\varepsilon}_\infty \quad ; \quad \mathbf{E}=\boldsymbol{\varepsilon}_\infty^{-1}\mathbf{B}$$

$$\mathbf{F}=-\boldsymbol{\varepsilon}_\infty^{-1}\frac{\mathbf{A}}{\varepsilon_0} \quad ; \quad \mathbf{G}=2\,j\boldsymbol{\varepsilon}_\infty^{-1}\mathbf{B}\;\boldsymbol{\delta}_p\mathbf{B}^{-1}\frac{\mathbf{A}}{\varepsilon_0} \quad ; \quad \mathbf{H}=\boldsymbol{\varepsilon}_\infty^{-1}\,\mathbf{B}\,\boldsymbol{\omega}_\mathbf{p}^2\,\mathbf{B}^{-1}\frac{\mathbf{A}}{\varepsilon_0}$$

Eq. (2) is the eigenvalue equation, where $\mathbf{H}$ is the characteristic matrix composed of summitries and ω is frequency. For the parameter values of $\omega_p=1.256\cdot10^{10}$, $\delta_p=1.256\cdot10^{9}$, and $\varepsilon_s=8.9$, in the band structure calculations shown in Fig. 1 and Fig. 2, the FDFD and FDTD are compatible for lower eigenmodes. FDFD obtains very accurate values for all the eigenmodes; however, FDTD has low accuracy for higher eigenmodes as shown irregular dotted values for higher eigenmodes.

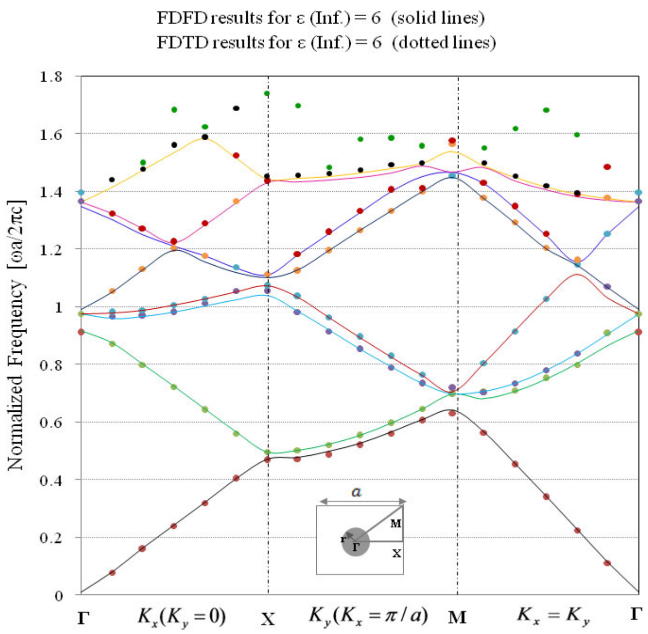

Fig. 1 Comparison of the FDFD and FDTD for $\varepsilon_\infty=6$.

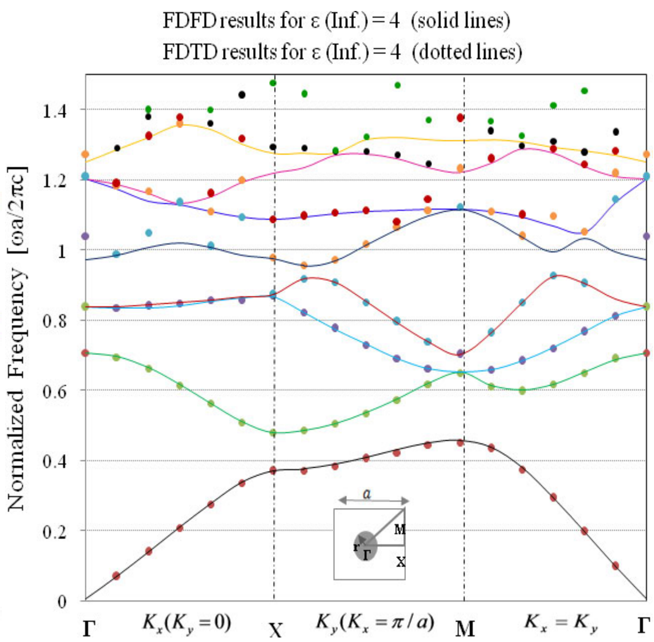

Fig. 2 Comparison of the FDFD and FDTD for $\varepsilon_\infty=4$.

REFERENCES

[1] F. Yang and Y. Rahmat-Samii, *Electromagnetic Band Gap Structures in Antenna Engineering*, Cambridge University Press, New York, 2009

[2] K. Yasumoto, *Electromagnetic Theory and Application for Photonic Crystal*s, CRC press, Boca Raton, FL, 2006.

[3] K. Sakoda, *Optical Properties of Photonic Crystals*, 2nd Ed., Springer-Verlag,Berlin Heidelberg, 2005

[4] A. Taflove and S. C. Hagness, *Computational Electrodynamics: The Finite-Difference Time -Domain Method*, 3rd Ed., Artech House, Norwood, MA, 2005.

[5] T. Uno, *Finite-Difference Time – Domain Method for Electromagnetic Field and Antenna Analysis*, Corona Publishing Co. LTD. 1998 (in Japanese).

[6] A. G. Hanif, T. Uno, and T. Arima, "Finite-Difference Frequency-Domain Algorithm For Band Diagram Calculation of 2-D Photonic Crystals Composed of Debye Type Dispersive Materials" *IEEE Antenna and Wireless Propagat. Lett.*, Vol. 11, 41-44, 2012.

Construction of Dirac Points Using Triangular Supercrystals

Mohammad Hasan Aram[1], **Roya Mohajeri**[1], **and Sina Khorasani**[1*]
[1]School of Electrical Engineering, Sharif University of Technology, Tehran, Iran
[*]corresponding author: khorasani@sina.sharif.edu

Abstract-We show a methodology on how to construct Dirac points as they occur at the corners of Brillouin zones as the Photonic counterparts of Graphene. We used a triangular lattice with circular holes on Silicon substrate to create a Coupled Photonic Crystal Resonator Arrray (CPCRA) which its cavities play the role of Carbon atoms in Graphene. In this structure each cavity has six cavities in neighborhood. We used tight binding method to obtain the band structure of our CPCRA. For this purpose we first designed a cavity which its resonant frequency is approximately at the middle of the first H-polarization band gap of our basis triangular lattice. Then we obtained dipole modes and magnetic field distribution of this cavity using finite element method. Finally we drew two bands that construct the Dirac points together with the frequency contour plots for both bands and compare to the Plane Wave Expansion (PWE) result.

The CPCRA lattice that is studied in this paper is shown in Figure 1. As it can be seen holes diameter to holes separation distance ratio is 0.7. This fraction is 0.4 for cavities that are shown by red circles in the figure.

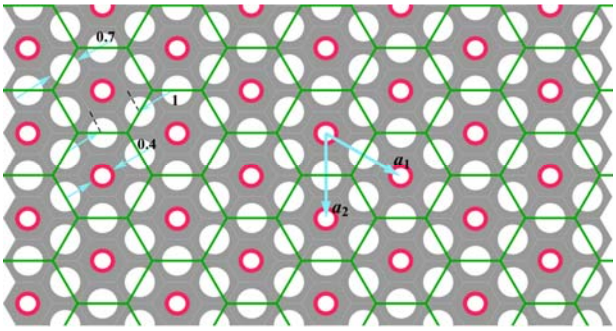

Figure 1- CPCRA lattice that we show has a Dirac point in its band structure

a_1 and a_2 are lattice primitive vectors and green hexagons are primitive cells. Using the standard degenerate tight-binding method we reached the following eigenvalue equation which its eigenvalues are proportional to square of frequency.

$$\nu^2 \left[A(\mathbf{k})\right] \begin{bmatrix} b_1 \\ b_2 \end{bmatrix} = \omega^2(\mathbf{k}) \left[B(\mathbf{k})\right] \begin{bmatrix} b_1 \\ b_2 \end{bmatrix} \tag{1}$$

In this equation $\left[A(\mathbf{k})\right]$ and $\left[B(\mathbf{k})\right]$ are 2×2 matrices that depend on the overlap field of two near cavities. ν is the resonant frequency of each cavity. Since the size of matrices are 2 this equation has two eigenvalues; one for each band. Figure 2 shows contour plots of constant ω in reciprocal lattice for the first and second band. The band structure which shows the Dirac point is also drawn in Figure 3. Figure 4 shows the same from PWE calculations for comparison. The importance of the existence of Dirac points cannot be overemphasized, and in fact has been studied in the microwave regime using metamaterials [1].

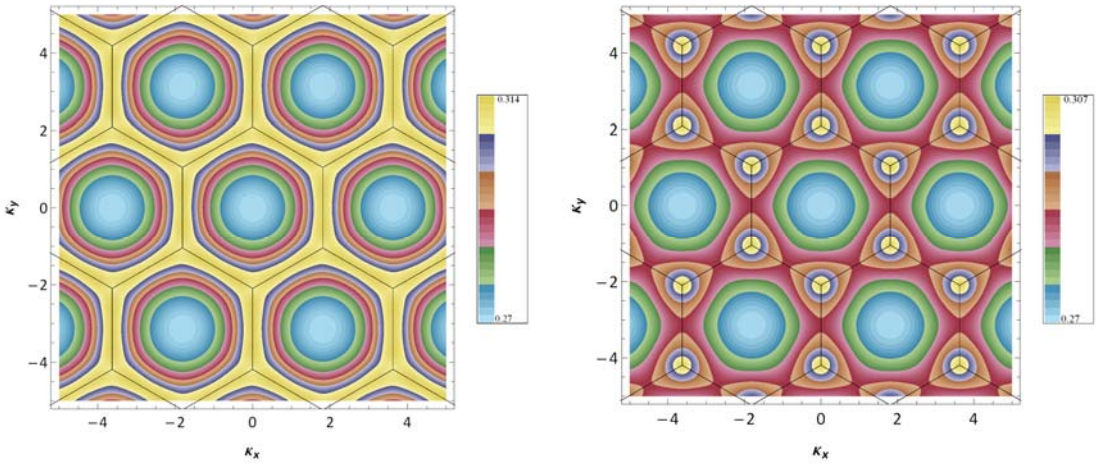

Figure 2- contour plots of constant frequency in reciprocal lattice

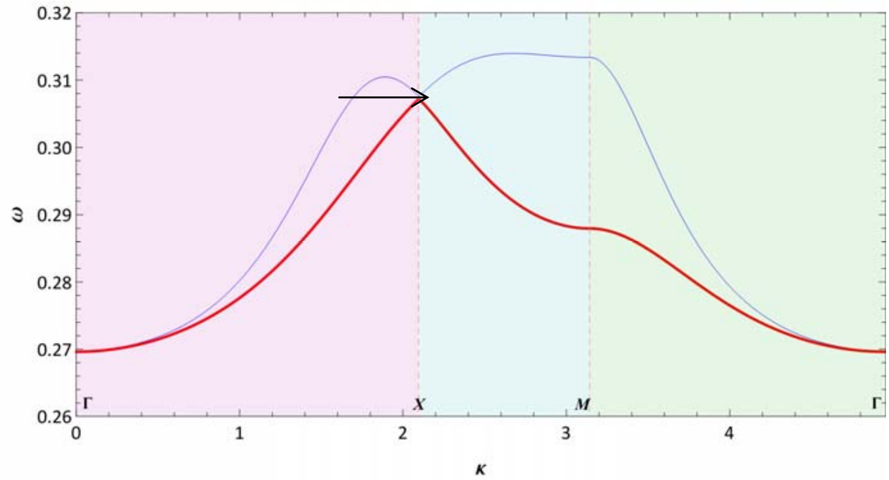

Figure 3- Band structure of CPCRA introduced in Fig.1 using the degenerate Tight-Binding Method.

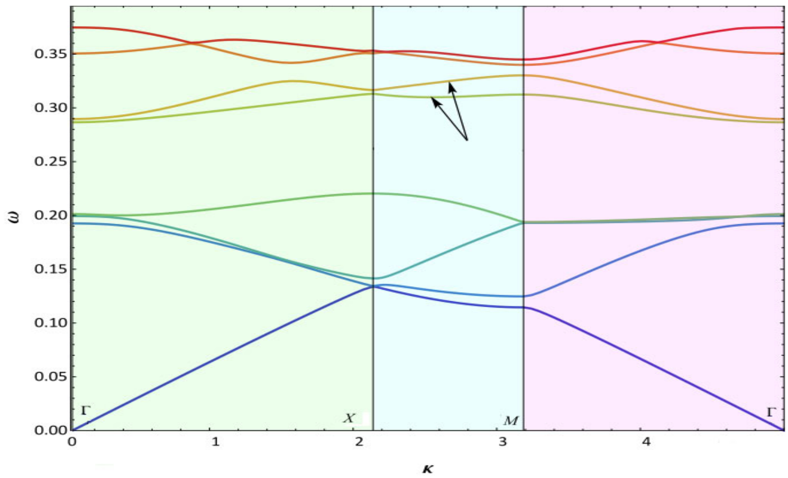

Figure 4- Band structure of CPCRA in photonic crystal basis introduced in Fig.1 using the PWE.

REFERENCES

1. Khanikaev, A. B., Mousavi, S. H., Tse, W.-K., Kargarian, M., MacDonald, A. H., Shvets, G. “Photonic topological insulators,” *Nature Mat.* doi:10.1038/nmat3520 (2012).

Inverse design and topology optimization of novel Photonic Crystal broadband pasive devices for Photonic Integrated Circuits

I. Andonegui* and **A. J. Garcia-Adeva**

Departamento de Fisica Aplicada I, E.T.S. de Ingenieria de Bilbao, UPV/EHU, Spain

*imanol_andonegui@ehu.es

Abstract—

We report on the application of various Monte Carlo algorithms as a very promising approach for the realization of true integrated optics devices by means of inverse design. We show that these techniques provide a global optimum towards one or various functional objectives at a reasonable computational cost. The results obtained by these methods are far beyond intuitive design procedures and clearly outperform trial-and-error based models. We illustrate their performance by using a series of inverse-designed practical photonic devices.

Photonic crystals (PC) have generated a surge of interest in the last decades as they offer the possibility to control the propagation of light to an unprecedented level. The prospect of attaining a fully functional photonic device that tackles light propagation in subwavelength scale requires breaking the spatial symmetry of PCs. These topologies enhance additional functionalities and enable a higher level of control in complex light paths, albeit, creating novel designs based upon aperiodic PC clusters entails dealing with numerous sensitive and correlated parameters. In addition, investigating all feasible combinations of structural parameters for a particular application demands a lot of computational effort, which scales exponentially with the number of parameters. Therefore, the challenging problem of designing such PC structures belongs to the class of the NP-complete optimization problems. On the other hand, currently, the process of designing a PC structure that ultimately complies with a certain required objective is still based on intuitive assumptions rather than using a rigorous mathematical technique. Generally, these methodologies start with the election of a particular dielectric arrangement which supports appropriate characteristics. Then, its parameters are iteratively tuned, one at a time, until a maximum in the desired objective function is achieved. However, this method lacks of certain thoroughness in its foundations. First of all, the starting geometry is somehow arbitrarily chosen. Besides, a trial and error technique is very inefficient in large design spaces and an iterative exhaustive search is highly time consuming. Moreover, designing structures founded on intuition, usually yields to non-optimum scenarios. Beyond these assumptions, creating PC structures to fulfill multiple conflicting objectives highly hinders the design procedure.

In contrast with intuition-based approaches, we found that global optimization heuristic and evolutionary algorithms are specially well suited to deal with the noisy and non-linear nature of disordered PCs. In this work, we report a number of inverse designed novel passive devices using two alternative heuristic methods, namely the fast simulated annealing technique (FSA) [1] and the harmony search (HS) [2] algorithm and one fast elitist multi-objective Genetic Algorithm (GA) approach [3]. The optimized complex systems obtained by means of these techniques clearly outperform intuitive based models. These procedures support a constrained search of the parameter space and hence they can render PC topologies that are fully compatible with CMOS fabrication technology. We found that these methods are easily applicable to most of PC engineering design problems since they do not require any detailed knowledge of the structure of the problem and they can rely on the solver of the problem as a black-box. Therefore, we exploit the advantages of implementing a stochastically-driven optimization process and the rapidity and accuracy of the finite element method (FEM) in order to design fully functional passive optical components: an abrupt and short stage of broadband PC waveguide taper, sharp PC waveguide bends, broadband PC beam splitters and Y-junctions, PC resonant cavities with high quality factors, and reduced modal volume and compact PC multiplexers, among others.

ACKNOWLEDGMENT

We would like to thank the Basque Government for financial support under the SAIOTEK 2012 (ref. S-PE12UN043) programme. One of us, I.A., wants to thank the Vicerrectorado de Euskara y Plurilinguismo de la UPV/EHU for financial support under the PhD Fellowships 2011 programme.

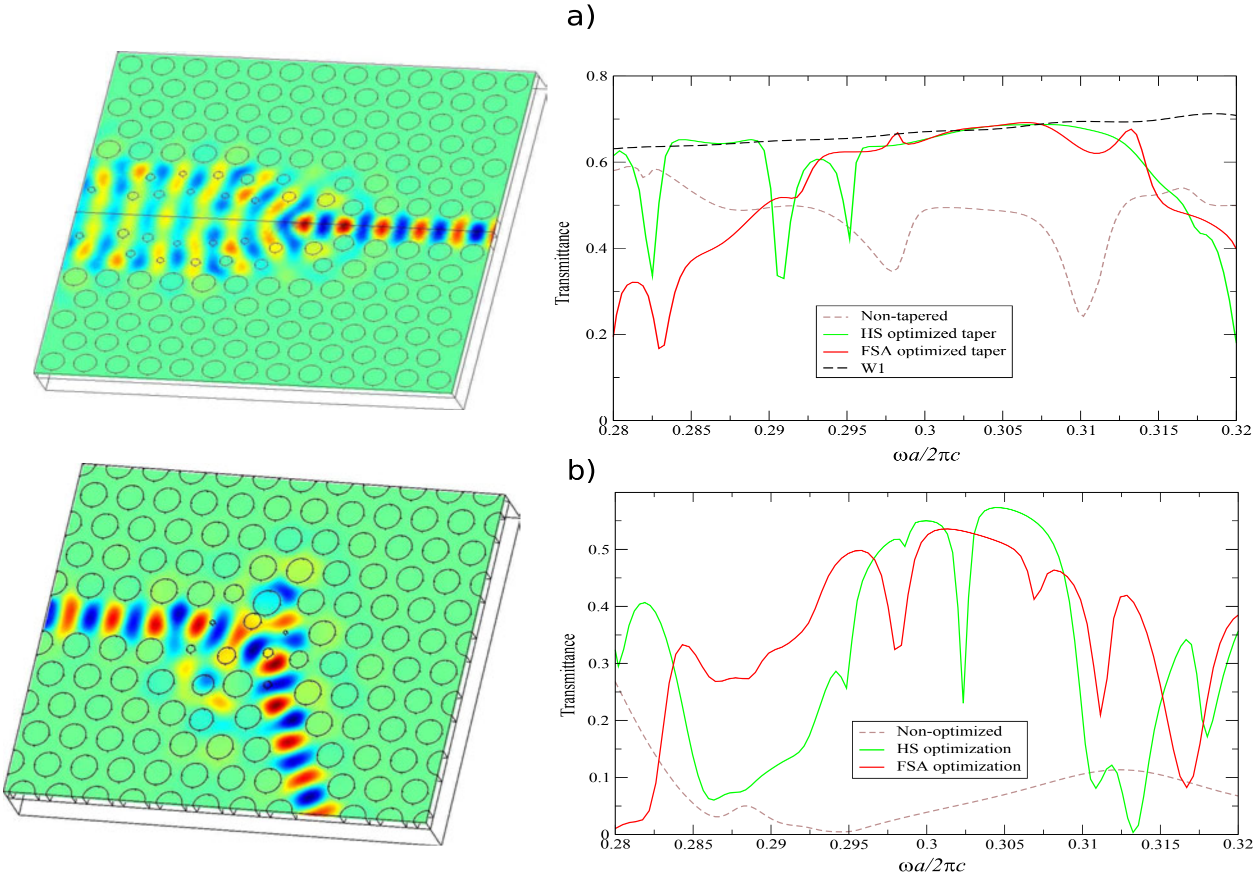

Figure 1: . a) On the left: representation of the H_z field through an inverse designed tapering section that enhances light coupling and mode matching of two highly different waveguide sections. On the right: transmittance diagram comparison for a non-tapered model and optimized models provided by FSA and HS methods. b) On the left: representation of the H_z field through an inverse designed sharp bend that maximizes the transmission. On the right: transmittance diagram comparison for a non-optimized bend and optimized FSA and HS model results.

REFERENCES

1. Szu, H. and Hartley R., "Fast simulated annealing", *Phys. Lett. A*, Vol. **122**, No. 3–4, 157–162, 1987.
2. Geem, Z. W., Kim, J. H., and Loganathan, G. V., "A New Heuristic Optimization Algorithm: Harmony Search", *Simulation*, Vol. **76**, No. 2, 60–68, 2001.
3. Deb, K., "A fast and elitist multiobjective genetic algorithm: NSGA-II", *IEEE Transactions on Evolutionary Computation*, Vol. **6**, No. 2, 182–197, 2002.

Electrically Tunable Photonic Crystal Using Modified Fe_3O_4/SiO_2 Nanoparticles in Nonpolar Solvents

Y. M. Kim, A. R. Joo, H. N. Lee, H. M. Cho, Y. S. Kim[*]

Display Components & Materials Research Center, Korea Electronics Technology Institute, #68 Yatap-dong, Bundang-gu, Seongnam-si, Gyeonggi-do, Korea

[*]corresponding author: vis4freedom@keti.re.kr

Abstract- The cationic Fe_3O_4/SiO_2 nanoparticles was synthesized through the silanization reaction and characterized by FT-IR and TGA. These colloids were well dispersed in nonpolar solvent and self assembled to produce photonic colors upon applying electric field. Remarkably, the reversible color change on the cathode was observed by changing the electric forces.

The photonic crystals have received much attention for their photonic band gaps which produced structural colors. Recently, the colors resulting from the colloidal assembly were readily tuned by the external stimuli such as magnetic and electric forces. The balance between the attractive interactions and the repulsive forces between particles changes the distance of them leading to the color change. In general, the structural colors were produced in polar solvent because charge separation which enhanced the repulsive forces between particles occurs. However, much effort has been made to disperse the colloids in nonpolar solvents in which the particles were supposed to be more stable than in polar solvents. Yin group has investigated the tunable photonic crystals in apolar solvent with the aid of a charge control agent which lowers the energy barrier for charge separation in the system. Here we reported the colloids which were decorated with the cationic groups and their electrophoretic behavior in apolar solvents.

The monodisperse Fe_3O_4/SiO_2 nanoparticles were synthesized by coating Fe_3O_4 colloidal nanoparticle clusters with SiO_2 shell. The thickness of the shell was carefully controlled by adjusting the reaction time. In the optimized conditions, the Fe_3O_4/SiO_2 nanoparticles with 170nm in size were prepared. FT-IR showed the broad band at *ca.* 1050 cm^{-1} confirming that the silica was formed. The silica coating was known to prevent the Fe_3O_4 nanopartilces from being oxidized. Furthermore, the silica surface could be easily modified with various functional groups through silanization reactions. We have treated the Fe_3O_4/SiO_2 colloids with cationic silanes to decorate the particles with cationic groups which were supposed to enhance the repulsive forces between them. As the Fe_3O_4/SiO_2 colloids were well dispersed in polar solvents, the silanization reaction was carried out in ethanol/water mixture. The FE-SEM image confirmed that the sizes of the resulting particles (cationic Fe_3O_4/SiO_2 (**1**)) were comparable to those of Fe_3O_4/SiO_2 colloids. The thermal gravimetric analysis showed that the mass loss of the compound at 110 °C and 280 °C, respectively. To maximize the amount of the grafted silane moiety, the cationic colloid **1** was dispersed in nonpolar solvent and treated with cationic silane. The resulting cationic Fe_3O_4/SiO_2 (**2**) was characterized by FT-IR spectrum and TGA. With this compound in hand, we have investigated the electrophoresis of it by fabricating the test cell. The cationic Fe_3O_4/SiO_2 in nonpolar solvent was injected into the gap between two ITO coated glasses separated by 50 μm. The cathode displayed the structural color while the anode was brown color upon applying electric field on the cell. The color was blue shifted from orange to blue by increasing the voltage. The increased voltage led the particles compressed on the cathode, which reduced the interpaticle distance to reflect blue color. Interestingly, the color change was reversible. The colorimetric properties of the colloidal assembly were measured by a Minolta CS1000 spectrometer. The reflective color expressed as chromaticity coordinates (x,y) according to the CIE standard colorimetric system. The CIE chromaticity coordinates (0.46, 0.43) and (0.31, 0.37) were obtained at 1.0V and 5.0V, respectively (Figure 1).

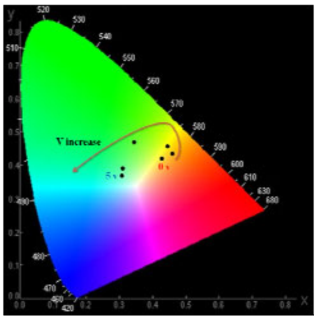

Figure 1. The change of the CIE chromaticity coordinates

Acknowledgements

This work was supported by an International Collaboration grant (No.Sunjin-2010-002) from the Korean Ministry of Knowledge Economy.

REFERENCES

1. Ge, J. and Yin, Y. “Responsive photonic crystals”, *Angew. Chem. Int. Ed.*, Vol. 50, No. 7, 1492-1522, 2011.
2. Ge, J., Hu, Y. and Yin, Y. “Highly tunable superparamagnetic colloidal photonic crystals”, *Angew. Chem. Int. Ed.*, Vol. 46, No. 39, 7428-7431, 2007.
3. Lee, I., Kim, D., Kal, J., Baek, H., Kwak, D., Go, D., Kim, E., Kang, C., Chung, J., Jang, Y., Ji, S., Joo, J., and Kang, Y. “Quasi-Amorphorus Colloidal Structures for Electrically Tunable Full-Color Photonic Pixels with Angle-Independency”, *Adv. Mat.*, Vol. 22, No. 44, 4973-4977, 2010.
4. Ge, J., He, L., Geobl, J. and Yin, Y. “Assembly of magnetically tunable photonic crystals in nonpolar solvents”, *J. Am. Chem.Soc*, Vol. 131, No. 10, 3484-3486, 2009.

Tunable Photonic Crystals in Nonpolar Solvents

Y. M. Kim, A. R. Joo, H. M. Cho, Y. S. Kim*

Display Components & Materials Research Center, Korea Electronics Technology Institute, #68 Yatap-dong, Bundang-gu, Seongnam-si, Gyeonggi-do, Korea

*corresponding author: vis4freedom@keti.re.kr

Abstract – To prepare the suspension of the nanoparticles in nonpolar solvents, the dispersion stability tests of Fe_3O_4/SiO_2 nanopartilces and SiO_2 nanoparticles in nonpolar solvents with various charge control agents were carried out. We found that the most stable suspension of Fe_3O_4/SiO_2 in tetrachlorethylene produced the structural colors under magnetic and electric fields. Interestingly, the encapsulated Fe_3O_4/SiO_2 suspension was assembled to ordered structure producing the structural colors.

Photonic crystals are of interest because the structural colors are produced when the periodic dielectric structure is satisfied with Bragg's law.[1] The use of nanoparticles was one way to create the photonic crystal structures. The self assembly of the nanoparticles featuring a narrow size distribution produced the reflective colors when the repulsive forces overcome the attractive forces between the particles.[2] Therefore, the manipulation of the forces could change the colloidal assembly with the concomitant color change of the reflective colors. Owing to the high charge density on the surface of the colloids, the repulsive forces enhanced leading the colloidal assembly in polar solvents. The aggregation of the colloids, however, was observed in apolar solvents because the high energy of the charge separation.[3] To resolve this problem, charge control agents (CCAs) were employed in nonpolar solvents. Recently, Yin group has investigated on the assembly of the colloids in nonpolar solvents with the aid of sodium di-2-ethylhexylsulfosuccinate (AOT).[3] Here, we report the colloidal assembly of Fe_3O_4/SiO_2 in nonpolar solvents. The structural colors resulting from the assembly was tuned by magnetic and electric forces.

The Fe_3O_4/SiO_2 was prepared by treating the Fe_3O_4 with TEOS in the presence of NH_4OH. Since the surface of Fe_3O_4 was coated with silica, the behavior of Fe_3O_4/SiO_2 in solution was expected to be similar to that of SiO_2 nanoparticles. Therefore, SiO_2 nanoparticles instead of Fe_3O_4/SiO_2 nanoparticles were used to test the dispersion stability in nonpolar solvents. We found that the SiO_2 nanoparticles were dispersed in nonpolar solvents such as isopar G and tetrachloroehtylene in the presence of OLOA 12000 and AOT as CCAs. Indeed, the Fe_3O_4/SiO_2 colloids were well dispersed in the same solutions and produced structural colors along with magnetic field. As the suspension of Fe_3O_4/SiO_2 colloids in teterachloroethylene with OLOA 12000 showed the most stable dispersion, we used that for fabricating the test cell to electrophoresis of them. The colloids in the cell were assembled upon applying the magnetic and electric field displaying reflective color in green (Figure 1). The reflectivity was *ca*. 10% at λmax = 580nm which was measured by the cm-3600d spectrophotometer using $BaTiO_3$ as a reference. Even though the color change was reversible, the reflectivity was in the range of 6-10%. Expecting the increased reflectivity, suspensions of the Fe_3O_4/SiO_2 colloids was encapsulated using gelatin / gum arabic coacervates. The resulting microcapsule was in the range of 76-143 um in size. Due to the Brownian motion of the colloids, the color was brown without external forces. The assembly of the colloids was observed upon applying magnetic field displaying the reflective color in green.

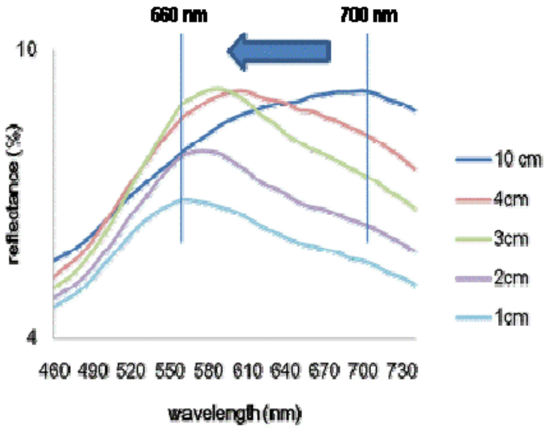

Figure 1. Reflectivity change of Fe_3O_4/SiO_2 particles under magnetic forces.

Acknowledgements

This work was supported by an International Collaboration grant (No.Sunjin-2010-002) from the Korean Ministry of Knowledge Economy.

REFERENCES

1. Ge, J. and Yin, Y. “Responsive photonic crystals”, *Angew. Chem. Int. Ed.*, Vol. 50, No. 7, 1492-1522, 2011.
2. Ge, J., Hu, Y. and Yin, Y. “Highly tunable superparamagnetic colloidal photonic crystals”, *Angew. Chem. Int. Ed.*, Vol. 46, No. 39, 7428-7431, 2007.
3. Ge, J., He, L., Geobl, J. and Yin, Y. “Assembly of magnetically tunable photonic crystals in nonpolar solvents”, *J. Am. Chem.Soc*, Vol. 131, No. 10, 3484-3486, 2009.

Chiral and bianisotropic materials

Ultrathin q-Wave Plates Based on Double-L Shape Plasmonic Nanoantennas

A. Kabiri[1*], E. Girgis[1], and F. Capasso[1]

[1]School of Engineering and Applied Sciences, Harvard University, Cambridge, MA 02138, USA

*Corresponding author: akabiri@seas.harvard.edu

Abstract- Double-L resonators are designed to achieve a strong anisotropic optical response. An ultrathin quarter wave plate for mid-infrared frequencies is demonstrated based on array of double-L shape plasmonic nanoantennas. Experimental results are in a good agreement with numerical simulations. The proposed design shows a relatively wide bandwidth (~20%) response which is suitable for many applications.

Many optical devices are polarization sensitive. For example, circular polarization, in particular, is a preferable polarization state in numerous advanced optical sensors due to its inherent robustness with respect to scattering and diffraction. The state-of-the-art in the design of circular polarizers is still based on birefringent materials [1]. Polarizers based on birefringence need specific thickness to accumulate required phase difference in orthogonal directions. Therefore, integration of relatively bulky polarizers in sensors and nanophotonic devices is very challenging [2]. Recent advancement in controlling light polarization has led to the design of various plasmonic-based polarizers such as crossed-resonant nanoantennas, corrugated elliptical gratings, patterned metallic films, planar chiral structures and metasurfaces with phase discontinuities with clear advances over currently available technology in terms of required thickness and/or bandwidth of operation [3-4]. In this work, we investigate an ultrathin plasmonic metasurface and demonstrate its applications in design of quarter-wave plates. Ultrathin plasmonic quarter-wave plates are suitable for the design of any polarizer with a desired polarization state.

In order to achieve a quarter-wave plate, a device for conversion between linear and circular polarization, equal amplitude and a 90^o phase difference in the two orthogonal components of the transmitted wave is required. A general transmission matrix of a quarter wave plate, according to Jones matrices, can be written as

$$S = \begin{pmatrix} \sigma & 0 \\ 0 & \pm i\sigma \end{pmatrix}. \qquad (1)$$

We designed an ultrathin metasurface operating according to (1). The proposed design is based on asymmetric double-L resonators (Figure 1-A) with incident polarization along any arm of resonators. Since the phase of the scattered fields abruptly varies with frequency around each arm's resonance, the desired phase shift between the reradiated waves from two arms of the L-shape can be adjusted by slightly changing their relative length. The double-L shape structure is suitable for detuning the arm resonances using the capacitive gap introduced between the arms. Computer System Technology (CST) Studio, commercial full-wave simulation software based on the finite integral technique (FIT), has been accommodated to simulate the structure and optimize the dimensions of L-shape resonators. The required phase shift and appropriate ratio of electric field components in transmission have been optimized. The structures were designed to operate at mid-infrared frequencies ($\lambda = 9\mu m$). The angular and bandwidth performance of such interfaces were studied. Figure 1-B demonstrates the phase difference and the ratio of co- to cross-polarized components of the transmitted electric field. The structures were fabricated using nano-lithography techniques. The double-L resonators are made of gold and printed on a Silicon wafer. Transmission coefficient at different polarization states was measured using a Fourier Transform Infrared Spectrometer. The measured data were used in the calculation of the ellipticity coefficient based on the Stokes' parameters method. Figure-2 demonstrates the SEM image of the fabricated structure and comparison of the numerical and experimental results. A good agreement was achieved between the numerical and experimental data. Moreover, the structure shows a relatively wideband response of about $2\mu m$ at the central wavelength of $9\mu m$. The optimal performance and the lithographic realization make the design a suitable candidate for integration in infrared sensors and other related technologies.

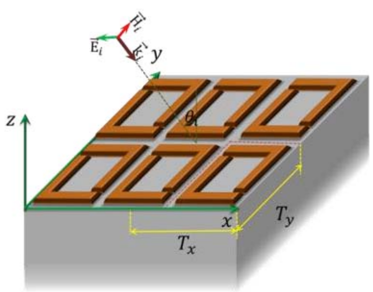

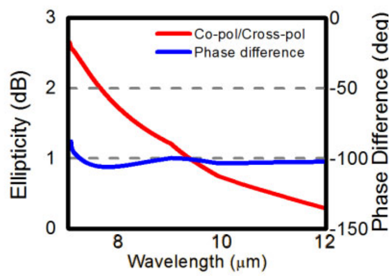

(A) (B)

Figure 1 - (A) Schematic of a quarter-wave plate based on a metasurface composed of double-L inclusions. (B) The plot shows the calculated ratio and phase difference of the transmitted signal polarized along x and y directions in Figure 1-A.

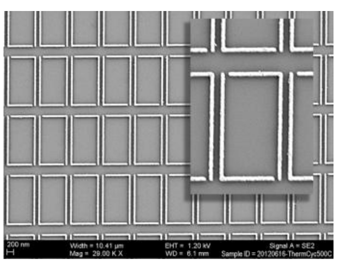

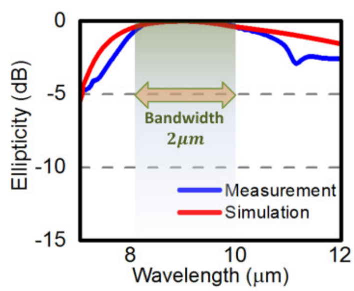

(A) (B)

Figure 2 - (A) SEM image of a metasurface composed of a double-L resonators array. (B) Depiction of numerical and experimental results of ellipticity factor of the designed quarter wave plate. The plot exhibits a $2\mu m$ bandwidth response.

Acknowledgements, The fabrication were performed at the Harvard Center for Nanoscale Systems, which is a member of the National Nanotechnology Infrastructure Network.

REFERENCES

1. Huang, Y. H. Zhou, Y. and Wu, S. T. "Broadband circular polarizer using stacked chiral polymer films" Optical Express Vol. 15, Vol. 10, 6414, 2007.
2. Drezet, A. Genet, C and Ebbesen, T. W. "Miniature Plasmonic Wave Plates", Physical. Review. Letter. Vol. 101, No 4, 043902, 2008.
3. Zhao, Y., Belkin, T. W. and Alù A. 'Twisted optical metamaterials for planarized ultrathin broadband circular polarizers", *Nature Communication* 3, 870, 2012.
4. Yu, N. et al, "A Broadband, Background-Free Quarter-Wave Plate Based on Plasmonic Metasurfaces", *Nano letters*, August 2012, DOI: 10.1021/nl302516v. Online.

Plasmon-enhanced photovoltaics, photocatalysis, and solar fuels

Broadband spectroscopy of nanoporous-gold promoter

S. Kuwano-Nakatani[1], Y. H. Han[1] , T. Takahashi[2] and T. Awano[1*]

[1] Tohoku Gakuin University, Japan

[2]Research Reactor Institute, Kyoto University, Japan

[*]corresponding author: awano@tjcc.tohoku-gakuin.ac.jp

Abstract- The efficiency of UV photocatalysis on TiO_2 particles was increased by mixing TiO_2 particles with nanoporous gold (NPG) with pore diameters of 10–40 nm. This means that NPG acts as a promoter in the photocatalytic reaction of TiO_2. Broadband spectroscopic results from millimeter wave to ultra violet of NPG membrane alone and NPG on TiO_2 are discussed to estimate plasmonic effect on the catalysis.

It is well known that bulk Au is inert. However, Au nanoparticles with several-nanometer-scale sizes are catalytically active for several chemical reactions such as the decomposition of formaldehyde and oxidation of CO[1,2]. The catalytic activity depends on the size of nanoparticles. The nanoparticles with diameters less than 3–5 nm show the highest activity for oxidation[3]. Nanoporous Au (NPG) with 10–50 nm pore size also shows catalytic activity for oxidation[3].

Recently, TiO_2 is being widely used for photocatalysis of various materials. TiO_2 has a different activity with crystal structure for different wavelengths. It has been reported that composite materials of TiO_2 with Au or Pt nanoparticles enhance TiO_2 catalytic activity[4]. TiO_2 plays an active role in the decomposition of water to generate OH radicals. It is supposed that the plasmonic electromagnetic effect of Au or Pt enhances the catalytic activity of TiO_2. In addition, since pores of NPG are able to trap the TiO_2 particles, NPG seems to be a photocatalytic nanocomposite because of enhancement of the catalytic activity by the electromagnetic effect. We have found that NPG acts as a promoter to produce OH radicals using TiO_2 [5]. We report optical properties of NPG and NPG/TiO_2 in this paper to investigate electromagnetic and plasmonic origin of the promotor effect.

Commentaire [A1]: The meaning of this sentence is unclear. Perhaps you mean “The activity of TiO_2 depends on its crystal structure and light wavelength.”

Commentaire [A2]: Does this edit convey your intended meaning?

NPG films were obtained by nitric acid etching of Ag from $Au_{35}Ag_{65}$ alloy films with about 100 nm thickness. The average pore diameter was 10–40 nm, according to the dealloying temperature and time. Figure 1 shows SEM images of NPG films with average pore diameters of 20 nm (a) and 42 nm (b). The other samples were confirmed to have average pore diameters of 11 and 33 nm.

Anatase (85 nm average diameter) and rutile (25 nm average diameter) TiO_2 particles were in the ratio 3:1. The mixture of NPG, TiO_2, and spin trapping agent was irradiated by UV light. The spectra for the estimation of the amount of induced OH radicals were measured by X-band ESR. No OH radical was formed by the $Au_{35}Ag_{65}$ alloy film or NPG film alone during the UV-light irradiation. Besides, the coexistence of TiO_2 particles and NPG films enhanced the production of the OH radical. ESR signals of the OH-radical spin adduct were observed, and it was

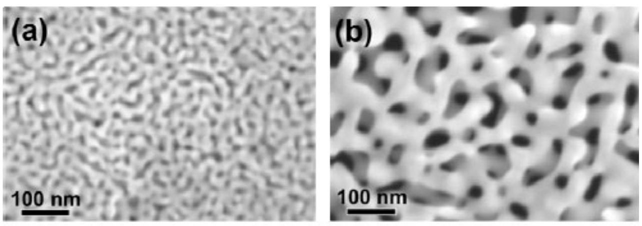

Figure 1. SEM images of NPG films. Pore diameter is (a) 20 nm and (b) 42 nm.

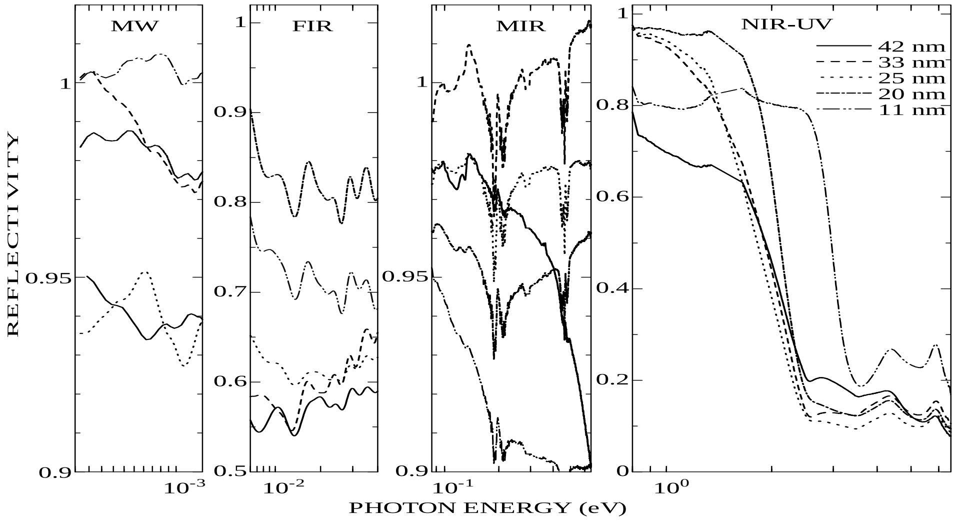

Figure 2. Reflectivity spectra of NPG membranes on quartz substrates. Average pore diameters of the five samples with each dealloying temperature and time from 40C&180min. to -30C&5min are shown in the NIR-UV figure. Fine structures in IR spectra are due to CO_2 and H_2O in atmosphere. Experimental error by surface imperfection occurred at several wavelength ranges in which reflectivity excess one.

confirmed that NPG is a promoter for photocatalysis on TiO_2. The maximum efficiencies normalized by that of an $Au_{35}Ag_{65}$ alloy film was 1.5 at average pore diameter of 20 nm. No enhancement was observed at pore diameters over 40 nm. This peak seems to be due to that the average particle diameter of the rutile TiO_2 particles, which are sensitive to the irradiated UV-light, was 25 nm. Therefore, the active rutile TiO_2 particles appear to dispersively infiltrate into the pores of Au and tightly stick to the pore surface. This seems to enhance the promoter effect of Au on TiO_2.

Commentaire [A3]: Is this edit correct, or do you mean "tightly block the pores"? Please check this.

Figure 2 shows broadband reflectivity spectra of NPG with various average pore sizes. Millimeter wave spectra showed no characteristic feature. FIR reflectivities were small as compared with normal plasmon reflection as millimeter wave region. Analysis of plasmonic effect is under way. Broadband spectroscopic measurement of NPGs on TiO_2 will be discussed to estimate contribution of rocalized surface plasmon effect on the catalysis.

Acknowledgements

Part of this work was done under the visiting researcher program of Research Reactor Institute, Kyoto-University and UVSOR facility of Institute for Molecular Science.

REFERENCES

1. Bierner, J. et al "Surface-chemistry-driven actuation in nanoporous gold,"*Nature Materials*, Vol. 8, 47–51, 2009.
2. Wittstock, A., V. Zielasek, J. Biener, C. M. Friend, M. Bäumer, "Nanoporous Gold Catalysis for Selective Gas-Phase Oxidative Coupling of Methanol at Low Temperature", *Science* Vol. 327, 319-322, 2003.
3. Haruta, M., "When Gold Is Not Noble: Catalysis by Nanoparticles", *Chem. Rec.*, Vol.3, 75-87, 2003.
4. Haruta, M., "Nanoparticulate Gold Catalysis for Low-Temperature CO Oxidation", *J. New Mat. Electrochem. Sys.* , Vol. 7, 163-172, 2004.
5. Kuwano-Nakatani S., T. Ando, K. Oba and Y.H. Han, to be published.

Design Consideration for Plasmonic Solar Cells Based on Ag Nanoparticles

Razan R. Nejm, and Mousa Hussein

Department of Electrical Engineering, United Arab Emirates University, Al Ain, , United Arab Emirates

Abstract

A plasmonic solar cell based on silver (Ag) nanoparticles is modelled and studied theoretically in this paper as a preliminary study for future experimental work. Ag nanoparticles were deposited on a silicon (Si) substrate surface and are exited by normally incident light source propagating from air into silicon surface. Three main parameters were the interest of study, nanoparticles (NPs) size, period and number, dielectric environment and the incident light tilt angle. NPs parameters and tilt angle value show enhancement in the forward scattering power, whereas dielectric environment can be controlled to enhance and tune the resonance region.

Numerical simulations using FDTD from Optiwave was used to carry on the analysis. Silver (Ag) nanoparticles (NPs) on a crystalline silicon (c-Si) substrate was modeled using Drude-Lorentz model. Using more than one NP in the study is due to the importance of inter-particle coupling effect which is neglected in most theoretical work. Observation area was selected to be in the middle of the substrate to show the normalized scattering power in the solar cell Fig. 1. All the results are depending on the calculated back/forward scattered fields as a function of wavelength normalized to the back/forward scattered fields in absence of nanoparticles.

NPs number, size, spacing between the particles, and type were studied. NPs number was varied with saving the distance from boundaries and other parameters to study the nanoparticles density effect only. The size effect was studied by changing the sphere diameter only without changing the spacing between the spheres or from the boundaries and the observation area. Then the period between the NPs was changed too. Finally Ag NPs changed to Au NPs for comparison.

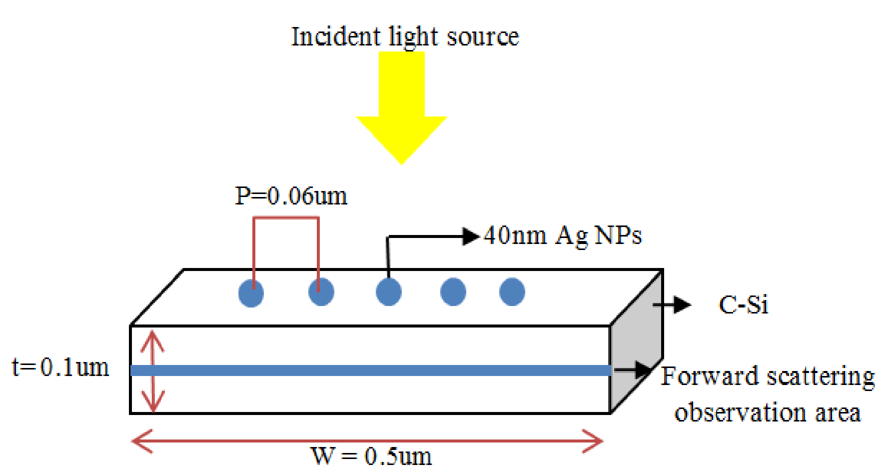

Figure 1: Reference device structure

Next, substrate thickness and width was varied too, to study the substrate effect on the scattering efficiency. Insulating layer between the NPs and the Si substrate was added to increase the distance between the nanoparticles and the substrate. Different substrate material were used SiO_2, TiO_2, Si_3N_4, Mica, GaAs and ITO with the constant thickness equal to 20nm to study the type effect only. Finally tilt angle of the incident light was varied which is in the direction of propagation (z-direction) and Y polarization.

It was found that increasing the nanoparticles number is not efficient as decreasing the particles diameter and the spacing between them. Also coating the substrate with high refractive index insulator layer increases its absorbance, by increasing the NPs spacing from the substrate. The latter is effective more than increasing the substrate thickness. Finally to get the best performance incident light must be ideally normal to the target device.

References:

[1] K. R. Catchpole and A. Polman, *Plasmonic solar cells*, Opt. Express 16, 21793-21800 (2008)
[2] Solarbuzz. Global PV Market. 2010; Available from: http://www.solarbuzz.com/facts-and-figures/market-facts/global-pv-market.
[3] Spinelli, P., et al., *Optical Impedance Matching Using Coupled Plasmonic Nanoparticle Arrays*. Nano Letters. 11(4): p. 1760-1765.
[4] Ferry, V.E., J.N. Munday, and H.A. Atwater, *Design Considerations for Plasmonic Photovoltaics*. Advanced Materials. 22(43): p. 4794-4808.
[5] Pillai, S. and M.A. Green, *Plasmonics for photovoltaic applications*. Solar Energy Materials and Solar Cells. 94(9): p. 1481-1486.
[6] Pillai, S., et al., *Surface plasmon enhanced silicon solar cells*. Journal of Applied Physics, 2007. 101(9): p. 093105-093105-8.

Enhanced Light Absorption in Thin-Film Tandem Solar Cells using a Bottom Metallic Nanograting

Xuanru Zhang[1], Randy J. Knize[3], Bin Xiang[2,*] and Yalin Lu[1,2,3]*

1 Advanced Applied Research Center, Hefei National Laboratory for Physical Science at the Microscale, University of Science and Technology of China, Hefei, Anhui, 230026, P. R. China

2 CAS Key Laboratory of Materials for Energy Conversion, Department of Material Science and Engineering, University of Science and Technology of China, Hefei, Anhui, 230026, P. R. China

3 Laser Optics Research Center, Physics Department, United States Air Force Academy, Colorado Springs, CO 80840, USA

*binxiang@ustc.edu.cn, yalin.lu@usafa.edu

Abstract: We introduced a metallic nanograting structure at the bottom of thin-film tandem solar cells, and carried out an investigation into the light absorption in the top and bottom cells via electromagnetic simulation. It indicated that broadband and polarization-insensitive light absorption enhancement was obtained in the bottom cell while the light absorption in the top cell remained unchanged by the influence of this metallic nanograting. It caused that overall carrier generation enhancement can be achieved as much as 60% for both polarization. This light absorption enhancement effect can survive in a wide range of cell thickness and nanograting geometries, which enables us to reduce the thickness of the bottom cell with minimal impact on light absorption. Thereby, it reduces the solar cell production cost in the meanwhile it enhances the solar cell efficiency by the decrease of light-generated carrier recombination rate.

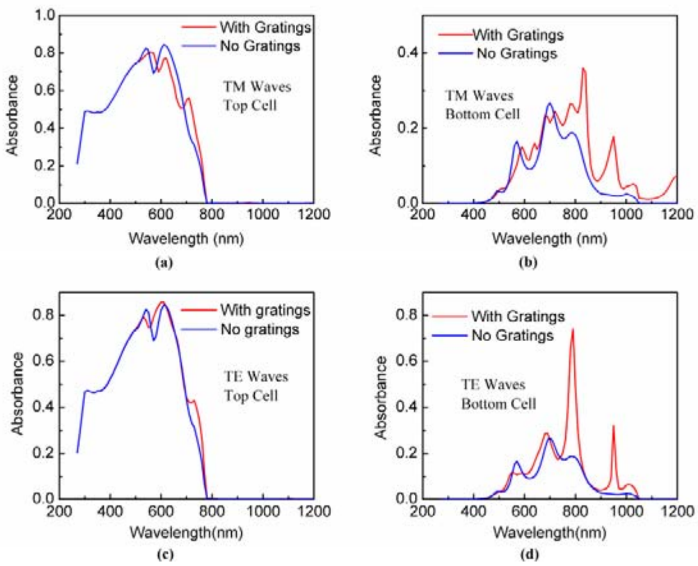

Absorbance of the top (a and c) and bottom (b and d) cells for both polarization, for the structure with and without the gratings. The geometric parameters are: T_4=200 nm, p=350 nm, w=100 nm, T_5=50 nm.

VO_2-based multilayers with enhanced luminous transmittance and switching properties

Y Zhao,[1] X R Zhang,[2] R J Knize, [3] Yalin Lu [1,2,3,*]

[1] CAS Key Laboratory of Materials for Energy Conversion, Department of Materials Science and Engineering, University of Science and Technology of China, Hefei 230026, P. R. China

[2] Advanced Applied Research Center, HeFei National Laboratory for Physical Sciences at the Microscale, University of Science and Technology of China, Anhui 230026, P. R. China

[3] Laser Optics Research Center, Physics Department, United States Air Force Academy, CO 80840, USA

[*] Corresponding author: yllu@ustc.edu.cn and yalin.lu@usafa.edu

Abstract: We studied the optical properties of VO_2/Al:ZnO(AZO)/glass multilayer films near the semiconductor-metallic (S-M) transition of VO_2, when changing the temperature across the S-M transition. It was found that both VO_2/AZO/glass films with a periodic VO_2 stripe grating and ZnO/VO_2/AZO/glass multilayer structures showed much enhanced luminous transmittance and the solar modulation ability. The optical transmission properties of the films could be tuned by changing either VO_2 or AZO layer thicknesses. The obtained results may lead to a potential application in thermochromic smart building windows for energy saving.

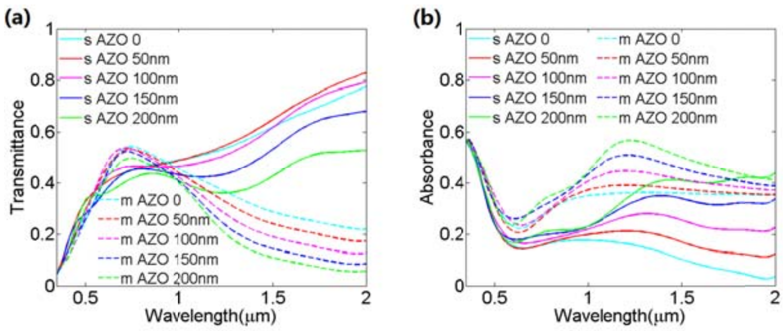

Transmittance (a) and absorbance (b) spectra for VO_2/AZO/glass films having different AZO layer thicknesses, with 's' standing for semiconducting VO_2 (25°C) and 'm' for metallic VO_2 (90°C). The VO_2 layer thickness 'h_1' is fixed at 40 nm.

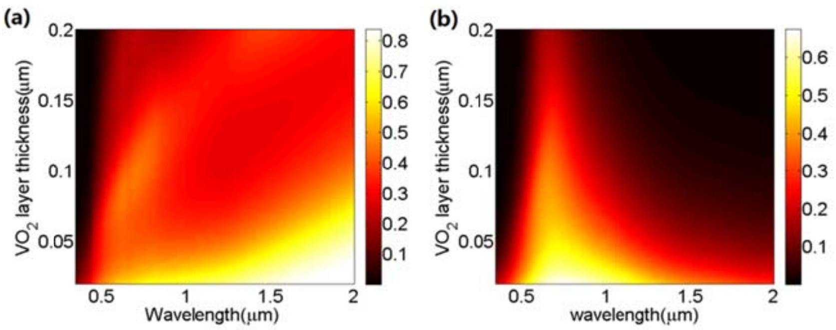

Mapping transmittance for VO_2/AZO/glass films with varying VO_2 layer thickness in semiconducting (a) and metallic phase (b). The AZO layer thickness 'h_2' is fixed at 75 nm.

Structured and disordered media

3D Photonic Amorphous Nanostructures

L. Cortese[1*], M. Burresi[1,2], K. Vynck[1] and D. S. Wiersma[1,2]
[1]LENS-European Laboratory for Non-Linear Spectroscopy, University of Florence, Via Nello Carrara 1, 50019 Sesto Fiorentino (Firenze), Italy
[2]Istituto Nazionale di Ottica (CNR-INO), Largo Fermi 6, 50125 Firenze, Italy
[*]cortese@lens.unifi.it

Abstract-We present an experimental and numerical study of light transport on engineered-disorder 3D photonic amorphous nanostructures. We prepare such structures by introducing spatial short-range correlations in disordered systems. The high-quality fabrication is achieved by Direct Laser Writing.

Studies on the interplay between order and disorder on the transport properties of light are extremely relevant for both fundamental research and applications, since a certain degree of disorder is ubiquitous in “ordered” systems and a certain degree of order is intrinsic in “disordered” systems, in particular in photonic nanostructures. In recent years systems which combine properties of both ordered and disordered features, like photonic amorphous systems, have been raising a lot of interest aiming to unravel the true nature of the formation of photonic band gaps[1,2,3,4] or to observe the occurrence of localization of light at optical wavelengths[1,5].

In this work we investigate the light transport properties in the weakly scattering regime of 3D photonic nanostructures starting from the introduction of order in a disordered structure (introducing short-range correlations between scatterers in a random media). In such a study a full control of the architecture of the structure is paramount to infer the transport properties of engineered-disorder systems. We achieve such a control by fabricating high-quality nanostructures with Direct Laser Writing. This technique exploits the 2-photon polymerization process induced by an ultrafast laser pulse focused on a photoresist. By controlling the position of the focal spot in the photoresist we are able to fabricate 3D polymeric high-quality photonic structures[6] and engineering order and disorder at will. Such a control gives us also the opportunity to theoretically investigate *exactly* the same disorder structures that we fabricate.

We fabricated correlated-disordered structures (Fig. 1), the so-called Photonic Amorphous Structures[2,3,4,7]. These are isotropic structures characterized by the lack of any long-range (translational and rotational) order and by the presence of short-range order. We are able to design and fabricate tetrahedrally connected dielectric networks (amorphous diamond geometry) with short-range correlation between scatterers (dielectric rods of less than 1 μm of average length and diameter less than 0.5 μm) having under control the degree of order of the systems. A such kind of photonic structure has been recently observed in nature and it is considered responsible of the particular coloration of certain animals[8]. It has been already theoretically predicted that the presence of correlation between the position of scatterers modifies the transport properties of the media, reducing the transport mean free

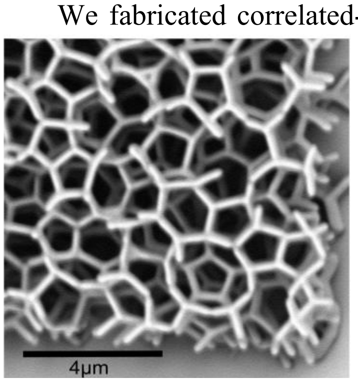

Fig. 1 *SEM image of a photonic amorphous structure*

path at wavelengths comparable with the correlation distance[9].

These studies are the first step to investigate the role of engineered-disorder in the strong light-matter interaction regime at optical wavelengths. The fabricated structures can be used as templates for silicon infiltration in order to produce high refractive index contrast material[10]. Such a novel photonic structures can lead to unambiguous observations of light localization. Moreover, high refractive index amorphous photonic structures are expected to exhibit a complete photonic bandgap, despite the lack of any periodicity[2,3,4,7]. Given their random nature, this novel photonic bandgap material will be less susceptible to imperfections in the fabrication procedure of material.

REFERENCES

1. John, S., *Phys. Rev. Lett.*, 58, 2486, 1987.
2. Florescu, M. et al., *PNAS*, 106, 20658-20663, 2009.
3. Edagawa, K. et al., *Phys. Rev. Lett.*, 100, 013901, 2008.
4. Imagawa, S. et al., *Phys. Rev. B*, 82, 115116, 2010.
5. Toninelli, C. et al., *Phys. Rev. Lett.*, 101, 123901, 2008.
6. Von Freymann, G. et al., *Advance. Functional Materials*, 20, 1038-1052, 2010.
7. Fatt Liew, S. et al., *Phys. Rev. A*, 84, 063818, 2011.
8. Yin, H et al., *PNAS*, 109,20798, 2012.
9. Fraden, S. et al., *Phys. Rev. Lett.*, 65, 512-515, 1990.
10. Ledermann, A. et al., *Nature Materials*, 5, 942-945, 2006.

Analysis of nanoparticles self-organization in microdroplets

M. Bogdanova [1*], S. Belousov[1], A. Afanasyev[2], and P. Lebedev-Stepanov[2,3]
[1]Kintech Lab, Moscow, Russia
[2]NRNU MEPhI, Moscow, Russia
[3]Photochemistry Center, RAS, Moscow, Russia
[*]corresponding author: bogdanpva@kintech.ru

Abstract-Spectrum of light transmission through a microdroplet made of polystyrene nanoparticles was calculated numerically and analyzed on the base of photonic crystal optical properties. Measuring of transmission spectrum can provide information about ordering quality of nanoparticles, number of layers and average lattice constant in a single layer.

Ordered assemblies are formed from microdroplets of a solution due to a nanoparticles self-assembly process [1–4]. Self-assembly technologies are based on the self-organization of nanoparticles into evaporated droplet of solution on a flat surface of a substrate. A multilayer face-centered cubic structure can form through self-organization of such particles. This structure has a lattice constant of the order of the size of its constituent nanoparticles. If the particles have a sufficiently regular shape and an equal size, this system will operate as a photonic crystal for electromagnetic radiation with a wavelength of the order of the lattice constant.

The shape of microcluster with self-organized nanoparticles and the quality of their ordering on a substrate may be controlled by parameters of a solvent and a substrate, value of surface electric charge of the particles, temperature of evaporation, contact line dynamics, etc. [5]. On Figures 1 and 2 two different droplets are presented. The first of them consists of very good periodic structured two layer system (especially in central area). The second one has a broken symmetry even in the central area.

a.
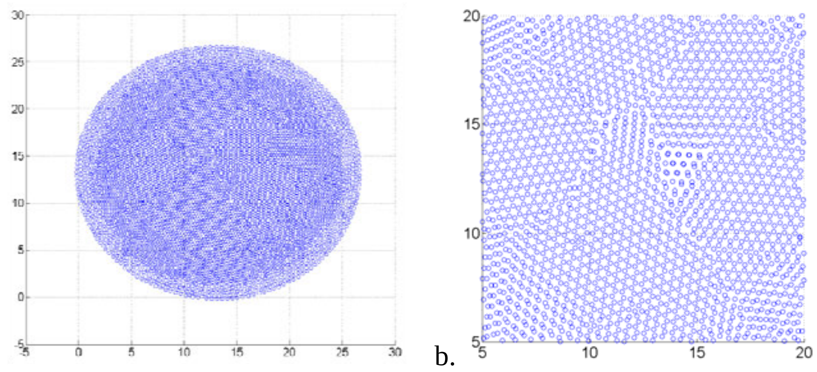

Figure 1. Nanoparticle locations in a microdrop (all scales are in microns). a: top view of the whole drop, b: top view of the central part.

Transmission spectrum gives a dip at the characteristic wavelength (Figure 3). The position of this dip provides information about average lattice period in a layer. The depth of this dip depends on the structure ordering. This method of diagnostics could be applied to characterize the self-assembled nanoparticles ordering in such droplets.

a. b.

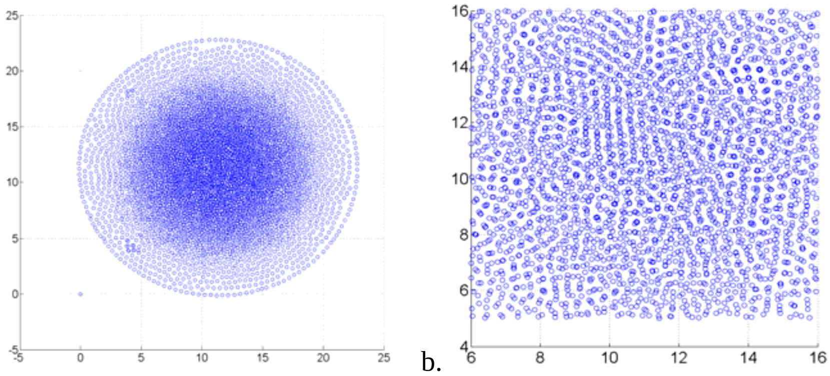

Figure 2. Nanoparticle locations in a microdrop (all scales are in microns). a: top view of the whole drop, b: top view of the central part.

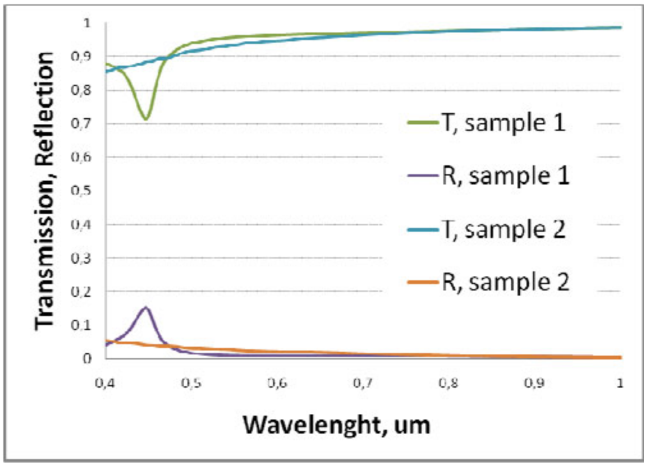

Figure 3. Transmission and reflection coefficient for two samples.

REFERENCES

1. G. Nicolis and I. Prigogine, *Self-Organization in Nonequilibrium Systems: From Dissipative Structures to Order through Fluctuations*,Wiley, New York, 1977.
2. J. Park, J. Moon, H. Shin, D. Wang, and M. Park,"Direct Write Fabrication of Colloidal Photonic Crystal Microarrays by Ink Jet Printing," *J. Colloid Interface Sci.* Vol. 298, 713–719, 2006.
3. L. V. Andreeva, D. A. Ivanov, D. S. Ionov, A. V. Koshkin, P. V. Lebedev-Stepanov, O. Yu. Rybakov, A. S. Sinitsky, A. N. Petrov, and M. V. Alfimov, "Investigations of Crystallization of Solutions in Microdroplets on an Affymetrix GMS 417 Arrayer Device," *Prib. Tekh. Eksp.*, No. 6, 1–8, 2006 [*Instrum. Exp. Tech.* Vol. 49, No. 6, 860–867, 2006].
4. L. V. Andreeva, A. V. Koshkin, P. V. Lebedev-Stepanov, A. N. Petrov, and M. V. Alfimov, "Driving Forces of the Solute Self-Organization in an Evaporating Liquid Microdroplet," *Colloids Surf. A: Physicochem. Eng. Aspects*, Vol. 300, 300–306, 2007.
5. P. V. Lebedev-Stepanov, S. P. Gromov, S. P. Molchanov, N. A. Chernyshov, I. S. Batalov, S. K. Sazonov, N. A. Lobova, N. N. Shevchenko, A. Yu. Men'shikova, M. V. Alfimov, Controlling the self-assemblage of modified colloid particle ensembles in solution microdroplets, *Nanotechnologies in Russia*, Vol. 6, Issue 9-10, 569-578, 2011.

Transformational electromagnetics

Right-angle bending and “carpet” cloaking of a surface electromagnetic wave

Hongyi Xu[1,2], Su Xu[3], Hongsheng Chen[3], Handong Sun[1,2], and Baile Zhang[1,2]*

1. Division of Physics and Applied Physics, School of Physical and Mathematical Sciences, Nanyang Technological University, Singapore 637371, Singapore.

2. Centre for Disruptive Photonic Technologies, Nanyang Technological University, Singapore 637371, Singapore

3. Department of Information Science & Electronic Engineering, Zhejiang University, Hangzhou, 310027, China

*corresponding author: blzhang@ntu.edu.sg

Abstract—A long-standing issue in plasmonics is that surface plasmonic polaritons (SPPs) are subject to large scattering loss when encountering a sharp corner or an obstacle on the propagation path. We address this problem by adopting the method of nonmagnetic transformation optics. A curved electromagnetic space is created with layered metamaterials to efficiently steer the propagation of SPPs through a right-angle, zero-radius bending corner with high transmission. Besides, SPPs can efficiently circumvent a bump on a flat surface as if the bump was not there. We experimentally tested the above strategies in microwave regime.

Plasmonics that studies surface plasmonic polaritons (SPPs) has the potential of many unprecedented applications. For example, it can break the diffraction limit in imaging and provide the possibility to produce ultra-compact optoelectronic devices. While bearing great expectations in next-generation photonics such as plasmonic circuitry, the wide application of SPP is still subject to a long-standing issue: SPPs are typically scattered when they encounter a sharp corner or an obstacle on the propagation path. This problem especially stands out in plasmonic on-chip applications where effective routing of surface plasmonic signal and compact interconnection of plasmonic components become highly demanding.

The problem of high scattering loss originates from the momentum mismatch at the location where the surface profile contains an abrupt change. For example, a right-angle sharp bending corner will introduce large momentum mismatch for SPPs propagation since the incident/outgoing wave vectors that are perpendicular to each other need to be matched in a very compact region. Traditional solutions generally use a bending adapter with large radius of curvature to gradually steer the incident wave and hence mitigate the momentum mismatch issue. Although being successful in obtaining high transmission, these solutions need to sacrifice the compactness of devices: in order to guarantee a high transmission the feature size of bending adapters has to be at least a few times larger than the wavelength, which is obviously undesirable in the efficient integration of plasmonic circuits.

Aiming at realizing a near-unit transmission across a sharp corner with zero radius of curvature, we electromagnetically ‘flatten’ a bent surface by applying nonmagnetic transformation optics[1]. A curved electromagnetic space is created by metamaterials; and in this space SPPs will be ‘cheated’ as if it propagates on a flat surface [Fig. 1(a)] rather than an bent one [Fig. 1(b)]. The electromagnetic momentum of input signal can be effectively steered to match that of the outgoing one in a compact area. As a result, a high transmission across a sharp corner can be expected [Fig. 1(c)].

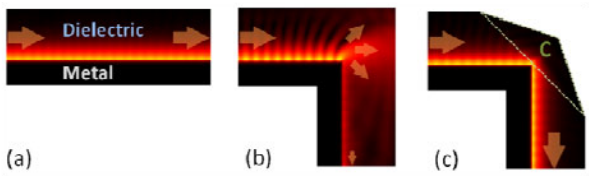

Figure 1 The simulated field distribution (magnetic field amplitude |**H**|) surface plasmon polaritons propagating (a) on a flat surface, (b) across a 90 degree sharp corner, and (c) across a sharp corner in a curved electromagnetic space C.[2]

Experimentally, two scenarios were investigated: firstly, guiding surface plasmonic polaritons through a sharp corner; secondly, cloaking a bump on a flat surface as if the bump were not there [Fig. 2]. Both of them were proved to have near-unity transmission, compared to a very low transmission in untransformed circumstances. The experiments were conducted in microwave regime where the concept of spoof SPPs is introduced.

To the best of our knowledge, this is the first time to successfully guide SPPs across ultra-sharp bending corners and the first demonstration of high transmission in “carpet” cloaking of SPPs.

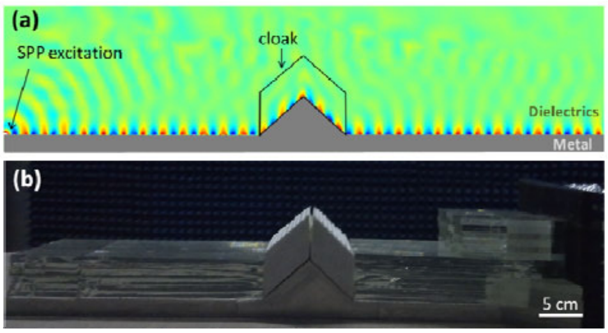

Figure 2 (a) The simulated field distribution (magnetic field **H**) of surface plasmon polaritons propagating through a bump lossless with the assistance from a cloak designed by nonmagnetic transformation optics. (b) The device working in microwave regime.

Reference

1. H. Xu, B. Zhang, T. Yu, G. Barbastathis, and H. Sun, "Dielectric waveguide bending adapter with ideal transmission: practical design strategy of area-preserving affine transformation optics," J. Opt. Soc. Am. B **29**, 1287-1290 (2012).
2. H. Xu, X. Wang, T. Yu, H. Sun, and B. Zhang, "Radiation-Suppressed plasmonic open resonators designed by nonmagnetic transformation optics," Sci. Rep. **2**, 784 (2012).

Fundamentals of designing Cylindrical High Order Transformation Optics Invisibility Cloaks using Silver-Silica Metamaterials

K. S. Elassy*

*Arab Academy for Science, Technology, and Maritime Transport, Egypt

kareemsalah@ieee.org

Abstract— **Metamaterials have effective properties that are distinctive from its composites. Understanding the properties of the MM composites is vital to be capable of engineering new effective parameters. We surveyed for the various techniques to control EM waves using MM, and then we perform a detailed study for the analytical analysis of the effective and the constituents' parameters of Silver-Silica MM at different sizes of the inclusions and volume fractions. We also propose a simple design technique for high order TO cylindrical cloak previously proposed in [4] highlighting the design constraints for this cloak.**

Metamaterials (MMs) are artificially structured arrangement of elements designed to achieve unusual electromagnetic properties. These extraordinary human-made materials provide an unprecedented ability to controlling electromagnetic (EM) waves. MMs can be constructed in many different shapes or designs to achieve similar results; for example, Chiral MMs and Negative Index Materials (NIMs) which can be either C-shaped MMs, nano strip pairs or split ring resonators. These are all different kinds and types of MMs that have been developed over the last decade.

Exciting applications of MMs came to life in 2000 when Pendry [1] firstly proposed a design of super resolution lens, or *Superlens*. Later on, more applications were developed by other scientific researchers, such as: hyperlenses, optical absorbers, optical black holes and finally the most interesting application which is invisibility cloaks.

Invisibility cloaks, in general, can be achieved by three main theoretical and mathematical approaches: quasi-conformal mapping, Mei scattering and transformation optics (TO). TO is a unique means of designing an optical device. Rather than relying on the standard tools of optics, we instead imagine warping the space in a manner so as to control the trajectories of light rays.

There are two types of TO: linear TO and high order TO. The latter is preferable because it reduces the impedance mismatching between the optical device and the free space, and thus produces better results and finer performance. Mathematical models and solutions for both cylindrical and spherical high order TO designs were proposed by Pendry *et al.* [2]. The solutions for both designs require a gradient-refraction index material with the boundary conditions: $n = 1$ at the outer radius and $n = 0$ at the inner radius, as shown in figure 1.

The fundamentals of designing a gradient-refraction index material were proposed by Shalaev *et al.* [3] in 2007. Later in 2008, a fully detailed interpretation of designing a silver-silica composite cylindrical optical cloaking device by using high order TO was also provided by Shalaev *et al.* [4]. Other proposed designs are also introduced by Shalaev [3,4].

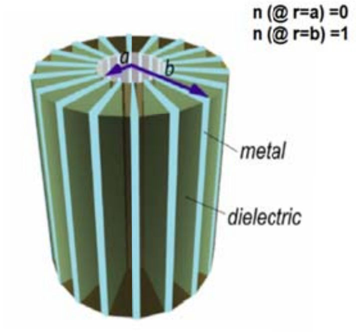

Figure 1 Cylindrical gradient-refraction index material

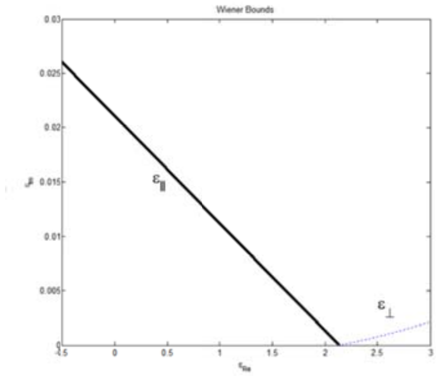

Figure 2 Wiener bounds graph of silver-silica composite

inclusion shape effect and the screening parameter κ expressed in (2).

$$f_1 \frac{\varepsilon_1 - \varepsilon}{\varepsilon_1 + \kappa\varepsilon} + f_2 \frac{\varepsilon_2 - \varepsilon}{\varepsilon_2 + \kappa\varepsilon} = 0 \tag{1}$$

$$\kappa = (1 - L)/L \tag{2}$$

, where f_1 and f_2 are the metal and dielectric volume fractions, respectively, ε_1 and ε_2 are the electric permittivity of the constituent materials, ε is the effective permittivity of the whole composite and L is the Lorentz depolarization factor

The last constraint is that the thickness of the metal plates should not exceed the skin depth of the material to allow the propagation of electromagnetic waves inside them.

References

[1] Pendry, J. B. “Negative Refraction Makes a Perfect Lens,” *Phys. Rev. Lett.*, Vol. 85, No. 18, 2000.

[2] Pendry, J. B., D. Schuring and D. R. Smith, “Controlling Electromagnetic Fields.” *Sci. Exp.*, 10.1126, science.1125907, 2006.

[3] Shalaev V. M., W. Cai, U. K. Chettiar, A. V. Kildishev, “Optical Cloaking with Metamaterials,” *Nat. Pho.*, Vol. 1, 2007.

[4] Shalaev V. M., W. Cai, U. K. Chettiar, A. V. Kildishev, “Designs for Optical Cloaking with High-Order Transformations,” *Birck and NCN Publications*, Paper 174, 2008.

Extraordinary transmission

Enhanced Emission of Plasmonic Thermal Emitter with Random Gold Nanoparticles

Che-Hsuan Cheng[1*], Yu-Cheng Chen[2], Hung-Hsin Chen[1], and Si-Chen Lee[1]

[1]*Graduate Institute of Electronics, National Taiwan University, Taipei City, Taiwan, R.O.C*
[2]*Molecular Imaging Center, National Taiwan University, Taipei City, Taiwan R.O.C*
[*]*corresponding author: r00943051@ntu.edu.tw*

Abstract- The enhanced emission of plasmonic thermal emitter with gold nanoparticles randomly distributed onto periodic metallic island arrays is investigated in the mid-infrared regime. Gold films with different thicknesses were deposited on top of the periodic structures and then annealed to form nanoparticles of random sizes. It was discovered that the infrared emission of plasmonic thermal emitter with these random nanoparticles is significantly enhanced. This design provides an efficient infrared light source which can be applied in biosensing area.

The emission properties of a tri-layer metal/dielectric/metal plasmonic thermal emitter (PTE) with periodic metallic island arrays as top layer have been studied [1-3]. This structure exhibits narrow thermal emission modes induced by localized surface plasmon (LSP) resonance, and the resonant wavelength can be tuned by varying the dimensions of the metallic patch. Owing to its tunability, this structure can be utilized as an ideal narrow band infrared light source. In recent years, gold nanoparticles have been applied to enhance the performance of various devices, i.e., biosensing [4], photovoltaics [5] and plasmonic devices, etc. It is demonstrated in this work that the emittance of a PTE can be efficiently enhanced by embedding randomly sized and distributed gold nanoparticles in periodic island arrays.

The PTE with periodic square islands was fabricated by e-gun evaporation and patterned using photolithography. A thin gold film was then thermal evaporated on the PTE and followed by rapid thermal annealing (RTA) at 400^{o}C for 2 minutes. The Mo film was deposited on the back side of the silicon substrate as a heating layer. A direct current was supplied into the Mo film which heated the PTE device and further excited the LSP modes. The thermal emittance spectra were measured by a FTIR spectrometer. The schematic view of the fabrication processes is shown in Fig. 1. The dimensions of the periodic island structure are fixed, the periods of the island arrays are 7 μm in both x and y directions, while the length of each square island is 4 μm. The thickness d of the gold film were varied from 1, 3 to 5 nm in order to form nanoparticles with different sizes.

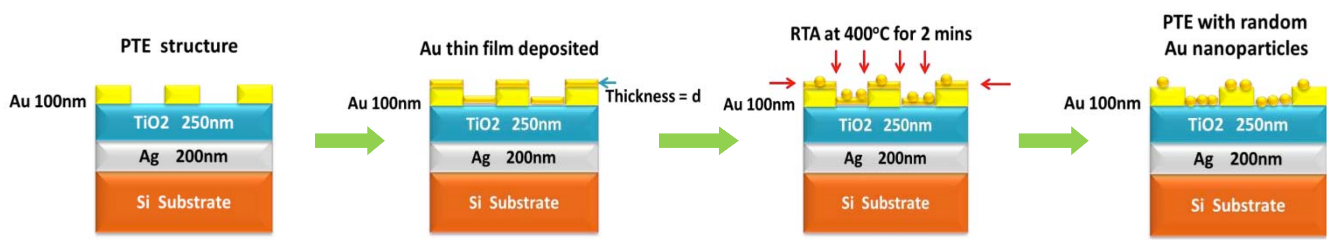

Fig. 1 Schematic fabrication process of a PTE with random gold nanoparticles.

Fig. 2(a) shows the OM image of the top view of a PTE with periodic island arrays, each square island acts as a Fabry–Pérot type resonator. Fig. 2(b) displays the AFM image of the sample with 1 nm gold film after RTA process and its corresponding landscape measurement. The sizes of the nanoparticles are between 5 to 30 nm.

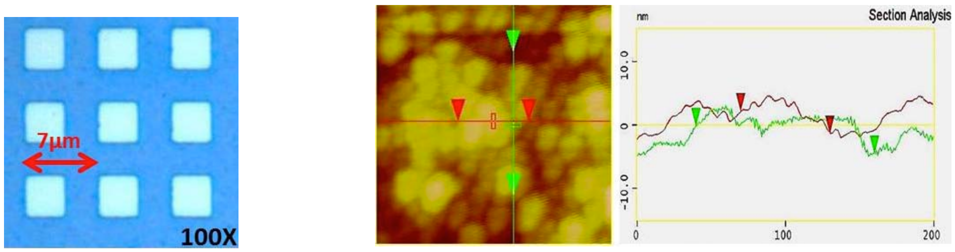

Fig. 2 (a) The OM image of square island arrays. **(b)** The AFM image and landscape measurement of the sample with 1 nm gold film after RTA.

The thermal emittance spectra of PTEs with 1, 3 and 5 nm gold films after RTA process denoted as A1, A2, and A3 are shown in Fig. 3(a), (b), and (c), respectively. The blue curves denoted as B1, B2, and B3 represent the emittance spectra of the original samples before gold film deposition and RTA process. The power inputs to each sample were fixed. It is obvious that the emittances of A1 and A2 are significantly enhanced after adding random gold nanoparticles. Emittances of fundamental LSP (1,0), (0,1) modes are increased by 25% and 39% for A1 and A2, respectively, while slightly decreased for A3. The random nanoparticles act as LSP resonators that accumulate radiation generated from the dielectric layer of a PTE and scatter back and forth between nanoparticles, resulting in enhanced emission. However, when the gold film is too thick (5 nm for A3) to form nanoparticles, it will block part of the radiation from emitting, thus reducing the emission. In summary, emission of a PTE can be efficiently enhanced through random gold nanoparticles formed by rapidly thermal annealing very thin gold film, and this device has the potential to be applied in biosensing area.

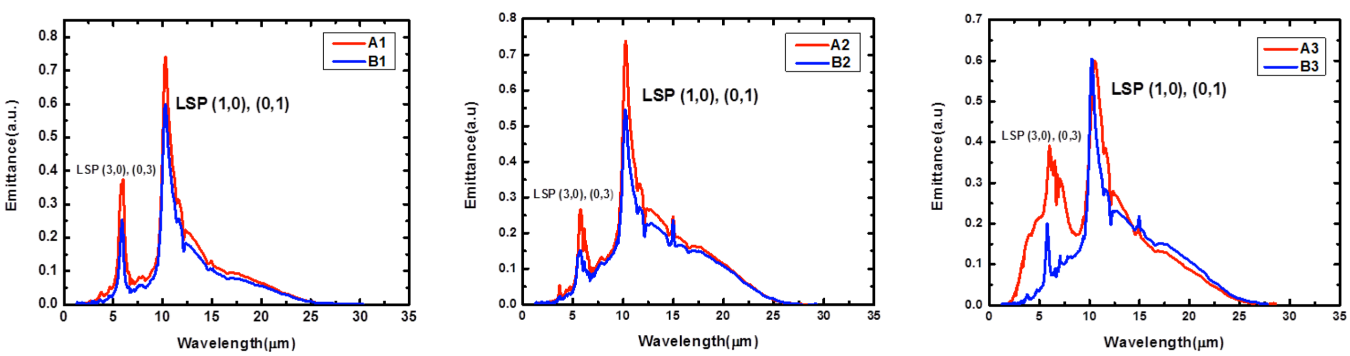

(a) (b) (c)

Fig. 3 Thermal emittance spectra of PTEs with (a) 1, (b) 3, and (c) 5 nm thin gold films after RTA process (red curves).

REFERENCES

1. W. L. Barnes, A. Dereux, and T. W. Ebbesen, "Surface plasmon subwavelength optics," Nature, vol. 424, pp. 824–830, Aug. 2003.
2. P. E. Chang, et al., "Wavelength selective plasmonic thermal emitter by polarization utilizing Fabry–Pérot type resonances," Appl. Phys. Lett., vol. 98, no. 7, pp. 073111-1–073111-3, 2011.
3. Y. H. Ye, et al., "Localized surface plasmon polaritons in Ag/SiO2/Ag plasmonic thermal emitter," Appl. Phys. Lett., vol. 93, no. 3, pp. 033113-1–033113-3, 2008.
4. Kiley A White, Nathaniel L Rosi, Gold nanoparticle-based assays for the detection of biologically relevant molecules, Nanomedicine, 2008, 3, 4, 543.
5. H. A. Atwater and A. Polman, "Plasmonics for improved photovoltaic devices," Nature Mater., vol. 9, no. 3, pp. 205–213, 2010.

A Study on the Properties of Chalcogenide Based Glasses for 8~12㎛ IR Region Aspherical Optical Lens Application

Dong-Sik Bae[1], Jong-Bin Yeo[2], and Hyun-Yong Lee[3*]

[1]Department of Advanced Chemicals and Engineering, Chonnam National University, Gwangju 500-757, Republic of Korea

[2]The Research Institute for Catalysis, Chonnam National University, Gwangju 500-757, Republic of Korea

[2]Faculty of Applied Chemical Engineering, Chonnam he Research Institute for Catalysis, Chonnam National University, Gwangju 500-757, Republic of Korea

[*]corresponding author: hyleee@chonnam.ac.kr

Abstract-The chalcogenide glass well known for infrared(IR) transmission materials and currently one of widely applied to optical materials. In recent years, many researchers have studied IR lenses using the chalcogenide glass. The chalcogenide glass has good optical properties of IR region transmittance. We determine the composition of GeSbSe chalcogenide glass for IR lenses and variety the effect of $Ge_{19}Sb_{23}Se_{58}$. Because this composite rate have good properties of optical, thermal, physical, and structural. The chalcogenide glass was compared quenching with annealing. The optical, structural and thermal properties were measured by Fourier transform infrared spectroscopy(FT-IR), X-ray diffraction(XRD), Differential scanning calorimeter(DSC), respectively. From the analysis result, We ascertained the feasibility as a molding materials for infrared optics.

An infrared optical lens material to the present Ge, Si, ZnS, ZnSe, MgF_2 been developed. But quite expensive and require a long time to manufacture, and when cutting a lot of material has the disadvantage of loss. So high light transmittance, chemically stable, 8 ~ 12μm wavelength range, especially with the application for the light transmittance chalcogenide glass has attracted attention. Chalcogenide elements of safety glass, or optical, thermal, and physical characteristics were considered to select the GeSbSe.

Bulk samples of $Ge_{19}Sb_{23}Se_{58}$ were prepared by a conventional melt quenching technique. The constituent elements weighed at given atomic-weight percentage ratios were sealed in an evacuated quartz ampoule, which was then placed in a furnace and respectively heated to 490k, 903k, 1231k for 2h, then it was raised to 1273K for 24h. The thin films were prepared by thermal evaporation of the bulk at a deposition rate of about 3 Å/s on p-type Si (100) and slide glass substrates kept in a vacuum of $\sim 10^{-4}$ Torr. The film thickness was fixed to be about 200 nm. The films were isothermally annealed from 150 °C to 390°C at intervals of 30°C. Heat treatment process progressed in 200 sccm N_2 atmosphere for 1 h in order to prevent oxidation of thin films. The structural phases of the thermal annealed films were evaluated by X-ray diffraction (XRD). Differential scanning calorimeter DSC(Perkin Elmer DSC-7) is used to determine the characteristic temperatures. The temperature precision of this equipment is ±0.1 K with an average standard error of about 1 K in the measured values. The masses of the samples varied between 2 and 3mg and were measured by weighing with an accuracy of about 100 mg. For the sample that has been examined and identified as a glass, a slice of the sample was mounted and then polished on both sides. The thickness of the slice was 2mm.

Glasses classified as Fig. 1 and Fig. 2 are those in which crystals were detected using X-ray diffraction pattern but which also showed a distinct crystallization temperature(T_c), glass transition temperature(T_g) in a DSC measurement. The crystalline structures of $Ge_{19}Sb_{23}Se_{58}$ films were characterized by XRD measurement and shown in Fig. 1. The typical DSC curves $Ge_{19}Sb_{23}Se_{58}$ chalcogenide glass were recorded at heat flow up(mW) are shown in Fig. 2. T_g peak(247°C) and the crystallization peak(342°C) were detected using DSC analysis. Fig. 3 shows the IR transmittance results of a 2mm thick slice of $Ge_{19}Sb_{23}Se_{58}$ glass. The transmittance for most wave numbers was about 73%. From the analysis result,We ascertained the feasibility as a molding materials for infrared optics.

In the future, aspherical lens will be processed by using fabricated bulk and will be evaluated properties of chalcogenide based surface roughness for aspherical lens.

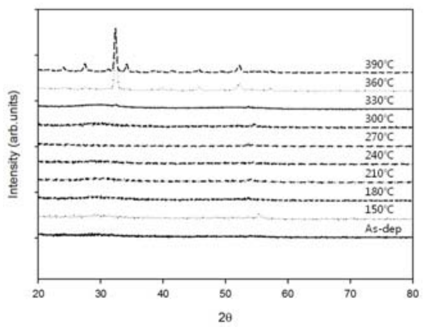

Fig. 1. XRD patterns of chalcogenide glass at annealing.

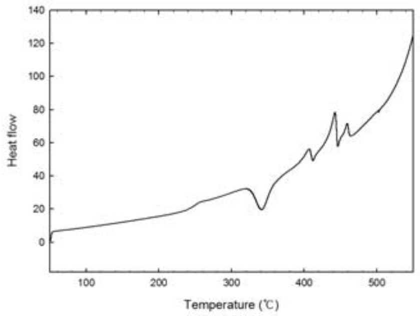

Fig. 2. DSC curve of chalcogenide glass at quenching.

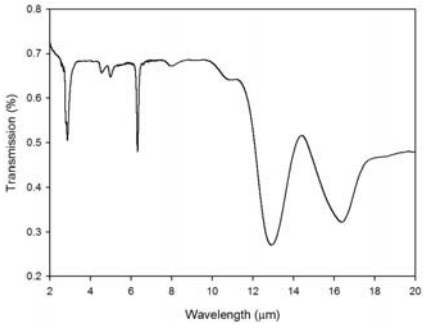

Fig. 3. Transmission curve of 2mm thick sample of chalcogenide glass at quenching.

Acknowledgements, This work was supported by Priority Research Centers Program through the National Research Foundation of Korea(NRF) funded by the Ministry of Education, Science and Technology(2009-0094055)

REFERENCES

1. A. M FARIED, S. S. FOUAD, A. H. AMMAR, "The structural properties of $Ge_xSb_{40-x}Se_{60}$system", JOURNAL OF MATERIALS SCIENCE : MATERIALS IN ELECTRONICS, 16, pp.97-101,(2005).
2. J. A. SAVAGE, P. J. WEBBE R, A. M. PITT, "An assessment of Ge-Sb-Se glasses 8 to 12㎛ infrared optical materials", JOURNAL OF MATERIALS SCIENCE, 13, pp.859-864, (1978).

Frequency selective structures and high impedance surfaces

Conception of CRLH Antenna

Oussama TABBABI, Mondher LABIDI and Fethi CHOUBANI
Innov'com Research Laboratory, Higher School of Communications of Tunis,
Sup'Com University of Carthage, Tunisia

Abstract-In This paper, a novel rectangular patch antenna is proposed and studied based on the Metamaterial Composite Right Left Handed (CRLH) transmission line (TL) model. It is a miniaturized Zeroth Order Resonance (ZOR) antenna designed on Reactive Impedance Surface (RIS). The miniaturization is provided by the use of mushrooms that increase the (LH) inductor and then push down the Left Handed (LH) region. Simulated result at zeroth order resonance show improvement in the antenna gain and bandwidth by increasing a number of vias.

Several Meatamaterial realizations were presented using Transmission Line (TL) theory. They were done by [1-4], where a mushroom structure [2] is used for the realization of the High Impedance Surface (HIS) [5]. Microstrip antenna loaded with this CRLH metamaterial is able to excite the negative order resonance and provide decreased resonance frequencies [6]. It is shown that they have a good radiation and small size.

The basic structure of the CRLH metamaterial antenna as shown in Figure 1 is consist of ground plane, substrate and patch on the top of the substrate, a mushroom connects the patch and the ground plane, and there is a gap between the adjacent patches. The Left Handed (LH) capacitance C_L is provided by coupling of adjacent top patches while the LH inductance is provided by a mushroom connected to the ground plane.

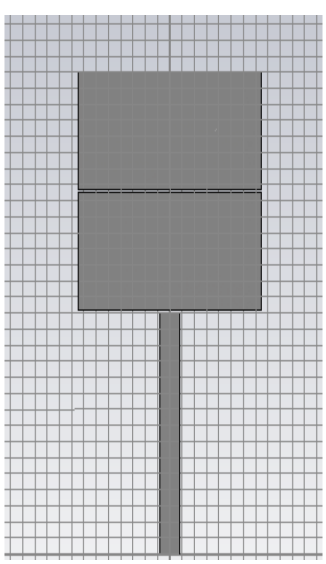

Fig 1. Microstrip antenna based on CRLH metamaterial.

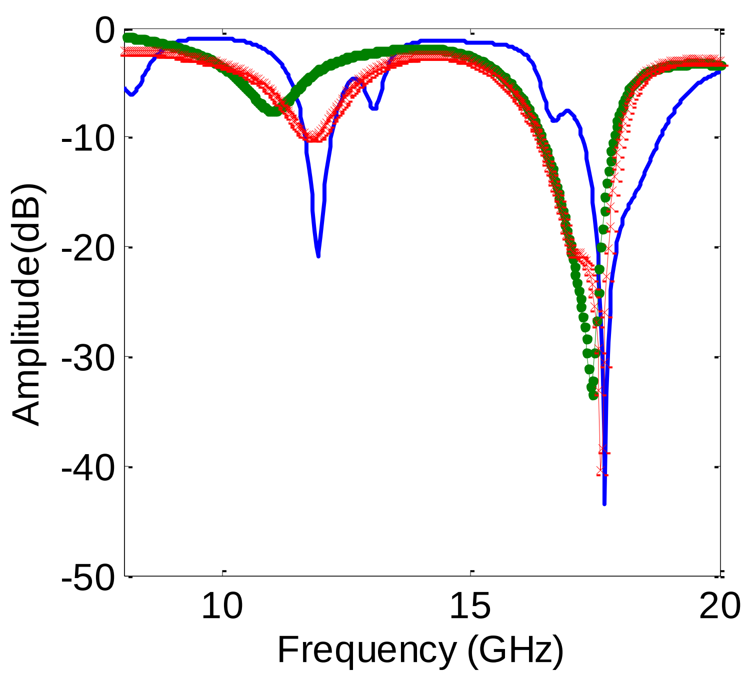

Fig 2. Effect of the mushroom on the return loss of the two patch antenna.

Figure 2 shows the comparison of the return loss between the two patches antenna only, antenna using 2 and 6 mushrooms. As shown in Fig 2, the structure is more compact and has a return loss of -45 dB with 6 mushrooms.

REFERENCES

1. A. Sanada, C. Caloz, and T. Itoh, Planar distributed structures with negative refractive index, *IEEE Trans Microwave Theory* Tech 52 (2004).
2. C. Caloz and T. Itoh, *Electromagnetic Metamaterials: Transmission Line Theory and Microwave Applications,* Wiley, Hoboken, NJ, 2006.
3. A. Lai, C. Caloz, and T. Itoh, Composite right/left-handed transmission line metamaterials. *IEEE Microwave Mag* (2004), 33–50.
4. F. Qureshi, M.A. Antoniades, and G.V. Eleftheriades, A compact and low-profile metamaterial ring antenna with vertical polarization, *IEEE Antennas Propag* Lett 4 (2005), 333–336.
5. D. Sievenpiper, L. Zhang, R. F. J. Broas, N. G. Alexopolus, and E. Yablonovitch, High-impedance lectromagnetic surfaces with a forbidden frequency band, *IEEE Trans. Microwave Theory Tech*., vol. 47, pp. 2059–2074, 1999.
6. H. R. Stuart and A. Pidwerbetsky, Electrically small antenna elements using negative permittivity resonators, *IEEE Trans. Antennas Propag*., vol. 54, no. 6, pp. 1644–1653, Jun. 2006.

High Gain Compact Helix Antenna in a Cylindrical Cavity for UHF RFID

N. Rimbault, A. Sharaiha and S. Collardey
IETR, Université de Rennes 1, Bat 11D, 263 Avenue du Général Leclerc, 35042 Rennes Cedex, France1Author
Narcisse.rimbault@univ-rennes1.fr, ala.sharaiha@univ-rennes1.fr, sylvain.collardey@univ-rennes1.fr

Abstract- Decreasing the size of the UHF Radio Frequency Identification (RFID) reader antenna without reducing the tag reading performance is a challenging problem. A low profile helix antenna (0.3λ) with high gain for RFID reader is presented. The size reduction and high gain are obtained by using cylindrical cavity combined with Frequency Selective Surfaces (FSS). The structure has a total size of 692x692x155mm3 and presents good performance, such as high gain of 14.8dBic over a large bandwidth with a good axial ratio.

Introduction

Radio Frequency Identification (RFID) system in Ultra High Frequency (UHF) band has been receiving much interest in several services industries, distribution logistic and goods flow system. In these applications, a reader must usually read passive tags with low gain antennas and low backscattered power and with a linear polarization. So, a high gain antenna with small angular aperture is required in order to increase the read range and, above, to avoid the detection of parasitic tags outside a restricted area. A circularl polarization is also needed to read a tag which can be located in any position.

Helix antennas are widely used in communication system, for their performances such as a high gain in axial direction and the quality of circular polarization [1]. However the high gain comes at the cost of an increase antenna height.

Fabry-Perot cavities [2] are usually fed by planar antennas or open waveguide and achieve high gain with a low profile structure in a small bandwidth. In this paper, a new structure is proposed, based on Fabry Perot cavity combined with FSS, to obtain a small helix antenna of 0.3 λ of height integrated in a cylindrical circularly polarized Fabry Perot cavity with a gain greater than 14 dBic.

Antenna design

The helix antenna is designed to operate at UHF RFID frequencies from 860 to 960MHz. The ground plane is a circular metallic plane of 300m diameter. The helix structure has been realized with 20mm width copper strips. According to previous studies and formulas, 10.8dB gain and 2.2dB axial ratio (AR) can be achieved with a helical antenna of 300mm height (4 turns) for a pitch angle of 12.5°.

In [3] we have shown that, the performances of the helix antenna can be improved if the circular ground plane is replaced by a cylindrical cavity, of diameter equal to D=2λ for a cavity height of 0.6λ (hcav), and helical antenna of 300mm height. For these dimensions, the gain is equal to 13.8dBic and the axial ratio achieves 1.2dB in a large bandwidth. Now, to reduce more the antenna and cavity heights, we propose to use a Fabry-Perot cavity. The height of the cavity is reduced to reach about λ/2. The height of the helix antenna is also reduced to be embedded into the cylindrical cavity which is closed by a frequency selective surface (FSS) to make a Fabry-Perot cavity.

The final structure is shown in Fig.1 (a). The height of the cavity is 0.44λ, its diameter is 2λ. The ratio of the grid is 0.03 between the width and periodicity. The height of the helix antenna is 100mm (0.3λ).
We showed that the cylindrical cup structure presents a 3dB gain higher than a gain of the structure with circular ground plane. The new solution Fabry-Perot cavity presents 1dB gain higher than the cylindrical cup gain, but in a narrower bandwidth. The Fabry-Perot cavity presents a higher axial ratio (less than 3.5 dB) due to the small helix height and to the FSS proximity, but it still interested. The Fig.1 (b) presents the radiation pattern of RHCP and LHCP gain.

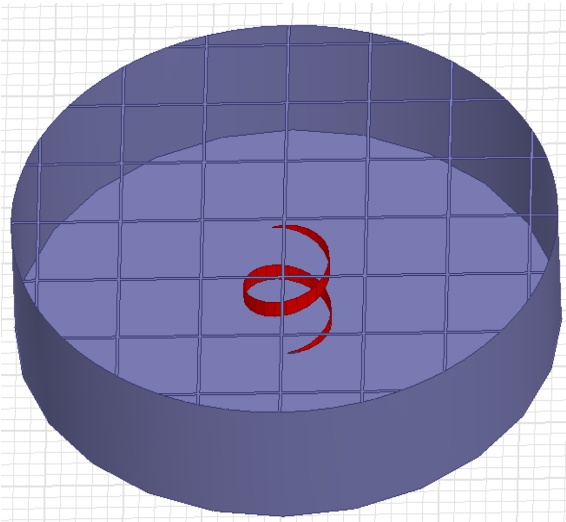

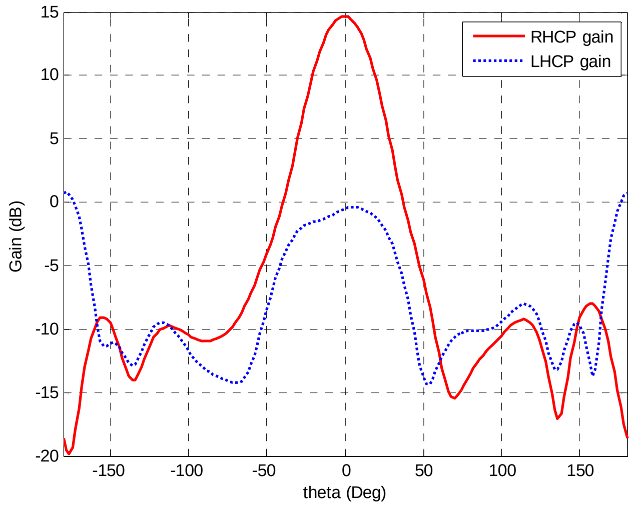

(a) **(b)**

Figure 1 (a) Fabry –Perot cavity, exited by helix antenna, (b) Radiation pattern of RHCP & LHCP Gain at F=865MHz and phi=0°

Conclusion

In this paper, we propose to integrate a helix antenna in Fabry- Perot cavity to obtain a very low profile structure (0.3λ height) with high gain in a large bandwidth compared to classical techniques using high helix antenna height (>λ). The axial ratio increases but stays acceptable for RFID applications. All performances are obtained by reducing the height system antenna by 50%. Complementary studies and measurement results will be presented in the final paper.

Acknowledgements, This work was done during Spinnaker project financed by OSEO with Tagsys as the main industrial partner.

REFERENCES

1. J.D. Kraus, "Antennas", *2nd ed., New York: McGraw-Hill*, 1988.
2. S.A. Muhammad, R. Sauleau, H. Legay, “Small-size shielde metallic Fabry-Perot cavity antennas with large bandwidth for space applications”, *IEEE Trans Antennas Propagat*, Vol.60, Feb 2012, pp.792-802
3. N. Rimbault, A. Sharaiha, S. Collardey, “High Gain Design of Small Axial Mode Helical Antenna Over a Cylindrical Cavity for RFID Applications”, *IEEE RFID-TA*,2012

Frequency selective surfaces based on substrate integrated waveguide with miniaturized elements

Fan-Cheng Huang[1] **and Yih-Peng Chiou**[1,2,3*]

[1]Graduate Institute of Photonics and Optoelectronics, [2]Graduate Institute of Communication Engineering, and [3]Department of Electrical Engineering, National Taiwan University, Taipei 10617, Taiwan
*ypchiou@ntu.edu.tw

Abstract— We demonstrate a miniaturized element FSS structure incorporated with substrate integrated waveguide (SIW) cavity. The resonance frequency of the structure is stabler and its roll-off response is sharper as compared that without SIW cavity.

Frequency selective surfaces (FSSs) have been widely studied by many researchers and utilized in various applications [1]. FSSs are usually periodic arrays comprising identical elements and perform high transmission or high reflection when electromagnetic waves propagate through FSSs. FSSs based on substrate integrated waveguides (SIW) are investigated, and they provide a low-cost architecture with a high quality factor and thus sharp roll-off at the passband edges [2], [3]. Recently, miniaturized element FSSs (MEFSS) are presented, which can reduce the size of FSSs to avoid bulky and heavy structures in low frequency applications [4], [5]. In addition, the problem of grating lobes can be effectively suppressed in MEFSSs and their frequency response is less sensitive to the incident angle incidence, since their periods are much smaller than the operating wavelength.

Here, we demonstrate a FSS structure with miniaturized elements bound within a SIW cavity as Fig. 1. Since the SIW vias can effective stop the propagatin waves, the SIW vias can be approximated with a perfect electric conductor (PEC) sheet. The FSS element comprises a single PEC surface with etched slot aperture on the top, a 1 mm thick FR4 substrate, a sheet PEC cavity with radius of $R_{cavity} = 2.15$ mm tunnelling the substrate. The period (Λ) of unit cell is 4.5 mm. The R_{in} and R_{out} of the miniaturized aperture are 0.65 mm and 2.0 mm, respectively. Slot width of the meander pattern is 0.15 mm. Simulation results by HFSS software with sheet cavity at different incidence angles and polarizations are shown in Fig. 2.

We further investigate the response of larger Λ with the rest parameters unchanged. Comparisons between cases of $\Lambda = 4.5$ and 6.0 mm with and without cavity are shown in Fig. 3. We can observe that the miniaturized element FSS with cavity is not very sensitive to incidence angles as Fig. 2 and resonance frequencies are relative stable compared with FSS cases without cavity as in Fig. 3. The cavity will provide good isolation between elements so that resonance frequencies are almost the same both of $\Lambda = 4.5$ and 6.0 mm cases. By contrast, frequency shift is larger in the case without cavity in Fig. 3(b). Another advantage is the sharper roll-off at the passband edges

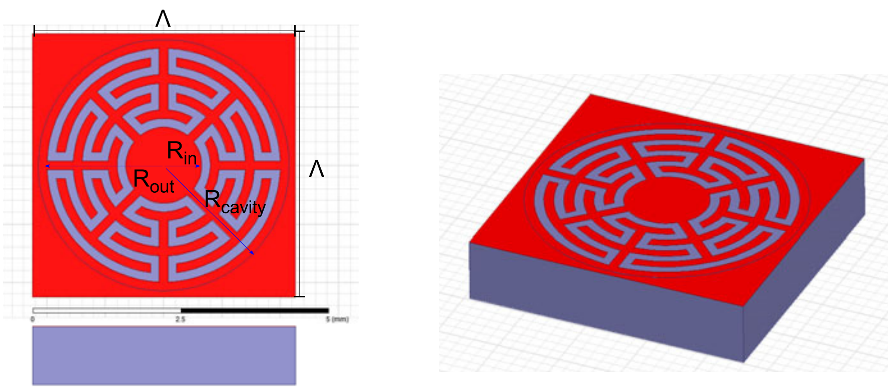

(a) (b)

Figure 1: Schematic diagrams of the SIW-MEFSS: (a) Top and side views. (b) Three dimensional view.

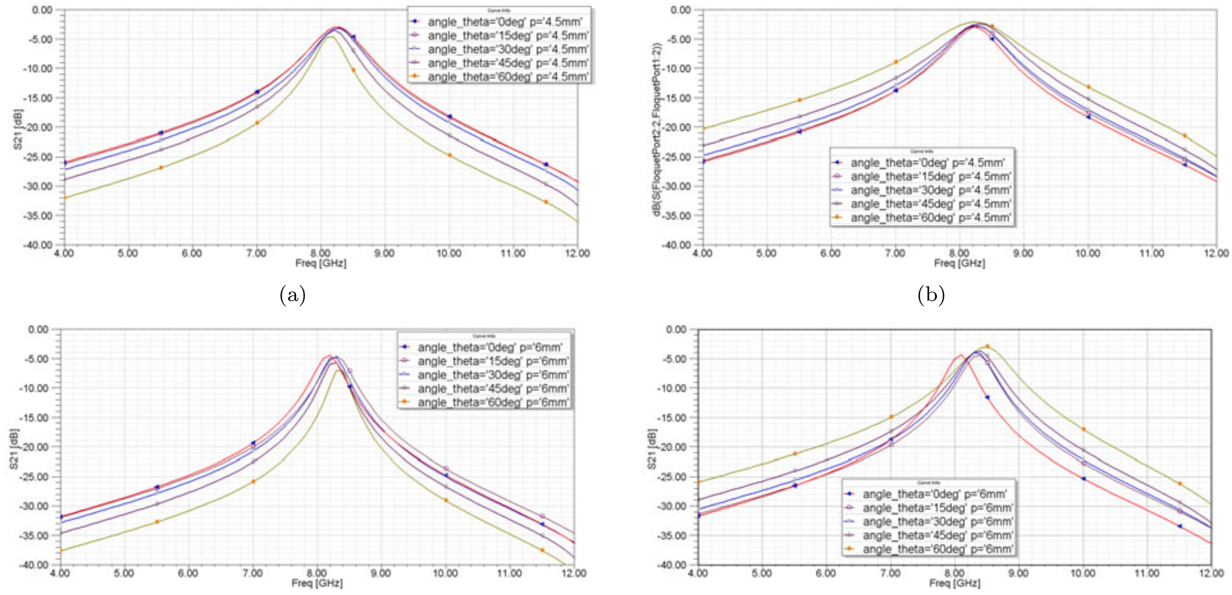

(a) (b) (c) (d)

Figure 2: S_{21} parameters for with (a) TE polarization and $\Lambda = 4.5$ mm, (b) TM polarization and $\Lambda = 4.5$ mm, (c) TE polarization and $\Lambda = 6.0$ mm (b) TM polarization and $\Lambda = 6.0$ mm. The angle theta and p in the legend are the incidence angle and period Λ, respectively.

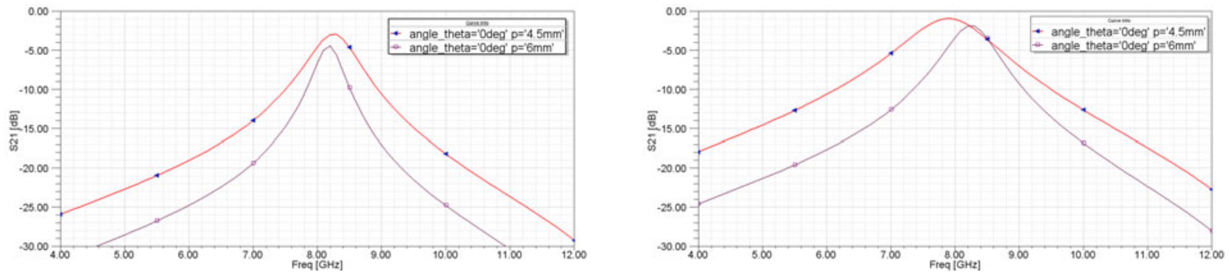

(a) (b)

Figure 3: Comparisons of S_{21} parameters between $\Lambda = 4.5$ mm and $\Lambda = 6.0$ mm. Normal incidence with TE polarization for (a) FSS with PEC cavity and (b) without PEC cavity.

indicating a better frequency resolution which is good for filters. Bandwidth of -10 dB of Fig. 3(a) $\Lambda = 4.5$ mm case is about 1.5 GHz and of Fig. 3(b) $\Lambda = 4.5$ mm case is about 3.3 GHz. We will demonstrate more results in the conference.

ACKNOWLEDGMENT

This work was supported in part by the National Science Council of the Taiwan under grant NSC 101-2120-M-110-006, NSC98-2221-E-002-170-MY3, and the Excellent Research Projects of National Taiwan University under Grant 101R89081. They are grateful to the National Center for High-performance Computing in Taiwan for computer time and facilities.

REFERENCES

1. Munk, B. A., *Frequency Selective Surfaces: Theory and Design*, Wiley-Interscience, New York, 2000.
2. Luo, G. Q., W. Hong, Z. C. Hao, B. Liu, W. D. Li, J. X. Chen, H. X. Zhou and K. Wu, "Theory and Experiment of Novel Frequency Selective Surface Based on Substrate Integrated Waveguide Technology," *IEEE Trans. Antennas Propag.*, Vol. 53, No. 12, 4035–4043, 2005.
3. Winkler, S. A., W. Hong, M. Bozzi and K. Wu, "Polarization Rotating Frequency Selective Surface Based on Substrate IntegratedWaveguide Technology," *IEEE Trans. Antennas Propag.*, Vol. 58, No. 4, 1202-1213, 2010.
4. Sarabandi, K. and N. Behdad, "A Frequency Selective Surface With Miniaturized Elements," *IEEE Trans. Antennas Propag.*, Vol. 55, No. 5, 1239–1245, 2007.
5. Al-Joumayly, M. and N. Behdad, "A New Technique for Design of Low-Profile, Second-Order, Bandpass Frequency Selective Surfaces," *IEEE Trans. Antennas Propag.*, Vol. 57, No. 2, 452–459, 2009.

Analytical model of a self-complementary connected array on high impedance surface

X. Begaud[1*], **F. Linot**[1,2], **M. Soiron**[3], **C. Renard**[2]
[1]Institut Mines Télécom, Télécom ParisTech - LTCI CNRS UMR 5141, France
[2]Thales Systèmes Aéroportés, France
[3]SART, France
[*]corresponding author: Xavier.Begaud@telecom-paristech.org

Abstract-This paper presents an analytical model to design a self-complementary connected array above artificial material. The purpose of this model is to facilitate and set parametric studies for a significantly shorter time than an electromagnetic simulator. In this work we have derived analytical models to design the proposed phased array antenna above high impedance surface, absorber or reactive. All the results have been verified to be accurate by numerical simulations done with Ansoft HFSS. These artificial materials can modify the antenna behavior by either increasing the bandwidth with control of an agile band or by adding several bandwidths.

This work has been realized in the framework of research on wideband and low-profile antenna arrays for airborne applications. It is well known that wideband behaviour can be achieved by choosing an appropriate antenna element shape. It is also well known that for achieving wideband behaviour an appropriate antenna element must be selected. Self-complementary antennas are a good choice to fix the input impedance of such an antenna [1]. In this work, the antenna element shape considered is a checkerboard. Designing unidirectional antennas is required on many platforms in order to obtain outward radiation and to preserve the interior against any electromagnetic pollution. For this, most common solutions in wideband applications locate the antenna above an absorbing reflector or an absorbing cavity, but these solutions are bulky particularly for low frequency applications. Another efficient technique is to use a reflector made of a very good electrical conductor to retrieve the radiation lost in the first solution. This technique is optimal at the middle of the bandwidth where a constructive interference phenomenon is obtained by placing the reflector at a quarter wavelength (at central frequency) from the antenna. But this solution is inherently limited in bandwidth and can rarely exceed an octave. Among artificial materials, High impedance Surfaces (HIS) have remarkable characteristics. While a highly conductive metal imposes a reflection phase of π, HIS do not introduce any phase shift. So it becomes possible to position the antenna closer to the new reflector. Consequently, the antenna is unidirectional and thin. In our work, an analytical model has been proposed to take into account an infinite self-complementary phased antenna array located above a HIS (Fig. 1). The antenna, with or without HIS, can be considered like a stack of dielectric and metallic layers. Here, we show that the transmission line theory allows the calculation of the Return Loss (RL) and the input impedance of the infinite antenna array. Each layer (metallic and dielectric) can be represented by an ABCD matrix [2]. Consequently, the input impedance of this structure can be determined by the relation between the input and output tension and currents. Luukkonen [3] proposed an analytical model to design artificial surfaces facilitating their use in different applications. HIS can be modelled as a parallel connection of grid impedance and surface impedance of the grounded dielectric slab. Finally, the complete model of the antenna above an HIS is made with the antenna model loaded by the HIS model. The several formulations to calculate an HIS will be presented in detail in the final version of the paper.

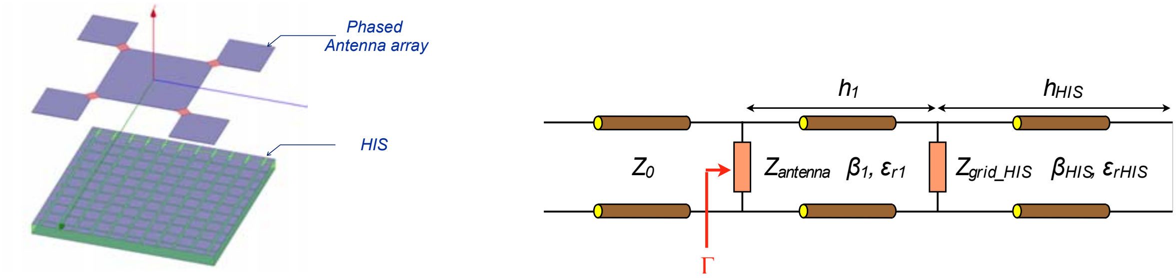

(a) (b)

Fig. 1: Self-complementary antenna above HIS: (a) Unit Cell, (b) Equivalent model

Hence, the infinite complete structure is characterized in receiving mode, i.e. all the generators have been replaced by their equivalent internal resistance. Cavalo et al. [4] have shown that the RL of an infinite phased array antenna can be calculated either in transmit or in receive mode. Fig. 2b shows the verification of the hypothesis: the RL of an infinite connected self-complementary array antenna above a ground plane is plotted in transmit and receive modes and results obtained with HFSS are compared with results obtained with our analytical model. The agreement between the numerical simulations and the analytical model is very good. The final paper will present the return loss for several incidence angles for both several polarizations and radiation patterns of the complete structure.

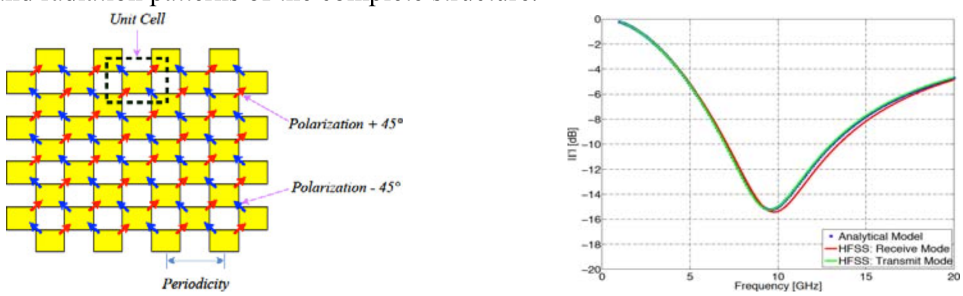

(a) (b)

Fig. 2: (a) Self-complementary connected phased antenna array, (b) Return Loss of the proposed antenna plotted on Fig. 1a above a ground plane placed at λ/4 at 6GHz

REFERENCES

1. Y. Mushiake, “Self-complementary antennas,” *IEEE Antennas Propagation Magazine*, Vol.34, No.6, pp.23-29, 1992.
2. D.M. Pozar, “Microwave Engineering”, 2nd Edition, Wiley, 1998, pp.206-213.
3. O. Luukkonen, C. Simovski, G. Granet, G. Goussetis, D. Lioubtchenko, A.V. Räisänen and S.A. Tretyakov, “Simple and Accurate Analytical Model of Planar Grids and High-Impedance Surfaces Comprising Metal Strips or Patches”, *IEEE Trans. on Antennas and Propagation*, Vol.56, No.6, pp.1624-1632, 2008.
4. D. Cavallo, A. Neto and G. Gerini, "Green's Function Based Equivalent Circuits for Connected Arrays in Transmission and in Reception," *IEEE Trans. on Antennas and Propagation*, Vol.59, No.5, pp.1535-1545, 2011.

Design and measurement of a thin and light absorbing material for space applications

Y. Pinto[1], J. Sarrazin[2], A.C Lepage[1], X. Begaud[1], N. Capet[3]
[1] Institut Mines-Télécom, Télécom ParisTech, France
[2] UPMC Univ. Paris 06, UR2, L2E, Paris, France
[3] Centre National d'Etudes Spatiales, France
[*] *corresponding author:* pintobal@telecom-paristech.fr

Abstract- This paper presents the design, realization and measurement of a thin lightweight absorbing material for space applications. Absorber design is based on High Impedance Surfaces (HIS) loaded with resistors and known as a Resistive High Impedance Surface (RHIS). The behaviour of RHIS is analysed at normal and oblique incidences for TE and TM polarizations. Final design has a reflection coefficient less than-15dB in S-Band [2-2.3GHz] at normal incidence. Simulation results are validated by measurement.

Absorbing material can be used to reduce the reflection of waves on a surface. For space applications, these materials may for example be placed on the satellite in order to reduce interference between antennas. Conventional design methods consist in the insertion of losses on the surface of the material. The Salisbury screen [1] is an example of this approach in which a resistive layer is placed on top of a metal surface at a distance equal to a quarter wavelength. The major drawback of this resonant structure is to operate on a narrow band of frequencies. The Jaumann absorbent [2], consisting of several resistive layers spaced approximately by a quarter wavelength, operates over a wide band. However, this technique greatly increases the thickness of the structure.

In 2002, Engheta proposes to introduce metamaterials in the design of absorbers [3]. This approach represents a technological breakthrough as it allows reducing drastically the thickness. Thus, in [4] the use of a High Impedance Surface (HIS) associated with a resistive material as absorbent is presented. This type of structure, called Resistive High Impedance Surface (RHIS), consists of a FSS (Frequency Selective Surface) over a grounded dielectric slab. The FSS is usually a periodic array of printed patterns loaded with resistors or resistive sheets in order to achieve absorption. Such a material has the advantage of being lightweight and thin.

In this article, RHIS is optimized for good absorption performance ($| S_{11} | < -15$dB in the band [2 - 2.3GHz] 14%) at normal incidence, while fulfilling specific constraints for space applications as a low mass density (<1kg/m²), a thickness less than 50 mm. This structure is also analyzed at oblique incidence for TE and TM polarizations. Figure 1 shows the unit cell of the RHIS structure. It is composed of square copper patches over Rogers RO4003 substrate ($\varepsilon_r = 3.38 + / -0.05$). Below, are a honeycomb layer ($\varepsilon_r = 1.08$) and the ground plane, consisting of a copper film. Interconnecting patches, resistors are formed with TICER resistive film with width $W_{res} = 0.53$mm, resistivity 100Ω/square and thickness t = 0.1µm which provides a resistance of 377 Ω. The structure is simulated and optimized using the CST Microwave Studio ® (frequency solver) [5]. Figure 2 shows the measurement setup and Figure 3 the prototype. Different layers (substrate with patches, honeycomb and copper) are added together using double-sided adhesive film.

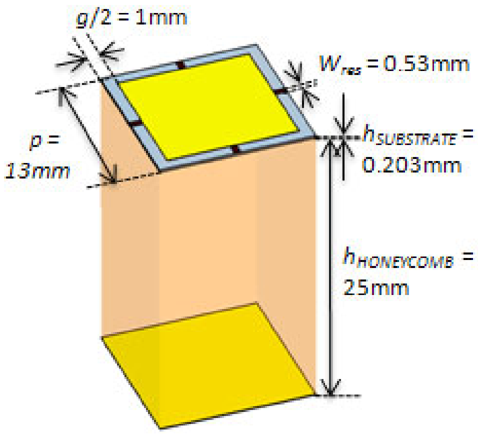

Fig. 1: RHIS unit-cell structure

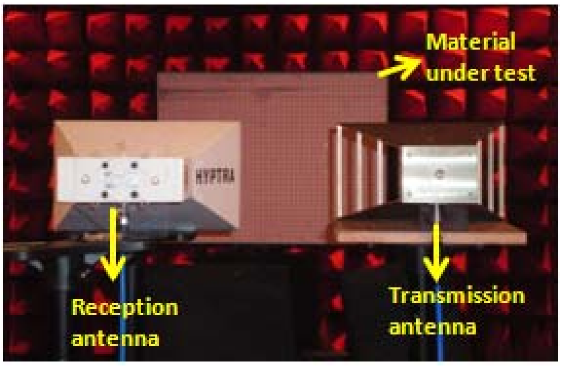

Fig. 2: Measurement setup

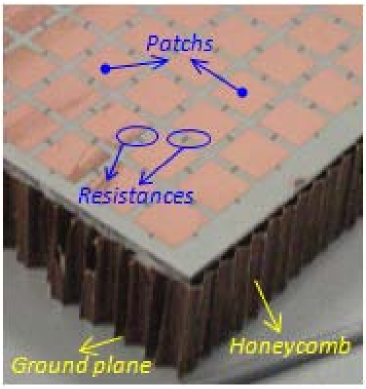

Fig. 3: Material prototype

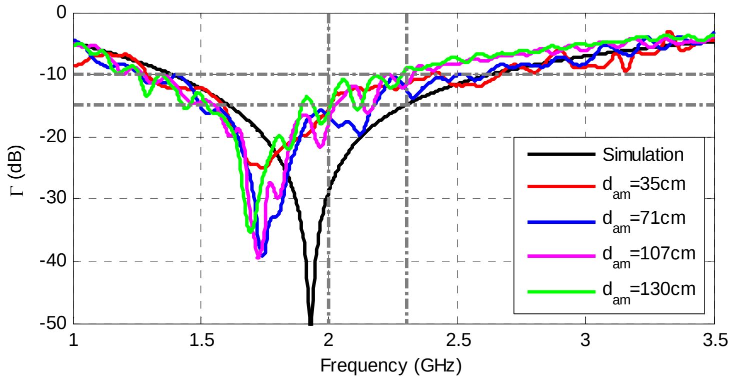

Fig. 4: Measurement results at normal incidence

An example of measurements made at normal incidence is presented on Figure 4. The measurement results for different distances between the antennas and the material (d_{am}) and the simulation result for an infinite RHIS are plotted on Figure 4. There is a good agreement, despite some differences in frequency and level. Shifts in frequency and level can be explained by the imperfections of realisation. In addition, the simulation does not take into account the presence of the glue. The resistance value is not accurate, it has a tolerance of + / - 10%. Finally, the simulated structure is supposed to be infinite and the edges effects and finitude are not analyzed.

In the final paper, all the results will be presented at normal and oblique incidences for TE and TM polarizations.

REFERENCES

[1] W. W. Salisbury, «*Absorbent body for electromagnetic waves*», U.S. Patent 2599944, June 1952.

[2] L. J. Du Toit, «*The Design of Jauman Absorbers*», IEEE Antennas and Propagation Magazine, vol. 36, no. 6, pp. 17-25, Dec. 1994.

[3] N. Engheta, «*Thin absorbing screens using metamaterial surfaces*», IEEE Antennas and Propagation Symposium, vol. 2, pp. 392-395, 2002.

[4] F. Costa, A. Monorchio, and G. Manara, «*Analysis and Design of Ultra Thin Electromagnetic Absorbers Comprising Resistively Loaded High Impedance Surfaces*», IEEE Transactions on Antennas and Propagation, vol. 58, no.5, pp.1551-1558, May 2010.

[5] F. Linot, X. Begaud, M. Soiron, C. Renard and M. Labeyrie, "*Characterization of a loaded high impedance surface*". International Journal of Microwave and Wireless Technologies, 1, pp 483-487, 2009.

Near-field optics and nano-optics

New materials for manufacturing solar cells

Aldabergenov M.K., Iskakova K.A., Kenes K.M.
Kazakh National University after Al-Farabi

Conversion of solar energy into electricity is the most promising and rapidly developing areas of renewable energy. Solar energy is widely available, has almost unlimited resources at its photoelectric conversion does not pollute the environment. For the direct conversion of solar energy into electrical energy using photoelectric effect in solar cells (solar cells), based on the structure of the p-n junction. To date, the maximum efficiency of certain types of semiconductor solar cell is over 30%.

Single solar cells generate limited capacity. To obtain the required energy performance elements are combined in series to each other in the modules and series-parallel fashion in the battery. Power modules and batteries composed of the output power of a single solar cell. Depending on the technology of photovoltaic cells, there are different types of solar cells. The most widely distributed crystalline photovoltaic cells made of mono-and multicrystalline silicon, and thin-film solar cells based on amorphous silicon, cadmium telluride, gallium arsenide, indium phosphide, and some other compounds. At present, the number of crystalline solar cells is about 93%, and thin-film - about 7%. But these technologies and materials are expensive and Rare. And the goal of our work is to obtain materials with a high efficiency and a new modification of the solar cell [1].

At this stage of the study new materials such as oxide (I) copper, cadmium sulfide and copper. These elements have long been known as semiconductors. But perfectly still unknown. There are many works with copper oxide, which were submitted in the period from 2000 to 2008 years [2].

Based on these materials, as well as the addition of new ideas to work on the production of the material. Eat as copper oxide solar cell stems from its chemical properties. It has long been known that copper semiconductor and used since ancient times. But full use in the industry is not yet in sight. It can be explained by the difficulty of obtaining pure. Such a description of the copper oxide does not exist. So getting the copper oxide and its use as a solar cell is not yet fully explored [3].

After receiving a few samples at the research stage, we can offer a few ideas and projects to create solar cells. In this case, increase the use of alternative energy and the production of solar panels. While the project is under study and experimentation. So, insert experiments are necessary aids to help better define the efficiency of solar cells, as well as use common type solar cell receiving-spraying.

The results obtained in the synthesis of copper oxide are ideal ie pure for further study of the topic. We used electrochemical and chemical methods of obtaining materials. Processed materials tested by X-ray analysis.

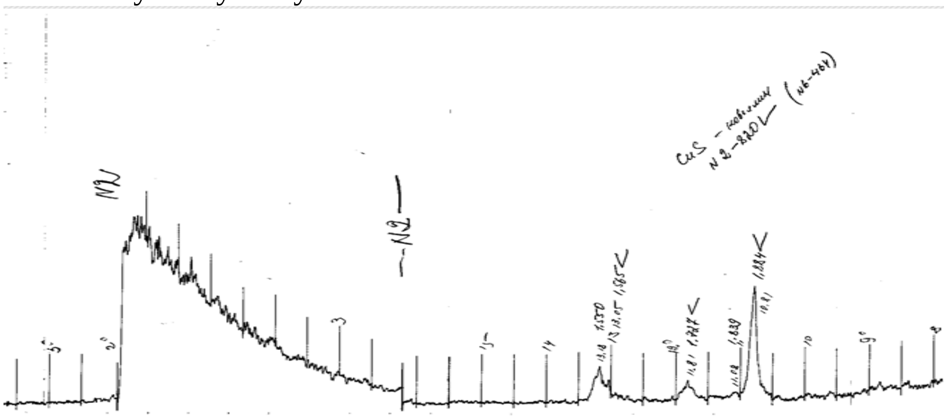

Figure -2 XRD results on samples of cadmium sulfide and copper

Reference:

1 A.S.Basin, A.V.Shishkin // Get the silicon wafers for the solar industry: methods and tehnologii. 2000. Novosibirsk-196 p.

2 F. Caballero-Brionesa, A. Palacios-Padrusa, O. Calzadilla, Fausto Sanzd. Evidence and analysis of parallel growth mechanisms in Cu_2O films prepared by Cu anodization. Electrochimica Acta 55 (2010) 4353-4358

3 N.V. Usoltseva, V.V. Korobochkin. Electrolysis by an alternating current as a method for the synthesis of copper-aluminum oxide system-I-th Russian-Kazakhstan International Conference on Chemistry and Chemical Engineering, p. 205-207

Analytic Explanation of Superresolution with Virtual Image in the Near Field

Y. Kiasat[1, 2*], **B. Luk'yanchuk**[3], **and E. P. Li**[1]
[1] Institute Of High Performance Computing (IHPC), Singapore
[2] National University of Singapore, Singapore
[3] Data Storage Institute, Singapore
[*] g0900296@nus.edu.sg

Abstract - Less than a year ago, by using dielectric microspheres as superlenses [1], a breakthrough in far-field sub-wavelength imaging $(\frac{\lambda}{8}-\frac{\lambda}{14})$ was reported in visible spectrum. However, an analytical insight to explain the image formation and magnification mechanisms was not given. To explain the mechanisms which reveal the maximum achievable resolution by this novel technique for the first time, the exact analytical explanation of near field virtual image formation is presented. Based on this given fundamental solution, the nanosphere's optimum radius and index of refraction for maximum possible magnification are calculated.

The last decade has witnessed numerous efforts to achieve the perfect image by beating the Abbe-Rayleigh diffraction limit. In spite of an impressive progress in this field, surface Plasmon Polariton (SPP) energy loss, sophistications in nanofabrication, specific laser sources, and parameter configuration of SPP excitation are the factors, which hamper the far-field sub-wavelength imaging in the whole visible spectrum [2-4].

Almost a year ago, a breakthrough in far-field sub-wavelength imaging with white light source was reported in nature communication [1]. The idea was based on overcoming the diffraction limit by using the ordinary SiO2 microspheres as superlenses. It created a magnified virtual image of the object in near field. As a result the diffraction limit was greatly overcome, and the resolution of 50 nm $(\frac{\lambda}{8}-\frac{\lambda}{14})$ was reported with a conventional optical microscope. However, to the best of our knowledge, the near field virtual image formation and magnification mechanism which reveal the ultimate achievable sub-wavelength resolution are not discussed so far.

Although it is simple to find the virtual image under approximation of geometrical optics, it is difficult to find the virtual image in the near field. Here we present a complete analytical explanation of near-field virtual image formation for the first time. The phenomenon is explained by the exact solution of Maxwell equation for the given configuration in figure 1. It is shown that only evanescent waves, which carry the high frequency spatial sub-wavelength information, are responsible for the formation of near field image. It is also demonstrated analytically that while the evanescent waves improve the resolution of the real image, the remarkable imaging performance is due to nanoscope's sub-wavelength near field focusing size.

The final achievable resolution is found by solving the Maxwell equations for the scattering problem in figure 1. First the field scattered by nanoscope is calculated by using multipole expansion technique [5]. The incident field is radiated by two arbitrarily located and oriented Hertzian dipoles set apart by distance *d*. It is known that for near field virtual image formation, the geometry optics and prolonging stray rays are not valid anymore and Poynting vector lines should be prolonged instead [1]. Based on the reciprocity principle [6], the total Poynting vector outside the nanosphere is back propagated with an algorithm developed in Mathematica to form the virtual of dipoles at the point of convergence. Consequently, the limit is found when the virtual images of two dipoles begin to overlap. In the last step, the optimum radius r_{opt} and index of refraction n_{opt} for maximum achievable magnification are calculated.

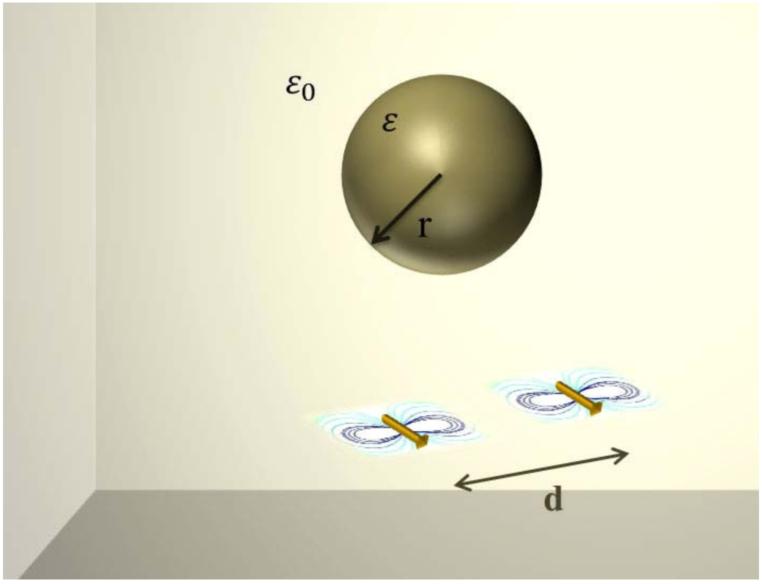

Figure1. The incident field is generated by two Hertzian dipoles spaced by *d*. The dielectric microsphere operates as a superlens to create magnified virtual image of two dipoles.

Acknowledgements: The support of Agency for Science Technology and Research (A*STAR) Singapore, Metamaterial Research Program Grant No. 0821410039 and SERC Program on Superlens, grant no. 092 154 0099; SERC grant no.TSRP-1021520018; and the grant no. JCOAG03-FG04-2009 from the Joint Council of A*STAR are acknowledged.

REFERENCES

1. Wang, Z.B. *et al.,*"Optical virtual imaging at 50 nm lateral resolution with a white-light nanoscope*", Nature Communications **2**, 218* (2011).
2. Smolyaninov *et al*, "Magnifying superlens in the visible frequency range," *Science* **315**, 1699 (2007).
3. Jacob, Z *et al*,"Optical hyperlens: Far-field imaging beyond the diffraction limit", *Optics Express* **14**, 8247 (2006).
4. Fang, N *et al*, "Sub-diffraction-limited optical imaging with a silver superlens", *Science* **308**, 534 (2005).
5. Jackson, J. D., "*Classical Electrodynamics*", (Wiley, 3 Edition, 1998).
6. Potton, R. J., "Reciprocity in optics", *Rep. Prog. Phys.* **67,** 717, 2004.

Analytical and numerical modelling of complex materials and structure

Theory and Simulation of Cavity Quantum Electro-Dynamics in Multi-partite Quantum Complex Systems

M. A. Shahraki[1], **and S. Khorasani**[1*]
[1]School of Electrical Engineering, Sharif University of Technology, P. O. Box 11365-9363, Tehran, Iran
[*]corresponding author: khorasani@sina.sharif.edu

Abstract- Cavity quantum electrodynamics of complex systems, consisting of arbitrary number of emitters and modes is analyzed. We solve the system in Schrödinger space and for the first time, observe a chaotic behavior in ultrastrong regime.

In this article, the general behavior in cavity quantum electrodynamics of complex systems is analyzed. Such quantum optic multi-partite systems normally consist of an arbitrary number of quantum dots in interaction with an arbitrary number of cavity modes. Initially, the coefficients matrix of the system is computed and numerically measured. For this purpose, the general time-dependent state of the most general possible system has been rigorously specified and solved in Schrödinger space. For the first time, we have observed that plotting the system trajectory in the phase space reveals a chaotic behavior in the so-called ultrastrong coupling regime. Results are presented and discussed for the behavior of a real quantum optic system (Fig. 1) and a multi-partite system consisting of six quantum dots in interaction with one cavity mode (Fig. 2).

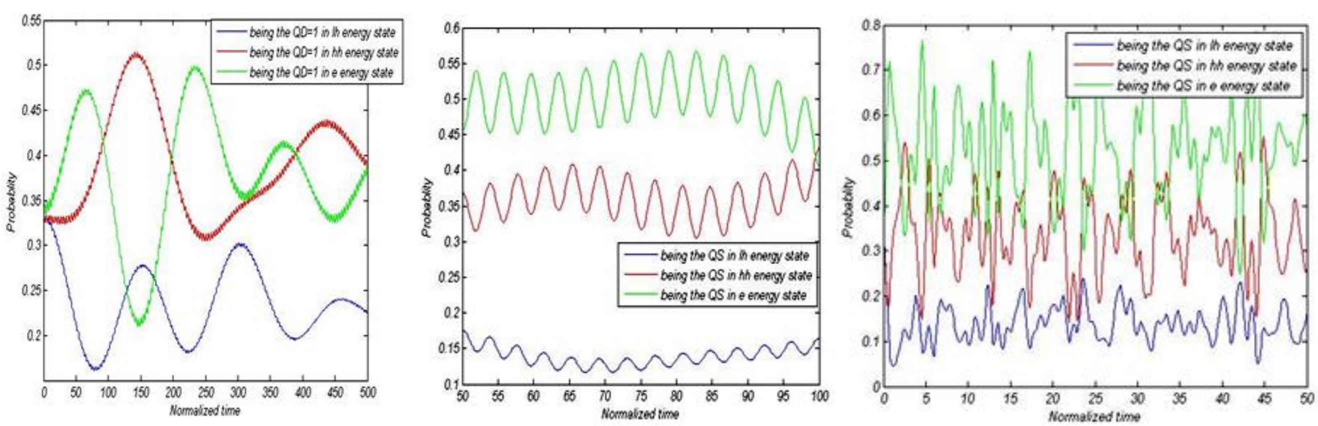

Figure 1. Probablities of occupation of the heavy-hole (hh), light-hole (lh), and conduction (e) states in a AlGaAs quantum well. From left to right: weakly, strongly, and ultrastrongly coupled systems.

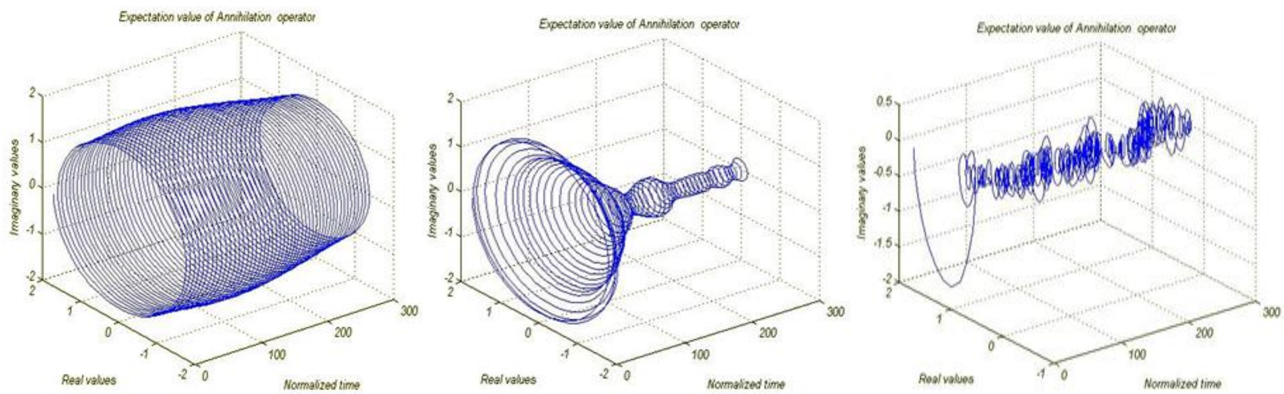

Figure 2. Three-dimensional plot of the real and imaginary values of the expectation of the field annihilation operator in a multi-partite complex quantum optical system with seven sub-systems, comprising of six double-state quantum dots and one radiation field with a maximum occupancy of eight photons. From left to right: weakly, strongly, and ultrastrongly coupled systems.

The quantum optical [1] theoretical foundation of this work has been based on an extension of the JCM model [2,3]. For this purpose, a special notation and formulation has been invented by our group [4], in conjunction with a major correction to the JCM model [5-7] which accounts for a less known mathematical error in the context. We successfully identify this error [5-7] and show that it could be avoided by solving the system directly in the Schrödinger's, rather than the Heisenberg's interaction picture [8,9]. To the best of our knowledge, this work presents the first complete and most accurate simulation of quantum multi-partite systems.

Acknowledgements: This work has been supported in part by Iranian National Science Foundation.

REFERENCES

1. Schleich, W. P., *Quantum Optics in Phase Space*, Wiley-VCH, Berlin, 2001.
2. Jaynes, E. T., and F.W. Cummings, "Comparison of quantum and semiclassical radiation theories with application to the beam maser," *Proc. IEEE*, Vol. 51, No. 1, pp. 89-109, Jan. 1963.
3. Paul, H., "Induzierte Emission bei starker Einstrahlung," *Ann. Phys.*, Vol. 466, pp. 411-412, 1963.
4. Sadeghi, A. H., A. Naqavi, and S. Khorasani, "Interaction of Quantum Dot Molecules with Multi-mode Radiation Fields," *Scientia Iranica*, Vol. 17, pp. 59-70, 2010.
5. Ahmadi, E., H. R. Chalabi, A. Arab, and S. Khorasani, "Cavity Quantum Electrodynamics in the Ultrastrong Coupling Regime," *Scientia Iranica*, Vol. 18F, No. 3, pp. 820-826, 2011.
6. Ahmadi, E., H. R. Chalabi, A. Arab, and S. Khorasani, "Revisiting the Jaynes-Cummings-Paul model in the limit of ultrastrong coupling," *Proc. SPIE* , Vol. 7946, 79461W, 2011.
7. Arab, A., and S. Khorasani, "Fully automated code for exact and efficient analysis of quantum optical systems in the regime of ultrastrong coupling," *Proc. SPIE*, Vol. 8268, 82681M, 2012
8. Alidoosty, M. "Behavior Patterns Analysis of Cavity Quantum Electro-Dynamics in Complex Systems for Different Coupling Regimes," MSc thesis, School of Electrical Engineering, Sharif University of Technology, Tehran, Iran, 2012.
9. Karimi, F. "Analysis of Ultra-Strong Coupling in Optical Waveguides," MSc thesis, School of Electrical Engineering, Sharif University of Technology, Tehran, Iran, 2012.

Angular dependence of the optical response of a magnetic anisotropic material: analytical/numerical analysis

M. Warenghem[1*]**, J.F. Blach**[1]**, S. Nemer**[1]**, J. F. Henninot**[1]
Unité de Catalyse et de Chimie du Solide (UCCS Artois), UMR CNRS 8181
Université d'Artois, Faculté des sciences; Lens cedex; France
[*]corresponding author: marc.warenghem@univ-artois.fr

Abstract- We propose a 3 steps method to analyze the role of anisotropy (dielectric and magnetic). The two first consists in finding analytical expressions for propagation elements and their link with measurable quantities. The third step consists in comparing those results, which involve constitutive relationships, to results which do not involve any effective optical parameters. In this communication, we focus on the first two steps to lay the foundation for this approach.

The response of the so-called metamaterials to an optical excitation quite often exhibits a complex dependence on the angle of incidence and polarization of the input beam. As the origin of that dependence is not clearly established, the behavior of any device using such materials will be difficult to predict and obviously this is a drawback for applications. There are potentially several possible origins for that dependence: anisotropy, periodicity or more sophisticated coupling between basic pattern of the lattice, if any. Anisotropy concerns the pattern itself and periodicity accounts for repetition of this pattern. Since most of the structures developed up to now are geometrically asymmetric, they should be anisotropic. Moreover, the metamaterials are also supposed to present some magnetic properties which are most likely anisotropic as well. Prior to account for periodicity, which is usually treated using Bloch modes approach as in photonic crystals, or Fourier transform approach, it is preferable to check first to which extend the anisotropy (dielectric and magnetic) plays a role in the observed angular dependence. To analyze that aspect, we propose a method, which consists in three steps. The two first consists in finding analytical expressions for propagation elements and their link with measurable quantities. The third step consists in comparing those results, which involve constitutive relationships, to results which do not involve any effective optical parameters. They can be either experimental measurements or results obtained using numerical simulation such as finite elements. In this communication, we focus on the first two steps to lay the foundation for this approach.

First, using Berreman method, we find analytical expressions for the different elements of propagation (index and angle of refraction, Poynting's vector, reflection and transmission coefficients of a slab etc...) for a material dielectrically and magnetically anisotropic, satisfying the constitutive relationship (1), assuming that both tensors are diagonal in the same frame, named R_{dia}. The analytical calculation is possible as the material is aligned in such a way that the material frame (R_{dia}) coincides with the frame (R_{lab}) in which the input beam lies in the oyz plane, as shown on the figure 1.

$$\vec{D} = \vec{\vec{\varepsilon}}.\vec{E} \qquad \vec{B} = \vec{\vec{\mu}}.\vec{H} \qquad 1$$

Apart the propagation elements, which, at our best knowledge, have not been expressed for such materials, it is shown that, in case of magnetic anisotropy, both TE and TM modes have indices that depend on angle of incidence, contrarily to usual dielectric anisotropic material for which only the TM mode is angle dependent.

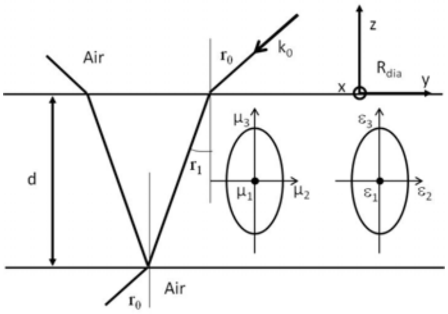

Figure 1. Geometry and frame. Both tensors **ε** and **μ** are diagonal in the R_{dia} frame. The incident wave vector lies in the oyz plane of that frame

Second, we show that it is possible to get the 6 diagonal elements of dielectric and magnetic tensors from reflection and transmission measurements in extending to anisotropic material and slanting incidence the retrieving procedures [1, 2, 3, 4]. Most of the usual methods that are all deriving the optical parameters from the reflexion and transmission coefficients do not use the anisotropic expressions for those coefficients, which we do herein.

Third, and this will be detailed in a forthcoming paper, we develop the "numerical" sample concept, which allows checking whether or not a sample follows up the tensorial effective medium concept.

Acknowledgements,

This work is/has been carried out within the NANODIELLIPSO project n°ANR-09-NANO-003 funded by the French National Agency (ANR) in the frame of its 2009 programme in Nanosciences, Nanotechnologies and Nanosystems (P3N2009).

REFERENCES

1. Abeles, F. "Physics of Thin Films" Vol. 6 (eds Francombe, M. H. & Hoffman, R. W.) Ch. V–-VII (Academic, New York, 1971).
2. Nicolson A.M. and G.F. Ross, "Measurement of the intrinsic properties of materials by time-domain techniques", IEEE Trans. Instrum. Meas., vol. 19, pp. 377382, 1970
3. Smith D.R., Shultz S., Markos P. and C. M. Soukoulis, "Determination of effective permittivity and permeability of metamaterials from reflection and transmission coefficients", Phys. Rev. B, vol. 65, 195104, 2002
4. Menzel C., Rockstuhl C., Paul T., Lederer F. and T. Pertsch, "Retrieving effective parameters for metamaterials at oblique incidence", Phys. Rev. B 77, 195328, 2008

Effective Bilayer Slab Retrieval for Asymmetric Scattering Response

Muhammad Amin and Hakan Bağcı
Division of Computer, Electrical, and Mathematical sciences and Engineering,
4700 King Abdullah University of Science and Technology
Thuwal 23955-6900, Saudi Arabia.
*corresponding author: muhammad.amin@kaust.edu.sa

Abstract- A method to retrieve effective medium properties from the scattering parameters of a metamaterial unit cell with asymmetry along the direction of propagation is proposed. The method searches for a slab consisting of two layers with different wave impedances, z_1 and z_2, and the same refractive index, n. Since the condition $z_1 \neq z_2$ is now allowed, the (possible) asymmetry in the response of the metamaterial can be accounted for by the effective two-layer slab. The method is applicable to arbitrary shaped unit cells consisting of a single or cascaded multiple scattering elements; this is demonstrated via application of the proposed method to several examples.

The unusual dispersion characteristics of metamaterials are typically achieved using carefully designed, intricate, and complicated geometries. Atypical response of the metamaterial structure to electromagnetic excitation is the combined response of periodically located individual unit cells involving these geometries. Numerical or theoretical analysis of such geometrically complicated metamaterial structures can be significantly simplified if one can come up with an effective medium that would have the same response as the layer(s) of the periodically located unit cells. Most of the time, this effective medium is a slab with an equivalent refractive index, which generates the same scattering parameters as the metamaterial.

Numerous techniques have been developed to retrieve the effective medium properties, i.e., refractive index n and wave impedance z, of this equivalent slab [1-3] from measured or computed scattering parameters, S_{11}, S_{12}, S_{21}, and S_{22}, of the metamaterial strucure. Since the response of a slab is always symmetric along the propagation direction of normally incident electromagnetic excitation, these retrieval methods cannot be used when the metamaterial's scattering parameters satisfy the condition, $S_{11} \neq S_{22}$. This happens when the unit cell has geometrical asymmetry along the direction of propagation. Retrieval methods that search for bianisotropic constitutive material properties have often been used to alleviate this problem [4]. However, for problems, where the asymmetry in the response is not necessarily due to the bianisotropy of the field interactions in the unit cell, these retrieval methods unnecessarily complicate the inverse problem of finding the effective medium parameters.

The retrieval method proposed in this work searches for a slab consisting of two layers with different wave impedances, z_1 and z_2, and the same refractive index, n. Since condition $z_1 \neq z_2$ is now allowed, the asymmetry in the scattering response of the metamaterial can be accounted for by the equivalent two-layer slab. The proposed method is used for determining the effective medium parameters of cascaded multiple heterogeneous scattering elements and single scattering element with asymmetry in propagation direction.

REFERENCES

1. Smith, D. R., Vier, D. C., Koschny, T., and Soukoulis, C. M. "Electromagnetic parameter retrieval from inhomogeneous metamaterials," *Phys. Rev. E*, vol. 71, no. 3, 036617, 2005.
2. Smith, D. R., Schultz, S., Markoš, P., and Soukoulis, C. M, "Determination of effective permittivity and permeability of metamaterials from reflection and transmission coefficients," *Phys. Rev. B*, vol. 65, no.19, 195104, 2002.
3. Chen, X., Grzegorczyk, T. M., Wu, B. I., Pacheco Jr, J., and Kong, J. A., "Robust method to retrieve the constitutive effective parameters of metamaterials," *Phys. Rev. E*, vol. 70, no. 1, 016608, 2004.
4. Li, Z., Aydin, K., and Ozbay, E. "Determination of the effective constitutive parameters of bianisotropic metamaterials from reflection and transmission coefficients," *Phys. Rev. E*, vol. 79, no. 2, 026610, 2009.

The investigation of the photonic waveguide structure made of silicon carbide by means of the method of the Singular Integral Equations

T. Gric[1, 2*], **L. Nickelson**[1, 2]
[1]Center for Physical Sciences and Technology, Semiconductor Physics Institute, Vilnius, Lithuania
[2]Vilnius Gediminas Technical University, Vilnius, Lithuania
[*]corresponding author: tatjana.gric@gmail.com

Abstract- Here we present the investigation of the photonic waveguide structure by means of the method of the Singular Integral Equations. We discovered peculiarities of the dispersion characteristics.

The semiconductor photonic waveguide devices have been constructed in [1]. The article [2] reports on the numerical analysis of the reflectivity of electromagnetic waves for several one-dimensional photonic crystal structures. A waveguide consisting of one-dimensional photonic crystal is shown to be promising for optical interconnection on a semiconductor wafer. The fabrication of optical directional couplers with the waveguides and their fundamental characteristics are demonstrated in [3]. The photonic waveguide structures have the wide area of applications. Our contribution is the investigation of the photonic waveguide structures made of silicon carbide (SiC). SiC waveguides operating at the microwave range are presently being developed for advantageous use in high-temperature, high-power, and high-radiation conditions. SiC however, has superior properties for power devices, compared to silicon. A change of technology from silicon to silicon carbide will revolutionize the power electronics. We have investigated the photonic waveguide structure made of SiC (Fig. 1) by means of the method of the Singular Integral Equations (SIE).

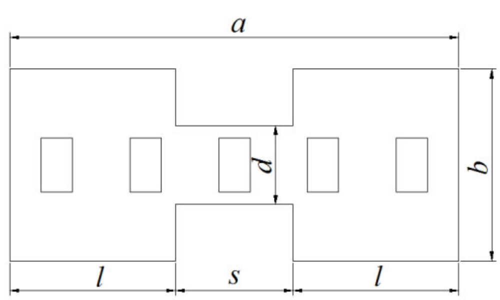

Fig. 1 The photonic waveguide structure

Firstly we have calculated the waveguide structures without air holes. In this case the $a = b = 7$ mm, $s = d = 1$ mm, $l = 3$mm. We have calculated the complex dispersion characteristics (Fig. 2). We have calculated the dispersion characteristics at three different temperatures T. Here we present characteristics of the main modes only. The dispersion curves of the main mode at T=1500ºC are denoted by the red colour. The permittivity of the SiC is 8-2j in this case [4] at the cutoff frequency of the main mode. The dispersion curves at T=1000ºC and

20ºC are denoted by the blue and green lines correspondingly. The permittivity of the SiC is 7-j and is 6-0.5j in these cases. We discovered special dependencies of structure losses (Fig. 1) upon the sizes and location of slots.

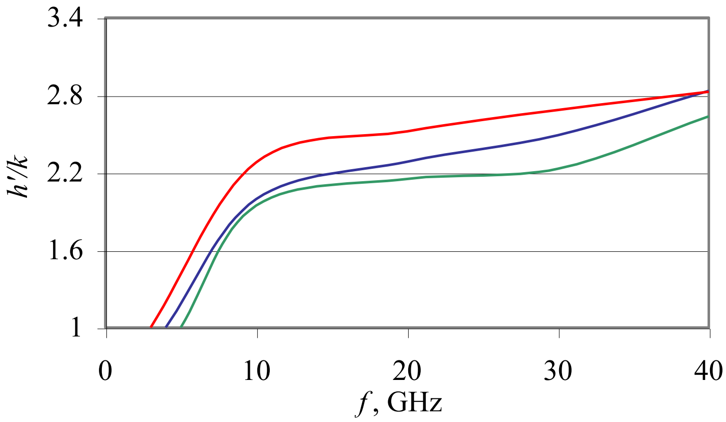

(a)

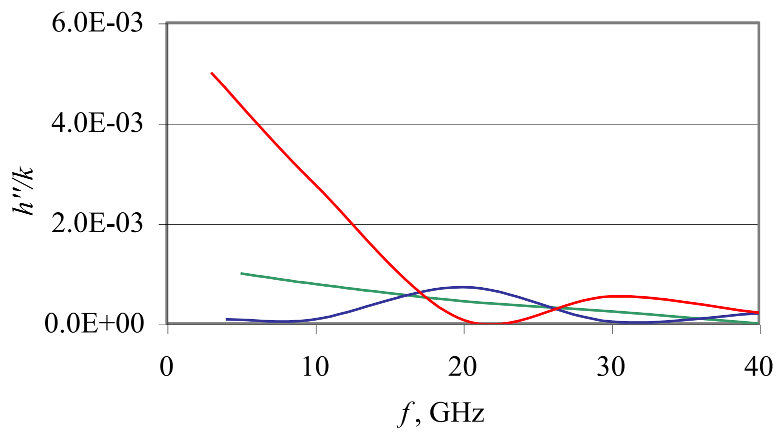

(b)

Fig. 2 The complex dispersion characteristics of the waveguide structure without air holes: (a) – the dependence of the normalized real part of the complex propagation constant upon the frequency, (b) - the dependence of the imaginary part of the complex propagation constant (the losses) upon the frequency

REFERENCES

1. Oku, S., and Y. Shibata, "Semiconductor photonic waveguide structures made by a reactive beam etching technique," in *Proceedings of Indium Phosphide and Related Materials International Conference*, Nara, Japan, May 2001, 75–78.
2. Taniyama, H. "Waveguide structures using one-dimensional photonic crystal," *J. Appl. Phys.,* Vol. 91, No. 6, 3511-3515, 2002.
3. Yamada, H., T. Chu, S. Ishida and Y. Arakawa, "*Si* photonic wire waveguide devices," *IEEE J. Sel. Top. Quant.,* Vol. 12, No. 6, 1371–1379, 2006.
4. Baeraky, T. A. "Microwave measurements of the dielectric properties of silicon carbide at high temperature," *Egypt. J. Sol.*, Vol. 25, No. 2, 263–273, 2002.

Electrodynamical analysis of metamaterial waveguides coated with silicon carbides

L. Nickelson[1, 2*]**, A. Bubnelis**[1, 2], **S. Asmontas**[1]
[1] State Research Institute Center for Physical Sciences and Technology, Lithuania
[2] Vilnius Gediminas Technical University, Lithuania
[*]corresponding author: lucynickelson@gmail.com

Abstract-Here we present our calculation results of dispersion characteristics and electromagnetic (EM) field distributions of open two-layered cylindrical waveguides. Waveguides are made of metamaterial (UCSD30815) core [1] which coated with a silicon carbide (SiC) layer [2]. We analyzed electrodynamical characteristics at several metamaterial core radii 0.1, 0.5, 0.7, 1.0, 1.5, 2.0, 3.0 mm. We discovered the very important feature that can be only one propagating mode in the range from 11 to 16 GHz. The particularity of the dispersion characteristics at certain metamaterial core radii can be used for creation of microwave filters.

We investigated open two-layer cylindrical metamaterial-SiC waveguides in frequency range 11–16 GHz. As it known SiC has privileges because it can operate at high-temperature, high-power, high-radiation conditions and SiC does not feel the impact of any acids or molten salts up to 800°C. Outer radius of waveguides are constant and equal to $R = 5$ mm. The radius of metamaterial core is changing. The real part of complex propagation constant *h=h'-ih"* dependencies on the frequency at two metamaterial core radii are shown in Fig. 1 a, b. We see that dispersion curves are unusual intricate shapes. We are going to present also the imaginary part of propagation constant (losses) of metamaterial waveguide because waveguide materials are characterized by the complex permittivity and permeability [1], [2]. Our computer program, that is written in Matlab language, let us take into account high value losses of materials.

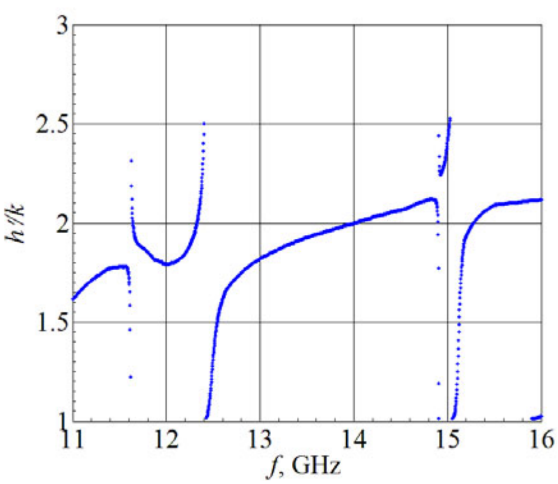

(a)

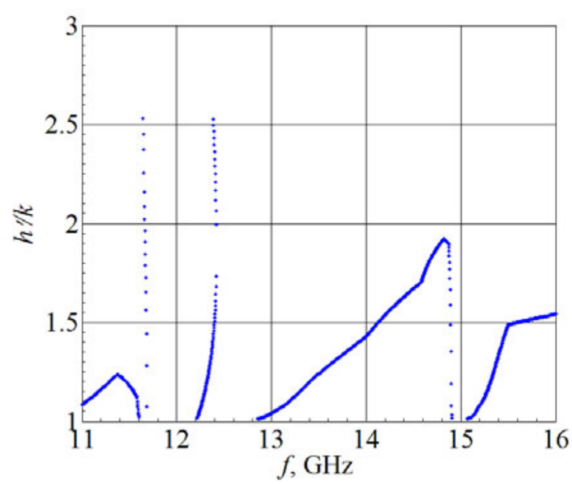

(b)

Fig 1 Normalized phase constant frequency dependences of metamaterial-SiC waveguide when metamaterial core radius is $r = 0.5$ mm (a) and $r = 2$ mm (b)

Electric and magnetic fields distributions of the main hybrid mode when the metamaterial core radius is 2 mm and the thickness of SiC layer is 3 mm are presented in Figs 2 and 3.

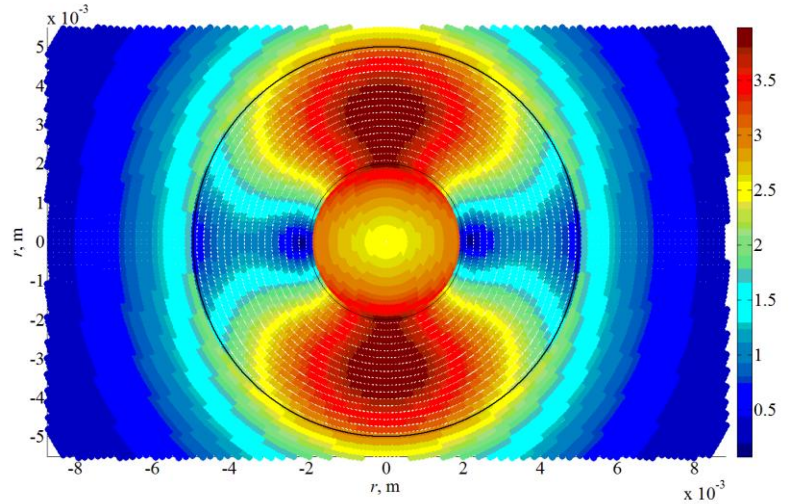

Fig. 2 Electric field distribution at frequency $f = 14.5243$ GHz, when metamaterial core radius is 2 mm

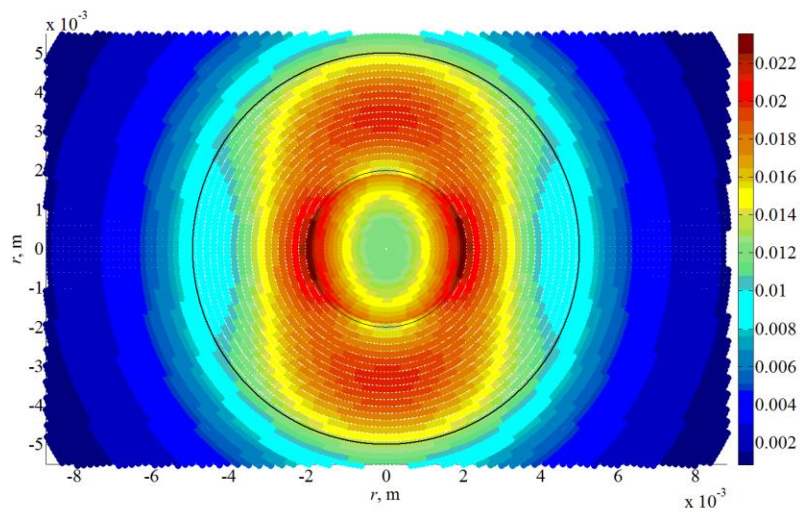

Fig. 3 Magnetic field distribution at frequency $f = 14.5243$ GHz, when metamaterial core radius is 2 mm

We see that the strongest concentration of the electric and magnetic fields are in the area of the metamaterial core surface but it is in the different places of the core perimeter. The maximum magnitudes of electric and magnetic fields are in the SiC layer area which is resistant to temperatures.

REFERENCES

1. Smith D. R. and et al. “Design and Measurement of Anisotropic Metamaterials that Exhibit Negative Refraction,” *IEICE Trans. Electron.* Vol. E87-C, No. 3, 359–370, 2004.
2. Baeraky, T. A. “Microwave measurements of the dielectric properties of silicon carbide at high temperature,” *Egypt. J. Sol.,* Vol. 25, No. 2, 263–273, 2002.

Microwave scattering diagrams of three-layered SiC-metamaterial/ gyrotropic ferrite-SiC cylinders

J. Bucinskas[1], **L. Nickelson**[2, 3]

[1]Physics Department, Vilnius University, Vilnius, Lithuania
[2]Center for Physical Sciences and Technology, Semiconductor Physics Institute, Vilnius, Lithuania
[3]Vilnius Gediminas Technical University, Vilnius, Lithuania
*corresponding author: lucynickelson@gmail.com

Abstract - We present the rigorous solution of boundary diffraction problem about the microwave scattering by a multilayered cylinder. The material permittivity or/and permeability of any layer may be made of isotropic or uniaxial anisotropic or gyrotropic materials. The number and thickness of layers is not limited in our solution. Using the obtained solution we calculated scattering diagrams (a radial component of real part of the Poynting vector) inside and outside of cylinder. Here we present scattering diagrams from three- layered cylinder made of SiC and metamaterial UCSD30815 or saturate magnetized ferrite ISCh4. Diagrams were computed for angles between cylinder axis and incidence wave direction θ=π/2, π/3, π/6 inside of metamaterial/ferrite layer at the distance 1 mm and outside of cylinder at the distance 2.5 mm from the cylinder axis.

Here we present the scattering microwave power diagrams of three-layered cylinder (Figs 1-3). The core of cylinder has radius 0.5 mm, the middle layer radius is 1.5 mm and the external cylinder radius is 2.0 mm. Numerical calculations were made for the incident plane harmonic monochromatic microwave with the operating frequency f =12 GHz.

The core of cylinder and it external layer are made of SiC material. This material is useful because it can operate at high-temperature, high-power, high-radiation conditions. The SiC permittivity ε_1=6.5-i0.0005 and the permeability μ_1=1 were taken from [1]. The middle layer can be made from a metamaterial or a gyrotropic ferrite. The metamaterial permittivity ε_2= -4.95- i0.2 and the permeability μ_2= -2.5+ i0.25 were taken from [2].

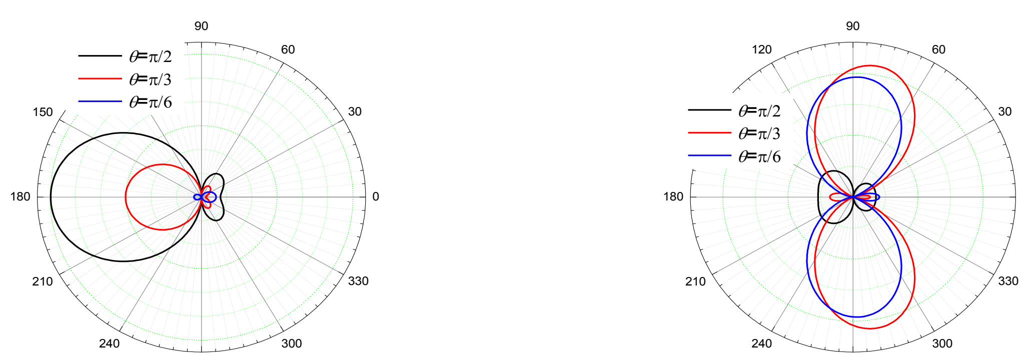

(a) (b)

Fig. 1 Scattering diagrams of SiC-metamaterial-SiC layered cylinder at the distance from the axis of cylinder equal to 1mm for parallel (a) and perpendicular (b) polarizations.

When the middle layer of cylinder is the gyrotropic ferrite then the permeability tensor components after the diagonalization of the tensor are expressed as $\mu_{jj} = <\mu_{+1}, \mu_{-1}, \mu_p>$, where μ_{+1} =6.757-i0.00301 and μ_{-1} =3.814-i0.00072, μ_p =1 and ε_{fer}=13.5-i0.0005. The variation of the scattering power of microwave at different points on cylindrical surfaces of radius *r* is shown in Figs 1-3. Here are given the scattering power distributions at angles: θ=π/2 (denoted by the black line), θ=π/3 (red), θ=π/6 (blue).

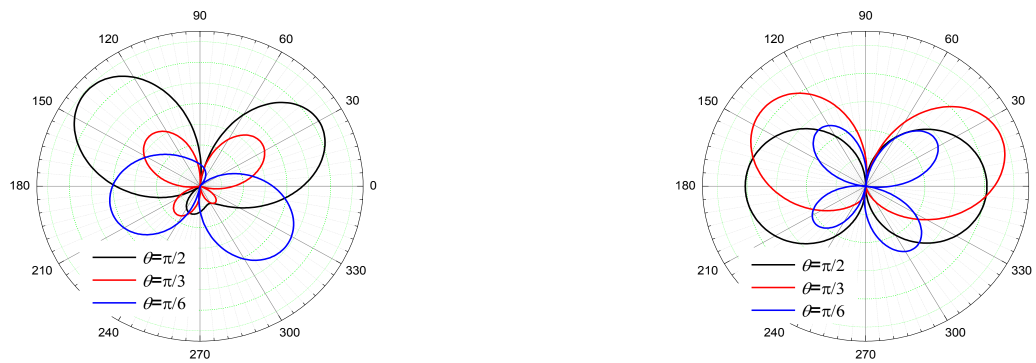

(a) (b)

Fig. 2 Scattering diagram of SiC- gyrotropic ferrite -SiC layered cylinder at the distance from the cylinder axis equal to 1mm for parallel (a) and perpendicular (b) polarizations.

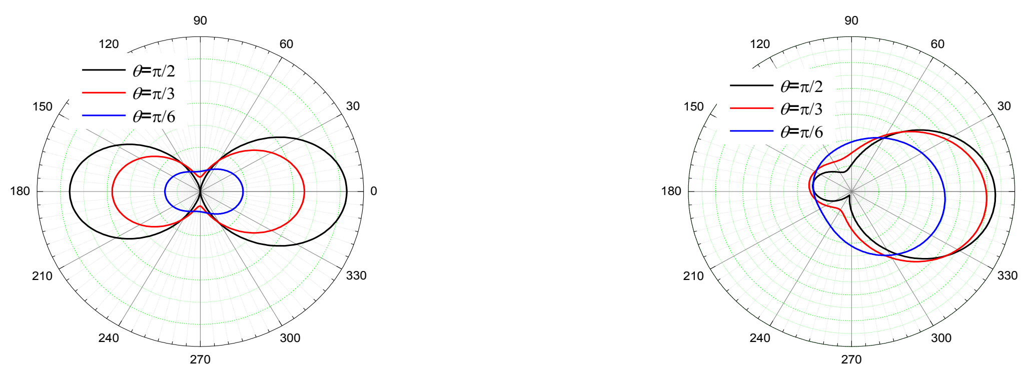

(a) (b)

Fig. 3 Scattering diagrams of layered cylinder at the distance from the cylinder axis equal to 2.5 mm for parallel polarizations when cylinder made of SiC- metamaterial -SiC (a) and SiC- gyrotropic ferrite –SiC (b).

The comparison of scattering diagrams of cylinders with the different middle layers (the metamaterial or the gyrotropic ferrite) shows that exist strong dependencies of the scattering characteristics on the middle layer electrical parameters and the incident microwave polarization. On the base structures like the considered cylinders can be created controllable by magnetic field antenna reflectors that can re-direct a radiation.

REFERENCES

1. Smith D. R. and et al. "Design and Measurement of Anisotropic Metamaterials that Exhibit Negative Refraction," *IEICE Trans. Electron.* Vol. E87-C, No. 3, 359–370, 2004.
2. Baeraky, T. A. "Microwave measurements of the dielectric properties of silicon carbide at high temperature," *Egypt. J. Sol.,* Vol. 25, No. 2, 263–273, 2002.

The wave functions of the energy bands of the crystal lattice

Iskakova K.A., Ahmaltdinov R.F., Amanova A.E.
Kazakh National Pedagogical University after Abai

According to the Pauli principle and the theory of closed shells it follows that have equilibrium atom electron configuration. During the formation of of the crystal, being collectivized, the electron, leaving the atomic orbitals forms a defect in the electronic configuration, which leads to an increase in the width of the empty valence band [1-4]. In the crystal, when approaching of the ions to each other their impenetrability violated quantum mechanical effects. On an unfilled configuration electron shell of copper in a state 4s has one valence electron.

Let us assume that in the equilibrium state of the crystal for each intercore gap has one electron. Part of the intercore element, the surrounding ions are identical and have the same form in the shape of a cone with a concave base. Electron shell contains copper twenty-nine electrons. Every two electrons with opposite spins have their own shell. The transition of an electrically charged object through this barrier is impossible. This property explains the preservation of the structure of a solid. But, due to the quantum mechanical effects transition of the probe electron through the electron shells occurs. In the even-numbered states (in the 2nd and 4th) are clearly visible envelopes plane wave.

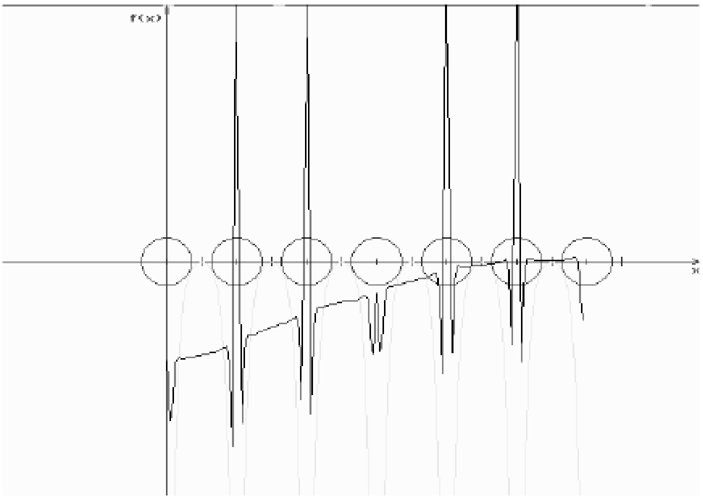

Figure 1 shows the wave function for a copper crystal state n = 2.

In these states, the geometry of the crystal (fcc lattice) increases the total contribution of all the cores and intercores into the amplitude of envelope of the wave (core-intercore-lattice acts as a resonator of amplitudes).

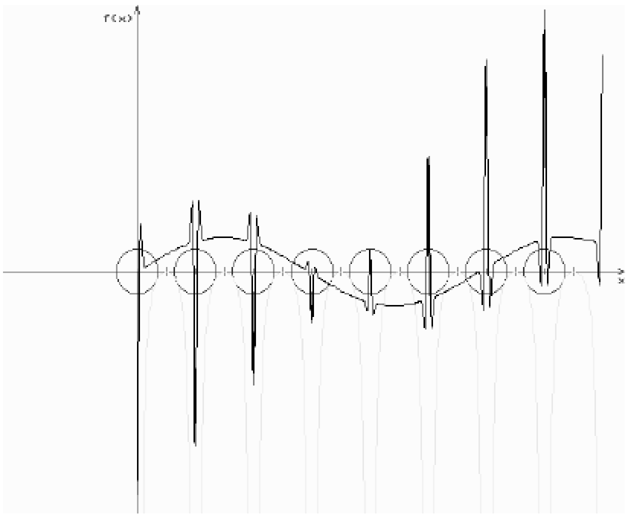

Figure 2 shows the wave function for a copper crystal state n = 4.

Imaginary and real parts are obtained periodical. Imaginary and real parts of the calculated wave function without the use of assumptions about its frequency are obtained periodical with a period equal to the lattice constant. The amplitudes of the wave functions with increasing values of energy in energy bands increase in the crystal lattice.

Reference:

1. J. Slater wave functions in a periodic potential field // Phys. Rev., 1937, V. 51, P. 846.
2. Berman R. Thermal conductivity of solids, Moscow, Moscow, 1979.
3. AN Kushnirenko Introduction to Quantum Field Theory, Moscow High School, 1983.
4. Born, M., Huang Kun. Dynamical Theory of Crystal Lattices, Clarendon Press, Oxford, 1958. 488.

Analytical modeling of wave-guiding in semiconductor nano-lasers

Z.A.Sattar[1*], and K.A.Shore[1]
[1] Bangor University, School of Electronic Engineering, Bangor, LL57 1UT, Wales, UK
[*]corresponding author: z.a.sattar@bangor.co.uk

Abstract-Analytical modeling of cylindrical semiconductor nano-lasers has been undertaken accommodating local gain variations in the active region of the device. Specifically modal gain calculations have been performed using the cylindrical transfer matrix method (cTMM). For representative gold-clad $In_{0.2}Ga_{0.8}As$ structures it is shown that for lower order TE and TM mode, modal gains of order 1500 cm^{-1} and 130 cm^{-1} can be achieved thereby providing the opportunity to support lasing with appropriately chosen device lengths.

Summary

The design process for advanced laser structures [1-3] is reliant on accurate modeling of the physical processes underpinning the operational characteristics of candidate semiconductor nano-laser designs. Crucial issues in this regard are the identification of structures which enable effective light confinement and thereby enable gain in nano-scale cavities. In general the modeling of such aspects requires the adoption of numerical techniques in order to provide accurate predictions of the behaviour of proposed nano-lasers. In that context, a numerical model that emulates a cylindrical metal-clad nano-laser using TMM (transfer matrix method) [4-5] has been used for this work to evaluate the modal gain for TE_{01} and TM_{01} mode of metal-clad nano-lasers by incorporating annular core geometry. The model which has been developed for this work allows for the definition of an arbitrary number of layers in the active core semiconductor region.

The structure under consideration is a cylindrical annular core metal-clad nano-laser. In previous work such a structure has been studied assuming a uniform core [1-2]. The structure comprises of an inner core and *N* outer core regions to take into account spatial variations in gain in the active region. The cross-section of such a structure is illustrated in Fig. 1, where the core semiconductor material is assumed to be $In_{0.2}Ga_{0.8}As$ with a refractive index of *3.6* with an overall core radius $r_N = 200nm$ and $100nm$ for TE and TM mode respectively at λ = 1μm. The overall core radius r_N, was kept constant by keeping the inner core radius r_1 at a constant value with variation in the thickness of the outer core layers. The metal cladding is taken to be gold with a refractive index n_{metal} of *0.22– j6.71* and the thickness t_m of metal-clad is assumed to be *20nm*. For the analysis of the structure, the transverse field component for the TM and TE mode is expressed in terms of E_z *and* H_z respectively,

$$E_{zi} = [U_i J_o(\gamma_i r_i) + V_i Y_o(\gamma_i r_i)] \tag{1}$$

$$H_{zi} = [W_i J_o(\gamma_i r_i) + Q_i Y_o(\gamma_i r_i)] \tag{2}$$

Where J_o and Y_o are the zero order Bessel functions of the first and second kind respectively. U_i, V_i, W_i, Q_i are constants, *i = 1, 2, 3…..N, N+1, N+2* representing the regions in the structure and γ_i is represented in the form of material and modal gain and is defined by;

$$\gamma_i = \gamma_o \sqrt{\left(Re(n_i) \pm j\frac{g_i}{2\gamma_o}\right)^2 - \left(Re(n_{eff}) \pm j\frac{G}{2\gamma_o}\right)^2} \tag{3}$$

Where, $\boldsymbol{\gamma_i}$ is the propagation constants of each layer and $\boldsymbol{\gamma_o}$ is free space propagation constant, $\boldsymbol{n_i}$ is the refractive index of each layer, $\boldsymbol{G}$ is the modal gain/loss, $\boldsymbol{n_{eff}}$ is the effective refractive index of the mode, and $\boldsymbol{g_i}$ is the material gain for the semiconductor core and loss for the metal. The variations in the material gain $\boldsymbol{g_i}$ of the active core is such that;

$$g_{inner\ core} > g_{outer\ core\ 1} > g_{outer\ core\ 2} \cdots\cdots > g_{outer\ core\ N} \tag{4}$$

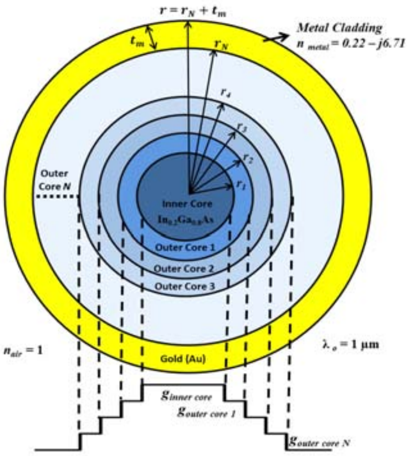

Fig. 1 Cross-section of the metal-clad nano-laser.

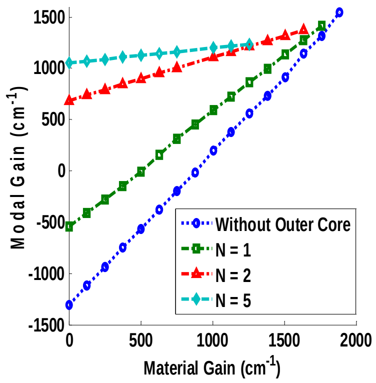

Fig. 2 TE_{01} Modal Gain vs Material Gain.

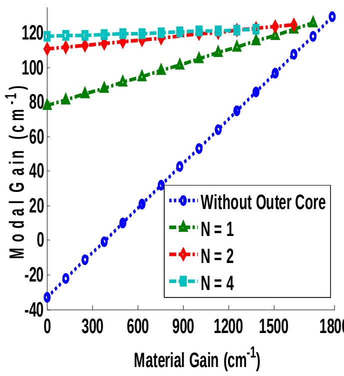

Fig. 3 TM_{01} Modal Gain vs Material Gain.

For the specific calculations performed, the inner core material gain for the structure is kept at 1885cm^{-1} whilst the respective material gains in the outer core(s) are varied and analyzed to evaluate modal gain for the structure. Our results highlight that increased number of outer core layers tends to shift the modal gain to the positive while after a specific range the overall modal gain becomes constant as shown in Fig 2 and Fig 3 for the TE_{01} and TM_{01} modes respectively. The model developed here provides the basis for more detailed nano-laser design and specifically is capable of extension to provide a self-consistent analysis of the wave-guiding and gain properties of such nano-lasers.

Acknowledgement

The work of Z. A. Sattar was supported from Bangor University, School of Electronic Engineering, Wales, UK and the Memon Communities in Pakistan.

REFERENCES

1. Krishnamurthy,V. and B. Klein, "Theoretical investigation of metal cladding for nanowire and cylindrical micropost lasers," *IEEE J. Quantum Electron*., vol. 44, no.1, pp. 67-74, Jan. 2008.
2. Ikeda ,K., Y. Fainman, K.A.Shore and H. Kawaguchi, "Modified long range surface plasmon polariton modes for laser nanoresonators."*J.Appl.Phys.*,vol. 110,no.6,pp.063106–(1)–6),Sep.2011.
3. Maslov,A. V. and C. Z. Ning, "Size reduction of a semiconductor nanowire laser by using metal coating," *Proc.SPIE*., vol.6468,pp. 646801–(1)–(7), 2007.
4. Yeh,P., A. Yariv, and E. Marom, "Theory of Bragg fiber," *J. Opt. Soc. Am.*,vol. 68,no.9,pp. 1196-1201,Sep.1978.
5. Yeh ,P., *Optical waves in layered media*. New York: John Wiley & Sons, Inc., 1988.

On the importance of higher order Bloch modes for the homogenization of periodically structured media

C. Menzel[1*], T. Paul[2], C. Rockstuhl[3], F. Lederer[3] and T. Pertsch[1]
[1]Institute of Applied Physics, Abbe Center of Photonics, Friedrich-Schiller-Universität Jena, Germany
[2]Fraunhofer Institute for Applied Optics and Precision Engineering, Jena, Germany
[3]Institute of Condensed Matter Theory and Solid State Optics, Abbe Center of Photonics, Friedrich-Schiller-Universität Jena, Germany
[*]corresponding author: Christoph.Menzel@uni-jena.de

Abstract- In this contribution we discuss the homogenization of periodically structured media, in particular metamaterials, by means of a Bloch mode analysis and prove the general importance of higher order Bloch modes. We show that the fundamental Bloch mode approximation is of paramount importance, since it provides probably the only way to derive unique effective parameters. The physical origin of common issues like the convergence of effective parameters with the thickness of the sample is resolved within this contribution.

In this contribution we review our work on the description of metamaterials (MM) response in terms of Bloch modes. We will show that from the Bloch mode perspective several issues and problems regarding the homogenization of MMs can be understood and explained easily. Most of the difficulties are shown to be related to a significant contribution of higher order Bloch modes to the response. Since higher order Bloch modes, which are always excited at the interface of a laterally structured medium, can be neglected for diluted materials with periods much smaller than the wavelength, their general importance is not obvious and sometimes misunderstood. Here we clarify typical misunderstandings and elaborate the regimes where higher order Bloch modes might be neglected, allowing for a homogeneous description of the MM under consideration.

The purpose of homogenization of periodically structured media might be understood as the reduction of the complex optical response to the smallest possible set of effective parameters, such that a stack of similar or dissimilar MMs can be properly described by a simple transfer matrix algorithm using their individual effective parameters. The weakest requirement on these effective parameters is their independence on the thickness, i.e. the number of layers used to build up the metamaterial. This is equivalent to the replacement of complex reflection and transmission coefficients by so called wave parameters k and Z which are the propagation constant and the impedance, respectively, and which are attributed to a single Bloch mode that shall dominate the response. We will show, that the latter is true if the fundamental mode approximation [1] holds, i.e., if higher order Bloch modes are excited at a negligible strength.

The language of Bloch modes is preferable for several reasons. First of all, Bloch modes are the native eigenfunctions for periodically structured media. Already known from photonic crystals the language has just to be marginally adjusted to account for the generally lossy metamaterials that usually rely in their design on resonant plasmonic particles. Furthermore, in the context of homogenization just a single Bloch mode accounts for the propagation inside the metamaterial, namely this Bloch mode which has the propagation constant k with the smallest imaginary part [2]. All quantities related to propagation the propagation of beams and pulses, i.e.

diffraction and dispersion, can be deduced from the dispersion relation of this fundamental mode [3]. If the coupling of an external field to the MM is dominated by this fundamental mode, the Bloch impedance derived from the values of Bloch-amplitude at the interface fully accounts for the coupling and, hence, determines reflection and transmission [1]. For the common case of plane wave incidence, the Bloch amplitude of this fundamental mode is then necessarily plane wave like at the interface and the overall response is reducible to a single value of k and Z for each eigen-polarization and frequency.

However, if multiple (higher order) Bloch modes are excited at the interface and, hence, the fundamental mode approximation is not valid, an exact treatment gets cumbersome and no unique effective parameters can be found that properly replace the complex reflection and transmission coefficients. Physically speaking, these higher order Bloch modes account for the near-field coupling between the unit cells and, hence, the environment, which necessarily prohibits unique parameters. In that sense, the effects of substrate-induced bianisotropy [4] and quasi-planar chirality [5] are due to the occurrence of higher order Bloch modes, too.

The treatment of periodically structured media by Bloch modes furthermore allows identifying the requirements which have to be fulfilled for using the S-parameter retrieval, also know as Nicholson-Ross-Weir method. The higher order Bloch modes are shown to be responsible, for the convergence of the effective parameters with an increasing thickness of the material. The so called Fabry-Perot artifacts [6], which occur dominantly within the effective impedance where the thickness of the metamaterial is a multiple of half of the wavelength, are also due to higher order Bloch modes. At this thicknesses the fundamental mode undergoes a Fabry-Perot resonance and, hence, (for lossless media) the reflection is supposed to vanish and the transmission becomes unity, such that the contribution of higher order Bloch modes to R and T increases, finally leading to the Lorentz-shaped artifacts.

Within this contribution we will discuss all these issues and problems at the most simple, rigorous numerically investigated example of a stack of dielectric or metallic stratified layers with a plane wave incident parallel to the multilayer stack, proving the importance for higher order Bloch in general and the importance of the fundamental mode approximation for the homogenization of periodically structured media and MMs.

Acknowledgements: The authors acknowledge financial support by the German Federal Ministry of Education and Research (PhoNa) and Thuringian Ministry of Education, Science and Culture (MeMa).

REFERENCES

1. T. Paul, C. Menzel, W. Śmigaj, C. Rockstuhl, P. Lalanne, and F. Lederer, Reflection and transmission of light at periodic layered metamaterial films, Phys. Rev. B **84**, 115142 (2011).
2. C. Rockstuhl, T. Paul, F. Lederer, T. Pertsch, T. Zentgraf, T. P. Meyrath, and H. Giessen, Transition from thin-film to bulk properties of metamaterials, Phys. Rev. B **77**, 035126 (2008).
3. T. Paul, C. Rockstuhl, C. Menzel, and F. Lederer, Anomalous refraction, diffraction, and imaging in metamaterials, Phys. Rev. B **79**, 115430 (2009).
4. D. A. Powell, and Y. S. Kivshar, Substrate-induced bianisotropy in metamaterials, Appl. Phys. Lett. **97**, 091106 (2010); M. Albooyeh, and C. R. Simovski, Substrate-induced bianisotropy in plasmonic grids, J. Opt. **13**, 105102 (2011).
5. S. I. Maslovski, D. K. Morits, and S. A. Tretyakov, Symmetry and reciprocity constraints on diffraction by gratings of quasi-planar particles, J. Opt. A: Pure Appl. Opt. **11**, 074004 (2009).
6. Xing-Xiang Liu, D. A. Powell, and A. Alù, Correcting the Fabry-Perot artifacts in metamaterial retrieval procedures, Phys. Rev. B **84**, 235106 (2011).

Simulation of outcoupling in OLEDs with structured cathodes with finite-difference time-domain method

S. Belousov[1,2*], M. Bogdanova[1], I. Valuev[1,3], and H. Greiner[4]

[1]Kintech Lab, Russia

[2]NRC "Kurchatov Institute", Russia

[3]Joint Institute for High Temperatures RAS, Russia

[2]Philips Research Europe, Germany

[*]corresponding author: belousov@kintechlab.com

Abstract-We study the optical performance of organic light emitting diodes (OLEDs) with the corrugated cathode. We model the outcoupling efficiency of OLEDs with two-dimensional periodic as well as random corrugations of the cathode. We show that outcoupling efficiency of vertically oriented emitters is greatly enhanced by the presence of corrugations, in accordance with experimental findings. The enhancement is strongly dependent on both geometry of corrugations and material parameters of the cathode.

Close proximity of an emitting layer to the metallic cathode (less than 100nm) in OLEDs (organic light emitting diodes) strongly affects the light outcoupling efficiency in these devices. The major loss channel is associated with the near field coupling of the dipole emitters to the nonradiative surface plasmon (SP) waves supported by the cathode [1]. Creating subwavelength corrugations at the cathode surface [1,2] opens up a radiative decay channel for the SP waves, leading to the enhanced light outcoupling from the device. In this study, we are concerned with both periodic and random corrugations. We consider a generic OLED design, which is shown on Fig.1. The modeled structure consists (from bottom to top) of a metallic cathode, organic electron transport layer (ETL) and hole transport layer (HTL), the transparent conducting cathode (ITO), and the glass substrate.

We assume that the emitters are confined to the ETL/HTL interface (Fig.1). The emitters are modeled as point dipole sources. The modeling is performed with our dedicated Electromagnetic Template Library (EMTL) [3] implementation of the finite-difference time-domain (FDTD) method [4].

Two types of two-dimensional corrugations are considered: 1) metal cylindrical bumps on the cathode surface, 2) cylindrical holes in the cathode surface. The cylindrical bumps (holes) are either arranged on a square grid, or randomly distributed over the cathode surface. We show, that strong outcoupling enhancement is achieved for the vertically oriented emitters (see Fig.2), in accordance with experimental findings [1]. We also investigate the influence of the cathode material parameters on the outcoupling efficiency. The modeling and optimization of such structures will help further improve the efficiency of OLED devices, particularly those with an oriented emitting layer.

The presented results are a part of our activities in the framework of the Russian/European IM3OLED project (Integrated Multidisciplinary Multiscale Modeling for OLEDs).

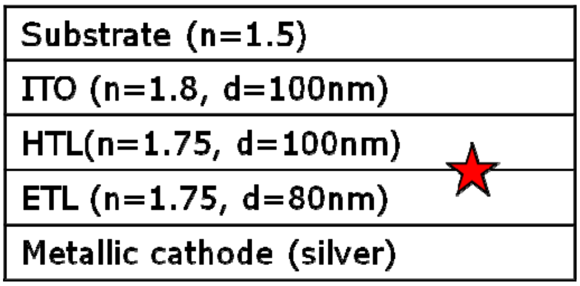

Figure 1. The sketch of the OLED design. Refractive indices and width (*d*) of the corresponding layers are shown in parentheses. Red star represents the emitter.

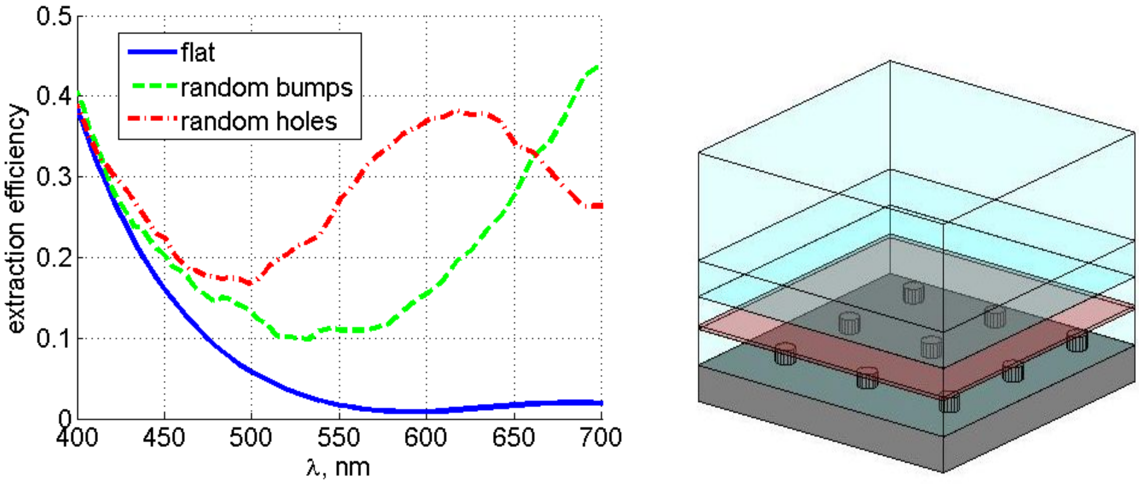

Figure 2. The extraction efficiency into the substrate of vertically oriented dipole emitters for a) flat cathode; b) cathode with the random cylindrical bumps (mean bump height 50nm, mean bump width 110nm, mean bump-to-bump distance 500nm); c) cathode with the random cylindrical holes (mean hole depth 50nm, mean hole width 110nm, mean hole-to-hole distance 500nm). OLED with bumps on the cathode is shown on the right.

Acknowledgements

The work is partially supported by The Ministry of Science and Education of Russia under the contract No.16.523.11.3004.

REFERENCES

1. Koo, W. H., Jeong, S. M., Araoka, F., Ishikawa, K., Nishimura, S., Toyooka, T., and Takezoe H., "Light extraction from organic light-emitting diodes enhanced by spontaneously formed buckles," *Nat. Photon.*, Vol. 4, 222 – 226, 2010.
2. Frischeisen, J., Niu, Q., Abdellah, A., Kinzel, J. B., Gehlhaar, R., Scarpa, G., Adachi, C., Lugli, P., and Brütting, W., "Light extraction from surface plasmons and waveguide modes in an organic light-emitting layer by nanoimprinted gratings," *Opt. Express*, Vol. 19, No.101, A7 – A19, 2010.
3. Electromagnetic Template Library (EMTL), Kintech Lab Ltd, http://fdtd.kintechlab.com
4. Taflove, A., and Hagness, S. H., *Computational Electrodynamics: The Finite Difference Time-Domain Method*, Artech House, Boston, 2000.

A convergence proof for dynamic homogenization

A. Bossavit[1]

[1]LGEP, CNRS, France
bossavit@lgep.supelec.fr

Abstract— We justify, by an asymptotic analysis, an homogenization method which applies to the Maxwell system of equations in the harmonic case at angular frequency ω. The method yields effective coefficients by solving the Maxwell system on a fundamental domain of the crystal-like metamaterial of interest, with appropriate periodic boundary conditions. The case of all-dielectric materials, with strong contrast, is especially addressed.

1. INTRODUCTION

'Dynamic homogenization' [1] should be understood, in this paper, as a procedure that delivers *frequency-dependent* effective coefficients $\epsilon_{\text{eff}}(\omega)$ and $\mu_{\text{eff}}(\omega)$ from a complete description of the local values of ϵ and μ inside the periodicity cell of a metamaterial. 'Static' homogenization, in contrast, is the kind of (non-trivial) spatial averaging of ϵ and μ described in classic work such as [2], which works fine in static situations, but cannot take into account the internal resonance phenomena that make metamaterials what they are.

In both cases, one first solves a so-called 'cell problem', on a periodicity cell of the material, with periodic boundary conditions, from which would-be effective coefficients are computed. One then replaces the macroscopic body, made of this material, by a homogeneous medium of the same shape, endowed with these effective coefficients, other elements of the situation (field generator(s), other homogeneous bodies present, air around, etc.), being unchanged.

Such a procedure needs justification, in the form of an appropriate asymptotic result: "When the size of the periodicity cell tends to 0, the solution of the Maxwell equations (over the whole setup) converges, in some sense, towards ...", etc. This is relatively easy (and now well known) in the static case, but much more of a challenge in dynamic homogenization, when all fields are time-harmonic at some definite angular frequency ω.

We propose here a way to state and prove such things in the dynamic case for a large family of metamaterial designs. (The case of bispherical dielectric inclusions [3, 4, 5], with strong contrast over the dielectric background, will serve as concrete example.) The main idea is that internal resonance phenomena should somehow be 'kept invariant' in the asymptotic analysis, in spite of the fact that letting the periodicity cell shrink to a point tends to move such resonances away from ω. Relations between Floquet–Bloch analysis (on periodic media) and Fourier analysis (over homogeneous ones) play a key role in the proofs [6].

2. DETAILS

Consider a lattice generated by three independent vectors $\partial_1, \partial_2, \partial_3$. Call C (the periodicity cell) the parallelepiped built on them, and suppose 3D space filled by a material for which $\mu(x + v) = \mu(x)$ and $\epsilon(x + v) = \epsilon(x)$ for all points x and all vectors v belonging to the lattice (a so-called "C-periodic" material). A source current, $j^s(x)$ at point x, is given.

Suppose j^s time-independent. Magnetostatics consists in solving for h and b such that $\operatorname{div} b = 0$, $b = \mu h$, $\operatorname{rot} h = j^s$. Call this "problem P_1". It can be embedded, conceptually, in a family of similar virtual problems P_α, for which the cell is C_α generated by the vectors $\alpha\partial_1, \alpha\partial_2, \alpha\partial_3$, with j^s unchanged. Using Bloch decomposition (relative to C_α), one can prove [6] that the solution (b_α, h_α) weakly converges, when the non-dimensional parameter α tends to 0, towards the solution (b_0, h_0) of the following "problem P_0":

$$\operatorname{div} b = 0, \quad b = \mu_{\text{eff}}\, h, \quad \operatorname{rot} h = j^s, \tag{1}$$

where μ_{eff} is the 3×3 matrix defined, for any nonzero vector$H$, by

$$\mu_{\text{eff}} H \cdot H = [\inf_\varphi \{ \int_C \mu |H + \operatorname{grad} \varphi|^2 \}]/\text{volume}(C), \tag{2}$$

where the infimum is taken with respect to all (smooth enough) C-periodic magnetic potentials φ living on C.

In practice, the material with C-periodic μ has finite extent, but this convergence result is enough to justify *homogenization*, i.e., the replacement of μ by μ_{eff} in the bulk metamaterial. In the dynamic case, where the excitation current at time t and point x is $\text{Re}[j^s(x)\exp(i\omega t)]$, the analogous procedure consists in solving the homogenized Maxwell equations (all fields b, h, etc., now complex-valued):

$$-i\omega d + \text{rot}\, h = j^s, \quad d = \epsilon_{\text{eff}}\, e, \;\; b = \mu_{\text{eff}}\, h, \quad i\omega b + \text{rot}\, e = 0 \tag{3}$$

where again ϵ_{eff} and μ_{eff} come from solving a preliminary cell problem, as follows. (We ignore the possibility of chiral behavior for the moment, see below.)

Let us denote by $U \times x$, where U is a given (complex) 3D vector, the vector *field* whose value at point x is the cross product $U \times \overrightarrow{cx}$, where c is the center of the cell C and $\overrightarrow{cx}$ the vector from c to x. (Remark that $\text{rot}(U \times x) = 2U$.) Now, given 3D vectors B and D, we solve on C for fields b, h, d, e such that $e + \frac{i\omega}{2} B \times x$ and $h - \frac{i\omega}{2}\, D \times x$ be C-periodic and

$$-i\omega\epsilon\, e + \text{rot}\, h = 0, \quad i\omega\mu\, h + \text{rot}\, e = 0 \;\text{ in } C. \tag{4}$$

(The C-periodicity conditions concern only the tangential components of the fields on the cell's boundary, and are easily dealt with, numerically, when using edge-based finite elements, cf. [7].) This done, we compute the following Lagrangian, a quadratic function of B and D:

$$\mathcal{L}(B, D) = (\textstyle\int_C [\mu\, h \cdot \overline{h} - \overline{\epsilon}\, \overline{e} \cdot e])/\text{volume}(C), \tag{5}$$

hence two (a priori, complex) vectors H and E, linearly depending on B and D, such that $\mathcal{L}(B, D)$ $= B \cdot \overline{H} - \overline{D} \cdot E$. The relation thus found between the pairs (B, D) and (H, E) is the desired homogenized law. Its general form is $B = \mu_{\text{eff}}\, H + \zeta_{\text{eff}}\, E$ and $D = \xi_{\text{eff}}\, H + \epsilon_{\text{eff}}\, E$, where μ_{eff}, ζ_{eff}, etc., are 3×3 complex matrices which do depend on ω. Note the possibility of anisotropy and of chirality (nonzero ζ_{eff} and ξ_{eff}).

We justify the procedure by a convergence result in the case (important in metamaterial studies, cf. [3, 4, 5]) when C contains a region C_1 in which $\epsilon(x) = \epsilon_1$, a large value with respect to ϵ_0, and $\epsilon(x) = \epsilon_0$ for x in $C - C_1$. Call P_1, again, the problem, set in the whole space,

$$-i\omega\epsilon\, e + \text{rot}\, h = j^s, \quad i\omega\mu_0\, h + \text{rot}\, e = 0. \tag{6}$$

The trick consists in embedding P_1 in a family P_α of similar problems, with $C^\alpha = \alpha C$ as periodicity cell, $\epsilon = \epsilon_0$ in $C_\alpha - \alpha\, C_1$, and $\epsilon = \epsilon_1/\alpha^2$ in αC_1. We also embed the cell problem (4)—call it CP_1— in a family CP_α set on the cell C (thanks to a rescaling move), with the same modified values of ϵ inside. The same Fourier–Bloch analysis as in the static case leads to a cell problem which is precisely the limit of CP_α, hence the desired asymptotic result. The 'contrast enhancement', so to speak, operated by dividing ϵ_1 by α^2, is the way by which one can keep the resonance values close to ω, as $\alpha \to 0$, in this category of problems with dielectric inclusions at strong contrast over the background.

REFERENCES

1. Bossavit, A., "On the homogenization of Maxwell equations", *COMPEL*, Vol. 14, No. 4, 23–26, 1996.
2. Bensoussan, A., Lions, J.L., Papanicolaou, G., *Asymptotic methods for periodic structures*, North Holland, Amsterdam, 1978.
3. Ahmadi, A., Mosallaei, H., "Physical configuration and performance modeling of all-dielectric metamaterials", *Phys. Rev. B,* Vol. 77, No. 4, 045104-(1–11), 2008.
4. Vendik, I., Odit, M., Kozlov, D., "3D Metamaterial Based on a Regular Array of Resonant Dielectric Inclusions", *Radioengineering*, Vol. 18, No. 2, 111–116, 2009.
5. Zhao, Q., Zhou, J., Zhang, F., Lippens, D., "Mie resonance-based dielectric metamaterials", *Materials Today*, Vol. 12, No. 12, 60–69, 2009.
6. Bossavit, A., "Homogenization of Split-Ring Arrays, Seen as the Exploitation of Translational Symmetry", in *Metamaterials and Plasmonics: Fundamentals, Modelling, Applications*, NATO SPS Series, Springer, Dordrecht, 2009, pp. 77–90.
7. Belyamoun, M.H., Dubrunfaut, S., Zouhdi, S., "Dynamic homogenization of split-ring metamaterials by Floquet–Bloch decomposition", *Appl. Phys. A*, Vol. 109, No. 4, 1043–1051, 2012.

Experimental characterization techniques

Raman scattering study of strain in nanostructure oxides

J. Belhadi[1], M. El Marssi[1,*], Y. Gagou[1], Yu. I. Yuzyuk[2], and I. P. Raevski[2]

[1] Laboratoire de Physique de la Matière Condensée, Université de Picardie Jules Verne, France
[2]*Faculty of Physics, Southern Federal University, Russia*
[*]mimoun.elmarssi@u-picardie.fr

Abstract- We report Raman scattering of ferroelectric $BaTiO_3$ (BT) film and superlattice (SL) consisting of BT and paraelectric $BaZrO_3$ (BZ). These nano-structures have been growth by a pulsed laser deposition. The epitaxial BT film and BT and BZ layers with a periodicity of 256Å were deposited on MgO substrate buffered with $La_{1/2}Sr_{1/2}CoO_3$ layer. The spectra revealed that the strain reduces considerably Ti^{4+} ions disorder and suggest a monoclinic phase in BT layers and polar phase in BZ layers for the SL.

Room-temperature Raman spectra of BT film SL were recorded in normal to substrate and side-view backscattering geometries and first should be compared with those of bulk tetragonal BT crystal. In the tetragonal ferroelectric BT point group C_{4v} polar axis is along Z, the zz component of the Raman tensor involves A_1 phonons exclusively. For the xx and yy components the A_1 and B_1 phonons are allowed simultaneously, while E modes are only allowed for zx and zy components. No Raman-active modes are allowed in the spectra corresponding to the xy component of the Raman tensor. In the tetragonal phase the E(1TO) soft mode is overdamped because the frequency value is about 34–38 cm^{-1} while the half-width is about 85–115 cm^{-1}. In the tetragonal BT crystals, the fully symmetrical A_1(TO) component of the soft mode at 276 cm^{-1} is heavily damped and coupled with low-frequency A_1(TO) hard mode at 180 cm^{-1}. As a result of this coupling the sharp dip exists in Y(ZZ)-Y spectrum while a sharp peak appears in the Y(XX)-Y spectrum of the single-domain BT crystals.

Room-temperature polarized Raman spectra of BT film recorded in Y(ZX)-Y, Y(ZZ)-Y, and Y(XX)-Y side-view back-scattering geometries were obtained. Like in BT single crystal, the overdamped soft mode is observed in Y(ZX)-Y spectrum, but its frequency is markedly shifted in BT film up to 60 cm^{-1} . In contrast to BT crystal Y(ZZ)-Y and Y(XX)-Y spectra are very similar and the interference structure at 180 cm^{-1} is the same for both these spectra. Examination in normal backscattering configuration Z(XY)-Z (not presented here) revealed Raman response very similar to that in Y(ZX)-Y one. This implies the absence of c-domain structure and more likely the BT film in either monoclinic r-phase or orthorhombic aa-phase as was predicted by first-principle and phenomenological calculations for epitaxial perovskites on cubic substrates. [1,2] For SL the Raman spectra obtained in Y(ZX)-Y, Y(ZZ)-Y, and Y(XX)-Y geometries are markedly different. The BZ layer is compressed within the SL due to significant mismatch between the alternating BZ and BT layers and the out-of-plane parameter slightly larger than in unconstrained BZ. As a consequence of this distortion, all triply degenerated modes of cubic BZ are split into Raman-active components. This is in agreement with the high-pressure study on BZ reported by Chemarin et al. [3] that shows that the Raman spectrum is sensitive to the hydrostatic pressure. They have attributed the spectral changes observed at 12 and 16 GPa to the pressure-induced structural phase transitions. It is worth noting that the Raman spectra of BT/BZ SLs is not a simple superposition of the BT and BZ spectra. All Raman-active modes of BT/BZ SL 256 Å exhibit an obvious narrowing with respect to those of BT film. The observed narrowing is a signature of the lattice ordering within the SLs due the coupling between the constituent layers. Two sharp peaks at about 136 and 170 cm^{-1} are perfectly polarized exclusively in Y(ZX)-Y geometry. No signature on this doublet was detected in Y(XX)-Y spectra and only weak leakage of these lines was detected in Y(ZZ)-Y and Z(XY)-Z geometries. The E(1TO) soft mode is markedly altered with respect to single BT film and appears as underdamped peak at about 200 cm^{-1} in Y(ZX)-Y geometry. Like in BT/BTZ SL [4] the strains imposed by the epitaxial SL construction reduce considerably Ti disorder, as follows from the underdamped character of the soft mode. It seems that this soft mode is not degenerated in the SL since weak contributions with a little bit higher wave number can be traced in diagonal geometries.

Such a high value of soft mode frequency is typical for BT crystals in the fully ordered low-temperature rhombohedral phase. Since the latter phase is forbidden by symmetry in epitaxial films, one can suggest that monoclinic phase r the most similar to the rhombohedral is stable in SL. Polarization-dependent Raman spectra of these SLs are in agreement with monoclinic symmetry.

REFERENCES

[1] O. Diéguez, K. M. Rabe, and D. Vanderbilt, Phys. Rev. B 72, 144101 (2005)
[2] V. B. Shirokov, Yu. I. Yuzyuk, B. Dkhil, and V. V. Lemanov, Phys. Rev. B 75, 224116 (2007)
[3] C. Chemarin, N. Rosman, T. Pagnier, and G. Lucaseau, J. Solid State Chem. 149, 298 (2000).
[4] F. De Guerville, M. El Marssi, I. P. Raevski, M. G. Karkut, and Yu. I. Yuzyuk, Phys. Rev. B 74, 064107 (2006)

Plasmon damping characterized with a nanoprobe

M. Bosman[1*], S.F. Tan[2], J.K.W. Yang[1], and C.A. Nijhuis[2]

[1]Institute of Materials Research and Engineering, A*STAR (Agency for Science, Technology and Research), 3 Research Link, 117602, Singapore

[2]Department of Chemistry, National University of Singapore, 3 Science Drive 3, 117543, Singapore

[*]corresponding author: michel.bosman@gmail.com

Abstract- A novel analysis method is introduced for the quantitative analysis of plasmon damping, based on monochromated electron energy-loss spectroscopy. The damping of localized surface plasmons in a large (>50) series of single gold nanoparticles was performed with nanometer spatial accuracy, confirming and expanding earlier theoretical predictions.[1]

The damping properties of localized surface plasmon resonances are critical in determining their interaction time and frequency range. Plasmons resonate in a narrow frequency band when their damping is low; a broadband frequency response results from strong damping. With the advances in fabrication and synthesis of plasmon-active structures, nanometer control over shape and inter-particle distance has become possible. Here, we present results where the plasmon dephasing was analyzed—for the first time—with nanometer spatial precision on single plasmon modes in individual particles.

Monochromated electron energy-loss spectroscopy (EELS) has become a popular technique for the local analysis of surface plasmon modes.[2-5] An electron probe with a diameter of 1 nm is used to excite surface plasmons, and the losses that occur in the process are recorded in EELS spectra. A novel analysis routine was used here to analyze the spectral response of any selected plasmon mode, in a large series of single nanoparticles. Figure 1 shows an example where EELS was performed on a gold nanorod, showing two clear resonance modes in this case. For each separate plasmon mode, the analysis routine allows the calculation of the dephasing time, as shown. Our results from the series of gold nanoparticles confirm the strong energy-dependence of the plasmon damping.[1] Remarkably, the experiments combine nanometer spatial precision with 60 meV spectral resolution and cover a broad spectral range that includes the near-infrared (down to 0.4 eV), the visible, and the ultraviolet, giving access to a much broader range of frequencies, at a much higher spatial resolution than is possible with all-optical experiments.

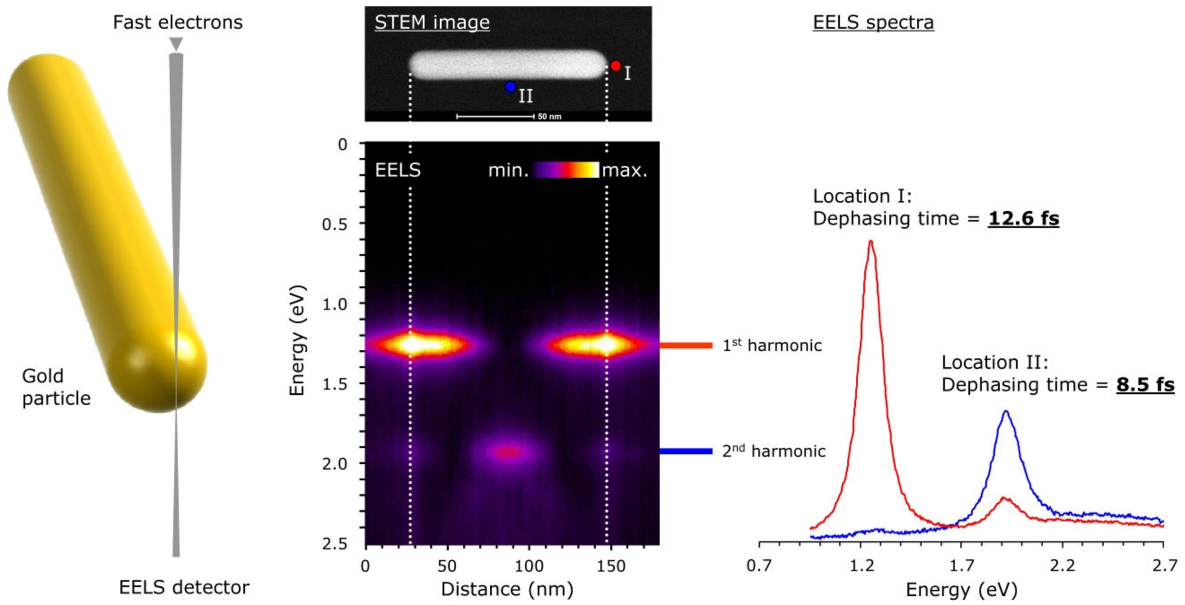

Figure 1: ***Localized surface plasmons in a single gold nanorod.*** *A fast electron traverses a gold particle, exciting localized surface plasmons that are then analyzed with EELS. Each plasmon mode has a distinct spatial distribution of anti-nodes plotted here as a function of distance along the gold rod,[5] corresponding to the aligned scanning TEM image. The presented analysis routine allows an accurate determination of the plasmon dephasing times, confirming earlier optical experiments,[6] and theoretical predictions.[1]*

Acknowledgements, The National Research Foundation (NRF) is kindly acknowledged for supporting this research under the CRP program (award No. NRF-CRP 8-2011-07)

REFERENCES

1. Myroshnychenko, V.; Rodríguez-Fernández, J.; Pastoriza-Santos, I.; Funston, A.M.; Novo, C.; Mulvaney, P.; Liz-Marzán, L.M.; García de Abajo, F.J. “Modelling the optical response of gold nanoparticles,” *Chem. Soc. Rev*. 37, 1792–1805, 2008.
2. García de Abajo, F. J. “Optical Excitations in Electron Microscopy,” *Rev. Mod. Phys*. 82, 209-275 2010.
3. Bosman, M.; Keast, V. J.; Watanabe, M.; Maaroof, A. I.; Cortie, M. B. “Mapping Surface Plasmons at the Nanometre Scale with an Electron Beam,” *Nanotechnology* 2007, 18, 165505.
4. Nelayah, J.; Kociak, M.; Stéphan, O.; García de Abajo, F. J.; Tencé, M.; Henrard, L.; Taverna, D.; Pastoriza-Santos, I.; Liz-Marzán, L. M.; Colliex, C. “Mapping Surface Plasmons on a Single Metallic Nanoparticle,” *Nat. Phys*. 3, 348-353, 2007.
5. Rossouw, D.; Couillard, M.; Vickery, J. Kumacheva, E.; Botton, G.A. “Multipolar Plasmonic Resonances in Silver Nanowire Antennas Imaged with a Subnanometer Electron Probe,” *Nano Lett*., 11, 1499-1504, 2011.
6. Sönnichsen, C.; Franzl, T.; Wilk, T.; von Plessen, G.; Feldmann, J. “Drastic Reduction of Plasmon Damping in Gold Nanorods,” *Phys. Rev. Let*., 88, 077402, 2002.

Technologies and applications

Nano-aperture design to enhance optical transmission using the shape optimization procedure

H. Lim[1]**, N. Heo**[1]**, J. Choi**[2] **and J. Yoo**[3*]

[1]Graduate School of Mechanical Engineering, Yonsei University, Seoul, Korea
[2]Samsung Electronics, Co. Ltd., Suwon, Korea
[2]School of Mechanical Engineering, Yonsei University, Seoul, Korea
[*]corresponding to: yoojh@yonsei.ac.kr

Abstract- This study suggests a systematic design approach of a nano-aperture for the purpose of improving optical transmission by adopting the phase field method based shape optimization procedure using an Allen-Cahn equation. Through the design process, we have designed an unprecedented form of the aperture and compared its performance was with traditional shapes.

As the fabrication technology regarding the nano-scaled metallic aperture has advanced, various types of aperture have been developed such as making a slit in the vicinity of the aperture[1] and changing the shape of the aperture[2]. Those types were invented using the principles of the surface plasmon resonance (SPR) to improve the transmission rate[3].

In this study, we have considered a sub-wavelength scale slit as the initial prototype shape and designed the final shape using the shape optimization procedure based on the phase field method applying the Allen-Cahn equation[4]. The governing equation for numerical analysis is represented as the two-dimensional wave equation of TM mode as below:

$$\frac{\partial}{\partial x}\left(\frac{1}{\varepsilon_r}\frac{\partial}{\partial x}H_z\right)+\frac{\partial}{\partial y}\left(\frac{1}{\varepsilon_r}\frac{\partial}{\partial y}H_z\right)=\frac{\omega^2}{c^2}H_z \tag{1}$$

where H_z is the z-directional magnetic field intensity, c is the wave speed and ε_r is the relative value of the electric permittivity.

The incident light wavelength is fixed to 850nm, which is in near infrared wavelength range, goes from the upper air portion and passes through the nano-aperture and propagates a-Si(amorphous silicon) layer as displayed in figure 1(a). The design domain is defined 75nm depth silver layer designated in the red box. Table 1 shows relative electric permittivity values of the materials used for the analysis. The design objective is to maximize the field strength intensity in the measuring domain in figure 1(a) and we evaluated it by calculating the Poyinting vector value of the area. The prototype model is set as the whole design domain is filled with Ag material.

Table 1. Material properties used for the analysis

Material	Air	Ag (silver)	a-Si
Relative permeability	1	-32.2222+1.7279*i*	14.6211+0.4964*i*

During the design process, refractive index values in the design domain are changed according to the variation of the design variable, i.e., the level set function Φ based on the following formulation:

$$n'_{Ag} + (n'_{SiO_2} - n'_{Ag})\phi + i\left\{n''_{Ag} + \left(n''_{SiO_2} - n''_{Ag}\right)\phi\right\} \tag{2}$$

where ε'_{Ag} and ε'_{SiO2} are real parts of the electric permittivity of the Ag layer and the a-Si part, respectively, and ε''_{Ag} and ε''_{SiO2} are their imaginary parts. Figure 1(b) illustrates the optimal material distribution where the black and the white parts represent the a-Si and Ag portion, respectively. The model shown in figure 1(b) gives more than two times performance improvement based on the Poynting vector value of the measuring domain in comparison with the prototype model.

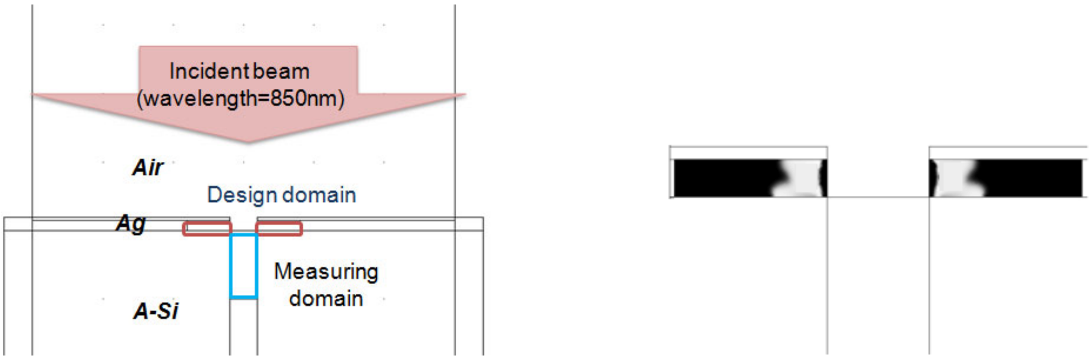

(a) (b)

Figure 1. (a) Schematic model for analysis with the design domain (in red colored box) and the measuring region (in blue colored box) and (b) optimal material distribution in the design area (SiO_2: black, Ag: white).

Acknowledgements This work was supported by the National Research Foundation of Korea(NRF) grant funded by the Korea government(MEST) (No. 2012-0005701).

REFERENCES

1. Garcia-Vidal, F. J., H. J. Lezec, T. W. Ebbesen and L. Martin-Moreno, "Multiple paths to enhance optical transmission through a single subwavelength slit ", *Physical Review Letters*, Vol. 90, No. 21, 213901, 2003.
2. Matteo, J. A., D. P. Fromm, Y. Yuen, P. J. Schuck, W. E. Moemer and L. Hesselink, "Spectral analysis of strongly enhanced visible right transmission through single C-shaped nanoapertures", *Applied Physics Letters*, Vol. 85, No. 4, 648-640, 2004.
3. Raether, H., *Surface plasmons on smooth and rough surfaces and on gratings*, Springer, Berlin, 1988.
4. Yamada, T., K. Izui, S. Nishiwaki, A. Takezawa, "A topology optimization method based on the level set method incorporating a fictitious interface energy", *Computer Methods in Applied Mechanics in Engineering*, Vol. 199, 2876-2891, 2010.

Twisting a focused light spot with a nano-spiral

H. Liu[1†], M. Q. Mehmood[2†], Cheng-Wei Qiu[2], L. Ke[1], and J. H. Teng[1*]

[1]Institute of Materials Research and Engineering, Agency for Science, Technology and Research (A*STAR), 3 Research Link, Singapore 117602.

[2]Department of Electrical and Computer Engineering, National University of Singapore, 4 Engineering Drive 3, Singapore 117576.

† These Authors contributed equally to this work.

*corresponding author: jh-teng@imre.a-star.edu.sg

Abstract- In this work, we report an experimental demonstration and analytical study on a deterministic aperiodic nanostructure (DANS) of spiral, which is able to focus as well as twist light in far field. The 100-nm thick Au spiral structure was patterned by electron beam evaporation and electron beam lithography followed by dry etching. It was optically characterized by confocal imaging microscopy with an incident light of 633 nm wavelength. Both experimental and simulation results demonstrate that this work provides an innovative way for light manipulation.

Light would be twisted around its axis of travel, which occurs when it interacts with specific matters in space. This phenomenon has been extensively studied in the past from fundamental researches to technological applications. Specifically, it has incubated quite a few attractive developments in optical manipulation/trapping[1-2], optical tweezers[3], optical vortex knots[4], telecommunication[5], imaging[6], astronomy[7-8] and quantum information processing[9-10].The intriguing properties of twisted light are attributed to the interaction of spin angular momentum (SAM) and orbital angular momentum (OAM). SAM is associated with polarization state, a manifestation of photon spin, which was theoretical elucidated by Poynting in 1909[11] and experimentally demonstrated by Berth in 1936[12], respectively. OAM originating from light's helical wavefront structure was conceptualized by Allen *et al* in a much later time at 1992, and comparatively it was related to spatial field distribution. The discovery of OAM has remarkably boosted the study of its unique properties and the interesting phenomena associated with spin-orbital interaction[13].

At optical frequency, light waves can be twisted when they impinge on spiral nanostructures, which are one type of deterministic aperiodic nanostructures (DANS) offering new avenues for creation and manipulation of complex scattering resonances and localized optical field at nanoscale. From a mathematic point of view, DANS interpolate a tunable class between periodicity and randomness, while in an optic context they refer to inhomogeneous metal-dielectric structures where their optical properties (refractive index, transmission and reflection, etc.) alter over manifold dimensional scales, either comparable or less than the wavelength of incident light. Furthermore, their structural complexity is multivarian in comparison with periodical and disordered or random matters. In view of these, typical DANS, i.e., spiral nanostructures of various shapes, have been investigated and characterized in terms of scattering[14], plasmonic chirality[15] and polarization response[16], which have shown potentials for thin film solar cells, optical biosensors, plasmonic photodetector and polarization analyzers.

In this work, a specifically designed spiral nanostructure was fabricated and characterized as a light twister. 100nm-thick Au film was evaporated onto quartz substrate following by spin-coated with ZEP resist. Subject to electron-beam lithography, spiral structure was patterned onto resist and further transferred into Au film by a dry etching process. Eventually, a 100nm thick Au spiral structure with a minimum feature size of about 50 nm was created on quartz. Then, its confocal imaging was optically characterized by a photon scanning tunneling microscopy (PSTM) with an incident light of 633 nm wavelength. Based on the depth scan results in a distance from 0 to 25 μm above sample surface, it was observed that a focal spot rotated at the far-field around its axis of travel (z-axis), while light twisted as well. A detailed analysis on the geometry effect and near-field coupling will be presented and a discussion on the SAM-OAM interaction will be given based on the simulation of the electric field distribution along z-axis. This work unveils a novel way of optical manipulation by twisting a focused light in far field via a spiral nanostructure. The results may have potential applications in optical tweezers and optical chirality analyzer.

Acknowledgements We acknowledge Dr. J. Deng and Mr. C. C. Choy from IMRE and Dr. M. Zhang from Data Storage Institute, A*STAR. The work is financially supported by Agency for Science, Technology and Research (A*STAR) under grant number 0921540099 and 1021740172.

REFERENCES

1. Grier, D. G., "A revolution in optical manipulation," *Nature* 424, 810-816, 2003.
2. Paterson, L., MacDonald M. P., Arlt, J., Sibbett, W., Bryant P. E., Dholakia, K., "Controlled rotation of optically trapped microscopic particles," *Science* 292, 912–914, 2001.
3. Padgett, M., Bowman, R., "Tweezers with a twist," *Nature Photon*. 5, 343–348, 2011.
4. Dennis, M. R., King, R. P., Jack, B., O'Holleran, K. and Padgett, M. J., "Isolated optical vortex knots," *Nature Phys*. 6, 118–121, 2010.
5. Wang, J., Yang, J., Fazal, I. M., Ahmed, N., Nan, Y., Huang, H., Ren, Y., Yue, Y., Dolinar, S., Tur, M. and Willner, A. E., "Terabit free-space data transmission employing orbital angular momentum multiplexing," *Nature Photon*. 6, 488-496, 2012.
6. Bernet, S., Jesacher, A., Fu¨rhapter, S., Maurer, C., and Ritsch-Marte, M., "Quantitative imaging of complex samples by spiral phase contrast microscopy," *Opt. Express* 14, 3792–3805, 2006.
7. Tamburini, F., Thide, B., M-Terriza, G., and Anzolin, G., "Twisting of light around rotating blackholes," *Nature Phys*. 7, 195-197, 2011.
8. Grover A. S. J., Erin L. F., Rukiah S. A.-M., Laird M. C., Mary, A. P., David, M. P. and Daniel W. W., "Astronomical demonstration of an optical vortex coronagraph," *Opt. Express* 16,10200-10207, 2008.
9. Barreiro, J. T., Wei, T.-C. and Kwiat, P. G., "Beating the channel capacity limit for linear photonic superdense coding," *Nature Phys*. 4, 282–286, 2008.
10. Leach, J., Jack, B., Romero J., Jha A. K., Yao, A. M., Franke-Arnold, S., Ireland, D. G., Boyd, R. W., Barnett, S. M., Padgett, M. J., "Quantum correlations in optical angle-orbital angular momentum variables," *Science* 329, 662–665, 2010.
11. Poynting, J., "The wave motion of a revolving shaft, and a suggestion as to the angular momentum in a beam of circularly polarised light." *Proc. R. Soc. Lond. A* 82**,** 560–567, 1909.
12. Beth, R., "Mechanical detection and measurement of the angular momentum of light," *Phys. Rev.* 50**,** 115–125, 1936.
13. Shitrit, N., Bretner, I., Gorodetski, Y., Kleiner, V., and Hasman, E., "Optical spin Hall effects in plasmonic chains," *Nano Lett*. 11, 2038–2042, 2011.
14. Trevino, J., Gao, H., and Negro, D., "Circularly symmetric light scattering from nanoplasmonic spirals," *Nano Lett*. 1, 2008-2016, 2011.
15. Ohno, T., and Miyanishi, S., "Study of surface plasmon chirality induced by Archimedes' spiral grooves," *Opt. Express* 14, 6285-6290, 2006.
16. Gorodetski, Y., Niv, A., and Hasman, E., "Observation of the spin-based plasmonic effect in nanoscale structures," *Phys. Rev. Lett*. 101, 043903, 2008.

Simulation and Design of a Bandpass Filter on Metasubstrates

V. P. Silva Neto*, C. F. L. Vasconcelos, M. R. M. L. Albuquerque, and A. G. D'Assunção
Federal University of Rio Grande do Norte, Brazil
*valdemir.neto@yahoo.com.br

Abstract-This work presents the analysis of a microstrip bandpass filter on metamaterial substrates. The filter is composed of two ring resonators with quarter-wavelength side-coupled sections. The filter input is provided, as well as the output port, using a quarter-wavelength side-coupled microstrip line section. Simulation by finite element method is proposed to verify the effect of the metamaterial substrate properties on the filter performance and to compare these results to those obtained considering isotropic substrate.

Metamaterials have received a great deal of attention due to their unusual electromagnetic properties unavailable in conventional materials. These engineered materials can be used in a variety of printed circuit applications such as filters, impedance transformers, couplers, and antennas.

Planar microwave filters are attractive for use in several microwave circuits and systems. Bandpass filters with one-wavelength ring resonator fed by side-coupled lines on isotropic substrates were reported in [1]. In this work, a filter geometry composed of two one-wavelength ring resonators is proposed (Fig. 1). Basically, this geometry is composed of two coupled ring resonators and three quarter-wavelength side-coupled sections. Microstrip lines of 50 Ω are considered. The design is performed using equivalent circuit theory and scattering parameters. The filter performance is controlled by the characteristic impedances of the rings and by the even- and odd-mode characteristic impedances of the side-coupled line sections. Numerical computation is performed considering homogeneous metamaterial substrates.

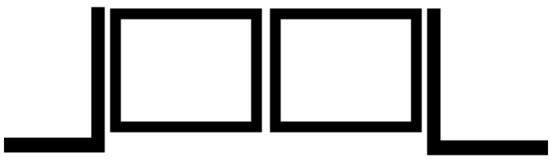

Figure 1 – Bandpass microstrip filter geometry.

In this work, we consider that homogeneous anisotropic metamaterials used as substrates in planar filter design are modeled according to the analytical formulation presented in [2], with enhanced positive values of electric permittivity and magnetic permeability for microwave applications. The parameter extractions are accomplished using metamaterial unit cell containing spiral loop embedded in a dielectric substrate (ε_r = 10.7, h=1.57mm). The spiral loop geometry is shown in Fig 2.

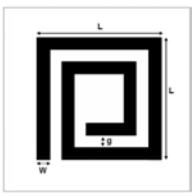

Figure 2 – Spiral loop geometry used in modeling the planar filter metamaterial substrate (L = 16 mm, W = g = 0.12 mm).

The metamaterial substrate is characterized by two uniaxial tensors with the optical axes on z-direction, as follows:

$$\ddot{\varepsilon} = \varepsilon_0 \begin{bmatrix} \varepsilon_{xx} & 0 & 0 \\ 0 & \varepsilon_{yy} & 0 \\ 0 & 0 & \varepsilon_{zz} \end{bmatrix} \qquad \ddot{\mu} = \mu_0 \begin{bmatrix} \mu_{xx} & 0 & 0 \\ 0 & \mu_{yy} & 0 \\ 0 & 0 & \mu_{zz} \end{bmatrix} \tag{1}$$

where $\varepsilon_{xx} = \varepsilon_{yy} \neq \varepsilon_{zz}$ and $\mu_{xx} = \mu_{yy} \neq \mu_{zz}$.

Fig. 3 shows the frequency responses for the designed filter using isotropic and metamaterial substrates that are 1.7 mm thick. Microstrip lines of 50 Ω were assumed. For the filter on isotropic material, in the first band (centered at 1.7 GHz) return loss is -18 dB, while the insertion loss is -2 dB. In the second band (centered at 2.04 GHz) the filter response is not a good one, because it is not properly adapted to the input port (S_{11} = -8 dB). For the filter on a metamaterial substrate a very good response was obtained in both frequency bands. In the first band (centered at 1.92 GHz) the insertion loss is -3 dB, and the return loss is -22 dB. In the second band (centered at 2.21 GHz) return loss is -28 dB and insertion loss is -2 dB.

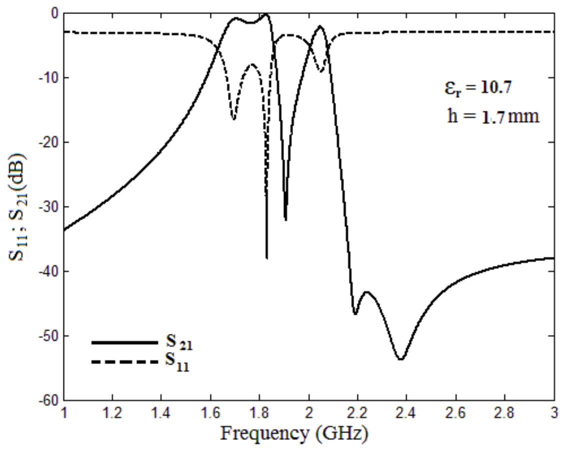

(a)

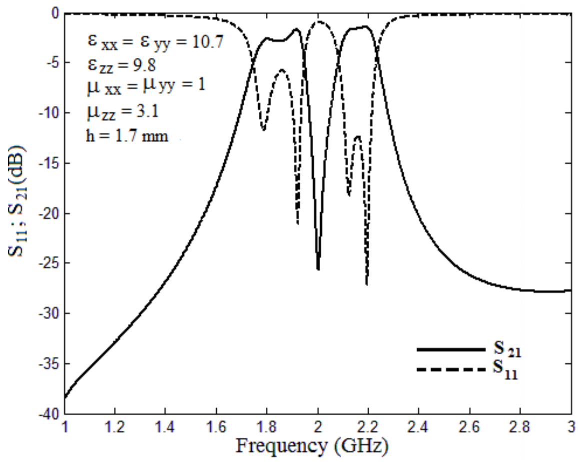

(b)

Figure 3 - Frequency response of the filter on: (a) isotropic and (b) metamaterial substrate.

As can be seen from Fig. 3, the designed filters exhibit a dual band behavior. The first band is due to the lengths of the two rings that are both approximately equal to one-wavelength (λ) at the central frequency of this band. The second one is due to the coupling between the two ring resonators. From Fig. 3(b), we can conclude that the filter on metasubstrate has a potential application as a duplex component, because it exhibits a good frequency response with two close frequency bands.

REFERENCES

1. Salleh, M. K. M., G. Prigent, O. Pigaglio, and R. Crampagne, "Quarter-wavelength side-coupled ring resonator for bandpass filters," *IEEE Trans. Microwave Theory Tech.*, Vol. 56, No. 1, 156-162, 2008.
2. Buell, K., H. Mosallaei and K. Sarabandi, "A substrate for small patch antennas providing tunable miniaturization factors," *IEEE Trans. Microwave Theory Tech.*, Vol. 54, No. 1, 135-146, 2006.

Metamaterial-Inspired Displacement Sensor with High Dynamic Range

Zahra Shaterian, **Ali K. Horestani**, **and Christophe Fumeaux**

School of Electrical & Electronic Engineering, The University of Adelaide, Adelaide, Australia
zshaterian@eleceng.adelaide.edu.au

Abstract— Split Ring Resonators (SRRs) are ideal structures for realization of compact high resolution sensors because of their high quality factor resonance, compact size and sensitivity to changes in the constituent materials and physical dimensions. This article presents a displacement sensor based on broadside coupled SRRs coupled to a microstrip line. In contrast to previous SRR-based displacement sensors, the proposed sensor benefits from a high dynamic range limit and since the displacement sensing is based on the shift in the resonance frequency, rather than change in the depth of resonance, the proposed sensor benefits from a higher immunity to noise.

Metamaterials were originally proposed as artificially engineered bulk materials composed of electrically small particles that are able to create a specified material's effective permittivity and/or permeability [1]. The metamaterial basic elements, such as split ring resonators (SRRs), have also found applications for high-quality resonators [2] and compact filters [3]. Because of their high quality factor resonance, subwavelength dimensions, and the sensitivity of the resonance to the constituent materials and physical dimensions, SRRs are also appropriate to be used in the design of high sensitivity and high resolution sensors [4, 5, 6]. Recently, displacement sensors based on SRR-loaded coplanar waveguide (CPW) have been proposed [7, 8]. This paper proposes a displacement sensor based on a microstrip line loaded with broadside coupled SRRs (BC-SRRs). In contrast to the previous displacement sensors in which a fundamental dynamic range limit was dictated by the CPW's lateral dimension, the proposed sensor has virtually no dynamic range limit. It is also shown that the sensitivity of the sensor can be increased by using tipped SRRs.

Figures 1(a) and (b) illustrate the side and top view of the proposed displacement sensor, which is composed of a microstrip line loaded with a pair of BC-SRRs. Each BC-SRR is composed of two U-shaped split-rings printed on different layers, on top of each other and open in opposite directions. Note that in the proposed structure one of the rings is printed on the same layer as the microstrip line, so it is fixed, and the second one is on the top layer of a second substrate, which can be displaced along the direction of the microstrip line, as shown by the red arrows in the figure. The aim of the proposed sensor is to measure this displacement. The BC-SRR can be modeled as a parallel LC resonator [9], in which the equivalent capacitance corresponds to the capacitance of the overlapping metallic area of the two U-shaped rings and the equivalent inductance corresponds to the rectangular loop formed by the two U-shaped rings. In the configuration shown in the figure, an increase in the displacement d of the upper ring results in a decrease in the equivalent capacitance and an increase in the equivalent inductance of the BC-SRR. However, as will be shown in the simulation results, the change in equivalent capacitance is dominant, which results in shifting the resonance frequency to higher frequencies. The shift in the resonance frequency can therefore be used to sense the amount of displacement along the direction of the microstrip line.

Based on this sensor concept, a specific geometry is designed by electromagnetic simulations using Rogers RO4003 substrates with relative permittivity of 3.38 and copper metallization with thickness of $35\,\mu$m. The thickness of the bottom and top substrates are 1.524 mm and 0.203 mm, respectively. The width of the microstrip line is $w = 3.3\,\mathrm{mm}$ which corresponds to a $50\,\Omega$ characteristic impedance. The dimensions of the BC-SRRs are mentioned in the caption of Fig. 1.

Fig. 1(c) depicts the simulated transmission coefficients of the sensor for the displacement d varying from 0 mm to 9 mm in steps of 1 mm. The figure demonstrates the increase in resonance frequency for increasing displacement d. The resonance frequency can thus be used as measure for the amount of displacement. The dynamic range of the proposed sensor is not limited and can be increased by using longer BC-SRRs.

Fig. 1(d) and (e) illustrate the side and top view of an improved version of the sensor with tipped BC-SRRs in which, compared to the uniform BC-SRR, a higher rate of change of capacitance versus displacement is achieved. Fig. 1(f) depicts the simulated transmission coefficients of the sensor for the displacement d varying between 0 mm and 9 mm in steps of 1 mm. Comparing the total frequency shift for 9 mm displacement in Fig. 1(c) and (f), the sensor with tipped BC-SRRs achieve a 29% improvement in the displacement sensitivity in terms of frequency, i.e. 1060 MHz shift vs. 820 MHz shift for the sensor with uniform resonators.

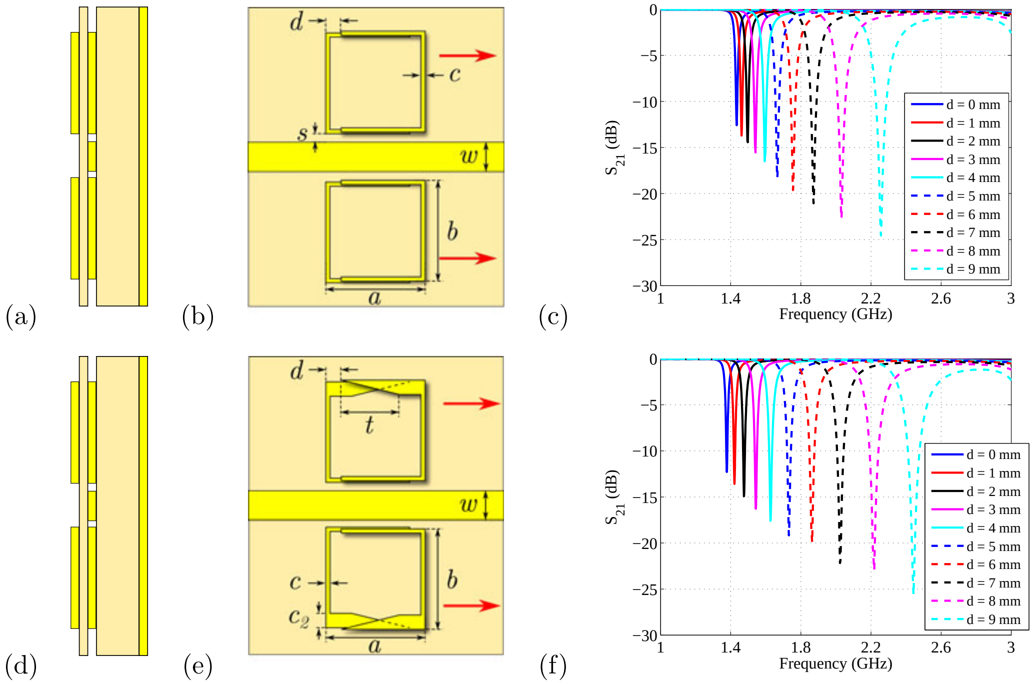

Figure 1: (a) Side view and (b) top view of the displacement sensor based on uniform BC-SRRs. Dimensions of the structure are $a = 10.2$ mm, $b = 12.4$ mm and $c = 0.4$ mm. (c) Simulated transmission coefficients of the structure for different displacements $d = 0$ mm to $d = 9$ mm in steps of 1 mm. (d) Side view and (e) top view of the displacement sensor based on tipped BC-SRRs. All dimensions are the same as in (b) except the tipped part of the resonator for which $c_2 = 3$ mm and $t = 7.7$ mm. (f) Simulated transmission coefficients of the structure for different displacements $d = 0$ mm to $d = 9$ mm in steps of 1 mm.

Conclusion

This work has presented a high dynamic range displacement sensor based on U-shaped BC-SRR. The proposed sensor benefits from a dynamic range that can be tailored to suit applications, without the limitations of previously published SRR-based displacement sensors. Furthermore, it has been shown that the sensitivity of the sensor can be significantly improved by using tipped BC-SRRs.

REFERENCES

1. J. J. Yang, M. Huang, and J. Sun, "Double negative metamaterial sensor based on microring resonator," *IEEE Sensors Journal*, vol. 11, no. 10, pp. 2254–2259, 2011.
2. A. Horestani, Z. Shaterian, S. Al-Sarawi, and D. Abbott, "High quality factor mm-wave coplanar strip resonator based on split ring resonators," in *36th International Conference on Infrared, Millimeter and Terahertz Waves (IRMMW-THz)*. IEEE, 2011, pp. 1–2.
3. A. Horestani, Z. Shaterian, W. Withayachumnankul, C. Fumeaux, S. Al-Sarawi, and D. Abbott, "Compact wideband filter element-based on complementary split-ring resonators," in *Smart Nano-Micro Materials and Devices*. International Society for Optics and Photonics, 2011, pp. 820 431–820 431.
4. M. Huang and J. Yang, "Microwave sensor using metamaterials," *Wave Propagation*, pp. 13–36, 2011.
5. W. Withayachumnankul, K. Jaruwongrungsee, C. Fumeaux, and D. Abbott, "Metamaterial-inspired multichannel thin-film sensor," *IEEE Sensors Journal*, no. 5, pp. 1455–1458, 2012.
6. S. A. Taya and M. M. Shabat, "Sensitivity enhancement in optical waveguide sensors using metamaterials," *Applied Physics A: Materials Science and Processing*, vol. 103, no. 3, pp. 611–614, 2011.
7. J. Naqui, M. Durán-Sindreu, and F. Martín, "Novel sensors based on the symmetry properties of split ring resonators (SRRs)," *Sensors*, vol. 11, no. 8, pp. 7545–7553, 2011.
8. A. Horestani, C. Fumeaux, S. Al-Sarawi, and D. Abbott, "Displacement sensor based on diamond-shaped tapered split ring resonator," *IEEE Sensors Journal*, in print 2013.
9. R. Marqués, F. Mesa, J. Martel, and F. Medina, "Comparative analysis of edge- and broadside-coupled split ring resonators for metamaterial design-theory and experiments," *IEEE Transactions on Antennas and Propagation*, vol. 51, no. 10, pp. 2572–2581, 2003.

Planar metamaterial-based MIMO Antennas

D. A. Ketzaki[1], **D. K. Ntaikos**[1], **I. T. Rekanos**[2] **and T. V. Yioultsis**[1*]
[1] Dept. of Electrical and Computer Engineering, Aristotle University of Thessaloniki, Greece
[2] Physics Div., Dept. of Mathematics, Physics, and Computational Sciences, Aristotle Univ.Thessaloniki, Greece
[*]corresponding author: traianos@auth.gr

Abstract-A systematic design of planar MIMO antennas with significantly reduced mutual coupling is presented, based on the concept of metamaterials. Split ring resonators are placed in the space between antenna elements, providing high levels of isolation without essentially affecting the simplicity and planarity of the antennas. The designs are further explained and justified by a rigorous parameter retrieval, based on a proper inverse problem methodology, thus addressing the problem of material characterization for 1D rows of resonators or single resonators.

The concept and application of metamaterials, i.e. periodic formations with synthetic material properties has drawn significant attention over the last years [1]. Among many applications, they have been utilized to enhance antenna characteristics, including metamaterial-based small antennas [2]. Metamaterial properties and particularly their ability to control electromagnetic wave propagation have been used to reduce mutual coupling in multiple-input multiple output (MIMO) antennas [3]. However, the resulting structures can be bulky and hard to fabricate. On the other hand, metamaterial properties seem to manifest themselves even at a single-cell level. This fact is utilized here to propose a systematic process and a series of designs for entirely planar metamaterial-enhanced MIMO monopole antennas, by properly placing split ring resonators (SRRs) in the space between individual monopoles.

The antenna design is based on the property of negative permeability, by first tracing the primary paths of wave propagation. The next step involves the design of the resonator elements to be placed between the antennas. The geometric parameters of the ring resonator are carefully selected by a finite-element based computational analysis to achieve resonance close to the frequency of 2.45 GHz. This will provide the basic mechanism to suppress the substrate modes that induce coupling. Finally, individual ring resonators are placed between the antennas, acting in a sense as a metamaterial “shell” or “screen” that can either enhance the individual antenna radiation properties or regulate coupling between them. We note that the applied parameter retrieval procedure addresses the problem of 1D rows of metamaterial unit cells or single SRRs, by a properly designed computational inverse problem formulation, as it is it is impossible to employ any simple slab EM analysis formulas in such a case. Thus, we attempt to address the fundamental question whether it is the periodic metamaterial aggregate that provides the meta-behavior or an indication of its properties can be traced at the level of rows of unit cells or single resonators.

The antenna designs are based on planar printed microstrip-fed monopole antennas (Fig. 1). The comparison between coupling before and after the insertion of the metamaterial structure is shown in Fig. 1a and 1b. Obviously, coupling is considerably reduced, while matching is also achieved in a wide frequency band. Most importantly, SRRs can be designed not only to reduce but also regulate coupling, with the aim of maximizing channel capacity (Fig. 1c).

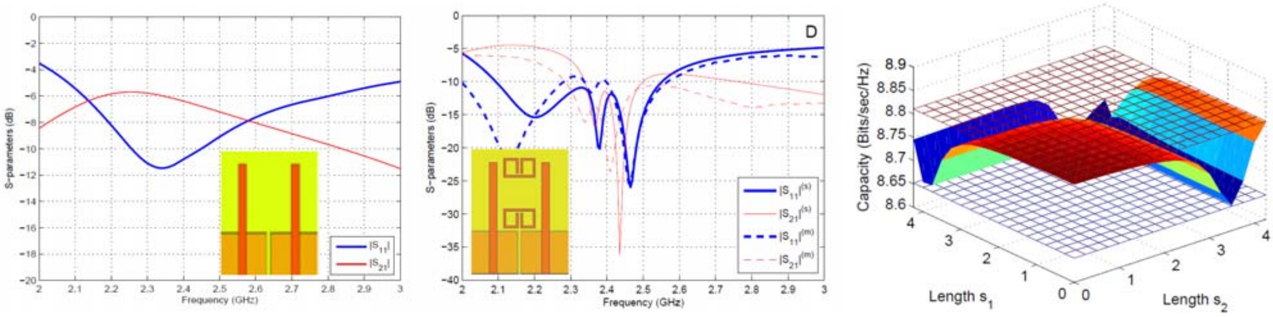

Fig. 1. Reflection and transmission (coupling) of the two element MIMO monopole antenna, (a) before and (b) after the insertion of the metamaterial structure. (c) Computed channel capacity for combinations of the SRR reentrant faces' lengths.

Other, more complex variations have been also fabricated, like the four-element ultra compact MIMO antenna (Fig. 2), where metamaterial samples are used to make individual elements compact, while other ones are invoked to result in particularly low values of correlation coefficients.

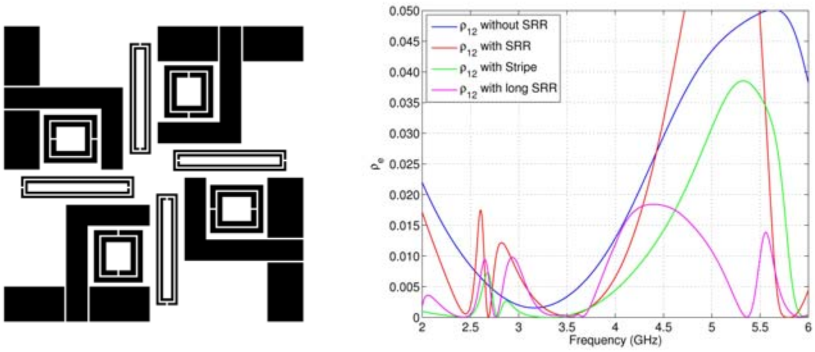

Fig. 2. A four element compact MIMO and the obtained values of correlation coefficients.

In general, the proposed design process is simple and straightforward, since it deals with the unit cell only, without the need of a complete optimization. The resulting antennas are entirely planar and simple to fabricate, thus being promising for modern MIMO-based wireless communications.

Acknowledgement: This research has been co-financed by the European Union (European Social Fund - ESF) and Greek national funds through the Operational Program "Education and Lifelong Learning" of the National Strategic Reference Framework (NSRF) - Research Funding Program: THALES: Reinforcement of the interdisciplinary and/or inter-institutional research and innovation (Project ANEMOS).

REFERENCES

1. Smith D. R., Padilla W. J.,. Vier D. C, Nemat-Nasser S. C. and Schultz S., "Composite medium with simultaneously negative permeability and permittivity," *Phys. Rev. Lett.*, vol. 84, no. 18, 4184–4187, 2000.
2. Erentok A. and Ziolkowski R. W., "Metamaterial-inspired efficient electrically small antennas," *IEEE Trans. Antennas Propag.*, vol. 56, no. 3, 691–707, 2008.
3. Bait-Suwailam M. M., Boybay M. S. and Ramahi O. M., "Electromagnetic coupling reduction in high–profile monopole antennas using single–negative magnetic metamaterials for MIMO applications," *IEEE Trans. Antennas Propag.*, vol. 58, 2894–2902, 2010.

Experimental demonstration of evanescent waves enhancement inside wire metamaterial slab

Alexey P. Slobozhanyuk, Irina V. Melchakova*, and Pavel A. Belov
National Research University of Information Technologies, Mechanics and Optics,
Kronverkskiy pr. 49, 197101, St. Petersburg, Russia
*corresponding author: melchakova-i@yandex.ru

Abstract- Being motivated by theoretical proposal of evanescent waves enhancement inside wire medium slab, we provide an experimental verification of this phenomenon in the microwave frequency range. The enhancement is originated by resonant pumping of standing waves inside the wire medium. Excellent agreement between the experimental data and numerical results is found.

The amplification of evanescent spatial harmonics inside of a wire medium slab with half-wavelength thickness has been predicted in [1]. The physics of the phenomenon are drastically different as compared to the amplification observed for the slabs of left-handed media [2]. The amplification of evanescent waves in the slab of left-handed material appears due to resonant excitation of the surface plasmons at the interfaces of the slab. This effect is extremely sensitive to the losses in the left-handed material. The amplification in wire medium slab happens because of resonant excitation of the standing waves inside of the slab, that is why this regime is not sensitive to losses in the metamaterial. The enhancement effect may be used for sub-surface imaging and creation of subwavelength imaging devices of new generation [3,4], including magnetic resonance imaging (MRI) systems and mechanical near-field microwave scanners.

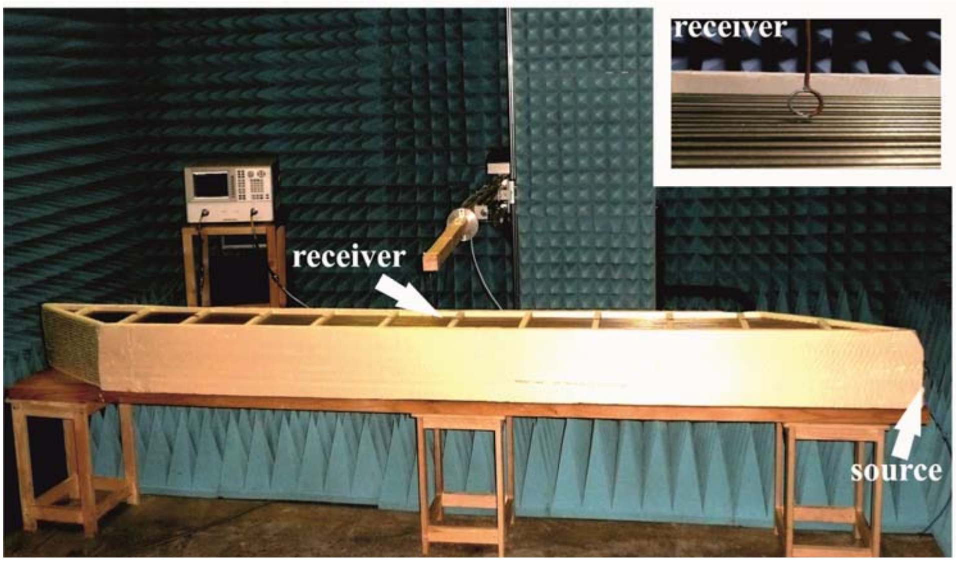

Fig.1: Experimental setup of measurement of magnetic field inside wire medium lens.

We designed a tilted wire medium lens [5, 6] as shown in Fig. 1, consisting of an array of 20×20 parallel brass wires with an equal length of 2,5 m. The period of the array is 10 mm. The radius of the wires is 1 mm.

The wires are supported by thin foam slabs with thickness of 20 mm and relative permittivity close to unity at the frequency of operation (60 MHz). The angle between the wires direction and the interface planes of the tilted lens is 30 degrees. The aperture of tilted lens is 200×400 mm^2.

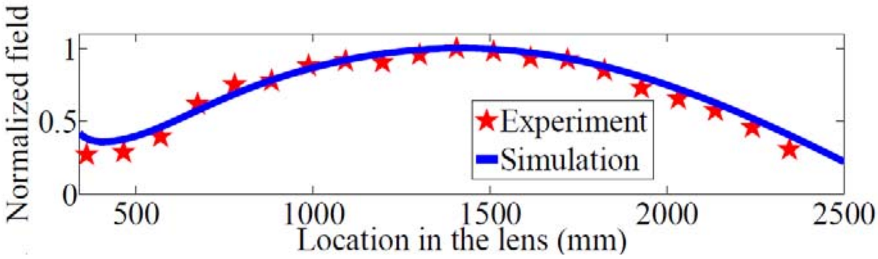

Fig. 2 Distribution of magnetic field inside wire medium lens

The lens was excited by a magnetic loop antenna, with radius 20 mm, which was placed at 3 mm distance from the front interface of the lens in the wires planes, so that the magnetic field of the loop is normal to the wires. The field distribution inside the lens was scanned by an automatic mechanical near-field scanner with magnetic probe (loop diameter 10 mm) made from a coaxial cable with 2 mm diameter and a vector network analyzer Agilent E8362C PNA. The results of the scan together with simulation results are shown in Fig.2. One can see that the evanescent waves of the source are dramatically enhanced by the wire medium slab. The maximum enhancement appears in the center of the lens.

We have experimentally verified the phenomenon of evanescent waves enhancement inside wire medium lens in the microwave frequency range. This phenomenon can be employed for improvement of the canalization regime of subwavelenth imaging by wire medium lenses [4] through using internal imaging approach [3]. Without any change in the structure, wire medium lenses are capable of imaging a source with sub-wavelength resolution located at certain distance from the device, but the image in this case has to be detected inside the slab. We suppose that this concept can be applied for improvement of magnetic resonance imaging through enhancement of amplitude of RF signal near detecting coil of the device and this will lead to application of wire metamaterials [4] in real industrial applications.

REFERENCES

1. Belov, P.A., Y. Zhao, Y. Hao, C. Parini, “Enhancement of evanescent spatial harmonics inside of materials with extreme optical anisotropy”, *Optics Letters*, vol. 34, 527-529, 2009.
2. Pendry, J. “Negative refraction index makes perfect lens”, *Phys. Rev. Lett.*, vol. 85, 3966-3969, 2000.
3. Zhao, Y., P.A. Belov and Y. Hao, “Subwavelength internal imaging by means of a wire medium”, *Journal of Optics A: Pure and Applied Optics*, Vol. 11, 075101 (1-6), 2009.
4. Simovski, C.R., P.A. Belov, A.V. Atrashchenko, Yu.S. Kivshar, "Wire metamaterials: Physics and Applications", *Advanced Materials*, Vol.24, No. 31, 4229-4248, 2012
5. Morgado, T. A. and M. G. Silveirinha, “Transport of an arbitrary near field component with an array of tilted wires”, *New J. Phys.*, Vol.11, 083023 (1-21), 2009.
6. Morgado, T. A., J. S. Marcos, M. G. Silveirinha and S. I. Maslovski, “Experimental verification of full reconstruction of the near-field with a metamaterial lens”, *Appl. Phys. Lett.* , Vol.97, 144102 (1-3), 2010.

Parallel Plate Lens
with Metal Hole Array for Terahertz Wave Band

Takehito Suzuki[1*], Hiroki Yonamine[1] , Takuya Konno[1], John C. Young[2], Keisuke Takano[3], and Masanori Hangyo[3]

[1]Department of Electrical & Electronic Engineering,
Ibaraki University, 4-12-1 Nakanarusawa, Hitachi, Ibaraki 316-8511, Japan
[2]Electrical and Computer Engineering, University of Kentucky, Lexington, Kentucky 40506-0046, USA
[3]Institute of Laser Engineering, Osaka University, 2-6 Yamadaoka, Suita, Osaka 565-0871, Japan
[*]E-mail: takehito@mx.ibaraki.ac.jp

Abstract- This paper presents the proposal and analysis of a parallel plate lens with metal hole array for the terahertz wave band. The full wave analysis at a design frequency of 0.5 THz is performed by Ansys HFSS. The fast wave effect can be controlled by the sizes of the hole array on the metallic plates and the width of the parallel plates. The light focusing due to the fast wave effect is verified by the analysis.

Optical devices for terahertz wave band from 0.1 to 10 THz are rapidly expanding and require better designs. It is not easy, however, to arbitrarily realize the desired refractive index using naturally-occurring materials. When materials are directly used as optical devices, the material properties themselves determine the optical characteristics. Typical lenses for the terahertz wave band are high density polymer lenses, Tsurupica lenses, and silicon lenses with refractive indices of 1.52, 1.56, and 3.41, respectively. Lenses composed of electromagnetic metamaterials have been proposed for microwave frequency bands in [1] and [2]. The work in [3] presents a metamaterial with an unnaturally high refractive index and that in [4] presents an antireflection coating in the terahertz wave band. The work in [5] proposes an artificial dielectric lens with metallic corrugated structures for the terahertz wave band. The fabrication of terahertz electromagnetic metamaterials by metallic processing and semiconductor etching is relatively easy compared with fabrication of metamaterials in the optical range since the dimensions of the unit element are on the order of microns. Furthermore, the unit cell of an electromagnetic metamaterial, which controls the refractive index, is of prime importance with respect to design flexibility and cost performance.

This paper proposes a parallel plate lens with a metal hole array as shown in Figure 1 and studies the focusing effect in the terahertz wave band. For a fixed y value, the hole radii increase in size along the x direction to a maximum value and then decrease again as shown in Fig. 1 (b). For all plates, the hole radii are constant along the propagation z direction for a fixed x direction. The separation of the parallel plates becomes wider toward the center of the lens as shown in Fig. 1 (c). The excitation is a TEM mode with E field parallel to the metallic plate such that TE_1 mode propagates as the dominant mode in the parallel plate. The fast wave effect [1], [6], which can produce a focusing effect, is controlled by the sizes of the holes and the separation of the parallel plates. Table 1 shows the lens parameters. The full wave analysis results shown in Figure 2 are obtained by Ansys HFSS, where the incident electric field is 1 V/m. The local maximum value is 6.2 times that of the incident wave at 1.02 mm (1.7λ) from the front of the lens. Due to symmetry, only one quarter of the analysis model is analyzed in order to reduce the problem size, and to further reduce analysis time. The dimensions of the full analysis model are small compared with those of the actual lens. The results verify that the parallel plate lens with metal hole array produces a focusing effect. We plan to fabricate this parallel plate lens with metal hole array and measure the focusing effect in the terahertz wave band.

ACKNOWLEDGMENT

This research was partially supported by a Grant-in-Aid for Scientific Research on Innovative Areas "Electromagnetic Metamaterial" (No. 23109505) from the Ministry of Education, Culture, Sports, Science and Technology (MEXT), Japan, the Strategic Information and Communications R&D Promotion Programme (SCOPE) (No. 122103011) from the Ministry of Internal Affairs and Communications, Accelerating Utilization of University IP Program (No. 439) from Japan Science and Technology Agency (JST), Program for Revitalization Promotion (No. 241FT0462) from Japan Science and Technology Agency (JST), the Takayanagi Memorial Foundation, the Yazaki Memorial Founda-tion for Science & Technology, and the Iketani Science and Technology Foundation.

REFERENCES

1. W. E. Kock, Bell Syst. Tech. J. **27**(1), 58-82 (1948)
2. S. S. D. Johns and J. Brown, Nature, **163**, 324-325 (1949)
3. M. Choi, et al., Nature 470, 369–374 (2011)
4. H.-T. Chen, et al., Phys. Rev. Lett. **105**, 073901-1–073901-4 (2010)
5. T. Konno, et al., Appl. Phys. A **109**(4), 1103-1108 (2012)
6. L. Josefsson, IEEE Trans. Antennas Propag., **41**(7), 845-850 (1993)

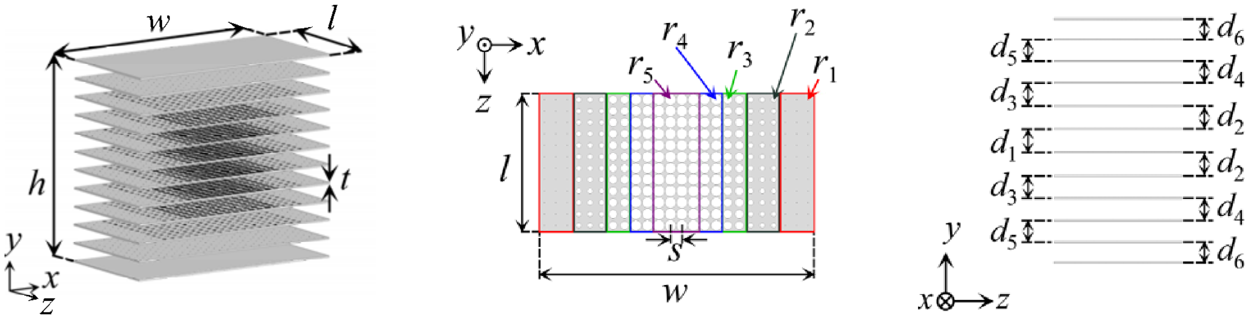

(a) Bird's-eye view (b) Top view (c) Side view

Fig. 1 Parallel plate lens with metal hole array.

Table 1 Lens parameters.

l	2.1 mm	d_1	360 µm
w	4.2 mm	d_2	350 µm
t	30 µm	d_3	340 µm
s	175 µm	d_4	330 µm
r_1	5.0 µm	d_5	320 µm
r_2	40 µm	d_6	310 µm
r_3	65 µm		
r_4	80 µm		
r_5	85 µm		

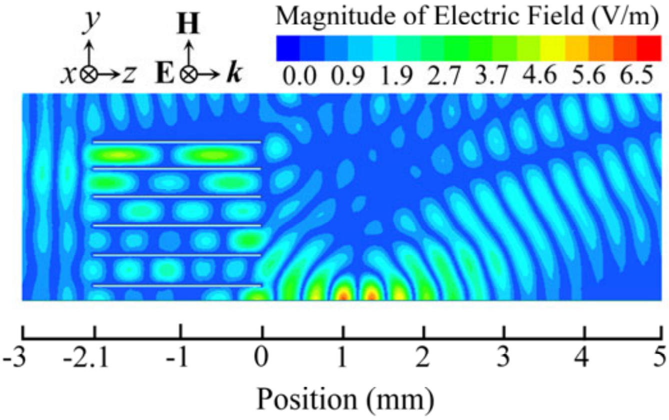

Fig. 2 Full wave analysis result.

A Novel Method for Implementation of the Waveguide Filters with Prescribed Transmission Zeros Using Metamaterial-Based Structures

H. S. Farahani *, A. Khaleghi, and R.A. Sadeghzadeh

Electrical and Computer Engineering Department, Khajeh Nasir Toosi University of Technology (KNTU), Tehran, Iran

**corresponding author, E-mail: sarbandifarahani@ee.kntu.ac.ir*

Abstract*- In this paper, a novel method for implementation of the waveguide filters with prescribed transmission zeros (TZs) is presented. The use of metamaterial-based periodic structure as an attractive way to mitigate the complexity of waveguide filter designs is proposed, evaluated and simulated. The main objective is to utilize metamaterial Groove and Ridge Gap waveguides and cavities to simplify the designing of the filters. A Ku-band filter with one and two prescribed TZs is designed and simulated to validate the proposed design procedure.*

Introduction*- the recent years, metamaterials periodic structures such as photonic band gap (PBG) has attracted numerous attentions of researchers all over the world due to their interesting characteristics [1]. By making some defects in the geometry of such periodic structures, the light propagation is suppressed along the specific direction and frequency bands. The PBGs have been investigated for waveguide, add-drop filters and many various applications [2]. The Groove and Ridge Gap waveguides and cavities are similar structure used for microwave frequencies [3]. In this paper, a new method for realization of the resonators required for the filter designs, along with cavities producing the prescribed TZs using groove and ridge gap structures are proposed for the first time. The full-wave high frequency structure simulator (Ansoft HFSS) and Computer simulation technology (CST) have been adopted to validate the primary claims.*

Proposed waveguide, cavity and filter design*- The proposed filter structure is comprised of both the groove and ridge gap structures. A ridge gap waveguide and several groove gap cavity resonators are shown in Fig. 1. The ridge and groove gap structures are basically made on a defected periodic structure, a bed of the metallic nails. It has been demonstrated in [3] that the ridge gap waveguide are comprised of two parallel metallic plates and in the bed of nails which exhibit good advantages of no electrical contact, simple and accurate design. As shown in Fig.1, periodicity, p, height, h, air gap, g and dimension of the nails are important parameters to achieve the required frequency band-gap in which the wave is suppressed. The important and optimized parameters of the designed filter are tabulated in Table. I. A schematic view of the proposed configuration for realization the filter with two cavities providing the prescribed zeros is shown in Fig. 1. Signal is propagated and suppressed along the ridge gap waveguide and between the periodic metallic nails, respectively. By placing the resonant cavities in the vicinity of the ridge gap waveguide, a part of the propagated EM wave corresponding with the resonant frequencies of the cavities is coupled into the cavities. It has been shown in our previous work that by placing a cavity in the vicinity of the ridge gap waveguide, the electromagnetic wave corresponding with the resonant frequency of the cavity is trapped in the cavity. Fig. 1, show the main idea of this paper so that by effectively employing the cavities, poles and zeros required for the filter design can be realized. In addition, the couplings between the resonant cavities are defined by changing the periodicity and/or* *height of the structure. Fig. 1(a) shows scattering parameters of the designed filter with two resonant cavities used for applying two prescribed TZs in the top and bottom of the pass band. It can be seen that good isolation, return and insertion loss have been achieved for the proposed structure.*

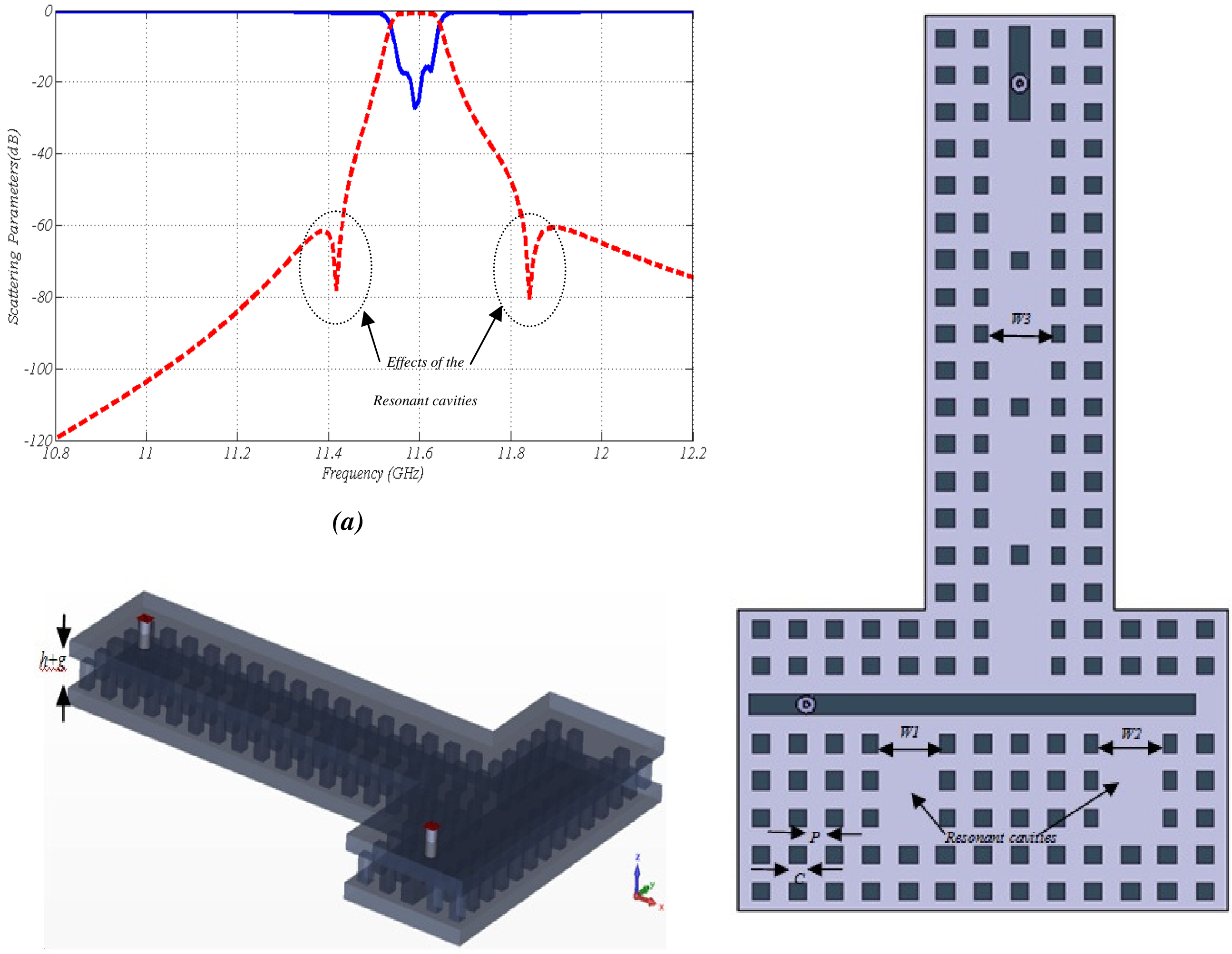

(a)

(b) ***(c)***

Figure 1: The proposed filters :(a) Scattering parameters, (b) Perspective and (c) Top, Schematic view.

TABLE I

Optimized Parameters of the Proposed Filter

Parameters	*C*	*g*	*h*	*W1*	*W2*	*W3*	*P*
Value(mm)	*3.9*	*1.3*	*6.5*	*14.5*	*15.5*	*14.55*	*4.5*

REFERENCES

1. *Y. Rahmat-Samii and F. Yang, "Electromagnetic Band Gap Structures in Antenna Engineering", Cambridge, U.K.,Cambridge Univ. Press, 2009.*
2. *M. Bahrami-Panah, H. S. Farahani, and A. Tadjali,"A Novel Tunable Photonic Crystal Filter Using Anisotropic Materials", IEEE APS-URSI, 2010.*
3. *A.U. Zaman, P.S. Kildal, and A. Kishk, "Narrow-Band Microwave Filter Using High-Q Groove Gap Waveguide Resonator With Manufacturing Flexibility and No Sidewalls", IEEE Trans.on Comp.,Packag & Manufac.Tech., 2012.*

Plenary Session

Magnet-less Non-Reciprocal Metamaterials

C. Caloz[1*], T. Kodera[2], and D. L. Sounas[2]

[1]École Polytechnique de Montréal, Montréal, Québec, H3T 1J4, Canada

[2]Yamaguchi University, Yamaguchi, Ube, 7558611, Japan

[*]corresponding author: christophe.caloz@polymtl.ca

Abstract - This paper presents a novel class of metamaterials, namely metamaterials exhibiting non-reciprocal gyrotropy without requiring a magnet. It describes the basic operation of this metamaterial and discusses some of its first applications.

Non-reciprocal microwave components, mainly isolators, circulators, gyrators, phase shifters, polarizers, switches, tunable resonators and tunable filters [1],[2], are ubiquitous in modern wireless applications, including communications, radar and sensor networks [3]-[5].

Over the past 60 years, the dominant technology for non-reciprocal microwave components has been based on ferrites, which are passive high-resistivity ferrimagnetic materials, such as YIG (yttrium iron garnet) or compounds of iron oxides and other elements such as aluminium, cobalt, manganese and nickel [1]-[3],[6]. However, ferrite components suffer of major drawbacks, associated with the ferrite materials and with the permanent magnet required to bias them: they are bulky, heavy, incompatible with integrated circuit technologies, expensive, sensitive to temperature detuning at lower microwave frequencies, and sometimes (case of ferromagnetic resonance based devices) inapplicable at higher microwave frequencies. Non-reciprocal active circuits intended to avoid these drawbacks have been reported [8]-[11], but they have served only as marginal alternatives to ferrite components due to fundamental issues.

Recently, we have proposed a magnetless non-reciprocal metamaterial (MNM) [12,13], which exhibits essentially the same properties as ferrites, including Faraday rotation, birefringence and field displacement, while overcoming the aforementioned drawbacks of ferrites. The principle of the MNM is illustrated in Fig. 1(a).

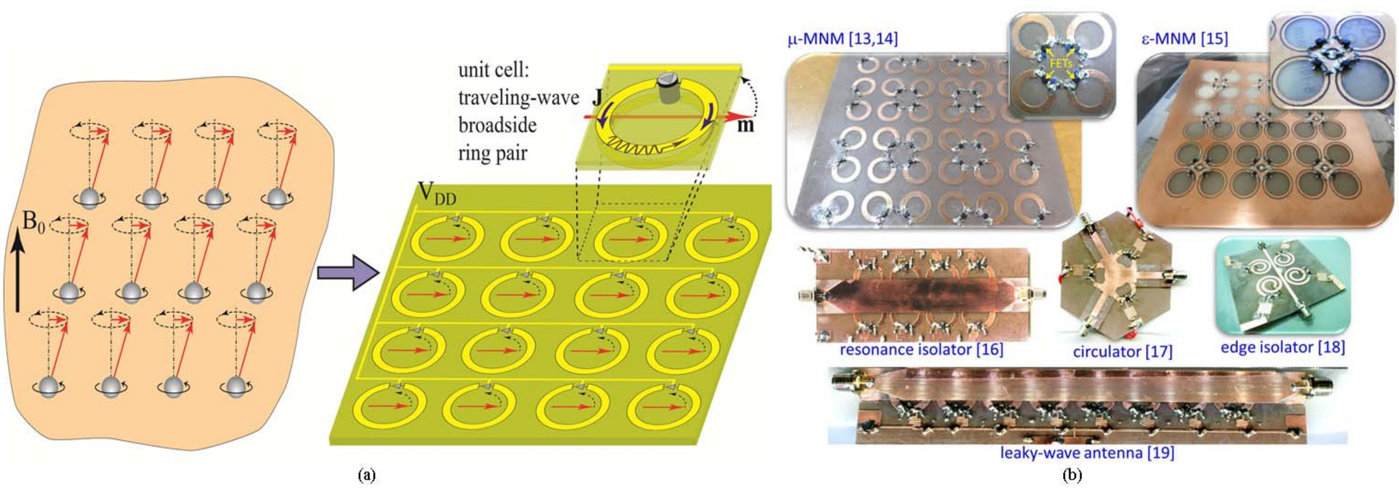

Fig. 1: (a) Principle of the magnet-less non-reciprocal metamaterial (MNM) (right), whose traveling-wave ring resonators support a rotating magnetic dipole moment mimicking precession in a ferrite material (left). (b) Proof-of-concept MNM structures and components.

The classical-picture current loops formed by spin electron precession in ferromagnetic materials is mimicked by electric current loops along conducting ring pairs loaded with a unilateral semiconductor component, typically a field-effect transistor (FET). The rotating magnetic dipole moments required for gyrotropy, and hence non-reciprocity, are produced in the mid-plane be-tween the two rings of each ring pair unit cell as a result of the traveling-wave propagation regime due to the FETs.

The MNM requires neither a ferrite nor a magnet. It is planar and has therefore a very low profile; it is lightweight, fully compatible with monolithic microwave integrated circuit (MMIC) technology, low-cost, insensitive to temperature detuning and applicable up to the upper millimeter-wave frequency range.

Its proof-of-concept has already been done in a number of structures and components [13]-[23], some of which are shown in Fig. 1(b), along with reference numbers. These applications include magnetic and electric MNM surfaces, resonance and edge isolators, circulators and non-reciprocal leaky-wave antennas, and many more applications will be devices in future. In addition to being a novel paradigm, the MTM represents a potentially disruptive technology to replace or/and complement existing ferrite-based non-reciprocal microwave components, as suggested by the interest of many companies.

Not requiring a magnet and being fully compatible with integrated circuits, MNMs have a great potential for microwave and millimeter-wave applications.

REFERENCES

[1] B. Lax and K. J. Button, *Microwave Ferrites and Ferrimagnetics*, McGraw Hill, 1962.

[2] A. Goldman, *Modern Ferrite Technology*, Springer, 2nd ed., 2010.

[3] D. M. Pozar, *Microwave Engineering*, Wiley, 4th ed., 2011.

[4] A. F. Molisch, *Wireless Communications*, Wiley-IEEE, 2nd ed., 2011.

[5] E. Lutz, M. Werner, and A. Jahn, *Satellite Systems for Personal and Broadband Communications*, Springer, 2000.

[6] A. G. Gurevich and G. A. Melkov, *Magnetization Oscillations and Waves*, CRC-Press, 1996.

[7] G. Carchon and B. Nanwelaers, "Power and noise limitations of active circulators," *IEEE Trans. Microw. Theory Tech.*, vol. 48, no. 2, pp. 316-319, Feb. 2000.

[8] Y. Ayasli, "Field effect transistor circulators," *IEEE Trans. Magn.*, vol. 25, no. 5, pp. 3242-3247, Sep. 1989.

[9] I. Bahl, "The design of a 6-port active circulator," *IEEE Trans. Magn. MTT-S Symp. Digest*, pp. 1011-1012, May. 1988.

[10] M. Smith, "GaAs monolithic implementation of active circulators," *IEEE Trans. Magn. MTT-S Symp. Digest*, pp. 1015-1016, May. 1988.

[11] S. Tanaka, N. Shimomura, and K. Ohtake, "Active circulators – the realization of circulators using transistors," *Proc. IEEE*, vol. 53, no. 3, pp. 260–267, March 1965.

[12] C. Caloz, T. Kodera, and D. Sounas, "Artificial magnetic material, artificial magnetic material device, artificial magnetic material reflecting wall, and artificial magnetic material transparent wall," *Patent* PCT/CA2011/001422, Dec. 2011, claiming priority over JP 2012-285353 (Dec. 2010).

[13] T. Kodera, D. L. Sounas, and C. Caloz, "Artificial Faraday rotation using a ring metamaterial structure without static magnetic field," *Appl. Phys. Lett.*, vol. 99, no. 3, pp. 031 114:1–3, Jul. 2011.

[14] D. L. Sounas, T. Kodera, and C. Caloz, "Non-reciprocal gyrotropic electrically–biased ring metasurface," *NC/USNC URSI National Radio Science Meeting*, Spokane, WA, USA, July 2011.

[15] T. Kodera, D. L. Sounas, and C. Caloz, "Faraday rotation by artificial electric gyrotropy in a transparent slot-ring metamaterial structure," in *IEEE AP–S Int. Symp.*, Chicago, IL, USA, July 2012.

[16] T. Kodera, D. L. Sounas, and C. Caloz, "Isolator utilizing articial magnetic gyrotropy," in *IEEE MTT–S Int. Microw. Symp. (IMS)*, Montréal, Canada, Jun. 2012.

[17] T. Kodera, D. Sounas, and C. Caloz, "Magnet-less Non-reciprocal ring metamaterial components," *under review*.

[18] T. Kodera, D. L. Sounas, H. V. Nguyen, H. Razavipour, and C. Caloz, "Field displacement in a traveling–wave ring resonator meta-structure," *XXXth URSI General Assembly and Scientific Symposium (GASS)*, Istanbul, Turkey, Aug. 2011.

[19] T. Kodera, D. L. Sounas, and C. Caloz, "Non-reciprocal magnet-less CRLH leaky-wave antenna based on a ring metamaterial structure," *IEEE Antennas Wirel. Propagat. Lett.*, vol. 10, pp. 1551–1554, Jan. 2012.

[20] T. Kodera, D. L. Sounas, and C. Caloz, "PEMC metamaterial surface whose gyrotropy is provided by travelling-wave ring resonators," *Int. Symp. Antennas Propag. (ISAP)*, Jeju, Korea, Oct. 2011.

[21] D. L. Sounas, T. Kodera, and C. Caloz, "Electromagnetic modeling of a magnet-less non-reciprocal gyrotropic metasurface," *IEEE Trans. Antennas propagat.*, *in press*.

[22] D. L. Sounas, T. Kodera, and C. Caloz, "Network modeling of multi-layer magnet-less non-reciprocal gyrotropic metamaterials," in *IEEE AP–S Int. Symp.*, Chicago, IL, USA, July 2012.

From classical to quantum kisses between optical nanoantennas

Javier Aizpurua
[1]Materials Physics Center (CSIC-UPV/EHU) and Donostia Int. Phys. Center (DIPC), San Sebastián, Spain
[*]aizpurua@ehu.es

Abstract-A review of the recent capabilities of strongly-coupled optical gap-nanoantennas as building blocks to provide near-field coherent control, ultrafast all-optical switching and addressing high-frequency transport, among others, will be provided. As separation distances between metallic nanoantennas reach subnanometric dimensions, strong nonlocal effects are triggered out and coherent electron tunneling between the nanoantenna blocks is produced. A quantum-corrected model revealing the quantum regime in tunneling plasmonics is described.

Optical gap-nanoantennas formed by strongly-coupled metallic nanoparticles provide the capability to tune the optical response on demand. A switch between a capacitive and conductive situation within the gap modifies the plasmonic modes allowing for a variety of applications such as all-optical switching, near-field coherent control of single emitters, or probing of transport properties at optical frequencies. Most of these effects can be tackled within a classical treatment of electrodynamics since the typical distances involved in the optical interactions of plasmonic gaps are nanometric.

As metallic nanoparticles come close together at subnanometric distances, the plasmonic nanogap enters a strong non-local regime. For separations of ~0.35nm electron quantum tunnelling across the gap modifies dramatically the optical response of the system. To account for the effect of the spill-out of the electrons at the surface of the metal as well as the coherent tunnelling that can be established across the gap, full quantum mechanical calculations of the optical response are necessary. However, quantum-mechanical calculations can tackle a limited number of electrons effectively limiting the size of the nanostructures that can be addressed. Time-dependent density functional theory (TDDFT) has been successfully applied to obtain the response of a few thousand electrons, but the billions of electrons present in a realistic plasmonic structure exceeds the current capabilities of quantum frameworks [1,2].

We present a new method to calculate quantum effects in large plasmonic systems based on parametric inputs derived from simpler full mechanical calculations. With this quantum corrected model (QCM) [3], it is possible to obtain extinction cross sections as well as near-field enhancements for situations involving subnanometric interactions, thus bridging the gap between classical and quantum plasmonics.

Furthermore, the quantum-corrected model has been successfully applied to describe the tunnelling regime in an experimental situation where two metallic particles are located in subnanometric proximity, almost kissing each other [4]. A simultaneous measurement of the transport properties and the optical characterization by dark-field microscopy allows for capturing the quantum regime in tunnelling plasmonics by means of a sudden blue-shift of the plasmonic modes as the gap distance is decreased. Classical descriptions fail to address the modal distribution and the field enhancement in plasmonic gaps separated by less than ~5 Å. The presence of quantum tunnelling screens the charge densities induced at the gap and reduces the field enhancement establishing a fundamental quantum limit to the minimum volume of a metallic cavity where light can be trapped.

Acknowledgements, Financial support from the ETORTEK project “nanoiker” from the Dept. of Industry of the Government of the Basque Country is acknowledged.

REFERENCES

1. Zuloaga J., Prodan E., and Nordlander P., “Quantum description of the plasmon resonances of a particle dimer", *Nano Lett.*, Vol. 9, 887 (2009).
2. Marinica, C., Kazansky A., Nordlander, P. Aizpurua, J. and Borisov, A.G., “Quantum plasmonics: nonlinear effects in the field enhancement of a plasmonic nanodimer”, *Nano Lett.*, Vol. 12, 1333, 2012.
3. Esteban R., Borisov A.G., Nordlander, P., and Aizpurua J., “Bridging quantum and classical plasmonics with a quantum-corrected model”, *Nat. Commun.*, Vol. 3, 825, 2012.
4. Savage K.J., Hawkeye M.M., Esteban R., Borisov, Aizpurua J., and Baumberg J.J., “Revealing the quantum regime in tunneling plasmonics”, *Nature*, Vol. 491, 574, 2012.

New frontiers for nanoplasmonic cavities

Stefan A Maier[1]
[1]Department of Physics, Imperial College London, London SW7 2AZ, UK

[*]corresponding author: s.maier@imperial.ac.uk

Abstract- Nanoplasmonic cavities, also known as optical nanoantennas, are efficient transducers from the far to the near field, harvesting light to the nanoscale. This talk will touch upon a variety of new concepts, including transformation optics design, non-local effects, direct imaging of ultra-confined modes, and new design geometries for broadband spectroscopies and nonlinear optics.

When metallic nanostructures come in close contact with each other, plasmon hybridization leads to the establishment of spatially highly confined optical fields, also known as electromagnetic hot spots. The mathematical framework of transformation optics has revolutionized our understanding of light localization on this deep sub-wavelength scale [1], demonstrating that cavities with structural singularities lead to a broadband light harvesting response. This talk will summarize our present understanding on how to exploit this framework for cavity design, highlighting both extensions towards practical structures, as well as fundamental physical limitations in performance due to non-local effects [2, 3].

We will then discuss the imaging of highly confined plasmon modes sustained by nanoantennas using electron energy loss spectroscopy (EELS). Examples of complete mode mapping of both bright and dark modes will be shown, focusing on structures with nanometric gaps at the limits of the classical electromagnetic treatment [3].

Lastly, practical applications of nanoantennas for nonlinear optics and sensing will be presented. Here we focus on two novel approaches, log periodic optical antennas for broadband second harmonic generation and spectroscopy [5, 6], and hybrid plasmonic-photonic cavities combining high spatial mode confinement with high quality factors typical of Fabry-Perot type resonators [7].

REFERENCES

1. Pendry, J.B., Aubry, A., Smith, D.R., & Maier, S.A., Transformation optics and subwavelength control of light, *Science* 337, 549 (2012)
2. Férnandez-Domínguez, A.I., Wiener, A. García-Vidal, F.J., Maier, S.A., & Pendry, J.B., A transformation optics description of non-local effects in plasmonic nanostructures, *Physical Review Letters* 108, 106802 (2012)
3. Ciracì, C., Hill, R.T., Mock, J.J., Urzhumov, Y., Fernández-Domínguez, A.I., Maier, S.A., Pendry, J.B., Chilkoti, A., & Smith, D.R., Probing the ultimate limits of plasmonics enhancement, *Science* 337, 1072 (2012)
4. Duan, H., Fernández-Domínguez, A.I., Bosman, M., Maier, S.A., & Yang, J.K.W., Nanoplasmonics:

classical down to the nanometer scale, *Nano Letters* 12, 1683 (2012)
5. Navarro-Cia, M., & Maier, S.A., Broad-band near-infrared plasmonic nanoantennas for higher harmonic generation, *ACS Nano* 6, 3537 (2012)
6. Aouani, H., Navarro-Cia, M., Rahmani, M., Sidiropoulos, T.P.H., Hong, M., Oulton, R.F., & Maier, S.A., Multiresonant broadband optical antennas as efficient tunable nanosources of second harmonic light, *Nano Letters* 12, 4997 (2012)
7. Schmidt, M.A., Lei, D.Y., Wondraczek, L., Nazabal, V., & Maier, S.A., Hybrid nanoparticle-microcavity-based plasmonics nanosensors with improved detection resolution and extended remote-sensing ability, *Nature Communications* 3, 1108 (2012), doi:10.1038/ncomms2109

Antenna-based Infrared Nanoscopy - From Nanoscale Chemical Identification to Real-Space Mapping of Graphene Plasmons

Rainer Hillenbrand
CIC nanoGUNE Consolider, San Sebastian, Spain
Ikerbasque, Basque Science Foundation, Bilbao, Spain
*corresponding author: r.hillenbrand@nanogune.eu

Abstract- Scattering-type scanning near-field optical microscopy brings the analytical power of visible, infrared and THz imaging and spectroscopy to the nanometer scale. The spatial resolution of about 10 - 20 nm opens a new era for modern nano-analytical applications such as chemical identification and near-field mapping of plasmonic structures. Recent applications in biospectroscopy, real-space imaging of graphene plasmons and antenna mode mapping will be presented.

Optical spectroscopy has tremendous impact in science and technology, particularly in the infrared (IR) and terahertz (THz) spectral range, where photons can probe molecule vibrations, phonons, as well as plasmons and electrons in non-metallic conductors. However, diffraction limits the spatial resolution to the micrometer scale, thus strongly limiting its application in nano- and biosciences. To overcome this drawback, we developed near-field microscopy based on elastic light scattering from atomic force microscope tips (scattering-type scanning near-field optical microscopy, s-SNOM) [1]. Collection of the tip-scattered light yields nanoscale resolved IR and THz [2] images, beating the diffraction limit in the terahertz spectral range by more than three orders of magnitude.

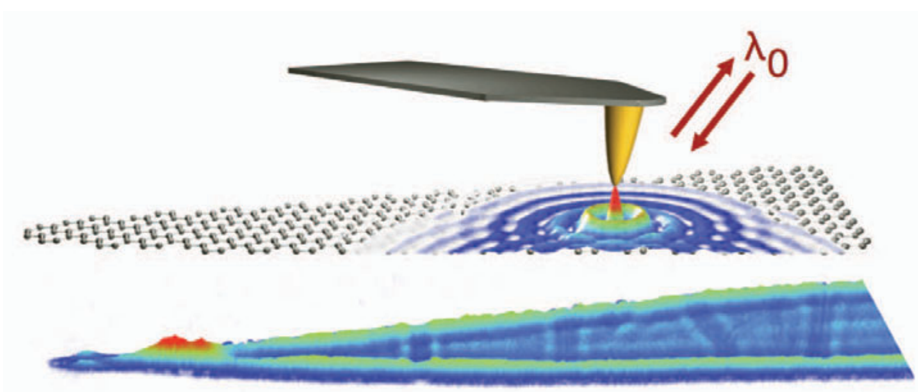

Figure 1: Figure: Optical nanoimaging of graphene plasmons. Upper panel: Sketch of the imaging method. A laser illuminated scanning tip launches plasmons on graphene. Detection is by recording the light backscattered from the tip. Lower panel: Optical image of graphene, where the fringes visualize the interference of the graphene plasmons.

For nanoscale infrared dielectric mapping and vibrational spectroscopy we employ metalized AFM tips acting as infrared antennas. The illuminating light is converted into strongly concentrated near fields at the tip apex (nanofocus), which provides a means for localized excitation of molecule vibrations, plasmons or phonons in the sample surface. Spectroscopic mapping of the scattered light thus allows for nanoscale chemical recognition of (bio)materials, mapping of free-carrier concentration in semiconductor nanodevices [2] and nanowires [3] or nanoimaging of strain.

Using broadband IR illumination and Fourier-transform (FT) spectroscopy of the tip-scattered light, we are able to record IR spectra with nanoscale spatial resolution (nano-FTIR), even when employing the weak radiation from an incoherent thermal source [4]. Particularly, we demonstrate that nano-FTIR can acquire near-field absorption spectra of molecular vibrations throughout the mid-infrared fingerprint region at a spatial resolution of 20 nm. To that end, we employ a novel laser-based continuum source and perform spectroscopic imaging and identification of polymer nanostructures [5]. First results on biological nanostructures such as viruses, membranes and fibrils will be presented.

s-SNOM also enables the launching and detecting of propagating and localized plasmons in graphene nanostructures (Fig. 1). Spectroscopic real-space images of the plasmon modes allow for direct measurement of the ultrashort plasmon wavelength and for visualizing plasmon control by gating the graphene structures [5,6].

Another application of s-SNOM is the imaging of the vectorial infrared near-field distribution of plasmonic nanostructures. In this application, a dielectric tip scatters the near fields at the sample surface, allowing for mapping the hot spots in plasmonic infrared gap antennas [8] or for verifying IR energy transport and compression in nanoscale transmission lines [9]. Combining s-SNOM and far-field spectroscopy of individual infrared-resonant nanoantennas, we verify experimentally the spectral shift between near- and far-field peak intensities.

REFERENCES

1. F. Keilmann, R. Hillenbrand, Phil. Trans. R. Soc. Lond. A 362, 787 (2004)
2. A. J. Huber, et al., Nano Lett. 8, 3766 (2008)
3. J. M. Stiegler, et al., Nano Lett. 10, 1387 (2010)
4. F. Huth, M. Schnell, J.Wittborn, N. Ocelic, R. Hillenbrand, Nature Mater. 10, 352 (2011)
5. F. Huth, et al., Nano Lett. 12, 3973 (2012)
6. J. Chen, et al., Nature 487, 77 (2012)
7. Z. Fei, et al., Nature 487, 82 (2012)
8. P. Alonso-González, et al., Nat. Commun. 3:684 doi: 10.1038/ncomms1674 (2012)
9. M. Schnell, et al., Nature Photon. 5, 283 (2011)

Homogenization of Wire Media for the Efficient Analysis of Practical Metamaterial Structures at Microwave and Terahertz Frequencies

A. B. Yakovlev[1*], S. I Maslovski[2], M. G. Silveirinha[2], C. S. R. Kaipa[1], G. W. Hanson[3], P. A. Belov[4,5], O. Luukkonen[6], I. S. Nefedov[7], C. R. Simovski[7], S. A. Tretyakov[7], Y. R. Padooru[1] and E. Forati[3]

[1]Dept. of Electrical Engineering, The University of Mississippi, Mississippi 38677-1848, USA

[2]Dept. de Eng. Electrotécnica da Universidade de Coimbra, Instit. de Telecomunicações, 3030 Coimbra, Portugal

[3]Dept. of Electrical Engineering, University of Wisconsin-Milwaukee, Milwaukee, WI 53211, USA

[4]National Research Univ. of Information Tech., Mechanics and Optics, St. Petersburg 197101, Russia

[5]School of Electronic Engin. and Computer Science, Queen Mary University of London, London, E1 4NS, UK

[6]Nokia Research Center, P. O. Box 407, FIN-00045 Nokia Group, Finland

[7]Aalto University, School of Electrical Engineering, P. O. Box 13000, 00076 Aalto, Finland

[*]corresponding author: yakovlev@olemiss.edu

Abstract – This review paper is intended to demonstrate that the interaction of electromagnetic waves with wire media based metamaterial structures can be analyzed in a simple and efficient manner, providing physical insight into exotic wave phenomena. The analysis is based on the homogenization theory of spatially dispersive wire media with additional boundary conditions derived for different interface scenarios. Various applications at microwave and terahertz frequencies are demonstrated, including subwavelength imaging, super lenses, Casimir forces in nanowires, artificial impedance surfaces, carbon-based nanomaterials, and many others.

We review our most recent advances in the homogenization theory of spatially dispersive wire media (WM) and focus on the analysis of complex WM based metamaterial structures at microwave and terahertz frequencies.

An important feature of WM is its ability to conduct electric current along the wires such that the wave propagation in WM is accompanied with the propagation of wave of conduction current. This results in the local accumulation of charge along the wires, leading to strong *spatial dispersion* (SD) in the WM at microwave and low-terahertz frequencies, and even in the quasi-static regime [1]. Various analytical and numerical approaches have been proposed for the analysis of WM based metamaterial structures, which in general lack physical insight or are limited to some canonical applications. Recently, a homogenization theory of WM, based on the quasi-static approximation that operates with the per-unit length inductance and capacitance of the wires has been developed [2], and the additional boundary conditions (ABCs) at various interfaces (including truncation, termination, lumped impedance insertions, resistive loads or graphene) have been formulated in a general framework [3,4]. The theory [2] is applicable to lattices of highly conducting wires at microwaves, as well as to plasmonic rods at THz and optics. In [3], a local framework for nonlocal WM has been proposed that introduces the additional degrees of freedom of the quasi-static model [2] (the wire additional potential and the wire current) into the classical macroscopic electromagnetic field equations. With this approach, boundary value problems involving WM, as well as point source radiation problems in WM can be solved in a simple and elegant way [5] because a non-uniform or truncated WM is described with a local system of first-order partial differential equations, in contrast to the spatially dispersive permittivity formulation [1] which leads to integral equations. A “local” model has also been developed based on the drift-diffusion equation, leading to a current density that includes both the local electric field via a local conductivity and the gradient of charge [6] (which accounts for spatial dispersion). The drift diffusion approach leads to an integro-differential equation that is much easier to solve than the usual convolution-type integral equation of nonlocal media; we show via measurements that this formulation provides good accuracy for three-dimensional wire medium scatterers.

With a general analytical framework developed for WM, here we demonstrate that exotic wave phenomena can be efficiently and accurately modeled in a wide frequency range. This includes wire lenses to provide a canalization of the near field to distances of several wavelengths at microwaves [7] and terahertz [8] frequencies, wire lenses based on the evanescent waves amplification [9], negative refraction phenomena [10], artificial mushroom-type impedance surfaces [11], broadband microwave absorbers with stable angle characteristics [4], periodic arrays of metallic carbon nanotubes [12], Casimir forces in nanowires [13], and many others.

REFERENCES

1. Belov, P. A., R. Marques, S. I. Maslovski, I. S. Nefedov, M. G. Silveirinha, C. R. Simovski, and S. A. Tretyakov, “Strong spatial dispersion in wire media in the very large wavelength limit,” *Phys. Rev. B*, v. 67, p. 113103, 2003.
2. Maslovski, S. I. and M. G. Silveirinha, “Nonlocal permittivity from a quasistatic model for a class of wire media,” *Phys. Rev. B*, v. 80, p. 245101, 2009.
3. Maslovski, S. I., T. A. Morgado, M. G. Silveirinha, C. S. R. Kaipa, and A. B. Yakovlev, “Generalized additional boundary conditions for wire media,” *New J. Phys.*, v. 12, p. 113047, 2010.
4. Padooru, Y. R., A. B. Yakovlev, C. S. R. Kaipa, G. W. Hanson, F. Medina, F. Mesa, and A. W. Glisson, “New absorbing boundary conditions and analytical model for multilayered mushroom-type metamaterials: Applications to wideband absorbers,” *IEEE Trans. Antennas Propag.*, v. 60, Dec. 2012 (in press).
5. M.G. Silveirinha and S.I. Maslovski, “Radiation from elementary sources in a uniaxial wire medium,” *Phys. Rev. B,* v. 85, pp. 155125(1-10), 2012.
6. Hanson, G. W., E. Forati, and M. G. Silveirinha, “Modeling of spatially-dispersive wire media: transport representation, comparison with natural materials, and additional boundary conditions,” *IEEE Trans. Antennas Propag.*, v. 60, pp. 4219-4232, Sept. 2012.
7. Belov, P. A., Y. Zhao, S. Tse, P. Ikonen, M. G. Silveirinha, C. R. Simovski, S. Tretyakov, Y. Hao, and C. Parini, “Transmission of images with subwavelength resolution to distances of several wavelengths in microwave regime,” *Phys. Rev. B*, v. 77, p. 193108, 2008.
8. Silveirinha, M. G., P. A. Belov, and C. R. Simovski, “Subwavelength imaging at infrared frequencies using an array of metallic nanorods,” *Phys. Rev. B*, v. 75, p. 035108, 2007.
9. Kaipa, C. S. R., A. B. Yakovlev, S. I. Maslovski, and M. G. Silveirinha, “Near-field imaging with a loaded wire media,” *Phys. Rev. B*, v. 86, p. 155103, 2012.
10. Silveirinha, M. G. “Broadband negative refraction with a crossed wire mesh,” *Phys. Rev. B*, v. 79, p. 153109, 2009.
11. Luukkonen, O., M. G. Silveirinha, A. B. Yakovlev, C. R. Simovski, I. S. Nefedov, and S. A. Tretyakov, “Effects of spatial dispersion on reflection from mushroom-type artificial impedance surfaces,” *IEEE Trans. Microwave Theory Tech.*, v. 57, pp. 2692-2699, Nov. 2009.
12. Nefedov, I. S. and S. A. Tretyakov, “Ultrabroadband electromagnetically indefinite medium formed by aligned carbon nanotubes,” *Phys. Rev. B*, v. 84, p. 113410, 2011.
13. Maslovski, S. I. and M. G. Silveirinha, “Mimicking Boyer’s Casimir repulsion with a nanowire material,” *Phys. Rev. A*, v. 83, p. 022508, 2011.

Nano-Plasmonics: Material Models and Computational Methods

Kurt Busch
Humboldt-Universität zu Berlin, Institut für Physik, AG Theoretische Optik & Photonik
Newtonstraße 15, 12489 Berlin, and
Max-Born-Institut, Max-Born-Straße 2A, 12489 Berlin, Germany
*corresponding author: kurt.busch@physik.hu-berlin.de

Abstract-An overview of the Discontinuous Galerkin Time-Domain with an emphasis on applications to nano-photonic systems is provided.

Nano-Photonic systems provide novel routes for controlling the propagation of light and light-matter interaction via large tailored dispersion relations, strong field confinement, and field enhancement effects. In view of the increasing sophistication of fabrication and spectroscopic characterization, quantitative computational approaches face challenges which include the adequate representation of complex geometries and the development of material models that describe the (potentially) strongly nonlocal and/or nonlinear optical response of the constituent materials as well as the strongly modified light-matter interaction that is mediated by them.

The recently developed Discontinuous-Galerkin Time-Domain (DGTD) method [1,2] represent an computational tool to address the above challenges within a time-domain approach. The adaptive finite-element meshing together with concurrent high-order spatial and temporal discretization allows quantitative analyses of nano-photonic systems [3,4,5,6]. Advanced feature include the efficient modeling of complex geometric features via curvilinear elements [7], the determination of electron-energy loss spectra from plasmonic systems[8,9]. In addition and owing to its nature as a time-domain method, DGTD allows for the realization of advanced material models that allow capture the above-mentioned nonlocal and nonlinear effects – for instance, by way of a hydrodynamic model of the conduction electrons in plasmonic systems.

REFERENCES

1. J. S. Hesthaven and T. Warburton, J. Comput. Phys. **181** (2002)
2. K. Busch et al., Laser Photonics Rev. **5**, 773 (2011)
3. J. Niegemann et al., J. Opt. A **11**, 114015 (2009)
4. J. Niegemann et al., Photon. Nanostruct. **7**, 2 (2009)
5. K. Stannigel et al., Optics Express **17**, 14934 (2009)
6. K. R. Hiremath et. Al. Optics Express **19**, 8641 (2011)
7. M. Husnik et al., Phys. Rev. Lett., in press
8. C. Matyssek et al., Photon. Nanostruct. **9**, 367 (2011)
9. F. von Cube et al., Optical Materials Express **1**, 1009 (2011)

Plasmonic Metamaterials for Enhanced Spectroscopy and Biosensing

H. Altug[1,3*], R. Adato[1.3], S. Aksu[2], A. E. Cetin[1], A. Artar[1]

[1]Department of Electrical and Computer Engineering, Boston University, 8 St. Mary's St. Boston, MA, USA
[2]Material Science and Engineering Division, Boston University, 8 St. Mary's St. Boston, MA, 02215, USA
[3] Bioengineering Department, Ecole Polytechnique Federale de Lausanne, CH-1015, Switzerland

[*]corresponding author: altug@bu.edu

Abstract- Biosensing technologies that can study biological systems and their dynamic interactions are important for understanding of fundamental biological process and our ability to diagnose and treat diseases. In this talk we demonstrate plasmonic metamaterials can be used to dramatically increase sensitivities of biosensors and infrared absorption spectroscopy technique thus enable to monitor monolayer of proteins and protein interactions in real-time within aqueous solutions.

Sensing of proteins and identification of their interactions is fundamental to our understanding of cellular biology and could greatly contribute to early diagnosis of complex diseases and as well as to the discovery of most effective drugs. Current toolkit for biosensing & spectroscopy is comprised predominantly of fluorescence, label free techniques and vibrational spectroscopy methods.

Fluorescence is one of the most popular techniques as it is sensitive & versatile. But there are some fundamental problems associated with it. Firstly, it relies on using fluorescent labels. Labels often sterically interfere with molecular binding interactions and lead to inaccurate measurements. Secondly, photo-bleaching and quenching of labels also cause further limitations for real-time and quantitative. To get around these issues, various label-free sensing techniques have been introduced, such as optical resonator based nanosensors relying on detection of resonance wavelength shifts. When a molecule sticks to the sensor surface the local refractive index increases, which results in red-shifting of the resonance wavelength. The nice feature here is that aside from having to capture the molecule, there's no label. And, most importantly, the frequency change is easily read out via a peak shift that can be directly and quantitatively related to a mass accumulation or height change in a molecular film.

Another label-free optical detection method is based on vibrational spectroscopy. These are based on the fact that every molecular bond has a set of vibrational modes associated with it. In the case of infrared spectrum, these modes directly result in absorption at specific frequencies. So the absorption in the IR gives spectra gives signal that is intrinsic to the most fundamental part of the sample – its molecular structure. This information is so desirable due to the fact that in biology, the theme of structure being intimately related to function is very important. This is especially true for proteins, which are critical because they are the primary machinery of living organisms. Structural information is important to a number of applications and fields, from fundamental biophysical questions to drug discovery. Unfortunately, most of these studies are limited to relatively large quantities of protein. Generally films a few um thick are needed due to sensitivity limitations. Fundamentally, this is because Beer's law governs the signal due to some absorbing molecule, so that it is reduced with path length to the point where it can be negligible for monolayers or single molecules. Additionally, due to the strong absorption of water in the IR, measurements in fluid are cumbersome, requiring specialized equipment and extremely high analyte concentrations. Plasmonic metamaterials supporting resonances at mid-IR wavelengths offer an attractive means with which to overcome many of these limitations. In particular, plasmonic resonances result in strongly enhanced near-field intensities confined to the surface of metallic particles, which allow one to dramatically increase the absorption signal of molecules.

In this talk we will describe by leveraging the engineered resonances obtained by top down fabrication of plasmonic nanostructures, we can dramatically increase sensitivity of infrared absorption spectroscopy and reliability detect absorption signals from even monolayers of proteins with high SNR [1]. We will show that using Fano-resonances of high Q-factors with asymmetrically designed nanoantennas, we can extract structural orientation of proteins [2-3]. We will then demonstrate multi-band nanoantennas, capable of simultaneously probing several vibrational bands [4].

References

[1] Adato et al., PNAS Vol. 106, pp 19227-18232 (2009).

[2] Wu et al., Nature Materials Vol. 11, pp 69-75 (2012).

[3] Aksu et al., to be submitted (2012).

[4] Chen et al., ACS Nano Vol. 6, pp 7998-8006 (2012)

Classical optics in a new light: Flat photonics based on metasurfaces

Federico Capasso

School of Engineering and Applied Sciences, Harvard University, USA

capasso@seas.harvard.edu

Abstract- Metasurfaces consisting of optically thin arrays of sub-wavelength-size and –spaced resonators such as optical antennas have unique potential to design the wavefront of the scattered light by local control of the amplitude, phase and polarization of the scattered light. Generalized laws of reflection and refraction have been demonstrated for such surfaces along with a new class of flat metadevices. Finally for surfaces with nanometer-thin coatings, in the presence of optical loss, classical thin film interference is dramatically modified leading to remarkable coloring of metals and to perfect absorption in a single VO_2 thin film, as the temperature is changed across the metal-insulator transition.

Conventional optical components such as lenses rely on gradual phase shifts accumulated during light propagation to shape light beams. We have recently shown how new degrees of freedom in optical design can be attained by introducing in the optical path abrupt phase changes over the scale of the wavelength [1], [2]. Such phase discontinuities enable wavefront engineering with unprecedented flexibility, which is promising for a wide variety of planar optical components. Specific devices that have been implemented will be discussed such as lenses free of spherical aberrations [3], axicons [3], background free broadband quarter wave plates [4], spiral phase plates that create optical vortices [5] and metasurfaces with giant birefringence [6].

We have recently also shown that the phenomenon of thin film interference, known for hundreds of years, which gives rise to vivid coloring when the thickness is on the scale of the wavelength, under appropriate conditions can persist in ultrathin, highly absorbing films of a few to tens of nanometres in thickness. We have demonstrated a new type of optical coating comprising such a film on a metallic substrate, which selectively absorbs various frequency ranges of the incident light [7]. These coatings have a low sensitivity to the angle of incidence and require minimal amounts of absorbing material that can be as thin as 5–20nm for visible light. This technology has the potential for a variety of applications from ultrathin photodetectors and solar cells to optical filters, to labeling, and even the visual arts and jewelry.

In a parallel and related study we have demonstrated that perfect absorption can be achieved in a system comprising a single lossy dielectric layer of thickness much smaller than the incident wavelength on an opaque substrate by utilizing the nontrivial phase shifts at interfaces between lossy media [8]. This design is implemented with an ultra-thin ($\sim\lambda/65$) vanadium dioxide (VO_2) layer on sapphire, temperature tuned in the vicinity of the VO_2 insulator-to-metal phase transition, leading to 99.75% absorption at $\lambda = 11.6\,\mu$m. In the vicinity of this transition VO_2 behaves like a tunable metamaterial with a refractive index that changes significantly with temperature. The structural simplicity and large tuning range (from ~80% to 0.25% in reflectivity) are promising for thermal emitters, modulators, and bolometers.

References

1. N. Yu, et al. *Science* **334,** 333 (2011)
2. F. Aieta, et al. *Nano Lett.* **12,** 1702 (2012)
3. F. Aieta et al. *Nano Lett.* Aug. 15, 2012; DOI**:** 10.1021/nl302516v
4. N. Yu et al. *Nano Lett.* Nov. 6, 2012; D**OI:** 10.1021/nl303445u
5. P. Genevet, et al. *Appl. Phys. Lett.* **100,** 13101 (2012)
6. M. A. Kats, *PNAS* **109**, 12364 (2012)
7. M. A. Kats et al. *Nature Materials* PUBLISHED ONLINE: 14 OCTOBER 2012 | DOI: 10.1038/NMAT3443
8. M. A. Kats et al. *Appl. Physics Lett.* **101**, 221101 (2012)

Anisotropic Plasmonic Metamaterials

Anatoly V Zayats

Department of Physics, King's College London, Strand, London WC2R 2LS, United Kingdon

email:a.zayats@kcl.ac.uk; http://www.nano-optics.org.uk

Guiding and manipulating light on length scales below the diffraction limit requires structural elements with dimensions much smaller than the wavelength. Recently, plasmonic metamaterials have been developed based on arrays of aligned gold nanorods and other anisotropic shapes, nanocrosses, slits, elliptical features. Such metamaterials provide a flexible platform with tuneable resonant optical properties across the visible and telecom spectral range. Such metamaterials, with a controllable and engineered plasmonic response, can be used instead of conventional plasmonic metals for designing plasmonic waveguides, plasmonic crystals, label-free bio- and chemo-sensors and for development nonlinear plasmonic structures with the enhanced nonlinearities. In this talk we will overview fundamentals and applications of anisotropic plasmonic metamaterial for controlling both intensity and polarization of light, including active control with temperature, loss/gain-induced anisotropy and magneto-optical properties. Plasmonic metamaterials allow one to achieve polarization manipulation in deep subwavelngth thin structures in both reflection and transmission, otherwise impossible with naturally occurring anisotropic materials.

1. M. Kauranen and A. V. Zayats, "Nonlinear plasmonics," *Nature Photonics, vol.* **6**, 2012, pp. 737-742.
2. P. Ginzburg, F. J. Rodríguez Fortuño, A. Martínez, A. V. Zayats, "Analogue of the quantum Hanle effect and polarisation conversion in non-Hermitian plasmonic metamaterials," Nano Lett. vol. 12, 2012, pp. 6309–6314.
3. J.-S. Bouillard, S. Vilain, W. Dickson, G.A. Wurtz, A.V. Zayats, "Broadband and broadangle SPP antennas based on plasmonic crystals with linear chirp," Sci. Rep. 2, 2012, 829.
4. Y. Veniaminova, A. A. Stashkevich, Y. Roussigné, S. M. Chérif, T. V. Murzina, A. P. Murphy, R. Atkinson, R. J. Pollard, A. V. Zayats, "Brillouin light scattering by spin waves in magnetic metamaterials based on Co nanorods," Opt. Mater. Expr. 2, 2012, pp. 1260-1269.
5. A. N. Poddubny, P. A. Belov, P. Ginzburg, A. V. Zayats, Yu. S. Kivshar, "Microscopic model of the Purcell enhancement in hyperbolic metamaterials," Phys. Rev. B, vol. 86, 2012, 035148.
6. J.-S. Bouillard, G. A. Wurtz, W. Dickson, D. O'Connor, A. V. Zayats, "Low-temperature plasmonics of metallic nanostructures," Nanoletters, vol. 12 , 2012, pp. 1561-1565.

Active Nanophotonic Metamaterials

From Loss-Compensation to Ultrafast Nano-Lasing

Ortwin Hess*
The Blackett Laboratory, Department of Physics, Imperial College London, SW7 2AZ, United Kingdom
*corresponding author: o.hess@imperial.ac.uk

Abstract-New theoretical insights and experimental advances show that quantum gain media may efficiently be integrated into nanophotonic metamaterials, compensating losses and allowing for ultrafast light sources on the nanoscale.

Nanophotonics and optical metamaterials have in the last decade emerged as a new paradigm in condensed matter optics and nanoscience, offering a fresh perspective to the optical world. They enable the efficient coupling of light fields to the nanoscale, the world of biological or other inorganic molecules [1]. This tight light localisation on truly nanoscopic dimensions enhances its interaction with mater, paving the way for a multitude of classical and quantum nano-optical applications. However, metal optics suffers from inherent dissipative losses, which have persistently hampered many of the envisaged applications. Advances in the theoretical understanding and experimental fabrication of gain-enhanced nano-plasmonics and optical metamaterials, now promise to lead to novel nanophotonic components and devices.

Recent theoretical [2,3] and experimental [4] works have recently shown that it is realistically possible to overcome dissipative losses of nanoplasmonic metamaterials, even in the exotic negative-index regime. Moreover, we have recently shown that the strong coupling of the excited (bright) modes of optical metamaterials to the radiative continuum opens up a broad window within which we can achieve full loss compensation and amplification in the steady-state regime [3].

When the gain supplied by the active medium embedded within the fabric of an active nano-fishnet metamaterial structure (inset, Figure 1) is sufficient to overcome dissipative and radiative losses, the nano-fishnet structure can indeed function as a coherent emitter of surface plasmons and light over the whole ultrathin 2D area, well below the diffraction limit for visible light [5,6]. Both, bright and dark plasmonic lasing states can be generated, coupling either strongly or weakly to the continuum. Which one eventually dominates can be controlled by the design of the metametaterial structure.

The dynamic, nonlinear competition between such lasing states is illustrated in Figure 1. One can clearly see the initial buildup of the bright-mode energy (external and internal; red), followed by the damped-amplitude, ps-period relaxation oscillations. The then leads to steady-state emission which is, however, interrupted (at around 50 ps) by the instability of the dark mode (only internal; yellow). Eventually, steady-state emission is reached again. This interplay of bright and dark light demonstrates that gain-enhanced nanoplasmonics and optical metamaterias constitute an exciting new frontier in nanophotonics and nanoscience, and are precursors towards active, intergrated quantum nano-optics [1].

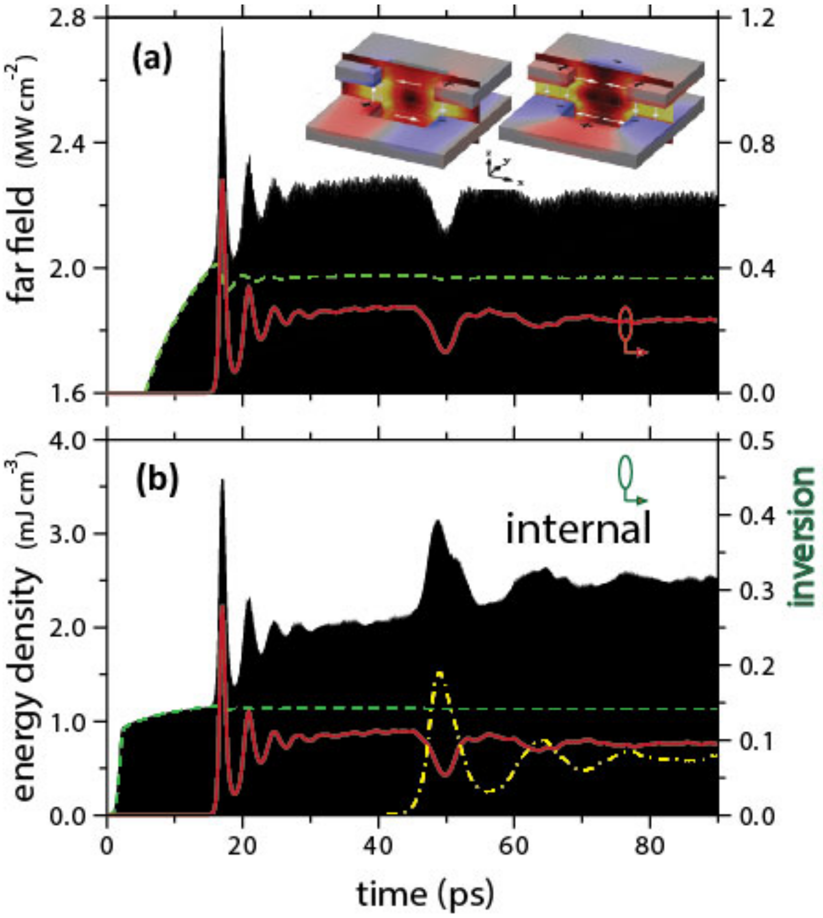

Figure 1: Dynamics of bright and dark lasing states in gain-enhanced nano-fishnet metamaterials. (a) External (far field emission). (b). Internal dynamics of the energy density of bright (red) and dark (yellow) light and inversion (green).

Moreover, bringing gain on the nanoscale is anticipated to improve the performance of a host of active nano-components, such as electro-optic modulators and light sources, but also passive ones, such as plasmonic waveguides or sensors featuring intensified plasmonic hotspots for single-emitter spectroscopy.

Acknowledgements, Support by the Leverhulme Trust and the EPSRC is gratefully acknowledged.

REFERENCES

1. Hess, O., et al., "Active nanoplasmonic metamaterials," *Nature Materials*, Vol. 11, 573 – 584, 2012.
2. S. Wuestner, A. Pusch, K. L. Tsakmakidis, J. M. Hamm, and O. Hess, Overcoming losses with gain in a negative refractive index metamaterial, *Phys. Rev. Lett.* **105**, 127401 (2010).
3. Hamm, J. M., S. Wuestner, K. L. Tsakmakidis, and O. Hess, "Theory of Light Amplification in Active Fishnet Metamaterials", *Phys. Rev. Lett.*, Vol. 107, 167405, 2011.
4. Xiao, S., *et al*., "Loss-free and active optical negative-index metamaterials". *Nature* Vol. 466, 735, 2010.
5. Pusch, A., S. Wuestner, J. M. Hamm, K. L. Tsakmakidis, and O. Hess, "Coherent Amplification and Noise in Gain-Enhanced Nanoplasmonic Metamaterials: A Maxwell-Bloch Langevin Approach", *ACS Nano* Vol. 6, 2420, 2012.
6. Wuestner, S., *et al*., "Control and dynamic competition of bright and dark lasing states in active nanoplasmonic metamaterials", Phys. Rev. B Vol. 85, 201406(R), 2012.

Electromagnetic surface wave manipulation by plasmonic metasurface

Wei Ting Chen[1,2], Yao-Wei Huang[1,2], Pin Chieh Wu[1,2], Kuang Yu Yang[2,3], Shulin Sun[2,4], Chia Min Chang[1,2,3,5], Ming Lun Tseng[1,2], Bo Han Cheng[3,6], Yen Ju Liu[2,3], Yueh-Hung Cheng[2], Chun Yen Liao[2], Hung-Kuei Tsai[2], Kuang Sheng Chung[2], Yu Lim Chen[2], Hung Yi Chung[3], Yung-Chiang Lan[6], Ding-Wei Huang[5], Ai Qun Liu[7], Chih-Ming Wang[8], Guang-Yu Guo[2], Lei Zhou[9], Din Ping Tsai[1,2,3,*]

[1]Graduate Institute of Applied Physics, National Taiwan University, Taipei 10617, Taiwan
[2]Department of Physics, National Taiwan University, Taipei 10617, Taiwan
[3]Research Center for Applied Sciences, Academia Sinica, Taipei 115, Taiwan
[4]National Center for Theoretical Sciences at Taipei, National Taiwan University, Taipei 10617, Taiwan
[5]Graduate Institute of Photonics and Optoelectronics, National Taiwan University, Taipei 10617, Taiwan
[6]Department of Photonics, National Cheng Kung University, Tainan 701, Taiwan
[7]School of Electrical and Electronic Engineering, Nanyang Technological University, Singapore
[8]Institute of Opto-electronic Engineering, National Dong Hwa University, Hualien 97401, Taiwan
[9]Physics Department, Fudan University, Shanghai 200433, China
[*]corresponding author: dptsai@phys.ntu.edu.tw

Abstract- Using plasmonic nanostructures to manipulate the scattered light from the SPP and free-space impinging waves is demonstrated. The curved arrangement of Au nanobumps can scattered the surface plasmon waves and focused into spots in three-dimensional space. The light can be modulated into desired light patterns. For the free-space impinging waves, a gradient meta-surface supports broadband (750-900 nm) anomalous light reflections at ~850nm wavelength with high conversion efficiency (~80%) is realized.

Using nanostructures to manipulate surface plasmon polariton (SPP) plane waves is an important issue. Recently, three-dimensional focusing and diverging of SPP waves by a quarter circular structure composed of Au nanobumps were studied [1]. The Au nanobumps confer additional three-dimensional propagating wave vectors (kx, ky, kz) on SPP wave for departing from surface. In this work, we manipulate the scattering of SPP waves by various plasmonic structures composed of arranged nanobumps on a gold thin film [2]. Upon controlling the geometry of the plasmonic structures, the height, position, and pattern of scattered light can be modified as desired. It provides a simple and efficient way to project a specific light pattern into free space, and demonstrate the capability of three-dimensional light manipulation.

Gradient-index meta-surfaces were found to exhibit extraordinary light-manipulation abilities, governed by a generalized Snell's law with an additional parallel wave vector provided by the radiation phase gradient of the meta-surface. Recently, we showed that a new type of gradient meta-surface can convert a propagating wave to a surface wave with 100% efficiency provided that the phase gradient is large enough, and experimentally verified the idea in the microwave regime [3]. In this work, we designed and fabricated a gradient meta-surfaces working in visible region (~850nm) with broad-band functionality (750-900nm), and demonstrated by both experiments and numerical simulations that it can redirect an input light to a non-specular channel with high efficiency (~80%) [4].

In summary, we introduce two ways of light manipulation by the designed plasmonic nanostructures.

Engineering the scattering properties of these nanostructures with the SPP or free-space impinging waves, the novel light-manipulation abilities can be achieved. Our results can lead to many practical applications, such as plasmonic beam splitters, three-dimensional plasmonic circuitry, holography, etc.

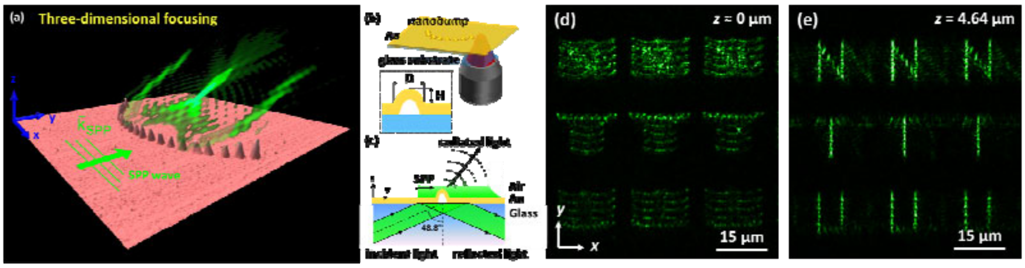

Figure 1: Schematic illustrations of (a) three-dimensional focusing, (b) laser processing for nanobump, and (c) the scattering from the interactions between SPP wave and an individual nanobump under TIR condition. The TIRM images of the designed structures observed at (a) z = 0 μm and (b) z = 4.64 μm, respectively.

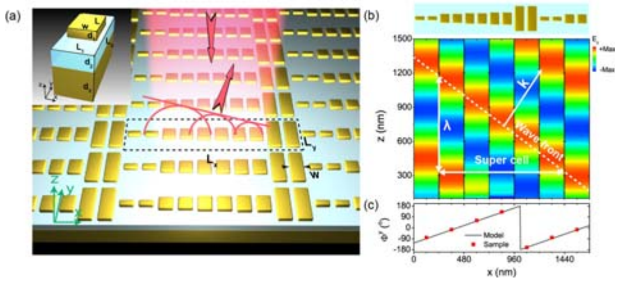

Figure 2: Schematic illustrations of (a) Geometry and working mechanism of our meta-surface. The designed sample consisting of Au nanorods (yellow) and a continuous Au film (yellow) separated by the MgF_2 spacer (blue). (b) FDTD simulated scattered Ey field patterns of the gradient meta-surface under the normal incident of a y-polarized light with λ = 850 nm (c) Reflection phase of each structural unit within a super cell.

Acknowledgements

The authors acknowledge financial support from *National Science Council*, Taiwan under grant numbers 100-2923-M-002-007-MY3, 101-2112-M-002-023-, 101-2911-I-002-107 and 101-3113-P-002-021- respectively. They are also grateful to *National Center for Theoretical Sciences*, Taipei Office, *Molecular Imaging Center of National Taiwan University*, *National Center for High-Performance Computing*, Taiwan, and *Research Center for Applied Sciences*, *Academia Sinica*, Taiwan for their support.

REFERENCES

1. C. M. Chang, C. H. Chu, M. L. Tseng, Y.-W. Huang, H. W. Huang, B. H. Chen, D.-W. Huang, and D. P. Tsai, “Light manipulation by gold nanobumps,” *Plasmonics*, Vol. 7, No. 3 563–569, 2012.
2. C. M. Chang, M. L. Tseng, B. H. Cheng, C. H. Chu, Y. Z. Ho, H. W. Huang, Y.-C. Lan, D.-W. Huang, A. Q. Liu, D. P. Tsai, “Three-Dimensional Plasmonic Micro Projector for Light Manipulation,” *Adv. Mater.*, Early View, DOI: 10.1002/adma. 201203308, 2012.
3. S. Sun, Q. He, S. Xiao, Q. Xu, X. Li, and L. Zhou, “Gradient-index meta-surface as a bridge linking propagating waves and surface waves,” *Nature Materials* Vol. 11, 426, 2012.
4. S. Sun, K.-Y. Yang, C.-M. Wang, T.-K. Juan, W. T. Chen, C. Y. Liao, Q. He, S. Xiao, W.-T. Kung, G.-Y. Guo, L. Zhou, and D. P. Tsai, “High-efficiency Broadband Anomalous Reflection of Light by Gradient Meta-surfaces,” *Nano Lett.* Vol. 12, 6223-6229, 2012.

Recent progress on numerical methods for metamaterial analysis

A Robustness Analysis of the Numerical Computation of Green's Dyadics in Bianisotropic Media

I. Bogaert

Ghent University, Belgium
Ignace.Bogaert@intec.UGent.be

Abstract— The robustness of a previously developed numerical algorithm for the computation of the four Green's dyadics in homogeneous bianisotropic materials is analyzed. The lossy bianisotropic materials are identified as a class of materials for which the numerical computation is provably robust. This is of practical importance because many bianisotropic materials are lossy.

The most general linear constitutive equations in classical frequency-domain electromagnetics are those of bianisotropic materials:

$$\boldsymbol{d}(\boldsymbol{r}) = \bar{\bar{\varepsilon}} \cdot \boldsymbol{e}(\boldsymbol{r}) + \bar{\bar{\xi}} \cdot \boldsymbol{h}(\boldsymbol{r}), \tag{1a}$$

$$\boldsymbol{b}(\boldsymbol{r}) = \bar{\bar{\zeta}} \cdot \boldsymbol{e}(\boldsymbol{r}) + \bar{\bar{\mu}} \cdot \boldsymbol{h}(\boldsymbol{r}). \tag{1b}$$

Therefore, piecewise homogeneous bianisotropic scatterers are the most general scatterers that can be handled with boundary integral equation methods. However, the absence of analytical expressions for the Green's dyadics poses a serious practical problem and has severely hindered the development of boundary integral equations for bianisotropic materials. It is worthwhile to point out that analytical expressions for Green's dyadics exist for many materials [1–3], but not for all of them.

To circumvent the need for analytical expressions, an all-numerical scheme to compute the Bianisotropic Scalar Green's Function (BSGF) was introduced in [4, 5]. The BSGF is defined as

$$G(\boldsymbol{r}) = \frac{1}{8\pi^3} \int_{\mathbb{R}^3} \frac{e^{j\boldsymbol{s}\cdot\boldsymbol{r}}}{D(\boldsymbol{s})} \mathrm{d}\boldsymbol{s}, \tag{2}$$

with $D(\boldsymbol{s})$ the so-called Helmholtz determinant [6]

$$D(\boldsymbol{s}) = \mathrm{Det}\left[\mathsf{P}(\boldsymbol{s})\right], \tag{3}$$

which is defined by means of the 6×6 matrix

$$\mathsf{P}(\boldsymbol{s}) = \begin{bmatrix} \bar{\bar{\varepsilon}} & \bar{\bar{\xi}} - \boldsymbol{s} \times \mathbb{1} \\ \bar{\bar{\zeta}} + \boldsymbol{s} \times \mathbb{1} & \bar{\bar{\mu}} \end{bmatrix}. \tag{4}$$

The symbol $\mathbb{1}$ denotes the 3×3 unit matrix, such that

$$\boldsymbol{s} \times \mathbb{1} = \begin{bmatrix} 0 & -s_z & s_y \\ s_z & 0 & -s_x \\ -s_y & s_x & 0 \end{bmatrix}. \tag{5}$$

It can be shown that the components of the Green's dyadics, which relate electric and magnetic currents with the electric and magnetic fields they generate, are linear combinations of at most fourth-order partial derivatives of this BSGF [4]. Hence, the numerical computation of the Green's dyadics can be accomplished if the BSGF and its derivatives (up to fourth order) can be numerically computed in a stable and efficient way.

It will now be shown that the integral in (2) can be computed in a robust manner if the bianisotropic material is lossy. A bianisotropic material is called lossy if

$$\Im\left\{\boldsymbol{V}^H \cdot \begin{bmatrix} \bar{\bar{\varepsilon}} & \bar{\bar{\xi}} \\ \bar{\bar{\zeta}} & \bar{\bar{\mu}} \end{bmatrix} \cdot \boldsymbol{V}\right\} < 0, \forall \boldsymbol{V} \in \mathbb{C}^6 \setminus \{\mathbf{0}\}. \tag{6}$$

The proof hinges on two properties:

- a sufficient speed of convergence to zero of $\frac{1}{D(\boldsymbol{s})}$ for $||\boldsymbol{s}|| \to \infty$ in every direction of $\mathbb{R}^3$.
- the nonexistence of real zeros for the Helmholtz determinant $D(\boldsymbol{s})$,

It is clear that, if both properties are satisfied, an adaptive integration routine can be applied to (2), which is very robust. The first property will be proved in the final version of this paper. The second property is proved by assuming that there exists a real zero $\boldsymbol{s}_0$ of the Helmholtz determinant and showing that this results in a contradiction. If

$$D(\boldsymbol{s}_0) = 0, \tag{7}$$

then, by the definition of the Helmholtz determinant (3), there exists a complex vector $\boldsymbol{V}_0 \in \mathbb{C}^6$ such that

$$\begin{bmatrix} \bar{\bar{\varepsilon}} & \bar{\bar{\xi}} - \boldsymbol{s}_0 \times \mathbb{1} \\ \bar{\bar{\zeta}} + \boldsymbol{s}_0 \times \mathbb{1} & \bar{\bar{\mu}} \end{bmatrix} \cdot \boldsymbol{V}_0 = \boldsymbol{0}. \tag{8}$$

Taking the imaginary part of the inner product with $\boldsymbol{V}_0^H$ yields

$$\Im\left\{\boldsymbol{V}_0^H \cdot \begin{bmatrix} \bar{\bar{\varepsilon}} & \bar{\bar{\xi}} - \boldsymbol{s}_0 \times \mathbb{1} \\ \bar{\bar{\zeta}} + \boldsymbol{s}_0 \times \mathbb{1} & \bar{\bar{\mu}} \end{bmatrix} \cdot \boldsymbol{V}_0\right\} = 0. \tag{9}$$

However, if $\boldsymbol{s}_0$ is real, then

$$\Im\left\{\boldsymbol{V}_0^H \cdot \begin{bmatrix} 0 & -\boldsymbol{s}_0 \times \mathbb{1} \\ \boldsymbol{s}_0 \times \mathbb{1} & 0 \end{bmatrix} \cdot \boldsymbol{V}_0\right\} = 0, \tag{10}$$

regardless of what $\boldsymbol{V}_0$ may be, because the matrix in between the two vectors is hermitian. Therefore, (9) simplifies to

$$\Im\left\{\boldsymbol{V}_0^H \cdot \begin{bmatrix} \bar{\bar{\varepsilon}} & \bar{\bar{\xi}} \\ \bar{\bar{\zeta}} & \bar{\bar{\mu}} \end{bmatrix} \cdot \boldsymbol{V}_0\right\} = 0, \tag{11}$$

which contradicts the criterium for lossyness (6). This robustness result for (2) immediately extends to the approach in [4, 5].

To conclude, the numerical computation of the BSGF and its derivatives is robust for all lossy bianisotropic materials. Since all passive bianisotropic materials exhibit at least some loss at nonzero frequencies, this shows that the numerical computation strategy introduced in [4, 5] has wide applicability, e.g. for modeling circulators or other microwave components.

ACKNOWLEDGMENT

The work of Ignace Bogaert is supported by a postdoctoral grant from the Fund for Scientific Research Flanders (FWO-Vlaanderen).

REFERENCES

1. F. Olyslager and I. V. Lindell, "A pedigree of bianisotropic media." in *Proceedings of the 8th International Conference on Electromagnetics of Complex Media (Bianisotropics 2000), 27-29 September 2000, Lisbon, Portugal*, 2000, pp. 153–158.
2. F. Olyslager and I. Lindell, "Electromagnetics and exotic media: a quest for the holy grail," *Antennas and Propagation Magazine, IEEE*, vol. 44, no. 2, pp. 48 –58, apr 2002.
3. I. Lindell and F. Olyslager, "Generalized decomposition of electromagnetic fields in bi-anisotropic media," *Antennas and Propagation, IEEE Transactions on*, vol. 46, no. 10, pp. 1584 –1585, oct 1998.
4. I. Bogaert, "Accurate Computation and Tabulation of the Scalar Green Function for'Bi-anisotropic Media and its Derivatives," in *Proceedings of the conference of the Applied Computational Electromagnetics Society*, Columbus, Ohio, USA, 10-14 April 2012.
5. ——, "Computing Green's Functions for Bianisotropic Materials," in *Proceedings of the International Conference on Electromagnetics in Advanced Applications*, Cape Town, South Africa, 2–7 September 2012.
6. B. Jakoby and F. Olyslager, "Asymptotic expansions for greens dyadics in bianisotropic media," *Progress on Electromagnetics Research*, vol. 12, pp. 277–302, 1996.

Selective mode suppression in microstrip differential lines by means of electric-LC (ELC) and magnetic-LC (M-LC) resonators

J. Naqui, M. Durán-Sindreu, and F. Martín*
GEMMA/CIMITEC, Departament d'Enginyeria Electrònica, Universitat Autònoma de Barcelona, 08193-BELLATERRA (Barcelona), Spain
*corresponding author: Ferran.Martin@uab.cat

Abstract-In this paper, it is demonstrated that the so-called electric-LC (ELC) resonators, and their dual counterparts, the magnetic-LC (MLC) resonators, are useful for the selective suppression of either the differential or the common mode in microstrip differential lines. The key point to mode suppression is the alignment of the electric (differential mode) or magnetic (common mode) walls of the line with the resonator. It is shown that by simply rotating the resonators 90^o we can selectively choose the suppressed mode at the resonator's fundamental resonance frequency. The theory is validated through full-wave electromagnetic simulation.

Split-ring resonators (SRRs) [1] and their complementary counterparts (CSRRs) [2] have been extensively used for the implementation of metamaterials and many devices based on them [3]. SRRs/CSRRs exhibit bianisotropy, and thus they can be excited by means of a uniform axial time-varying magnetic/electric field, or by means of an electric/magnetic field orthogonally applied to the symmetry plane of the particle. As compared to SRRs or CSRRs, the so-called electric-LC resonator, ELC (Fig. 1a) [4], or its complementary particle, the magnetic-LC resonator, MLC (Fig. 1b), do not exhibit bianisotropy. Moreover, such particles are bisymmetric, one of the symmetry planes being a magnetic wall and the other one being an electric wall at the fundamental resonance (see Fig. 1).

As it was discussed before [5], if a transmission line is loaded with a symmetric resonator with aligned symmetry planes, and the symmetry plane of the line and resonator are of the same nature (electric or magnetic walls), signal propagation at the fundamental resonance is inhibited (i.e., a transmission zero appears). However, the line is transparent if such symmetry planes are distinct. In particular, if we consider a microstrip differential line, there are 4 cases of interest for selective mode suppression, depicted in Fig. 2. In Figs. 2(a) and (b), the differential line is loaded with an ELC etched on the upper side of the substrate, with a relative orientation of 90^o between the loading elements. According to these orientations, it is expected that the structure of Fig. 2(a) is transparent for the common mode and produces a notch for the differential mode, contrarily to Fig. 2(b). In Figs 2(c) and 2(d), the differential line is loaded with an MLC resonator etched in the ground plane. In this case the situation is reversed since the electric and magnetic walls of ELCs and MLCs are interchanged.

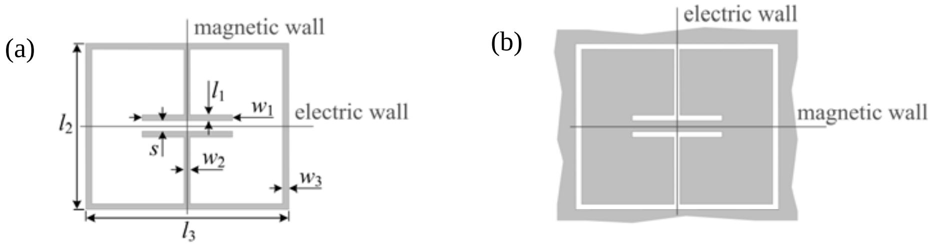

Figure 1. Typical topology of a ELC (a) and MLC (b) resonator. The nature of the symmetry planes is indicated.

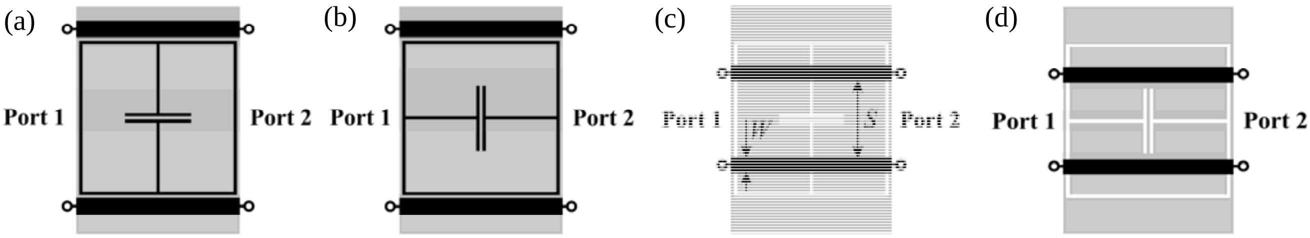

Figure 2. Microstrip differential line loaded with an ELC with the electric (a) and magnetic (b) wall aligned with the symmetry plane of the line, and microstrip differential line loaded with an MLC with the magnetic (c) and electric (d) wall aligned with the line. The substrate is *Rogers RO3010* with thickness h = 1.27 mm and dielectric constant ε_r = 10.2. Line dimensions are: W = 1.1 mm and S = 10.4 mm [(a) and (b)], and W = 1 mm and S = 5 mm [(c) and (d)]. Resonator dimensions are: w_1 = 4 mm, $w_2 = w_3 = l_1 = s$ = 0.2 mm, and $l_2 = l_3$ = 10 mm.

The transmission coefficients for the differential (S_{dd21}) and common (S_{cc21}) modes of the structures of Fig. 2 have been inferred by means of the *Agilent Momentum* commercial software. These results (depicted in Fig. 3), validate the selective mode suppression achievable in these differential lines by merely rotating the resonators 90^o. These resonators are of interest for the common mode noise suppression in such differential lines, or for the implementation of balanced notch filters.

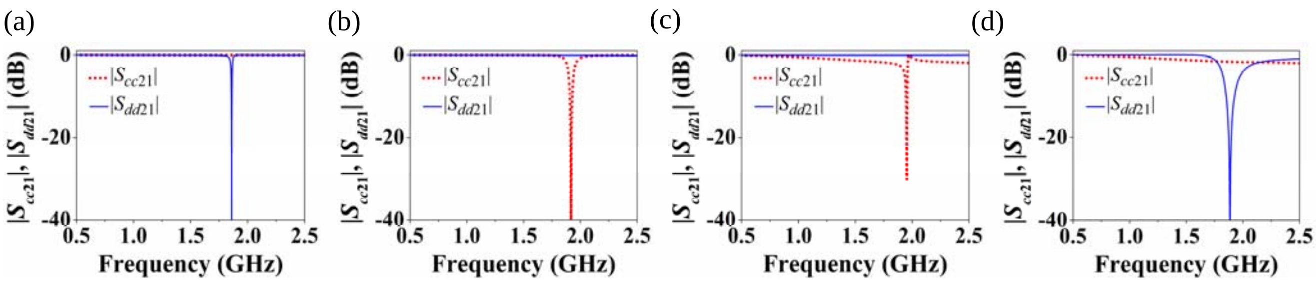

Figure 3. Transmission coefficient (full-wave EM simulation) of the structures depicted in Fig. 2.

Acknowledgements. This work has been supported by MINECO under projects CSD2008-00066, TEC2010-17512 and TEC2011-13615-E, and by AGAUR, through project 2009SGR-421.

REFERENCES

1. Pendry, J.B., *et al.*, “Magnetism from conductors and enhanced nonlinear phenomena”, *IEEE Trans. Microw. Theory Tech.*, vol. 47, pp. 2075-2084, Nov.1999.
2. Falcone, F, *et al.*, “Effective negative-epsilon stop-band microstrip lines based on complementary split ring resonators”, *IEEE Microw. Wireless Compon. Lett.*, vol. 14, pp. 280-282, June 2004.
3. Marqués, R.; Martín, F.; Sorolla, M., *Metamaterials with negative parameters: theory, design and microwave applications*, John Wiley & Sons Inc., USA, 2008.
4. Schurig, D.; Mock, J.J.; and Smith, D.R.; “Electric-field-coupled resonators for negative permittivity metamaterials.” *Appl. Phys. Lett.*, vol. 88, paper 041109, 2006.
5. Naqui, J., *et al.*, “Common mode suppression in microstrip differential lines by means of complementary split ring resonators: theory and applications”, *IEEE Trans. Microw. Theory Techn.*, vol. 60, pp. 3023-3034, Oct. 2012.

Enhanced circuit modeling of metasurfaces

F. Mesa[1], **R. Rodríguez-Berral**[1], **F. Medina**[2], **and M. García-Vigueras**[3]

[1]Dpt. of Applied Physics 1, University of Seville, Seville, Spain
[2]Dpt. of Electronics & Electromagnetism, University of Seville, Seville, Spain
[3]Lab. Electromagnetics & Acoustics, École Polytechnique Fédérale de Lausanne, Switzerland
mesa@us.es, rrberral@us.es, medina@us.es, mariagv1@gmail.com

Abstract— This paper presents some recent advances in the circuit modeling of 1-D and 2-D periodic metasurfaces. Most of these advances are focused in the obtaining of a fully-analytical equivalent circuit model for the scattering of an obliquely-incident plane wave on a metasurface composed of a periodically patterned metallic surface embedded in a layered dielectric environment. Our approach also provides the "exact" topology of the network that models the reflection/transmission effects of the metasurface.

Recently the authors have presented in [1] a fully analytical equivalent circuit to model the scattering of an obliquely incident plane on a 1-D periodic array of strips/slits in a metal screen embedded in a multilayered dielectric environment. As shown in Fig. 1(a), the periodicity of the problem under consideration allows us to view the original scattering problem as a problem of a waveguide with certain discontinuities (Fig. 1(a) shows the particular case of normal incidence and magnetic field parallel to the direction of the slits). The validity of the approach in [1] extends up to frequencies well inside the grating-lobe regime provided that the ratio of the obstacle with respect to the operating wavelength is small (roughly $d/\lambda_0 \lesssim 1/5$; several examples showing the accuracy and range of validity of this approach can be found in [1]). It should be noted that this approach can give the reflection/transmission properties of the metasurface in different frequency ranges (low-frequencies, microwaves, millimeter waves, Terahertz) as long as the material characteristic (dispersion, losses,...) are included in the lumped elements of the network. This can easily be done for dielectric losses and ohmic losses under the strong skin effect approximation, but not when the metallic parts of the screen cannot be considered as good conductors. In this latter case, other simplified analysis could be carried out [2].

In the previous problem, the thickness of the metallic screen was neglected. However, this thickness and even certain internal structure inside the metallic screen can readily be accounted for by an appropriate cascade of lumped elements and transmission-line sections, as shown in Fig. 1(b). The capacitances that appear in the corresponding equivalent circuit can be found in closed form. As an example of the efficiency of the equivalent circuit approach Fig. 2(a) shows the transmission spectrum given by our analytical approach and HFSS for the structure shown in the inset of the figure.

The equivalent circuit approach can also be extended to metasurfaces with 2-D periodicity. Although this topic has been studied for long time for many antenna applications [3], a renewed interest arose since the discovery of the extraordinary transmission phenomenon. A previous approach reported by some of the authors in [4] has recently be extended in [5] to deal with layered dielectric environment and non-rectangular holes/scatterers. In the present work it is shown in Fig. 2(b) the practical case of a metasurface composed of a 2-D periodic array of rectangular metallic dipoles printed on a metal-backed dielectric substrate. Following the guidelines in [5] (with just $N_{\mathrm{TE}} = 1, N_{\mathrm{TM}} = 0$) we have obtained a very good agreement between our results and those given by HFSS (the effect of the ground plane is implicitly taken into account in our approach).

All the above equivalent circuits can be very useful for the design/analysis of metasurfaces since we have provided fully analytical approaches to find both the topology of the network of lumped elements and the values of the necessary parameters.

ACKNOWLEDGMENT

This work has been supported by the Spanish Ministerio de Ciencia e Innovación and European Union FEDER funds (projects TEC2010-16948 and Consolider CSD2008-00066).

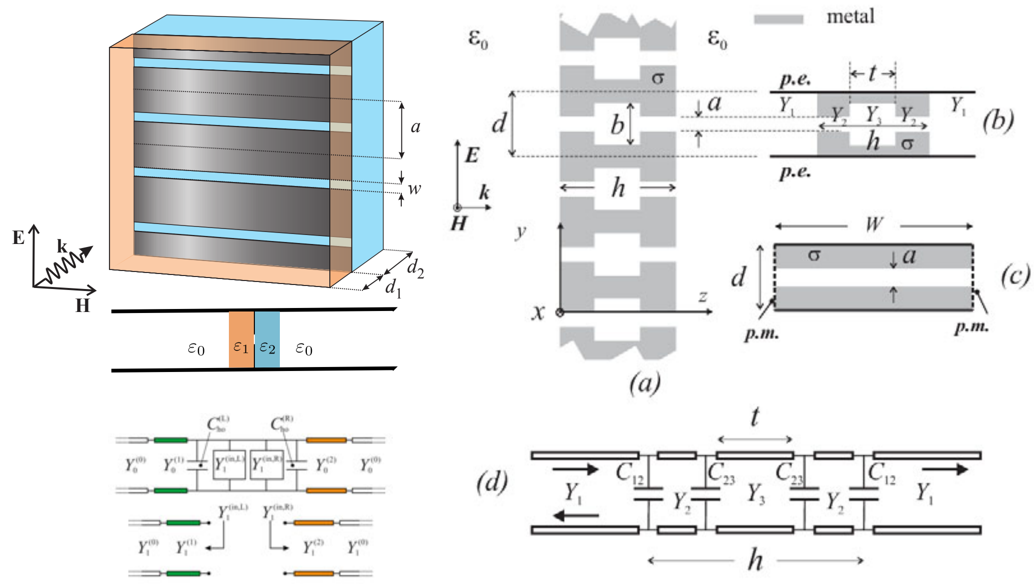

(a) (b)

Figure 1: Equivalent circuits of the scattering of a plane wave by a 1-D periodically slitted metallic screen of (a) zero thickness embedded in a layered dielectric environment and (b) non-zero thickness and an eventual internal structure.

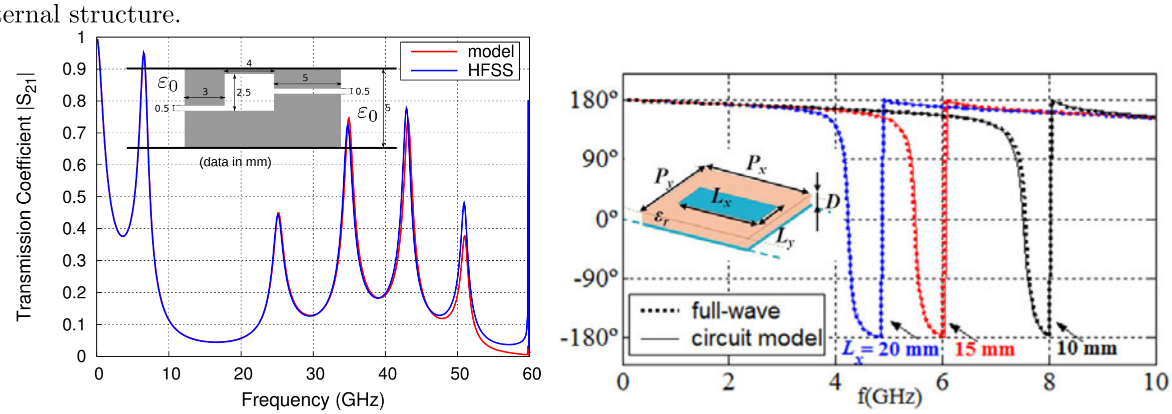

(a) (b)

Figure 2: (a) Magnitude of the transmission coefficient of a normally incident plane wave on a 1-D metallic metasurface [see Fig. 1(b)] with the internal structure shown in the inset. (b) Phase of the reflection coefficient of an obliquely incident plane wave (30°) on a 2-D array of metallic dipoles ($P_x = P_y = 30$ mm, $L_y = 10$ mm) printed on a grounded substrate with $\varepsilon_r = 3$ and $D = 1.524$ mm (Rogers substrate RO4230).

REFERENCES

1. Rodríguez-Berral, R., C. Molero, F. Medina and F. Mesa, "Analytical wideband model for strip/slit gratings loaded with dielectric slabs," *IEEE Trans. Microw. Theory Techn.*, Vol. 60, No. 12, 2012.
2. Delgado, V and R. Marqués, "Surface impedance model for extraordinary transmission in 1D metallic and dielectric screens," *Opt. Exp.*, Vol. 19, No. 25, 25290-25297, 2011.
3. Munk, B.A., *Frequency Selective Surfaces: Theory and Design*, John Wiley, 2000.
4. Medina, F., F. Mesa and R. Marqués, "Extraordinary transmission through arrays of electrically small holes from a circuit theory perspective," *IEEE Trans. Microw. Theory Techn.*, Vol. 56, No. 12, 3108-3120, 2008.
5. García-Vigueras, M., F. Mesa, F. Medina, R. Rodríguez-Berral and J. L. Gómez-Tornero, "Simplified circuit model for arrays of metallic dipoles sandwiched between dielectric slabs under arbitrary incidence," *IEEE Trans. Antennas Propag.*, Vol. 60, No. 10, 4637-4649, 2012.

Multifrequency and Low Profile Metamaterial-Inspired Antennas

S. DAKHLI[1, 2]. H. RMILI[3*], J. M. FLOC'H[4], F. CHOUBANI[1] and K. MAHDJOUBI[2]

[1]Innov'Com Laboratory, SUPCOM,University of Carthage, Tunis, Tunisia.

[2]IETR, University of Rennes 1, #263, Av. Général Leclerc, CS 74205, 35042 Rennes Cedex, France.

[3]King Abdulaziz University, Electrical and Computer Engineering Department, Jeddah, Saudi Arabia.

[4]IETR, INSA, #20 avenue buttes des coësmes, 35043 Rennes Cedex, France.

[*]Hatem RMILI: hmrmili@kau.edu.sa

Abstract-In this paper several low profile and multifrquency metamaterial inspired antennas are designed. All these antennas are based on the electric coupling between the parasitic element and the driven monopole element. The simulated and measured results of the return loss are given. Results dealing with of efficiency and radiation patterns are under study.

1. Introduction

The rapid progress of wireless devices for communication has increased the requirement of efficient, low profile, light weight and low cost electrically small antennas [1]. In this work, we use new type of parasitic elements with different shapes in order to obtain a multifrequency behavior. This technique leads to new resonance frequencies lower than that of the exciting monopole. Three families of antennas are studied: each one is composed of a monopole antenna and parasitic element(s).

2. Antennas Design and Fabrication

Figure.1 presents the structures of the proposed antennas A1, A2 and A3. For all these antennas, we have used a Rogers Duroid TM 5880 substrate of thickness 0.8mm and relative permittivity $\varepsilon_r = 2.2$, and a monopole antenna of length 25mm and width 1.5mm, with a resonance frequency of 2.45GHz and a bandwidth of 400MHz. The antennas are simulated by ANSYS-HFSS software.

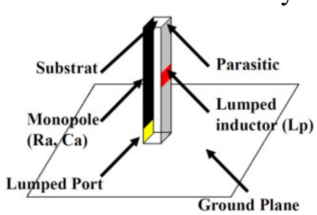

Antenna A1 [2]

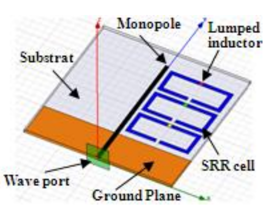

Antenna A2

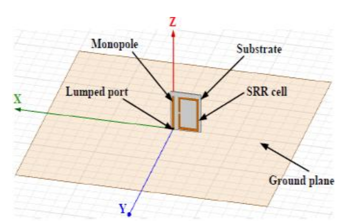

Antenna A3

Figure 1. The structures of the three proposed antennas.

Antenna A1

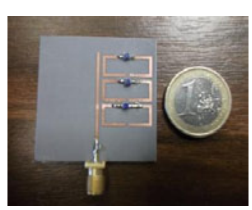

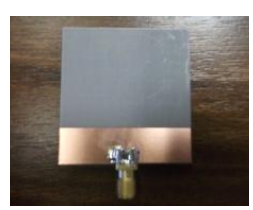

Antenna A2: Top View ; Bottom View

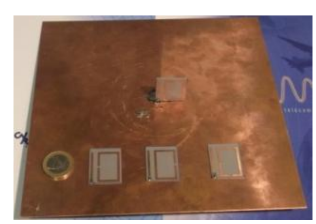

Antenna A3

Figure 2. Photos of the realized prototypes.

3. Equivalent Circuit Model

An equivalent circuit model (Fig.3) is proposed in order to describe the operation of the antenna system.

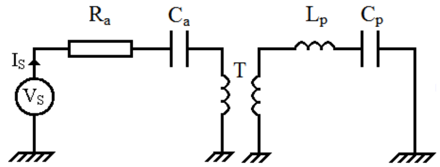

Figure.3. Equivalent circuit model of the antenna system.

To a lower frequency, the monopole and the coupling elements are electrically small. The monopole acts as a RC circuit (R_a,C_a). Whereas the parasitic element acts like a LC circuit (L_p,C_p).The coupling between the two elements is ensured by a transformer T. The resonant frequency of the circuit model is approximately [3]:

$$f_{res} = \frac{1}{2\pi}\sqrt{\frac{C_a+C_p}{L_p(C_a C_p)}} \qquad (1)$$

4. Results

Figure.4 illustrates the measured and simulated return loss for the different antennas.

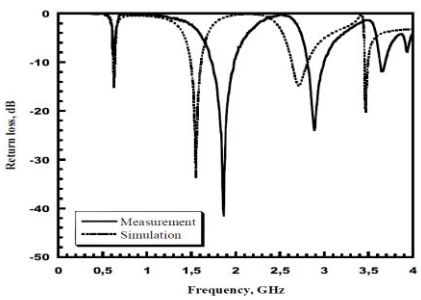

Antenna A1

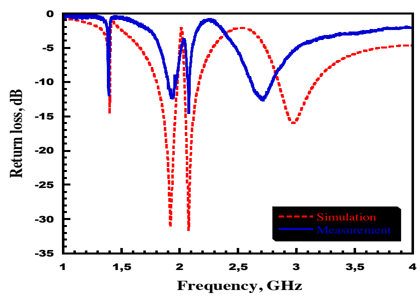

Antenna A2

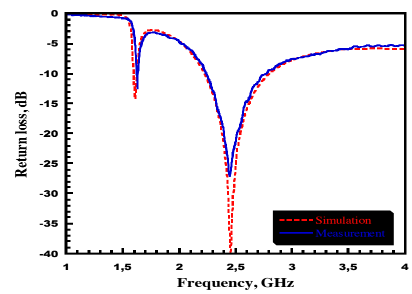

Antenna A3

Figure 4. Measured and Simulated Return loss for the three prototypes.

According Fig.4, the addition of the parasitic elements generates a new resonance frequencies lower than that of the exciting monopole. We can notice a good agreement between numerical and experimental results.

5. Conclusion

A family of low profile and multifrequency metamaterial inspired antennas is reported. We have used different shape of parasitic elements to reduce the profile of the monopole antenna and/or to create multifrequency behavior.In the long version of this paper we will add both measured and simulated results of efficiency, gain and radiation patterns. We will also analyze the proposed circuit model in order to explain the operation of the antenna systems.

REFERENCES

1. Jin, P. and Ziolkowski, R.W. «Broadband, Efficient, Electrically Small Metamaterial-Inspired Antennas Faciltated by Active Near Field Resonant Parasitic Elements, » *IEEE Trans. Antennas Propag.,* vol. 58, pp 318-327, Feb. 2010.
2. Dakhli, S. Mahdjoubi, K. Rmili, H. Floc'h, J.M and Zangar, H. «Compact, Mulifunctional Metamaterial-Inspired Monopole Antenna, » *European Conference on Antennas and Propagation, EUCAP,* Prague, Czech Republic, proceeding, pp 1967-1970, Mar.2012.
3. Ziolkowski, R.W. «Efficient Electrically Small Antenna Facilitated by a Near-Field Resonant Parasitic, » *Antenna and Wireless Propagation Letters IEEE*, vol. 7, pp. 581 - 584, Sep. 2008.

Numerical evaluation of coordinate transformation based devices using the FDTD method

Wenxuan Tang[1, 2], **Yang Hao**[2*]
[1]State Key Laboratory of Millimetre Waves, School of Information Science and Engineering, Southeast University, Nanjing 210096, China
[2]Department of Electronic Engineering, Queen Mary, University of London, Mile End Road, London, E1 4NS, United Kingdom
[*]corresponding author: yang.hao@eecs.qmul.ac.uk

Abstract-The coordinate transformation has been employed to create new functional devices for microwave engineering and antenna systems. Numerical simulation is an important step during the designing procedure as it serves to predict and to guarantee the performance of designed devices. In this work, we discuss the features of such kind of devices in terms of composing materials and dispersive property, and study the schemes to evaluate their performance using the dispersive FDTD method.

The concept of coordinate transformation has been employed to engineer the propagation of electromagnetic waves and consequently to bring in new devices with unique functions [1, 2], from the well-known “cloak of invisibility” to a series of antenna modules [3-5]. The general coordinate transformation could be termed as the “analytical coordinate transformation (ACT)” because the transformation media are calculated by an analytical method based on Maxwell’s equations. This method usually leads to devices composed of anisotropic and inhomogeneous metamaterials with less-than-unity permittivities and/or permeabilities. A specified form of the coordinate transformation is the discrete coordinate transformation (DCT) [6, 7], which discretises the transformation space and decides the transformation media using conformal mapping. For TE polarization, all-dielectric devices are achievable under some approximations through this method. Nevertheless, in both cases, dielectrics and metamaterials are required to have spatially-varying material properties, and, each of them have pros and cons in terms of material fabrication and device performance. For instance, metamaterials are probably easier to be manufactured with controlled material properties but often spatially and frequency-dispersive, while gradient dielectric materials can be made isotropic and homogeneous but difficult to be fabricated in the lab.

Therefore, numerical simulation is an efficient tool to validate the performance of coordinate-transformation based devices. The Finite-Difference Time-Domain (FDTD) method has been successfully applied to model metamaterials and to evaluate the performance of both ACT and DCT based devices [8]. Firstly, the basic FDTD method can be extended to simulate both spatially and spectrally dispersive media. Secondly, this time-domain method is appropriate for modelling broadband electromagnetic responses. In the rest of this paper, we will discuss several key aspects of evaluating a coordinate transformation based device.

Dispersion: Most ACT based devices (and some DCT based devices) contain areas with permittivity and/or permeability values less than the unity. To simulate this special kind of problem, dispersive FDTD techniques have been developed [9]. The material parameters are mapped with a well-known and widely-used Drude dispersive material model, and the required parameter values occur at center frequency. In practice, such devices are composed of metamaterials, which are strongly frequency-dispersive and consequently have an essential limitation of operating bandwidth. The performance of a flat reflector will be presented as an example to show the dispersive property of transformation devices.

Bandwidth: Bandwidth is one of the key features of a device. In the numerical simulation, a band-limited Gaussian pulse with zero DC content can be applied to evaluate the broadband performance of both ACT and DCT devices. The Fourier spectrum of this pulse has even symmetry around the center frequency. Received signals at observation positions are recorded at each time step, and their Fourier spectra are compared to that of the input signal in order to calculate the scattering parameters (S11 and S21) against frequencies. It should be pointed out that since the less-than-unity parameters are dispersive, the center frequency of the dispersive FDTD simulation should be carefully decided to guarantee the accuracy of modelling.

Far-field Performance: The FDTD method can efficiently calculate the electromagnetic responses of a structure to its surrounding environment. However, to test the radiating property of an antenna, for example the radiation pattern of a reflector, the electromagnetic field in the far-field region is required. Therefore, the near-to-far-field (NTFF) transformation is needed to obtain the far-field parameters [10]. For an antenna design, the directivity can also be used to evaluate its operating bandwidth.

REFERENCES

1. U. Leonhardt, "Optical conformal mapping," *Science,* vol. 312, pp. 1777-1780, 2006.
2. J. B. Pendry, D. Schurig and D. R. Smith, "Controlling electromagnetic fields," *Science*, vol. 312, pp. 1780-1782, 2006.
3. F. Kong, B. Wu, J. Kong, J. Huangfu, S. Xi, and H. Chen, "Planar focusing antenna design by using coordinate transformation technology," *Appl. Phys. Lett.*, vol. 91, p. 253509, 2007.
4. N. Kundtz and D. Smith, "Extreme-angle broadband metamaterial lens," *Nat. Mater*., vol. 9, pp. 129-132, 2010.
5. H. F. Ma and T. J. Cui, "Three-dimensional broadband and broad-angle transformation-optics lens," *Nat. Commun.*, vol. 1, pp. 124-130, 2010.
6. J. Li and J. Pendry, "Hiding under the carpet: A new strategy for cloaking," *Phys. Rev. Lett.*, vol. 101, no. 20, p. 203901, 2008.
7. W. Tang, C. Argyropoulos, E. Kallos, W. Song, and Y. Hao, "Discrete coordinate transformation for designing all-dielectric flat antennas," *IEEE Trans. Ant. Propag.*, vol. 58, no. 12, pp. 3795-3804, 2010.
8. Y. Hao and R. Mittra, *FDTD Modelling of Metamaterials: Theory and Applications*, Artech House, MA, 2009.
9. Y. Zhao, C. Argyropoulos, and Y. Hao, "Full-wave finite-difference time-domain simulation of electromagnetic cloaking structures," *Opt. Express*, vol. 16, no. 9, pp. 6717-6730, 2008.
10. A. Taflove and S. C. Hagness, *Computational electrodynamics: the finite-difference time-domain method*, 3rd Edition. Artech House, 2005.

Efficient and Accurate Analysis of Arbitrary Metamaterials with Three-dimensional Crystal Elements

R. Mittra[1, 2], R. K. Arya[1] , C. Pelletti[1] and T. Dong[1]

[1]EMC Laboratory, The Pennsylvania State University, USA

[2]Hi-Ci Professor, King Fahd University of Petroleum and Minerals, Dhahran - Saudi Arabia

rajmittra@ieee.org

Abstract - In this paper we present a numerically efficient and accurate technique for the analysis of doubly-infinite periodic arrays of elements, which find applications as Frequency Selective Surfaces (FSSs), Electronic Bandgap (EBGs) structures and Metamaterials (MTMs). The principal advantages of the proposed method, which is not based on the use of the Periodic Boundary Condition (PBC), are its versatility--since it can analyze Metamaterials with 3D crystal elements that can be inhomogeneous --and its ability to handle arbitrary incidence angles in an efficient way, regardless of how large that angle is.

Periodic structures are typically modeled as doubly-infinite arrays of scatterers, and are commonly analyzed by imposing the periodic boundary condition on a unit cell to reduce the original problem to a manageable size [1-2]. The conventional Method of Moments (MoM) [3] is well suited for simulating FSSs with thin planar PEC elements; but it becomes very inefficient when handling inhomogeneous and complex-shaped elements that are more amenable to convenient analysis via the use of Finite Methods.

In this paper we present a technique based on the "*generalized*" waveguide simulator (GWS) approach, for calculating the transmission and reflection coefficients of doubly-infinite periodic arrays. It is well known that the waveguide modes can be viewed as superposition of two obliquely incident plane waves whose angles depend upon the transverse dimension of the waveguide. The waveguide simulator approach has been extensively used in the past to analyze periodic structures, though only for limited number of angles.

In this paper we modify the above approach in a way that not only circumvents the limitations of the waveguide simulator (WGS) technique mentioned above, but to also do it in a time-efficient manner by utilizing the strategy described in [4-5] for MoM-based analysis of thin-wire elements.

Let us consider a truncated version of a two dimensional periodic array of elements--with spatial periodicities D_x and D_y along *X*- and *Y*-axes, respectively--which can be excited with a plane wave incident at an arbitrary angle. We begin by placing the truncated array inside a waveguide, as shown in Figure 1, and using the waveguide simulator approach, in which the effective angle of incidence is determined by the transverse dimension of the waveguide and the operating frequency without the side wall of the waveguide.

Next, we solve the above scattering problem by using a Finite Method, e.g., FDTD or FEM to compute the scattered fields along the longitudinal directions. We can show, by invoking the Floquet's theorem, that the wave numbers of these fields are associated with the Floquet modes of the infinite periodic structure. The total field on the incident side of the waveguide ($z<0$) is a summation of the incident and scattered (reflected) fields comprising of these modal (Floquet) fields, while only the transmitted fields exist in the other side ($z>0$).

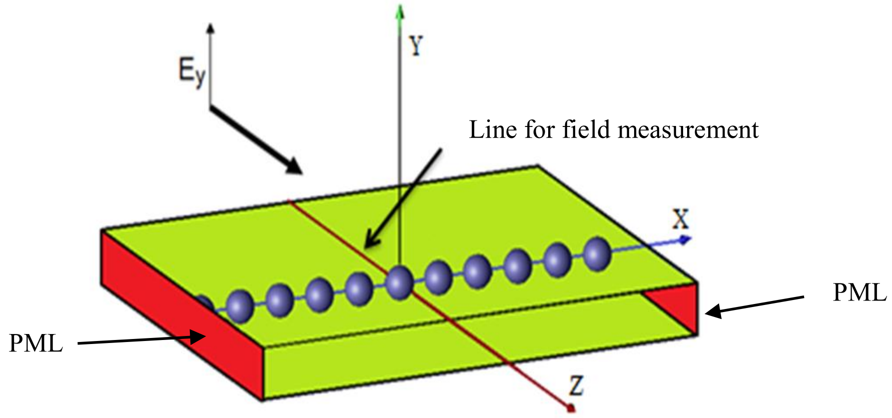

Figure 1: Modified Waveguide Geometry (the Z-axis is normal to the open ends of the waveguide and top- bottom are PEC boundaries).

The fields within region z<0 are decomposed into their incident and reflected components, by using Generalized Pencil of Functions (GPOF) [6]. The weights of the transmitted and reflected fields associated with the dominant Floquet harmonic yield the transmission and reflection coefficients for the truncated array. We then extrapolate these results, taking a cue from [4], to derive the desired values of the reflection and transmission coefficients R and T, for the infinite array. As an example, we consider a periodic array of spheres and calculate reflection coefficient. In Figures 2(a) and 2(b), we show the results for an array of PEC and dielectric (ε_r=9) spheres with diameter of 0.5 λ_0, at the operating frequency of 5 GHz respectively. The dimensions of the unit cell are: $D_x = D_y = 0.75\ \lambda_0$. The reflection coefficients obtained via this method are plotted and are compared against those obtained from a commercial FEM solver.

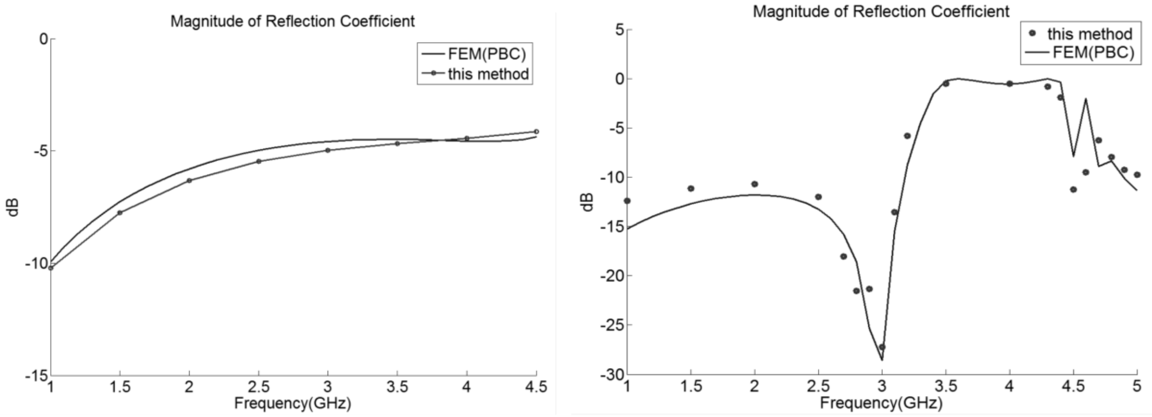

(a) (b)

Figure 2 Magnitude of Reflection coefficient derived by using the present method and compared with those from a commercial FEM (PBC) solver for 20 degree incidence angle for (a) PEC spheres and (b) dielectric spheres

It is evident from Figure 2 that good agreement has been achieved between the results obtained with a commercial FEM solver and those computed by using the introduced algorithm, despite the fact the use of PBCs has been totally avoided in the present method. Thus, this approach does not suffer from the difficulty encountered in the FDTD method when dealing with oblique incidence angles while simulating periodic structures; furthermore, in contrast to the conventional FDTD, the proposed algorithm it does not demand a reduction of the time-step in the FDTD simulations when we increase the angle of incidence.

Finally, we turn to the problem of modeling periodic structures in the optical regime, a topic that is of considerable importance today in the wake of recent interest in Optical Metamaterials. Unlike microwave frequency cases that we have discussed above, where the FSS elements are either PEC or dielectric types, the elements at optical wavelengths are comprised of plasmonic materials; hence they are highly dispersive as well as lossy. As a result, their response characteristics are often very different from those of their PEC counterparts. Nonetheless, we show that the concepts of using the Characteristic Basis Function Method (CBFM) to reduce the number of unknowns (see [4]), as well as the prediction of the asymptotic behavior of truncated arrays to obtain the characteristics of infinite doubly-periodic arrays, continues to be a viable and efficient approach, even at optical wavelengths. What is more, the technique can be modified to address the important problem of modeling periodic structures with statistical variations in their geometries, as is typically the case with Metamaterial structures at optical wavelengths where the difficulties in their fabrication almost always introduce small variations in the dimensions of the elements that comprise the "periodic" array.

REFERENCES

1. Mittra, R., C. H. Chan and T. Cwik, "Techniques for Analyzing Frequency Selective Surfaces-a Review," *IEEE Proc.*, Vol. 76, No. 12, 1593-1615, 1988.
2. B.A. Munk, *Frequency selective surfaces: Theory and design*, Wiley, New York, 2000.
3. R. F. Harrington, *Field Computation by Moment Method*, New York: The Macmillan Company, 1968.
4. K. Yoo, N. Mehta and R. Mittra, "A new numerical technique for analysis of periodic structures," *Microwave* and Optical Technology Letters, Vol. 53, No. 10, 2332-2340, Oct. 2011.
5. R. Mittra, C. Pelletti, N. L. Tsitsas, G. Bianconi, "A new technique for efficient and accurate analysis of FSSs, EBGs and metamaterials," Microwave and Optical Technology Letters, Vol. 54, No. 4, 1108-1116, Oct. 2011.
6. Y. Hua, T. Sarkar, "Generalized Pencil-of-Functions Method for Extracting Poles of an EM System from Its Transient Response," IEEE Trans. Antennas and Propag., Vol. 37, No. 2, pp. 229-234, Feb. 1989.

Efficient Integral Equation Approach for Periodic Multilayered Metamaterial Structures

N. A. Ozdemir[1], C. Craeye[1*], K. Ehrhardt[2] and A. Aradian[2]
[1]ICTEAM Université catholique de Louvain, Belgium
[2] Centre de Recherche Paul Pascal CNRS, Université de Bordeaux , France
[*]corresponding author: {nilufer.ozdemir, christophe.craeye}@uclouvain.be

Abstract- This study exploits the surface equivalence principle to obtain a reduced system of equations for a problem that includes doubly periodic infinite arrays of multilayers of core-shell nanoparticles, illuminated by a plane wave, above a dielectric substrate. The proposed approach allows different host medium for each layer of core-shell nanoparticles without employing multilayered media Green's function.

Metamaterials and, more generally, nanostructured materials, form an extremely active field of research in the optics and photonics community. One approach that is being increasingly developed is the "bottom-up" route: the desired optical properties are obtained through assemblies of plasmonic nanoparticles, synthesized by chemical means; they create local resonances controlling the global effective properties of the fabricated material, for instance to obtain strong variations of permittivity, or create artificial permeability in the optical range, or even negative index of refraction. Often, dense assemblies with high resonator concentration are required, and it is then convenient to work with "core-shell" nanoparticles: these have a core made of the plasmonic material (e.g., gold or silver) surrounded by a dielectric shell (e.g., silica). The shell in itself has no particular electromagnetic property, but it serves as a geometrical spacer in the design: when particles come into contact in the dense assembly, the distance between cores is controlled by the shell thickness (see Figure 1). It is thereby a very efficient way to control the overall filling fraction of plasmonic resonators in the material. There is therefore a need for numerical methods able to efficiently compute electromagnetic properties (such as field and local currents) for systems with core-shell geometries.

Integral equation approaches such as the Method of Moments (MoM) are an appropriate technique applied in the numerical analysis of periodic structures such as metamaterials because (i) the underlying analytical results are represented in the form of Green's functions, (ii) the radiation condition is fulfilled implicitly and (iii) unknowns are limited to interfaces between piecewise homogeneous media. The periodic Green's functions can be efficiently determined with the help of plane-wave decompositions for observation points above the array plane, with an exponential convergence, and cylindrical wave decompositions for observation point very close to or on the array plane [1]-[2]. This method appears to be more efficient for the gradient of the Green's functions, needed for the analysis of plasmonic nanoparticles, where the surface equivalence principle is exploited [3] for penetrable objects. In this study, the surface equivalence is exploited at two different levels. First, core-shell particles are analyzed via equivalent currents placed on the interfaces between media; interactions between media not directly touching each other are zero. Second, when the structures are embedded in multiple layers, a possible approach would consist of exploiting layered-media Green's functions. However, in that case the Green's function is no longer invariant with respect to the absolute vertical position, which hence requires 4D tabulation instead of 3D tabulation. That is why an equivalence plane is placed at every interface between layers (see arrows representing equivalent currents on Figure 1). In this case, the medium in a given layer can be treated as a homogeneous unbounded medium and 3D tabulation is sufficient.

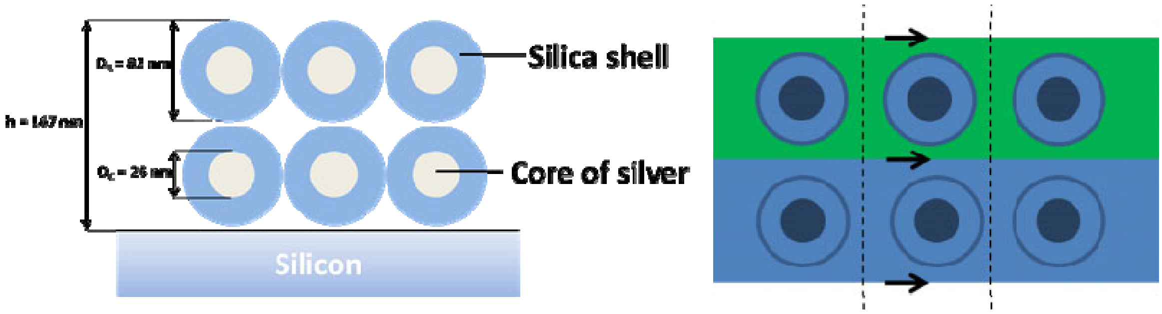

Figure 1. Surface equivalence for a multi-layered configuration of core-shell nanoparticles

We obtain the reflection and transmission coefficients of a doubly periodic infinite array of 2 layers of core-shell nanoparticles above 1μm thick silicon substrate, with a unit cell as illustrated in Figure 1, when illuminated by a normally-incident plane wave. The unit cell size is 84 nm in both x and y directions. The surface of the silver core and the outer surface of the silica shell are discretized into 48 and 150 RWG basis functions, respectively. The surface of the substrate and the equivalent surfaces in the multi-layered configuration are discretized into 512 rooftop basis functions. Figure 2 shows the reflection and transmission coefficients of the infinite array in [250-575] THz region. The error in energy conservation is less than 0.0002. The method can be applied to different morphological configurations of core-shell nanoparticles, which will be the subject of the prospective study.

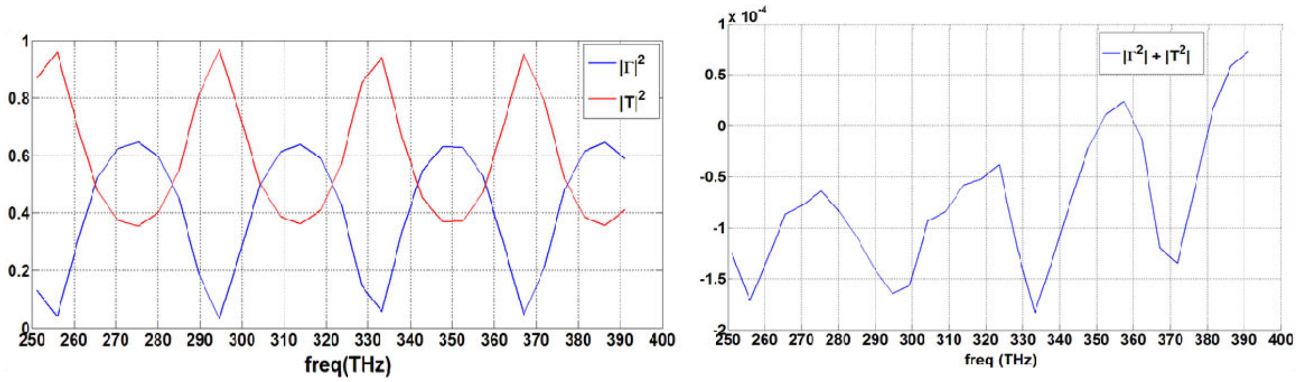

Figure 2. Magnitude of reflection and transmission coefficients is shown in the frequency range [250-575] THz.

This study has been funded by the European Union's Seventh Framework Programme (FP7/2008) under METACHEM project with grant agreement no 228762.

REFERENCES

1. Singh, S. and Singh R., "On the use of Levin's transform in accelerating the summation series representing the free-space periodic Green's function," *IEEE Trans. Microw. Theory Tech.*, Vol. 41, No. 5, 884–886, 1993.
2. Guérin N., Craeye C., Dardenne X., "Accelerated computation of the free space Green's function gradient of infinite phased arrays of dipoles," *IEEE Trans. Antennas Propag.*, Vol. 57, 3430–3434, 2009.
3. Dardenne X. and Craeye C., "Method of moments simulation of infinitely periodic structures combining metal with connected dielectric objects," *IEEE Trans. Antennas Propag.*, Vol. 56, No. 8, 2372–2380, 2008.

Analytical Modeling of a Magnetless Non-Reciprocal Metasurface Under Oblique Plane-Wave Incidence

D. L. Sounas[1,2], B. Gurlek[1], T. Kodera[3], and C. Caloz[1]

[1]École Polytechnique de Montréal, Montréal, Québec, Canada
[2]The University of Texas at Austin, Austin, Texas, USA
[3]Yamaguchi University, Ube, Japan
dsounas@gmail.com

Abstract— A non-reciprocal metamaterial exhibiting essentially the same properties as ferrites but without requiring a static magnetic bias has been recently introduced. The metamaterial consists of an array of ring-pair particles loaded with unilateral chip components and supporting rotating magnetic dipole moments, like atoms in ferrites. An analytical model for a metamaterial single layer under oblique plane wave incidence is presented. Effective surface magnetization and polarization densities are derived from the ring currents, calculated via a circular transmission line model for each ring.

Non-reciprocal components, such as isolators and circulators, are essential parts of telecommunication systems. Since the 1950's, the most common way to achieve non-reciprocity has been through magnetized ferrites [1]. However, the need of a static magnetic bias, usually provided by permanent magnets, makes ferrite-based components bulky, heavy and incompatible with integrated-circuit technology. In order to overcome these issues, the authors have recently proposed a magnet-less non-reciprocal metamaterial (MNM), which exhibits properties identical to those of ferrites but without requiring a static magnetic bias [2]. The constituent particle of the MNM is a pair of rings loaded with a field effect transistor (FET), as shown in Fig. 1(a). When the transistor is biased with by an appropriate voltage, it operates as a unilateral component and the ring-pair supports a rotating magnetic moment, similar to the rotating magnetic moment due to electron spin precession in magnetized ferrites, as illustrated in Fig. 1(b). An accurate analytical model for the MNM under normal plane-wave incidence was developed in [3]. Here, we extend this model for obliquely-incident plane waves.

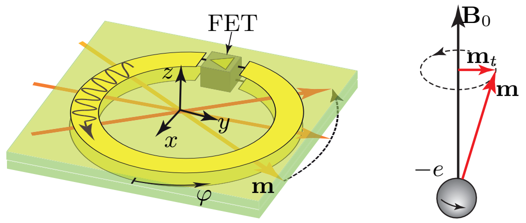

Figure 1: Principle of the MNM. (a) Rotating magnetic moment in the MNM as a result of the FET-loading of the constituent particle of the metamaterial. (b) Rotating magnetic moment in a magnetized ferrite as a result of the electron spin precession.

The MNM has two modes of operation, an odd one with antiparallel currents along the two rings, excited by a magnetic field parallel to the rings, and an even one with parallel currents along the two rings, excited by an electric field parallel to the rings. The current and the field of the odd mode are sketched in Fig. 2(a). The odd mode supports a rotating radial magnetic moment and hence provides the gyrotropic properties of the MNM. Furthermore, the mid-plane between the rings is a virtual perfectly electric conducting (PEC) plane and each ring can therefore be considered as a microstrip transmission line with substrate thickness half of the distance between the rings. If L and C is the per-unit angle inductance and capacitance of the ring microstrip line, respectively, the ring current satisfies the wave equation

$$\frac{d^2 I}{d\varphi^2} + \frac{\omega^2}{\omega_0^2} I = -j\omega C V^{\text{ext}}, \tag{1}$$

where $\omega_0 = 1/\sqrt{LC}$ and $V^{\text{ext}} = (j\omega\mu_0 Rt/2)H_\rho^{\text{ext}}$ is the voltage induced in the ring by the external field. Equation (1) is accompanied by the boundary conditions

$$I(\varphi_1) = a_{11}I(\varphi_2) + a_{12}I'(\varphi_2), \quad I'(\varphi_1) = a_{21}I(\varphi_2) + a_{22}I'(\varphi_2), \tag{2}$$

where a_{11}, a_{12}, a_{21} and a_{22} depend on the S-parameters of the FET. Equations (1) and (2) constitute a Sturm-Liouville problem with the solution

$$I(\varphi) = -j\omega C \sum_m \frac{\omega_0^2}{\omega^2 - \omega_m^2} I_m(\varphi) \left\langle I_m^\dagger(\varphi'), V^{\text{ext}}(\varphi') \right\rangle \tag{3}$$

where ω_m and $I_m(\varphi)$ are frequency and the current distribution of the m-th resonant mode of the ring, respectively, $I_m^\dagger$ is the m-th mode of the adjoint problem, and $\langle f, g\rangle = \int_{\varphi_1}^{\varphi_2} f(\varphi)g(\varphi)d\varphi$. Once $I(\varphi)$ has been found, the magnetic moment is calculated as $\mathbf{m} = \int_c I(\varphi)\mathbf{r} \times \hat{\boldsymbol{\varphi}}dl$. Note that the ring pair also exhibits an electric quadrupole moment $\bar{\bar{Q}}^e$ related to $\mathbf{m}$ according to $j\omega\hat{\mathbf{z}} \times \hat{\mathbf{z}} \cdot \bar{\bar{Q}}^e = 2\mathbf{m}$ [3].

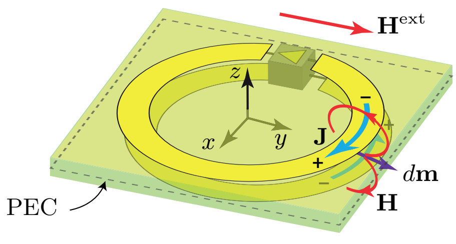

(a)

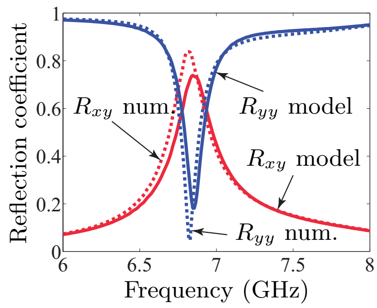

(b)

Figure 2: Odd mode of the MNM. (a) Current, magnetic field and effective infinitesimal magnetic dipole moment. The mid-plane between the rings is a virtual PEC plane. (b) Analytically and numerically calculated reflection coefficient of a PEC-backed single-ring metasurface under excitation by an y-polarized normally incident plane wave.

Consider now that the metamaterial is illuminated by an obliquely incident plane wave $\mathbf{E}^{\text{inc}} = \mathbf{E}_0 e^{-j(\mathbf{k}_t\cdot\hat{\boldsymbol{\rho}}+k_z z)}$, where $\mathbf{k}_t$ is the transverse wave-vector and $k_z = \sqrt{k_0^2 - k_t^2}$. The excitation voltage is then $V^{\text{ext}} = (j\omega\mu_0 Rt/2)H_\rho^{\text{ext}} e^{j\mathbf{k}_t\cdot\hat{\boldsymbol{\rho}}}$, where H_ρ^{ext} is the superposition of the incident field and the field generated by the induced effective magnetization $\mathbf{M}$ in the metasurface. As shown in [3], $\bar{\bar{Q}}^e$ equally contributes to $\mathbf{M}$ as $\mathbf{m}$, hence $\mathbf{M} = 2\mathbf{m}/p^2$, where p is the periodicity. For oblique incidence, the electric quadrupole moment also creates an electric polarization $\mathbf{P} = [j\mathbf{k}_t \cdot (\hat{\mathbf{z}} \cdot \bar{\bar{Q}}^e)/2p^2]\hat{\mathbf{z}}$. The field generated by $\mathbf{P}$ is proportional to k_t^2, hence it corresponds to a second order spatial dispersion effect.

Figure 2(b) presents the analytically and numerically calculated reflection coefficient of a PEC-backed single-ring metasurface under excitation by a y-polarized normally incident plane wave. An x-polarized component is generated in the reflected field by the rotating dipole moment, meaning that the polarization plane of the incident wave is rotated by the metasurface. The agreement between the analytical and numerical results is very good. Results for the general case of oblique incidence will be presented during the conference.

REFERENCES

1. Lax, B. and Button, K. J., *Microwave ferrites and ferrimagnetics,* McGraw-Hill, New York, 1962.
2. Kodera, T., Sounas, D. L., and Caloz, C., "Artificial Faraday rotation using a ring metamaterial structure without static magnetic field," *Appl. Phys. Lett.*, Vol. 99, 031114(1–3), 2011.
3. Sounas, D. L., Kodera, T., and Caloz, C., "Electromagnetic modeling of a magnet-less non-reciprocal gyrotropic metasurface," *IEEE Trans. Antennas Propag.*, 2012, To be published.

On the use of a Hierarchical Multi-level Building Block Basis Function Scheme in Periodic Plasmonic Structures

X. Zheng[1], V. K. Valev[2], V. Volskiy[1], G. A. E. Vandenbosch[1*] and V. V. Moshchalkov[3]
[1]Department of Electrical Engineering (ESAT – TELEMIC), KU Leuven, Leuven, Belgium
[2]Cavendish Laboratory, Department of Physics, University of Cambridge, Cambridge, United Kingdom
[3]Nanoscale Superconductivity and Magnetism, Pulsed Fields Group, Department of Physics, KU Leuven, Leuven, Belgium
[*]corresponding author: guy.vandenbosch@esat.kuleuven.be

Abstract – A Volumetric Method of Moments (V-MoM) algorithm is applied to predict the electromagnetic properties of plasmonic metamaterials. It is based on the use of a multi-level building block basis function scheme, in combination with a dedicated Kummer transformation. The hierarchical scheme is applied to a period structure for the first time, and the dedicated so-called "asymptotic functions" used in the Kummer transformation have been introduced very recently. The algorithm is demonstrated by analyzing a Ninja Star periodic structure. Circular Dichroism (CD) is observed by both simulations and experiments.

Nano-plasmonic metamaterials have been constantly drawing attentions from physicists, chemists, and electrical engineers in the last decade, due to their exotic electromagnetic properties induced by surface plasmons. Aside from the quantum mechanical explanations of the problem, in general the interaction of light with nano-metallic (plasmonic) structures can be modeled in the framework of classical electrodynamics. Thus, the classic Method of Moments (MoM) algorithm can be adapted and applied in the field of nano-plasmonic applications, by noticing the dispersive properties of metals at optical frequencies and the volumetric nature of the current in the nanoplasmonic structures. As shown in Fig. 1, the surface plasmons induced by left and right circularly polarized light in a Ninja Star [1] nanostructure are calculated with our in-house developed Volumetric Method of Moments (V-MoM) based software, MAGMAS [2] [3].

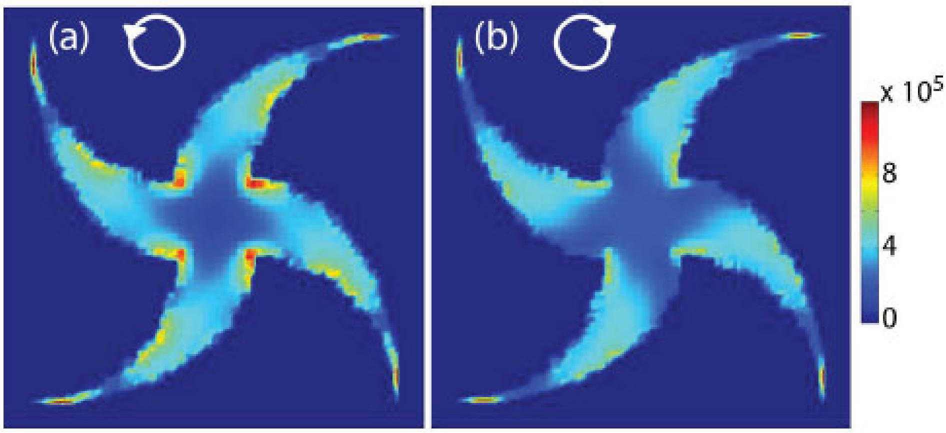

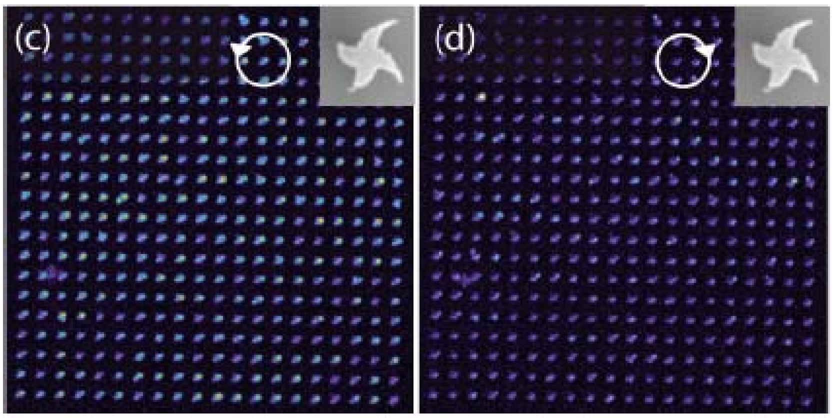

Fig. 1: (a) and (b): The induced surface plasmon by left and right circularly polarized light (simulated by MAGMAS); (c) and (d) SHG microscopy.

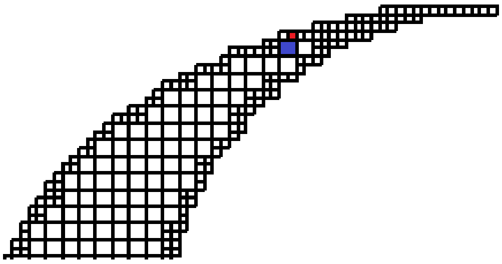

Fig. 2: Multi-level building block scheme: Blue (large) block is always paired by two red (small) blocks.

In order to depict the curved boundaries of the Ninja star in detail, small building blocks must be employed. However, the use of small building blocks implies a coupling matrix of larger dimensions, thus larger memory usage and longer matrix inversion time. By noticing the volumetric nature of the current in the nanoplasmonic structures, i.e. the stand-alone surface charges do not induce singularities; a scheme of mixing blocks with small and large sizes can be applied, as shown in Fig. 2. The multi-level building block scheme together with a dedicated calculation of the periodic Green's functions, involving a very recently introduced Kummer transformation, renders a good agreement between simulations and experiments, that is, Ninja stars whose arms screw in the clockwise direction are more sensitive to the left circularly polarized light than the right circularly polarized light, as shown both in Fig. 1 (a) and (b). The theoretical concepts used will be explained in much more detail in the full paper.

REFERENCES

1. Valev, V. K. , et al., "The role of chiral local enhancements below the resolution limit of Second Harmonic Generation microscopy," *Opt. Exp.*, Vol. 20, No. 1, 256 -264, 2012.
2. Schols, Y. and G. A. E. Vandenbosch, "Separation of horizontal and vertical dependencies in a surface/volume integral equation approach to model quasi 3-d structures in multilayered media," IEEE Trans. Antennas Propag., VOL. 55,NO. 4, pp. 1086–1094, 2007.
3. Volskiy, V. and G. A. E. Vandenbosch, "Quasi 3D Mixed Potential Integral Equation Formulation for periodic structures," IEEE Trans. Antennas Propag., Vol. 61, No. 4, April 2013.

Characterization of the opened left- and right-handed transmission channels in stacked subwavelength apertures

E. Ozbay*, A. O. Cakmak, and E. Colak
Bilkent University, Nanotechnology Research Center, 06800 Ankara, Turkey
*corresponding author: ozbay@bilkent.edu.tr

Abstract-The hybridization of the unit lattices along the propagation direction in stacked subwavelength apertures produces a left-handed transmission band in the absence of the contributions from higher order diffractions. The left-handed propagation channel is governed by the stacked resonators. The numerical results confirm that the designed structure is scalable to near-infrared wavelengths. A right-handed transmission channel can also be opened for the periodic structures by making use of the Fabry-Perot based cavity modes.

The extraordinary transmission (EOT) through periodic subwavelength aperture arrays has been previously studied for stacked fishnet configurations without making a clear distinction between the designs with homogenized and hybridized unit lattice variations [1,2]. The present study aims to categorize these configurations by investigating the physical origins of the observed EOT. In one case (configuration 1), the holes on metallic screens have a periodicity that is relatively larger than the subwavelength openings. The first two bands in the dispersion graph (black and red colored lines, respectively) in Fig. 1(a) have negative slopes ($\partial\omega / \partial k < 0$), indicating anti-parallel group and phase velocities, which is a characteristic feature of the metamaterials. Consequently, EOT bands are spotted around 13.85 GHz and 15.5 GHz in the simulated transmission spectrum for configuration 1 in Fig. 1(c). A modal analysis for the propagating modes reveals that the inductive TE_{20} and capacitive TM_{02} modes are the contributing higher orders of the artificial waveguide below the cutoff frequency of the individual holes (21.42 GHz). This particular artificial waveguide stems from the periodicity and EOT relies on the LC tank formation of the respective modes regardless of the hybridization of the unit lattice. On the other hand, a secondary design with a dense hole distribution (configuration 2) destroys the EOT band by acting solely as a frequency selective surface in the new condition. A transmission channel with a negative slope appears only after the hybridization of the unit lattice which is carried out by arranging different volumetric proportions of different dielectric media (not air) between the alternating metallic screens. The left-handed (LH) transmission regime is located at 14.27 GHz and the electric fields are localized at the sandwiched layer with the higher dielectric constant in Fig. 1(f). The LH transmission line model that could be applicable to describe the propagation along the stacking direction, as in the case of Fig. 1(e), is no longer valid. In contrast, the overall design constitutes a series of coupled LC tank resonators. The inductance arises from the induced surface currents while the capacitance is due to the inserted dielectrics. The analysis of these resonators shows that EOT emerges at f_R that is given in Eq. (1). The shortening of the cascaded metallic screens to each other obstructs the EOT band [see red colored line in Fig. 1(d)], which further confirms the resonance nature of the EOT band. Conversely, the shortening has little effect on configuration 1. The two configurations are scaled up to infrared wavelengths [see Fig. 1(g) and (h)]. It has been shown that Eq. (1) can still be used in order to scale the EOT band from microwave frequencies to optical wavelengths for configuration 2.

$$f_R = \frac{1}{2\pi\sqrt{LC}} \propto \sqrt{\frac{1}{\varepsilon} \times \left(\frac{1}{a_{y2}(a_{y2}-w)} + \frac{(a_{x2}-w)}{a_{x2}a_{y2}w}\right)}\,. \tag{1}$$

Yet, the dispersive characteristics of the metals cause slight shifts [compare purple colored line with the others in Fig. 1(j)]. A more precise value for the EOT peak is found by allowing the normal incident wave to be coupled to the surface plasmons $k_{SPP}=2\pi m/a_{x4}$ (m is an integer). Then, the peak value is given by $\lambda_0 = \lambda_{SPP}\sqrt{\varepsilon_2 \times (t_2 + 2\coth(\omega_p t_m/c)/(\omega_p t_2/c))}$, where ε_2 is associated with the higher dielectric constant. The homogenous unit lattice case is simulated in Fig. 1(i), for which the EOT band is located right after the Rayleigh-Wood anomaly [3]. Finally, a cavity mode at 15.4 GHz can be realized by creating a defect site. This defect site forms a Fabry-Perot resonator, for which a certain relation between the total phase change (Φ, inside the cavity) and the phase change due to the reflections (ψ) at the walls of the cavity must be satisfied [4]. In the end, transmission channels can be simultaneously opened and measured as in the case of Fig. 1(l) by combining these two regimes in hybrid unit lattice fishnet metamaterials.

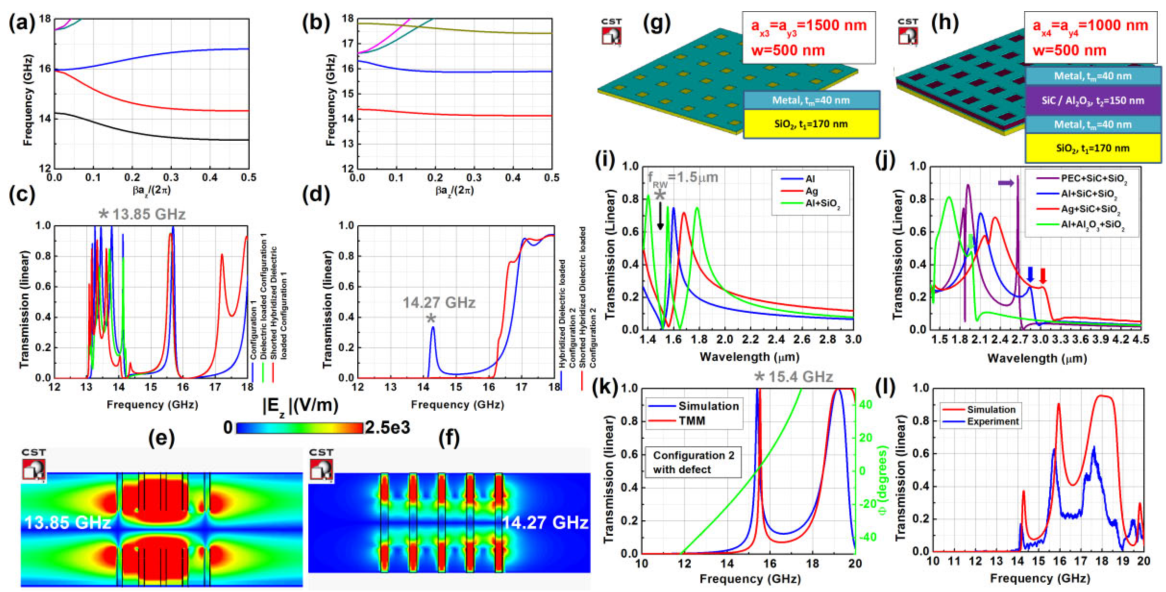

Figure 1. The designs have square lattices with equal periodicity on metal planes (x-y plane): $a_{x1}=a_{y1}=21$ mm, $a_{x2}=a_{y2}=14$ mm perpendicular to the propagation direction (z-axis). The unit lattice separation $a_z=4$ mm. The aperture window is $w=7$ mm for both cases, the dielectric is Teflon with $\varepsilon=2.16$. Dispersion results, simulated transmission spectrum, electric field distributions for configuration (a), (c), (e) 1 and (b), (d) and (f) 2. The scaled designs at optical wavelengths and their respective transmission spectrum for configuration (g), (i) 1 and (h), (j) 2. (k) The transmission spectrum with the defect site. Transfer Matrix Method (TMM). (l) The simultaneously opened transmission channels, simulation and experimental results.

REFERENCES

1. Beruete M. *et al.* "Extraordinary transmission and left-handed propagation in miniaturized stacks of doubly periodic subwavelength hole arrays," *Opt. Express*, Vol. 15, No. 3, 1107-1114, 2007.
2. Kafesaki M. *et al*. "Left-handed metamaterials: the fishnet structure and its variations," *Phys. Rev. B*, Vol. 75, No. 23, 235114, 2007.
3. At this particular wavelength the modal expressions for the propagating waves tend to cancel each other.
4. $\Phi = \beta \cdot L + \psi = m \cdot \pi$ (L and β are the cavity length and propagation constant)

A general approach to determine the constitutive parameters of bi-anisotropic metamaterials

M. Śmierzchalski[1*], K. Mahdjoubi[1]
[1]Univeristy of Rennes 1, Institute of Electronic and Telecommunication of Rennes (IETR), France
[*]corresponding author: maciej.smierzchalski@univ-rennes1.fr

Abstract- A systemic method is proposed for the characterization of constitutive parameters of bi-anisotropic (BA) metamaterials. The main contributions of the method are: i) the generalization of the inversion of the interface conditions for continuous BA medium and, ii) the proper definition of wave admittances and propagation constants for discontinuous (i.g. periodic) medium by considering the Bloch admittance for taking into account the spatial dispersion.

1-Introduction

The medium made of periodic lattice of resonating particles with period much smaller than the wavelength of propagating wave inside is commonly known as a metamaterial (MM) medium. The MMs have found large attractiveness because they can offer non natural properties. A typical example of MM medium is a lattice of split rings resonators (SRR), equivalent to a bi-anisotropic (BA) homogeneous material, which is capable to behave like a left-handed medium.

In BA media, the propagation constant and/or the wave impedance can depend on the propagation direction. Hence, unlike the propagation inside the isotropic media, the incident (forward) and reflected (backward) waves can be quite different from each other. Therefore, the classical NRW method [1], which supposes that the forward and backward waves have identical impedance and wave number, cannot be used to extract the constitutive parameters of BA materials. The second problem related with the metamaterials is that they are often, made of lattices of resonating particles like SRRs. The E and H fields inside the unit cell is highly non uniform and the E / H ratio is often non constant. Under these conditions, the wave characteristics, such wave impedance, are not trivial to define. These problems will be addressed in this communication.

2-A general approach for retrieving constitutive parameters of continuous bi-anisotropic media

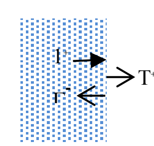

a) + direction

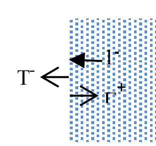

b) − direction

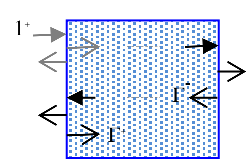

c) Slab of BA materials

The problem of characterisation of BA metamaterials has been investigated by several research groups [2-5]. In contrast with these investigations, the approach proposed here considers the proper inversion of the interface conditions by considering the BA properties. Consider the air-material interface of figures (a) and (b). For isotropic materials, these two configurations give the same results for the reflection (Γ) and transmission (T) coefficients. For BA materials, as the wave characteristics (wave numbers and impedances) depend on the propagation direction, these two configurations lead to different coefficients ($\Gamma^+ \neq \Gamma^-$, $T^+ \neq T^-$). Taking into account the right coefficients at each interface, we have established the S parameters for a slab of BA materials (Fig. c) and then, inversed their expressions in a way similar to that of NRW method, to extract correctly the wave numbers and wave impedances.

3-Metamaterials as discontinuous bi-anisotropic media

As mentioned before, the metamaterials are often made of lattices of resonating particles like SRRs. Under the condition of $kp < 0.01$ (k = wave number in the medium and p = period) the material is supposed to behave as continuous (homogeneous) medium [3]. However, even under this condition. The E and H fields inside the unit cell is highly non uniform, the field ratio E/H is often non constant and hence, the wave impedance is difficult to be identified or defined. Therefore, the Bloch impedance (admittance) is introduced by averaging the field on the unit periodic, and then the scattering parameters are adjusted by the transmission line technique [6] to define correctly the boundary conditions on the slab edge.

4-Example of Results

The SRRs medium used in this example is similar to that proposed in [2], however in the measurements are introduce forward and backward direction of excitation. The scattering parameters are obtained by the electromagnetic simulation HFSS of a given unit SRR cell.

In retrieving method it is needed to determinate surface impedances, Bloch impedances and refractive index which all have to satisfy physical laws [8, 9]. For the comparison, constitutive parameters are defined for two cases: with and without considering the spatial dispersion (long wave regime), i.e. respectively with Bloch impedance or with usual wave impedance. The refractive index is assumed to be the same for both methods.

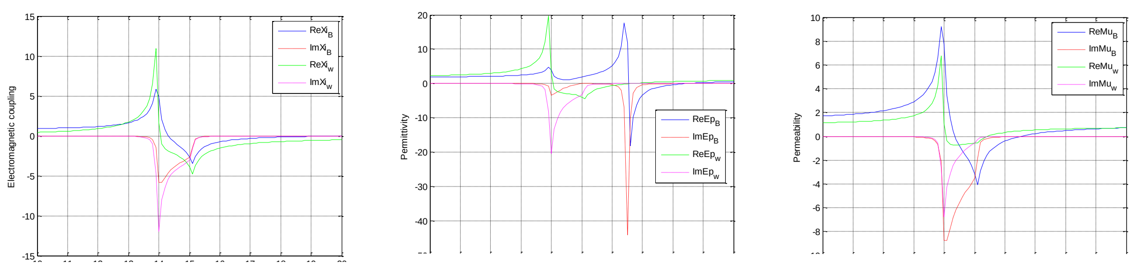

Figure 1. Real and imaginary parts of retreived constituvie paramters from surface impedace (green and pink) and Bloch impedace (blue and red). a) electromagnetic coupling term, b) permititvity and c) permability.

All the presented parameters satisfy physical laws. The main deference is observed for retrieved permittivity. responses obtained with Bloch impedance (B subscript in the figure 1) are more accurate to the model of MMs.

Conclusions

A proposed method of determination of local constitutive parameters has been presented. The approach was verified by comparison two approaches with and without consideration of quasi-static limit approximation. In the method is introduced Bloch impedance which allows to homogenize the medium when spatial dispersion occurred. The obtained results validate physical laws and theoretical assumption of behaviour for SRR medium.

REFERENCES

1. Nicholson A. M. and Ross G. F., "Measurement of Intrinsic Properties of Materials by Time Domain Techniques", IEEE Trans. Instrum. Meas., Vol. IM-19, 377-382, 1970.
2. Chen X., Wu B. I., Kong J. A., and Grzegorczyk T. M., "Retrieval of the effective constitutive parameters of bianisotropic metamaterials", Phys. Rev.

E, Vol. 71, 046610, 2005.

3. Simovski C. R. and Tretyakov S. A., “Local constitutive parameters of metamaterials from an effective-medium perspective Phys. Rev. B, Vol. 75, 195111, 2007.
4. Silveirinha M. G., Baena J. D., Jelinek L. and Marqués R., “Nonlocal homogenization of an array of cubic particles made of resonant rings”, Metamaterials, Vol. 3, pp. 115-128, 2009.
5. Caminita F., Martini E., Sardi G.M. and Maci S., “Metadispersion in anisotropic and bianisotropic media,“ XXXth URSI, 2011.
6. Pozar D. M., “Microwave Engineering”, Addison-Wesley Publishing, 1993.
7. Caloz C. and Itoh T., “Electromagnetic Metamaterials: Transmission Line Theory and Microwave Applications”, John Wiley and Sons., New Jersey, 2006.
8. Landau L.D. and Lifshitz E. M., “Electromagnetics of Continous Media”, Pergamon, New York, 1984.
9. Alù A., Yaghjian A. D., Shore R. A., and Silveirinha M. G., “Causality relations in the homogenization of metamaterials”, Phys. Rev. B, Vol. 84, 054305, 2011.

EM Models for Multisurface Metamaterial Homogenization

Giovanni M. Sardi, Enrica Martini, Stefano Maci
Department of Information Engineering and Mathematical Sciences
University of Siena
Siena, Italy
macis@ing.unisi.it

***Abstract*— This work presents a quasi-analytical approach to the homogenization of metamaterials realized by the superposition of identical periodic planar surfaces. It is based on the definition of an equivalent admittance matrix for the single layer, combined with the application of the Bloch theory for the analysis of the periodically loaded equivalent transmission line modelling the layered structure. Different theoretical definitions of equivalence are discussed in connection with practical applications of the homogenization concept. It is shown that the uniqueness of the equivalent homogeneous medium depends on the final objective of the homogenization procedure, i.e. on the specific metamaterial behavior to be mimicked.**

I. INTRODUCTION

The continuous interest on metamaterials, started more than a decade ago, has in parallel inspired a lot of work about their modeling, and the most proper and efficient methods of analysis and design [1]-[2]. The development of a reliable and accurate approach for the modeling of the electromagnetic behavior of artificial materials is a key point to fully exploit their potential. Considerable effort has been made to represent these artificial structures as effective homogeneous media, described by a set of equivalent constitutive parameters [3]-[7]. This approach may reveal very useful in the design of metamaterial-based devices. However, the procedure for the retrieval of the equivalent parameters is not univocally defined; in fact, different techniques can be used depending on the metamaterial characteristics and on the goal of the homogenization process. In this framework, different models can be set up relying on the definition of different "homogenization equivalences".

Volumetric metamaterials can be realized by cascading a number of periodic surfaces made of patch- or slot-type elements, as shown in Fig. 1. This kind of surfaces is widely known and is indicated with different denominations depending on the application, as for instance Frequency Selective Surfaces (FSS) [8], Partially Reflecting Surfaces (PRS) and, more recently, with the new exotic denomination of MetaSurfaces [9]. This class of volumetric metamaterials is particularly interesting due to the ease of fabrication, and the wide variety of realizable electromagnetic behaviors. In this work we describe a general approach for the homogenization of these artificial materials, and we show how it can be applied to satisfy different homogenization equivalences.

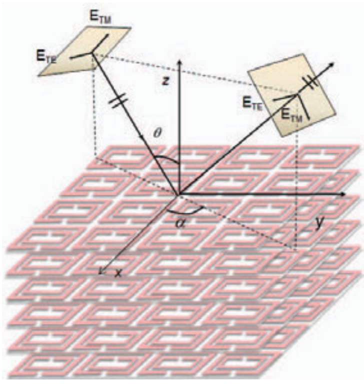

Fig. 1. Geometry for the multilayer structure under analysis.

II. DEFINITION OF THE EQUIVALENCE MODELS

The definition of "homogenization equivalence" actually depends on the final objective of the homogenization procedure, since this latter determines which characteristics of the artificial media must be also exhibited by the effective homogeneous medium. In most of the cases, the definition of the equivalent parameters is based on a scattering analysis; in some other cases, the effective homogeneous medium is required to match the dispersion properties of the metamaterial. Moreover, the capability of the homogenization model to correctly represent the structure of the supported fields could also be important.

Starting from these considerations, we can define three different homogenization equivalences, namely:

- External Equivalence: slabs of the artificial multilayer material and of the equivalent homogeneous medium possess the same scattering and transmission matrices as a function of frequency and wavenumber.
- Dispersion Equivalence: the artificial multilayer material and the equivalent homogeneous medium admit the same solutions of the dispersion equation for the two dominant eigenmodes.
- Modal equivalence: the field structure of the two modes supported by the equivalent homogeneous medium matches the one of the two dominant eigenmodes of the artificial multilayer material.

In the following, a general homogenization procedure that can be adapted to match the different types of equivalence is presented.

III. Homogenization Procedure

The class of artificial media described above can be conveniently analyzed resorting to an equivalent periodically loaded transmission line model, in which each layer is modeled via the equivalent admittance [10], Fig. 2. Applying the Bloch theory for periodic structures [11] it is possible to define an equivalent uniform transmission line, which satisfies both the External equivalence and the Dispersion equivalence.

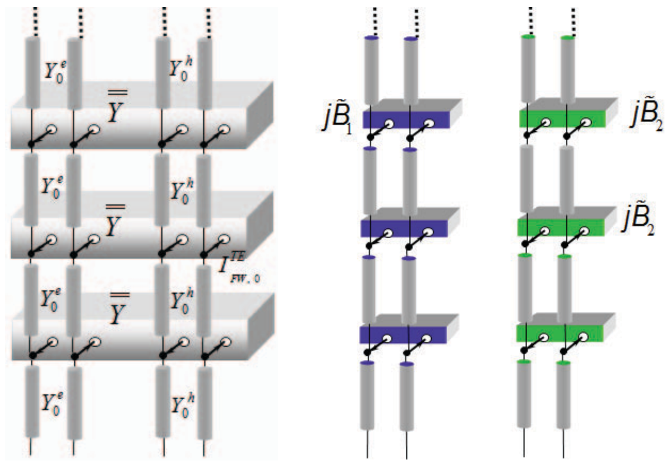

Fig. 2. (a) Equivalent transmission line model of the multilayer artificial material; (b) eigenmode transmission line for the definition of the homogenization equivalences.

A. External Equivalence

The "External Equivalence" approach leads to the definition of a set of equivalent constitutive parameters capable of providing the correct prediction of the scattering from a metamaterial slab consisting of an arbitrary number of periodic layers [6]. The Bloch theory provides the propagation constant and characteristic impedance of an equivalent uniform transmission line with the same scattering coefficients of the periodically loaded transmission line. Hence, this transmission line parameters can be used to define a set of constitutive parameters satisfying the external equivalence.

This approach to homogenization is intrinsically ambiguous, due to the fact that the scattering is only determined by the components of the fields that are tangential to the interface. This ambiguity can also be explained in terms of volumetric equivalent currents, since different equivalent media are associated with different sets of equivalent currents, but any set of non-radiating currents do not affect the scattering properties of the slab.

B. Dispersion Equivalence

The "Dispersion Equivalence" leads to the definition of an equivalent homogeneous medium which admits the same solutions of the dispersion equations (i.e. the same relationship between the propagation vector components and the frequency) as for the two dominant modes of the artificial material. The "Dispersion Equivalence" can provide useful results in applications where the focus is on the characterization of the propagation inside the unbounded material

As a general rule, the scattering coefficients from a given material slab do not univocally identify the dispersion relation of the material, since there is an ambiguity in the definition of the longitudinal component of the propagation constant. This means that the "External Equivalence" does not automatically guarantees the "Dispersion Equivalence". It is noted however that by imposing that the homogeneous medium is described by the same equivalent transmission line model of the multilayer material it is possible to simultaneously satisfy both the "External Equivalence" and the "Dispersion Equivalence". The homogeneous medium defined through this procedure is not univocally defined, but it possesses all the properties requires for some particular applications, like for instance the design of planar lenses, filters and polarizers. In fact, in these cases, the knowledge of the transfer function of a metamaterial slab is the key point for the analysis and/or design processes.

C. Modal Equivalence

The "External Equivalence" and the "Dispersion Equivalence" leave an ambiguity in the definition of some entries of the equivalent tensors.

In order to complete the definition of the equivalent medium, a "Modal Equivalence" can be set by considering also the longitudinal field components. In this respect, we can distinguish two cases: the "Single Mode Equivalence" and the "Full Modal Equivalence". The first one consists in matching all the field components for one of the two dominant eigenmodes, and it is appropriate when only one mode is of interest, e.g. when only one dominant mode is propagating. The second one consists in matching all the field components of the two dominant eigenmodes with a unique couple of tensors. This latter equivalence can always be rigorously established when TE and TM modes are decoupled in the artificial medium. In the most general case, it is approximately achievable under the assumption that the metamaterial is not bianisotropic and presents a low degree of spatial dispersion.

In the proposed homogenization approach, the definition of the implementation of the Modal equivalence requires the determination of the average longitudinal fields in the metamaterial. This step can be done in quasi analytical form if a spectral MoM is used for the analysis of the planar periodic layers.

Fig. 3 shows the set representation of the homogenization equivalences.

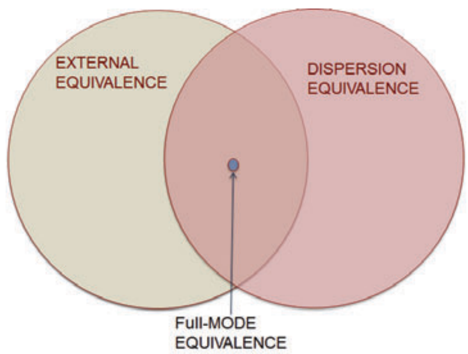

Fig. 3. Set theory representation of the relationship between the three different homogenization equivalences and corresponding equivalent parameters.

IV. CONCLUSIONS

A quasi-analytical homogenization procedure has been presented for volumetric metamaterials consisting of planar periodic layers. Different approaches to the definition of equivalent constitutive parameters can be applied depending on which characteristics of the metamaterial must be also exhibited by the effective homogeneous medium. A first methodology defines an equivalent medium by matching the scattering properties of an artificial medium slab. A second one obtains the equivalent parameters by matching the solutions of the dispersion equation for the two dominant eigenmodes (Bloch modes). A third approach also considers the average longitudinal field and uses this information to identify a unique couple of equivalent tensors that match the fields of the two dominant Bloch modes.

ACKNOWLEDGMENT

This work is co-financed by U.S Army Research Laboratory in the framework of research contract W911NF-11-1-0469.

REFERENCES

[1] N. Engheta and R. Ziolkowski, *Metamaterials: Physiscs and Engineering Exploration*, New Wiley, 2009.

[2] S. Maci and A. Cucini, "FSS-based EBG Surfaces", in *Electromagnetic metamaterials: physics and engineering aspects*, N. Engheta and R. Ziolkowski, John Wiley, 2005.

[3] M.G. Silveirinha, "Generalized Lorentz-Lorenz formulas for microstructured metamaterials", *Physical Review B*, vol. 76, 2007.

[4] A. Ishimaru, S.W Lee, Y. Kuga and V. Jandhyala, "Generalized Constitutive Relation for Metamaterials Based on the Quasi-Static Lorentz Theory", *IEEE Trans. On Antennas and Propagation*, vol. 51, no. 10, pp. 2550-2557, October 2003.

[5] A.D. Scher and E.F. Kuester, "Extraxcting the bulk effective parameters of a metamaterial via the scattering froma single planar array of particles", *Metamaterials*, vol. 3, pp. 44-55, 2009

[6] D.R. Smith, S. Schultz, P. Markos, and C.M. Soukoulis, "Determination of effective permittivity and permeability of metamaterials from reflection and transmission coefficients", *Phys. Rev. B*, vol. 65, n. 195104, 2002.

[7] C.R. Simovski and S. Tretyakov, "Local constitutive parameters of metamaterials from an effective-medium perspective", *Physical Review* B, vol. 75, 195111, 2007.

[8] B.A. Munk, *Frequency Selective Surfaces: Theory and Design*, John Wiley and Sons, New Yotk, 2000.

[9] S. Maci, G. Minatti, M. Casaletti, and M.Bosiljevac, "Metasurfing: Addressing Waves on Impenetrable Metasurfaces,"*Antennas and Wireless Propagation Letters, IEEE*, vol.10, no., pp.1499-1502, 2011.

[10] S. Monni, G. Gerini, A. Tijhuis, and A. Neto, "Multimode Equivalent Networks for the Design and Analysis of Frequency Selective Surfaces," *IEEE Trans. on Antennas and Propagation*, vol. 55, no. 10, pp. 2824-2835, October 2007.

[11] R.E. Collin, *Field Theory of Guided Waves*, IEEE Press, New York, 1991.

Novel applications of transformation electromagnetics

Experiments on transformation thermodynamics: Molding the flow of heat

R. Schittny[1*], M. Kadic[1], S. Guenneau[2], and M. Wegener[1,3]

[1]Institute of Applied Physics, Karlsruhe Institute of Technology (KIT), 76128 Karlsruhe, Germany
[2]Institut Fresnel, CNRS, Aix-Marseille Université, Campus Universitaire de Saint-Jérôme, 13013 Marseille, France
[3]Institute of Nanotechnology, Karlsruhe Institute of Technology (KIT), 76128 Karlsruhe, Germany
[*]corresponding author: robert.schittny@kit.edu

Abstract— It has recently been shown theoretically that the time-dependent heat conduction equation is form-invariant under curvilinear coordinate transformations. Thus, the concepts of transformation electrodynamics can be applied to thermodynamics as well. Following these ideas, we design, fabricate and characterize a thermal cloaking device that molds the flow of heat around an object in a metal plate. The object is protected from heating while the downstream heat flow is preserved as if no object was there.

In transformation thermodynamics, the propagation of waves is controlled by (real-space) metamaterial distributions resembling fictitious curved space [1, 2, 3, 4]. This is possible due to the form-invariance of the hyperbolic wave equation under curvilinear coordinate transformations. Recently it was shown theoretically that this form-invariance holds true also for the parabolic time-dependent heat conduction equation [5]. Thus, the known concepts of transformation electrodynamics can be applied just as well to heat conduction, opening up the field of transformation thermodynamics. Inspired by our recent experiments on mechanical thin-plate cloaking [6], we design and fabricate a thermodynamic cloak that protects an object in a metal plate from transient heating while maintaining a temperature distribution in the surrounding as if no object was there.

Following the theoretical considerations in Ref. [5], we obtain an inhomogenous and anisotropic heat conductivity distribution for the area of the cloak [7]. This is then mapped onto a multilayer metamaterial structure made by drilling rings of holes into a copper plate and filling them with polydimethylsiloxane (PDMS), leaving a solid copper region inside the cloak. The high contrast in heat conductivity between the constituent materials (more than 2600 for copper and PDMS) makes the fabrication of highly anisotropic thermal metamaterials much easier than in other systems. The copper plate is furthermore coated with a thin layer of PDMS which serves as a high-emissivity layer and makes characterization by thermal imaging possible. Fig. 1 shows a blueprint of the cloak design and a photograph of the fabricated structure.

For characterization, the plate is heated locally by immersing one side in a tank filled with hot water while keeping the other side in a tank filled with room-temperature water [7]. The time-dependent temperature profile is recorded with a conventional infrared heat camera. Fig. 2 shows the measured temperature distributions in a false-color scale for two different times t after exposing the sample to the heat baths at $t = 0\,\mathrm{s}$. The cloaking structure (left-hand side column) as well as a reference structure (right-hand side column) consisting only of the solid central region and one isolating ring are depicted. The cloak obviously succeeds in protecting the central region from heating and maintains a temperature distribution in the surrounding as if nothing was there, as indicated by the nearly vertical white iso-temperature lines. In sharp contrast to systems exhibiting wave phenomena, effects like scattering, shadowing or interference are absent for the reference structure in the right-hand side column of Fig. 2. Instead, only a distortion of the iso-temperature lines is observed, which can be seen as the thermal counterpart of wave fronts.

In conclusion, we have applied the concepts of transformation thermodynamics and realized a cloak that molds the flow of heat around an object as if no object was there [7]. Such thermal cloaks might find future application in, e.g., temporarily protecting a chip or electrical circuit from excessive heating. Furthermore, we have experimentally shown that the concepts of transformation electrodynamics are not restricted to wave phenomena but can also be applied to thermal conduction, which might pave the way towards cloaking for other diffusion processes in chemical and biological engineering.

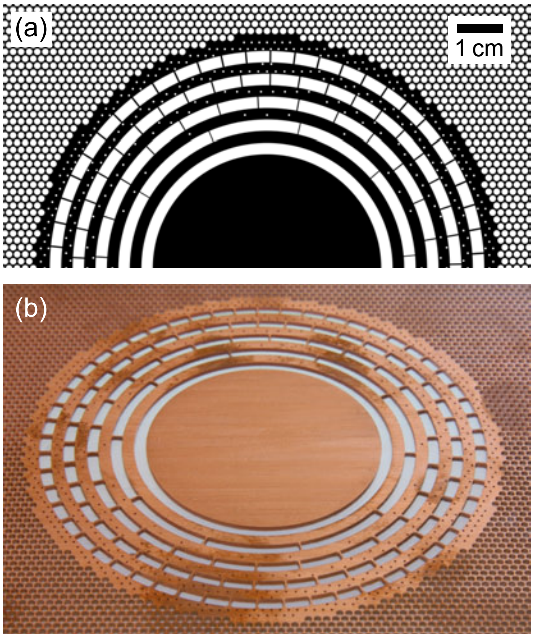

Figure 1: (a) Blueprint of the thermal cloak structure. Black regions resemble copper, white regions polymethyldisiloxan (PDMS). (b) Photograph of the fabricated cloak structure. Taken from Ref. [7]

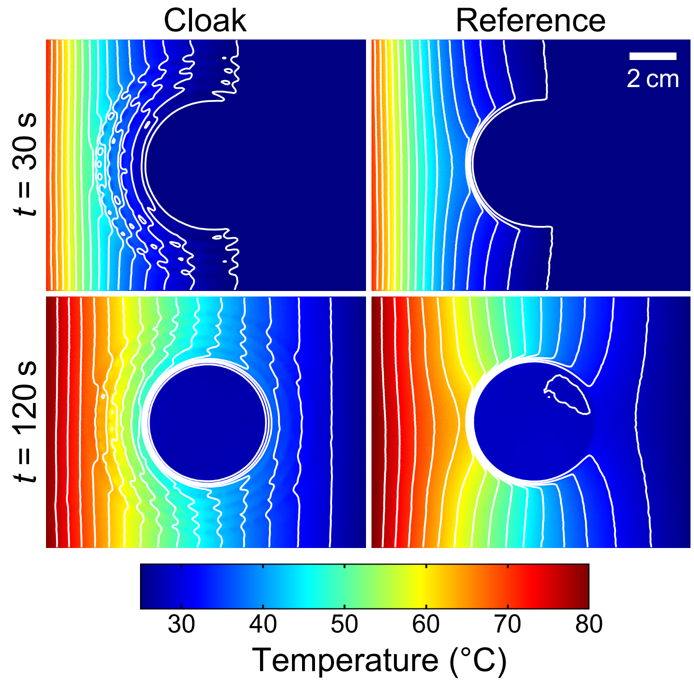

Figure 2: Measured temperature distributions at different times t after starting with a homogenous room-temperature distribution at $t = 0\,\mathrm{s}$. The left-hand side column depicts the complete cloaking structure as shown in Fig. 1(b), the right-hand side column shows results for a simplified reference structure consisting of only the solid central part and the first ring shown in Fig. 1(a). Iso-temperature lines are drawn in white with a spacing of 3° C. Taken from Ref. [7]

REFERENCES

[1] J. B. Pendry, D. Schurig, and D. R. Smith, Science **312**, 1780 (2006).
[2] M. Farhat, S. Enoch, S. Guenneau, and A. B. Movchan, Phys. Rev. Lett. **101**, 134501 (2008).
[3] G. W. Milton, M. Briane, and J. R. Willis, New J. Phys. **8**, 248 (2006).
[4] S. Zhang, D. A. Genov, C. Sun, and X. Zhang, Phys. Rev. Lett. **100**, 123002 (2008).
[5] S. Guenneau, C. Amra, and D. Veynante, Opt. Express **20**, 8207 (2012).
[6] N. Stenger, M. Wilhelm, and M. Wegener, Phys. Rev. Lett. **108**, 014301 (2012).
[7] R. Schittny, M. Kadic, S. Guenneau, and M. Wegener, arXiv:1210.2810 (2012).

Transformation optics: a new paradigm for nanoplasmonic cavity design

Stefan A Maier[1]
[1]Department of Physics, Imperial College London, London SW7 2AZ, UK

*corresponding author: s.maier@imperial.ac.uk

Abstract-The application of transformation optics to the field of nanoplasmonic cavities will be discussed. Generally, it will be shown how systems with structural singularities can be related to infinite geometries sustaining surface plasmon polaritions, and that this implies a broadband light harvesting response. The ramifications of blunting out singularities, as well as of non-local effects, will be elucidated.

Transformation optics allows us to manipulate electric and magnetic field lines, instead of rays, and opens up new avenues for the design of efficient light harvesting nanoplasmonic cavities. We have recently shown that a general class of two- and three-dimensional cavities with at least one geometrical singularity exhibits a broadband light collection response, which can intuitively be understood via a geometry transformation to an infinite system [1]. In this talk we will examine prominent incarnations of such cavities, such as touching nanowires and spheres, cavity-on-groundplane geometries, elucidate the fundamental physics of their superfocusing abilities, and present experimental realizations.

We will further show how the broadband response is removed when the relevant singularities are blunted out, focusing on the example of a crescent with rounded end corners [2]. In these situations, transformation optics can provide valuable design criteria for the development of experimentally realizable cavities with a desired spectral response.

Finally, we will show how non-local effects, a consequence of the smearing out of the surface charge over the characteristic lengthscale of the Thomas Fermi screening length, sets an ultimate limit to the light collection capabilities of plasmonics nanocavities [3, 4]. The talk will close with a discussion on the implementation of quantum effects related to electron tunneling into the transformation optics framework.

REFERENCES

1. Pendry, J.B., Aubry, A., Smith, D.R., & Maier, S.A., Transformation optics and subwavelength control of light, *Science* 337, 549 (2012)
2. Luo, Y. Lei, D.Y., Maier, S.A., & Pendry, J.B., Broadband light harvesting nanostructures robust to edge bluntness, *Physical Review Letters* 108, 023901 (2012)
3. Férnandez-Domínguez, A.I., Wiener, A. García-Vidal, F.J., Maier, S.A., & Pendry, J.B., A transformation optics description of non-local effects in plasmonic nanostructures, *Physical Review Letters* 108, 106802 (2012)
4. Ciracì, C., Hill, R.T., Mock, J.J., Urzhumov, Y., Fernández-Domínguez, A.I., Maier, S.A., Pendry, J.B., Chilkoti, A., & Smith, D.R., Probing the ultimate limits of plasmonics enhancement, *Science* 337, 1072

(2012)

Transformation Electromagnetics for Efficient Solution of Rough Surface Scattering Problems by Finite Methods

O. Ozgun[1*], **and M. Kuzuoglu**[2]
[1]TED University, Dept. of Electrical and Electronics Engineering, Ankara, Turkey
[2]Middle East Technical University, Dept. of Electrical and Electronics Engineering, Ankara, Turkey
[*]corresponding author: ozlem.ozgun@tedu.edu.tr

Abstract-A computational model is presented by combining the principles of transformation electromagnetics and finite methods (such as finite element method or finite difference methods) for efficient Monte Carlo simulation of rough surface scattering problems. Unlike the conventional Monte Carlo approach, the proposed approach utilizes the salutary features of the transformation electromagnetics to eliminate the need of mesh generation for each surface. A single mesh is created assuming a smooth surface and ignoring the actual surface, and thereafter, a transformation medium is designed on the smooth surface. This new problem becomes equivalent to the original problem by defining the material parameters of the transformation medium according to the actual surface through a coordinate transformation. A simple, single and uniform mesh is employed through repeated Monte Carlo realizations. Hence, the computation time is reduced to a great extent. The technique is demonstrated via various finite element simulations.

Since no real surface is perfectly smooth in physical world, it is of considerable interest to analyze the extent to which electromagnetic waves are affected by surface roughness. This problem is important especially in the design of radar systems, as well as in areas such as optics, acoustics, astronomy, etc. In general, the ongoing research in this area deals with three cases: (i) Scattering from a rough sea or ground surface, (ii) scattering from a composite problem where smooth objects are located on/above random rough sea or ground surface (i.e., perfectly smooth objects are in a random medium), and (iii) scattering from a rough-surface object in a deterministic or random medium. The analysis of such problems requires some statistical or stochastic techniques. A commonly-used technique is the Monte Carlo method, which is performed by producing a set of random rough surfaces from a given probability distribution, and by solving the problem corresponding to each surface by using a numerical technique. The results are collected and formed as a random process (or random field since the domain of the underlying parameter is space rather than time). The random process is analyzed to determine the average behavior of the problem (such as mean, variance, etc). One difficulty in implementing the Monte Carlo method is the large amount of computational resources required to realize the repeated solutions for each surface. For instance, while implementing the Monte Carlo method by finite methods, the mesh is generated anew for each surface and the problem is solved afterwards. Hence, the computation time increases dramatically especially in electrically large problems.

The purpose of this study is to present a computational model that makes efficient the Monte Carlo simulation of the rough surface scattering problem by combining the principles of transformation electromagnetics and finite methods. The studies in the field of transformation electromagnetics are intended to tune electromagnetic waves in a desired manner by designing application-oriented transformation media (or metamaterials) by using the form invariance property of Maxwell's equations under coordinate transformations [1-4]. If the spatial space is modified by defining a coordinate transformation, this medium equivalently turns into an anisotropic medium in which Maxwell's equations keep the same mathematical form. The material parameters of the transformation medium are determined by the Jacobian of the coordinate transformation. The main steps of the proposed approach are as follows: (i) Generate a single and uniform mesh on the assumed smooth surface of the object; (ii) Place a transformation medium on the smooth surface; and (iii) Compute the material parameters of the medium by applying a coordinate transformation that maps the points within the transformation medium to the actual space around the rough surface. In other words, a "virtual" equivalent problem working with a smooth surface and an anisotropic medium is created, which mimics the behavior of the original problem working with the rough surface. To illustrate the idea, an example is shown in Fig. 1. The coordinate transformation for this example is defined as follows:

$$\vec{r} \rightarrow \tilde{\vec{r}} = \mathrm{T}(\vec{r}) = K(\vec{r} - \vec{r}_{\mathrm{c}}) + \vec{r}_{\mathrm{b}}, \qquad \text{where } K = \|\vec{r}_{\mathrm{a}} - \vec{r}_{\mathrm{b}}\| / \|\vec{r}_{\mathrm{a}} - \vec{r}_{\mathrm{c}}\|. \tag{1}$$

Here, $\vec{r}$ and $\tilde{\vec{r}}$ are the position vectors of the points P and $\tilde{\mathrm{P}}$ in the original and transformed coordinate systems, respectively; and $\vec{r}_{\mathrm{a}}$, $\vec{r}_{\mathrm{b}}$ and $\vec{r}_{\mathrm{c}}$ are the position vectors of the points $\mathrm{P_a}$, $\mathrm{P_b}$ and $\mathrm{P_c}$, through the unit vector $\hat{a}$. The unit vector is originating from a point inside the innermost domain (e.g., the center-of-mass point) in the direction of the point P inside the layer. The main advantage of the approach is the ability to use the same mesh in all realizations of the Monte Carlo simulation. Each time the surface changes, only the material parameters are modified. We have explored the performance of the method by several finite element simulations.

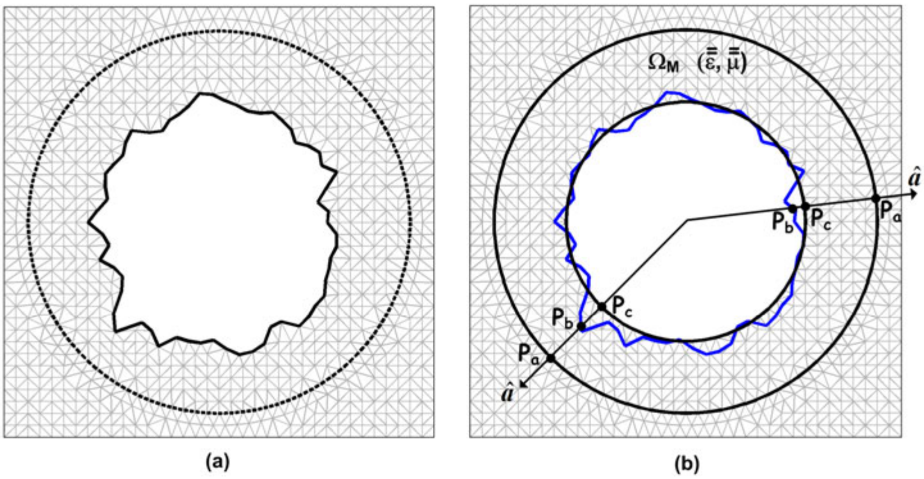

Figure 1: Circular cylinder with rough surface: (a) Original problem (the mesh is adapted to the actual rough surface), (b) Equivalent problem with transformation medium (the mesh is adapted to the smooth surface). (Roughness scale is exaggerated and a coarse mesh is used for better visualization.)

REFERENCES

1. Pendry J.B., D. Schurig, and D.R. Smith, "Controlling electromagnetic fields", *Science*, Vol. 312, 1780-1782, 2006.
2. Leonhardt U., "Optical Conformal Mapping", *Science*, Vol. 312, 1777-1780, 2006.
3. Ozgun O., and M. Kuzuoglu, "Electromagnetic metamorphosis: Reshaping scatterers via conformal anisotropic metamaterial coatings", *Microwave Opt. Technol. Lett.*, Vol. 49, No. 10, 2386-2392, 2007.
4. Ozgun O., and M. Kuzuoglu, "A Transformation Media Based Approach for Efficient Monte Carlo Analysis of Scattering from Rough Surfaces with Objects", *IEEE Trans. Antennas Propagat.*, (scheduled for) Vol. 61, No. 3, 2013.

Designing Antennas and Cloaks for Real-World Applications Using the Field Manipulation Technique

Raj Mittra[1, 2*], **and Yuda Zhou**[1]
[1] EMC Laboratory, The Pennsylvania State University, University Park, PA–16802, USA
[2] Distinguished Professor (Adjunct), King Fahd University of Petroleum and Minerals, Dhahran, Saudi Arabia
[*]corresponding author: rajmittra@ieee.org

The purpose of this paper is to discuss a technique for addressing the real-world problems of designing flat-lenses, high-performance horns, cloaks, *etc*., that are frequently handled by using the Transformation Optics (TO) algorithm [1-50]. The TO offers an elegant approach to designing these devices by morphing the geometry of a given object, which is located in the physical domain, into a target shape in the virtual domain that has the desired radiation or scattering characteristics. For instance, in the scattering case, the virtual domain object may be a cylinder (or sphere) with a vanishingly small radius r, embedded in free space, such that its cross-section as seen by an incoming wave is very small. Its physical domain counterpart could be a scaled-up version of the same, *i.e.*, one whose radius is larger by a scale factor of a, and which we are trying to cloak to render it invisible to an incoming wave by letting the virtual domain radius r tend to 0 in the limit. The TO approach capitalizes on the invariance of Maxwell's field equations to determine the material parameters of the medium surrounding the object in the physical domain, so that its scattering or radiation characteristics mimic those of the one in the virtual domain.

While the TO paradigm is elegant, simple to understand, and to implement on paper, there are a few hurdles which we need to overcome when we attempt to apply the algorithm to design real-world problems, *e.g.*, a flat lens or a cloak. For instance, we face issues pertaining to narrow bandwidth, strong dependence on polarization of the incoming wave, difficulty in acquiring materials with characteristics dictated by the TO, and controlling the thickness of the cloak (or the lens), to the level we desire. As an example, the thickness of a TO-designed cloak may be on the order of a wavelength (or larger), and its bandwidth may be only a few percent, while our design goal may be a cloak whose thickness is a small fraction of a wavelength, and whose bandwidth is several hundred percent—typically frequency range of interest in the radar world being 2 to 18 GHz. Furthermore, realizing the requisite permittivity and permeability values, dictated by the TO, may be totally infeasible, even if we use metamaterials, because of losses and dispersion effects in such materials that result in very narrow bandwidths and loss in efficiency and/or directivity.

In addition, while the application of the TO to design cloaks for objects with simple shapes has been discussed extensively in the literature, the problem of systematically deriving as well as realizing cloaks (or blankets) for *arbitrarily shaped* objects using materials that have realistic properties, namely ε and μ parameters, has not been thoroughly addressed yet. This provides us the incentive to explore ways to handle this practical problem, which is one of the objectives of this effort.

An alternative form of cloak, namely the "carpet cloak," transforms a surface with a "bump" to a flat planar surface, again by using the TO approach. Although the realizability issue may not be as critical in this case as it is for the conventional cloaks, the problem of realizing carpet cloaks is not altogether without its own difficulties either. The required ε and μ values for these cloaks can be less than unity at some locations, and be unreasonably high at others, making it difficult to realize them by either using available materials or metamaterials, since it is difficult to locate materials that are polarization-insensitive, non-dispersive and have the desired frequency characteristics over the band of interest. Furthermore, there appears to be no systematic approach that helps us in our attempt to reduce the thicknesses of either of these cloaks, which can easily be several wavelengths, to one that is a small fraction of the wavelength, as we typically desire.

In this work is present a new strategy that builds on the concepts of the TO to design radar absorbers that are tailored for arbitrarily shaped objects, and not just infinite planar surfaces, as has been the case in the past when designing such absorbers. We begin by using the conventional approach to designing absorbers for planar surfaces, employing realistic materials that can be fabricated in a Materials Lab by using realistic ingredients. We transform the original object to one with a relative smooth surface (but not to a scaled down version of the original object as is typically the case in TO), which is relatively close in shape *and size* to that of the original one. We then use the planar absorber that we have designed earlier to wrap it around the transformed object to determine how well it maintains its performance without any modifications. (We have demonstrated in the past that this is indeed the case, very often, by performing a large number of numerical experimentations, carried out for a wide variety of object shapes.) Finally, to complete the design process, we optimize the design (if performance improvement is warranted) by using a variant of the TO that we have developed, which does not explicitly rely on the Jacobian matrix of the coordinate transformation, but utilizes the integral form of Maxwell's equations instead to determine the modifications in the material parameters of the blanket for the desired object. It is intuitively clear that the if the two object shapes are close to each other, then the transformation of one geometry into another would not require a dramatic change in the desired material properties of the absorber from the original design; hence, the needed materials would be relatively easy to realize, because the adjustment from the original blanket is expected to be relatively minor.

The alternative TO, proposed herein, is based on impedance modification as opposed to geometry modification, and it transforms the very low impedance presented by a PEC object to one that is close to free space. The method can handle arbitrary objects, and the designed blankets are both physically realizable and realistic. Also, the blankets so designed are: (i) orders of magnitude thinner than those realized by using the TO; (ii) able to handle arbitrary polarization; and, (iii) have much larger bandwidths than those of the cloaks that have been reported in the literature to-date. The presentation will include the details of the proposed strategy as well as illustrative examples that show its application.

The paper will then go on to discuss the problem of designing lenses and other types of aperture antennas, again by using an alternative strategy rather than the coordinate transformation. This time we use field manipulation, to transform the distribution of the field in the input aperture, which originates from a given source of the incident field, into a desired distribution in the exit aperture plane, by deriving the material properties of the intervening medium located between these planes. Once again, the method we follow avoids the pitfalls of having to deal with unrealistic ε and μ parameters; hence, circumvents the bandwidth and loss problems that often plague the metamaterials-based designs. Illustrative examples that incorporate the above design procedure will be included in the presentation.

REFERENCES

1. Leonhardt, U. Optical conformal mapping. Science 312, 1777–1780 (2006).
2. Pendry, J. B., Schurig, D. & Smith, D. R. Controlling electromagnetic fields. Science 312, 1780–1782 (2006).

3. Chen, H., Chan, C. T. and Sheng, P. Transformation optics and metamaterials. Nature Materials 9, 387-396 (2010).
4. Post, E. G. Formal Structure of Electromagnetics: General Covariance and Electromagnetics (Interscience Publishers, 1962).
5. Lax, M. & Nelson, D. F. Maxwell equations in material form. Phys. Rev. B 13, 1777–1784 (1976).
6. Schurig, D., Pendry, J. B. & Smith, D. R. Calculation of material properties andray tracing in transformation media. Opt. Express 14, 9794–9804 (2006).
7. Shalaev, V. M. Transforming light. Science 322, 384–386 (2008).
8. Leonhardt, U. & Philbin, T. G. Transformation optics and the geometry of light. Prog. Opt. 53, 69–152 (2009).
9. Cummer, S. A. et al. Full-wave simulations of electromagnetic cloaking structures. Phys. Rev. E 74, 036621 (2006).
10. Schurig, D. et al. Metamaterial electromagnetic cloak at microwave frequencies. Science 314, 977–980 (2006).
11. Chen, H. S. et al. Electromagnetic wave interactions with a metamaterial cloak. Phys. Rev. Lett. 99, 063903 (2007).
12. Ruan, Z. C. et al. Ideal cylindrical cloak: perfect but sensitive to tiny perturbations. Phys. Rev. Lett. 99, 113903 (2007).
13. Liang, Z. X. et al. The physical picture and the essential elements of the dynamical process for dispersive cloaking structures. Appl. Phys. Lett. 92, 131118 (2008).
14. Chen, H. Y. & Chan, C. T. Time delays and energy transport velocities in three dimensional ideal cloaking devices. J. Appl. Phys. 104, 033113 (2008).
15. Leonhardt, U. Notes on conformal invisibility devices. New J. Phys.8, 118 (2006).
16. Cai, W. S. et al. Optical cloaking with metamaterials. Nature Photon.1, 224–227 (2007).
17. Cai, W. S. et al. Nonmagnetic cloak with minimized scattering. Appl. Phys. Lett. 91, 111105 (2007).
18. Yan, W. et al. Coordinate transformations make perfect invisibility cloaks with arbitrary shape. New J. Phys. 10, 043040 (2008).
19. Jiang, W. X. et al. Arbitrarily elliptical–cylindrical invisible cloaking. J. Phys. D 41, 085504 (2008).
20. Kwon, D.-H. & Werner, D. H. Two-dimensional eccentric elliptic electromagnetic cloaks. Appl. Phys. Lett. 92, 013505 (2008).
21. Nicolet, A., Zolla, F. & Guenneau, S. Electromagnetic analysis of cylindrical cloaks of an arbitrary cross section. Opt. Lett. 33, 1584–1586 (2008).
22. Lai, Y. et al. Complementary media invisibility cloak that cloaks objects at adistance outside the cloaking shell. Phys. Rev. Lett. 102, 093901 (2009).
23. Chen, H. Y. et al. Extending the bandwidth of electromagnetic cloaks. Phys. Rev. B 76, 241104 (2007).
24. Yaghjian, A. D. & Maci, S. Alternative derivation of electromagnetic cloaks and concentrators. New J. Phys. 10, 115022 (2008).
25. Kildishev, A. V. et al. Transformation optics: Approaching broadband electromagnetic cloaking. New J. Phys. 10, 115029 (2008).
26. Chen, H. Y. & Chan, C. T. Electromagnetic wave manipulation by layered systems using the transformation media concept. Phys. Rev. B 78, 054204 (2008).
27. Li, J. & Pendry, J. B. Hiding under the carpet: A new strategy for cloaking. Phys. Rev. Lett. 101, 203901

(2008).
28. Kallos, E., Argyropoulos, C. & Hao, Y. Ground-plane quasicloaking for free space. Phys. Rev. A 79 063825 (2009).
29. Liu, R. et al. Broadband ground-plane cloak. Science 323, 366–369 (2009).
30. Valentine, J. et al. An optical cloak made of dielectrics. Nature Mater. 8, 568–571 (2009).
31. Gabrielli, L. H. et al. Silicon nanostructure cloak operating at optical frequencies. Nature Photon. 3, 461–463 (2009).
32. Leonhardt, U. & Tyc, T. Broadband invisibility by non-Euclidean cloaking. Science 323, 110–112 (2009).
33. Chen, H. Y. & Chan, C. T. Transformation media that rotate electromagnetic fields. Appl. Phys. Lett. 90, 241105 (2007).
34. Chen, H. Y. et al. Design and experimental realization of a broadband transformation media field rotator at microwave frequencies. Phys. Rev. Lett. 102, 183903 (2009).
35. Roberts, D. A. et al. Transformation-optical design of sharp waveguide bends and corners. Appl. Phys. Lett. 93, 251111 (2008).
36. Rahm, M. et al. Transformation-optical design of adaptive beam bends and beam expanders. Opt. Express 16, 11555–11567 (2008).
37. Jiang, W. X. et al. Arbitrary bending of electromagnetic waves using realizable inhomogeneous and anisotropic materials. Phys. Rev. E 78, 066607 (2008).
38. Mei, Z. L. & Cui, T. J. Arbitrary bending of electromagnetic waves using isotropic materials. J. Appl. Phys. 105, 104913 (2009).
39. Yan, M., Yan, W. &Qiu, M. Cylindrical superlens by a coordinate transformation. Phys. Rev. B 78, 125113 (2008).
40. Jiang, W. X. et al. Layered high-gain lens antennas via discrete optical transformation. Appl. Phys. Lett. 93, 221906 (2008).
41. Kwon, D.-H. & Werner, D. H. Flat focusing lens designs having minimized reflection based on coordinate transformation techniques. Opt. Express 17, 7807–7817 (2009).
42. Roberts, D. A., Kundtz, N. & Smith, D. R. Optical lens compression via transformation optics. Opt. Express 17, 16535–16542 (2009).
43. Kwon, D.-H. & Werner, D. H. Polarization splitter and polarization rotator designs based on transformation optics. Opt. Express 16, 18731–18738 (2008).
44. Lai, Y. et al. Illusion optics: The optical transformation of an object into another object. Phys. Rev. Lett. 102, 253902 (2009).
45. Chen, H. Y. & Chan, C. T. “Cloaking at a distance” from folded geometries in bipolar coordinates. Opt. Lett. 34, 2649–2651 (2009).
46. Tretyakov, S. et al. Broadband electromagnetic cloaking of long cylindrical objects. Phys. Rev. Lett. 103, 103905 (2009).
47. Miller, D. A. B. On perfect cloaking. Opt. Express 14, 12457–12466 (2006).
48. Vasquez, F. G., Milton, G. W. & Onofrei, D. Active exterior cloaking for the 2D Laplace and Helmholtz equations. Phys. Rev. Lett. 103, 073901 (2009).
49. Alitalo, P. & Tretyakov, S. Electromagnetic cloaking with metamaterials. Mater. Today 12, 22–29 (2009).
50. Tang, W. Hao, Y. & Mittra, R. Design of A Carpet Cloak to Conceal an Antenna Located Underneath, IEEE Trans. Ant. Propag., vol. 60, no. 9, p. 4444, 2012.

Analytic Expression of Electromagnetic Fields in a Planar Layered Medium Obtained Using Transformation Electromagnetics

Joshua Le-Wei Li[1,2] and Zhi Wang[1]

[1]Institute of Electromagnetics & School of Electronic Engineering

University of Electronic Science and Technology of China, Chengdu, China

[2]Department of Electrical & Computer Systems Engineering

Monash University, Victoria, Australia and Selangor, Malaysia

Characterizations of electromagnetic fields in a multilayered medium have been an important, but tough research topic in various applications spanned from low frequency, via microwave frequency, millimeter wave frequency, terahertz, and optical wave frequency. The difficulty in the problem is the rigorous and/or exact solutions of the electromagnetic fields in such a planar layered material. There were many different approaches developed to obtain the solutions, either asymptotic or relatively accurate. However, there is no standard or widely valid solution available in the literature. To overcome the problem, the transformation electromagnetics approach is proposed in this paper to covert the layered planar structures to the spherically layered geometries. As the electromagnetic fields in spherically layered medium has exact solutions expressed in terms of the spherical harmonics, such a transformation electromagnetics approach will lead to the rigorous solution to the planar structures when the spherical radially are electrically large (versus the operating wavelength.

With this approach, all the 3 components of electromagnetic fields in the layered problems are obtained and expressed explicitly and the convergence issues of the slow convergent series are to be considered. The solution is found to be general enough for all the radiation antennas, and in some specific cases, we have considered practical examples for which we obtained our own results and compared them with these data commonly available in literature. Also, the convergence issues were be discussed.

Focusing properties of the Maxwell fish eye lens

R. C. Mitchell-Thomas[1], **O. Quevedo-Teruel**[1], **and Y. Hao**[1*]
[1] Department of Electronic Engineering and Computer Science,
Queen Mary University of London, United Kingdom
[*]corresponding author: yang.hao@eecs.qmul.ac.uk

Abstract – This summary outlines the origin and design of the Maxwell fish eye lens as a sub-wavelength image system, and its association with non-Euclidean transformations. A brief discussion of the focusing property is given, which is supported by two simulation techniques: 1) ray tracing illustrating the focusing in the limit of geometrical optics; and 2) a finite element method simulation, showing that the focusing property is retained for wave optics.

The refractive index profile of the Maxwell fish eye lens can be derived if the propagation of rays confined to the surface of a sphere is transformed into a flat surface by a geometrical projection [1]. Assuming that the rays will follow the surface of a sphere, if the rays are emitted from a point source at any arbitrary point, then they will diverge until they reach the mid-point of the sphere, and upon crossing this boundary the rays will converge to form a focus on the opposite side of the sphere. If a non-Euclidean transformation is applied to this curved surface to change it to a flat one, the outcome will be a profile that extends to infinity (where the refractive index reaches zero).

To circumvent this problem, the addition of a mirror around the circumference of the lens at a radius equal to that of the original sphere, and this gives the benefit of negating the need for metamaterials (and consequently, the losses and dispersive characteristics associated with them), and also makes the lens a finite size [2,3]. This index profile, truncated at the aforementioned radius, is plotted in figure 1(a), showing that the required refractive index range can be achieved with dielectric materials.

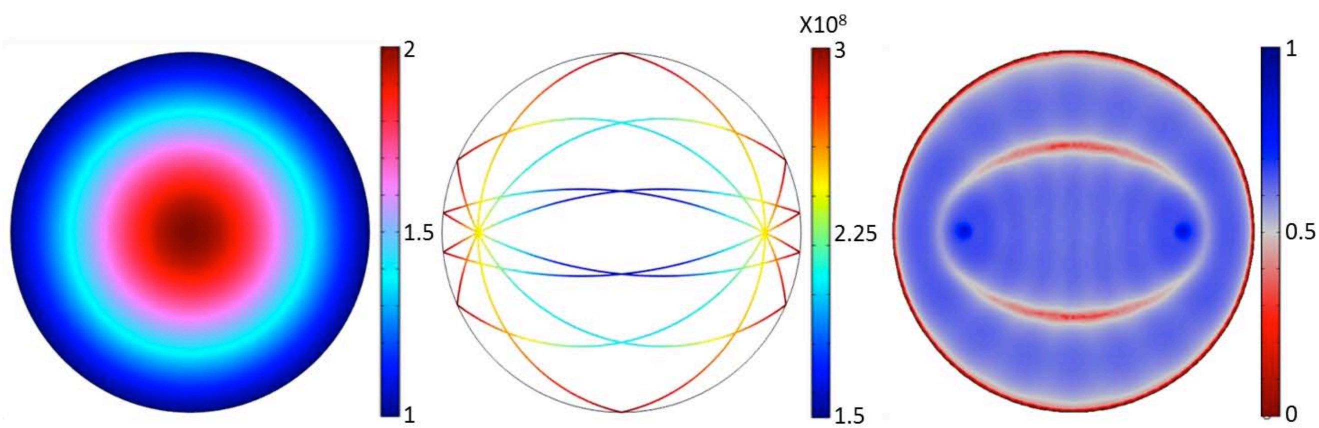

(a) (b) (c)

Figure 1. (a) Refractive index distribution of the Maxwell fish eye lens. (b) Ray tracing in the lens, where the colour bar indicates the phase velocity of the ray in the medium. (c) Normalized field intensity in the presence of an emitting source on the left hand side (dark blue point), and a passive, matched drain on the right hand side (dark blue point).

The index profile is surrounded by a mirror, which reflects the rays so that the once circular ray paths now have trajectories that follow arcs and they are each reflected by the mirror once, before converging at the image point, as shown in figure 1(b) with a ray tracing simulation. The color of the traced ray path denotes the speed of the ray, and it can be appreciated that although the ray paths have different lengths, the change in speed ensures that the phase on arrival at the image point is matched.

If this property is to be harnessed in a device, then a method of radiating, and capturing the electromagnetic wave needs to be employed. Here, a simple monopole antenna has been utilized, created from a coaxial cable, with the inner conductor exposed [4,5]. This is used for both the source (radiating) and the drain (non-radiating, passive). A full wave simulation (finite element method) was undertaken to illustrate the performance of the lens for wave optics and in figure 1(c) is illustrated by the field intensity in the device. It can be seen that the emitting source on the left side of the lens is reconstructed on the right hand side of the lens. This shows that for this simple scenario, the lens is capable of imaging an object.

Claims that the Maxwell fish eye lens is capable of imaging that can beat the diffraction limit [2,3] has created some disagreement in the literature [6-9], but this work shows that under certain conditions the sub-wavelength resolution can be achieved, specifically for a single source and drain. Analysis of the field intensity at the focal point in figure 1(c) shows that the width of the peak is a fraction of the wavelength in the medium. Previous work has also illustrated that the imaging is dependent upon frequency [10], however for discrete frequency bands, sub-wavelength imaging is once again achievable.

This work was funded by the Engineering and Physical Sciences Research Council (EPSRC), UK under a Programme Grant (EP/I034548/1) “The Quest for Ultimate Electromagnetics using Spatial Transformations (QUEST)”.

REFERENCES

1. Sarbort M., T. Tyc "Spherical media and geodesic lenses in geometrical optics," *Journal of Optics,* Vol. 14, 075705, 2012.
2. Leonhardt U. "Perfect imaging without negative refraction," *New Journal of Physics,* Vol. 11, 093040, 2009.
3. Leonhardt U., T. G. Philbin "Perfect imaging with positive refraction in three dimensions," *Physical Review A,* Vol. 81, 011804, 2010.
4. Ma Y. G., S. Sahebdivan, C. K. Ong, T. Tyc, U. Leonhardt "Evidence for subwavelength imaging with positive refraction," *New Journal of Physics,* Vol. 13, 033016, 2011.
5. Ma Y. G., S. Sahebdivan, C. K. Ong, T. Tyc, U. Leonhardt "Subwavelength imaging with materials of in-principle arbitrarily low index contrast," *New Journal of Physics,* Vol. 14, 025001, 2012.
6. Blaikie R. J. "Perfect imaging without refraction?," *New Journal of Physics,* Vol. 13, 125006, 2011.
7. Kinsler P. "Active drains and causality," *Physical Review A,* Vol. 82, 055804, 2010.
8. Merlin R. "Maxwell's fish-eye lens and the mirage of perfect imaging," *Journal of Optics,* Vol. 13, 024017, 2011.
9. Sun F., S. He "Can maxwell's fish eye lens really give perfect imaging?," *Progress in Electromagnetics Research-Pier,* Vol. 108, 307-22, 2010.
10. Quevedo-Teruel O., R. C. Mitchell-Thomas, Y. Hao "Frequency dependence and passive drains in fish-eye lenses," *Physical Review A,* Vol. 86, 053817, 2012.

Some theoretical and practical developments in controlling waves

S. A. R. Horsley[1],

[1]Electromagnetic and Acoustic Materials Group, Department of Physics, University of Exeter, Stocker Road, UK
s.horsley@exeter.ac.uk

Abstract In the first part of this talk we give an account of two developments in the theory of electromagnetic waves in continuous media: (i) the extension of transformation optics to chiral media; and (ii) the derivation of fundamental limits on the allowed constitutive relations for chiral, and generally bi anisotropic media from quantum mechanical principles. In the second part of the talk we discuss some early experimental work implementing transformation optics recipes to control the propagation of surface waves.

1. BI–ANISOTROPIC MEDIA AND TRANSFORMATION OPTICS

The original presentation of transformation optics [1] provides a means of finding the material parameters necessary to perform a given deformation of the electromagnetic field. It has the advantage that it is intuitive, and it has arguably been the most fruitful avenue for metamaterial device design.

However there are certain optical functions that cannot be straightforwardly understood in terms of a coordinate transformation. For example, focussing parallel rays to a point would require a transformation of an initial Cartesian grid that at one position compresses an axis to a point. This would certainly lead to undesirable material parameters. In such cases, one needs to use a broader understanding of transformation optics (*non–Euclidean transformation optics*), where the medium is understood as being equivalent to a *curved* space [2]. Such extra freedom has led to alternative designs for cloaking [3], and lensing [4].

Yet it is possible to go further with the geometrical understanding of Maxwell s equations, and this is the first subject of this talk. Differential geometry is fundamentally concerned with how vectors are transported around a space, and there are some geometrical properties that have not been examined in the context of transformation optics. One such property is known as *torsion*, and can be understood as the inherent twist of a space, causing vectors to rotate as they are transported. One finds this property is equivalent to chiral and Tellegen (of which, topological insulators provide a potential example) media [5]. In the case of chiral media it is found that the torsion (T_{ijk}) is related to the chirality (κ) as follows,

$$T_{ijk} = -2\mu_0\epsilon_{ijk}\frac{\kappa}{c} \tag{1}$$

In this manner chirality can be incorporated into transformation optics based designs, geometrically independent from ϵ and μ. This can be used to manipulate the polarization in some specific way without affecting the ray trajectories [5], and may lead to a new perspective on old problems [6].

After applying transformation optics one should then ask whether the material parameters appearing in the designs are realistic. Sometimes the required materials are very difficult to produce, but it is also possible that the constitutive relations violate a fundamental physical principle: in such a case they cannot be even approximately realised. We shall discuss the restrictions on chiral media (and bi anisotropic media in general) that emerge from considerations of quantum electromagnetism [7, 8]. The restrictions on the susceptibilities are found to be,

$$\boldsymbol{\chi}_{\text{EB}} - \boldsymbol{\chi}^{\dagger}_{\text{BE}}\ {}_{ij} \leq \ \boldsymbol{\chi}_{\text{EE}} - \boldsymbol{\chi}^{\dagger}_{\text{EE}}\ {}_{ii}\ \boldsymbol{\chi}_{\text{BB}} - \boldsymbol{\chi}^{\dagger}_{\text{BB}}\ {}_{jj} \tag{2}$$

where $\boldsymbol{\chi}_{\text{EB}}$ and $\boldsymbol{\chi}_{\text{BE}}$ are the bi anisotropic susceptibilities, $\boldsymbol{\chi}_{\text{EE}}$ is the electric susceptibility, and $\boldsymbol{\chi}_{\text{BB}}$ the magnetic susceptibility. This is a restriction on the dissipation within the medium, but via the Kramers Kronig relations one can also observe restrictions on the reactive part of the bi anisotropy, in turn this restricts the parameters used in some transformation optics based designs.

2. CONTROLLING SURFACE WAVES WITH TRANSFORMATION OPTICS

As well as being concerned with the fundamentals of controlling waves with geometry, we are now working towards putting transformation optics into practice within a model system. The experimental set–up is illustrated in figure 1i, where spoof surface plasmons [9] (surface waves) can be launched on a metal ground plane covered in vertical wires, upon which are attached square patches. It can be shown that in the isotropic case, the effective geometry (optical length dl, coordinates, $d\boldsymbol{x}$) seen by these surface waves is determined by the surface impedance of the structure, $\mathcal{Z}$,

$$dl^2 = \left(1 - \frac{\mathcal{Z}^2}{\eta^2}\right) d\boldsymbol{x}^2 \tag{3}$$

where η is the impedance of free space. Through changing the dimensions of the surface structure, $\mathcal{Z}$ can be tailored to manipulate the waves. Figure 1ii shows the experimental results from a surface that is designed to perform the function of a Luneberg lens.

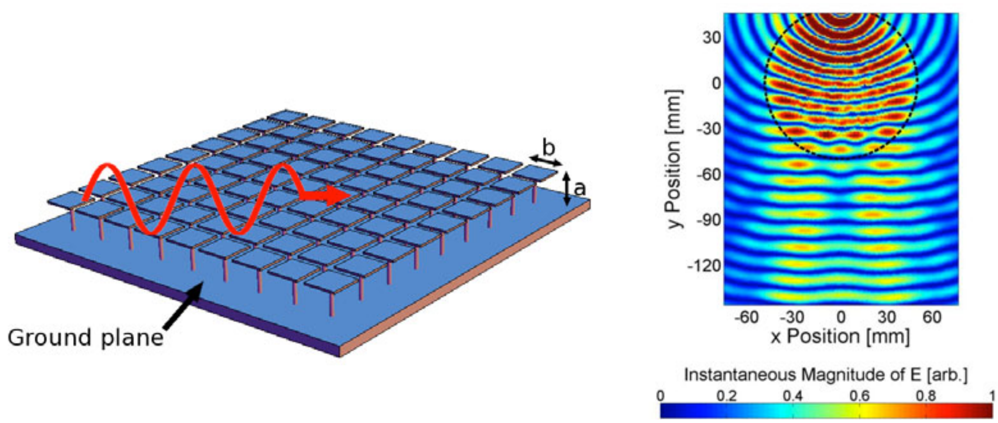

(i) (ii)

Figure 1: (i) Schematic of the experimental sample. Copper patches of cross–sectional area b^2 are attached through their centre to a ground plane via thin wires of length, a. The surface impedance of this structure, $\mathcal{Z}$ is determined by the values of a and b, and gives the effective geometry seen by the surface waves, via (3). (ii) Field plot of TM surface waves launched on a sample where the patch area within the dashed circle has been tailored to give the effective index profile of a Luneberg lens. The circular wavefronts of the point source at the top of the figure are clearly deformed into plane wave fronts as the wave passes through the device. The diffraction within the output wave is due to the small scale of the device relative to the wavelength.

To summarize, we show how chiral and Tellegen media may be incorporated into transformation optics, and derive fundamental limitations on the physically allowed chiral and bi–anisotropic media. We also illustrate some early experimental work to implement some transformation optics designs for surface waves.

ACKNOWLEDGMENT

This work was carried out while the author was supported by an EPSRC postdoctoral fellowship.

REFERENCES

1. Pendry, J. B., Schurig, D., and Smith, D. R., "Controlling Electromagnetic Fields," *Science*, Vol. 312, 1780, 2006.
2. Leonhardt, U. and Philbin, T. G., "General Relativity in Electrical Engineering," *New J. Phys.*, Vol. 8, 247, 2006.
3. Leonhardt, U. and Tyc, T., "Broadband Invisibility by Non–Euclidean Cloaking," *Science*, Vol. 323, 110, 2009.
4. Yao, K. and Jiang, X. and Chen, H., "Collimating lenses from non–Euclidean transformation optics," *New J. Phys.*, Vol. 14, 023011, 2012.

5. Horsley, S. A. R., Transformation optics, isotropic chiral media and non Riemannian geometry, *New J. Phys.*, Vol. 13, 053053, 2011.
6. Cory, H., Chiral devices - an overview of canonical problems, *J. Electromag. Wav. Appl.*, Vol. 9, 805, 1995.
7. Philbin, T. G., Canonical quantization of macroscopic electromagnetism, *New J. Phys.*, Vol. 12, 123008, 2010.
8. Horsley, S. A. R., Consistency of certain constitutive relations with quantum electromagnetism , *Phys. Rev. A*, Vol. 84, 063822, 2011.
9. Pendry, J. B., Martin-Moreno, L. and Garcia-Vidal, F. J., Mimicking Surface Plasmons with Structured Surfaces , *Science*, Vol. 305, 847, 2004.

Metasurfaces designed by coordinate transformations

Enrica Martini [1], Stefano Maci [2]

[#] *Department of Information Engineering and Mathematical Sciences, University of Siena*
Via Roma 56, Siena, Italy

[1] `martini@dii.unisi.it`

[2] `macid@dii.unisi.it`

***Abstract*—Metasurfaces are thin metamaterial layers characterized by unusual reflection properties of plane waves and/or dispersion properties of surface/guided waves. Properly modulated metasurfaces can be used to transform an incoming surface wave field into a different wavefield configuration with desired properties. This work proposes a systematic approach to design a large number of metasurface-based devices based on a metasurface transformation theory. This approach represents an extension of the Transformation Optics method to control the wavefront of surface waves through the use of modulated metasurfaces.**

I. Introduction

Metamaterials are artificial media which can be engineered to achieve electromagnetic behaviours which can not be found in nature. These artificial media can be formed by periodically arranging many small inclusions in a dielectric host environment. This concept can be extended to two dimensional lattices on a surface, thus realizing thin metamaterial layers characterized by unusual reflection properties of plane waves and/or dispersion properties of surface/guided waves. This surface version of a metamaterial is referred to in the literature as "metasurface" [1].

Metasurfaces can be realized at microwave frequencies by printing a dense periodic texture of small elements on a grounded slab, with or without shorting vias. The basic assumption in the conventional analysis of metasurfaces is the periodical distribution of the constituent elements with a period small in terms of the wavelength. Under this condition, the metasurface can be accurately characterized in terms of an equivalent surface impedance tensor relating the tangential components of the average electric and magnetic fields [2]. By introducing a modulation of the equivalent surface impedance it is possible to engineer the interaction of a given incoming field with the metasurface, thus realizing a large class of devices [3]. For instance, through the application of the holographic concept, modulated metasurfaces can be used to produce leaky-wave radiation [4-5]. Moreover, metasurfaces can be designed to achieve a prescribed equivalent refractive index profile, thus realizing planar lenses [6], or horns with increased directivity [7]. Many other applications are feasible, provided one is capable of defining the equivalent impedance pattern needed to obtain a desired wavefield transformation. This work proposes a systematic approach to metasurface design based on an extension of the Transformation Optics concept.

Transformation Optics is a systematic approach that makes use of coordinate transformations to design electromagnetic devices capable of controlling the propagation of electromagnetic waves [8]. This control is achieved on the basis of macroscopic equivalent constitutive tensors of a volumetric anisotropic material. The TO methodology has been applied, for instance, to design invisibility cloaks, i.e. shells of anisotropic materials capable of rendering any object within their interior cavities invisible to detection from outside [9, and references therein]. However, the technological difficulties in controlling the variation of the equivalent constitutive tensors of volumetric metamaterials, together with anisotropy and extreme values of the parameters, complicate the engineering implementation of TO in practical devices.

This work shows how the TO approach can be extended to control the propagation of design surface waves (SW) through properly designed modulated metasurfaces, with a significant increase in technological simplicity.

II. Metasurface Design based on a Coordinate Mapping

In order to extend TO theory to metasurfaces, let us consider two half-spaces: a "virtual" one, and a "real" one. Both half-spaces are filled by *free space*, however, they have two *different boundary conditions*. We assume that the virtual space possesses boundary conditions described by a *uniform* scalar reactive surface-impedance jX_S.

We define a coordinate transformation from the real to the virtual space. This transformation leaves unchanged the coordinate orthogonal to the surface impedance, so that it can be actually described by a 2D mapping. Similarly to what happens in the TO approach, the wavefronts of a SW propagating in the virtual space would be distorted in the real space according to the aforementioned coordinate mapping. This effect can be obtained by imposing in the real space boundary conditions described by a modulated anisotropic reactive impedance $j\underline{\underline{\mathbf{X}}}_{eq}$, whose entries are univocally related to the coordinate transformation. This relationship is obtained by matching the metasurface local dispersion equation to the one associated with the transformed wavefront.

It is noted that the direct application of a two dimensional version of TO would imply a variable compression of the medium in the direction normal to the surface, with a consequent inhomogeneity of the surrounding medium. In order to simplify the practical implementation we have instead assumed *a priori* the presence of free space above the impedance surface, and we have compensated this assumption by changing the value of the reactance tensor. The process suggested here is not exact; however, it is possible to identify the parameters of the coordinate transformation that reveal the accuracy of the approximation and to define the condition to avoid radiation losses.

A. Conformal Mappings

In the proposed approach, conformal mappings result in an isotropic equivalent surface impedance. In these cases, it is possible to identify an equivalent refractive index and to apply an effective Fermat's principle formulation to determine the ray paths. A similar approach can be also used for quasi-conformal mappings [10].

Isotropic metasurfaces can be realized at microwave frequencies by printing a dense periodic texture of small symmetric elements on a grounded slab. The modulation is obtained by gradually changing the geometry of the elements in contiguous cells. Figure 1 illustrates examples of practical realizations of modulated metasurfaces, consisting of square or circular patches with different sizes printed on a grounded slab.

Due to the small dimensions of the unit cell, the impedance variation can be assumed to be almost continuous. The value of the equivalent surface impedance at a given unit cell is obtained by considering the relevant constituent element as embedded in a uniform periodic structure which locally matches the geometry.

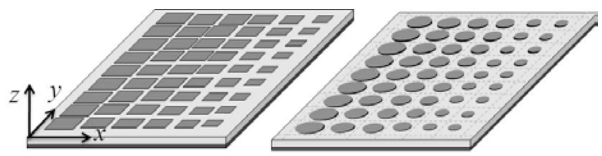

Fig. 1 Modulated metasurfaces at microwave frequencies consisting of small patches with variable sizes printed on a grounded slab.

B. Non Conformal Mappings

In the proposed approach, non-conformal mapping s lead to anisotropic equivalent impedance tensors. A specific anisotropic behaviour of the metasurface can be obtained by using asymmetric constituent elements. These elements typically exhibit two non-dimensional parameters, which primarily affect the principal values and the principal axes of the impedance tensor, respectively. The first parameter is the ratio between a characteristic length of the patch, and the side length of the periodic cell. Increasing this parameter implies increasing the magnitude of the principal values of the impedance tensor. The second parameter is the orientation angle and it mostly influences the orientation of the principal axes of the tensor. Figure 2 shows the entries of the equivalent impedance tensor for a screw-head patch as a function of the two aforementioned parameters. These maps have been obtained by assuming the patch embedded in a periodic Cartesian lattice and applying a periodic Method of Moment (MoM) analysis for a limited but sufficiently high number of prameter pairs.

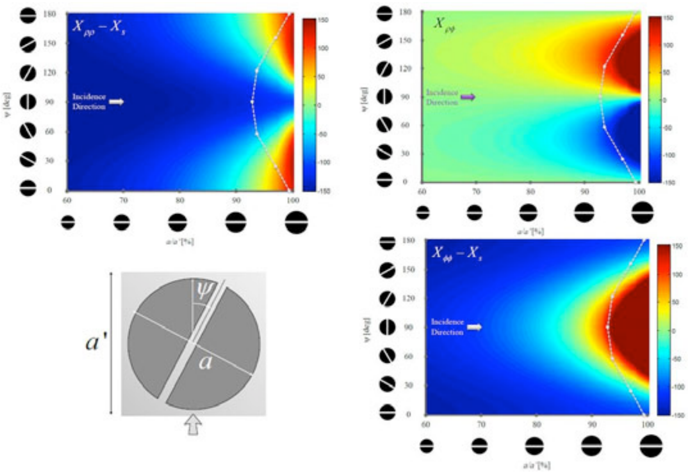

Fig. 2: Maps (in ohms) of the reactance tensor components $X_{ee}-\bar{X}_{ee}, X_{hh}-\bar{X}_{hh}, X_{eh}$; where $\bar{X}_{ee}, \bar{X}_{hh}$ are average values around 300 Ohms for the circular slotted element in the inset (results from [5]).

III. CONCLUSION

A systematic approach based on a generalization of the transformation optics concept has been presented for the design of metasurface based devices. As the outputs of the conventional TO approach are the metamaterial constitutive parameters able to perform a certain modification of the ray-field path, here the outcomes are the components of the equivalent impedance tensor capable to create a prescribed curved wavefront surface wave.

REFERENCES

[1] C.L. Holloway, E.F. Kuester, J.A. Gordon, J. O'Hara, J. Booth, and D.R. Smith, "An overview of the theory and applications of metasurfaces: the two-dimensional equivalents of metamaterials," *IEEE Antennas Propagat. Magazine*, vol. 54, no. 2, pp. 10-35, 2012.

[2] S. Maci, A. Cucini, "FSS-based EBG surfaces" In *Electromagnetic Metamaterials: Physics and Engineering Aspects* R.W. Ziolkowski, N. Engheta N eds, New York: Wiley Interscience, ch. 13, 2006.

[3] S. Maci S, G. Minatti, M. Casaletti, M. Bosiljevac, "Metasurfing: addressing waves on impenetrable metasurfaces," *IEEE Antennas Wireessl Propag. Lett.*, vol. 10, pp. 1499 – 1502, 2011.

[4] B.H. Fong, J.S. Colburn, J.J. Ottusch, J.L. Visher, D.F. Sievenpiper, "Scalar and tensor holographic artificial impedance surfaces," *IEEE Trans. Antennas Popagat.*, vol. 58, no. 10, pp. 3212 – 3221, 2010.

[5] G. Minatti, S. Maci, P. De Vita, A. Freni, M. Sabbadini, "A circularly-polarized isoflux antenna based on anisotropic metasurface," *IEEE Trans. Antennas Propagat.,* vol. 60, no.11, pp. 4998 – 5009, 2012.

[6] M. Bosiljevac, M. Casaletti, F. Caminita, Z. Sipus, and S. Maci, "Non-uniform metasurface Luneburg lens antenna design," *IEEE Trans. Antennas Propagatat.*, vol. 60, no. 9, pp. 4065-4073, 2011.

[7] M. Casaletti, F. Caminita, S. Maci, M. Bosiljevac and Z. Sipus, "New type of horn based on variable metasurface," *2011 IEEE AP-S*, pp. 1048-1050, 2011.

[8] J.B. Pendry, D. Schurig, D.R. Smith, "Controlling electromagnetic field," *Science*, vol. 312 (5781), pp. 1780-1782, 2006.

[9] A.D. Yaghjian, S. Maci, "Alternative derivation of electromagnetic cloaks and concentrators," *New J Phys*. Vol. 10, pp. 1-29, 2008.

[10] J. Li and J. B. Pendry, "Hiding under the carpet: a new strategy for cloaking," *Phys. Rev. Lett*., vol. 101, no. 20, 203901, 2008.

Plasmonic antennas

Broadband and hybrid plasmonic/dielectric cavities for sensing and spectroscopy

Stefan A Maier[1]
[1]Department of Physics, Imperial College London, London SW7 2AZ, UK

[*]corresponding author: s.maier@imperial.ac.uk

Abstract- A new design approach for plasmonic nanoantennas covering a spectral range from the visible to the mid-infrared is presented, based on a log periodic geometry. Examples in higher harmonic generation as well as surface enhanced infrared absorption spectroscopy are shown. We also demonstrate how the figure of merit of localized surface plasmon resonance sensors can be significantly increased via hybridization of the plasmonic modes with higher-order Fabry Perot resonances of an underlying dielectric thin film. Applications in nanometrology will be discussed.

We have recently introduced the translation of log perioidic antenna designs from the RF to the visible and the near-infrared regime [1]. Due to their broadband response, such antennas are efficient transducers from the far to the near field over a broad spectral range, which makes them particularly useful for the enhancement of nonlinear processes. In this regard we will present and elucidate recent results on highly efficient second harmonic generation from silver log periodic antennas, with efficiencies close to those of conventional macroscopic crystals [2]. The broadband nature of the field concentration allows efficient generation over a spectral width of about one micron, due to simultaneous enhancement of both the exciting laser field, and the nonlinear susceptibility at the 2nd harmonic frequency.

The broadband nature of the field enhancement also makes log periodic antennas an ideal substrate for surface enhanced spectroscopies, as molecular fingerprinting usually requires the simultaneous observation of spectrally separated absorption lines. In this regard we will present first results on surface enhanced infrared absorption spectroscopy (SEIRA) over a spectral width of about 3 microns, and discuss how the spectral window can be broadened to span from the visible to the mid-infrared, with the prospect of enhancements of fluorescence, surface enhanced Raman, and surface enhanced infrared absorption spectroscopies on the same substrate.

Lastly, we demonstrate how a hybrid plasmonic/dielectric-cavity nanosensor combines both the high spatial field confinement of plasmonics with high cavity quality factors of dielectric cavities, resulting in an improved overall figure of merit for refractive index sensing. Our design is based on the dipolar plasmon mode of a Au nanoparticle hybridized with higher-order Fabry Perot modes of an underlying dielectric thin film [3]. Detailed studies on sensitivity will be presented, together with applications in thin film nanometrology.

REFERENCES

1. Navarro-Cia, M., & Maier, S.A., Broad-band near-infrared plasmonic nanoantennas for higher harmonic generation, *ACS Nano* 6, 3537 (2012)

2. Aouani, H., Navarro-Cia, M., Rahmani, M., Sidiropoulos, T.P.H., Hong, M., Oulton, R.F., & Maier, S.A., Multiresonant broadband optical antennas as efficient tunable nanosources of second harmonic light, *Nano Letters* 12, 4997 (2012)
3. Schmidt, M.A., Lei, D.Y., Wondraczek, L., Nazabal, V., & Maier, S.A., Hybrid nanoparticle-microcavity-based plasmonics nanosensors with improved detection resolution and extended remote-sensing ability, *Nature Communications* 3, 1108 (2012), doi:10.1038/ncomms2109

Optical responses of three dimensional plasmonic nanoantenna arrays

X. X. Xia[1*], Z. Liu[1], J. J. Li[1], H. F. Yang[1], B.G. Quan[1], and C. Z. Gu[1]

[1]Beijing National Laboratory for Condensed Matter Physics, Institute of Physics, Chinese Academy of Sciences, Beijing 100190, China

[*]corresponding author: xiaong@aphy.iphy.ac.cn

Abstract-Nanoantenna metamaterial can be used for many important applications in photonics and optoelectronics. However, most of previous nanoantenna structures are simple wires or rods due to the limitation of nanofabrication. In this work, a series of hexagonal three dimensional gold nanoantenna arrays were fabricated. The optical responses of such nanoantenna arrays were systematic studied by varying the incidence polarization, geometry parameters of nanoantenna structure and dielectric-loads. It would improve the manipulation ability of nanoantenna metamaterials with more freedom and flexibility.

The interaction of light with designed metallic nanostructures provides an opportunity to manipulate light for novel applications in photonics and optoelectronics. Due to the unique optical resonances in such metallic nanostructures, the so-called metamaterials have become a topical focus of intense current interest. Nanoantenna arrays with simple one-dimensional metallic structures such as nanorods or nanowires can function as a metamaterial with tunable optical properties by dielectric load [1, 2]. Such nanoantenna metamaterial can be used for many applications such as surface enhanced Raman scattering, sensing, imaging and optical nonlinearity enhancement. However, in previous studies, most nanoantenna structures still are simple arrays of wires, rods or dots because of limitation in nanofabrication. Due to the essential geometry-dependence of its optical resonances, the study on three dimensional nanoantenna structures becomes extremely urgent and important.

In this work, a series of three dimensional gold nanoantenna arrays were fabricated. The unit cell of hexagonal array was consisted of crossing nanowires and standing nanorods, as shown in Fig. 1. By using a negative electron resist hydrogen silsesquioxane (HSQ) and gray-tone e-beam lithography, the three dimensional structure was realized in HSQ resist, and then was transferred onto a gold film by an inductively coupled plasma reactive ion etcher. Fig. 2. shows the SEM pictures of the gold three dimensional nanoantenna array, the linewidth of the unit structure is 40 nm. The optical responses of such nanoantenna arrays were systematic studied by varying the incidence polarization, geometry parameters of nanoantenna structure and dielectric-loads. This study would improve the manipulation ability of nanoantenna metamaterials with more freedom and flexibility.

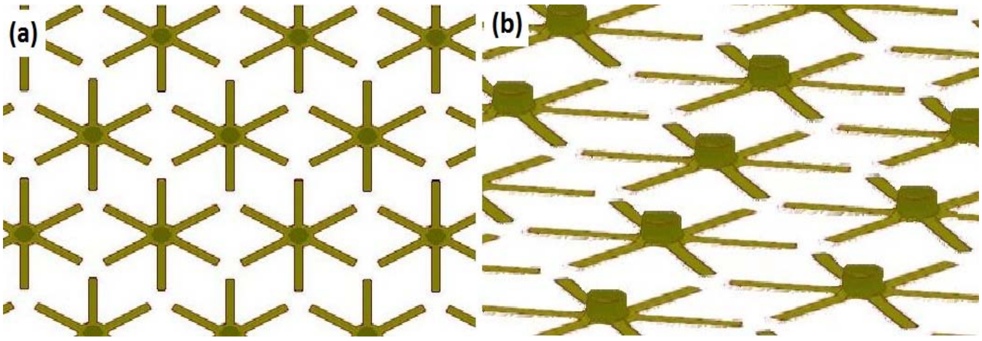

Figure 1 Schematic of the 3D nanoantenna arrays: (a) top view and (b) side view

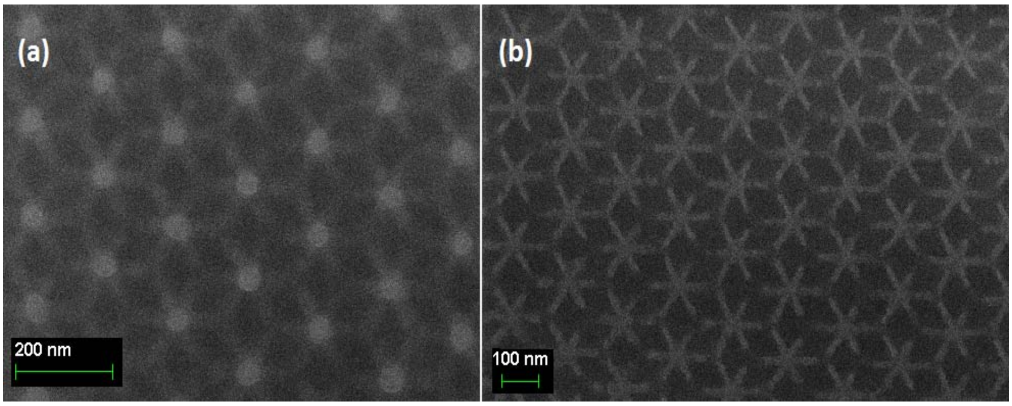

Figure 2 SEM pictures of the top view of 3D nanoantenna arrays:
(a) focused on the top; (b) focused on the bottom

Acknowledgements This work was supported by National Natural Science Foundation of China (Grants No. 50825206, 1083401, 60871045，61001045, 50825206 and 91023041) and the National Basic Research Program of China (Grant No.2009CB930502) and the Knowledge Innovation Project of CAS (Grant No. KJCX2-EW-W02).

REFERENCES

1. Dickson, W., G. A. Wurtz, P. Evans, D. O’Connor, R. Atkinson, R. Pollard, and A. V. Zayats, “Dielectric-loaded plasmonic nanoantenna arrays: A metamaterial with tuneable optical properties,” *Physical Review B*, 76, 115411, 2007.
2. Alu, A., and N. Engheta, “Tuning the scattering response of optical nanoantennas with nanocircuit loads,” *Nature Photonics*, Vol. 2, 307–310, 2008.

Ultrafast index modulation of a terahertz graphene metamaterial

Seung Hoon Lee[1], Jeongmook Choi[2], Hyeon-Don Kim[1], Hyunyong Choi[2*], and Bumki Min[1*]
[1]Mechanical Engineering, KAIST, Republic of Korea
[2]Electrical and Electronic Engineering, Yonsei University, Republic of Korea
[*]corresponding author: hychoi@yonsei.ac.kr, bmin@kaist.ac.kr,

Abstract We demonstrate significant amount of ultrafast index modulation by optically exciting nonequilibrium Dirac fermions in the graphene layer integrated onto the high index metamaterial. Furthermore, an extremely-large electrical modulation of refractive index up to $\Delta n \sim -3.4$ (at 0.69 THz) is achieved by electrical tuning of the density of equilibrium Dirac fermion in the graphene metamaterial.

Refractive index control in natural materials has attracted considerable attention in the field of holographic imaging systems and data storage [1] as well as for numerous photonic applications. Change of refractive index under external stimuli has been intensively studied in various transparent nonlinear crystals [2] and light-sensitive materials [3]. However, these natural materials inherently have small index change due to high-order nonlinearities known as Pockels or Kerr effects and insignificant modification of molecular structures in polymers. Therefore, promising alternatives to the natural materials for ultrafast index modulation with large contrast are highly desirable.

In order to actively control of the refractive index, here we propose terahertz (THz) metamaterial where an array of meta-atoms, an atomically thin graphene layer, and an array of metallic wire gate electrodes are functionally configured together into an ultra-compact, thin, and flexibly polymeric substrate [4] as shown in Fig. 1a. As can be confirmed by the image of the saturated electric field in Fig. 1d, a large number of surface charges accumulate on the edge of the hexagonal metallic frame, which induces a huge polarization by strong capacitive coupling between the unit cells [5]. Among the accumulated charges, some portion of the charge carries leak into the attached graphene layer, resulting in a reduction of the induced polarization, which determines the initial refractive index of the graphene metamaterial. When the Fermi level of graphene is tuned by proper electrical gating or optical pumping, the induced polarization is altered because the intraband optical conductivity of graphene is highly sensitive to its Fermi level, and the conductivity change modifies the capacitance between the meta-atoms. With this principle of polarization change, the effective permittivity, and thus the refractive index of

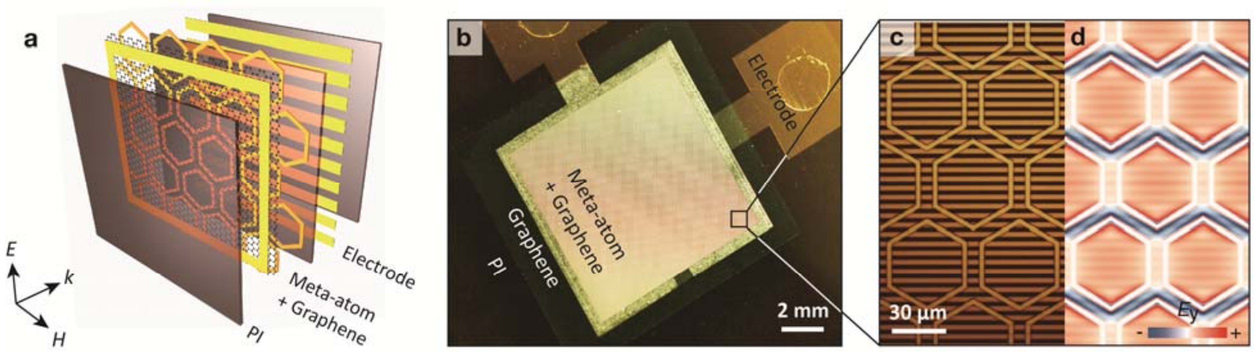

Fig. 1. Schematic view and OM image of high index graphene metamaterials. **(a)** Schematic rendering of a graphene metamaterial shows that a monolayer graphene directly attached to hexagonal gold meta-atoms (a 60-µm-size unit cell with 3-µm-width and a 100-nm-thick gold frame with a 5-µm-width gap between adjacent meta-atoms) and transparent wire electrodes (periodicity = 6 µm, metal width = 4 µm) are fully embedded in a thin and flexible polyimide (PI) substrate. The total thickness of the graphene metamaterial is ~3.2 µm which shows a high index of refraction above 10 at the THz range. Both the ultrafast optical pump beam and electrical gating contribute to the modulation of the high index of refraction with large index contrast. **(b)** Optical image of the fabricated high index graphene metamaterial. **(c)** Optical micrograph of the fabricated metamaterial for a clear understanding of the realistic structure of the field image of **(d)** where in-plane electric field component (at 0.5 THz) of the graphene metamaterial is plotted at the charge neutral point (CNP).

the graphene metamaterial can be modulated both by electrical and optical means. An image of the fully integrated device is shown in Figs. 1b and c, and the geometrical parameters of the fabricated metamaterial are given in the caption of Fig. 1.

Figures 2a shows electrically-controlled refractive index Re(n) extracted from the THz-TDS measurement with an iterative algorithm considering multi-pass transmission [5]. At charge neutral point (CNP), a strong electrical resonance was observed with a peak refractive index of 13.8 at a frequency of 0.58 THz and of 12.1 at the quasi-static limit where the loss of the metamaterial has a minimum value. With increasing $|\Delta V|$, where $\Delta V = V_g - V_{CNP}$ and V_g is the applied gate voltage, the refractive index gradually decreased from 12.4 to 9.0 (ΔRe(n) ~ −3.4) at 0.69 THz due to remarkable change of the capacitance between the meta-atoms. To investigate optically-controlled ultrafast index modulation in the graphene metamaterial, we employ an ultrafast optical-pump THz-probe spectroscopy (upper panel in Fig. 2c). As displayed in Fig. 2b, the pump-induced $\Delta E(t)$ traces show substantial field reshaping compared to the $E_0(t)$. Negligible phase shifts of $\Delta E(t)$ were observed in the low-frequency part of early THz field delay (t < 0) while apparent phase shifts were shown in the high-frequency component of the THz field (t > 0) because of resonance arising from the meta-atoms. The resonant response is further characterized in order to corroborate the electrical index modulation. As shown in Fig. 2c, when the pump fluence is 18.7 μJ/cm^2 for example, the photo-induced refractive index change shows a large index contrast ΔRe(n) ≃ −2.4 near the frequency at around 0.61 THz, and the modulation depth is highly sensitive to the applied gate voltages.

In conclusion, we demonstrated both electrical and optical control of the refractive index of graphene-hybrid THz metamaterials showing that the unprecedented index contrasts were much larger than that of any natural photorefractive polymers or nonlinear crystals. This graphene-based tunable metamaterials may have a great advantage in the ultrafast operation of various THz devices as well as tunable transformation optics.

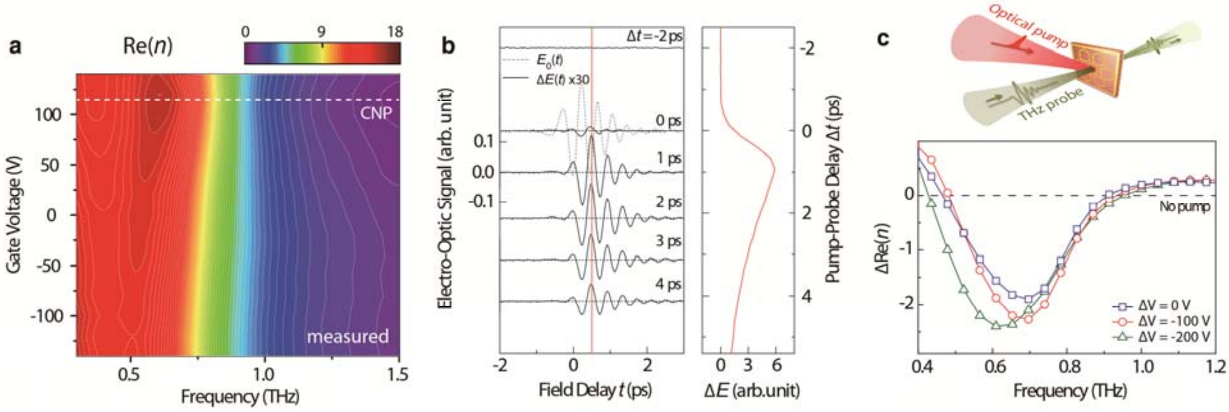

Fig. 2. Electrically and optically control of the refractive indices of the graphene metamaterial. **(a)** Electrical control: measured refractive index spectra are plotted as a function of gate voltages (electrically). With increase the quasi-static carrier density, the refractive index decrease near resonance frequency (at 0.69 THz). **(b)** Optical control: the THz field through the graphene metamaterial without a pump $E_0(t)$ (gray dot) and with a pump (black line) are shown at different pump-probe delay Δt. **(c)** Upper: a schematic of the optical-pump THz-probe spectroscopy is shown. Lower: the photo-excited refractive index changes as a function of gate-voltages at Δt = 1 ps with a pump fluence of 18.7 μJ/cm^2. The large index contrast ΔRe(n) ≃ −2.4 and the red-shift of the resonance are clearly visible due to decrease of the graphene's intraband optical conductivity.

REFERENCES

1. Haw, M. "Holographic data storage: The light fantastic," *Nature*, Vol. 422, No. 6932, 556–558, 2003.
2. Ashkin, A. et al. "Optically-induced refractive index inhomogeneities in $LiNbO_3$ and $LiTaO_3$," *Appl. Phys. Lett.*, Vol. 9, No. 1, 72–74, 1966.
3. Würthner, F. *et al.* "ATOP dyes. Optimization of a multifunctional merocyanine chromophore for high refractive index modulation in photorefractive materials. *J. Am. Chem. Soc.* Vol. 123, No. 12, 2810-2824, 2001.
4. Lee, S. H. *et al.* "Switching terahertz waves with gate-controlled active grpahene metamaterials," *Nature Mater.*, Vol. 11, No. 11, 936–941, 2012.
5. Choi, M. et al. " A terahertz metamaterial with unnaturally high refractive index," *Nature*, Vol. 470, No. 7334, 369–373, 2011.

Gradient index devices for terahertz waves and terahertz surface waves

M. Volk[1], T. Fip[1], B. Reinhard[1], M. Höh[1], J. Neu[1], and M. Rahm[1,*]
[1]Department of Electrical and Computer Engineering and Research Center OPTIMAS, University of Kaiserslautern, Germany
[*]corresponding author: marco.rahm@eit.uni-kl.de

Abstract-Gradient index devices provide versatile means to actively manipulate the electromagnetic properties of both freely propagating terahertz (THz) waves and tightly bound surface waves. In this context, we investigated meta-surfaces with specific gradient index structures that were designed to focus confined surface waves along their path on the surface. Further applications of gradient index devices, as for example surface wave bends and switchable mirrors, are discussed.

The idea of implementing optics by using materials with a spatial gradient of the refractive index reaches back to at least the 19th century when Maxwell already studied various examples of such gradient index (GRIN) optics in 1854 [1]. Back then, these concepts could not be readily technologically implemented due to a lack of available materials and fabrication methods. Although the development of sophisticated growing and doping methods enabled the fabrication of more conventional GRIN optics, the invention of metamaterials finally added considerable freedom to the design and fabricability of GRIN devices and brought this concept to another level. GRIN optics has been successfully demonstrated for a number of examples in the microwave [2], terahertz [3] and even in the infrared spectral region where most recently holograms were experimentally demonstrated by use of metamaterial-based gradient index diffractive optics [4,5].

In the presentation, we show how gradient index design concepts can be used to technologically implement in-plane optics for tightly bound terahertz surface waves on meta-surfaces. Although various examples for such devices are presented in the presentation, we only focus on a gradient index lens for terahertz surface waves in this summary.

Fig. 1(a) shows a schematic of the gradient index design of a meta-surface that supports strongly confined surface waves. In the experiment, we excited the surface waves by a grating coupler which constitutes the excitation region of the implemented GRIN meta-surface. Along the propagation zone we devised the meta-surface to exhibit a lateral index gradient with a higher index in the center line of the propagating surface wave and a decreasing index towards the border. That way, a propagating plane wave is converted into a focusing wave along the meta-surface. Fig. 1(b) illustrates the near field measurement of the electric field of the surface wave. As can be seen, the phase fronts of the electric field obtain a converging curvature during the propagation and the surface wave is focused in the focal plane from which it diverges during the subsequent travel. The deviation of the surface wave from the original propagation direction behind the focus is an artifact of the measurement and results from varying distances of the measurement tip from the slightly curved metasurface during the measurement.

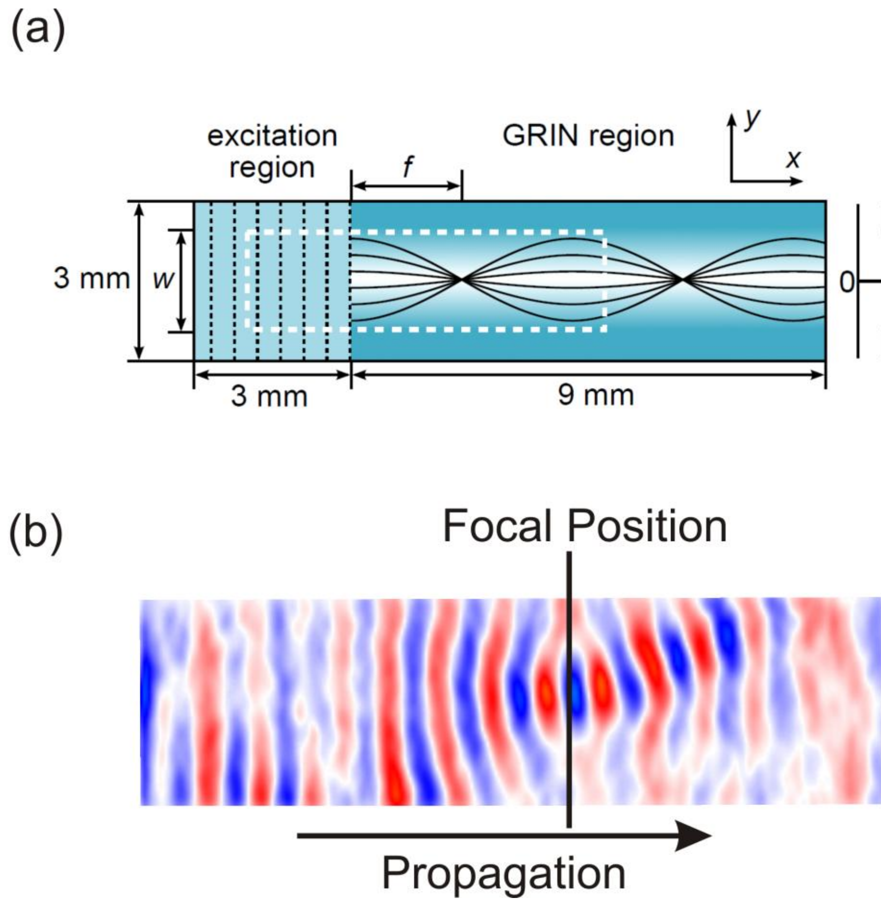

Fig. 1: (a) Schematic of the design of a GRIN lens for terahertz surface waves. The surface waves are excited by grating coupling in the excitation zone and propagate from left to right. Due to a lateral gradient, the surface waves are focused along their path on the metasurface. (b) Experimental demonstration of the focusing behavior of the GRIN metasurface. The picture shows the phase fronts of the electric field. In this case, only the region which is denoted by the white rectangle in (a) has been measured.

REFERENCES

1. J. C. Maxwell, "Solutions of problems," Cambridge Dublin Math. J.8, 188–195 (1854).
2. D. R. Smith, J. J. Mock, A. F. Starr, and D. Schurig, "Gradient index metamaterials," Phys. Rev. E 71, 036609 (2005).
3. J. Neu, B. Krolla, O. Paul, B. Reinhard, R. Beigang, and M. Rahm, " Metamaterial-based gradient index lens with strong focusing in the THz frequency range," Opt. Express 18, 27748 (2010).
4. Yu-Ju Tsai, Stéphane Larouche, Talmage Tyler, Guy Lipworth, Nan M. Jokerst, and David R. Smith, "Design and fabrication of a metamaterial gradient index diffraction grating at infrared wavelengths," Optics Express 19, 24411-24423 (2011).
5. S. Larouche, Y.-J. Tsai, T. Tyler, S. Dhar, N. M. Jokerst, D. R. Smith, "Infrared metamaterial hologram", Nature Materials 11, 450 (2012).

Long-range interaction of localized surface plasmons from periodic to random Au nano-disk patterns

Y. Nishijima[1], **L. Rosa**[2], **and S. Juodkazis**[2,3]

[1]Department of Electrical and Computer Engineering, Graduate School of Engineering, Yokohama National University, Japan
[2]Faculty of Engineering and Industrial Sciences, Swinburne University of Technology, Australia
[3]Melbourne Centre for Nanofabrication, Australia
nishijima@ynu.ac.jp

Abstract— The plasmon resonance of periodic/random arrays of Au-nanodisks has been investigated experimentally and numerically. During the randomization, plasmon resonance spectra become broadened, however the electro-magnetic field enhancement is augmented by a factor of 10-10^2 times as shown by the finite elements time domain (FDTD) calculations. The randomized structures are promising for the applications in opt-electronics and sensing.

The localized surface plasmon resonances (LSPRs) are generated by nanostructures of noble metals such as gold, silver and copper, which are attractive and promising materials in the field of opto-electronics, photochemistry, and sensing. Recently configuration of a nano-pattern has been paid much of attention for controlling the wide-angle light-plasmon coupling. In the case of periodic arrays of nanostructures which are widely produced by top-down nanotechnology techniques, the Bragg diffraction strongly affects scattering and plasmon resonances. The diffracted light departs from surface and is lost for light harvesting. However, when periodicity of pattern is broken by randomization, spectroscopic properties and electromagnetic field enhancement are modified favorably for light harvesting. In this study, we demonstrate the optical extinction spectra of well-defined square lattice arrays of gold nano-disks and their random configurations at a gradually increasing disorder. The experimental results are analyzed numerically [1, 2, 3].

Arrays of nano-disks were fabricated by top-down approach using electron beam (EB) lithography lift-off technique as reported earlier [1]. EB resist (ZEP-520A ZEON Co.) was coated on the glass substrate by spin coating (3000 rpm for 2 min.). Top of resist was covered with charge dissipating agent. Patterns of gold nano-disks are CAD generated by the random-walk method starting from a perfectly periodic arrangement. After EB drawing process and development, 2 nm of Cr (as the adhesion layer) and 25 nm of Au has been coated with thermal evaporation. Then, EB resist with residual metal over-coating was removed by organic solvent; the obtained gold nano-disc structures were used for experiments. Transmission spectra were measured with a confocal microscope system, composed of a microscope ($10^{\times}$ objective lens with numerical aperture $NA = 0.5$, pinhole of 0.1 mm diameter from Optiphoto, Nikon Co.) and an optical spectrum analyzer (Q8381A, Advantest Co.). Numerical simulations by finite-difference time domain (FDTD) method were carried out with 5×5 nano-discs; the configuration was obtained from the CAD design used in EB.

Figure 1 shows the optical dark field images and scanning microscopy images of 500 nm periodic/random arrays. During the randomization, green color (which is caused by the Bragg diffraction of 500 nm periodic pattern) has disappeared and a red color (scattering of light by plasmon resonance) gradually appeared. Typical extinction features of periodic and randomization effect is shown in Fig. 2. When increasing the periodicity from 450 to 750 nm, an extinction peak shifts, at first to the red and then to the blue spectral side. This is caused by the coupling of plasmon resonance and Bragg diffraction [1, 4]. During the randomization process, plasmon resonance slightly blueshifts and broadens. As shown in the optical microscopic image, internal Bragg diffraction has disappeared with randomization. Reducing the order of initially periodic patterns affects the plasmon resonance, its spectrum, and electro-magnetic field enhancement. The electro-magnetic field enhancement is up to 10-10^2 times larger in partly disordered patterns. In the case of a random structure, each nano-disk has a slightly different resonance wavelength because of different long-range interaction, thus the randomly-scattered light is spread over wide range of wavelengths. Spectrally broader plasmon resonances are favorable in practical light harvesting applications. In contrast, periodic nano-disk arrays show an increase of the LSPR resonance, relative to the random configuration, larger Q-factor and longer dephasing time.

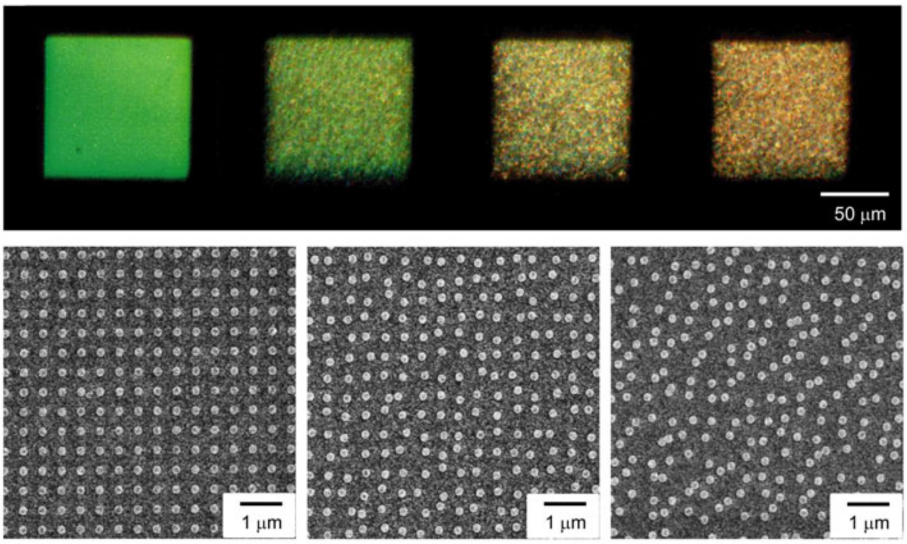

Figure 1: Dark field (100×100 μm^2) and SEM image of a gradually randomized periodic gold nano-disc array structures.

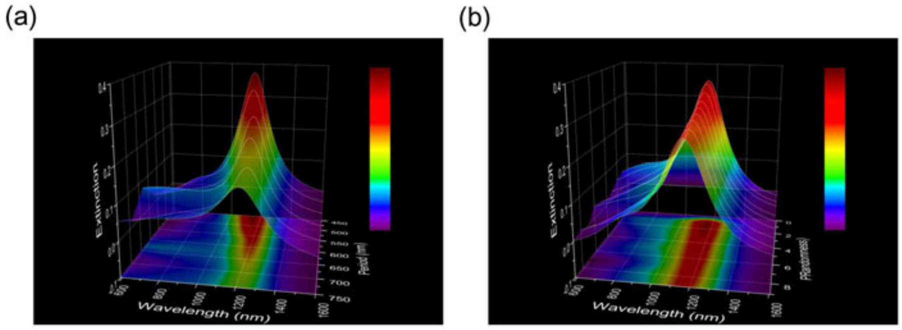

Figure 2: Extinction spectra of periodic array (a) and randomization for the 500 nm period structure. Extinction color scale spans from 0 to 0.4; linear scale.

In this study, we have demonstrated the effect of periodic and random particle patterns on the plasmonic resonance. An increase of extinction and a broader plasmon resonance occur at with increasing the randomness. FDTD calculations show an augmentation of the enhancement by more than two order of magnitude for the random configuration of nano-disks, however, those hot-spots are more sparsely distributed on the surface.

ACKNOWLEDGMENT

This work was financially supported by the Amada Foundation, the Research Foundation for Opt-Science and Technology, and The Ministry of Education, Culture, Sports, Science and Technology(MEXT), Japan.

REFERENCES

1. Y. Nishijima, L. Rosa, and S. Juodkazis, "Surface plasmon resonances in periodic and random patterns of gold nano-disks for broadband light harvesting," *Opt. express*, Vol. 20, No. 10, 11466–11477, 2012.
2. J. B. Khurgin and G. Sun, "Impact of disorder on surface plasmons in two-dimensional arrays of metal nanoparticles," *Appl. Phys. Lett.*, Vol. 94, No. 22, 22111, 2009.
3. W. Khunsin, B. Brian, J. Dorfmuller, M. Esslinger, R. Vogelgesang, C. Etrich, C. Rockstuhl, A. Dmitriev, and K. Kern, "Long-distance indirect excitation of nanoplasmonic resonances," *Nano Lett.*, Vol. 11, No. 7, 2765-2769, 2011.
4. B. Lamprecht, G. Schider, R. T. Lechner, H. Ditlbacher, J. R. Krenn, A. Leitner, and F. R. Aussenegg, "Metal nanoparticle gratings: Influence of dipolar particle interaction on the plasmon resonance," *Phys. Rev. Lett.*, Vol. 84, No. 20, 4721-4724, 2000.

Terahertz super thin planar optical elements based on metasurface

Yan Zhang*, Jiasheng Ye, Dan Hu, Xinke Wang, Shengfei Feng, and Wenfeng Sun
Beijing Key Lab for Terahertz Spectroscopy and Imaging, Key Laboratory of Terahertz Optoelectronics, Ministry of Education, and Department of Physics, Capital Normal University, Beijing, 100048 China
*Email: yzhang@mail.cnu.edu.cn

Abstract-A cylindrical lens, a spherical lens, optical interconnector, and phase holograms with the arrays of complementary V-shaped slit antennas have been designed and fabricated for terahertz radiation modulation. The thickness of these elements is only 1/4000th of the working wavelength. Experiment results demonstrate that these elements can achieve the preset functions well.

Terahertz (THz) radiation has been found to have many potential applications. Many efforts have been made to develop THz sources, detector, and elements. However, due to the long wavelength property of the THz radiation, the size of the optical elements for dominating the THz beam is relatively large. The large size of the THz element limits the application of the THz radiation due to the difficulty of the system integration. Based on the diffractive optics theory, the thickness of an element, for example, a lens can be reduced from several millimeters of the bulk elements to several hundred micrometers of the diffractive optical elements. However, this size is still too large for some applications. It is eager to reduce the thickness of the THz elements further.

Both bulk elements and diffractive phase elements achieve the phase modulation via the gradual phase changes accumulated the optical paths. If the large refractive indices materials are adopted, the thickness of the elements can be reduced. But the high refractive index causes the high reflection loss. The phase changes can also be introduced by an optical resonator such as electromagnetic cavities, nanoparticles cluster, and plasmonic attennas.

The abrupt phase change over the scale of the wavelength at the metasurface, where the plasmonic antennas array was arranged on, had been proposed. Based on this method, we selected eight basic complementary V-shaped slit antennas to generate the desired phase changes (from 0 to 2π with $\pi/4$ intervals) and equal intensity modulation for the cross polarized light. Then several THz elements with different functions, including cylindrical lenses, spherical lenses, optical interconnector, and phase holograms, were designed for 0.75 THz radiation (corresponding wavelength is 400 μm). The phase values of the desired elements were wrapped into the range of 0 to 2π and quantized to eight values. A set of complementary V-shaped antennas was selected according to the desired phase shift. Each element (with area of 8 mm× 8 mm) had 40×40 cells.

The elements are fabricated in the gold films (with a thickness of 100 nm) deposited on a double-sided polished silicon substrate (with a thickness of 500 μm) using the conventional photolithography and metallization processes. The performance of the designed cylindrical lens was theoretically verified using the FDTD method and experimentally tested with the focal plane imaging system. The result for a cylindrical lens is shown in Fig. 1.

As a conclusion, several ultrathin planar elements were designed and fabricated for the THz wavefront manipulation. The thickness of the elements was only 1/4000th of the illuminating wavelength. It is expected that this method can be used for design more optical devices.

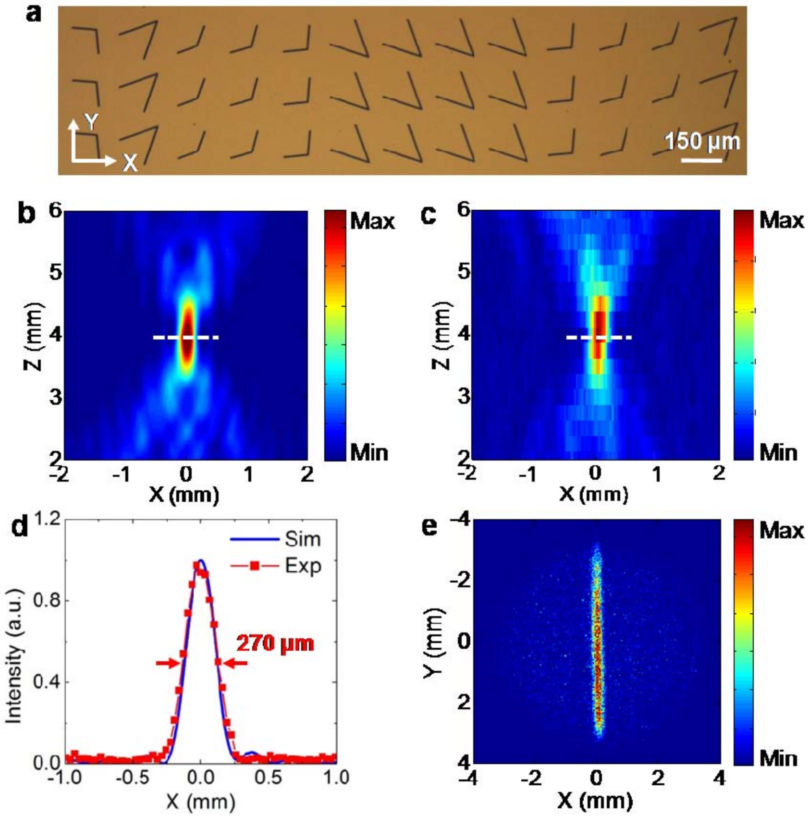

Fig. 1 Performances of a cylindrical lens. a) Photograph of a part of the fabricated cylindrical lens. b) Intensity distribution of the cross polarized light for the designed cylindrical lens along the z direction as simulated using commercial software according to the FDTD method. c) Experimental measurement of the intensity distribution of the cross polarized light for the fabricated cylindrical lens on the x-z plane. d) Intensity distributions along the white dashed lines shown in b) and c). e) The line focus of the cylindrical lens on the preset focal plane in experiments.

Acknowledgements This work was supported by the 973 Program of China (No. 2011CB301801), the National Natural Science Foundation of China (No.10904099, 11204188, 61205097, and 11174211), and the Beijing Natural Science Foundation (No. KZ201110028035).

REFERENCES

1. Tonouchi, M., "Cutting-edge terahertz technology," *Nature Photon.* 1, 97-105 2007.
2. Yu N. F, Genevet P., Kats M. A., Aieta F., Tetienne F, Capasso F., Gaburro Z., "Light propagation with phase discontinuities: Generalized laws of reflection and refraction," Science 334, 333-337 2011.
3. Zhu Q. F., Ye J. S., Wang D. Y., Gu B. Y., and Zhang Y., "Optimal design of SPP-based metallic nanoaperture optical elements by using Yang-Gu algorithm," *Opt. Express,* 19, 9512-9522 2011.
4. Wang X. K., Cui Y., Sun W. F., Ye J. S., and Zhang Y., "Terahertz polarization real-time imaging based on balanced electro-optic detection," *J. Opt. Soc. Am. A* 27, 2387-2393 2010.

Non Lorentzian-profile filters by two-handed metamaterials

Yi-Ju Chiang[1], Tseng-Yu Huang[1], Ting-Tso Yeh[1], and Ta-Jen Yen[1,*]
[1]Department of Materials Science and Engineering, National Tsing Hua University, Taiwan
[*]corresponding author: tjyen@mx.nthu.edu.tw

Abstract- We presented a two-handed metamaterial (THM) by two metallic discs sandwiching a dielectric layer. Such a THM exhibited two distinct sets of EM responses simultaneously, one right-handed and the other left-handed, mainly resulting from its multiple resonance modes. After elucidating the nature of the various resonance modes in the THM, we further engineered its electromagnetic properties and demonstrated various filters beyond the limit of conventional Lorentzian-profile filters, including dual-band bandpass filters, high-ratio bandwidth square-wave-like bandpass filters, ultra-wide bandpass filters, and sharp-transition bandpass filter.

It is an interesting observation what dominates in nature is the right-handed systems− for example, the major population of right-handed people, the right-handed helix of deoxyribonucleic acids (DNA) traced by the sugar-phosphate backbone and certainly, electromagnetic (EM) responses of materials in which electric field **E**, magnetic field **H**, and wave vector **k** form a right-handed triplet of vectors. Although rare, the left-handed systems do exist such as left-handed people and left-handed helical DNAs, and the left-handed EM response achieved by negative-refractive-index metamaterials. More interestingly, naturally occurring systems in fact allow the co-existence of both right-handed and left-handed sets (e.g., clearly observed in human beings and DNAs). As a consequence, to further enrich the possible EM properties of materials, in this talk we present a highly symmetric two-handed metamaterial (THM; Fig. 1) to exhibit two distinct sets of EM responses.[1] Not only does the THM exhibit two distinct allowed bands with right-handed and left-handed electromagnetic responses, but posses a further advantage of being independent to the polarizations of external excitations. In addition, the THM automatically matches the wave impedance in free space, leading to maximum transmittances about 0.8 dB in the left-handed band and almost 0 dB in the right-handed band, respectively. Such a THM can be employed for diverse electromagnetic devices including dual-band bandpass filters,[1] high-ratio bandwidth square-wave-like bandpass filters[2] (Fig. 2), ultra-wide bandpass filters[3] (Fig. 3), and sharp-transition bandpass filter[4] (Fig. 4) beyond conventional Lorentzian-profile filters.

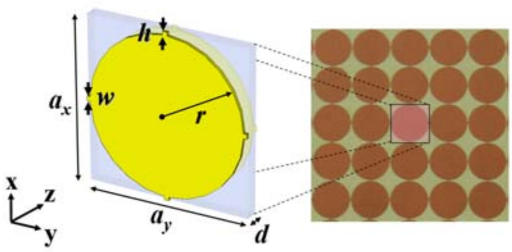

Fig. 1. The fabricated THM (right panel) and the perspective view of a unit cell (left panel). The THM shows a four-fold symmetric sandwiched structure.

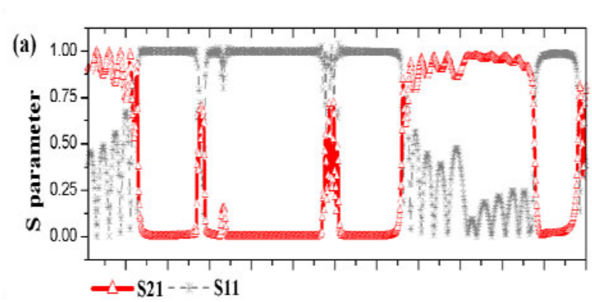

Fig 2. Diagram of complex transmittance. A multi-allowed band bandpass filter is presented.

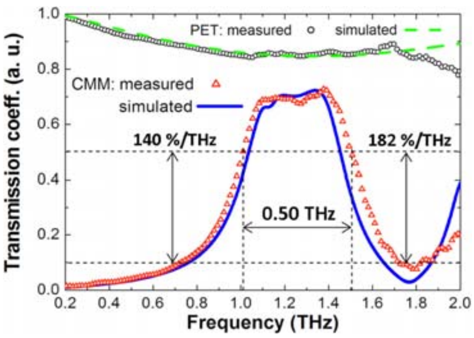

Fig. 3. Transmission spectrum of the broadband THz bandpass filter from the measurement (red triangles) and the simulation (blue solid line).

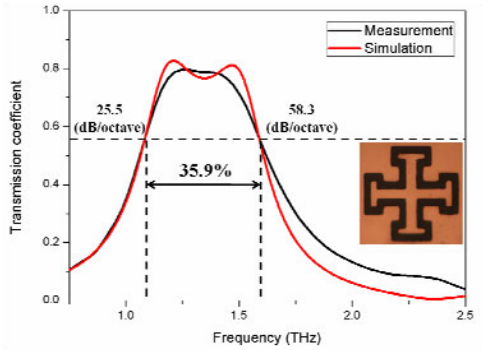

Fig. 4. The transmittance spectra of the MDM Jerusalem cross slot. The inset shows the OM image of the fabricated sample.

Acknowledgements

The authors would like to gratefully acknowledge the financial support from the National Science Council, the Ministry of Education and National Tsing Hua University in Taiwan.

REFERENCES

1. Y. J. Chiang and Ta-Jen Yen***, *Optics Express,*** Vol. 16 (17), pp. 12764-12770 (2008)
2. T.-Y. Huang and T.-J. Yen*, ***PIER Letters***, Vol. 21, pp. 19-29 (2011)
3. Yi-Ju Chiang, Chan-Shan Yang, Ci-Ling Pan and **Ta-Jen Yen***, ***Appl. Phys. Lett***. Vol 99, 191909, (2011)
4. Ta-Jen Yen***** *et al.*, ***Optics Express,*** Vol. 20 (7), pp. 7580-7589 (2012)

A High-performance Terahertz Spatial Light Modulator based on Reconfigurable Mesh Filters

(Invited Paper)

M. Unlu[1], C. W. Berry[1], S. Li[1], S.-H. Yang[1], M. R. Hashemi[1], and M. Jarrahi[1*]

[1]University of Michigan, Ann Arbor, MI, USA

[*]mjarrahi@umich.edu

Abstract- A terahertz spatial light modulator based on MEMS-reconfigurable mesh filters is presented, which offers record-high modulation depths and modulation bandwidths without a compromise on modulation speed and modulation voltage through a fully integrated device configuration.

We present and experimentally demonstrate a terahertz spatial light modulator, which offers more than 67% modulation depth over a 1.5 THz frequency band, under a modulation voltage of 30 V and modulation speeds exceeding 20 KHz. The achieved modulation depth is the highest reported among previously demonstrated terahertz intensity modulators, in general, and 5 times higher than the demonstrated broadband terahertz modulators with similar modulation voltages and modulation speeds, specifically. The key advantage of our design in comparison with the previously demonstrated terahertz modulation schemes based on tunable metamaterials [1-6] is reconfiguring the device's geometry, which enables radical changes in the device scattering parameters over a broad range of frequencies [7, 8]. Device geometry reconfiguration is made possible through integration of a double-layered mesh filter with an array of electrostatically actuated MEMS switches. In contrast to the previously demonstrated MEMS-reconfigurable terahertz metamaterials [4-6], the electromechanical displacement required for geometry reconfiguration is less than 250 nm in the presented terahertz modulator, enabling device operation at low modulation voltages and high modulation speeds.

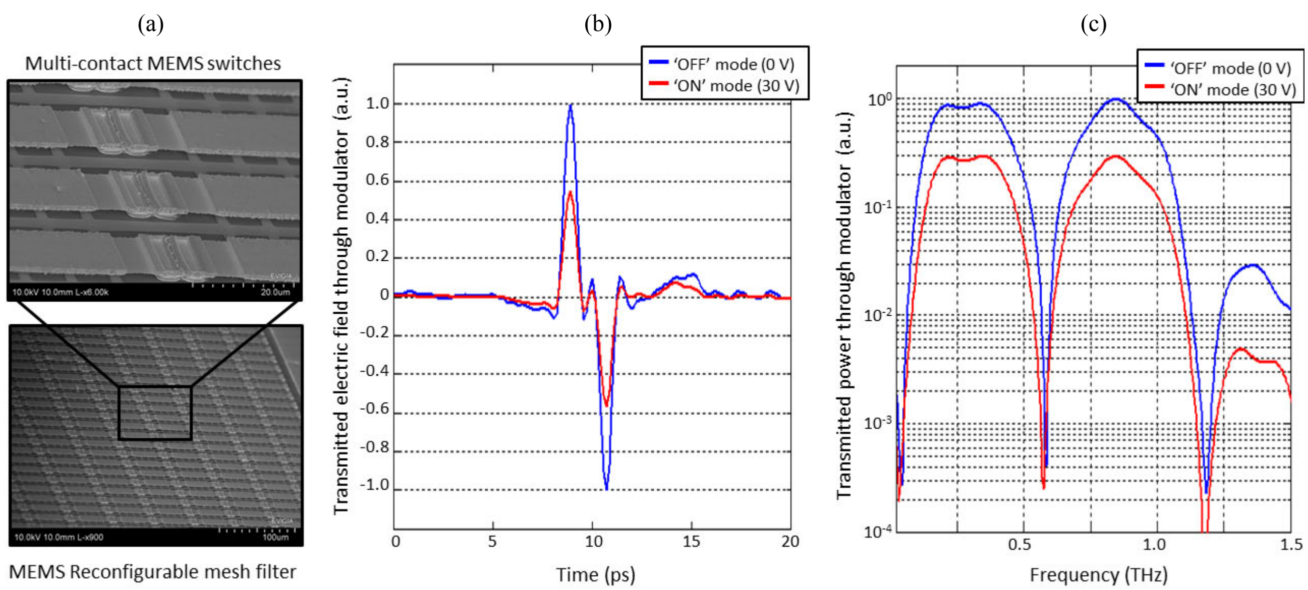

Fig. 1 (a) SEM image of the implemented terahertz modulator, transmitted electric field and power spectrum of a terahertz pulse through the implemented terahertz modulator is shown in (b) and (c). Spectral dips are the result of the apertures used for focusing the terahertz pulse onto the modulator.

Figure 1a shows the SEM image of the implemented terahertz modulator [9]. It consists of two layers of capacitive mesh filters integrated with an array of multi-contact MEMS switches. The geometry of the capacitive mesh filters, which behave as low-pass filters, is designed to allow efficient terahertz transmission over a 1.5 THz bandwidth during the MEMS switch non-contact mode (modulation 'OFF' mode). During the MEMS switch contact mode (modulation 'ON' mode), the two layers of capacitive mesh filters are connected to form an inductive mesh filter, which behaves as a high-pass filter. As a result, terahertz transmission is significantly attenuated over the 1.5 THz bandwidth. We fabricated the MEMS-reconfigurable multi-layered mesh filter on a high resistivity silicon substrate and characterized its performance in a time-domain terahertz spectroscopy setup. By measuring the electric field of a transmitted terahertz pulse through the implemented terahertz modulator (Fig. 1b) we have calculated the spectrum of the transmitted power during the modulation 'ON' and 'OFF' modes (Fig. 1c), which indicate more than 67% modulation depth over the 1.5 THz frequency band. The high efficiency and broadband operation of the presented terahertz spatial light modulator could have a significant impact on future terahertz imaging, spectroscopy and communication systems.

REFERENCES

1. H. Tao, W. J. Padilla, X. Zhang, and R. D. Averitt, "Recent progress in electromagnetic metamaterial devices for terahertz applications," *IEEE Journal of Selected Topics in Quantum Electronics* 17, 92-101 (2011).
2. H. T. Chen, W. J. Padilla, J. M. O. Zide, A. C. Gossard, A. J. Taylor, and R. D. Averitt, "Active terahertz metamaterial devices," *Nature* 444, 597-600 (2006).
3. H. T. Chen, W. J. Padilla, M. J. Cich, A. K. Azad, R. D. Averitt, and A. J. A. Taylor, "A metamaterial solid-state terahertz phase modulator," *Nature photonics* 3, 148-151 (2009).
4. W. L. Chan, H. T. Chen, A. J. Taylor, I. Brener, M. J. Cich, and D. M. Mittleman, "A spatial light modulator for terahertz beams," *Applied Physics Letters* 94, 253111 (2009).
5. T. D. Drysdale, I. S. Gregory, C. Baker, E. H. Linfield, W. R. Tribe, and Dr. R. S. Cumming, "Transmittance of a tunable filter at terahertz frequencies," *Applied Physics Letters* 85, 5173-5175 (2004).
6. H. Tao, A. C. Strikwerda, K. Fan, W. J. Padilla, X. Zhang, and R. D. Averitt, "Reconfigurable terahertz metamaterials," *Physical Review Letters* 103, 147401 (2009).
7. C. W. Berry, J. Moore, and M. Jarrahi, "Design of Reconfigurable Metallic Slits for Terahertz Beam Modulation," *Optics Express* 19, 1236-1245 (2011).
8. M. Jarrahi, "Broadband terahertz modulators based on reconfigurable metamaterials and their potential application in terahertz imaging," *Proc. International Symposium on Electromagnetic Theory*, 640-642 (2010).
9. M. Unlu, C. W. Berry, S. Li, S.-H. Yang, M. R. Hashemi, M. Jarrahi, "Broadband terahertz modulators based on MEMS-reconfigurable mesh filters," arXiv:1212.6562v1 (2012).

PLASMONICS FOR THE DESIGN OF ACTIVE NANODEVICES

G. Wurtz, and A. Zayats*

Nano Optics Group, Department of Physics, King's College London
Stand, WC2R 2LS, London, United Kingdom
*corresponding author: g.wurtz@kcl.ac.uk

Abstract
Plasmonic nanomaterials show promise to revolutionize nanotechnology, in particular in the area of information technology. Their potential in the design of active nanodevices with the speed of photonic devices and the nanoscale dimension of semiconductor electronics, will open a new technological era not constrained by the limitations in size and speed photonics and electronics devices currently show. In this presentation we will discuss the potential of complementary plasmonic structures in providing solutions in the development of active nanodevices.

Our ability to control and manipulate electromagnetic energy at the nanoscale, both dynamically and in real-time through low-energy external control signals is a missing link in our aim to develop a fully integrated sub-wavelength optical platform. To date, plasmonic systems demonstrating active functionalities, incorporating thermo- and electro-optic media, quantum dots, and photochromic molecules, are achieving incremental progress in switching and modulation applications [1, 2]. However, high switching times (>nanosecond) [3, 4] or the need for relatively strong control energy (~μJ/cm^2) to observe sensible signal modulation (35% to 80%) [2, 5] limit the practical use of such structures as signal processing or other active opto-electronic nanodevices. In order for active plasmonics to offer a viable technological platform, both the magnitude and the speed of the measured non-linearity, as well as the spectral/spatial tunability of the effect must be improved.

In this context, this work will present several plasmonic geometries showing relevant dynamical optical properties. One example consists of an optically-controlled plasmonic switch based on a resonant cavity structure incorporating a nonlinear material. The switching mechanism is governed by a nonlinear Kerr effect in the cavity. Depending on cavity geometry, an average refractive index change on the order of 10^{-3} allows for the controlled transmission of a surface plasmon polariton mode over a dynamic range of up to 15 dB, corresponding to a transmission change of approximately 97% [6]. Here we provide a detailed discussion on the switching mechanism originating from the interplay between photonic and plasmonic eigenmodes of the structure. Several other plasmonic structures, including plasmonic metamaterial and waveguides will be discussed as well.

References:
[1] K. F. MacDonald, Z. L. Samson, N. I. Zheludev, Active plasmonics: current status. *Laser Photonics Rev.* **4**, 562–567 (2009)
[2] G. A. Wurtz, R. Pollard,W. Hendren, G. P. Wiederrecht, D. J. Gosztola,V. A. Podolskiy and A.V. Zayats, Designed ultrafast optical nonlinearity in a plasmonic nanorod metamaterial enhanced by nonlocality, *Nature Nanotechnology* **6**, 107–111 (2011)

[3] T. Nikolajsen, K. Leosson, and S. I. Bozhevolnyi, Surface plasmon polariton based modulators and switches operating at telecom wavelengths. *App. Phys. Lett.* **85**, 5833 (2004)
[4] G. A. Wurtz, R. Pollard, and A. V. Zayats, Optical Bistability in Nonlinear Surface-Plasmon Polaritonic Crystals. *Phys. Rev. Lett.* **97**, 057402 (2006)
[5] K. F. MacDonald, Z. L. Sámson, M. I. Stockman, N. I. Zheludev, Ultrafast active plasmonics. *Nat Photon* **3**, 55-58 (2009)
[6] C. McPolin, D. O'Connor, J.-S. Bouillard, W. Dickson, G. Wurtz, and A.V. Zayats, manuscript in preparation

Experimental Verification of the Shift between Near-Field and Far-Field Peak Intensities in Plasmonic Nanoantennas

P. Alonso-González[1], P. Albella[1,2], F. Neubrech[3], J. Chen[1,2], F. Golmar[1,4], F. Casanova[1,5], L. E. Hueso[1,5], A. Pucci[3], J. Aizpurua[2], and R. Hillenbrand[1,5]

[1] CIC nanoGUNE, 20018 Donostia – San Sebastián, Spain

[2] Kirchhoff Institute for Physics, University of Heidelberg, Im Neuenheimer Feld 227, 69120 Heidellberg, Germany

[3] Centro de Fisica de Materiales (CSIC-UPV/EHU) and Donostia International Physics Center (DIPC), 20018 Donostia-San Sebastián, Spain

[4] I.N.T.I.–CONICET, Av. Gral. Paz 5445, Ed. 42, B1650JKA, San Martín, Bs As, Argentina

[5] IKERBASQUE, Basque Foundation for Science, 48011 Bilbao, Spain

*corresponding author: r.hillenbrand@nanogune.eu

Abstract- Recently, the distinct spectral shift between the near- and far-field optical response of plasmonic antennas has become subject of theoretical studies. By near-field optical microscopy and far-field optical spectroscopy of individual infrared-resonant nanoantennas we verify this spectral shift experimentally. We also discuss its implications.

Plasmonic nanoantennas show a large potential for application in optical microscopy, sensing and communication on the nanometer scale, owing to the strongly enhanced near-fields in the antenna vicinity and their strong far-field extinction. Recently, a distinct spectral shift between the near- and far-field optical responses of plasmonic antennas has been predicted [1] and indicated by a few experimental studies [2]. Here, we will present a combined study of near-field optical microscopy and far-field spectroscopy of individual infrared-resonant nanoantennas that provides an experimental verification of this spectral shift (Fig. 1). Numerical calculations corroborate our experimental results. We will also discuss the implications of this effect in surface-enhanced infrared absorption spectroscopy (SEIRA).

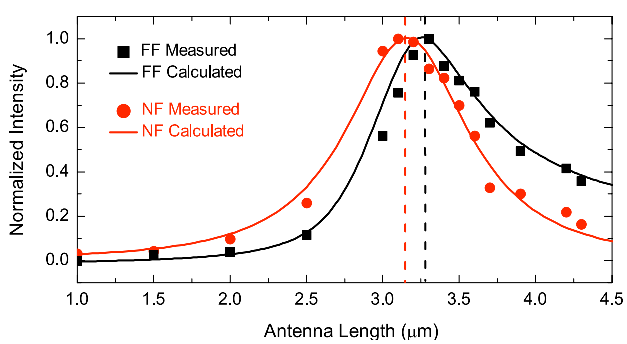

Figure 1: Experimental verification of the shift between near- and far-field peak intensities in individual plasmonic nanoantennas. The red symbols show the near-field intensity obtained by near-field microscopy, while the black symbols show the far-field extinction obtained from transmission measurements.

REFERENCES

1. J. Zuloaga, and P. Nordlander, *Nano Lett.*, 11, 1280, 2011.
2. J. Chen, P. Albella, Z. Pirzadeh, P. Alonso-González, F. Huth, S. Bonetti, V. Bonanni, J. Åkerman, J. Nogués, P. Vavassori, A. Dmitriev, J. Aizpurua, and R. Hillenbrand, *Small*, 7, 2341, 2011.

Metamaterial Patch Antenna Radiation Pattern Agility

S. M. CHAKER, M. BOUZOUAD.

Telecommunication Signal and Systems Laboratory,
BP 37G, Route de Ghardaïa, 03000, Laghouat, Algérie.
*corresponding author, E-mail: m.bouzouad@mail.lagh-univ.dz

Abstract

In this paper we address the introduction of antenna radiation pattern agility using an agile metamaterial. The agile metamaterial has two different behaviors which can be controlled by an external command. This agile metamaterial is used to design an agile lens which comprises two grids each composed of two regions: the first one constitutes a focusing zone (FZ) and the second one the lens body. The focusing zone parameters—refraction index, size, shape and position in the grid— can be modified using an external switching system (OFF or ON stat) by modifying the FZ parameters one can control the patch antenna radiation pattern main lobe beamwidth and direction (pointing angle) in E and H planes.

1. Introduction

Among the most important metamaterial applications in the antenna field we can mention the antenna performances enhancement and size reduction [1], [2], [3]. However, antenna characteristics control remains a major challenge of metamaterial use in the antenna domain. The goal is to design agile antennas [4], of which it is possible to change the radiation characteristics using an external control system. This makes telecommunications systems more flexible. We are interested in this study, with the patch antenna radiation pattern agility. The aim is to control the radiation pattern using a lens based on an agile metamaterial (programmable). Generally, in this kind of structures, switching elements (diodes, MEMs, etc…) are used to ensure the agility.

2. Antenna radiation pattern Agility

Figure 1 shows the studied agile radiation pattern antenna. The structure is formed by a patch antenna atop of which is disposed an agile metamaterial lens. The elementary cell of the agile metamaterial is made of a disconnected cross like conducting strips, printed on a dielectric substrate. The disconnected branches of the cross can be joined with a switching device (Diodes, MEMs, etc…). This modifiable unit cell (Figure 1-a and -b) allows us introducing the metamaterial agility. According to the switches state (ON or OFF), the unit cell has two different commutable behaviors. The first one corresponding to the disconnected cross type (switch ON) behaving like an effective medium with a refraction index n_1 higher than unity and the second one corresponding to the connected cross type (switch OFF) having a positive and close to zero refraction index n_2. The obtained programmable metamaterial is used to design the grids of the agile lens. These grids are made up of two regions (Figure 2- a), the first one forming a focusing zone (FZ) and the second one, the lens body (host medium). The refraction index (n_1 or n_2), the size, shape and position of the FZ can be programmed by acting on the switching devices (state ON or OFF). Modifying the FZ parameters (size, shape, position, and refraction index), allows us to control the antenna radiation pattern properties (main lobe direction (pointing angle)) and beamwidth in both E- and H-plane.

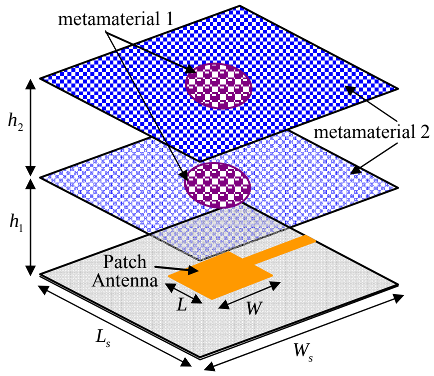

(a)

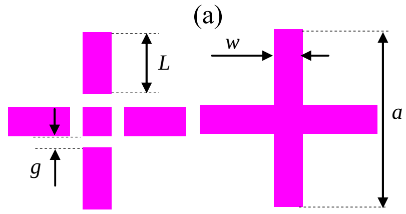

(b)

Figure 1: a) Agile radiation pattern radiating structure, b) agile metamaterial elementary cell (disconnected and connected cross).

3. Agile metamaterial characterization

The metamaterial elementary motifs (Figure 1- b) are printed on a dielectric substrate of permittivity $\varepsilon_r = 2.2$ and a thickness $h = 0.8$ mm [5]. The cross branch conducting strips are separated by a gap g and have a width w, a metallization thickness $t = 0.035$ mm.

3.1. The metamaterial unit cell size determination

The patch antenna operating frequency is 40 GHz, hence the corresponding wavelength in free space is 8 mm. Accordingly, the greatest dimension of the metamaterial unit cell must be much lower than the operating wavelength, to respect the homogenization conditions **Erreur ! Source du renvoi introuvable.**. It is fixed to 2 mm (lower than $\lambda/3 \approx 2.66$ mm). We used a parametric study to obtain the unit cell optimum sizes, of the two metamaterials types, to attain the desired refraction indexes profiles (Figure 2). The study shows also that the agile radiating structure directivity is maximum when the host mediums of the two agile lens grids are based on a connected cross type metamaterial and the FZs are based on a disconnected cross type metamaterial.

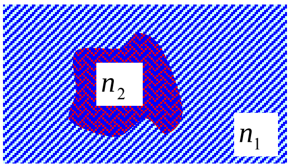

(a)

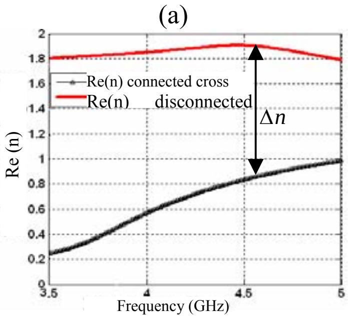

(b)

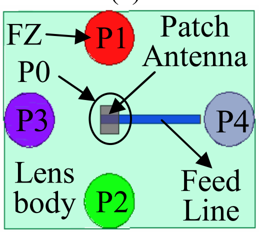

(c)

Figure 2: a) Agile lens grid: host medium with refraction index n_1 and FZ with index n_2, b) Used metamaterial refraction indices profiles, c) different positions of the FZ.

Constitutive parameters (ε_{reff} and μ_{reff}) of the agile metamaterial are obtained using the Fresnel inversion method starting from the S parameters, obtained by the HFSS simulation software (commercial code).

4. Results and discussion

Table 1. Agile antenna radiation pattern main angle direction θ_{max} versus FZ positions.

FZ positions	E-Plan	H-Plan
	θ_{max} (deg)	θ_{max} (deg)
Position P0	0	4.3
Position P1	-15.5	7.23
Position P2	15.4	7.23
Position P3	0,47	12.97
Position P4	0,56	2

Figure 3 shows the agile radiating antenna radiation pattern steering, obtained by the positioning of the FZ. When placed between positions P1 and P2, the FZ acts only on E-plane of the radiation pattern.The main lobe is rotated on both sides of the $\theta = 0°$direction. The amplitude of the rotation angle is about 15° (Table 1). Whereas, when placed between positions P3 and P4 the FZ acts only on the H-plane of the radiation pattern. The FZ positioned in P3 rotates the main beam pattern by 8° in the counter-clockwise and by 2° clockwise rotation if positioned in P4.

5. Conclusion

In this study, we highlight the possibility of introducing patch antenna radiation pattern agility by using an agile metamaterial lens. The metamaterial agility is obtained using a modifiable elementary unit cell based on a disconnected cross shape equipped with MEMs switches. According to the state of the MEMs switches (ON or OFF), the metamaterial refraction index flips between two values $n_1 \approx 0$ and $n_2 > 1$.

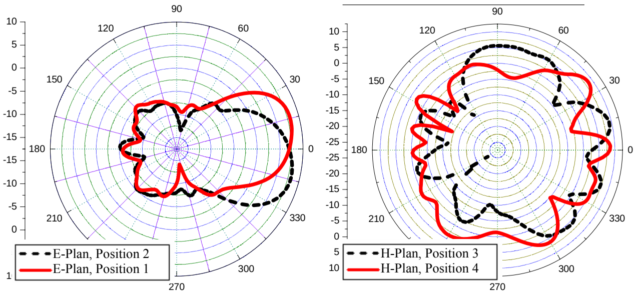

Figure 3: a) Radiation pattern steering of the agile radiating structure by positioning the FZ.

References

[1] J. Dalin, "Gain improvement of a microstrip patch antenna using metamaterial superstrate with the zero refractive index", International Conference on Microwave and Millimeter Wave Technology (ICMMT), May 2012; China.

[2] M. Bouzouad. « Analyse et conception d'antennes microruban sur des substrats bandes interdites électromagnétique ». Thèse de Doctorat d'État. École nationale polytechnique d'Alger, décembre 2007.

[3] J. Cha and Y. Kuga. "A steerable array antenna using controllable 4-bit dielectric slab phase shifters on a coplanar waveguide at 24 Ghz", Microwave and optical technology letters, Vol.49, n°12, 2007.

[4] L. Mercier, « Synthèse de propriété d'agilité électromagnétique par des matériau artificiel périodique intégrant des micocomposants : Application à la conception d'antenne à résonateur BIE configurable », Doctorat d'université de limoges, 2005.

[5] F. Bendelala, M. Bouzouad, A. Benabdelkrim, I. Huynen, « Optimisation des dimensions du motif élémentaire d'une grille métamatériau utilisée pour améliorer la directivité d'une antenne imprimée travaillant à 43 GHz », 17èmes Journées Nationales Microondes, 18-19-20 Mai 2011 - Brest.

[6] C.R. Simovski et al., "Homogenization of Planar Bianisotropic Arrays on the dielectric interface", Electromagnetics, 2002. 22: p. 177-189.

Active Terahertz Metamaterials

Optically Switchable Metamaterials in the Terahertz Regime

Ekmel Ozbay, and Mutlu Gokkavas

Nanotechnology Research Center, Bilkent University, Bilkent, 06800 Ankara, Turkey
Fax: + 90-312290105; email: ozbay@bilkent.edu.tr

Abstract

In this talk, we report the design, fabrication and experimental characterization of optically tunable metamaterials in the terahertz (THz) regime. The metamaterial design is based around electric-field-coupled inductor capacitor (ELC) resonators. This results in two potential resonance states, and the photoconductive semiconductor (silicon) settled in the critical region plays the role of intermediary for switching the resonator from mode 1 to mode 2. The metamaterials were fabricated on commercially available silicon-on-sapphire (SOS) wafers. The thin silicon layer was removed by RIE etching of all areas expect the 6x6 micron photoconductive region. In order to measure the tunable response of the metamaterial, an optical pump beam (800 nm) was used to excite photocarriers in the silicon. We observed a tuning range of the fabricated device as high as 26% (from 0.76 THz to 0.96 THz) by controlling the conductivity of the silicon layer via optical illumination. Numerical simulations yielded a simulated resonance around 0.69 THz. Following the increasing pump fluxes, we selected different corresponding values of Si to roughly reproduce the experimental results. The resonance has then shifted close to the final frequency of 0.96 THz. The simulations showed an all-optical blueshift with the tuning range of 40%, compared to 26% in the experiments. The realization of broadband blueshift tunable metamaterial offers opportunities for achieving switchable metamaterials with simultaneous redshift and blueshift tunability and cascade tunable devices. Our experimental approach is compatible with semiconductor technologies and can be used for other applications in the THz regime.

Short Abstract:

We report optically tunable metamaterials in the terahertz (THz) regime. We experimentally observed a tuning range of 26% (from 0.76 THz to 0.96 THz) by optically controlling the conductivity of a thin silicon layer.

Author Information

1) Ekmel Ozbay

Nanotechnology Research Center, Bilkent University, Bilkent, 06800 Ankara, Turkey
Phone: + 90-312-290-1966
Fax: + 90-312-290-1015;
email: ozbay@bilkent.edu.tr

2) Mutlu Gokkavas

Nanotechnology Research Center, Bilkent University, Bilkent, 06800 Ankara, Turkey
Phone: + 90-312-290-1966
Fax: + 90-312-290-1021;
email: gokkavas@bilkent.edu.tr

Terahertz band gaps based on TEM mode by photonic crystals inside parallel-plate waveguide

Eui Su Lee and Tae-In Jeon*
Division of Electrical and Electronics Engineering, Korea Maritime University, Busan 606-791, South Korea
*corresponding author: jeon@hhu.ac.kr

Abstract- We report an experimental and simulation study of terahertz (THz) band gap properties by using slits and grooves inside tapered parallel-plate waveguide (PPWG) with TEM mode. The Bragg and non-Bragg stop bands obtained from the slits embedded between the two surfaces of the PPWG can be used as notch filters and low-pass filters (LPFs). When the air gap between the metal plates of the PPWG is controlled using a motor controlled translation stage or piezo-actuator, a tunable THz notch filter can be obtained.

We use experimental measurements and FDTD simulations to investigate the THz band gaps properties by positioning metal slits at the center of the air gap or metal grooves on the surface of PPWG [1,2]. Recently, THz notch filter properties have been studied using single groove inside a PPWG [3]. The frequency of notch filter was very sensitive according to the air gap variation in the PPWG, leading to a feasibly tunable THz notch filter. We report the first experimentally demonstrated THz notch filter which is tunable by adjusting the air gap using a piezo-actuator. Therefore, the frequency of the tunable notch can be controlled by adjusting the DC voltage by means of the piezo-actuator.

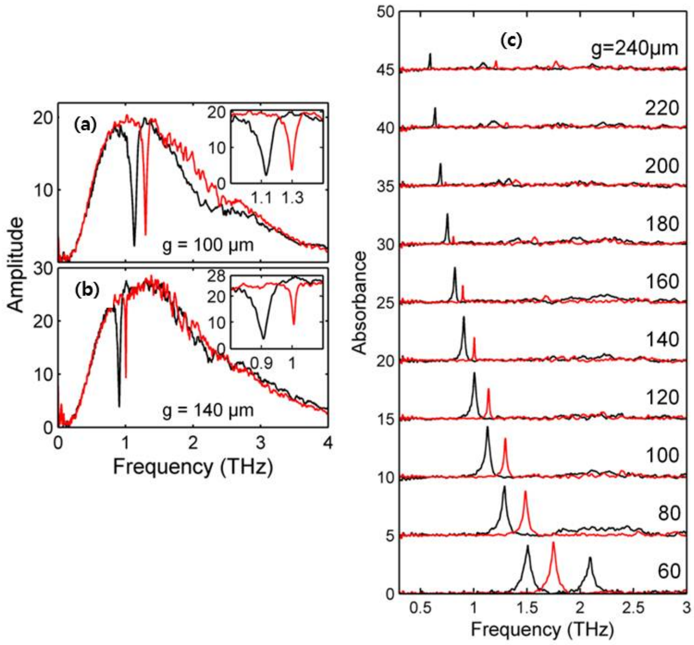

Fig. 1. THz notch filter properties by single groove inside PPWG. (a) 100 μm air gap (sample A: upper red, sample B: lower black). (b) 140 μm air gap. (c) Absorbance spectra in samples A and B when varying the air gaps from 60 to 240-μm.

Figure 1(a) and (b) show the amplitude spectra of the measured THz pulses with the 100- and 140-μm air gaps, respectively, for samples A (red) and B (black) where sample A has a 70 μm wide and a 28 μm deep groove, and sample B has a 105 μm wide and a 40 μm deep groove. When the air gaps are increased, the resonance frequencies shift to lower frequency region and also the resonance width gradually becomes narrower. Like the property of the notch filter resonance in the TE_1 mode, that in the TEM mode is also excellent. Unlike the TE_1 mode, which has a cutoff frequency, the notch filter resonances of the TEM mode can be obtained for the entire frequency region by adjusting the air gap. Figure 1(c) shows the absorbance of the notch filter resonance with different air gaps ranging from 60 to 240 μm. The resonant frequency shifts to a low frequency range and the absorbance becomes small with an increase in the air gap.

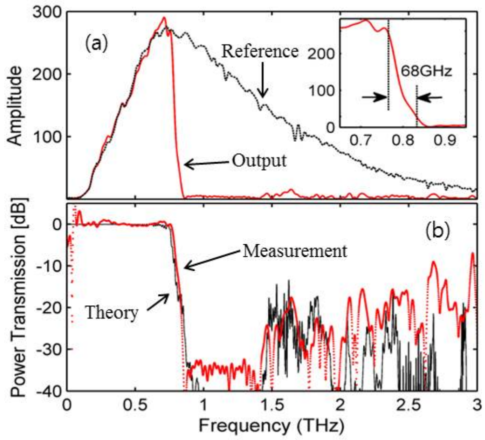

Fig. 2. (a) The spectra of the reference and output. The inset shows expended figure near the cutoff frequency. (b) Comparison of power Transmission in the measurement and FDTD simulation.

A THz beam propagating along slits with a period P inside a PPWG has a Bragg stop band with strong resonance at a Bragg frequency. The bandwidth of the Bragg stop band broadens as the period gets narrower at the Bragg stop band positions in the high frequency range. Using such characteristics, if slits with different periods are arrayed in a line on a metal sheet, an LPF can be implemented to completely eliminate the high frequency component after cutoff frequency. Figure 2(a) shows the amplitude of the output spectrum with cutoff frequency at 0.78 THz. As shown in the inserted figure, the magnitude response changes from pass band to stop band. The transition width is about 68 GHz. The power transmission in the cutoff region of the LPF is measured at about 35 dB. The experimental result is in good agreement with the FDTD simulation, which is represented with a measurement as shown in Fig. 2(b).

REFERENCES

1. E. S. Lee, S. G. Lee, C. S. Kee, and T.-I. Jeon, "Terahertz notch and low-pass filters based on band gaps properties by using metal slits in tapered parallel-plate waveguides," *Opt. Express, Vol. 19,*, 14852-14859, 2011.
2. E. S. Lee, J. K. So, G. S. Park, D. S. Kim, and T.-I. Jeon, "Terahertz band gaps induced by metal grooves inside parallel-plate waveguides," *Opt. Express*, Vol. 20, 6116-6123, 2012.
3. E. S. Lee, and T.-I. Jeon, "Tunable THz notch filter with a single groove inside parallel-plate waveguides," *Opt. Express*, Vol. 20, 29605-29612, 2012.

Nonlinear Terahertz Metamaterials

I. Al-Naib*
INRS-EMT, 1650 Boul. Lionel-Boulet, Varennes, Québec J3X 1S2, Canada
*corresponding author: alnaib@emt.inrs.ca

Abstract-Nonlinear effects caused by an intense terahertz waves on the transmission response of metamaterials are presented. We show experimentally that the transmission amplitude depends strongly on the intensity of the terahertz field. The proposed concept holds promise for future active terahertz metamaterials, as well as for ultrafast terahertz devices.

In recent years, metamaterials (MMs) have drawn considerable attention. They can be engineered to achieve tunable electromagnetic properties that are not available in natural materials. Planar metamaterials are of great interest for a variety of applications, such as filtering, the realization of modulators, sensing, slow light devices, and negative refraction. Controlling terahertz (THz) metamaterials response dynamically is highly desirable. Hence, thermal, electrical, and optical schemes have been proposed to achieve some degree of active control. However, the effective parameters in the aforementioned devices do not depend on the intensity of the applied field and they are typically quite slow processes. Obviously, the ability to dynamically control the response of such devices on the time scale of the light cycle is highly desirable.

In this work, we investigate the nonlinear effects induced by an intense terahertz field on the transmission response of double concentric ring metamaterial resonators (CRRs) on optically-pumped silicon. The terahertz electric field exhibits high confinement due to the CRRs, and hence modify the transmission response. Moreover, this kind of resonators exhibits a polarization- and angle-independent transmission response, a very important property for a wide range of filter applications [1]-[2]. The resonators are patterned on a 200 nm thick layer of gold deposited on a high resistivity silicon substrate. The measurements are performed using an optical-pump terahertz-probe setup (OPTP) coupled to the intense THz $LiNbO_3$ source available at the Advanced Laser Light Source (ALLS) facility recently established at INRS [3]. Experimentally, we measured the transmission response at different THz electric field from 0.4 kV/cm to 90 kV/cm. A very distinct behavior is observed around the resonance frequency where the transmission dip becomes significantly deeper as the THz intensity increases. We interpret that to a decrease in the conductivity of the thin photo-excited layer due to THz-field-induced inter-valley scattering, similar to the bleaching effect previously observed in GaAs [4]. The proposed concept could be employed for future active terahertz metamaterials, as well as ultrafast modulation in the terahertz regime.

REFERENCES

1. N. Papasimakis et al., Applied Physics Letters 94, 211902 (2009).
2. I.A.I. Al-Naib et al., Applied Physics Letters 98, 091107 (2011).
3. F. Blanchard et al., IEEE Journal of Selected Topics in Quantum Electronics 17, 5 (2011).
4. F. H. Su et al., Optics Express 17, 9620 (2009).

Terahertz Detection Sensitivity Enhancement by Use of Plasmonic Photoconductive Detectors

(Invited Paper)

N. Wang[1], C. W. Berry[1], M. R. Hashemi[1], and M. Jarrahi[1*]
[1]University of Michigan, Ann Arbor, MI, USA
[*]mjarrahi@umich.edu

Abstract- A novel photoconductive terahertz detector based on plasmonic contact electrode gratings is presented, which offers more than one order of magnitude higher detection sensitivities compared to conventional photoconductive terahertz detectors.

Photoconduction has been one of the most commonly used techniques for detecting terahertz waves [1]. One of the main limitations of conventional photoconductive terahertz detectors is their low detection sensitivity, which is the result of the inherent tradeoff between high quantum efficiency and ultrafast operation of conventional photoconductors. To address this limitation, we have developed a novel photoconductive terahertz detector that incorporates plasmonic contact electrodes. By reducing the photocarrier transport path to the photoconductor contact electrodes [2, 3], the plasmonic photoconductive terahertz detector offers significantly higher detection sensitivities compared to conventional photoconductive terahertz detectors. An additional advantage of the presented plasmonic photoconductive terahertz detector is that the device active area can be increased without a significant increase in the photoconductor capacitive parasitic and, therefore, higher detection sensitivity levels can be achieved at higher optical pump powers.

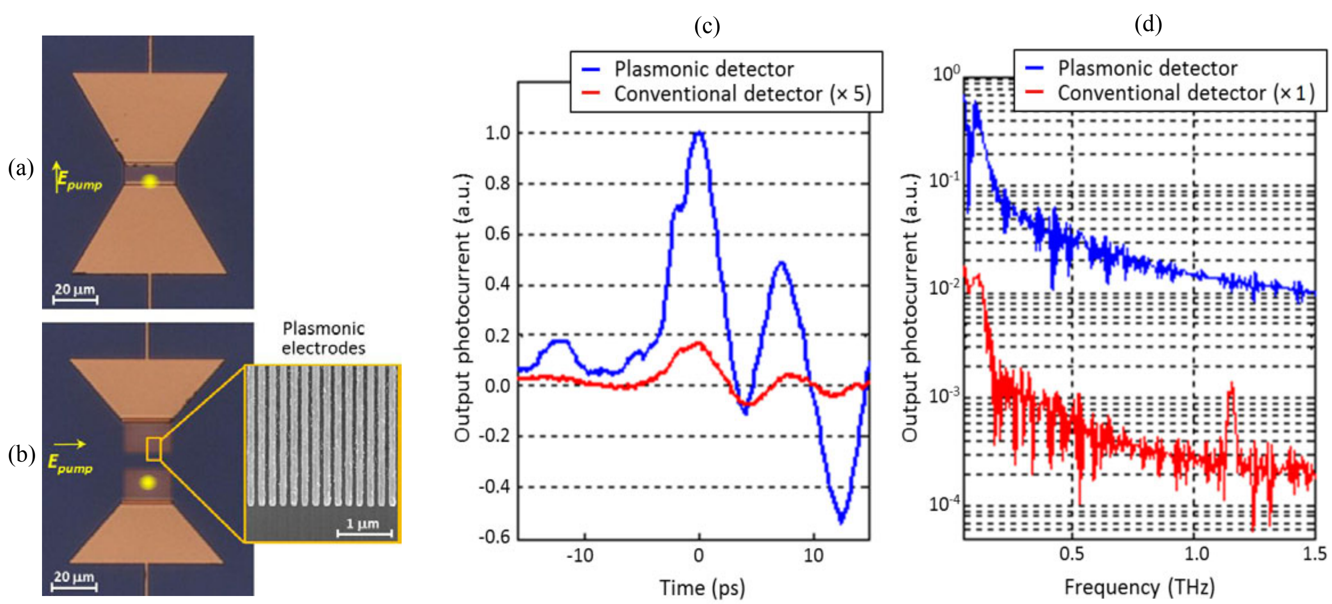

Fig. 1 (a) Conventional and (b) plasmonic photoconductive terahertz detector prototypes. The plasmonic photoconductive detector incorporates plasmonic contact electrode gratings with 100 nm metal width and 100 nm spacing. Measured output photocurrent of the detector prototypes in the (c) time domain and (d) frequency domain, indicate more than 30 fold detection sensitivity enhancement through use of plasmonic electrodes.

To evaluate the impact of plasmonic contact electrodes in enhancing the sensitivity of photoconductive terahertz detectors, prototypes of photoconductive detectors with and without plasmonic contact electrodes are built and integrated with equivalent bowtie terahertz antennas with the same radiation properties on a LT-GaAs substrate (Fig. 1a and 1b). The performance of the photoconductive terahertz detector prototypes is characterized in a time-domain terahertz spectroscopy setup. A Ti:sapphire mode-locked laser which generates 200 fs pulses at 800 nm is used for pumping a photoconductive terahertz emitter and the photoconductive terahertz detector prototypes at the same time. Experimental results show that incorporating plasmonic contact electrodes offers more than 30 times higher detection sensitivities over a 0.1-1.5 THz frequency band (Fig. 1c and 1d). The demonstrated terahertz detection sensitivity enhancement through use of plasmonic contact electrodes would have a significant impact on future time-domain and frequency-domain terahertz imaging and spectroscopy systems [4-6].

REFERENCES

1. Y. Cai, I. Brener, J. Lopata, J. Wynn, L. Pfeiffer, J. B. Stark, Q. Wu, X. C. Zhang, and J. F. Federici, “Coherent terahertz radiation detection: Direct comparison between free-space electro-optic sampling and antenna detection,” *Appl. Phys. Lett.*, 73, 444 (1998).
2. C. W. Berry and M. Jarrahi, “Terahertz generation using plasmonic photoconductive gratings,” *New J. Phys.*, 14, 105029 (2012).
3. C. W. Berry, M. R. Hashemi, M. Unlu, and M. Jarrahi, “Significant Radiation Enhancement in Photoconductive Terahertz Emitters by Incorporating Plasmonic Contact Electrodes,” arXiv:1209.1680v1 (2012).
4. P. R. Smith, D. H. Auston, and M. C. Nuss, “Subpicosecond photoconducting dipole antennas,” *IEEE J. Quantum Electron.* 24, 255 (1988).
5. M. van Exter and D. Grischkowsky, “Characterization of an optoelectronic terahertz beam system,” *IEEE Microwave Theory Technol.* 38, 1684 (1990).
6. B. B. Hu and M. C. Nuss, “Imaging with terahertz waves,” *Opt. Lett.* 20, 1716-1718 (1995).

Recent Advances in Nano-Particle Configurations

Polarization-independent Fano resonance in oligomer structures

B. Hopkins, W. Liu, and A. E. Miroshnichenko*
Nonlinear Physics Centre, Research School of Physics and Engineering,
Australian National University, Canberra, ACT 0200, Australia
*corresponding author: aem124@physics.anu.edu.au

Abstract-We study the optical responses of plasmonic and all-dielectric oligomers structures that have an n-fold symmetry. Under certain conditions oligomer structures may support well-pronounced Fano resonance. In the limit of the discrete-dipole approximation we analytically prove that all the cross-sections (extinction, scattering and absorption) are independent of the angle of polarization of the linearly-polarized plane wave. However, the near-field distribution does depend on the incident polarization. Such polarization independence reveals the peculiar origin of the Fano resonance in oligomer-like structures.

The current surging interest in various applications of nanoscale light-matter interactions, including biosensing, nanoantennas, photovoltaic devices and many others, has triggered enormous effort into the old and fundamental problem of manipulation of a particle's scattering and absorption characteristics. In the recently emerging fields of nanophotonics, various novel phenomena have been demonstrated involving interaction of nanoparticles with light, such as super-scattering, control of the direction of the scattered light by metasurface, coherent perfect absorption of light by surface plasmons, Fano resonances in plasmonic and all-dielectric oligomers [1]. At the same time, the interest in artificial magnetic responses that was fostered by the field of metamaterials has lead to the observation of artificial magnetic modes in nanoparticles [2] and, since then, many related novel scattering features based on the interplay of both electric and magnetic responses have been demonstrated [3].

To make further breakthroughs in different applications based on the particles scattering, there is a fundamental challenge to overcome: polarization dependence. The dependence of an optical response on polarization comes from the fact that most structures have dominantly electric responses, which are highly dependent on the polarization of the incident field. The simplest structure that does not exhibit polarization-dependent scattering properties is a single spherical particle. According to the Mie theory the total extinction, scattering and absorption cross-sections do not depend on the incident polarization angle, although the scattering diagram will exhibit some angle-dependent properties. However, it is possible to achieve polarization-independent scattering diagram by overlapping of an electric and magnetic dipole responses of a single spherical nanoparticle [4], but such effects can be only achieved by rigorous structure engineering and can happen only in specific spectral regime. It has also been experimentally observed that some plasmonic oligomer structures exhibit polarization-independent extinction cross-sections. This all leads to the question of what the necessary conditions are for an arbitrary system to have polarization-independent scattering properties.

In our study we perform a systematic investigation on the optical responses of structures with an n-fold rotational symmetry. Such n-fold symmetry implies that the optical properties of the system will be identical when rotating the whole structure by $2\pi/n$ radians. But, as we analytically prove, for structures with $n>2$ symmetries the extinction, scattering and even absorption cross-sections are all identical for rotation on *any* angle. Such structures can, therefore, be considered as being *polarization-independent* [5].

The extinction and scattering cross-sections are defined in the far-field, but absorption can be calculated by two independent ways - as an energy balance between the far field scattered and incident fields, and as integration of losses in the near field. Both approaches produce the same result. In the near field, the full profile of the electromagnetic field should be taken into account, while in the far field only the leading order will survive. The polarization-independent absorption is, then, quite counter-intuitive because the near field profile of the electromagnetic field does depend on the incident polarization yet the overall absorption cross-section does not. It implies that the variation of the near field with the incident polarization does not affect the overall integral absorption cross-section. Thus, the near field distribution still follows some symmetry properties of the entire structure. We are able to trace such peculiar relations using the dipole approximation because it is able to show the key aspects of the observed phenomena.

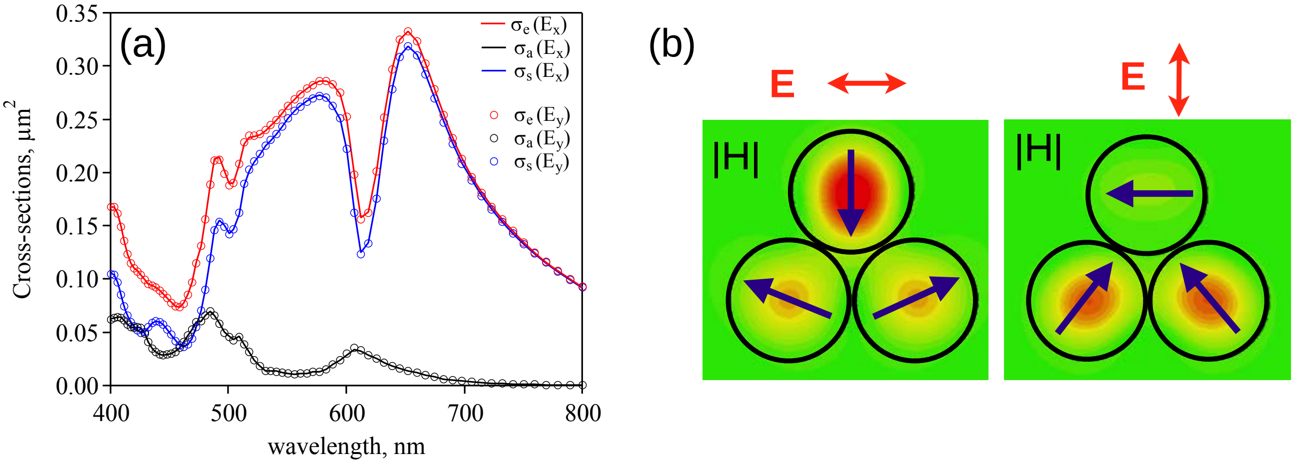

Fig.1 (a) Extinction, scattering and absorption cross-sections for two orthogonal polarizations for a trimer structure made of touching Si nanopartices of radii R=75nm. (b) Corresponding magnetic field distribution at the Fano resonance for two orthogonal polarizations together with induced magnetic dipole moments.

It has the main implication to the origin of the Fano resonance in oligomer-like structures. By studying the near-field and discrete dipole modes distribution we reveal the necessary conditions for the Fano resonance to occur in such structures.

This work was supported by the Australian Research Council.

REFERENCES

1. Miroshnichenko, A. E. and Y. S. Kivshar, "Fano resonances in all-dielectric oligomers," *Nano Letters*, available ASAP, 2012.
2. Kuznetsov A. I, *et al.* "Magnetic lignt," *Sci. Rep.*, Vol. 2, 492 , 2012.
3. Miroshnichenko, A. E., B. S. Luk'yancuk, S. A. Maier, and Y. S. Kivshar, "Optically Induced Interaction of Magnetic Moments in Hybrid Metamaterials," *ACS Nano*, Vol. 6, No. 1, 837–842, 2012.
4. Liu, W., A. E. Miroshnichenko, D. N. Neshev, and Y. S. Kivshar, "Broadband Unidirectional Scattering by Magneto-Electric Core–Shell Nanoparticles," *ACS Nano*, Vol. 6, No. 6, 5489–5497, 2012.
5. Hopkins, B., W. Liu, and A. E. Miroshnichenko, "Polarization-independent responses of systems with rotational symmetry," *arxiv:1211.3182*, 2012.

Nanometric gaps in plasmonics nanostructures: Mode visualization, the classical limit, and transformation optics treatment

Stefan A Maier[1]
[1]Department of Physics, Imperial College London, London SW7 2AZ, UK

*corresponding author: s.maier@imperial.ac.uk

Abstract- Recent progress in nanofabrication has enabled the generation of metallic nanoantennas with gaps on the order of only a few nanometers. Even structures such as the simple bow tie can sustain a number of bright and dark plasmon modes, revealed via electron energy loss spectroscopy. We further discuss the limits of the classical electromagnetism framework on this length scale.

Plasmonic nanostructures composed out of two or more elements can sustain bright and dark plasmon modes, due to hybridization between the individual parent plasmons. Due to their small (or vanishing) dipole moment, dark modes do not couple strongly to far-field radiation, and are hence difficult to reveal via optical techniques. We will present studies of using electron energy loss spectroscopy (EELS) for the mapping of the complete mode spectrum of bow tie cavities, focusing on ever decreasing gaps [1], hence approaching the quantum regime. We show that down to gap sizes of 1 nm, the classical description suffices for numerical simulations of the expected spectral behavior.

Transformation optics has recently been developed into an excellent tool to investigate light confinement on spatial scales far below the wavelength, particularly with a viewpoint of creating a broadband light harvesting response [2]. After a brief review of the main achievements of this new design paradigm, we will focus on experimental implementations of transformation-optics-designed structures in the THz regime of the spectrum [3]. Lastly, we will discuss how the incorporation of spatial non-locality is necessary on this length scale in order to take consideration of the effect of surface charge smearing due to the finite Thomas Fermi screening length [4], and discuss experimental observations of this effect [5].

REFERENCES

1. Duan, H., Fernández-Domínguez, A.I., Bosman, M., Maier, S.A., & Yang, J.K.W., Nanoplasmonics: classical down to the nanometer scale, *Nano Letters* 12, 1683 (2012)
2. Pendry, J.B., Aubry, A., Smith, D.R., & Maier, S.A., Transformation optics and subwavelength control of light, *Science* 337, 549 (2012)
3. Hanham, S.M., Férnandez-Domínguez, A.I., Teng, J.H., Ang, S.S., Lim, K.P., Yoon, S.F., Ngo, C.Y., Klein, N., Pendry, J.B., & Maier, S.A., Broadband terahertz plasmonic response of touching InSb disks, *Advanced Materials* 24, OP226 (2012)
4. Férnandez-Domínguez, A.I., Wiener, A. García-Vidal, F.J., Maier, S.A., & Pendry, J.B., A transformation optics description of non-local effects in plasmonic nanostructures, *Physical Review Letters* 108, 106802

(2012)

5. Ciracì, C., Hill, R.T., Mock, J.J., Urzhumov, Y., Fernández-Domínguez, A.I., Maier, S.A., Pendry, J.B., Chilkoti, A., & Smith, D.R., Probing the ultimate limits of plasmonics enhancement, *Science* 337, 1072 (2012)

A cloak from self-assembled metallic nanoparticles

C. Rockstuhl[1], S. Mühlig[1], M. Farhat[1], S. Bin Hasan[1], A. Cunningham[2], T. [2], J. Dintinger[3], T. Scharf[3], and F. Lederer[1]

[1] Institute of Condensed Matter Theory and Solid State Optics,
Abbe Center of Photonics, Friedrich-Schiller-Universität Jena, D-07743 Jena, Germany

[2] , Quai Ernest-Ansermet 30,
- 4, Switzerland

[3] Optics & Photonics Technology Laboratory, École Polytechnique Fédérale de Lausanne (EPFL),
CH-2000 Neuchâtel, Switzerland

*corresponding author: carsten.rockstuhl@uni-jena.de

Abstract- We present the theory, the realization, and the successful experimental characterization of a cloak that was fabricated using self-assembling techniques from the field of colloidal nanochemistry. The cloak essentially consists of plasmonic nanoparticles that decorate the object to be cloaked, which is a dielectric sphere. It is shown that the cloak almost perfectly suppresses the scattering response of the dielectric sphere in the electric dipolar limit. Extensions to cloak more macroscopic objects are additionally discussed.

Cloaking is potentially the most fascinating application that has come within reach with metamaterials. Once the idea sparked, various strategies were established to actually achieve, meaning fabricating, cloaks. If a macroscopic object shall be concealed from an external observer, materials are usually required that possess a highly anisotropic inhomogeneous permittivity and permeability. Carpet cloaks - that conceal objects above ground plates - diminish these requirements and can be made from dielectrics only [1]. A metallic shell suffices to suppress the scattering field from small dielectric core objects and hence to cloak them. The purpose of the metallic shell is to generate a scattered dipole field that is equal in amplitude to the scattered dipole field from the core but oscillating π-out-of-phase [2]. Whereas implementations at radio frequencies demonstrated the validity of the approach, implementations for visible light remain challenging [3]. The subtlety and the nanoscale extension of the structure render its fabrication with top-down methods really difficult. Here, we overcome these obstacles and detail theory, fabrication, and successful characterization of a scattering cloak that operates in the visible regime. The key to success was a fabrication with a bottom-up approach based on electrostatic forces.

To self-assemble the cloak, we fabricated negatively charged silver nanoparticles according to a modified Lee-Meisel method. Dielectric spheres, suitably functionalized to render them positively charged, are then exposed to the silver nanoparticle solution which readily adsorb with a high filling fraction at the surface - forming the structure shown in the left-hand image - essentially an effectively metallic shell. The shell possesses at a particular frequency a suitable effective permittivity which nullifies the total scattering. This frequency is slightly detuned from the particle plasmon resonance such that parasitic absorption is weak. Directly in resonance, where a secondary working frequency exists, large absorption prevents the cloak from being functional. The suppression of the simulated scattered field at the suitable frequency is shown in the central figure. The experimentally measured scattering signals from the spherical object with and without cloaking shell are shown in the right figure. A clear suppression of the scattering signal was observed [4,5].

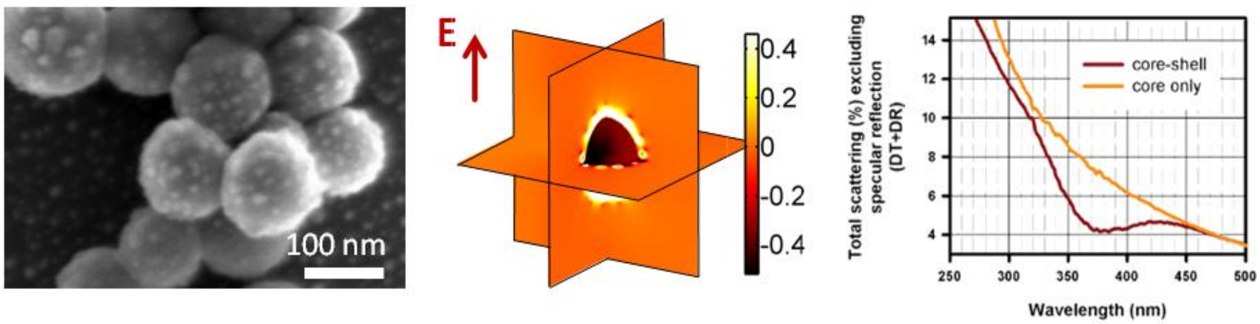

Figure 1: (left) Scanning electric micrograph image of a fabricated cloak. The structure consists of silver nanoparticles that decorate a dielectric core sphere. (center) The rigorously calculated total near-field upon illuminating the cloak with a plane wave at a suitable frequency. The figure shows the intensity on a logarithmic scale. A clear suppression of the scattered field can be seen, i.e. the field outside the cloak corresponds only to the illumination. (right) Measured total scattering cross section of the core object with and without the cloak.

A self-assembled cloak that hides optically small particles is an achievement in its own rights. It is, nevertheless, naturally desirable to have a clear strategy in mind that also allows the cloaking of more macroscopic objects. Therefore, we also present the results of a theoretical study where a cloak is designed that allows the suppression of not only the electric dipolar scattering response from the object, but also its magnetic dipolar response. The key that allows the implementation of such cloaks is the use of nanoparticles in the shell material that are made from a polaritonic material, i.e. a material with a large permittivity in a certain frequency interval. These nanoparticles sustain as lowest order Mie resonance a magnetic dipole response. This suggests that a shell made from such nanoparticles can generate a magnetic dipolar response that can cancel the magnetic dipole contribution from the core object in the far-field [6].

In summary, our specific contribution is the demonstration of a self-assembled cloak. The structure may find applications in cloaked sensors or in optical nanoantenna arrays with strongly suppressed cross-talk. The more general contribution is to establish new design and fabrication paradigms that exploit bottom-up approaches to realize nanooptical devices. Extensions to cloak more macroscopic objects are presented as well.

Financial support from the European Union FP7 project NANOGOLD and the German Federal Ministry of Education and Research (PhoNa) is acknowledged.

REFERENCES

1. Wegener M. and Linden S. "S g o c l c w l" *Physics Today* Vol. 63, 32-, 2010.
2. Alù A. and Engheta N. " l o c l clo k g : c l c o l" *J. Opt. A* Vol. 10, 093002, 2008.
3. Rainwater D., Kerkhoff A. , Melin K., Soric J., Moreno G., and Alù A. "Ex l f c o of three-dimensional plasmonic cloaking in free- c " *New J. of Phys.* Vol. 14, 013054, 2010.
4. Mühlig S. l. "A lf bl c lo k" o .
5. Mühlig S., Farhat M., Rockstuhl C., and Lederer F. " lo k g l c c c l obj c b ll of metallic nanoparticles" *Phys. Rev. B* Vol. 83, 195116, 2011.
6. F M. Mü l g S. Rock l . L F. "Sc g c c l l o of g c o l f l f o c o c o c " *Opt. Express* Vol. 20, 13896, (2012).

Enhanced optical absorption of nanoparticles in multiple scattering regime

J.P. Hugonin[1], M. Besbes[1], M. Langlais[1,2] and P. Ben-Abdallah[1*]

[1]Laboratoire Charles Fabry, UMR 8501, Institut d'Optique, CNRS,
Université Paris-Sud 11, 2, Avenue Augustin Fresnel, 91127 Palaiseau Cedex, France

[2]Total New Energies, R&D, Tour Michelet, 92078 Paris La Défense Cedex, France

[*]corresponding author: pba@institutoptique.fr

Abstract-Using the coupled multipoles theory and a finite element solver of Maxwell equations we compute the apparent absorption of nanoparticles in two-dimensional nanoparticles lattices immersed inside semi-infinite transparent materials. For metallic nanoparticles we demonstrate that this absorption can be enhanced in the visible range by more than one order of magnitude compared with isolated particles thanks to multiple interactions with the neighbourhoods particles. These multiple interaction mechanisms pave the way to a new strategy for engineering light absorption.

Engineering light interactions with subwavelength objects is a longstanding problem in physics which is of prime importance for numerous technological applications among which are the photovoltaïc energy conversion[1], the optical manipulation of nanoobject[2] or the quantum information treatment[3]. Since the pioneer work of Purcell[4−6] it is well known that the emission of a quantum emitter can be tailored by local modifications of its close environment. Recently Castanié et al.[7] have shown that the presence of an interface in the neighbourhood of a nanoparticle can drastically change its absorption pattern and can be used to control both the resonance frequency and the level of absorption.

In the present work we study how the absorption cross section of metallic nanoparticles embedded in a two dimensional lattice (Fig. 1-a) changes thanks to multiple interactions with their counterpart. In presence of electric and magnetic current density $\bar{j}_E$ and $\bar{j}_H$, the power absorbed inside a particle at a frequency ω is given by

$$P = \sum_{A=E,H} \int_V \mathrm{Re}[\bar{j}_A(r,\omega).\bar{A}^*(r,\omega)]dr \qquad (1)$$

where $\bar{A}$ denotes either the local electric or magnetic field. This expression has been calculated using both the coupled multipoles theory and a finite element solver of the Maxwell equations and compared with the power absorbed by a single particle in the same local environment. The results plotted in Fig. 1-(b) and Fig. 1-(c) demonstrate that the absorption level of nanoparticles within such lattices can be strongly enhanced. They show that the multiple interaction mechanisms between nanoparticles can be used to design a new generation of light absorbers by engineering the configurational resonances which depend on the spatial and size distribution of particles.

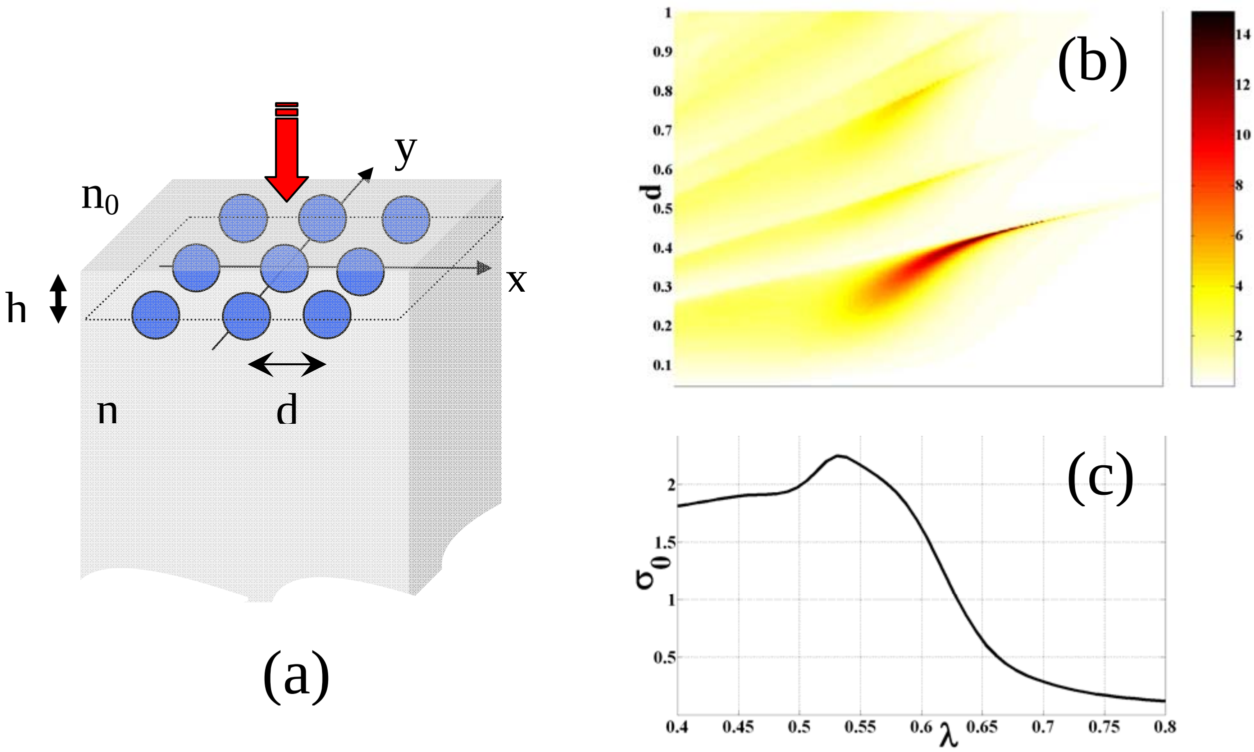

Figures 1: (a) Sketch of a 2D square nanoparticles lattice immerged inside a semi-infinite transparent medium of refractive index n which is highlighted from the top at normal incidence. (b) Map of losses (normalized by $d^2/(\pi r^2)$) in gold particles (r=50 nm) versus both the wavelength λ and separation lattice period d when the lattice is embedded in a semi-infinite medium of index $n=1.5$ at a distance h=100 nm from its surface. The surrounding medium is vacuum ($n_0=1$). (c) Losses inside an isolated particle at the same distance from the surface.

REFERENCES

1. Atwater H. A. and Polman A., Plasmonics for improved photovoltaic devices, Nature Materials, Vol. 9, 205-2013, 2010.
2. Ashkin A., Dziedzic J. M., Bjorkholm J. E. and Chu S., Observation of a single-beam gradient force optical trap for dielectric particles, Opt. Lett., Vol. 11, 288–290, 1986.
3. Poddubny A. N., Belov P. A. and Kivshar Y. S., Spontaneous radiation of a finite-size dipole emitter in hyperbolic media, Phys. Rev. A, Vol. 84, 023807, 2011.
4. Purcell E. M., Spontaneous emission probabilities at radio frequencies, Phys. Rev., Vol. 69, 681, 1946.
5. Drexhage K. H., Kuhn H., and Schäfer F. P., Variation of the Fluorescence Decay Time of a Molecule in Front of a Mirror, Ber. Bunsenges. Phys. Chem., Vol. 72, 1179, 1968.
6. Chance R. R., Prock A., and Silbey R., Molecular fluorescence and energy transfer near interfaces, Adv. Chem. Phys., Vol. 37, 1, 1978.
7. Castanié E., Vincent R., Pierrat R., and Carminati R., Absorption by an optical dipole antenna in a structured

environment, Int. J. Opt., 452047, 2012.

Plasmonic nanoparticles as dielectric tuner, sub-wavelength light confiner and heat generator

M. Elbahri [1,2]

[1] Nanochemistry and Nanoengineering, Institute for Materials Science, Faculty of Engineering, University of Kiel, Kaiserstrasse 2, 24143 Kiel, Germany

[2] Institute of Polymer Research, Helmholtz-Zentrum Geesthacht, Max-Planck-Str. 1, 21502 Geesthacht, Germany

[*]corresponding author: me@tf.uni-kiel.de

Abstract-Plasmonic nanoparticles drawn the attention in the last few decades due to their exotic properties ranging from sub-wavelength optics up to guiding of the light and heat generation. In this work, the great potential of nanoparticles as a refractive index tuner, light trapper and heat generator will be thoroughly discussed.

When a metal nanoparticle is illuminated, part of the intercepted light is scattered in the surroundings, while the other part gets absorbed and ultimately dissipated into heat as described in Figxy. Therefore, understanding the absorption and scattering cross sections of the nanoparticles is crucial to predict which pathways are most probable. It is known that the small particle (<5 nm) tend to absorb more light whereas in the bigger one (>50 nm) scattering is dominant. This size dependency means that one can engineer and tune the plasmonic properties of any device from localized hot state to re-radiated one by implementing small and big particles in the system, respectively. In other word, the overall response of any plasmonic device would rely on the nature of the plasmon resonance which can be either radiative or non-radiative (or the combination of both). Figure 1 demonstrate a new application of plasmonic nano-particles as a heat generator which make the possiiblity of healing the cracked polymer with low intensity laser (details will be discussed in the talk).

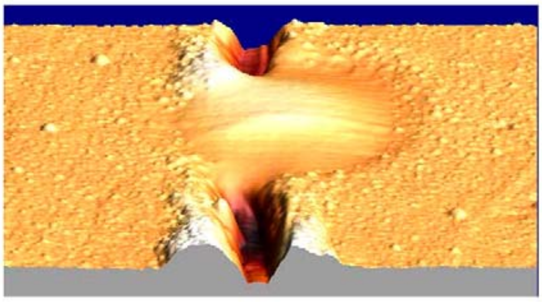 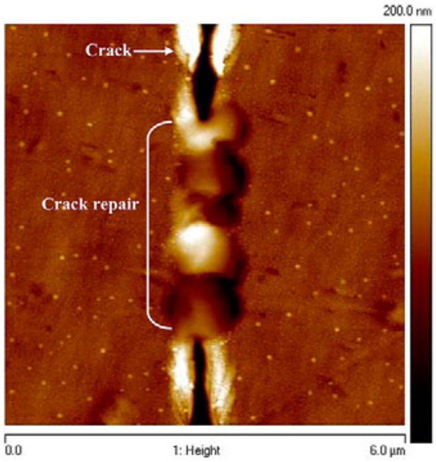

Figure 1: (left) 3D view for the concept of crack repair where the softened material fills in the crevice (AFM height profile). (right) Multiple overlapping spots made by 532 nm laser using 5 mW power were made to fill in the crack [1].

REFERENCES

1. Zillohu, A. U., Abdelaziz, R., Hedayati, M. K., Emmler, T., Homaeigohar, S., Elbahri, M., "Plasmon-Mediated Embedding of Nanoparticles in a Polymer Matrix: Nanocomposites Patterning, Writing, and Defect Healing," *J. Phys. Chem. C* Vol. 116, 17204-17209, 2012.

Multiple-Source Excitation of Active Coated Nano-Particles

S. Arslanagić
Department of Electrical Engineering, Electromagnetic Systems
Technical University of Denmark, Ørsteds Plads, Bldg. 348, DK-2800 Kgs. Lyngby, Denmark
E-mail: sar@elektro.dtu.dk

Abstract – The present work investigates the resonance and transparency effects that occur in electrically small active coated nano-particles in the case of multiple-dipole excitation. While the resonance effects are found for dipole locations both inside, as well as outside, the nano-particles, the transparency is only in evidence for dipole locations exterior to particles. Furthermore, the work reports on interesting pattern-rotation possibilities when several dipoles, of different orientations and locations, excite a super-resonant active coated nano-particle.

.

1. Introduction

A variety of passive and active canonical coated nano-particle (CNP) systems have been studied as source and scattering problems using analytical based solutions. Both plane wave and electric Hertzian dipole excitations of these CNPs have been investigated.

Most nano-particle configurations have been examined under the more common plane wave source excitation, and solutions have been obtained for potential use, for instance, in the design of sub-wavelength nano-particle lasers [1] and optical metamaterials [2]. In these designs, both silver and gold coatings and canonical and three-level atom gain models were considered.

Recently, the less common electric Hertzian dipole excitation problem solutions have also been obtained and used to design a variety of highly sub-wavelength nano-amplifiers and nano-sensors [3]. In particular, these works have shown that appropriate gain inclusion in CNP configurations may lead to profound localizations of electromagnetic power density inside the CNPs, as well as enhancements of the power radiated by the respective sources; these are all features highly desirable for efficient fluorescent nano-sensors and nano-antennas with properties significantly surpassing those of their passive-based counterparts. The impact of the metal choice on the performance of nano-amplifiers and nano-sensors was accounted for in [4]. Aside from the significantly enhanced values of the power radiated by a single dipole, the CNP configurations studied in [3] was also found to decrease significantly the radiated power (in the far-field region) of the dipole when it is located outside the CNP, thereby effectively cloaking the dipole emitter to a far-field observer. This property was further addressed in [5] where even lower power levels were observed for the case of multiple dipole excitations of spherical active CNPs when all dipoles were placed outside the CNP. These cloaking and super-resonant properties of active CNP might be of great potential interest in suppressing the emission lines of certain molecules, while enhancing those of others – another very useful nano-sensing application.

The present work further examines active coated nano-particles in the presence of multiple electric Hertzian dipoles. Attention is devoted to the resonance effects, which are found for dipole locations both inside and outside the nano-particles, and, to some extent, to transparency effects which only occur for the exterior dipole locations. In addition hereto, several interesting pattern-rotation possibilities are reported when two dipoles, of different locations and orientations, excite a super-resonant active CNP.

2. Results and discussion

The spherical CNP configuration is shown in Fig. 1. It consists of a 24 nm radius silica nano-core (green region) covered concentrically by a 6 nm thick silver nano-shell (red region), and is excited by one or more electric Hertzian dipoles (EHDs); the figure only shows the case with the two-EHD excitation. For the plasmonic nano-shell, the size-dependency of the permittivity was taken into account. The active CNPs are simulated by incorporating the canonical, constant frequency, gain model inside the silica nano-core [1].

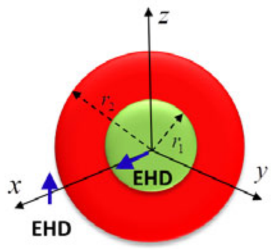

Figure 1.
The CNP configuration.

Fig. 2 shows the magnitude of the θ-component of the electric field for the case of two-EHD excitation. In Fig. 2(b), the two dipoles are both z-oriented, and are located along the positive x-axis, one being inside the nano-core at 12 nm and the other being outside the CNP at 36 nm. In Fig. 2(d), the dipole locations are the same as in Fig. 2(b), but the EHD outside the CNP is now x-oriented. For reference purposes, the corresponding free-space results for these two-EHD configurations are included in Fig. 2(a) and (c), respectively. Comparing the results of Fig. 2(a) and (b) we observe a very strong response in Fig. 2(a) where a resonant dipole mode have been excited inside the CNP. Due to the z-orientation of the exciting EHDs, the resulting pattern of the whole system resembles the one of a very strong z-oriented EHD at the center of the CNP. However, when the orientation of one of the dipoles changes, so that the exterior EHD is now x-oriented, the resulting pattern flips as shown in Fig. 2(d). A deeper account on these results, as well as the results for additional EHD locations and/or orientations will be shown at the presentation.

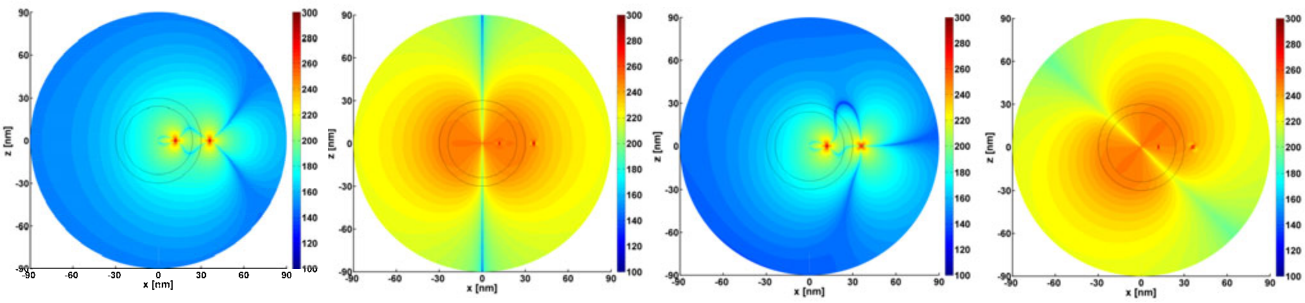

(a) (b) (c) (d)

Fig. 2. Electric field distributions of several, two-EHD, free-space and CNP configurations. See the main text for further explanations.

REFERENCES

1. J. A. Gordon and R. W. Ziolkowski, “The design and simulated performance of a coated nano-particle laser,” *Opt. Express*, Vol. 15, 2622-2653, 2007.
2. J. A. Gordon and R. W. Ziolkowski, “CNP optical metamaterials,” *Opt. Express*, Vol. 16, 6692-6716, 2008.
3. S. Arslanagic and R. W. Ziolkowski, “Active coated nano-particle excited by an arbitrarily located electric Hertzian dipole – resonance and transparency effects,” *J. Opt. A*, Vol. 12, 024014, 2010.
4. S. Arslanagic and R. W. Ziolkowski, “Active coated nano-particles: impact of plasmonic material choice,” *Appl. Phys. A*, Vol. 103, 795-798.
5. S. Arslanagic and R. W. Ziolkowski, “Jamming of quantum emitters by active coated nano-particles,” Submitted to *IEEE Journal of Selected Topics in Quantum Electronics*, July, 2012.

An overview of sum rules and physical limitations for passive metamaterial structures

Mats Gustafsson

Lund University, Sweden
mats.gustafsson@eit.lth.se

Abstract— Metamaterials offer many new possibilities to design structures and devices with improved performance. In this paper, we present an overview of physical limitations for passive structures. The physical limitations relate the product between performance and bandwidth with the size of the structure. They are derived from sum rules that relate a weighted all spectrum integral of the performance with the low- and high-frequency responses. We present results for extinction cross sections, radar absorbers, high-impedance surfaces, extraordinary transmission, antennas, and temporal dispersion of metamaterials. The results provide a tradeoff between possible performance and bandwidth. As they are derived solely using passivity and linearity, the results also state when it is necessary to use active or non-linear media.

Passivity is inherent in many physical processes. Here, we consider an input output system that can be written on convolution form $u = R * v$, that follow from the assumptions of linearity, time-translational invariance, and continuity [14]. The time-domain characterizations for admittance passivity and scattering passivity are

$$\mathcal{E}_{\mathrm{adm}}(T) = \int_{-\infty}^{T} u(t)v(t)\,\mathrm{d}t \geq 0 \quad \text{and } \mathcal{E}_{\mathrm{scatt}}(T) = \int_{-\infty}^{T} |v(t)|^2 - |u(t)|^2\,\mathrm{d}t \geq 0, \tag{1}$$

respectively, where the inequality should hold for all T and v [14]. It is clear that time-domain passivity implies causality. The Laplace (or Fourier) transform of a passive system introduces a transfer function that is related to a positive real function or Herglotz function [1].

Herglotz functions, $h(z)$, are holomorphic in the upper half plane $\operatorname{Im} z > 0$ and map the upper half plane into itself, *i.e.*, $\operatorname{Im} h(z) \geq 0$, see [1, 11]. Here, we also restrict the analysis to symmetric Herglotz function $h(z) = -h^*(-z^*)$. Their asymptotic expansions are of the form

$$h(z) = \sum_{n=0}^{N_0} a_{2n-1} z^{2n-1} + \mathrm{o}(z^{2N_0-1}) \quad \text{as } z \hat{\to} 0 \quad \text{and } h(z) = \sum_{n=0}^{N_\infty} b_{1-2n} z^{1-2n} + \mathrm{o}(z^{1-2N_\infty}) \quad \text{as } z \hat{\to} \infty \tag{2}$$

for some $N_0 \geq 0$ and $N_\infty \geq 0$, see [1], where $\hat{\to}$ denotes limits for $0 < \alpha \leq \arg(z) \leq \pi - \alpha$. The expansions (2) guarantee that $\operatorname{Im}(x)$ satisfy the integral identities

$$\frac{2}{\pi}\int_0^\infty \frac{\operatorname{Im}\{h(x)\}}{x^{2n}}\,\mathrm{d}x = a_{2n-1} - b_{2n-1} = \begin{cases} -b_{2n-1} & n < 0 \\ a_{-1} - b_{-1} & n = 0 \\ a_1 - b_1 & n = 1 \\ a_{2n-1} & n > 1, \end{cases} \tag{3}$$

where $n = 1 - N_\infty, ..., N_0$ and $a_{2n-1} = b_{1-2n} = 0$ for $n < 0$, see [1] for details. Note that a simplified notation is used here where the limits in (3) are dropped, *i.e.*, the integrand is the limit $h(x + \mathrm{i}y)$ as $y \to 0$. The non-negative constraint, $\operatorname{Im} h \geq 0$, imply the inequity $\frac{2}{\pi}\int_{x_1}^{x_2} \operatorname{Im}\{h(x)\} x^{-2n}\,\mathrm{d}x \leq a_{2n-1} - b_{2n-1}$.

The identity (3) is the foundation for deriving sum rules and limitations on a many physical systems [1], see also [3, 12, 13]. In short; it is sufficient to identify a passive system and to determine its low- and/or high-frequency asymptotics. In the presentation, we illustrate the use of sum rules and physical bounds for various passive electromagnetic systems. We present an overview of results that answer questions such as

- What limits the scattering and absorption of electromagnetic waves by finite objects over a frequency interval [13]?
- How does the ultimate bandwidth depend on the size and volume of antennas [5, 6]?
- What are the tradeoffs between thickness and bandwidth for; absorbers [12], high-impedance surfaces [2, 7], total cross sections [10], and blockage of EM waves [9]?
- How does the aperture size and shape related to the bandwidth for extraordinary transmission of electromagnetic waves through apertures in thin sheets [8]?
- What is the ultimate bandwidth for negative refraction [4]?
- How is the bandwidth related to the permeability in artificial magnetism [4]?

The derived sum rules and physical bounds are useful as they relate the dynamic response to the often much simpler low- or high frequency properties. The asymptotic values can also often be determined analytically and are related to simple parameters of the structure, such as the thickness [7, 12] or polarizability [13]. The derived bounds offer simple tradeoffs between performance and bandwidth for many cases [4–7, 12]. The results are also useful as they show fundamental limits for linear and passive structures and hence indicate when it is necessary to utilize active or non-linear devices.

REFERENCES

1. A. Bernland, A. Luger, and M. Gustafsson. Sum rules and constraints on passive systems. *J. Phys. A: Math. Theor.*, **44**(14), 145205, 2011.
2. C. R. Brewitt-Taylor. Limitation on the bandwidth of artificial perfect magnetic conductor surfaces. *Microwaves, Antennas & Propagation, IET*, **1**(1), 255–260, 2007.
3. R. M. Fano. Theoretical limitations on the broadband matching of arbitrary impedances. *Journal of the Franklin Institute*, **249**(1,2), 57–83 and 139–154, 1950.
4. M. Gustafsson and D. Sjöberg. Sum rules and physical bounds on passive metamaterials. *New Journal of Physics*, **12**, 043046, 2010.
5. M. Gustafsson, C. Sohl, and G. Kristensson. Physical limitations on antennas of arbitrary shape. *Proc. R. Soc. A*, **463**, 2589–2607, 2007.
6. M. Gustafsson, C. Sohl, and G. Kristensson. Illustrations of new physical bounds on linearly polarized antennas. *IEEE Trans. Antennas Propagat.*, **57**(5), 1319–1327, May 2009.
7. M. Gustafsson and D. Sjöberg. Physical bounds and sum rules for high-impedance surfaces. *IEEE Trans. Antennas Propagat.*, **59**(6), 2196–2204, 2011.
8. M. Gustafsson, D. Sjöberg, and I. Vakili. On the extraordinary transmission through subwavelength apertures in perfectly conducting sheets. In *International Conference on Electromagnetics in Advanced Applications (ICEAA)*, Turin, Italy, September 12–16 2011.
9. M. Gustafsson, C. Sohl, C. Larsson, and D. Sjöberg. Physical bounds on the all-spectrum transmission through periodic arrays. *EPL Europhysics Letters*, **87**(3), 34002 (6pp), 2009.
10. M. Gustafsson, I. Vakili, S. E. B. Keskin, D. Sjöberg, and C. Larsson. Optical theorem and forward scattering sum rule for periodic structures. *IEEE Trans. Antennas Propagat.*, **60**(8), 3818–3826, 2012.
11. H. M. Nussenzveig. *Causality and dispersion relations.* Academic Press, London, 1972.
12. K. N. Rozanov. Ultimate thickness to bandwidth ratio of radar absorbers. *IEEE Trans. Antennas Propagat.*, **48**(8), 1230–1234, August 2000.
13. C. Sohl, M. Gustafsson, and G. Kristensson. Physical limitations on broadband scattering by heterogeneous obstacles. *J. Phys. A: Math. Theor.*, **40**, 11165–11182, 2007.
14. A. H. Zemanian. *Distribution theory and transform analysis: an introduction to generalized functions, with applications.* Dover Publications, New York, 1987.

A sparse scattering model for nanoparticles on rough substrates

M. Karamehmedović[1*], P.-E. Hansen[2], and T. Wriedt[3]
[1]Foundation Institute of Materials Science (IWT), Department of Production Engineering,
University of Bremen, Germany
[2]Danish Fundamental Metrology, Denmark
[3]Institut für Werkstofftechnik, Germany
[*]corresponding author: mirza@iwt.uni-bremen.de

Abstract-We present and validate an efficient forward scattering model for nanoparticles on rough contaminated substrates.

The technology of functional nanomaterials relies on the rapid nondestructive characterization of nanostructures on substrates using Optical Diffraction Microscopy (ODM). The roughness and the contamination of the substrate typically increase the ill-posedness of the inverse scattering problem inherent in ODM, as well as complicate the use of numerical scattering methods in the forward computations [1]. We here present a forward scattering model that employs a heuristic transfer-function description of the substrate roughness and contamination to enable the use of the efficient Discrete Sources Method [1–5] for scattering computation. The performance of the model is validated against experimental Bidirectional Reflectance Distribution Function (BRDF) data, obtained at Danish Fundamental Metrology, for a Pt submicron wire on a Si substrate, shown in Figure 1.

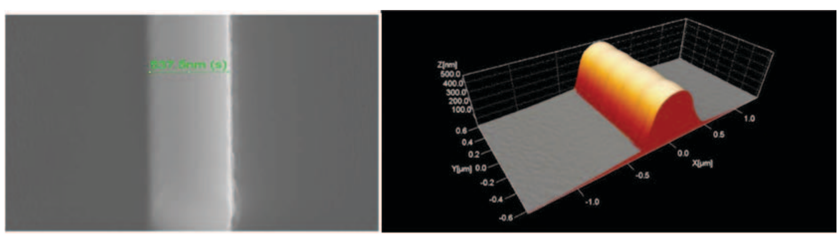

Figure 1. Pt submicron wire on Si substrate. a) SEM image. b) AFM image.

As illustrated in Figure 2a), we decompose the original scattering process into two idealized setups. The substrate roughness and contamination are described in terms of a heuristic transfer function H_{rough} computed by fitting the reflected power pattern $I_{\mathrm{sca},0}$ observed *in the absence of the nanostructure*, see Figure 3a). The transfer function H_{nanostr}, describing the scattering by the nanostructure on a *smooth* substrate, is computed using the numerically efficient Discrete Sources Method [1–5] with complex images [6], see Figure 2b). Here, essentially, the reflected field is expressed in terms of fields radiated by a set of electric line currents and their complex images,

$$\mathbf{E}^{\mathrm{ref}}\left(\mathbf{x}_\mu\right) = \sum_\nu C_\nu H_0^{(1)}\left(k_0\left|\mathbf{x}_\mu - \mathbf{r}'_\nu\right|\right) + \sum_\nu D_\nu H_0^{(1)}\left(k_0\left|\mathbf{x}_\mu - \tilde{\mathbf{r}}'_\nu\right|\right).$$

The product transfer function $H_{\mathrm{rough}}H_{\mathrm{nanostr}}$ is then used to model the total scattering process. Figure 3b) compares the measured BRDF against the predicted reflected power patterns $I_{\mathrm{sca,1,ROUGH}}$ and $I_{\mathrm{sca,1,SMOOTH}}$ obtained with and without taking the substrate roughness and contamination into account, respectively. The root mean square error in the predicted patterns is improved from 0.6386 to 0.3754 when using our composite model, with virtually no decrease in the computational efficiency.

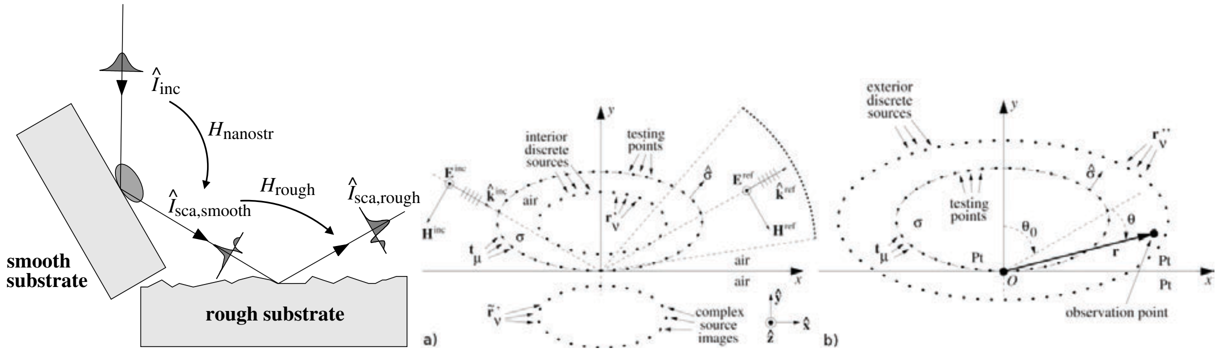

Figure 2. a) Decomposing the scattering process. b) Discrete sources formulation.

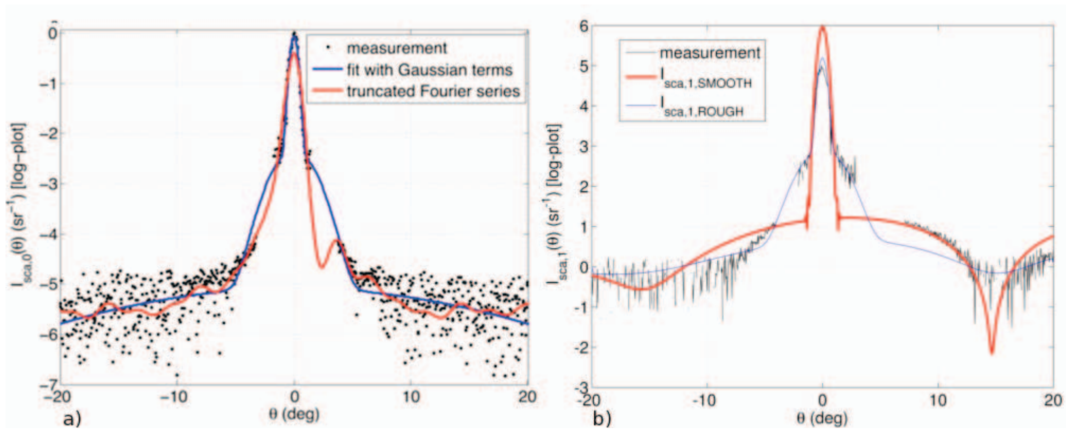

Figure 3. a) The heuristic roughness model. b) Validation against experimental BRDF data.

Acknowledgment-This work was supported by German Research Foundation (DFG grant no. WR 22/36-2) and by the European Commission and the EURAMET e. v. (support code no. 912/2009/EC).

REFERENCES

1. Karamehmedović, M., P.-E. Hansen and T. Wriedt, “An efficient rough-interface scattering model for embedded nano structures,” *Thin Solid Films*, accepted, 2012. http://dx.doi.org/10.1016/j.tsf.2012.11.048
2. Karamehmedović, M., P.-E. Hansen, K. Dirscherl, E. Karamehmedović and T. Wriedt, “Profile estimation for Pt submicron wire on rough Si substrate from experimental data,” *Opt. Express*, Vol. 20, No. 19, 21678–21686, 2012.
3. Karamehmedović, M., P.-E. Hansen and T. Wriedt, “A fast inversion method for highly conductive submicron wires on a substrate,” *J. Eur. Opt. Soc. – Rapid*, Vol. 6, 11039, 2011.
4. Karamehmedović, M., P.-E. Hansen and T. Wriedt, “An efficient scattering model for PEC and penetrable nanowires on a dielectric substrate,” *J. Eur. Opt. Soc – Rapid*, Vol. 6, 11021, 2011.
5. Karamehmedović, M., M.-P. Sørensen, P.-E. Hansen and A. V. Lavrinenko, “Application of the method of auxiliary sources to a defect-detection inverse problem of optical diffraction microscopy,” *J. Eur. Opt. Soc. – Rapid*, Vol. 5, 10021, 2010.
6. Lindell, I.V., and E. Alanen, “Exact Image Theory for the Sommerfeld Half-Space Problem, Part I: Vertical Magnetic Dipole,” *IEEE Trans. Antennas Propag.*, Vol. AP–32, No. 2, 126–133, 1984.

Gold Nanoparticle Doped Polymer Materials for Micro- and Nanofabrication

S. V. Fischer[1], N. Masuda[1], S. S. Keller[1], B. Uthuppu[1], M. H. Jakobsen[1]

[1]Department of Nanotechnology, DTU, Kgs. Lyngby, Ørsteds plads, 2800, DK
Mogens.Jakobsen@nanotech.dtu.dk

New bottom-up approach to fabricate metal nanoparticle doped polymer photoresist (polymer nanocomposite) is presented. The nanocomposite holds a potential to fabricate hierarchically structured materials which have tailored functionalities spanning multiple length, scales and dimensions. Such materials will enable exiting new applications in micro- and nanotechnology1. However, simple mixture of nanoparticles with many polymers leads to non-uniform distribution, particle clustering or aggregation that impairs desired properties in the composite material[2].

Gold nanoparticle SU-8 composite was structured by UV photolithography and attained the lithographic resolution of 3.5 µm by soft contact (Figure 1). Point-wise light scattering was observed through dark field microscopy (Figure 2). Plasmonic extinction peaked at 550 nm and similar response was observed by brief Mie calculation at n=1.63, (Figure 3). Spherical gold nanoparticle possesses isotropic feature. However, the composite showed polarization dependency to incident light, indicating that the particles were self-organized chemically and/or physically during the fabrication. The material is speculated to be useful in various fields, such as biomedical optics and photonics. The technique may be a break-through for cost-effective and scalable development for plasmonic sensing devices for example, SPR spectroscopy/SERS substrate and ultra-thin photonic crystals which sometimes relay on time consuming top-down approach for the fabrication. Since SU-8, PVP/VA and gold nanoparticles have low biological toxicity there may be applications in life science and medicine with this technique[4, 5].

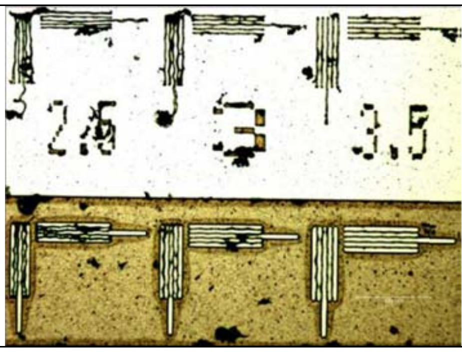

Figure 1: Bright field image from two SU-8 structures. Lithographic resolution, 3.5µm was achieved

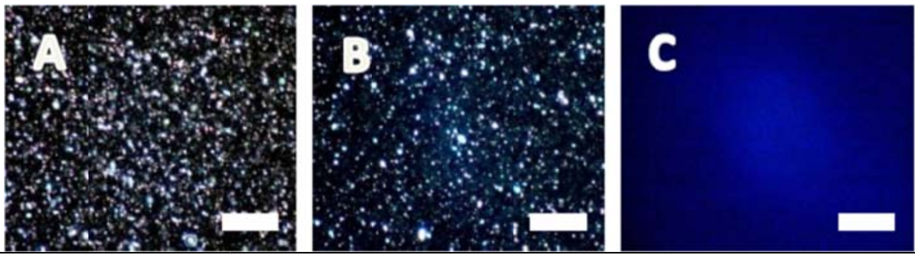

Figure 2: The image from dark field microscopy. From left to right, pictures were taken with (A) 1w/w% (8mg), (B) 0.25w/w (2mg) and (C) control respectively. The white bar is the scale bar (10μm).

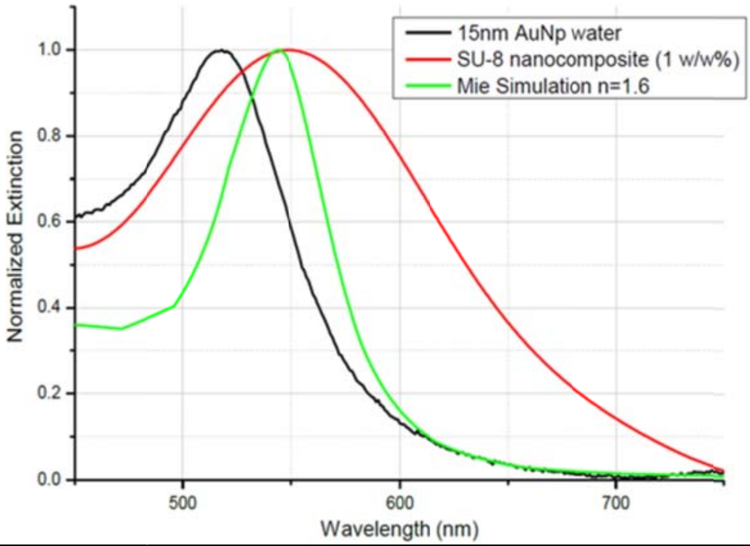

Figure 3: Normalized excitation spectra from 5um SU-8/15nm gold nanoparticle composite. From black, red to green spectra corresponds to phase in water, SU-8 nanocomposite (1 w/w %) and theoretical spectra from 15nm particle at n=1.6 respectively.

1. O.D. Velev & S. Gupta, *Adv. Mater.*, Vol.21, p.1897 (2009).
2. A.C. Balazs, T. Emrick & T.P. Russell, *Science*, Vol.314, p.1107 (2006).
3. B. Bilenberg, T. Nielsen, B. Clausen & A. Kristensen, *J. Micromech. Microeng.*, Vol.14, p.814 (2004).
4. C. Leuner, & J. Dressman, Eur. *J. Pharm. Biopharm.*, Vol.50, p.47 (2000).
5. G. Voskerician et al., *Biomaterials*, Vol.24, p.1959 (2003).

A bottom-up approach towards metamaterials and plasmonics

Stretchable and Tailored Optical Metamaterial made by Self-Assembly

S. Salvatore[1*], S. Vignolini [1], Sang Soon Oh[2], Angela Demetriadou[2], Sebastian Wuestner[2], M. Stefik[3], U. Wiesner[3], Ortwin Hess[2], J. J. Baumberg[1*], and U. Steiner[1*]

[1]Cavendish Laboratory, Department of Physics, University of Cambridge, J.J. Thomson Avenue, Cambridge CB3 0HE, UK

[2]Blackett Laboratory, Department of Physics, Imperial College London, South Kensington Campus, London SW7 2AZ, UK

[3]Department of Materials Science & Engineering, Cornell University, Ithaca, New York 14853 US

[*]corresponding author: ss880@cam.ac.uk

Abstract - The creation of metamaterials working at visible light requires the assembly of architectures with structural control on the 10-nm length scale. Here we present a three-dimensional optical metamaterial, created by a metal replica of a template made by block copolymer self-assembly. This particular architecture can be tailored to tune the optical properties and exploited to create a stretchable metamaterial.

Artificially engineered metamaterials allowed the observation of completely new effects in light-matter interactions[1,2]. Many different experimental methods have been pursued or proposed for the fabrication of such materials throughout the electromagnetic spectrum from the GHz to visible light[3]. However the creation of such structure at visible frequencies is problematic since it requires complex architecture at the nanometer scale. This order of magnitude matches the typical dimensions of the features in block copolymers self-assembly (from 10 to 150 nm).

In this work we present the realization of a three dimensional gold metamaterial based on block copolymer self-assembly[4,5] that can be tuned and applied for stretchable and flexible devices. The complex architecture obtained by self-assembly is exploited as a scaffold to create a perfect gold replica. In order to do so we start with an *isoprene-block-styrene-block-ethylene oxide* (*ISO*) copolymer that, for opportune conditions forms two chemically distinct, interpenetrating gyroid networks (*I,O*) of opposite chirality embedded in a matrix of the third block (*S*). The *I* network is then selectively removed by UV degradation and back-filled with gold by electrodeposition. The remaining polymer is finally removed by plasma etching.

Thus the final device consists of a continuous, triply periodic network of gold; see Figure 1(a). The dimension of the unit cell can be varied from 35 to 50 nm, which is far below optical wavelengths. A complete optical characterization reveals the plasma frequency of such gold ”holey” structure far reduced respect to solid gold. An analytical model[6] and FDTD calculations[6] are in perfect agreement with the experimental data.

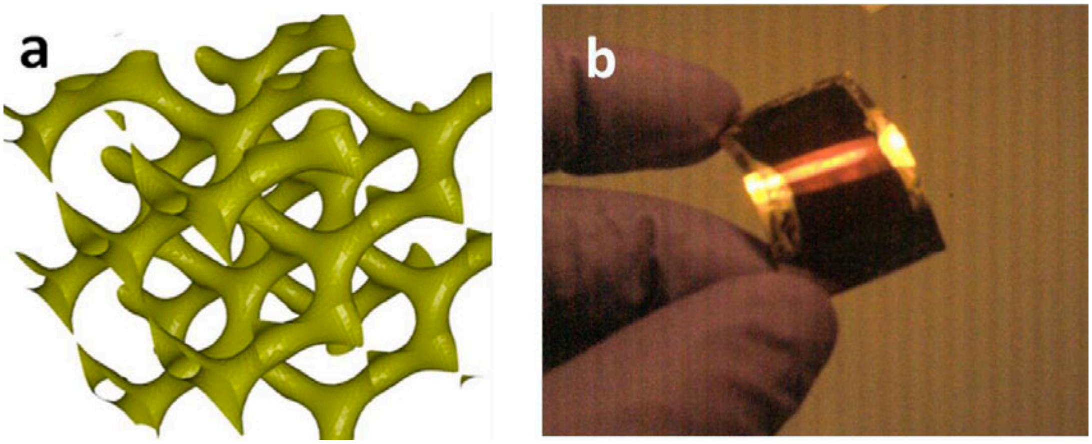

Figure 1 - Single gyroid metamterial. (a) Schematic representation of the three dimensional structure. (b) Photo of the final device showing the flexibility of this optical metamaterial.

The optical response of this metamaterial is strictly correlated with the structural parameters. We are able to control all the dimensions of this architecture in order to finely tailor the optical properties.

Moreover, the continuity of this structure in three dimensions is exploited to obtain a perfectly flexible and stretchable metamaterials that paves the way for the practical use of optical metamaterials, which can lead to a variety of large scale applications.

REFERENCES

[1] V.G. Veselago, *The electrodynamics of substances with simultaneously negative values of ε and μ.* Soviet Physics Us- pekhi **10**, 509 (1968).

[2] J. B. Pendry, *Negative refraction makes a perfect lens.* Phys. Rev. Lett. **85**, 3966–3969 (2000).

K.R. Thomas *et . al*. *Function of blue iridescence in tropical understorey plants.* J. Roy. Soc. Int. **7** 1699-707 (2010).

[3] N. Engheta, R. W. Ziolkowski, *Metamaterials: physics and engineering,* John Wiley and Sons (2006).

[4] F. S. Bates and G. H. Fredrickson, *Block copolymers—designer soft materials*. Physics Today **52**, 32–38 (1999).

[5] S.Vignolini *et al*. *A 3D Optical Metamaterial Made by Self-Assembly*. Adv. Mat. DOI: 10.1002/adma.201103610 (2011).

[6] Demetriadou, A.; Oh, S. S.; Wuestner, S.; Hess, O. New Journal of Physics 2012, 14, DOI: 10.1088/1367–2630/14/8/083032.

[7] Oh, S. S.; Demetriadou, A.; Wuestner, S.; Hess, O. Advanced Materials 2012, Doi: 10.1002/adma.201202788.

Eutectic metamaterial THz waveguides and dynamically tunable modulators

M. Massaouti,[1] A. A. Basharin,[1,2] M. Kafesaki,[1,3] M. F. Acosta,[4] R. I. Merino,[4] V. M. Orera,[4] E. N. Economou,[1,5] C. M. Soukoulis[1,6] and S. Tzortzakis[1,3,*]

[1]*Institute of Electronic Structure and Laser (IESL), Foundation for Research and Technology - Hellas (FORTH),P.O. Box 1527, GR-71110 Heraklion, Greece*

[2]*National Research University "Moscow Power Engineering Institute", 112250 Moscow, Russia*

[3]*Department of Materials Science and Technology, University of Crete, GR-71003, Heraklion, Greece*

[4]*Instituto de Ciencia de Materiales de Aragón, Universidad de Zaragoza, E-50009 Zaragoza, Spain*

[5]*Department of Physics, University of Crete, GR-71003 Heraklion, Greece*

[6]*Ames Laboratory, Department of Physics and Astronomy, Iowa State University, Iowa 50011, USA*

[*]corresponding author: *stzortz@iesl.forth.gr; http://unis.iesl.forth.gr*

Abstract- We present and analyze unique phenomena of enhanced THz transmission through a sub-wavelength LiF dielectric rods lattice embedded in an epsilon-near-zero KCl host. Our experimental results in combination with theoretical calculations show that sub-wavelength waveguiding of terahertz radiation is achieved within an alkali-halide eutectic metamaterial as result of the coupling of Mie-resonance modes arisen in the dielectric lattice.

Metamaterials, have drawn extensive attention during the last decade due to their novel and unique electromagnetic properties, such as negative permittivity/permeability, negative index of refraction, giant chirality, etc. [1]. Recently, a particular interest is noted to the so-called Epsilon-Near-Zero (ENZ) metamaterials which possess a number of intriguing properties associated to the near zero permittivity they exhibit [2]. Among these properties are their ability to “squeeze” electromagnetic waves (E/M) in ultra-narrow ENZ channels [3], to shape the radiation phase pattern of arbitrary sources [4], to control leaky wave radiation from waveguides made by embedding defects in ENZ materials [5], etc.

Here we demonstrate, both experimentally and theoretically, enhanced transmission and sub-wavelength guiding and propagation of THz waves through self-organized eutectic systems made of a LiF rods lattice in a KCl host, exploiting the ENZ response of the polaritonic KCl [6]. According to a recent theoretical study [7] an enhancement of E/M wave transmission through an ENZ material is expected if dielectric cylinders are embedded in it. This enhanced transmission has a resonant character and it is associated with the occurrence of sub-wavelength Mie-resonances in the cylinders which exhibit electrical permittivity much higher than the permittivity of the surrounding ENZ medium. In a periodic system of such cylindrical particles (photonic lattice), the resonances of the nearby particles are combined to give a transmission band, in the same way that the atomic orbitals are combined to give a propagation band for electrons in a tight-binding scheme.

An additional feature characterizing this resonant response is associated with an electric field which is strongly confined along the direction of the incident wave. Thus, sub-wavelength waveguiding is expected.

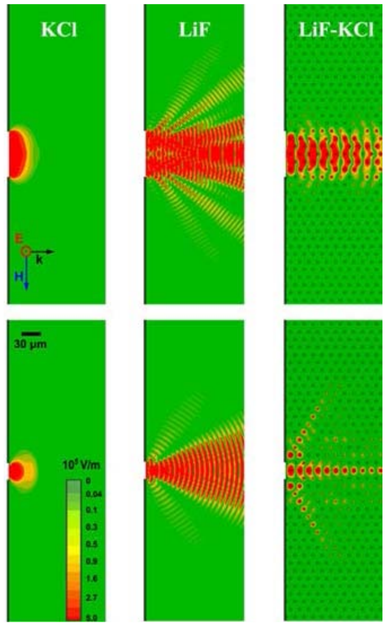

Figure 1: The electric field amplitude distribution of a plane wave (6 THz) propagating in a pure KCl medium (left), in pure LiF (middle) and in the KCl/LiF eutectic (right). The E/M radiation passes through a 50 μm slit (top row) and 15 μm slit (bottom row).

This waveguiding is demonstrated in Figure 1, where we present the field amplitude distribution of a plane THz wave, as propagating through homogeneous KCl and LiF bulks and through a LiF/KCl microstructured system with geometrical features as in the experimentally characterized sample. In all three cases the system is excited by a plane wave of 6 THz frequency, passing through a slit 50 μm wide (top row of Figure 1) and 15 μm wide (bottom row). The strong confinement, waveguiding, in the case of our eutectic lattice is evident.

Acknowledgements: We acknowledge financial support of this work through the following EU research projects: ENSEMBLE (grant n° 213669), NIMNIL (grant n° 228637), CHARISMA (grant n° 228330), “LASERLAB-EUROPE” (grant n° 284464), and Aristeia “FTERA”(grant n° 2570).

REFERENCES

1. Pendry, J. B., “Negative Refraction Makes a Perfect Lens,” Physical Review Letters, 85(18), 3966-3969 2000.
2. Ziolkowski, R. W., “Propagation in and scattering from a matched metamaterial having a zero index of refraction,” Physical Review E, 70(4), 046608 2004.
3. Silveirinha, M., and Engheta, N., Tunneling of Electromagnetic Energy through Subwavelength Channels and Bends using ε-Near-Zero Materials, Physical Review Letters, 97(15), 157403 2006.
4. AlĚ, A., Silveirinha, M. G., Salandrino, A. *et al*., “Epsilon-near-zero metamaterials and electromagnetic sources: Tailoring the radiation phase pattern,” Physical Review B, 75(15), 155410 2007.
5. Nguyen, V. C., Chen, L., and Halterman, K., “Total Transmission and Total Reflection by Zero Index Metamaterials with Defects,” Physical Review Letters, 105(23), 233908 2010.
6. Massaouti, M., Basharin, A. A., Kafesaki, M. *et al*., “Eutectic Epsilon-Near-Zero metamaterial THz waveguides,” Optics Letters *Submitted* 2013.
7. Basharin, A. A., Kafesaki, M., Economou, E. N. *et al*., “Epsilon Near Zero Based Phenomena in Metamaterials,” Physical Review B, 2012.

Optical properties of self-assembled anisotropic plasmonic nanocomposites

C. Tallet[1], K. Ehrhardt[1], J. Vieaud[1, 2], Z. Zheng[1], O. Merchiers[1], P. Barois[1], Y. Borensztein[3], M. Warenghem[4], A. Aradian[1] and V. Ponsinet[1*]

[1] Centre de Recherche Paul Pascal, Univ. Bordeaux and CNRS, UPR 8541, 115 avenue Schweitzer, 33600 Pessac, France

[2] Research Center for Materials Nanoarchitectonics (MANA) - National Institute for Materials Science (NIMS), 1-1 Namiki, Tsukuba, Ibaraki 305-0044, Japan

[3] Institut des NanoSciences de Paris, CNRS and UPMC Univ. Paris 6, UMR 7588, 4 place Jussieu, 75252 Paris Cedex 05, France

[4] Unité de Catalyse et de Chimie du Solide (UCCS Artois), Université d'Artois and CNRS, UMR 8181, 62307 Lens cedex; France

[*]corresponding author: ponsinet@crpp-bordeaux.cnrs.fr

Abstract- We study the relation between structure and optical properties in self-assembled lamellar plasmonic nanocomposites. The nanocomposites are produced by the assembly of plasmonic nanoparticles templated by ordered matrices of block copolymers and have a periodic lamellar structure of period between 50 and 100 nm. Their structure is studied by X-ray scattering and electron microscopy. Their optical properties are determined by spectroscopic ellipsometry and analyzed by appropriately developed effective medium models. Possible applications in metamaterials are discussed.

Novel optical properties in the visible range are foreseen when organizing nanoresonators[1], which can be performed by template-assisted self-assembly of plasmonic nanoparticles. In this presentation, we will describe the preparation and study of thin films of nanocomposites of polymers and gold nanoparticles. We will relate the structure of the composite and in particular the nature, density and spatial organization of the gold nanoparticles, with their optical index, as determined by spectroscopic ellipsometry using appropriately developed analysis methodologies.

We first study the optical response of gold nanoparticles deposited as a monolayer on top of a polymer layer above a silicon wafer (cf. Fig. 1), and show that the absorption cross-section of the particles are enhanced when the polymer spacer between the particles and the high index substrate is thin.

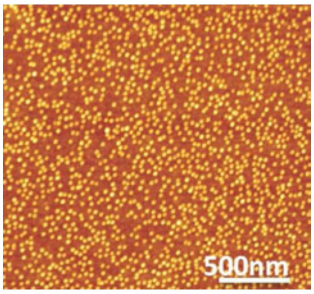

Figure 1: Atomic force microscopy image (top view) of a monolayer of gold nanoparticles of diameter 14nm, deposited on top of a polymer layer above a silicon wafer. The mean density is 330 nanoparticles per µm^2.

In a second step, we show that the optical properties of disordered nanocomposites of gold particles dispersed in a polymer matrix can be satisfactorily described by an effective medium model modified from the Maxwell-Garnett law in order to take into account some disordered couplings between neighboring nanoparticles. Moreover, such nanocomposites present, in the concentrated regime, a negative dielectric permittivity in a spectral range close to the plasmon resonance of the nanoparticles, as is illustrated on the. Fig. 2.

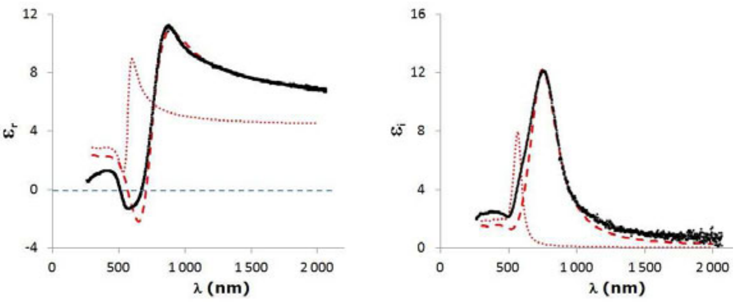

Figure 2: Real ε_r and imaginary ε_i parts of the dielectric permittivity of a composite film (thickness 50 nm) of polymer and gold nanoparticles (volume fraction 25%), extracted from the spectroscopic ellipsometry data. Comparison with a simple Maxwell-Garnett model (dotted red line), and a modified model (dashed red line) accounting for some degree of plasmonic coupling between nanoparticles.

Several methodologies[2,3,4] allows to use self-assembled templating matrices of block copolymers to organize nanoparticles. We thus produce ordered gold/polymer nanocomposites with long-range lamellar order and characteristic sizes between 50 and 100nm. The structural study of the nanocomposite films performed by X-ray reflectivity, atomic force microscopy and transmission electron microscopy provides a full description of the aligned lamellar structure, consisting of alternating layers of pure polymer and layers of polymer/gold nanoparticle composite (cf. Fig. 3). Using the methodology developed for the disordered nanocomposites, we analyze the spectroscopic ellipsometry measurements performed on the layered systems in terms of anisotropic plasmonic properties of these materials. This allows to discuss their potential interest in the fields of metamaterials applications.

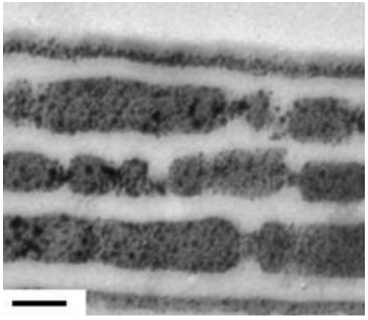

Figure 3: Transmission electron micrograph (side view) of a thin lamellar nanocomposite film. Bar = 100nm.

Acknowledgements: We acknowledge the support of the Région Aquitaine, the French Agence Nationale de la Recherche (ANR-09-NANO-003), the European Union's 7th Framework Program (FP7/2008) under grant agreement n° 228762 (METACHEM).

REFERENCES

1. Ponsinet, V., A. Aradian, P. Barois, and S. Ravaine, *Self-assembled and nanochemistry techniques for the fabrication of metamaterials*, in Metamaterials Handbook, F. Capolino, Ed., CRC Press, 2009
2. Chiu, J. J., J. K. Bumjoon, E. J. Kramer and D. J. Pine “Control of Nanoparticle Location in Block Copolymers”, *J. Am. Chem. Soc.*, Vol. 127, 5036-5037, 2005.
3. Maxit, B., D. Bendejacq and V. Ponsinet, "Facile formulation of high density well-ordered nanoparticle–copolymer nanocomposites", *Soft Matter*, Vol.8, 1317-1320, 2012.
4. Sohn, B. H. and B. H. Seo, "Fabrication of the Multilayered Nanostructure of Alternating Polymers and Gold Nanoparticles with Thin Films of Self-Assembling Diblock Copolymers", *Chem. Mater.*, Vol. 13, 1752–1757, 2001.

Plasmonics for Solid State Lighting

Jaime Gómez Rivas

FOM Institute for Atomic and Molecular Physics AMOLF, c/o Philips Research, High Tech Campus 4, Eindhoven, The Netherlands

During recent years, developments in light emitting materials have opened the door for white-light LEDs, in which several wavelengths are combined to mimic the solar spectrum. The most extended route to achieve white-light emitting LEDs consists in using a material, the so-called phosphor, which absorbs a fraction of the light emitted by a blue LED and re-emits at a longer wavelength. The mixing of the non-absorbed blue light with the emission of the phosphor provides a white spectrum. In order to develop efficient light sources based on LEDs, research efforts have mainly focused on both improving the intrinsic quantum efficiency (QE) and the stability of light emitters,[i] and on light extraction mechanisms.[ii] We have recently demonstrated that metallic nanoparticles can significantly improve the performance of highly efficient dyes employed in SSL by measuring up to a 60-fold enhancement of the emission in certain directions.[iii] Specifically, we made use of square arrays of nanoparticles that sustain localized surface plasmon polaritons. These localized resonances couple with each other through diffracted orders in the periodic array, leading to collective plasmonic modes. The collective resonances are responsible for large field enhancements that extend into the surroundings of the particles, where the phosphor is located, shaping the spectrum of the emitted light and beaming most of this emission into very small solid angles.

---

[i]. S. Reineke, F. Lindner, G. Schwartz, N. Seidler, K. Walzer, B. Lussem, & K. Leo, *Nature* **459**, 234 (2009)
[ii]. J. J. Wierer, A. David & M. M. Megens, *Nat. Photon*. **3**, 163-169 (2009)
[iii]. G. Lozano, D.J. Louwers, S.R.K. Rodríguez, S. Murai, O.T.A. Jansen, M.A. Verschuuren & J. Gómez Rivas. Light: Science & Applications (in press).

3D laser-made nanostructures

Maria Farsari
IESL-FORTH, N. Plastira 100, 70013, Heraklion, Crete, Greece

*corresponding author: mfarsari@iesl.forth.gr

Abstract- We present our most recent work on Direct fs Laser Writing and its applications in Photonics, Metamaterials and Biomedicine.

We present a new method for increasing the resolution of direct fs laser writing by multiphoton polymerization, based on quencher diffusion. This method relies on the combination of a mobile quenching molecule with a slow laser scanning speed, allowing the diffusion of the quencher in the scanned area and the depletion of the multi-photon generated radicals. We use this method to fabricate dielectric, metallic and quantum-dot doped photonic crystals and we show that the results are comparable to those produced by direct laser writing based on stimulated-emission-depletion microscopy, the method considered today as state-of-the-art in 3D structure fabrication. We model the quencher diffusion and we show that radical inhibition is responsible for the increased resolution. Finally, we discuss applications of Direct fs Laser Writing in photonics[1], metamaterials [2,3] (Fig.1a,b), biomedical implants [4,5], and 3D models (Fig. 1c).

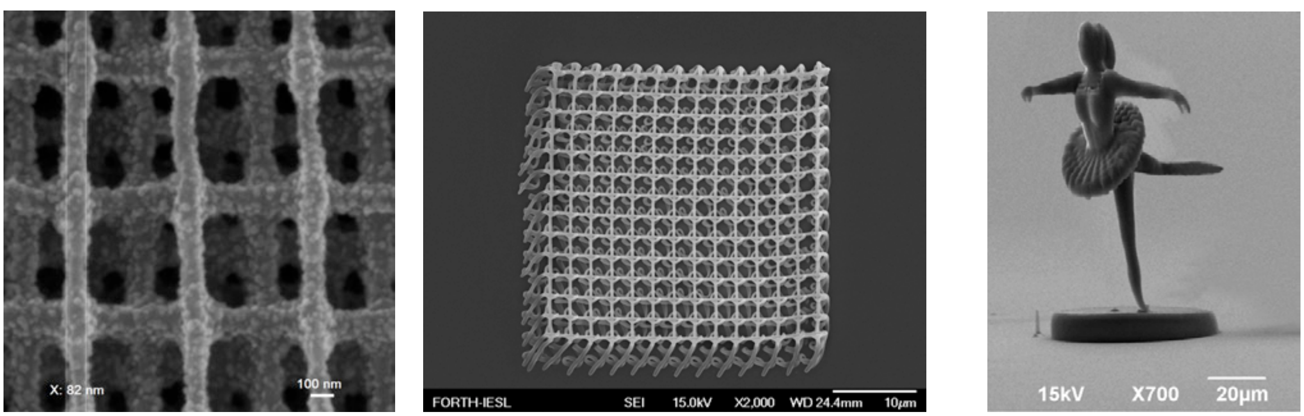

(a) (b) (c)

Fig. 1: (a) A metallic photonic crystal with optical bandgaps. (b) A spiral photonic crystal. (c) A micro-dancer

Acknowledgements, This work was partly funded by the EOARD Grant 113090 and by the GSRT grant Heraklitos

References

1 Sakellari, I. *et al.* Diffusion-Assisted High Resolution Direct Femtosecond Laser Writing. *ACS Nano* **6**, 2302-2311 (2012).

2 Terzaki, K. *et al.* 3D Conducting Nanostructures Fabricated Using Direct Laser Writing. *Opt. Mater.*

Expr. **1**, 586-597 (2011).
3 Vasilantonakis, N. *et al.* Three-Dimensional Metallic Photonic Crystals with Optical Bandgaps. *Adv. Mater.* **24**, 1101-1105 (2012).
4 Melissinaki, V. *et al.* Direct laser writing of 3D scaffolds for neural tissue engineering applications. *Biofabrication* **3**, 045005 (2011).
5 Turunen, S. *et al.* Pico- and femtosecond laser-induced crosslinking of protein microstructures: evaluation of processability and bioactivity *Biofabrication* **3**, 045002 (2011).

Oriented Assembly of Polyhedral Plasmonic Nanoparticle Clusters

J. Henzie[1,2*] **and Peidong Yang**[2]

[1]National Institute for Materials Science (NIMS), WPI-MANA, Tsukuba, Ibaraki 305-0044, JAPAN

[2]Department of Chemistry, University of California, Berkeley, CA 94720, USA

[*]corresponding author: HENZIE.Joeladam@nims.go.jp

Abstract-Shaped colloids can be used as nanoscale building blocks for the construction of plasmonic metamaterials that are completely assembled from the bottom up. I will describe how the shape, orientation and connectivity of polyhedral particles are controlled with nanoscale precision, reproducibly generating a range of nanoparticle clusters that strongly couple to light. Strikingly, electron microscopy shows that during self-assembly, these atomically smooth Ag polyhedra generate large, uniform nanoscale gaps that exhibit strong EM field enhancements that dominate their optical properties.

Si-nanorod-based plasmonic metamaterials: modeling, fabrication, and characterization

S. Peruch, J.S. Bouillard , D. O'Connor, W. Dickson, G. Wurtz, and A. Zayats*
Nano Optics and Near-field spectroscopy Group, Department of Physics, King's College London, Strand WC2R 2LS, London, United Kingdom

X. Han, and T. Akalin
IEMN CNRS UMR 8520, Lille 1 University, Lille, France

[*]corresponding author: a.zayats@kcl.ac.uk

Silicon is characterized by a high refractive index and a low intrinsic absorption at NIR wavelengths, two features that make it ideal for photon concentration, guiding, and detection. Moreover, light emission from Si and Si-compatible materials can be enhanced, leading to the possibility of using Si-based devices for optical amplification. Since the radiative rates for absorption and emission of light in Si remain well below those of direct gap semiconductors, plasmonic effects can be used to modify its absorption cross-section, radiative decay rate, and quantum efficiency, due to the high local electromagnetic fields produced. In addition, the reduced surface plasmon wavelength can enable high quality factor microcavities that confine light well below the diffraction limit. Combined, these plasmonic effects have enabled novel devices for on-chip nonlinear optics, quantum optics, and lasing.

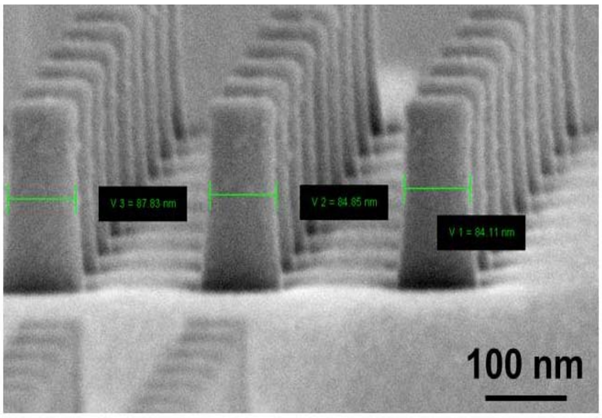

Figure: Au-coated Si nanorod assemblies.

Plasmonic metamaterials based on assemblies of metallic nanoparticles (MNPs) offer promising avenues to design nanodevices. They provide finely tunable optical properties, which can be tailored for different applications, from sensing to waveguiding [1], [2]. When arranged as an array of aligned particles, a new spectrum of delocalized modes arises [3]. Coated nanorods open up an even greater range of applications, exhibiting cavity mode resonances whose wavelengths depend on the shell to diameter thickness ratio. Here we investigate the optical properties of several Si-based plasmonic structures, including cavities and waveguides using both model calculations and experimental results.

References:

[1] J. McPhillips, A. Murphy, W. R. Hendren, R. Atkinson, A. V. Zayats, R. Pollard, M. P. Jonsson and F. Hook, *Acs. Nano* **4,** 2210 (2010).
[2] A. V. Kabashin, P. Evans, S. Pastkovsky, W. Hendren, G. A. Wurtz, R. Atkinson, R. Pollard, V. A. Podolsky and A. V. Zayats, *Nat. Mater*.**8**, 867 (2009).
[3] G. A. Wurtz, W. Dickson, D. O'Connor, R. Atkinson, W. Hendren, P. Evans, R. Pollard and A. V. Zayats, *Opt. Express* **16,** 7460 (2008).

NanoParticle Direct Doping: Novel method for manufacturing three-dimensional bulk plasmonic nanocomposites

Marcin Gajc*, **Katarzyna Sadecka, Andrzej Kłos, Barbara Surma, Dorota A. Pawlak***
Institute of Electronic Materials Technology (ITME)
133 Wolczynska Str, 01-919 Warsaw, Poland
*corresponding author: Marcin.Gajc@itme.edu.pl; Dorota.Pawlak@itme.edu.pl

Abstract- Metallodielectric materials with plasmonic resonances at optical and infrared wavelengths are attracting interest, due to their potential novel applications in photonics, plasmonics and photovoltaics. However, simple and fast fabrication methods for volumetric plasmonic nanocomposites that offer control over the size, shape and chemical composition of the plasmonic elements have been missing. Here, we present such a manufacturing method with experimental realisations of volumetric nanocomposites doped with plasmonic nanoparticles that exhibit resonances at VIS/IR wavelengths.

Nanocomposites of metallic/semiconducting nanoparticles embedded in dielectric matrix with resonances at optical and NIR wavelengths have been the subject of increasing interest due to their prospective exploitation for photonic/plasmonic applications [1-9]. Despite major developments, the fabrication of volumetric nanoplasmonic composites remains a challenge. There are several chemical (indirect) methods of manufacturing such composites based on doping dielectric glasses with metallic nanoparticles. However, such aspects as: (i) homogeneity of the obtained materials, (ii) doping with non-metallic nanoparticles (lower losses than metallic at some resonant frequencies [10]), and (iii) doping with anisotropic particles, are at the very beginning of development.

Here we demonstrate a fast, low-cost, bottom-up method for manufacturing nanoplasmonic composites - NanoParticle Direct Doping (NPDD) (see Fig. 1) [11]. This method is based on the direct doping of dielectric matrices with plasmonic nanoparticles and enables the fabrication of volumetric three-dimensional materials through a non-chemical process.

This relatively simple method enables:
(i) self-dispersion of the nanoparticle agglomerates;
(ii) manufacturing of nanoplasmonic materials doped with metallic and/or non-metallic particles;
(iii) control of the nanoelements size and shape;
(iv) co-doping with other chemical agents, such as rare earth ions;
(v) manufacturing of materials in which the nanoparticles are protected mechanically and chemically by the matrix;
(vi) very versatile crystal growth strategies, readily transferable to other industrial technological fields.

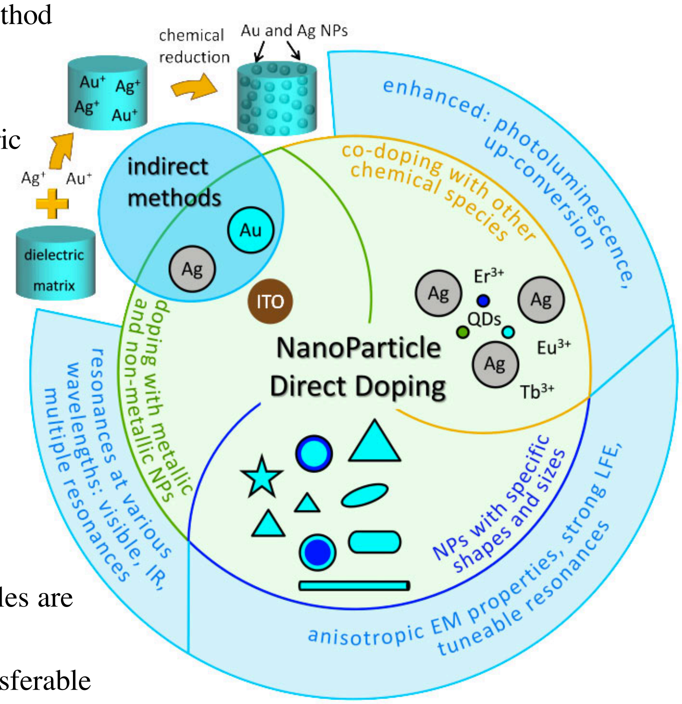

Fig 1. Comparison of the possibilities offered by indirect (chemical) methods of manufacturing dielectric matrices doped with nanoparticles with NanoParticle Direct Doping method (NPDD).

Figure 2 shows the NBP-glass rod doped by NPDD with 0.15 wt.% silver nanoparticles. Against a white background, the observer sees the rod as yellow in the transmitted light. When the rod is placed on a black background, however, light goes through the rod and is absorbed by the background—only scattered light reaches the observer. The material now appears blue. The observed colours originate from the LSPR of the silver nanoparticles, which occurs at a violet-blue wavelength.

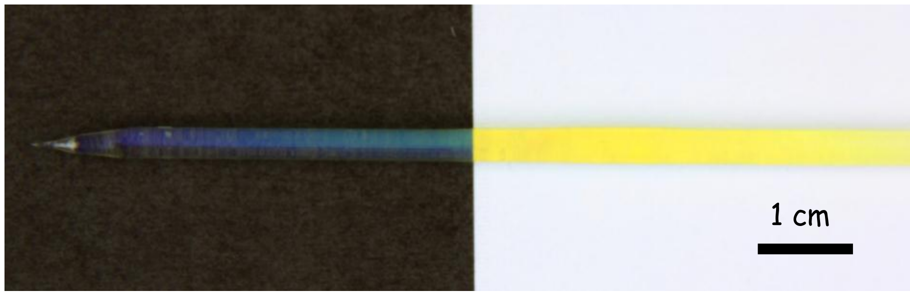

Fig. 2. NBP glass rod doped by NPDD with 0,15 wt. % Ag (20 nm, spherical) nanoparticles

Our approach may enable rapid and cost-efficient manufacturing of bulk nanoplasmonic composites with single or multiple resonances at various wavelength ranges. These composites could be isotropic or anisotropic, and potentially co-doped with other chemical agents, in order to enhance different optical processes such us photoluminescence.

References

[1] Maier, S. A. *Plasmonics: Fundamentals and Applications,* Centre for Photonics and Photonic Materials Department of Physics, University of Bath, UK, Springer, 2007.

[2] Atwater, H. A. & Polman, A. Plasmonics for improved photovoltaic devices. Nature Mater. 2010, 9, 205-213.

[3] Lal, S., Clare, S. E. & Halas, N. J. Nanoshell-Enabled Photothermal Cancer Therapy: Impending Clinical Impact. Accounts Chem. Res. 2008, 41, 1842-1851.

[4] Anker, J. N., Hall, W. P., Lyandres O., Sahah, N. C., Zhao, J. &. Van Duyne, R. P. Biosensing with plasmonic nanosensors. Nature Mater. 2008, 7, 442–453.

[5] Stockman, M. & Bergman, D. J. Surface plasmon amplification by stimulated emission of radiation: quantum generation of coherent surface plasmon in nanosystems. Phys. Rev. Lett. 2003, 90, 027402-1-4.

[6] O'Connor, D. & Zayats, A. V. Data storage: The third plasmonic revolution. Nature Mater. 2010, 5, 482-483.

[7] Hryciw, A., Jun, Y. Ch. & Brongersma M. Electrifying plasmonics on silicon. Nature Mater. 2010, 9, 3-4.

[8] Okamoto, K., Niki, I., Shvartser, A., Narukawa, Y., Mukai, T. & Scherer A. Surface-plasmon-enhanced light emitters based on InGaN quantum wells. Nature Mater. 2004, 3, 601-605.

[9] Henzie, J., Lee, M. H. & Odom, T. W. Multiscale Patterning of Plasmonic Metamaterials. Nature Nanotechn. 2007, 2, 549-554.

[10] Boltasseva, A., Atwater, H. A. Low-Loss Plasmonic Metamaterials, Science 2011, 331, 290-291

[11] Gajc, M., Surma, H. B., Klos, A., Sadecka, K., Orliśnski, K., Nikolaenko, A. E., Zdunek, K., Pawlak, D. A. NanoParticle Direct Doping: Novel method for manufacturing three-dimensional bulk plasmonic nanocomposites Adv. Funct. Mater., 2013, 10.1002/adfm.201203116

Effective optical properties of polymer-gold nanoparticle films: Theory and experiments

O. Merchiers[1], **J. Vieaud**[1], **K. Ehrhardt**[1], **M. Warenghem**[2], **Y. Borensztein**[3], **V. Ponsinet**[1] and **A. Aradian**[1]

[1] Centre de Recherche Paul Pascal - CNRS & Univ Bordeaux
[2] UCCS - Université d'Artois
[3] Institut des Nanosciences de Paris - Université Pierre et Marie Curie
aradian@crpp-bordeaux.cnrs.fr

Abstract— We study the effective optical properties of composite films made of spherical gold nanoparticle in a polymer matrix, both in dilute (5% gold fraction) and dense (20%) regimes. Even in the dilute regime, nanoagregation effects occur in the samples, which entail couplings between particles; we propose to take these into account in a simple way using a modified MG formula based on a distribution of ellipsoids. This modified Maxwell Garnett model allows for very good fits of the experimental data in the dilute regime, and rather satisfactory ones even in the dense regime.

Developments in designs over the past couple of years have brought the field of metamaterials into a stage where, besides usual lithography-based approaches, new "bottom-up" fabrication techniques based on nanochemistry and material science can now be effectively explored [1]. Expected benefits from bottom-up approaches include assembling true three-dimensional (3D) metamaterials or natively synthetizing resonators with sizes appropriate for the optical range. In the present work, we study the effective optical properties of composite materials made of spherical gold nanoparticles (GNP) randomly dispersed into a polymer host matrix. Such composite films, for high enough filling fractions, are expected to display an adjustable, near-zero or negative effective permittivity band around the particle plasmon resonance.

The composite material is made of a hydrosoluble polymer (poly-vinyl alcohol) embedding 14 nm spherical gold nanoparticles (GNPs). Films are made by spin-coating mixed dispersions of polymer and GNPs onto silicon wafers, so as to obtain dilute or dense films. The optical properties are measured from variable-angle spectroscopic ellipsometric measurements, and the permittivity of the film ε is extracted using a suitable ellipsometric model and a lambda-by-lambda numerical inversion procedure.

Experimental results are shown in Figure 1 for two typical samples in the dilute ($f \simeq 6\%$) and dense ($f \simeq 20\%$) regimes. In the dilute sample [Figure 1 (a) and (b)], the plasmonic resonance of the GNPs can be distinctly observed, but has a small amplitude. For the dense sample [Figure 1 (c) and (d)], the resonance has a much greater amplitude and the response displays a near-zero permittivity region in the short wavelength range which becomes negative around 600 nm with $\mathrm{Re}(\varepsilon)\big|_{\mathrm{min}} \simeq -2$. This is interesting behaviour, as it means that the composite has a hybrid macroscopic optical response: it responds like a metal over a finite frequency band, and like a dielectric elsewhere. Finally, we also note that both resonances have a significant linewidth, with more or less redshifted resonance wavelengths, denoting the presence of couplings between GNPs in the sample.

Trying to reproduce our experimental data with the help of the classical MG law [2] fails as shown on Fig. 1 (red lines). This is clearly due to the couplings taking place inside the samples, which are due to structural nanoagregation effects. As depicted schematically in Fig. 1 (e), in an empirical way, couplings between particles can be seen as deforming the initially isotropic polarizability of the nanospheres into ellipsoidal ones; this is a reflection of the local field distorsions induced by the couplings. Therefore, a simple-minded approach to improve the model is to introduce ellipsoidal polarizabilities in the MG model [5]: we take a distribution of ellipsoids to represent the variety of couplings at work (we choose a log-normal-like distribution), and we assume that the orientations of the coupling-induced ellipsoids are random.

We see in Fig. 1 (blue lines) that this modified MG model reproduces much better the experimental data. For the dilute sample, there are only two fitting parameter which are the global gold filling fraction f and the width of the log-normal ellipsoidal distribution; the ellipsoidal distribution is centered on the undisturbed, isotropic polarizability of the individual nanospheres. For the dense

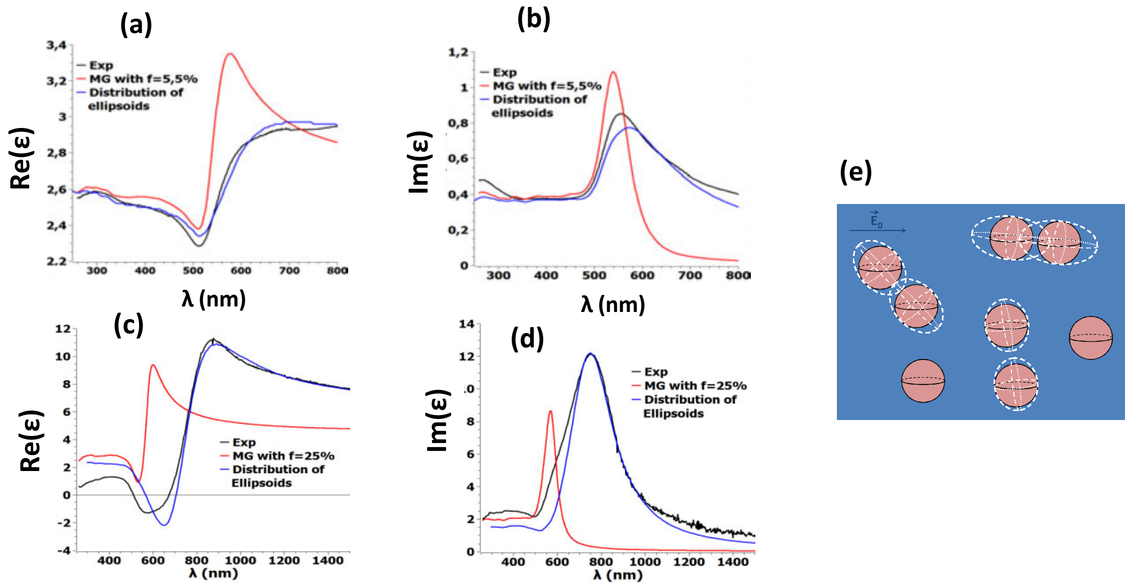

Figure 1: (a) and (b) Real and imaginary parts of the permittivity versus wavelength λ for a dilute sample with $f \simeq 6\%$. Black line: experiment; Red line: classical MG model; Blue line: modified MG with distribution of ellipsoidal polarizabilities. (c) and (d) Real and imaginary parts of the permittivity for a dense sample with $f \simeq 20\%$. Black line: experiment; Red line: classical MG model; Blue line: modified MG with distribution of ellipsoidal polarizabilities. (e) Ellipsoidal polarizabilities as empirical representations of electromagnetic couplings between neighbouring particles.

samples, because couplings are much stronger, it is necessary to center the ellipsoidal distribution on a mean ellipsoidal polarizability, reflecting the fact that no particle is free from coupling, even in average. The proper mean ellipsoid is first found by adjusting its resonance frequency on the observed experimental resonance, then an ellipsoidal distribution is taken around this mean ellipsoid, and the distribution width is adjusted for the theoretical curve to fit the experimental curve. Hence, for the dense samples, there are four free parameters: the total gold filling fraction f, the two depolarization factors of the mean ellipsoid, and the width of the distribution.

ACKNOWLEDGMENT

The support of the Région Aquitaine, the Délégation Générale de l'Armement, the Agence Nationale de la Recherche (Nanodiellipso project Anr-09-Nano-003) and the European FP7-NMP-2008 program under the Metachem project (grant agreement Nr. 228762) is acknowledged.

REFERENCES

1. V. Ponsinet, A. Aradian, P. Barois and S. Ravaine, Self-assembly and nanochemistry techniques towards the fabrication of metamaterials, in *Handbook of metamaterial,* vol. 2, F. Capolino Ed., Boca Raton, USA: CRC Press, 2009.
2. A. Sihvola, *Electromagnetic mixing formulas and applications,* London, United Kingdom: The Institution of Electrical Engineers, 1999.
3. P.B. Johnson and R.W. Christy, Optical constants of the noble metals, *Phys. Rev. B,* Vol. 6, p. 4370, 1972.
4. E.A. Coronado and G.C. Schatz, Surface plasmon broadening for arbitrary shape nanoparticles: A geometrical probability approach , *J. Chem. Phys.,* Vol. 119, p. 3926, 2003.
5. G. Bohren and D. Huffman, *Absorption and Scattering of Light by Small Particles*, New York, USA: John Wiley and Sons, 1983.

Genetic Algorithm Design and Holographic Fabrication of 3D Photonic Crystals and Optical Metamaterials

P. V. Braun[1*]
[1]Department of Materials Science and Engineering, University of Illinois at Urbana-Champaign, 1304 West Green Street, Urbana, IL 61801, USA
[*]corresponding author: pbraun@illinois.edu

Abstract-We have developed a genetic algorithm method for designing the diffractive optics used in phase mask lithography and performed exposures through this phase mask to realize various complex 3D structures, include helices. The structures were converted to both high refractive index materials and metallic materials through various materials replacement and infilling strategies.

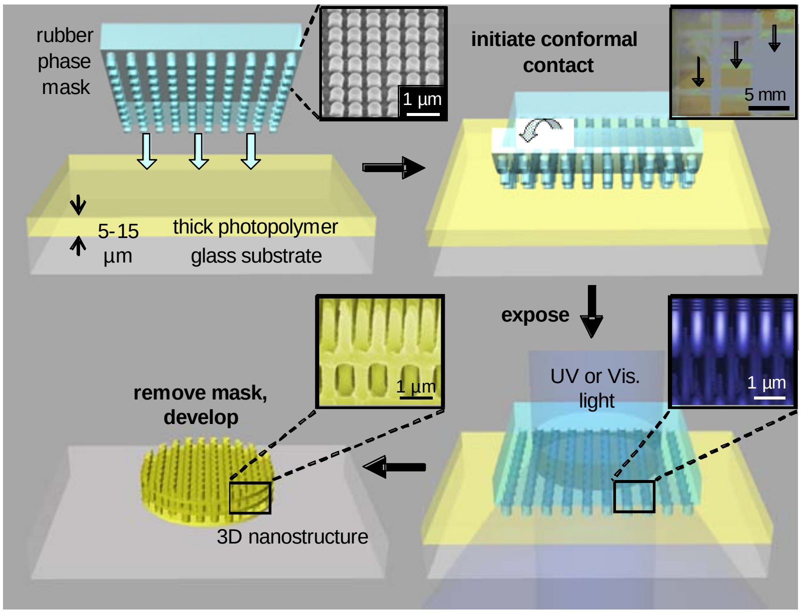

Fig. 1. PnP process whereby the 3-D spatially varying intensity distribution created by an elastomeric phase mask is replicated by a photopolymer.

Using a method that we refer to as Proximity field NanoPatterning (PnP), we demonstrated the use of elastomeric binary diffractive phase masks to form 3-D holographic micro- and nano-structures in photosensitive polymers (Fig. 1).[1] Light passing through the phase mask creates a three dimensional distribution of intensity in the photosensitive layer through its thickness, which can be developed yielding a 3-D replica of the intensity distribution. Design of a manufacturable phase mask for a given resultant 3-D structure, for example one that exhibits a complete 3-D photonic band gap, is complicated, and difficult to directly calculate. Using a genetic algorithm (GA) based phase mask approach that makes directly possible the design of phase masks for nearly arbitrary 3-D structures.[2] First, the surface relief profile and the incident polarization are encoded into a binary representation called a “chromosome”. Then, a random population of these chromosomes is generated and each chromosome is assigned a “fitness” score. Here, fitness quantifies how closely a given chromosome produces the desired target structure. Chromosomes having superior fitness are selected to “reproduce” and “mutate” with greater frequency, providing the necessary driving force toward improved phase mask designs over several generations. Importantly, the manufacturability of the phase mask can be included as part of the fitness factor. The optical response of the resulting structure can also be used as part of the fitness factor, with the only complication the time required to simulate the optical properties of every structure which at least to date has limited this approach to simple dielectric structures.

To date, two different structures using the GA design approach have been targeted: rod-connected diamond (fcc) and spiral (hexagonal). Several different designs have been generated, two of which are shown in Fig. 2. Both of the resultant structures match the target structure to better than 90%. The phase mask design generated using the GA is applied as follows. First, a film of polymethylmethacrylate (PMMA) is patterned using e-beam lithography, forming a "master" (Fig. 3a). The master, which contains the desired surface relief profile, is then used to fabricate a conformable polydimethylsiloxane (PDMS) mold (Fig. 3b). This mold is then applied to a film of SU-8 photoresist softened with a drop of ethanol. After the ethanol evaporates, the PDMS mold is removed, leaving behind the desired relief pattern embossed into the resist surface (Fig. 3c). Next, a layer of TiO2 is evaporated onto the patterned SU-8 (Fig. 3d). TiO2 has a higher refractive index than SU-8 increasing the phase mask diffraction efficiency (for some designs, the TiO2 layer is not necessary). Finally, the surface patterned SU-8 is exposed via a two-photon process using a 800 nm pulsed laser and developed, yielding the structure shown in Fig. 3e using the prescribed polarization and dose. Note the excellent match of experiment and theory.

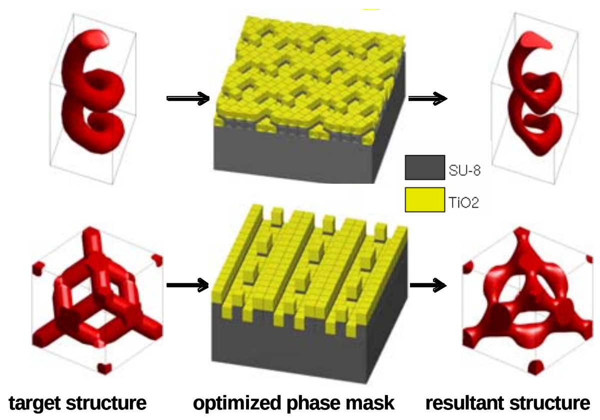

Figure 2. GA based phase mask design processs. Simulation indicates these designs produce high quality replicas (right column) of the target structures.

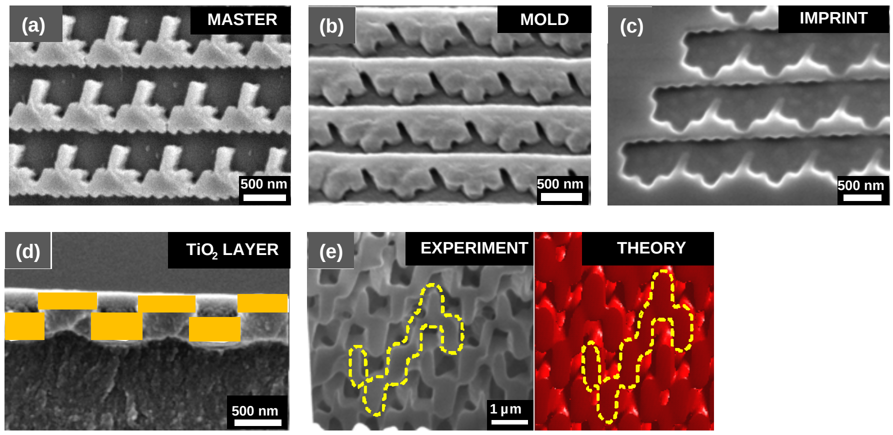

Fig. 3. Fabrication steps for producing holographic phase mask structures. a) GA designed pattern master is made by e-beam patterning a film of PMMA. b) Master is used to generate a flexible PDMS mold. c) PDMS mold stamps the desired pattern into a film of SU-8. d) Film of TiO_2 (yellow) is evaporated onto the patterned SU-8. e) The patterned film is exposed and developed. Note the excellent agreement of experiment and theory. The dotted yellow line is used to guide the eye. Figures a) – c) are top views, and d), e) are cross-sectional views.

REFERENCES

1. S. Jeon, J.-U. Park, R. Cirelli, S. Yang, C. E. Heitzman, P. V. Braun, P. J. A. Kenis, J. A. Rogers, Proceedings of the National Academy of Sciences 101, 12428-12433 (2004).
2. 2 J. W. Rinne, P. Wiltzius, Optics Express 14, 9909-9916 (2006).

Optical Chirality in Self-Assembled Nanoplasmonic Metamaterials

S. S. Oh[1], A. Demetriadou[1], S. Wuestner[1] and O. Hess[1*]
[1]The Blackett Laboratory, Department of Physics, Imperial College London, SW7 2AZ, United Kingdom
[*]corresponding author: o.hess@imperial.ac.uk

Abstract-Metamaterials with chiral geometry at the nanometer scale, fabricated using a recently demonstrated self-assembly technique, may enable a new way of achieving strong chirality at optical wavelengths. On the basis of our tri-helical metamaterial model, we theoretically predict the band structure and plasma frequency of the single gyroid metamaterial.

Chirality in a resonant medium can lead to negative refraction for one circular polarization [1]. Although strong chirality was demonstrated in several chiral metamaterials, such as Swiss Rolls [2] and gammadion structures [3], the unique property of artificial chirality has for some time been limited to terahertz and even lower frequencies due to the complexity of top-down fabrication of chiral geometries. Recent advances in self-assembly techniques now allow for the fabrication of chiral plasmonic structures at the nanometer scale with a view towards optical wavelength applications. The most notable example is the nanoplasmonic gyroid [4,5], which is composed of several helices oriented along multiple directions and connected to each other. To clarify the origin of the chiral behaviour of nanoplasmonic single gyroid (SG) metamaterials, we have developed an analytical model for a tri-helical metamaterial (THM), (i.e. three helices aligned with the three orthogonal axes) [6]. The THM model gives valuable insight into the physics of chiral metamaterials from microwave to the visible regime.

Here, we explain the physical mechanisms underlying the nanoplasmonic gyroid's chiral behaviour at optical wavelengths on the basis of the THM model, supporting our conclusions with numerical simulation results for the SG. In addition, using simulation results for a gold gyroid approximated by the Drude model, we show the impact of realistic metals on the propagation of EM waves in the SG and fully characterize the SG's electromagnetic and chiral behaviour.

In a single gyroid, there are two types of helices with different radii [7]. The smaller helices determine the optical properties close to the cut-off frequency. This cut-off frequency originates from the continuous nature of the metallic helices and is called plasma frequency, ω_p. Propagation in the gyroid is prohibited for frequencies below the plasma frequency, leading to high reflection. Conversely, there are three propagating modes just above the plasma frequency which are highly localized around the smaller helices. As a result, the plasma frequency is determined by the geometric parameters of the smaller helices and is given by the following equation derived using the THM model applied to optical wavelengths [8,9].

$$\omega_p^2 \approx \frac{c_0^2 4\pi^2}{a^2 c_1^2}\left(\frac{1}{\varepsilon_{Au} f c_2} + \frac{c_3}{n^2\left[c_4\sqrt{f} - \sqrt{c_5 + c_6 \ln\left(c_7/\sqrt{f}\right)}\right]^2}\right)$$

where a, f, c_1-c_7 are the lattice constant and filling fraction of SG and geometrical constants. ε_{Au} and n are the permittivity of gold and refractive index of the surrounding medium [6,9].

In Fig. 1a, band structures for single gyroid with different filling fractions are shown. The three propagating modes just above the plasma frequency are indentified as doubly degenerate transverse modes and one longitudinal mode. Above these propagating modes, there is a frequency region with high mode density due to localized plasmonic modes in the SG. This flat band region, which corresponds to wavelengths shorter than 570nm, shows very strong absorption due to its plasmonic nature. In Fig 1b, analytical plasma wavelengths are compared with the numerically retrieved plasma edge wavelengths for different filling fractions and show very good agreement.

The work presented here provides a good understanding of light propagation in gyroids at optical frequencies as well as a useful tool in estimating the plasma frequency in nanoplasmonic chiral structures.

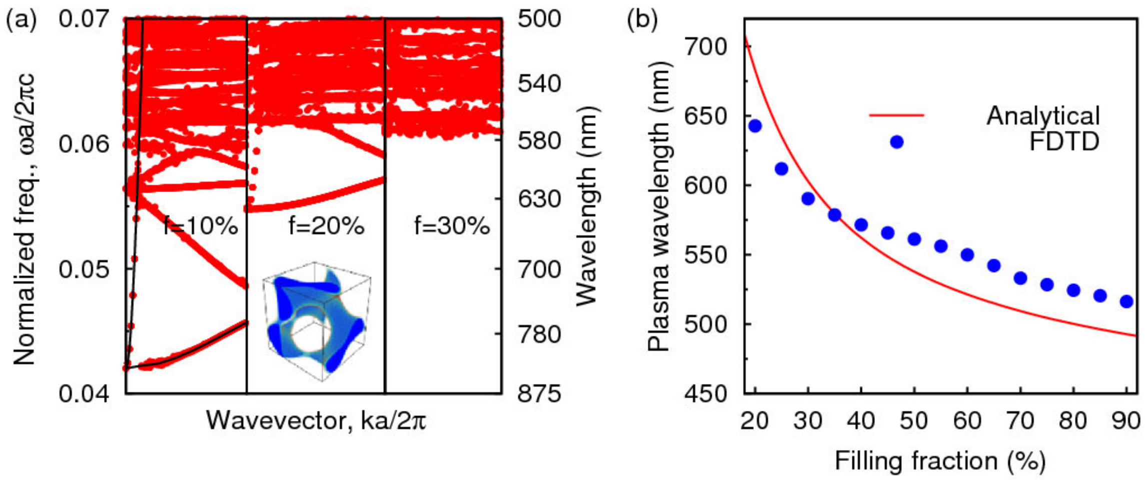

Figure 1: Filling fraction change of the Au SG. (a) Band structures with transverse (1st band) and longitudinal (2nd band) modes. (Inset) unit cell of the SG. (b) Plasma wavelengths for different filling fractions.

Acknowledgements, Support by the Leverhulme Trust and the EPSRC is gratefully acknowledged.

REFERENCES

1. Pendry, J. B. "A chiral route to negative refraction," *Science*, Vol. 306, 1353, 2004.
2. Demetriadou, A. and J. B. Pendry, "Extreme chirality in swiss roll metamaterials," *J. Phys.: Condens. Matter*, Vol. 21, 376003, 2009.
3. Zhao, R., *et al.*, "Conjugated gammadion chiral metamaterial with uniaxial optical activity and negative refractive index," *Phys. Rev. B.*, Vol. 83, 035105, 2011.
4. Vignolini, S., *et al.,* "A 3D optical metamaterial made by self-assembly," *Adv. Mater.*, Vol. 24, OP23, 2011.
5. Salvatore, S., A. Demetriadou, S.Vignolini, S. S.Oh, S.Wuestner, N. Yufa, M. Stefik, U. Wiesner, J. Baumberg, O. Hess, and U. Steiner, "Tunable 3D-Extended Self-Assembled Gold Metamaterials with Enhanced Light Transmission," *Submitted*.
6. Demetriadou, A., S. S. Oh, S. Wuestner and O. Hess, "A tri-helical model for nanoplasmonic gyroid metamaterials," *New J. Phys.*, Vol. 14, 083032, 2012.
7. Oh, S. S., A. Demetriadou, S. Wuestner and O. Hess, "On the origin of chirality in nanoplasmonic gyroid metamaterials," *Adv. Mater.*, doi: 10.1002/adma.201202788
8. Novotny, L. "Effective Wavelength Scaling for Optical Antennas," *Phys. Rev. Lett.,* Vol. 98, 266802, 2007.
9. Demetriadou, A. and O. Hess, "Analytical theory of optical nano-plasmonic metamaterials," *Submitted.*

Plasmonic super-radiance and collective resonance state at the loss compensation condition near metal nanoparticle

V. Pustovit*[1], A. Chipouline [2] and A. M. Urbas[1]

[1]Materials and Manufacturing Directorate, Air Force Research Laboratory, Wright Patterson Air Force Base, Ohio 45433, United States

[2] Institute of Applied Physics, Friedrich Schiller University Jena, Max-Wien-Platz 1, D-07743 Jena, Germany

[*]corresponding author: pustovit@icnanotox.org

Abstract- We here present the first unified theory of the response of plasmonic nanoshells assisted by optical gain media. We identify mechanism of plasmonic super-radiance of the aggregate similar to conventional Dicke effect with reduced intraband relaxation bandwidth due to the loss compensation in the system. We demonstrate that mechanism of the total loss compensation leads to the laser resonator type collective resonance state that could cause a stimulated radiative emission.

Radiation of a dipole near a metal nanostructure supporting a surface plasmon (SP) is attracting renewed interest due to possible biosensing and metamaterials applications [1]. While early studies mainly focused on fluorescence of molecules near rough metal films, recent advances in near-field optics and in chemical control of molecule-nanostructure complexes spurred a number of experiments on single metal nanoparticles (NPs) linked to dye molecules or semiconductor quantum dots [2]. Emission of a photon by a dipole-NP complex involves two competing cooperative processes: enhancement due to resonance energy transfer (RET) from an excited dipole to the SP and quenching due to energy exchange with optically inactive excitations in the metal. These decay channels are characterized by radiative and nonradiative decay rates, respectively, and their balance is determined by the separation **d** of the emitter from the metal surface. The primary mechanism of cooperative emission is resonant energy transfer between emitters and plasmons rather than Dicke radiative coupling between emitters. The emission is dominated by three superradiant states with the same quantum yield as a single emitter, leading to a drastic reduction of ensemble radiated energy down to just thrice of that by a single emitter, the remaining energy being dissipated in the metal through subradiant states [3-4]. We establish a complete description of the optical response of the system based on Green's functions, which allows us to investigate high molecular coverage of metal nanoparticle with either regular or random distribution of dye molecules, taking into account not only the interactions between NP (treated in a multipolar approach) and dye dipoles, but also between dyes molecules, either directly or via the nanoparticle. Then we obtain the interaction Hamiltonian of the core-shell aggregate that composed from the direct response from the nanoparticle and the contribution rising from the energy transfer mechanism. We show that applied total loss compensation conditions lead to appearance of collective resonance state similar to the laser resonator with ability to induce stimulated emission.

REFERENCE

1. Lakowicz J.R., *Principles of Fluorescence Spectroscopy,* Plenum, 1999.
2. Dulkeith E., Ringler M., Klar T. A. and Feldmann J.., "Gold Nanoparticles Quench Fluorescence by Phase Induced Radiative Rate Suppression", *Nano Lett.* 5, 585-589 , 2005.
3. Pustovit V.N. and Shahbazyan T. V., "Plasmon-mediated superradiance near metal nanostructures", *Phys.Rev.* B 82, 075429, 2010
4. Pustovit V.N. and Shahbazyan T. V., "Resonance energy transfer near metal nanostructures mediated by surface plasmons", *Phys. Rev B*, 83, 085427, 2011.

Polaritonic materials for THz metamaterials

M. Kafesaki[1,2]**, A. Basharin**[1]**, A. Reyes-Coronado**[1]**, E. N. Economou**[1,] **C. M. Soukoulis**[1,3]
[1]Institute of Electronic Structure and Laser, Foundation for Research and Technology, Hellas (FORTH), P.O. Box 1385, Heraklion, Crete, Greece
[2]Department of Materials Science and Technology, University of Crete, Greece
[3]Ames Lab and Dept of Physics and Astronomy, Iowa State University, Ames, IA, USA
*corresponding author: kafesaki@iesl.forth.gr

Abstract-We present a variety of phenomena and possibilities that can be realized in metamaterials based on polaritonic materials. Such phenomena include hyperlensing, subwavelength resolution imaging based on backward propagation, and subwavelength guiding and propagation based on epsilon-near-zero response.

Polaritonic materials are becoming recently a more and more valuable component of THz metamaterials. This is due the rich electromagnetic response of those materials, which includes regions of very high permittivity, of negative permittivity and of permittivity near zero. This rich permittivity response, which is a result of the phonon-polariton resonance that polaritonic materials exhibit in the THz regime, allows a variety of metamaterial-based properties and capabilities in structures made of polaritonic materials. In this talk we will present some of those properties and capabilities, which include hyperbolic dispersion relation, backward radiation, total transmission or reflection and subwavelength guiding and collimation. The systems that we employ to demonstrate those properties are two-dimensional periodic alkali-halide systems made of LiF rods in KCl or in NaCl. Such systems can be easily fabricated in subwavelength scale by employing a self-organization approach of eutectic mixtures.

The negative permittivity response of a polaritonic material, if the material is structured in the form of a two-dimensional periodic system of sub-wavelength-scale rods, it can lead to an anisotropic effective permittivity tensor of both negative and positive components, and thus to hyperbolic dispersion relation. Hyperbolic dispersion relation is well-known to offer subwavelength-resolution imaging, known as hyperlensing, as well as possibility of large absorption, suitable for thermophotovoltaic applications. Here we demonstrate subwavelength resolution imaging due to hyperbolic dispersion relation in 2D periodic systems of LiF rods (of micrometer scale) in NaCl. Such systems have been fabricated using eutectics directional solidification and have been characterized by FTIR and THz time domain spectroscopy. The characterization results, in very good agreement with corresponding simulation data, confirm hyperbolic dispersion relation response in the frequency regime 9-11 THz. Demonstration of subwavelength propagation and imaging due to hyperbolic dispersion is shown in Fig. 1.

Another interesting effect that can be observed in negative electrical permittivity materials is backwards propagation and radiation in waveguides made by such materials if the permittivity of the material has small negative values. This backwards radiation can be exploited to give beams of subwavelength confinement and collimation in a system of parallel cylindrical waveguides, as is demonstrated in Fig. 2 for a system of LiF rods (material of small negative permittivity) in KCl host.

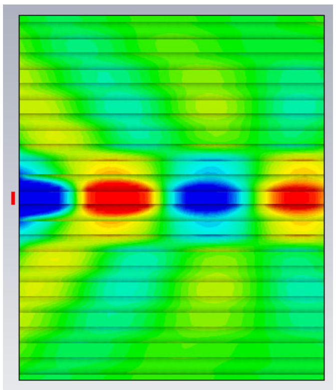

Figure 1. Subwavelength propagation (λ/4) of a TM wave emitted by a point source (left-side) through a polaritonic material of LiF circular rods in NaCl, in hexagonal lattice. Rod radius and lattice constant are few μm. The wave has frequency ~10 THz, where the system shows hyperbolic dispersion relation

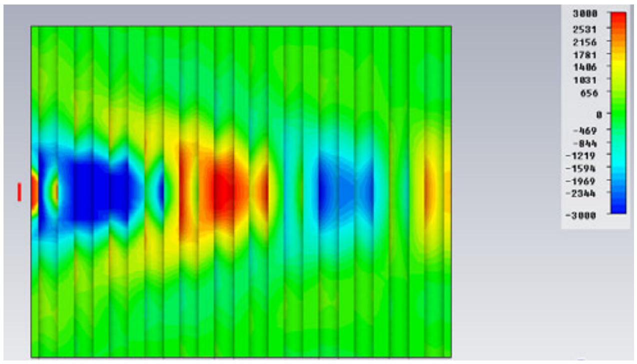

Figure 2. Subwavelength propagation due to backwards radiation in in a system of LiF rods in NaCl. The source (left-side) emits a TM wave (of frequency 15 THz) which is guided perpendicularly to the rods.

Another rich category of phenomena that become possible with polaritonic materials is phenomena based on epsilon-near-zero (ENZ) response. Such phenomena can be total transmission and reflection for dielectric scattereres embedded in a ENZ host, as well as subwavelength guiding in chains of dielectric scattereres in a ENZ material. Here we demonstrate these phenomena in LiF rods in KCl host, in the frequency regime where KCl shows ENZ response (there LiF has positive epsilon). Such a demonstration is shown in Fig. 3.

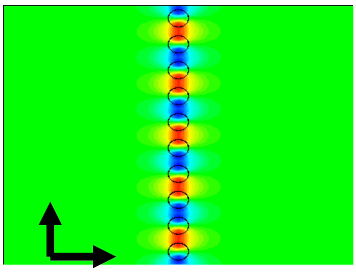

Figure 3. Sub-wavelength guiding along a chain of dielectric rods embedded in an epsilon near zero host (KCl at ~6 THz). The guiding takes place due to the excitation of Mie-resonances in the rods and the coupling of those resonances between neighboring rods.

Acknowledgements, authors acknowledge financial support by EU-project ENSEMBLE and by Greek GSRT, through project ERC-02 EXEL.

REFERENCES

1. Reyes-Coronado, A. et. al., "Self-organization approach for THz polaritonic metamaterials", *Opt. Express,* Vol. 20, 14663-14682, 2012.
2. Basharin, A.A., Kafesaki, M., Economou E.N., and Soukoulis, C.M., "Backward wave radiation from negative permittivity waveguides and its use for THz subwavelength imaging", *Opt. Express*, Vol. 20, 12752-12760, 2012.
3. Basharin, A.A., Kafesaki M., Economou, E.N., and C. M. Soukoulis, C.M., "Epsilon-near-zero based phenomena in metamaterials", submitted to *Phys. Rev. B.*

Engineering plasmonic nano- and metamaterials for ultasensitive biosensing and imaging

K. Maximova[1], A. Aristov[1], D. Grojo[1], P. Delaporte[1], P. Blandin[1], V. Kravets[2], M. Sentis[1], A. N. Grigorenko[2], A. V. Kabashin[1*]

[1]Aix Marseille University, CNRS, LP3 UMR 7341, Campus de Luminy - Case 917, Marseille cedex 9, 13288 Marseille, France

[2]School of Physics and Astronomy, University of Manchester, Manchester, M13 9PL, UK

[*]corresponding author: kabashin@lp3.univ-mrs.fr

Abstract- This presentation will review our activities in the frame of bio-plasmonics project, which implies the development of methods for biosensing and imaging using plasmonic nano/meta materials. For the synthesis of plasmonic materials, we use a series of bottom-up laser assisted methods involving fs laser ablation from a gold target (or from gold colloids) in deionized water to form "ultrapure" colloidal gold nanoparticles; or near field laser ablation through self-assembled microspheres to form plasmonic metamaterial arrays. All laser-fabricated structures are now actively used in sensing, imaging and SERS tasks. We also developed a series of phase-sensitive plasmonic sensing methods relying on the detection of biological binding events on gold through refractive index (RI) monitoring. Profiting from singular phase behavior in conditions of Surface Plasmon Resonance (SPR) or diffractive-coupled Localized Plasmon Resonance (LPR), phase-sensitive plasmonic or plasmonic metamaterial-based sensors promise an unprecedented detection limit (down to single molecular level) and can be used for the detection of small molecular weight compounds (drugs, proteins) or ultra-small concentrations of larger compounds.

Due to unique optical properties associated with the excitation of plasmons, gold-based plasmonic nano- and metamaterials (nanoparticles, nanorods, core-shells, designed arrays) become increasingly popular for tasks of biosensing, imaging and therapy. In particular, extremely efficient optical scattering of gold nanostructures has been employed for the formation of optical contrast in bio imaging [1], while strong electric field enhancement near nanoparticles and designed arrays is actively used in SERS applications [2]. Finally, a strong dependence of conditions of SPR and LPR excitation on RI of the adjacent medium contacting gold can be used to follow biological binding events on gold, giving rise to label-free plasmonic biosensing [3-5]. Further advancement of plasmonic-based biosensing and imaging modalities requires the synthesis of new plasmonic materials, which are free of toxic sub-products or impurities (especially, for in vivo or SERS applications), and the exploration of novel transduction mechanisms enabling a much improved sensitivity and additional functionalities (size selectivity, spectral tuneability, compatibility with modern nano-bioarchitectures etc).

Our on-going bio-plasmonic project is focused on clean synthesis of novel promising plasmonic materials and the development of methods for biosensing and imaging using plasmonic nano/meta structures. As the main nanofabrication approach, we use various laser-assisted roots, which can offer unique conditions for cost-efficient and "clean" production of nanoparticles and nanoparticle arrays [6]. In particular, we actively employ ultra-short (ps, fs) laser ablative methods for the synthesis of colloidal nanomaterials in deionized water [7,8], which make possible a purely physical control of size characteristics of synthesised nanomaterials and the reduction of nanoparticle size dispersion. The synthesized materials exhibit not only exceptional purity in the absence of even a trace of contaminant, unique surface chemistry and biocompatibility, but also prominent optical properties (absorption/scattering, multiphoton excitation fluorescence, SERS etc), which makes them promising candidates for sensing and imaging. As another laser nanofabrication approach, we use self-assembled silica microspheres as masks to perform near-field laser ablation and thus form nanofeatures [9]. The nanofeatures are then covered by a gold layer and standard photolithography tools are applied to form plasmonic nanoarrays. Advantages of this approach include cost-efficient production arrays on a large area (several mm^2).

As the main biosensing approach we use the concept of phase-sensitive plasmonic transducer, which was originally introduced for conventional thin film-based SPR geometry [10,11] to offer 1-2 orders of magnitude improvement of sensitivity to RI changes. We recently demonstrated further possibilities for the sensitivity improvement of plasmonic transducers by using diffraction-coupled LPR in designed plasmonic metamaterials [12]. These metamaterials present regular arrays of submicron-scale structures made from Au displaying LPR in the visible spectrum. If pumping light beam covers many dots, diffraction-coupled LPR can lead to extremely narrow resonance feature, yielding to Heaviside-like phase jump. Extracting phase information within this jump by ellipsometry or interferometry [10-12], one can obtain a drastic improvement of phase response compared to SPR geometry. In fact, the detection limit can be lowered down to sub 10^{-9} RIU level opening access to single molecular label-free detection (as we demonstrated in Graphene hydrogenation model, the areal mass sensitivity at a level of less than fg/mm^2, which is orders of magnitude better compared to LPR or SPR).

REFERENCES

1. Hirsch, L. R. et. al. “Nanoshell-mediated near-infrared thermal therapy of tumors under magnetic resonance guidance”, *Proc. Nat. Acad. Sci.*, Vol. 100, 13549-13554, 2003.
2. Kneipp, K. "Surface-Enhanced Raman Scattering", Physics Today, Vol. 60, 40-47, 2007.
3. Liedberg, B. et. al. "Biosensing with SPR - how it all started", *Biosens. Bioelect*. Vol. 10, i, 1995.
4. Anker, J. N. et. al. R. P. "Biosensing with plasmonic nanosensors", *Nature Mater*., Vol. 7, 442-453, 2008.
5. Kabashin, A. V.; Evans, P.; Patskovsky, S.; Wurtz, G.; Hendren, W.; Dickson, W.; Pollard, R. J.; Podolsky, V.; Zayats A. V., "Plasmonic nanorod metamaterials for biosensing". *Nature Mater.,* Vol. 8, 867-871, 2009.
6. Kabashin, A. V., Delaporte, P., Perreira, A., Grojo, D., Torres, R., Sarnet, T., Sentis, M. "Nanofabrication with pulsed lasers", *Nanoscale Res. Lett*., Vol. 5, 454–463, 2010.
7. Kabashin, A. V., Meunier, M., “Synthesis of colloidal nanoparticles during femtosecond laser ablation of gold in water”, *J. Appl. Phys.*, Vol. 94, 7941-7943, 2003.
8. Besner, S., Kabashin, A. V., Meunier, M. “Fragmentation of colloidal nanoparticles by femtosecond laser-induced super continuum generation”, *Appl. Phys. Lett*. Vol. 89, 233121-233123, 2006.
9. Pereira, A., Grojo, D., Chaker, M., Delaporte, P., Guay, D., Sentis, M., "Laser-Fabricated Porous Alumina Membranes for the Preparation of Metal Nanodot Arrays", *Small*, 4, 572 (2008).
10. Kabashin, A. V., Nikitin, P. I., "Interferometer based on a surface-plasmon resonance for sensor applications", *Quant. Electon*. 27, 653-654 (1997)
11. Kabashin, A. V., Patskovsky, S., Grigorenko, A. N. “Phase and amplitude sensitivities in Surface Plasmon Resonance bio- and chemical sensing”, *Opt. Express*, Vol. 17, 21191-21204 (2009)
12. Kravets, V. G., Schedin, F., Jalil, R., Britnell, L., Gorbachev, R. V., Ansell, D., Thackray, B., Novoselov, K. S., Geim, A. K., Kabashin, A. V., Grigorenko, A. N. "Singular-phase nanooptics in plasmonic metamaterials for single molecular detection", *Nature Mater*., doi:10.1038/nmat3537 (2013).

Fabrication and optical properties of arrays of caped Au multi-step-nano-holes

Benzhong Wang[1*], Hongwei Gao[2], Ning Xiang[2] and Soo Jin Chua[1,2]
[1]Institute of Materials Research and Engineering A*STAR (Agency for Science, Technology and Research), Singapore
[2]National University of Singapore, Singapore
[*]bz-wang@imre.a-star.edu.sg

Abstract-A facile method to fabricate unique nanostructures, multi-step nano-hole with a cap of Au, has been described, where a self-assembled monolayer of nanospheres is employed as masks in dry etching processes. A sample with two-step structures has been obtained, which show strong extraordinary optical transmission at wavelength of 635 nm, while it appears at 945 nm for the one-step structures.

The observation of enhanced optical transmission (EOT) through metal subwavelength hole arrays[1] has generated significant interest in nanophotonics and contributed insight into the interaction between light and materials at the nanoscale.[2–4] These fundamental studies have demonstrated that rationally engineered surfaces can manipulate and focus light well below the diffraction limit and have led to emerging applications in photonics[5–7] and chemical and biological analysis.[8, 9] Here, we report an approach to fabricate unique metal nanostructures, arrays of caped Au multi-step-nano-holes, and its optical properties.

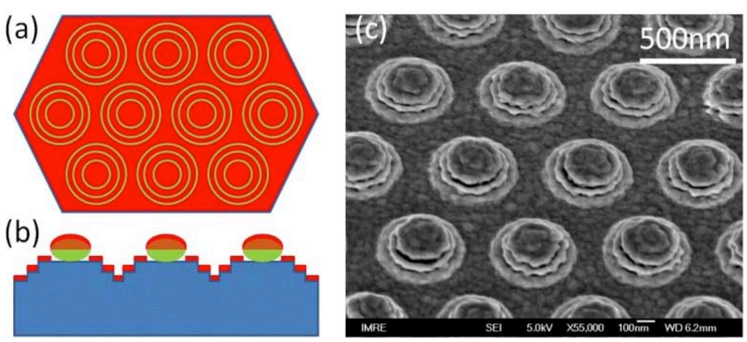

Fig 1, (a) and (b), top and side view of schematic of the caped Au two-step-nano-holes with caps (c), tilted view of SEM picture of a the Au structures which created through 600 nm PS spheres.

Fig. 1 shows the top (a) and side (b) view of schematic of the caped Au multi-step-nano-holes. A self-assembled monolayer of 600 nm polystyrene (PS) nanosphere was used as mask to fabricate such structures. A microscope glass sheet was used as substrate. The diameter of the PS sphere was reduced by Oxygen RIE firstly, then RIE etching was done to create first step on the glass sheet. After that, the diameter of the PS spheres was further reduced on site and the glass sheet was etched to create second step. In principle, many steps can be created by repeating the process although only one- and two-step structures have been fabricated in our experiments. The diameter of the PS spheres was reduced again on site before Au deposition. Finally, a 100 nm Au was evaporated onto the two-step nanostructures. Fig. 1 (c) shows a SEM image of the two-step Au nanostructures.

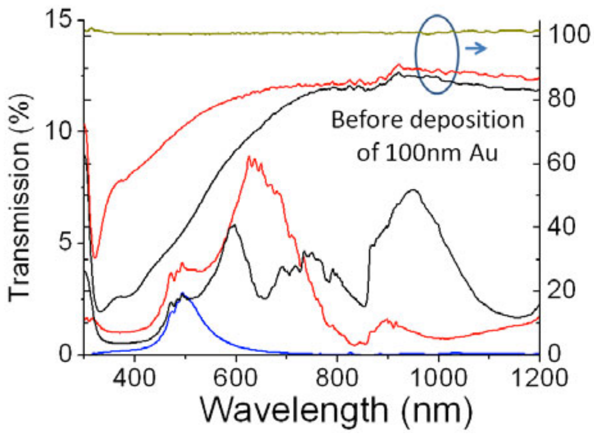

Fig 2. Transmission spectra measured at normal incidence for a glass sheet (dark yellow) which served as a substrate (normalized to 100% in the measured region), one-step (black) and two-step (red) structures before (right y-scale) and after (left-scale) 100 nm Au deposition, and a 100 nm Au deposited on a normal glass sheet (blue).

Fig. 2 displays the results of transmission spectra of the sample with one and two steps. The glass transmission was normalized to 100% in our experimental region (yellow line). For both samples the transmission reduced much in the short wavelength region due to the creation of the nanostructures.

Strong transmission has been observed after a 100 nm Au deposited on the structures. For comparison, transmission spectrum of 100 nm Au film deposited on a flat glass sheet is displayed (blue curve). Only one peak located around wavelength of 500 nm is observed on the Au film, which can be attributed to bulk Au plasmon. For the nanostructured samples, both of one and two steps, strong transmission peaks have been observed at longer wavelength side, which can be attributed to the coupling of light with plasmons—electronic excitations—on the surface of the periodically patterned metal film. However, the peak characters are much different for the two samples. The stronger peak appears at the wavelength of around 945 nm for the wafer with one-step structures, while it appears at the wavelength of around 635 nm for the wafer with two-step structures, although the periodicity of both samples is the same 600 nm, the diameter of original PS spheres.

REFERENCES

1. Ebbesen, T.W., Lezec, H. J., Ghaemi, H. F., Thio, T., Wolff, P. A., *Nature* 1998, 391, 667–669.
2. Barnes, W. L., Dereux, A., Ebbesen, T.W., *Nature* 2003, 424, 824–830.
3. Gao, H., Henzie, J., Odom, T.W., *Nano Lett*. 2006, 6, 2104–2108.
4. Pendry, J. B., MartEn-Moreno, L., Garcia-Vidal, F. J., *Science* 2004, 305, 847–848.
5. Bozhevolnyi, S. I., Volkov, V. S., Devaux, E., Laluet, J.-Y., Ebbesen, T.W., *Nature* 2006, 440, 508–511.
6. Lezec, H. J., Degiron, A., Devaux, E., Linke, R. A., Martin-Moreno, L., Garcia-Vidal, F. J., Ebbesen, T.W., *Science* 2002, 297, 820–822.
7. Ozbay, E., *Science* 2006, 311, 189–193.
8. Brolo, A. G., Arctander, E., Gordon, R., Leathem, B., Kavanagh, K. L., *Nano Lett*. 2004, 4, 2015–2018.
9. Rindzevicius, T., Alaverdyan, Y., Dahlin, A., Hook, F., Sutherland, D. S., Kall, M., *Nano Lett*. 2005, 5, 2335–2339.

A facile approach to form Ag particles in an ordered fashion

Benzhong Wang[1*], **Hongwei Gao**[2], **Ning Xiang**[2] **and Soo Jin Chua**[1,2]

[1]Institute of Materials Research and Engineering A*STAR (Agency for Science, Technology and Research), Singapore

[2]National University of Singapore, Singapore

[*]bz-wang@imre.a-star.edu.sg

Abstract-A facile method to fabricate ordered silver nanoparticles has been described, where a self-assembled monolayer of nanospheres is employed as a template to form SiO_2 honeycomb network on a Si substrate, which was further used as second template to guide the Ag particle formation. Our experimental results indicate that the particle size and distribution strongly depends on deposited silver thickness and anneal temperature.

Noble metal nanostructures on different length scales exhibit a variety of optical properties ranging from plasmon resonance [1] and Raman enhancement [2,3] to fluorescence [4-6] providing novel opportunities for bioimaging and sensing [7-9]. In a regime where the particle size is larger than electron mean free path length (50 nm for silver and gold), collective excitations of electrons become dominant, leading to plasmon resonance. Recent development of robust methods for fabrication of nanostructures, e.g. nanospheres, nanostructured substrate surface, etc., have increased the possibility of controlling an optical field in both aspects of localization and enhancement mediated with the light scattering. However it is desired to fabricate ordered NPs particles which provides other way to modify its optical properties due to 2D photonic crystal and coupling effects. However, how to form such ordered arrays of the Ag nanoparticles in interesting regions efficiently is still a big challenge.

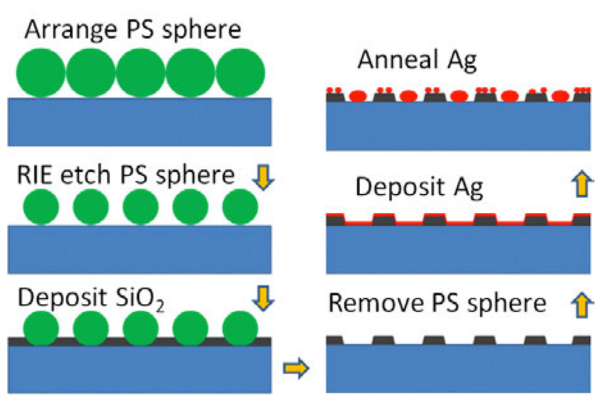

Fig 1, schematic of the process to create ordered Ag nanoparticles arrays.

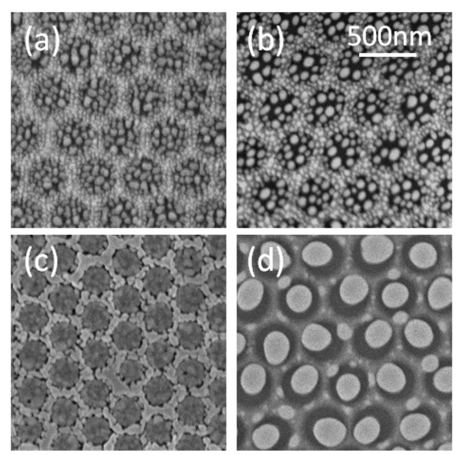

Fig 2. SEM images of the ordered Ag particles. (a), 10 nm Ag deposition, (b), after annealing at 500 °C, 30 min. (c), 30 nm Ag deposition, and (d), after annealing at 700 °C, 30 min.

Here, we described a facile approach to form ordered Ag particles on a Si substrate through modified nanosphere lithography. As shown in Fig. 1, a monolayer of 300 nm polystyrene (PS) nanospheres was self-assembled on a Si substrate. Then the diameter of the PS sphere was reduced to ~250 nm by Oxygen RIE. ~50 nm SiO_2 was deposited onto the Si substrate by E-beam evaporator to form honeycomb network. Ag film with varied thickness (10-30 nm) was evaporated on the ordered SiO_2 nanoholes after removing the PS sphere. Finally, annealing process was performed to form the ordered Ag particles.

The formation of the ordered Ag particles has investigated systemically. The particle size and distribution depend on not only annealing temperature, but also deposited thickness. Fig. 1 (a) shows a SEM image of the sample with 10 nm Ag deposition. It is clearly observed that a separated island-like film was formed on both Si and SiO_2 surface. However, the size of the islands formed on the SiO_2 surface is much smaller than that on the Si surface. After 500 ^{o}C, 30 min annealing [Fig. 2 (b)], the Ag islands become smooth and tend to be round on both Si and SiO_2 surface, but the number almost no change. When increase annealing temperature (not shown here), the islands on the SiO_2 surface tend to disappear, while the islands on the Si surface tend to be large.

Fig. 2 (c) shows a SEM image of the sample with 30 nm Ag deposition. It is clearly observed that the Ag film was formed on both Si and SiO_2 surface, close lined islands formed on the SiO_2 surface. After 700 ^{o}C, 30 min annealing [Fig 2 (d)], only one big particle formed inside the SiO_2 holes, while some small particles formed on the SiO_2 surface. Optical properties of the ordered Ag nanoparticles were also investigated which shown unique features.

REFERENCES

1. Kreibig, U.; Vollmer, M., *Optical Properties of Metal Clusters*; Springer: Berlin, 1995; Vol. 25.
2. Haynes, C. L.; McFarland, A. D.; Van Duyne, R. P., *Anal. Chem*. 2005, 77, 338A–346A.
3. Moskovits, M., *J. Raman Spectrosc*. 2005, 36, 485–496.
4. Fedrigo, S.; Harbich, W.; Buttet, J., *J. Chem. Phys*. 1993, 99, 5712–5717.
5. Peyser, L. A.; Vinson, A. E.; Bartko, A. P.; Dickson, R. M., *Science* 2001, 291, 103–106.
6. Zheng, J.; Dickson, R. M., *J. Am. Chem. Soc*. 2002, 124, 13982–13983.
7. Mirkin, C. A.; Letsinger, R. L.; Mucic, R. C.; Storhoff, J. J., *Nature* 1996, 382, 607–609.
8. Sonnichsen, C.; Reinhard, B. M.; Liphardt, J.; Alivisatos, A. P., *Nat. Biotechnol*. 2005, 23, 741–745.
9. Qian, X. M.; Peng, X. H.; Ansari, D. O.; Yin-Goen, Q.; Chen, G. Z.; Shin, D. M.; Yang, L.; Young, A. N.; Wang, M. D.; Nie, S. M., *Nat. Biotechnol*. 2008, 26, 83–90.

Bottom-up plasmonic metasurfaces: Macroscopic thermal management, thin-film photovoltaics and control of the interband absorption

Alexandre Dmitriev
Applied Physics, Chalmers University of Technology, Göteborg, Sweden, alexd@chalmers.se

In numerous applications of light transformation into heat the focus recently shifted towards highly absorptive materials featuring nanoplasmons. It is currently established that noble metals-based absorptive plasmonic platforms deliver significant light-capturing capability and can be viewed as super-absorbers of optical radiation. However, direct experimental evidence of plasmon-enabled *macroscopic* temperature increase that would result from these efficient absorptive properties is lacking so far. I will present a general quantitative method of characterizing light-capturing properties of a given heat-generating absorptive layer by macroscopic thermal imaging. We monitor macroscopic areas that are homogeneously heated by several degrees with plasmonic nanostructures that occupy a mere 8% of the entire surface, evidencing significant heat generation capability of nanoplasmon-enabled light capture and its direct applicability in thermophotovoltaics and other applications.

As a second example, I will discuss the engineering of front and back plasmonic electrodes and reflectors for thin-film photovoltaic technology. Particular applications are organic [1], crystalline [2] and amorphous thin-film solar cells.

Finally, I will present the concept of ‘interband nanoplasmonics’. Plasmonic metals like gold and silver show two distinct regions in their dielectric functions, one with dominant free electron contribution and one with dominant bound electron contribution. The former can be explained by Drude term while Lorentzian oscillator describes the latter. Certain metals also exhibit spectrally well-defined interband transitions – examples are Al (1.5eV), Cu (2.1eV), Fe (2.5eV) or Ni (4.7eV). We examine the interaction between the free and bound electrons and show both theoretically and experimentally that the optical response, related to the interband transition, is remarkably affected by the presence of localized plasmon resonance. We see stark modification of the absorption, associated with the interband transition, while we by design spectrally approach plasmon resonance to the IB transition to steer their coupling. We foresee that these effects can be used to understand the fundamentals and control the optical response of the transition metals, and might find exciting applications in catalysis and photovoltaics.

[1] B. Niesen et al., *Adv. Energy Mater.*, doi 10.1002/aenm.201200289 (2012)
[2] O. El Daif et al., *Sol. Ener. Mat. Sol. C* 104, 58 (2012).

Birth of a Plasmon

Terry P. Bigioni

Department of Chemistry,
Wright Center for Photovoltaics Innovation and Commercialization,
The University of Toledo, Toledo, OH 43606

The bottom-up approach to making plasmonic metamaterials begins with individual nanoparticles, however the fundamental nature of plasmons is still poorly understood. The emergence and size evolution of plasmons in noble metal nanoparticles remains elusive due to the difficulty of accurately resolving the spectral features as a function of size. This is primarily due to the challenge of preparing a series of atomically precise clusters over a size range from small clusters to colloidal nanoparticles. This is further exacerbated by the complex physical and chemical interactions between the metal core and surrounding media. Here, we present a complete and systematic series of spectra for discrete Ag magic-number clusters that bridge the molecular and plasmonic regimes and are capped with different ligand shells. The structured spectra of the smallest clusters were found to evolve with increasing size, ultimately collapsing into a single plasmonic peak for the largest particles in the series. These results will be discussed in the context of recent theory describing the nature of plasmonic excitations as single-electron excitations.

[†]current address: Department of Chemistry, Ohio State University, Columbus, OH 43210

Plasmonic Nanocomposites

Tunable Plasmonics: A New Route towards Optical Metamaterials

R. Caputo[1,*], L. De Sio[1], U. Cataldi[2], L. Pezzi[1] and C. Umeton[1]

[1]LICRYL (Liquid Crystals Laboratory, IPCF-CNR),
Center of Excellence CEMIF.CAL and Department of Physics
University of Calabria, 87036 Arcavacata di Rende (CS), Italy

[2]Dèpartement de Chimie Physique, Universitè de Genève, Quai Ernest-Ansermet 30, 1211 Gèneve, Switzerland.

[*]corresponding author: roberto.caputo@fis.unical.it

Abstract- Fabrication of samples showing plasmonic properties is fundamental for the realization of devices exhibiting peculiar electromagnetic properties. A hot-topic is the fabrication of devices whose plasmonic functionalities are also tunable. Several examples are provided here, confirming this possibility: depending on the specific system, the plasmonic tunability can be achieved by applying external electric fields, mechanical stresses or by changing the temperature of the considered sample.

Wide interest is actually devoted to the realization of materials showing Plasmonic properties. These materials are of great interest for many applications such as integrated optics [1], plasmonic circuits [2], biosensing [3] and quantum information processing [4]. Their unique properties derive from the collective oscillation of the free conduction electrons induced by the interaction of metallic nanoparticles with an external electromagnetic field, the so-called Localized Surface Plasmon Resonance (LSPR). The plasmonic response of a system containing metal nanoparticles (NPs) is usually evidenced by a very intense color, absent in the bulk material, as well as in individual atoms. Control of the spectral position of the plasmonic resonance is a hot-topic and can be enabled by modifying size and shape of NPs or their distribution.

In order to fabricate above mentioned materials, a possible choice is a top-down approach (e-beam or photo-lithography) but, due to the long processing times, the resulting useful area is way too small. A bottom-up approach is then preferable: NPs can be combined with host materials that have the ability to induce self-organization of particles through chemical or physical mechanisms. A very intriguing possibility is the use of an "active" host, through which it is possible to control the spectral position of the NPs plasmonic resonance. Much effort has been recently spent to design host materials that can exercise such an influence on NPs. Here we report on our attempts to realize tunable plasmonic systems by combining "hard" and "soft" matter.

A convenient way to dynamically modify the plasmonic resonance frequency of a homogeneous (surface or bulk) distribution of mono-dispersed metal NPs is to vary the dielectric permittivity of the medium surrounding the NPs. Indeed, the optical properties of spherical nano-particle dispersions can be predicted by the Mie theory [5], which states that, for small and isolated metal particles, the spectral position of the plasmonic absorption peak depends on the refractive index of the medium surrounding them. A modification of the dielectric function of the host material corresponds, therefore, to a tuning action of the plasmonic resonance frequency. The outstanding properties of Liquid Crystals (LCs) make them an ideal candidate for this role; indeed, these materials represent an excellent example of reconfigurable medium where the refractive index can be finely controlled by means of external stimuli. A demonstration of the use of LCs as a tunable host for gold NPs can be found in [6]. In that case, the (electrically or thermally) induced variation of the refractive index of a Cholesteric Liquid Crystal doped with gold nanoparticles strongly influences the position of the plasmonic absorption peak of NPs. Fig. 1 shows that both blue- and red-shift can be achieved depending whether the tunability is obtained through the application of an external electric field or by changing the sample temperature.

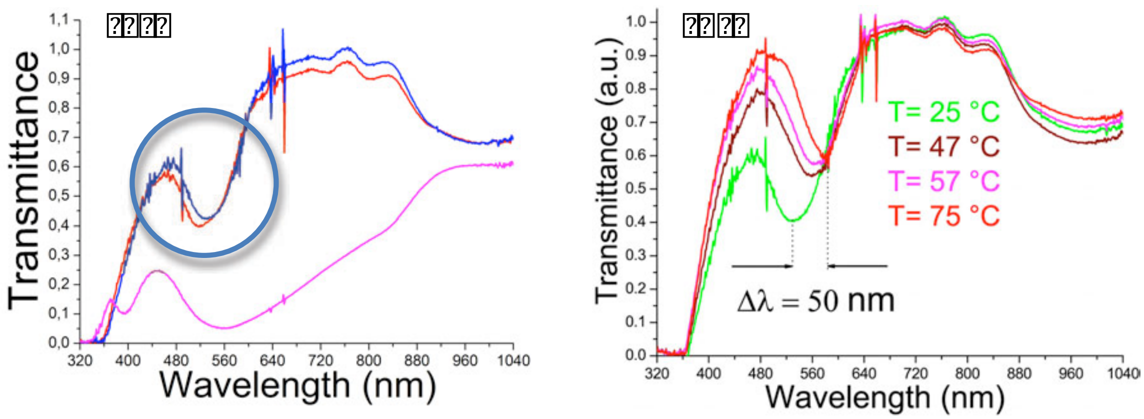

Fig. 1. Plasmonic tunability of a sample made of Cholesteric Liquid Crystal doped with gold NPs. The application of an external electric field produces a blue shift of the plasmonic resonance peak (a); by changing the temperature of the sample, a pronounced red shift of the same peak takes place (b).

Another way to exploit the plasmonic tunability of a metal NPs array is to act on NPs inter-distance. This idea has been implemented by coating a Polydimethylsiloxane (PDMS) substrate with mono- or multi-layers of gold NPs. The fabricated system is sensitive to mechanical stresses and, depending on NPs size and density, and on the number of gold layers, it is possible to induce a plasmonic shift as well as modifications of the shape of the resonance curves [7]. All above-mentioned systems show tunable plasmonic functionalities in the visible range of the spectrum, due to the collective action of a very large number of metal nanoparticles. In our opinion, these results hold promises for the realization of optical metamaterials.

Acknowledgements

The research leading to reported results has received funding from the European Union’s Seven Framework Programme (FP7/2007-2013) under grant agreement n°228455.

REFERENCES

1. V.M. Shalaev, S. Kawata, Nanophotonics with Surface Plasmons (Advances in Nano-Optics and Nano-Photonics). Elsevier, 2007.
2. T.W. Ebbesen, C. Genet, S.I. Bozhevolnyi, Phys. Today 2008, 61, 44.
3. J.N. Anker, W.P. Hall, O. Lyandres, N.C. Shah; J. Zhao, R.P. Van Duyne, Nat. Mater. 2008, 7, 442.
4. L. Childress, J. M Taylor, A. S. Sorensen, M. D. Lukin, Phys. Rev. A 2005, 72, 052330.
5. G. Mie, Ann. Phys 1908, 25, 377.
6. L. De Sio, R. Caputo, U. Cataldi and C. Umeton, J. Mat. Chem. 2011, 21, 47, 18967.
7. U. Cataldi, P. Cerminara, L. De Sio, R. Caputo and C. Umeton, Mol. Cryst. Liq. Cryst. 2012, 558, 1, 22.

3–dimensional arrays of silver nanoparticles: Bottom-up fabrication and optical properties.

P. Barois[1*], L. Malassis[1], P. Massé[2], M. Tréguer-Delapierre[2], and S. Mornet[2]
[1]Université de Bordeaux, CNRS, Centre de Recherche Paul Pascal, France
[2]Université de Bordeaux, CNRS, Institut de Chimie de la Matière Condensée de Bordeaux, France
[*]corresponding author: barois@crpp-bordeaux.cnrs.fr

Abstract - Meta-atoms constituted of silver nanoparticles are self-assembled in 2D and 3D arrays. A fine control of the plasmonic coupling is obtained by encapsulation of the particles in a silica shell. The optical response of the films exhibits a sharp collective plasmon band which is blue-shifted and narrower than the absorption band of the particles in solution. The influence of the shell thickness is discussed. Values of the refractive index lower than 1 are obtained for moderate fraction of silver.

Metamaterials are constituted of electromagnetic resonators (meta-atoms) whose dimensions must be much shorter than the operating wavelength. For visible light, nanoparticles made of noble metals such as gold or silver (which is less lossy) are good candidates as they exhibit localized plasmon resonances (LSPR) in the visible range. Moreover, self-assembly appears as an efficient way to assemble the huge number of resonators required for the fabrication of bulk metamaterials. It has been shown indeed that random dispersions of silver nanoparticles can generate extreme values of the real part of the dielectric permittivity [1].

In order to study and understand the effect of the structural parameters on the optical properties of the self-assembled materials, it is important to control with a high precision the size of the resonators and the distance between them, which both affect strongly the plasmonic response. Clustering usually results in red-shifting whereas polydispersity causes broadening. We developed a fabrication method that controls as much as possible these important structural parameters. Figure 1 illustrates the basic principle of this method. Silver-silica core-shell nanoparticles are first synthesized by nanochemistry and subsequently assembled in dense films by a self-assembly method derived from the Langmuir-Blodgett technique. The silver cores provide the wanted LSPR whereas the silica shells ensure a constant distance between the cores, and hence a constant coupling strength.

The optical properties of the films have been studied by experimental measurements of the reflectance at normal incidence versus wavelength, shell thickness and film thickness. We show that the optical response is well described by an effective model based on a single Lorentz oscillator. A blue shift and a narrowing of the resonance are observed. This effect is consistent with numerical [2] and experimental [3] studies reported on 2D arrays of silver particles. It is however observed for the first time in 3D films and for dimensions much shorter than the wavelength. This is a direct consequence of the fine control of the regular distribution of the resonators in space.

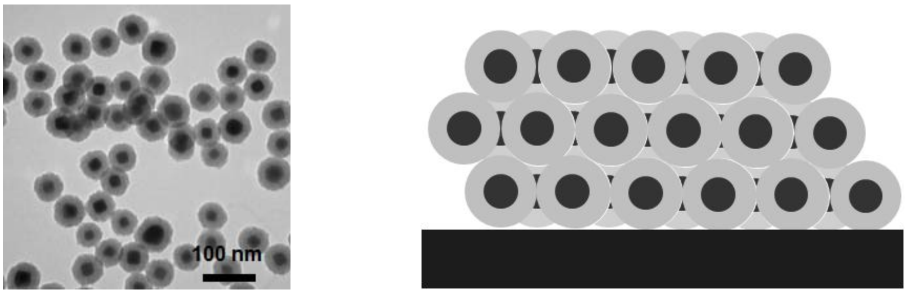

Figure 1: Left**:** Electron Microscopy view of core-shell nanoparticles used in this study. The silver core is clearly visible at the center of the silica shell. Right: sketch of the structure of a film showing how the silica shell fixes the distance between the silver cores.

The effective refractive index extracted. Values of the real part lower than 1 are obtained for moderate fraction of silver.

Acknowledgements, this work was funded by the European FP7 collaborative project Metachem under grant # 228762.

REFERENCES

1. J. Dintinger, S. Mühlig, C. Rockstuhl and T. Scharf, “A bottom-up approach to fabricate optical metamaterials by self-assembled metallic nanoparticles”, *Opt. Mater. Express*, *2*, 269, 2012.
2. Zhao, L., Kelly, K. L. & Schatz, G. C. “The Extinction Spectra of Silver Nanoparticle Arrays: Influence of Array Structure on Plasmon Resonance Wavelength and Width”. *J. Phys. Chem. B*, 107, 7343–7350 (2003).
3. S. Malynych and G.Chumanov, “Narrow plasmon mode in 2D arrays of silver nanoparticles self-assembled on thin silver films”, *Journal of Microscopy*, Vol. 229, 567–574, 2008.

A first-principles study of surface enhanced Raman spectra of molecules adsorbed to plasmonic nanocomposites

M. Thomas[2,3], **S. Mühlig**[1], **E. Hebestreit**[1], **T. Deckert-Gaudig**[3,4], **V. Deckert**[3,4], **P. Marquetand**[2], **and C. Rockstuhl**[1]

[1] Institute of Condensed Matter Theory and Solid State Optics,
Abbe Center of Photonics, Friedrich-Schiller-Universität Jena, D-07743 Jena, Germany

[2] Institute of Theoretical Chemistry, University of Vienna, Währinger Str. 17, 1090 Vienna, Austria

[3] Institute of Physical Chemistry, Friedrich-Schiller-Universität Jena, Helmholtzweg 4, 07743 Jena, Germany

[4]Institute of Photonic Technology e.V., Albert-Einstein-Str. 9, 07745 Jena, Germany

[*]corresponding author: carsten.rockstuhl@uni-jena.de

Abstract- Surface enhanced Raman scattering is a well established analytical tool to identify the presence, the composition, and the concentration of molecules. However, the particular interplay between various enhancement mechanisms that eventually contribute to the signal is not fully understood yet. Here, we use real time time-dependent density functional theory combined with rigorous electromagnetic simulations to unravel how the chemical and the electromagnetic mechanisms enhance the measurement signal at the important example of para-Nitrothiophenol.

Raman scattering suggests that upon exciting a molecule with external light at a fixed frequency, the scattered radiation comprises frequency components at a higher or lower energy, depending on whether a quanta of energy is transferred to a vibrational level of the molecule or vice versa. The Raman spectrum provides a fingerprint for the molecule. Unfortunately, the cross section is usually weak and mechanisms are required to enhance the signal. It has been identified, approximately 40 years ago, that by adsorbing molecules to metallic surfaces, the Raman spectra is enhanced by orders of magnitude [1]. Surface plasmon polaritons, as sustained by metallic nanostructures, are usually identified as an important contribution to the effect. Phenomenologically, it can be shown in a lowest order approximation that the Raman signal depends on the fourth power of the exciting local electric field as perceived by the molecule. However, in an ongoing debate arguments were also raised that suggest that it is not just a pure electromagnetic effect that causes the enhancement, but the modification of the vibrational levels of the molecules upon adsorption on the metallic surface can cause an enhancement as well. The latter effects are summarized as chemical enhancement. The disentanglement of both contributions is an important topic for nanoscience. Only if both effects are sufficiently well understood, they can be tailored at will to unfold their efficiency at its maximum.

In response to this need, various efforts were put in place to grasp both effects simultaneously in devoted simulations. Among others, the metallic nanoparticle can be modeled by effective charges that are included in the molecular Hamiltonian [2], a many body Green's function can be used to model the interaction of the molecule and the conduction electrons of the metal nanoparticle [3], or a combined description of the metal nanoparticle by the finite-difference time-domain method with a two-level model for the molecule within the random phase approximation can be used [4]. However, potentially the most advanced technique, pioneered by the group of G. C. Schatz, combines rigorous electromagnetic and quantum chemical simulations where the evolution of the local electric field close to the metal nanostructure is explicitly included in the Hamiltonian of the molecule via time-dependent density functional theory [5,6]. This allows deriving predictions of all measurable quantities that can be compared to experiments. While considering in such analysis additional atoms in the Hamiltonian that describe a fraction of the metallic nanoparticle close to the molecule of interest, the chemical and electromagnetic enhancement can be studied simultaneously.

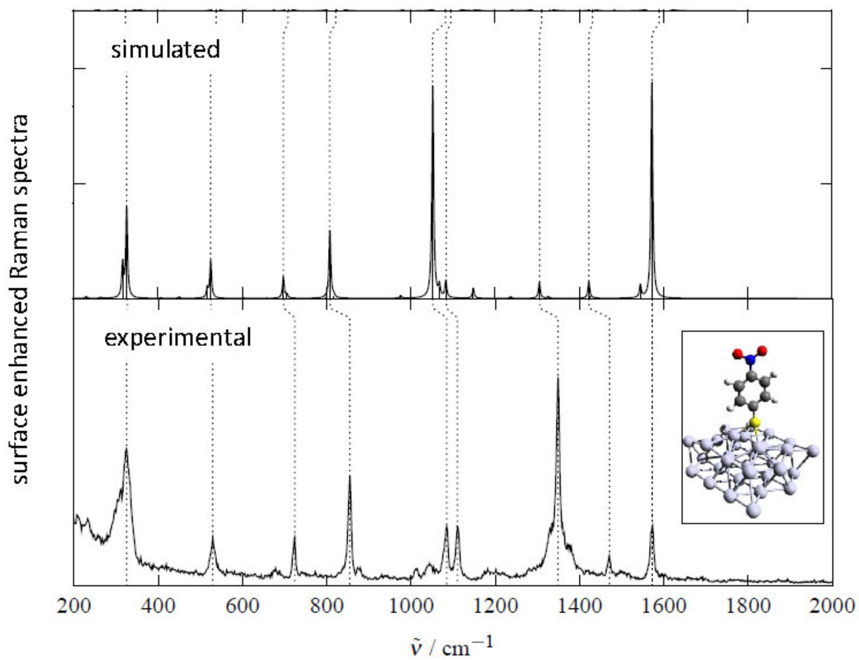

Figure 1: Simulated and measured Raman spectra of para-Nitrothiophenol. In the simulations, not just the molecule is taken into account but also its adsorption to the surface of the metallic nanoparticle, as indicated in the inset.

Here we exploit such methodology to study the surface enhanced Raman spectra of molecules adsorbed on the surface of a plasmonic nanocomposite. Emphasis is put on distinguishing electromagnetic and chemical enhancement effects. Particularly, we show for para-Nitrothiophenol that the first effect enhances the signal, whereas the latter causes a deviation of the Raman spectra of the adsorbed molecule with respect to the isolated one [7]. A referential result for such analysis is shown in Fig. 1. Beyond this distinction, we also study the impact of the arrangement of the molecule relative to the plasmonic nanocomposite and try to assess the predictive power of more approximate theories, e.g. those that only rely on the analysis of the electric field at the spatial position of the molecule. In its simplest version the considered plasmonic nanocomposite consists of an isolated metallic nanoparticle; but eventually more complicated structures should be considered as well. Examples thereof are coupled metallic nanoparticles, i.e. dimers, or metallic nanoparticles close to a planar metallic surface.

REFERENCES

1. Fleischmann M., Hendra P., and McQuillan A., *Chem. Phys. Lett.* Vol. 26, 163–166, 1974.
2. Corni S. and Tomasi J., *J. Chem. Phys.* Vol. 114, 3739–3751, 2001.
3. Masiello D. J. and Schatz G. C., *Phys. Rev. A* Vol. 78, 042505, 2008.
4. Lopata K. and Neuhauser D. J., *Chem. Phys.* Vol. 130, 104707, 2009.
5. Chen H., McMahon J. M., Ratner M. A., and Schatz G. C., *J. Phys. Chem. C* Vol. 114, 14384–14392, 2010.
6. Mullin J. et al., *J. Phys. Chem. A*, Vol. 116, 9574–9581, 2011.
7. Thomas M. et al, submitted to *J. Raman. Spect.*

Coupling of Surface Plasmon with GaAs/InGaAs Quantum Well Emission by Random Gold Nanoparticle Arrays

Hongwei GAO[1], Jinghua TENG[2], Soo Jin CHUA[1,2], Ning XIANG[1]

[1]National University of Singapore, Singapore,
[2]Institute of Materials Research and Engineering, Singapore

Abstract: Coupling effect of surface plasmon (SP) with InGaAs/GaAs QW emission is demonstrated experimentally. The SP resonance is generated by fabricating a random Au nanodisk arrays on InGaAs/GaAs QW surface. The thickness of cap layer of QW is 20 nm. More than 2-fold QW PL enhancement is observed. Theoretical simulations confirm that the PL emission is enhanced by surface plasmon coupling.

Recently large amount of attention has been attracted to the effects of field enhancement in the vicinity of metallic nanostructures. Narrowed directional extinction resonances has been predicted[1] and observed [2,3] in ordered arrays of metallic nanoparticles which separated by distances comparable to the free space wavelength of radiation. However, only a very small part of the surface can actually experience the local field enhancement for nanoparticles characterized by only a fraction of a wavelength in diameter but a separation of a full wavelength from each other. Thus closely spaced arrays of nanoparticles appeared in which the electric field over most of the area would have been strongly enhanced. It would be useful for some applications due to the advantage of strength and directionality generated by ordered arrays [4,5]. While for fluorescence enhancement applications, which is very important and be our interested field, the arrays are at a significant disadvantage because the energy from the excited molecules gets dissipated due to coupling into dark modes.

Here we introduce the randomly distributed metallic nanostructure on the surface of InGaAs/GaAs QW to observe the photoluminescence enhancement, of which emission wavelength located in near infrared range. Due to this disorder caused by the randomness, the phases of different modes spread. This expansion would have benefit in enhancing the luminescence of molecules placed in the vicinity of random metallic arrays. In our experiment, more than 2-fold PL enhancement has been obtained. Numerical simulation is also performed to verify experimental result.

Acknowledgement: This work is supported by Singapore Ministry of Education (grant number MOE2009-T2-1-086).

References

1 S. Zou, N. Jarel, and G. C. Schatz, J. Chem. Phys. **120**, 10871 (2004).
2 Y. Chu, E. Schonbrun, T. Yang, and K. B. Crozier, Appl. Phys. Lett. **93**,181108 (2008).
3 B. Auguié and W. L. Barnes, Phys. Rev. Lett. **101**, 143902 (2008).
4 S. A. Maier, M. L. Brongersma, P. G. Kik, and H. A. Atwater, Phys. Rev.B **65**, 193408 (2002).
5 G. A. Wurtz, J. S. Im, S. K. Gray, and G. P. Widerrecht, J. Phys. Chem. B**107**, 14191 (2003).

Bottom-up organisation of metallic nanoparticles for metamaterials applications

T. Bürgi[1*], **A. Cunningham**[1]
[1]Department of Physical Chemistry, University of Geneva, 30 quai Ernest-Ansermet, 1211 Geneva, Switzerland

[*]corresponding author: Thomas.buergi@unige.ch

Abstract- The means to fabricate both large scale metallic nanoparticle arrays and core shell nanoparticle clusters is discussed. The preparations developed afford high degrees of control, to almost nanometre precision, over important material parameters such as particle size and separation. The optical properties of the structures have been extensively characterised yielding results that show excellent agreement with theory.

The self-organisation of metallic nanoparticles into assemblies of interest to the metamaterials community has been studied. A variety of colloidal nanochemistry techniques were developed to fabricate structures proposed by theoreticians working in the field. Spectroscopic techniques were then employed to fully probe the optical properties of these structures and evaluate the extent to which they could be used to advance metamaterials research. The coupling of metallic nanoparticles within the structures, which determines the optical properties of the materials, can be described both quantitatively and qualitatively by plasmon hybridisation theory,[1] an analogous model to that used in molecular orbital theory, which describes the mixing and splitting of the dipolar localised surface plasmon resonances (LSPR) exhibited by metallic nanoparticles.

Large scale planar arrays of metallic nanoparticles were fabricated on a variety of functionalised substrates such as glass, silicon, polymers and transparent conducting oxides, using electrostatic interactions. Several means to control the overall filling fraction were also investigated. Arrays encapsulating a variety of densities, from extremely isolated nanoparticles through to closely packed structures approaching monolayers, were successfully fabricated.

The construction of three-dimensional structures, one of the principal challenges faced by researchers attempting to fabricate metamaterials through more conventional top-down techniques, was then achieved. The deposition concepts referred to above were combined with the layer-by-layer deposition [2] of charged polymer layers to build up multiple arrays of metallic nanoparticles. The distances between arrays could be accurately tuned, with almost nanometre precision, allowing the magnitude of the electromagnetic coupling, and therefore the optical properties, between separate arrays to be controlled. Only limitations of a practical nature restrict the overall number of metallic nanoparticle arrays and their relative separations. Several parameters, including array separation and nanoparticle size, were investigated using this system. [3] A similar structure was also used to probe asymmetric coupling between gold and silver nanoparticle arrays. The optical properties of these structures were studied as a function of both the angle of incidence of the probing beam and, again using polyelectrolytes, array separation.

The importance of magnetic resonances to the field of metamaterials also led to research on core-shell nanoclusters. [4] Prepared in an analogous fashion to the planar arrays described above, this research was motivated by several theoretical papers outlining the magnetic dipole moment that such spherical organisations of metallic nanoparticles should exhibit and the importance of this in preparing negative refractive index materials. These assemblies were fabricated both in solution and as large scale arrays on suitably functionalised substrates and were also investigated for their potential cloaking properties.

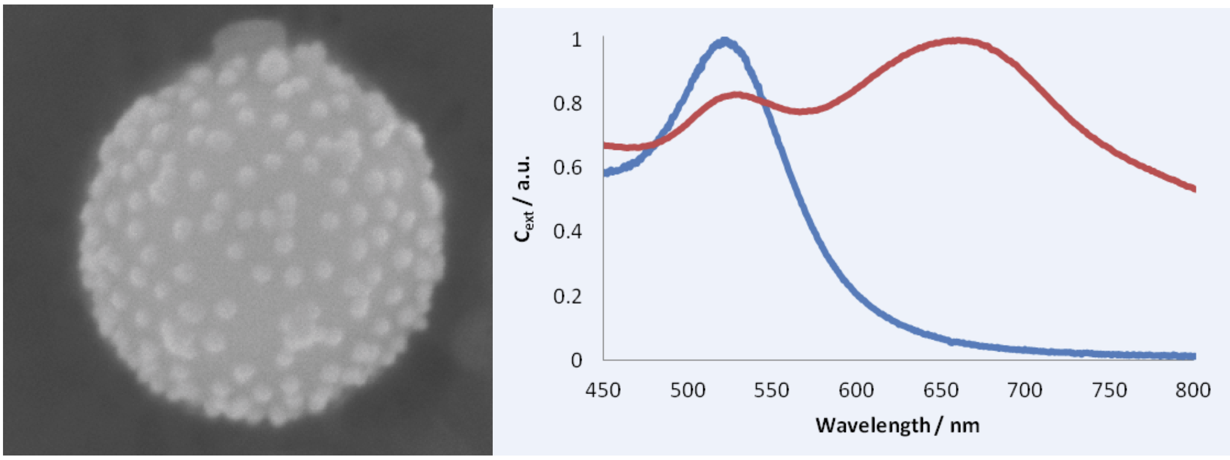

Figure: SEM micrograph of core-shell gold nanoparticle cluster (left) and extinction spectra of both GNPs and core shell gold nanoparticle clusters (right). [4]

Acknowledgements: Financial support from the European Union FP7 project NANOGOLD is kindly acknowledged.

REFERENCES

1. Prodan, E., Radloff, C., Halas, N. J. and Nordlander, P., "A hybridization model for the plasmon response of complex nanostructures", *Science*, Vol. 302, 419, 2003.
2. Decher, G., "Fuzzy nano-assemblies: Toward layered polymeric multicomposites", *Science*, Vol. 277, 1232, 1997.
3. Cunningham, A., Mühlig, S., Rockstuhl, C. and Bürgi, T. "Coupling of plasmon resonances in tunable layered arrays of gold nanoparticles," *J. Phys. Chem. C*, Vol. 115, 8955, 2011.
4. Mühlig, S., Cunningham, A., Scheeler, S., Pacholski, C., Bürgi, T., Rockstuhl, C. and Lederer, F., "Self-Assembled plasmonic core-shell clusters with isotropic magnetic dipole response in the visible range." *ACS Nano*, Vol. 5, 6586, 2011.

Complex DNA Plasmonics

N. Liu[1*] and B. Q. Ding[2]
[1]Max-Planck-Institute for Intelligent Systems, Heisenbergstr. 3, D-70569 Stuttgart, Germany
[2]National Center for Nanoscience and Technology, Beijing, China
[*]corresponding author: laura.liu@is.mpg.de

Abstract-We demonstrate the realization of three-dimensional plasmonic chiral nanostructures through programmable transformation of gold nanoparticle-dressed DNA origami. The concept of combining the know-how in plasmonics and biology opens a new pathway to the design of smart artificial plasmonic nanostructures for answering intriguing biological questions.

Advanced designs of nanomaterials require a large amount of control over the assembly of nanoscale components. Structural DNA nanotechnology, which utilizes the programmability of DNA, offers a compelling approach towards fully addressable nanopatterning. In particular, the DNA origami technique can create arbitrary two- or three-dimensional DNA nano-architectures with well-defined sizes, shapes, and spatial addressability. Most remarkably, DNA origami allow for rational organization of nanocrystals in three dimensions, which remains a significant challenge for top-down techniques.

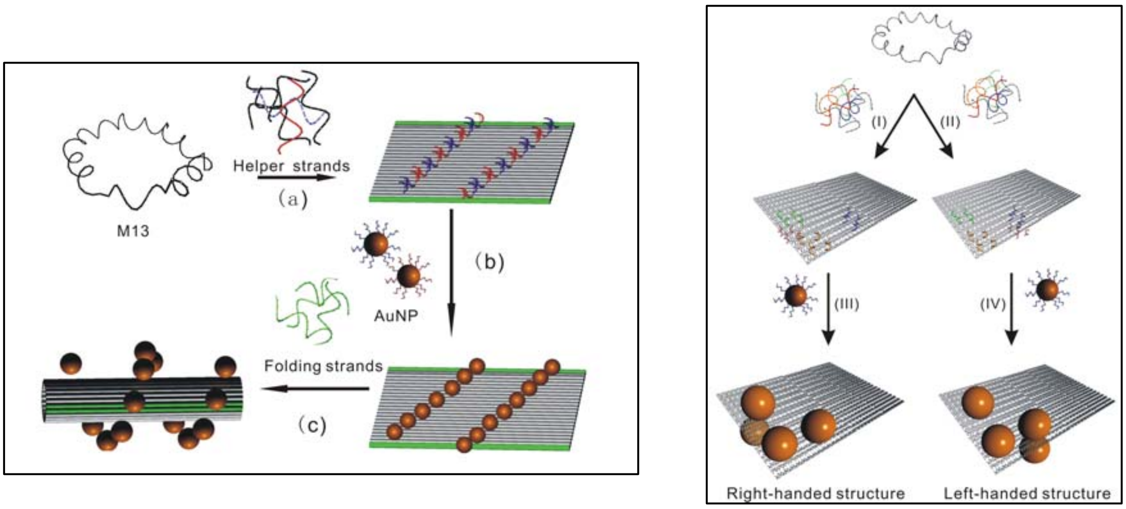

Fig. 1: Left: Experimental scheme for constructing 3D plasmonic spirals. M13 DNA and helper strands form the origami, leading to a plasmonic spiral. Right: Experimental scheme for constructing left- and right-handed 3D plasmonic tetramers.

We show in this contribution the experimental implementation of 3D plasmonic chiral structures, which display distinct circular dichroism in the visible range. The first example is 3D plasmonic spirals that are constructed through programmable transformation of gold nanoparticles (AuNP)-dressed DNA origami [1]. A rectangular DNA origami template is functionalized with two linear AuNP chains at specific positions. The process is then followed by rationally rolling and stapling the planar DNA rectangular origami into tubular DNA origami. After rolling, the AuNPs are automatically organized into a 3D helix on the tubular DNA origami (Fig. 1 left). The second example is 3D plasmonic tetramers [2], in which four identical AuNPs are assembled at four desired binding sites on a rigid DNA origami template with accuracy on the nanometer scale. The left- and right-handed structures are obtained by arranging the four binding sites in left- and right-handed fashion, respectively (Fig. 1 right). In both cases, optical circular dichroism has been found in isotropic liquid solutions of our plasmonic structures.

Our method opens up a number of possibilities to realize programmable 3D plasmonic structures with desired optical properties. These 3D chiral nanomaterials will enable a new generation of 3D plasmon rulers in that CD spectra are notably sensitive on 3D conformational changes. For example, subtle spatial changes can be reported in real time by monitoring the CD spectrum change, resulting from the binding or cleavage of a specific staple strand on the origami by enzymes or proteins. Also, rationally designed DNA origami templates can be further modified to precisely organize multiple components in three dimensions including different metallic nanoparticles, magnetic nanoparticles, quantum dots, and proteins for various functionalities and applications.

Acknowledgements, N. Liu was supported by the Sofja Kovalevskaja Award from the Alexander von Humboldt-Foundation. B. Ding was supported by National Basic Research Program of China (973 Program, 2012CB934000), 100-Talent Program of Chinese Academy of Sciences, National Science Foundation China (21173059, 91127021) and Beijing Natural Science Foundation (2122057).

REFERENCES

1. X. Shen, Chen Song, Jinye Wang, Dangwei Shi, Zhengang Wang**,** Na Liu, Baoquan Ding, “Rolling up gold nanoparticle dressed DNA origami into three-dimensional plasmonic chiral nanostructures.”*J. Am. Chem. Soc*. Vol. 134, 146-149, 2012.
2. X. Shen, Ana Asenjo-Garcia, Qing Liu, Qiao Jiang, F. Javier García de Abajo, Na Liu, and Baoquan Ding, submitted, 2012.

Liquid crystal based plasmonic metamaterials

T. Scharf[1], J. Dintinger[1], B.J. Tang[2], G. H. Mehl[2], X. Zeng[3], G. Ungar[3], S. Mühlig[4], T. Kienzler[4] and C. Rockstuhl[4]

[1]Optics & Photonics Technology Laboratory, Ecole Polytechnique Fédérale de Lausanne (EPFL), Switzerland

[2]Department of Chemistry, University of Hull, United Kingdom

[3]Department of Engineering Materials, University of Sheffield, United Kingdom

[4]Institute of Condensed Matter Theory and Solid State Optics, Abbe Center of Photonics, Friedrich-Schiller-Universität Jena, Germany

[*]corresponding author: toralf.scharf@epfl.ch

Abstract- The optical properties of metamaterials can be tailored by a choice of materials and the geometry of constituents as well as their orientation on different length scales. In our contribution we study composite plasmonic metamaterials containing resonant metallic nanoparticles that show organization. The non-conventional properties derive from a self-organization of nanoparticles on short distance by mesogens that form liquid crystals. We compare the properties of such materials with other model systems containing organized nanoparticles. Theoretical insight of the electromagnetic properties is provided and we give details on the pathway to design such structures and to adjust their optical and mechanical properties.

Nowadays, most metamaterials are often realized as complex nanostructured metasurfaces. Their functionality is based on a combination of plasmonic resonances sustained by metallic nanostructures. Novel concepts of bottom up fabrication using liquid crystal self-organization promise the realization of bulk metamaterials, inks and paints. Our aim is a material that derives its spectral response from the close coupling of its resonant entities that can potentially be influenced by external forces just in the same way as in liquid crystal display technology. Plasmonic metal nanoparticles are used in combination with organic linker molecules to realize the functional material. Only very few composite self organizing materials based on liquid crystals are demonstrated up to now. Several problems have to be considered when using liquid crystals for self-organization. Most notably, there is a considerable size difference between the liquid crystal molecule and the plasmonic nanoparticle. If the particle is small it can be easily incorporated into material designs leading to self-organization [1-4]. In such materials the plasmonic resonance is weak and they are optically not efficient. If particles are large and show strong electromagnetic resonances their self-organization gets more and more challenging. Often mixtures of a liquid crystal host and functionalized nanoparticles are studied [5]. But mixtures have the disadvantage that phase separation presents a serious problem leading to mixtures with only low concentration of nanoparticles that can be made. The precise control of distance of nanoparticles and their electromagnetic coupling in mixtures is equally difficult. Nevertheless examples exist that promise success to create coupled resonances of plasmonic particles with a narrow parameter window for particle size and particle concentration. In our approach we are seeking an entire material, having phase transitions and coupling of plasmonic resonances. Such a material needs rather larger plasmonic particles with diameters bigger than 3 nm, short distance order to keep the particles in place and a distance control mechanism between nanoparticles to allow high nanoparticle filling factor and to assure coupling. In our contribution we will present a first material with mesogen coated gold nanoparticles that fulfils these requirements.

In detail we use rod like nematic liquid crystal molecules that are grafted onto gold nanoparticles via spacers with adapted properties such as length and stiffness. Structural analysis is done by X-ray scattering experiments that revealed an arrangement of the nanoparticles in chains similar to the ones found in columnar phases but with short range order only. The short range order mediates the plasmonic coupling. Optical characterization with spectroscopic polarization microscope is done on oriented samples and allows for the determination of the combined effect of the ligands birefringence and the anisotropic arrangement of the plasmonic nanoparticles. For the material presented here, strong polarization dependence of the material's optical properties is found. A model is developed to understand the electromagnetic response based on structural date and supplementary measurements. The material studied is not a mixture but an entire material that is not affected by structural in-homogeneities known from liquid crystal defects. Our results demonstrate the ability to fabricate a self ordered and tunable metamaterial by chemical engineering of the nanoparticles with liquid crystalline mesogen ligands incorporating plasmonic resonances.

A B C D

Figure: Concept for the electromagnetic response evaluation of liquid crystalline metamaterials. A) The metallic nanoparticle (gold) is surrounded by different linker molecules that might carry mesogens which form liquid crystalline phases. B) This building blocks are described by optical uniform materials and positioned in space in C) as found by x-ray structural analysis. D) The electromagnetic response can be calculated for different incident polarizations and shows pronounced resonant behaviour.

This work received financial support from the European Union FP7 framework program under grant agreement No. 228455 NANOGOLD.

REFERENCES

1. L. Cseh and G. H. Mehl, „Structure–property relationships in nematic gold nanoparticles" J. Mater. Chem., 17, 311-315, 2007,
2. L. Cseh and G. H. Mehl, " The Design and Investigation of Room Temperature Thermotropic Nematic Gold Nanoparticles " J. Am. Chem. Soc., 128, 13376-13377, 2006
3. M. Wojcik, W. Lewandowski, J. Matraszek, et al. "Liquid-Crystalline Phases Made of Gold Nanoparticles" Angew. Chem., , 48, 5167-5169, 2009
4. J. W. Goodby, et al. "Transmission and Amplification of Information and Properties in Nanostructured Liquid Crystals." Angew. Chem. Int. Ed., 47: 2754–2787, 2008
5. H. K. Bisoyi and S. Kumar "Liquid-crystal nanoscience: an emerging avenue of soft self-assembly" Chem. Soc. Rev., 40, 306–319, 2011
6. G. L. Nealon, et al. "Liquid-crystalline nanoparticles: Hybrid design and mesophase structures" Beilstein J. Org. Chem. 8, 349–370, 2012

Effective index engineering using metal-dielectric metamaterials for silicon photonics applications

N. Dubrovina[1], X. Le Roux[1,2], R. Salas-Montiel[3], S. Blaize[3], A. de Lustrac[1], G. Lerondel[3], A. Lupu[1,2]
[1]Univ. Paris-Sud, Institut d'Electronique Fondamentale, UMR 8622, 91405 Orsay Cedex, France
[2]CNRS, Orsay, F-91405, France
[3]Laboratoire de Nanotechnologie et d'Instrumentation Optique, Institut Charles Delaunay, Université de Technologie de Troyes, 12 rue Marie Curie, BP 2060, 10010 Troyes Cedex, France
*anatole.lupu@u-psud.fr

Abstract- We report experimental and modeling results for the behavior of metallic metamaterials (MMs) in a guided wave configuration aimed to explore their potential for silicon photonics applications in the near-infrared (λ=1.5µm). The investigated approach consists in using a hybrid guiding structure made of metamaterial layer over a high index slab waveguide, as for instance silicon on insulator (SOI) in the present case. It is namely demonstrated that the effective index and the loss level in such hybrid waveguides can be carefully controlled with planar metallo-dielectric MMs.

There is sustained interest for the application of MMs due to their ability for an efficient tailoring of such an artificial composite media effective index [1-5]. Here we discuss the potential of hybrid MMs waveguides for silicon photonics applications. We consider the case of a composite guiding structure made of a single film of metamaterial above a silicon waveguide (Fig. 1). In such a configuration only the evanescent tail of the field interacts with the MMs layer, which acts essentially as a perturbation. Its role is to modify the effective index of the composite waveguide structure. The advantage of such a solution is to significantly reduce the propagation losses since the main part of the electromagnetic energy do not interact directly with the metallic part of the metamaterial.

The appropriate approach for modeling such a hybrid composite waveguide was described in our recent contributions [6,7]. It consists in approximating the entire structure that is, the Si layer and the metallic cut wires on top of it as a single dielectric slab guiding the signal by total internal reflection.

For our experiments we considered a 2D array of gold cut wires placed on the top of a silicon waveguide (Fig. 1a). The transmission spectral measurements performed in the spectral range between 1.25 and 1.64µm using an end-fire coupling setup, revealed a marked dip for TE polarized light, corresponding to the MMs resonance frequency obtained using HFSS numerical modeling. No such a dip in transmission was observed for TM polarized light, i.e. when the electric filed is perpendicular to the layers interface and the orientation of the cut wires.

The scanning near field optical microscopy experiments (SNOM), performed in the same spectral range, revealed for TE polarized light a strong enhancement of the electric field confined in the region between the end of the adjacent cut wires (Fig. 1b right). These results confirm the efficient excitation of the MMs resonance in a guided wave configuration for TE polarization.

The extraction of the MMs slab effective parameters, performed either from numerical simulations or experimental results, show that an array of gold coupled cut wires over a slab waveguide leads to a significant local variation of the slab effective index in the vicinity of the resonance. The ability for the local engineering of the effective index based on the interaction of the evanescent tail with the MMs layer and control in such a way the light flow in a guiding slab layer constitutes a real opportunity to design a novel class of photonic devices.

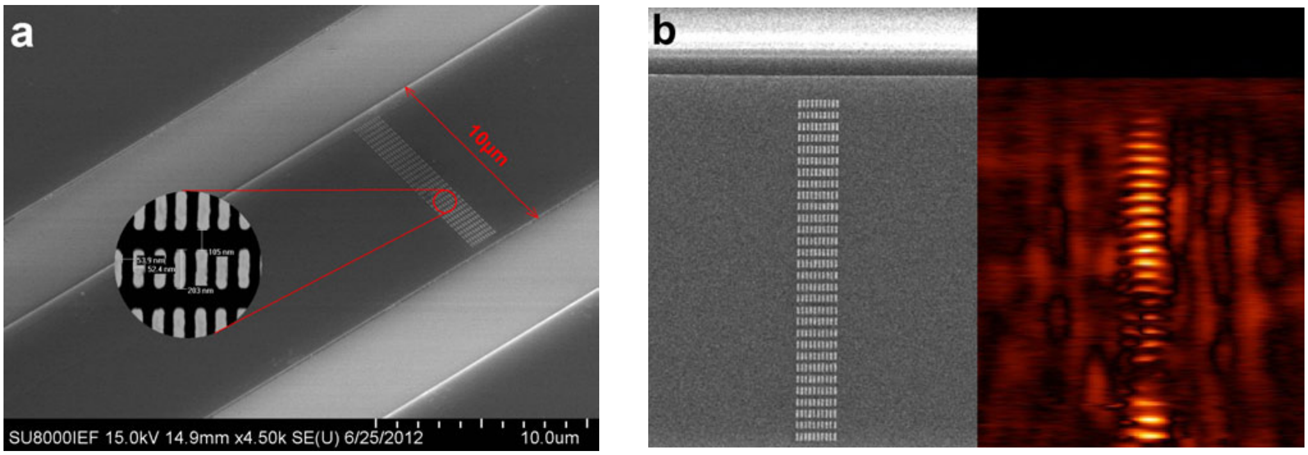

Fig. 1. a) SEM view of a 10µm wide SOI waveguide with MM area (inset); b) MM area on SOI waveguide SEM view (left) and SNOM view (right).

In summary, the investigated approach shows that dispersion and guiding properties of photonic waveguides can be carefully controlled with planar metallo-dielectric MMs, paving thus the way for new optical functionalities.

Acknowledgements

This work was supported by the French National Research Agency (ANR Metaphotonique, contract number 7452RA09) and the Champagne-Ardenne region.

REFERENCES

1. J.B. Pendry, “Negative refraction makes a perfect lens,” Phys. Rev. Lett. **85**, 3966 (2000).
2. J. Zhou, T. Koschny, M. Kafesaki, and C. M. Soukoulis, “Negative refractive index response of weakly and strongly coupled optical metamaterials,” Phys. Rev. B **80**, 035109 (2009).
3. C. Menzel, C. Rockstuhl, T. Paul, and F. Lederer, “Retrieving effective parameters for metamaterials at oblique incidence,” Phys. Rev. B **77**, 195328 (2008).
4. C. Menzel, R. Singh, C. Rockstuhl, W. Zhang, and F. Lederer, “Effective properties of terahertz double split-ring resonators at oblique incidence,” J. Opt. Soc. Am. B **26**, B143-B147 (2009).
5. N. Dubrovina, L. Le Cunff, N. Burokur, R. Ghasemi, A. Degiron, A. De Lustrac, A. Vial, G. Lerondel, and A. Lupu, “Single metafilm effective medium behavior in optical domain: Maxwell-Garnett approximation and beyond,” Applied Physics A **109**, 901-906 (2012).
6. A. Lupu, N. Dubrovina, R. Ghasemi, A. Degiron, and A. de Lustrac, “Metal–dielectric metamaterials for guided wave silicon photonics,” Opt. Express **19**, 24746–24761 (2011).
7. A. Lupu, N. Dubrovina, R. Ghasemi, A. Degiron, A. de Lustrac, “Metal-dielectric metamaterials for guided optics applications,” Proc. SPIE 8423, 842306 (2012).

Laser welding of polymer foils by using plasmon resonance of gold nanoparticles

Andreas Heilmann
Fraunhofer Institute for Mechanics of Materials IWM
Walter-Hülse-Straße 1, 06120 Halle (Saale), Germany
andreas.heilmann@iwmh.fraunhofer.de

The optical properties of metallic nanoparticles embedded in organic matrices are determined by their size and shape distribution as well as by their spatial arrangement in the surrounding media [1]. Additionally, the optical properties of the surrounding matrix have to be considered to describe the optical properties of the composite media [2]. If the nanoparticles are embedded in an optical transparent medium (e.g. polymers), laser irradiation can induce structural changes at the irradiated areas [3,4]. The Laser irradiation can stimulate diffusion processes like reshaping and coalescence and, finally, melting of the nanoparticles. Otherwise, melting and finally pyrolysis of the embedding media can occur. By using ultra-short laser pulses, parallel arrangements of nanoparticles can be achieved by spatially limited diffusion processes [5].
Laser welding of transparent polymer materials requires an optical absorber placed in the interface between the two welding partners. Usually, dye molecules with absorption properties adapted to the laser wavelength are used as absorbers. At a well-defined temperature, the dye molecules will be chemically modified, and transparent laser welding seams can be achieved.
On samples of ethylene-tetrafluoroethylene foils (thickness 200 µm), gold nanoparticles were deposited by radio frequency (r.f.) magnetron sputtering at high vacuum (10^{-3} Pa) conditions. Using different positions of the samples in the reactor geometry, nanoparticle layers with homogeneous metal content or with a continuous gradient of the metal area filling factor were achieved. Simple mask technologies were used to get line-wise coatings with different widths for laser irradiation and formation of welding seams. Finally, a layer with a thickness of about 50 nm was deposited by r.f. plasma polymerization of the monomer hexamethyldisilazane (HMDSN). This optical transparent protection layer stabilizes the gold layer against mechanical influences.
For laser welding, a coated ETFE foil and an uncoated foil were brought into direct contact. These foils were irradiated line-wise in perpendicular incidence. A continuous wave diode laser at 808 nm wavelength was moved over the foils. The nearly Gaussian intensity profile of the laser beam was split to a laser spot diameter of approximately 3 mm. The excitation of the plasmon resonance and the following heating of the interface between two joining partners are sufficient to weld polymer foils with high melting points. After laser irradiation, the welding seams become transparent, caused by a new metal nanoparticle arrangement.
The morphology of the gold nanolayer before and after Laser welding was determined by transmission electron microscopy (TEM). Optical properties of the multilayer system before and after the laser welding were recorded in the UV-Vis wavelength range by a conventional double beam spectrometer. For determination of the mechanical tensile strength R_m of the welding seams, tensile tests were performed on strip samples by using a universal testing machine. The tensile strength is with $R_m \approx 30$ N/mm² lower than that of conventional thermal welding seams (42 N/mm²). but substantially higher than the limit for technical application. Up to now, similar results were found for other noble metals like silver and copper. It was the longtime mechanical properties of the laser welds fulfill the requirements which are necessary for applications.

[1] U. Kreibig; M. Vollmer: Optical Properties of Metal Clusters (Springer , Berlin, 1995)
[2] A. Heilmann: Polymer Films with Embedded Metal Nanoparticles (Springer, 2003)
[3] A. Heilmann, J. Werner, F. Homilus, F. Mueller, J. Adhes. Sci. Technol., 9, 1181 (1995).
[4] M. Sendova-Vassileva, M. Sendova, A. Troutt, Applied Physics A 81, 871-875 (2005)
[5] K. Loeschner, G. Seifert, A. Heilmann, J. Appl. Phys. 108, 073114 (2010)

Fabrication approaches for plasmon-improved photovoltaic cells

C. Gritti[1], **R. Malureanu**[1*], **B. Kardynal**[2], **A. V. Lavrinenko**[1]
[1] Department of Photonics Engineering, Technical University of Denmark, Kgs. Lyngby 2800, Denmark
[2] FZ-Juelich, Forschungszentrum Jülich, Wilhelm-Johnen-Strasse 52425 Jülich, Germany
[*]corresponding author: rmal@fotonik.dtu.dk

Abstract-During this talk we will present various fabrication approaches to improve the performance of photovoltaic (PV) cells by using metallic nanoparticles in order to generate photocurrent below the bandgap. This effect is possible due to the generation of surface plasmon polaritons (SPPs) in optimized nanoparticles.

Small metal nanoparticles(NPs) may, in certain conditions, absorb the incoming photons and generate SPPs that add to the photocurrent generated within a PV cell [1-3]. Since the frequency of the absorbed light is defined by the particle size, shape and placement, it can be adjusted such that it lies below the bandgap of the photovoltaic cell material. This way the light that would otherwise be lost is used for increasing the PV cell efficiency [4, 5].

Our initial choice of metal was Au. Although Au is not the best metal available for SPP propagation, it has the advantage of being a noble metal thus its properties are not changing in time as for example the ones of Ag do. Still, the low surface adhesion of Au on GaAs or Si, the materials of choice for PV cells, introduces an extra step in the fabrication process. Thus, before Au deposition, a thin layer of Ti must be used. We believe that this thin Ti layer may limit the Au performance to a point where the increase in absorption is hardly observable. During the talk we will present several attempts where the Au nanoparticles, although similar in shape and size and matching the dimensions of the simulated ones, show no absorption increase (see figure 1).

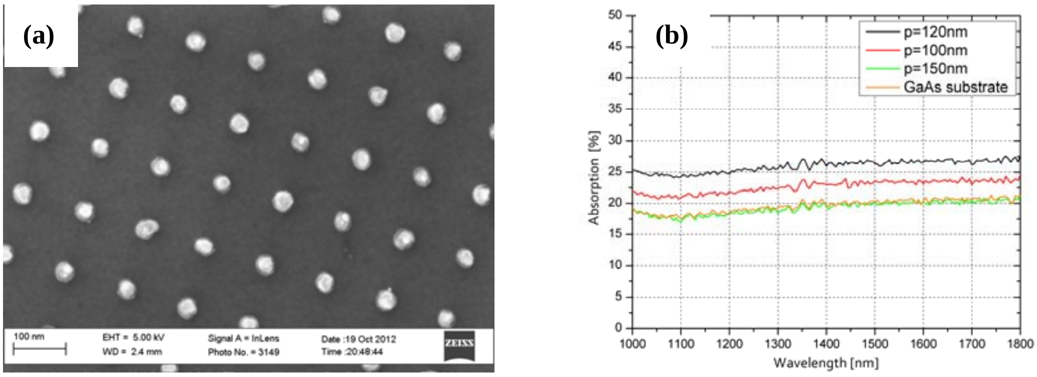

Figure 1. (a) SEM image of typical Au nanoparticles. The period of the particles is 100nm while their size is of 35nm. (b) absorption graphs for Au nanoparticles with different periodicities. Although measured in a big frequency range, the nanoparticles show no resonant absorption.

Due to these difficulties in utilizing Au NPs, as well as better behavior of the Ag particles [6] we decided to switch to Ag ones. The change in materials came with new challenges. On one side, the Ag is less stable than Au thus the deposition process needs to be altered. Also, the dimensions of the particles are now at the limit of the electron beam lithography(EBL) technique, thus making them more expensive and difficult to fabricate. Due to these two aspects we decided to try, apart from the EBL technique, electroless deposition of Ag nanoparticles on the desired substrate. This deposition method has the advantage of being cheap, large scale and the particle size can be accurately controlled. Also, the stability of the grown particles is much higher than the one of the evaporated ones. The disadvantage of this technique is brought by its sensitivity to the NP growth to the surface chemistry. Thus, the same recipe will give completely different results in terms of crystal size and shape if used for Si or GaAs substrates (see figure 2). Thus, although the filling fraction is of about 46% for both cases, in the Si one the average particle size is about 8 times smaller than in the GaAs one. During the talk we will present various approaches for controlling the growth on these substrates.

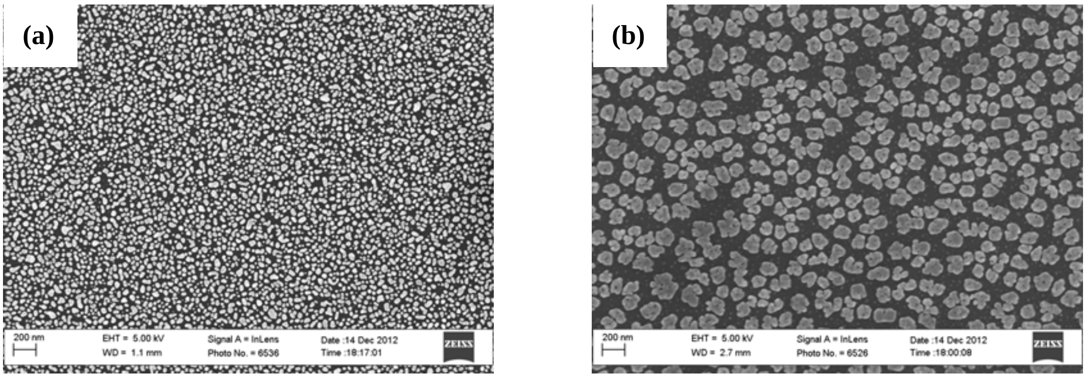

Figure 2. Difference in the growth of the nanoparticles on Si(a) and GaAs(b). The two samples were fabricated in the same time and using the same recipe thus the only varying parameter is the surface property one.

Acknowledgements, R.M., and A.L. wish to acknowledge the FTP THzCOW project for partial financial support.

REFERENCES

1. Atwater, H.A., and Polman, A., “Plasmonics for improved photovoltaic devices,” *Nat. Mat.*, Vol. 9, 205-213, 2010.
2. Moulin, E., Luo, P., Pieters, B., Sukmanowski, J., Kirchhoff, J., Reetz, W., Muller, T., Carius, R., Royer, F.–X., and Stiebig, H., “Photoresponse enhancement in the near infrared wavelength range of ultrathin amorphous silicon photosensitive devices by integration of silver nanoparticles,” *Appl. Phys.Lett.,* Vol. 93, 033505, 2009.
3. Nishijima, Y., Ueno, K., Yokota, Y., Murakoshi, K., and Misawa, H., “Plasmon-Assisted Photocurrent Generation from Visible to Near-Infrared Wavelength Using a Au-Nanorods/TiO2 Electrode,” *J. Phys. Chem. Lett.*, Vol. 1, 2031-2036, 2010
4. Novitsky, A., Uskov, A. V., Gritti, C., Protsenko, I. E., Kardynał, B. E., and Lavrinenko, A. V., “Photon absorption and photocurrent in solar cells below semiconductor bandgap due to electron photoemission from plasmonic nanoantennas,” *Progress in Photovoltaics*, doi: 10.1002/pip.2278
5. Nakayama, K., Tanabe, K., and Atwater, H. A., “Plasmonic nanoparticle enhanced light absorption in GaAs solar cells,” *Appl. Phys. Lett.*, Vol. 92, 121904, 2008
6. Yu E.T., *Nanoplasmonics for Photovoltaic Applications*, CRC Press, 2010

Plasmonic nanocomposites based on branched gold nanoparticles within mesoporous silica thin films

P. C. Angelomé,[1] I. Pastoriza-Santos,[1] J. Pérez-Juste,[1] A. Zelcer,[2] G. Soler-Illia,[2] and L. M. Liz-Marzán[1,3,4]
[1] Departamento de Química Física, Universidade de Vigo, 36310, Vigo, Spain
[2] Gerencia de Química, Centro Atómico Constituyentes, Comisión Nacional de Energía Atómica, Av. Gral Paz 1499, B1650KNA, San Martín, Buenos Aires, Argentina
[3] Bionanoplasmonics Laboratory, CIC biomaGUNE, Paseo de Miramón 182, 20009 Donostia-San Sebastián, Spain
[4] Ikerbasque, Basque Foundation for Science, 48011 Bilbao, Spain
[*]corresponding author: pastoriza@uvigo.es

Abstract- Composite materials made of mesoporous oxide thin films containing metallic nanoparticles are of high interest in various fields, including catalysis, biosensing and non-linear optics. We demonstrate in this work the fabrication of such composite materials containing a sub-monolayer of gold nanoparticles (GNPs) of various shapes covered with mesoporous silica thin films.

In this work we have demonstrated that it is possible to obtain composite materials containing a submonolayer of gold nanoparticles with arbitrary shapes covered with mesoporous silica thin films. We have also demonstrated that the shape of the particles, and thus their optical properties, can be modified by standard seeded growth. By adjusting the CTAB and ascorbic acid concentration the anisotropy of the grown nanoparticles can be varied (see Figure 1), so that they can branch through the pores of the mesoporous silica film, which is also influenced by the pore size of the mesoporous film. When the interpore distance is increased from 6 up to 12 nm, the final morphology varies from isotropic to anisotropic or branched structures. The obtained composite materials combine the interesting optical properties of metal nanoparticles (which can be tuned through the reaction conditions), the filtering ability of mesoporous thin films and the chemical reactivity of silica. All these properties combined in one single composite material opens up the possibility of applications in several fields, including catalysis, (bio)sensing and non-linear optics.

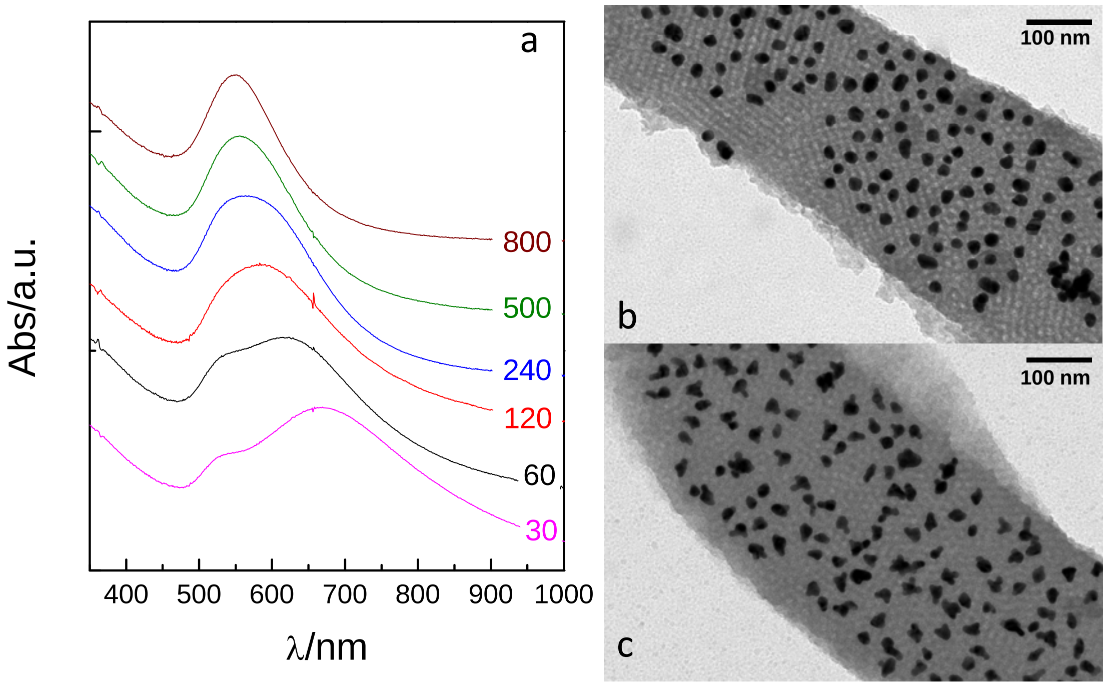

Figure 1. Effect of [CTAB] on the growth of mesoporous thin films with Au (**a**) UV-visible spectra as a function of [CTAB]/[Au] (as indicated in the labels) after 6h of reaction. Representative TEM images of the highest (**b**) and the lowest (**c**) [CTAB].

Photoswitchable perfect absorber at visible frequency

M. K. Hedayati[1], **M. Javaherirahim**[1], **M. Elbahri**[1, 2]

[1] Nanochemistry and Nanoengineering, Institute for Materials Science, Faculty of Engineering, University of Kiel, Kaiserstrasse 2, 24143 Kiel, Germany

[2] Institute of Polymer Research, Helmholtz-Zentrum Geesthacht, Max-Planck-Str. 1, 21502 Geesthacht, Germany

*corresponding author: me@tf.uni-kiel.de

Abstract- Here in this work, we show a new class of photo-switchable perfect absorber working at visible frequency whereas its resonance peak could be broaden upon illumination by ultraviolet light. The structure is simply composed of a optically thick gold film covered by a thin polymer-spirophenanthrooxazine composite film. The as-deposited film have a high absorption band in UV to green part of spectrum whilst the band-width can be broaden up to 600nm wavelength by few seconds UV irradiation and at the same time the absorption intensity enhances. Because of the fast response of the system to light, it might pave the way for implementation of perfect absorber as an efficient optical sensor and smart imaging devices.

The absorption loss is generally obviated as an obstacle against the improvement of Metamaterial's (MM) performance, nevertheless it has received wide-spread research attention once its potential for host of application recognized. Since the first experimental results on fabrication of highly MM absorber, different strategy have been proposed and implemented to realize perfect absorber composite at different frequency ranging from GHz to visible. So far most of the trends oriented in way to improve the efficiency of passive metamaterials, but due to the ever-increasing demand of fast nonlinearities for switching light with light and control of the electromagnetic properties of matter with external stimuli, the new field of active metamaterials (aka Metadevices) drawn the attentions. The well known idea for design and fabrication of metadevices is structure tunable metamaterials [1-2] however its response is slow. Up to now variety of fast response metadevices have been realized so far working at Gigahertz [3], Mid-Infrared [4], Terahertz [5], but realization of active metamaterials working at visible is difficult. In this work, we implement a new coating layer which is a composite out of a dispersive molecules (spirophenanthrooxazine (SPO)) as a photochromic molecule) which can tune the reflectivity of the base layer by UV or white light [6]. The composite with proper thickness and composition can diminish the reflection of metal down to 10% by UV illumination and turn the optically thick gold film (block the light transmission) to a photo-switchable super absorber (Figure 1 (left)). On the other hand, having illuminated the film by a UV light source, the SPO molecules turns to photomerocyanine (PMC) and absorb the light at 600nm wavelength enhancing the absorption of the system which illustrate the dynamic functionality of the stack. Although the absorption of molecule deposited on glass does not exceed 20% after UV irradiation (Figure 1(right)), it enhances around 4 times of initial magnitude reaching 90% when it comes close to metallic film. In addition, the absorption band of the molecule deposited on glass which appeared at 568nm shift to 584nm once it get close to gold film. The interaction of polarized molecule (PMC) and its induced charges into the metallic film is mainly the origin of the mentioned phenomena which will be discussed in details.

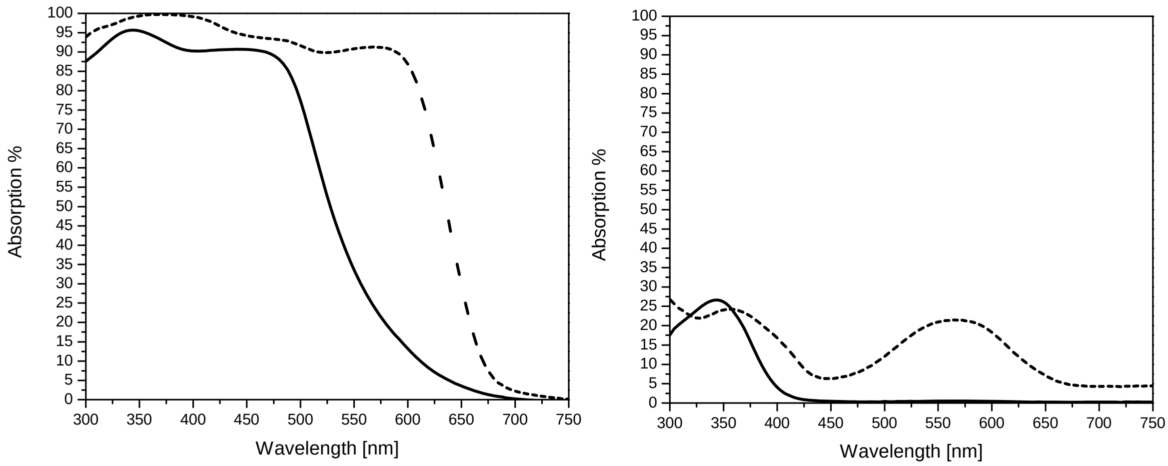

Figure 1: Absorption spectra of PS-SPO composite with 50% concentration (solid line) as deposited, (dashed line) upon UV irradiation deposited on (left) 100nm gold, (right) glass.

Acknowledgements, We gratefully acknowledge the financial support by the German Research Foundation (DFG) through the projects EL 554/1-1 and SFB 677 (C1,C9). M.E. would like to thank the Initiative and Networking Fund of the Helmholtz Association's (grant No. VH-NG-523) for providing the financial base for the start-up of his research group. We wish also to express our gratitude to Prof. Faupel who allowed us to use his Lab's facilities and equipments.

REFERENCES

1. Powell, D. , Gorkunov, M., Shadrivov, I., Marqués, R., Kivshar, Y., "Structural tunability in metamaterials," *Appl. Phys. Lett.*, Vol. 95, 084105 (2009)
2. Boardman, A. D., Grimalsky, V. V., Kivshar, Y. S., Koshevaya, S. V., Lapine, M., Litchinitser, N. M., Malnev, V. N., Noginov, M., Rapoport, Y. G. and Shalaev, V. M., "Active and tunable metamaterials," , *Laser & Photon. Rev.* Vol. 5, 287 (2010)
3. Zhu, B., Feng, Y., Zhao, J., Huang, C. and Jiang, T., "Switchable metamaterial reflector/absorber for different polarized electromagnetic waves,", *Appl. Phys. Lett.*, Vol. 97, 051906 (2010)
4. Miao, X., Passmore, B., Gin, A., Langston, W., Vangala, S., Goodhue, W., Shaner, E. and Brener, I., "Doping tunable resonance: Toward electrically tunable mid-infrared metamaterials," *Appl. Phys. Lett.*, Vol. 96, 101111 (2010)
5. Chen, H., Padilla, W. J., Zide, J. M. O., Gossard, A. C., Taylor, A. J. and Averitt, R. D., "Active terahertz metamaterial devices," *Nature* Vol. 444, 597 (2006)
6. Jamali, M., Hedayati, M.K., Mozooni, B., Javaherirahim, M., Abdelaziz, R., Zillohu, A.U., Elbahri, M., "Photoresponsive Transparent Conductive Metal with a Photobleaching Nose," *Adv. Mater.*, Vol. 23, 4243 (2011)

Design, fabrication and characterization of a new transparent conductor based on plasmonic nanocomposite

M. K. Hedayati[1], M. Javaherirahim[1], T. Strunskus[2], F. Faupel[2] and M. Elbahri [1,3]

[1] Nanochemistry and Nanoengineering, Institute for Materials Science, Faculty of Engineering, University of Kiel, Kaiserstrasse 2, 24143 Kiel, Germany

[2] Multicomponent Materials, Institute for Materials Science, Faculty of Engineering, University of Kiel, Kaiserstrasse 2, 24143 Kiel, Germany

[3] Institute of Polymer Research, Helmholtz-Zentrum Geesthacht, Max-Planck-Str. 1, 21502 Geesthacht, Germany

[*]corresponding author: me@tf.uni-kiel.de

Abstract-Plasmonic nanoparticles are widely recognized as heat generator due to their large optical cross section and low quantum yield. Their strong localized electric field routing from the excitation of plasmon resonance which is dependent on the type, size and shape of the particles. Even though nanoparticles have been extensively studied for variety of application, implementation of particles with diameter much smaller than the incident wavelength (<10nm) for guiding the light (energy) is discredited because of their huge intrinsic losses. Here in this work, we showed fabrication and characterization of a transparent conductor (TC) based on a plasmonic nanocomposite out of metallic particles smaller than 5 nanometers and thin metallic film showing a wide-band transparency in visible spectrum. Despite a little loss in blue part of spectrum, the particles tune the dielectric of the hosting matrix and provide high optical transparency (compared to the bare film) demonstrating an efficient plasmonic TC which can leverage using of ultra-small nanostructure for photovoltaic applications.

Traditionally, indium tin oxide (ITO) has been widely implemented as a standard transparent conductor (TC) in different kinds of optoelectronic devices. Due to the increasing demand of ITO for consumer electronics and the low abundance of indium, the price of ITO has continually increased throughout the past decade. Therefore great efforts have been made to develop new kind of TCs to replace ITO. In this regard different materials and composite proposed and studied including conductive polymers [1], carbon nanotubes (CNTs), graphene [2], metal grids [3], and random networks of metallic nanowires [4]. But so far none of them could be used as a replacing material, since either they are fragile and brittle or their electrical conductivity is below the typical ITO.

Thin metallic films due to their high electrical conductivity could be one of the best replacing materials for ITO, however their poor transparency makes their application as TCs limited. Recently a new plasmonic coating method is developed in our group to improve the optical transparency of the thin metallic film with the aid of dipole-dipole interaction [5]. Here, based on our recent finding, we tried to improve the performance of the developed structures and analyze its optical performances thoroughly.

With the optimized condition, the relative transparency enhancement up to 100% achieved in a limited range of visible spectrum. The electrical conductivity measurement also showed that the resistance of the structure is comparable to bulk metal showing that this device could be used as a new transparent conductive film.

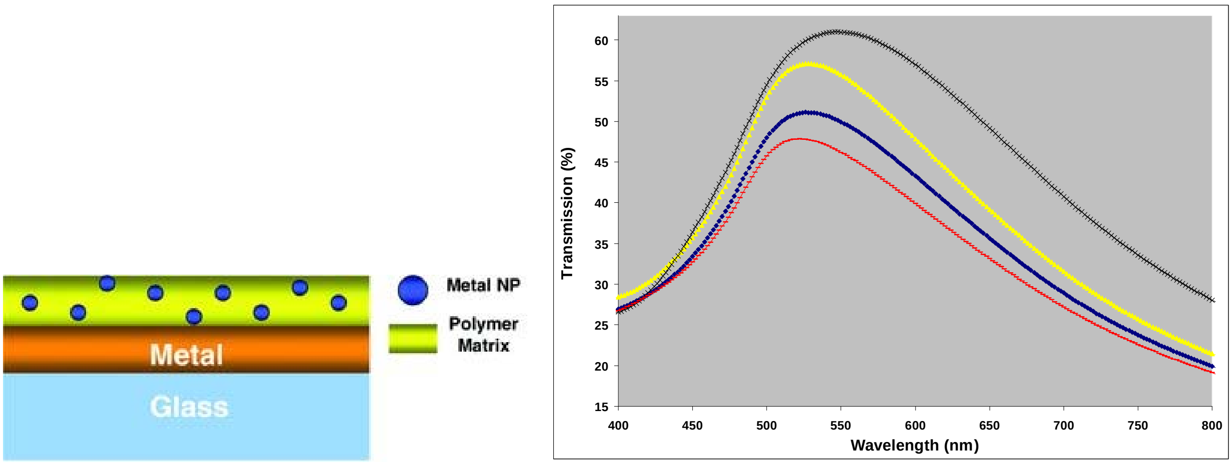

Figures 1: (left) schematic of the multi-stack layer used in the present study which is composed of 20nm thin gold (or silver) metallic film and 20 nm nanocomposite (silver-Teflon or Silver-Silicon dioxide) atop. (right) Transmission spectra of the multi-stack for different thickness and composition. Red curve is the transmission spectra of 20nm gold film shown as reference.

REFERENCES

1. Fehse, K. Walzer, K., Leo, K., Lövenich, W., Elschner, A., "Highly Conductive Polymer Anodes as Replacements for Inorganic Materials in High-Efficiency Organic Light-Emitting Diodes," *Adv.Mater.,*Vol. 19, 441-444, 2007.
2. Kim, K. S., Zhao, Y., Jang, H., Lee, S. Y., Kim, J. M., Kim, K. S., Ahn, J, Kim, P., Choi, J., Hong, B. H., "Large-scale pattern growth of graphene films for stretchable transparent electrodes," *Nature* Vol. 457, 706-710, 2009.
3. Kang, M., Kim, M., Kim, J., Guo, L., "Organic Solar Cells Using Nanoimprinted Transparent Metal Electrodes," *Adv.Mater.,*Vol. 20, 4408-4413, 20088.
4. De, S., Higgins, T., Lyons, P., Doherty, E., Nirmalraj, P., Blau, W., Boland, J, Coleman, J., " Silver Nanowire Networks as Flexible, Transparent, Conducting Films: Extremely High DC to Optical Conductivity Ratios," *ACS nano* Vol. 3, 1767-1774, 2009.
5. Elbahri, M., Hedayati, M. K., Chakravadhanula, V. S. K., Jamali, M., Strunkus, T., Zaporochentko, V., Faupel, F., " An Omnidirectional Transparent Conducting-Metal-Based Plasmonic Nanocomposite," *Adv.Mater.,*Vol. 23, 1993-1997, 2011.

Manipulation of Light Scattering by Plasmonic Nanocomposite Structures

Venkata Ananth Tamma, Yonghao Cui, Jianhong Zhou and Wounjhang Park*
Department of Electrical Computer and Energy Engineering, University of Colorado,
Boulder CO, 80309-0425, U.S.A.
*corresponding author: won.park@colorado.edu

Abstract-We present two different types of plasmonic nanostructures that could significantly modify light scattering. One is an array of gold nanowires offering a plasmonic cover to achieve cancellation of induced dipole moments. The other is hepmaters made of gold nanorods which enables unique orientation dependence. Detailed theoretical and experimental results will be presented.

Recently, there has been much interest in plasmonic molecules in which individual plasmon resonances couple together to form new resonances extended over the entire structures in a manner analogous to the formation of molecular orbitals. One of the representative structures widely studied by many groups is a heptamer composed of seven nanoparticles in a hexagonal configuration. One of the unique properties of a heptamer is the Fano resonance it supports. Fano resonance results from the interaction between bright and dark modes and typically manifests itself as a strongly suppressed scattering cross-section at the resonance wavelength. Recently, we have studied the effect of symmetry on the Fano resonance and shown that the nature of the modes is preserved even under the lowered symmetry.[1] In this presentation, we will further probe the nature of the plasmon hybridization by constructing the heptamer structure with nanorods instead of nanocylinders. In nanorods, the originally degenerate modes of nanocylinder are split and thus we can control the hybridization with the orientation of the nanorods.

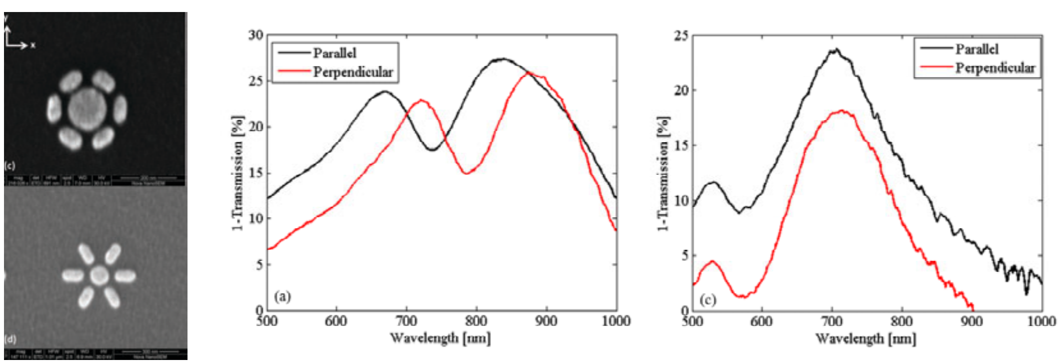

(a) (b) (c)

Fig. 1. (a) Scanning electron micrographs of nanorod heptamers with nanorods arranged azimuthally (top) and radially (bottom). Experimentally measured extinction spectra for (b) azimuthal and (c) radial heptamers.

Fig. 1(a) shows the scanning electron micrographs (SEMs) of nanorod heptamers with nanorods arranged azimuthally and radially. The fabrication was initially done on silicon substrate and later transferred to a flexible elastomer for application of mechanical stress. Fig 1(b) and (c) are experimentally measured extinction spectra for the azimuthal and radial heptamers. It was apparent azimuthal heptamer supported Fano resonance and radial heptamer did not. We confirmed this observation by conducting extensive numerical simulations over a wide range of structural parameters. This result indicates that the Fano resonance observed in circular heptamer structures originates from the azimuthally aligned dipole modes and radial components do not contribute. Also, we conducted group theoretical analysis on both azimuthal and radial heptamer structures and show how the symmetry lowering affects the resonances. In particular, we show an originally optically inactive mode is transformed into an optically active mode by symmetry lowering.

The second part of this presentation will discuss the use of gold nanorwires to cancel induced dipole moment and achieve scattering reduction. When the scattering object is small enough, the light scattering is dominantly determined by the induced dipole moment which in turn is related to the permittivity of the material. If the object is coated with a negative permittivity material, it is possible to achieve a zero net dipole moment and thus zero scattering cross-section.[2] To implement this, it is required to have a material with modest negative permittivity, which in our work was accomplished by an array of nanowires. Fig 2(a) shows the SEM of gold nanowires fabricated on the sidewall of a silicon nanorod. This was accomplished by a combination of electron-beam lithography and focused ion beam milling.

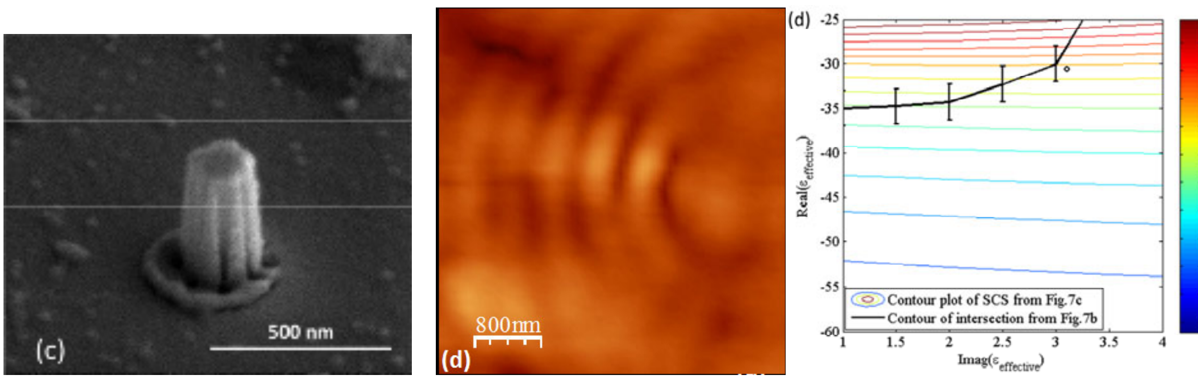

(a) (b) (c)

Fig. 2 (a) SEM of gold nanowire coated silicon nanorod for scattering cancellation device (b) NSOM image of the interference fringes due to the scattered light. (c) Contour plot of scattering cross-section for real and imaginary part of permittivity. Open circle shows the measured value, which corresponds to scattering reduction of 9.5 dB.

The light scattering was then measured by near-field scanning optical microscope which accurately determined the interference fringes produced by the scattering light, as shown in Fig. 2(b). We developed a theory relating the interference fringe curvature to the scattering cross-section so that we can determine the scattering cross-section from the measured fringe curvature. The result is summarized in Fig. 2(c) where the scattering cross-section and fringe curvature are calculated for a range of effective complex permittivity of the coating layer. The solid line is the contour of complex permittivity values that should result in the measured fringe curvature. The graph clearly shows there is a cutoff, indicating that the measured value of curvature indicates a minimum of ~7 dB scattering reduction. Comparing with other data such as the positions of the fringe peaks and valleys, we were able to determine the scattering reduction in our device was 9.5 dB, as indicated by an open circle in Fig. 2(c). Details of the analysis and additional data concerning the reference samples will be presented and discussed at the conference.

REFERENCES

1. Y. Cui, J. Zhou, V. A. Tamma, and W. Park, "Dynamic Tuning and Symmetry Lowering of Fano Resonance in Plasmonic Nanostructure," ACS Nano **6**, 2385–2393 (2012).
2. A. Alù and N. Engheta, "Cloaking a Sensor," Phys. Rev. Lett. **102**, 233901 (2009).

Tailoring Plasmonic Nanocomposites by Vapor Phase Deposition

M. K. Hedayati[2], A. Biswas[1,4], H Takele[1,5] T. Strunskus[1], M. Elbahri[2,3], and F. Faupel[1]*

[1]Christian-Albrechts University at Kiel, Institute for Materials Science - Multicomponent Materials, Kaiserstr. 2, 24143 Kiel, Germany

[2]Christian-Albrechts University at Kiel, Institute for Materials Science -Nanochemistry and Nanoengineering, Kaiserstr. 2, 24143 Kiel, Germany

[3]Institute of Polymer Research, Helmholtz-Zentrum Geesthacht, Max-Planck-Str. 1, 21502 Geesthacht, Germany

4now: Center for Nano Science and Technology, University of Notre Dame

[5]now: Oled Technologies & Solutions B.V.

*ff@tf.uni-kiel.de

Abstract-Plasmonic nanocomposites containing metallic nanoparticles in a dielectric matrix can be tailored by vapor phase co-deposition. Formation of the nanostructure occurs through self-organization and does not require e-beam lithography. Examples presented include transparent conducting metal coatings, perfect plasmonic absorbers, and photoswitchable nanocomposites.

Plasmonic nanocomposites consisting of metal nanoparticles embedded in a dielectric organic or inorganic matrix have a host of applications ranging from simple color filters to complex metamaterials. The present talk is concerned with vapor phase deposition of nanocomposites [1] and the resulting plasmonic properties. Deposition techniques include evaporation [2] and magnetron co-sputtering [3] of the matrix and metallic components and the combination of a gas phase aggregation cluster source with plasma polymerization or magnetron sputtering. In contrast to the production of plasmonic nanostructures by e-beam lithography, the nanocomposites form by self-organization which allows large-scale deposition. It will be shown how the plasmonic properties can be tailored via the incorporation of metallic clusters with well-defined composition, filling factor, and filling factor profile into various matrices [4-8]. Examples involve transparent conducting metal coatings [9], perfect plasmonic absorbers [10] and photoswitchable nanocomposites.

Acknowledgements-We will always remember Vladimir Zaporojtchenko who was strongly involved in all our work on functional nanocomposites and who passed away much too soon. Financial support by DFG within the Collaborative Research Centers TR24 and SFB 677 is acknowledged.

REFERENCES

1. F. Faupel, V. Zaporojtchenko, T. Strunskus, M. Elbahri, “Metal-Polymer Nanocomposites for Functional Applications”, *Adv. Eng. Mater.* 12, 1177, 2010.
2. A. Biswas, Z. Márton, J. Kruse, J. Kanzow, V. Zaporojtchenko, F. Faupel, and T. Strunskus, “Controlled generation of Ni nanoparticles in the capping layers of Teflon AF by vapor phase tandem evaporation”, *Nano Letters* 3, 69, 2003.
3. U. Schürmann, H. Takele, V. Zaporojtchenko, and F. Faupel, “Optical and electrical properties of poymer metal nanocomposites prepared by magnetron co-sputtering”, *Thin Solid Films* 515, 801, 2006.
4. A. Biswas, O. C. Aktas, U. Schürmann, U. Saeed, V. Zaporojtchenko, T. Strunskus, and F. Faupel, “Tunable

multiple plasmon resonance wavelengths response from multicomponent polymer-metal nanocomposite systems", *App. Phys. Lett.* 84, 2655, 2004.

5. H. Takele, H. Greve, C. Pochstein, V. Zaporojtchenko, and F. Faupel, "Plasmonic properties of Ag nanoclusters in various polymer matrices", *Nanotechnology* 17, 3499, 2006.
6. V. S. K. Chakravadhanula, M. Elbahri, U. Schürmann, H. Greve, H. Takele, V. Zaporojtchenko, and F. Faupel, "Equal intensity double plasmon resonance of bimetallic quasi-nanocomposites based on sandwich geometry", *Nanotechnology* 19, 225302/1, 2008.
7. H. Takele Beyene, V.S.K. Chakravadhanula, C. Hanisch, M. Elbahri, T. Strunskus, V. Zaporojtchenko, L. Kienle, and F. Faupel, "Preparation and plasmonic properties of polymer based composites containing Ag-Au alloy nanoparticles produced by vapor phase co-deposition" J. Mater. Sci. 45, 5865, 2010.
8. H. T. Beyene, V. S. K. Chakravadhanula, C. Hanisch, T. Strunskus, V. Zaporojtchenko, M. Elbahri, and F. Faupel "Vapor Phase Deposition, Structure, and Plasmonic Properties of Polymer-Based Composites Containing Ag-Cu Bimetallic Nanoparticles", *Plasmonics* 7, 107, 2012.
9. M. Elbahri, M. K. Hedayati, V. S. K. Chakravadhanula, M. Jamali, T. Strunkus, V. Zaporojtchenko, and F. Faupel, "An Omnidirectional Transparent Conducting-Metal-Based Plasmonic Nanocomposite" Adv. Mater., 23, 1993 2011.
10. M. K. Hedayati, M. Javaherirahim, B. Mozooni, R. Abdelaziz, A. Tavassolizadeh, V. S. K. Chakravadhanula, V. Zaporojtchenko, T. Strunskus, F. Faupel, and M. Elbahri, "Design of a Perfect Black Absorber at Visible Frequencies Using Plasmonic Materials", Adv. Mater. 23, 5410, 2011.

Metamaterials for Broadband Linear Polarization Conversion and Near-Perfect Anomalous Reflection and Transmission

Nathaniel Grady[1], Jane Heyes[1], Dibakar Roy Chowdhury[1], Yong Zeng[2], Antoinette J. Taylor[1], Diego A. R. Dalvit[2], and Hou-Tong Chen[1*]

[1] Center for Integrated Nanotechnologies, Los Alamos National Laboratory, Los Alamos, New Mexico 87545, USA
[2] T-4, Los Alamos National Laboratory, Los Alamos, New Mexico 87545, USA
*Corresponding author: chenht@lanl.gov

Abstract-We demonstrated high efficiency broadband metamaterial linear polarization converter using planar metamaterial structures in the terahertz frequency range. The structures were further used to demonstrate nearly perfect anomalous reflection and transmission by introducing a phase gradient in the metamaterials. Results from numerical simulations, experimental measurements, and semi-analytical modeling revealed excellent agreement.

The polarization state is one of the basic properties of electromagnetic waves conveying valuable information that is important in transmitting signals and making sensitive measurements. There have been a few efforts in exploiting metamaterials for polarization control and manipulation. Many metamaterial basic building blocks, such as split-ring resonators, are essentially anisotropic exhibiting birefringence effect, which can be used to construct wave plates when multi-layered planar metamaterials are employed. They attracted particular interest in the terahertz frequency range [1,2], due to the lack of suitable materials for functional device applications [3]. However, they are usually with narrow bandwidth and quite often suffer from high insertion loss due to reflection.

Chiral metamaterials are another class of metamaterials that are suitable and promising for polarization control and manipulation, though they are typically fabrication challenging. Chiral metamaterials cause the breaking of degeneracy between the two circularly polarized waves. These metamaterials can serve as broadband circular polarizers [4,5]. By integrating semiconducting materials into the metamolecules, recent demonstrations have revealed that optical activity can be dynamically controlled through photoexcitation [6,7]. In these cases, however, the energy of the unwanted polarization is lost, while they are in general not able to convert the polarization states or rotate the linear polarization direction. To date, polarization conversion was demonstrated only by employing multi-layered planar metamaterials [8-10] over a narrow bandwidth.

Using the cross-polarization coupling in anisotropic resonators and based on our recent theoretical modeling of few-layered metamaterials [11-13], we demonstrate broadband linear polarization converters with very high conversion efficiency. The metamaterial devices are capable of rotating the polarization to its orthogonal direction for an incident linearly polarized electromagnetic wave. The experimentally demonstrated power conversion is higher than 50% over a bandwidth of more than two octaves, and the efficiency is only limited by the metal and dielectric losses in the materials being used. They operate either in reflection or transmission mode with nearly zero co-polarization reflection or transmission, which suggests high polarization purity of the output wave. The demonstration is in the terahertz frequency range, and it is easy to be extended to other relevant frequency regimes. The phase of the converted cross-polarization is determined by the geometry of the resonators, and it can be expanded over a 2π range by metamaterial structural design. This further enables the demonstration of near-perfect anomalous reflection and transmission, phenomenon that have been demonstrated recently [14,15]. In contrast to the previous demonstrations where the regular reflection and transmission beams carry most of the power, our approach reveals that anomalous reflection or transmission beam carries >50% of the incident power, and the regularly reflected or transmitted beams are almost completely suppressed.

We acknowledge the support in part from the Los Alamos National Laboratory LDRD Program and the Center for Integrated Nanotechnologies.

REFERENCES

[1] A. C. Strikwerda, K. Fan, H. Tao, D. V. Pilon, X. Zhang, and R. D. Averitt, "Comparison of birefringent electric split-ring resonator and meanderline structures as quarter-wave plates at terahertz frequencies," *Opt. Express* **17**, 136-149 (2009).

[2] X. G. Peralta, E. I. Smirnova, A. K. Azad, H. T. Chen, A. J. Taylor, I. Brener, and J. F. O'Hara, "Metamaterials for THz polarimetric devices," *Opt. Express* **17**, 773-783 (2009).

[3] H. T. Chen, J. F. O'Hara, A. K. Azad, and A. J. Taylor, "Manipulation of terahertz radiation using metamaterials," *Laser Photon. Rev.* **5**, 513-533 (2011).

[4] J. K. Gansel, M. Thiel, M. S. Rill, M. Decker, K. Bade, V. Saile, G. von Freymann, S. Linden, and M. Wegener, "Gold helix photonic metamaterial as broadband circular polarizer," *Science* **325**, 1513-1515 (2009).

[5] Y. Zhao, M. A. Belkin, and A. Alu, "Twisted optical metamaterials for planarized ultrathin broadband circular polarizers," *Nat. Commun.* **3**, 870 (2012).

[6] S. Zhang, J. F. Zhou, Y. S. Park, J. Rho, R. Singh, S. Nam, A. K. Azad, H. T. Chen, X. B. Yin, A. J. Taylor, and X. Zhang, "Photoinduced handedness switching in terahertz chiral metamolecules," *Nat. Commun.* **3**, 942 (2012).

[7] J. F. Zhou, D. R. Chowdhury, R. K. Zhao, A. K. Azad, H. T. Chen, C. M. Soukoulis, A. J. Taylor, and J. F. O'Hara, "Terahertz chiral metamaterials with giant and dynamically tunable optical activity," *Phys. Rev. B* **86**, 035448 (2012).

[8] J. M. Hao, Y. Yuan, L. X. Ran, T. Jiang, J. A. Kong, C. T. Chan, and L. Zhou, "Manipulating electromagnetic wave polarizations by anisotropic metamaterials," *Phys. Rev. Lett.* **99**, 063908 (2007).

[9] J. Y. Chin, M. Z. Lu, and T. J. Cui, "Metamaterial polarizers by electric-field-coupled resonators," *Appl. Phys. Lett.* **93**, 251903 (2008).

[10] Y. Q. Ye and S. He, "90° polarization rotator using a bilayered chiral metamaterial with giant optical activity," *Appl. Phys. Lett.* **96**, 203501 (2010).

[11] H. T. Chen, "Interference theory of metamaterial perfect absorbers," *Opt. Express* **20**, 7165-7172 (2012).

[12] H. T. Chen, J. F. Zhou, J. F. O'Hara, F. Chen, A. K. Azad, and A. J. Taylor, "Antireflection coating using metamaterials and identification of its mechanism," *Phys. Rev. Lett.* **105**, 073901 (2010).

[13] L. Huang, D. R. Chowdhury, S. Ramani, M. T. Reiten, S. N. Luo, A. K. Azad, A. J. Taylor, and H. T. Chen, "Impact of resonator geometry and its coupling with ground plane on ultrathin metamaterial perfect absorbers," *Appl. Phys. Lett.* **101**, 101102 (2012).

[14] N. F. Yu, P. Genevet, M. A. Kats, F. Aieta, J. P. Tetienne, F. Capasso, and Z. Gaburro, "Light propagation with phase discontinuities: generalized laws of reflection and refraction," *Science* **334**, 333-337 (2011).

[15] X. J. Ni, N. K. Emani, A. V. Kildishev, A. Boltasseva, and V. M. Shalaev, "Broadband light bending with plasmonic nanoantennas," *Science* **335**, 427-427 (2012).

Active functionalities with hybrid plasmonic nanostructures

W. Dickson, G. A. Wurtz, A. V. Zayats

Department of Physics, King's College London, Strand, London WC2R 2LS,

United Kingdom

http://www.nano-optics.org.uk

Optical properties of metallic nanostructures are in many cases determined by one or another type of plasmonic excitations such as surface plasmon polaritons, localized surface plasmons, particle plasmons, etc. The coupling of light to such excitations, that are collective electronic modes in metallic nanostructures, allows one to confine the electromagnetic field on the sub-wavelength scales and manipulate it with high precision both spectrally and spatially. Hybritization of plasmonic nanostructures with functional materials, such as ferroelectric, magneto-optical, nonlinear optical materials and molecular species, results in metamaterials or stand-alone nanostructures whose photonic response can be actively controlled by application of external stimuli. Plasmonic dispersion and, thus, optical properties of such nanostructures and their response to applied control signals can be designed in a straightforward and controllable way by the appropriate structuring of the metallic host and choice of active dielectric. In this talk we will overview magneto-optical, all-optical and electro-optical functionalities achievable with hybrid plasmonic nanostructures. Photonic functionalities in nanoscale plasmonic devices are important for nanophotonic applications, controlling light on the nanoscale as well as for development of tuneable and functional optical metamaterials.

1. M. Kauranen and A. V. Zayats, "Nonlinear plasmonics,“ *Nature Photonics, vol.* **6**, 2012, pp. 737-742.
2. P. Ginzburg, F. J. Rodríguez Fortuño, A. Martínez, A. V. Zayats, "Analogue of the quantum Hanle effect and polarisation conversion in non-Hermitian plasmonic metamaterials," Nano Lett. vol. 12, 2012, pp. 6309–6314.
3. J.-S. Bouillard, S. Vilain, W. Dickson, G.A. Wurtz, A.V. Zayats, "Broadband and broadangle SPP antennas based on plasmonic crystals with linear chirp," Sci. Rep. 2, 2012, 829.
4. Y. Veniaminova, A. A. Stashkevich, Y. Roussigné, S. M. Chérif, T. V. Murzina, A. P. Murphy, R. Atkinson, R. J. Pollard, A. V. Zayats, "Brillouin light scattering by spin waves in magnetic metamaterials based on Co nanorods," Opt. Mater. Expr. 2, 2012, pp. 1260-1269.
5. G. A. Wurtz, R. Pollard, W. Hendren, G. P. Wiederrecht, D. J. Gosztola, V. A. Podolskiy, A. V. Zayats, "Designed ultrafast optical nonlinearity in a plasmonic nanorod metamaterial enhanced by nonlocality," Nature Nanotech., vol. 6, 2011, pp. 107-111.
6. J.-S. Bouillard, G. A. Wurtz, W. Dickson, D. O'Connor, A. V. Zayats, "Low-temperature plasmonics of metallic nanostructures," Nanoletters, vol. 12 , 2012, pp. 1561-1565.

Tunable metamaterials and plasmonics devices

Analytical Modeling of Realistic Conformal Metasurface Cloaks with a Line-Source Excitation

Y. R. Padooru[1], A. B. Yakovlev[1*], P.-Y. Chen[2], and A. Alù[2]
[1]Department of Electrical Engineering, The University of Mississippi, Mississippi 38677-1848, USA
[2]Department of Electrical and Computer Engineering, The University of Texas at Austin, Austin, Texas 78712, USA
[*]corresponding author: yakovlev@olemiss.edu

Abstract – Here, we report on the analytical modeling and physical properties of conformal metasurface cloaks excited by an electric line source. The realistic metasurface cloaks are formed with 2-D periodic arrays of printed (patches or Jerusalem crosses) and slotted (meshes or Jerusalem cross slots) sub-wavelength elements. It is demonstrated that the analytical grid-impedance expressions, originally derived for planar metasurfaces and plane-wave incidence, may be successfully applied in the analysis of cylindrical conformal mantle cloaks illuminated by near-field sources.

Based on the concept of mantle cloaking or a cloaking by a surface [1], in [2] we have proposed a simple and accurate analytical model to design various practical metasurface cloaks, which provides a clear analytical recipe for the collective response of individual periodic elements that constitute metasurfaces conformal to cylindrical objects. In the present work, we extend the rigorous analytical treatment of [2] to the case of an electric line source placed in close proximity of a cloaked cylindrical object. We demonstrate that the design rules obtained in [2] for plane-wave incidence are still very effective for near-field excitation, for both dielectric and conducting cylinders covered with slotted and printed metasurface mantle cloaks. We consider a variety of 2-D arrays with sub-wavelength periodic elements, such as mesh grids and patches, and Jerusalem crosses. The scattering problem is solved using the analytical eigenfunction-expansion method, which employs sheet impedance boundary conditions on the surface of the mantle cloak. Our analytical results are then accurately validated with full-wave simulations (HFSS [3]).

A detailed study in regard to the applicability of the homogenized grid-impedance expressions, originally derived and validated for planar surfaces and plane-wave incidence (with the summary of analytical expressions provided in [2]), is presented for the case of an electric line source. Conditions on the accuracy of these analytical expressions (which depend on the position of the line source and the observation point with respect to the cloaked object) are discussed and confirmed based on the comparison between analytical and full-wave numerical simulations. It is shown that very good agreement is obtained, which expectedly deteriorate when sources or observation points are located at distances less than the period of the metasurface sub-wavelength inclusions.

In Figure 1, we demonstrate the robustness of the metasurface cloaks (with the use of 2-D printed and slotted arrays of Jerusalem crosses) for dielectric and conducting cylinders with the line-source excitation. The analytical results for cloaked and uncloaked scenarios are compared with full-wave numerical simulations (HFSS) demonstrating very good agreement even for observation points in close proximity to cylindrical objects.

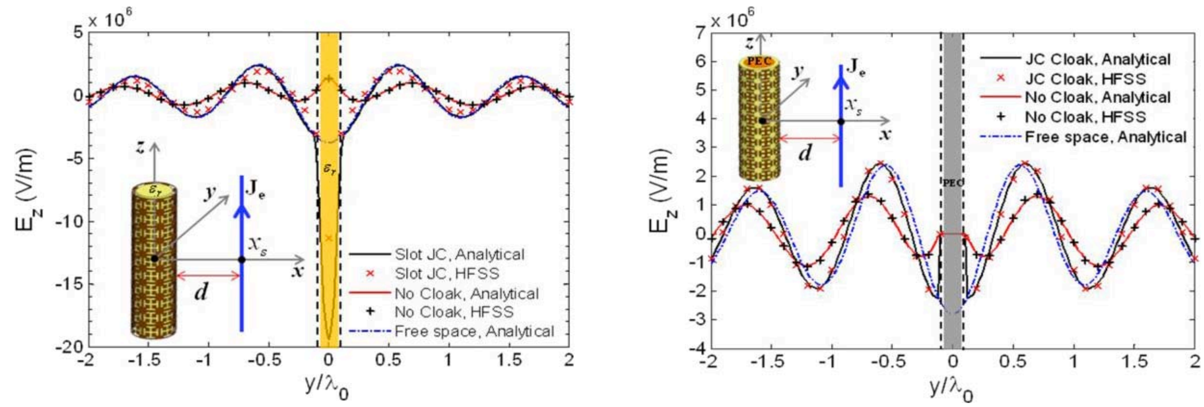

(a) (b)

Fig. 1. Electric field distribution E_z along the y-axis: (a) the vertical dashed bold lines represent the position of the slotted Jerusalem cross cloak, and the shaded region represents the dielectric cylinder and (b) free space, conducting cylinder without cloak, and conducting cylinder covered with Jerusalem cross cloak. The distance of the line source from the cloak interface is d = $0.1\lambda_0$. The analytical results are represented by solid and dash-dot lines, full-wave HFSS simulations by symbols (crosses and plus signs).

In Figure 2, the analytical results of the electric-field distribution in the ϕ-plane are shown for dielectric and conducting cylinders with and without metasurface cloaks, clearly demonstrating that the scattered field from the cylinders can be drastically reduced with the presence of the cloaks even for the near-field source placed in close proximity to the objects.

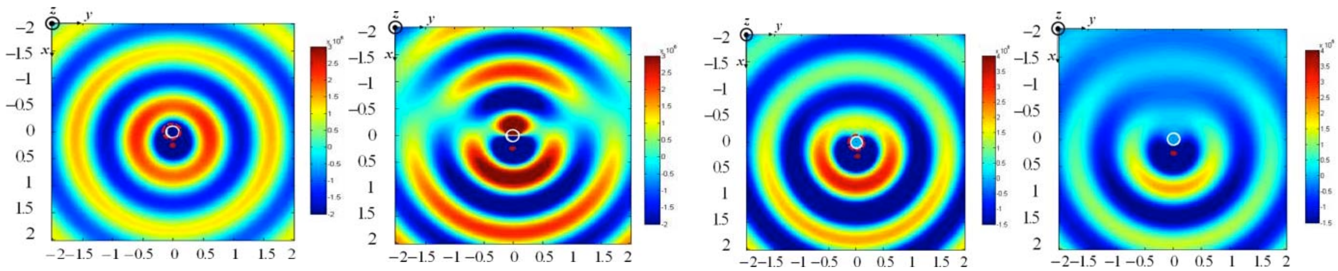

(a) (b) (c) (d)

Fig. 2. Analytical results of magnitude of E-field distributions in the ϕ-plane for a dielectric cylinder due to a line source: (a) with the slotted Jerusalem crosses cloak and (b) without the cloak; for a conducting cylinder: (c) with the Jerusalem crosses cloak and (d) without the cloak. The distance of the line source from the cloak interface is $d = 0.1\lambda_0$.

We have investigated mantle cloaking of dielectric and conducting cylinders covered by practical metasurfaces realized by printed and slotted sub-wavelength periodic elements due to line-source excitation. A detailed study has been performed to understand the validity and limitations of the analytical model for cylindrical conformal mantle cloaks placed in the near field of a line source.

REFERENCES

1. AlĚ, A. "Mantle cloak: Invisibility induced by a surface," *Phys. Rev. B*, Vol. 80, 245115(1-5), Dec. 2009.
2. Padooru, Y. R., A. B. Yakovlev, P.-Y. Chen, and A. AlĚ, "Analytical modeling of conformal mantle cloaks for cylindrical objects using sub-wavelength printed and slotted arrays," *J. Appl. Phys.*, Vol. 112, 034907(1-13), Aug. 2012.
3. High Frequency Structure Simulator (HFSS) ver 12.0, Ansoft Corporation, PA, 2010. [Online]. Available: http://ansoft.com

All-Graphene Terahertz Interconnects, Devices and Circuits

P. Y. Chen[*], and A. Alù

Dept. of Electrical and Computer Engineering, University of Texas at Austin, Austin, TX 78712, USA

[*]corresponding author: pychen@utexas.edu

Abstract- We propose here the concept and design of terahertz (THz) nanocircuit devices and components utilizing four-terminal gated graphene-based transmission line, which support the tightly-confined quasi-transverse electromagnetic (quasi-TEM) mode. We theoretically demonstrate that the active graphene transmission line may allow the real-time control of propagation constant, phase velocity, and impedance, enabling tuanble, bandwidth-configurable THz nanodevices and nanocircuits. We envision an all-graphene transmitter front-end, which presents a fundamental step towards design architectures and protocols for innovative THz sensing and communications.

Graphene is an emerging electronic nanomaterial, which is ultimately dominated by quantum effects. Graphene's ultrahigh carrier mobility, excellent thermal stability, and unusual carrier-density-dependent surface conductivity show promise to fill the THz gap, which is a transition region between electric and photonic sources. Graphene-based interconnects or transmission-lines may present much shorten effective guided-wavelength and long propagation length, due to engineered plasmonic properties. Ultra-compact dimensions of graphene devices may therefore be applied to future chip-scale CMOS integrated circuits. The exciting tunability on graphene interconnect's propagation constant, phase velocity and characteristic impedance via the gate bias may further enable various THz devices and components, such as phase shifters, modulators, interconnects, THz antennas, and bandwidth-configurable filters and matching networks. The quantum behavior of graphene transistors near the scaling limit, such as the voltage-dependent quantum capacitance, may be exploited to design analog and THz circuits, such as frequency multipliers, mixers, voltage-controlled oscillators and varactor-tuned phase-locked loops. Sich nonlinear behavior may also realize a rectifier for the self-charged energy harvesting circuitry. To envision the graphene's potential future applications, we have proposed the all-graphene phased array and THz transmitter front-end for applications in THz wireless data transmission, inter-/intra-chip communication, sensing and actuating.

A Hybrid Gold-Graphene Metamaterial Design for Generating Fano Resonances at THz Frequencies

Muhammad Amin, Mohamed Farhat, and Hakan Bağcı
Division of Computer, Electrical, and Mathematical sciences and Engineering,
4700 King Abdullah University of Science and Technology
Thuwal 23955-6900, Saudi Arabia.
*corresponding author: muhammad.amin@kaust.edu.sa

Abstract- In this work, a hybrid gold-graphene metamaterial capable of supporting a tunable Fano resonance at Terahertz (THz) frequencies is proposed. The destructive interference between the broad dipole mode of the gold ring and the much narrower dipole mode of the graphene patch generates a Fano resonance and leads to THz equivalent of Electromagnetic Induced Transparency. This hybrid metamaterial design demonstrates that Fano resonance can be achieved by interference of two bright modes contrary to most of the traditional plasmonic Fano resonators. Additionally, the spectral location and line shape of the Fano resonance supported by the hybrid metamaterial are highly and easily tunable; this is simply achieved by applying a gate voltage to the graphene patch. The effective group index of the hybrid gold-graphene metamaterial has been shown to be extremely high suggesting potential applications in design of ultrasensitive bio-chemical sensors.

Design of devices capable of supporting Fano resonances at Terahertz (THz) and optical frequencies has recently become a research focus because of these devices' potential applications in bio-chemical sensing, switching, filtering, and enhancement of nonlinear effects [1]. Plasmonic Fano resonances are typically generated by coupling either two antiparallel dipole modes or broad dipolar modes to narrower higher order ones [2]. For the latter mechanism, originally dark modes are typically excited via symmetry breaking. For both of these mechanisms, the term "mode" refers to the surface plasmon generated on a noble metal surface. In this work, for the first time, surface plasmons generated on gold and graphene surfaces are "coupled" to generate a highly and easily tunable Fano resonance at the THz frequencies.

The unit cell of the hybrid gold-graphene metamaterial is depicted in the inset of Fig. 1(a). The proposed metamaterial consists of a square gold ring and a smaller graphene patch, which support broad and narrow dipolar surface plasmon modes within the THz part of the spectrum, respectively. The dipole mode of the graphene patch, which acts as a "dark" mode, destructively couples to the "bright" dipole mode of the gold ring and generates a Fano resonance. It should be noted here that the geometrical parameters of the structure are carefully selected to ensure a spectral overlap of the two dipole resonances. The spectral location and the line shape of the Fano resonance can be tuned by varying the graphene's chemical potential between 500meV-2500meV. This can simply be achieved by applying a gate voltage to the graphene patch [Fig. 1 (a)]. This easy tunability can be utilized as a way to make switches at THz frequencies.

The retrieved effective group index of the hybrid metamaterial is shown in Fig. 1 (b). The figure clearly demonstrates highly dispersive nature of field interactions. Especially, at the Fano resonance, the group index exceeds 1200 demonstrating the potential of the hybrid metamaterial in slow light applications, including ultrasensitive detection of bio-molecules at THz frequencies.

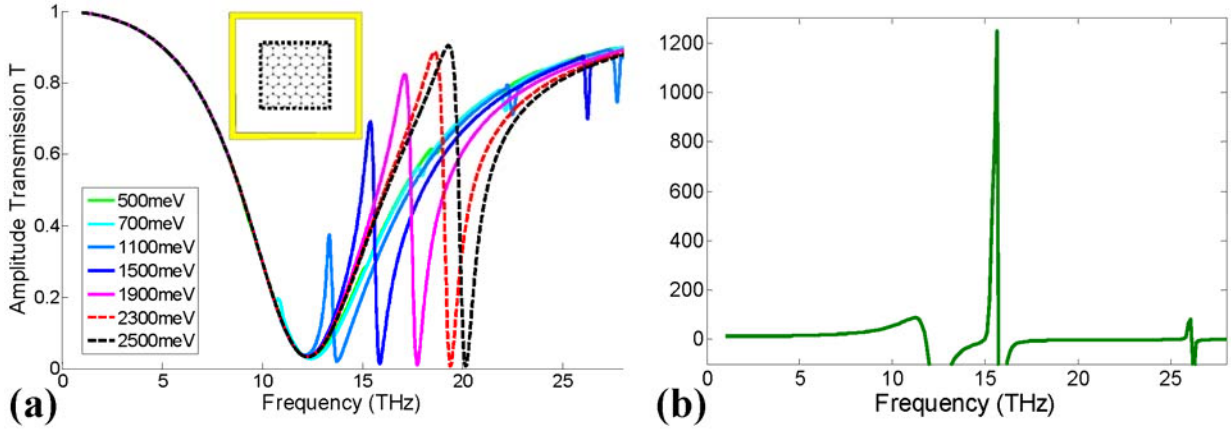

Figure 1. (a) Inset: Geometry of the proposed hybrid graphene-gold metamaterial's unit cell. The width, thickness, and height of the square gold ring are 5.5μm, 100nm, 30nm, respectively. The width of the square graphene patch is 1.6μm. Transmission from the structure for various values of chemical potential (500-2500meV) demonstrates the tunability of the Fano resonance. (b) Retrieved group index of the device.

REFERENCES

1. Rahmani, M., B. Luk'yanchuk, and M. Hong. "Fano resonance in novel plasmonic nanostructures." *Laser & Photon. Rev.*, 2012. DOI 10.1002/lpor.201200021
2. Luk'yanchuk, B., Zheludev, N. I., Maier, S. A., Halas, N. J., Nordlander, P., Giessen, H., and Chong, C. T. "The Fano resonance in plasmonic nanostructures and metamaterials." *Nat. Mater.,* vol. 9, no. 9, pp. 707-715, 2010.
3. Grigorenko, A. N., Polini, M., and Novoselov, K. S., "Graphene Plasmonics," *Nat. Photonics.*, vol. 6, pp. 749–758, 2012.
4. Amin, M., Farhat, M., Bağcı, H., "Hybrid graphene tunable Fano resonators at THz frequencies," submitted to *Appl. Phys. Lett.*

Plasmonic Graphene-Antenna Photodetector and Transistor

Zheyu Fang,* Yumin Wang, Peter Nordlander, Naomi J. Halas, Xing Zhu.
School of Physics, Peking University, Beijing, China, 100871
Department of Electrical and Computer Engineering, Laboratory for Nanophotonics, Rice University, Houston, Texas 77005, United States.
[*]corresponding author: zhyfang@rice.edu

Abstract- Graphene monolayer with plasmonic antenna to form a sandwich photodetector realizes 800% photocurrent enhancement and 20% internal quantum efficiency in the visible and NIR frequency, can be further used for graphene-based optically induced electronics.

Nanoscale antennas sandwiched between two graphene monolayers yield a photodetector that efficiently converts visible and near-infrared photons into electrons with an 800% enhancement of the photocurrent relative to the antennaless graphene device.[1] The antenna contributes to the photocurrent in two ways: by the transfer of hot electrons generated in the antenna structure upon plasmon decay,[2] as well as by direct plasmon-enhanced excitation of intrinsic graphene electrons due to the antenna near field. This results in a graphene-based photodetector achieving up to 20% internal quantum efficiency in the visible and near-infrared regions of the spectrum. This device can serve as a model for merging the light-harvesting characteristics of optical frequency antennas with the highly attractive transport properties of graphene in new optoelectronic devices.

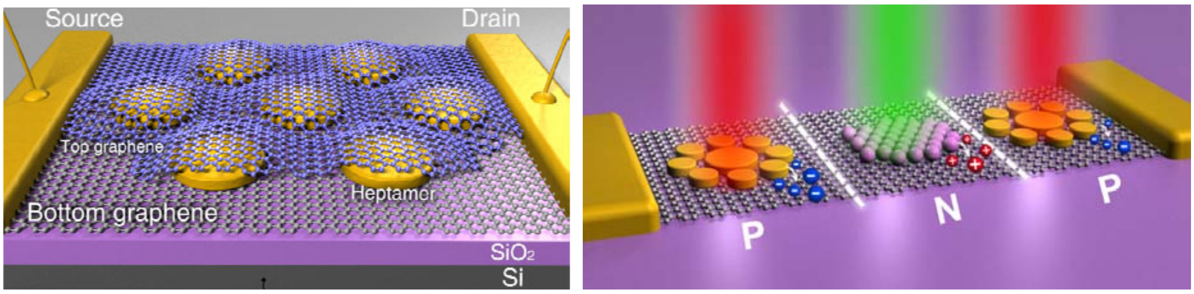

Fig.1. (a) Schematic illustration of a single gold heptamer sandwiched between two monolayer graphene sheets. (b) Schematic illustration of optically induced electronics (OIE) by nanoantenna *n*-doping and quantum dot *p*-doping for an *n*-*p*-*n* transistor.

References:

1. Zheyu Fang, Zheng Liu, Yumin Wang, Pulickel M. Ajayan, Peter Nordlander, and Naomi J. Halas, **Nano Lett.** *12*, 3808, 2012.
2. Zheyu Fang, Yumin Wang, Zheng Liu, Andrea Schlather, Pulickel M. Ajayan, Frank H. L. Koppens, Peter Nordlander, and Naomi J. Halas, **ACS Nano**, 2012, doi: 10.1021/nn304028b

Fano-resonant nanoplasmonic cavities and metamaterials: from fundamentals to active control

Stefan A Maier[1]
[1]Department of Physics, Imperial College London, London SW7 2AZ, UK

[*]corresponding author: s.maier@imperial.ac.uk

Abstract- A general modeling approach of Fano resonances applicable to a wide class of cavity geometries will be described, based on an intuitive Hamiltonian description. Various experimental realizations of Fano cavities will be presented, with a particular focus on actively tunable electromagnetically induced transparency in a terahertz metamaterial.

Fano resonances form via the coupling of bright and dark plasmonics modes in a variety of metallic cavity nanosystems, and recently there has been an large amount of research interest in this general class of resonances [1]. Due to the spectral sharpness of the Fano response, such systems show unique opportunities for optical sensing, or for the control of light transmission in metamaterial geometries.

We will present a general modeling approach of Fano resonances based on a Hamiltonian description of the coupling process between a bright and a dark mode [2], and apply it to a variety of prominent Fano cavity geometries such as dolmens, disk/ring cavities, nanoparticle clusters, and the coupling of grating to localized resonances. This approach allows a clear identification of the underlying parent resonances, and hence for the rational design of Fano cavities.

Active control of Fano resonances, particularly in the regime of deep modulation (also known as a classical analogue of electromagnetically induced transparency), is possible when the spectral characteristics of at least one of the underlying parent resonances can be tuned. We will present an example of such control in a terahertz metamaterial allowing all-optical control of the transparency response [3].

REFERENCES

1. Luk'yanchuk, B., Zheludev, N.I., Maier, S.A., Halas, N.J., Nordlander, P., Giessen, H., & Chong, C.T., The Fano resonance in plasmonic nanostructures and metamaterials, *Nature Materials* 9, 707 (2010)
2. Francescato, Y., Giannini, V., & Maier, S.A., Plasmonic systems unveiled by Fano resonances, *ACS Nano* 6, 1830 (2012)
3. Gu, J., Singh, R., Liu, X., Zhang, X., Ma, Y. Zhang, S., Maier, S.A., Tian, Z., Azad, A., Chen, H.-T., Taylor, A.J., Han, J., & Zhang, W., Active control of electromagnetically induced transparency in terahertz metamaterials, *Nature Communications* 3, 1151 (2012), doi:10.1038/ncomms2153

Active metamaterial device based on complementary split ring resonators for controllable light modulation

Z. Liu[1], X. X. Xia[1], J. J. Li[1], H. F. Yang[1], B.G. Quan[1], and C. Z. Gu[1*]
[1]Beijing National Laboratory for Condensed Matter Physics, Institute of Physics, Chinese Academy of Sciences, Beijing 100190, China
[*]corresponding author: czgu@aphy.iphy.ac.cn

Abstract-Active metamaterial devices consisted of double layer complementary split ring resonators (CSRRs) were studied. They were fabricated by ion beam etching method on Au-SiO_2-Au films, and the biased voltage can be applied on the top and bottom electrodes of the device. Light amplification was observed in transmission spectra for different incident polarizations. The results show the potential applications for CSRR device such as biomaterial sensing and surface enhanced Raman scattering.

Optical property of metamaterials has attracted attentions in many application fields, such as sensors, modulators, switches, filters and so on. Complementary split ring resonator (CSRR) is a promising metamaterial structure, which was put forward as the complementary structure of split ring resonator (SRR) based on Babinet principle [1]. The transmission property of CSRR has been studied from microwave to visible range with the development of microfabrication, and has been applied as filters and sensors [2, 3]. However, the optical responses are mainly related to the geometry and material of CSRR, which is not flexible for controlling the responses. In recent years, active devices were proved to give compensation for losses in metamaterials [4]. CSRR metamaterials, with hollow patterns in continuous metal films, can be conveniently used as electrode. However, up to now, active devices based on CSRR have not been reported yet.

In this work, the CSRR-based active devices were fabricated on Au-SiO_2-Au films, Fig. 1 shows the schematic of the device. Au films were deposited on quartz substrate by electron beam evaporation, and SiO_2 films were grown by plasma enhanced chemical vapor deposition. After spin-coating of PMMA resist and electron beam lithography, U-shaped patterns were formed on resist. The patterns were then transformed onto the Au-SiO_2-Au films by ion beam etching method. Figure 2 gives the scanning electron microscope images of CSRRs. The line width is 50 nm and unit size is 200 nm. Transmission spectra of the device were measured by applying biased voltage on the two layers. The coupling between the resonators in different layer was studied under different incidences and applied electric fields.

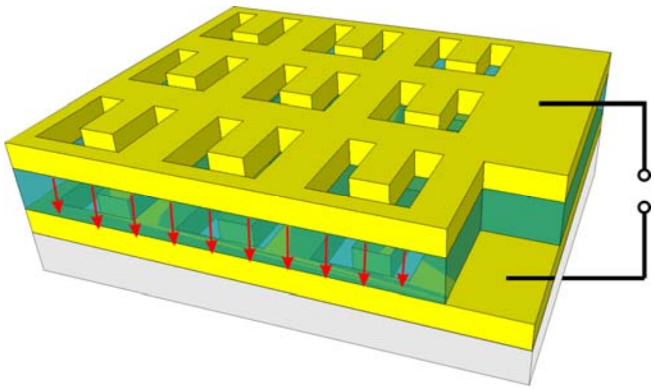

Figure 1 The schematic of CSRR-based active device.

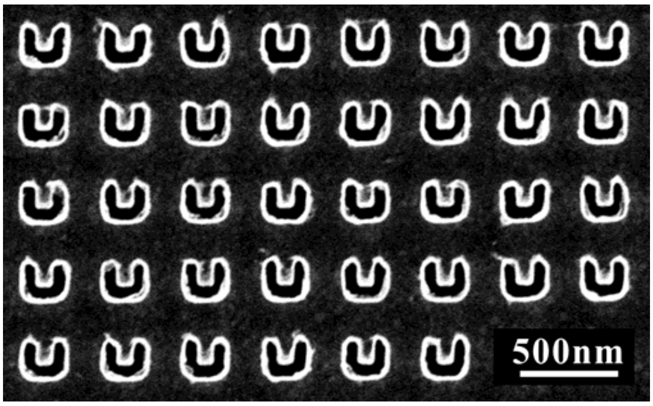

Figure 2 The SEM image of CSRR structures on active device

Acknowledgements This work was supported by National Natural Science Foundation of China (Grants No. 50825206, 1083401, 60871045，61001045, 50825206 and 91023041) and the National Basic Research Program of China (Grant No.2009CB930502) and the Knowledge Innovation Project of CAS (Grant No. KJCX2-EW-W02).

REFERENCES

1. Falcone, F., T. Lopetegi, M. A. G. Laso, J. D. Baena, J. Bonache, M. Beruete, R. Marques, F. Martin, and M. Sorolla, “Babinet Principle Applied to the Design of Metasurfaces and Metamaterials,” *Phys. Rev. Lett.*, Vol. 93, No. 19, 197401, 2004.
2. Kim, K. T., J. H. Ko, K. Choi and H. S. Kim, “Optimum Desing of Wideband Bandpass Filter With CSRR-Loaded Transmission Line Using Evolution Strategy,” *IEEE T. Magn.*, Vol. 48, No. 2, 811-814, 2012.
3. Liu, Z., X. Xia, Y. Sun, H. Yang, R. Chen, B. Liu, B. Quan, J. Li and C. Gu, “Visible transmission response of nanoscale complementary metamaterials for sensing applications,” *Nanotechnology*, Vol. 23, 275503, 2012.
4. Hamm, J. M., S. Wuestner, K. L. Tsakmakidis and O. Hess, “Theory of Light Amplification in Active Fishnet Metamaterials,” *Phys. Rev. Lett.*, Vol. 107, 167405, 2011.

Tuning in plasmonic antennas: control of the position of hot-spots in a plasmonic trimer and control of the directivity

B. Rolly, B. Stout, N. Bonod[1*]
[1]Institut Fresnel, Domaine UNIVERSITAIRE DE Sain tjérôme, 13397 Marseille
[*]corresponding author: Nicolas.bonod@fresnel.fr

Abstract-We show that we can control the position of a hot spot in a linear trimer of metallic nanoparticles by tuning the angle of incidence or the illuminated frequency of an impinging plane wave. We also show that the forward/backward scattering of metallic particles can be controlled by tuning the distance between a dipolar emitter and the particle. We derive an analytical model able to accurately predict the scattering property of a single antenna.

Optical antennas attracted a lot of attention due to their ability to concentrate light energy into very small volume when illuminated in far field. Reciprocally, when they are illuminated from the near field region, they permit to strongly enhance the decay rates of quantum emitters and to shape their emission pattern. We will first consider a linear trimer of metallic particles behaving as electric dipoles. We will study first the scattering cross-section of this linear trimer with respect to the illuminating frequency when illuminated in oblique incidence. We will then plot the light intensity in the two neighboring nano-gaps with respect to the frequency, without modifying the angle of incidence. We will discover that surprisingly, light intensity in one nano-gap can be entirely vanished while it can be strongly enhanced in the other nano-gap (Fig.1). This result proves that we can control the light intensity position in a trimer antenna by simply modifying the angle of incidence, while the distance between the two nano-gaps is around the tenth of the incident wavelength [1]. By considering slightly larger particles it could be possible to control the position of the so-called hot spot without modifying the angle f incidence but by tuning the frequency.

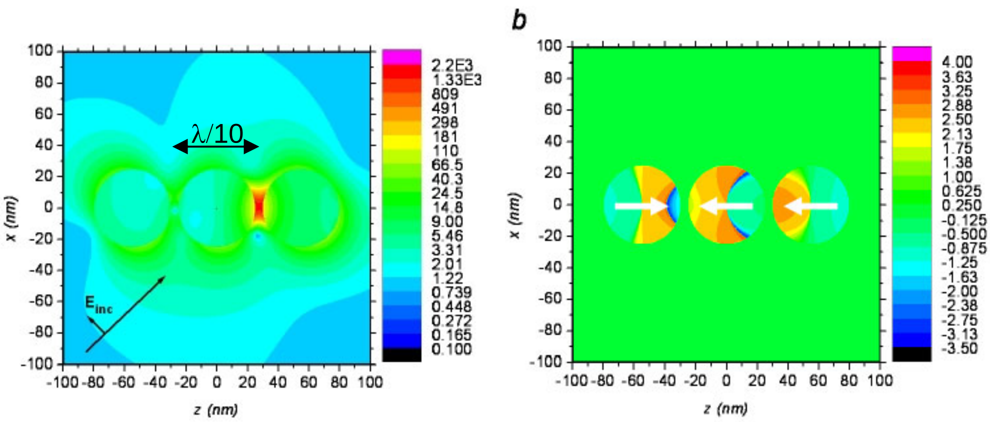

Fig.1. Left. Light intensity in the vicinity of a linear trimer of metallic particles. Right: reconstruction of the phase of the induced electric dipoles.

The second part of the talk will be dedicated to the control of the backward/forward scattering of a dipolar metallic antenna by tuning the distance between the emitter and the particle. We will evidence the fact that for particles illuminated at frequencies smaller than the plasmon resonance frequency, light can be collected or reflected by tuning the emitter/particle distance at a $\lambda/50$ scale (Fig.2).

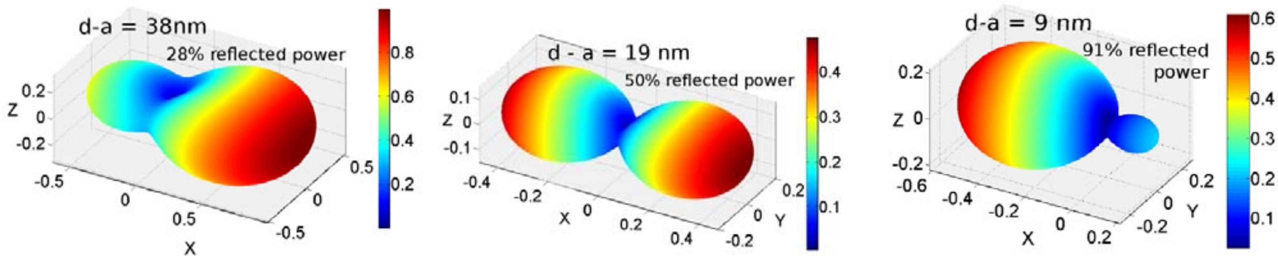

Fig.2. Radiation pattern of a dipolar emitter coupled with a single metallic particle. Left: distance between the emitter and the particle surface: 38 nm, collector behaviour, middle: distance emitter surface: 19 nm, symmetric emission, right: reflector behaviour.

We will derive an analytical dipolar model that is able to accurately predict the scattering property of a single metallic particle. This model shows that the radiation pattern results from an interference effect between the two electric dipoles. The far field contributing terms are then considered. But the difference of phase between the two dipoles must take into account the three fundamental terms of the dipolar emission: near field, intermediate field, and far field. As a consequence, this phase term is non linear and highly dependent on the distance between the two neighboring dipoles. This non linear dependence explains why a plasmonic antenna can either collect or reflect light with a high efficiency, depending on its distance to the emitting source [2-3].

REFERENCES

1. B. Rolly, B. Stout, S. Bidault, N. Bonod, "Crucial role of the emitter–particle distance on the directivity of optical antennas," Opt. Lett. **36**, 3368-3370 (2011)
2. N. Bonod, A. Devilez, B. Rolly, S. Bidault, B. Stout, "Ultracompact and unidirectional metallic antennas," Phys. Rev. B **82**, 115429 (2010).
3. A. Devilez, B. Stout, N. Bonod, "Mode-balancing far-field control of light localization in nanoantennas," Phys. Rev. B **81**, 245128 (2010).

Subwavelength focusing of surface acoustic wave using a locally resonant metastructure

Abdelkrim Khelif[1*], Mohammed A. Al-Lethawe[1], Mahmoud Addouche[1] , Sébastien Guenneau[2]
[1] Institut FEMTO-ST, UMR CNRS 6174, Université de Franche-Comté, F25044, France
[2] Institut Fresnel, UMR CNRS 6133, Universitaire de Saint-Jérome F13397 Marseille, France
[*]corresponding author: abdelkrim.khelif@femto-st.fr

Abstract- We describe an all-angle negative refraction effect for surface acoustic waves (SAW) in 2D phononic crystals made of cylindrical pillars assembled in a square lattice and deposited on the surface of a semi-infinite substrate. The iso-frequency contours convexity of some branches leads to a NR effect. A flat lens for SAW has been designed demonstrating the focusing of an acoustic source into an image on the other side with an image resolution of λ/4, which overcomes the diffraction limit.

In this paper, we report on the negative refraction of surface acoustic wave in pillars-based phononic crystals, occurring at the frequencies where both group velocity and a refractive index are positive. We consider a 2D phononic crystal consisting of cylinder pillars deposited on the surface of a semi-infinite medium, which have been studied experimentally and theoretically in [1, 2]. The substrate and pillars form a monolith made of Lithium Niobate with XY 128 cut.

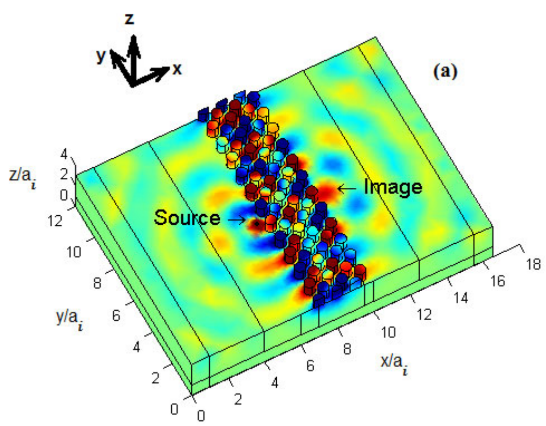

Figure 1: Out-of-plane displacement field of a point source and its image across a pillar-based phononic crystal flat lens. Dimensions are given according to the interface-parallel period. The point source operates at f1.a = 1075m/s for pillar relative high h=a equals to 1.

The main advantage of such AANR is the possibility to design a flat lens that can focus a point source into an image on the other side of the lens. To study the focusing properties of the lens for surface acoustic wave, we built a finite size of the pillars-based structure with 13 "**a**i" of width and six layers thick. A point source is placed close to the left side of the flat lens and is operating, according to the considered pillar height, at the reduced frequencies f1.a = 1075m/s Fig. 1. The frequency of the incident wave is chosen where all-angle negative refraction may occur.

Practically, an out-of-plane excitation is applied on one node of the meshing at 5.55**a** in X direction and 6.55**a** in Y direction. It is important to note that the width of the point source is smaller than the wavelength of the surface at the operating frequency, making it suitable for the investigation of t he super-resolution properties of the flat lens. In Fig. 1, we plot the field pattern of the out-of-plane displacement of the emitting wave and their images a cross the finite size structure. We observe a high quality image formed in the opposite side of the finite size of the structure with an image resolution of $\lambda/4$, which overcomes the Rayleigh diffraction limit.

REFERENCES

[1] A. Khelif, Y. Achaoui, S. Benchabane, V. Laude, and B. Aoubiza, Phys. Rev. B 81, 214303 (2010).
[2] Y. Achaoui, A. Khelif, S. Benchabane, and V. Laude, Phys. Rev. B 83, 104201 (2011).

Broadly tunable metasurfaces based on phase change materials

Federico Capasso, Mikhail Kats, Shiram Ramanathan

School of Engineering and Applied Sciences, Harvard University, USA

capasso@seas.harvard.edu

Abstract

The effect of the insulator to metal transition (IMT) on the optical properties of thin films of Vanadium Oxide on sapphire is studied and shown to lead to a perfect absorber at specific wavelengths. By patterning the same films with optical antennas significant tunability of the antenna resonances due the IMT is demonstrated

We demonstrate that the resonances of plasmonic antennas can be tuned or turned off by taking advantage of the thermally-driven insulator-to-metal phase (IMT) transition in vanadium dioxide (VO_2). Y-shaped antennas were fabricated on a 180nm film of VO_2 over a sapphire substrate, and their resonances were shown to depend on the temperature of the VO_2 film in proximity of the phase transition, in good agreement with full-wave simulations. We achieved tunability of the resonance wavelength of approximately 10% (>1 μm at $\lambda \sim 10$ μm). In parallel and related study we have demonstrated that perfect absorption can be achieved in the same system by utilizing the nontrivial phase shifts at interfaces between lossy media [1]. This design is implemented with an ultra-thin ($\sim\lambda/65$) vanadium dioxide (VO_2) layer on sapphire, temperature tuned in the vicinity of the VO_2 insulator-to-metal phase transition, leading to 99.75% absorption at $\lambda = 11.6\,\mu$m. In the vicinity of this transition VO_2 behaves like a tunable metamaterial with a refractive index that changes significantly with temperature. The structural simplicity and large tuning range (from ~80% to 0.25% in reflectivity) are promising for thermal emitters, modulators, and bolometers.

Collaborations with R. Blanchard, P. Genevet, Jiao Lin, D. Sharma, Zheng Yang, M. Mumtaz Qazilbash and D. N. Basov

References

1. M. A. Kats et al. *Appl. Physics Lett.* **101**, 221101 (2012)

Liquid-crystal tunable long-range surface plasmon polariton waveguides and directional couplers

D. C. Zografopoulos & R. Beccherelli*
Consiglio Nazionale delle Ricerche, Istituto per la Microelettronica e Microsistemi (CNR-IMM), Rome, Italy
*corresponding author: romeo.beccherelli@artov.imm.cnr.it

Abstract- *Long Range Surface Plasmon Polariton devices tuned by means of the electro-optic effect in liquid crystal are numerically investigated. Waveguides and 2x2 directional couplers, both in vertical and coplanar configuration are discussed. Application of a control voltage allows modifies the dielectric tensor profile and allows for the control of the devices, with low power consumption, high extinction ratio and insertion loss as low as 1 dB.*

A variety of *Long Range Surface Plasmon Polariton (LR-SPP)* tuneable devices relying on the thermo-optic control of the background polymer refractive index, controlled via current injection through the metal waveguide [1, 2, 3] devices has been thus far demonstrated. We propose an alternative route towards dynamically tunable photonic devices based on the use of nematic liquid crystals (NLCs), inherently anisotropic materials whose properties can be extensively controlled via the application of external fields.

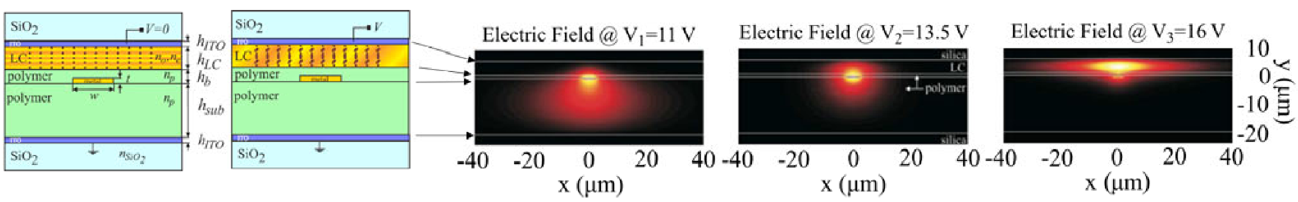

Figure 1 Cross section of the LR-SPP waveguide. An LC cell of thickness h_{LC} is situated above the gold stripe, separated by a buffer layer of thickness h_b: at rest state ($V = 0$), the LC molecules lie along the z−axis, while an applied voltage V induces molecular reorientation. Electric field profile at three values of V ($h_b = 1$ μm).

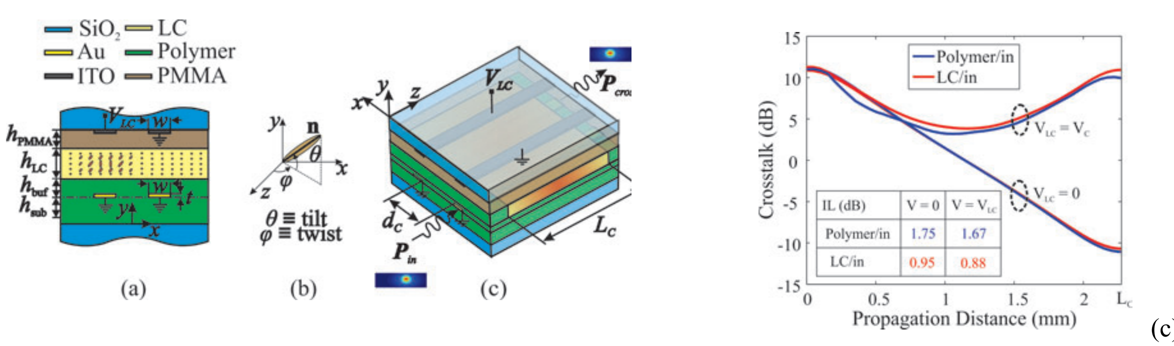

Figure 2: (a) Cross-sectional view of the proposed LC-based plasmonic directional coupler and definition of material and structural parameters. (b) Definition of tilt and twist angles that describe the nematic director local orientation. (c) Three-dimensional view of the pro- posed coupler. The interaction/coupling length is equal to *LC* and the separation between the two metal stripes is *dC*.

Already established in the design and fabrication of dielectric-based photonic guided-wave electro-optic components [4,5], functional LC-based plasmonic components, such as variable attenuators, phase-shifters and switches have been theoretically demonstrated in a variety of waveguide platforms [6], [7], [8]. As they are based on capacitive operation, LC-plasmonic devices are not only free from current injection issues, such as electromigration or thermal diffusion crosstalk, but, more importantly, they allow for extremely low-power consumption, which may reach several orders of magnitude lower than their thermo-optic counterparts, in the nW range.

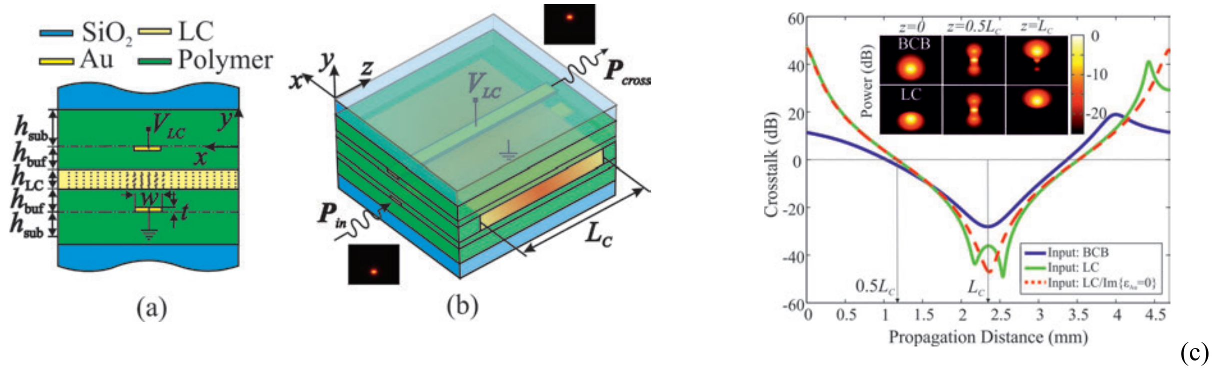

Figure 3: (a) Cross-section and (b) perspective view of the vertical liquid-crystal plasmonic directional coupler. (c) Crosstalk evolution along propagation, when the coupler is excited by the LC- and BCB-reference LRSPP modes, at 1.55 m, where LC = 2.348 mm. The ideal lossless case is also included for comparison. Inset shows modal power profiles at the input, output of the coupler and after a propagation distance z = 0.5LC

REFERENCES

1. Nikolajsen, T. K., Leosson, K. and Bozhevolnyi, S. I. “Surface plasmon polariton based modulators and switches operating at telecom wavelengths,” *Appl. Phys. Lett.* Vol. 85, 5833–5835, 2004.doi:10.1063/1.1835997

2. Boltasseva, A. and S. I. Bozhevolnyi, “Directional couplers using long-range surface plasmon polariton waveguides,” *IEEE J. Sel. Top. Quant. Electron.* Vol. 12, 1233–1241, 2006. doi: 10.1109/JSTQE.2006.882659

3. Charbonneau, R., Scales, C., Breukelaar, I., Fafard, S., Lahoud, N. Mattiussi, G. and Berini P.,“Passive integrated optics elements based on long-range surface plasmon polaritons” *J. Lightwave Technol.* Vol. 24, 477–494, 2006. doi:10.1109/JLT.2005.859856

4. Bellini B. and Beccherelli R. "Modelling, design and analysis of liquid crystal waveguides in preferentially etched silicon grooves", *J. Phys. D: Appl. Phys*, Vol. 42 No. 4, art. 045111 (2009) doi:10.1088/0022-3727/42/4/045111

5. Zografopoulos, D. C., Asquini, R. Kriezis, E. E., d’Alessandro, A. and Beccherelli R. “Guided-Wave Liquid-Crystal Photonics”, *Lab on a Chip* Vol. 12, 3598-3610 2012 doi:10.1039/C2LC40514H

6. Zografopoulos, D. C., Beccherelli, R., Tasolamprou A. C. and Kriezis, E. E. “Liquid-Crystal Tunable Waveguides for Integrated Plasmonic Components” *Photonics and Nanostructures – Fundamentals and Applications* on-line, 20th September 2012 doi:10.1016/j.photonics.2012.08.004

7. Zografopoulos, D. C. and Beccherelli R. “Liquid-Crystal Tunable Waveguides for Integrated Plasmonic Components”, *Plasmonics* on-line. 2nd September 2012. doi:10.1007/s11468-012-9440-7

8. Zografopoulos, D. C. and Beccherelli R. “A vertically-coupled liquid-crystal long-range plasmonic optical switch” (submitted) arXiv:1211.6071v1

Tunable Nanoplasmonics

(Invited)
M. A. Swillam

Department of Physics, School of Science and Engineering,
The American University in Cairo, Egypt
*corresponding author: m.swillam@aucegypt.edu

Abstract-In this paper we present novel mechanisms for tuning and controlling the response of plasmonic waveguide made using metal-insulator-metal (MIM) configuration. These mechanisms allow for full control on the transmission response from these waveguide based structures. This control can be done optically or mechanically. The applications and advantages of these mechanisms are discussed in details.

Plasmonics waveguides have shown unique advantages to guide the light while confined in subwavelength area. This unique advantage provides make the plasmonics waveguide attractive candidate for various applications. These applications include high density integration for optical interconnects applications, on-chip biosensing, and nonlinear applications.

Among various plasmonics waveguides, metal-insulator metal (MIM) is considered as a suitable candidates for the aforementioned applications. The 3D version of this configuration is the plasmonic slot waveguide (PSW) as shown in Fig.1.

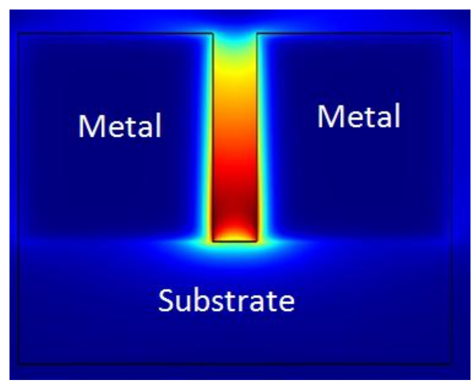

Fig. 1 The field profile in a 50 nm slot mode waveguide with an air gap between two metal layers

This waveguide configuration has been utilized in various proposed configurations to attain different filter responses. However real realization of these waveguides is challenging. Moreover, good coupling efficiency to this waveguide with few nanometers gap is the bottleneck of using such waveguides. Recently, a novel coupling mechanism is proposed, fabricated and tested with very good coupling efficiency [1],[2].

This novel coupling mechanism provides a suitable solution for accessing and fabricating these waveguide and integrate it with silicon waveguides on the same substrate. In general tuning or controlling the response of PSW is challenging and never been discussed before.

In this paper we propose different mechanism to control and tune the light inside the PSW. One of these mechanisms is to exploit another optical signal to modify the interference condition created inside a mesh created of these PSWs. In this approach another optical source is utilized to allow all optical control of the created PSW mesh. Wide band tunability is obtained using this approach.

Another possible mechanism is through micro electromechanical systems (MEMS) in this mechanism an inline resonance filter is utilized with tunable length. Varying the length of the resonator is done through mechanical motion for the reflectors. A wide tunable range is obtained.

These novel approaches open the door for wide range of applications such as tunable filters, tunable lasers, spectrum analyzer, and biosensing.

REFERENCES

1. B. Lau, M. A. Swillam, and A. S. Helmy, "Hybrid orthogonal junctions: wideband plasmonic slot-silicon waveguide couplers," Opt. Express, vol. 18, 27048-27059, December 2010.
2. C. Lin, H. Wong, B. Lau, M. Swillam, A. S. Helmy, "Efficient broadband energy transfer via momentum matching at hybrid junctions of guided-waves," Appl. Phys. Lett., 123115, (2012).

Label-free, coupler-free, scalable and intracellular bio-imaging by multi-mode plasmonic resonances

Yueh-Chun Lai[1], Hsin-Cheng Lee[1], Shu-Wen Kuo[2], Cheng-Kuang Chen[1], Hsieh-Ting Wu[1], Oscar K. Lee[2] and Ta-Jen Yen1,*

[1]Department of Materials Science and Engineering, National Tsing Hua University, Taiwan

[2]Institute of Clinical Medicine, National Yang-Ming University, Taiwan

[*]corresponding author: tjyen@mx.nthu.edu.tw

Abstract-From direct electric excitations on SRR structures, we demonstrated multi-mode plasmonic resonances that can be quantitatively described by our standing-wave plasmonic resonance model. We further manifest that the lower-order modes possess greater sensitivity associated with stronger localized electromagnetic field leading to greater sensitivity, while the higher-order modes present mediate sensitivity with micron-scale detection lengths to allow intracellular bio-events detection. These unique merits enable the SRR-based sensor a label-free, coupler-free, scalable and intracellular sensing/imaging device.

The SRR structure was first proposed by J. B. Pendry, which is excited by the time-varying H-field parallel to its axial direction (i.e., grazing-angle incidence)[1]. To date, the SRR remains the most common artificial structure to give rise to the absent negative as well as high-frequency magnetic responses[2] in nature; nevertheless, it is obvious that this H-field coupling to the resonance is quite difficult to perform in particularly beyond microwave frequencies because of the extremely small thickness of the SRR for the grazing-angle incident excitation. Under the electric excitations at normal incidence, we demonstrated multiple resonance modes and reported a general model of standing-wave plasmonic resonances[3] beyond the conventional gap-capacitive LC circuit model to interpret the multiple responses in SRRs (Fig. 1). Next, deduced from this standing-wave plasmonic resonance model, we presented a multi-functional SRR-based plasmonic sensor, and investigated its sensitivity and detection lengths with respect to multiple resonance modes (Fig. 2), indicating that the lower-order modes possess greater sensitivity associated with stronger localized electromagnetic field leading to greater sensitivity, while the higher-order modes present mediate sensitivity with micron-scale detection lengths[4]. In the end, we present a first-ever intracellular plasmonic imaging by exciting multi-mode resonances in spilt-ring resonators (Fig. 3). The demonstrated SRR microscopy possesses the key advantages beyond other optical microscopy such as label-free and real-time diagnosis (vs. fluorescent and Raman scattering techniques), coupler-free to avoid the issues of coupling oil leakage and dispersion, great detection lengths (vs. SPP techniques), and scalable operation frequencies (vs. LSPR techniques) in particular in IR regimes to prevent strong absorption from bio-agents, providing the possibility for the live cells imaging technique, including the observation of cellular proliferation and differentiation process[5].

Acknowledgements

The authors would like to gratefully acknowledge the financial support from the National Science Council, the Ministry of Education and National Tsing Hua University in Taiwan.

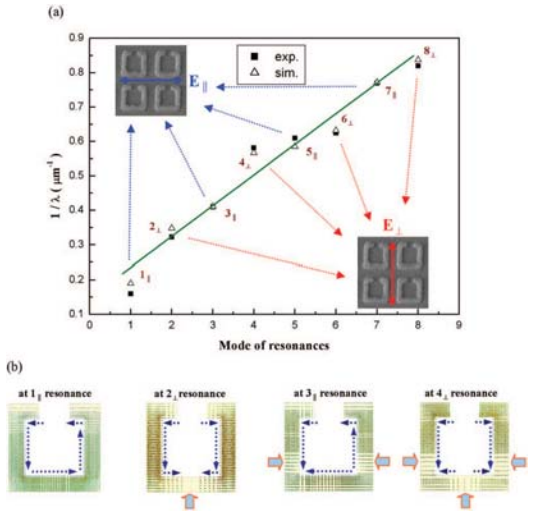

Fig. 1. (a) The plot of reciprocal values of multiple resonance wavelengths versus the mode numbers, showing a clear linear relationship. (b) Simulated distributions of the induced currents for the first four resonances, respectively.

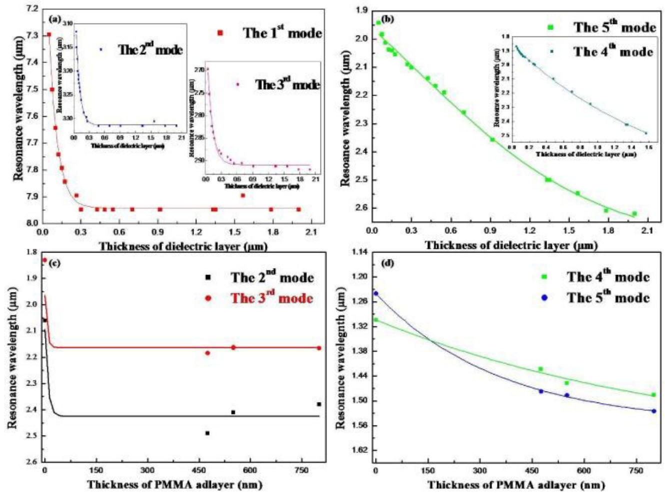

Fig. 2 (a,b) Simulated results of the varied detection lengths with respect to 1^{st} to 5^{th} resonance modes. (c) Measured thickness effect of 2^{nd} and 3^{rd} resonance modes. (d) Measured thickness effect of left 4^{th} and 5^{th} resonance modes.

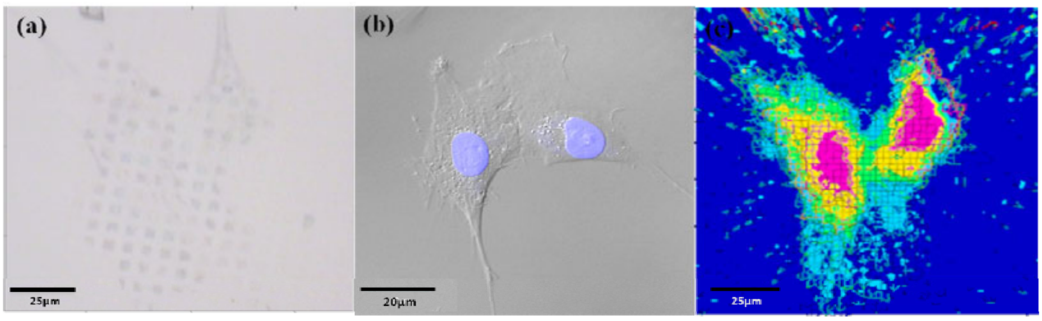

Fig. 3. (a) The non-labeled optical microscopic image of hMSCs on the SRR substrate. (b) The confocal fluorescent microscopic image of hMSCs. The purple part is the nuclei of hMSCs labeled by 4'-6-diamidino-2-phenylindole (DAPI). (c) The designed SRR samples with hMSCs grown on surface sample area has been measured in reflection mode at the wavenumber 1850-2400 cm^{-1} using the FT-IR imaging system equipped with a focal plane array detector (64 x 64 detector elements) and a 15x objective (NA=0.4).

REFERENCES

1. J. B. Pendry, A. J. Holden, D. J. Robbins, and W. J. Stewart, IEEE Trans. Microwave Theory Tech. **47**, 2075 (1999).
2. T. J. Yen *et al*., *Science 303*, pp.1494 (2004)
3. C. Y. Chen, S. C. Wu, T. J. Yen, *Appl. Phys. Lett*., *93*, 034110 (2008)
4. Ta-Jen Yen *et al*., ***Optics Express***, Vol. 18, pp. 9561-9569 (2010)
5. Ta-Jen Yen *et al*., ***Advanced Materials***, Vol. 24 (23), pp. OP148-OP152, (2012)

Near-field optical properties of graphene-based heterosystems: application to thermophotovoltaic energy conversion

R. Messina and P. Ben Abdallah

Laboratoire Charles Fabry, Institut dOptique, CNRS, Université Paris-Sud,
Campus Polytechnique, RD128, 91127 Palaiseau Cedex, France
riccardo.messina@institutoptique.fr

Abstract— We study the modifications to the optical properties of a silicon carbide (SiC) surface induced by a single layer of graphene. To this aim we consider the electromagnetic local density of states in proximity of the graphene-modified surface, as a function of the distance from the surface and of the chemical potential of graphene. Finally, the use of graphene for the enhancement of the efficiency of a thermophotovoltaic cell is proposed.

The recent discovery of graphene has generated a broad interest coming from several domains of physics toward the study of its surprising features. In particular, it has proved to possess interesting electrical [1, 2] and optical [3, 4, 5, 6] properties. Moreover, these properties can be often easily tailored by means of an active control of its chemical potential, achievable for example by using an externally imposed voltage difference.

We focus here our attention on the optical properties of graphene. In order to describe them we study the electromagnetic local density of states (LDOS), a fundamental tool of optics allowing to deduce several important physical quantities, such as the electromagnetic energy density and the free energy [7]. Moreover, its knowledge is strictly connected to the field scattered by a dipolar tip near a surface, paving the way to the theoretical modeling of near-field scanning optical microscopy experiments, aiming at mapping the near field in proximity of a sample [8]. In presence of a material supporting surface plasmons, the associated resonances correspond, especially in near-field regime, to peaks in the LDOS.

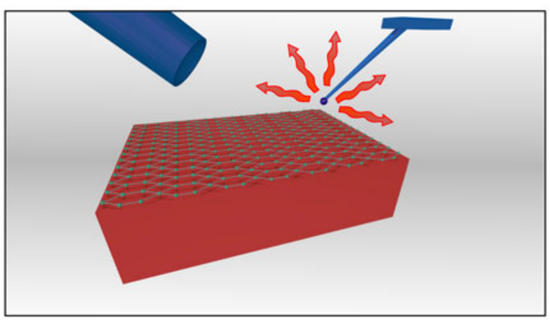

(a) Scheme of a typical LDOS measurement

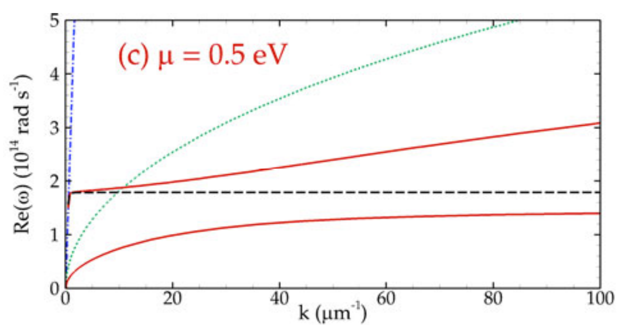

(b) Graphene-modified dispersion relation of surface modes

Figure 1: We show in (a) the basic principle for measuring the LDOS above a surface: an AFM tip scatters the evanescent field in proximity of the sample into a propagative contribution, which is then collected by a probe aperture. In (b) the dispersion relations for the surface modes of SiC alone (black dashed), a single sheet of graphene (green dotted) and graphene-modified SiC (solid red) are presented. The chemical potential of graphene is $\mu = 0.5\,\mu$eV and the blue dot-dashed line represents the light cone in vacuum.

We study how the LDOS in proximity of a silicon carbide (SiC) planar surface is modified by the deposition of a presence of a monolayer sheet of graphene [9] (see figure 1(a)). As a first step, we compare the dispersion relations of surface resonances for a SiC surface to those of a suspended graphene sheet and of the composite SiC-graphene sample (see figure 1(b)). Guided by these results, we calculate and discuss the LDOS in the three cases, showing the appearance of a new peak as well as a tunable shift of the existing ones, whose dependence on the chemical potential is discussed.

Finally we propose an application of graphene to the standard scheme of a thermophotovoltaic (TPV) cell, in which the near-field heat exchange between a source (supporting a surface resonance) and a cell (a gap semiconductor) is exploited to produce an electric current [10]. We theoretically show that by covering the surface of the cell with a sheet of graphene (see figure 2(a)), we partially solve the well-known problem of mismatch between the surface resonance of the source and the gap of the cell [11]. This simultaneously produces a significant enhancement of the electric power produced in the cell as well as of the overall efficiency of the device [12] (see figure 2(b)).

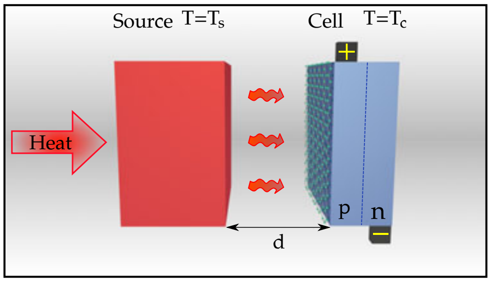

(a) Scheme of the graphene-modified NTPV cell

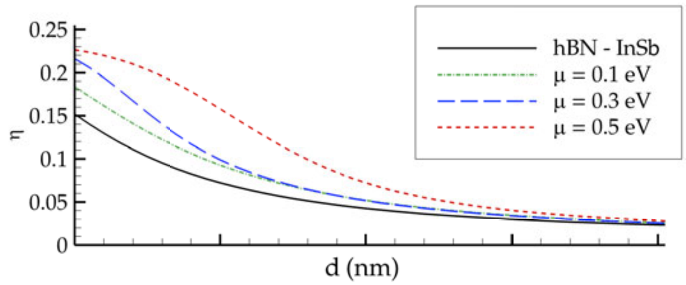

(b) Cell efficiency in absence and in presence of graphene

Figure 2: Our proposal of graphene-modified TPV cell is presented in (a). We show in (b) the dependence of the efficiency η of the cell as a function of distance between source and cell and of the chemical potential.

REFERENCES

1. A. K. Geim and K. S. Novoselov, Nature Mater. **6**, 183 (2007).
2. A. K. Geim, Science **324**, 1530 (2009).
3. T. Stauber, N. M. R. Peres, and A. K. Geim, Phys. Rev. B **78**, 085432 (2008).
4. L. A. Falkovsky, J. Phys. Conf. Ser. **129**, 012004 (2008).
5. M. Jablan, H. Buljan, and M. Soljačić, Phys. Rev. B **80**, 245435 (2009).
6. R. J. Koch, T. Seyller, and J. A. Schaefer, Phys. Rev. B **82**, 201413(R) (2010).
7. K. Joulain *et al.*, Surf. Sci. Rep. **57**, 59 (2005).
8. Y. De Wilde *et al.*, Nature **444**, 740 (2006).
9. R. Messina *et al.*, preprint arXiv 1211.3145 (2012).
10. S. Basu, Y.-B. Chen, and Z. M. Zhang, Int. J. Energy Res. **31**, 689 (2007).
11. A. Narayanaswamy and G. Chen, Appl. Phys. Lett. **82**, 3544 (2003).
12. R. Messina and P. Ben-Abdallah, preprint arXiv 1207.1476 (2012).

New Advances in Optically Magnetic Materials for Nanophotonics

Photon management in two-dimensional disordered media

M. Burresi[1,2*], K. Vynck[1], F. Pratesi, F. Riboli[1], and D. S. Wiersma[1,2]

[1]European Laboratory for Non-linear Spectroscopy (LENS), 50019 Sesto Fiorentino (FI), Italy.

[2]Istituto Nazionale di Ottica (CNR-INO), Largo Fermi 6, 50125 Firenze (FI), Italy.

[*]corresponding author: burresi@lens.unifi.it

Abstract-We present a novel nanophotonic strategy based on disorder to greatly augment the absorption of thin-film materials over a large range of wavelengths. The introduction of a properly engineered 2D random structure in thin-slabs gives rise to guided disordered modes, which traps light impinging from the third direction, thus enhancing the absorption. Furthermore, by properly introducing correlations in the random structure we are able to control spectrally and angularly the coupling properties of the photonic disordered structure.

Given the ever-growing demand of green energy, many efforts of the industrialized societies are spent in the development of new technologies for renewable energy. In particular, the nanophotonic community has been producing a great deal of alternative strategies to improve the performance of various photovoltaic technologies. Thin-film solar cells are the current state-of-the-art in solar energy technologies, made out of different, sometimes very expensive, materials (e.g. CdTe, CIGS), for which nanophotonics is particularly suited for improving their performance. These so-called third-generation solar cells generally have high quantum efficiency, thereby yielding more electric current per absorbed photon. However, given the small thickness of the film (less than 1 μm), the probability for a photon to be absorbed is low, yielding a small net production of electric current, in spite of high quantum efficiencies. Nanophotonics aims to find reliable solutions to enhance the absorption of light in thin films. Engineering the absorbing material at the nanoscale indeed leads to interferences that can significantly increase light absorption [1,2].

In this talk, we will present a novel photonic architecture to improve the absorption of thin films based on disordered structures, which provide performances comparable to their deterministic (periodic) counterparts. We will show that the introduction of a two-dimensional random structure yields to disordered modes, created by the in-plane multiple scattering. Such guided modes are characterized by an enhanced coupling with the surrounding environment and confines light in the slab for a specific lifetime. Hence, the material becomes optically 'thicker', increasing the probability of light to be absorbed [3]. Furthermore, the introduction of correlations in the random distribution of holes, which leads to a short-range statistical order, provides us an additional degree of control which can be exploited to tune the optical properties of the photonic structures. In these correlated-disordered photonic materials a strong reshaping of the absorption spectrum occurs, providing an absorption enhancement which compares with its deterministic counterpart.

In this presentation we will also show our latest experimental results which aims to verify the theoretical predictions. We will study the absorption of a-Si thin-films as a function of different geometries and realization of disorder by probing the material at wavelengths relevant for photovoltaic applications with different impinging angle and polarizations [4].

This new nanophotonic architecture can be applied to many of the state-of-the-art third-generation photovoltaic technologies, since it is not affected by the kind of material employed. Given its random nature, the structure is inherently 'optically robust' and does not require a high degree of fabrication accuracy, crucial point for large scale production. Furthermore, with a fine engineering of the disorder, e.g. introducing correlations, the coupling efficiency and the operative spectral range can be tuned at will and still be insensitive to the exact structural parameter.

REFERENCES

1. Zongfu Yu *et al*, “Fundamental limit of nanophotonic light-trapping in solar cells”, PNAS (2010)
2. Zongfu Yu *et al*, “Thermodynamic Upper Bound on Broadband Light Coupling with Photonic Structures”, PRL (2012)
3. Vynck *et al*, “Photon management in two-dimensional disordered media”, Nature Materials (2012).
4. M. Burresi *et al*, Under Review (2012).

Negative refraction, perfect lenses and new objectives in metaatom research

Manuel Nieto Vesperinas*
Instituto de Ciencia de Materiales de Madrid, CSIC,
Cantoblanco, 28049 madrid, Spain.
www.icmm.csic.es/mnv

Artificial composites with electromagnetic properties experienced an upsurge about thirteen years ago with the proposal of negative refractive index media and their use for imaging superresolution. Nevertheless, their inherent highly lossy transmission characteristics has precluded so far their efficient use as refractive elements.

However, in recent times a new perspective is being undertaken by employing their magnetic response to illuminating waves, on the one hand; as well as their high absorption of incident energy. While the former property conveys effects that lead to a harnessing of electromagnetic waves by interference between induced electric and magnetic dipoles and higher order multipoles, like Fano resonances, Kerker-like suppression of scattered intensities in given directions, or highly directional scattering; the latter characteristics suggested devising new concepts for storage and emission of electromagnetic energy. In this talk I shall overview these facts

On the electromagnetic scattering by magnetodielectric small spherical particles

J.M. Geffrin [1], B. García-Cámara [2,3], R. Gómez- Medina [4], P. Albella[5], L.S. Froufe-Pérez[6], C. Eyraud[1], A. Litman[1], R. Vaillon[7] , F. González[3], M. Nieto-Vesperinas[8], J.J. Sáenz [4,5] and F. Moreno[3]

[1] Institut Fresnel, CNRS, Aix-Marseille Université, Ecole Centrale Marseille, Campus de St Jérôme, 13013 Marseille, France

[2] Research Center on Nanoscience and Nanotechnology CIN2(CSIC) and CIBER-BBN, Campus UAB, 08193 Bellaterra, Barcelona, Spain

[3] Grupo de Óptica, Departamento de Física Aplicada, Universidad de Cantabria, Avda. de Los Castros s/n, 39005 Santander, Spain

[4] Departamento de Física de la Materia Condensada and Instituto "Nicolás Cabrera", Universidad Autónoma de Madrid. Campus de Cantoblanco, 28049 Madrid, Spain.

[5] Material Physics Center CSIC-UPV/EHU and Donostia International Physics Center DIPC, Paseo Manuel de Lardizabal 5, Donostia-San Sebastián 20018, Spain.

[6] Instituto de Estructura de la Materia, Consejo Superior de Investigaciones Científicas CSIC, Serrano 121, 28006 Madrid, Spain

[7] Université de Lyon, CNRS, INSA-Lyon, UCBL, CETHIL, UMR5008, F-69621, Villeurbanne, France

[8] Instituto de Ciencia de Materiales de Madrid, Consejo Superior de Investigaciones Científicas CSIC, Campus de Cantoblanco, 28049 Madrid, Spain.

Abstract- We analyze the light scattering by a magnetodielectric subwavelength isolated sphere and its capacity to show non-usual scattering properties, like the inhibition of backward scattered intensity and the almost inhibition of the scattered intensity in the forward direction. The possible relevance of this study in micro and nano- technological fields will be presented.

Magnetodielectric small spheres present unusual electromagnetic scattering features, theoretically predicted a few decades ago by Kerker et al. [1]. However, achieving such behavior has remained elusive, due to the non-magnetic character of natural optical materials or the difficulty in obtaining low-loss highly permeable magnetic materials in the gigahertz regime. Here we present unambiguous experimental evidence that a single low-loss dielectric subwavelength sphere of moderate refractive index ($n\approx 4$ like some semiconductors (Si, Ge) at near-infrared) radiates fields identical to those from equal amplitude crossed electric and magnetic dipoles, and indistinguishable from those of ideal magnetodielectric spheres. The measured far-field scattering radiation patterns (see Fig. 1(a)) and degree of linear polarization (3–9 GHz/33–100mm range) show that, by appropriately tuning the a/λ ratio, zero-backward ('Huygens' source) or almost zero-forward ('Huygens' reflector) radiated power can be obtained [2]. Also, the near-field scattering distributions and their correlation with those measured in far-field, are numerically calculated and analyzed (see Fig. 1(b)). These Kerker scattering conditions [1] only depend on a/λ. Our results open new technological challenges from nano and micro-photonics to science and engineering of antennas, metamaterials and electromagnetic devices.

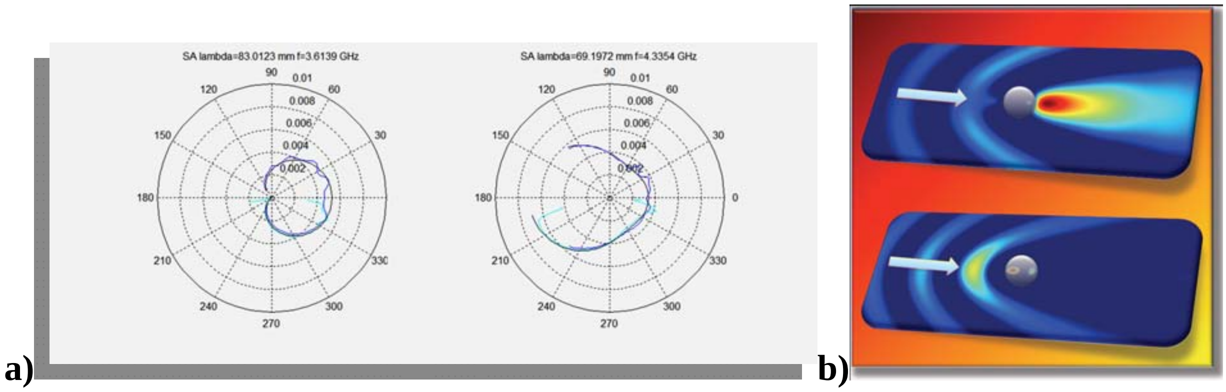

Figure 1- (a) Far-Field (experiment (blue line), theory (black line)) and (b) Near field intensity distributions of a subwavelength dielectric sphere (refractive index≈4+0i), illuminated by a linearly polarized monochromatic wave (white arrow), for the two Kerker frequencies: Zero-backward: 3.6GHz (left in (a), top in (b)) and near zero-forward: 4.3GHz (right in (a), bottom in (b)).

Acknowledgements, We acknowledge helpful discussions with I. Suárez-Lacalle and José Mª Saiz. R.V., and J.M.G. acknowledge the technical expertise brought and the work done by B. Lacroix (CETHIL) over recent years to improve some parts of the measurement device. This work was supported by the Spanish Ministerio de Ciencia e Innovación through grants: Consolider NanoLight (CSD2007-00046), FIS2009-13430-C01 and C02, FIS2010-21984, as well as by the Comunidad de Madrid (Microseres-CM, S2009/TIC-1476). B.G.-C. acknowledges his post-doctoral grant from the University of Cantabria, B.G.-C. and L.S.F.-P. acknowledge the financial support from the JAE-Program of the Spanish Council for Scientific Research (CSIC) co-funded by the European Social Fundation (ESF).

REFERENCES

1. Kerker, M., Wang, D.S. & Giles, L. Electromagnetic scattering by magnetic spheres. *J. Opt. Soc. Am.* 73, 765–767 (1983)
2. Geffrin, J.M. et al. Magnetic and electric coherence in forward- and back-scattered electromagnetic waves by a single dielectric subwavelength sphere. *Nat. Commun.* 3:1171 doi: 10.1038/ncomms2167 (2012).

Towards homogeneous magnetic metamaterials - a comprehensive multipole analysis

C. Menzel[1*], E. Hebestreit[2], S. Mühlig[2], S. Burger[3,4], C. Rockstuhl[2], F. Lederer[2] and T. Pertsch[1]

[1]Institute of Applied Physics, Abbe Center of Photonics, Friedrich-Schiller-Universität Jena, Germany

[2] Institute of Condensed Matter Theory and Solid State Optics, Abbe Center of Photonics, Friedrich-Schiller-Universität. Jena, Germany

[3]Zuse Institute Berlin (ZIB), Takustraße 7, D-14195 Berlin, Germany

[4]JCMwave GmbH, Bolivarallee 22, D-14050 Berlin, Germany

[*]corresponding author: Christoph.Menzel@uni-jena.de

Abstract- The availability of local, homogeneous metamaterials is of utmost importance for most devices that rely on metamaterials. The desired locality of the response, however, is usually not proven or actually even not questioned. Here, we present a promising set of meta-atoms that provide the desired local artificial magnetic response by exploiting the extremely strong coupling regime. We discuss their properties, possibilities, and limitations comprehensively in terms of a multipole expansion technique.

Artificial magnetic resonances in the visible and near IR regime are of prime interest for metamaterials (MMs) and, more generally, for nano-plasmonic devices. Having a material at hand that offers a nontrivial response to the magnetic field allows tailoring the optical response at will. Based on such MMs, an enormous number of novel and promising devices have been proposed. In particular, huge effort is made to realize an artificial magnetic response in the visible and thereby a possible negative refractive index [1]. The shift of these magnetic resonances, that were first demonstrated in the microwave or radiofrequency regime, to higher frequencies such as the terahertz and eventually to the optical regime, was accomplished by using derivatives of canonical geometries of the split-ring resonator, namely fishnet or cut-wire-type structures. However, whereas at low frequencies the size of the unit cell with respect to the operating wavelength is fairly small and the effective material thereof can be safely assumed as being characterized by local properties, the important issue of locality of these MMs was usually underestimated in the visible. In fact, most optical sub-wavelength MMs proposed so far suffer from the nonlocality, i.e. strong spatial dispersion and, hence, an angular dependence of their effective parameters [2]. This dramatically increases the complexity of an effective description of the optical response and inhibits the realization of the proposed MM based devices.

Recently, it has been shown that homogeneous, local, artificially magnetic MMs might be realized by exploiting the concept of extremely strong coupling [3] between resonant metal plates. There, the metallic plates are brought in very close proximity, i.e. in the order of one or a few nanometers, to allow for an intensive coupling. Here, this concept is further developed by investigating two strongly coupled gold discs as shown in Fig. 1a. These inhomogeneous plasmonic meta-atoms support a magnetic resonance. They are brought in such close proximity that the effective metal-insulator-metal waveguide built by the spacing layer between the particles supports a mode with very large propagation constant [4]. For finite particles this results in cavities which are resonant at a very large wavelength-to-cell-size-ratio of approx. 10-40 and eventually enables the use of local material parameters.

In this contribution we will comprehensively discuss this mechanism of the coupling, its opportunities and general limitations on analytical and numerical grounds. To this end, the optical response of the isolated meta-atom is computed in numerical simulations and described in terms of a multipole expansion [5]. This appears to be a versatile and invaluable tool that provides clear insight into the physics of the excited eigenmodes in the investigated meta-atoms (see Fig.1b and c). These investigations reveal, e.g., that the contribution of higher-order moments to the scattering response, in particular, that of the electric quadrupole moment, is significantly reduced in the extreme coupling regime (see Fig.1d), which is of fundamental importance for the assignment of local parameters. Furthermore, the dependence of the multipole moments on parameters like the radius of the discs or the metal thickness provides limits for this artificial magnetism with respect to the overall particle size. To sum up, we will discuss the question of local material parameters of MMs for a specially designed meta-atom by using extended analytical and numerical techniques. The results can be seen as a general roadmap, to design and fabricate arbitrary MMs that can be described by local material parameters and offer a magnetic response in the visible and near IR.

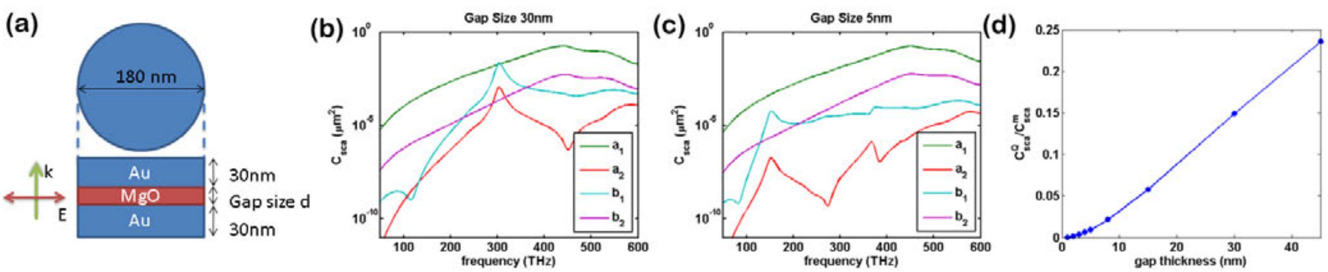

Figure 1: (a) Schematic sketch of the investigated meta-atom made of two extremely coupled discs with variable gap size *d*. (b)-(c) contribution of the spherical multipole moments (a_1 - electr. dipole, a_2 - electr. quadrupole, b_1 - magnetic dipole, b_2 - magnetic quadrupole) to the scattering cross section of the particle for different gap sizes. Note, the shift of the bluish magnetic resonance (b_1) to small frequencies for decreasing gap size *d*. (d) Ratio of electric quadrupole and magnetic dipole contributions to the scattering cross section at the lowest magnetic resonance (in (b) 300THz, in (c) 150THz) which is rapidly decreasing for decreasing gap size *d*.

Acknowledgements: The authors acknowledge financial support by the German Federal Ministry of Education and Research (PhoNa) and Thuringian Ministry of Education, Science and Culture (MeMa).

REFERENCES

1. C. M. Soukoulis, S. Linden, and M. Wegener, Negative refractive index at optical wavelengths, Science 315, 47, 2007.
2. C. Menzel, T. Paul, C. Rockstuhl, T. Pertsch, S. Tretyakov, and F. Lederer, Validity of effective material parameters for optical fishnet metamaterials, Phys. Rev. B. 81, 035320, 2010.
3. C. Menzel, R. Alaee, E. Pshenay-Severin, C. Helgert, A. Chipouline, C. Rockstuhl, T. Pertsch, F. Lederer, Genuine effectively biaxial left-handed metamaterials due to extreme coupling, Opt. Lett. 37, 596, 2012.
4. R. Filter, Jing Qi, C. Rockstuhl, and F. Lederer, Circular optical nanoantennas: an analytical theory, Phys. Rev. B 85, 125429, 2012.
5. S. Mühlig, C. Menzel, C. Rockstuhl, and F. Lederer, Multipole analysis of meta-atoms, Metamaterials 5, 64-73, 2011.

Quantum effects in small plasmonic particles

R. Alcaraz de la Osa, J. M. Sanz, J. M. Saiz, F. González and F. Moreno

Grupo de Óptica, Dpto. de Física Aplicada. Universidad de Cantabria
Avda. de los Castros s/n, Santander, Spain
alcarazr@unican.es

Abstract We examine the plasmonic properties of silver and gold nanospheres and dimers, with radii ranging from 10 nm to 1 nm, extending from the classically described regime to the quantum size regime. We have studied the spectral extinction cross-section by using the T-matrix method. The results indicate an increasingly substantial change in nanoparticle permittivity as the radius is reduced below 5 nm, showing a clear blueshift and weakening of the plasmon resonances for both silver and gold.

The remarkable growth of nanotechnology has been driven by the ability to alter material properties as dimensions are reduced towards the atomic scale. Nanomaterials exhibit physical and chemical properties very different from those of their bulk counterparts, often resulting from enhanced surface interactions or quantum confinement. Therefore, the plasmonic properties of particles in the quantum size regime (radii below 10 nm) have recently received a renewed attention [1], fueled by the race of technologies towards the low nano-scale domain. For instance, it has been shown that cancer treatments based on delivering drugs using nanoparticles (NPs) with radii below 10 nm showed better antitumour efficiency than those using larger particles [2]. In this work, we examine the plasmonic properties of both individual nanospheres and dimers made of silver and gold, with radii ranging from 10 nm to 1 nm, extending from the classically described regime to the quantum size regime. We have studied the spectral extinction cross-section by using the T-matrix method [3]. To model the optical properties of quantum-sized plasmonic particles, a revised expression for the permittivity is required. In our analysis, the standard Drude model is recast with Lorentzian terms that are defined quantum mechanically (QM), based on fundamental physical phenomena, such as electron transition frequencies ω_{if} and oscillator strengths S_{if} [4]. The overall permittivity expression can then be described as follows [4]:

$$\varepsilon(\omega) = \varepsilon_{\mathrm{IB}} + \omega_p^2 \sum_i \sum_f \frac{S_{if}}{\omega_{if}^2 - \omega^2 - i\gamma\omega} \tag{1}$$

, where $\varepsilon_{\mathrm{IB}}$ is a frequency-dependent correction term to account for the contribution of the d-band valence electrons to interband transitions at higher energies, ω_p is the plasma frequency ($9.01\,\mathrm{eV}/\hbar$ for silver [1] and $9.0\,\mathrm{eV}/\hbar$ for gold [5]) and γ is the scattering frequency, dependent on the nanosphere dimension (particle radius) and the empirical constant γ_{bulk} ($0.016\,\mathrm{eV}/\hbar$ for silver [1] and $0.07\,\mathrm{eV}/\hbar$ for gold [5]).

Fig. 1 shows the real and imaginary parts of the relative electric permittivity of silver as we increase the particle radius, for three different energies of the incident radiation. The values of the electric permittivity have been calculated following Eq. (1). A clear convergence to the bulk values (Johnson & Christy [6] and Palik [7]) is observed. The inset of Fig. 1 clearly shows how at $R = 10\,\mathrm{nm}$ the QM corrected results already converge to bulk results, except for the remain of a small bump belonging to the series of period $\approx 2\,\mathrm{nm}$.

Fig. 2 shows the spectral extinction efficiency (cross-section normalized by the total geometric section) for these systems, calculated with both bulk and QM corrected optical properties. The most remarkable feature of the spectral dependence of Q_{ext} shown in Fig. 2 is the fact that, when including QM corrections, resonances shift to smaller wavelengths (blueshift [1]) and also become weaker (lower peaks). The redshift and the peak increment of the dimer resonance with respect to the isolated particle persist in the QM results.

As a summary, the introduction of QM corrected optical properties becomes in blueshifted [1] and weaker resonances as shown in Fig. 2. The case of silver allows us to test our calculations, while the case of gold shows how important these quantum considerations may be when treating very small particles close to resonance. As a direct consequence, two particles close to each other with quantum corrected optical properties interact less, therefore producing smaller shifts and lower peak increments in the far-field cross-sections.

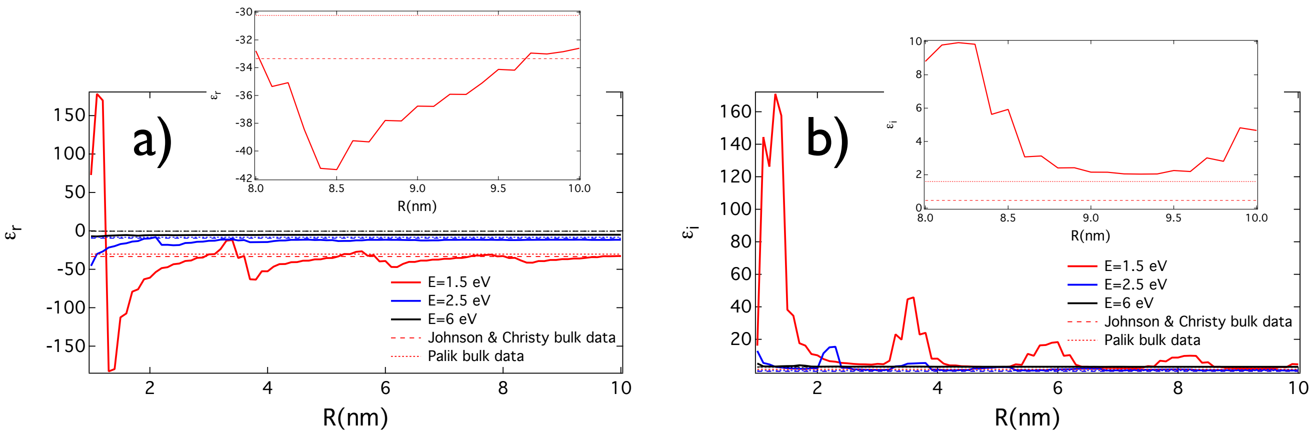

Figure 1: Real (a) and imaginary (b) parts of the relative electric permittivity of silver as a function of the particle radius for three different energies. Bulk values taken from Johnson & Christy [6] as well as Palik [7] are also shown. The insets show zoomed areas between $R = 8\,\text{nm}$ and $R = 10\,\text{nm}$.

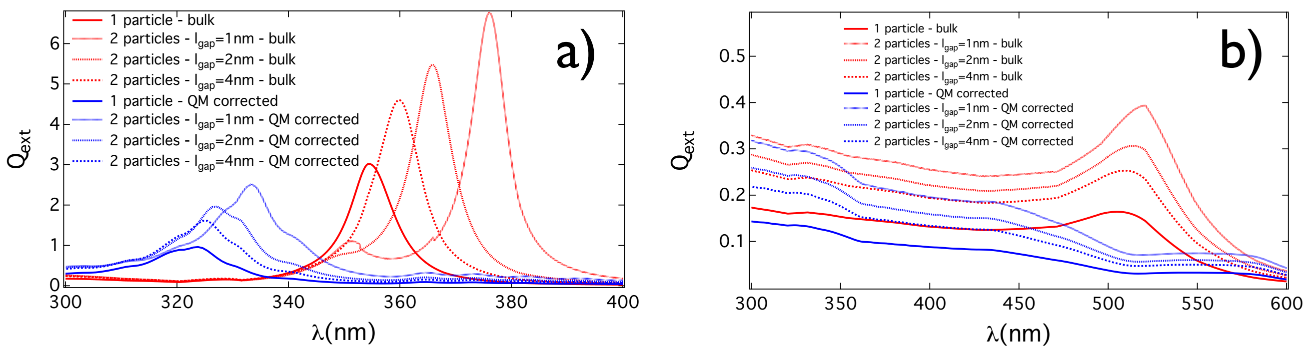

Figure 2: Spectral extinction efficiency for both single particles and dimers of radius $R =$ 4nm made of a) silver and b) gold, calculated with both bulk and QM corrected optical properties.

ACKNOWLEDGMENT

This research has been supported by MICINN under project #FIS2010-21984. R. Alcaraz de la Osa also thanks the Ministry of Education of Spain for his FPU grant.

REFERENCES

1. J. A. Scholl, A. L. Koh, and J. A. Dionne, "Quantum plasmon resonances of individual metallic nanoparticles," Nature **483**, 421 (2012).
2. C. J. Cheng, and W. M. Saltzman, "Downsizing tumour therapeutics," Nature Nanotechnology **7**, 346 (2012).
3. D. W. Mackowski, and M. I. Mishchenko, "Calculation of the T matrix and the scattering matrix for ensembles of spheres," J. Opt. Soc. Amer. A **13** 2266-2278 (1996).
4. W. A. Kraus, and G. C. Schatz, "Plasmon resonance broadening in small metal particles," J. Chem. Phys. **79**, 6130 (1983).
5. S. Berciaud, L. Cognet, P. Tamarat, and B. Lounis, "Observation of Intrinsic Size Effects in the Optical Response of Individual Gold Nanoparticles," Nano Letters **5** (3), 515 (2005).
6. P. B. Johnson, and R. W. Christy, "Optical constants of the noble metals," Phys. Rev. B **6**, 4370 (1972).
7. E. D. Palik, *Handbook of Optical Constants of Solids* (Academic Press, Boston, 1985).

Magnetic light: Optical magnetism of dielectric nanoparticles

A. E. Miroshnichenko*[1], A. I. Kuznetsov[2], B. Luk'yanchuk[2], and Y. S. Kivshar[1]
[1]Nonlinear Physics Centre, Research School of Physics and Engineering,
Australian National University, Canberra, ACT 0200, Australia
[2]Data Storage Institute, 5 Engineering Drive I, Singapore
*corresponding author: aem124@physics.anu.edu.au

Abstract Dielectric nanostructures makes a new twist on light scattering phenomena. Subwavelength particles made of high-dielectric materials exhibit very strong magentic response in visible range, which has been recently demonstrated experimentally. Dielectric nanoparticles with strong magnetic response can be used as building blocks to explore new types of interactions at nanoscales. The lower losses, compared to plasmonic counterparts, allow to employ dielectric nanostructures for a variety of applications spanning from optical nanotantennas towards metamaterials.

The magnetic response of many natural materials at optical frequencies is very weak. Thus, only the electric component of light is directly controlled in many optical devices. However, *artificial magnetism* can be achieved at high frequencies in nanostructured materials. One of the canonical examples is a split-ring resonator (SRR), an inductive metallic ring with a gap (a building block of a majority of metamaterials) that can support an oscillating current giving rise to an optically-induced magnetic moment. Unfortunately, intrinsic losses of metals set the fundamental limit for the use of SRRs at optical frequencies. This is where spherical silicon nanoparticles with the sizes of hundred nanometers make an attractive alternative, Fig.1. Dielectric nanoparticles were predicted to exhibit strong magnetic resonances in the visible [1]. The basic physics of the excitation of such modes is similar to that of SRRs, but silicon nanoparticles have much lower losses. A magnetic resonance originates from the excitation of a particular electromagnetic mode inside the nanoparticle with a circular displacement current of the electric field. This mode is excited when the wavelength of light is comparable to the particle's diameter. It has an antiparallel polarization of the electric field at the opposite sides of the particle while the magnetic field is oscillating up and down in the middle [see Fig.1(a)]. Recently, this fundamental phenomenon of strong magnetic resonances was experimentally observed throughout the whole visible spectral range from blue to infra-red for silicon nanoparticles with sizes ranging from 100 to 270 nm [2]. Similar results in red and infra-red spectral region for Si particles ranging from 200 to 265 nm have also been published in [3].

Dielectric nanoparticles with strong magnetic response can be used as building blocks to explore new types of interactions at nanoscales. Coupling of silicon nanoparticles and SRRs allows for control of the magnetic interaction between optically-induced dipole moments. If the spacing between a nanoparticle and SRR becomes smaller than a critical value, the induced magnetization can be inverted. This leads to a staggered pattern of magnetic moments, Fig.1(c), with a unique possibility for light-induced artificial *antiferromagnetism* at optical frequencies [4]. This approach can be generalized to construct a variety of hybrid structures supporting and controlling optically induced spin waves. Another manifestation of the magnetic interaction of dielectric particles is the existence of the Fano resonance in all-dielectric oligomer structures [5].

Interaction of magnetic and electric dipoles may lead to entirely new scattering properties. In particular, an interference between two optically induced dipole resonances results in azimuthally symmetric unidirectional scattering, that can be realized in layered nanoparticles with metal cores and dielectric shells [6]. A superposition of electric and magnetic resonances of a single core-shell nanoparticle may result in the suppression of the backward scattering and unidirectional emission by a single subwavelength element [6]. The directivity can be further enhanced by forming a chain of such nanoparticles. Together with low losses of dielectric materials, this property suggests a novel principle of optical nanoantennas made of dielectric nanoparticles [7]. Such all-dielectric nanoantennas exhibit much higher radiation efficiency than their plasmonic counterparts allowing more compact designs.

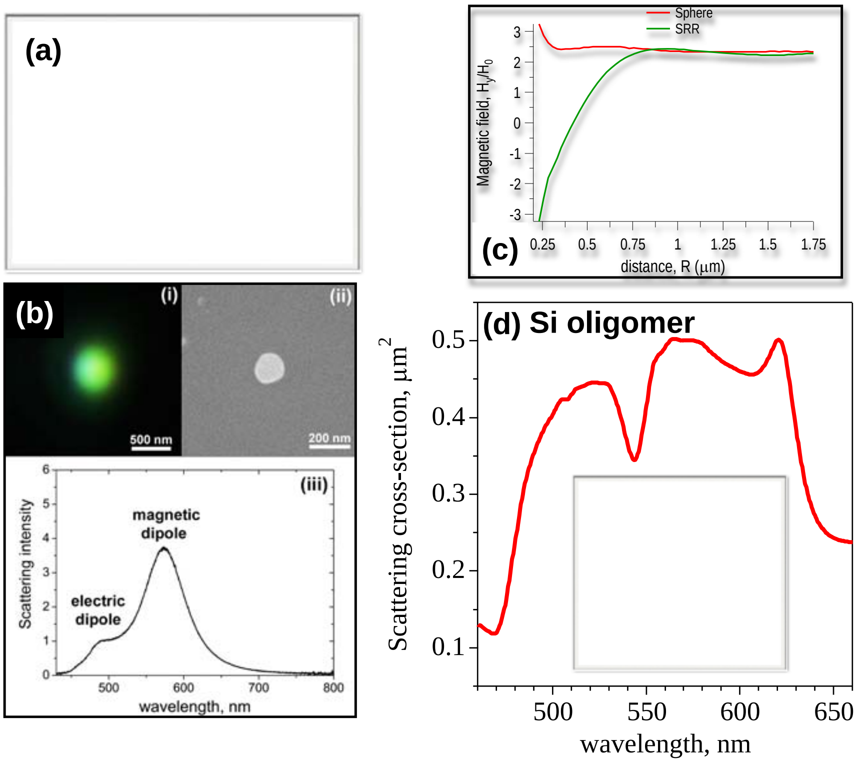

Fig.1 Optically induced magnetic response of high-refractive index dielectric nanoparticles.
(a) Schematic of electric (yellow) and magnetic (blue) field distributions inside a high-refractive index dielectric nanoparticle at the magnetic resonance.
(b) Close-view dark-field microscope: (i) and SEM (ii) images of a single Si nanoparticle with experimental dark-field scattering spectra (iii) exhibiting very strong magnetic dipole (md) resonance.
(c) Dependence of the optically induced magnetization of the dielectric sphere and SRRs on the separation distance at the magnetic resonance frequency. Below the critical distance, the optically induced ferromagnetic-like magnetization is replaced by an antiferromagnetic pattern.
(d) Scattering cross-section of a Si heptamer exhibiting strong Fano resonance. Insert shows the magnetic field distribution at the Fano resonance.

REFERENCES

1. Evlyukhin, A. B. *et al.* "Optical response features of Si-nanoparticle arrays" *Phys. Rev. B*, 82, 045404, 2010.
2. Kuznetsov, A. I. *et. al.*, “Magnetic light”, *Sci. Rep.* Vol. **2**, 492 (2012).
3. Evlyukhin, A. B. *et al.* "Demonstration of magnetic dipole resonances of dielectric nanospheres in the visible region", *Nano Lett.* Vol. 12, 3749 (2012).
4. Miroshnichenko, A. E., B. Luk’yanchuk, and Yu. S. Kivshar,” Optically induced interaction of magnetic moments in hybrid metamaterials,” ACS *Nano*, Vol. 6, 837 (2012).
5. Miroshnichenko, A. E., and Yu. S. Kivshar, “Fano resonance in all-dielectric oligomers,” *Nano Lett.*, available ASAP, (2012).
6. Liu, W., A. E. Miroshnichenko, D. Neshev, and Yu. S. Kivshar, “Broadband unidirectional scattering by magneto-electric core–shell nanoparticles,” *ACS Nano*, Vol. 6, 5489 (2012).
7. Krasnok, A. E., A. E. Miroshnichenko, P. Belov, and Yu. S. Kivshar, “All-dielectric optical nanoantennas,” *Optics Express* Vol. 20, 20599 (2012).

Exotic optical properties of metallo-dielectric core-shell nanospheres and nanowires. Application to negative refraction

R. Paniagua-Domínguez[1], D. R. Abujetas[1], F. López-Tejeira[1], L. Froufe-Pérez[1], R. Marqués[2], J. A. Sánchez-Gil[1*]

[1] Instituto de Estructura de la Materia (CSIC), Serrano 121, 28006 Madrid, Spain

[2] Departamento de Electrónica y Electromagnetismo, Universidad de Sevilla, Sevilla, Spain

[*]corresponding author: j.sanchez@csic.es

Abstract- Here we propose a 2D and 3D isotropic metamaterials with strong electric and magnetic responses in the optical regime, based on hybrid metallo-dielectric core-shell nanospheres and nanowires. The magnetic response stems from the lowest, magnetic-dipole resonance of the dielectric shell with high refractive index, and can be tuned to coincide with the plasmon resonance of the metal core, responsible for the electric response. Also, their scattering properties are investigated in connection with directionality and invisibility.

Artificial materials showing electromagnetic properties not attainable in naturally occurring media, the so called metamaterials, are among the most active fields of research in optical and material physics. One of the major challenges found is to obtain truly three-dimensional isotropic negative index metamaterials (NIM) at optical frequencies.

We report the possibility to use a certain class of core-shell (CS) nanospheres as building blocks of such NIM, operating in the near infrared. These CS, made of a metallic core and a high permittivity shell, are doubly-resonant, allowing for a spectral overlap of their first electric and magnetic dipolar resonances. The strong diamagnetic response is due to the lowest, dipolar magnetic resonance of the shell, where the electric field is forced to rotate as a consequence of the abrupt continuity conditions between the shell and the surrounding medium. The electric resonance is due to the excitation of a localized surface plasmon resonance in the core (see Fig. 1).

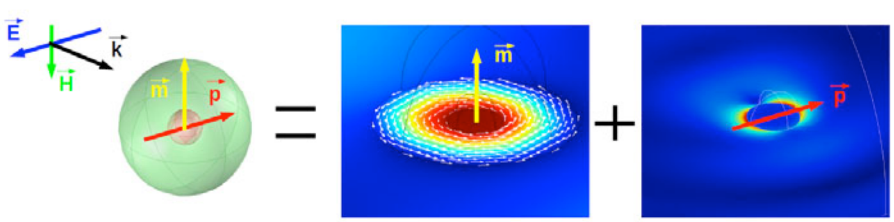

Figure 1: Scheme of the underlying physical mechanism operating in the doubly-resonant metallo-dielectric core-shell nanosphere considered in this work.

Since the responses do not depend on the interaction between constituents, no particular arrangement is needed to build the metamaterial, which is, moreover, intrinsically isotropic and polarization independent. We study realistic designs with silver in the core, and silicon or germanium in the shell. We show that, for certain geometrical parameters and filling fractions, metamaterials composed by such CS nanospheres can have simultaneously negative permittivity and permeability between 1.2-1.55 μm [1].

Moreover, we have extended our study to metallo-dielectric core-shell nanowires, revealing similar properties when incident light wavevector and polarization are both normal to the nanowire axis. The metallic core (localized surface plasmon) resonance provides again the negative electric response; the dielectric shell yields a magnetic resonance, which nonetheless does not exhibit a proper magnetic dipolar character. The resulting metamaterial then behaves in certain frequency range and fixed polarization, as a 2D isotropic NIM, exhibing very low losses (f.o.m. up to 200) [2].

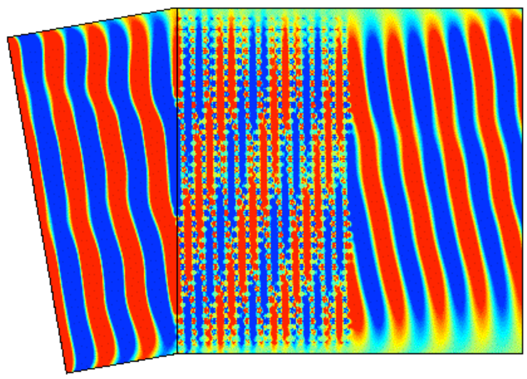

Figure 2: A negative-refraction-index slab made of core-shell (Ag@Si) nanowires operating at λ_0=1.35μm.

Finally, the far-field scattering properties of a single core-shell nanosphere or nanowire are also explored in the spectral region where both (electric and magnetic) resonances either overlap or become negligible. Resonance overlap may lead to Kerker scattering conditions [3], and has been recently proposed as means for broadband focusing [4]; on the other hand, scattering efficiency minima may lead to invisibility domains [5].

Acknowledgements: Spanish "Ministerio de Economía y Competitividad" (CSD2008-00066, FIS2009-11264, and FIS2012-31070), "Comunidad de Madrid" (S2009/TIC-1476), and CSIC (JAE-Pre grant).

REFERENCES

1. R. Paniagua-Domínguez, F. López-Tejeira, R. Marqués and J. A. Sánchez-Gil, "Metallo-dielectric core–shell nanospheres as building blocks for optical three-dimensional isotropic negative-index metamaterials," *New. J. Phys.* 13, 123017, 2011.
2. D. R. Abujetas, R. Paniagua-Domínguez, and J. A. Sánchez-Gil, "Ultra low-loss, isotropic 2D optical negative-index metamaterial based on hybrid metal-semiconductor nanowires," arXiv:1210.8410.
3. J. M. Geffrin, B. García-Cámara, R. Gómez-Medina, P. Albella, L. S. Froufe-Pérez, C. Eyraud, A. Litman, R. Vaillon, F. González, M. Nieto-Vesperinas, J. J. Sáenz, and F. Moreno, "Magnetic and electric coherence in forward- and back-scattered electromagnetic waves by a single dielectric subwavelength sphere," *Nature Communications* 3, 1171, 2012.
4. W. Liu, A. E. Miroshnichenko, D. N. Neshev, and Yu. S. Kivshar, "Broadband unidirectional scattering by magneto-electric core-shell nanoparticles," *ACS Nano* 6, 5489-5497, 2012.
5. D. R. Abujetas, R. Paniagua-Domínguez, L. S. Froufe-Pérez, J. J. Sáenz, and J. A. Sánchez-Gil, preprint.

Dielectric gap-nanoantennas as building blocks for magnetic dipolar emission

P. Albella[1], M. A. Poyli[1], M. K. Schmidt[1], S. Maier[2], F. Moreno[3], J. J. Saenz[4], and J. Aizpurua[1*]
[1]Materials Physics Center (CSIC-UPV/EHU) and Donostia Int. Phys. Center (DIPC), San Sebastián, Spain
[2]Experimental Solid State Group, Department of Physics, Imperial College London, UK
[3]Dep. de Física Aplicada, Universidad de Cantabria, Avenida de los Castros s/n, Santander, Spain
[4]Dep. de Física de la Materia Condensada and Inst. Nicolás Cabrera, Universidad Autónoma de Madrid, Spain
[*]aizpurua@ehu.es

Abstract-Dielectric nanostructures composed of high-refractive index materials show very intense magnetic resonances that make them ideal candidates to interact with magnetic emitters. When two of these dielectric nanoantennas are located in close proximity, the electric and magnetic modes can interact generating the ability to control the properties of light scattering as well as to discriminate the polarization and nature of the emission from a single emitter. We analyze here the optical response of two Si spheres forming a dielectric gap-nanoantenna.

Dielectric spheres composed of high-refractive index materials show fundamental magnetic resonances at lower energies than their electric counterparts [1,2]. These magnetic resonances can be used to enhance the radiative decay of magnetic emitters as demonstrated recently [3]. When two of these dielectric spheres are coupled together at close proximity, the electric and magnetic resonances get coupled producing new spectral features that require some interpretation. A sample of the optical response of such a coupled system is shown in Fig. 1(a), where the resonances of a Si dimer are displayed as a function of separation distance. As the particles get closer together, new spectral features emerge giving rise to blue- and red-shifted coupled resonances.

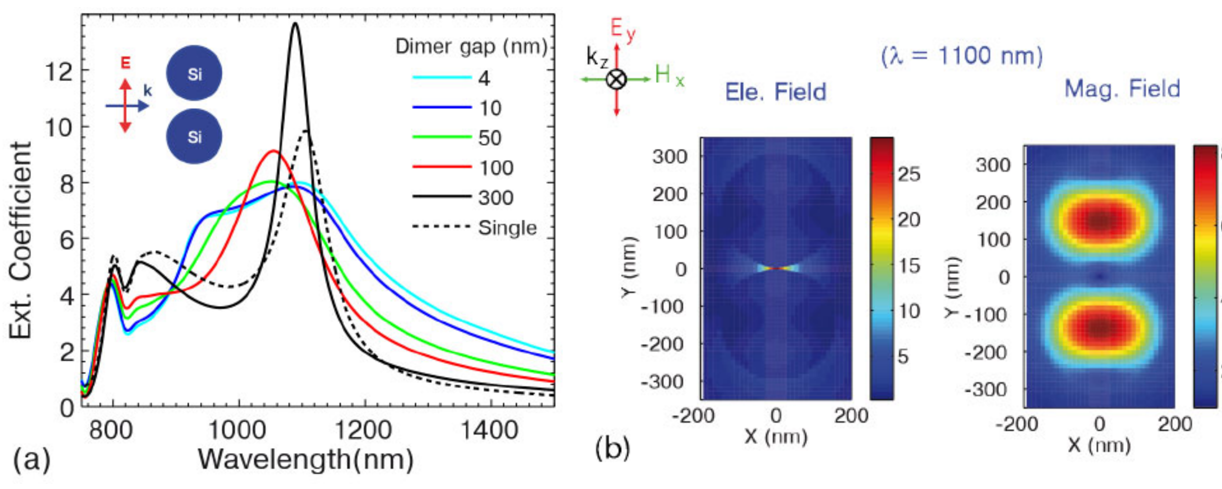

Figure 1: (a) Extinction coefficient of a Si dimer as a function of separation distance. The polarization and incidence of the incoming planewave are displayed in the inset. (b) Near-field distribution of the electric and magnetic fields in a Si dimer separated 4nm at resonance λ=1100nm. The polarization is shown in the inset.

These hybridized resonances can be explained as due to the coupling of the dipolar electric and magnetic resonances induced at each particle. The electric dipoles are excited via the generation of magnetic dipoles at the other particle. A self-consistent solution of all the dipoles explains the complex structure of the far-field.

The structure of the electric and magnetic near-fields at resonance can be observed in Fig. 1(b) with clear localization of the electric field at the Si dimer gap, and of the magnetic field inside the dielectric particles.

Another interesting aspect of these antennas is the enhancement and control of electromagnetic radiation from single emitters. We study the decay rates of single magnetic emitters located at the gap of the dimer for parallel and perpendicular position with respect to the dimer axis. The Si dimer shows the ability to enhance dramatically the emission of a single magnetic emitter located at the gap when it is positioned parallel to the axis of symmetry, whereas other complementary modes are more efficient for perpendicular positioning of the emitter. This allows selective excitation of magnetic modes based on the relative orientation of the emitter, thus opening the path to obtain polarization-selected fluorescence from magnetic emitters, a novel aspect in nanophotonics.

Acknowledgements, Financial support from the ETORTEK project “nanoiker” of the Dept. of Industry of the Government of the Basque Country and from the Spanish Ministerio de Ciencia e Innovación through grant FIS2010-21984 are acknowledged.

REFERENCES

1. Garcia-Etxarri A., Gómez-Medina R., Froufe-Pérez L. S., López C., Chantada L., Scheffold F., Aizpurua J., Nieto-Vesperinas M., and Sáenz J.J., “Strong magnetic response of submicron Si particles in the infrared", *Opt. Express*, Vol. 19, 4815 (2012).
2. Geffrin J.M., García-Camara B., Gómez-Medina R., Albella P., Froufe-Pérez L. S. Eyraud C., Litman A., Vaillon R., González F., Nieto-Vesperinas M., Sáenz J.J., and Moreno F., “Magnetic and electric coherence in forward- and back-scattered electromagnetic wave by a single dielectric subwavelength sphere”, *Nat. Commun*, Vol. 3, 1171, 2012.
3. Schmidt M. K., Esteban R., Sáenz J.J., Suárez-Lacalle I., Mackowski S. and Aizpurua J., “Dielectric antennas - a suitable platform for controlling magnetic dipolar emission”, *Opt. Express*, Vol. 20, 13636, 2012.

Scattering forces on magneto-dielectric particles and the electromagnetic momentum density

Manuel I. Marqués[1*] **and Juan José Sáenz**[2]
[1]Departamento de Física de Materiales & Instituto Nicolás Cabrera,
Universidad Autónoma de Madrid, 28049, Madrid, Spain
[2]Departamento de Física de la Materia Condensada & Instituto Nicolás Cabrera,
Universidad Autónoma de Madrid, 28049, Madrid, Spain

[*]corresponding author: manuel.marques@uam.es

Abstract- In this paper we analyze the non-conservative forces on magneto-dielectric particles in special configurations where the scattering force is not proportional to the average value of the Poynting vector. Based on these results, we revisit the concept of electromagnetic momentum density.

Light energy and momentum can be transferred to particles, molecules, and atoms. After the pioneering experimental work by Ashkin [1], the mechanical action of light on small particles has been extensively used to trap and manipulate small particles with optical tweezers [2–4]. Light forces on a small particle may be described as the sum of the dipole or gradient force and the radiation pressure or scattering force [5,6]. Radiation pressure is traditionally considered proportional to the Poynting vector. However, for inhomogeneous waves, there is an additional contribution to the scattering force that can play an important role in determining the actual forces on nanometer sized particles [7]. Recently, this additional contribution has been shown to be a non conservative force proportional to the curl of the spin angular momentum of the light field [8], that affects to dielectric and magneto dielectric particles [9]. Both radiation pressure and spin forces must be considered in order to understand the scattering forces in the focal volume of microscope objectives [10,11].

As we will show, in some specific cases like, for example, crossed circularly polarized standing waves, the field distribution shows regions in which the electric and magnetic fields are parallel corresponding to a null Poynting vector [12]. Although the average value of the momentum density, proportional to the Poynting vector, is zero in these regions, there are scattering forces acting on small dielectric particles due to light's spin force (see Fig.1). The total scattering force suggests a new definition of the average value of the momentum density, for free propagating electromagnetic fields, proportional to the full scattering forces. We extend these results to small, highly refractive, lossless dielectric particles, which presents both an electric and magnetic response [13,14]. We will discuss the differences between crossed linear [15-17] and circularly polarized waves and the intriguing interplay between the momentum and spin densities and the actual force on magneto-dielectric particles.

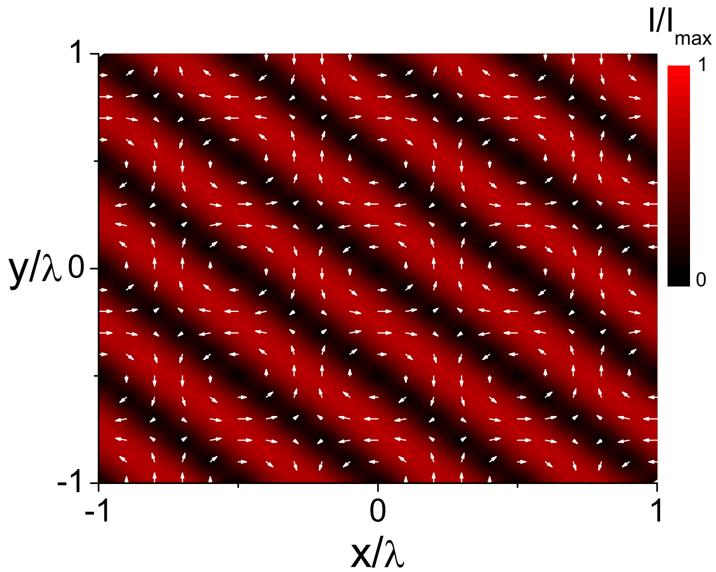

Figures 1: Intensity map for the configuration consisting in two perpendicular, circularly polarized, stationary waves with wavelength λ propagating in the X–Y plane and with a difference on the phase $\phi = \pi/2$. Values are normalized to the maximum intensity value. The map also shows the time-averaged scattering forces induced by the electromagnetic radiation. Note how scattering forces different from zero, coming from the curl of the spin density of the light field, show up in null intensity regions

Acknowledgement, This work was supported through grants FIS2009-13430-C02 and CSD2007-00046 (Consolider NanoLight) and by the Comunidad de Madrid Microseres project S2009/TIC-1476.

REFERENCES

1 . A. Ashkin, Phys. Rev. Lett. 24, 156 (1970).
2 . A. Ashkin, J. M. Dziedzic, J. E. Bjorkholm, and S. Chu, Opt. Lett. 11, 288 (1986).
3 . D. G. Grier, Nature 424, 810 (2003).
4 . K. C. Neuman and S. M. Block, Rev. Sci. Instrum. 75, 2787 (2004)
5 . L. Novotny and B. Hecht, Principles of Nano-Optics (Cambridge University, 2012).
6 . M. Nieto-Vesperinas, P. C. Chaumet, and A. Rahmani, Phil. Trans. R. Soc. A 362, 719 (2004).
7 . V. Wong and M. Ratner, Phys. Rev. B 73, 075416 (2006).
8 . S. Albaladejo, M. I. Marqués, M. Laroche, and J. J. Sáenz, Phys. Rev. Lett. 102, 113602 (2009).
9 . M. Nieto-Vesperinas, J. J. Sáenz, R. Gómez-Medina, and L. Chantada, Opt. Express 18, 11428 (2010).
10. I. Iglesias and J. J. Sáenz, Opt. Commun. 284, 2430 (2011); Opt. Express 20, 2832 (2012).
11. A. Bekshaev, K. Y. Bliokh, and M. Soskin, J. Opt. 13, 053001 (2011).
12. M. I. Marqués and J. J. Sáenz, Opt. Lett. 37, 2787 (2012).
13. A. García-Etxarri et al., Opt. Express 19, 4815 (2011).
14. J.M. Geffrin et al., Nat. Commun. 3, 1171 (2012).
15. R. Gómez-Medina, M. Nieto-Vesperinas, and J. J. Sáenz, Phys. Rev. A 83, 033825 (2011).
16. S. Albaladejo, M. I. Marqués, F. Sheffold, J. J. Sáenz, Nanoletters, 9, 3527 (2009).
17. S. Albaladejo, M. I. Marqués, J. J. Sáenz, Optics Express 19, 11471 (2011).

Magneto-electric optical antennas

B. Rolly[1], S. Varault[1], G. Boudarham[1], B. Stout[1], S. Bidault[2], N. Bonod[1*]

[1]Institut Fresnel, CNRS UMR 7249, Domaine Universitaire de Saint Jérôme, 13397 Marseille, France

[2]Institut Langevin, ESPCI ParisTech, CNRS UMR 7587, 75005 Paris

[*]corresponding author: nicolas.bonod@fresnel.fr

Abstract-In this talk, we will describe the decay rates of electric and magnetic dipolar emitters coupled with electric and magnetic, dipolar and quadrupolar resonators. We will show the explicit relations and will focus on the inter-coupling between electric decay rates and magnetic modes. In the second part of the talk, we will emphasize on the directivity offered by magneto-electric antennas and will evidence the benefit of considering electric and magnetic contributions in order to boost the directivity. The last part of the talk will be focused on the recent advances on non dielectric magneto-electric antennas.

Lanthanide ions (e.g. Eu3+ cations around 0.59 µm, Er3+ cations around 1.54 µm wavelengths) present magnetic dipole (MD) transitions, but those transitions are competing with an electric dipole (ED) transition from the same excited state. In order to investigate and use those MD transitions, a better control of the percentage of the energy radiated as an ED or MD is needed [1]. It has been recently shown that purely dielectric particles could present both electric and magnetic induced dipoles of high quality [2]. We proposed [3] to use high-index dielectric spheres or particles (the general results we obtain can be extended to non-spherical shapes) in order to promote either the MD or the ED transition of a lanthanide ion in the visible to near infrared regime. The rather large quality factor of electric and magnetic quadrupolar resonances of high index dielectric particles compensates their low field confinement compared to the plasmon resonances of metallic particles. Using lossless material permits to exploit those resonances, once again contrary to the case of metallic particles in which nonradiative channels dominate in quadrupolar resonances. In a host matrix of refractive index n = 1.45, and when the emitter is placed at the center of a dimer of Si spheres, we obtain enhancement factors of the magnetic decay rates over the electric decay rates of 4 (around the 1.54 µm wavelength of the MD transition of Er3+), considering an isotropic distribution of the emitter orientations

Kerker set up some conditions on the electric and magnetic Mie coefficients predicting total forward or backward scattering for far-field illumination, with the requirement of the nanoparticle being magneto-electric (in the sense that $\varepsilon r \neq 1$ and $\mu r \neq 1$) [4]. Then Gomez-Medina et al. showed that purely dielectric particles could support strong magnetic dipole resonances, allowing Kerker-like conditions at spectral positions where the induced electric and magnetic dipole resonances overlap [5]. These predictions were very recently nicely measured experimentally in the microwave regime [6]. Nevertheless, with the goal of optical antenna design, near-field illumination has to be considered. Again, a somewhat accurate description can be given using Mie theory, considering the near-field interaction of the emitting dipole with the induced electric and magnetic dipoles inside the dielectric sphere. Computing the far-field time-averaged Poynting vector then yields [7]:

$$\mathbf{P}(x,y,z) = \frac{k^3\omega}{32\pi^2\epsilon_0\epsilon_m r^2}\left[(1-x^2)|1+\gamma_e\bar{\alpha}e^{-jkdz}|^2 + (1-y^2)|\gamma_m\bar{\beta}|^2 + 2z\Re\left\{(\gamma_m\bar{\beta}e^{-jkdz})^*(1+\gamma_e\bar{\alpha}e^{-jkdz})\right\}\right]\hat{\mathbf{e}}_\mathbf{r}$$

The first term represents the interference between the emitting and induced electric dipoles, the second term the radiation of the induced magnetic dipole, and the last term the interference between the induced magnetic dipole and the two electric ones. Searching the conditions for which the Poynting vector goes to zero in the forward or the backward directions, one can then deduce the extended Kerker conditions for near-field illumination, yielding:

$$e^{-jkdz} + \gamma_e \tilde{\alpha} \approx \gamma_m \tilde{\beta}$$

and:

$$e^{+jkdz} + \gamma_e \tilde{\alpha} \approx -\gamma_m \tilde{\beta}$$

Finally applying those Kerker conditions allows for the design of highly directive antennas. Highly efficient and compact nano-antennas can then be designed by coupling a dielectric sphere to a highly radiative near-field source.

The previous studies show how working on the magnetic contribution of nanoparticles can bring new means in the design of highly radiative and directive nano- antennas. In this context, our group is currently investigating alternatives to dielectric spheres in order to design some new type of magneto-electric nanoantenna. We will thus present the latest advances.

REFERENCES

[1] S. Karaveli and R. Zia, "Spectral Tuning by Selective Enhancement of Electric and Magnetic Dipole Emission", Optics letters 106, 193004 (2011)

[2] A. Garcia-Etxarri, R. Gomez-Medina, L. S. Froufe-Perez, C. Lopez, L. Chantada, F. Scheffold, J. Aizpurua, M. Nieto-Vesperinas, and J. J. Saenz, “Strong magnetic response of submicron silicon particles in the infrared”, Opt. Express 19, 4815–4826 (2011)

[3] B. Rolly, B. Bebey, S. Bidault, B. Stout, and N. Bonod, “Promoting magnetic dipolar transition in trivalent lanthanide ions with lossless Mie resonances”, Phys. Rev. B, 85, 245432 (2012)

[4] M. Kerker, D.-S. Wang, and C. L. Giles, “Electromagnetic scattering by magnetic spheres”, J. Opt. Soc. Am. 73, 765–767 (1983)

[5] R. Gomez-Medina, B. Garcia-Camara, I. Suarez-Lacalle, F. Gonzalez, F. Moreno, M. Nieto-Vesperinas, and J. Jose Saenz, “Electric and magnetic dipolar response of germanium nanospheres: interference effects, scattering anisotropy, and optical forces”, Journal of Nanophotonics 5, 053512 (2011)

[6] J.M. Geffrin et al.,” Magnetic and electric coherence in forward- and back-scattered electromagnetic waves by a single dielectric subwavelength sphere,” Nat. Comm. 3, 1171 doi: 10.1038/ncomms2167 (2012).

[7] B. Rolly, B. Stout and N. Bonod, “Boosting the directivity of optical antennas with magnetic and electric dipolar resonant particles”, Optics Express, Vol. 20, 20376–20386 (2012)

Scattering anisotropy, mean free paths and effective refractive index of a disordered dispersion of lossless semiconductor nanospheres

Miztli Yépez [1], Yan Zhang [1], Luis S. Froufe-Pérez [2], Raquel Gómez-Medina [1], Frank Scheffold [3], Manuel Nieto-Vesperinas [4] and Juan José Sáenz [1,*]

[1] Departamento de Física de la Materia Condensada
and Centro de Investigación en Física de la Materia Condensada (IFIMAC),
Universidad Autónoma de Madrid, Campus de Cantoblanco, 28049 Madrid, Spain.

[2] Instituto de Estructura de la Materia, Consejo Superior de Investigaciones Científicas CSIC,
Serrano 121, 28006 Madrid, Spain.

[3] Department of Physics, University of Fribourg, Chemin du Muse 3, 1700 Fribourg, Switzerland

[4] Instituto de Ciencia de Materiales de Madrid, Consejo Superior de Investigaciones Científicas CSIC, Campus de Cantoblanco, 28049 Madrid, Spain.

[*]corresponding author: juanjo.saenz@uam.es

Abstract- Lossless dielectric nanospheres (made of nonmagnetic materials) with moderate refraction index may present strong electric and magnetic dipolar resonances. We analyze the light scattering from a dilute dispersion of dipolar semiconductor spheres. We show that there is an optical frequency range in which the scattering asymmetry parameter is negative and hence the dispersion acquires a transport mean free path smaller than its scattering mean free path. The Physics behind the effective refractive index and Fresnel reflection and transmission coefficients of a disordered thin film based on a disordered dispersion of dipolar semiconductor spheres will be discussed.

Our current understanding of the diffusive transport through nonabsorbing media is based on the knowledge of two key quantities: the transport and scattering mean free paths (MFPs). The scatter density and cross section define the scattering MFP l_S. The relevant scattering length for diffusive light power transport is the transport MFP l^*. Both quantities are connected by the scattering asymmetry parameter g defined [1] as the average of the cosine of the scattering angle. Isotropic Rayleigh scattering of small particles leads to $g \sim 0$ while it is frequently argued that for Mie particles (or human tissue) [1] scatter strongly in the forward direction (small scattering angles) and hence $g \sim 1$. The unusual observation of negative g has been limited to systems with appropriate short-range correlations [2].

Recently it has been shown that subwavelength spheres made of nonabsorbing dielectric material with relatively low refractive index produce strongly asymmetric angular distributions of scattered intensity [3,4] with unusual properties like the inhibition of backward scattered intensity and the almost inhibition of the scattered intensity in the forward direction. As we will see, these particles can present negative-g values in specific wavelength regions around the condition near-zero forward scattering i.e., a random dispersion of such particles will show the unusual characteristic of having $l^* < l_S$ even in the absence of positional correlations [5]. The intriguing effective optical properties of a thin film made of a disordered dispersion of such particles at the zero-backwards scattering condition will be discussed in detail.

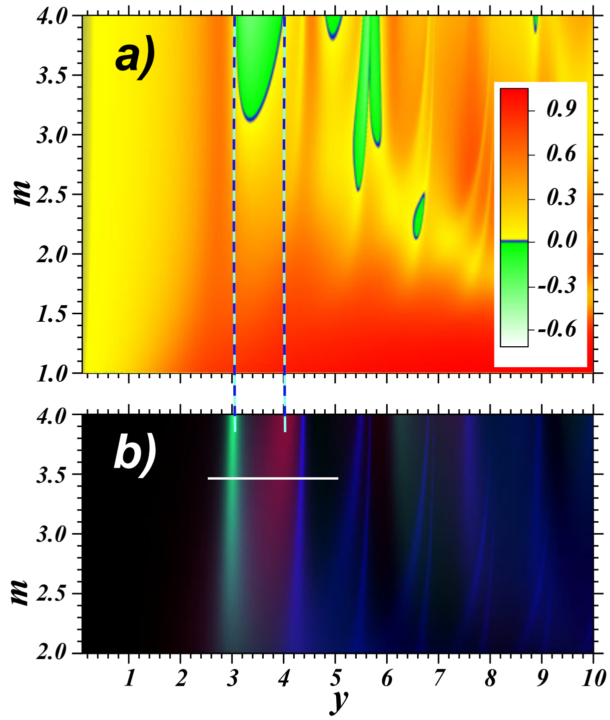

Figure 1- (a) Color map of the g factor for spherical absorptionless particles as a function of their refractive index m and size parameter y = mka. As seen in the attached scale, green areas correspond to negative values of g. (b) Color map of the sphere scattering cross section. Red corresponds to dominant electric dipole contributions to the scattering cross section. Green corresponds to dominant magnetic dipole contributions, while blue sums up all higher-order multipole terms. Vertical dashed lines coincide with y parameter for maximum electric dipole contribution (right vertical line) and maximum magnetic dipole contribution (left vertical line). The white horizontal line at m ≈ 3.5 which corresponds to a silicon sphere. (After Ref.[5]).

Acknowledgements, This work was supported by the Spanish Ministerio de Ciencia e Innovación through grants: Consolider NanoLight (CSD2007-00046), FIS2009-13430-C01-C02 as well as by the Comunidad de Madrid (Microseres-CM, S2009/TIC-1476). M.Y. thanks the Mexican Consejo Nacional de Ciencia y Tecnología for a postdoctoral grant (No. 000000000162768).

REFERENCES

1. C. F. Bohren and D. R. Huffman, *Absorption and Scattering of Light by Small Particles,* Wiley, N.Y., 1983.
2. Rojas-Ochoa, L. et al. “Photonic properties of strongly correlated colloidal liquids”, *Phys. Rev. Lett.,* Vol. 93, 073903 (2004).
3. Garcia-Etxarri A. et al. “Strong magnetic response of submicron Si particles in the infrared", *Opt. Express*, Vol. 19, 4815-4826 (2011).
4. Geffrin, J.M. et al. “Magnetic and electric coherence in forward- and back-scattered electromagnetic waves by a single dielectric subwavelength sphere”, *Nat. Commun.,* Vol. 3, 1171-1178 (2012).
5. Gomez-Medina, R. et al. “Negative scattering asymmetry parameter for dipolar particles: Unusual reduction of the transport mean free path and radiation pressure”, *Phys. Rev. A*, Vol. 85, 035802 (2012).

Magnetic response of Si nanoparticles in the visible spectral region

A. B. Evlyukhin, U. Zywietz, T. Birr, R. Kiyan, C. Reinhardt, and B. N. Chichkov

Laser Zentrum Hannover e.V., Hollerithallee 8, D-30419 Hannover, Germany
a.b.evlyukhin@daad-alumni.de

Abstract— Strong resonant light scattering by individual spherical Si nanoparticles is experimentally demonstrated, revealing pronounced resonances associated with the excitation of magnetic and electric modes in these nanoparticles. The fabrication of Si nanoparticles is based on laser transfer from bulk and film substrates. Influences of the particle sizes, shapes, and environments on the spectral positions of the electric and magnetic dipole resonances are discussed by comparison of experimental and theoretical results. The scattering properties are measured by single particle spectroscopy. Theoretical investigations are performed using a recently developed numerical approach, allowing analyzing the role of different multipole modes in the extinction and scattering spectra of arbitrary shaped nanoparticles located either in a homogeneous surrounding or on a substrate surface. It is shown that it is possible to design silicon particles for which the electric dipole and magnetic dipole resonances are located at the same wavelength under certain propagation directions of incident light.

It has been shown theoretically that spherical silicon nanoparticles can have two optical resonances (electric dipole and magnetic dipole) in the visible [1] or near infrared [2] spectral ranges, depending on their sizes. This is a principal result of Mie theory, demonstrating the possibility of optical magnetism on the base of Si nanoparticles. In this work, we present experimental results which demonstrate strong resonant optical magnetic and electric response of individual spherical Si nanoparticles with radii in the range of 60-100 nm. The Si nanoparticles are fabricated on glass substrates by laser-induced transfer (LIT) and characterized using linear transmission and reflection spectroscopy with high spatial resolution. A schematic presentation of the experimental arrangement used for LIT can be found for example in [3]. The fabricated Si nanoparticles accquire a spherical shape due to the high surface tension of the molten silicon. Figure 1 demonstrates SEM image of a spherical Si nanoparticles with different radii and their corresponding scattering spectra. The scattering spectra are recorded by a fibre-coupled spectrometer in combination with a dark field microscope showing clearly the electric an magnetic dipole resonances around 520 nm and 630 nm, respectively. Theoretical analysis of the experimental spectra show that resonant peaks correspond to excitation of electric and magnetic dipole modes of the nanoparticle. Note that the dark-field image of Si nanoparticles fabricated on a glass substrate can have different colors, being associated to nanoparticles with different diameters. This indicates a strong dependence of the scattering resonances on the particle size [3, 4].

In order to analyze the influence of different parameters, including particle sizes and shapes, on the spectral positions of the scattering resonances of Si nanoparticles, we apply a new theoretical approach, allowing the role of multipole modes in the extinction and scattering spectra of arbitrary shaped nanoparticles [5] to be analyzed. The approach is based on the discrete dipole approximation (DDA). Within DDA, nanoparticles are represented as a three-dimensional arrayed ensemble of point dipoles in a local domain with dimensions smaller than the scattered wavelength. One can then represent the scattered fields (radiated fields by the dipoles) approximately as a series of multipole contributions. Our approach can be applied to the cases when the scattering nanoparticles are located in a homogeneous environment or in close proximity to a substrate surface. In the frame of this approach, the extinction cross section σ_{ext} of an arbitrary-shaped scatterer can be presented as a sum of multipole terms:

$$\sigma_{ext} = \sigma_{ext}^{p} + \sigma_{ext}^{Q} + \sigma_{ext}^{m} + \sigma_{ext}^{M} + \sigma_{ext}^{O} + \dots\,, \tag{1}$$

where σ_{ext}^{p}, σ_{ext}^{Q}, σ_{ext}^{m}, σ_{ext}^{M}, σ_{ext}^{m} are the cross sections corresponding to the electric dipole (ED), electric quadrupole (EQ), magnetic dipole (MD), magnetic quadrupole (MQ), and electric octupole (EOC) contributions, respectively. Multipole decomposition of the extinction cross sections into

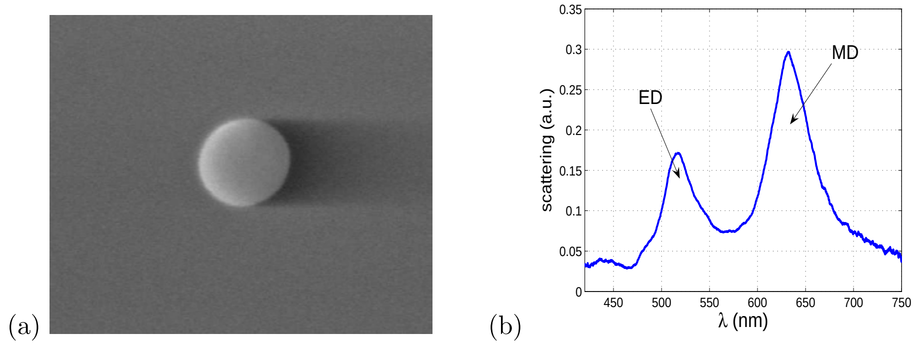

Figure 1: (a) SEM image of spherical Si nanoparticle (radius of 75 nm) on a glass substrate. (b) Scattering spectrum of the nanoparticle. Two peaks correspond to electric dipole (ED) and magnetic dipole (MD) resonant scattering.

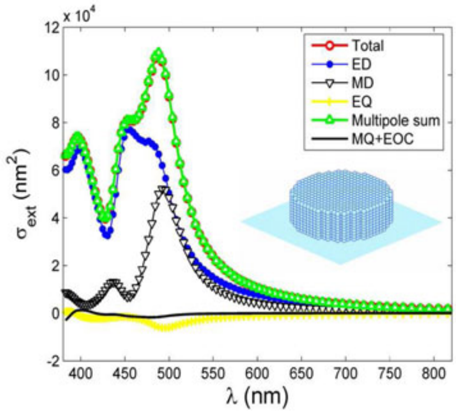

Figure 2: Extinction cross-section spectra of cylindrical silicon nanoparticles located in air on glass substrate. The particle dimensions: height 70 nm, diameter 140 nm. Linearly-polarized light plane waves propagate along the cylinder symmetry axis and normally to the substrate surface. The graphs present the total ECS, separate contributions of different multipole modes (ED-electric dipole, MD-magnetic dipole, EQ-electric quadrupole, MQ-magnetic quadrupole, EOC-electric octupole), and the multipole sum.

different multipole contributions allows classifying the resonances and evaluating their relative efficiencies. As an example, Figure 2 demonstrates the extinction cross section of cylindrical Si nanoparticles on a flat glass substrate. We see that the ED and MD resonances overlap and generate a hybrid electromagnetic state in the nanoparticle. Here, we will discuss the influences of the mutual spectral positions of electric and magnetic dipole resonances for particles of different shapes as well as possible constructions of artificial optical media with Si nanoparticles as building blocks are discussed.

REFERENCES

1. Evlyukhin, A. B., C. Reinhardt, A. Seidel, B. S. Luk'yanchuk, and B. N. Chichkov , "Optical response features of Si-nanoparticle arrays," *Phys. Rev. B* Vol. 82, 045404, 2010.
2. García-Etxarri, A., R. Gómez-Medina, L. S. Froufe-Pérez,2 C. López, L. Chantada, F. Scheffold, J. Aizpurua, M. Nieto-Vesperinas, and J. J. Sáenz, "Strong magnetic response of submicron Silicon particles in the infrared," *Opt. Express* Vol. 19, 4815–4826, 2011.
3. Evlyukhin, A. B., S. M. Novikov, U. Zywietz, R. L. Eriksen, C. Reinhardt, S. I. Bozhevolnyi, and B. N. Chichkov, "Demonstration of magnetic dipole resonances of dielectric nanospheres in the visible region," *Nano Lett.* Vol. 12, 3749–3755, 2012.
4. Kuznetsov, A. I., A. E. Miroshnichenko, Y. H. Fu, J. Zhang, and B. Luk'yanchuk, "Magnetic light," *Sci. Rep.* Vol. 2, 492, 2012.
5. Evlyukhin, A. B., C. Reinhardt, and B. N. Chichkov , "Multipole light scattering by non-spherical nanoparticles in the discrete dipole approximation," *Phys. Rev. B* Vol. 84, 235429, 2011.

Magneto-optical response of nanoparticles and some potential use in active nanophotonics

R. Carminati[1], **H. Marinchio**[1], **R. Vincent**[2] **and J.J. Sáenz**[3]

[1]Institut Langevin, ESPCI ParisTech, CNRS, France
[2]Université de Technologie de Troyes, France
[3]Universidad Autónoma de Madrid, Spain
remi.carminati@espci.fr

Abstract— We discuss the magneto-optical response of nanoparticles, and their potential use in plasmonics and for the control of non-radiative energy transfer in molecular fluorescence. Our results provide theoretical proofs of concept for applications of magneto-optics to active nanophotonics.

One aspect of active nanophotonics is the control of the optical response of a nanostructure using an external parameter. Among various possible approaches, the use of a magneto-optical response, with the external static magnetic field as a control parameter, is receiving increasing attention. In this talk, we focus on the magneto-optical response of nanoparticles and discuss their potential use in plasmonics and for the control of non-radiative energy transfer in molecular fluorescence.

We discuss the optical response of nanoparticles based on the concept of dressed polarizability, both for the "dielectric" isotropic response (dielectric or metallic nanoparticles) [1] and for the magneto-optical response (magnetic nanoparticle) [2, 3]. We show that the magneto-optical response of a nanoparticle in the vicinity of a flat substrate can be enhanced by near-field interactions, with respect to the purely dielectric contribution. In the case of metallic surfaces, we identify the role of surface-plasmon polaritons in the enhancement process [3]. We show that a magnetic nanoparticle can also be used to locally excite surface plasmons. We identify a scheme allowing to produce a directional excitation even with a single spherical nanoparticle [4].

We study the the potential use of magnetic nanoparticles to control non-radiative energy transfer in molecular fluorescence (Förster resonance energy transfer or FRET). We show that the distance dependence, the orientation dependence and the strength of the FRET efficiency can be changed substantially by the magneto-optical response of the nanoparticle [5]. In particular the distance dependence is controlled by a new distance R_p that depends of the polarization properties of the nanoparticle, and that replaces the usual Förster radius.

Our results provide theoretical proofs of concept for applications of magneto-optics to active nanophotonics. The road towards effective devices rely on the design of nanoparticles with large magneto-optical activity (compared to that of usual ferromagnetic materials).

REFERENCES

1. E. Castanié, R. Vincent, R. Pierrat and R. Carminati, "Absorption by an optical dipole antenna in a structured environment", *Int. J. Opt.*, Vol. 2012 (special issue), 452047, 2012.
2. S. Albaladejo, R. Gómez-Medina, L.S. Froufe-Pérez, H. Marinchio, R. Carminati, J.F. Torrado, G. Armelles, A. García-Martín and J.J. Sáenz, "Radiative corrections to the polarizability tensor of an electrically small anisotropic dielectric particle", *Opt. Express*, Vol. 18, 3556, 2010.
3. H. Marinchio, J.J. Sáenz and R. Carminati, "Light scattering by a magneto-optical nanoparticle in front of a flat surface: Perturbative approach" , *Phys. Rev. B*, Vol. 85, 245425, 2012.
4. R. Vincent and R. Carminati, in preparation, 2012.
5. R. Vincent and R. Carminati, "Magneto-optical control of Förster energy transfer", *Phys. Rev. B*, Vol. 83, 165426, 2011.

Progress in all-dielectric optical nanoantennas

A. E. Krasnok[1], **P. A. Belov**[1,♯], **A. E. Miroshnichenko**[2], **Yu. S. Kivshar**[1,2]

[1]National Research University of Information Technologies, Mechanics and Optics (ITMO), St. Petersburg 197101, Russia

[2]Nonlinear Physics Centre, Research School of Physics and Engineering, Australian National University, Canberra ACT 0200, Australia

♯ email: belov@phoi.ifmo.ru

Abstract— We suggest and verify experimentally a novel type of optical nanoantennas made of high-permittivity low-loss dielectric spheres. In addition to the electric resonances, they exhibit very strong magnetic resonances at the nanoscale. By placing a point-like dipole source near a single dielectric particle driven at the magnetic resonance results the radiation pattern similar to that of a Huygens source with the enhanced forward and vanishing backward emission. This feature can be employed in the Yagi-Uda geometry for highly efficient optical nanoantennas.

The recently emerged field of optical nanoantennas is promising for its potential applications in various areas of nanotechnology [1]. The ability to redirect propagating radiation and transfer it into localized subwavelength modes at the nanoscale makes the optical nanoantennas highly desirable for efficient solar cells, biological and chemical sensing, quantum communication systems, molecular spectroscopy and, in particular, for the emission enhancement and directionality control over a broad wavelength range. We suggest [2, 3] a novel type of optical nanoantennas made of all-dielectric elements and argue that, since the source of EM radiation is applied externally, dielectric nanoantennas can be considered as the best alternative to their metallic counterparts. First, dielectric materials exhibit low loss at the optical frequencies. Second, as was suggested earlier [4], nanoparticles made of high-permittivity dielectrics may support both electric and magnetic resonant modes. This feature may greatly expand the applicability of optical nanoantennas for, e.g. detection of magnetic dipole transitions of molecules. In our study we concentrate on nanoparticles made of silicon.

The mentioned above properties of dielectric nanoparticles allow to realize optical Huygens source [6] consisting of a point-like electric dipole operating at the magnetic resonance of a dielectric nanosphere (Fig.1a). Such a structure exhibits high directivity with vanishing backward scattering and polarization independence, being attractive for efficient and compact designs of optical nanoantennas.

In Fig. 2a we show the dependence of the Directivity versus wavelength for a single dielectric nanoparticle excited by a electric dipole source. The inserts demonstrate 3D angular distribution of the radiated pattern corresponding to local maxima. One can clearly see, that in case the system radiates mostly in the forward direction at $\lambda = 590$ nm, while in another case, the radiation is predominantly in the backward direction at $\lambda = 480$ nm.

By adding more elements to the single silicon nanoparticle it is possible to enhance the nanoantenna performance. Next we consider the dielectric analogue of the Yagi-Uda like design, shown in Fig. 1b. It consist of four directors and one reflector. The radius of the directors and the reflector

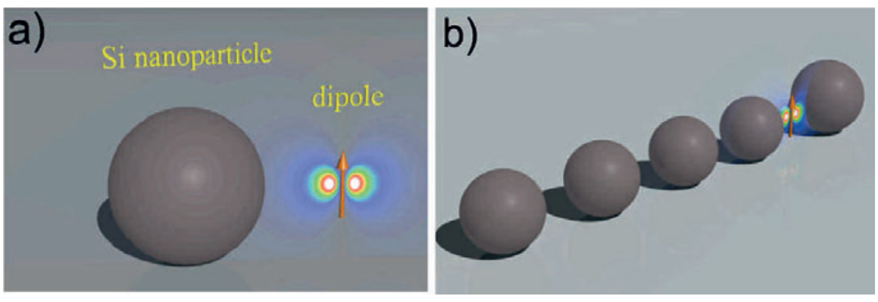

Figure 1: Huygens element (a) and dielectric Yagi-Uda nanoantenna (b) based on silicon nanoparticles.

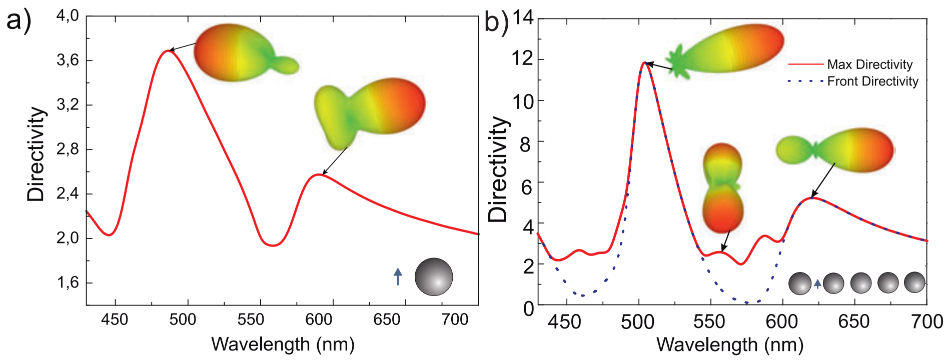

Figure 2: Directivity of the dielectric Huygens element (a) and Yagi-Uda nanoantenna for the separation distance G = 70 nm (b) vs wavelength. Insert demonstrates 3D radiation pattern diagrams at particular wavelengths.

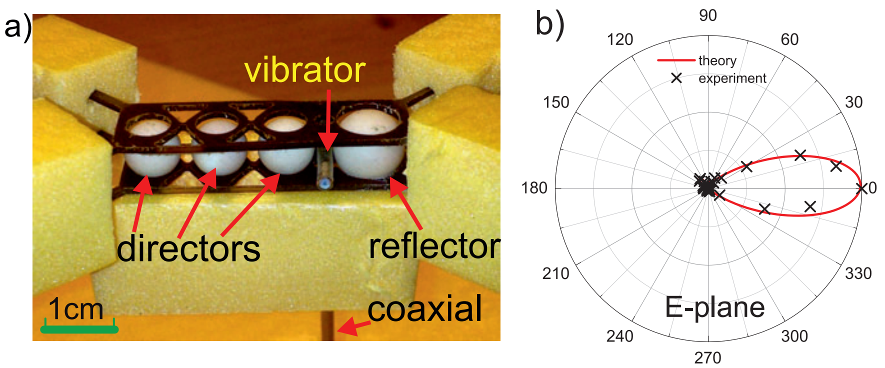

Figure 3: Photographs of the all-dielectric Yagi-Uda microwave antenna placed in a holder(a) and experimental radiation pattern of the antenna in E-plane (b).

should be chosen is such a way to achieve the maximal constructive interference in the forward direction along the directors chain. In Fig. 2b we plot the directivity of the dielectric Yagi-Uda nanoantenna versus wavelength with the separation distance G = 70 nm. The strong maximum is obtained at $\lambda = 500$ nm. The main lobe is extremely narrow with the beamwidth about 40° and the backscattering is negligible, as it can be seen from the corresponding insert.

We scale the dimensions and provide the first experimental verification of the concept of all-dielectric nanoantennas. Figures 3a show the photographs of the fabricated all-dielectric Yagi-Uda antenna. To mimic the silicon spheres at the microwave frequency range, we employ MgO-TiO_2 ceramic which is characterized by dielectric constant of 16 and dielectric loss factor of (1.12-1.17)10^{-4} measured at 9-12 GHz frequency range. As a source, we use a half-wavelength vibrator. We study experimentally both the radiation pattern and directivity of the antenna.

The antenna radiation patterns in the far field (at the distance $\simeq 3$ m, $\simeq 100\lambda$) are measured in an anechoic chamber by a horn antenna and rotating table. The measured radiation patterns of the antenna in E- and H-planes at the frequency 10.7 GHz are shown in Fig. 3b. The measured characteristics agree very well with the numerical results.

REFERENCES

1. L.Novotny and N. van Hulst, "Antennas for light", *Nat. Photon.,* vol. 5, p. 83, 2011.
2. A. E. Krasnok, A. E. Miroshnichenko, P. A. Belov and Yu. S. Kivshar, "All-dielectric optical nanoantennas", *Opt. Express,* vol. 20, p. 20599, 2012.
3. D. S. Filonov1, A. E. Krasnok, A. P. Slobozhanyuk, P. V. Kapitanova, E. A. Nenasheva, Yu. S. Kivshar, and P. A. Belov, "Experimental verification of the concept of all-dielectric nanoantennas", *APL,* vol. 100, p. 201113, 2012.
4. A. B. Evlyukhin, C. Reinhardt, A. Seidel, B. S. Lukyanchuk and B. N. Chichkov, "Optical response features of Si-nanoparticle arrays", *Phys. Rev. B,* vol. 82, p. 045404, 2010.
5. E. Palik, *Handbook of Optical Constant of Solids,* San Diego, Academic, 1985.
6. C. Balanis, *Antenna theory: analysis and design,* New York ; Brisbane : J. Wiley, 1982.

Emerging technology in plasmonics

Multi-level 3-D Plasmonic Nano-Circuits

M.H. Bakr[1], M. H. El Sherif[1*], O. S. Ahmed[1], and M. A. Swillam[2]

[1] Department of Electrical and Computer Engineering, McMaster University, Hamilton, Ontario L8S 4K1, Canada.

[2] Department of Physics, The American University in Cairo, P.O. Box 74 New Cairo 11835, Cairo, Egypt.

[*]corresponding author: elsherm@mcmaster.ca

Abstract- A novel and compact surface plasmon polarization-controlled beam splitter is proposed. The beam splitter is designed based on the orthogonal junction coupling between silicon nanowires and plasmonic slot waveguides (PSWs). It couples light with different polarizations from a silicon nanowire to multi-level plasmonic set-ups. Two orthogonal PSWs are employed to guide each polarization to its respective port. This ability of controlling polarization can be exploited to achieve 3-D multi-level plasmonic circuits and polarization controlled chip to chip channel.

Surface Plasmon Polariton (SPP) devices can be miniaturized below the diffraction limit [1], bridging the gap between electronics and optics. They are proposed for optical circuits to replace the copper interconnects. The fabrication and integration of these plasmonic devices is done on silicon on insulator (SOI), which leads to an evolution in integrating optical and electronic devices. The routing and data transfer are done using optical interconnects without affecting the functionality of the electronic circuit [1].

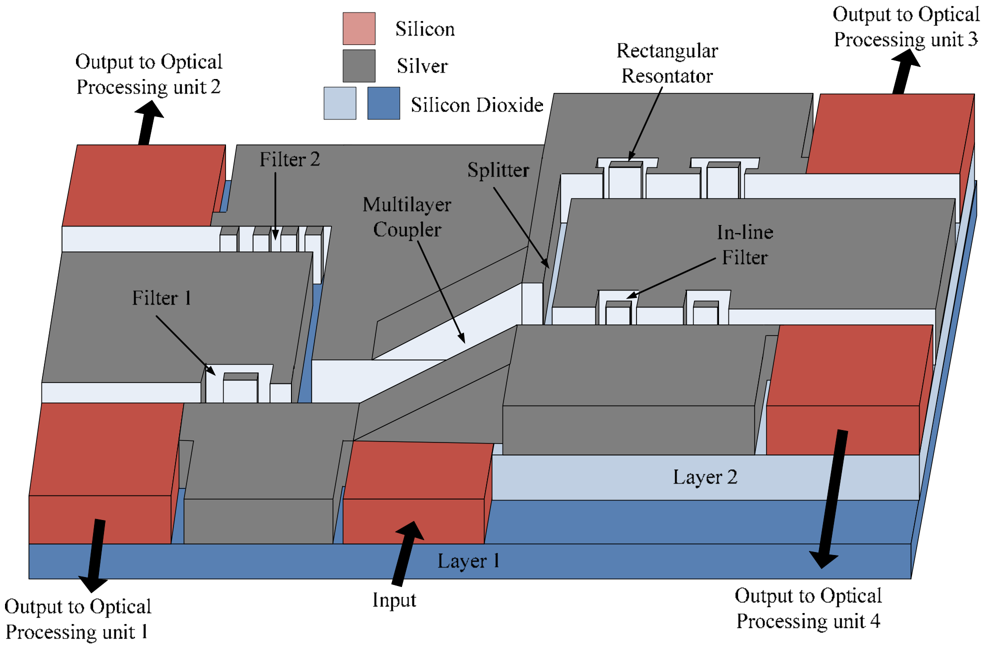

Figure 1. A 3-D plasmonic chip

The interfaces between electronic and optical components are challenging for dense device integration. An all-optical chip can be exploited to realize a complete optical computation and communication system. The number of optical components placed on a chip is limited by the cross talk between the closely placed components [2], thus limiting the efficiency of in-plane chips. An approach to solve this issue is stacking the optical chips in order to have multiple levels as shown in Fig. 1. By stacking multiple circuits, highly dense photonic optical circuits with faster processing and wider functionality can be realized.

Several approaches for realizing 3-D optical chips have been proposed using the conventional Silicon on Insulator (SOI) [2]. They are limited in size, subject to cross talk, and sensitive to fabrication [3]. A potential alternative is to exploit plasmonic to provide high density integration with minimal cross talk. Little work has been done in realizing 3-D chips using plasmonics. 3-D plasmonic chips are limited to the polarization dependence of the SPP waves. Signal manipulation utilizes only one polarization of the input field. The other polarization does not couple to the SPP structures. This is a serious drawback that obstructs using quadrature functionalities.

We propose a novel structure for realizing multilevel plasmonic chips based on the right angle coupling configuration demonstrated in [4]. The structure acts as a surface plasmon polarization beam splitter. The main functionality of this device is to allow both polarizations of the input field to be manipulated using plasmonic structures by routing each one to a different horizontal plane. A conventional silicon nanowire is utilized as the input waveguide. By controlling the light polarization at the nanoscale, on-chip communication becomes much faster. Moreover, this will introduce a quadrature space that provides multifold of the current capacity. The proposed device helps in realizing 3-D plasmonic chips that are compact and with high integration and density.

The proposed structure is shown in figure 2. A -4.5 dB transmission efficiency at a wavelength of 1.55 μm is obtained for the different polarizations in the respective output ports. A transmission efficiency of -21 dB is achieved in the subsidiary port. We analyze and simulate the structure using the FDTD method with silver and aluminum as the materials for the PSWs. The proposed device can be utilized in integrated chips for optical signal processing and optical computations.

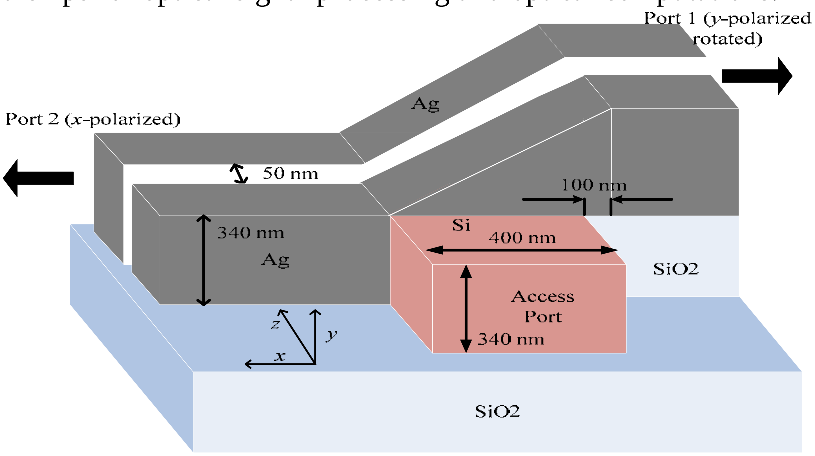

Figure 2. The structure of the polarization splitter for multilevel coupling

REFERENCES

1. Maier, S. A. and M. L. Brongersma, P.G. Kik, S. Meltzer, A. A. G. Requicha, and H. A. Atwater, “Plasmonics-a route to nanoscale optical devices,” *Adv. Mater.*, Vol. 13**,** No. 19, 1501-1505, 2001.
2. Raburn, M., B. Liu, K. Rauscher, Y. Okuno, N. Dagli, and J. E. Bowers, “3-D photonic circuit technology,” *IEEE J. Sel. Toics Quantum Electron.*, Vol. 8, No. 4, 935-942, 2002.
3. Garner, S. N., S. Lee, V. Chuyanov, A. Chen, A. Yacoubian, W. H. Steier, and L. R. Dalton, “Three-dimensional integrated optics using polymers,” *IEEE J. Quantum Electron.*, Vol. 35, No. 8, 1146-1155, 1999.
4. Lau, B., M. A. Swillam, and A. S. Helmy, “Hybrid orthogonal junctions: wideband plasmonic slot-silicon waveguide couplers,” *Opt. Express*, Vol. 18, No. 26, 27048-27059, 2010.

Accurate Finite Difference Analysis of Novel Trenched Channel Plasmonic Waveguides

A. M. Heikal, M.F.O. Hameed, S.S.A.Obayya*

Centre for Photonics and Smart Materials, Zewail City of Science and Technology, Sheikh Zayed District, 6th of October City, Giza, Egypt. E-mail: sobayya@zewailcity.edu.eg

Abstract- In this paper, accurate modal analysis of a novel design of three trenched single mode channel plasmon polariton is introduced and analyzed. The simulation results are obtained using accurate full-vectorial finite difference method for linear oblique and curved interface which overcomes staircase problem of the conventional finite difference methods. The suggested design has a good confinement behavior similar to the V-grove structure with improved propagation length. However, the reported structure is easier in fabrication and design with lower propagation loss.

Plasmons are defined as electromagnetic excitations coupled to the charges of a conductive medium. Many optical devices operates on telecommunication wavelength nowadays depends on the channel plasmon polariton (CPP) [1] such as waveguide bends, and splitters. One of the most popular CPP is the V-shaped grove which is drilled in the top side of the metal [1]. The V-shaped grove has a well confined field inside the grove while it is difficult for fabrication with a moderate propagation length.

In this paper, a comprehensive study has been done to investigate the dispersion characteristics of a novel design of CPP based on three-trenched-type grove. Figure 1(a) shows the suggested novel three-trenched grove CPP structure. The reported CPP consists of three-trenches drilled vertically on the top surface of the gold metal with three different widths W_1, W_2 and W_3. The depths of each grove are d_1, d_2, and d_3. However, the conventional V shape structure is shown in Fig. 1(b). The refractive index of the Gold metal is calculated using Drude Model [2]. It is evident from Fig.1 (b) that the V-shaped structure has oblique interfaces. In addition, the conventional full vectorial finite difference method (FVFDM) [3] deals with horizontal and vertical interface. Therefore, the conventional FVFDM suffers from staircase problem when dealing with the V- shaped grove. Therefore, accurate FVFDM for linear oblique and curved interface (FVFDM-LOCI) [4] with perfect matched layer boundary conditions is used to analyze the V-shaped grove and the suggested three-trenched-type grove. Throughout this paper, the propagation length L_{prop}=1/Imaginary(β/k) is calculated using complex propagation constant β and free space wave number k. In addition, the confinement of the field inside CPP waveguides based on air groove can be well explained by studying the lateral (parallel to the x-axis) mode radius r_{3dB} which is defined as the distance of -3dB power drop point from the waveguide symmetrical plane. Moreover, the figure of merit (FOM) has been used and defined as FOM = L_{prop}/ r_{3dB}.

Figure 2 shows the variation of the propagation length and real part of complex effective index n_{eff} of the V-shaped structure with the meshing size using conventional FVFDM [3] and FVFDM-LOCI [4]. In this study, the meshing size Δx in x direction is equal to meshing size Δy in y direction. In addition, the width W and depth d of the V grove are taken as 0.5 μm, 1.2 μm, respectively. It is revealed from Fig. 2 that the FVFDM-LOCI is more accurate than the conventional FVFDM in studying the CPP with oblique interfaces. As the meshing size decreases, n_{eff} decreases while the propagation losses increases until convergence occurs at meshing size of Δx=

Δy=0.003 μm. Therefore, meshing size Δx= Δy=0.003 μm is used in the subsequent simulations throughout this work.

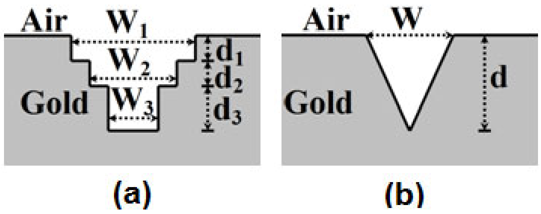

Figure 1 Schematic diagram of (a) novel three-trenched grove structure (b) V-shaped structure

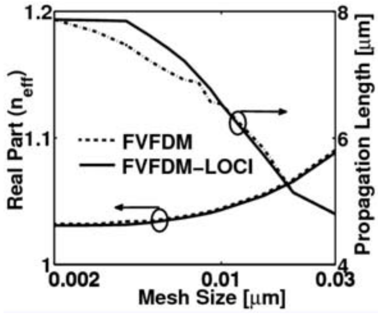

Figure 2 Variations of the propagation length and effective index of the V-shaped structure with the meshing size

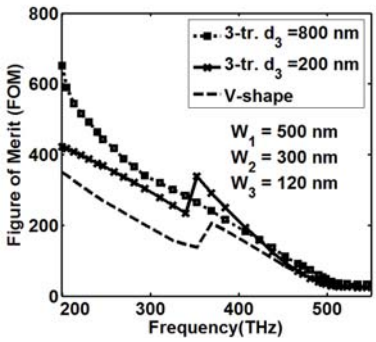

Figure 3 Variation of frequency dependent FOM for the V-grove, and three trenched grove waveguides with two different depths d_3.

The variation of the frequency dependent FOM for the V-groove and the three trenched groove waveguide with two different depths d_3, 200 μm and 800 μm is shown in Fig. 3. In this study, d_1 of the suggested grove is set to 200 nm and d_2+d_3 are fixed to 1.0 μm. In addition, W_1, W_2 and W_3 are taken as 500 nm, 300 nm, and 120 nm, respectively. It is revealed from Fig.3 that the V-groove with d=1.2 μm and W=500 nm is the most efficient groove with the highest FOM for frequency greater than 500 THz. However, in the frequency range from 350 to 400 THz, the propagation length for the 3-tenched groove with d_3 = 200 nm is greater than that of all other grooves. When the frequency decreases below f = 350 THz, r_{3dB} for the three trenched groove with a short d_3=200 nm starts to increase causing the FOM to drop down suddenly. More results will be presented in the conference including the effect of the structural geometrical parameters on the real part of effective index n_{eff}, propagation length, lateral mode radius r_{3dB} and FOM.

REFERENCES

1. Moreno, E., F. J. Garcia-Vidal, S. G. Rodrigo, L. Martin-Moreno, and S. I. Bozhevolnyi, "Channel plasmon polaritons: modal shape, dispersion, and losses," *Opt. Lett*., Vol.31, 3447-3449, 2006
2. Kubo, S., A. Diaz, Y. Tang, T. S. Mayer, I. C. Khoo, and T. E. Mallouk, "Tunability of the Refractive Index of Gold Nanoparticle Dispersions", *Nano Letters*, Vol. 7, No. 11, 3418-3423, 2007.
3. Fallahkhair, A. B., Li, and T. E. Murphy, "Vector Finite Difference Mode solver for Anisotropic Dielectric Waveguides," *IEEE J.Lightwave Technol*., Vol.26, No.11, 1423-1431, 2008.
4. Chiang, Y. C., Y. P. Chiou and H. C. Chang, "Improved full-vectorial finite-difference mode solver for optical waveguides with step-index profiles," *IEEE J. Lightwave Technology,* Vol.20, 1609- 1618, 2002

Novel Symmetric Mixed Finite Element Analysis for Hybrid Dielectric-Loaded Plasmonic Waveguide Structures

Shaymaa.I.H.Ibrahim, S.S.A.Obayya*
Centre for Photonics and Smart Materials, Zewail City of Science and Technology, Sheikh Zayed District, 6th of October City, Giza, Egypt. E-mail: sobayya@zewailcity.edu.eg

Abstract- A modified symmetric mixed finite element is introduced to be utilized in the modeling of metal-based nanophotonic structures, namely nanoplasmonic waveguides. Besides the benefits of conventional curl conforming mixed elements, the symmetric element has the advantage of being independent on the selection of facet related basis functions. Numerical results show the effectiveness of the proposed symmetric elements in simulating plasmonic structures.

Since their first introduction [1], mixed finite elements have received a great attention. These elements are able to accurately apply boundary conditions to prohibit spurious modes, and also satisfy Nedelec's constraints to eliminate unnecessary degrees of freedom. A wide variety of vector basis functions are deduced either following the definition of the element given by Nedelec [2], or not [3].

Figure 1 shows a second order vector element. The element has six tangential unknowns along with two facet unknowns. The facet related basis is hence asymmetric. This asymmetry may cause some problems: the choice of any two of possible three facet functions may influence the numerical accuracy of results. Special attention must be paid to numerical implementation of the asymmetric elements.

Koshiba *et al*. have successfully used the second order vector elements by Lee [3] and Peterson [2], to model guided wave problems [4]. While the later satisfies the Nedelec's constraints, both are asymmetric elements in which each selection of two facet functions forms a different modeling space.

Trying to use the facet related functions in [2] to deduce a set of basis that satisfy the dependence relation:

$$\sum_{i=1}^{3} W_i = 0 \tag{1}$$

where W_i is the facet basis function.

Thus we get a symmetric element with facet basis:

$$\begin{aligned} W_1 &= L_1 L_2 \nabla L_3 - L_2 L_3 \nabla L_1 \\ W_2 &= L_2 L_3 \nabla L_1 - L_3 L_1 \nabla L_2 \\ W_3 &= L_3 L_1 \nabla L_2 - L_1 L_2 \nabla L_3 \end{aligned} \tag{2}$$

The importance of this modification becomes very clear when modeling structures containing metals such as plasmonic waveguides. A hybrid dielectric-loaded plasmonic waveguide (HDLPW) has become one of the most important plasmonic waveguides due to their superior properties. HDLPW has a very low propagation loss as well as subwavelength confinement. Therefore HDLPW is an ideal candidate for the design of high-performance, low-loss, highly integrated nanophotonic components [5]. A precise modal characterization of a planar HDLPW is extremely important as it forms the building block for almost all other circuitry components.

To validate our developed finite elements technique, we have analyzed the structure shown in Fig. 2(a). It consists of a thin low-index SiO_2-stripe with 50 nm thickness and refractive index n_2=1.44, sandwiched between a high-index Si nanowire of 150 nm thickness and 200 nm width and n_1=3.48 and a 100 nm silver film with n_3=0.145+11.359i sitting on a SiO_2 substrate, operating at 1550 nm wavelength.

Figure 2(b) shows the field discontinuities at the semiconductor-oxide interface and at metal-semiconductor interfaces of the planar HDLPW. The mode effective index (n_{eff}) and propagation length (L_{prop}) have been calculated using different functions selections for the second order element in [2] and our modified element. As shown in Table 1, different choices of facet basis functions in our modified element has less effect on the real part of the effective index than on the other element. On the other hand the imaginary part is most influenced by different selections which reflects strongly on the calculation of the propagation length.

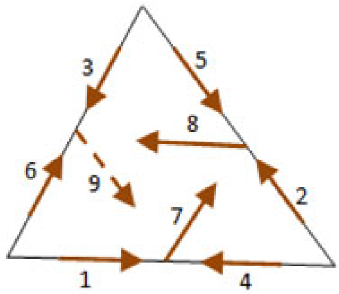

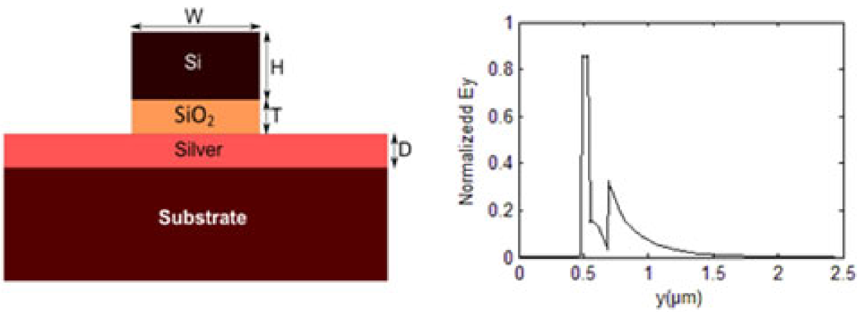

Figure 1 Second order mixed finite element.   Figure 2(a) A Planar HDLPW structure, (b) Field discontinuities at HDLPW interfaces.

Table 1: Results of the calculated effective index (n_{eff}) and propagation length (L_{prop}) using different choices of facet basis functions.

	[2]			**Modified symmetric element**		
Selection	W_1-W_2	W_2-W_3	W_3-W_1	W_1-W_2	W_2-W_3	W_3-W_1
n_{eff},	1.245451881	1.2454791226	1.245465538	1.245467874	1.245469097	1.245465694
Error	1.358E-05	-1.358E-05	1.365E-05	1.223E-06	3.403E-06	2.180E-06
L_{prop}	130.0490504	130.0541633	130.0406681	130.0480514	130.0483769	130.0486127
Error	0.013495236	0.013495236	0.008382319	0.0003255	0.0002357	0.0005613

REFERENCES

1. Nedelec. J. C. "Mixed finite elements in R^3," *Numerische Mathematik*, Vol. 35, 315–341, 1980.
2. Peterson, A.F.; , "Vector finite element formulation for scattering from two-dimensional heterogeneous bodies," *IEEE Transactions on Antennas and Propagation*, Vol.42, No.3, 357-365, 1994.
3. Lee, J.-F.; Sun, D.-K.; Cendes, Z.J.; , "Full-wave analysis of dielectric waveguides using tangential vector finite elements," *IEEE Transactions on Microwave Theory and Techniques*, Vol.39, 1262-1271, 1991.
4. Koshiba, M.; Tsuji, Y.; , "Curvilinear hybrid edge/nodal elements with triangular shape for guided-wave problems," *IEEE Journal of Lightwave Technology*, Vol.18, No.5, 737-743, 2000.
5. H. S. Chu, Y. A. Akimov, P. Bai, E. Li, and W. R. Hoefer, "Ultracompact wavelength-selective silicon-based plasmonic components," *Quantum Electronics and Laser Science Conference*, OSA Technical Digest 2011.

Nano-Plasmonic Biosensors and Photodetectors

Ekmel Ozbay

Nanotechnology Research Center, Bilkent University, Bilkent, 06800 Ankara, Turkey
Fax: + 90-312290105; email: ozbay@bilkent.edu.tr

Abstract

In this talk, we will present our recent work on nanoplasmonic based biosensors and photodetectors. We will present a label-free, optical nano-biosensor based on the Localized Surface Plasmon Resonance (LSPR) effect that is observed at the metal-dielectric interface of silver nano-cylinder arrays located periodically on a sapphire substrate by E-Beam Lithography (EBL), which provides high resolution and flexibility in patterning. Firstly, the size and period dependency of the LSPR wavelength was studied. Secondly, the surface functionalization studies were carried out on an array with a selected size and period. Finally, the concentration dependency of the LSPR shifts was observed by changing the avidin concentrations to be sensed in the target solution. The sensing mechanism is based on the detection of refractive index change, due to the binding of biotin that is immobilized on the silver nano-cylinders to the avidin in the target solution, by observing the shifts in the LSPR wavelength. Our results show that such a plasmonic structure can be successfully applied to bio-sensing applications and extended to the detection of specific bacteria species. A highly tunable design for obtaining double resonance substrates to be used in Surface Enhanced Raman Spectroscopy will also be presented. Tandem truncated nano-cones composed of Au-SiO2-Au layers are designed, simulated and fabricated to obtain resonances at laser excitation and Stokes frequencies. Surface Enhanced Raman Scattering experiments are conducted to compare the enhancements obtained from double resonance substrates to those obtained from single resonance gold truncated nano-cones. The best enhancement factor obtained using the new design is 3.86 x10E7. The resultant tandem structures are named after “Fairy Chimneys” rock formation in Cappadocia, Turkey. The integration of plasmonic structures with solid state devices has many potential applications. It allows the coupling of more light into or out of the device while decreasing the size of the device itself. Such devices are reported in the VIS and NIR regions. However, making plasmonic structures for the UV region is still a challenge. Here, we report on a UV plasmonic antenna integrated metal semiconductor metal (MSM) photodetector based on GaN. We designed and fabricated Al grating structures. Well defined plasmonic resonances were measured in the reflectance spectra. Optimized grating structure integrated photodetectors exhibited more than eight-fold photocurrent enhancement.

Active Surface Plasmon Photonics

Pierre Berini
School of Electrical Engineering and Computer Science, and Department of Physics, University of Ottawa, Ottawa, Canada
*corresponding author: berini@eecs.uottawa.ca

Abstract- Active planar structures enabling stimulated emission or amplification of surface plasmon-polaritons (SPPs) are of strong current interest, as are structures for their detection. Both types of active structures are discussed.

Stimulated emission of SPPs propagating along planar metallic waveguides can be achieved via interaction with an adjacent optically-pumped dipolar gain medium [1-11]. Physically realisable arrangements based on the single-interface and on symmetric thin metal films and stripes supporting long-range SPPs are described, along with the conditions required to achieve complete SPP loss compensation and SPP gain at visible and infrared wavelengths [12].

The detection of SPPs can be achieved via absorption in semiconductors [13], in an organic medium [14] or in metals [15-17]. The detection of SPPs using a Schottky contact detector implemented as a thin asymmetric metal stripe on Si is discussed. SPPs localised at the bottom metal/semiconductor interface are launched along the stripe via end-fire coupling at energies below the bandgap of Si (infrared wavelengths) and are detected via internal photoemission.

REFERENCES

1. J. Seidel et al., *Phys. Rev. Lett.* **94**, 177401 (2005)
2. M. A. Noginov et al., *Phys. Rev. Lett.* **101**, 226806 (2008)
3. J. Grandidier et al., *Nano Lett.* **9**, 2935 (2009)
4. I. P. Radko et al., *Opt. Express* **18**, 18633 (2010)
5. P. M. Bolger et al., *Opt. Lett.* **35**, 1197 (2010)
6. G. Winter et al., *New J. Phys.* **8**, 125 (2006)
7. I. De Leon and P. Berini, *Phys. Rev. B* **78**, 161401 (2008)
8. M. Ambati et al., *Nano Lett.* **8**, 3998 (2008)
9. I. De Leon and P. Berini, *Nature Photonics* **4**, 382 (2010)
10. I. De Leon and P. Berini, *Opt. Express* **17**, 20191 (2009)
11. M. C. Gather et al., *Nature Photonics* **4**, 457 (2010)
12. P. Berini, I. De Leon, *Nature Photonics*, Vol. 6, 16-24, 2012
13. P. Neutens et al., *Nature Photonics* **3**, 283 (2009)
14. H. Ditlbacher et al., *Appl. Phys. Lett.* **89**, 161101 (2006)
15. A. Akbari, R. N. Tait, and P. Berini, *Opt. Express* **18**, 8505 (2010)
16. C. Scales, and P. Berini, *IEEE J. Quant. Electr.* **46**, 633 (2010)
17. P. Berini, A. Olivieri, C. Chen, *Nanotechnol.* **23**, 444011 (2012)

Optimizing Silicon-Plasmonic Waveguides for $\chi^{(3)}$ Nonlinear Applications

A. Pitilakis[1], **O. Tsilipakos**[1], **and E. E. Kriezis**[1*]

[1]Department of Electrical and Computer Engineering, Aristotle University of Thessaloniki, Greece
*corresponding author: mkriezis@auth.gr

Abstract—Hybrid silicon-plasmonic waveguides constitute an appealing platform for integrated photonic circuitry. They merge the technical maturity and prevalence of the SOI platform with the subwavelength confinement of plasmonic waveguides, essential for accessing enhanced nonlinear response at micron length-scales. Employing full-wave numerical simulations complemented with Schrödinger equation techniques, we propose nonlinear waveguide designs for Kerr-effect applications exhibiting minimized impairments due to free-carrier effects, thus raising the power-ceiling imposed on standard silicon waveguides.

Nonlinear phenomena emanating from the third order susceptibility $\chi^{(3)}$ hold the key to efficient all-optical signal processing in integrated photonics. Circuitry based on standard silicon-on-insulator (SOI) waveguides [1] presents limited potential for micron-length-scale Kerr-type nonlinear applications due to the large interaction length-scales required: typically longer than 1 mm [2]. Furthermore, silicon exhibits two-photon absorption (TPA) in the telecom band, which in turn, apart from introducing additional losses, gives rise to free-carrier effects (FCEs), namely dispersion (FCD) and, more importantly, absorption (FCA). The magnitude of FCEs increases quadratically with the optical power. Thus, FCA limits the maximum on-chip power to a few tens of milliwatts; above this threshold, it drastically quenches the optical power. On the other hand, purely plasmonic waveguides can allow for subwavelength confinement significantly boosting the nonlinear response and thus reducing the required interaction length. However, they suffer from substantial Ohmic losses, a fundamental barrier for any nonlinear application.

Hybrid silicon-plasmonic waveguides [3] present a fair compromise between silicon and plasmonic traits, with respect to the potential for Kerr-type nonlinear applications [4]. Fusing index-contrast and plasmonic guiding mechanisms, they confine the optical field in a nanosized low-index dielectric gap, formed between a metal and a high-index silicon area. If the dielectric additionally possesses a high nonlinear index n_2, then the nonlinear parameter γ quantifying the Kerr-effect strength acquires orders-of-magnitude larger values than those typical of SOI waveguides ($\sim 100\ \mathrm{m}^{-1}\mathrm{W}^{-1}$). More importantly, hybrid silicon-plasmonic waveguides offer a two-fold advantage over SOI ones with respect to FCE impairments. Specifically, as the optical field is confined primarily inside the dielectric gap, not only is the relative TPA magnitude (r_{TPA}) decreased, but, in addition, TPA-generated free-carriers (residing only inside the silicon area) do not significantly overlap with the optical field. The latter means that the overall FCE perturbation is decreased even further, and this is reflected onto the carrier-field overlap factor Π_{Si} [1].

In this work, we define a nonlinear-waveguide figure-of-merit (FoM) that provides a qualitative measure of the impact of all discussed nonlinear phenomena, namely, the Kerr effect, TPA and FCEs. We start off with a basic FoM for TPA-free waveguides defined as $F = \gamma \times L_{\mathrm{prop}}$ measured in W^{-1}. L_{prop} is the propagation length, i.e., the e-folding distance of the optical power, due to linear propagation losses. It can be shown that the power-level required for a particular Kerr-type nonlinear application (e.g., self-phase-modulation-induced spectral-broadening, cross-phase modulation, four-wave mixing, etc.) is proportional to the inverse of this FoM. Subsequently, in order to include the influence of TPA and FCEs, we derive a power-dependent FoM: $F' = \gamma' \times L'_{\mathrm{prop}}$. For this purpose, we introduce the effective quantities γ' and L'_{prop}, by applying correction terms to the nonlinear parameter and propagation length, respectively. Specifically, FCD counteracts the self-focusing Kerr-effect leading to a reduced effective nonlinear parameter ($\gamma' < \gamma$), while both TPA and FCA are responsible for additional losses that lower the effective propagation length ($L'_{\mathrm{prop}} < L_{\mathrm{prop}}$). The relative importance of FCEs increases with the dimensionless factor $r_{\mathrm{TPA}} \times \Pi_{\mathrm{Si}}$.

We base our hybrid silicon-plasmonic waveguide design on the planar conductor-gap-silicon (CGS) waveguide [3] and extend the dielectric and metal regions laterally. For the dielectric gap material, we select the DDMEBT nonlinear polymer [2] possessing linear and nonlinear indices of $n = 1.8$ and $n_2 = 1.7 \times 10^{-17}$ m^2/W, respectively, while the metal is silver for minimal Ohmic losses at $\lambda = 1550$ nm ($n_{\mathrm{Ag}} = 0.14 - j11.4$). In order to boost the plasmonic confinement even further, we introduce an inverted metal rib [4] or wedge, laterally aligned with the underlying silicon waveguide [Fig. 1(a),(b)]. The corresponding intensity distributions (TM_{00} mode) are plotted in Fig. 1(c),(d).

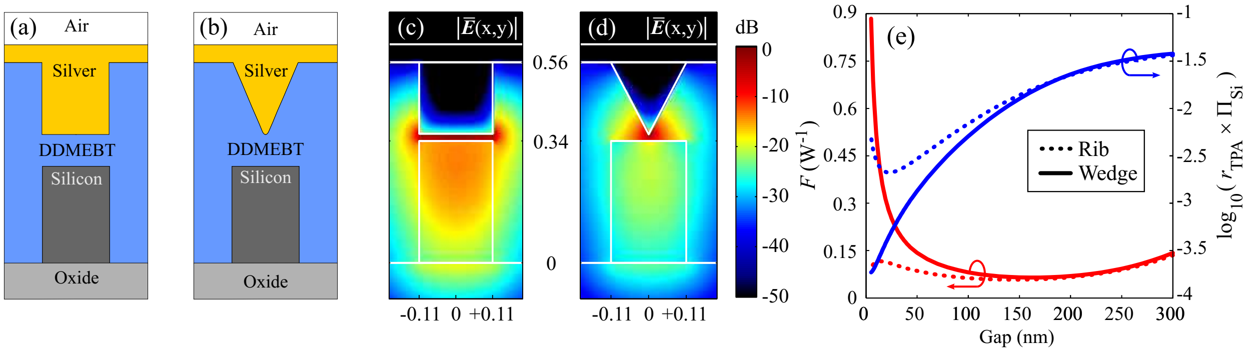

Figure 1: (a)-(b) Cross-sections of the inverted metal-rib/-wedge hybrid silicon-plasmonic waveguide designs. (c)-(d) Typical intensity distributions of the fundamental TM_{00} mode supported for a 20 nm gap. (e) FoM and factor $r_{\mathrm{TPA}} \times \Pi_{\mathrm{Si}}$ quantifying the relative importance of FCEs as a function of gap, for the two waveguide designs. The silicon ridge is in all cases $W \times H = 220$ nm $\times$ 340 nm, the silver film is 50 nm thick and the inverted metal-rib/wedge is $W \times H = 220$ nm $\times$ 200 nm. The wedge angle is approximately 57° and its tip curvature is 1 nm.

The most crucial parameter of these hybrid silicon-plasmonic waveguide designs is the gap size. Thus, in Fig. 1(e) we plot both the FoM and the factor $r_{\mathrm{TPA}} \times \Pi_{\mathrm{Si}}$ quantifying the impact of FCEs for a broad range of gap sizes (5–300 nm). One can readily confirm that the metal-wedge design offers considerable improvement in the FoM compared to the metal-rib design, especially for gaps smaller than 50 nm. As an example, for a gap of 20 nm the wedge design exhibits $\gamma \approx 6.7 \times 10^3$ m^{-1}W^{-1} (thus significantly outperforming standard SOI waveguides) and $L_{\mathrm{prop}} \approx 43$ μm, amounting to $F = 0.3$ W^{-1}. The factor $r_{\mathrm{TPA}} \times \Pi_{\mathrm{Si}}$ is approximately 5×10^{-4} indicating that the relative importance of FCEs is rather limited. This finding is corroborated by our full-wave beam-propagation method simulations revealing that FCEs become important for power-levels above 1 W (CW), assuming a typical effective carrier-lifetime of 1 nsec [1]. As a benchmark comparison, typical SOI waveguides have an FCE-ceiling in the order of 10 mW ($r_{\mathrm{TPA}} \times \Pi_{\mathrm{Si}} > 0.1$), i.e., 100 times smaller. They provide a higher FoM ($F \approx 5$ W^{-1}), but on substantially longer length scales ($L_{\mathrm{prop}} \approx 1$ cm). Finally, addressing some fabrication considerations, we note that the wedge-tip curvature-radius and the lateral offset between wedge and Si-rib do not have a major effect on the nonlinear FoM. Note also that acute wedges lead to improved performance, as do small gaps.

ACKNOWLEDGMENT

This research has been co-financed by the European Union (European Social Fund – ESF) and Greek national funds through the Operational Program "Education and Lifelong Learning" of the National Strategic Reference Framework (NSRF) — Research Funding Program: Heracleitus II. Investing in knowledge society through the European Social Fund.

REFERENCES

1. Daniel, B. A. and G. P. Agrawal, "Vectorial Nonlinear Propagation in Silicon Nanowire Waveguides: Polarization Effects," *J. Opt. Soc. Am. B*, Vol. 27, No. 5, 956–965, 2010.
2. Koos, C., P. Vorreau, T. Vallaitis, P. Dumon, W. Bogaerts, R. Baets, B. Esembeson, I. Biaggio, T. Michinobu, F. Diederich, W. Freude, and J. Leuthold, "All-Optical High-Speed Signal Processing with Silicon-Organic Hybrid Slot Waveguides," *Nat. Photonics*, Vol. 3, 216–219, 2009.
3. Wu, M., Z. Han, V. Vien, "Conductor-Gap-Silicon Plasmonic Waveguides and Passive Components at Subwavelength Scale," *Opt. Express*, Vol. 18, 11728–11736, 2010.
4. Pitilakis, A., O. Tsilipakos, and E. E. Kriezis, "Nonlinear Effects in Hybrid Plasmonic Waveguides," in *Proceedings of 14th International Conference on Transparent Optical Networks*, Coventry, United Kingdom, July 2012, Art. No. 6254436.

Functional nano-scale plasmonic slot waveguides networks

Amr S. Helmy[1*]

[1] The Edward S. Rogers Sr. Department of Electrical and Computer Engineering and the Institute of Optical Sciences, University of Toronto, Toronto, Ontario M5S 3G4, Canada

(Invited)

[*]*corresponding author: a.helmy@utoronto.ca*

Abstract- In this talk, I will present our recent developments for networks made out of PSWs as the basis for an integrated platform for functional devices. These devices are designed using an equivalent circuit model, which we developed. It is capable of predicting the response of any arbitrary PSW network with similar accuracy as FDTD. This model is independent of FDTD-extracted parameters and provides a means for rapid network design, optimization and tolerance analysis. Initial devices demonstrating record low insertion loss into this class of devices will also be presented. This work ushers in the era of incorporating plasmonics circuits into conventional electronics computer aided design packages.

Plasmonic slot waveguides (PSW) provide the unique ability to confine light within a few nanometers and allow for near perfect transmission through sharp bends as well as efficient light distribution between intersecting waveguide junctions. These features motivate the utilization of PSW for various nanoscale applications. Devices including optical splitters, switch matrices, filters, modulators amongst others will be discussed using this platform. A depiction of PSWs in a network format can be seen in Fig. 1, where multi-input multi-output PSW schematic network is shown.

Despite the promise that MIM mesh structures hold for nanophotonic circuits, their design process is primarily based on the time-intensive, numerical Finite-Difference Time-Domain (FDTD) technique. Mesh structures have also been modeled using the Scattering Matrix (S-matrix) method but it still relies on numerically extracted parameters to create a precompiled library of waveguides and junctions dispersion [1]. Analytical model for MIM bends and splitters based on waveguide impedance [2] have good agreement with their numerical counterparts but does not account for waveguide loss nor provides phase information, which is crucial if the model is to be extended to analyze interference effect in MIM mesh structures. In this work, we develop and evaluate a generic analytical model for MIM mesh structures that incorporates a modified impedance model into the S-matrix formalism. The model enables parameterization of plasmonic mesh structures and results in closed-form expressions that are only dependent on the mesh topology. The model does not require FDTD extracted parameters and is able to handle arbitrary combination of junctions with realistic design and optimization cycle duration. This can enable the incorporation of these structures into standard electronic computer aided design packages for their utilization as a platform for developing interconnect technologies.

Fig. 1 A depiction of a plasmonic slot waveguide network. The waveguides are defined with metallic regions, where the core in this example is with air gaps.

A major bottleneck that hinders the design of PSW-based optical devices is the lack of efficient coupling mechanism for PSW mode excitation due to the momentum mismatch as well as modal shape and size differences between PSW and dielectric waveguide. Attempts based on endfire coupling with modified silicon waveguide facet have been proposed but the coupling efficiency is wavelength-dependent [3]. Taper structures have been proposed to alleviate the resonance effect and allows for near 100% coupling efficiency but such design suffers in term of the overall device footprint [4].

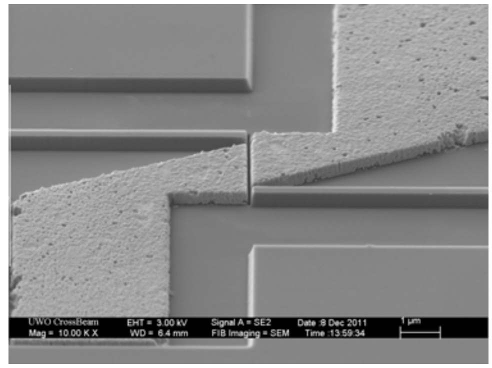

Fig. 2. Scanning electron microscope image of the orthogonal hybrid junction platform with 1 μm long PSW.

Recently we proposed a wideband, non-resonant, and highly efficient coupling scheme between PSW and silicon waveguides by placing them in an orthogonal fashion (Fig. 2) [5]. The longitudinal momentum component of the silicon waveguide can be phased matched to that of the PSW. Moreover the orthogonal configuration results in a nanoscale footprint while resolving the modal size mismatch, which results in coupling efficiencies of up to 70% at each junction and 50% after input and output junctions (Fig. 3) [6]. In this work, we also present the experimental realization of the orthogonal hybrid plasmonic junction. This novel coupling scheme provides the interface between low-loss silicon technology and sub-wavelength plasmonic structures, paving the way for wide range of silicon plasmonic hybrid interconnect applications.

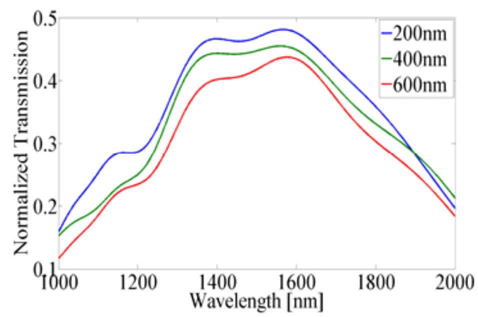

Fig. 3. Theoretical transmission spectra of the orthogonal hybrid junction platform between 400nm wide input/output Si waveguides and PSW of varying

In summary this work will focus on devices demonstrating record insertion loss into this class of devices. Also recent developments for networks made out of PSWs as the basis for an integrated platform for functional devices will be overviewed. These devices are designed using an equivalent circuit model, which is capable of predicting the response of any arbitrary PSW network with similar accuracy as FDTD.

REFERENCES

1. M.A. Swillam, and A.S. Helmy, “Feedback Effects in Plasmonic Slot Waveguides Examined Using a Closed-form Model,” Photonics Technology Letters, vol. 24, pp. 497-499, (2012).
2. C. Lin, M. Swillam, A. S. Helmy, ‘Analytical Model for Metal-Insulator-Metal Mesh Waveguide Architectures,’ J. OSA B, vol. 29, 3157-3169 (2012).
3. G. Veronis, and S. H. Fan, “Theoretical investigation of compact couplers between dielectric slab waveguides and two-dimensional metal-dielectric-metal plasmonic waveguides,” Opt. Express, vol. 15, 1211–1221, February 2007.
4. J. Tian, S. Yu, W. Yan, and M. Qiu, “Broadband high-efficiency surface-plasmon-polariton coupler with silicon-metal interface,” Appl. Phys. Lett., vol. 95, 013504, July 2009.
5. B. Lau, M. A. Swillam, and A. S. Helmy, "Hybrid orthogonal junctions: wideband plasmonic slot-silicon waveguide couplers," Opt. Express, vol. 18, 27048-27059, December 2010.
6. C. Lin, H. Wong, B. Lau, M. Swillam, A. S. Helmy, ‘Efficient broadband energy transfer via momentum matching at hybrid junctions of guided-waves,’ Appl. Phys. Lett., 123115, (2012).

Quantum effects and magnetic modes in resonant metallic nanostructures

J.A. Dionne[1*]**, J. A. Scholl**[1]**, A. Garcia-Etxarri**[1]**, S. Sheikholeslami**[1]**, and A. L. Koh**[1]

[1]Stanford University, USA

[*]corresponding author: jdionne@stanford.edu

Abstract- We explore optical-frequency quantum and magnetic plasmon modes. Our results demonstrate the quantum-to-classical transition in individual nanoparticles and in nanoparticle dimers, as well as the emergence of optical-frequency magnetism in a metamaterial fluid.

Electrons and photons can coexist as a single entity called a surface plasmon—an elementary excitation found at the interface between a conductor and an insulator. While most plasmonic applications – ranging from plasmon photovoltaics to plasmonic optical tweezers - rely on classical effects, quantum phenomena can also strongly influence the plasmonic properties of nanometer-scale systems. In this presentation, I'll describe our efforts to probe plasmon modes spanning both classical and quantum domains.

We first explore the plasmon resonances of individual metallic nanoparticles as they transition from a classical to a quantum-influenced regime. We investigate individual ligand-free silver nanoparticles using aberration-corrected transmission electron microscope (TEM) imaging and monochromated scanning TEM electron energy-loss spectroscopy (STEM EELS). This technique allows direct correlation between a particle's geometry and its plasmon resonance. As the nanoparticle diameter decreases from 20 nm to less than 2 nm, the plasmon resonance exhibits a blue-shift from 3.3 eV to 3.8 eV, with particles smaller than 10 nm showing a substantial deviation from classical predictions. We present an analytical quantum-mechanical model that well describes the plasmon resonance shift due to a change in particle permittivity. Our results highlight the unique quantum plasmonic properties of small metallic nanospheres, with direct application to understanding and exploiting catalytically-active and biologically-relevant nanoparticles.[1]

Furthermore, using TEM EELS, we can observe the plasmonic properties of multi-particle systems. Using excitation from the electron beam, ligand-free silver particles are capable of moving on silicon nitride substrates, allowing dynamic monitoring of plasmonic resonances as the particles approach each other and coalesce. This strategy provides a straightforward method for studying dimer interactions at variable separation distances, including quantum-sized separations. Because individual sets of particles can simultaneously imaged and spectrally analyzed, we can directly probe the crossover from classical to quantum plasmon resonances in particle dimers. For separations smaller than 0.5 nm, we observe the effects of quantum tunneling between particles on their plasmonic resonances.[2] We extend our analysis to probe quantum effects of multi-particle geometries, including those sustaining a magnetic mode.

Finally, using the properties of coupled metallic nanoparticles, we demonstrate the colloidal synthesis of an isotropic metafluid that exhibits a strong magnetic response at visible frequencies. The strength of the metafluid magnetic dipole is nearly 15% that of the electric dipole, and is tunable with interparticle separation. Our analysis provides a framework for controlling electric and magnetic light-matter interactions spanning classical and quantum domains, with applications ranging from molecular electronics to catalysis.

Acknowledgements: Funding from an AFOSR YIP grant (FA9550-11-1-0024) and NSF CAREER award (DMR-1151231) are gratefully acknowledged.

REFERENCES

1. Scholl, J. A., Koh, A. L. , Dionne, J.A., “Quantum Plasmon Resonances of Individual Metallic Nanoparticles,” *Nature*, 483, 421 (2012)
2. Scholl, J. A., Garcia-Etxarri, A., Koh, A. L. , Dionne, J.A., “Observation of Quantum Tunneling between Two Plasmonic Nanoparticles,” *Nano Letters*, http://dx.doi.org/10.1021/nl304078v

Hybrid Plasmonics: Theory and Applications

M. Mojahedi[*1], **J.S. Aitchison**[1]
[1]Department of Electrical and Computer Engineering, University of Toronto, Toronto, Canada
[*]corresponding author: Mojahedi@waves.utoronto.ca

Abstract- A review of the modes supported by the hybrid plasmonic waveguides and devices designed and fabricated based on this structure is given. It is seen that hybridization of the plasmonic and the dielectric waveguide modes can lead to a set of diverse and advantageous field profiles. The hybrid plasmonic structure can be used to design variety of nano-photonic devices such as TE- or TM- pass polarizers, polarization independent coupler, and polarization rotator, to name a few.

A hybrid plasmonic waveguide (HP) – a structure which can support plasmonic mode, dielectric modes, and/or a hybridization of the two aforementioned modes – has been a subject of much interest in recent years [1-3]. The HP waveguide was first introduced by our group in 2007 as a compromise between the propagation length and confinement of a mode in the context of plasmonic guiding schemes [1]. It is well known that there is a tradeoff between the *propagation length* (inversely proportional to the propagation loss) and *confinement* of plasmonic modes – i.e. increasing one is accompanied by a decrease in the other. The HP waveguide can then be viewed as a structure which facilitates hybridization of plasmonic and dielectric waveguide modes, where such a hybrid mode enjoys the *optimum combination of propagation length and confinement*. Although there is variety of proposed HP waveguides, the most commonly used structure consists of a metallic layer separated from a high index material by a thin low index spacer layer, as shown in Fig. 1.

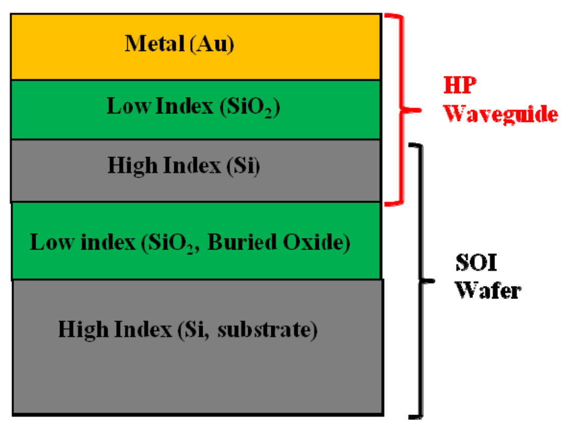

Fig. 1: Cross section of a HP waveguide built on a SOI platform

The basic structure shown in Fig. 1 has three distinctive advantages which are very useful in designing photonic devices. a) It can be used to fabricate extremely compact (both in transverse and/or longitudinal directions) optical components. b) By properly choosing the layers – for example, gold for the metal, Si for the high index, and SiO_2 for the low index layers – fabrication of photonic devices based on the HP platform is compatible with the standard Si and silicon-on-insulator (SOI) technologies. C) It turns out that the basic polarization modes, i.e. transverse magnetic (TM) and transverse electric (TE), mostly reside in two different layers – TM in the low index (SiO_2) and TE in the high index (Si) regions. This property will allow us to use the HP to design a variety of polarization dependent photonic devices.

HP platform has been used to design and fabricated various passive and active optical devices [4], [5, and references there in]. In this presentation we begin by describing the diverse modes supported by the HP waveguide. We then will discuss a few HP-based photonic devices such as TE- or TM-pass polarizers, polarization independent coupler, broadband coupler, and polarization rotator designed and fabricated in our laboratories.

HP Waveguide Modes: We provide a brief review of the modes supported by the HP structure. We investigate variations of the effective mode indices and field profiles for the guided modes when the thickness of the high and low index layers are changed. We categorize and summarize the modal characteristics and show how these modes can be understood in terms of a coupling between the plasmonic mode supported by the metallic layer and dielectric waveguide modes supported by the high index layer.

TE- or TM-pass Integrated Polarizers: Since the TE and TM modes are concentrated in different layers these layers can be engineered such that one particular polarization is passed through while the other is extinguished. As an example, Fig. 2 shows a cross section of a compact SOI compatible TE-pass polarizer fabricated in our laboratories. The polarizer is only 30 μm long and is characterized for the wavelength range of 1.52 to 1.58 μm. The extinction ratio in this wavelength range varies from 23 to 28 dB and the insertion loss for the TE mode is 2 to 3 dB. The device performance compares favorably against previously reported silicon based integrated polarizers.

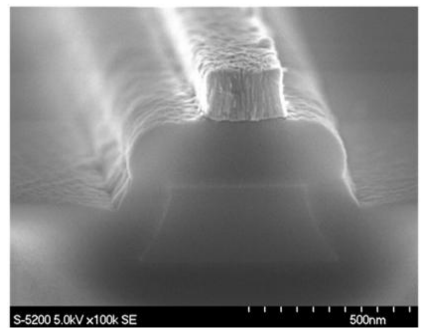

Fig. 2: A cross section of the TE-pass polarizer

Polarization Independent Coupler: Separation of TM and TE modes in different layers can be used to design a polarization independent coupler. In this case, the waveguide dimensions are chosen properly to ensure equal coupling lengths (the length required for complete power transfer from one guide to the other) for both TM and TE polarizations. As an example, we present the design of a 3 dB coupler for which the power transfer ratio for the two polarizations differs by less than 0.5 dB at 1.53 to 1.57μm wavelength range. The insertion loss – which includes material loss and also the coupling loss at both ends of the coupler – for both polarizations is less than 0.5 dB over the entire range. In addition to being compact, operation of the HP based coupler is more immune to fabrication imperfections as compare to other existing designs.

Polarization Rotator: The HP structure can be used to design an ultra-compact integrated polarization rotator operating at 1.55 μm. This extremely short rotator (~ 5 μm) combines the advantages of both mode evolution and mode interference schemes, while at the same time demonstrating a low insertion loss (~2 dB). The rotator consists of three sections: the first section is a short taper which transforms the TM silicon waveguide mode into a HP mode. The polarization rotation happens in the second section, where the metallic layer moves sideway and downward relative to the silicon nanowire. This movement can be interpreted as a rotation of the metal around the silicon waveguide. In the last section the metal is terminated and the silicon waveguide linearly tapers out to its original width.

REFERENCES

1. M. Z. Alam, J. Meier J, J. S. Aitchison and M. Mojahedi "Super mode propagation in low index medium," *CLEO/QELS*, http://www.opticsinfobase.org/abstract.cfm?uri=CLEO-2007-JThD112, 2007.
2. R. F. Oulton, *et al.* "A hybrid plasmonic waveguide for subwavelength confinement and long range propagation," *Nature Photonics*, Vol. 2, pp. 496, 2008.
3. M. Z. Alam, J. Meier, J. S. Aitchison and M. Mojahedi "Propagation characteristics of hybrid modes supported by metal-low-high index waveguides and bends," *Optics Express*, Vol. 18, pp. 12971, 2010.
4. R. F. Oulton, *et al.* "Plasmon lasers at deep subwavelength scale," Nature, Vol. 461, pp. 629, 2009.
5. M. Z. Alam, J. S. Aitchison and M. Mojahedi, "Theoretical Analysis of Hybrid Plasmonic Waveguides," *Journal of Selected Topics in Quantum Electronics, Nanoplasmonics*, accepted for publication, JSTQE-CON-NP-04490-2012, 2013.

Rigorous characterization of surface plasmonic waveguides and guided-wave devices for THz systems

C. Themistos, A. Quadir, C. Markides, H. Tanvir and B M A Rahman
City University London, Northampton Square, London EC1V 0HB, UK
Email: B.M.A.Rahman@city.ac.uk

Abstract: The design of low loss-waveguides, simple power splitters and narrow band filters, suitable for the THz frequency band, along with the optimization of the active region of a quantum cascade laser, are presented here.

1. Introduction

The terahertz (THz) region occupies a large portion of the electromagnetic spectrum, located between the microwave and optical frequencies and normally is defined as the band ranging from 0.1 to 10 THz. In recent years, this intermediate THz radiation band has attracted considerable interest, because it offers significant scientific and technological potential for applications in many fields, such as sensing, imaging and spectroscopy. However, waveguiding in this intermediate spectral region is a major challenge and strong dielectric and conductive losses in the terahertz frequency range have been a major problem in long distance waveguiding. However, plasmonic mode in metal clad waveguides and devices are showing a promise. In this paper, various types of metal coated waveguides supporting plasmonic modes are evaluated and design optimization of Quantum Cascade Lasers, MMI-based power splitters and narrow-band filters are presented.

2. THz waveguides

In the THz band, most of the dielectric materials or metallic regions have high dielectric or conductive losses, which restrict the opportunity to design low-loss waveguides for this THz frequency band. With limited materials availability for this frequency band the waveguide engineering becomes a major challenge. Earlier we have collaborated with Rutgers University in the design optimization of a low-loss metal-clad air-core plasmonic circular waveguides [1], which was fabricated and experimentally verified. In our more recent work [2], we have shown that similarly a polarization maintaining rectangular core air-core dielectric-clad metal-coated waveguide can also be less lossy. A thin metal coating would support plasmonic modes, but these are relatively lossy. However, a Teflon coating on the gold layer can draws field away from the lossy conducting layer and loss may reduce considerably. Figure 1 shows the variation of the loss value with the Teflon thickness for the H^x_{12} mode in an air-core 1 mm x 0.6 mm rectangular waveguide with 0.7 μm gold coating at 2.5 THz. It can be seen that at the optimum 21 μm Teflon thickness, the loss value can be 3.5 dB/m, one of the lowest reported so far [2]. The evolution of third order mode for no Teflon coating to a near Gaussian profile for 18 μm Teflon coating are shown as insets.

3. THz devices

Similar to the VLSI, MMIC or PIC technology as used for semiconductors, microwave or optical frequencies, if we want to develop compact guided-wave THz systems, it would also be necessary to design and fabricate such integrated components. The MMI principle has been widely used to design compact optical power splitters and a similar approach is shown here. The evolution of field at the center of the waveguide along the axial direction is shown in Fig. 2 for a 1.0 mm by 3.0 mm metal-coated dielectric clad hollow-core multimoded THz waveguide, similar as reported earlier [1]. It can be observed here that at a distance of 37.2 mm, a neat 1 x 2 power splitting can be achieved. Similarly, THz filters can be used for on-chip signal processing and sensing. The variation of the Insertion Loss with the operating frequency for a microstrip-based THz filter is shown in Fig.3, which clearly illustrate the fundamental resonating frequencies of two 192 μm and 82 μm long filter stubs with 5 μm width.

During the last decade, Quantum Cascade Lasers (QCL) have emerged as one of the best compact sources for the generation of useful amount of power in this frequency band. Although, it was observed that a wider QCL yields a lower threshold, but the differential gain-threshold with higher order modes are small, which may cause mode hoping during any environmental variations. We have considered to engineer the upper metal layer and the gain threshold for 4 lower modes for etched and slotted electrodes are shown in Fig.4. This figure clearly shows the differential gain threshold can be substantially increased for a slotted electrode which will prevent mode hopping. All these simulations shown here have been carried out by using numerically efficient finite element based mode solver [5] and beam propagation methods [6].

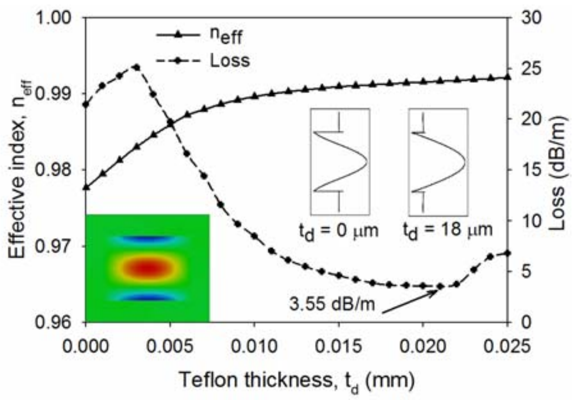

Fig.1 Effective index and loss with the Teflon thickness for the H^x_{12} mode

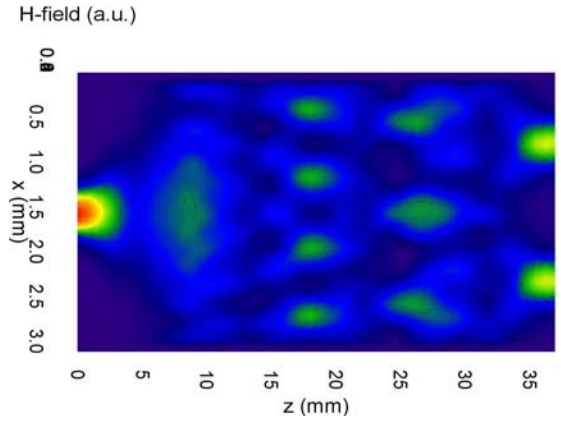

Fig.2 BPM Simulation of the MM-based THz 3dB coupler.

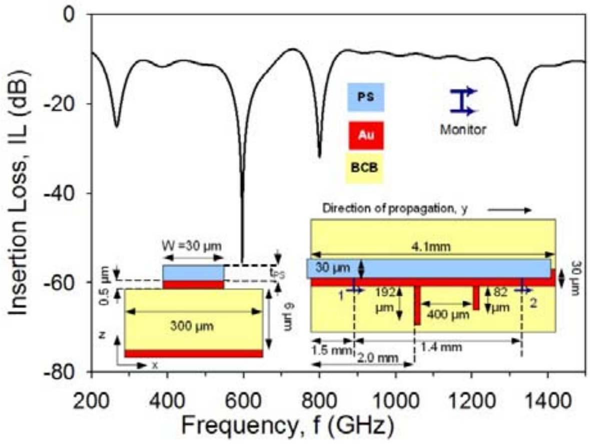

Fig.3 Insertion Loss with frequency for the microstrip filter.

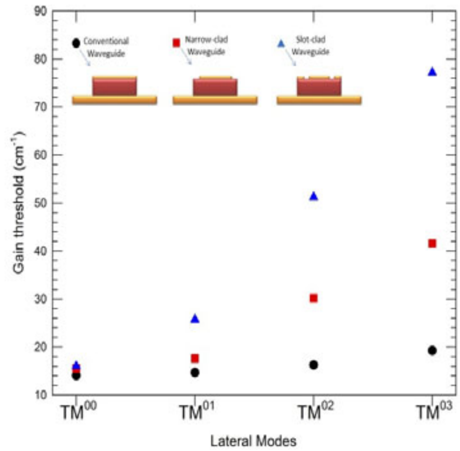

Fig. 4 Gain Threshold of the lasing modes for different electrode arrangements

4. Conclusions

Although, most of the present THz systems are free-space based but a guided-wave system would be more efficient and flexible and will have significant advantages over the present systems. For that, first of all it is essential to develop low-loss THz waveguides and subsequently guided-wave devices to process the THz interactions. In this work rigorous full-vectorial numerical methods are used to optimize the design of low-loss THz waveguides and guided-wave devices for future compact THz systems.

5. References

[1] C. Themistos, B. M. A. Rahman, M. Rajarajan, K. T. V. Grattan, B. Bowden, and J. Harrington, "Characterization of Silver/Polystyrene (PS)-coated hollow glass waveguides at THz frequency," IEEE/OSA J. Lightwave Technol., vol. 25, no. 9, pp. 2456–2462, 2007.

[2] B. M. A. Rahman, A. Quadir, H. Tanvir, and K. T. V. Grattan, Characterization of Plasmonic Modes in a Low-Loss Dielectric-Coated Hollow Core Rectangular Waveguide at Terahertz Frequency," IEEE Photonics J., vol.3, No.6, pp.1054,, 2011

[3] H. Han, H. Park, M. Cho, and J. Kim, "Terahertz pulse propagation in plastic photonic crystal fiber," Appl. Phys. Lett, 80, no.15, pp.2634-2636, 2002.

[4] H. Tanvir, B.M.A. Rahman, N. Kejalakshmy, A. Agrawal and K.T.V. Grattan, "Evolution of Highly Confined Surface Plasmon modes in Terahertz Quantum Cascade Laser Waveguides," IEEE/OSA J. Lightwave Technol., vol. 29, no. 14, pp. 2116-2125, 2011.

[5] B.M.A. Rahman and J.B. Davies, "Finite-element solution of integrated optical waveguides," J. Lightwave Technol. 2, pp. 682-688, 1984.

[6] S. S. A. Obayya, B. M. A. Rahman and H. A. El-Mikati, "New Full-Vectorial Numerically Efficient Propagation Algorithm Based on the Finite Element Method," IEEE/OSA J. Lightwave Technol., vol.18, no.3, pp.409-415, 2000.

Singularities & broken symmetries of systems with gain and loss structu

Discrete solitons in $\mathcal{PT}$-symmetric networks of optical waveguides

V. V. Konotop[1], **D. E. Pelinovsky**[2], **and D. A. Zezyulin**[1]

[1]Centro de Física Teórica e Computacional, Faculdade de Ciências, Universidade de Lisboa, Avenida Professor Gama Pinto 2, Lisboa 1649-003, Portugal

[2]Department of Mathematics and Statistics, McMaster University, Hamilton, Ontario, L8S 4K1, Canada

konotop@cii.fc.ul.pt

Abstract— We present a proof of existence of discrete solitons in infinite parity-time ($\mathcal{PT}$-) symmetric lattices, which describe stationary light propagation in networks of waveguides with dissipation and gain. The energy balance between dissipation and gain implies that in the anticontinuum limit the solitons are constructed from elementary $\mathcal{PT}$-symmetric blocks such as dimers, quadrimers, or more general oligomers. We consider in detail a chain of coupled dimers, analyze bifurcations of discrete solitons from the anticontinuum limit and show that the solitons are stable in a sufficiently large region of the lattice parameters. The approach is illustrated on two examples of networks of quadrimers, for which stable discrete solitons are also found.

We consider an array of waveguides with gain and losses described by the $\mathcal{PT}$-symmetric discrete nonlinear Schrödinger (DNLS) equation

$$i\frac{dq_n}{dt} + c_n(q_{n+1} - q_n) + c_{n+1}(q_{n-1} - q_n) - |q_n|^2 q_n + i(-1)^{n+1}\gamma q_n = 0, \tag{1}$$

where q_n is a dimensionless field in the waveguide n, t means the propagation coordinate, the positive constants $c_n = 1$ for $n = 2p$ and $c_n = \epsilon$ for $n = 2p+1$ describe the two alternating couplings between neighbor waveguides normalized to 1 and to $\epsilon > 0$, and it is assumed that all odd (even) sites have loss (gain) which is characterized by $\gamma > 0$ [Fig. 1, left panel].

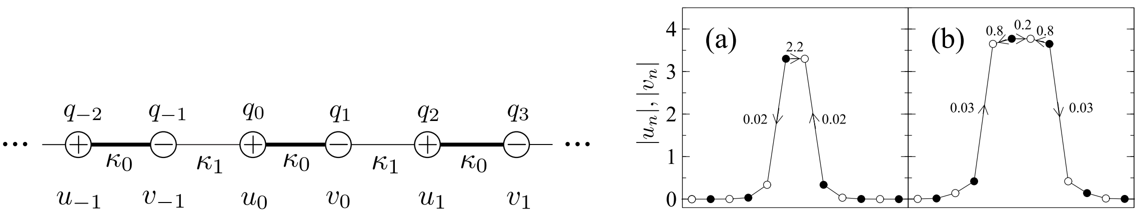

Figure 1: Left panel: Graph presentation of the $\mathcal{PT}$-symmetric array of waveguides with gain, "+", and losses, "−". Right panel: Amplitude and currents for (a) an unstable soliton of Eq. (3) at $\epsilon = 1$, (the respective energy flow $P = \sum_n(|u_n|^2 + |v_n|^2) \approx 22$) and (b) a stable soliton at $\epsilon = 3.32$ (respectively $P \approx 56$). For the both solitons $\mu = 10$ and $\gamma = 0.1$. Filled and empty circles correspond to sites with gain (i.e. u_n) and losses (i.e. v_n), respectively. Arrows show directions and amplitudes of the largest currents in the system.

The model (1) is conveniently rewritten in terms of the variables

$$q_{2n}(t) = u_n e^{-i(\kappa_0+\kappa_1+\mu)t}, \qquad q_{2n+1}(t) = v_n e^{-i(\kappa_0+\kappa_1+\mu)t}, \tag{2}$$

where μ is a constant and we assume that u_n and v_n do not depend on t and satisfy zero boundary conditions: $u_n, v_n \to 0$ as $n \to \pm\infty$. Then Eq. (1) can be rewritten in the matrix form:

$$H\mathbf{w}_n + \epsilon\,(\sigma_-\mathbf{w}_{n-1} + \sigma_+\mathbf{w}_{n+1}) = F(\mathbf{w}_n)\mathbf{w}_n, \tag{3}$$

where

$$\mathbf{w} = \begin{pmatrix} u_n \\ v_n \end{pmatrix},\ H = \begin{pmatrix} \mu - i\gamma & 1 \\ 1 & \mu + i\gamma \end{pmatrix},\ \sigma_- = \begin{pmatrix} 0 & 1 \\ 0 & 0 \end{pmatrix},\ \sigma_+ = \begin{pmatrix} 0 & 0 \\ 1 & 0 \end{pmatrix},\ F(\mathbf{w}_n) = \begin{pmatrix} |u_n|^2 & 0 \\ 0 & |v_n|^2 \end{pmatrix}.$$

Starting with the anti-continuum limit (where $\epsilon = 0$) we proof the existence of the localized solutions of (3) (i.e. consider analytical continuation for $\epsilon > 0$), whose examples are illustrated in the right panel of Fig. 1, describe the families of such solutions, as well as their dynamical stability.

Further we generalize the consideration to more complex networks like the ones illustrated in the left panels of Fig. 2, and construct their soliton solutions whose graphical illustration is given in the right panels of Fig. 2.

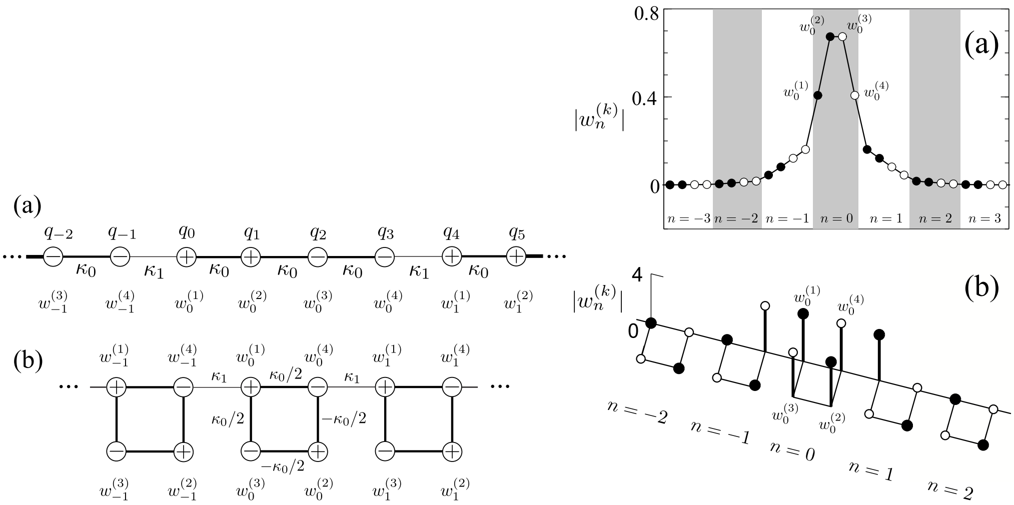

Figure 2: (Left panels) Two examples of $\mathcal{PT}$-symmetric networks, which consists of a set of disconnected quadrimers in the anticontinuum limit and are identical from the point of view of the spectral properties in the linear limit [1]. (Right panels) Stable solitons for the network shown in the left panels (a) at $\epsilon = 0.5$, $\gamma = 0.25$ and $\mu = 2$ and (b) at $\epsilon = 1.6$, $\gamma = 0.1$ and $\mu = 10$. Filled (empty) circles correspond to sites with gain (losses).

We thus show that the idea of analytical continuation from the anticontinuum limit (for all technical details see [2]) can be applied to networks of $\mathcal{PT}$-symmetric optical waveguides, offering analytical proof of the existence of discrete optical solitons. Such solitons obey the $\mathcal{PT}$-symmetric shape and can be found stable. The considered systems allow for further straightforward generalizations, say to chains of clusters with more than one links among the neighbor ones, or to chains of oligomers, i.e. clusters with more than four sites. Furthermore, the approach of continuation from the anticontinuum limit can be used for developing of a classification of intrinsic localized modes, as well as analytical theory of the nonlinear stability of such modes.

ACKNOWLEDGMENT

VVK and DAZ acknowledge the support of the FCT (Portugal) Grants No. SFRH/BPD/64835/2009, No. PTDC/FIS/112624/2009, and No. PEst-OE/FIS/ UI0618/2011

REFERENCES

1. Zezyulin, D. A. and Konotop, V. V. "Nonlinear Modes in Finite-Dimensional $\mathcal{PT}$-Symmetric Systems," *Phys. Rev. Lett.*, Vol. 108, 213906 (2012).
2. Konotop, V. V., Pelinovsky, D. E., and Zezyulin, D. A., "Discrete solitons in $\mathcal{PT}$-symmetric lattices," *EPL*, (in press)

Nonlinear modes in $\mathcal{PT}-$symmetric metamaterials

G. P. Tsironis[1*], **and N. Lazarides**[1]

[1]Department of Physics, University of Crete and Institute of Electronic Structure and Laser, FORTH
P. O. Box 2208, Heraklion 71003, Greece
*gts@physics.uoc.gr

Abstract— We introduce a nonlinear metamaterial with matched gain and loss. The linearized system has a band gap and experiences a phase transition from an exact dynamical phase to a broken phase where the band extend reduces. In the nonlinear case we find that there is generation of novel type of intrinsic localized modes.

Synthetic systems with matched gain and loss may form parity-time ($\mathcal{PT}$)-symmetric metamaterials described through non-hermitian Hamiltonians and showing a phase transition in between an exact and a broken phase as a function of the gain/loss power [1].The $\mathcal{PT}-$symmetry breaking has been experimentally observed in optical lattices [2]. We introduce a $\mathcal{PT}$-symmetric metamaterial consisted of split-ring resonator (SRR) dimers, one with loss and the other with equal amount of gain, coupled magnetically while nonlinearity and gain are introduced through tunnel Esaki diodes. Within the framework of the equivalent circuit model [3], extended for the $\mathcal{PT}-$ dimer chain, the dynamics of the charge q_n accumulated in the capacitor of the $n-$th SRR is governed by

$$\lambda'_M \ddot{q}_{2n} + \ddot{q}_{2n+1} + \lambda_M \ddot{q}_{2n+2} + q_{2n+1} = \varepsilon_0 \sin(\Omega\tau) - \alpha q_{2n+1}^2 - \beta q_{2n+1}^3 - \gamma \dot{q}_{2n+1} \tag{1}$$

$$\lambda_M \ddot{q}_{2n-1} + \ddot{q}_{2n} + \lambda'_M \ddot{q}_{2n+1} = \varepsilon_0 \sin(\Omega\tau) - \alpha q_{2n}^2 - \beta q_{2n}^3 + \gamma \dot{q}_{2n} \tag{2}$$

where λ_M, λ'_M are the magnetic interaction coefficients, α and β are dimensionless nonlinear coefficients, γ is the gain/loss coefficient ($\gamma > 0$), ε_0 is the amplitude of the external driving voltage, while Ω and τ are the driving frequency and temporal variable, respectively, normalized to the inductive-capacitive (LC) resonance frequency ω_0 and inverse LC resonance frequency ω_0^{-1}, respectively, $\omega_0 = 1/\sqrt{LC_0}$ with C_0 being the linear capacitance.

In the absense of nonlinearity, for fixed λ_M, λ'_M, the bandwidths as a function of the gain/loss parameter γ show the onset of the $\mathcal{PT}-$ phase transition and a resulting band modification. The presense of noninearity may induce nonlinearly localized modes in the form of discrete breathers with the largest part of the total energy concentrated into two neighboring sites belonging to the same gain/loss dimer [3]. The $\mathcal{PT}-$ symmetric nonlinear metamaterial may be used for dynamic tuning in the range of the modified band and switching to the broken phase.

ACKNOWLEDGMENT

We acknowledge partial support by the "THALES" Project ANEMOS, funded by the ESPA Program of the Ministry of Education of Greece.

REFERENCES

1. R. El-Ganainy,et al., Opt. Lett. **32**, 2632 (2007); K. G. Makris, et al, Phys. Rev. Lett. **100**, 103904 (2008).
2. A. Guo *et al.*, Phys. Rev. Lett. **103**, 093902 (2009); C. E. Rüter *et al.*, Nature Physics **6**, 192 (2010); A. Szameit, et al., Phys. Rev. **A 84**, 021806(R) (2011).
3. N. Lazarides, M. Eleftheriou, and G. P. Tsironis, Phys. Rev. Lett. **97**, 157406 (2006); N. Lazarides and G. P. Tsironis, cond. mat. 1210.2410v1.

Soliton scattering in the chain of optical waveguides including $\mathcal{PT}$ - symmetric defect

S. V. Suchkov[1], **S. V. Dmitriev**[1], **A. A. Sukhorukov**[2], **and Yu. S. Kivshar**[2]

[1]Institute for Metals Superplasticity Problems, Russian Academy of Sciences, Ufa 450001, Russia
[2]Nonlinear Physics Centre, Research School of Physics and Engineering, Australian National University, Canberra, ACT 0200, Australia
sergey.v.suchkov@gmail.com

Abstract— We study the propagation of nonlinear waves in an optical waveguide array with an embedded pair of waveguides with gain and loss satisfying the so-called parity-time symmetry condition. We demonstrate that in the case of small soliton amplitudes, the linear theory describes the scattering of solitons with a good accuracy. We also show that by exciting a large-amplitude localized mode, it is possible to perform phase-sensitive control of soliton scattering and amplification of the localized mode.

It was shown by Bender [1] that non-Hermitian Hamiltonians can have an entirely real eigenvalue spectrum under the parity-time ($\mathcal{PT}$) symmetry constraint. This mathematical observation can have deep physical consequences. It turns out that for optical structures the necessary condition for the $\mathcal{PT}$-symmetry of a Hamiltonian with a complex potential, $V(x)$, can be reduced to the condition $V(x) = V^*(-x)$ [2]. Those systems can be realized in the most straightforward way in optics, by combining a spatially symmetric profile of the refractive index with symmetrically positioned gain and loss regions. Photonic structures composed of coupled waveguides with loss and gain offer new possibilities for shaping optical beams and pulses compared to conservative structures. Such structures can be designed as optical analogues of complex $\mathcal{PT}$- symmetric potentials, which can have a real spectrum corresponding to the conservation of power for optical eigenmodes, however the beam dynamics can demonstrate unique features distinct from conservative systems due to nontrivial wave interference and phase transition effects [2]. Recently the possibility of creation of $\mathcal{PT}$ - symmetric optical coupler, a pair of waveguides with gain in one of them and loss in another, was demonstrated experimentally [3, 4]. In our study we demonstrate that such coupler can play a role of optical controller for the propagating beams in optical waveguide arrays.

We consider a chain of optical waveguides which includes one $\mathcal{PT}$ - symmetric coupler. The scheme of considered system is presented in Fig. 1. Beam dynamics is governed by a system of

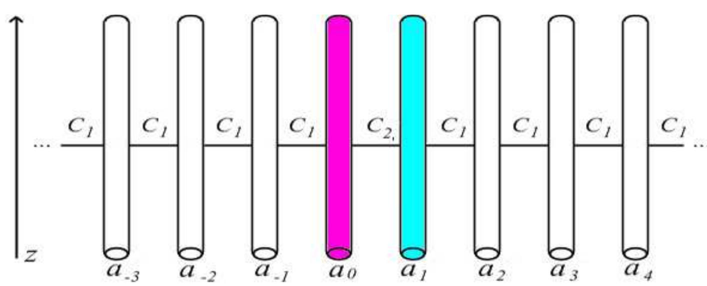

Figure 1: Scheme of optical waveguide array including $\mathcal{PT}$ - symmetric coupler composed of a waveguide with loss at the position $j = 0$ and a waveguide with gain at $j = 1$.

discrete nonlinear Schrodinger equations

$$\begin{aligned} \frac{da_j}{dz} &= i|a_j|^2 a_j + iC_1 a_{j-1} + iC_1 a_{j+1}, \quad j \neq 0,1 \\ \frac{da_0}{dz} &= -\rho a_0 + i|a_0|^2 a_0 + iC_1 a_{-1} + iC_2 a_1, \\ \frac{da_1}{dz} &= \rho a_1 + i|a_1|^2 a_1 + iC_1 a_2 + iC_2 a_0, \end{aligned} \tag{1}$$

where ρ is the gain/loss coefficient, C_1 - coupling constant between conservative waveguides, C_2 - coupling constant between the loss and gain waveguides of the $\mathcal{PT}$ coupler, a_j - optical mode amplitude at j-th waveguide.

We investigate the scattering of solitons on the defect in the case of strong nonlinearity. We confirm that linear theory developed in Ref. [5] describes with a good accuracy the scattering of small-amplitude solitons for a wide range of model parameters. Importantly, we find that the high-amplitude solitons can excite a mode localized on the defect. In Fig. 2 two characteristic cases of soliton scattering are presented. In panel (a) one can see that the soliton with the amplitude $A = 0.2$ does not excite a localized mode, while in panel (b) it is clearly seen that the mode is excited by the soliton with the amplitude $A = 0.5$. Next, we investigate how the intensity of the

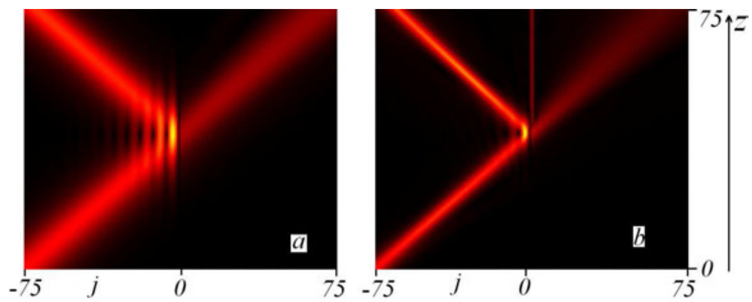

Figure 2: Scattering of soliton on the $\mathcal{PT}$ - symmetric coupler. Brighter colors show larger light intensity. Model parameters: $C_1 = 2$, $C_2 = 4$, $\rho = 1.5$. In panel (a) the soltion amplitude is $A = 0.2$, while in (b) $A = 0.5$. For both cases soliton's velocity is $v = 0.5$.

localized mode, which appears after the soliton passes through the defect, depends on the soliton's amplitude and loss/gain parameter ρ. Since the incident soliton can excite a localized mode it is interesting to investigate the interaction of the soliton with the high-amplitude localized mode. We show that the interaction dynamics is sensitive to the soliton's phase and thus, the localized mode can be used for phase-sensitive control of the soliton scattering.

In summary, we conclude that the presented optical system with the $\mathcal{PT}$ - symmetric element can be used for active control of propagating signals, particularly for amplification, filtering, and for all-optical switching.

REFERENCES

1. C. M. Bender, C. Boettcher, *Phys. Rev. Lett*, Vol. 80, 5243–5246, 1998.
2. R. El-Ganainy, K. G Makris, D. N. Chistodoulides, and Z. H. Musslimani, *Opt. Lett.* Vol. 32, 2632, 2007.
3. C. E. Ruter, K. G. Makris, R. El-Ganainy, D. N. Christodoulides, M. Segev, D. Kip, *Nature Physics* , Vol. 6, 192–195, 2010.
4. A. Guo, G. J. Salamo, D. Duchesne, R. Morandotti, M. Volatier-Ravat, V. Aimez, G. A. Siviloglou D. N. Cristodoulides, *Phys. Rev. Lett.* Vol. 103, 093902, 2011.
5. S. V. Dmitriev, S. V. Suchkov, A. A. Sukhorukov, Yu. S. Kivshar, *Phys. Rev. A*, Vol. 84, 013833, 2011.

Optical response of gain-assisted plasmonic nanoparticles

V. Pustovit[1], A. Veltri[1], F. Capolino[2] and A. Aradian[1]

[1] Centre de Recherche Paul Pascal - CNRS & Univ Bordeaux, France
[2] Department of Electrical Engineering and Computer Science, University of California Irvine, USA
aradian@crpp-bordeaux.cnrs.fr

Abstract— The resonant behaviour of single plasmonic nanoparticles in contact with gain media is studied theoretically. Two approaches are presented. The first , simple description is based on a quasi-static continuum description of the gain medium. The second model describes the situation of a metallic gold nanoparticle, surrounded with a corona of dyes, taking into account interactions through a Green function formalism. The amplification of the hybrid modes of the particle-and-dye system are studied.

The physics of localized plasmons in metal nanoparticles has been recently fueled by the rapid development of new techniques for producing small particles and by the applicability of these objects in the realization of visible range metamaterials. One of the main issues in using metallic nano-structures for metamaterial applications at optical frequencies is their high level of losses. A most promising strategy to circumvent this obstacle is loss compensation, where the particles are coupled to active compounds (such as pumped dye molecules or quantum dots) which are able to transfer them energy and therefore amplify the desired response. Research along this line has gained momentum in the past couple of years, resulting for example in the first demonstration of a nanoscale spaser using gain-assisted core-shell nanoparticles [1, 2].

In the first theoretical model presented [3], we approach the problem of the optical response of metallic nanoparticles immersed in a gain medium (externally pumped dye solution) in a"macroscopic" approach. We describe the behaviour of the particle using the classical, long-wavelength formula for the static polarisability of a sphere. Under these conditions, we investigate in detail the response for this polarisability when the embedding medium contains gain, and we produce a rational chart of all possible behaviours, as a function of material parameters and gain level. This reveals that although the plasmonic resonance can be strongly sharpened in the presence of gain [4], it will not reproduce "ideal" plasmons which would be obtained from lossless metals. Also, new types of responses appear, including one whose real part has a bell-like, Lorentzian shape and the imaginary part, a sigmoidal behaviour (we call this the "conjugate" from a usual plasmon). We compare our results for gold and silver particles: these two metals show some significant differences, with important practical consequences. We also prove analytically that these phenomena are in fact related to Fano resonances [5], with the nanoparticle and gain medium forming an interesting case of a"self-tuned" and unusual Fano system.

We extend this macroscopic approach by studying a core-shell geometry for the nanoparticle, with a metal core and dye-doped silica shell, much closer to experimental realizations [6]. Similar results conclusions can be drawn for the shape of the predicted resonances. Whereas previous results were obtained with a particle in an infinite gain medium, it is clear physically that only the gain molecules or elements close enough to the particle will contribute to the loss compensation. In this geometry, we are therefore able to evaluate an "effective gain" radius. We also evaluate the number of molecules needed to achieve best loss compensation with the number of gain molecules that can be geometrically packed in the silica shell – a crucial point for the chemical fabrication of such nanoparticles, with drastically different outcomes for gold versus silver.

The second theoretical description we study is based on a detailed microscopic description of the optical response of metal nanoparticles surrounded by gain elements, in contrast with the above-described work which was macroscopic in spirit. We assume here that the metal nanoparticle is decorated by a monolayer corona made of dye molecules (or quantum dots) which are externally pumped, and that dyes and metal are separated by a protective silica shell. A system of equations is derived accounting for all dye-nanoparticle interactions (multipolar) as well as dye-dye interactions, both directly and cooperatively mediated by the nanoparticle, using a proper dyadic Green function [7]. We then derive the expression for the effective polarizability of the whole metal-silica shell-dye ensemble, which involves a set of hybrid dye-nanoparticle eigenmodes describing the collective electromagnetic behaviour of the aggregate. In some cases, one specific collective mode will be highly amplified and dominate the whole response, giving sharp resonant features, reminiscent of nano-laser response.

ACKNOWLEDGMENT

This work was supported by the FP7-NMP-2008 European project METACHEM under grant agreement nr. 228762 and the SAMM project of the GIS-Advanced Materials in Aquitaine network.

REFERENCES

1. Noginov, M. A., G. Zhu, A. M. Belgrave, R. Bakker, V. M. Shalaev, E. E. Narimanov, S. Stout, E. Herz, T. Suteewong and U. Wiesner, “Demonstration of a spaser-based nanolaser,” *Nature*, Vol. 460, No. 7259, 1110–1112, 2009.
2. Bergman, D. J. and M. I. Stockman, “Surface Plasmon Amplification by Stimulated Emission of Radiation: Quantum Generation of Coherent Surface Plasmons in Nanosystems,” *Phys. Rev. Lett.*, Vol. 90, No. 2, 027402-1–027402-4
3. Veltri, A and A. Aradian, “Optical response of a metallic nanoparticle immersed in a medium with optical gain,” *Phys. Rev. B.*, Vol. 85, No. 11, 115429-1–115429-5.
4. Lawandy, N. M., “Localized surface plasmon singularities in amplifying media,” *Appl. Phys. Lett.*, Vol. 85, No. 21, 5040–5042, 2004.
5. Lukyanchuk, B, N. Zheludev, S. A. Maier, N. J. Halas, P. Nordlander, H. Giessen and C. T. Chong, “The Fano resonance in plasmonic nanostructures and metamaterials,” *Nature Mat.*, Vol. 9, 707–715, 2010.
6. De Luca, A, M. Ferrie, S. Ravaine, M. La Deda, A. Veltri, A. Aradian, N. Scaramuzza, M. Infusino, A. R. Rashed and G. Strangi, “Gain functionalized core-shell nanoparticles: the way to selectively compensate absorptive losses,” submitted.
7. Pustovit, V. N. and T. V. Shahbazyan, “Resonance energy transfer near metal nanostructures mediated by surface plasmons,” *Phys. Rev. B*, Vol. 83, 085427-1–085427-5, 2011.

One way propagation manipulation by complex Parity-Time photonic crystals

Ming-Hui Lu[1] , Liang Feng[1, 2], Ye-Long Xu[1] and Yan-Feng Chen[1,*],

1. National Laboratory of Solid-State Microstructures and Department of Materials Science and Engineering, Nanjing University, Nanjing 210093 China
2. Department of Electrical Engineering, California Institute of Technology, Pasadena CA91125, USA

[*]corresponding author: yfchen@nju.edu.cn

Abstract- Artificial structures exhibiting exotic optical properties not found in nature have gotten much attention due to their great potential applications. Among them, photonic crystals have been developed to control the propagation of electromagnetic waves with allowed and forbidden frequency band structures. It has been also extend to the design of metamaterials, which has subwavelength character dispersion and can be used to realize objects invisible or super-resolution imaging. In the past, photonic crystals mean widely a kind of artificial structural materials with the spatial distribution of the refractive index across passive optical components. In this talk, we describe our recent theoretical and experimental work regarding the complex photonic crystals, which might be a big step forward in the concept of photonic crystals and metamaterials. We will show some design and experiment progress about the Parity-Time symmetric (PT) photonic crystals in this talk. Different from the conventional photonic crystals, by modulating both the real and the imaginary part of the refractive index indicating either amplification (gain) or absorption (loss) of light within a material, a new class of optical structure is proposed to realize in optical system the recently developing concept of PT symmetry — a property of physical systems that are invariant under time inversion and parity symmetry. Such PT symmetry was originally introduced in quantum field theories, which reminded as an open question fundamentally; meanwhile the concept has been extended to optical system by the modulation of complex optical potential with symmetric real part and anti-symmetric imaginary part. We present our artful design and the experiment implementation of such PT-symmetric CMOS compatible devices in silicon optical chips, which show some unique optical phenomena, such as unidirectional coupler, mode converter and one-way reflectionless invisibility.

Acknowledgements, the National Basic Research of China (no. 2012CB921503 and no. 2013CB632702), the National Nature Science Foundation of China (no. 11134006)

REFERENCES

1. L. Feng et al., “Nonreciprocal Light Propagation in a Silicon Photonic Circuit,” *Science*, Vol. 333, 729, 2011.
2. L. Feng et al., “Experimental demonstration of a unidirectional reflectionless parity-time metamaterial at optical frequencies” *Nature Mater.*, Advanced online, DOI: 10.1038/NMAT3495

Surface plasmon components for parity-time symmetric systems

Pierre Berini

School of Electrical Engineering and Computer Science, and Department of Physics, University of Ottawa, Ottawa, Canada

*corresponding author: berini@eecs.uottawa.ca

Abstract- Passive and active long-range surface plasmon waveguide components are of interest for the implementation of parity-time (PT) symmetric systems. We review recent work on passive integrated elements such as straight waveguides, bends, couplers and Bragg gratings, and on the prospects of incorporating gain in such elements in order to achieve PT symmetric systems.

Surface plasmon polaritons (SPPs) are transverse-magnetic (TM) polarized surface waves that propagate, typically, along the interface of a dielectric and a metal at optical wavelengths. Long-range surface plasmon polaritons (LRSPPs) supported by thin narrow metal stripes are of interest in this paper [1], as are passive integrated components based on the stripe, such as S-bends, couplers and Bragg gratings [2], and active waveguides such as amplifiers [3]. The symmetric metal stripe shown in front cross-sectional view in Fig. 1, is the generic structure of interest. It consists of a thin metal stripe of thickness t, width w and permittivity ε_1, surrounded by an optically infinite dielectric of permittivity ε_2. One of the fundamental modes supported by the metal stripe, identified as the ss_b^0 mode [1], can propagate over a long range (i.e., with low loss) compared to the single-interface SPP if the metal stripe is thin enough. The distribution of the main transverse electric field component of the long-range ss_b^0 mode over the waveguide cross-section resembles a 2-D Gaussian distribution enabling efficient end-fire coupling to dielectric waveguides.

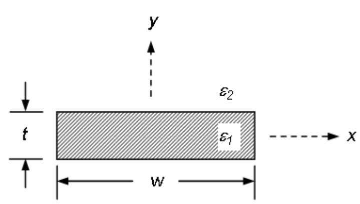

Fig. 1. Cross-sectional sketch of a metal stripe surface plasmon waveguide.

The metal stripe provides confinement in the (2D) plane transverse to the direction of propagation, enabling integrated components similar to those found in conventional integrated optics. Much work has already been done to establish various functions using metal stripes, including straight waveguides, passive elements and Bragg gratings [1,2]. Fig. 2(a) shows a sketch of a directional coupler designed by placing two metal stripes of width w in parallel over a length CL and separated from each other (edge to edge) by S. Fig. 2(b) shows measured outputs from the through and coupled ports at λ_0 = 1550 nm for a series of couplers as a function of S for S = 8 to 2 μm in steps of 1 μm [2]. The input port was excited by end-fire coupling to PM-SMF. The Au stripe dimensions were w = 8 μm, t = 25 nm and they were embedded in optically infinite SiO_2. Bragg gratings are most easily implemented as "step-in-width" structures, where the width of the stripe is stepped periodically over a prescribed length [1]. This architecture provides a weak perturbation so the gratings are about 0.5 to 1 mm long but they produce a very narrow linewidth (~0.2 nm) and a high reflectance ($R > 0.9$).

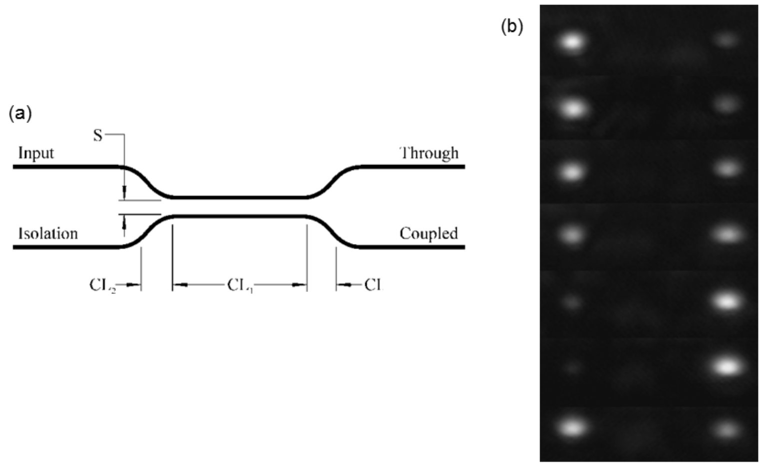

Fig. 2. (a) Sketch of coupled metal stripes. (b) Measured outputs as a function of stripe separation S; $S = 8$ to 2 μm in steps of 1 μm (top to bottom).

Recently, the amplification of LRSPPs has been demonstrated in the near IR (~880 nm) using a dye gain medium placed in contact with a metal stripe [3]. A reasonable dye concentration and pump intensity produced an LRSPP mode power gain of ~ 8 dB/mm.

By combining the above capabilities, two routes to achieving PT-symmetric LRSPP devices appear feasible: (*i*) The incorporation of gain uniformly along one arm of the coupled section of a coupler (*cf*. Fig. 2(a)) in an amount that is asymmetrical with the LRSPP loss in the other arm (equal in magnitude but of opposite sign) [4]. This produces a system which satisfies $\varepsilon(-x) \sim \varepsilon(x)^*$ with respect to the longitudinal plane of symmetry separating the coupled waveguides (x being the transverse axis along the width). (*ii*) The incorporation of gain uniformly along a step-in-width Bragg grating in an amount that provides LRSPP gain in one section of each period (say the narrowest) but LRSPP loss in the other (say the widest), such that a structure with periodic modulation of the real and imaginary parts of the effective permittivity is realized [5]. This produces a system which satisfies $\varepsilon(-z) \sim \varepsilon(z)^*$ within each grating period with respect to the period bisector (z is the propagation direction). Both of these structures could be realized, in principle, using doped PMMA as the gain medium as in LRSPP lasers [6].

REFERENCES

1. Berini, P., "Long-range surface plasmons," *Adv. Opt. Phot.*, Vol. 1, 484-588, 2009.
2. Charbonneau, R. *et al*., "Passive Integrated Optics Elements Based on Long-Range Surface Plasmon Polaritons," *J. Lightwave Technol.*, Vol. 24, 477-494, 2006.
3. De Leon, I., Berini, P., "Amplification of long-range surface plasmons by a dipolar gain medium," *Nature Photonics*, Vol. 4, 382-387, 2010
4. Benisty, H. *et al*., "Implementation of PT symmetric devices using plasmonics: principle and applications," *Opt. Express*, Vol. 19, 18004-18019, 2011.
5. Kulishov, M. *et al*., "Nonreciprocal waveguide Bragg gratings," *Opt. Express*, Vol. 13, 3068-3078, 2005.
6. Karami Keshmarzi, E., Tait, R. N., Berini, P., "Long-range surface plasmon single-mode laser concepts, » *J. Appl. Phys.*, Vol. 112, 063115, 2012.

Guided-wave devices with fixed losses inspired by PT-symmetry and their spectrum singularity

H. Benisty[1*], A. Lupu[2], and A. Degiron[2]
[1]LCF IOGS, Palaiseau, France
[2]IEF, Univ. Paris-Sud and CNRS, Orsay, France
[*]corresponding author: henri.benisty@institutoptique.fr

Abstract- Guided-wave devices with plasmonic-type fixed losses can be adapted to exploit the singular point behavior well known for exact PT symmetric guides. Coupled guides having fixed losses and variable gain fail to exhibit a singular point in their eigenvalues if the guides' effective indices coincide. We show how to "heal" this situation and restore singularity by detuning among the guides. We also present a frame inspired by Kogelnik's representations of alternate $\Delta\beta$ couplers to usefully account for several configurations.

We investigate the possible benefits of guided wave devices, such as couplers made of two coupled guides, but inspired by the PT symmetric configuration which is well known to produce a singular point in the eigenvalue spectrum evolution vs. the gain/loss parameter. In actual coupled waveguides, it is generally delicate, if not impossible, to impose gain and losses accurately while maintaining a good mode coupling between the two guides. Therefore, it is tempting to investigate the capability to retain the essential features of the singularity of eigenvalues with a more practical guide that features only fixed losses, and notably a plasmonic waveguide.

In the simplest 1D coupled-wave view, we first remark that the singularity is maintained for a guide with fixed losses ($g= -|g|$, of course coupled to a gain guide), but that the singular point itself lies at zero modal gain ($\gamma=0$) only if the coupling strength is related to the fixed losses according to the rule $|g| =\kappa$. The transfer function can then be plotted (Fig.1(a)) in a map whose axis are (L, $|g|/\kappa$), i.e. guide length L and gain to coupling ratio. Compared to a similar map for an exact PT system, most major features are preserved [1]. The tracks of the underlying eigenvalues are indicated below these figures.

However, if we model actual coupled waveguides, e.g. a plasmonic and a dielectric waveguide, the track of eigenvalues in the complex plane avoids the singularity by a variable amount. We interpret this effect as a complex coupling, the coupling constants are affected by the variable gain in the concerned waveguide.

Correspondingly, some of the transitions manifested in Fig.1 are smoother than they would be ideally. Thus, it would be advantageous to "heal" the waveguides in such a way as to restore the singularity.

We showed very recently [2] that this is simply done by detuning the two waveguides. Then, the interplay of variable gain with both the real and imaginary parts of the system's eigenvalues can lead to a "compensation", causing the eigenvalues trajectories to experience a perfect singularity.

We will give a graphical interpretation of this "healing" mechanism, and we will exemplify its operation in several model cases, with either model dielectric guides or more realistic configurations involving plasmons or involving the recently proposed hybrid plasmonic waveguide geometry that we have termed "PIROW" (Plasmonic Inverse-Rib Optical Waveguide) [3].

In the last part of this talk, we will attempt to present a variant of PT symmetric guides that is analog to Kogelnik's alternate-$\Delta\beta$-couplers presented decades ago [4]. The main merit of this approach and of the associated diagrams in the (L, $|g|/\kappa$) plane is to show how the extra complexity allows both "cross" and "bar" states in a coupler that does *not* operate at the right length, coupling, or wavelength by modifying the gain/loss parameters. Indeed "bar" and "cross" refer to passive waveguides and these denominations should be generalized for PT symmetric systems, as we shall explain.

As a hint, we note that one essential feature of the commutation diagram for a PT system is the genesis of two branches originating from each singular cross state at the g=0 axis. These two branches open the possibility to either get the usual "reciprocal" cross-bar switching found in conventional passive coupled waveguides, or get an asymmetric switching that can be fruitfully exploited to implement a dynamical buffer memory as proposed by Kulishov in 2005 [5].

Thus, the introduction of alternating gain/loss sections along the propagation direction in the variant PT system leads to an extra feature in the transfer diagram. As more alternating PT sections are defined, regularly spaced stripes of high gain regions emerge close to the G=0 axis inside regions that featured lower gain in the non-alternating case of Fig. 1(a). The origin of this phenomenon and its potential applications will be discussed.

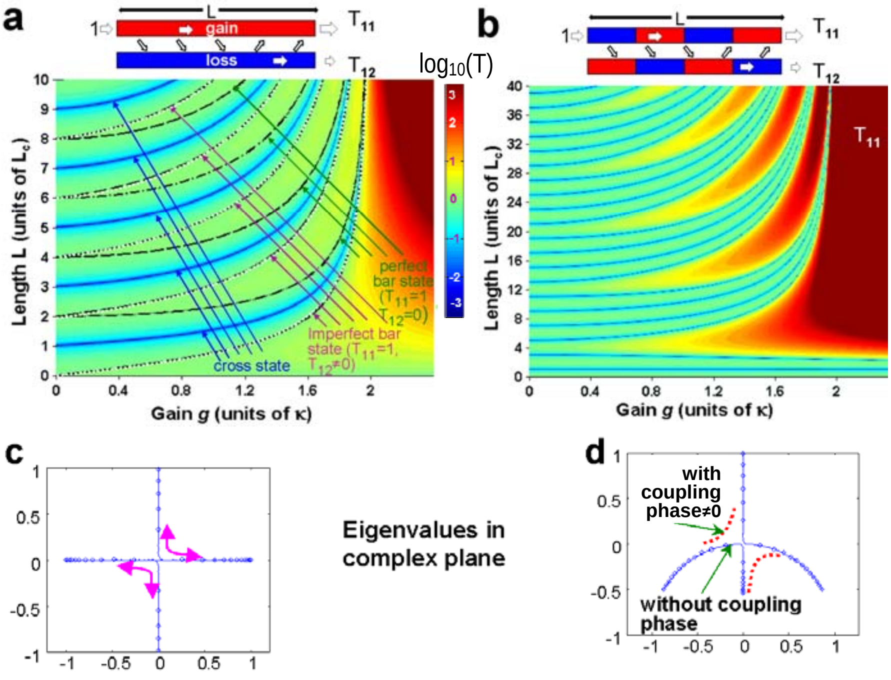

Figure 1 :
(a) Ideal transfer diagram of a PT symmetric system : the color map is that of T_{11};
(b) Similar transfer diagram but with 4 alternating PT sections coupler.
The two bottom graphs (c,d) show the respective eigenvalue evolutions in the complex plane. The presence of a coupling phase causes an avoided crossing, thus no good operation window unless the fixed losses are "healed".

REFERENCES

1. H. Benisty, A. Degiron, A. Lupu, A. De Lustrac, S. Chénais, S. Forget, M. Besbes, G. Barbillon, A. Bruyant, S. Blaize, and G. Lérondel, "Implementation of PT symmetric devices using plasmonics: principle and applications," Opt. Express **19**, 18004−18019 (2011).
2. H. Benisty, C. Yan, A. Degiron and A. Lupu, "Healing near-PT-symmetric structures to restore their characteristic singularities : analysis and examples," Journal of Lightwave Technology **30**, 2675 - 2683 (2012).
3. H. Benisty and M. Besbes, "Confinement and optical properties of the plasmonic inverse-rib waveguide," J. Opt. Soc. Amer. B **29**, 818–826 (2012).
4. H. Kogelnik and R. V. Schmidt, "Switched directional couplers with alternating Δβ," IEEE J. Quantum Electron. QE-**12**, 396-401 (1976).
5. M. Kulishov, J. M. Laniel, N. Bélanger, and D. V. Plant, "Trapping light in a ring resonator using a grating assisted coupler with asymmetric transmission," Opt. Express 13, 3567–3578 (2005).

Exploring effective PT-symmetric Hamiltonians using metamaterials

Ming Kang[1], Fu Liu[1], and Jensen Li[1,2*]

[1]*Department of Physics and Materials Science, City University of Hong Kong, Hong Kong*

[2] *School of Physics and Astronomy, University of Birmingham, Edgbaston, Birmingham B15 2TT, UK*

*corresponding author: j.li@bham.ac.uk

Abstract- We theoretically investigate the analog of PT-symmetric non-Hermitian quantum mechanical systems using metamaterials, which can provide a flexible testing ground for PT-symmetry. We show that spontaneous PT-symmetry breaking can be achieved by exploring the interplay between the near-field coupling and material absorption or gain. An ideal PT-symmetry can also be established effectively in a passive system. Coherent perfect absorption and amplification are demonstrated as examples.

Complex Hamiltonians respecting a parity-time symmetry, [PT,H] = 0, can have real eigenenergies depending on an adjustable parameter [1]. It provides a generalization of Hermitian Hamiltonians with much richer properties. Although it may not be easy to realize a PT-symmetric Hamiltonian in quantum mechanics, there can be optical analogies. For example, a pair of optical waveguides with balanced gain and loss can be well represented by a 2×2 PT-symmetric Hamiltonian matrix with complex conjugate pairs in both the diagonal and off-diagonal elements. Here, we seek how such a Hamiltonian can be effectively established for metamaterials, which can provide a flexible platform for studying PT-symmetry. For a metamaterial slab at normal incidence without polarization conversion, the optical response can be expressed using a 2×2 scattering matrix S as

$$\begin{pmatrix} b_+ \\ b_- \end{pmatrix} = S \begin{pmatrix} a_+ \\ a_- \end{pmatrix}, \tag{1}$$

with Figure 1(a) defining all the out-of-plane E-field amplitudes for the incoming and outgoing waves. Here, we further use a thin metamaterial slab consisting an electric atom (with electric dipole p responding to a local electric field) and a magnetic atom (with magnetic dipole m responding to a local magnetic field) with the same resonating frequency ω_0 in each unit cell as an example. The two atoms are coupled through near fields with coupling strength κ. For such a case, it can be proved that a family of effective Hamiltonians (with different values of n) can be defined by

$$H_n = \begin{pmatrix} \omega_0 - i\gamma_1 & \kappa \\ \kappa & \omega_0 - i\gamma_2 \end{pmatrix} + n \begin{pmatrix} i\gamma_1^{(s)} & 0 \\ 0 & i\gamma_2^{(s)} \end{pmatrix}, \tag{2}$$

where $\gamma_i = \gamma_i^{(s)} + \gamma_i^{(loss)}$ (i = 1,2) is the total resonating linewidth as a sum of the scattering part and the absorption part (positive for absorption, negative for gain) for each atom. Then, an eigenfrequency problem of H_n corresponds to an eigenvalue problem of S as

$$H_n\begin{pmatrix} p \\ im \end{pmatrix} = \omega\begin{pmatrix} p \\ im \end{pmatrix} \Leftrightarrow \frac{n-2}{n}\begin{pmatrix} a_+ \\ a_- \end{pmatrix} = S\begin{pmatrix} a_+ \\ a_- \end{pmatrix}. \tag{3}$$

For example, we can have a Hamiltonian H_2 exhibiting effective PT-symmetry when we have

$$\gamma_1^{(s)} - \gamma_1^{(loss)} = \gamma_2^{(loss)} - \gamma_2^{(s)}. \tag{4}$$

It can be satisfied when we have a "bright" atom 1 with scattering more than absorption and a "dark" atom 2 with absorption more than scattering. Then, coherent perfect absorption [4,5] can occur with zero scattered fields when we have real eigenfrequencies. In a more general situation, Figure 1(b) shows the phase map (varying κ and γ_2) for where we can get real eigenfrequencies (solid lines: blue/black/red color for H_0/H_1/H_2) with fixed parameters: ω_0 = 402.5THz, γ_1 = 15THz, $\gamma_1^{(loss)}$ = 1.75THz, and $\gamma_2^{(s)}$ = 0THz. The vertical red line at γ_2 = 11.5THz indicates the condition we have an ideal PT-symmetric H_2. The two separate regions, solid/dashed line above/below $\kappa = \gamma_2$, indicate the so-called spontaneous PT-symmetry breaking process when real eigenfrequencies are transited to complex eigenfrequencies. We will construct metamaterial structures for numerical demonstrating the PT-symmetry and we will also discuss the cases of other values for n to achieve other PT-related phenomena such as coherent perfect amplification with gain incorporated into the system.

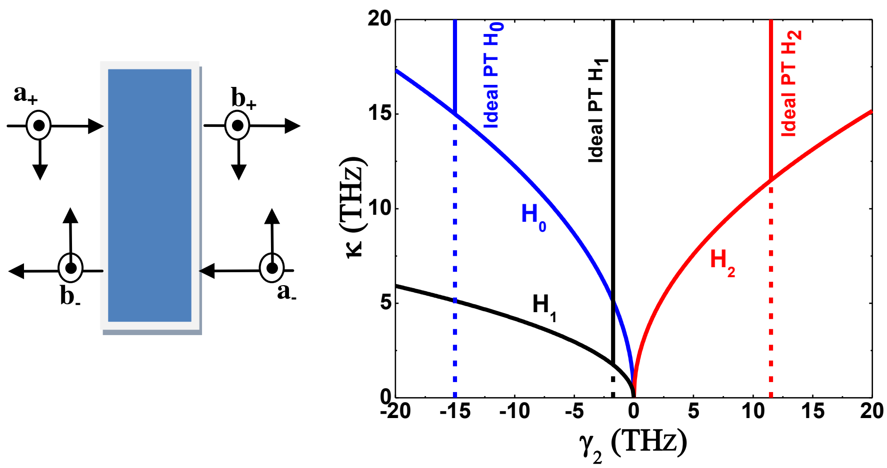

Figure 1. (a) Schematic of the metamaterial at normal incidence with incoming E-field (out-of-plane) amplitudes of a_+, a_- and outgoing amplitudes of b_+, b_-; (b) Parametric evolution of the metamaterial for different H_n. Vertical lines indicate the ideal PT-symmetric condition (a particular γ_2) for different H_n. The curved solid lines show the general condition in getting real eigenfrequencies for H_n.

This work is supported by Hong Kong Research Grants Council (GRF grant CityU 102012).

REFERENCES

1. C. M. Bender and S. Boettcher, Phys. Rev. Lett. 80, 5243 (1998).
2. A. Guo, et al., Phys. Rev. Lett. 103, 093902 (2009).
3. C. E. Ruter, et al., and D. Kip, Nat. Phys. 6, 192 (2010).
4. Y. D. Chong, L. Ge, and A. D. Stone, Phys. Rev. Lett. 106, 093902 (2011).
5. S. Longhi, Phys. Rev. A 82, 031801(R) (2010).

Full-vector analysis of photonic gain/loss structures

J. Čtyroký
Institute of Photonic and Electronics, AS CR, v.v.i. Czech Republic
ctyroky@ufe.cz

Abstract-Photonic waveguide structures with a balance of gain and loss have been mostly analyzed either in a 2D approximation in which the electromagnetic field is decoupled into TE and TM polarization, and each of them is fully determined by a single scalar function, or by using of the coupled mode theory in which the vectorial character of modal fields is usually not considered in detail. In this contribution we present results of a “rigorous” (numerical) full-vector analysis of several waveguide structures with a balance of loss and gain and show that the basic character of gain/loss structures – the existence of a critical gain/loss value at which the behaviour of the structures is dramatically changed – is fully retained also in this case.

Probably the first analysis of photonic waveguide structure with balanced loss and gain was described in [1] and [2] as a modelling task for benchmarking BPM methods. Within last years, a close formal relationship between photonic structures with the balance of loss and gain and quantum-mechanical structures with $\mathcal{PT}$ symmetry has been recognized and utilized in the analysis of several pertinent photonic, plasmonic as well as quantum systems [3-7]. Here we consider only the basic photonic aspects of interesting physical phenomena in gain/loss waveguide structures.

In [1, 2, 8] it has been shown that in a planar (2D) two-layer two-mode waveguide structure with complex permittivity distribution satisfying the relation $\varepsilon(-x) = \varepsilon^*(x)$, the two (super)modes propagate with two different real propagation constants (i.e., without loss or gain) as long as the gain/loss parameter (e.g., the imaginary part of the waveguide permittivities, ε'') is small. However, for a particular (critical) value $\varepsilon'' = \varepsilon''_{crit}$, *both propagation constants as well as the mode fields merge into a single one*. As ε'' further increases, the propagation constants become complex conjugate, which means that one mode becomes attenuated while the second one becomes amplified. The mode field distributions are modified correspondingly – the individual eigenmode fields are ever more concentrated in the media with loss and gain, respectively.

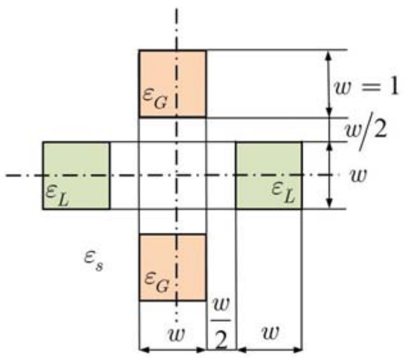

Figure 1. The cross section of the waveguide structure

In this contribution we show by “rigorous” (numerical) solution that this behaviour takes essentially place also for vector eigenmodes of channel waveguides, and – for a particular group of modes – also for 2D complex permittivity distributions satisfying the relations

$$\varepsilon(-x, y) = \varepsilon(x, -y) = \varepsilon^*(x, y)\,. \tag{1}$$

As an example, let us consider the structure composed of four rectangular channel waveguides, the cross-section of which is shown in Figure 1. The permittivities of the waveguides are $\varepsilon_{L,G} = 3.35^2 \pm \varepsilon''$, the permittivity of the surrounding medium is $\varepsilon_s = 3.30^2$. The structure was chosen so as to enable a very simple full-vector numerical modelling using the Fourier Modal Method [9]. At the wavelength of 1.55 μm, there are 8 localized eigenmodes – “supermodes” of the structure. As it follows from the (quasi)-symmetry of the structure, the modes are very nearly polarization degenerated, i.e., there is essentially no difference between horizontally (TE) and vertically (TM) polarized modes with the corresponding mode field distributions.

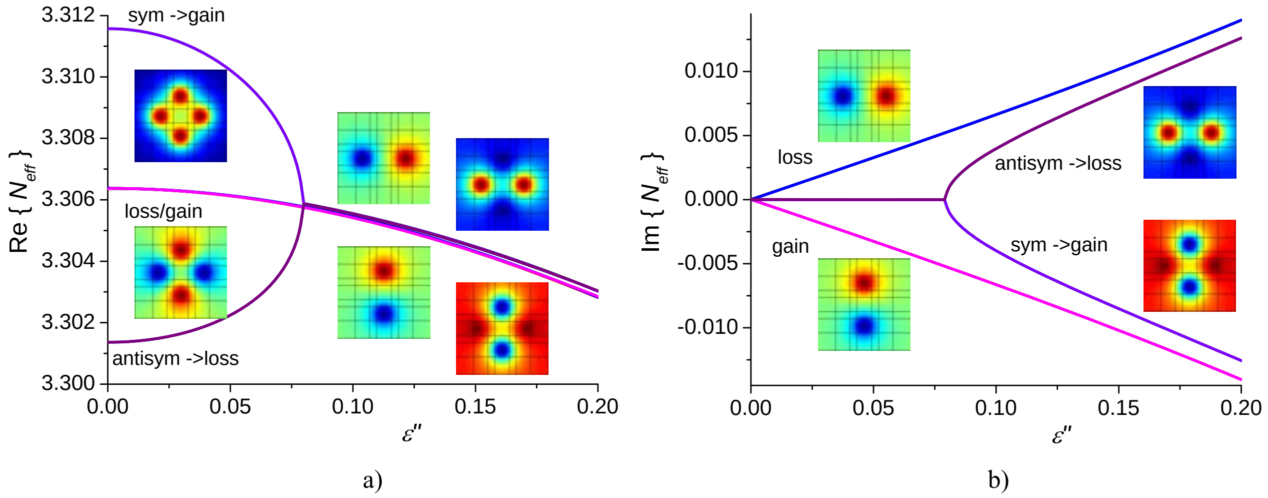

Figure 2. Real (a) and imaginary (b) parts of effective refractive indices of supermodes of the waveguide structure in Figure 1.

The calculated dependences of the real and imaginary parts of the effective indices of the (super)modes on ε'' are plotted in Figure 2. The distributions of the dominant electric field intensity components are shown in the insets. It is apparent that only one half of modes of the structure exhibit the characteristic gain/loss singularity.

Acknowledgements

Financial support by the Czech Science Foundation under project P205/10/0046 is acknowledged.

REFERENCES

[1] H.-P. Nolting, G. Sztefka, M. Grawert, and J. Čtyroký, "Wave Propagation in a Waveguide with a Balance of Gain and Loss," in *Integrated Photonics Research '96*, Boston, USA, 1996, pp. 76-79.

[2] G. Guekos, Ed., *Photonic Devices for telecommunications: how to model and measure*. Berlin: Springer, 1998, p.^pp. Pages.

[3] R. El-Ganainy, K. G. Makris, D. N. Chrisodoulides, and Z. H. Musslimani, "Theory of coupled optical PT-symmetric structures," *Optics Letters,* vol. 32, pp. 2632-2634, 2007.

[4] K. G. Makris, R. El-Ganainy, and D. N. Chrisodoulides, "Beam Dynamics in PT Symmetric Optical Lattices," *Physical Review Letters,* vol. 100, pp. 103904(1)-103904(4), 2008.

[5] C. E. Rüter, K. G. Makris, R. E-Ganainy, D. N. Christoulides, M. Segev, and D. Kip, "Observation of parity–time symmetry in optics," *Nature Physics,* vol. 6, pp. 192-195, 2010.

[6] H. Benisty, A. Degiron, A. Lupu, A. De Lustrac, S. Chenais, S. Forget*, et al.*, "Implementation of PT symmetric devices using plasmonics: principle and applications," *Optics Express,* vol. 19, pp. 18004-18019, Sep 2011.

[7] A. A. Sukhorukov, S. V. Dmitriev, S. V. suchkov, and Y. S. Kivshar, "Nonlocality in PT-symmetric waveguide arrays with gain and loss," *Optics Letters,* vol. 37, pp. 2148-2150, 2012.

[8] J. Čtyroký, V. Kuzmiak, and S. Eyderman, "Waveguide structures with antisymmetric gain/loss profile," *Optics Express,* vol. 18, pp. 21585-21593, 11 October 2010 2010.

[9] J. Čtyroký, "3-D Bidirectional Propagation Algorithm Based on Fourier Series," *Journal of Lightwave Technology,* 2012, DOI 10.1109/JLT.2012.2226208.

Plasmonic Biosensors

Metal island film based structures for sensing using spectrophotometry and ellipsometry

V. Janicki[1,2*], J. Sancho-Parramon[1,2], S. Bosch[2] and H. Zorc[1]
[1]Ruder Boskovic Institute, Croatia
[2]University of Barcelona, Spain
[*]corresponding author: janicki@irb.hr

Abstract-Metal island films (MIF) are good candidates for sensors due to environment refractive index sensitive localized surface plasmon resonance. The strong near field enhancement in the vicinity of the island surface can be even higher if metal layer (ML) is placed close to MIF. Structures containing MIF with and without ML are prepared and sensitivities of spectrophotometric and ellipsometric features of the measurements compared. It is shown that simple MIF is preferable for ellipsometric and including ML for spectrophotometric sensing.

Metal island films (MIFs), consisting of two-dimensional ensembles of metal particles deposited on a substrate, have strong potential for plasmonic biosensing. The localized surface plasmon resonance (LSPR) of isolated particles is highly sensitive to refractive index changes of the environment, enabling to detect presence of different analytes [1]. The strong near field enhancement taking place close to the island surface, allows amplification of Raman signal [2] or infrared absorption [3] of closely located molecules. The near field enhancement is largest for very small particles and inter-particle distances, which are typically few nanometers in the case of MIFs. Strong coupling between LSPR of metal nanoparticles and propagating surface plasmon of a nearby metal film, enhances this electric near field largely [4]. MIFs are attractive candidates for the production of performance- and cost-efficient sensors. Sensing using MIFs is typically based on the LSPR band central wavelength shift upon changes of dielectric environment [1].

This work compares sensitivity of MIFs-based plasmonic structures to the quantity of dielectric material surrounding the metal nanoparticles. The first type of structure is substrate/MIF/SiO_2 (MIF* serial) and the second substrate/Au/SiO_2/MIF/SiO_2 (AuMIF* serial). The samples within one serial differ in the mass thickness of capping SiO_2 layer (d_{capp}). All the corresponding layers are prepared in the same electron beam deposition process. Therefore, their thicknesses and optical parameters in the both structures are assumed to be the same.

Spectroscopic (reflectance *R* and transmittance *T*) and ellipsometric measurements of two series of samples are analysed. *R* and *T* are measured in the range 300-1100 nm, and ellipsometric functions Ψ and Δ in the range 4.35-0.57 eV (that corresponds to 285-2175 nm), at incidence angles 25°, 45°, 55°, 65° and 80°. Additionally, *T* is measured at ellipsometer in the same range as Ψ and Δ, at normal incidence. Absorption *A* is calculated from spectroscopic measurements as $A = 1 - R - T$. The maxima or minima in the spectra having significant central wavelength (λ_o) shift or change of the intensity (I_o) with d_{capp} were analysed. Sensitivity was calculated as S_x=dx/dd, where x denotes λ_o or I_o of the extreme point of interest and d is mass thickness of SiO_2 deposited above Au islands.

It is found that AuMIF* serial transmittance peak shift sensitivity $S_{\lambda 0}(T_{AuMIF*})$ is higher than the one of MIF*. This makes AuMIF* structure more practical for sensing purposes, as *T* measurements are simple and widely available. $S_{\lambda 0}(A_{AuMIF*})$ also shows higher value than the one of MIF*. However, $S_{\lambda 0}$ (R_{MIF*}) has the highest sensitivity of all the spectrometric measurements. Generally, S_I shows lower values for this kind of measurements than $S_{\lambda 0}$, S_I(AuMIF*) being higher than S_I(MIF*). Regarding ellipsometric measurements, shift sensitivities of MIF* are significantly higher than for AuMIF*. In the case of S_I the situation is opposite. However, comparing shift and intensity sensitivities obtained from ellipsometry, S_I values are lower. Overall, AuMIF* structure is preferable for sensing in the case of spectrometric measurements, while ellipsometric measurements give advantage to MIF* structure. These results offer a guideline for design of MIF based sensing structures depending on the availability of optical measurements.

Acknowledgements

Vesna Janicki would like to thank European Science Foundation (ESF) for the activity entitled 'New Approaches to Biochemical Sensing with Plasmonic Nanobiophotonics (PLASMON-BIONANOSENSE) Exchange Grant 3853.

REFERENCES

1. Vaskevic, A. and I. Rubinstein, “Localized Surface Plasmon Resonance Sensing (LSPR) Spectroscopy in Biosensing,” *Handbok of Biosensors and Biochips*, Wiley, 2007.
2. Moskovits, M., "Surface-enhanced Raman spectroscopy: a brief retrospective," J. Raman Spectrosc., Vol. 36, No. 36, 485-496, 2005.
3. Osawa, M., "Surface Enhanced Infrared Absorption," Topics Appl. Phys., Vol. 81, 163-187, 2001.
4. Chu, Y. and K. B. Crozier, "Experimental study of the interaction between localized and propagating surface plasmons," *Opt.Lett*., Vol. 34, No. 3, 244-246, 2009.

Plasmonic response in InSb sub-wavelength structures

J. H. Teng
Institute of Materials Research and Engineering, Agency for Science, Technology and Research (A*STAR),
3 Research Link, Singapore 117602.
*jh-teng@imre.a-star.edu.sg

Abstract- This talk will introduce the plasmonic response in InSb sub-wavelength structures. InSb touching disks are used to demonstrate broadband THz response while direct tuning of plasmonic response is realized by optical excitation of an InSb sub-wavelength grating.

There have been intense research interests on terahertz (THz) electromagnetic radiation for its fingerprint spectral range for molecules and the important applications in bio-sensing, imaging, and spectroscopy. Recently, the development of plasmonics and metamaterials gives new perspectives in manipulating THz waves. Significant progress has been achieved in THz technology development based on plasmonics and metamaterials, such as ultra-high refractive index THz metamaterials [1], high efficiency THz photomixer [2], near field on-chip THz detector [3], high extinction ratio THz polarizer [4], and tunable THz metamaterials [5-7]. The strong field confinement and localization by surface plasmon are especially attractive for THz sensors. Surface plasmons in THz range can be generated either through surface structured metals [8] or by using semiconductor materials [9], while the latter one is more versatile in terms of tuning the plasmon properties and forming active THz plasmonic devices. InSb is an excellent material for THz plasmonics and can be viewed as classic solid-state plasma with its plasma frequency lies within the THz frequency range and its permittivity resembles that of noble metals in optical frequencies. More importantly, as a semiconductor material, the carrier concentration of InSb can be easily tuned by optical and electrical excitation, which in turn tune the permittivity and consequently plasmonic resonant frequency. In this paper, we will introduce the broadband plasmonic response from InSb touching disks [10] and the direct optical tuning of the plasmonic response of InSb subwavelength gratings in THz range [11].

Whereas sharp localized surface plasmon resonance (LSPR) has been reported, the realization of broadband plasmonic antennas implementing transformation optics recipes remains a challenge. The use of LSPR in the THz regime offers the potential to overcome the restriction posed by the diffraction limit and the relatively long wavelength, and allow its application towards deep sub-wavelength sensing. For example, large biomolecules have a broad dielectric response in the THz range rather than narrowband resonances. A broadband LSPR based sensor would allow for the detection of biomolecules and other substances in low concentrations with high sensitivity. Touching disks structures were designed by transformation optics and fabricated by semiconductor processing. The structure showed a broadband absorption response consistent with the theoretical predictions of transformation optics for gold nanostructures at visible frequencies. Simulations demonstrated that InSb touching dimers display strong field enhancement and sub-wavelength confinement in the gap between the disks over a broad THz range.

InSb subwavelength gratings are also fabricated and demonstrated direct optical tuning of the transmission spectra in THz range. Under TM polarization, LSPR occur and result in a dip in the transmission spectrum, which can have the intensity and position tuned by optical excitation. Full wave electromagnetic simulations were performed to illustrate the physics underlying transmision peak shift. Carrier lifetime of the InSb material was characterized by optical-pump THz-probe spectroscopy to get the modulation speed. Dependence of plasmonic effects on grating geometies, such as carrier concentration, grating period, thickness, duty cycle, etc. was investigated numerically. The direct all optical tuning and modulation of the plasmonic response of InSb provides more flexibilities in THz sensing device development.

Acknowledgements, The work is supported by the A*STAR Metamaterials Program and in collaborations with S. Maier from Imperial College London and S. J. Chua from the National University of Singapore.

REFERENCES

1. M. Choi, S. H. Lee, Y. Kim, S. B. Kang, J. Shin, M. H. Kwak, K.-Y. Kang, Y.-H. Lee, N. Park, B. Min, "A terahertz metamaterial with unnaturally high refractive index," *Nature*, Vol. 470, No. 7334, 369-373, 2011.
2. H. Tanoto, J. H. Teng, Q. Y. Wu, M. Sun, Z. N. Chen, S. A. Maier, B. Wang, C. C. Chum, G. Y. Si, A. Danner and S. J. Chua, "Greatly enhanced continuous-wave terahertz emission by nano-electrodes in a photoconductive photomixer," *Nature Photonics*, Vol. 6, 121-126, 2012.
3. Y. Kawano, K. Ishibashi, "An on-chip near-field terahertz probe and detector," *Nature Photonics*, Vol. 2, No.2, 618-621, 2008.
4. L. Y. Deng, J. H. Teng, Q. Y. Wu, H. Liu, X. H. Zhang, and S. J. Chua, "Extremely high extinction ratio terahertz broadband polarizer using bilayer subwavelength metal wire-grid structure," Applied Physics Letters, Vol. 101, 011101, 2012.
5. W. M. Zhu, A. Q. Liu, T. Bourouina, D. P. Tsai, J. H. Teng, X. H. Zhang, G. Q. Lo, D. L. Kwong, and N. I. Zheludev, "Microelectromechanical Maltese-cross metamaterial with tunable terahertz anisotropy," *Nature Communications*, DOI: 10.1038/ncomms2285, 2012.
6. H.-T. Chen, W. J. Padilla, J. M. O. Zide, A. C. Gossard, A. J. Taylor, R. D. Averitt, "Active terahertz metamaterial devices," *Nature,* Vol. 444, No. 1017, 597-600, 2006.
7. W. M. Zhu, A. Q. Liu, X. M. Zhang, D. P. Tsai, T. Bourouina, J. H. Teng, X. H. Zhang, H. C. Guo and H. Tanoto, T. Mei, G. Q. Lo and D. L. Kwong "Switchable Magnetic Metamaterials Using Micromachining Processes," *Advanced Materials*, Vol. 23, 1792–1796, 2011.
8. C. R. Williams, S. Andrews, S. Maier, A. Fernández-Domínguez, L. Martín-Moreno, F. García-Vidal, "Highly confined guiding of terahertz surface plasmon polaritons on structured metal surfaces," *Nature Photonics*, Vol. 2, 175-179, 2008.
9. Vincenzo Giannini, Audrey Berrier, Stefan A. Maier, José Antonio Sánchez-Gil, and Jaime Gómez Rivas, "Scattering efficiency and near field enhancement of active semiconductor plasmonic antennas at terahertz frequencies," *Optics Express,* Vol.18, No. 3, 2797-2807, 2009.
10. S. M. Hanham, A. I. Fernández-Domínguez, J. H. Teng, S. S. Ang, N. Klein, J. B. Pendry, K. P. Lim, S. F. Yoon, C. Y. Ngo and S. A. Maier, "Broadband Terahertz Plasmonic Response of Touching InSb Disks," *Advanced Materials*, Vol. 24, No. 35, OP226–OP230, 2012.
11. L. Y. Deng, J. H. Teng, H. W. Liu, Q. Y. Wu, J. Tang, X. H. Zhang, S. A. Maier, K. P. Lim, C. Y. Ngo, S. F. Yoon and S. J. Chua, "Direct Optical Tuning of Terahertz Plasmonic Response of InSb Subwavelength Gratings," *Advanced Optical Materials*, DOI: 10.1002/adom.201200032, 2012.

Nano-Micro Ribbon Structure and Probe Localization Effect for BioPlasmonic Sensing

M. Chamtouri , M. Besbes, J. Moreau and. M. Canva[*]
Laboratoire Charles Fabry,
Institut d'Optique Graduate School, Univ Paris Sud, CNRS
[*]corresponding author: michael.canva@institutoptique.fr

Abstract - In order to overcome the intrinsic limitations of purely propagating plasmonic (PP) sensing devices, nano and micro structuration of the substrates is investigated in order to make also use of localized plasmons (LP) and possible coupling in between those modes, PP and LP. It is demonstrated that to really take advantage of nano-micro structured plasmonic gratings, it is also required to localize the sensing probes where the target capture will affect the most the plasmonic sensor response.

Plasmonic sensors based on uniform gold film substrates have become major surface interaction characterization tools, using mono or multi-channel configuration as well as imaging set-ups. In this later case, application to biochip reading has been demonstrated and implemented. The model case often chosen being the diagnostic of genetic point mutations using ssDNA interactions [1-3]. However some end users are requiring always more performing instrumentation and in particular addressing the issue of low quantity and concentration of targets to characterize. Unfortunately, propagating plasmon sensors have reached their limits with current technology [4] even if sensitivity of the order of few 10^{-7} R.I.U. has been achieved, and effective DNA sequence diagnostic conducted on a bioarray format with ssDNA concentration as low as 0.1 nM [5]. To overcome such limitations much research effort has been and is currently devoted to the study and use of localized plasmon modes, initially on nanoparticles and also more recently on arrays of nano-antenna structured surface. We have focused our efforts on the intermediate regime [6, 7] where propagating plasmon (PP) and localized plasmon (LP) can effectively co-exist and coupled trough quasi propagating plasmon (QPP) mode as well as Coupled Localized Plasmon modes (CLP).

We have exhaustively mapped the dimensions parameters impact of nano-micro grating 1D grating on bioplasmonic sensitivity, varying the widths w1 and w2 associated to gold thickness of h1 and h2 of the plasmonic substrate. Home-made simulations hybrid tools make use of Fourier Modal Analysis (FFM) and Finite Element Method (FEM) were developed and used for computation. Different physical regimes are clearly shown, associated to very different modes and sensitivities. Furthermore, locating the probe sensing material not all over the plasmonic substrate but in specific places, in particular, either on top of ridges, bottom of grooves or side wall in the precedent structure, lead to significantly different sensing performances. As example, Figure 1 shows, for the case of 20 nm ridges and at λ=850 nm, the sensitivity enhancement factor of the sensor response to the biomolecules target capture in such specific areas. It can be seen that the gain in terms of sensitivity of the target bounded to such ridge, top and sidewalls, is significantly greater than the one from the base of the structure. These points will be emphasis at the conference.

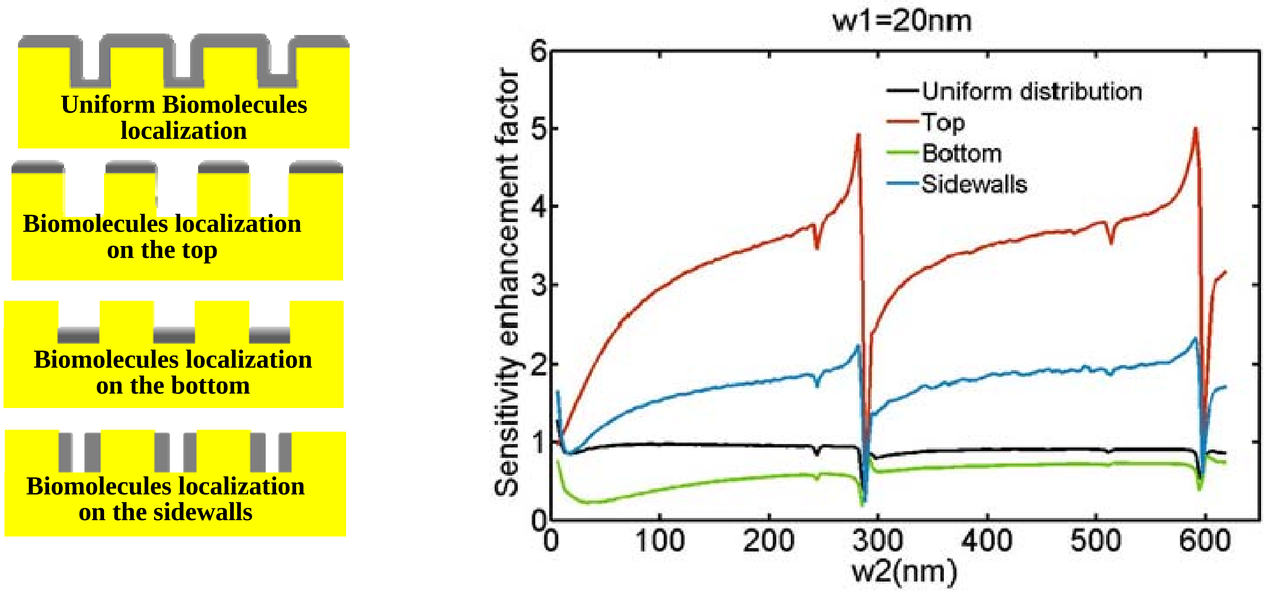

Figure 1: Sensitivity enhancement factor corresponding to different target binding configurations: all the surface, top, bottom or sidewalls of the nanostructure.

Acknowledgements, Institut d'Optique Graduate School/CNRS is part of the European Network of Excellence in BioPhotonics, Photonics for Life, P4L – the work conducted on genetic diagnostic of cystic fibrosis was conducted with Michel Goossens *et al.* from the Henri Mondor Hospital.

REFERENCES

1. Mannelli I., V. Courtois, P. Lecaruyer, G. Roger, M.C. Millot, M. Goossens and M. Canva, "Surface plasmon resonance imaging (SPRI) system and real-time monitoring of DNA biochip for human genetic mutation diagnosis of DNA amplified samples", *Sensors and Actuators B*, Vol. 119, 583-591 (2006).
2. Hottin J., J. Moreau, G. Roger, J. Spadavecchia, M.C. Millot, M. Goossens and M. Canva, "Plasmonic DNA: towards genetic diagnosis chips", *Plasmonics*, "Plasmonics and DNA" special issue, Vol. 2, 201-215 (2007).
3. Hottin J., J. Moreau, A. Bellemain and M. Canva, "Biochip data normalization using multifunctional probes", *Analyst,* Vol. 137, 3119-3125 (2012).
4. Piliarik M., J. Homola, "Surface plasmon resonance (SPR) sensors: approaching their limits?", *Optics Express*, Vol. 17, 16505-16517, (2009).
5. Bardin F., A. Bellemain, G. Roger and M. Canva, "Surface plasmon resonance spectro-imaging sensor for biomolecular surface interaction characterization", *Biosensors and BioElectronics*, Vol. 24, 2100-2105 (2009).
6. Nakkach M., A. Duval, B. Ea-Kim, J. Moreau and M. Canva, "Angulo spectral surface plasmon resonance imaging of nanofabricated grating surfaces", *Optics Letters*, Vol. 35(13), 2209-2211 (2010).
7. Dhawan A., A. Duval, M. Nakkach, G. Barbillon, J. Moreau, M. Canva and T. Vo-Dinh,, "Deep UV Nano-Micro-Structuration of Substrates for Surface Plasmon Resonance Imaging", *Nanotechnology*, Vol. 22, 165301 8pp (2011).

Plasmonic biosensing for deciphering cellular pathways

L.M. Lechuga

Nanobiosensors and Bioanalytical Applications Group

Research Center on Nanoscience and Nanotechnology (CIN2) CSIC & CIBER-BBN, Barcelona, Spain

Corresponding author: Laura.lechuga@cin2.es

Abstract-Plasmonic biosensing is one of the most powerful techniques for label-free analysis of biomolecular interactions in real time. Besides the standard approach of analyzing concentration of chemical and biological substances, we have recently proposed the use of plasmonic sensing as an unconventional strategy for deciphering main cell pathways gaining knowledge and understanding of different biological levels influencing diseases progression. Plasmonic biosensing could help in improving the diagnosis and follow-up of therapies for diseases as cancer.

Surface Plasmon Polaritons (SPPs) excited on thin metal films and Localized Surface Plasmon Resonances (LSPR) of nanostructures have attracted a remarkable interest for label-free biosensing applications due to their high sensitivity and multiplexing capabilities. Based on standard SPPs on thin gold films, we have developed fully-automated and portable sensing platforms. Moreover, based on metal nanostructures, as suspended nanodisks, we have developed a multiplexed LSPR configuration, which could afford a robust, simple and cost-effective sensing platform by using large-scale nanofabrication of nanoplasmonic sensing surfaces [1].

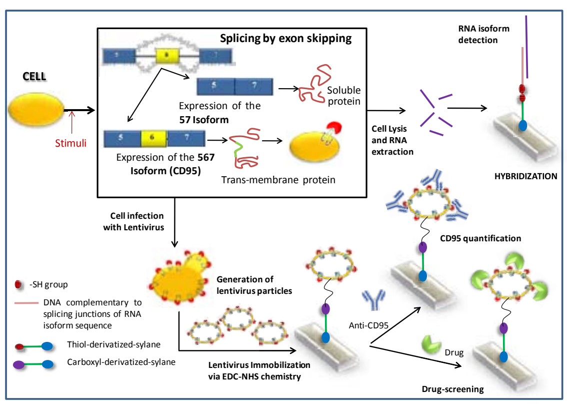

Fig. 1. Scheme of some of the cellular pathways analyzed by plamonic sensing

One of the key aspects in plasmonic biosensing is the optimization of the biofunctionalization procedure which directly affects the reproducibility, selectivity and resolution of the results. Biofunctionalization must guarantee an efficient coverage of the sensor surface, while keeping intact the functionality of the biological receptor. Moreover, real applications as clinical or environmental diagnosis require well-defined surfaces, minimizing non-specific adsorptions from complex samples. We have developed several techniques to ensure a proper functionalization of the plasmonics sensors for evaluating real samples [2,3]. During last years, we have demonstrated the suitability of our plasmonic devices for clinical and environmental diagnostics, as for the detection of DNA single mutations in cancer-related genes, pituitary hormones, protein tumour biomarkers or toxic environmental pollutants, among others [4-8]. In all cases, plasmonic sensing method has shown excellent robustness with high reproducibility, rendering in a valuable tool for fast diagnostics.

Recently we have proposed to employ plasmonic sensing as an unconventional strategy to deciphering the expression pathways in eukaryotic cells. We are analyzing gene expression at several cellular pathway levels see Fig. 1): (i) splicing routes and splicing variants level; (ii) epigenetics as DNA methylation; (iii) interaction with non-coding RNA regulators such as microRNAs; and (iv) interactions between native surface cell receptors with key molecules, as regulating factors or therapeutic drugs (see Fig. 2). Monitoring of these events of gene expression is relevant to the diagnosis and therapeutic outcome of several diseases, as cancer. With such integral knowledge better therapies could be designed to overcome the apoptosis-resistance of tumours, which in turn could improve the clinical outcome in cancer patients. Albeit these biological events could all be analysed separately using state-of-the-art technology, this would require unification of a diverse array of complex, time-consuming and costly techniques, and consequently, would not be amenable to systematic analysis of individual cancer patients.

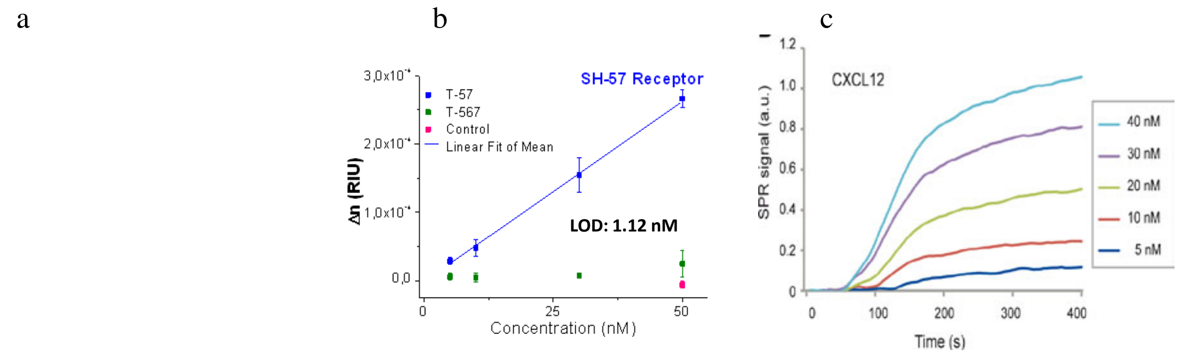

Fig. 2. a) Detection of highly structured RNA sequences at pM level. b) Differentiation of alternative splicing RNA isoforms. c) Specific CXCL12 ligand interaction with virions-supporting native cellular receptors.

REFERENCES

1. Otte, M.A., M.C. Estevez, L.G. Carrascosa, A.B. González-guerrero, L.M. Lechuga and B. Sepúlveda, “Improved biosensing capability with novel suspended nanodisks”, J. Phy. Chem C,115, 5344-5351, 2011.
2. de Juan-Franco, E., A. Caruz, J.R. Pedrajas and L. M. Lechuga, “Site-directed antibody immobilization using a protein A-gold binding domain fusion protein for enhanced SPR immunosensing”, Analyst, *In Press*.
3. TreviĖo, J., A. Calle, J.M. Rodriguez-Frade, M. Mellado and L.M. Lechuga, “Surface plasmon resonance immunoassay analysis of pituitary hormones in urine and serum samples”, Clin. Chim. Acta Vol. 403, 56-62, 2009.
4. Carrascosa, L.G., A. Calle and L.M. Lechuga, “Label-free detection of DNA mutations by SPR: Application to the early detection of inherited breast cancer”, Anal. Bioanal. Chem. Vol. 393, 1173-1182, 2009.
5. Olguín, Y. et al., “Detection of flagellin by interaction with human recombinant TLR5 immobilized in liposomes”, Anal. Bioanal Chem, DOI 10.1007/s00216-012-6523-4, 2012.
6. Mauriz, E., C. García-Fernández, J.V. Mercader, A. Abad-Fuentes, A.M. Escuela and L.M. Lechuga, “Direct Surface Plasmon Resonance immunosensing of Pyraclostrobin residues in untreated fruit juices”, Anal. Bioanal Chem. Vol 404, 2877–2886, 2012.
7. Carrascosa, L.G. , S. Gómez-Montes, A. AviĖó, A. Nadal, M. Pla, R. Eritja and L.M. Lechuga, “Sensitive and label-free biosensing of RNA with predicted secondary structures by a triplex affinity capture method”, Nucleic Acids Res 40, e56/1-11, 2012.
8. Vega, B., et al., “Technical Advance: Surface plasmon resonance-based analysis of CXCL12 binding using immobilized lentiviral particles”, J. Leukocyte Biol. Vol. 90, 399-408, 2011.

Synthesis of Au nanostars and their applications for sensing

I. Pastoriza-Santos
Departamento de Química Física, Universidade de Vigo, 36310, Vigo, Spain
*corresponding author: pastoriza@uvigo.es

Abstract- Metal nanoparticles display interesting optical properties related to localized surface plasmon resonances (LSPRs), which give rise to well-defined absorption and scattering peaks in the visible and near-IR spectral range. Such resonances are strongly dependent on the particle size and shape, but are also extremely sensitive towards dielectric changes in the near proximity of the particles surface. Another interesting feature of LSPRs is the generation of very high electromagnetic fields at the nanoparticles' surface. Besides, the localization and intensity of such fields can also be modulated through the morphology of the particles. Thus, particles with sharp edges and tips show intense and highly focalized electromagnetic fields.

In this communication, the synthesis of gold nanostars (with tailored both dimensions and optical properties) using a seed-mediated method in N,N-dimethylformamide (DMF) is presented. Additionally, some examples showing that potential of gold nanostars for sensing applications are presented.

Plasmon-Modulated Photoluminescence of Individual Plasmonic Nanostructures

Hailong Hu[1], Huigao Duan[2], Joel K. W. Yang[2,*], Ze Xiang Shen[1,*]

[1] Centre for Disruptive Photonic Technologies & School of Physical and Mathematical Sciences Nanyang Technological University, 21 Nanyang Link, 637371 Singapore

[2]Institute of Materials Research and Engineering, A*STAR (Agency for Science, Technology and Research), 3 Research Link, 117602 Singapore

*Address correspondence to:
zexiang@ntu.edu.sg, and yangkwj@imre.a-star.edu.sg.

Energy conversion between photons and electrons through plasmonic nanostructuce is one of central research topics. Photoluminescence of metal nanostructures is now gaining more interest [1-4], providing useful information about the energy transfer from non-equilibrium electrons into photons. Plasmon resonances of metal nanostructures have been observed to play an important role in this generation of luminescence. However, the underlying mechanism of the PL process and the exact role of plasmons are still not fully understood.

In this work, we performed a systematic study on the photoluminescence and scattering spectra of individual gold nanostructures that were lithographically defined. We identify the role of plasmons in photoluminescence as modulating the energy transfer between excited electrons and emitted photons. By comparing photoluminescence spectra with scattering spectra, we observed that the photoluminescence of individual gold nanostructures showed the same dependencies on shape, size and plasmon-coupling as the particle plasmon resonances, as shown in Fig.1 a. Our results provide conclusive evidence that the photoluminescence in gold nanostructures indeed occurs via radiative damping of plasmon resonances driven by excited electrons in the metal itself. Moreover, we provide new insight on the underlying mechanism based on our analysis of a reproducible blue shift of the photoluminescence peak (with respect to the scattering peak), and observation of an incomplete depolarization of the photoluminescence.

In addition, a four-step process was used to describe the PL mechanism including two important aspects, the modulation of particle plasmon resonance and thermalization of non-equilibrium electrons. And a simple prediction of PL was proposed as follows.

PL ~ population profile of thermalized electrons × DOS

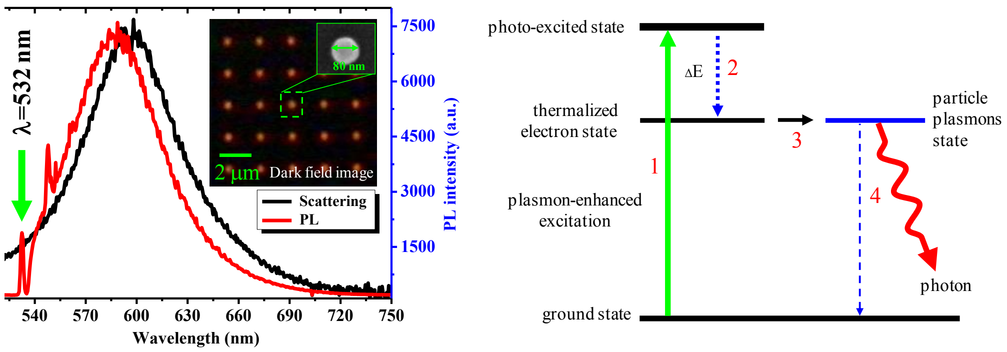

(a) **(b)**

Fig. 1: (a) Single photoluminescence (red) and scattering (black) spectra of single 80 nm Au nanoparticles. The insert represents the dark field optical and SEM images. (b) Mechanism model for plasmon luminescence, showing a four-step process: 1) Plasmon enhanced excitation of electrons; 2) thermalization of excited electrons; 3) excitation of particle plasmons by non-equilibrieum electrons; 4) radiation damping of plasmon into photon.

[1]. E. Dulkeith, et al. *Physical Review B*, 2004, 70, 205424-4.
[2]. A. Tcherniak et al. *J. Phys. Chem. C*, 2011, 115, 15938-15949.
[3]. Yorulmaz et al. *Nano Lett* 2012, ASAP, DOI:10.102/nl302196a.
[4]. Fang et al. *Acs Nano* 2012, ASAP, DOI: 10.1021/nn3022469.

Near field coupling in plasmonic sensor designs

Zhengtong Liu[1*], **Erping Li**[1]
[1]Institute of High Performance Computing, Singapore
[*]corresponding author: liuzt@ieee.org

Abstract-Near field coupling in plasmonic nanostructures has been studied and applied to design of nanoantenna-superlens system for sensing applications. The study shows that the near field coupling is significant and has to be taken into account when modeling and designing plasmonic nanostructures. By using near field coupling we have designed nanoatenna-superlens sensing devices that can overcome the limitation of permittivity matching and work at arbitrary wavelength.

Plasmonic nanostructures, such as superlens, gratings, and nanoantennas, have attracted great research interests due to their unique light-matter interaction behaviors [1-3]. Their near field properties are of particular interest, and many applications, such as super-resolution imaging and subwavelength light focusing, are results of near field manipulation. When several plasmonic nanostructures are combined to form a new device, their near fields interact and the overall performance is different from simple combination of each individual component's functionality. We have studied a nanowire-superlens system to show the effect of near field coupling [4]. The theoretical analysis clearly shows that when dealing with near fields of plasmonic nanostructures, the near field coupling effect has to be taken into account, and a plasmonic system that consists of several components has to be studied as a whole.

Inspired by this finding, we have revisited one of our earlier sensor designs [5]. In the previous work we proposed that by combining a superlens and nanoantennas we can make a sensor for fluorescence and surface enhanced Raman scattering (SERS). However we had to use metal-dielectric composite to match the permittivity of silicon at the working wavelength. In light of the finding of near field coupling, we have redesigned the sensor using only pure metal and made it work at arbitrary wavelength. The new sensor design is illustrated in Fig. 1.

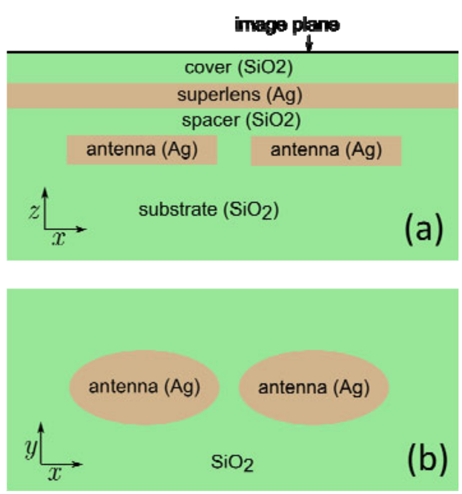

Fig. 1 The side view (a) and top view (b) of a unit cell of the nanoantenna array with superlens.

The dimensions of the design have been optimized to give highest field enhancement at the image plane. The resultant field maps are show in Fig. 2 for two different wavelengths: 633 nm and 647 nm. Hotspots are clearly shown in the field maps. From the field maps we draw conclusions that even with mismatched permittivities, it is possible to design superlens-nanoantenna systems to create near field enhancement for sensing applications.

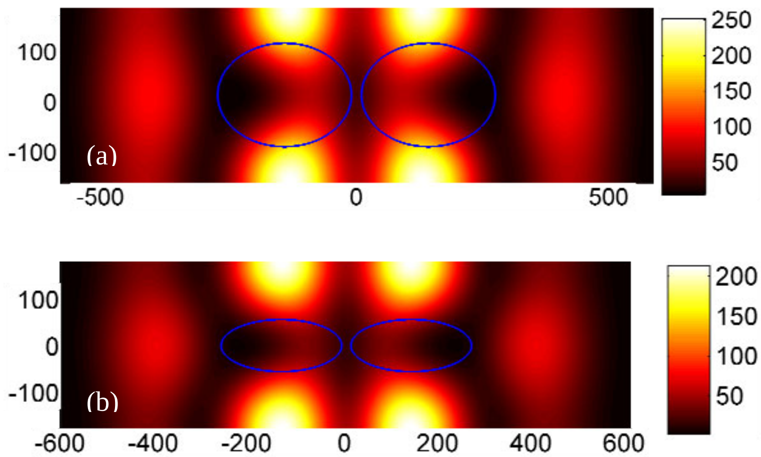

Fig. 2 The electric field enhancement of the optimized system at the image plane for (a) 633 nm and (b) 647 nm.

REFERENCES

1. Pendry, J. B., "Negative Refraction Makes a Perfect Lens," *Phys. Rev. Lett.* Vol. 85, 3966–3969, 2000.
2. Fang, N., Lee, H., Sun, C., and Zhang, X., "Sub-diffraction-limited optical imaging with a silver superlens, " *Science*, Vol. 308, 534–537, 2005.
3. Liu, Z., Boltasseva, A., Pedersen R. H., Bakker R., Kildishev. A. V., Drachev V. P., and Shalaev. V. M., "Plasmonic nanoantenna arrays for the visible," *Metamaterials*, Vol. 2, 45–51, 2008.
4. Liu, Z., Shalaev, V. M., and A. V. Kildishev. "Coupling effect in a near-field object–superlens system" *Appl Phys A*, Vol. 107, 83–88, 2011.
5. Liu, Z., Thoreson, M. D., Kildishev, A. V., and Shalaev, V. M., "Translation of nanoantenna hot spots by a metal-dielectric composite superlens," *App. Phys. Lett.* Vol. 95, 033114, 2009.

Graphene elliptical-pair antenna for THz sensing

H. Z. Liu[1*], Z. T. Liu[1], and E. P. Li[1]
[1]A*STAR Institute of High Performance Computing, Singapore
[*]corresponding author: liuh@a-star.ihpc.edu.sg

Abstract-In this paper, a graphene-based elliptical-pair antenna is reported. Numerical analysis with methods of moment demonstrates that its resonant frequency can be increased by either decreasing the major axis radius or increasing the minor axis radius. Furthermore, strong electric field enhancement is observed at the gap between two elements, which is found to be inversely proportional to the gap size. The designed antenna is ideal for THz sensing applications.

In the past decade, metallic nanoantennas with the ability to support localized surface plasmon polaritons at optical frequencies have been developed for a plethora of applications, such as sensing and spectroscopy. However, due to the inherently high loss of noble metals at lower frequencies, little work has been performed at THz. Nevertheless, it is worthwhile to explore equivalent sensors at THz frequencies since the vibrational frequencies of many biological molecules lie in this range. In particular, graphene, being an atomic thick material composed of hexagonally arranged carbon atoms, has manifested great potential for antenna applications at THz [1] with distinct merits of large plasmon confinement, long lifetime and good tunability via electrostatic gating. Liu et al. presented a graphene ring antenna with good electric field enhancement at THz frequencies. [2] In this work, we attempt to design a THz graphene antenna using elliptical-pair structure, analogous to its metallic counterpart discussed in [3].

The graphene conductivity is obtained under local-random phase approximation [4] with intrinsic relaxation time $\tau = \mu E_F / e v_F^2$ where $E_F = 0.5$eV is the Fermi level used in this work, $v_F \approx c/300$ denotes Fermi velocity, $\mu = 10000\,\mathrm{cm}^2/\mathrm{Vs}$ refers to the measured DC mobility. Here, surface impedance model is adopted to model graphene with equivalent surface impedance $Z_s = 1/\sigma$. [5] Numerical analysis is performed using method of moments with surface equivalence principle through the commercial software *FEKO*. As shown in Figure 1, a z-travelling plane wave polarized along the x-axis is incident on a self-standing graphene antenna consisting of two elliptical patches. The major axis of the elliptical patches lies along the x-axis and minor axis is parallel to the y-axis. The major axis radius, minor axis radius and gap size of the antenna are denoted by r_1, r_2 and g, respectively.

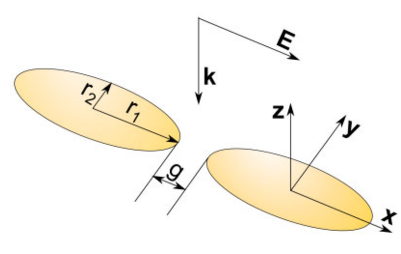

Figure 1 Schematic of graphene elliptical-pair antenna.

As shown in Figure 2(a), the resonant frequencies are investigated with varying antenna parameters. It is found that the resonant frequency is most sensitive to the major axis radius. The resonant frequency is raised by decreasing major axis radius and increasing minor axis radius. In general, as the parameters become larger, the resonant frequency is less sensitive to their variations. Moreover, the resonant frequency is slightly increased with increasing gap size when the gap size is small and remains almost invariant when the gap size goes beyond 30nm. This is in great contrast to metallic nanoantennas where the resonant frequency is highly sensitive to variations in gap size when the gap size is small.[3] In Figure 2(b), the electric field enhancement at the center of the gap is examined. It can be observed that the field enhancement is inversely proportional to the gap size since the coupling between the two elements is enhanced as they are shifted closer to each other. On the other hand, the field enhancement is slightly improved with increasing radii of major and minor axis. In Figure 3, the near-field distribution of electric field is presented, where the magnitude of the electric field is found to be well above 100V/m near the gap.

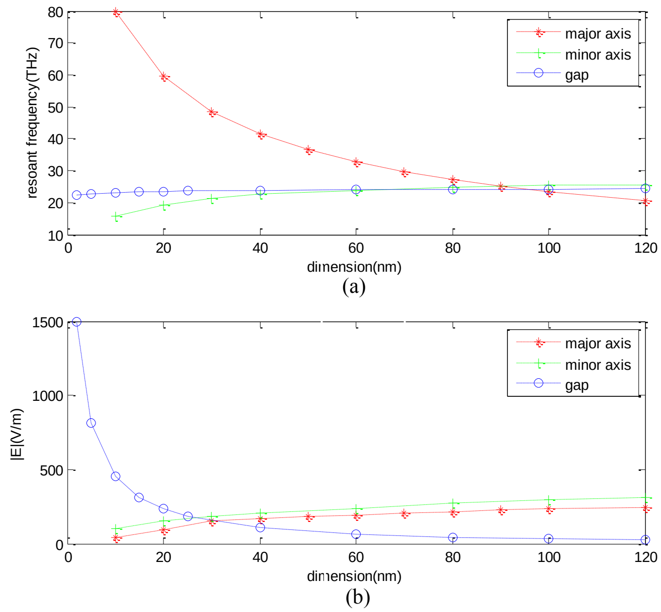

Figure 2 (a) The resonant frequencies as a function of antenna parameters; (b) The magnitude of electric field at the center of the gap as a function of antenna parameters.

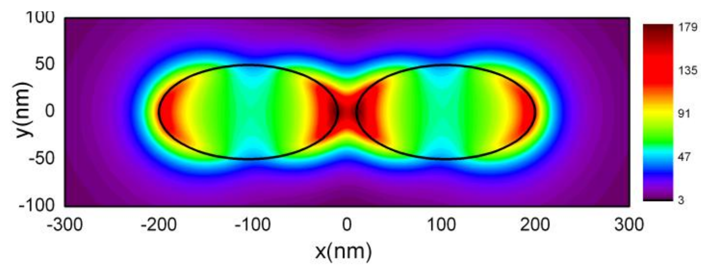

Figure 3 Distribution of the magnitude of electric field in a plane 10nm above the antenna of r_1 = 60nm, r_2 = 50nm, g = 20nm at 32.79THz.

In conclusion, a graphene nanoantenna with a pair of elliptical elements has demonstrated good electric field enhancement in the gap region. Results suggest that graphene nanoantennas are a good candidate for THz sensing applications, analogous to metallic nanoantennas at optical frequencies.

REFERENCES

1. Perruisseau-Carrier, J., “Graphene for antenna applications: opportunities and challenges from microwaves to THz,” in *Loughborough Antennas & Propagation Conference*, Loughborough, UK, November 2012.
2. Liu, P. et al., “Tunable terahertz optical antennas based on graphene ring structures,” *Appl. Phys. Lett.*, Vol. 100, No. 153111, 2012.
3. Liu, Z. T. et al., “Plasmonic nanoantenna arrays for the visible,” *Metamaterials*, Vol. 2, No. 1, 45–51, 2008.
4. Gan, C. H. et al., “Synthesis of highly confined surface plasmon modes with doped graphene sheets in the midinfrared and terahertz frequencies,” *Phys. Rev. B*, Vol. 85, No. 12, 125431, 2012.
5. Llatser, I. et al., “Graphene-based nano-patch antenna for terahertz radiation,” *Photon. Nanostruct.: Fundam. Appl.*, Vol. 10, No. 4, 353-358, 2012.

Plasmonic metamaterials and applications

Transparent electrodes in the terahertz regime – a new approach

R. Malureanu[1, 3*], Z. Song[2, 3], M. Zalkovskij[1, 3], C. Gritti[1], A. Andryieuski[1], Q. He[2], L. Zhou[2], P. U. Jepsen[1], A. V. Lavrinenko[1]

[1] Department of Photonics Engineering, Technical University of Denmark, Kgs. Lyngby 2800, Denmark

[2] State Key Laboratory of Surface Physics, Key Laboratory of Micro and Nano Photonic Structures (Ministry of Education), Fudan University, Shanghai 200433, China

[3] These authors contributed equally to the work

[*]corresponding author: rmal@fotonik.dtu.dk

Abstract-We suggest a new possibility for obtaining a transparent metallic film, thus allowing for completely transparent electrodes. By placing a complementary composite layer on top of the electrode, we can cancel the back-scattering of the latter thus obtaining a perfectly transparent structure. For ease of fabrication, we performed the first experiments in the THz regime, but the concept is applicable to the entire electromagnetic waves spectrum. We show that the experiments and theory match each other perfectly.

Using the effective medium theory, the permittivity of a composite 2D layered material where the electric field is perpendicular to the layers is given by [1]:

$$\frac{1}{\varepsilon_{AB}} = \frac{1}{\varepsilon_A}\frac{W_A}{P} + \frac{1}{\varepsilon_B}\frac{W_B}{P} \tag{1}$$

Where W_A, W_B are the widths of each material, $P = W_A + W_B$ is the periodicity of the structure and ε_A, ε_B are the permittivities of each layer. With the advent of the metamaterials field, at least one of the initial ε values can be negative thus hugely expanding the range the composite material permittivity can reach.

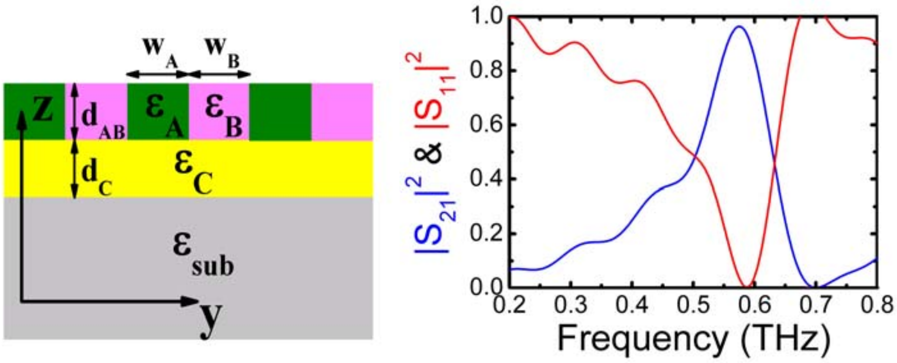

Figure 1. (a) the design considered for simulations; The A layer is silica, the B one is the composite mesh while the C is the electrode. The polarization is parallel to the y axis. (b) S-parameters results showing high transmittivity at 0.6THz

In this example, we defined the B layer as a metallic mesh with, in the THz regime; a permittivity $\varepsilon_B = 3.85 - (3.06/f)^2$ and the A layer as a dielectric with a constant permittivity of 3.85. This resulted in a dielectric function of the composite material as: $\varepsilon_{AB} = 3.85 + 4.19/(0.74^2 - f^2)$. The widths of the stripes were 10 and 30μm for the A and B layers respectively (see figure 1(a)) and f is the frequency in THz.

Employing the standard transfer matrix method [2] and considering the C layer a uniform metallic mesh with

$\varepsilon_C = 3.85 - (4.98/f)^2$ we obtain, for a frequency of 0.6THz, perfect transmission through a complex structure placed on a Si substrate (see figure 1(b)).

The simulated structures were fabricated using aligned optical lithography and thin layer depositions. The fabrication flow will be presented during the conference. Figure 2 shows the fabrication results for the C mesh as well as the AB complex layer. [3]

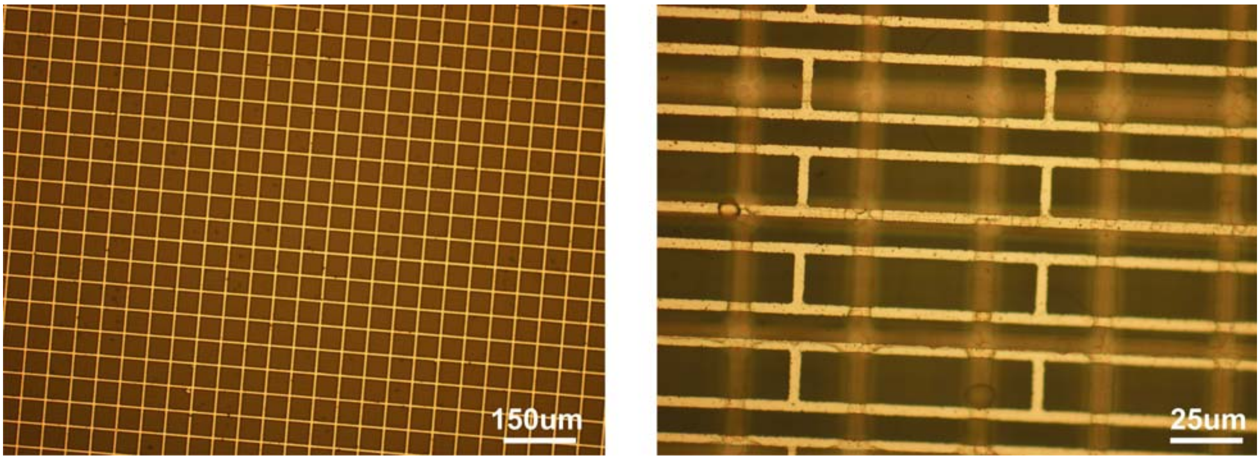

Figure 2. Fabricated structure showing high alignment accuracy and high quality of the structure.

The obtained experimental results are in almost perfect match with the predicted theory ones thus showing that our approach for designing such structures is viable. The experimental results as well as the challenges in measurements will be discussed during the conference.

Acknowledgements, R.M., M.Z., A.L. wish to acknowledge the FTP THzCOW project for partial financial support. Z.Y.S, Q. H. and L. Z. thank the financial supports from NSFC (60990321, 11174055)), Program of Shanghai Subject Chief Scientist (12XD1400700) and MOE of China (B06011). A.A. acknowledges the Danish Council for Technology and Production Sciences for partial financial support via the FTP GraTer project.

REFERENCES

1. Bergman, D., "The dielectric constant of a composite material - a problem in classical physics," *Phys. Rep.*, Vol. 43, 377–407, 1978.
2. Busch, K., Chan, C. T., and Soukoulis, C. M., *Photonic band gap materials*, Kluwer, Dordrecht, 1996.
3. Malureanu, R., Zalkovskij, M., Song, Z., Gritti, C., Andryieuski, A., He, Q., Zhou, L., Jepsen, P. U., and Lavrinenko, A. V. "A new method for obtaining transparent electrodes" *Opt.Exp.*, Vol. 20, 22770-22782, 2012

MAGNETOPLASMONICS: COMBINING MAGNETIC AND PLASMONIC FUNCTIONALITIES

Gaspar Armelles, Alfonso Cebollada, Antonio García-Martín, Jose Miguel García-Martin, María Ujué González, David Meneses-Rodriguez.

IMM-Instituto de Microelectrónica de Madrid (CNM-CSIC), Isaac Newton 8, PTM, E-28760 Tres Cantos, Madrid, Spain.

Nanosystems with combined magnetic and plasmonic functionalities have in recent years become an active topic of research. In these new structures, know as magneto-plasmonics, magnetic and plasmonic properties are intertwined, allowing for example plasmonic properties to become tunable upon de application of a magnetic field (active plasmonics) [1], or the Magneto-Optical (MO) effects to be largely increased by plasmon resonance excitation, as a consequence of the enhancement of the electromagnetic (EM) field in the MO active component of the structure [2,3]. In this last case, the study of the enhanced MO activity in structures with subwavelength dimensions is especially interesting since they may be viewed as nanoantennas in the visible range with MO functionalities. The light harvesting properties of these systems upon plasmon resonance excitation bring as a consequence an enhanced EM field in its interior, and more interestingly in the region where the MO active component is present [4]. At this stage, optimizing the EM field distribution within the structure by maximizing it in the MO components region while simultaneously minimizing it in all the other, non MO active, lossy components, will allow for the development of novel systems with even larger MO activity with reduced optical losses [5].

References

[1] V. V. Temnov, G. Armelles, U. Woggon, D. Guzatov, A. Cebollada, A. Garcia-Martin, J. M. Garcia-Martin, T. Thomay, A. Leitenstorfer, R. Bratschitsch, *Nat. Photonics* **4** (2010) 107–111.
[2] G. Armelles, A. Cebollada, A. García-Martín, J.M. García-Martín, M.U. González, J.B. González-Díaz, E. Ferreiro-Vila, and J.F. Torrado, *Journal of Optics A: Pure and Applied Optics* **11** (2009) 114023.
[3] G. Armelles, A. Cebollada, A. García-Martín, M.U. González,. *Advanced Optical Materials*, in press
[4] D. Meneses-Rodríguez, E. Ferreiro-Vila, P. Prieto, J. Anguita, M.U. González, J.M. García-Martín, A. Cebollada, A. García-Martín, and G. Armelles, *Small* **7**(2011), 7, 3317.
[5] J.C. Banthí, D. Meneses-Rodríguez, F. García, M.U. González, A. García-Martín, and G. Armelles, *Advanced Materials* **24**(2012) OP36.

Advances in directional solidification based approach towards plasmonic materials and metamaterials

Dorota A. Pawlak*, Paweł Osewski, Marcin Gajc, Katarzyna Sadecka, Andrzej Kłos, Krzysztof Orlinski, Andrzej Stefanski, Barbara Surma

Institute of Electronic Materials Technology (ITME)
133 Wolczynska Str, 01-919 Warsaw, Poland
*corresponding author: Dorota.Pawlak@itme.edu.pl

In recent years, novel research areas have been developed in the field of photonics: metamaterials and nanoplasmonics. By utilizing the ideas developed in these research areas and using specially-designed materials, unusual electromagnetic properties such as artificial magnetism, negative refractive index, cloaking and squeezing photons through subwavelength holes have been demonstrated. These novel fields need new material fabrication techniques, especially bottom-up approaches such as self-organization. Two novel bottom-up manufacturing methods will be presented based on: (i) directional solidification of eutectic composites and (ii) doping dielectric matrices with plasmonic nanoparticles. Eutectics are simultaneously monolithic and multiphase materials forming self-organized micro/nanostructures, which enable: (i) the use of various component materials including oxides, semiconductors, metals, (ii) the generation of a gallery of geometrical motifs and (iii) control of the size of the structuring, often from the micro- to nanoregimes. On the other hand, the novel method of direct doping of dielectric matrices with nanoparticles utilizing directional solidification may provide three-dimensional nanoplasmonic materials enabling doping with nanoparticles of various chemical composition, various size and shape, as well as co-doping with other chemical agents. In both cases we apply one of the crystal growth methods - the micro-pulling down method - to create the material. Materials with plasmonic resonances at visible and IR wavelengths, as well as anomalous refraction will be presented. Our new approach may lead to novel manufacturing solutions for photonic applications in areas such as metamaterials, plasmonics, as well as photovoltaics and

Near-field imaging and spectroscopy of plasmonic excitations at infrared frequencies

Y. De Wilde[1], **A. Bousseksou**[2], **R. Colombelli**[2], **K. Joulain**[3], **J.-J. Greffet**[4], **P.-O. Chapuis**[5],
[1] Institut Langevin, ESPCI ParisTech, CNRS, 75238 Paris Cedex 05, France
[2] Institut d'Electronique Fondamentale, Univ. Paris Sud, CNRS UMR8622, 91405 Orsay, France
[3]Institut P', CNRS, Université de Poitiers, 86022 Poitiers, France
[4] Laboratoire Charles Fabry, Institut d'Optique, CNRS, Université Paris-Sud, 91127 Palaiseau, France,
[5] Centre de Thermique de Lyon (CETHIL), CNRS, INSA Lyon, UCBL, 69621 Villeurbanne, France
*corresponding author: yannick.dewilde@espci.fr

Abstract- Compact plasmonic devices using mid-infrared quantum cascade lasers (λ=7.5 μm), and near-infrared tensile-strained quantum well diode lasers (λ=1.3 μm) have been realized for the generation of surface plasmons. We investigate the building blocks of these active plasmonic devices using near-field microscopy. We also discuss the combination of a scattering near-field microscope with a Fourier transform infrared spectrometer to investigate the spectrum of thermal emission in the near-field. The later is quasi-monochromatic on silicon carbide due to the contribution of surface phonon polaritons.

The paper will first describe the development of active sources of surface plasmons and their investigation in the near-field using near-field scanning optical microscopy (NSOM). The first devices which we have investigated operate at mid-infrared frequencies, where ohmic losses in metals are moderate. Quantum cascade lasers (λ=7.5 μm) combined with a DFB metal grating have been shown to produce hybrid surface plasmons [1]. The hybrid surface plasmons are coupled with a passive waveguide by means of a grating coupler. We have performed a slit-doublet experiment by launching two counter-propagating surface plasmons on a passive gold stripe and characterized the various sections of the devices using apertureless NSOM [2]. We also show that at mid-infrared wavelength, the patterning of the waveguide allows achieving a subwavelength confinement of the surface plasmons at the surface of the guide [3]. The experience gained at mid-infrared frequencies has been used to develop active sources of surface plasmons which operate at near-infrared frequencies in the telecom range (λ=1.3 μm) using near-infrared tensile-strained quantum well diode lasers. Aperture NSOM has been used to demonstrate the generation of surface plasmons and their launching on a passive waveguide using a grating coupler [4]. It has also been used to investigate the transverse distribution of the mode in the cavity of a laser with a DFB grating combined with an ultra-thin top cladding, by scanning the facet of the device. Our results show that the metal patterning produces a hybrid mode in which the field is repelled far from the metal, which produce a significant loss reduction.

Surface polaritons can also be thermally excited. We had shown previously that mapping the near-field thermal emission using a thermal radiation scanning tunnelling microscope (TRSTM) enables one to image the electromagnetic local density of states (EM-LDOS) of surface polaritons [5]. Here, we show that combining TRSTM with Fourier transform infrared spectroscopy enables one to obtain near-field thermal emission spectra, which probe the frequency dependence of the EM-LDOS. Near-field thermal emission spectra measured on silicon carbide (SiC) show a quasi-monochromatic peak due to the thermal excitation of surface phonon polaritons, in agreement with theoretical predictions [6].

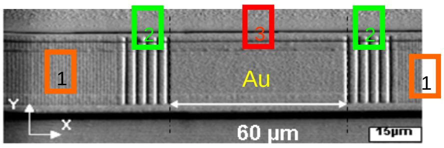

Figure 1 : Topography of the metallic top electrode of a semiconductor laser designed for the generation of surface plasmon polaritons (SPPs). (1) Generator of hybrid SPPs; (2) Grating coupler; (3) Passive waveguide. This device performs a slit doublet experiment with two counter propagating SPPs. The concept has been validated both at mid-infrared (λ=7.5 µm) and at telecom (λ=1.3 µm) wavelengths [2,4].

Figure 2: Spectrum of the near-field thermal emission measured on silicon carbide (SiC) showing the partial temporal coherence due to thermally excited surface phonon polaritons [6]. The demodulation frequency with respect to the tip oscillation frequency Ω_{tip} is indicated.

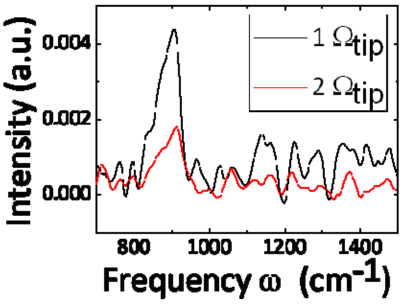

Acknowledgements: This work is supported by the French National Research Agency (Grant Nos. ANR-07-NANO-039 “NanoFtir” and ANR-09-NANO-020), by the Region Ile-de-France in the framework of DIM Nano-K, and by LABEX WIFI (Laboratory of Excellence within the French Program "Investments for the Future") under reference ANR-10-IDEX-0001-02 PSL.

REFERENCES

1. Bousseksou, A., Colombelli, R., Babuty, A., De Wilde, Y., Chassagneux, Y., Sirtori, C., Patriarche, G., Beaudoin, G., Sagnes, I., “A semiconductor laser device for the generation of surface-plasmons upon electrical injection”, *Optics Express*, Vol. 17, 9391- 9400, 2009.
2. Babuty, A., Bousseksou, A. , Tetienne, J.−P., Moldovan Doyen, I. , Sirtori, C., Beaudoin, G. , Sagnes, I. , De Wilde, Y., Colombelli, R., “Semiconductor Surface Plasmon Sources”, *Physical Review Letters*, Vol. 104, 226806, 2010.
3. Bousseksou, A., Babuty, A., Tetienne, J.−P., Moldovan Doyen, I., Braive, R., Beaudoin, G., Sagnes, I., De Wilde, Y., Colombelli, R., 1.“Sub-wavelength energy concentration with electrically generated mid-infrared surface plasmons”, *Optics Express*, Vol. 20, 13738 - 13747, 2012.
4. Costantini, D., Greusard, L., Bousseksou, A., Rungsawang, R., Zhang, T. P., Callard, S., Decobert, J., Lelarge, F., Duan, G.-H., De Wilde, Y., and Colombelli, R., “In Situ Generation of Surface Plasmon Polaritons Using a Near-Infrared Laser Diode”, *Nano Letters*, Vol. 12, 4693 - 4697, 2012.
5. De Wilde, Y., Formanek, F., Carminati, R., Gralak, B., Lemoine, P.-A., Mulet, J.-P., Joulain, K., Chen, Y., Greffet, J.-J., “Thermal radiation scanning tunnelling microscopy”, *Nature* , Vol. 444, 740 - 743, 2006.
6. Babuty, A., Joulain, K., Chapuis, P.-O., Greffet, J.-J., De Wilde, Y., “Blackbody spectrum revisited in the near-field”, submitted, 2013.

Multilayer infrared metamaterials for optical devices

R. Ghasemi[1], A. Degiron[1,2], A. Lupu[1,2], and A. de Lustrac[1,*]

[1]Univ. Paris-Sud, Institut d'Electronique Fondamentale, UMR 8622, 91405 Orsay Cedex, France

[2] CNRS, Orsay, F-91405, France

[*]corresponding author: andre.de-lustrac@u-psud.fr

Abstract- The coordinate transformation approach can be applied to design optical devices in the near IR telecom domain. In this design we use metamaterials where we need to control separately the permittivity and the permeability. We propose in this paper a technology to realize a multilayer metamaterial with these properties. Numerical simulations and experimental realizations are performed in order to validate the concept and the realization feasibility.

Metamaterials have recently attracted considerable interests because of their unusual properties, not encountered with conventional materials and allowing their applications in a novel class coordinate transformation based devices [1-3]. Despite these very attractive features, there is a number of issues limiting MMs implementation, especially in the optical domain. These structures are often metallic with important losses due to the high absorption coefficient of metals in the infrared and visible domains. In addition, the fabrication of these composite materials having subwavelength dimensions requires nanoscale precision control [4]. Given the current state of nanotechnology, optical MMs can be realized in a simple way by planar monolayer structures. In a precedent study we have demonstrated that planar MMs can be used in guided wave configuration by placing a sheet of MMs on the top of a silicon slab waveguide [5]. In this study we propose a technology to realize a multilayer metamaterial with these properties. Numerical simulations and experimental realizations are performed in order to validate the concept and the realization of materials.

In view of the realization of devices designed by transformation optics, we start to develop a fabrication process of optical infrared MMs in a clean room. As show in figure 1, we think make the final device with layers of metallic cut wires, whose dimensions vary to achieve the space transformation. At this stage of our study, we were able to fabricate a multilayer metamaterial made of metallic cut wires on planar substrate, as shown in the views of SEM in figure 1.

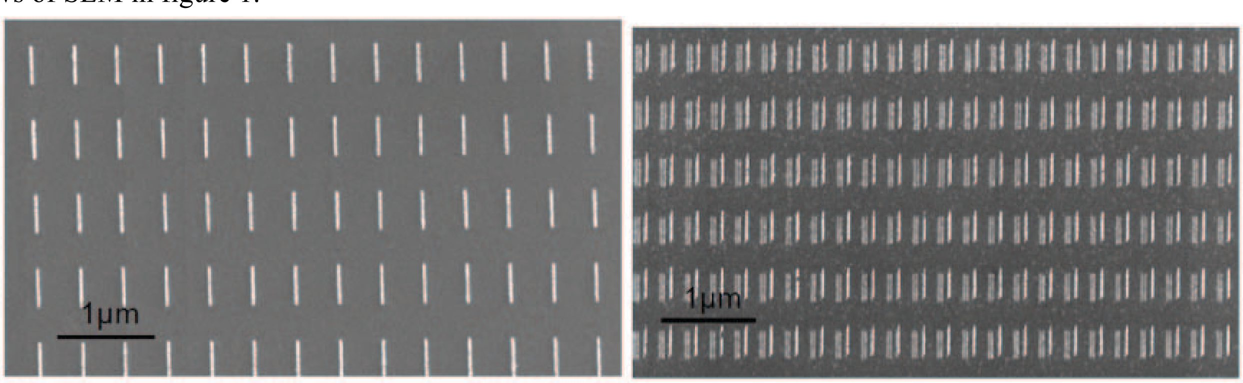

(a) (b)

Fig. 1 : (a) monolayer metamaterial made of gold wires, length 440nm, width 30nm, thickness 50nm (a). Multilayer metamaterial made of 4 layers of gold wires, separated by a 65nm dielectric layer (b).

The dimensions and the period of the cut wires are sub-micron so that the entire layer behaves as a homogeneous medium at a wavelength of 1.55μm. Therefore, these structures can be performed by electron beam lithography followed by metallization (Ti-Au) and a lift-off procedure (figure 1(a)). Looking to develop the fabrication, we arrive to realize multilayer structures (up to 4 layers) on a glass substrate (figure 1(b)). We should mention that the thickness of the wires is 50nm; their width is about 30 nm and their length 440nm. We control the position of each wire layer with respect to its neighbors. So we can obtain different optical index easily [6, 7]. Figure 2 presents the numerical simulations and experimental results of these structures.

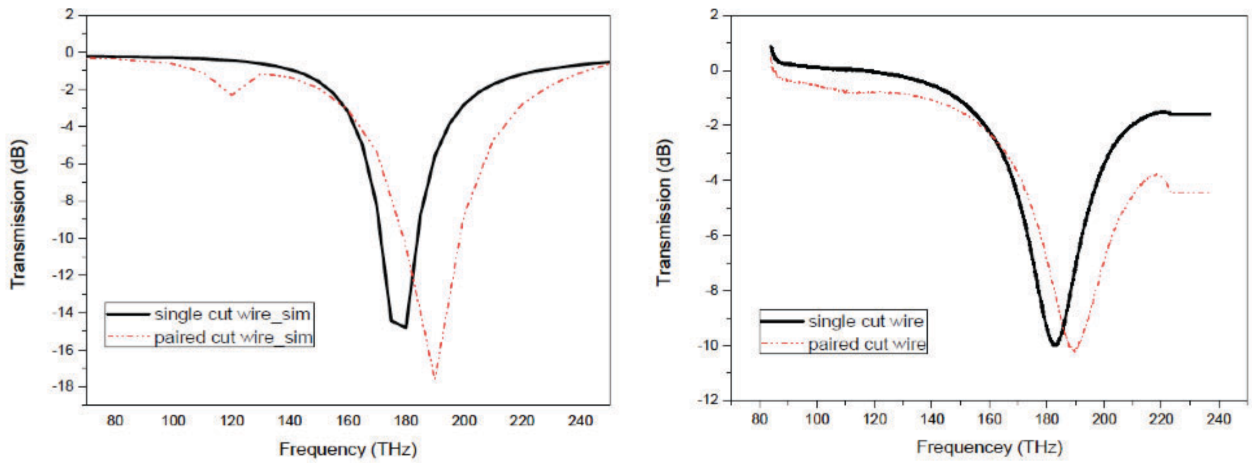

(a) (b)

Figure 2: Calculated (a) and measured (b) transmission for a monolayer of gold cut wire: length 440nm, width 30nm, thickness 50nm and for 4 layers of gold cut wire made on a glass substrate separated by a 65 nm dielectric layer.

Acknowledgements: This work was supported by the French National Research Agency (ANR Metaphotonique, contract number 7452RA09).

REFERENCES

1. Veselago V. G., "The electrodynamics of substances with simultaneously negative values of ε and μ", Soviet Phys. USPEKHI, 10, 509-514, 1968.
2. Pendry J. B., A. J. Holden, D. J. Robbins et al., "Magnetism from conductors and enhanced nonlinear phenomena", IEEE TRANSACTIONS ON MICROWAVE THEORY AND TECHNIQUES, 47, 2075-2084, 1999.
3. Pendry J. B., A. J. Holden, D. J. Robbins et al., "Low frequency plasmons in thin-wire structures", JOURNAL OF PHYSICS-CONDENSED MATTER, 10, 4785-4809, 1998.
4. Soukoulis M. C., M. Wegener, "Past achievements and future challenges in the development of three-dimensional photonic metamaterials", Nature Photonics, 5, 523-530, 2011.
5. Ghasemi R., P. H. Tichit, A. Degiron, A. Lupu and A. de Lustrac, "Efficient control of a 3D optical mode using a thin sheet of transformation optical medium", Opt. Express, 18, 20305, 2010.
6. Burokur S. N., A. Sellier, B. Kante, A. de Lustrac, "Symmetry breaking in metallic cut wire pairs for negative refractive index", Appl. Phys. Lett,. 94:201111, 2009.
7. Kante B., S. N. Burokur, A. Sellier and A. de Lustrac and J.-M Lourtioz, "Controlling Plasmon Hybridization for Negative Refraction Metamaterials", Phys. Rev. Lett. B., 79:075121, 2009.

Dynamical study and group velocity picture for metamaterials and devices

Xunya Jiang[1,2,3]

[1] Dept. of Illuminating Engineering and Light Sources, School of Information Science and Engineering, Fudan University , Shanghai, China
[2] Engineering Research Center of Advanced Lighting Technology, Fudan University, Ministry of Education , Shanghai, China
[3] State Key Laboratory of Functional Material for Informatics, SIMIT, CAS, Shanghai, China

Abstract

The wave propagation in the meta-material is so strange that many arguments appear when a kind of new material or a new effect is found, e.g. "Could the material exist in real world?" or "Is the effect real real?" etc.. Researchers have difficulties to find which side is correct. In this presentation, we will give several examples， such as superlens, hyperlens and cloak, to show that the dynamical study is the key method to solve such problems. From dynamical study, it can be revealed that how the fields evolve inside or at the interface of the meta-material and how the "beams" become stable after the relaxation process. The essential physical value behind these phenomena is group velocity (or energy velocity), which is obtained from the dispersion relation and determines the propagation direction of the beams. We will also demonstrate that some simulation results in frequency domain is misleading while the simulation in time domain is much more believable, since the causality restriction is forced to be satisfied in the time-domain simulation.

Plasmonic photocoupler for infrared optoelectronics

Zhenghua An
State Key Laboratory of Surface Physics and Key Laboratory of Micro and Nano Photonic Structures (Ministry of Education), Institute of Advanced Materials,, Fudan University, Shanghai 200433, China

**Email address: anzhenghua@fudan.edu.cn*

Plasmonic resonances are favorable for trapping photons efficiently into optoelectronic devices and therefore boost their performance, as has been proposed or demonstrated by many groups.[1] So far, most of reported works have mainly concentrated on the visible light (or near-infrared) region partially due to the urgent demands from green energy industry. However, in the longer-wavelength region, i.e., infrared and terahertz regions, the surface electromagnetic waves, known as Sommerfeld or Zenneck waves are characterized by poor confinement to surfaces and are therefore ineffective in enhancing the coupling strength of light-semiconductor interaction. By patterning the metal surface with subwavelength periodic features can markedly reduce the asymptotic surface plasmon frequency, leading to 'spoof' surface plasmons with subwavelength confinement at infrared wavelengths and beyond, which mimic surface plasmons at much shorter wavelengths. The usefulness of spoof surface plasmons for infrared optoelectronic devices have been evidenced by reported smaller divergence (reduced from $\sim 180^0$ to $\sim 10^0$) and higher directivity (~10 decibels) in terahertz quantum cascade lasers[2] and larger photo-responsivity (~130%) of a photodetector at 8.8μm [3] . On the other hand, however, the spatial confinement of the spoof surface plasmons in the reported works was still weak if we compare their decay length with the thickness of photo-active semiconductor layers. It is therefore anticipated that further improvement to the performance of plasmonic infrared optoelectronics might be possible if additional confinement is introduced.

We demonstrate that a plasmonic cavity consisting of a perforated metal film and a flat metal sheet separated by a semiconductor spacer is particularly suitable for multicolor infared light detection, due to the excellent spectral tunability, spatially distinct field distributions and absorption enchancement [4,5]. Three different types of optical modes are clearly identified --- the propagating and localized surface plasmons on the perforated metal film and the Fabry-Perot modes inside the cavity. Interactions among them lead to a series of hybridized eigenmodes exhibiting excellent spectral tunability and spatially distinct field distributions, which cannot be achieved by convential grating photo coupler. As an example, we design a two-color detector protocol with calculated photon absorption efficiencies enhanced by more than 20 times at both colors, reaching ~42.8% at 15μm (in wavelength) and ~46.2% at ~10.2 μm for a 1 μm total thickness of sandwiched quantum wells. The rich plasmonic-photonic hybridization effects discovered here provide plenty of opportunities to optimize light harvesting efficiencies for modern ultra-small infrared optoelectronic devices with subwavelength dimensions.

References:

1. For example, V. E. Ferry, L. A. Sweatlock, D. Pacifici, and H. A. Atwater, *Nano Letters*. **2008**, 8, 4391.
2. N.F. Yu, Q.J.Wang, M.A.Kats, *et al*, *Nature Materials* **2010**, 9, 730.
3. C. C. Chang, Y. D. Sharma, Y. S. Kim, J. A. Bur, R. V. Shenoi, S. Krishna, D. H. Huang, and S. Y. Lin, *Nano Letters*. **2010**, 10, 1704.
4. H.L.Wang, Zhenghua An, Che Qu *et al*, *Plasmonics*, **6**, 319(2011).
5. Feilong Mao, Jinjin Xie, *et al*, *Optics Express* **21**(1), 295 (2013).

Metamaterials to bridge propagating waves with surface waves and control electromagnetic waves

Qiong He[1], Shulin Sun[2], Shiyi Xiao[1], Xin Li[1], Din Ping Tsai[2] and Lei Zhou[1*]

[1] Department of Physics, Fudan University, Shanghai 200433, P. R. China

[2] Department of Physics, National Taiwan University, Taipei 10617, Taiwan

* phzhou@fudan.edu.cn

Abstract- We review our recent efforts in employing metamaterials to control electromagnetic (EM) waves. In particular, we show that a carefully designed gradient-index meta-surface can covert an incident propagating wave to a surface wave bounded on the meta-surface with 100% efficiency. We also demonstrate experimentally high-efficiency anomalous reflections for near-infrared light following the generalized Snell's law.

Controlling electromagnetic (EM) waves freely is a dream for researchers. While manipulating propagating waves (PWs) or surface waves (SWs) has separately become possible using transformation optics, a bridge that can link PWs with SWs at will has not yet been found and is highly desired to make the full control over EM waves possible. Recently, graded structures were widely used to control EM waves, leading to trapped rainbows, lensing, beam bending and deflection, but none of them was focused on bridging a PW with an SW. Here, we demonstrate that a specific gradient-index meta-surface can convert a PW to an SW with theoretically 100% efficiency [1]. Distinct from conventional devices such as prism or grating couplers, here the momentum mismatch between PW and SW is compensated by the reflection-phase gradient of the meta-surface, and perfect PW-SW conversion can happen for any incidence angle larger than a critical value. Experiments, including both far-field and near-field characterizations, are performed to verify this idea in the microwave regime, which are in excellent agreement with full-wave simulations. In addition, we demonstrated that such SWs bounded on the meta-surfaces, which are driven by incident PWs, can be guided out to flow as surface plasmons on another system supporting eigen surface EM modes. Our findings may pave the road for many applications, including high-efficiency surface plasmon couplers, anti-reflection surfaces, light absorbers, and so on.

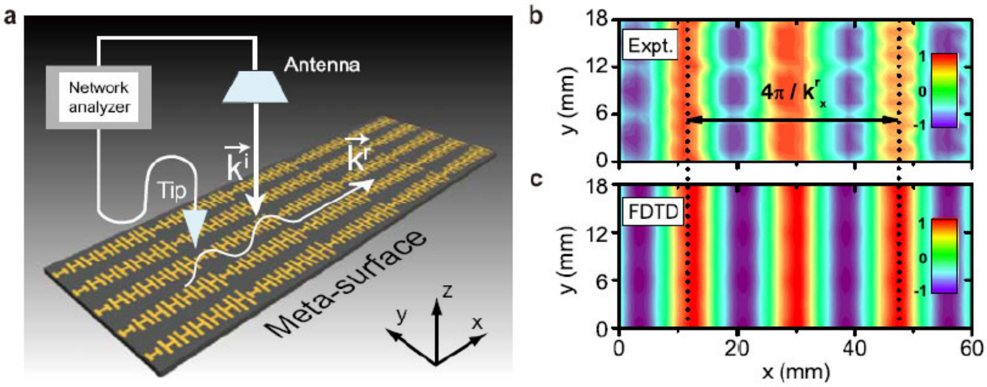

Fig 1. (a) Schematic picture showing the near-field characterizations of the PW-SW conversion. (b) Measured and simulated Ez field distributions on the meta-surface under the illumination of a normally incident PW.

We will also present our latest efforts in realizing the noted phenomena in optical frequency regime [2]. We combine theory and experiment to demonstrate that a carefully designed gradient meta-surface supports high-efficiency anomalous reflections for near-infrared light following the generalized Snell's law[3], and the reflected wave becomes a bounded surface wave as the incident angle exceeds a critical value. Compared to previously fabricated gradient meta-surfaces in infrared regime, our samples work in a shorter wavelength regime with a broad bandwidth (750−900 nm), exhibit a much higher conversion efficiency (~80%) to the anomalous reflection mode at normal incidence, and keep light polarization unchanged after the anomalous reflection. Finite-difference-timedomain (FDTD) simulations are in excellent agreement with experiments. Our findings may lead to many interesting applications, such as antireflection coating, polarization and spectral beam splitters, high-efficiency light absorbers, and surface plasmon couplers. And finally, We will show that a flat metasurface with a parabolic reflection-phase distribution based on gradient metasurface idea can focus an impinging plane wave to a point image in reflection geometry [4].

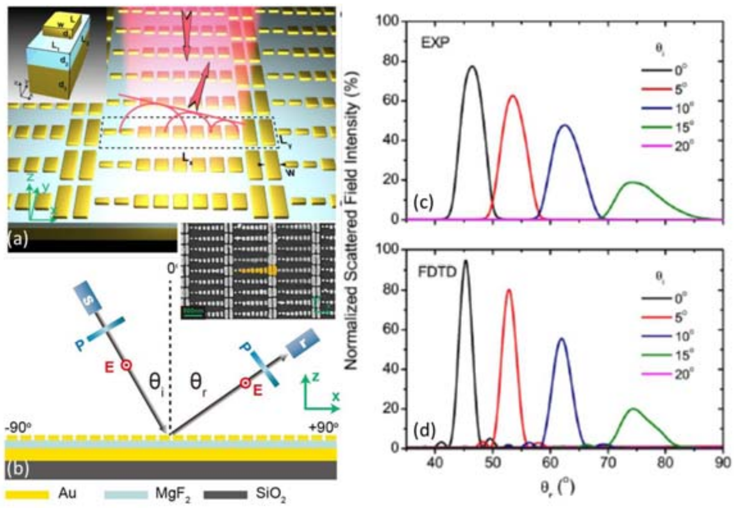

Fig2. (a) Schematics of the designed sample with a unit cell (inset) consisting of an Au nano-rod (yellow) and a continuous Au film (yellow) separated by the MgF2 spacer (blue). (b) Experimental setup for the far-field measurement. (c) and (d) Measured and simulated normalized scattered electric field intensity 0 for the gradient meta-surface under the illuminations a y-polarized light at λ=850 nm with different incident angles, respectively.

Acknowledgements: This work was supported by NSFC (60990321, 11174055, 60990324, and 11204040) and the Program of Shanghai Subject Chief Scientist (12XD1400700). The co-authors from Taiwan acknowledge financial support from National Science Council, under Grant Nos. 99-2120-M-002-012, 99-2911-I-002-127, 100-2120-M-002-008, and 100-2923-M-002-007-MY3, 100-2112-M-004-002, 100-2923-M-004-001-MY3, and 101-2221-E-259-024-MY3, 101-2120-M-259-002.

REFERENCES

1. Shulin Sun, Qiong He, Shiyi Xiao, Qin Xu, Xin Li & Lei Zhou, "Gradient-index meta-surfaces as a bridge linking propagating waves and surface waves", Nature Materials 11, 426-431 (2012).
2. Shulin Sun, Kuang-Yu Yang, Chih-Ming Wang, Ta-Ko Juan, Wei Ting Chen, Chun Yen Liao, Qiong He, Shiyi Xiao, Wen-Ting Kung, Guang-Yu Guo, Lei Zhou, and Din Ping Tsai, "High-Efficiency Broadband Anomalous Reflection by Gradient Meta-Surfaces" ,Nano Lett. 12, 6223−6229 2012.
3. N. Yu, P. Genevet, M. a. Kats, F. Aieta, J.-P. Tetienne, F. Capasso and Z. Gaburro, "Light propagation with phase discontinuities: generalized laws of reflection and refraction."Science 334, 333-337 (2011)
4. Xin Li, Shiyi Xiao, Bengeng Cai, Qiong He, Tie Jun Cui, and Lei Zhou, "Flat metasurfaces to focus electromagnetic waves in reflection geometry" , Opt. Lett 37, 4940, 2012

Acoustic metamaterials and phononic crystals

Anisotropic versions of pentamode structures: Towards transformation elastodynamcis

R. Schittny[1*], M. Kadic[1], T. Bückmann[1], and M. Wegener[1,2]

[1]Institute of Applied Physics, Karlsruhe Institute of Technology (KIT), 76128 Karlsruhe, Germany
[2]Institute of Nanotechnology, Karlsruhe Institute of Technology (KIT), 76128 Karlsruhe, Germany
*corresponding author: robert.schittny@kit.edu

Abstract— Pentamode metamaterials are artificial structures which—despite being solids—approximately resemble the mechanical properties of a liquid, having a finite bulk but vanishing shear modulus. Anisotropic versions of these structures are a promising candidate for applications in transformation-elastodynamics. We theoretically discuss possibilities for introducing anisotropy into three-dimensional pentamode structures and show examples of corresponding fabricated macro- as well as microstructures.

Liquids have a finite bulk yet a vanishing shear modulus, making them hard to compress but easy to deform. Ideal liquids in three dimensions can be seen as *pentamode* materials, having only one mode of propagation for elastic waves, namely the compression mode, while all five ("penta") other shear-related modes are absent. In 1995, Milton and Cherkaev proposed that these properties can also be approximated by artificial solid structures [1], which have been fabricated recently [2].

Fig. 1 a) shows a sketch of an ideal isotropic pentamode fcc unit cell, consisting of a diamond-like lattice with lattice constant a connected by double cones. In the ideal case, the connection points P between the double cones are point-like (marked with a green dot in Fig. 1 a)). While this theoretically gives rise to a shear modulus of exactly zero, such a structure can of course not be fabricated, since it would fall apart immediately. Thus, for fabrication, a small deviation of the perfect structure has to be introduced by making the connection points finite in size. Fig. 1 b) and c) show pictures of a macroscopic pentamode structure, fabricated with a commercial 3D printing system. The diameter of the connection point volume is $d = 0.25\,\mathrm{mm}$ and the lattice constant $a = 15\,\mathrm{mm}$. Corresponding microstructures with parameters $d = 0.55\,\mu\mathrm{m}$ and $a = 37.3\,\mu\mathrm{m}$ have been fabricated with direct laser writing (not depicted here) [2].

In sharp contrast to real liquids, artificial pentamode structures can also be made intentionally inhomogenous [3] as well as anisotropic. Anisotropy is an important prerequisite for several suggestions on transformation-elastodynamic architectures such as for example three-dimensional elastic cloaking [4, 5, 6, 7, 8, 9]. Here, we study the option to introduce anisotropy into three-dimensional pentamode structures by moving the position of the connection point P of the double cones inside the primitive unit cell. Fig. 1 d) shows a sketch of an ideal (meaning a point-shaped connection P) yet anisotropic version of a pentamode structure, where P was shifted along the space diagonal of the cubic fcc cell, while panels e) and f) of Fig. 1 again show corresponding fabricated macrostructures (same parameters as in Fig. 1 b) and c)).

The anisotropy resulting from the shifted position of P is studied using numerical calculations with the commercial software package Comsol Multiphysics. We calculate three-dimensional phonon band structures for a systematic variation of the connection point position and find anisotropic longitudinal-wave phase velocities that differ by a factor of nearly ten for experimentally accessible structures. At the same time, the shear-related transverse-wave phase velocities (which originate from the finite size of the connection point P) are always smaller than the longitudinal ones, although only by a factor of two for the case of maximum anisotropy. Furthermore, we find that in static continuum mechanics, a transition from anti-auxetic pentamode materials (Poisson's ratio $\nu = 0.5$) to an auxetic (Poisson's ratio $\nu < 0$) material is possible in dependence of the position of P, creating another possible application of anisotropic versions of pentamode structures.

In conclusion, we theoretically study anisotropic versions of pentamode structures and show them to be realistically accessible both for microscopic and macroscopic fabrication. While the numerical studies show promising results, even greater anisotropy might be needed for transformation-elastodynamic architectures, leading to further challenges in the fabrication. Experiments on the characterization of the fabricated structures are ongoing.

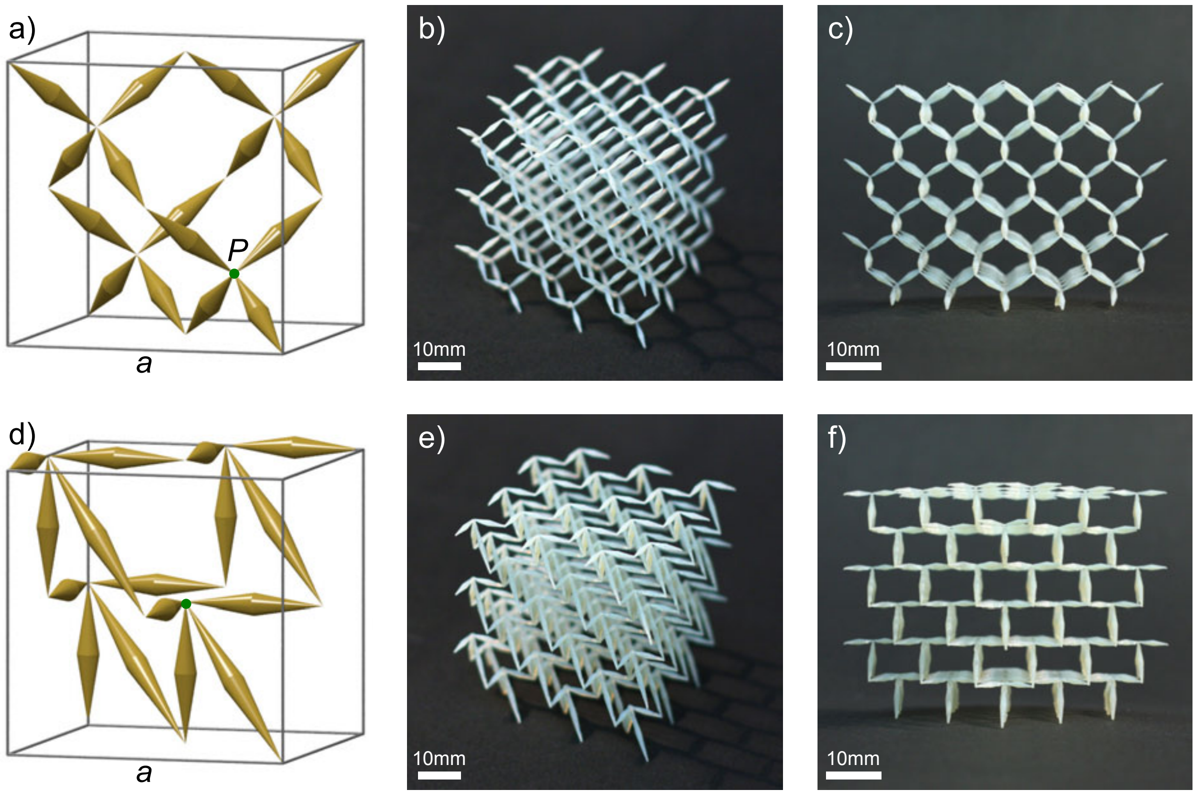

Figure 1: Examples of isotropic and anisotropic versions of pentamode structures. Panel a) shows a sketch of an isotropic pentamode fcc unit cell with the connection point P marked with a green dot. The connections between the double cones are point-shaped, resembling the ideal yet unrealistic pentamode case. Panels b) and c) show a macroscopic version of the same structure from two different angles, fabricated with a commercial 3D printing system on a much bigger scale ($a = 15\,\mathrm{mm}$). Panels d) to f) exhibit anisotropic versions of pentamode structures where the connection point in each unit cell has been shifted along the space diagonal of the cubic fcc cell. Panel d) again shows a sketch of the ideal structure while panels e) and f) display images of a corresponding fabricated macrostructure.

REFERENCES

[1] G. W. Milton and A. V. Cherkaev, J. Eng. Mater. Technol. **117**, 483 (1995)
[2] M. Kadic, T. Bückmann, N. Stenger, M. Thiel, and M. Wegener, Appl. Phys. Lett. **100**, 191901 (2012)
[3] A. Martin, M. Kadic, R. Schittny, T. Bückmann, and M. Wegener, Phys. Rev. B **86**, 155116 (2012)
[4] G. W. Milton, and M. Briane, and J. R. Willis, New. J. Phys. **8**, 248 (2006)
[5] A. N. Norris, Proc. R. Soc. Am. **464**, 2411 (2008)
[6] A. N. Norris, Proc. R. Soc. Am. **125**, 839 (2009)
[7] M. Brun, S. Guenneau, and A. B. Movchan, Appl. Phys. Lett. **94**, 061903 (2009)
[8] C. L. Scandrett, J .E. Boisvert, and T. R. Howarth, J. Acoust. Soc. Am. **127**, 2856 (2010)
[9] N. H. Gokhale, J. L. Cipolla, and A. N. Norris, J. Acoust. Soc. Am. **132**, 2932 (2012)

Nanoparticles and nanosystems

Nanophotonics in photovoltaic cells for solar or indoor light trapping

R. Peretti[1,2], T. Deschamps[1,2,3], G. Gomard[1,2,3], X. Meng[1,2,3], L. Lalouat[1,2,3], F. Mandorolo[1,3], A. Fave[1,3], E. Drouard[1,2], C. Seassal[1,2*]

[1]Université de Lyon, Institut des Nanotechnologies de Lyon (INL), UMR 5270, CNRS-INSA-ECL-UCBL, France

[2]Ecole Centrale de Lyon, 36 Avenue Guy de Collongue, 69134 Ecully Cedex, France

[3]INSA de Lyon, Bat. Blaise Pascal, 7 Avenue Capelle, 69621 Villeurbanne, France

[*]corresponding author: christian.seassal@ec-lyon.fr

Abstract- We first introduce selected approaches, concepts and technological strategies to control light collection and absorption in photovoltaic ultrathin film cells for both solar and indoor light harvesting. We then illustrate light trapping into photonic crystal structures with examples of structures and devices, including 100nm thick hydrogenated amorphous silicon and 1µm thick crystalline layer solar cells. Finally, we discuss on the interest of photonic crystal structures to enhance non linear optical processes like down conversion for 3rd generation solar cells.

During the past decades, research in the field of photovoltaic (PV) solar cells was mainly driven by material development, technological upgrading and cost reduction. New challenges have emerged with third generation PV devices, with a view to achieving very high efficiency and low cost systems by using a wider spectral range. In this scope, the recent development of Nanophotonics has triggered the emergence of novel concepts for light management in photovoltaic cells. This includes incident light trapping and strategies to control light absorption in thin film photovoltaic cells especially with Photonic Crystal (Ph.C.) [1]: it enables to reach higher absorption increase with a high angular tolerance, over the whole solar spectrum that enables to reach a very high absorption increase, over the whole solar spectrum. These approaches allow facing specification of light absorption for both solar and indoor light. In the first case, the major issue is to enable a broadband absorption enhancement mostly under a normal incidence while in the second case, the Ph.C parameters are adjusted to achieve a robust optical response over a broad range of solid angles as well as to match the particular emission spectra of the indoor light sources.

a) b)

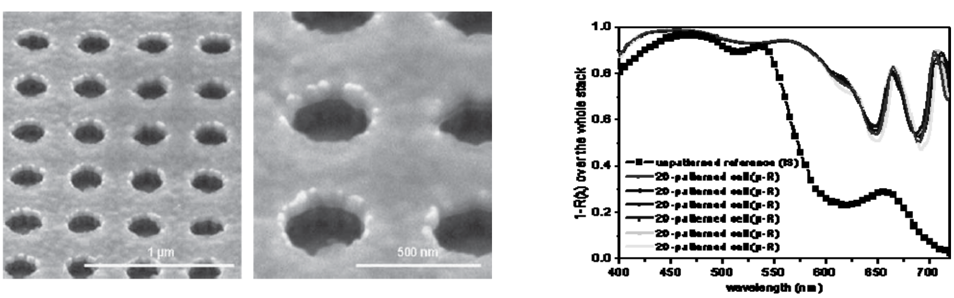

Figures 1. SEM views of the photonic crystal structure (a), and absorption spectra under normal incidence measured for the reference and patterned structures (b).

In this communication, we will first introduce the design [2], fabrication, and optical characterization of photonic crystal hydrogenated amorphous silicon (a-Si:H) solar cells structures using 1D [3] or 2D Ph.C. [4, 5] as shown in fig 1. Such a corrugation of the cell allow to a broader spectral absorption but also a better angular response allowing being good candidate in both solar and indoor photovoltaic.

Then, we introduce designs and experimental results obtained for solar cell structures based on crystalline silicon layers with thicknesses in the micrometer range [6] demonstrating spectral and angular absorption enhancement.

In parallel, and to go further in the complexity of the cells, a better understanding of the phenomenon playing a role in light absorption in PV cell was studied [7, 8]. We used the “time domain coupled mode theory” to model light absorption in our device especially focusing in 2 modes interaction.

Lastly, as an outlook, we discuss on the possibility to assist UV light absorption and IR light emission, using a down conversion layer [9], especially useful in the case of indoor photovoltaic cells. For instance, rare earth doped thin layers can absorb UV light and convert down to IR light with an efficiency upper than 1 (1.3 in our case), which is more efficiently converted into an electrical current by a c-Si solar cell. The efficiency of this process can be greatly increased if, e.g., UV light absorption can be strongly enhanced by photonic crystals.

To conclude, using the possibility to take control of the properties of optical modes, including their photon lifetime and their radiation pattern, is a great opportunity to generate novel generations of photovoltaic cells exhibiting specifically designed characteristics that can handle absorption enhancement in both solar and indoor light harvesting.

Acknowledgements, This work was supported by Orange Labs Networks contract 0050012310-A09221, by the European Union (EU) PhotoNVoltaics project (Grant Agreement No. 309127), by the ANR “Sparcs” and “Nathisol” project and by the “Repcop” IMUST project.

REFERENCES

1. Park, Y., Drouard, E., Daif, O. E., Letartre, X., Viktorovitch, P., Fave, A., Kaminski, A., Lemiti, M., and Seassal, C. Aug 2009 *Opt. Express* **17(16)**, 14312–14321.

2. Gomard, G., Drouard, E., Letartre, X., Meng, X., Kaminski, A., Fave, A., Lemiti, M., Garcia-Caurel, E., and Seassal, C. (2010) *Journal of Applied Physics* **108(12)**, 123102.

3. Daif, O. E., Drouard, E., Gomard, G., Kaminski, A., Fave, A., Lemiti, M., Ahn, S., Kim, S., iCabarrocas, P. R., Jeon, H., and Seassal, C. Sep 2010 *Opt. Express* **18(S3)**, A293–A299.

4. Gomard, G., Meng, X., Drouard, E., Hajjam, K. E., Gerelli, E., Peretti, R., Fave, A., Orobtchouk, R., Lemiti, M., and Seassal, C. (2012) *Journal of Optics* **14(2)**, 024011.

5. Meng, X., Gomard, G., Daif, O. E., Drouard, E., Orobtchouk, R., Kaminski, A., Fave, A., Lemiti, M., Abramov, A., iCabarrocas, P. R., and Seassal, C. (2011) *Solar Energy Materials and Solar Cells* **95, Supplement 1(0)**, S32 – S38.

6. Meng, X., Depauw, V., Gomard, G., Daif, O. E., Trompoukis, C., Drouard, E., Jamois, C., Fave, A., Dross, F., Gordon, I., and Seassal, C. Jul 2012 *Opt. Express* **20(S4)**, A465–A475.

7. Peretti, R., Gomard, G., Seassal, C., Letartre, X., and Drouard, E. (2012) *Journal of Applied Physics* **111(12)**, 123114.

8. Peretti, R., Gomard, G., Seassal, C., Letartre, X., and Drouard, E. (2012) Proceeding SPIE, volume **8425**, : SPIE p. 84250Q.

9. Deschamps, T., Guille, A., Drouard, E., Mazurczyk, R., Orobtchouk, R., Jamois, C., Fave, A., Peretti, R., Pereira, A., Moine, B., and Seassal, C. In Photonic West 2013 San Francisco (U.S.A.) number 8620-15.

Characterization of nano metal-semiconductor interfaces

M. Rezeq[1*], M. Ismail[1*], I. Lababidi[1] and Kh. Eledlebi[1]

[1]Khalifa University of Science Technology and Research, Abu Dhabi, Country
[*]corresponding author: mohd.rezeq@kustar.ac.ae.

Abstract- The I-V characteristics of nano-metal semiconductor contacts have showed unusual behaviors compared to conventional Schocttky contacts. We have studied the characterization of nano metal semiconductor interfaces when the contact size is reduced from micro to sub 10 nm range. We have performed analytical and numerical analyses to investigate the effect of the size of the contact on the energy band structure at the interface and found that the main depletion region parameters are direct functions of the nano metal size.

There is a growing interest in scaling down the basic electronic devices to a few nano meter range, which would result in minimum operation currents and voltages, and thus minimum energy consumption. Devices based on nano Schottky contacts have the capability to replace the conventional CMOS devices as the latter have some limitations in device scaling due to some technical difficulties, like controlling the dopant concentration around various junctions in sub 20 nm area. However, some preliminary analyses have been made to investigate the nano metal semiconductor contacts [1-4]. Here, we present a rigorous model that describes the metal semiconductor interface, which is based on visualizing a nano metal particle, with a spherical shape, embedded in a semiconductor substrate. As an example, we will consider a substrate made of an n-doped semiconductor, with a uniform doping concentration (N_d). The depletion region around the nano metal particle will look like a spherical shell with a positive charge density (ρ) equals to the dopant concentration, thus $\rho = q\ N_d$, as illustrated in Figure. 1. At electrostatic equilibrium enough charges (electrons) have transferred into the metal side until the Fermi levels on both sides are aligned up. However, since the nano metal particle size is limited, unlike the planar metal contacts, the amount of charge required to transfer to the metal is less than that required for the planar surface. Consequently this results in a narrower depletion region for the nano M-S contacts. The schematic in Figure 2 depicts the energy band structure through the transition from a planar metal-semiconductor (M-S) interface to a nano (M-S) interface.

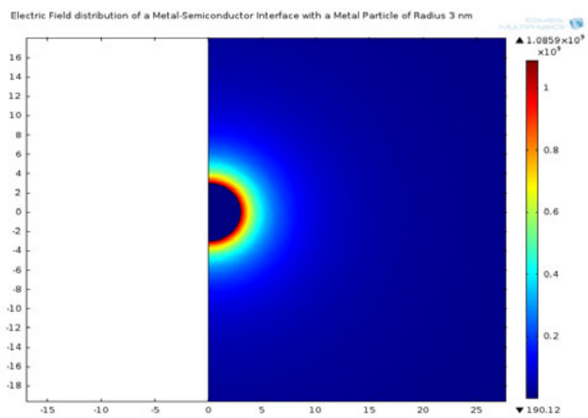

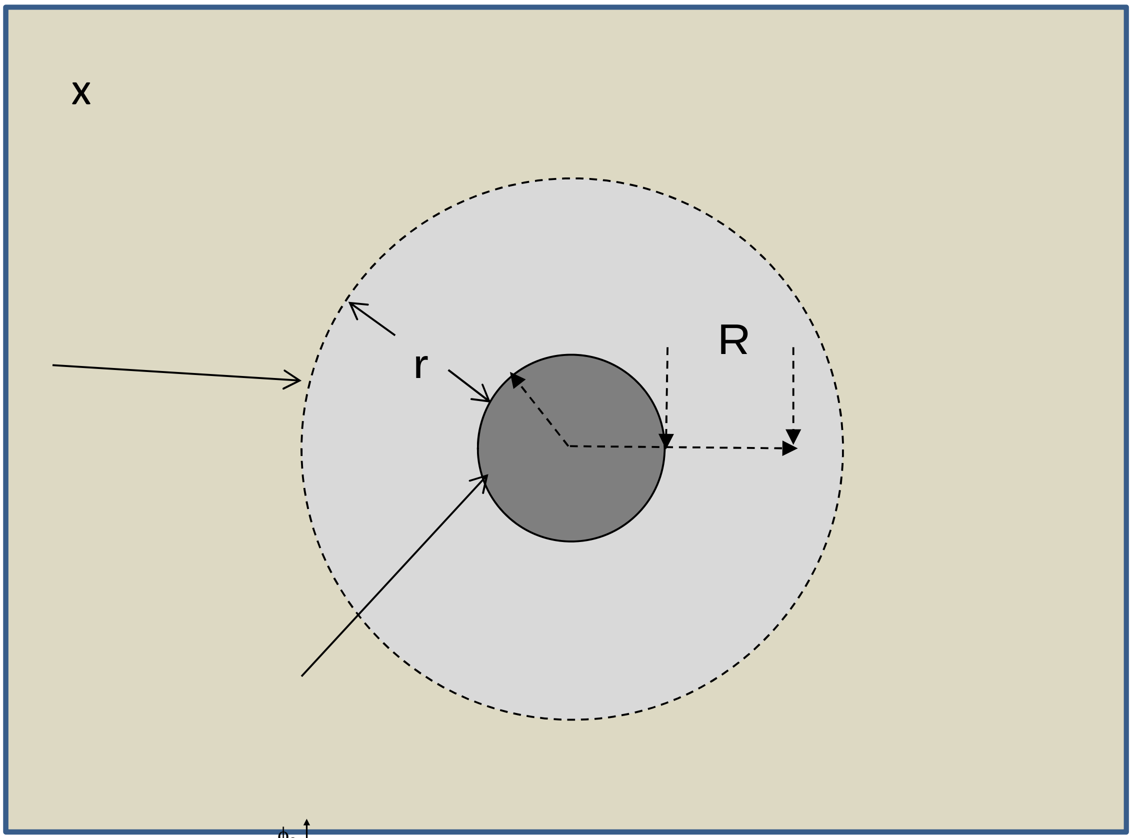

Figure 1: (left) Two-dimensional model of nano metal-semiconductor interface, (right) Finite element simulation model.

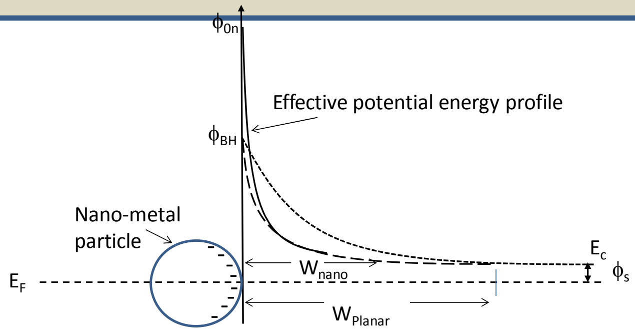

Figure 2: The enhancement of the potential energy at the interface as the depletion width is reduced from the planar value, due to the high surface charge density on the nano particle, to a maximum value ϕ_{0n}.

By applying Poisson's equation on the model [5] we have calculated the crucial parameters in the interface region, like the depletion width, the maximum electric field (E_{0n}) and the built-in potential (V_{bn}), for two different substrates with N_d = $1x10^{16}$ cm^{-3} and $1x10^{18}$ cm^{-3}. We have found that the depletion width decreases significantly with the decrease of the metal size, whereas this effect is less pronounced in the case of the high dope substrate. The electric field at the metal surfaces also enhances drastically as the metal size decreases from 50 μm to 3 nm. In the case of low dope, the maximum interface field compared to the planar interface field of the same substrate type is about three orders of magnitude higher. For instance, the maximum field is in the range of 1 V/nm for a nano particle radius = 3 nm. This effect is less significant in the case of high dope as the field enhancement over the same radius range is just about one order of magnitude. We have also calculated the effective barrier width which is taken at Full Width Half Maximum (FWHM) of the potential profile and found out that the effective barrier is in the range of the nano metal particle radius R, when R < 10 nm, and this barrier width increases rapidly and reaches smoothly the conventional planar contact values at large values of R, R > 1000 nm.

In conclusion, we have found out that the main interface parameters, w, E_{0n} and V_{bn} are direct functions of the radius of the metal contact which has more effect in low dope samples. The reduction of the barrier width and the field enhancement at the nano metal-semiconductor interface accounts for the reversed I-V characteristics that have observed for nano metal-semiconductor junctions.

REFERENCES

1. Song Q., Ding T., Li J., Cai Q., “Scanning tunneling microscope study of nanosized metal-semiconductor contacts between $ErSi_2$ nanoislands and Si(001) substrate,” *Surf. Sci.*, vol. 604, pp. 361-365, 2010.
2. .Kuikka M. A, Li W., Kavanagh K. L., Yu H-Z., “Nanoscale Electrical and Structural Characterization of Gold/Alkyl Monolayer/Silicon Diode Junctions,” *J. Phys. Chem. C*, vol. 112, pp. 9081-9088, 2008.
3. Smit G. D. J., Rogge S., and Klapwijk T. M., “Scaling of nano-Schottky-diodes,” *Appl. Phys. Lett.* Vol., no. 20, pp. 81, 3852-3854, Nov. 2002.
4. Sze S. M. and Ng K. K., “physics of semiconductor devices”, John Wiley and Sons, Hoboken, New Jersey, 2007
5. Rezeq M. and Ismail M., “The significant effect of the size of a nano-metal particle on the interface with a semiconductor substrate”, in *Proceedings of IEEE NANO2012 conference*, Birmingham, UK, August 2012, 1-5.

Nanoassemblies from Metallic and Semiconducting Nanocrystals

C. von Borczyskowski*

Department of Optical Spectroscopy and Molecular Physics, Institute of Physics,
Chemnitz University of Technology
Chemnitz, Germany

*corresponding author: borczyskowski@physik.tu-chemnitz.de

Abstract- Optical properties of nanomaterials such as semiconductor and metal quantum dots are important for sensor and photovoltaic applications. They often show quantum size effects. We report on optical, microscopic and AFM investigations on single quantum objects and the preparation of functionalized nanostructures via lithography. Of special interest is the investigation of semiconductor-organic dye nanoassemblies.

Modern material science focuses on nanostructures and even single atoms or molecules. Such materials are important for (molecular) electronics, photovoltaic, and analytics in medicine. Both, bottom-up and bottom-down preparation techniques are presently developed. In each case they need a high level of sensitivity to monitor material properties, related dynamics and functionalities. One mayor field of such investigations are optical properties related e.g. to sensors in medicine or environmental monitoring, photo-electrical devices, and quantum computing. The talk will outline the principle optical detection schemes for single semiconductor nanocrystals via scanning optical microscopy and spectroscopy. Applications for self-aggregated quantum dots and organic dye molecules will be discussed. This includes charge and excitation energy transfer, which are important aspects for photovoltaic devices. General models for electric charging of nanocrystals and semiconductor interfaces will be outlined. Applications such as lithographically functionalized interfaces for storage of electric charges, control of diffusion and selective molecular binding for sensors will also be presented.

Central aspects of nanomaterials are size dependent properties. Quantum size effects control the optical properties of many semiconductor and metallic quantum dots such as band gap energies and relaxation path ways. Many of these aspects can be investigated by optical single quantum object detection. One of the outstanding phenomena reported are luminescence intermittency and blinking [1]. The origin of these phenomena is the splitting-up of the electron-hole pair of an excited exciton.

The physical nature of intermittency is related to localisation of in most cases the electron at the interface of the quantum dot to the embedding environment. On the other hand, the properties of the interface are controlled by crystal defects, bonding properties or ligands. This gives rise to a competition of exciton states and surface states. The tunnelling probability of the excited excition wavefunction will control the population or even formation of surface states finally showing up as intra-band gap states [2] [3]. We will discuss varies aspects of the competion of charge localisation and radiationless transitions for the class of colloid CdSe/ZnS quantum dots.

Since localisation of excitons plays a prominent role in quantum dot physics we will discuss this matter with respect to those mechanisms, which are responsible for the localisation process itself. The representative class of silicon nanoparticles shows that electron-phonon coupling is the driving interaction [4, 5]. It depends both on the size of the quantum dot and the physico-chemical nature of the interface.

A comparison of both classes of quantum dots shows that some features are inherent to localisation processes, that are electron-phonon coupling and near-band edge-state formation. Both can be controlled by chemical and physical manipulation of the interface. All together we aim at a comprehensive description and modelling of complex interactions at quantum dot surfaces. A full understanding is mandatory for further material design and optimisation.

Finally we will report on the preparation of nanostructures via lithography and their functionalization via optical active organic dye molecules and quantum dots [6].

REFERENCES

1. F. Cichos, C. von Borczyskowski, M. Orrit, "Power-law intermittency of single emitters", *Current Opinion in Colloid and Interface-Science*, 12, 272-284, 2007.
2. T. Blaudeck, E. I. Zenkevich, F. Cichos, C. von Borczyskowski, "Probing Wave Functions at Semiconductor Quantum-Dot Surface by NON-FRET Photoluminescence Quenching", *Journal of Physical Chemistry C,* 20251-20257 *,2008*.
3. D. Kowerko, J. Schuster, N. Amecke, M. Abdel-Mottaleb, R. Dobrawa, F. Würthner, C. von Borczyskowski, "FRET and ligand related NON-FRET processes in single quantum dot-perylene bisimide assemblie", *PhysChemChemPhys*, 12(16), 4112, 2010.
4. J. Martin, F. Cichos, F. Huisken, C. von Borczyskowski, "Electron-Phonon Coupling and Localization of Excitons in Single Silicon Nanocrystals", *Nanoletters,* 8, 656-660, 2008.
5. N. El-Kork, F. Huisken, C. von Borczyskowski, "Dielectric effects on the optical properties of single silicon nanocrystals", J. Appl. Phys., 110( ), 074312, 2011.
6. T. Baumgärtel, H. Graaf and C. von Borczyskowski, "Effect of chemical termination of self-assembled organic monolayers on the tip induced local anodic oxidation of silicon(100)", Thin Solid Films, 519(11), 3443-3447, 2011.

Dissolution and Agglomerate Morphology of Protein-Stabilized Silver Nanoparticles

M. N. Martin[1*]
[1]Khalifa University of Science, Technology, and Research, United Arab Emirates
[*]corresponding author: matthew.martin@kustar.ac.ae

Abstract- Stability limits, and thus the destabilization of silver nanoparticles (AgNPs) is poorly understood, mostly because effects such as dissolution, agglomeration, and sedimentation compete, making it technically challenging to quantify the destabilization process. By utilizing *in situ* ultra-small angle X-ray scattering (USAXS), we were able to simultaneously measure dissolution, agglomeration, and stability limits of AgNPs coated with a highly protective protein: bovine serum albumin (BSA). Intermediate agglomerate morphologies during the destabilization process were examined as well.

Silver nanoparticles (AgNPs) are the focus of intense scientific research [1] because they have unique biological and environmental properties that are not present in their elemental and bulk counterparts. Unlike gold, elemental Ag is a natural biocide and, at the nanoscale, the chemical activity is amplified due to the increased ratio of surface to volume atoms. However, aqueous AgNPs are not inert, unlike gold; AgNPs agglomerate, precipitate, and dissolve in water if not carefully stabilized. Since silver ions are known to be toxic to cells, or useful for disinfecting wounds, and are now being incorporated as AgNPs into medicines, there exists a critical need for quantification of the amount of silver released from nanoparticle form [2] and under what conditions.

Probing gently around BSA's stability limits revealed the likely mechanism of BSA coating breakdown in which individual particles disappear as a whole. Many insights were gained into the stabilization ability of proteins as well. This study can be extended to a wide variety of metal nanoparticle systems and coating molecules to survey their stability limits.

Acknowledgements Funding from NIST-ARRA Fellowship Program Award, NIST Materials Measurement Lab, and use of the Advanced Photon Source at Argonne National Laboratory.

REFERENCES

1. Tolaymat, T. M., El Badawy, A. M., Genaidy, A., Scheckel, K. G., Luxton, T. P., Suidan, M. "An Evidence-based Environmental Perspective of Manufactured Silver Nanoparticle in Syntheses and Applications: A Systematic Review and Critical Appraisal of Peer-reviewed Scientific Papers." *Science of the Total Environment*, 408, 999–1006, 2010.
2. Liu, J.; Hurt, R. H. Ion Release Kinetics and Particle Persistence in Aqueous Nano-Silver Colloids. *Environmental Science & Technology*, 44, 2169–2175, 2010.

Integrated plasmonics: towards zeptogram-scale colorimetric sensing

J. Proust[1], J. Martin[1], D. Gérard[1], J-L Bijeon[1] and J.Plain[1,*]
[1]LNIO, Université de technologie de Troyes, France
[*]corresponding author: jerome.plain@utt.fr

Abstract- We report on the fabrication of single metal plasmonic sensors made of a single metallic nanoparticle integrated at the top of a axicon lens. This system allows to optimize efficiently the excitation of a plasmonic nano-object and the collection of its far-field collected signal. Finally, the use of such a nanosystem as very sensitive colorimetric sensor is demonstrated.

Due to the Localized Surface Plasmon Resonance (LSPR), light is intensively absorbed and scattered by metal nanoparticles. LSPR phenomenon confers to MNPs extremely attractive nano-optical properties and the subsequent technological applications are various. As it is well known, LSPR is extremely sensitive to the dielectric environment of the MNPs paving the way to highly sensitive sensors. Consequently, any optical change in the environment will induce a measurable shift of the plasmon resonance. This property is widely used to develop plasmon-based nanosensors[1]. In general, plasmon-based nanosensors are developed as an array of nanoparticles in order to get an easily measurable signal[2]. Unfortunately, the quality factor of the LSPR of such an array is strongly reduced due to various phenomena. Such damping can be partially limited by using a single nanoparticle in place of an array as nanosensor. Using single MNP as an active nano-optical device relies in the development of efficient techniques to measure their optical properties with a good signal-to-noise ratio.

In order to significantly optimize our signal, our single MNP-based nanosensor is integrated into a system shown figure 1a[3]. It allows to efficiently couple the far field excitation to the single particle and then to efficiently collect the transmitted light. Our approach is based on the integration of the MNP-based nanosensor onto an axicon lens (see figure 1b)[4]. We report a limit of detection of about some tens of zeptograms as shown figure 1c.

As a conclusion, we clearly show the ability to measure a signal variation induced by some tens of zeptogram of organic material absorbed onto a single metal nanoparticule-based nanosensor.

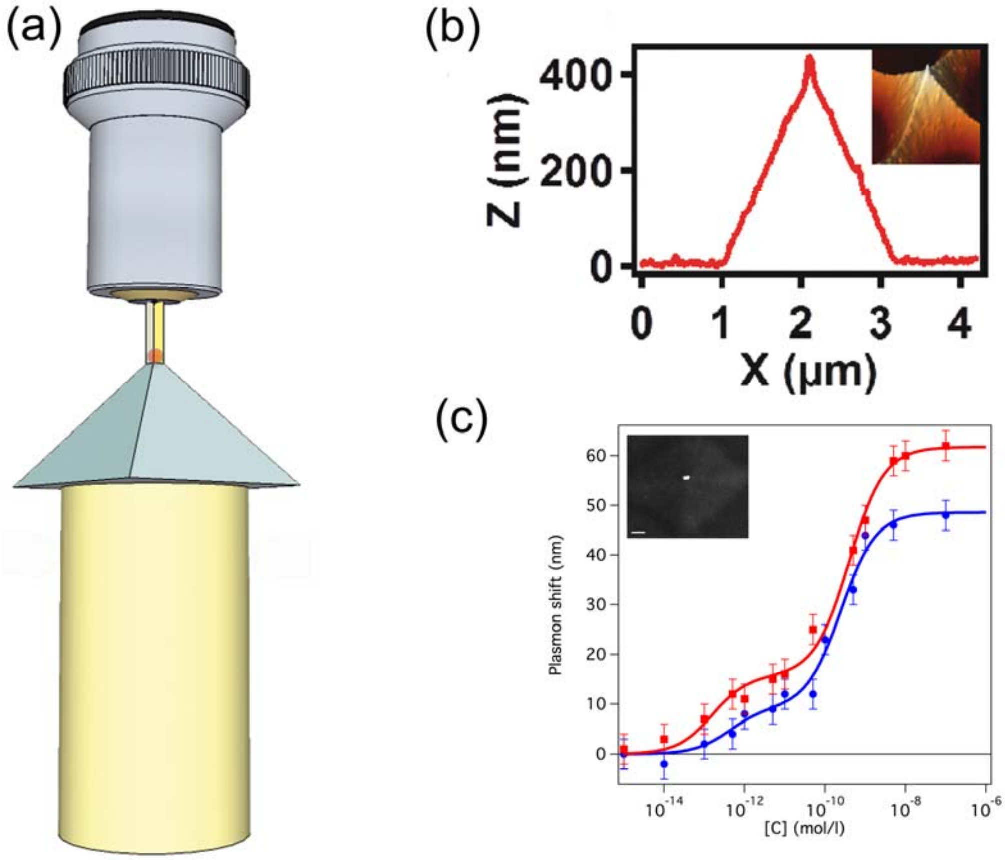

Figure 1: (a) Schematic representation of the developed system. (b) Atomic force microscopy image showing one axicon lens functionalized with a single gold nanoparticle. (c) Limit of detection measured onto a dimer for both polarizations (longitudinal polarization in red and transverse polarization in blue).

Acknowledgements. This work has been funded by the European community (FEDER funds), the « conseil général de l'Aube » and the « Conseil Régional Champagne-Ardenne »: grant NANO'MAT (www.nanomat.eu).

REFERENCES

1. Anker, J. N.; Hall, W. P.; Lyandres, O.; Shah, N. C.; Zhao, J.; Van Duyne, R. P. "Biosensing with Plasmonic Nanosensors." *Nature Materials* 7, 442–453, 2008.
2. Barbillon, G.; Bijeon, J.-L.; Plain, J.; Lamy De La Chapelle, M.; Adam, P.-M.; Royer, P. "Biological and Chemical Gold Nanosensors Based on Localized Surface Plasmon Resonance." *Gold Bull* 40, 240–244, 2007.
3. Barbillon, G.; Bijeon, J.; Lerondel, G.; Plain, J.; Royer, P. "Detection of Chemical Molecules with Integrated Plasmonic Glass Nanotips." *Surface Science* 602, L119–L122, 2008.
4. Martin, J.; Proust, J.; Gerard, D.; Bijeon, J.-L.; Plain, J. "Intense Bessel-Like Beams Arising From Pyramid-Shaped Microtips." *Opt Lett* 37, 1274–1276, 2012.

Surface enhanced spectroscopies : from SERS to MEF/SEF

P. M. Adam[1],
[1]Author Institut Charles Delaunay - Université de technologie de Troyes, CNRS FRE 2848,
Laboratoire de Nanotechnologie et d'Instrumentation Optique,
12 rue Marie Curie, BP 2060 – 10010 Troyes Cedex, France
E.mail : adam@utt.fr

Abstract-Plasmonics is a field connected to optics dealing with the properties and applications of surface plasmons which are modes of metal dielectric interfaces. Nanoplasmonics concerns the excitation, manipulation and detection of the surface plasmons at the nanometric scale. It has highly potential applications for ultrasensitive biochemical sensing. Surface enhanced spectroscopies are the ultimate sensor tools as they can reach single molecule sensitivity. We will present in this paper our results towards the realization of highly controllable and reproducible nanoplasmonics substrates.

1. Introduction

Plasmonics is now well established field finding numerous applications in pharmacology, biology, optoelectronics and metamaterials among others. For the sensitive detection of molecules or markers Surface Enhanced Spectroscopies are well widespread [1].

Among them, Surface Enhanced Raman Spectroscopy (SERS) and Metal Enhanced Fluorescence (MEF) or Surface Enhanced Fluorescence (SEF) are the most used for applications. Both these enhanced spectroscopies are based on local field enhancement entailed in the near vicinity of metallic nanoparticles when Surface Plasmon oscillations are driven for a specific optical wavelength. SERS can achieve single molecule detection when two or more metallic nanoparticles are near-field coupled, resulting in enhancements ranging between 8 and 10 orders of magnitude, even if absolute magnitude of enhancement is still a subject of debate. However, these particular SERS substrates are difficult to reproduce.

Less enhancement is obtained with MEF/SEF but usually the intrinsic fluorescence cross section of a molecule is 14 orders of magnitude more important than that of its Raman cross-section. In MEF/SEF one has to take into account the finite lifetime of the excited levels of the molecule of interest, which results in quantum yield (modifications in the presence of the metallic nanoparticles. Quantum yield can be enhanced or even reduced leading in the latter case to a competition with local field excitation enhancement and thus the possibility of quenched fluorescence of the emitters.

Another approach for detecting various molecules is biochemical sensors relying on the detection of the spectral shift of the Surface Plasmon resonance of metallic nanoparticles after the adsorption of these same molecules. This technique, even if not reaching single molecule detection so far, has the advantage of being not limited to specific types of molecules. This contribution will show the ties between SERS, MEF and sensors. Some of the works of the LNIO laboratory in that direction will also be presented. [2-4].

2. Results and discussions

There is definitely a parallel between SERS [2] and MEF [3] as both types of spectroscopies deal with enhancement of incoherent spontaneous phenomena: spontaneous emission for fluorescence, spontaneous scattering for Raman. Both phenomena can thus be treated the same way from the theoretical point of view [5]. The main difference resides in the fact that SERS involves virtual levels while MEF/SEF involve real levels of the molecule of interest.

When performing SERS or MEF experiments the emitting or scattering molecules do necessarily, by their presence in the near vicinity of the metallic nanoparticles, entail a shift in the surface plasmon resonance of the latter. This is indeed the principle of nanoplasmonic biochemical sensors [4]. This shift is due to the modification of the refractive index of the surroundings of the metallic nanoparticles. As a comparison traveling surface plasmons on plane interfaces exhibit a dispersion law and such planar surface waves do depend on the dielectric properties of both adjacent media of the interface.

3. Conclusions

Nanoplasmonics is an emerging branch of nanoptics with a high potential for applications in biochemistry. It is also worth mentioning that from the fundamental point of view m any new effects have been recently observed and this will pave the way to other possible directions for applications in sensors and enhanced spectroscopies.

Acknowledgements: The author thanks the financial support of NanoMat (www.nanomat.eu) by the "Ministère de l'enseignement supérieur et de la recherche," the "Conseil régional Champagne-Ardenne," the "Fonds Européen de Développement Régional (FEDER) fund," and the "Conseil général de l'Aube" is acknowledged. including all funding information, should be gathered into a brief statement at the end.

REFERENCES

1. K. M. Kosuda, J. M. Bingham, K. L. Wustholz, and R. P. Van Duyne, Chapter 10, in "Handbook of Nanoscale Optics and Electronics"; Wiederrecht, G., Ed., Elsevier, Amsterdam (2010).
2. J. Grand, J., M. Lamy de la Chapelle, J.L. Bijeon, P.M. Adam, A. Vial, P. Royer, Phys. Rev. B, 72, 033407 (2005)
3. P. Viste, J. Plain, R. Jaffiol, A. Vial, P.-M. Adam, P. Royer, ACS Nano, 4, 759 (2010)
4. G. Barbillon, J.L. Bijeon, J. Plain, M. Lamy de la Chapelle, P.M. Adam, P. Royer, Surf. Sci., (2007), vol.601, p. 5057-5061.
5. S. Gaponenko "Introduction to Nanophotonics", chapter 13, Cambridge University Press 2010.

The study of magnetic properties of Ge nanoparticles

Yung. Liou[1]

[1]Institute of Physics, Academia Sinica, Taipei, Taiwan, ROC
[*]corresponding author: yung@phys.sinica.edu.tw

Abstract- Room-temperature ferromagnetism was observed in Ge nanoparticles fabricated by different methods. The saturation magnetization was determined by both the size and inter-particle distance of Ge nanoparticles.

In this study, room-temperature ferromagnetism was observed in Ge nanoparticles. Ge nanoparticles with various sizes were fabricated by different methods, such as thermal evaporation, inert gas condensation, co-sputtering and so on. By depositing different thick Ge films on rough surfaces, such as polystyrene nanospheres covered Si substrates, the ferromagnetism in Ge films was observed. The saturation magnetization in Ge films depended on both the thickness of the film and the size of underneath nanospheres. The ferromagnetism disappeared when Ge films were thicker than 10 nm or the sizes of nanospheres were larger than 50 nm. The largest saturation magnetization was measured in the sample with 5 nm thick Ge film on the nanosphere with 20 nm in diameter. From the observations of the atomic force microscope and transmission electron microscope, we believed the Ge films were broken into different sizes of nanoparticles due to the rough surface underneath and the structure of the Ge nanoparticles was mostly amorphous. The sizes and the distributions of Ge nanoparticles were manipulated by the sizes of the polystyrene nanospheres and the thickness of the Ge films.

Similar results were also observed when we replaced the polystyrene nanospheres with silica nanoballs. Different Ge nanoparticles have also been collected in inert gas condensation method by adjusting the helium pressures. The saturation magnetization of these samples was affected by both the size and the density of Ge nanoparticles. By co-sputtering, Ge nanoparticles have been mixed into other different matrix materials, such as Al, Cu, Sb, Bi and SiO_2, and the magnetic properties have been investigated. The magnitudes of the saturation magnetization in these samples were different from the other methods, but the largest saturation magnetizations were always measured in samples with smaller sizes and higher densities of Ge nanoparticles. The ferromagnetism always disappeared if large Ge particles or Ge continuous films were formed. The room-temperature ferromagnetism was attributed to the magnetic coupling among Ge nanoparticles, in which magnetic moments in Ge nanoparticles might arise from the size effect however both the defect and surface effects might also be included.